B. B. Das
Christy P. Gomez
Benu G. Mohapatra   *Editors*

Recent Developments in Sustainable Infrastructure (ICRDSI-2020)— Structure and Construction Management

Conference Proceedings
from ICRDSI-2020 Volume 1

Lecture Notes in Civil Engineering

Volume 221

Lecture Notes in Civil Engineering (LNCE) publishes the latest developments in Civil Engineering - quickly, informally and in top quality. Though original research reported in proceedings and post-proceedings represents the core of LNCE, edited volumes of exceptionally high quality and interest may also be considered for publication. Volumes published in LNCE embrace all aspects and subfields of, as well as new challenges in, Civil Engineering. Topics in the series include:

- Construction and Structural Mechanics
- Building Materials
- Concrete, Steel and Timber Structures
- Geotechnical Engineering
- Earthquake Engineering
- Coastal Engineering
- Ocean and Offshore Engineering; Ships and Floating Structures
- Hydraulics, Hydrology and Water Resources Engineering
- Environmental Engineering and Sustainability
- Structural Health and Monitoring
- Surveying and Geographical Information Systems
- Indoor Environments
- Transportation and Traffic
- Risk Analysis
- Safety and Security

To submit a proposal or request further information, please contact the appropriate Springer Editor:

– Pierpaolo Riva at pierpaolo.riva@springer.com (Europe and Americas);
– Swati Meherishi at swati.meherishi@springer.com (Asia - except China, and Australia, New Zealand);
– Wayne Hu at wayne.hu@springer.com (China).

All books in the series now indexed by Scopus and EI Compendex database!

More information about this series at https://link.springer.com/bookseries/15087

B. B. Das · Christy P. Gomez · Benu G. Mohapatra
Editors

Recent Developments in Sustainable Infrastructure (ICRDSI-2020)—Structure and Construction Management

Conference Proceedings from ICRDSI-2020
Volume 1

Editors
B. B. Das
Department of Civil Engineering
National Institute of Technology Karnataka
Surathkal, India

Christy P. Gomez
Department of Construction Management
Universiti Tun Hussein Onn Malaysia
Batu Pahat, Johor, Malaysia

Benu G. Mohapatra
School of Civil Engineering
KIIT Deemed University
Bhubaneswar, India

Contents

Prediction of Carbonation on Precast Concrete Exposed to Severe Environmental Conditions

T. Jena, K. C. Panda, and C. R. Panda

1 Introduction

Concrete structures are highly vulnerable in marine environment. The off-shore and on-shore structures are always at high risk for different types of chemical attacks in tidal zones near marine site. The wind blowing from sea regions is containing saline water vapours and attacking on structural components that produced chloride induced corrosion which is too harmful for concrete to sustain under such a marine exposure condition. A good compaction, well-made construction joints etc. are among disparate points which can help increasing the durability of concrete in sea water. For better quality if it is possible then the use of high pressure steam-cured prefabricated concrete elements is necessary. Chemical attack is defining as leaching or attack by acid or sulphate chloride, carbonate, bicarbonate, alkalinity, magnesium, leaching and attack by acid the dissolution of lime is associated with the use or lean permeable concrete in cold water. When carbon dioxide from the air enters into concrete and reacts with calcium hydroxide which forms calcium carbonates is known as "carbonation". Carbon dioxide carbonates the concrete in huge amount and reduces the alkalinity nature of concrete. The hardened cement paste's pH-value was around 13 shall be reduced to 9.0. Further the value reduced to about 8.3, when all the $Ca(OH)_2$ has become carbonated. When pH-value becomes low, the protective layers of concrete get destroyed and the steel reinforcement gets corroded.

Research papers related to carbonation are summarized here. Jena and Panda [1] studied the durability properties of precast concrete exposed to sea water. Prusty et al [2] reviewed many papers regarding durability properties of concrete using

T. Jena (✉) · C. R. Panda
SOA (Deemed To Be University), ITER, Bhubaneswar, Odisha, India
e-mail: trilochanjena@soa.ac.in

K. C. Panda
Department of Civil Engineering, GCEK, Bhawanipatna, Odisha, India

agro- waste products. Finally the authors reported that there was an increasing trend for depth of carbonation when the substitution of agro-waste in concrete and mortar increases. But it can be decreased by reducing the water cement ratio. Morandeau et al [3] studied the accelerated carbonation tests with concentration of 10% CO_2 at 25 °C and 62% relative humidity (RH) on FA blended cement pastes. Experiments were performed to study the carbonation depth at the ages of 1 to 16 weeks in order to quantify key parameters such as mercury intrusion porosimetry (MIP), thermo gravimetric analysis (TGA) and gamma ray attenuation method (GRAM). The authors reported that the highest contents of 60% FA decrease total porosity with a rearrangement of the microstructure due to carbonation and development of big capillary pores in the paste. Jena and Panda [1, 4–6] studied the utilization of silpozz upto 30% replaced with OPC to improve the durability of marine concrete and found an alternative material which can be used as a substitute material of silica fume (SF). Panda and Prusty [7] found the development of strength properties using silpozz as a partial replacement of OPC. Won et al [8] developed precast concrete panels after partial replacement of BFS ranges from 50%, 60% and 70% by weight with cement and steam curing was given for 4, 5, 6 and 8 h of interval. The result showed that 60% BFS and 6 h duration of steam curing sample performed better than control mix. The reduction in CO_2 emission was 33.8% as compared to control mix. Kari et al [9] verified the experimental carbonation data with the theoretical modeling approach consists of thermo dynamic model and statistical methodology after exposing the sulphate resisting Portland cement concrete specimens for 13 years to natural carbonation. The author investigated that thermo dynamic model proved to be well over the statistical methodology. The author also suggested that the carbonation phenomenon is too complex to predict by conventional diffusion equation. Frias and Goni [10] studied the depth of carbonation at 100% CO_2, 65% RH and 20 ± 1 °C for a period of 30 days using OPC, activated paper sludge and FA.

2 Materials and Methods

The materials composed of OPC 43 grade, Silpozz, FA, fine aggregate, coarse aggregate, sea water and super plasticizer. The experimental physical properties of OPC such as standard consistency 34%, initial setting time 165 min, final setting time 360 min, fineness 333 m^2/kg and specific gravity 3.15 are determined confirming to IS 8112:1989 [11]. The physical properties of coarse aggregates obtained as per IS: 383-1970 [12] such as fineness modulus 7.0, water absorption 0.2%, specific gravity 2.86, and crushing value 23.3% as well as the properties of fine aggregates such as fineness modulus 3.03 (Zone-III), water absorption 0.4% and specific gravity 2.67. High end super plasticizer CERA HYPERPLAST XR-W40 is used.

When FA is used as partial replacement with OPC in blended concrete, low heat is produced and staggers through pozzolanic reactions and ultimately reduces microcracking thus improves soundness of concrete. Silpozz can be used as an effective mineral admixture to make special concrete mixes and also improves the durability of

Table 1 Materials properties (chemical and physical)

Oxides (%)	OPC	Silpozz	FA
SiO_2	20.99	88.18	58.13
Al_2O_3	6.05	1.61	31.00
Fe_2O_3	6.01	0.56	4.10
Carbon	–	2.67	–
CaO	62.74	1.59	0.60
MgO	1.33	1.63	0.10
K_2O	0.40	1.67	0.90
Na_2O	0.04	–	0.05
SO_3	1.82	–	0.12
TiO_2	0.025	–	1.63
Others	–	2.09	0.011
Moisture content (%)	–	0.79	3.0
Loss on ignition (%)	1.14	0.04	0.29
Physical properties			
Bulk Density (gm/cc)	1.43	0.23	1.2
Specific gravity	3.15	2.3	2.12
Particle size (Micron)	35	25	34
Specific surface, m^2/g	0.33	17	33
Color	Gray	Gray black	Gray

marine concrete. The heat of hydration is lowered by as much as 30% when Silpozz is added to concrete, as well as prevents formation of cracks during casting. The chemical and physical properties of FA and silpozz given by the supplier are shown in Table 1.

2.1 Mix Proportions and Identifications

The minimum grade of concrete is M30 which is suitable for marine environment and designed as per Indian Standard code 10,262–2009 [13]. The proportion of material ratio was (1:1.44:2.91), w/b 0.43. The reduction of water was observed by 20% after several trial mixes in order to maintain the slump in between 25–50 mm. The first blended concrete samples were made 0% FA and the silpozz replacement varied from 10–40% with OPC. The second blended concrete samples were made 10% FA and the replacement of silpozz varied from 10–40% with OPC. The third blended concrete samples were made 20% FA and replacement of silpozz varied from 10–30% with OPC. The fourth blended concrete samples were made 30% FA and silpozz varied from 10–20% with OPC. The control mix prepared with 100% OPC. The percentage of cementitiuos materials with SP are given in Table 2.

Table 2 Percentage of cementitiuos materials with SP

Proportions of cementitious materials	Mix identity
Cement 100% + FA 0% + Silpozz 0% + SP 0%	MC100F0S0
Cement 90% + FA 0% + Silpozz 10% + SP 0.20%	M1C90F0S10
Cement 80% + FA 0% + Silpozz 20% + SP 0.29%	M1C80F0S20
Cement 70% + FA 0% + Silpozz 30% + SP 0.40%	M1C70F0S30
Cement 60% + FA 0% + Silpozz 40% + SP 0.45%	M1C60F0S40
Cement 80% + FA 10% + Silpozz 10% + SP 0.22%	M1C80F10S10
Cement 70% + FA 10% + Silpozz 20% + SP 0.33%	M1C70F10S20
Cement 60% + FA 10% + Silpozz 30% + SP 0.47%	M1C60F10S30
Cement 50% + FA 10% + Silpozz 40% + SP 0.72%	M1C50F10S40
Cement 70% + FA 20% + Silpozz 10% + SP 0.25%	M1C70F20S10
Cement 60% + FA 20% + Silpozz 20% + SP 0.38%	M1C60F20S20
Cement 50% + FA 20% + Silpozz 30% + SP 0.56%	M1C50F20S30
Cement 60% + FA 30% + Silpozz 10% + SP 0.30%	M1C60F30S10
Cement 50% + FA 30% + Silpozz 20% + SP 0.46%	M1C50F30S20

3 Prediction of Carbonation

The most external agents are chlorides that intrude into concrete and carbonation induced corrosion causing structural damage in marine environments. The carbonation induced corrosion occurred in marine concrete when carbon dioxide intrusion takes place into concrete cover and reaches the reinforcement causing corrosion in presence of moisture and oxygen. The durability properties in term of carbonation depth measurement are presented for SWC pre-cast concrete samples at 28, 90, 180 and 365 days. The depth of carbonation is measured by spraying a phenolphthalein indicator on fresh concrete chiseled and cleaned by wire brush. The phenolphthalein solution will remain unchanged where concrete is carbonated and turn pink where concrete is not carbonated. At least the average of four measurements is reported for each sample of carbonation. The depth of carbonation is increased with time of exposure at all ages. It is found that as the percentage of FA increases, the depth of
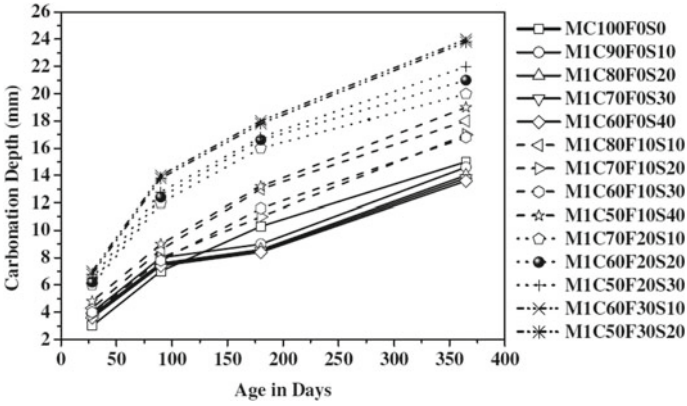
Fig. 1 Carbonation depth verses age in days

Fig. 2 Carbonation coefficient verses concrete mix
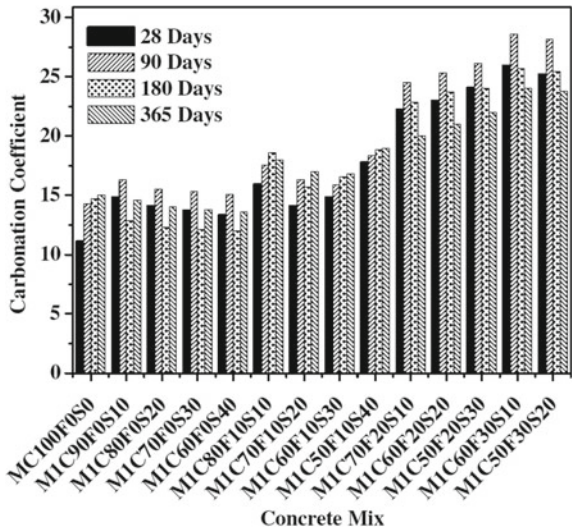
carbonation increases which is agreed with Ho and Lewis [14]. The carbonation coefficient is calculated using the relationship, $X = K \sqrt{T}$, where, X is the carbonation depth in mm, T is the exposure period in years and K is the carbonation coefficient.

4   Results and Discussions

The carbonation depth verses age in days is given in Fig. 1. The coefficient of carbonation verses concrete mix is shown in Fig. 2. Papadakis [15] observed that the coefficient of carbonation increases with increase in FA content. When silpozz is replaced with OPC, the coefficient of carbonation is decreasing. The higher cement content increase the alkali content and reduces the carbonation rate. The depth of carbonation is increased with time of exposure at all ages.

Tha concrete mix versus carbonation depth for different curing periods is shown in Fig. 3.

All silpozz based samples with SP contributes less carbonation depth as compared to control sample. When OPC is replaced by silpozz with desired doses of SP, the coefficient of carbonation is decreasing. The higher cement content increases the alkali content and reduces the carbonation rate. Due to the increase in alkalinity, the passivating layer around the reinforcement does not destroyed and hence reduces the carbonation rate. The lower cement content provides lower depth of carbonation as FA and silpozz is replacing with OPC.

Fig. 3 Types of mix verses depth of carbonation
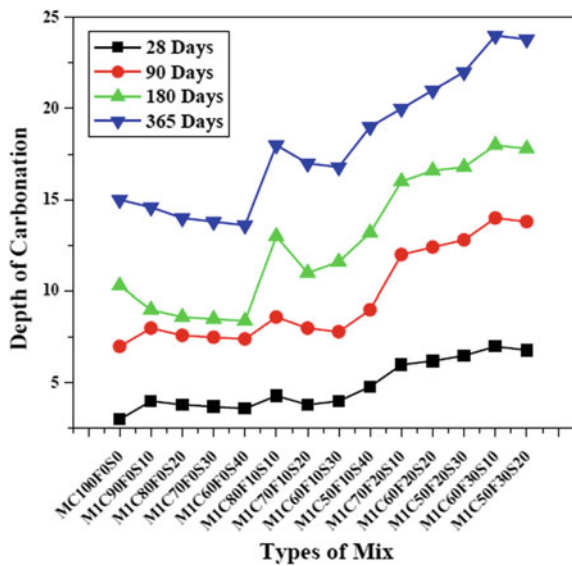
5　Conclusions

A few concluding remarks may be drawn from this article:

- As the replacement of FA increases the carbonation depth increases irrespective of cement content.
- The depth of carbonation decreases when silpozz replacement increases upto 30% irrespective of FA.
- The combined replacement of 10% FA and upto 30% silpozz with OPC combats carbonation.
- The depth of carbonation increases as the replacement of FA with OPC increases but the incorporation of silpozz upto 30% restricts the diffusion of carbonation. The same trend is found for the coefficient of carbonation.

References

1. Jena T, Panda KC (2018) Mechanical and durability properties of marine concrete using fly ash and silpozz. Adv Concrete Constr 6(1):47–68
2. Prusty JK, Patro SK, Basarkar SS (2016) Concrete using agro-waste as fine aggregate for sustainable built environment—a review. Int J Sustain Built Environ 5:312–333
3. Morandeau A, Thiery M, Dangla P (2015) Impact of accelerated carbonation on OPC cement paste blended with fly ash. Cem Concr Res 67:226–236
4. Jena T, Panda KC (2015) Effect of fly ash and silpozz on strength and durability properties of concrete in sea water. Indian J Sci Technol 8(29):1–7
5. Jena T, Panda KC (2015) Influence of sea water on strength and durability properties of concrete. Adv Struct Eng 3:863–1873
6. Jena T, Panda KC (2017) Compressive strength and carbonation of sea water cured blended concrete. Int J Civil Eng Technol 8(2):153–162
7. Panda KC, Prusty SD (2015) Influence of silpozz and rice husk ash on enhancement of concrete strength. Adv Concrete Constr 3(3):203–221
8. Won JP, Kim HH, Lee SJ, Choi SJ (2015) Carbon reduction of precast Concrete under the marine environment. Constr Build Mater 74:118–123
9. Kari OP, Puttonen J, Skantz E (2014) Reactive transport modelling of long-term carbonation. Cement Concr Compos 52:42–53
10. Frias M, Goni S (2013) Accelerated carbonation effect on behaviour of ternary Portland cement. Compos Part B: Eng 48:122–128
11. IS: 8112–1989, 43 grade OPC specifications (first revision). Bureau of India Standards, New Delhi, India
12. IS: 383–1970, Indian Standard Specification for course and fine aggregates from naturalsources for concrete (second revision). Bureau of Indian Standards, New Delhi, India
13. IS: 10262–2009, Guide lines for concrete mix design proportioning. Bureau of Indian Standards, New Delhi, India
14. Ho DWS, Lewis RK (1987) Carbonation of concrete and its prediction. Cem Concr Res 17:489–504
15. Papadakis VG (2000) Effect of supplementary cementing materials on concrete resistance against carbonation and chloride ingress. Cem Concr Res 30(2):291–299

Effects of Ultra-fine Material on Workability, Particle Packing Density and Compressive Strength of Mortar

Vinay Mohan Agrawal and Purnanand P. Savoikar

1 Introduction

Use of cement in building and construction industry is increasing with a rapid rate. Cement is an important ingredient of concrete which is the second largest used material only after water [8]. Cement is mainly composed of natural materials which are under the verge of depletion due to over exploitation. In addition to this, the production of cement is not an eco-friendly process as it emits huge quantity of harmful carbon-di-oxide into the environment [7, 10]. Hence, there is a need to find a suitable alternative of cement with confirmation to desirable structural properties. However, complete or full replacement of cement is difficult, rather partial replacement of cement has been proved to be feasible and beneficial. The usage of industrial and agricultural by-products such as ground granulated blast furnace slag, fly ash, metakaolin, silica fume, rice husk ash, bagasse ash, palm oil fuel ash, lime stone powder and many such wastes are being used as supplementary cementitious material in cement and concrete.

The two widely used industrial by-products—fly ash and slag, both possess pozzolanic and hydraulic property and hence are used as an alternative to cement. Several studies have been done in the past to confirm the suitability of fly ash in cement mortar and concrete [9, 11, 7]. Use of slag in mortar and concrete is also been studied extensively by many researchers [6, 15, 1]. By incorporating certain changes in physical characteristics, specifically by reducing the particle size of fly ash and slag, several properties of mortar and cement concrete can be enhanced [12, 14, 13]. The limitation of fly ash and slag is their inability to exhibit strength at early

V. M. Agrawal · P. P. Savoikar (✉)
Civil Engineering Department, Goa College of Engineering, Farmagudi, Goa, India

V. M. Agrawal
NICMAR Goa Campus, Ponda, Goa 403401, India

9

age. This limitation/drawback can be addressed with incorporation of ultra-fine material as binder component [4, 3]. With the usage of fine or ultra-fine supplementary cementitious materials, the packing density is evidently enhanced. This improvement in microstructure results in higher mechanical strengths and offers better durability characteristics to mortar and concrete [5, 2, 16].

In the present study, ultra-fine fly ash (UFFA) and ultra-fine slag (UFS) has been used to partially replace ordinary Portland cement in binary combinations. The effect of 5, 10, 15 and 20% replacement of ordinary Portland cement with each UFFA and UFS is examined in terms of workability, particle packing density and compressive strength of mortar. The results of same are compared and discussed with the control or reference mortar containing 100% ordinary Portland cement. The best alternative that satisfies both early and later age strengths is concluded with experimental facts.

2 Materials and Methods

Cementitious material or binders used in the present study are—ordinary Portland cement (OPC), ultra-fine fly ash (UFFA) and ultra-fine slag (UFS). These binders are commercially available in the market. The chemical compositions of OPC, UFFA and UFS are presented in Table 1.

The specific gravity of UFFA and UFS was observed as 2.36 and 2.86 respectively. The specific gravity of OPC was found as 3.15. The Blain's fineness of UFFA and UFS was observed as 650 m^2/kg and 900 m^2/kg respectively whereas the fineness of OPC was observed as 320 m^2/kg.

The mean particle size (d_{50}) of UFFA and UFS was found to be equal to 10.50 and 8.25 μm determined using particle size analyser. Commercially available fine aggregate, also known as M-sand is used for the present research.

In order to understand the particle packing density of supplementary cementitious materials, Puntke test was conducted in all combinations of cementitious materials. The test determines the compactness of cementitious material achieved by filling the coarser pores by finer particles. This study is significantly beneficial when coarse particles of ordinary Portland cement are mixed with ultra-fine material such as UFFA and UFS. The voids created by OPC particles will tend to get filled by UFFA and UFS.

The mortar combinations studied in this research have 1:3 binder to sand ratio, with a constant water to binder ratio of 0.40. In order to achieve adequate workability,

Table 1 Chemical composition of binders

Binder	SiO_2 (%)	Al_2O_3 (%)	Fe_2O_3 (%)	CaO (%)	MgO (%)	Na_2O (%)	K_2O (%)
OPC	20.50	7.25	3.50	64.20	1.80	0.20	0.35
UFFA	52.80	23.50	3.85	7.55	1.85	0.60	2.45
UFS	31.50	19.25	1.35	35.50	6.90	0.03	0.50

Table 2 Details of mix design with particle packing density and flow value

Mix designation	OPC (%)	UFFA (%)	UFS (%)	Particle packing	Flow value (mm)
C	100	–	–	0.675	150
F5	95	5	–	0.725	165
F10	90	10	–	0.765	175
F15	85	15	–	0.825	180
F20	80	20	–	0.750	185
S5	95	–	5	0.785	145
S10	90	–	10	0.805	140
S15	85	–	15	0.850	130
S20	80	–	20	0.790	120

PCE based superplasticizer with a dosage of 0.4 % of binder content is used in all mortar combinations. One control mix with 100 % OPC is used as reference mortar, this is denoted as 'C'. Four mixes each with varying percentage of UFFA and UFS is studied in binary combinations. In all, total nine combinations were studied for particle packing density, workability and compressive strengths. The proportion of binders of binary combinations are presented is Table 2. C denotes the control mix, F and S represents UFFA and UFS in binder followed by their respective percentage in total binder content. For example S15 represents binary mortar with 15% UFS and 85% OPC.

The workability of mortar in terms of flow value is determined using flow table test. The compressive strength of mortars were identified using specimen mould of 70.6 mm cube under laboratory scale compression testing machine. The compressive strength is determined at the age of 3, 7, 28, 56 and 90 days. The experimental results are discussed in the sections below.

3 Results and Discussion

The particle packing density is obtained as the water required to completely saturate the cementitious mixture with water. The binders are dry mixed in desired proportion for 2 minute in a tumbler. Water is added slowly by gently stirring the mixture with the help of a spoon. The water added will coat the surface of binders and additional water will fill the voids of binders. In this process, the mixture will become saturated after a definite volume of water is added to it. Any further addition of water will result in bleeding. Hence water is added drop by drop in order to achieve this point of saturation. The tumbler is tapped over hard surface for 20 times when saturation is about to reach, this is desired for expelling the entrapped air. Saturation of binder is confirmed by appearance of a shiny layer of water at the top after subsequent tapping. Finally the volume of water added will be calculated at saturation point. The particle

packing density is the ratio of initial dry weight of the binder to the final saturated weight of the binder. The desired value of particle packing density is calculated and reported in Table 2. The graphical representation of particle packing density is shown in Fig. 1.

It can be observed from the graph that with usage of UFFA and UFS, the particle packing density has significantly improved. The maximum improvement was shown by F15 and S15 among all combinations. A significant increment of 22.2% and 25.9% was observed by F15 and S15 respectively as compared to reference mix. The particle packing has seen to reduce when the replacement percentage is more than 15% for both the binders. The increment in particle packing is majorly attributable to smaller particle size of UFFA and UFS.

Workability of mortars was measured using flow table where the average spread of mortar was noted as flow value. The flow values for all combinations are presented in Fig. 2.

It is observed that the workability in terms of flow value for reference mix is 150 mm. The flow value increases with the addition of UFFA as shown in Fig. 2. This is due to spherical shape of UFFA. The flow values for UFS combinations have shown a reducing trend. This is attributable to angular shape of UFS. Inclusion of UFFA could reduce the water dement to meet the desired workability where as in case of UFS the water demand will tend to increase.

Compressive strength of all mortar combinations was investigated. The strengths were examined after 3, 7, 28, 56 and 90 days. Table 3 shows the observed compressive strength results for control and binary mixes with UFFA and UFS at different ages.

Figure 3 shows the compressive strength of control and binary mortars with 5, 10, 15 and 20% UFFA. It can be observed that, none of the binary combination with UFFA has been able to meet the early strength (3 and 7 day) capacity of control mixture. At 28 days, only F15 combination has been able to reach the strength equivalent to that of control mixture. At later age (56 days and beyond) the strengths of F15 and F20 are higher than that of control mixture. The combinations F5 and F10 have not been

Figure 1 Particle packing density of reference and binary mix with UFFA and UFS
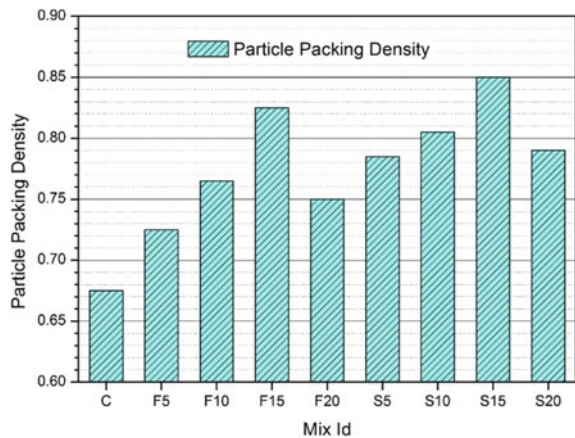
Figure 2 Workability or flow value of reference and binary mixes
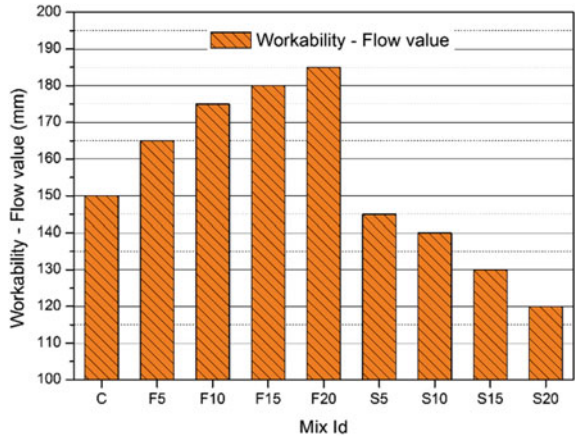
Table 3 Compressive strengths of control and binary mortar mixes

Mix id	Compressive strength (MPa)				
	3 day	7 day	28 day	56 day	90 day
C	20.02	33.78	52.55	60.06	65.06
F5	11.26	20.02	37.54	52.55	58.81
F10	15.01	25.02	42.54	55.05	62.56
F15	15.03	28.81	52.61	62.63	68.89
F20	13.80	22.58	47.66	61.46	66.47
S5	16.28	27.55	40.08	51.35	57.61
S10	17.54	30.07	42.60	53.87	62.64
S15	23.84	43.91	57.71	66.49	74.02
S20	26.37	38.92	52.73	65.29	70.31

Figure 3 Compressive strengths of control and binary mortars with UFFA
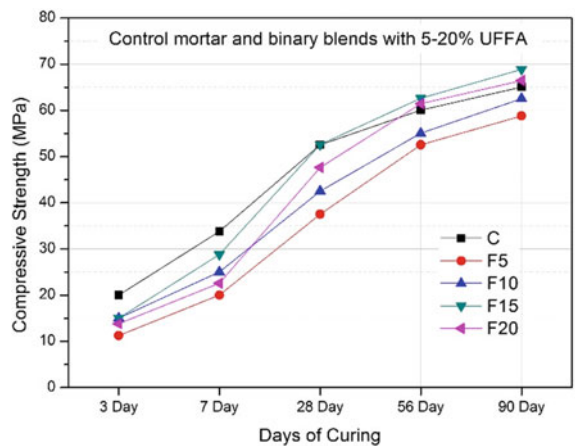
Figure 4 Compressive
strengths of control and
binary mortars with UFS
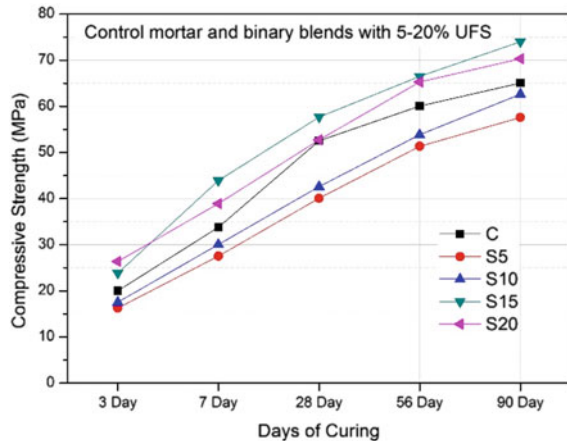
able to meet the strength criteria at any duration and hence cannot be considered as replacement alternative. The rate of strength development is slow in the initial days and it gets increased beyond 28 days, this is due to slow pozzolanic effect of fly ash at early age.

The effect of addition of UFS in binary combinations is shown in Fig. 4. It is observed that due to addition of UFS in the binary combination, the compressive strength at early age is significantly improved by S15 and S20. The 28 day and later age strengths have shown a similar rising trend for both these combinations. The maximum strength is gained by S15 combination as compared to reference mix.

The mix S5 and S10 does not meet strength requirement at any age and hence cannot be considered as replacement alternative. The higher strengths at early and later age for combination with 15 and 20% UFS is attributable to hydraulic and pozzolanic property of slag. In addition, UFS have very fine particle size hence it reacts much faster than cement particles. The binary combination S15 can be considered as the best alternative in terms of compressive strength requirements. S15 performs better in comparison to F15 as well, and hence it is the best alternative among the chosen binary mixes.

4   Conclusions

The present study with control mix, 4 binary mixes each with UFFA and UFS, have concluded following major findings.

- The use of UFFA and UFS significantly improves the particle packing of binder as compared to control mix. This is due to finer particle size of UFFA and UFS. The increment in particle packing results in denser concrete. This improves the mechanical property of structure.

- Increase in workability in terms of flow value is observed due to UFFA addition. Whereas, the workability reduces with addition of UFS.
- Early age compressive strength requirement is met only with UFS mortar. UFFA mortars demonstrated less strength as compared to control mix at 3 and 7 days.
- Compressive strength at 28 days and beyond is satisfied by 15% and 20% binary replacement of UFFA and/or UFS. Both binders have been able to give better compressive strength.
- Maximum increment in compressive strength is obtained by 15% UFS combination. The increment observed is 13.77% as compared to control mixture at the age of 90 days. Hence, S15 combination can be the preferred alternative binder composition as per the present study.

References

1. Benhelal E et al (2013) Global strategies and potentials to curb CO_2 emissions in cement industry. J Clean Prod 51:142–161
2. Chindaprasirt P et al (2007) Effect of fly ash fineness on microstructure of blended cement paste. Constr Build Mater 21(7):1534–1541
3. Escalante JI et al (2001) Reactivity of blast-furnace slag in Portland cement blends hydrated under different conditions. Cement Concrete Res 31(10):1403–1409
4. Escalante-García JI, Sharp JH (2001) The microstructure and mechanical properties of blended cements hydrated at various temperatures. Cement Concrete Res 31(5):695–702
5. Kara De Maeijer P et al (2020) Effect of ultra-fine fly ash on concrete performance and durability. Constr Build Mater 263:120493
6. Korde C et al (2019) Activated slag as partial replacement of cement mortars: effect of temperature and a novel admixture. Constr Build Mater 216:506–524
7. Kurtoglu AE et al (2018) Mechanical and durability properties of fly ash and slag based geopolymer concrete. Adv Concrete Constr 6(4):345–362
8. Paliwal Gopal, Maru Savita (2017) Effect of fly ash and plastic waste on mechanical and durability properties of concrete. Adv Concrete Constr 5(6):575–586
9. Sakai E et al (2005) Hydration of fly ash cement. Cement Concrete Res 35(6):1135–1140
10. Scrivener KL et al (2018) Eco-efficient cements: potential economically viable solutions for a low-CO_2 cement-based materials industry. Cement Concrete Res 114:2–26
11. Sevim Özer, Demir İlhami (2019) Physical and permeability properties of cementitious mortars having fly ash with optimized particle size distribution. Cement Concrete Compos 96:266–273
12. Sharmila P, Dhinakaran G (2016) Compressive strength, porosity and sorptivity of ultra fine slag based high strength concrete. Constr Build Mater 120:48–53
13. Teng S et al (2013) Durability and mechanical properties of high strength concrete incorporating ultra fine ground granulated blast-furnace slag. Constr Build Mater 40:875–881
14. Ting L et al (2019) Effects of ultra-fine ground granulated blast-furnace slag on initial setting time, fluidity and rheological properties of cement pastes. Powder Technol 345:54–63
15. Yi H et al (2012) An overview of utilization of steel slag. Proc Environ Sci 16:791–801
16. Yu J et al (2017) Mechanical properties of green structural concrete with ultrahigh-volume fly ash. Constr Build Mater 147:510–518

Compressive Strength Prediction of Aluminosilicate Precursors Based Geopolymers Through Artificial Neural Network (ANN)

Sourav Kumar Das and Sandeep Shrivastava

1 Introduction

Geopolymers are the 3D structured artificial polymers which are generated due to the alkali activation of aluminosilicate sources [4]. The most advantageous benefits of geopolymer production that it uses wastage from industries, construction sites and demolition sites [4]. Geopolymer products like concrete [17], mortar [1], bricks [12], tiles [24], etc. have already proven its better candidacy against the same product made from ordinary Portland cement (OPC) its terms of mechanical and durability properties. During the last two decades, a series of wastes which are high in silica (Si) and alumina (Al) are analyzed for there geopolymeric potential at different age of curing depending on the curing temperature, exposure condition, molarity of alkali and mix ratios of different alkalis [22, 10, 18, 21]. But the production of geopolymers creates uncertainty in the expected outcome due to the use of a waste product which generates in an uncontrolled environment so changing the alkali proportions and curing temperature by trial and error finally helps us to achieve the required outcome. Which consumes a huge amount of time and effort which could certainly affect the economical and time constraints of a project.

To optimize the effect of the chemical composition of the waste on the required end product needed to be solved by a machine learning approach which will save both time and effort to identify the mix proportions. In the machine learning (ML) approach, Artificial Neural Network (ANN) technology, which belongs to a family of huge parallel architectures, designed to solve difficult and diversified civil engineering applications via appropriately interconnected artificial neurons is a beneficial method

S. K. Das
Department of Civil Engineering, Manipal University Jaipur, Jaipur, India

S. K. Das · S. Shrivastava (✉)
Department of Civil Engineering, Malaviya National Institute of Technology Jaipur, Jaipur, India
e-mail: sshrivastava.ce@mnit.ac.in

17

[14]. The most interesting capability of the ANN approach is its efficiency to train itself from the available novel data and to understand the highly complex connectivity among different parameters. This understanding potential of ANN helps it to apply the concept to different civil engineering problems where the data extraction is tough to achieve or the data is noisy or insufficient [25]. Also, the basic strategy to apply ANN Models to different material-based approaches in civil engineering domain is to train the model through the experimented results obtained to comprehend the behaviour of the material [26]. This trained model can not only replicate the experimental results but can also generate approximate results by the generalisation of various materials [27].

Now, ANN has been effectively used to create different models to process the expected outcome from different sources of wastage by considering the parameters like curing temperature, the molarity of sodium of potassium hydroxide (NaOH or KOH), mix ratio of different alkali solutions for geopolymer applications. For example, Saridemir [25] forecasted the compressive strength of silica fume and metakaolin based concrete by developing two ANN models with one hidden layer and two hidden layers and reported an R^2 value of 0.98 between the training and testing compressive strength of the models. Eskandari-Naddaf and Kazemi [6] tried to predict the compressive strength of cement mortar depending on the different cement classes using the ANN approach with a reported R^2 value of 0.94. Hammoudi et al. [8] puts an innovative approach by predicting the effect of recycled aggregate concrete on cement concrete and thus comparing between ANN and Response Surface Methodology (RSM), where ANN method is more constructive than the later one with an R^2 value of 0.998. From the durability analysis of concrete through ANN approach, Boukhatem et al. [9] explored the effect of carbonation on fly ash based concrete by taking six input parameters which were water/binder ratio, binder content, fly ash content, humidity, CO_2 concentration and exposure duration. Narazi and Rihari [16] developed ANN model to study the impact of TiO_2 nanoparticles on the water penetrability of high strength concrete and compare it with the genetic programming (GP). In the ANN Model developed by Nazari and Rihari [16], eight input neurons were taken into consideration with two hidden layers of neurons and finally one output layer which is the compressive strength. Though the method employed gives commendable output in considering the TiO_2 nanoparticle inclusion percentage but conclude that depending on the R^2 value ANN showed better prediction than the GP approach.

Considering the soft computing techniques i.e. ANN approach for predicting the outcome required for geopolymer products very few research articles have been published to date. Few like Nagajothi and Elavenil [14] studied the effect of aluminosilicates on the strength properties of geopolymer concrete. Yadollahi et al. [28] developed ANN models to predict the compressive strength of ground pumice based geopolymers and obtained an R^2 value of 0.958. So, based on the literature survey on employing ANN models to forecast the compressive strength of geopolymers very limited applications were revealed and left a scope to develop model(s) considering the different important parameter which actively affects the compressive strength and durability of geopolymers.

In this article, the authors developed four ANN models depending on the input-target values obtained from previous works [3]. A total of 396 data were collected and randomly split up into 278, 59, and 59 for testing, validation, and testing purpose. Input parameters considered were the chemical compositions ($SiO_2\%$, $Al_2O_3\%$ and $CaO\%$) depending on the type of precursors, curing age, the molarity of NaOH, alkali mixture ratio of NaOH to Na_2SiO_2 ratio, $Na_2O\%$ and silicate modulus. A single output parameter i.e. compressive strength is kept for assessment of the prediction level for each model.

2 Data Collection

The data required for the training, validation and testing purpose of the ANN models were collected from previously published work. Different types of aluminosilicate sources (fly ash, clay brick with adhered mortar, ground granulated blast furnace slag and glass waste) were identified to keep the source material from the same domain i.e. aluminosilicates, for appropriate model generation.

3 The Architecture of Artificial Neural Network (ANN)

"ANNs are non-linear statistical data Modeling tools for relations between input and output data, which can be an adaptive system that changes its structure based on information that flows through the network during the learning phase [6]". These neurons are the data processing elements which process the data from the input layer to the output layer via one or more hidden layers. Feedforward network-based ANN Models are generally multilayered, where the layers are arranged horizontally. This multilayered ANN Models consist of one input layer, one or multiple hidden layers and one output layer. Where the input layer consists of multiple neurons which are equal to the parameters upon which the prediction is to be calculated but no data processing occurs in this layer. Data process and re-production starts at the hidden layer and finally the re-produced data flows through the output layer. But interestingly there will be no connectivity between the neurons within the same layer. In the hidden layer, the input data are given different input weightage values which were summed. A nonlinear sigmoid or hyperbolic tangent function is used to transfer data from input to output layer of the ANN model. Figure 1 shows the architecture of the neural network developed for Model—4 with seven input neurons at the input layer, two hidden layers with 14 neurons and one output layer with one neuron which is the expected result. Finally, the ANN Model create a loop from the input to the output layer. In this article, horizontal layers were defined following the feed-forward with backpropagation technique. The backpropagation is the mostly accepted training algorithm for multilayer perceptron, where it follows the gradient descent technique
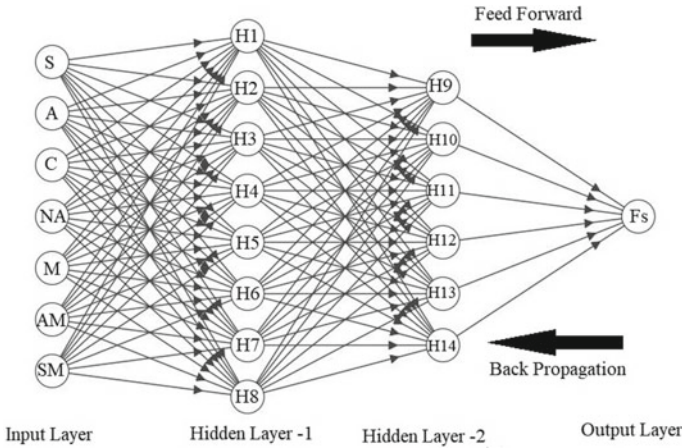
Fig. 1 ANN architecture of Model—4

by minimizing the error for a certain training pattern thus by adjusting the weightage in a small amount every time of propagation (Nazari and Pacheco Torgal).

Now, this weighted sum is the sum of the weightage given to the input data, varying on the effect of the input to the process layer or hidden layer. The weighted sums function thus being calculated by using Eq. (1) which calculates the net response that goes to a neuron (Murat Günaydın and Zeynep Doğan).

$$(net)_j = \sum_{i=1}^{n} w_{ij} x_i + b \tag{1}$$

where $(net)_j$ is the weighted sum of the jth neuron for the response obtained from the former layer with *n* neurons. w_{ij} is denoted as the weight between the jth neuron of the preceding layer, x_i is the output of the ith neuron in the preceding layer, *b* is a fixed internal addition value and S represents the summation function [19, 20]. Now the activation function is the one which processes the net input received from the summation function and determines the output of the neuron. Generally, for multilayered feed-forward ANN Model, the activation function is being sigmoid activation function type. The jth output of the output layer $(out)_j$ is being calculated by utilizing the sigmoid activation function which is mentioned as Eq. (2) [19].

$$(out)_j = f(net)_j = \frac{1}{1 + e^{-\alpha(net)j}} \tag{2}$$

where α is a constant which is used to influence the slope of the semi-linear region and along with the constant α the nonlinear sigmoid function remains active in each layer other than the input layer [11].

4 ANN Model and Parameters

Total four ANN Models developed in this research article consist of seven input neurons which are the parameters upon which the compressive strength prediction is established. The seven parameters which are taken into consideration are $SiO_2\%$ (S), $Al_2O_3\%$ (A) and $CaO\%$ (C) of the aluminosilicate precursors utilized, and molarity of NaOH solution (M), alkali mixture (AM) ratio of sodium silicate (Na_2SiO_3) to sodium hydroxide (NaOH) solution, total $Na_2O\%$ both from precursor and alkali solution (NA) and silicate modulus (SM). The output neuron is the predicted compressive strength (Fs). Table 1 gives the range of input and output parameters. Two hidden layers are taken with two different combinations of neuron which are (a) 6–4 neurons and (b) 8–6 neurons in each hidden layer. Summary of the parameters i.e. number of neurons in each hidden layer and epoch involved for each model generation is given in Table 2. The reason behind considering two hidden layers in the multilayer neural architecture is because it gives the minimum absolute percentage error values for both training and testing phase [14, 16]. Table 3 gives the input variable details maintained for each model.

Once the input values are supplied, it proceeds to the next layers i.e. hidden and output layer until the desired prediction is obtained. If the predicted value is not same as the target value than the difference is calculated as error and the data back propagates to the input neurons and again feed-forward layer by layer with a new

Table 1 Input and output variables range considered for Model–1 to Model–4

Sl. No	Variable	Range
1	$SiO_2\%$ (S)	44.35–58.65%
2	$Al_2O_3\%$ (A)	5.5–12.1%
3	$CaO\%$ (C)	5.75–30.35%
4	$Na_2O\%$ (NA)	5.15–16.35%
5	Molarity of NaOH solution (M)	6-16 M
6	Alkali mixture ratio (AM)	1.5–3.5
7	Silicate modulus (SM)	0.65–2.7
8	Compressive strength (Fs)	1.5–44.2

Table 2 Summary of models created to forecast the compressive strength

Symbol	Number of neurons		Termination epoch
	Hidden layer—1	Hidden layer—2	
Model—1	6	4	1000
Model—2	8	6	1000
Model—3	6	4	439
Model—4	8	6	219

Table 3 Value of parameters used for each ANN model

Parameters	ANN
No. of input neuron	7
No. of output neuron	1
No. of hidden layer	2
Momentum rate	0.88
Learning rate	0.7

weightage assigned at the hidden layer. The architecture of ANN is design in a manner that the error is being distributed to all the neurons in the hidden layer to make them accountable for the error (Nagajothi and Elavenil).

The total prediction approach of an ANN architecture depends on three steps which are (a) Training, (b) Validation and (c) Testing. Generally, the maximum amount of experimented data are provided to the training steps as this step will train the model by changing the weightage of the input parameters depending on the target value provided. Next is the validate and testing steps which generally kept the same where the trained model will validate the data and will predict in the testing phase. To make a model most accurate the quantity of hidden layers and neurons in each hidden layer is to be assigned through trial and error process only, as no reliable approach is present still now and it is mostly done on previous experiences [25].

In this article, Matlab-2019 is used to prepare the four ANN models. The description of the models is given in Table 2. A total of 396 data sets were taken into consideration from previous studies where 278 data sets were being used for training, 59 data sets for validation and 59 data sets for testing purpose. To make an effective prediction from a Model, two different approaches are employed where Model 1 and 2 were trained for the maximum number of epochs i.e. 1000, and Model 3 and 4 were trained till the minimum error is obtained by the neural network (ref. Table 2). As discussed the training phase of any model developed using ANN is the most important phase, so Lavenberg-Marquardt (LM) training algorithm is followed in this study, which is the most effective algorithm and also been supported by previous researchers [5, 23, 7]. Also, the performance of a Model is determined by the different types of errors such as Root Mean Square Error (RMSE), Mean Absolute Percentage Error (MAPE) and Mean Absolute Error (MAE), which are calculated by Eqs. (3)–(5).

$$\text{RMSE} = \sqrt{[\frac{1}{n} \sum_{i=1}^{n} |x_i - y_i|^2]} \tag{3}$$

$$\text{MAPE} = \frac{100}{n} \sum_{i=1}^{n} \frac{|x_i - y_i|}{x_i} \tag{4}$$

$$\text{MAE} = \frac{1}{n} \sum_{i=1}^{n} |x_i - y_i| \tag{5}$$

where 'n' is the number of total values, 'x' is the experimented value and 'y' is the expected value.

5 Result and Discussions

A comparison between the experimented and predicted values for four differently approached ANN models with regression analysis are shown in Figs. 2 and 3 for the prediction of compressive strength. Table 4 summarized the R^2 values from where it is observed that all the models were well trained and effectively predicts the compressive strength. The optimum R^2 values are given by Model—4, which consist of 8–6 neurons in the two hidden layers and the Model was let to stop training automatically when minimum error value was obtained. Though the same approach was applied for Model—3 but the neurons in the hidden layer was reduced to 6–4. The neurons in the hidden layer play a vital role in training a perfect Model for ANN architecture, which has been already accepted by previous researchers and as there is no exact method to ascertain the required quantity of neurons so it is done by purely trial and error basis [23, 25, 15]. The statistical values which are R^2, RMSE, MAPE and MAE for each Model are given in Table 4. The best R^2 value of 0.9994 is obtained for Model—4, whereas the minimum RMSE, MAPE and MAE values of 0.6455, 2.635 and 0.2854, respectively are attained by Model—2. Though for R^2 value between Model—2 and 4 there are no significant differences. The minimum R^2
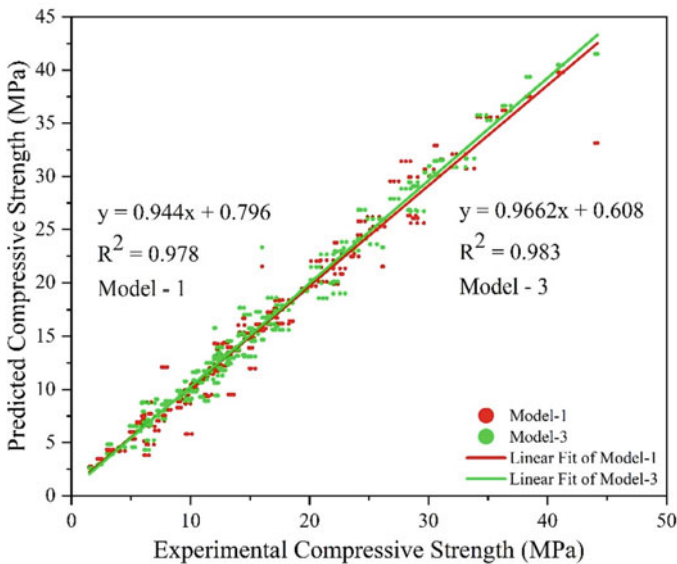
Fig. 2 Performance of testing phase of Model—1 and Model—3
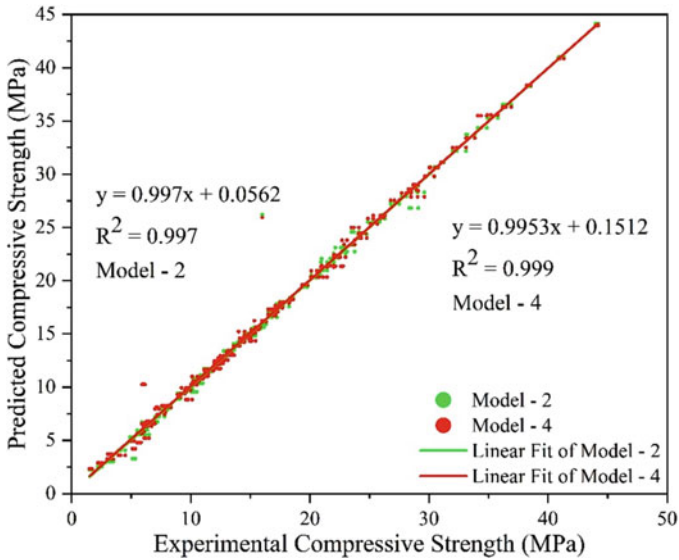
Fig. 3 Performance of testing phase of Model—2 and Model—4

Table 4 Statistical calculation of Model—1 to Model—4 for the testing phase

Model	R^2	RMSE	MAPE	MAE
Model—1	0.97768	1.6882	8.838	1.0652
Model—2	0.99758	0.6455	2.635	0.2854
Model—3	0.98270	1.3267	8.825	1.0083
Model—4	0.99940	0.7623	3.794	0.3732

and maximum RMSE, MAPE and MAE value of 0.97768, 1.6882, 8.834 and 1.0652, respectively are given by Model—1. So, depending on the statistical values for each model both Model—2 and Model—4 are suitable for the prediction of geopolymers compression strength. Finally, the prediction of compressive strength of geopolymers through ANN approach depicts that the models are mostly governed by the number of neurons in the hidden layer which effectively distribute the error to the neurons when feedforward—backpropagation method is employed for model generation.

6 Conclusion

Soft computing practices such as Artificial Neural Network have been widely accepted machine learning tool to predict different parameters. In this study, the same approach was adopted to predict the compressive strength of geopolymers made of

different types of aluminosilicates where seven different input parameters were identified and their effect on the final compressive strength was predicted through four differently approached ANN models. The conclusions drawn from the present study are summarized below:

1. In an ANN model, the quantity of neurons in the hidden layer plays a key role in effectively predicting the compressive strength of geopolymers, as the compressive strength of geopolymers is strongly influenced by many factors.
2. Feedforward-Backpropagation algorithm is the most effective algorithm in developing an ANN model.
3. Model—4 is the most effective model in terms of R^2 value among the four models developed, where the model was let to stop training when the minimum error value was obtained.
4. Model—4 could be further utilized in effectively predicting the compressive strength of geopolymer depending on the range provided (Table 1) for developing the model.

References

1. Al-Majidi MH et al (2016) Development of geopolymer mortar under ambient temperature for in situ applications. Constr Build Mater 120:198–211. https://doi.org/10.1016/j.conbuildmat.2016.05.085
2. Das SK (2018) Parametric study of flyash based geopolymer concrete. Int J Eng Technol (UAE) 7(2). https://doi.org/10.14419/ijet.v7i2.31.13439
3. Das SK, Sandeep S (2020) Siliceous fly ash and blast furnace slag based geopolymer concrete under ambient temperature curing condition. Struct Concrete suco.201900201. https://doi.org/10.1002/suco.201900201
4. Das SK, Sandeep S (2020) A study on the viability of fly ash and construction and demolition waste as geopolymerized masonry mortar and their comparative analysis. Mater Today: Proc 32(4):574–583, Elsevier Ltd. https://doi.org/10.1016/j.matpr.2020.02.402
5. Duan ZH et al (2013) Using artificial neural networks for predicting the elastic modulus of recycled aggregate concrete. Constr Build Mater 44:524–532. https://doi.org/10.1016/j.conbuildmat.2013.02.064
6. Eskandari-Naddaf H, Kazemi R (2017) ANN prediction of cement mortar compressive strength, influence of cement strength class. Constr Build Mater 138:1–11. https://doi.org/10.1016/j.conbuildmat.2017.01.132
7. Haddad R, Haddad M (2020) Predicting fiber-reinforced polymer–concrete bond strength using artificial neural networks: a comparative analysis study. Struct Concrete suco.201900298. https://doi.org/10.1002/suco.201900298
8. Hammoudi A et al (2019) Comparison of Artificial Neural Network (ANN) and Response Surface Methodology (RSM) prediction in compressive strength of recycled concrete aggregates. Constr Build Mater 209:425–436. https://doi.org/10.1016/j.conbuildmat.2019.03.119
9. Kellouche Y et al (2019) Exploring the major factors affecting fly-ash concrete carbonation using artificial neural network. Neural Comput Appl 31(S2):969–988. https://doi.org/10.1007/s00521-017-3052-2
10. Koenig A et al (2017) Resistance of alkali-activated binders to organic acid attack: assessment of evaluation criteria and damage mechanisms. Constr Build Mater 151:405–413. https://doi.org/10.1016/j.conbuildmat.2017.06.117

11. Liu SW et al (2002) Detection of cracks using neural networks and computational mechanics. Comput Methods Appl Mech Eng 191(25–26):2831–2845. https://doi.org/10.1016/S0045-7825(02)00221-9
12. Madani H et al (2020) Geopolymer bricks made from less active waste materials. Constr Build Mater 247:118441. https://doi.org/10.1016/j.conbuildmat.2020.118441
13. Murat Günaydın H, Zeynep Doğan S (2004) A neural network approach for early cost estimation of structural systems of buildings. Int J Project Manag 22(7):595–602. https://doi.org/10.1016/j.ijproman.2004.04.002
14. Nagajothi S, Elavenil S (2020) Influence of aluminosilicate for the prediction of mechanical properties of geopolymer concrete—artificial neural network. SILICON 12(5):1011–1021. https://doi.org/10.1007/s12633-019-00203-8
15. Nazari A, Torgal FP (2013) Predicting compressive strength of different geopolymers by artificial neural networks. Ceram Int 39(3):2247–2257. https://doi.org/10.1016/j.ceramint.2012.08.070
16. Nazari A, Riahi S (2011) Prediction split tensile strength and water permeability of high strength concrete containing TiO2 Nanoparticles by artificial neural network and genetic programming. Compos B Eng 42(3):473–488. https://doi.org/10.1016/j.compositesb.2010.12.004
17. Ng C et al (2018) A review on microstructural study and compressive strength of geopolymer mortar, paste and concrete. Constr Build Mater 186:550–576. https://doi.org/10.1016/j.conbuildmat.2018.07.075
18. Niibori Y et al (2000) Dissolution rates of amorphous silica in highly alakline solution. J Nuclear Sci Technol 37(4):349–357. https://doi.org/10.1080/18811248.2000.9714905
19. Öztaş A et al (2006) Predicting the compressive strength and slump of high strength concrete using neural network. Constr Build Mater 20(9):769–775. https://doi.org/10.1016/j.conbuildmat.2005.01.054
20. Pala M et al (2007) Appraisal of long-term effects of fly ash and silica fume on compressive strength of concrete by neural networks. Constr Build Mater 21(2):384–394. https://doi.org/10.1016/j.conbuildmat.2005.08.009
21. Phoo-ngernkham T et al (2015) Effects of sodium hydroxide and sodium silicate solutions on compressive and shear bond strengths of FA–GBFS geopolymer. Constr Build Mater 91:1–8. https://doi.org/10.1016/j.conbuildmat.2015.05.001
22. Pilehvar S et al (2018) Physical and mechanical properties of fly ash and slag geopolymer concrete containing different types of micro-encapsulated phase change materials. Constr Build Mater 173:28–39. https://doi.org/10.1016/j.conbuildmat.2018.04.016
23. Rajeshwari R, Mandal S (2019) Prediction of compressive strength of high-volume fly ash concrete using artificial neural network. Lect Notes Civil Eng 25:471–483. https://doi.org/10.1007/978-981-13-3317-0_42
24. Reggiani A (2019) Geopolymer roof tile. Ceram Eng Sci Proc 39(3):225–232. https://doi.org/10.1002/9781119543381.ch20
25. Sarıdemir M (2009) Prediction of compressive strength of concretes containing metakaolin and silica fume by artificial neural networks. Adv Eng Softw 40(5):350–355. https://doi.org/10.1016/j.advengsoft.2008.05.002
26. Siddique R et al (2011) Prediction of compressive strength of self-compacting concrete containing bottom ash using artificial neural networks. Adv Eng Softw 42(10):780–786, https://doi.org/10.1016/j.advengsoft.2011.05.016
27. Topçu İB, and Mustafa S (2008) Prediction of compressive strength of concrete containing fly ash using artificial neural networks and fuzzy logic. Comput Mater Sci 41(3):305–311. https://doi.org/10.1016/j.commatsci.2007.04.009
28. Yadollahi MM et al (2015) Prediction of compressive strength of geopolymer composites using an artificial neural network. Mater Res Innov 19(6):453–458. https://doi.org/10.1179/1433075X15Y.0000000020

Load-Settlement Behaviour of Stone Column with Varied Spacing

Jijo James and S. V. Sivapriya

1 Introduction

Stabilisation of soil becomes mandatory when the site soil posses deprived shear strength. The soil can be stabilised by two methods, i.e. mechanical and chemical. In mechanical stabilisation the stiffness of the soil is changed by installing a column making it as a composite ground. Whereas in chemical stabilisation, the properties of the soil is modified by adding admixtures. The main parameters considered while selecting the stabilisation methods are soil properties, type of super structure, water table, settlement characteristics etc.

Stone column technique is used to stabilise soft clay, silts and loose silty sand mechanically. It reduces foundation settlement, increases the stiffness and shear strength of the soil thereby reducing the permeability [1]. The undrained shear strength of the soil around the stone column influences the load carrying capacity of the stone column [2]. When loading a stone column vertically, the stress transferred to the column dissipates excess pore pressure and reduces consolidation [3].

With increase in length of the column, the capacity increases and the column shared a major load by the passive resistance against bulging (4D at the top of the column).When the L/D ratio exceeds 10, there is no influence of stone column in settlement characteristics [4]. Hence it is not preferable for heavy structures as it cannot stress the soil to a deeper depth [5]. The capacity of stone column found by conducting the test in direct shear box is half the calculated shear strength [6]. The bearing capacity of the column increases with increase in friction angle as well as diameter [7].

In the current study, number of stone column with varied diameter and spacing with same length laboratory study was conducted.

J. James · S. V. Sivapriya (✉)

Associate Professor, Department of Civil Engineering, Sri Sivasubramaniya Nadar College of Engineering, Chennai 603110, India

Table 1 Properties of soil sample

Properties	IS code	Values
Specific gravity	[8] 2720—Part III/2	2.57
Liquid limit, %	[9] 2720—Part V	43.5
Plastic limit, %		29.37
Grain size analysis	[10] 2720—Part VI	Gravel–0.28% Sand–43.64% Coarse sand–4.585% Medium sand–18.314% Fine sand–20.745% Silt and Clay–56.07%
Proctor compaction maximum dry density, kN/m^3 optimum moisture content, %	[11] 2720—Part VIII	16.3 12.63
Classification	[12] 1498	CI

2 Materials and Methodology

2.1 Materials

The properties of the soil used for stabilisation is given in the Table 1.

3 Methodology

The soil with particle size less than 425 microns is mixed thoroughly with water and filled in the CBR mould of 150 mm diameter and 125 mm of height. Commercially available PVC pipe of varied diameter (1 and 1.25 inch) is installed at two location with varied spacing (5, 7 and 9 cm) and 5 mm stone chips is filled inside the pipe by tamping to ensure the column formation; upon filling the stone chips inside the tube, the column is removed from unit cell (Fig. 1).

The unit cell set up is then placed in a loading frame of 50 kN capacity and uniform load is applied through proving ring of 10 kN capacity with a constant strain rate of 0.625 mm /min.
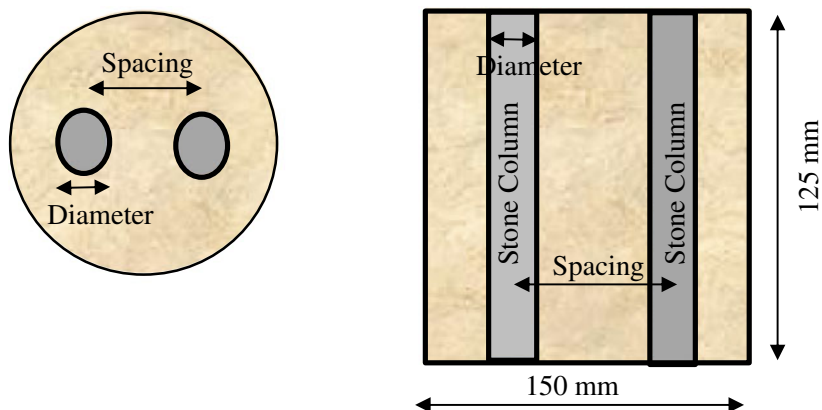
Fig. 1 Schematic representation of stone column

4 Results and Discussion

Considering the permissible settlement of single pile foundation as 12 mm, the load corresponding to it is observed and discussed. The parameters varied are tabulated in Table 2.

From the graph (Fig. 2) of load Vs settlement, with increase in spacing between the column the load carrying capacity increases. It is observed with diameter of stone column 2.54 cm, there is large increase in load beyond 12 mm settlement, whereas for stone column of 3.18 cm diameter the load comes to a same point indicating higher capacity proving ring should be used. Considering the load at 12 mm settlement, there is a linear increase in load with increase in spacing; however for 3.18 cm diameter stone column there is a slight non -linearity.

For the same condition with single column from the previous study for the two diameter is observed as 123.17 kg and 164.37 kg for 2.54 and 3.18 cm diameter stone column respectively [7]; the capacity increases by 41.2%. There is a increase in capacity by 59.55, 94.81 and 103.78% with increase in spacing compared with single pile for 2.54 mm diameter pile. For a 3.18 mm, the capacity increases by 21.55, 32.62 and 103.64% for the same increase in spacing. The results shows when the

Table 2 Parametric study

Diameter, cm	Spacing between two columns, cm	Denotation
2.54	5	D1S1
	7	D1S2
	9	D1S3
3.18	5	D2S1
	7	D2S2
	9	D2S3
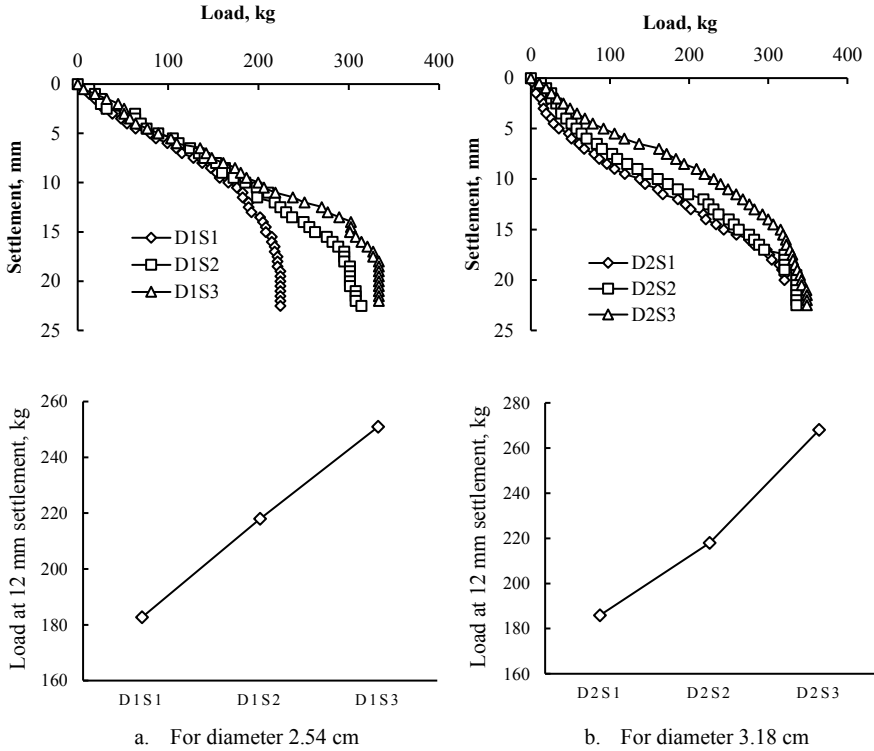
Fig. 2 Load Settlement graph

spacing increases from 2-3.5 D for smaller diameter and 1.5–3 D for large diameter stone column.

The area ratio (AR) is defined as the ratio of area of the stone column to the area of the unit cell. The area ration for 2.54 mm is 5.73 and for 3.18 mm spacing it is 8.99. The area ratio increases with increase in spacing but the both the values are negligible.

5 Conclusion

Laboratory test is conducted in a CBR mould conceptualised as unit cell with two different stone column with three different spacing. The load corresponding to 12 mm settlement is noted and inferred. With increase in diameter of the stone column, the capacity increases.

When the spacing between the stone column increases beyond 3D, the load carrying capacity increases by double; indicating the applied load is taken care by the installed column, preventing the soil from any settlement failure.

References

1. Keller (2020) Vibro stone columns, Keller Co.Uk. 1–8. https://www.keller.co.uk/expertise/tec hniques/vibro-stone-columns
2. Van-Impe WF (1989) Soil improvement techniques and their evolution
3. Jie H, Ye S-L (2001) Simplified model for consolidation rate of stone column reinforced foundations. J Geotech Geo 127:597–603
4. Malarvizhi I (2007) Comparative study on the behavior of encased stone column and conventional stone column. Soils Found Japanese Geotech Soc 47:873–885. https://doi.org/10.3208/sandf.47.873
5. Hughes JMO, Withers NJ (1974) Reinforcing of soft cohesive soil with stone columns. Gr Eng 7
6. Murugesan S, Rajagopal K (2009) Shear load tests on stone columns with and without geosynthetic encasement. Geotech Test J 32:76–85. https://doi.org/10.1520/GTJ101219
7. Sivapriya SV, James J (2019) Numerical study on static behaviour of a stone column under uniformly distributed load. AIP Conf Proc 2161. https://doi.org/10.1063/1.5127649.
8. Bureau of Indian Standards (1997) IS 2720(Part III/2) Determination of specific gravity for fine, medium and coarse grained soil
9. Bureau of Indian Standard (1995) IS 2720 (Part V) Determination of liquid and plastic limit
10. Bureau of Indian Standard (1995) IS 2720 (Part IV) Methods of test for soil—grain size analysis
11. Bureau of Indian Standard (2006) IS 2720 -Part 8 : Determination of water content—dry density relation using heavy compaction
12. Bureau of Indian Standard (2002) IS 1498-1970 (Reaffirmed 2002) Classification and indentification of soil

Study on Fracture Parameters of Basalt Fiber Reinforced Concrete Beam by Using Finite Element Method

Shilpi Shukla, Meena Murmu, and S. V. Deo

1   Introduction

Cracking in concrete is a very complex mechanism, which substantially differs from the cracking behaviour of other materials, such as steel. Suitable fracture mechanics models, as well as test configurations to determine the fracture parameters of quasi-brittle materials, have only been established during the last few decades. The issues which are now in solid structures, similar to void pores, considerations, and miniature splits are areas of break inception and can cause de-holding of particles of totals from the concrete grid. The field of fracture mechanics (FM) involves such a profound understanding and thus provides the ability to prevent unexpected or undesirable collapses. Cracking in concrete is a very complex mechanism, which substantially differs from the cracking behaviour of other materials, such as steel. Suitable fracture mechanics models, as well as test configurations to determine the fracture parameters of quasi-brittle materials, have only been established during the last few decades.

The design of concrete structures is commonly based on strength criteria, using elastic analysis which considers allowable stress or plastic limit analysis. In other words: a material is thought to be sufficient if its quality is more noteworthy than the normal applied pressure. Failure of concrete, however, essentially involves a rather complex mechanism of crack formation and crack growth. These fracture processes are important when regarding the ultimate load characteristics of concrete and hence are relevant to ultimate limit state analysis. As stated by Bazant (2005), split inception may rely upon pressure, however the real development of breaks requires vitality (crack vitality). Consequently, vitality rules ought to likewise be thought about. Actually, when a solid structure with an underlying break is exposed to stacking, the applied burden brings about a vitality discharge at the tip of the split, which comprises of two bits: the vitality rate devoured in making two crack

S. Shukla (✉) · M. Murmu · S. V. Deo
Civil Engineering Department, NIT Raipur, Raipur 492001, India

surfaces, and the energy rate to overcome the cohesive stresses in further separating the surfaces (Murthy et al., 2009). So essentially, FM is a failure concept which uses energy criteria and which makes allowances for failure propagation through the structure (Bazant, 2005). Furthermore, instead of strength, the most relevant material property is fracture toughness (Anderson, 2005).

The study of FM fundamentally started during World War I, when Griffith attempted to clarify the disappointment of fragile materials (for example glass) (Griffith, 1921). Based on the hypothesis that these materials contain elliptical micro-cracks & established an energy-based relationship between applied stress and crack length. When the strain-vitality change, the results from an addition of split development and which is adequate to defeat the surface vitality of the material. This defect gets flimsy and possess crack. In answer to certain weaknesses with respect to different materials, for example, metals, Irwin later built up an altered variant of Griffith's vitality balance approach. Westergaard demonstrated that the burdens and relocations close to the split tip can be portrayed by a solitary steady, identified with the vitality discharge rate, which is currently called the pressure power factor.

Only during the 1960s, the first efforts to apply FM to stone and concrete took place. While Kaplan tried to use conventional linear elastic fracture mechanics (Kaplan, 1961), Clintock and Walsh introduced the concept of friction between crack faces (Clintock et al., 1962). Rice later on proposed a new crack growth criterion in order to characterize the non-linear material behaviour ahead of a crack (Rice, 1968). By glorifying plastic twisting as non-direct versatile, indicated that the non-straight vitality discharge rate might be communicated by methods for J-basic, assessed along a discretionary shape around the break. The following serious step forward in solid FM was made Hillerborg et al., 1976. In view of the plans of Dugdale and Barenblatt in the mid1960s about the presence of a plastic zone of limited length at the break front, incorporated the pressure mellowing measure zone through an invented split in front of the previous split in which shutting powers act so that there is no pressure fixation at the tip of the all-encompassing break (Hillerborg et al., 1976).

1.1 Fracture Mechanics

Fracture mechanics is nothing but describing the science of how a crack starts and continues when the loads are applied to an engineering materials which are glasses, rocks, concrete and ceramics. Crack mechanics is consistently utilized in the field of studies of the planet, for example, oil building, geographical designing, mining designing and structural designing. Concrete is a material developed from a stone with permitting a mixture of cement, FA and gravel or other aggregate and when added with water it hardens and form a desired structure shape. Concrete is most used and popular material in the field of civil engineering for many reasons, which are less aggregate cost, availability of materials and for its higher compressive strength, but also the hardened concrete will be brittle and tensile strength when compared with the compression strength.

Besides an ideal sharp break tip with limitlessly little indent range is expected So as to measure the pressure state in a split body, exposed to outer powers, the pressure force factor (K) is utilized. The size of K (or the pressure circumstance) relies upon the example calculation, the size and area of the break, and the stacking setup. There are three sorts of stacking a break can understanding opening, in-plane shear, and out-of-plane shear, alluded to as mode I, mode II, and mode III.

1.2 *Linear Fracture Mechanics*

The basic concept of the linear elastic theory for crack propagation is reasoned from the knowledge that creating crack surfaces consumes energy. Bearing in mind the law of conservation of energy, Griffith formulated the following equilibrium equation: in order to overcome the surface energy of a linear elastic material and cause a crack to extend, sufficient potential energy must be available (Wang, 1996). In other words, crack propagation is induced by an energy transfer from external work and/or strain energy to surface energy. The critical stress level at which the crack becomes unstable decreases with crack length and depends on the material's toughness (related to the surface energy).

For determining the stress, strain, and displacement fields, associated to a crack or dislocation in an elastic solid, various techniques exist, amongst which the stress function of Westergaard is the most commonly applied one (Tada et al., 2000). Loading conditions (i.e. fracture mode), crack size, and geometry of the cracked body are of great interest and can be incorporated through the stress intensity factor K, describing the stress condition at the crack tip. The critical state at which failure will occur, corresponding to the material's resistance to fracture, is called the critical stress intensity factor Kc, and is an environment and load rate dependent material property (Murakami, 1987).

The stress intensity factor K based on linear elastic fracture mechanics has become an important parameter when evaluating the strength of a structure, since it represents the strength of the stress field at the crack tip and has a critical value which determines whether or not the crack will propagate.

2 Experimental Work

2.1 *Material*

The basalt fiber reinforced concrete beam was cast for concrete with M42.5 mix proportion was adopted and design mix used in the specimen was as per IS: 456 and IS: 10,262:2019 is used to cast the beams and properties. The cement used was 42.5 grade ordinary Portland (P.O) cement. Table 1 presents its properties. The used fly ash

Table 1 Properties of Portland cement

Cement type	Strength grade	Compressive strength 28 days (Mpa)
Ordinary Portland (P.O.)	42.5	45.2

Fig. 1 6 mm Basalt Fiber

Table 2 Properties of Basalt fiber

Diameter (μm)	Length (mm)	Tensile strength (MPa)	Elasticity (GPa)	Elongation (%)	Density (kg/m^3)
17.4	6	≥2000	≥85	2.5	2699

has ignition loss of 2.6%, moisture content of 0.1%. Coarse aggregate (CA) and fine aggregate (FA) are natural aggregate and crushed pebbles. FA with fineness modulus of 3.0 and bulk density of 2680 kg/m3 has saturate surface dry (SSD) bulk density of 2670 kg/m3. The SSD bulk density of CA is 2660 kg/m3. The high range water reducer (HRWR) and air entraining admixture (AEA) were employed to improve workability of concrete. The adopted basalt fiber (BF) is in length of 6 mm as shown in Fig. 1 and its properties are shown in Table 2. The water reducer and air entraining agent are 1% and 0.04% in mass of the amount of cement and fly ash, respectively. The volumetric ratio of BF was used to investigate the effect of BF dosage on fracture mechanical properties of BFRC.

2.2 Test Method

Check the strength of concrete cube for 7 and 28 days. Stress strain relationship between different basalt fiber dosages is shown in Fig. 2. Three point twisting test was performed on the precast scored beam example of two unique sizes given in Table 3. Regardless the dimensions of the specimen, three point bending test procedure remains identical. By exerting a linear, vertical load onto the middle of the
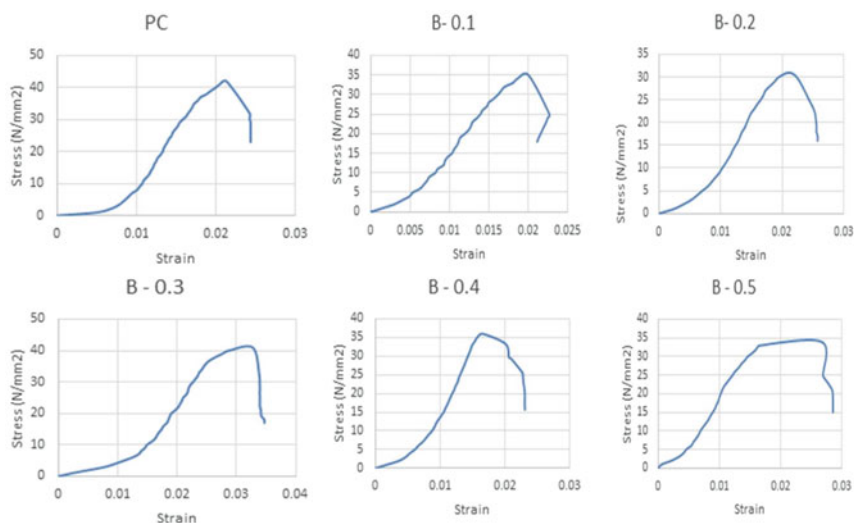
Fig. 2 Relationship between stress-strain

Table 3 Detail of specimen size

Group	Specimen size			a0 (mm)	S (mm)
	l (mm)	h (mm)	t (mm)		
I	480	180	60	36	400
II	640	240	80	48	540

beam's top surface, the line supported sample starts cracking at the notch tip until failure occurs. The starting tallness proportion of score and example (a0/h) is 0.2. The score was cut by a solid center shaper with a thick sharp edge. Width of score is 4 mm the radii of stacking head and two backings are 12 and 15 mm individually and shown in Fig. 3.

In the blending of basalt fiber fortified solid, dry fiber blending technique was completed to improve the consistency of fiber appropriation. Basalt fiber was included into concrete with 6 diverse volumetric proportions to concrete for example 0.0, 0.1, 0.2, 0.3, 0.4, and 0.5% two copies were tried for every basalt fiber measurements and example size.
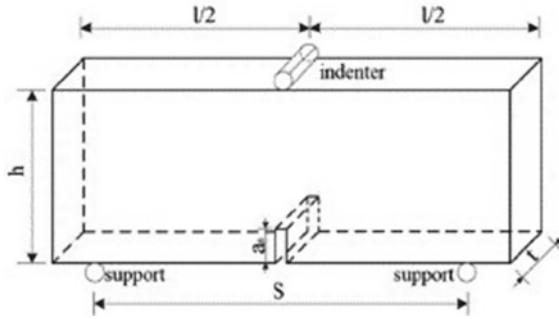
Fig. 3 Specimen detail for three point bending test

3 Results and Discussion

3.1 Load and Deflection

The impact of different basalt fiber measurement on load-break mouth opening removal bend were acquired from the tests as appeared in Fig. 4. For numerical investigation and comparison Load- Deflection curve is used [32]. Stage I, the heap and relocation were in straight relationship. Stage II, with load proceeding, the miniature splits happened under consistent proliferation until a definitive burden was reached. Stage III, unsteady break took over in split proliferation until the breaks created over the entire bar.
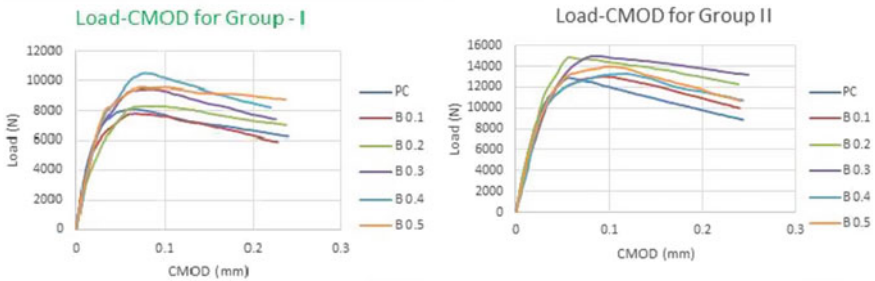
Fig. 4 Load-Crack mouth opening displacement curve

3.2 Calculation of Fracture Parameters

3.2.1 Double-K Fracture Parameters

(1) Initiation toughness

Initiation toughness can be expressed by Eqs. (1) and (2).

$$K_{IC}^{Q} = \frac{1.5\left(P_a + \frac{mg}{2} * 10^{-2}\right) * 10^{-3} * S\sqrt{a_o} * f(a)}{h^2} \tag{1}$$

$$f(a) = \frac{1.99 - \alpha(1-\alpha)\left(2.15 - 3.93\alpha + 2.7\alpha^2\right)}{(1+2\alpha)(1-\alpha)^{1.5}} \tag{2}$$

$$a = \frac{a_o}{h}$$

where K_{IC}^{Q} is initiation toughness (MPa m1/2); m is mass of mid-span specimen (kg); PQ is crack initiation load (kN) and equals to 0.67 Pmax. Pmax is peak load (kN).

(2) Unstable toughness

Unstable fracture toughness can be calculated by Eqs. (3) and (4).

$$K_{IC}^{S} = \frac{1.5\left(P_a + \frac{mg}{2} * 10^{-2}\right) * 10^{-3} * S\sqrt{a_C} * f(a)}{h^2} \tag{3}$$

$$f(a) = \frac{1.99 - \alpha(1-\alpha)\left(2.15 - 3.93\alpha + 2.7\alpha^2\right)}{(1+2\alpha)(1-\alpha)^{1.5}} \tag{4}$$

$$a = \frac{a_C}{h}$$

where, K^S is unstable fracture toughness (MPa m1/2); ac is effective crack length (m)

$$a_c = \frac{2}{\pi}(h + h_o)arctan\sqrt{\frac{\in V_c}{32.6 P_{max}}} - 0.1135 - h_o \tag{5}$$

where, h0 is thickness of the blade on the clip extensometer (m); Vc is critical value of CMOD (µm); E is elasticity modulus (GPa).

$$e = \frac{1}{C_i}\left(3.70 + 32.6 * tan2 * \left(\frac{\pi}{2} * \frac{a_o + h_o}{h + h_o}\right)\right)$$

$$C_i = \frac{V_i}{P_i}$$

where ci is the ratio of displacement to load in the linear phase (µm/kN) (Tables 4 and 5).

Expansion the measurement of basalt fiber from 0.0% to 0.5% inception strength increment after 0.1% and afterward diminished. The commencement sturdiness of BFRC was more prominent than that of plain concrete. Notwithstanding of example size the inception strength was greatest at 0.4% measurement for Group-I. At the point when the basalt fiber at 0.1% the commencement sturdiness was moderately less for Group-II. Reason may be that the fiber mass caused deformities, for example, miniature breaks and voids in concrete. By and large, thinking about the hour of break advancement, most ideal measurements of basalt fiber was 0.2%. Basalt fiber could expand the commencement durability since it have more quality and malleability than the plain concrete. Basalt strands disseminated and associated with one another in solid grid, which could forestall the improvement of miniature breaks, voids and the frail interface of mortar and totals, increment the direct proliferation and the inception durability. It is discovered that if basalt strands are not conveyed homogeneously and assembled, they won't forestall the improvement of miniature splits, voids and

Table 4 Fracture parameters of Basalt fiber reinforced concrete

Group-I	W (N-m)	PQ (KN)	Pmax (KN)	Critical CMOD (µm)	E (GPa)	ac (mm)	f(α)
PC	1.4	5.427	8.1	58	49.66	0.064	2.089
B-0.1	1.346	5.237	7.816	64	47.14	0.061	2.16
B-0.2	1.431	5.595	8.350	78	41.36	0.046	2.155
B-0.3	1.610	6.342	9.466	80	49.72	0.055	2.189
B-0.4	1.739	7.046	10.516	80	45.99	0.053	2.013
Group-II	W (N-m)	PQ (KN)	Pmax (KN)	Critical CMOD (µm)	E (GPa)	ac (mm)	f(α)
PC	2.13	8.643	12.9	56	42.06	0.073	1.941
B-0.1	2.060	8.263	12.33	119	49.20	0.062	2.278
B-0.2	2.551	9.983	14.9	56	45.68	0.060	1.885
B-0.3	2.588	10.072	15.033	83	36.30	0.054	1.948
B-0.4	2.210	8.922	16.316	120	36.93	0.065	2.233

Table 5 Double-k parameters

Group-I	Initiation toughness (MPa.m$^{1/2}$)	Unstable toughness (MPa.m$^{1/2}$)
PC	0.63	1.48
B-0.1	0.61	1.5
B-0.2	0.660	1.62
B-0.3	0.710	1.81
B-0.4	0.756	1.725
Group-II	Initiation toughness (MPa.m$^{1/2}$)	Unstable toughness (MPa.m$^{1/2}$)
PC	0.68	1.34
B-0.1	0.64	1.733
B-0.2	0.723	1.612
B-0.3	0.748	1.578
B-0.4	0.657	1.698

the frail interface of mortar and totals and decline the inception sturdiness. This is connected with the voids and the low rubbing in filaments.

Unsteady Fracture Toughness, succeeding direct proliferation, Basalt fiber strengthened cement began insecure break until it arrives at its definitive burden and fizzled. The variety of unsteady crack durability with various basalt fiber dose. As the augmentation in load, the splits in basalt fiber strengthened solid finishes direct stage and starts nonlinear stage. In this stage, abandons like the miniature splits, voids and the feeble interface of mortar and totals continue to create. Break and other deformity created in the mortar, with the goal that sand and interface of solidified concrete glue were harmed, this returns splits proliferation into slurry. On the off chance that slurry harmed example fizzled. The disappointment furthest reaches of basalt fiber fortified concrete is rely upon shaky burden and insecure sturdiness, this imperative to dissecting break execution. It is very well observed from the greatest unsteady break durability at 0.3% for bunch I and for bunch II was at 0.1%. Basalt fiber can influence the precarious break sturdiness of cement. Its instrument is that basalt filaments disseminated and associated with one another in solid framework. At the point when break begins proliferate and harms, basalt fiber holds up the split engendering by using the vitality during break spread which clarify the crack cycle of basalt fiber fortified cement.

3.3   Finite Element Model (ANSYS)

After pre-processing, ANSYS requires input information for material properties of cement and basalt fiber, as the model age, including coinciding is finished. It is prepared to start the arrangement period of the ANSYS meeting. To start with, the
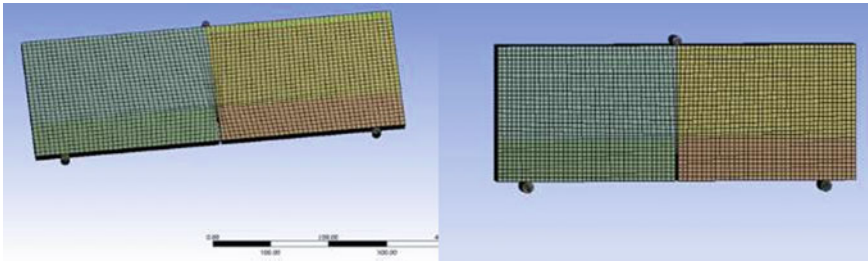
Fig. 5 Meshing of beam

Table 6 Unstable toughness for FEM

Specimen ID	Group-I	Group-II
PC	1.3494	1.3271
B-0.1	1.4863	1.729
B-0.2	1.579	1.4724
B-0.3	1.8877	1.57
B-0.4	1.755	1.7317
B-0.5	1.7397	1.7604

investigation type is determined static. To begin an examination after the underlying run or burden step has been finished. In ANSYS for examination the technique for applying the complete burden to limited component model into arrangement of burden increase which is characterized as burden step. In this examination heap of 50 kN was applied and load was sub partitioned in 50 stage it was applied for 1 s which implies 1kN was given in 0.023 s. The solidness network of the model is balanced toward the finishing of each gradual arrangement in basic firmness for reflecting changes before heading off to the following steady burden. ANSYS Workbench utilizes Newton–Raphson mathematical strategy cycles for refreshing the model firmness (Fig. 5; Table 6).

In FEM analysis, the increment of basalt fiber dosage the minimum toughness showed linear arise for Group II while the increment of basalt fiber dosage unstable toughness showed an irregular differences but greater than plain concrete. The expansion the measurement of basalt fiber from 0.0% to 0.5% inception strength increment and afterward diminished after 0.1% for Group II then again starts increasing. The commencement sturdiness of BFRC was more prominent than that of plain concrete. It shows that under loading, the value initially increase linearly and then rise up nonlinearly until they reach the maximum load (Fig. 6).
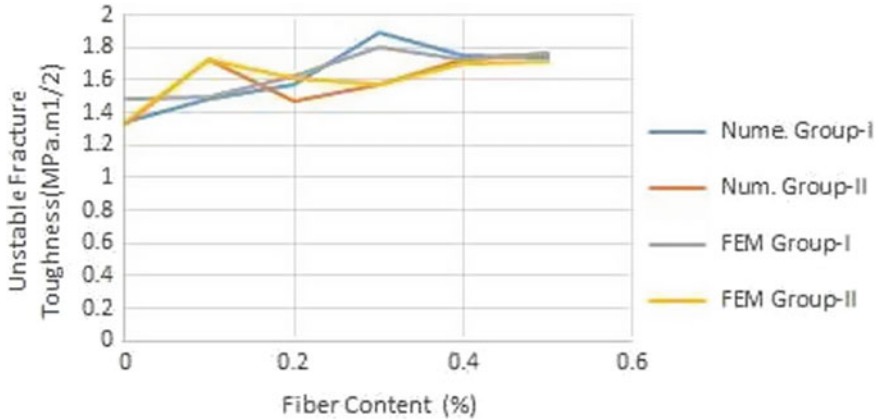
Fig. 6 Comparison of results from FEM and analytical

4 Conclusion

Basalt fiber can enhance the initiation toughness and unstable toughness of concrete. It can prevent the development of weak interface, micro-cracks, voids due to basalt fiber and increasing the crack resistance of concrete. It can be uniformly distributed in the concrete matrix to prevent these defect.

Load-crack mouth opening displacement curves established, on the basis of state of crack propagation initial crack load was obtained. And the initiation toughness calculated by the initial crack load. It is found that basalt fiber enhanced initiation toughness. Basalt fiber increased unstable toughness. According to load-crack mouth opening displacement curves, specimen starts fail when load reaches its maximum value. Unstable fracture toughness determined by failure load. As the increment of basalt fiber dosage the initiation toughness showed linear arise while unstable toughness showed an irregular differences but greater than plain concrete. Notched beam of different sizes, with the rise of height of specimen the initiation toughness increased, but unstable toughness was not appreciable. Three point bending test were analysed by using ANSYS. There may chance of error in analytical data. ANSYS can help out to model more complicated structure in less time which shows benefit over experimental study. FEM software can save both time and cost.

References

1. McCreath DR (1968) Imperial college of science and technology, Fracture mechanics ofconcrete, London
2. Philip George Meredith (1983) Geology department imperial college. A fracture mechanics study of experimentally deformed crustal rocks, London

3. Mikheevskiy S (2009) Elastic-plastic fatigue crack growth analysis under variable amplitude loading. Waterloo, Ontario, Canada
4. Linsbauer HN, Institute of large dams and hydraulic structures, University of Technology Vienna, Karlsplatz 13, A-1040 Vienna, Austria. Application of the methods of fracture mechanics for the analysis of cracking in concrete dams
5. Sharan A, Dung TAD (2012) Department of mechanical engineering national institute of technology Rourkela 2012, Prediction of fatigue crack propagation in circumferentially cracked pipe specimen using Casca and Franc2d
6. Saifuldin M, Manan A (2008) Department of mechanical engineering university college London. Fracture Mechanics Analysis of Multiple Edge Cracks
7. Vorechovsky M (2004) Stochastic fracture mechanics and size effect
8. Nunez D (2003) J-integral computation for linear elastic fracture mechanics in h, p, k Mathematical and computational framework. The University of Kansas, Lawrence, KS
9. Deepa PP, Baby A, Analysis of steel fibre reinforced concrete beam without conventional shear reinforcement
10. Kumar S, Barai SV, Size-effect of fracture parameters for crack propagation in concrete: a comparative study
11. Wafa FF, Associate Professor, Civil Engineering Department, Faculty of Engineering, King Abdulaziz University, Jeddah, Saudi Arabia, Properties and Applications of Fiber Reinforced Concrete
12. Ramos IS, Duque OAS, Gomez de Merodio MCH, Pozhilova N, Cracking study of a reinforced concrete beam
13. Sun X, Gao Z, Cao P, Zhou C, Ling Y, Wang X, Zhao Y, Diao M, Fracture performance and numerical simulation of basalt fiber concrete using three-point bending test on notched beam. Constr Build Mater
14. Zhao Y, Sun X, Cao P, Ling Y, Gao Z, Zhan Q, Zhou X, Diao M, Mechanical performance and numerical simulation of basalt fiber reinforced concrete (BFRC) using double-k fracture model and virtual crack closure technique
15. Chao Z, Cao P, Li J, Cao Y Numerical simulation to evaluate fatigue fracture behavior of concrete beam with initial crack
16. Nasrnia A, Aboutalebi FH Experimental investigation and numerical simulations of Unotch specimens under mixed mode loading by the conventional and extended finite element methods
17. Wu Y, Xu S, Li Q, Ruiz G, Yu RC (2016) Estimation of real fracture parameters of a dam concrete with large size aggregates through wedge splitting tests of drilled cylindrical specimens
18. Zhao Y-R, Wang L, Lei Z-K, Han X-F, Shi J-N (2018) Study on bending damage and failure of basalt fiber reinforced concrete under freeze-thaw cycles
19. Hu X-Z, Mai Y-W, Cotterell B, A statistical theory of time-dependent fracture for brittle materials.
20. Zhang C, Gao D, Gu Z (2017) Fatigue behavior of steel fiber reinforced high-strength concrete under different stress levels
21. Xin H, Veljkovic M (2019) Fatigue crack initiation prediction using phantom nodes- based extended finite element method for S355 and S690 steel grades
22. Al-Rousan R, Fatigue performance of reinforced concrete beams strengthened with CFRP sheets. Constr Build Mater
23. Reinhardt HW, Xu S, Crack extension resistance based on the cohesive force in concrete
24. Wang G, Lu W, Zhou C, Zhou W, The Influence of initial cracks on the crack propagation process of concrete gravity dam-reservoir-foundation systems
25. Wang JG, Ju DY, Sun MJ, Li SL (2011) A new analytical method for stress intensity factors based on in situ measurement of crack deformation under biaxial tension
26. Broek D (1986) Elementary engineering fracture mechanics
27. Shi J, Abaqus implementation of extended finite element method using a level set representation for three-dimensional fatigue crack growth and life predictions
28. Wang HW, Qin QH, Zhou HW, Miao H, Damage progress simulation in unidirectional composites by Extended Finite Element Method (XFEM).

29. Fu Y, Li Y-L, Tan Y-Q, Parametric analysis of dynamic crack propagation of concrete bending beam based on the extended finite element method
30. Lee MK, Barr BIG (2004) An overview of the fatigue behaviour of plain and fibre reinforced concrete
31. Xu S, Determination of fracture parameters for crack propagation in concrete using an energy approach
32. Yin Y, Qiao Y, Hu S (2019) Four-point bending tests for the fracture properties of concrete
33. Bangash MYH (1989) Concrete and concrete structures. Elsevier Science Publishers Ltd., London
34. Dahmani L, Khennane A, Kaci S (2010) Crack identification in reinforced concrete beams using ANSYS software. ISSN 0556-171X.
35. Huei HL (2015) Finite element simulations with ANSYS workbench 16
36. Hyndavi CH , Sai Kumar AVS, Sreedgar S (2015) Flexural strength of reinforced concrete beam with coupled rebars. ISSN: 2349-6010

Nonlinear Vibration of Functionally Graded CNT-Reinforced Composite Plate Under Nonuniform In-Plane Loading

Vishal Singh, Rajesh Kumar, Benu G. Mohapatra, Malay Saha, and S. N. Patel

1 Introduction

Composite has a significant impact in this modernized world, where engineers look for light but stiff materials for the design of different structural members. The composite materials have good strength and stiffness quality than any other individual material. New material is in great demand nowadays in different disciplines like - civil, aerospace, mechanical, and naval industries due to its extraordinary properties; it is known as carbon nanotube (CNT). CNT was discovered by Japanese scientist [1], and then it is adopted by many researchers in the progress of their work in increasing the mechanical properties along with the strength and stiffness of the CNTRC plate [2–5]. In this context, [6] investigated an FG-CNTRC plate loaded with parabolic loading for the analysis of buckling load, where the plate was modeled using first order shear deformation theory (FSDT) using the Ritz method. From the above discussion, it can be observed that how beneficial CNT is in developing the composite as advanced material. But the increasing strength and stiffness of the composite plates are not only the design criteria of a plate, with that the nonlinear vibration analysis needs to be included, which plays a vital role in the design criteria of the plate under periodic loading. In this viewpoint, [7, 8] investigated the nonlinear free vibration of a simply supported composite plate using the hierarchical finite element method (HFEM) along with the harmonic balance method (HBM). Again, a moderately thick, unsymmetrically laminated composite plate was

V. Singh (✉) · R. Kumar · S. N. Patel
Department of Civil Engineering, Birla Institute of Technology and Science, Pilani 333031, India
e-mail: p20180012@pilani.bits-pilani.ac.in

B. G. Mohapatra
School of Civil Engineering, KIIT University, Bhubaneswar 751024, India

M. Saha
Department of Civil Engineering, SIEM, Siliguri 734009, India

modeled based on FSDT and solved using FEM for free vibration response [9]. Cheung et al. [10] adopted IHB and Hsu's methods to investigate their effectiveness in the cubic nonlinear systems that govern many engineering applications like large-amplitude vibration of beam and plate. Darabi and Ganesan [11] studied the nonlinear vibration of the internally thickness tapered plate subjected to parametric excitation using the Galerkin method.

From the existing literature survey, the nonlinear vibration of the FG-CNTRC plate exposed to different types of nonuniform periodic loadings is not yet investigated. This study aims to investigate the nonlinear vibration of the FG-CNTRC plate exposed to nonuniform in-plane loading. The impact of different parameters like types of CNTs distribution profiles, volume fraction of CNT, types of nonuniform in-plane loadings, and compression pre-loading on the nonlinear vibration of the FG-CNTRC plates are studied.

2 Formulation

In the current study, an FG-CNTRC plate is semi-analytically analyzed for its nonlinear vibration behavior using the formulation, as stated in this section. The constituents used in each lamina are SWCNT (chiral indices $(n_0, m_0) = (10, 10)$) and polymer matrix (epoxy resin). The effective mechanical properties of the lamina (CNT embedded matrix) are obtained implementing the extended rule-of-mixture technique as given in the next subsection. Figure 1 shows the pictorial representation of the FG-CNTRC plate where a, b and h as length, width and thickness respectively, and also CNTs distribution across the thickness of the plate.

2.1 The Extended Rule-Of-Mixture

As per extended rule-of-mixture, the effective mechanical properties of the FG-CNTRC plate are estimated as [8],

$$E_{11} = \eta_1' V_{CNT} E_{11}^{CNT} + V_m E_m \tag{1}$$

$$\frac{\eta_2'}{E_{22}} = \frac{V_{CNT}}{E_{22}^{CNT}} + \frac{V_m}{E_m} \tag{2}$$

$$\frac{\eta_3'}{G_{12}} = \frac{V_{CNT}}{G_{12}^{CNT}} + \frac{V_m}{G_m} \tag{3}$$

$$V_{CNT} + V_m = 1 \tag{4}$$
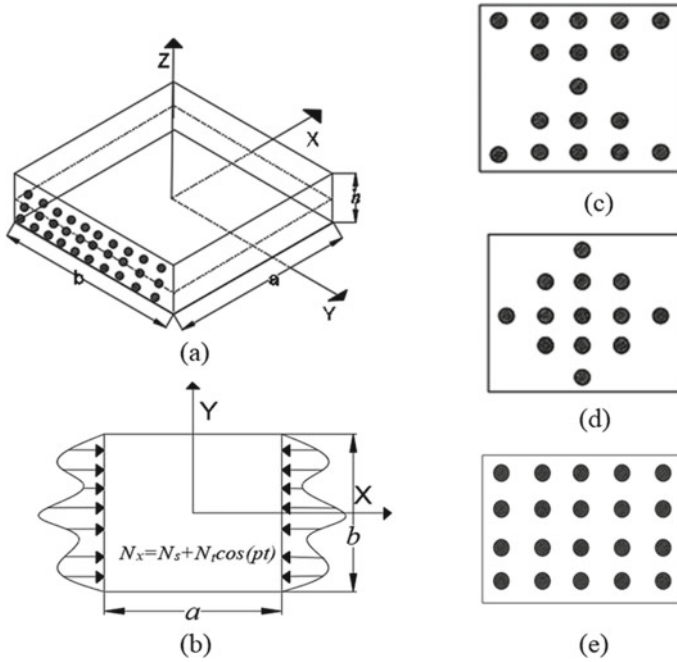
Fig. 1 Schematic view of (**a**) UD-CNTRC plate, (**b**) nonuniform in-plane loading (**c**) FG-X CNTRC, (**d**) FG-O CNTRC, and (**e**) UD-CNTRC

Table 1 Profiles for the three cases of CNTs distribution as a function of "z"	CNTs distribution within FG-CNTRC plate	V_{CNT} (Kiani, 2017)
	UD	$V_{\_cnt}$
	FG-O	$2V_{\_cnt}\left(1 - 2\frac{|z|}{h}\right)$
	FG-X	$4V_{\_cnt}\frac{|z|}{h}$

$$\mu_{12} = V_{\_cnt}\mu_{11}^{CNT} + V_m\mu_m \tag{5}$$

$$\rho_{hm} = V_{CNT}\rho_{CNT} + V_m\rho_m \tag{6}$$

where, η_1', η_2' and η_3' are the efficiency parameters. Here, E_{11}^{CNT}, E_{22}^{CNT}, and G_{12}^{CNT} are Young's and shear moduli of the CNT, respectively. E_m and G_m are Young's and shear moduli of the epoxy, respectively. V_{CNT} and V_m denote the volume fraction of CNT and epoxy, respectively. ρ_{CNT} and ρ_m denote the density of CNT and epoxy, respectively. The profiles for the different cases of CNTs distribution, such as UD,

FG-O, and FG-X, are presented in Table 1. Here, the volume fraction of all three cases of CNTs distribution is equal to V_{cnt}.

2.2 Kinematics of the FG-CNTRC Plate

The CNTRC plate in the current study is modeled as per HSDT which was developed by [12]. The displacement fields are considered based on HSDT for the rectangular plate, such that the transverse shear strains (in case of the thick plate) at the plate's top and bottom surfaces becomes zero, are expressed as:

$$u = u^0 + z\varphi_x - \frac{4z^3}{3h^2}\left(\varphi_x + w^0_{,x}\right) \tag{7}$$

$$v = v^0 + z\varphi_y - \frac{4z^3}{3h^2}\left(\varphi_y + w^0_{,y}\right) \tag{8}$$

$$w = w^0 \tag{9}$$

where u, v, and w denote the displacements of the point at a distance z from the neutral surface, and u^0, v^0 and w^0 denote the displacements of the point on the neutral surface. φ_x and φ_y represent the rotation of the cross-section normal to the x-axis and y-axis, respectively. In the above equations, $(\varphi_x + w^0_{,x})$ and $(\varphi_y + w^0_{,y})$ are represented by ϕ^0_x and ϕ^0_y, respectively. As per [13], the above equations are written as,

$$u = u^0 - zw^0_{,x} + f(z)\phi^0_x \tag{10}$$

$$v = v^0 - zw^0_{,y} + f(z)\phi^0_y \tag{11}$$

$$w = w^0 \tag{12}$$

where $f(z) = z\left(1 - \frac{4z^2}{3h^2}\right)$. The strain displacement equations of the CNTRC plate is expressed as:

$$\varepsilon_{xx} = \varepsilon^0_{xx} - zw^0_{,xx} + f(z)\phi^0_{x,x} \tag{13}$$

$$\varepsilon_{yy} = \varepsilon^0_{yy} - zw^0_{,yy} + f(z)\phi^0_{y,y} \tag{14}$$

$$\gamma_{xy} = \gamma^0_{xy} - 2zw^0_{,xy} + f(z)\phi^0_{x,y} + f(z)\phi^0_{y,x} \tag{15}$$

$$\gamma_{xz} = u_{,z} + w_{,x} = f^{'}(z)\phi_x^0 \tag{16}$$

$$\lambda_{yz} = v_{,z} + w_{,y} = f'(z)\phi_y^0 \tag{17}$$

where, ε_{xx}^0, ε_{yy}^0 and γ_{xy}^0 are the strains at the neutral surface of the plate defined as,

$$\varepsilon_{xx}^0 = u_{,x}^0 + \frac{1}{2}\left(w_{,x}^0\right)^2 \tag{18a}$$

$$\varepsilon_{yy}^0 = v_{,y}^0 + \frac{1}{2}\left(w_{,y}^0\right)^2 \tag{18b}$$

$$\gamma_{xy}^0 = u_{,x}^0 + v_{,y}^0 + w_{,x}^0 w_{,y}^0 \tag{18c}$$

The force resultants $\mathbf{N}^T = \{N_{xx}, N_{yy}, N_{xy}\}$, moment resultants $\mathbf{M}^T = \{M_{xx}, M_{yy}, M_{xy}\}$, additional moment resultants due to additional changes in curvatures $\mathbf{M}^{aT} = \{M_{xx}^a, M_{yy}^a, M_{xy}^a\}$ and shear resultants $\mathbf{Q}^T = \{Q_{yz}, Q_{xz}\}$ are related respectively to the membrane strains $\boldsymbol{\varepsilon}^{0T} = \{\varepsilon_{xx}^0, \varepsilon_{yy}^0, \varepsilon_{xy}^0\}$, bending strains $\boldsymbol{\kappa}^T = \{-w_{,xx}^0, -w_{,yy}^0, -2w_{,xy}^0\}$, additional bending strains $\boldsymbol{\kappa}^{aT} = \{\phi_{x,x}^0, \phi_{y,y}^0, \phi_{x,y}^0 + \phi_{y,x}^0\}$ and shear strains $\boldsymbol{\gamma}^T = \{\gamma_{yz}, \gamma_{xz}\}$, through the constitutive relations,

$$\mathbf{N} = \mathbf{A}\boldsymbol{\varepsilon}^0 + \mathbf{B}\boldsymbol{\kappa} + \mathbf{C}\boldsymbol{\kappa}^a \tag{19}$$

$$\mathbf{M} = \mathbf{B}\boldsymbol{\varepsilon}^0 + \mathbf{D}\boldsymbol{\kappa} + \mathbf{E}\boldsymbol{\kappa}^a \tag{20}$$

$$\mathbf{M}^a = \mathbf{C}\boldsymbol{\varepsilon}^0 + \mathbf{E}\boldsymbol{\kappa} + \mathbf{F}\boldsymbol{\kappa}^a \tag{21}$$

$$\mathbf{Q} = \mathbf{H}\boldsymbol{\gamma} \tag{22}$$

Here, bold upright letters are denoting matrices and vectors. In the above Eqs. (19)–(22), $\mathbf{A}$ (A_{ij}, $i,j = 1,2,6$), $\mathbf{B}$ (B_{ij}, $i,j = 1,2,6$), $\mathbf{C}$ (C_{ij}, $i,j = 1,2,6$), $\mathbf{D}$ (D_{ij}, $i,j = 1,2,6$), $\mathbf{E}$ (E_{ij}, $i,j = 1,2,6$), $\mathbf{F}$ (F_{ij}, $i,j = 1,2,6$) and $\mathbf{H}$ (H_{ij}, $i,j = 4,5$) are stiffness matrices of the FG-CNTRC plate.

2.3 Problem of In-Plane Elasticity

The in-plane stress equilibrium equation as per Airy's stress approach assuming a suitable function (ϕ) for CNTRC plate is obtained by means of strain-compatibility

conditions and given as per [15]. The formation of an analytical expression for the pre-buckling stresses is not presented due to page constraints.

2.4 Governing Equations

The partial differential equations (PDEs) of the CNTRC plate is obtained using Hamilton's principle as follows:

$$\hat{\bar{N}}_{xx,x} + \hat{\bar{N}}_{xy,y} = \rho_g u^0{}_{,tt} \tag{23}$$

$$\bar{N}_{xy,x} + \hat{\bar{N}}_{yy,y} = \rho_g v^0{}_{,tt} \tag{24}$$

$$\bar{M}_{xx,xx} + 2\bar{M}_{xy,xy} + \bar{M}_{yy,yy} + \left(\hat{\bar{N}}_{xx} w_{,x} + \hat{\bar{N}}_{xy} w_{,y}\right)_{,x}$$
$$+ \left(\hat{\bar{N}}_{xy} w_{,x} + \hat{\bar{N}}_{yy} w_{,y}\right)_{,y} = \rho_g w^0{}_{,tt} \tag{25}$$

$$\bar{M}^a_{xx,x} + \bar{M}^a_{xy,y} - \bar{Q}^a_{xz} = \rho_h \phi^0{}_{x,tt} \tag{26}$$

$$\bar{M}^a_{xy,x} + \bar{M}^a_{yy,y} - \bar{Q}^a_{yz} = \rho_h \phi^0{}_{y,tt} \tag{27}$$

The expression for equations density in the equation given above are written as, $\rho_g = \int_{-h/2}^{h/2} \rho_{hm} dz$, $\rho_h = \int_{-h/2}^{h/2} \rho_{hm} z^2 dz$ and $\hat{N}_{ij} = [N_{ij} - n_{ij}]$, where i, j = (x, y) and n_{ij} are the internal stress resultants due to applied nonuniform in-plane loading, and the large deformation stress resultants are represented by N_{ij}. Hence, $\hat{N}_{ij}$ are the net stress resultants within the CNTRC plate. The above PDEs in Eqs. (23–27) are solved via the Galerkin method [16] to reduce them into nonlinear ordinary differential equations (ODEs) as described in the next subsection.

2.5 Solution Methodology

Galerkin method reduces the above governing PDEs of the plate into nonlinear ODEs. Finally, these ODEs of the FG-CNTRC plate are solved by Increment Harmonic Balance (IHB) method [10] to trace the nonlinear vibration response (frequency-amplitude curve) of the FG-CNTRC plate.

3   Results and Discussion

The material properties for epoxy and CNTs, and other necessary parameters considered in the current study are taken from [6]. In this section, various nonuniform in-plane edge loadings such as parabolic, concentrated, partial edge loadings are considered along with uniform loading for evaluating the free and forced vibration of the FG-CNTRC plate. The various nonuniform in-plane loading functions are given below,

The partial edge loading function is expressed as,

$$N_s = N_t = \overline{N}_0 \frac{b}{d} \left(\frac{d}{b} + \sum_{r=1}^{\infty} \frac{2}{\pi} \frac{1}{r} sin \frac{r\pi d}{b} cos \frac{2r\pi y}{b} \right) \tag{28}$$

Here, partial edge loading at the edge of the plate is modeled using a single Fourier series along the y-direction. In which 50 terms (i.e., $r = 1$ to 50) in Fourier series are considered for the converged pre-buckling stresses ($\sigma_{ij}, (i, j = x. y)$) within the FG-CNTRC plate.

Parabolic loading function is expressed as,

$$N_s = N_t = \frac{3}{2} \overline{N}_0 \left(1 - 4 \frac{y^2}{b^2} \right) \tag{29}$$

The concentrated loading function is expressed as,

$$N_s = N_t = \frac{\overline{N}_0}{c\sqrt{\pi}} exp \left(-\frac{y^2}{c^2} \right) \tag{30}$$

In this above expression, $c = 1/24$ is chosen based on converged pre-buckling stresses ($\sigma_{ij}, (i, j = x. y)$) within the FG-CNTRC plate. Here, the loading function for all the different types of loadings is considered in such a way that the total load (i.e., area due to the loading distribution at the edge of the plate) is the same.

3.1   Validation Study

To validate the effectiveness of the current semi-analytical model, the results of present formulation along with the published works, are presented in Table 2. The dimensionless fundamental frequencies parameter ($\Omega_n = \omega_n a^2 / h \sqrt{\rho_{ep}/E_{ep}}$) of a simply supported (SSSS) FG-CNTRC plates for various profiles of CNTs distribution and CNT's volume fraction (V_{cnt}) along with the results given by [17]. The edge-to-thickness is chosen as $b/h = 50$, and CNT's volume fraction (V_{cnt}) is considered as 0.11, 0.14 and 0.17. The results of current study and published one as given by Zhu et al. are well matched as shown in Table 2.

Table 2 Validation of dimensionless fundamental natural frequency ($\Omega_n = \omega_n a^2/h\sqrt{\rho_{ep}/E_{ep}}$) of a plate ($a/b = 1$, SSSS) with the different distribution of CNTs and $V_{\_cnt}$

$V_{\_cnt}$			0.11		0.14		0.17	
b/h	Distribution	Method	(1,1)	(1,2)	(1,1)	(1,2)	(1,1)	(1,2)
50	UD	Present	19.159	23.286	21.322	25.205	23.613	28.829
		[17]	19.233	23.408	21.354	25.295	23.697	28.987
	FG-X	Present	22.904	26.635	25.499	29.065	22.287	33.187
		[17]	22.91	26.66	25.555	29.192	22.416	33.434
	FG-O	Present	14.252	19.279	15.772	20.494	17.494	23.697
		[17]	14.302	19.373	15.801	20.563	17.544	23.783

3.2 Influence of CNT Distribution

Figures 2 and 3 represents the frequency-amplitude curve of the FG-X CNTRC plate ($a/b = 1$, $b/h = 50$, $\lambda_s = 0$; $\lambda_d = 0.5$, SSSS) exposed to parabolic in-plane loading where Fig. 2 is due to different volume fraction of CNTs. It can be seen from the plot of dimensionless excitation frequency (Ω) versus dimensionless amplitude (w/h) that the plate's stiffness increases with the rise in CNTs volume fraction, which further leads to the rise in the degree of hardening of the plate. Thus, the nonlinear curve for $V_{\_cnt} = 0.28$ shows a higher degree of hardening than the nonlinear vibration curves obtained for $V_{\_cnt} = 0.12$ and $V_{\_cnt} = 0.17$. The plots are presented with respect to the N_{cr} of $V_{\_cnt} = 0.12$. Again, Fig. 3 represents that for the different types of CNTs distribution, the curve for FG-X type of CNTs distribution shows a higher degree of hardening than the curve for FG-O and UD CNTs distribution. Here, the plots are represented with respect to the N_{cr} of FG-O type CNTs distribution.

Fig. 2 Impact of volume fraction of CNTs on non-linear vibration response at $V_{\_cnt} = 0.12$, 0.17 and 0.28 of a FG-X CNTRC plate ($a/b = 1$, $b/h = 50$, $\lambda_s = 0$; $\lambda_d = 0.5$, SSSS)
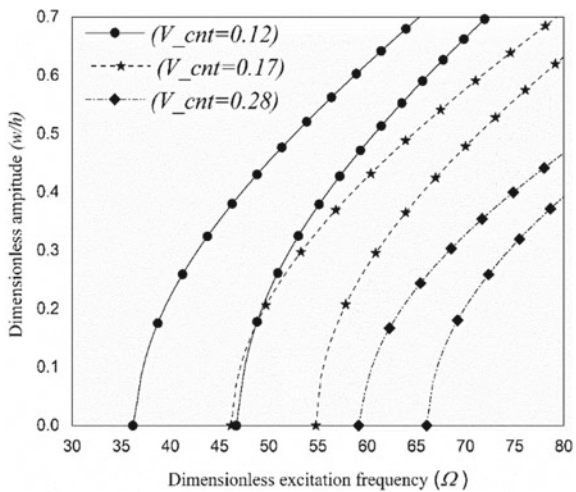
Fig. 3 Effect of CNTs distribution on non-linear vibration response at V_cnt = 0.17 of the FG-CNTRC plate ($a/b = 1$, $b/h = 50$, λ_s = 0; $\lambda_d = 0.5$, SSSS)
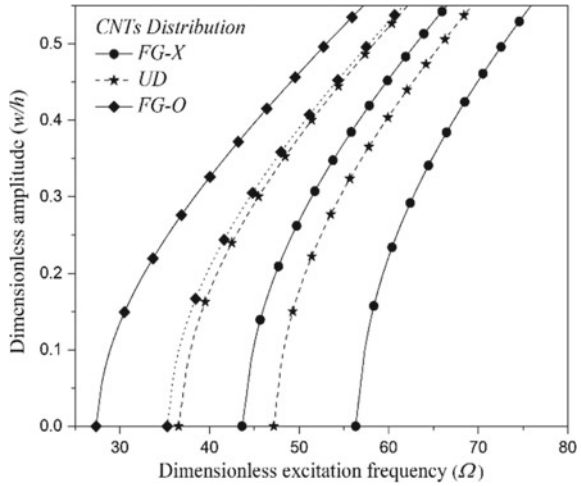
3.3 Influence of Static and Dynamic Load Factors

Both static and dynamic load factors have their own effect on the degree of hardening of the composite plate. The Fig. 4 shows the FG-X CNTRC plate ($a/b = 1$, $b/h = 50$, $\lambda_s = 0$, $V_{-cnt} = 0.17$, SSSS) which is exposed to parabolic in-plane loading with dynamic load factor as $\lambda_d = 0$, 0.4 and 0.8. Where plot with respect to $\lambda_d = 0$ shows the backbone curve (nonlinear free vibration response of FG-X CNTRC plate) with a single curve and $\lambda_d = 0.4$ and 0.8 shows the two curves for each dynamic load factor on both to the left and right-hand side of the backbone curve. It can be seen that as the dynamic load factor is increased, the plate's stiffness gets affected. The curve for nonlinear vibration to the right-hand side of the backbone curve shows an

Fig. 4 Effect of dynamic load factor on non-linear vibration response at $\lambda_d = 0$, 0.4 and 0.8 of an FG-X CNTRC plate ($a/b = 1$, $b/h = 50$, $\lambda_s = 0$, $V_{-cnt} = 0.17$, SSSS)
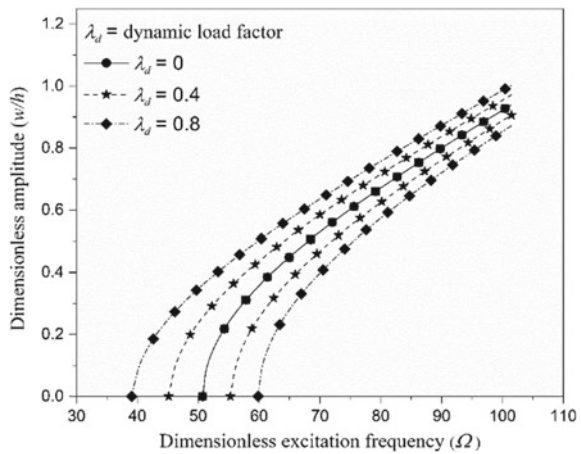
increase in the degree of hardening, while for the curve on the left-hand side, the rate of growth in amplitude is high with the frequency, which indicates a decrease in stiffness of plate and hardening as well, which is due to the change in resultant stiffness ($K = K_L + K_{NL} - N_{cr} (\lambda_s \pm 0.5\lambda_d) K_G$) with respect to λ_d.

3.4 Effect of Different Nonuniform Loadings

It can be observed from Fig. 5 that the type of loading has a significant impact on the nonlinear vibration behavior of the FG-X CNTRC plate. The buckling load (N_{cr}) for concentrated loading is found minimum compare to other types of nonuniform loadings means it affects the stiffness of the plate much more than other loading conditions. Thus, the graph is plotted with respect to the N_{cr} of concentrated loading. While curve due to uniform loading has a minimum value for buckling load, that means it has a minimum effect on the plate's stiffness. The sequence of decrease in stiffness which leads to the increase or decrease in degree of hardening of the FG-X CNTRC plate with respect to loading condition is as follows: uniform > parabolic > partial edge ($d/b = 0.5$) > partial edge ($d/b = 0.25$) > concentrated loading. The resultant stiffness (K) of the plate ($K = K_L + K_{NL} - N_{cr} (\lambda_s \pm 0.5\lambda_d) K_G$), where K mainly depends on the geometric stiffness (K_G) and " $\pm$ " sign of dynamic load factor (λ_d). Depending on the nature of loading concentration, the value of geometric stiffness (K_G) changes and which may increase or decreases the stiffness of the plate depending on the " $\pm$ " sign of λ_d for both the curves that generate for any dynamic load factor. Thus, the rate of increase in amplitude with an increase in frequency increases for the curve on the left-hand-side (" + " sign with λ_d), which shows a decrease in the degree of hardening of the FG-X CNTRC plate. While curve on the right-hand side ("−" sign with λ_d) shows an increase in the degree of hardening

Fig. 5 Plot of non-linear vibration response at $\lambda_s = 0$ for an FG-X CNTRC plate ($a/b = 1$, $b/h = 50$, $\lambda_d = 0.5$, $V_{-cnt} = 0.17$, SSSS) exposed to uniform and different nonuniform loading
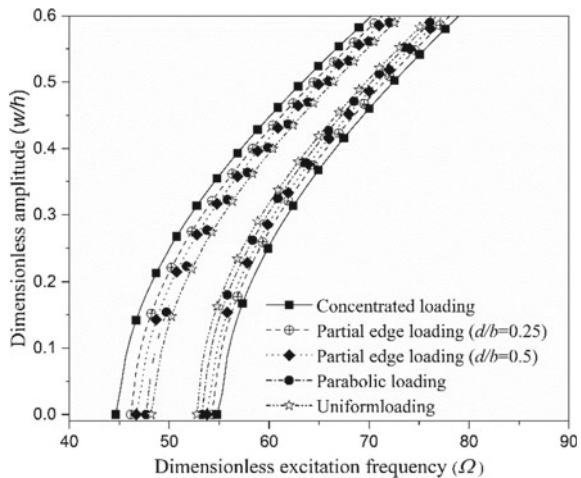
of the FG-X CNTRC plate as it's rate of increase in amplitude decreases with the increase in frequency. But for other loading conditions, the stiffness of the plate does not deteriorate as much as compared to concentrated loading conditions, and thus the plate's behavior for all other types of loading is shown in Fig. 5.

4   Conclusion

In this paper, the authors have tried to investigate the frequency-amplitude curve of an FG-CNTRC plate under uniform and various types of nonuniform in-plane loadings. Here, the effect of different parameters like CNTs volume fraction, types of nonuniform loadings, CNTs distribution profile (UD, FG-X or FG-O), and compression pre-loading on the nonlinear vibration of the CNTRC plate are studied. The remarks from the present investigation are summarized as,

- An increase in the *V_cnt*, the degree of hardening of the FG-CNTRC plate increases which further signifies the increase in stiffness of the plate.
- With the increase in dynamic load factor for any loading condition, the nonlinear curve to the right-hand-side shows an increase in the degree of hardening, which indicate an increase in stiffness of the FG-X CNTRC plate while the left-hand-side curve shows a different behavior where the rate of growth in amplitude with frequency is more due to the loss in stiffness of the FG-X CNTRC plate.
- Out of different loading conditions, the plate under concentrated loading shows the maximum and minimum degree of hardening for the FG-X CNTRC plate depending on the K_G and " $\pm$" sign of dynamic load factor (λ_d). However, comparing to all other types of loading conditions, uniform loading has maximum hardening behavior with minimum impact on FG-CNTRC plate's stiffness while concentrated loading has minimum hardening behavior with maximum impact on FG-CNTRC plate's stiffness with " $+$" sign of dynamic load factor (λ_d).

References

1. Iijima S (1991) Helical microtubules of graphitic carbon. Nature 354:56–58
2. Gojny FH, Wichmann MHG, Köpke U, Fiedler B, Schulte K (2004) Carbon nanotube-reinforced epoxy-composites: enhanced stiffness and fracture toughness at low nanotube content. Compos Sci Technol 64:2363–2371
3. Liew KM, Lei ZX, Zhang LW (2015). Mechanical analysis of functionally graded carbon nanotube reinforced composites: a review. Compos Struct 120:90–97
4. Shi DL, Feng XQ, Huang YY, Hwang KC, Gao H (2004) The effect of nanotube waviness and agglomeration on the elastic property of carbon nanotube-reinforced composites. J Eng Mater Technol Trans ASME 126:250–257
5. Tornabene F, Bacciocchi M, Fantuzzi N, Reddy JN (2017) Multiscale approach for three-phase CNT/Polymer/ fiber laminated nanocomposite structures. Polymer Compos 1–25

6. Kiani Y (2017) Buckling of FG-CNT-reinforced composite plates subjected to parabolic loading. Acta Mech 228:1303–1319

7. Ribeiro P, Petyt M (1999) Multi-modal geometrical nonlinear free vibration of fully clamped composite laminated plates. Journal of Sound and Vibration 225(1):127–152

8. Houmat A (2012) Nonlinear free vibration of a composite rectangular specially-orthotropic platewith variable fiber spacing. Compos Struct 94:3029–3036

9. Singh G, Raju KK, Rao GV, Iyengar NGR (1990) Nonlinear vibrations of simply supported rectangular cross-ply plates. J Sound Vibr 142(2):213–226

10. Cheung YK, Chen SH, Lau SL (1990) Application of the incremental harmonic balance method to cubic nonlinearity systems. J Sound Vibr 140(2):273–286

11. Darabi M, Ganesan R (2017) Nonlinear vibration and dynamic instability of internally-thickness-tapered composite plates under parametric excitation. Compos Struct 176:82–104

12. Reddy JN, Liu CF (1985) A higher-order shear deformation theory of laminated elastic shells. Int J Eng Sci 23(3):319–330

13. Soldatos KP (1991) A refined laminated plate and shell theory with applications. J Sound Vib 144(1):109–129

14. Jones RM (1975) Mechanics of composite materials. Hemisphere, Publishing Co., New York, NY

15. Kumar R, Banerjee B, Ramachandra LS (2016) Nonlinear stability and dynamics of composite skew plates under non-uniform loadings using differential quadrature method. Mech Res Commun 73:76–90

16. Kumar R, Tanish Dey, Panda SK (2019). Instability and vibration analyses of FG cylindrical panels under parabolic axial compressions. 31(2):187–199

17. Zhu P, Lei ZX, Liew KM (2012) Static and free vibration analyses of carbon nanotube-reinforced composite plates using finite element method with first order shear deformation plate theory. Compos Struct 94:1450–1460

Optimum Mix Design of Rice Husk Ash-Based Geopolymer Concrete Based on Workability, Setting Time, and Compressive Strength Cured in Ambient Temperature Condition

Mahapara Abbass and Gyanendra Singh

1 Introduction

Concrete similar to rock is artificially produced by mixing cement, water, and aggregates. The fresh state of concrete undergoes in the hydration process to create a hard structure like a rock. Concrete is the material used worldwide for the production of structural members having high compressive strength and durability characteristics like resistance against chemical attack. The cement used in the production of concrete while manufacturing produces one ton of carbon dioxide in the production of one ton of it, which is hazardous to the environment by inducing the greenhouse effect and global warming. As cement is an essential material for the production of concrete, it binds the aggregates together. Thus, to produce concrete with the replacement of cement by industrial wastes can reduce the carbon dioxide emission by cement production. These industrial wastes include those materials which have chemical composition almost similar or partly similar to cement. Viz; fly ash, ground granulated blast furnace slag, silica fume, rice husk ash, etc. when 100% cement is replaced by any of the by- products in concrete with the addition of the alkaline activators then it is termed as geopolymer concrete. The fly ash or rice husk ash or slag acts as source material, rich in alumina and silica, which undergoes polymerization in the presence of alkaline activator, which is the blend of either sodium hydroxide and sodium silicate or combinations of potassium hydroxide and potassium silicate. Geopolymer concrete, also termed as green concrete, is cement-free concrete; thus, environment friendly. Fly ash based Geopolymer concrete has the same compressive strength as conventional concrete [1]. The advantage of geopolymer concrete also depends on the concentration of sodium hydroxide, and it is also found that compressive strength increase by the increase in the level of sodium hydroxide [2]. In various studies, the blend of sodium hydroxide and sodium silicate has been used

M. Abbass (✉) · G. Singh
Department of Civil Engineering, DCRUST, Murthal, Sonipat, Haryana 131039, India

to improve strength and setting time of fly ash-based geopolymer concrete [2–4]. The ratio of sodium silicate to sodium hydroxide also plays an essential role in the strength properties of geopolymer concrete [5]. Superplasticizers are added to geopolymer mixes to increase workability at lesser water content [6, 7]. The optimized mix design of geopolymer concrete is the first step of the making geopolymer concrete with various parameters like concentration of sodium hydroxide, sodium silicate to sodium hydroxide ratio, alkaline activator to binder ratio, binder content [8–12]. The strength properties of geopolymer concrete also depend upon the fineness of source material; it has been found that higher the specific surface area of source material higher is the compressive strength [13, 14]. RHA can also replace cement in concrete in the presence of alkaline activators to produce geopolymer concrete [15–18]. In this study, the optimized mix design of RHA based geopolymer concrete has been found out by various experimentations using the Taguchi method [19] of design of experiments with the help of Qualitek 4 [20].

2 Experimental Program

2.1 Materials Used

2.2 Rice Husk Ash

RHA is a by-product of paddy grown as a staple food as rice is compulsory food all over the world, so its cultivation is mandatory for survival on this planet. After harvesting, about 25% of the rice paddy is an outer husk, which contains cellulose also, is removed and usually burnt either in the field or in a local power plant, resulting approximately 20% ash by weight of husk on burning. Therefore, the processing of 1 ton of rice will result in roughly 45–50kg of RHA, and rice husk ash is silica-rich. More than 90% of ash contains silica with pozzolanic properties and a desirable surface area. The amount of RHA produced through the burning process of husk depends on burning temperature, and the time of hold of burning (weather) amorphous or crystalline ash is provided. If the scorching heat is less, then there will be residual carbon content, and if the burning temperature is very high, then RHA produced will be crystalline. Rice husk ash used in this study was manufactured on a college campus by burning the raw rice husk. The physical properties and chemical composition of RHA are given in Tables 1 and 2, respectively.

Table 1 Physical properties of RHA

Colour	Specific gravity	Fineness (passing 45 μm)
Dark grey	2.13	97.00

Table 2 Chemical composition of RHA

SiO_2 (%)	Al_2O_3 (%)	Fe_2O_3 (%)	SO_3 (%)	CaO (%)	Na_2O (%)	LOI (%)
91.5	0.15	0.06	1.29	0.48	0.27	3.1

2.3 Alkaline Activators

In this experimental program, a blend of NaOH and Na2SiO3 as a soluble activator was used. The alkaline activators were supplied by a local commercial supplier. Sodium hydroxide flakes were mixed with water with a concentration of 14M, to produce sodium hydroxide solution and, which was kept invariable. The sodium silicate solution includes 15% of sodium oxide, 33.5% of silicate, and 48.5% solids. The (dry density) ρd of sodium silicate (Na2SiO3) answer was 1.54 g/cm^3. Superplasticizer used was master gelenium sky 8700.

2.4 Aggregates

Coarse aggregates used were of size greater than 10 mm less than 12.5 mm to provide better workability. Fine aggregates used were sand conforming to zone ii free of dirt, debris, and mud.

3 Optimum Mix Design

Taguchi method was used in this study for the optimal mix design of rice husk ash-based geopolymer concrete for the increase in compressive strength at ambient temperature. Qualitek 4 was used to perform a Taguchi experimental design. All the factors which influence the workability, setting time and compressive strength of RHA based geopolymer concrete were considered in this study. Three parameters keeping the concentration of NaOH constant as 14M, source material (400, 500 and 600 kg/m^3), Al'/Bd ratio (0.4, 0.5, and 0.6), SSi/SHd ratio (1.5, 2.0, and 2.5), (rate of H2O/Na2O was kept constant as 13) were considered (Table 3). Total 9 trial mixes

Table 3 Considerations and fractions used in Taguchi experimental design

Parameter	Fraction 1	Fraction 2	Fraction 3
RHA (kg/m^3)	400	500	600
Al'/Bd	0.4	0.5	0.6
NaOH/Na_2SiO_3	1.5	2.0	2.5
The concentration of NaOH (M)	14	14	14
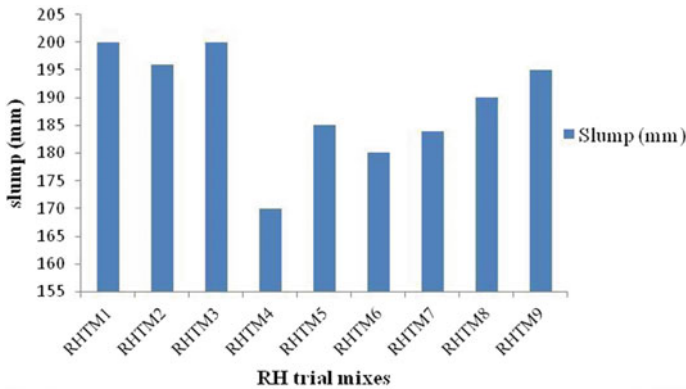
Fig. 1 Slump Values of the Trail Mixes

were prepared, 9 for setting time, and 9 for compressive strength. The component parameter was given for each trial mix (RHTM1–RHTM9) for setting time and (RHTM1–RHTM9) for compressive strength. Response index based on signal to noise ratio (S/N), from the Taguchi method, was used to obtain setting time and compressive strength from trial mixes of RHA based geopolymer concrete. Average of initial setting time and final setting time was used to determine the response index of each parameter, e.g., RHTM1, RHTM4, RHTM7 having an Al/Bd ratio of 0.4 (Figs. 1, 2, 3, 4, and 5; Table 4). The response index for trial mixes RHTM1, RHTM4, RHTM7 was equal to ((19.2 + 30.2 + 21.1)/3 = 23.5) (considering seven days compressive strength), which was higher as compared to the response index for Al/Bd ratio of 0.5 and 0.6 as shown in Fig.6. So, the optimum Al/ Bd ratio was 0.4. response index for all parameters was based on the s/n ratio was evaluated to determine the optimum mix design of RHA based geopolymer concrete, as shown in Figs. 2 and 4.

4 Specimen Preparation and Testing

For the preparation of RHA based geopolymer concrete specimens, all the dry ingredients viz; rice husk ash, sand, the coarse aggregate was mixed in the pan for 1 min, and afterwards, half of the water, alkaline activator prepared by the mixing of NaOH and Na2SiO3, and superplasticizer weighed as shown in Table 5 were added to the dry mixed ingredients and thoroughly diverse for 2 min after that left behind some of the liquid phase was added and remixed carefully for '2' min till the combination became homogeneous, the mixing procedure of geopolymer concrete was same as Rangan [21] casted specimens were cured under ambient temperature. The mix RHTM1 holds for the rice husk ash trail mix 1. The combination RHTM2 holds for the rice husk ash trail mix 2, the mix RHTM3 holds for the rice husk ash trail mix
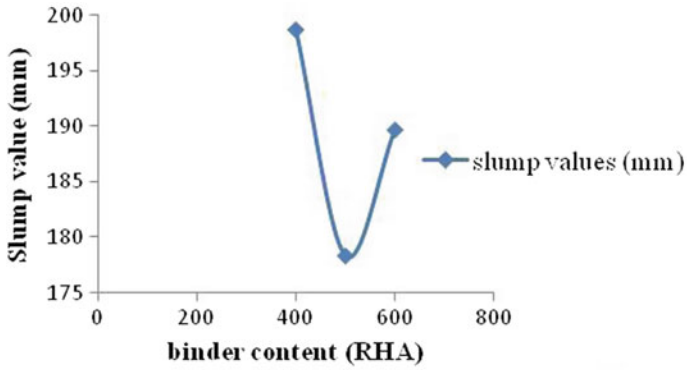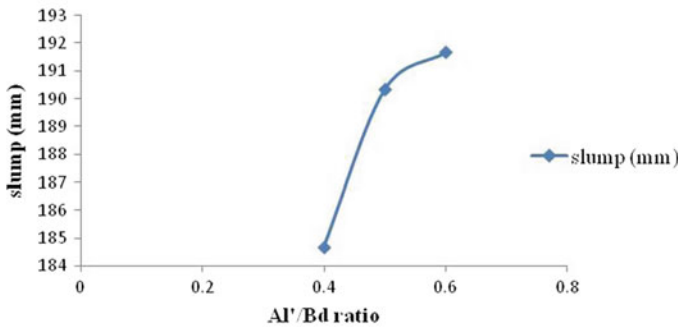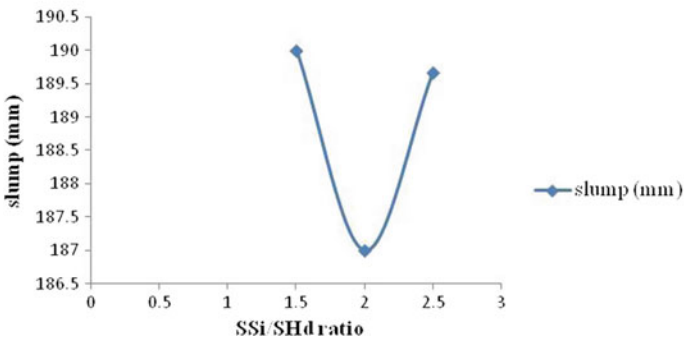
Fig. 2 Aspectual figures of the primary considerations that impact the slump values of RHA based geopolymer concrete paste. **a** Binder content. **b** Al'/Bd ratio. **c** SSi/SHd ratio
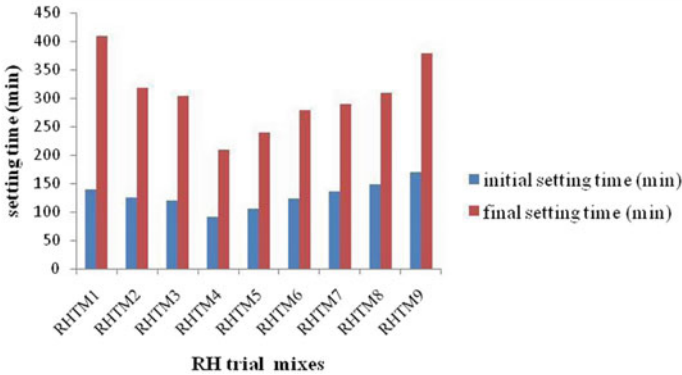
Fig. 3 Initial and final setting time of geopolymer specimens

3, the mix RHTM4 holds for the rice husk ash trail mix 4, the combination RHTM5 holds for the rice husk ash trail mix 5, the mix RHTM6 holds for the rice husk ash trail mix 6, the mix RHTM7 holds for the rice husk ash trail mix seven as given in Table 4.

5 Results and Discussion

In this study, the slump test to determine the workability of freshly mixed geopolymer concrete proportioned as given in (Tables 3, 4, and 5) was performed according to IS-1199-1959 [22]. The sump cone used was having a height of 300 mm, bottom diameter 200 mm, and top diameter 100 mm. The slump cone was filled in three layers, and each layer was tampered 25 times by tamping rod. High slump value indicates high workability but, as slump achieves higher costs, the workability increases, but compressive strength decreases. In this study, the highest slump value delivered was 200 mm, which was produced by RHTM1 and RHTM3 hence, more workable mixes. The lowest slump value was obtained by RHTM4, which was 170 mm. Thus, the slump values varied from 200 mm to 170 mm. The 170 mm to 200 mm slump denotes excellent workability for all mixes. The mixes RHTM2 and RHTM9 showed a slump of 196 mm and 195 mm, respectively, which is lesser than RHTM1 and RHTM3 but higher than RHTM5, RHTM7, RHTM6, and RHTM4. As shown in Fig. 1.

The factorial impact of different considerations on the workability of RHA based geopolymer concrete is shown in Figure 2a the impact of binder content (RHA) on slump value is displayed, when binder content was 400 kg/m^3 the average slump value of RHTM1, RHTM2, and RHTM3 was ((200 + 196 + 200)/3 = 198.67) 198.67 mm. When binder content was 500 kg/m^3, the average value of slump for RHTM4, RHTM5, and RHTM6 was ((170 + 185 + 180)/3 = 178.33) 178.33 mm.

(a)

(b)

(c)
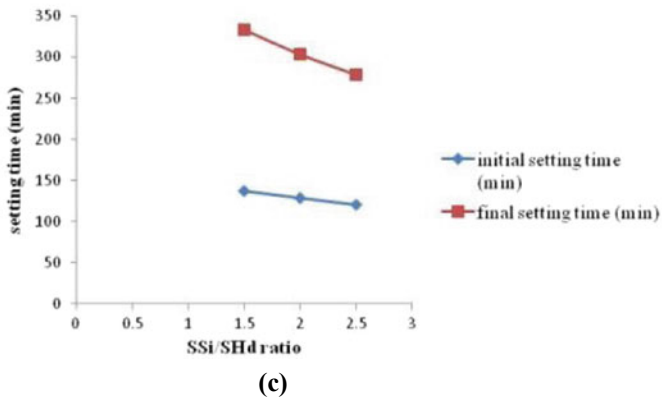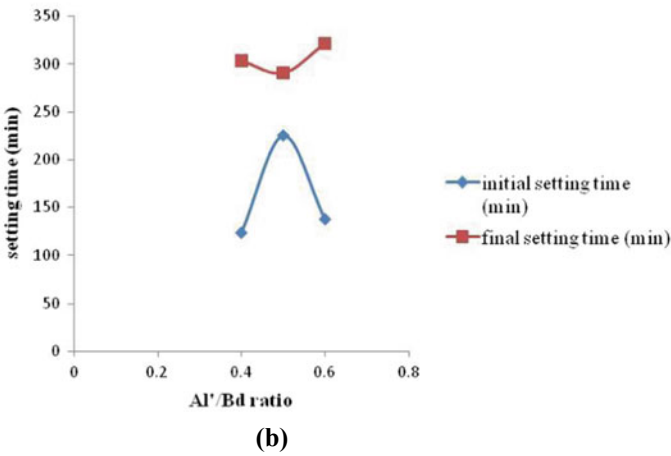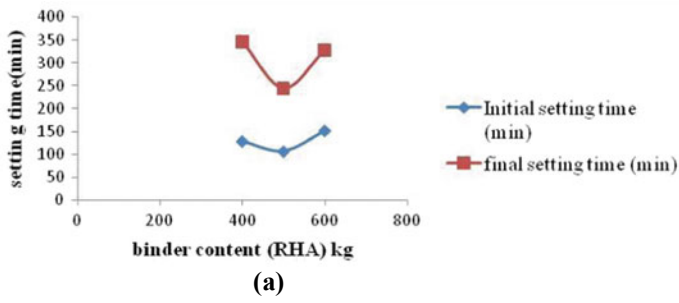
Fig. 4 Aspectual figures of the primary considerations that impact the initial and final setting time of RHA based geopolymer concrete. **a** Binder content (RHA). **b** Al'/Bd ratio. **c** SSi/SHd ratio
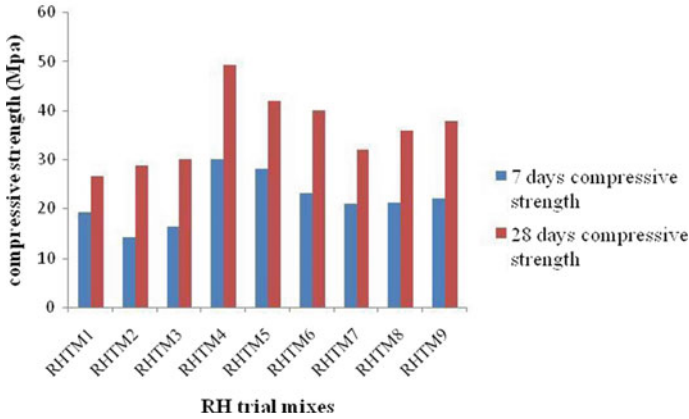
Fig. 5 Compressive strength (7 and 28 days) of RHA based geopolymer concrete specimens

Table 4 Considerations and assessments used in RHA based geopolymer concrete trail mixes

Experimental string	RHA content (kg/m^3)	Al'/Binder	NaOH/Na2SiO3	The concentration of NaOH(M)
RHTM1	400	0.4	1.5	14
RHTM2	400	0.5	2.0	14
RHTM3	400	0.6	2.5	14
RHTM4	500	0.4	2.0	14
RHTM5	500	0.5	2.5	14
RHTM6	500	0.6	1.5	14
RHTM7	600	0.4	2.5	14
RHTM8	600	0.5	1.5	14
RHTM9	600	0.6	2.0	14

When binder content was 600 kg/m^3, the average slump value for RHTM7, RHTM8, and RHTM9 was ((184 + 190 + 195)/3 = 189.66) 189.66 mm. The average slump value varied from 198.67 to 178.33 mm.

In Figure 2b, the effect of the Al'/Bd ratio on slump value is shown. When Al'/Bd ratio was 0.4 Table 6, the average slump value of the mixes (Table 3, 4, and 5) RHTM1, RHTM4, and RHTM7 ((200 + 170 + 184)/3 = 184.67) was 184.67 mm. When Al'/Bd ratio was 0.5, the average slump value of the mixes (Table 4) RHTM2, RHTM5, and RHTM8 ((196 + 185+ 190)/3 = 190.33) were 190.33 mm. When Al'/Bd ratio was 0.6, the average slump value of the mixes (Table 3, 4, and 5) RHTM3, RHTM6, and RHTM9 ((200 + 180 + 195/3) = 191.6) was 191.67 mm. In Figure 2c the effect of the SSi/SHd ratio (sodium silicate to sodium hydroxide ratio) on slump value is shown. When the ratio of SSi/SHd was 1.5, the average slump values of the mixes (Table 4, 5, 6) RHTM1, RHTM6, and RHTM8 ((200 + 180 +
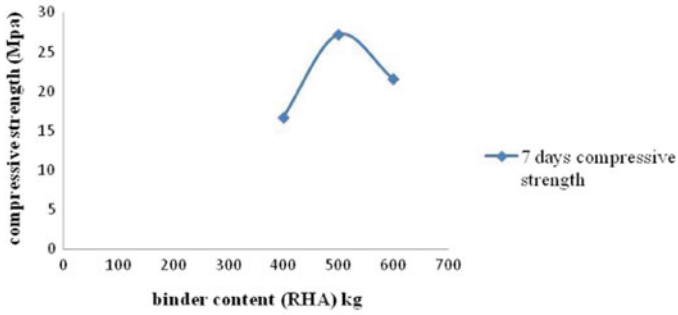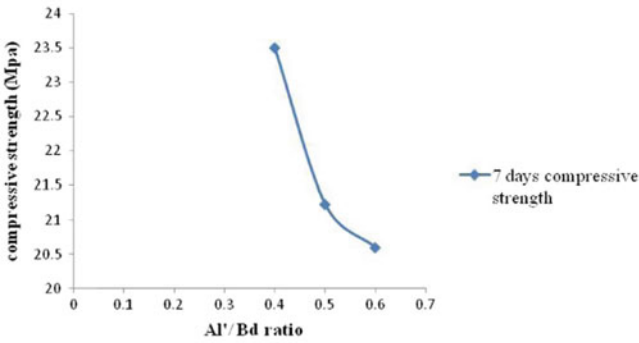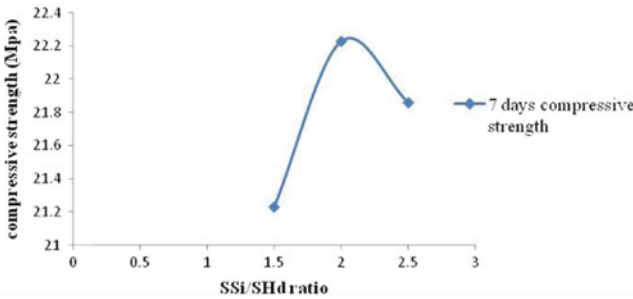
Fig. 6 Aspectual figures of the primary considerations that impact seven days compressive strength of the RHA based geopolymer concrete mixes. **a** Binder content (RHA). **b** Al'/Bd ratio. **c** SSi/SHd ratio

Table 5 Mix proportions of trial mixes

Mix	RHT M1	RHT M2	RHT M3	RHT M4	RHT M5	RHT M6	RHT M7	RHT M8	RHT M9
RHA (kg/m^3)	400	400	400	500	500	500	600	600	600
Al'/Bd	0.4	0.5	0.6	0.4	0.5	0.6	0.4	0.5	0.6
Na2SiO3 /NaOH	1.5	2.0	2.5	2.0	2.5	1.5	2.5	1.5	2.0
NaOH (kg/m^3)	64	66.67	68.57	66.67	71.43	120	68.57	120	120
Na2SiO3 (kg/m^3)	96	133.33	171.43	133.33	178.57	180	171.43	180	240
NaOH (M)	14	14	14	14	14	14	14	14	14
Superplasticizer (kg/m^3)	20	20	20	25	25	25	30	30	30
Additional Water	60	60	60	50	50	50	40	00	00
C.A. (kg/m^3)	1234	1143	1054	1047	933	782	900	685	553
F.A. (kg/m^3)	386	358	330	328	292	245	269	214	173
H$_2$ONa$_2$O	13	13	13	13	13	13	13	13	13

Table 6 Slump values of the mixes

Mix	RHTM 1	RHTM 2	RHTM 3	RHTM 4	RHTM 5	RHTM 6	RHTM 7	RHTM 8	RHTM 9
Slump(mm)	200	196	200	170	185	180	184	190	195

190)/3 = 190) were 190 mm. When the SSi/SHd ratio was 2.0, the average slump value of the mixes (Table 4, 5, 6) RHTM2, RHTM4, and RHTM9 ((196 + 170 + 195)/3 = 187) were 187 mm. When the ratio of SSi/SHd ratio was 2.5, the average slump value of the mixes (Table 4, 5, 6) RHTM3, RHTM5, and RHTM7 ((200 + 185 + 184)/3 = 189.67) was 189.67 mm. These slump values indicated that all trial mixes had excellent workability.

In this study, the Vicat apparatus was used to find out the initial and final setting time of RHA based geopolymer concrete [23]. Decreased value of initial and final setting time indicates that the hydration process or rate of polymerization is high, which means the formation of aluminosilicate hydrates is high, which induces earlier setting of geopolymer concrete. The first setting time of geopolymer mixes varied from 170 to 92 min, and the last set time of the geopolymer incorporates diverse from 410 to 210 min. (Table 7) shows the values of the first and last setting time of the mixes RHTM1 to RHTM9. From Figure 3, It can be predicted that the mix RH4 has the lowest first setting and last setting time. The mix RHTM1 and RHTM9 have the highest first and last setting time.

Figure 4 shows the factorial effect of various parameters on the first and last setting time of RHA based geopolymer concrete. The result of binder content on the first and last setting time is shown in Figure 4a. The effect of binder content (RHA) was found significant on the setting time of RHA based geopolymer concrete. When binder content was 400 kg/m^3, the average value of initial and final setting time for trial mixes RHTM1, RHTM2, and RHTM3 was 128.33 and 345 min, respectively. When binder content was 500 kg/m^3, the average value of first and last setting time for RHTM4, RHTM5, and RHTM6 was 106.67 and 243.67 min, respectively. When binder content was 600 kg/m^3, the average value of first and last setting time for RHTM7, RHTM8, and RHTM9 was 151.33 and 326.67 min, respectively. An increase in setting time is found when the binder content used was 500 kg/m^3, but when binder content was increased up to 600 kg/m^{3}the, the first and last setting time decreased significantly.

In Figure 4b the effect of the Al'/Bd ratio on the setting time is shown. When Al'/Bd ratio was 0.4 Table 6, the average value of first and last setting time for the mixes (Table 4) RHTM1, RHTM4, and RHTM7 was 123 and 303.33 min, respectively. When Al'/Bd ratio was 0.5, the average value of the first and last setting time of the mixes (Table 4) RHTM2, RHTM5, and RHTM8 was 225.33 and 290.33 min, respectively. When Al'/Bd ratio was 0.6, the average value of the first and last setting time for the mixes (Table 4) RHTM3, RHTM6, and RHTM9 was 137.33 and 321.67 min. There is an increase in the first and last setting time when the Al'/Bd ratio was 0.4. first setting time decreased when the Al'/Bd ratio was 0.5 and 0.6. In Figure 4c

Table 7 Initial (first) and final (last) setting time of trial mixes

Mix	RHTM 1	RHTM 2	RHTM 3	RHTM 4	RHTM 5	RHTM 6	RHTM 7	RHTM 8	RHTM 9
Initial settin g time (min)	140	125	120	92	105	123	137	148	170
Final settin g time (min)	410	320	305	210	241	280	290	310	380

Table 8 Compressive strength of RHA based geopolymer trial mixes under ambient curing conditions

Mix	Seven days compressive strength (Mpa)	28 days compressive strength (Mpa)
RHTM1	19.2	26.6
RHTM2	14.3	28.9
RHTM3	16.4	30.2
RHTM4	30.2	49.3
RHTM5	28.1	42.1
RHTM6	23.2	40.0
RHTM7	21.1	32.0
RHTM8	21.3	36.0
RHTM9	22.2	38.0

the effect of the SSi/SHd ratio on setting time is shown. When the rate of SSi/SHd was 1.5, the average first and last set time values of the mixes (Table 4, 5, 6) RHTM1, RHTM6, and RHTM8 were 137 and 333.33 min. When the SSi/SHd ratio was 2.0, the average first and last setting time value of the mixes (Table 4, 5, 6) RHTM2, RHTM4, and RHTM9 was 128.67 and 303.33. When the ratio of SSi/SHd ratio was 2.5, the average first and last setting time value of the mixes (Table 4, 5, 6) RHTM3, RHTM5, and RHTM7 was 120.67 and 278.67 min. When the SSi/SHd ratio was 1.5, the first setting time decreased, but the last setting time increased. The first and last setting time dropped when SSi/SHd ratio was 2.0.

The seven- and twenty-eight-days compressive strength of RHA based geopolymer concrete is given in Table 8. The compressive strength test was performed according to IS 516:1959 [22]. A compressive strength test was performed on the cubes of size 150 × 150 × 150 mm. In Figure 5 the seven- and twenty-eight-days compressive strength of trial mixes RHTM1 to RHTM9 is shown. The seven days compressive strength varied from 30.2 to 14.3 Mpa, and the twenty-eight days' compressive strength ranged from 49.3 to 26.6 Mpa. The trial mix RHTM4 gained the highest seven- and twenty-eight-days compressive strength as 30.2 Mpa and 49.3 Mpa, respectively due to the highest rate of polymerization and formation of aluminosilicate hydrates. The lowest seven days compressive strength was acquired by the mix RHTM2, which was 14.3 Mpa. The most moderate twenty-eight days compressive strength was gained by the mix RHTM1, which was 26.6 Mpa. However, the mix RHTM5 has also achieved good seven- and twenty-eight-days compressive strength but, less than RHTM4.

The Aspectual effect of various considerations on seven days compressive strength of concrete is shown in Figure 6 The result of binder content on seven days compressive strength is shown in Figure 6a. The impact of binder content (RHA) was found significant on the compressive strength of RHA based geopolymer concrete. When binder content was 400 kg/m^3, the middling assessment of seven days compressive strength for mixes RHTM1, RHTM2, and RHTM3 was 16.63 Mpa. When binder content was 500 kg/m^3, the average value of 7 days compressive strength for the

Table 9 Optimized mix design

Binder content (RHA) kg/m³	Al/Bd	SSi/SHd	Concentration of NaOH	Additional water kg/m³	Coarse aggregate kg/m³	Fine aggregate kg/m³
500	0.4	2.0	14 M	50	1047	328

mixes RHTM4, RHTM5, and RHTM6 was 27.16 Mpa. When binder content was 600 kg/m³, the average value of 7 days compressive strength for the mixes RHTM7, RHTM8, and RHTM9 was 21.53 Mpa. Increase in 7 days compressive strength was found while binder content used was 500 kg/m³, but when binder content was increased up to 600 kg/m³ the compressive strength decreased significantly.

In Figure 6b the impact of the Al/Bd ratio on the seven days compressive strength is shown. When Al'/Bd ratio was 0.4 Table 6, the average value of 7 days compressive strength for the mixes (Table 4) RHTM1, RHTM4, and RHTM7 was 23.5 Mpa, which is highest. When Al'/Bd ratio was 0.5, the middling assessment of 7 days compressive strength of the mixes (Table 4) RHTM2, RHTM5, and RHTM8 was 21.23 Mpa, which is lesser than Al'/Bd ratio of 0.4. When Al'/Bd ratio was 0.6, the average value of 7 days compressive strength for the mixes (Table 4) RHTM3, RHTM6, and RHTM9 was 20.6 Mpa, which is lesser than both the Al'/Bd ratios 0.4 and 0.5. Here was an increase in 7 days compressive strength while Al'/Bd ratio was 0.4. In Figure 6c the effect of the SSi/SHd ratio on seven days compressive strength is shown. When the rate of SSi/SHd was 1.5, the average seven days compressive strength of the mixes (Table 4, 5, 6) RHTM1, RHTM6, and RHTM8 was 21.23 Mpa. When the SSi/SHd ratio was 2.0, the average seven days compressive strength of the mixes (Table 4, 5, 6) RHTM2, RHTM4, and RHTM9 was 22.23 Mpa, which was highest. When the ratio of SSi/SHd ratio was 2.5, the average compressive strength of the mixes (Table 4, 5, 6) RHTM3, RHTM5, and RHTM7 were 21.86 Mpa, which was lower than when SSi/SHd ratio was 2.0. When the SSi/SHd ratio was 1.5, the seven days average compressive strength decreased. The higher value of 7 days compressive strength was obtained when SSi/SHd ratio was 2.0 (Table 9).

6 Conclusion

The experimental program draws the following conclusions:

(1) The RHA based geopolymer concrete with RHA (binder) content 500kg/m³, Al'/Bd ratio of 0.4, SSi/SHd ratio of 2.0 and sodium hydroxide concentration as 14M achieved seven- and twenty-eight- days compressive strength of 30.2 and 49.3 Mpa respectively which is highest than all other proportions at ambient curing conditions.

(2) The optimum mix with binder content 500kg/m^3, Al'/Bd ratio of 0.4, SSi/SHd ratio of 2.0 and concentration of sodium hydroxide as 14M attained excellent workability.

(3) The initial setting time of optimum mix that is having binder content 500kg/m^3, Al'/Bd ratio of 0.4, SSi/SHd ratio of 2.0, and concentration of sodium hydroxide as 14M was lesser as compared to all other mixes.

References

1. Jeevanandan K, Sreevidya V (2019) Experimental investigation on concrete and geopolymer concrete. Mater Today Proc no. XXXX, 2019. https://doi.org/10.1016/j.matpr.2019.05.448.
2. Das SK (2018) Parametric study of fly ash-based geopolymer concrete. Int J Eng Technol 7(2):196–198. https://doi.org/10.14419/ijet.v7i2.31.13439
3. Kurtoğlu AE et al (2018) Mechanical and durability properties of fly ash and slag based geopolymer concrete. Adv Concr Constr 6(4):345–362. https://doi.org/10.12989/acc.2018.6.4.345
4. Prabakaran PA, Premalatha J, Satheesh Kumar KRP (2017) Experimental investigation on flexural behaviour of geopolymer concrete. Int J Civ Eng Technol 8(8):1692–1706
5. Ravichandran G, Jegan M, Sivaraja M, Harihanandh M, Krishnaraja AR (2018) Article ID: IJCIET_09_04_148 varying temperature effect. Int J Civ Eng Technol 9(4):13161323. https://iaeme.com/Home/journal/IJCIET
6. Mithanthaya IR, Marathe S, Rao NBS, Bhat V (2017) Influence of superplasticizer on the properties of geopolymer concrete using industrial wastes. Mater Today Proc 4(9):9803–9806. https://doi.org/10.1016/j.matpr.2017.06.270
7. Karthi L (2017) A literature review on fiber reinforced geopolymer concrete. Artic Int J Sci Eng Res 8(2). http://www.ijser.org
8. Hadi MNS, Zhang H, Parkinson S (2019) Optimum mix design of geopolymer pastes and concretes cured in ambient condition based on compressive strength, setting time and workability. J Build Eng 23:301–313. https://doi.org/10.1016/j.jobe.2019.02.006
9. Farhan NA, Sheikh MN, Hadi MNS (2018) Experimental investigation on the effect of corrosion on the bond between reinforcing steel bars and fibre reinforced geopolymer concrete. Structures 14:251–261. https://doi.org/10.1016/j.istruc.2018.03.013
10. Pavithra P, Srinivasula Reddy M, Dinakar P, Hanumantha Rao B, Satpathy BK, Mohanty AN (2016) A mix design procedure for geopolymer concrete with fly ash. J Clean Prod 133:117–125. https://doi.org/10.1016/j.jclepro.2016.05.041
11. Of I et al., Chapter-3 mix design and strength properties of GPC, pp 65–83
12. Junaid MT (2012) A mix design procedure for alkali activated fly ash- based geopolymer concretes
13. Rajamane NP, Nataraja MC, Lakshmanan N (2011) An introduction to geopolymer concrete. Indian Concr J 85(11):25–28
14. Mustafa M, Bakri A, Mohammed H, Kamarudin H, Niza IK, Zarina Y (2011) Review on fly ash-based geopolymer concrete without Portland Cement. J Eng Technol Res 3(1):1–4
15. Kaur K, Singh J, Kaur M (2018) Compressive strength of rice husk ash-based geopolymer: the effect of alkaline activator. Constr Build Mater 169:188–192. https://doi.org/10.1016/j.conbuildmat.2018.02.200
16. Cheewaket T, Chalee W (2018) Utilization of rice husk ash-based geopolymer in hollow load-bearing concrete masonry block. J King Mongkut's Univ Technol. North Bangkok 29(2). https://doi.org/10.14416/j.kmutnb.2018.09.005
17. Mishra J, Kumar Das S, Mohammed Mustakim S (2018) Rice husk ash as a potential source material for geopolymer concrete: a review. http://www.ripublication.com

18. Hwang CL, Huynh TP (2015) Effect of alkali-activator and rice husk ash content on strength development of fly ash and residual rice husk ash-based geopolymers. Constr Build Mater 101:1–9. https://doi.org/10.1016/j.conbuildmat.2015.10.025
19. Athreya S, Venkatesh YD (2012) Application of taguchi method for optimization of process parameters in improving the surface roughness of lathe facing operation. Int Ref J Eng Sci 1(3):13–19. ISSN: 2319-1821
20. A. Design and T. Experiments, Qualitek-4 application guide
21. Rangan BV (2014) Fly Ash-based geopolymer concrete fly ash-based geopolymer concrete. Geopolymer Cem Concr 68–106
22. Kisan M, Sangathan S, Nehru J, Pitroda SG (1959) "म ⟶ नक,"
23. Kisan M, Sangathan S, Nehru J, Pitroda SG (1976) "म ⟶ नक,"

Formulation of Prediction Models for Mechanical Properties of Steel Fibre Reinforced Concrete

Y. Subasini, B. Nivetha, and S. Praveenkumar

1 Introduction

Concrete possess good compressive strength but very poor tensile strength since it is brittle in nature. Hence certain fibres can be introduced to overcome and improve the brittle nature of concrete. When the fibres are introduced, they will get distributed among the concrete matrix and will cause interruption to the growth of cracks. The fibres will slow down the growth of cracks and finally make them come to rest. This entire process is called as the crack bridging effect. This effect will tend to enhance the toughness property of concrete and it will improve the ability of the concrete to carry the load even after the first crack emerges. The structural integrity of the concrete will be enhanced by the addition of fibres. Among different types of fibres, steel fibres are used in this study because of its advantages. Addition of steel fibres tends to reduce the percentage of steel reinforcement and hence it proves to be economical. Steel fibres can also mitigate the growth of cracks and thus imparts durability to the concrete. Steel fibres can generally improve freeze- thaw resistance, impact and abrasion resistance and thus enhances the structural strength of the concrete. The aspect ratio of fibres influences the mechanical strength properties of the fibre reinforced concrete [14]. Inclusion of Steel fibres enhances the mechanical properties of concrete to a greater extent especially the splitting tensile and flexural strength. The optimum percentage of addition of steel fibres was found to be 1% that improves the splitting tensile and flexural strength (Tamilselvi, 2015). Concrete compressive strength, fibre content and

Y. Subasini · B. Nivetha
Post graduate student, Department of Civil Engineering, PSG College of Technology, Coimbatore, India

S. Praveenkumar (✉)
Assistant Professor (Senior Grade), Department of Civil Engineering, PSG College of Technology, Coimbatore, India
e-mail: spk.civil@psgtech.ac.in

75

the fibre aspect ratio are the important parameters that influence in determining the tensile strength of fibre reinforced concrete [5]. The incorporation of fibres generally increases the failure load and also ensures the ductile behaviour [11]. The inclusion of 0.75% steel and 0.45% polypropylene fibres shows improvement in the concrete strength. The effect of the hybrid system containing both steel and polypropylene fibres were investigated, and it was found that the optimum mix was attained with 0.85% steel and 0.15% polypropylene fibre [12, 13].

2　Research Significance

The main aim of this research is to determine the mechanical strength properties such as compressive strength, splitting tensile strength and flexural strength of the concrete reinforced with steel fibres with lengths of 30, 36 and 50 mm in volume fractions of 0.25, 0.35, 0.5 and 0.75%. This paper indicates the experimental results of a control mix and 12 different mixes, produced with the target compressive strength of 60 MPa. With the experimental results obtained, the prediction equations were developed considering concrete compressive strength, Fibre Volume fraction (FV_f) and Fibre Reinforcing Index (FRI) as the influencing parameters.

3　Experimental Program

3.1　Materials

Ordinary Portland cement (OPC) of grade 53 was used as the binder material in this study. The specific gravity of the cement used was found to be 3.2. M-sand was used as the fine aggregate whose specific gravity was 2.51 and bulk density was 1607.5 kg/m^3 and 1822.58 kg/m^3 in loose and rodded state respectively. The fineness modulus of M- sand was found to be 1.996 based on the results obtained from sieve analysis. Natural Aggregate of 20 mm size was used as the coarse aggregate, whose specific gravity was 2.76 and bulk density was 1504 kg/m^3 and 1734 kg/m^3 in loose and rodded state respectively. Hooked end steel fibres were used to reinforce the concrete and the properties of the fibres are tabulated in Table 1. A chemical admixture, based on poly carboxylic ether was added as Superplasticizer to increase the workability. Water used for both casting and curing of specimens was potable water (Fig. 1).

Table 1 Properties of fibres

Fibre	Shape	Length (mm) (l)	Diameter (mm) (d)	Aspect Ratio (l/d)	Density (kg/m^3)	Tensile strength (N/mm^2)
Steel	Hooked end	30	0.6	50	7.80	1050
Steel	Hooked end	36	0.45	80	7.80	1050
Steel	Hooked end	50	0.5	100	7.80	1050

Fig. 1 Steel fibres

3.2 Mix Proportions

In this research, a total of thirteen different mix proportions were prepared by varying the length and volume fraction of steel fibres. A control mix M0 was produced without the addition of steel fibres to compare the results with that of steel fibre reinforced concrete. Three different lengths of steel fibres such as 30 mm, 36 mm and 50 mm were used at four different volume fractions (0.25, 0.35, 0.5, 0.75%). Thus this results in 12 different mixes. The method proposed by P.C. Aitcin was used to determine the mix proportions for the concrete.

- M60 was taken as the characteristic compressive strength of the concrete
- The water-cement ratio of the concrete was taken as 0.33 for the mix design.

The derived mix proportions are tabulated in Table 2.

Table 2 Mix proportions

Component	Cement	Coarse aggregate	Fine aggregate	Superplasticizer	Water
Quantity	433 kg/m^3	1042 kg/m^3	823 kg/m^3	12 l/m^3	0.26 l/m^3

3.3 Test Procedures

A total of nine specimens were prepared for each mix (3 cubes of 150 mm × 150 mm 150 mm in size, 3 cylinders of 150 mm diameter and 300 mm height and 3 prisms of 100 mm × 100 mm × 400 mm). For each mix, 3 cubes were tested for compressive strength, 3 cylinders were tested for splitting tensile strength and the 3 prisms were tested for flexural strength and the average of the three specimens was determined. The cast specimens were left under curing conditions for 28 days and then tested. The hardened concrete properties such as compressive strength, flexural strength and splitting tensile strength were determined in accordance to IS: 516-1959—Indian standard Methods of Test for Strength of Concrete respectively [4].

4 Results and Discussion

The experimental test results of the hardened concrete properties are provided in Figs. 2, 3 and 4. The test results denote the average of the three specimens.
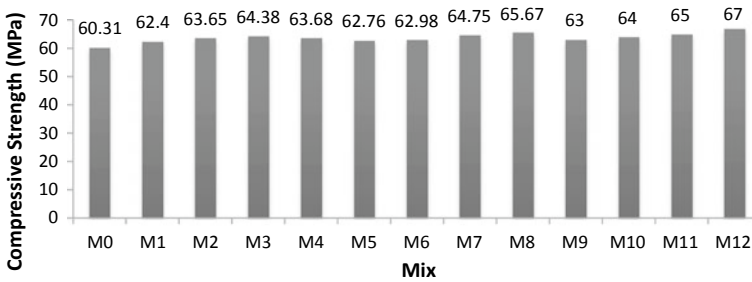
Fig. 2 Experimental test results of compressive strength
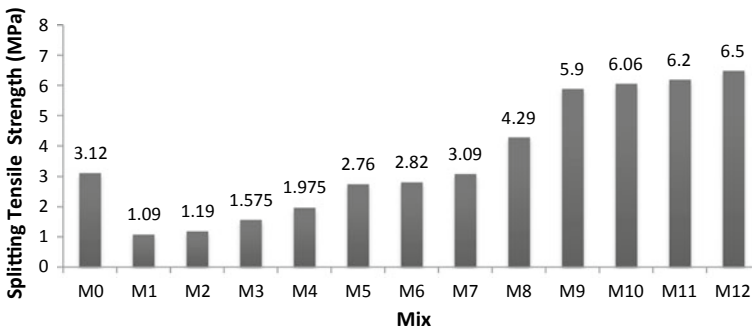
Fig. 3 Experimental test results of splitting tensile strength
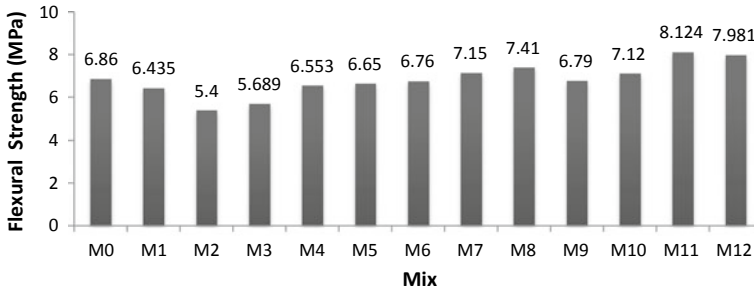
Fig. 4 Experimental test results of flexural strength

4.1 Compressive Strength (CS)

From the Fig. 2, it can be inferred that the compressive strength value increases as the volume fraction of the fibres increases, for a particular length of the fibre. It can also be concluded that the compressive strength value increases as the length of the fibres increases, for a particular volume fraction of the fibre. There is no drastic improvement in the values of compressive strength for the considered mixes. It was found that the gain in compressive strength for the mixes M1 to M11 was about 3–7% compared to the control specimen. The mix M12 which consists of fibres of length 50 mm and with a volume fraction of 0.75% showed maximum increment in compressive strength to about 11% compared to mix M0.

4.2 Splitting Tensile Strength (SP)

From Fig. 3, it can be inferred that the splitting tensile strength value initially decreases upon the addition of fibres (M1 to M7) but then increases for mixes M8 to M12, when compared to the control specimen. It can also be concluded that the splitting tensile strength value increases as the volume fraction of the fibres increases, for a particular length of the fibre. There is a decrease of about 30–60% for the mixes with fibres of length 30 mm and of about 0–10% for the mixes with fibres of length 36 mm. The splitting tensile strength is found to increase from the mix with fibres of length 36 mm and volume fraction of 0.75%. For mixes M7 to M11, the increment in splitting tensile strength is about 30–90%compared to M0. The maximum gain in the splitting tensile strength was about 108% for the mix M12.

4.3   Flexural Strength (FS)

From Fig. 4, it can be inferred that the flexural strength value initially decreases upon the addition of fibres (M1 to M6) and then increases for other mixes. The decrease in flexural strength was observed for mixes M1, M2, M3, M4, M5 and M6 to about 1–20% when compared to the control mix. The increase in flexural strength was observed for mixes M7, M8, M10, M11 and M12 to about 4–20% when compared to mix M0. There was a sudden decrease in the flexural strength for mix M9 to about 1%. The maximum increment in the flexural strength was about 18% for the mix M11.

4.4   Review of Prevailing Strength Models

Many researchers have conducted experiments and developed analytical equations to predict the mechanical properties such as compressive strength, splitting tensile strength and flexural strength of fibre reinforced concrete. A review was done on the prevailing strength models and the data are tabulated in Table 3, where CS_{cy} and CS_{cu} represents the compressive strength of cylinder specimen and cube specimen of plain concrete respectively, CS_{cyf} and CS_{cuf} represents the compressive strength of cylinder specimen and cube specimen of fibre reinforced concrete respectively, SP_f and SP represents the splitting tensile strength specimen of fibre reinforced concrete and plain concrete respectively, FS_f and FS represents the flexural strength specimen of fibre reinforced concrete and plain concrete respectively. The researchers have considered the mechanical properties of the control specimen, fibre reinforcing index (FRI_v and FRI_w), fibre volume fraction (FV_f) as the influencing parameters to derive at the analytical equations. FRI_v and FRI_w are the fibre reinforcing indices considering volume fractions (FV_f) and weight fractions (FW_f) of the fibres respectively.

$$FRI_v = FV_f \frac{1}{d} \tag{1}$$

$$FRI_w = FW_f \frac{1}{d} \tag{2}$$

where l and d denotes the length and diameter of the fibres respectively.

Table 3 Strength models from literatures

Author	CS	SP	FS
Abedel et al. [1]	$CS_{cyf} = CS_{cy} + 5.222\ FRI_v$	$SP_f = SP + 6.496\ FRI_v$	$FS_f = FS + 5.222\ FRI_v$
Ezeldin and Balaguru [2]	$CS_{cyf} = CS_{cy} + 3.51\ FRI_w$	–	–
Ghosh et al. [3]	–	$SP_f = 0.11\ CS_{cu}\ (1 - FV_f) + 0.573\ FRI_v + 0.571$	$FS_f = 0.15\ CS_{cu}\ (1 - FV_f) + 0.79\ FRI_v$
Nataraja et al. [7]	$CS_{cyf} = CS_{cy} + 2.16\ FRI_w$	-	–
Naryanan and Darwish [6]	–	$SP_f = CS_{cu}/(20 - \sqrt{FRI_v}) + 0.7 + \sqrt{FRI_v}$	–
Nuruddin et al. [8]	$CS_{cuf} = 1.03CS_{cu} - 0.03\ CS_{cu}\ FRI + 17.98\sqrt{(CRM)}$	$SP_f = 0.46CS_{cu} + 0.01\ FRI\ \sqrt{(CS_{cu})} + 2.58\sqrt{(CRM)}$	$FS_f = 0.46CS_{cu} - 0.011\ FRI\ \sqrt{(CS_{cu})} + 1.311\sqrt{(CRM)}$
Ou et al. [9]	$CS_{cyf} = CS_{cy} + 2.35\ FRI_v$	-	–
Padmarajaiah [10]	$CS_{cuf} = CS_{cu} + 1.998\ FRI_v$	$SP_f = \sqrt{CS_{cu}}\ /3 + 1.918\ FRI_v$	$FS_f = FS + 4.419\ FRI_v$
Song and Hwang [15]	$CS_{cyf} = CS_{cy} + 15.12\ FRI_v - 4.71\ FRI_v^{\,2}$	$SP_f = 5.8 + 3.01\ FV_f - 0.02\ FV_f^{\,2}$	$FS_f = 6.4 + 3.43\ FV_f + 0.32\ FV_f^{\,2}$
Thomas and Ramaswamy [16]	$CS_{cuf} = CS_{cu} + 0.014\ CS_{cu}\ FRI_v + 1.09\ FRI_v$	$SP_f = 0.63\ \sqrt{CS_{cu}} + 0.288\ FRI_v\ \sqrt{(CS_{cu})} + 0.052\ FRI_v$	$FS_f = 0.97\ \sqrt{CS_{cu}} + 0.295\ FRI_v\ \sqrt{(CS_{cu})} + 1.117\ FRI_v$
Wafa and Ashour [18]	$CS_{cyf} = CS_{cy} + 3.53\ FV_f$	$SP_f = 0.58\ \sqrt{CS_{cy}} + 3.02\ FV_f$	$SP_f = 0.99\ \sqrt{CS_{cy}} + 3.83\ FV_f$

4.5 Development of Strength Models

From the experimental data tested, new strength models were derived based on multiple regression analysis. Strength models were derived considering the plain concrete Compressive Strength (CS), Fibre Reinforcing Index (FRI) and Fibre Volume Fractions (FV_f) as the influencing parameters. The strength models were proposed for compressive strength, splitting tensile strength and flexural strength for the steel fibre reinforced concrete. The general form of the prediction equation is given by Eq. (3).

$$Strength\ of\ SFRC = x \times CS + y \times FRI + z \times FV_f \tag{3}$$

where x, y and z are the coefficients for regression. The fibre reinforcing index (FRI) is calculated from the formula,

$$\text{FRI} = \text{FV}_\text{f} \frac{1}{\text{d}} \tag{4}$$

where l and d are the length and diameter of the steel fibre respectively. The ratio of l/d is known as the aspect ratio of the fibre.

The derived prediction equations for compressive, splitting tensile and flexural strength of steel fibre reinforced concrete are represented in Eqs. (5), (6) and (7).

$$CS_f = 1.021\,CS + 6.078 \cdot FRI + 0.745\,FV_f \tag{5}$$

$$SP_f = 0.044\,CS + 16.82 \cdot FRI - 10.848\,FV_f \tag{6}$$

$$FS_f = 0.100\,CS + 6.004 \cdot FRI - 2.952\,FV_f \tag{7}$$

4.6   Comparing the Predicted and Experimental Results

To check the accuracy of the prediction equations, the values predicted from the equations are compared with the experimental test results. The comparison was done with the basic statistical parameters such as Mean Squared Error (MSE) and Average Absolute Error (AAE). The expressions to derive these above mentioned statistical parameters are represented by Eq. (8) and (9). In this study, various literatures were considered to compare the predicted results. But certain literatures have considered compressive strength of cylinder specimens instead of that of cube specimens. Thus compressive strength for cylinder is taken to be to 0.8 times of that of compressive strength of cube.

$$MSE = \frac{1}{N} \sum_{i=1}^{n} \left(\frac{Sf,\ \text{model},\ i - Sf,\ \text{exp},\ i}{Sf,\ \text{exp},\ i} \right)^2 \tag{8}$$

$$AAE = \frac{1}{N} \sum_{i=1}^{n} \left(\frac{Sf,\ \text{model},\ i - Sf,\ \text{exp},\ i}{Sf,\ \text{exp},\ i} \right) \tag{9}$$

where Sf, model represents the mechanical strength calculated from the model equation and Sf, exp represents the mechanical strength obtained from the experiments. The equations are used to calculate for compressive, splitting tensile and flexural strength separately. The calculated MSE and AAE values are tabulated in tables for compressive strength, splitting tensile strength and flexural strength respectively (Figs. 5, 6, and 7).
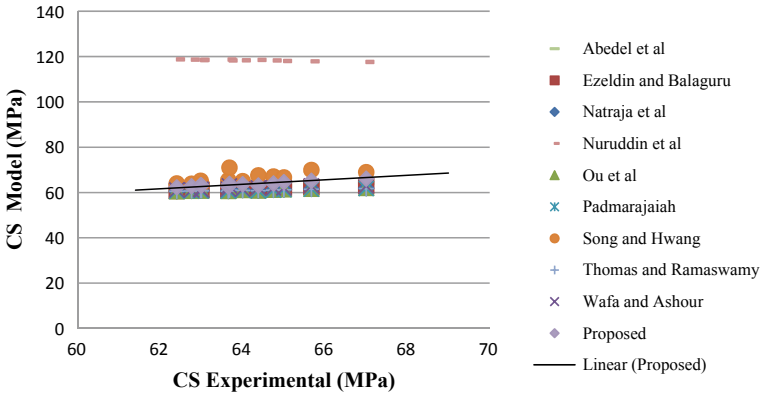
Fig. 5 Comparison of experimental and strength model values of compressive strength
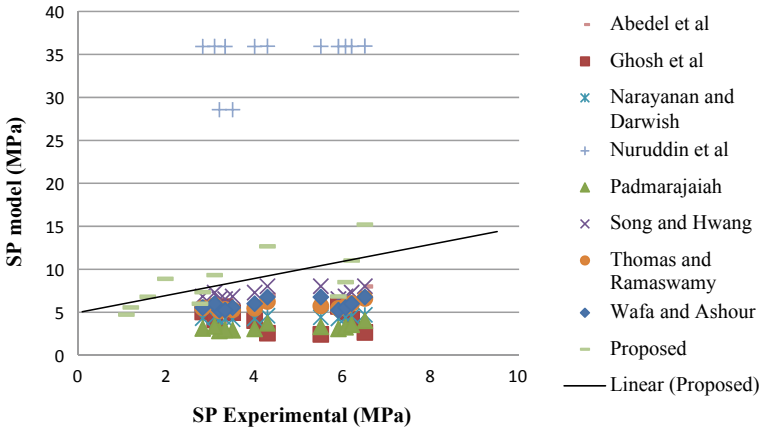
Fig. 6 Comparison of experimental and strength model values of splitting tensile strength
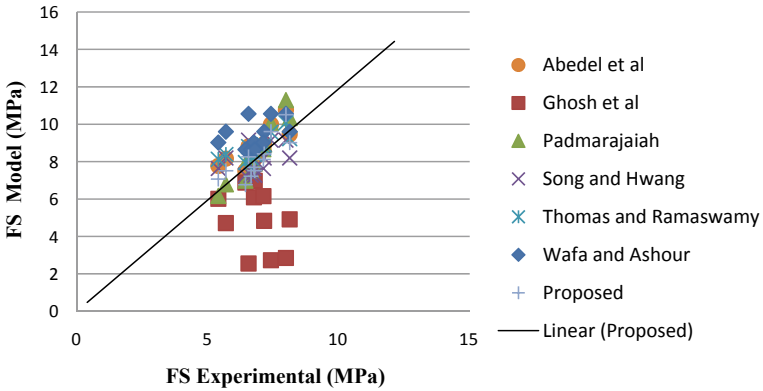
Fig. 7 Comparison of experimental and strength model values of flexural strength
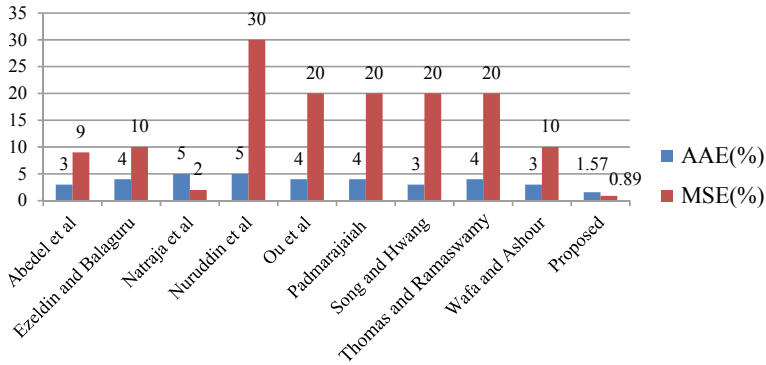
Fig. 8 AAE and MSE values for compressive strength

4.7 Evaluation of Strength Models

It can be clearly understood that the proposed strength models are effective in determining the mechanical properties of the steel fibre reinforced concrete, compared to the other literatures studied. This analysis is done based on the statistical parameters AAE and MSE [17].

4.7.1 Compressive Strength

From Fig. 8, it is seen that the calculated AAE and MSE values for the proposed strength model are 1.57% and 0.89% respectively. The AAE and MSE values range between 0.5 to 2% for the proposed strength model. The AAE and MSE values for the studied literatures range between 1–30%. The predicted models by Nuruddin et al., are less accurate in determining the compressive strength because it has a higher value of MSE to about 30%. Compared to the studied models, the proposed equations give more reliable results in determination of compressive strength due to its less value of AAE and MSE.

4.7.2 Splitting Tensile Strength

From Fig. 9, it is seen that AAE and MSE values for the proposed strength model are 2% and 4% respectively. The AAE and MSE values range between 1 to 4% for the proposed strength model. The AAE and MSE values for the studied literatures range between 8–40%. The predicted models by Wafa and Ashour, Thomas and Ramaswamy are less reliable in determining the splitting tensile strength because it has a higher value of AAE to about 40% and 35% respectively and high value of MSE of about 29% and 25% respectively. Comparing to the studied models, the
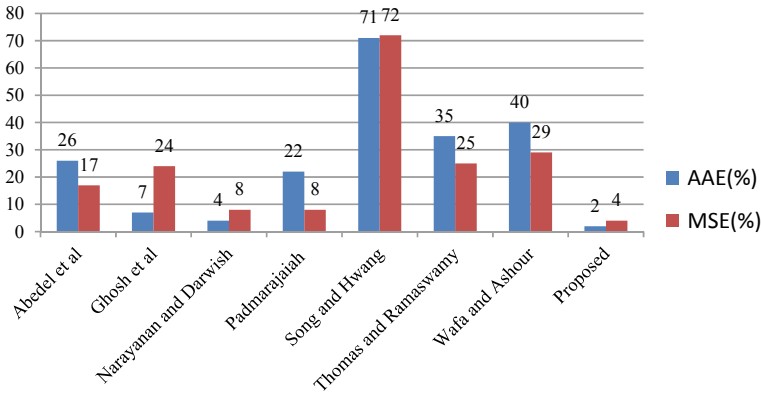
Fig. 9 AAE and MSE values for splitting tensile strength

proposed equations give more reliable results in determination of splitting tensile strength due to its less value of AAE and MSE.

4.7.3 Flexural Strength

From Fig. 10, it is seen that the AAE and MSE values for the proposed strength model are 1.09% and 0.32% respectively. The AAE and MSE values range between 0.2 to 1.5% for the proposed strength model. The AAE and MSE values for the studied literatures range between 5–40%. The predicted models by Wafa and Ashour are less reliable in determining the flexural strength because it has a higher value of AAE and MSE to about 40.52% and 18% respectively. Compared to the studied models, the
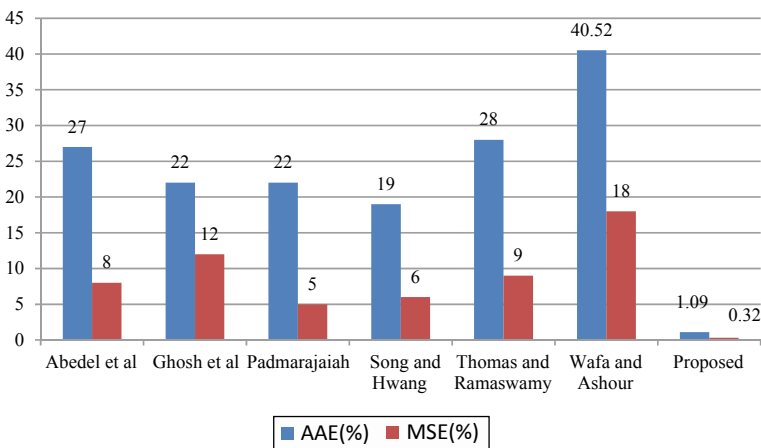
Fig. 10 AAE and MSE values for flexural strength

proposed equations give more reliable results in determination of flexural strength due to its less value of AAE and MSE.

5 Conclusions

From the study conducted, the following conclusions can be understood and interpreted.

- Fibre reinforced concrete enhanced the mechanical strength properties of the concrete since it has the ability to bridge the cracks and improve the brittle nature of concrete.
- Inclusion of steel fibres showed increments in the values of compressive, splitting tensile and flexural strength of concrete.
- The mix M12 which consists of fibres of length 50 mm and with a volume fraction of 0.75% showed maximum gain in compressive strength to about 11% compared to mix M0. The maximum increment in the splitting tensile strength was about 108% for the mix M12. The maximum increment in the flexural strength was about 18% for the mix M11
- New strength models were developed based on multiple regression analysis considering the plain concrete Compressive Strength (CS), Fibre Reinforcing Index (FRI) and Fibre Volume Fractions (FV$_f$) as the influencing parameters.
- The proposed strength models were found to be more reliable in predicting the mechanical properties of concrete than the prevailing strength models studied, due to its low values of AAE and MSE.

References

1. Abedel A, Abbas H, Almusallam T, Al-Salloum Y, Siddiqui N (2016) Mechanical properties of hybrid fibre reinforced concrete–analytical modelling and experimental behaviour. Mag Concr Res 823–843
2. Ezeldin AS, Balaguru PN (1992) Normal and high strength fiber reinforced concrete under compression. J Mater Civ Eng 415–429
3. Ghosh S, Battacharya C, Ray SP (1992) Tensile strength of steel fiber reinforced concrete. Inst Eng 222–227
4. IS:516-1959, Indian Standard—methods of test for strength of concrete
5. Mazen M (2013) Tensile strength of steel fiber reinforced concrete. Contemp Eng Sci 6(5):225–237
6. Narayanan R, Darwish IYS (1987) Use of steel fibers as shear reinforcement ACI Struct J 216–227
7. Nataraja MC, Dhang N, Gupta AP (1999) Stress-strain curves for steel-fiber reinforced concrete under compression. Cem Concr Compos 383–390
8. Nuruddin MF, Ullah Khan S, Shafiq N, Ayub T (2015) Strength prediction models for PVA fiber-reinforced high-strength concrete. J Mater Civ Eng 1943–5533

9. Ou Y-C, Tsai MS, Liu KY, Chang KC (2012) Compressive behavior of steel-fiber-reinforced concrete with a high reinforcing index. J Mater Civ Eng 24:207–215

10. Padmarajaiah SK (1992) Influence of fibers on the behavior of high strength concrete in fully/partially prestressed beams: an experimental and analytical study. PhD thesis, Indian Institute of Science

11. Praveenkumar S, Sankarasubramanian G (2019) Behavior of high performance fibre reinforced concrete composite beams in flexure. Roman J Mater 49(2):259–266

12. Praveenkumar S, Sankarasubramanian G (2020) Effect of fibers on strength and elastic properties of bagasse ash blended HPC composites. J Test Eval 48(2):922–937

13. Praveenkumar S, Sankarasubramanian G (2020) Performance evaluation of high performance fibre reinforced concrete composite beam column joint subjected to quasi-static loading. Asian J Civil Eng 351–365

14. Qian CX, Stroeven P (2000) Development of hybrid polypropylene-steel fibre-reinforced concrete. Cem Concr Res 30:63–69

15. Song PS, Hwang S (2004) Mechanical properties of high-strength steel fiber-reinforced concrete. Construct Build Mater 669–673

16. Thomas J, Ramaswamy A (2007) Mechanical properties of steel fiber-reinforced concrete. J Mater Civ Eng 19:385–392

17. Varghese A, Anand N, Prince Arulraj G, Johnson Alengaram U (2019) Influence of fibers on bond strength of concrete exposed to elevated temperature. J Adhes Sci Technol 1521–1543

18. Wafa F, Ashour SA (1992) Mechanical properties of high strength fiber reinforced concrete. ACI Mater J 449–455

Modelling and Prediction of Strength for Polypropylene Fiber Reinforced Concrete

B. Nivetha, Y. Subasini, and S. Praveenkumar

1 Introduction

Fibre-reinforced concrete increases the structural integrity of the structural components, due to the presence of fibrous materials. The fiber reinforcement improves the tensile properties of concrete [1, 2]. Fiber reinforced concrete will have enhanced mechanical properties [3]. The synthetic fibre used in our study is polypropylene fibre which arrests the crack and restrains them from further opening. In this research paper, strength models are proposed to forecast compressive, splitting tensile and flexural strengths of polypropylene fibre reinforced high performance concrete. Using multiple regression analyses, the strength models have been developed based on compressive strength of unreinforced concrete, fibre volume fraction (V_f) and fibre reinforcing index (RI) obtained from experimental results. The proposed strength models are also then compared with the existing strength models for compressive, splitting tensile and flexural strengths. The developed models are found to be more precise than the existing strength models. In the last several years, the use of synthetic non-metallic fibres has become more attractive and effective in improving the shear strength and more resistance to corrosion when compared with that of steel fibres [4]. Researches prove that polypropylene fibers (PPF) not only improve the strength of the structural elements, but also enhance the ductility and durability of the structure with increased load carrying capacity [3, 5]. PPF reinforced concrete assists in reducing the

B. Nivetha · Y. Subasini
Post Graduate Student, Department of Civil Engineering, PSG College of Technology, Coimbatore, India

S. Praveenkumar (✉)
Assistant Professor (Senior Grade), Department of Civil Engineering, PSG College of Technology, Coimbatore, India
e-mail: spk.civil@psgtech.ac.in

vapour pressure inside the concrete thus, providing improved sustainability towards fire damage [6, 7].

2 Research Significance

The current study evaluates the effect of polypropylene fibers (PPF) over the mechanical properties of concrete. To examine the impact of fiber aspect ratio and volume fraction, over the strength of concrete, polypropylene fibers of length 12 mm (diameter of 0.022 mm and 0.75) and 46 mm (diameter of 1.15 mm) are used in various volume fractions (0.25%, 0.35%, 0.5%, 0.75%). The strength prediction models based on the compressive strength of concrete specimen, fiber reinforcing index and volume fraction are derived and compared with the existing strength models.

3 Experimental Program

3.1 Materials and Methods

Ordinary Portland Cement (OPC) of grade 53 was used in this experiment. The specific gravity of the cement is tested and found to be 3.2. Sugarcane Bagasse Ash (SCBA) containing 50% cellulose, 25% of lignin, 25% of hemicellulose is used as Supplementary Cementitious Material (SCM). M-Sand as fine aggregate with specific gravity of 2.51 and coarse aggregate with specific gravity of 2.76 is used. To enhance the mechanical properties of concrete, polypropylene fiber is used [8]. To assist in the workability of fiber reinforced concrete, poly carboxylic ether based Master Glenium sky is used as superplasticizer. Table gives the proportion of various materials in the concrete mix per m^3. Polypropylene fibers are used in the concrete mix in various proportions to study its effect over the strength. Various mixes with fibers of length 12 mm in the diameter 0.022 mm (aspect ratio-545), 0.75 mm (aspect ratio-16)and of length 46 mm in the diameter 1.15 (aspect ratio-40) are used in the volume fraction of 0.25, 0.35, 0.5 and 0.75%. Thirteen concrete mixes including one control specimen are cast and their strengths at the age of 28 days are determined. The control mix is designated as M0, mixes with fiber length 12 mm and diameter 0.022 mm in the above mentioned volume fractions are designated M1, M2, M3, M4, mixes with fiber length 46 mm and diameter 1.15 mm in varying volume fractions are designated as M5, M6, M7, M8 and mixes with fiber length 12 mm and diameter 0.75 mm in varying volume fractions are designated as M9, M10, M11, M12. Table 1 represents the proportion of the materials constituting the concrete mix.

Table 1 Materials constituting concrete mix

Grade of Concrete	W/B Ratio	Cement (kg/m^3)	Coarse aggregate (kg/m^3)	Fine aggregate (kg/m^3)	Superplasticizer (l/m^3)	Water (l/m^3)
M$_{60}$	0.33	433	1042	823	12	0.26

3.2   Test Specimens

Three specimens for each mixture (cubes of 150 mm × 150 mm × 150 mm size, cylinder of 150 mm × 300 mm and prism of 100 mm × 400 mm dimension) are tested after 28-days of curing, to find the compressive strength, splitting tensile and flexural strengths. In accordance with IS standards [9], the consistency of fresh concrete is found by carrying out slump test. The compressive strength and splitting tensile are found by testing the cube 150 mm specimen and cylinder of 150 mm diameter and 300 mm length. The prism specimen is used to determine the flexural strength.

4   Results and Discussion

The experimental results are graphically represented from Figs. 1, 2 and 3 and these values are obtained from the average value of three specimens. The compressive strength is denoted by f_c' and splitting tensile by f_{sp}' and flexural strength by f_l' (modulus of rupture).
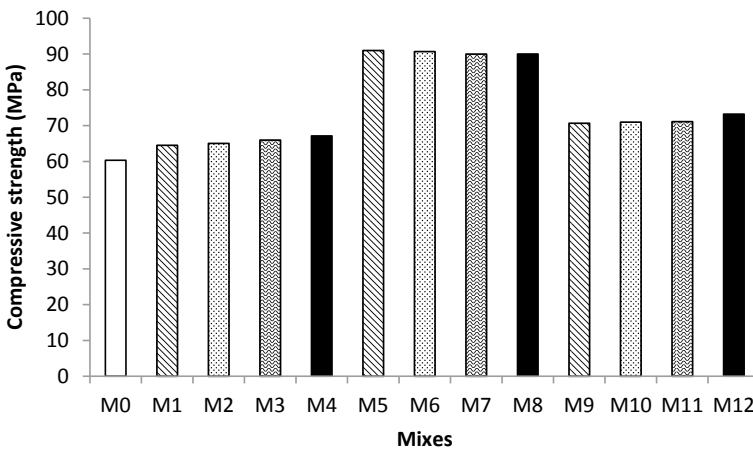
Fig. 1 Compressive strength of various mixes
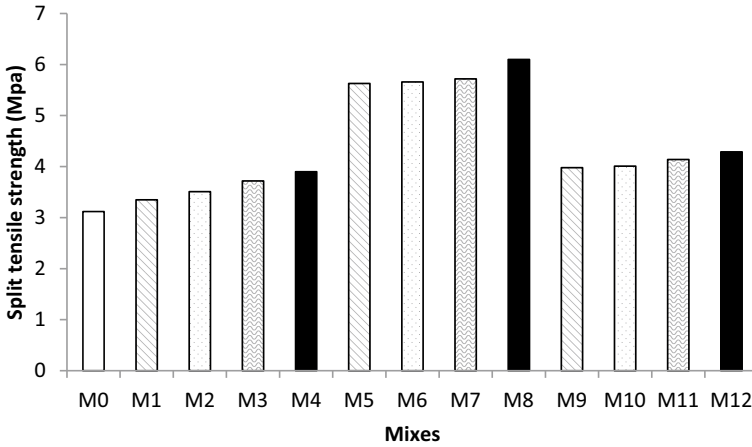
Fig. 2 Split tensile strength of various mixes
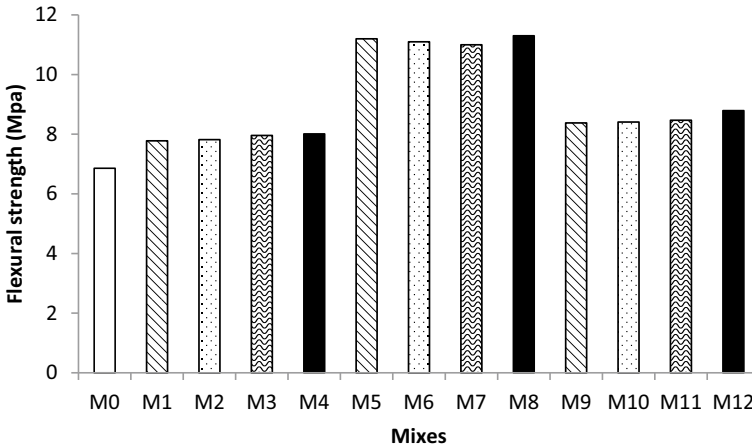
Fig. 3 Flexural strength of various mixes

4.1 Compressive Strength

In accordance with IS Standard, cube specimens are used to test the uniaxial compressive strength after 28 days curing. Figure represents the compressive strengths of various mixes at the age of 28 days. The following figure (Fig. 1) represents the compressive strength of the proposed mixes.

From the graph, it can be inferred that mixes with 46 mm PPF (M5–M8) shows an considerable increase in the compressive strength in the range from 50.8% to 49.2%. Mix with 46 mm PPF in the volume fraction of 0.25% (M5) shows an improved

compressive strength with an increase of 50.8%. Mixes from M1–M4 and M9–M12 shows an relative increase in the strengths in the ranges 6.9–11.3% and 17.1–21.4% with the increase in the volume fraction [10].

4.2 Splitting Tensile

Cylindrical specimens of dimension (150 mm × 300 mm) at the age of 28 days are used to test the splitting tensile strength in accordance with IS standard. The splitting tensile can be calculated using the Eq. (1):

$$f'_{sp} = \frac{2P}{\pi a^2} \tag{1}$$

where P and a are the applied load and dimension of the specimens.

Figure 2 represents the split tensile strength of various mixes.

The graph shows linear increase in strength with the increase in fiber fraction for the mixes with same aspect ratio. From the graph, it could be observed that mixes with 46 mm PPF (M5–M8) shows an abrupt increase in the split tensile strength in the range from 80.4 to 95.5%. Mix with 46 mm PPF in the volume fraction of 0.75% (M8) shows highest split tensile strength with an increase of 95.5%. Mixes from M1–M4 and M9–M12 shows an relative increase in the strengths in the ranges 7.3–25% and 27.5–37.5% with the increase in the fiber content.

4.3 Flexural Strength

Prism of 100 mm × 100 mm × 400 mm is used to determine the flexural strength of the fiber reinforced concrete as per the specifications in IS standard. The flexural strengths of the mixes are determined at the age of 28 according to the following formula.

$$f'_l = \frac{PL}{bd^2} \tag{2}$$

where f_l' is the flexural strength in N/mm^2, P is the applied load in N, L is the length, b is the width and d is the diameter of the prism in mm. Figure represents the flexural strength of the proposed mixes, at the age of 28 days. Figure 3 represents the flexural strength of the mixes.

It could be inferred from the graph that mixes M5 to M8 shows an increased flexural strength on comparison with other mixes. M8 with 46 mm PPF at the volume fraction of 0.75% shows the maximum flexural strength, with an increase of 64.7%.

Mixes from M1–M4 and M9–M12 shows relative increase in strength, in the ranges 13.4–16.7% and 22.1–28.1% with the increase in the volume fraction [11].

4.4 Strength Prediction Models

Based on the experimental results for PPF reinforced concrete, strength prediction models for compressive, split tensile and flexural strength are developed. The models are developed based on various parameters such as compressive strength of control specimen, Reinforcing Index (RI) and volume fraction of PPF. The basic equation representing the strength model for compressive, split tensile and flexure are given by Eqs. 3, 4 and 5.

$$f_{cu} = C_1 f'_c + C_2 V_f + C_3 RI \tag{3}$$

$$f_{sp} = C_4 f'_c + C_5 V_f + C_6 RI \tag{4}$$

$$f_l = C_7 f'_c + C_8 V_f + C_9 RI \tag{5}$$

where f_{cu} is the expected compressive strength, f_{sp} represents the expected split tensile strength, f_l is the expected flexural strength, f'_c is the compressive strength of specimen without fiber (M_0), V_f is the fiber volume fraction, RI is the fiber reinforcing index (Eq. 6) and C1, C2, C3, C4,C5, C6 are regression co-efficient obtained through regression analysis.

$$RI = V_f \frac{l}{d} \tag{6}$$

where l is the length of the fiber in mm and d is the diameter of the fibrin mm.

The strength prediction model developed in the current research is tabulated in Table 2 along with strength prediction models of various researchers.

Based on the proposed strength model, graphs comparing the existing strength models and developed model are plotted for compressive, split and flexural strengths. Figure 4, 5 and 6 represents the comparison graphs of the strengths for compressive, split and flexure respectively.

The developed strength model for compressive strength is found to be in-line with previously developed models except the strength model of [12]. He developed strength model for fiber reinforced concrete consisting cement replacement material, representing high compressive strength. His model is found to have a large deviation with every other models. Considering the comparison graph for split tensile, the proposed model is found to have good co-relation with every other proposed model, except, the models proposed by Nuruddin et al. [12] and Thomas & Ramaswamy

Table 2 Strength prediction models

Researcher	Compressive strength	Split tensile strength	Flexural strength
Proposed	$f_{cu} = 1.2369f'_c + 13.064V_f - 5.1424RI$	$f_{sp} = 0.1484f'_c + 1.8428V_f - 0.6628RI$	$f_l = 0.0678f'_c + 1.7847V_f - 0.4438RI$
Abedel et al. [12]	$f'_{cyf} = f'_{cy} + 5.222RI_v$	$f'_{sp} = f_{sp} + 6.496RI_v$	$f'_l = f_l + 5.222RI_v$
Nuruddin et al. [13]	$f'_{cuf} = 1.03f'_{cu} - 0.03f'_{cu}RI_v + 17.98\sqrt{CRM}$	$f'_{sp} = 0.46f'_{cu} + 0.01\sqrt{f'_{cu}}RI_v + 2.58\sqrt{CRM}$	$f'_l = 0.79f'_{cu} - 0.011\sqrt{f'_{cu}}RI_v + 1.311\sqrt{CRM}$
Ou et al. [14]	$f'_{cyf} = f'_{cy} + 2.35RI_v$	–	–
Thomas and Ramasamy [15]	$f'_{cuf} = f'_{cu} + 0.014\,f'_{cu}RI_v + 1.09RI_v$	$f'_{sp} = 0.63\sqrt{f'_{cu}} + 0.288\sqrt{f'_{cu}}RI_v + 0.052RI_v$	$f'_l = 0.97\sqrt{f'_{cu}} + 0.295\sqrt{f'_{cu}}RI_v + 1.117RI_v$
Song and Hwang [16]	$f'_{cyf} = f'_{cy} + 15.12V_f - 4.71V_f^2$	$f'_{sp} = 5.8 + 3.01V_f - 0.02V_f^2$	$f'_l = 6.4 + 3.43V_f + 0.32V_f^2$
Nataraja et al. [17]	$f'_{cyf} = f'_{cy} + 2.16RI_w$	–	–
Ezeldin and Balaguru [18]	$f'_{cyf} = f'_{cy} + 3.51RI_w$	–	–
Ghosh et al. [19]	–	$f'_{sp} = 0.11f'_{cu}(1 - V_f) + 0.573RI_v + 0.571$	$f'_l = 0.15f'_{cu}(1 - V_f) + 0.79RI_v$
Padmarajaiah [20]	$f'_{cuf} = f'_{cu} + 1.998RI_v$	$f'_{sp} = \frac{\sqrt{f'_{cu}}}{3} + 1.918RI_v$	$f'_l = f_l + 4.419RI_v$
Wafa and Ashour [21]	$f'_{cyf} = f'_{cy} + 3.53V_f$	$f'_{sp} = 0.58\sqrt{f'_{cy}} + 3.02V_f$	$f'_l = 0.99\sqrt{f'_{cy}} + 3.83V_f$
Narayanan et al. [22]	–	$f'_{sp} = \frac{f'_{cu}}{20 - RI_v} + 0.7 + \sqrt{RI_v}$	–
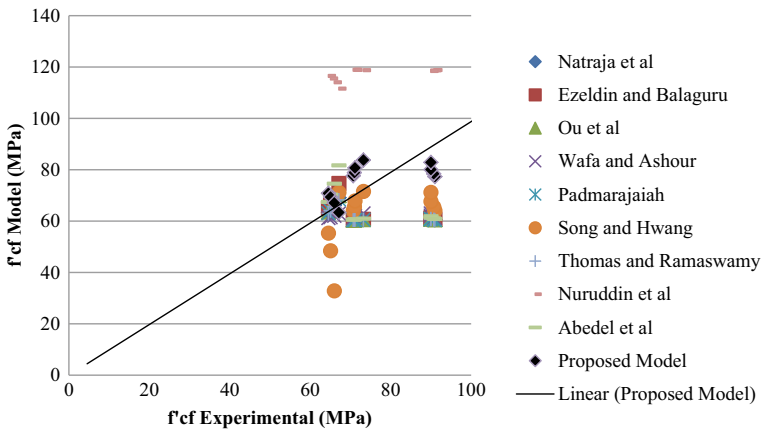
Fig. 4 Comparison graph of strength models for compressive strength
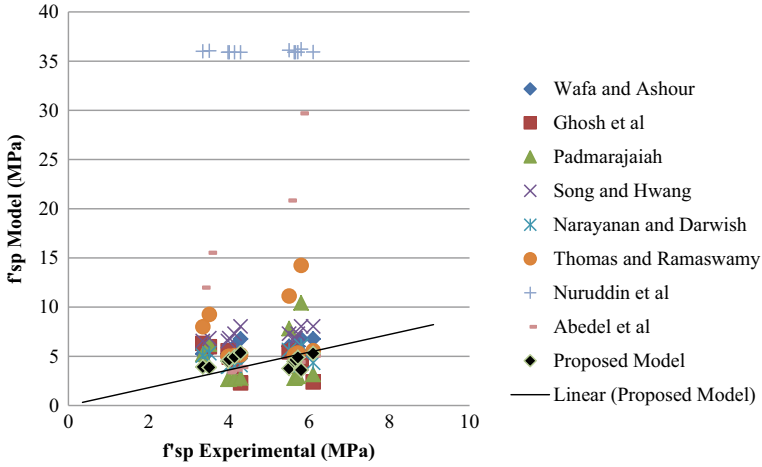
Fig. 5 Comparison graph of strength models for split tensile strength
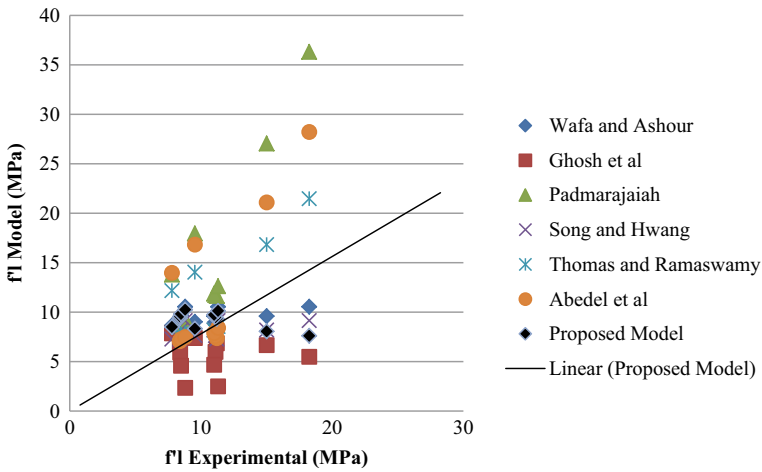
Fig. 6 Comparison graph of strength models for flexural strength

[15]. The strength model developed for predicting the flexural strength is found to deviate from the models of [12].

Padmarajaiah [20] and Thomas and Ramaswamy [15]. The accuracy of the proposed model can be evaluated by determining the mean (M), standard deviation (SD), Average Absolute Error (AAE) and Mean Squared Error (MSE). The formula to evaluate the AAE and MSE are given in the Eqs. 9 and 10.
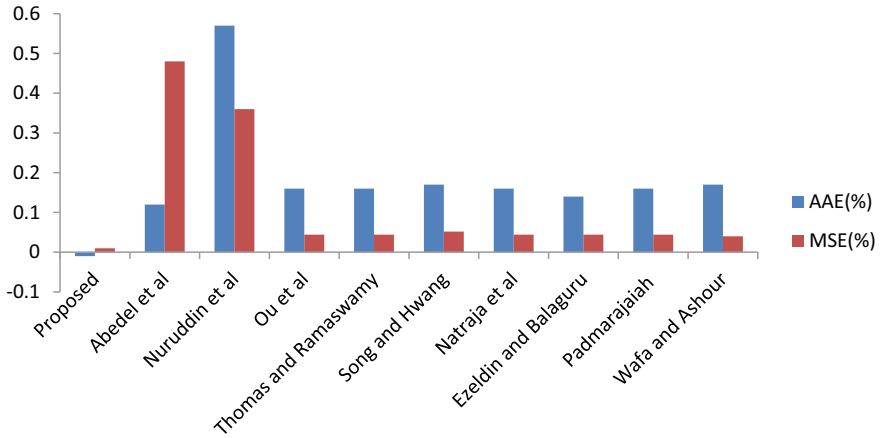
Fig. 7 Comparison graph of AAE and MSE for various strength models for compressive strength
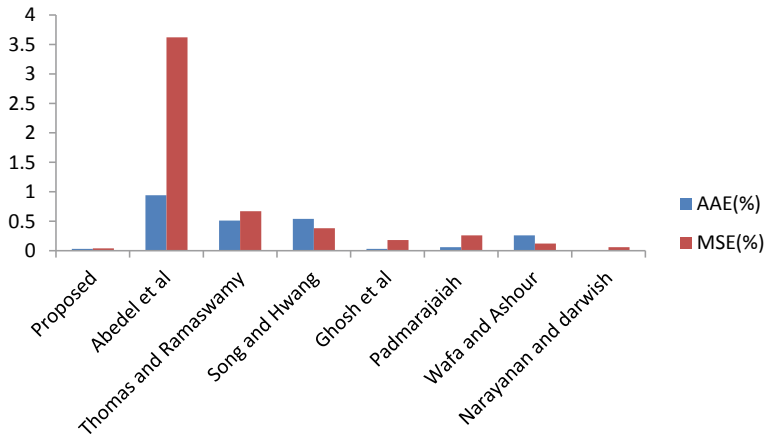
Fig. 8 Comparison graph of AAE and MSE for various strength models for split tensile strength

$$M = \frac{1}{N} \sum_{i=1}^{n} \frac{f'_{x,model,i}}{f'_{x,exp,i}} \tag{7}$$

$$SD = \sqrt{\frac{1}{N} \sum_{i=1}^{n} \left(\frac{f'_{x,model,i}}{f'_{x,exp,i}} - M \right)^2} \tag{8}$$

$$AAE = \frac{\sum_{i=1}^{n} \left[\frac{f'_{x,model,i} - f'_{x,exp,i}}{f'_{x,exp,i}} \right]}{N} \tag{9}$$
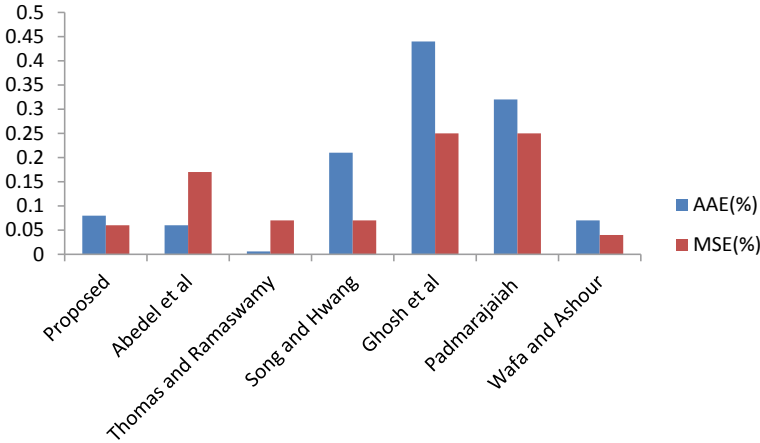
Fig. 9 Comparison graph of AAE and MSE for various strength models for flexural strength

$$\text{MSE} = \frac{1}{N} \sum_{i=1}^{n} \left(\frac{f'_{x,model,i} - f'_{x,exp,i}}{f'_{x,exp,i}} \right)^2 \tag{10}$$

where $f'_{x,model,I}$ represents the respective strengths obtained from the corresponding strength model, $f'_{x,exp,I}$ represents the respective strengths obtained from the experiment, at the age of 28 days. The AAE and MSE for the proposed model and existing strength models are calculated and represented in the figures from 7 to 9.

From the error comparison graph of compressive strength, it could be seen that AAE and MSE of proposed model is very low. The values are 0.01 and 0.01% (<0.05%). This reveals that the developed equation can be used to predict the compressive strength of fiber reinforced concrete. Out of existing strength models, the models developed by [12] and Nuruddin et al. [13] are found have more deviation from the test results. The value of AAE and MSE of them are 0.12, 0.48, 0.57, and 0.36%. The AAE of other models are found to be in the range of 0.14–0.17% and MSE to be 0.044–0.052%. The split tensile strength prediction of the proposed model in the current study is found to have the AAE and MSE value as 0.03–0.04% (<0.05%). In existing prediction models, the model proposed by Abedel et al. [12] is found to have the largest AAE and MSE value, 0.94–3.62%. These values of other models are found to be in the range of 0.005–0.54% and 0.06–0.67%. The model proposed by current study is found to be reliable to forecast the split tensile strength of fiber reinforced concrete. Among the strength predicting models for flexure, the one proposed by Ghosh et al. [19] are found be the highest with the value, 0.44% and 0.25%. The errors for the model proposed in the current study is 0.08 and 0.06% (<0.1%). These values for other models are found to be in the range 0.006–0.32% and 0.04–0.25%.

5   Conclusions

Considering the mechanical properties such as compressive, split and flexural strengths, the concrete with polypropylene reinforcement if found to have notifiable improvements. Highest rise in the compressive strength is observed for the mix M5, with percentile increase of 50.8%. Mix M8, is found to have high split tensile and flexural strength with an increase of 95.5–64.7%. Taking into account of the strength aspects, mixes with fiber length of 46 mm and fiber content in the range 0.25–0.75% is found to show good results. The strength models for forecasting the compressive, split tensile and flexural strength of the fiber reinforced concrete are found acceptable as their error values are found to be less than 0.1%. Thus the developed strength models can be safely used to prognosticate the strengths of fiber reinforced concrete which only requires the details of compressive strength of control specimen, length and diameter of the fiber and fiber proportion.

References

1. Wille K, Naaman AE, El-Tawil S, Parra-Montesinos GJ (2011) Ultra-high performance concrete and fiber reinforced concrete: achieving strength and ductility without heat curing. Mater Struct 45:309–324
2. Nili M, Afroughsabet V (2010) The effects of silica fume and polypropylene fibers on the impact resistance and mechanical properties of concrete. Construct Build Mater 927–933
3. Praveenkumar S, Gopalan S (2019) Behaviour of High Performance Fibre reinforced concrete composite beams in flexure. Romanian J Mater 459–466
4. Zahrani AH, Al-Tayyib J, Mesfer M-A (1990) Corrosion of steel reinforcement in polypropylene fiber reinforced concrete structures. Am Concrete Inst 108–113
5. Yermak N, Noumowe A (2017) Influence of steel and/or polypropylene fibres on the behaviour of concrete at high temperature: spalling, transfer and mechanical properties. Construct Build Mater 240–250
6. Varghese A, Anand N, Prince Arulraj G, Johnson Alengaram U (2019) Influence of fibers on bond strength of concrete exposed to elevated temperature. J Adhes Sci Technol 1521–1543
7. Kakooei S, Akil HMd, Jamshidi M, Rouhi J (2012) The effect of polypropylene fibers on the properties of reinforced concrete structures. Construct Build Mater 73–77
8. Dharan DS, Lal A (2016) Study the effect of polypropylene fiber in concrete. Int Res J Eng Technol (IRJET) 2395-0056
9. IS 516(1959): Method of Tests for Strength of Concrete [CED 2: Cement and Concrete]. (n.d.)
10. Praveenkumar S, Sankarasubramanian G (2020) Performance evaluation of high-performance fibre-reinforced concrete composite beam–column joint subjected to quasi-static loading. Asian J Civil Eng 351–365
11. Praveenkumar S, Sankarasubramanian G (2020) Effect of fibers on strength and elastic properties of bagasse ash blended HPC composites. J Test Eval 48(2):922–937
12. Abedel A, Abbas H, Almusallam T, Al-Salloum Y, Siddiqui N (2016) Mechanical properties of hybrid fibre-reinforced concrete–analytical modelling and experimental behaviour. Mag Concr Res (2016):823–843
13. Nuruddin MF, Ullah Khan S, Shafiq N, Ayub T (2015) Strength prediction models for PVA fiber-reinforced high-strength concrete. J Mater Civ Eng 1943–5533
14. Ou Y-C, Tsai MS, Liu KY, Chang KC (2012) Compressive behavior of steel-fiber-reinforced concrete with a high reinforcing index. J Mater Civ Eng 24:207–215

15. Thomas J, Ramaswamy A (2007) Mechanical properties of steel fiber-reinforced concrete. J Mater Civ Eng 19:385–392
16. Song PS, Hwang S (2004) Mechanical properties of high-strength steel fiber-reinforced concrete. Construct Build Mater 669–673
17. Nataraja MC, Dhang N, Gupta AP (1999) Stress-strain curves for steel-fiber reinforced concrete under compression. Cem Concr Compos 383–390
18. Ezeldin AS, Balaguru PN (1992) Normal and high strength fiber reinforced concrete under compression. J Mater Civ Eng 415–429
19. Ghosh S, Battacharya C, Ray SP (1992) Tensile strength of steel fiber reinforced concrete. Inst Eng 222–22.
20. Padmarajaiah SK (1992) Influence of fibers on the behavior of high strength concrete in fully/partially prestressed beams: An experimental and analytical study. PhD thesis, Indian Institute of Science (1992)
21. Wafa F, Ashour SA (1992) Mechanical properties of high strength fiber reinforced concrete. ACI Mater J 449–455
22. Narayanan R, Darwish IYS (1987) Use of steel fibers as shear reinforcement. ACI Struct J 216–227

The Use of Artificial Intelligence in High Strength Hybrid Fiber Self Compacting Concrete—An Approach to Function Approximation of Flexural Strength

V. Rajesh, Boppana. Narendra Kumar, and Vishal Singh

1 Introduction

Self-Compacting Concrete (SCC), when compared to normal concrete, is more brittle under the application of load. The tensile stresses which are caused due to environmental conditions and imposed loads are intensified at the boundary junction of cement matrix and aggregates [1]. The development of minute cracks occurs due to the brittleness of SCC, which is also responsible for the enhancement of their size as well as number [2]. These minute cracks propagate into the concrete matrix thereby giving rise to macro cracks. This macro and micro-crack can be minimized by the addition of arbitrarily distributed short fibers. The SCC that is obtained after the random orientation of the steel fibers is called Steel Fiber Reinforced Self Compacting Concrete (SFRSCC) and similarly, the SCC obtained after the random orientation of the glass fibers is called Glass Fiber Reinforced Self Compacting Concrete (GFRSCC) [3–5]. When more types of fibers are used or a mixture of two or more types of fibers are used together it is known as Hybrid Fiber Reinforced Self Compacting Concrete (HFRSCC). The inclusion of hybrid fibers helps to deal with the difficulties that occur when fibers are individually used in the mix. Like in the case of SFRSCC, the steel fibers get affected by the alkali content of the cement and in case of the GFRSCC, as the glass fibers are significantly less ductile when compared to steel fibers so they can only help in arresting the cracks without providing any remarkable increment in strength. Hence for hybrid fibers, these two problems are dealt with simultaneously as steel gives it the amount of strength required, and glass is not much influenced due to the alkali content of cement [3–5]. These types of

V. Rajesh · Boppana. N. Kumar (✉) · V. Singh
Department of Civil Engineering, VNR Vignana Jyothi Institute of Engineering & Tech, Telangana State, Hyderabad, India
e-mail: narendrakumar_b@vnrvjiet.in

concretes are currently being utilized in constructions such as rock slope stabilization, linings of tunnels, in Reinforced Cement Concrete (RCC) buildings, etc.

Machine learning is the application of artificial intelligence (AI) that helps in providing the systems and ability to learn and improve from experience without being explicitly programmed [6]. The learning process begins by observation of datasets to seek help from previous patterns and make better predictions for the subsequent samples. This process can be categorized into supervised and unsupervised learning methods. Supervised machine learning methods use samples of input and output to train the model. This model is then used to perform predictions on future data. Regression algorithms that we are using fall under this category. Regression analysis helps in estimating associations amidst variables, helping to enquire about the key patterns in large and diverse data sets and how they compare with each other.

MATLAB Machine Learning and Deep Learning toolkit provide many algorithms for regression which include linear regression models, regression trees, support vector machine (SVM), Gaussian process regression models and ensembles of trees. 5-fold cross-validation was performed on the models that were trained to find various efficiency parameters which include R-squared error, mean absolute error (MAE), mean squared error (MSE), and root means square error (RMSE) [7, 8].

2 Data Collections and Experiments

The experimental investigation is focused on understanding the performance of the material and structural behavior. To develop HSSCC mixes river sand was replaced by quartz sand in proportions of 0, 20, 40, 60, 80, and 100 [4, 5]. The hardened properties and fresh properties of the above mixes were determined to obtain optimized mix proportions [6]. By using this optimized mix proportion, and by working on differencing dosages of glass fibers and steel fibers the optimum fibrous powder content was determined [7]. It is noted that a dosage of 1.5% (0.75% glass fibers + 0.75% steel by weight) satisfies the fresh and hardened properties. After finalizing HSHFSCC and HSSCC mixes stress-strain of mixes was obtained. Flexural strength was determined including fresh properties.

3 Mix Proportions of HSHFSCC

Table 1 shows the mix proportions of the 8 mixes of HSHFSCC with varied range of steel and glass percentage incorporated in each mix.

Table 1 Mix Proportions of HSSCC Mixes with Fiber

Designation Of Mix	Cement (kg/m³)	Micro Silica (kg/m³)	Quartz powder (kg/m³)	Quartz Sand (kg/m³)	Coarse aggregate (kg/m³)	SP% of Powder content	VMA% of Powder content	W/P ratio	Fibres % of Powder content	
									Steel	Glass
HSSCC	640	64	160	910	800	1.5	0.5	0.21	–	–
HSSFSCC	640	64	160	910	800	1.5	0.5	0.21	1.5	–
HSHFSCC 1	640	64	160	910	800	1.5	0.5	0.21	1.35	0.15
HSHFSCC 2	640	64	160	910	800	1.5	0.5	0.21	1.20	0.30
HSHFSCC 3	640	64	160	910	800	1.5	0.5	0.21	1.05	0.45
HSHFSCC 4	640	64	160	910	800	1.5	0.5	0.21	0.90	0.60
HSHFSCC 5	640	64	160	910	800	1.5	0.5	0.21	0.75	0.75
HSHFSCC 6	640	64	160	910	800	1.5	0.5	0.21	0.60	0.90

4 Fresh Properties of HSHFSCC

The concrete has to be tested for passing ability, flowing ability and segregation resistance. Among other fresh properties, unit weight, air content and plastic shrinkage are noteworthy [8]. EFNARC guidelines for testing SCC were adopted for testing these properties. V Funnel test, L Box test and Slump Flow test are some of the test methods to characterize the workability properties and for the final acceptance of SCC mix proportions as per EFNARC [2005] (Figs. 1 and 2; Table 2).

Fig. 1 Flow table test

Fig. 2 L box test

Table 2 Shows the fresh properties with values of flow table, V funnel and L box for all the 8 mixes of HSHFSCC

Designation of Mix	Flow table data		V Funnel data		L box ratio
	Diameter (in mm)	T_{50} (in sec)	T_f (in sec)	T_{5min} (in sec)	
HSSCC	744	3	7	9	0.98
HSSFSCC	738	3	7	11	0.98
HSHFSCC-1	733	3	7	11	0.96
HSHFSCC-2	731	4	9	12	0.95
HSHFSCC-3	729	4	9	12	0.93
HSHFSCC-4	725	4	12	14	0.88
HSHFSCC-5	719	5	13	16	0.86
HSHFSCC-6	704	6	14	17	0.83

Table 3 Flexural strength of HSHFSCC

Mix designation	Flexural strength (MPa)			
	7 Days	28 days	90 days	180 days
HSSCC	7.32	10.44	11.05	11.21
HSSFSCC	7.44	10.64	11.24	11.49
HSHFSCC-1	7.58	10.85	11.59	11.84
HSHFSCC-2	7.77	11.12	12.05	12.29
HSHFSCC-3	8.03	11.46	12.39	12.73
HSHFSCC-4	8.32	11.84	12.87	13.17
HSHFSCC-5	8.61	12.37	13.62	13.98
HSHFSCC-6	8.23	11.47	12.41	12.97

5 Flexural Strength of HSHFSCC

In this study, six specimens of 500 mm × 100 mm × 100 mm were kept in flexural testing machine for three points loading and the load was applied until the specimen was failed at 7, 28 & 90 days of HSHFSCC respectively [8]. Table 3 shows the flexural strength for all the HSHFSCC specimens for 7, 28, 90 & 180 days respectively.

6 Modeling Methods

MATLAB Machine Learning and Deep Learning toolkit provide many algorithms for regression which include linear regression models, regression trees, support vector machine (SVM), Gaussian process regression models and ensembles of trees [7]. Fivefold cross-validation was performed on the models that were trained to find

various efficiency parameters which include R-squared error, mean absolute error (MAE), mean squared error (MSE), and root means square error (RMSE) [8].

7 Function Approximation of Flexural Strength of HSHFSCC by MATLAB

Table 4 shows that the assessment parameters including R-squared and RMSE of fine tree and Artificial Neural Networks higher level of reliability and accuracy of the model.

7.1 Graphs Between the Flexural Strength and Input Variables

Regression analysis was performed between flexural strength and input variables. Thus, the output is obtained as a graph between flexural strength and input variable. Input variables lie on X-axis and Flexural strength lies on Y-axis. Input variables for HSSCC are quantity of steel, the quantity of glass fibre and setting time of concrete. Function approximation is performed [4–6]. The points with true and predicted values are clearly shown as blue point denotes true value and orange point denotes predicted value [7, 8].

The below graphs depict the values to be predicted (flexural strength) on the Y axis and the input parameters (river sand, quartz sand, steel, glass and time) on the X axis for HSHFSCC (Figs. 3, 4, 5 and 6).

(a)   Decision tree Regressor (Fine tree) of HSHFSCC.

(b)   Artificial Neural Network (Plot fit) of HSHFSCC.

8 Function Approximation of Flexural Strength of HSHFSCC in Python

Concerning Table 5, It is observed that Fine tree regressor and Artificial Neural Networks (ANN) have yielded the best result. Therefore, approximation in python is also done on the same model [5].

The below graphs depict the predicted values of flexural strength for HSHFSCC by making use of two models i.e. Decision Regressor and Artificial Neural Network by giving input parameters such as percentage of steel, glass percentage, and setting time (Figs. 7, 8, 9, 10).

(a)   Decision Regressor (fine tree) of HSHFSCC
(b)   Artificial Neural Network of HSHFSCC

Table 4 Performance of various model for HSHFSCC in MATLAB

	RMSE		R-Squared		MSE		MAE	
	HSHF SCC	HS SCC	HSHF SCC	HS SCC	HSHF SCC	HS SCC	HSHF SCC	HS SCC
Linear Regression LR	1.13	1.25	0.53	0.32	1.82	1.57	1.22	1.11
Interactions L.R	1.79	1.52	0.17	0	3.21	2.31	1.59	1.3
Robust L.R	1.36	1.26	0.52	0.31	1.85	1.6	1.22	1.11
Stepwise L.R	1.31	1.19	0.55	0.39	1.73	1.42	1.19	1.06
Medium Tree	1.45	1.52	0.45	0	2.11	2.32	1.26	1.24
Coarse Tree	1.96	1.52	0	0	3.86	2.32	1.6	1.24
Linear SVM	1.6	1.29	0.33	0.28	2.58	1.68	1.17	0.8
Fine Tree	0.81	0.47	0.83	0.90	0.65	0.22	0.70	0.40
Quadratic SVM	1.24	1.31	0.6	0.26	1.54	1.72	0.98	0.94
Cubic SVM	1.2	1.41	0.62	0.14	1.45	1.99	0.98	1.1
Fine Gaussian SVM	1.86	1.68	0.1	0.21	3.46	2.82	1.43	1.35
Medium Gauss SVM	1.6	1.48	0.33	0.05	2.57	2.2	1.1	1.07
Coarse Gaussian SVM	1.65	1.36	0.29	0.2	2.74	1.87	1.12	0.83
Boasted Trees	1.5	1.24	0.41	0.33	2.26	1.55	1.26	1.06
Bagged Trees	1.08	1.07	0.69	0.5	1.18	1.16	0.92	0.88
Squar1ed Exponential	1.27	1.26	0.58	0.31	1.63	1.59	1.01	0.96
Matern 5/2 GPR	1.29	1.26	0.56	0.37	1.68	1.59	1.03	0.97
Exponential GPR	1.39	1.34	0.49	0.23	1.95	1.79	1.08	1.05
Rational GPR	1.27	1.26	0.58	0.31	1.63	1.59	1.01	0.96
ANN	0.34	0.004	0.97	0.99	-	-	-	-

9 Discussions and Results

In case of MATLAB Fine tree obtained R^2 value as 0.83 and Artificial Neural Network obtained R^2 value as 0.97. Therefore, in comparison with MATLAB, the Artificial Neural Network model is the best fit.
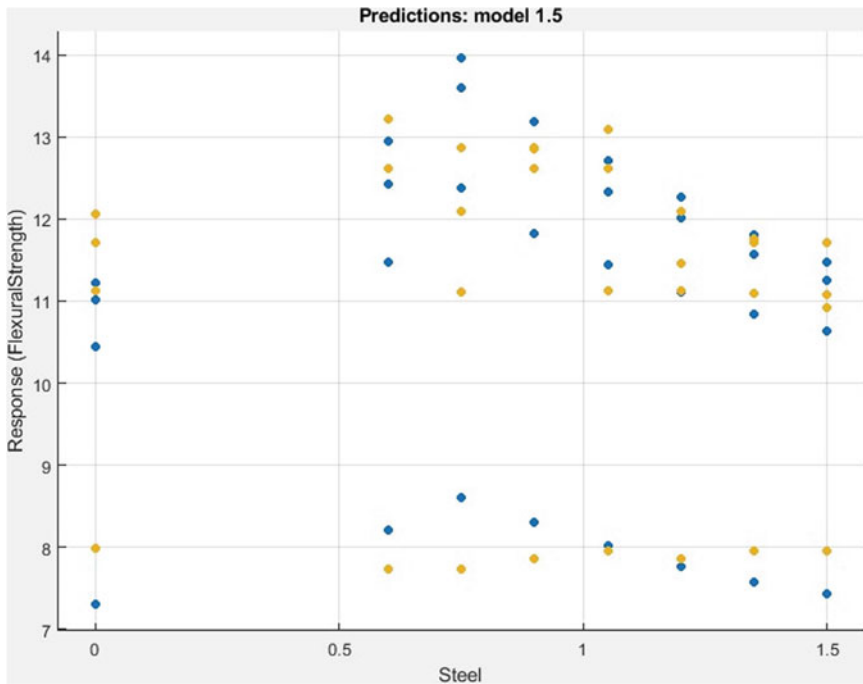
Fig. 3 Graph between flexural strength and steel percentage

In case of PYTHON Decision Tree Regression with the R^2 value as 0.945 and Neural Network with the R^2 value as 0.984, so with respect to PYTHON, the Neural Network model is the best fit.

By considering both MATLAB and PYTHON, it is observed that in PYTHON with Neural Network model (where the R^2 value as 0.984) is the best fit.

10   Conclusions

a.   Artificial intelligence has impacted many domains today. Its capacity to perform high-level analysis on data has shown it can be very impactful for predictions, given proper parameters that influence the prediction. We considered three input parameters to create the models and predict the compressive strength of the concrete.

b.   In this study, 24 samples were used to perform this experiment. These 24 samples were further divided int 16 samples for training and 8 samples for testing and validation. This is required to evaluate the performances of various models that are being tested.
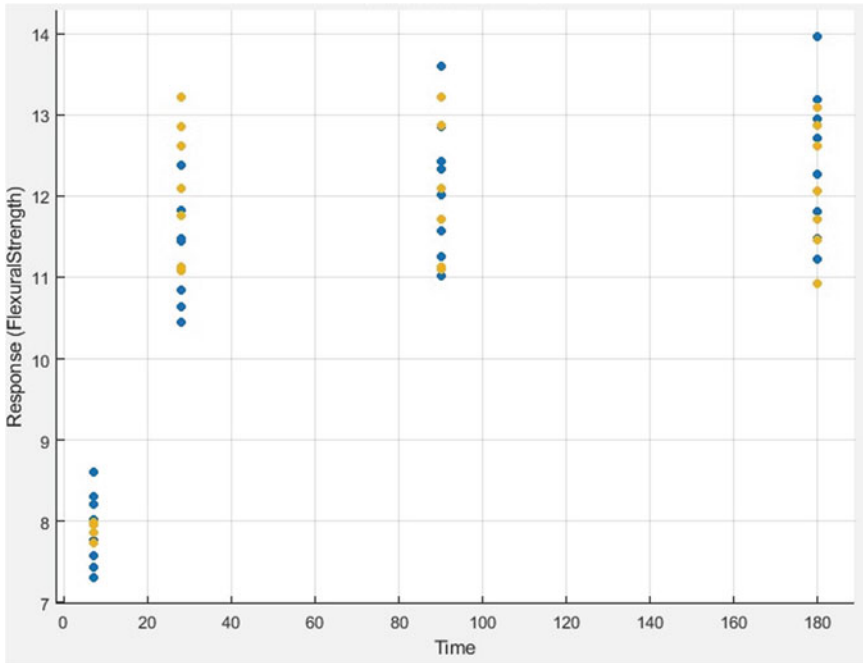
Fig. 4 Graph between time flexural strength and Setting time

c. It is observed that Artificial Neural Network model in MATLAB might serve as the most feasible prediction tool for predicting the Flexural Strength of HSSCC and Neural Network mode in PYTHON might serve as the most feasible prediction tool for predicting the Flexural Strength of HSHFSCC.
d. It can further increase the performances of these models by exposing them to larger datasets and fine-tuning the models for greater accuracy of prediction.
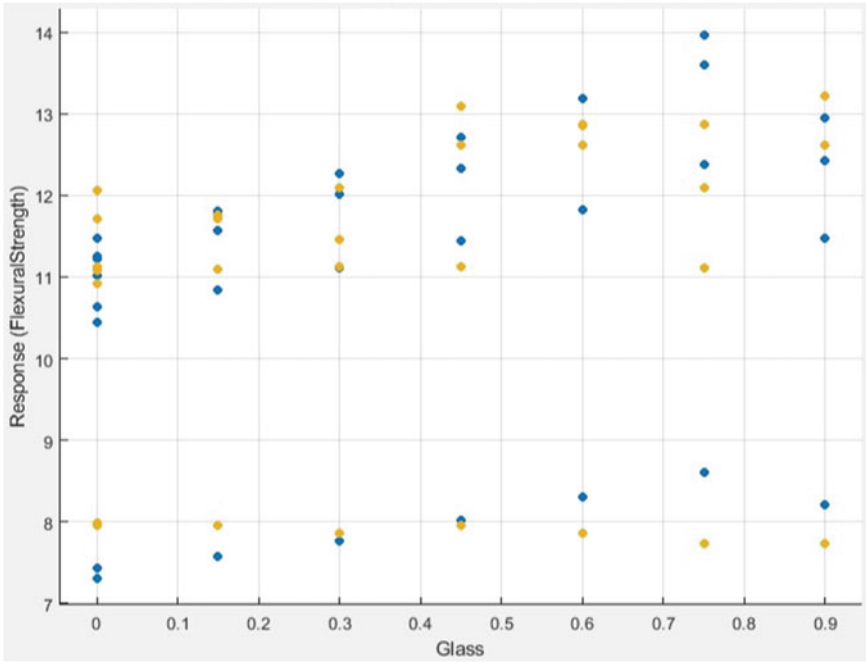
Fig. 5 Graph between time flexural strength and percentage of glass
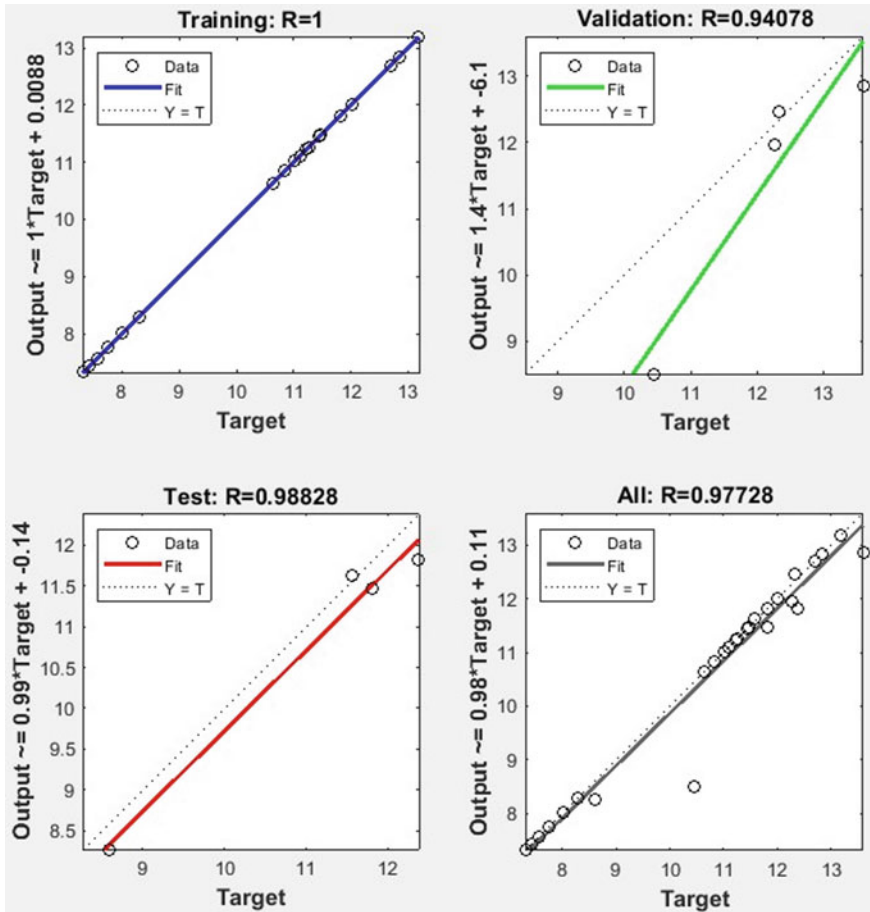
Fig. 6 Depicts the graph between real values and predicted fit for flexural strength

Table 5 Performance of models in Python

	R-squared	
	HSHFSCC	HSHFSCC
Decision tree regression	0.4913	0.945
Neural network	0.2489	0.984

Fig. 7 Depicts the graph between flexural strength and steel percentage
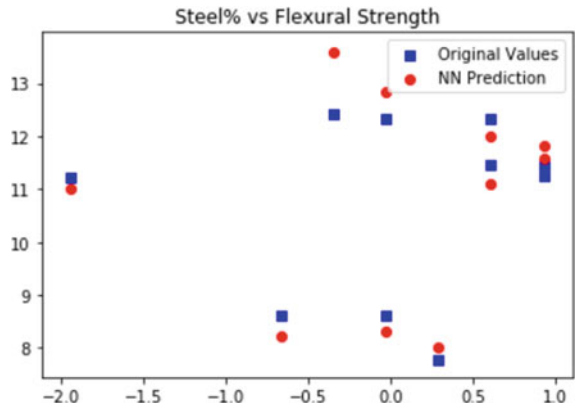
Fig. 8 Depicts the graph between flexural strength and glass percentage
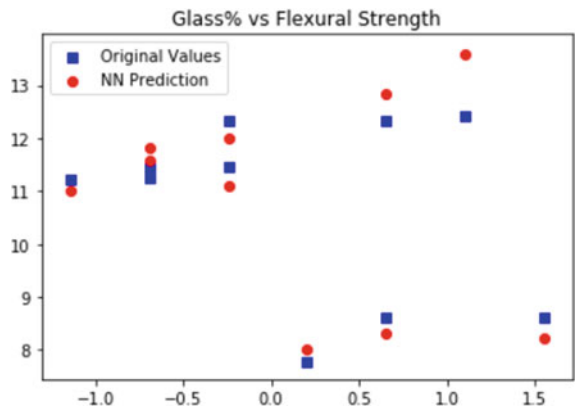
Fig. 9 Depicts the graph between flexural strength and amount of setting time
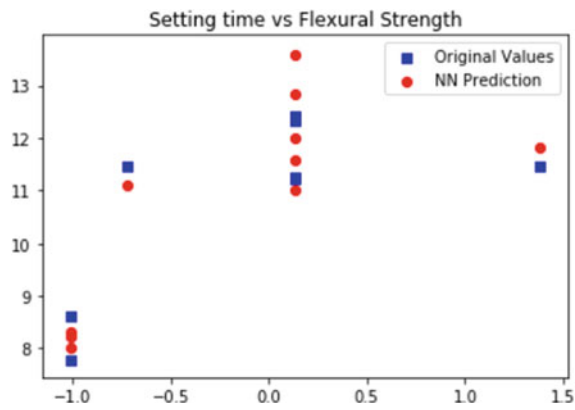
Fig. 10 Depicts the graph between setting time and flexural strength
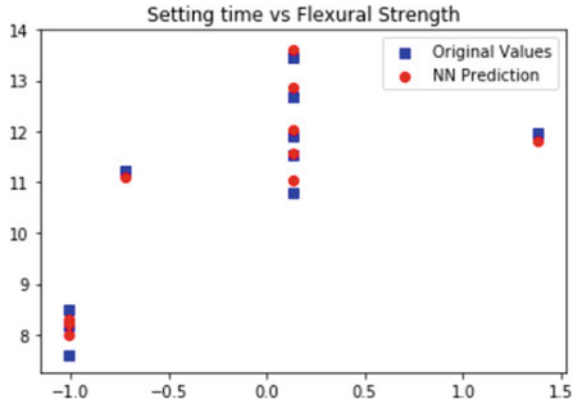
References

1. Application of neural network for prediction of compressive strength of silica fume concrete (2019) Int J Civil Eng Technol (IJCIET) 10(02)
2. Prediction of compressive strength of cement mortar in normal and aggressive environment using artificial neural network (2019) Int J Appl Eng Res ISSN 0973-4562 14(15)
3. Prediction of compressive strength of concrete using artificial neural network and genetic programming. Adv Mater Sci Eng 2016, Article ID 7648467)
4. Zhang J, Li D, Wang Y (2020) Predicting uniaxial compressive strength of oil palm shell concrete using a hybrid artificial intelligence model. J Build Eng 30
5. Hammoudi A, Moussaceb K, Belebchouche C, Dahmoune F (2019) Comparison of artificial neural network (ANN) and response surface methodology (RSM) prediction in compressive strength of recycled concrete aggregates. Constr Build Mater 209
6. Chou J-S, Pham A-D (2013) Enhanced artificial intelligence for ensemble approach to predicting high performance concrete compressive strength. Constr Build Mater 49
7. Murthy NRD, Seshu DR, Rao MVS (2007) Constitutive behavior of fly ash concrete with steel Cem-FIL Anti-Crak HD Glass fibers literature fibers in ordinary grade. IE(I) J, 41–46
8. Narendra Kumar B, Sinivasa Rao P (2013) Study on hardened properties of ultra high strength self compacting fiber reinforced concrete. IJCEA ISSN NO.2249-426x, 3(2)

Gradation of the Relative Significance of the Claims Obtained from Construction Industry

Pramodini Sahu, D. K. Bera, and P. K. Parhi

1 Introduction

The industry that plays a vital role in economy growth and employability of any country is the construction industry. At the same time, it is also the most complex sector due to involvement of different participants in the projects, which results difference in opinion and perceptions. The major participants of any construction project are the owner, contractor and consultant and all expect their own profit. Due to lack of unanimous decision, difference in perception conflict arises at different stages of construction. If not managed, these conflicts tend to arise of dispute and claims. The dispute may be due to contract condition (addition/omission/misinterpretation), delay in project, financial issues between two parties, project management dispute i.e. related to man/material/design, construction, dispute or conflict during execution of the project, maintenance dispute and involvement of local political parties. In last few decades the probability of dispute occurrence have been seen in survey and investigation stage, design and tendering stage, execution stage, post construction/maintenance stages of a construction project [1–3, 4, 5, 6, 7]. The unsolved disputes turn into claim. The success and failure of any construction project depends upon the management of the claims. The claims are solved either by reconciliation, Dispute Review Expert (DRE), Dispute Review Board (DRB), Arbitration, etc. If the claim is not solved by any of these methods, then it goes to the Court of Law.

The objective of this present research is to identify the major causes of the disputes in construction industry, types of claims, their occurrence and relative important index

P. Sahu · P. K. Parhi
College of Engineering and Technology, Bhubaneswar, India
e-mail: pkparhi@cet.edu.in

D. K. Bera (✉)
KIIT Deemed To Be University, Bhubaneswar, India
e-mail: dberafce@kiit.ac.in

in different stages of construction projects, the settlement process for the claims occurred in different construction projects and recommendations for minimising the disputes in construction projects.

2 Literature Review

The claim in construction may be defined as a demand by one party to the contract, for compensation for damages caused by failure of the other party to fulfil his part of obligations. The causes of claims in construction are: claims due to delay, increase in price, change in work order, inclusive of extra item, damage, profit and loss and withholding of deposits, etc. [8, 9]. The delay factors due to delay in issuing drawings, change of work order, subcontractor or other vendor and late release of running bills and mobilisation advances may cause the delay claims in construction projects in India [10]. The causes of disputes in construction industry identified by Khekale and Futane [11] are incorrect ground data, faulty and cryptic contract language, deviations of work, unprofessional behaviour or approach by both party and unfair risk distribution. On legal bases, the claim classified as contractual claim, extra-contractual claim and Ex-Gratia. Contractual claims fall within the contract. Extra contractual claims have no ground to contract, but these claims are the result from transgression of contract. Ex-Gratia claims have relationship with existing contract, but as per contractor, additional charge is there due to sudden price increase. The sources of claims are loophole in documents of contract, delay in work done, modification of work by the owner, liquidated damage and inclement weather. Mohamed et al. [12] surveyed to know the dispute causes in three forms i.e. behavioural problems, contractual problems and operational problems. They ranked these factors according to relative importance and found that the most caused claims are time over run, payment delay, work order variation, imperfect contract, poor communication and coordination.

Time over run was the major effect of increase in claims in Oman [13]. To minimise the claims in such projects, the author suggested that owner should evaluate their managing capability [14, 9]. Best delivery plan should be chosen for fulfilling the objective and for high level coordination among the parties. The disputes can be resolved by prevention i.e. by allocation of fair contract risk, correcting clauses related to resolution of dispute and team building; negotiation; standing neutral i.e. with the help of DRB (dispute review board and DRA (dispute resolution adviser); binding resolution i.e. providing neutral arbitrator or by arbitration; and litigation [11]. Prevention, negotiation, neutral stand, non-binding and private binding solution and arbitration to implement in EPC contract are six alternative solutions for minimising the disputes and claims in construction projects [15].

3 Research Methodology

Conflicts and claims for construction projects are becoming most vital part in the field of civil engineering for a fare course of action. Literature review and opinions from experts having experience of more than 30 years are the sources to prepare questionnaire for this pilot survey. The questionnaire has four sections. First section contains personal and professional information of the respondent; second section is related to the causes of dispute, stages in which, the claims arise in the project; third section includes the total number of claims in different stages of construction and fourth section contains causes of claim, its weightage, the resolve process of the claim and suggestion from the experts to minimise the claim. The questionnaire had been sent in Google form to different stakeholders involved in construction projects. The questionnaire was sent to different contractors, owners (clients), consultants involved in construction projects across India. More than 100 responds were being collected for the analysis.

Chan and Kumaraswamy [16] method for finding "relative importance index" (RII) has been adopted to determine the relative ranking of factors [17] of causes of claims in different stages of construction.

$$\text{Relative Importance Index RII} = \sum W/(A*N)$$
$$= (5n5 + 4n4 + 3n3 + 2n2 + 1n1)/5n$$

where W is the weighting given to each factor by the respondent, ranging from 1 to 5, (n1, n2, n3, n4 and n5) are the number of respondents for weight 1, 2, 3, 4 and 5, respectively). A is the highest weight (i.e. 5) and N is the total number of samples. The range for RII is 0 to 1.

4 Data Analysis and Discussion

4.1 General Characteristics of Respondents and Projects

For current study, a pilot survey was conducted by taking respondents as owners or clients, contractors and consultants having vast experience in handling construction projects. The respondents included 41.4% owners, 37.9% contractors and 20.7% consultants. These respondents were associated with different types of construction projects. These projects included 44.8% building projects, 13.8% road constructions, 6.9% railway projects, 10.3% water resource projects, 13.8% bridge projects and 10.3% other type such as ash pond construction etc., The details are shown in Fig. 1. Both completed and ongoing projects were considered for the study as shown in Fig. 2. The projects taken for analysis were related to both Government and private projects. Some of the projects were from Odisha PWD, Odisha state

Types of project
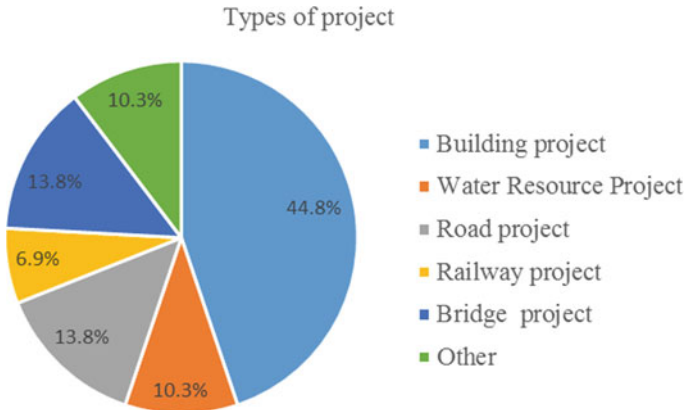
Fig. 1 Data collected from various projects

Fig. 2 Status of the projects
taken for survey

Status of the Projects
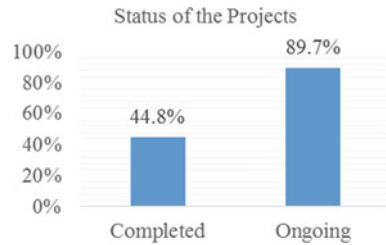
police housing and welfare corporation, THDC India Limited, Tehri, Uttarakhand, Heavy Water Plant Baroda, Department of Atomic Energy, Govt Of India, P R Dept. Bargarh, Rural works subdivision, Nimapara, Rail Vikash Nigam Ltd, Bhubaneswar, WRE Deptt Odisha, MR Construction, WhiteAnt Buildoneers Pvt Ltd, Consultorium Pvt. Ltd. M/S. Gupta & Co Vadodara-Gujrat, SM Consultant, Bhubaneswar (Project Management Consultant of RVNL) etc. The cost of the projects for survey varies from 50 lakhs to 5000Cr. The percentage of different types of project according to its cost is showing in Fig. 3.

4.2 Conflicts in Different Stages of Construction

Each construction project mainly consists of four stages i.e. survey and investigation stage, design and tendering stage, execution stage and post construction or maintenance stage. The total no of disputes or claims in each stage of construction project had been asked in the questionnaire. It was found that maximum conflicts were during execution stage. 55.2% of claims at the execution stage, 32% during

Cost of the project

10.3%

24.1%   48.3%

17.2%

- <10 Cr
- Between 10 Cr and 100 Cr
- Between 100 Cr and 1000 Cr
- >1000Cr

Fig. 3 Cost of the projects

Percentage of claim in different stages of construction project

5.7%

32.0%

55.2%

7.1%

- Survey and investigation Stage
- Design and Tendering Stage
- Execution Stage
- Post construction/Maintenance Stage
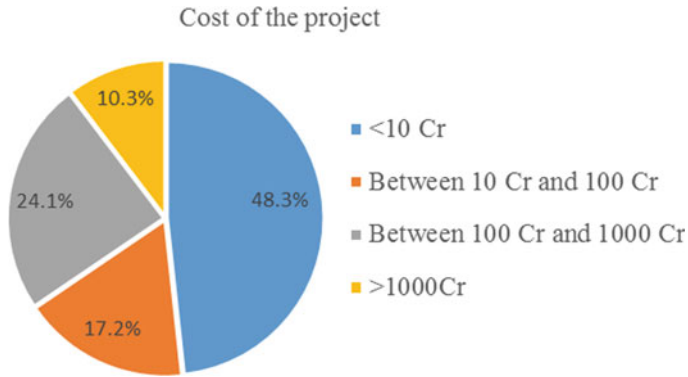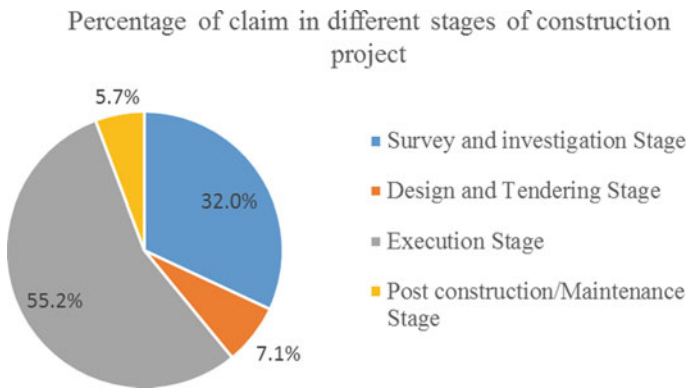
Fig. 4 Percentage of claims in different stages of construction

survey and investigation stage, 7.1% during design and tendering stage and 5.7% after completion of the work or maintenance stage are found as shown in Fig. 4

4.3 Types of Claims

In last few years, it has been seen that there is increse in claims in construction sector by either party which tends the deficiency in quality, cost over run and delay in delivery of the project [18]. In the current study, the claims were catagorised in to six groups for survey as shown in Fig. 5.
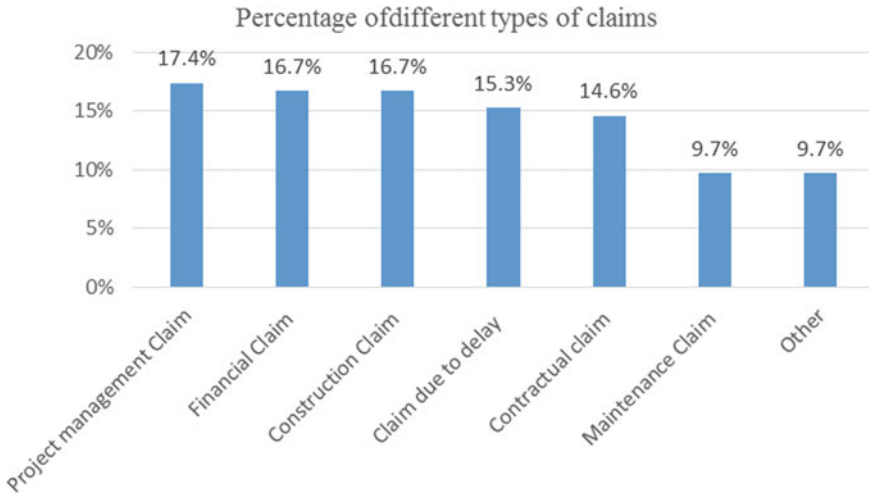
Fig. 5 Percentage of different types of claims

4.3.1 Contractual Claim

Contractual claim is related to construction contract agreement and arise by any of the party. This may be due to addition or omission of any clause, unforeseen circumstances, ambiguity clauses and insufficient information etc. In the current study 14.6% of total claims are contractual claims.

4.3.2 Financial Claim

In some construction projects financial claim arise due to late in supply of RA bill in which contractor suffers deficient in cash flow, additional of work, liquidated damage, sudden price hike in materials and delay in final payment etc. The present study shows 16.7% claims are financial claim.

4.3.3 Project Management Claim

Conflicts arise if there the resources of the project are not managed in proper way. Disputes related to drawings, man, material and machineries are very common for construction sector. Land dispute and problem in environmental clearance are the other major issues. If not handle properly, these disputes are converted to claim. From the survey these type of claims shares 17.4%.

4.3.4   Claim Due to Delay

Construction delays and claims are dependent to each other. Due to claim there is possibility of delay and also due to delay in construction or completion of project either party may claim for the loss. The reasons for delay in construction may be due to contractor, due to client, fault in design and drawings, late in supply of resources, price hike, environmental clearance, land dispute, natural calamities or political influence. 15.3% of total claims of this study are claim due to delay.

4.3.5   Construction Claim

During execution of work if any dispute arises and not solved at that time, it converts to claim. 16.7% claims of this study are related to the execution of the work. This claims affects the completion time.

4.3.6   Maintenance Claim (Post Construction)

After completion of all the work of the project by the contractor, the post construction claims arises. Failure to building code, poor work, defective materials, defect in design, physical damage after construction, final payment delay, delay in subcontractor payment etc. are the reasons for the post construction claims. The survey shows that 9.7% of total claims are post construction claims.

Some respondents mentioned some extra reasons for the claims which are not included in the above six types, such as force measures due terrorist affect by Maoist and involvement of local or political people. These reasons were included in other and contributes 9.7% claims of total.

Some more information had been collected from the stake holders, like major causes of claims as per owners are omissions of proper wordings in specific clauses of contract, unseen extra works, contractor not willing to do extra item of work due to dispute in agreement there by claiming extra cost, limitation of funds, land acquisition problem, shifting of electric utilities, financial issues, ego clash and differences in opinion on contract documents, Site condition for constructon, non Finalisations of balance payments, inadequete aminities of villages, price escalation due to delay and delay due to cash flow crisis of contractor, causing less deployment of manpower & machinery. As per contractors view the major claims are due to material cost escalation due delay in project execution, delay in completion, unavailability of materials, land dispute, delay in handing over problem free land, delay in project execution, change in layout and design, time extension, escalation, delay in payment to subcontractos, delay in final payment, delay in release of running bill, extra workdone, addition or omission of clauses in contract.

Table 1 Ranking of different types of claims as per RII

Types of claim	RII (%)	Rank
Contractual claim	28.97	5
Financial claim	68.28	2
Project management claim	71.03	1
Claim due to delay	55.17	4
Construction claim	57.24	3
Post construction or, maintenance claim	18.62	7
Other	19.31	6

4.4 Relative Important Index (RII) of Different Types of Claim

The respondents have given different weightage (1–5 scale) to the different types of claim in their project. The weightage has been given with respect to their effect on the time and cost overrun of the project. Form the data the relative important index of different types of claims are found and ranking has been done. Project management claims and financial claims affect the project in highest level. The RII values and ranking of different claims are shown in Table 1.

4.5 Resolution of Claim

As claim influences both time and cost overrun, it is required to be solved or settled as early as possible. Most of the claims in construction sector are settled in Reconciliation, if not it goes to next level for settlement i.e. to Dispute Review Expert (DRE). If the claim is not solved by DRE it goes to Dispute Review Board (DRB). If the parties are not satisfied with DRB, the claim is to go through Arbitration process for settlement. The claim goes to the Court of Law, if not settled by other four methods. The study shows that maximum claims were settled by reconciliation i.e. 69%, 13.8% by DRE, 10.3% by DRB, 3.4% through Arbitration and 3.4% were in at Court of law. Details are mentioned in Fig. 6.

5 Conclusion and Discussion

Analysis of claims in construction projects has been done from a field survey in questionnaire form which includes cost of project, status of project, disputes in different stages of project, types of claim, effect of the claim to time and cost overrun, and process of claim resolution. The ranking of different types of claim was done with respect to RII of each type. Data has been collected and interpreted for different

Type of Resolution of claim
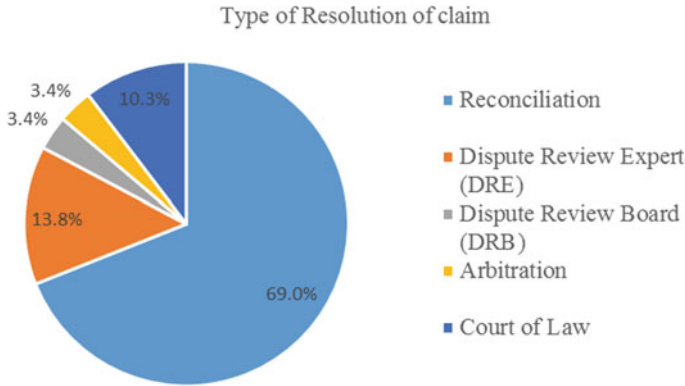
Fig. 6 Percentage of different types of resolution of claims

ongoing and completed projects. Maximum disputes identified in Execution stage i.e. more than 50%, in survey and investigation stage around 30% disputes found and in both Design, tender stage and post construction stage the conflicts were less than 10% each. Maximum claims are found in project management type i.e. 17.4% with respect to other types of claim.

With respect to RII value, ranking has been done. Project management claim and financial claims have more effect on time and cost of construction projects.

The survey shows most of the claims in construction sector resolved by reconcillation. 69% of claims of this study was solved by this process, 13.8% solved by Dispute Review Experts, 10.3% solved by Dispute Review Board, 3.4% through Arbitration and 3.4% goes to Court of law where some claims are still pending.

6 Recommendation by Experts

Special recomodations has been extracted from response of the stakeholders as mentioned below to minimise the claim.

- Contract documents must be outsourced to expert agency and must be reviewed inhouse.
- Financial health of contractors must be checked prior to bidding.
- Better liasoning with different departments for getting clearances.
- Drawing design and scope of work should be finalized before award of work so that no addition or alternation required during execution stage.
- Fixing of land boundary is much more important before execution of any project work to complete the project in schedule time without any variation of cost and extension of time.
- Work front should be released in time.

- Site condition should be properly assessed during estimation stage to avoid changes in design and layout.
- Going according to the agreement.
- If there is actual workdone falls behind as per schedule, proper bar chart and planning should be prpared to complete the project in time.
- Proper monitoring from beginning till end.
- There shouldn't be limitation of funds.
- Work should be done in a team for a win win situation among contractors consultants and clients
- More practical approach should be adopted than theoritical research.
- Careful in preplan and focus on the actual goals and probable hinderances like land issue n public participation on the planning process should be made mandatory.
- Use of modern technology and optimum use of local available materials should adopted.
- Construction in proper should be initiated only after land acquisition and rehabilitation and evacuation
- Both parties should obey the guidelines and payment should be given in proper time.
- Any dispute arises in a project should be amicably settled within contractor, consultants and client leaving aside the egos for better interest of project delivery in time n quality.

References

1. Pandey A, Chaudhary PK, Das BB (2021) Productivity analysis of shuttering works for sewage treatment plant. In: Select proceedings of TMSF 2019. Springer Publications Pte. Ltd
2. Akhil RP, Das BB (2019) Cost reduction techniques on MEP projects. In: Select proceedings of ICSCBM 2018. Springer Nature Singapore Pte Ltd., pp 495–517
3. Hegde AL, Jain A, Das BB (2021) Resource buffers in construction projects. In: Select proceedings of TMSF 2019. Springer Publications Pte. Ltd
4. Paul B, Tondihal S, Das BB (2021) Safety stock in inventory management and wastage analysis at construction sites. In: Select proceedings of TMSF 2019. Springer Publications Pte. Ltd
5. Upadhya PR, Das MS, Das BB (2021) Multi criteria decision making approach for selecting a bridge superstructure construction method. In: Select Proceedings of TMSF 2019. Springer Publications Pte. Ltd.
6. Reddy CP, Das BB (2019) Methods to monitor resources and logistic planning at project sites. In: Select proceedings of ICSCBM 2018. Springer Nature Singapore Pte Ltd., pp 793–802
7. Sushant S, Prince S, Das BB (2021) Developing a standard template for activity linkage and resource estimation of MEP works. In: Select proceedings of TMSF 2019. Springer Publications Pte. Ltd
8. Aziz BF, Kumar DS (2015) Impact of uncertainty factors in construction projects. Int J Adv Res Sci Eng 4(01):602–609
9. Shah A, Bhatt R, Bhavsar JJ (2014) Types and causes of construction claims. Int J Eng Res Technol 3(12):732–735
10. Chaphalkar N, Lyer KC (2014) Factors influencing decision on delay claims in construction contracts for Indian Senario. Aust J Construct Econ Build 14(1):32–44

11. Khekale C, Futane N (2015) Management of claims and disputes in construction industry. Int J Sci Res 4(5):848–856
12. Mohamed HH, Ibrahim AH, Soliman AA (2014) Reducing construction dispute through effective claims management. Am J Civil Eng Arch 2(6):186–196
13. Mohsin MA (2012) Claim analysis of construction projects in Oman. Int J Adv Sci Eng Inform Technol 2(2):73–78
14. Moza A, Poul VK (2018) Analysis of claims in public works construction contracts in India. J Construct Develop Countries 23(2):7–26
15. Zhow W (2019) The root cause of claims and disputes in construction industry and solution analysis. PM World J VIII(V):1–18
16. Chan DWM, Kumaraswamy MM (1997) A comprehensive study of causes of time overruns in Hong Kong construction projects. Int J project Manage 15(1):5563
17. Gunduz M, Nielsen Y, Ozdemir M (2013) Quantification of delay factors using the relative importance index method for construction projects in Turkey. J Manage Eng Am Soc Civil Eng 29(2):133–139
18. Naji HI (2017) Analysis of claims causing the quality deficiency and time overruns in construction projects. Int J Appl Eng Res 12(24):15347–15357
19. Qershi AMT, Kishore R (2018) Leading factors contributing to the generation of claims in Indian construction industry-consultant's perception. Civil Eng Res J 4(4)

Improvement of Concrete Strength by *Bacillus Cereus* Bacterium

Check for updates

S. Jena, B. Basa, and K. C. Panda

1 Introduction

When it was discovered that, in bacterial species, formation of crystal is a very natural phenomenon, bacteria have been used for useful purposes in sectors like civil and geological engineering, oil industries etc. [1]. A few instances of these applications are: blocking of rock for qualitative and quantitative increment in recovery of oil and preservation of stones [2–8]. These applications found carcinogenic bacteria to be useful, because they produced calcium carbonate or otherwise known as biologically produced calcium carbonate precipitation [9, 10]. It has been found that usage of self-healing microbiological increases the durability of concrete and helps in avoiding crack formation [11–15]. Twenty-first century is rightly said as the era of drastic infrastructural development. Concrete has earned its place as the most widely used ingredient for development. Even though there are a lot of reasons like availability, cost effectiveness for heavy usage of concrete in infrastructure development, modern day engineers found various drawbacks of it as well. One of the worst disadvantages of concrete is its low resistance to crack formation. Even a single crack if formed in concrete, it is never self-healed, rather it leads to corrosion and decrease in strength. Crack formation in concrete has been a reason of headache for the infrastructural sectors, because along with crack formation, comes the corrosion of reinforcement, that shortens the self life activity of concrete [16–21]. Cracks lead to the penetration of water and chloride which affects the concrete quality adversely [22–27]. Therefore, repairing the concrete as soon as possible is the wise decision. Once the cracks are formed it is quite impossible to heal them completely due to the penetration limit

S. Jena (✉) · B. Basa
Department of Civil Engineering, ITER, S'O'A (Deemed To Be University), Bhubaneswar, India

K. C. Panda
Department of Civil Engineering, GCE, Kalahandi, , Bhawanipatna, India

and the more time that the cracks remained unhealed, the more money they cause for their repair, which is not so economic.

As a solution to all these problems, comes the innovation of self-healing concrete that can be healed automatically, after the cracks are formed [28]. Concrete, to some extent, is capable of blocking the micro cracks formation, as it is autogenous healing. This method works by the mechanism of hydration of un-hydrated micro particles inside the concrete. This can also be done by the method of addition of some specific agents of healing [29]. But most of the components used in self-healing concrete are chemical bodies. Self-healing mechanism is now the most useful and the most effective mechanism for healing the cracks formed in the concrete. So, to get an environment friendly solution to the crack formation problem, the use of microbiological method and usage of microorganisms were taken into account. So far, there are mostly three types of bacterial metabolic activity which precipitate calcium carbonate successfully. With the help of enzymes, hydrolysis of urea is the basic one [30, 31]. Next one is oxidation of organic carbon [32–35]. Under anoxic condition, process of denitrification is the third one [36]. From all the mechanisms, hydrolysis of urea is the easiest and efficient one to carry out. Ramakrishnan et al. [37] first introduced the theory about the employment of microbiologically induced calcite ($CaCO_3$) precipitation by using it in crack reparation of concrete. When bacteria are introduced in concrete, layers of calcite which are water resistant or impermeable are seen on the concrete surface. For observing how bacteria affects concrete's strength, numerous tests have been performed by adding different kinds of microorganisms [38–41]. Tests were executed in the cement mortar by the addition of *Bacillus pasteurii* with various concentrations. As there was adequate amount of organic substances, after 28 days of curing there was 18% increase in compressive strength [20]. With the help of Shewanella species (thermophilic anaerobic bacteria) microorganism, 25–30% increase in compressive strength is obtained after a span of 28 days [39]. There was10% increment in strength with the combination of two bacteria i.e. *Bacillus cohnii* and *Bacillus pseudofirmus* [32]. With the addition of *Bacillus cohnii* bacteria upto definite cell concentration, strength increases. After that strength decreases [42]. When *Bacillus sp. CT-5* bacteria is added with mortar, the increase in compressive strength is 36% [43]. With both live as well as dead bacteria cell of *Sporosarcina Pasturii*, there was upto 10% increase in strength [44]. Concrete which contains fly ash as partial replacement of cement (10%, 20% and 30%), causes increment in strength in the presence of *Sporosarcina pasteurii* bacteria (10^3, 10^5 and 10^7 cells/ml). It may be due to the blockage of pores caused by the bacterial cells deposition [45]. There is 30.76, 46.15 and 32.21% rise in compressive strength and 13.75,14.28 and 18.35% increase in split tensile strength after 3,7 and 28 days in the presence of *Bacillus Sphaericus* bacteria (dormant condition) [46]. By using *Bacillus Pasturii* and *Bacillus Cereus*, it is seen that with *Bacillus Pasturii* increment in compressive strength was 29% and with *Bacillus Cereus* strength increases up to 38% [47]. With the use of *Bacillus subtilis* (10–10^6 cell/ml cell concentration), optimum strength was obtained at 10^5 cells/ml. Calcite formation ability of bacteria must be the reason of blockage of pores of concrete structure, which is eventually the reason for strength increment [48]. Two carrier compounds i.e. Light weight aggregate and Graphite

Nano platelets along with *Bacillus subtilis* were used in concrete. With respect to control specimen, there is 9.8% increase in strength when Graphite Nano platelets are used and 12% of increase in strength when Light weight aggregate are used [49]. The main reason of using self-healing concrete is its ability to recognize any damage in its initial stage and heal it in time.

2 Details of Experiment

2.1 Materials

Ordinary Portland cement (OPC) of Ramco make OPC-43 grade conforming to IS: 8112-1989 was used [50]. Table 1 represents the evaluated properties of cement.

In this particular research, the coarse aggregate of size ranging from 10 to 20 mm was used. Table 2 showcases the physical properties of fine and coarse aggregates. MCC, Pune supplied bacteria samples of *Bacillus cereus* which were present in freeze dried condition is presented in Fig. 1.

Table 1 Physical characteristics of cement

Characteristics	Test value
Normal consistency	32%
Initial setting time	40 min
Final setting time	120 min
Fineness	340
Compressive strength	
3 days	30 Mpa
7 days	43 Mpa
28 days	51 Mpa

Table 2 Physical attributes of NFA and NCA

Characteristics	Test value (as per IS:383–1970) [51]	
	NFA	NCA
Fineness modulus	2.73 (zone II)	6.92
Water absorption	0.85	0.24
Specific gravity	2.69	2.78
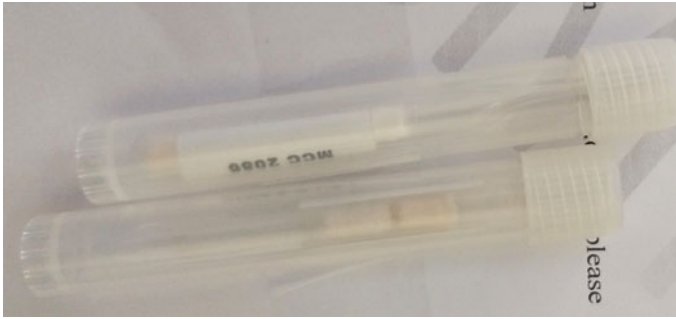
Fig. 1 Freeze dried bacteria

Table 3 Mix identity along with mix quantity of concrete (per m^3)

Identity	MB0	MB1	MB2	MB3	MB4	MB5	MB6
Cement (kg)	432.55	432.55	432.55	432.55	432.55	432.55	432.55
NCA (kg)	1226	1226	1226	1226	1226	1226	1226
NFA (kg)	628	628	628	628	628	628	628
Water (kg)	186	186	186	186	186	186	186
Bacteria cells (cells/ml)	0	10	10^2	10^3	10^4	10^5	10^6

2.2 Mix Proportion

According to standard specification IS: 10,262-1982, concrete (M30 grade) was outlined [52]. The mix proportion ratio that was used for the recent study is 1: 1.491: 2.690. In this study, seven varieties of sample concrete specimens in total were produced having six different bacterial concentrations, out of which, one is concrete specimen without bacterial mixture and other six mixtures are having *Bacillus Cereus* bacterium species. For the current work, Bacterial CFU (colony forming unit) of 10 cells/ml each time increasing by 10 times up to 10^6 cells/ml was used. Table 3 shows the concrete samples' mix identity along with mix calculation.

2.3 Bacterial Culture

For this research, the bacterial species that was used was of *Bacillus Cereus*. It was cultivated in agar. After the cultivation, a readymade Nutrient Hi Veg broth was used that helped in growth of bacteria. Bacterial cell concentration was calculated with the help of spectrophotometer. Prepared bacterial solution is shown in Fig. 2.

2.4 Casting and Testing of Specimen

The concrete mixer contained various materials such as OPC, NCA, NFA. These materials were measured and mixed together in dried condition until a homogeneous mixture is obtained. After that water and bacteria were added as per requirement. A slump test was done after the mixture was prepared. A table vibrator was used to vibrate the concrete samples and then they were cast into steel moulds. After an interval of 24 h, specimens were demoulded. After that, the concrete samples were let to cure for intervals of 7, 14 and 28 days.

3 Hardened Concrete Test Results

3.1 Compressive Strength

The compressive strength of concrete specimens is measured after 7, 14, 28 days' time intervals. A comparative study is done between control concrete and concrete mixed with *Bacillus cereus* for measuring compressive strength and the result is showcased in Fig. 3.

Addition of bacteria results in increased compressive strength with all cell concentration. But maximum strength is achieved with 10^5 cells/ml concentration of *Bacillus Cereus.* After adding *Bacillus Cereus* of 10^5 cells/ml when the strength is measured

Fig. 3 Analogy of
compressive strength of
control concrete and concrete
mixed with *Bacillus cereus*
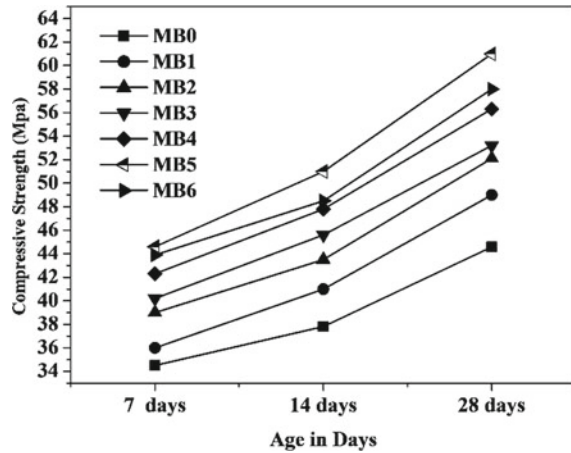
after 7, 14, 28 days the calculated value is increased 29.27%, 34.88% and 36.80% respectively. But with 10^6 cells/ml when the strength is measured after 7, 14, 28 days the value is found to be increased 27.24%, 28.27% and 30.07% respectively. The strength gradually increases upto 10^5 cells/ml and then decreases. The decreased value of strength obtained at 10^6 is still higher than that obtained at 10^4 cells/ml. Overall concrete added with *Bacillus Cereus* provides more strength than control concrete.

3.2   Split Tensile Strength

The split tensile strength of concrete specimens is measured after 7, 14, 28 days' time intervals. A comparative study is done between control concrete and concrete mixed with *Bacillus cereus* for measuring split tensile strength and the result is showcased in Fig. 4.

Addition of bacteria results in increased strength with all cell concentration. But maximum compressive strength is achieved with 10^5 cells/ml concentration of *Bacillus Cereus*. After adding *Bacillus Cereus* of 10^5 cells/ml when the strength is measured after 7, 14, 28 days the calculated value is increased 40.57%, 33.33% and 20.38% respectively. But with 10^6 cells/ml when the strength is measured after 7, 14, 28 days the value is found to be increased 33.73%, 28.33% and 16.37% respectively. The strength gradually increases upto 10^5 cells/ml and then decreases. The decreased value of strength obtained at 10^6 is still higher than that obtained at 10^4 cells/ml. Overall concrete added with *Bacillus Cereus* gives better strength as compared to control concrete.

Fig. 4 Analogy of split tensile strength of control concrete and concrete mixed with *Bacillus cereus*
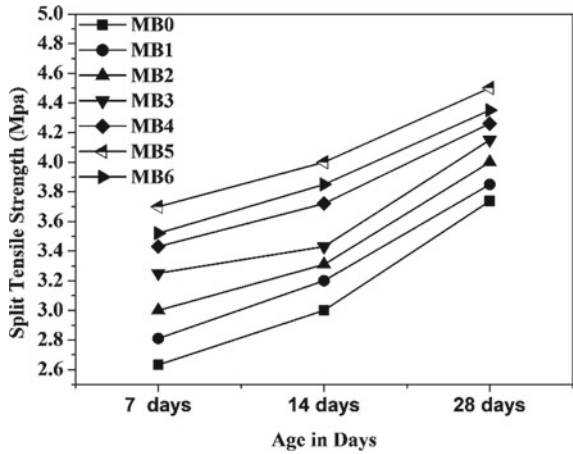
3.3 Flexural Strength

The flexural strength of concrete specimens is measured after 7, 14, 28 days' time intervals. A comparative study is done between control concrete and concrete mixed with *Bacillus cereus* for measuring flexural strength and the result is showcased in Fig. 5.

Addition of bacteria results in increased strength with all cell concentration. But maximum compressive strength is achieved with 10^5 cells/ml concentration of *Bacillus Cereus*. After adding *Bacillus Cereus* of 10^5 cells/ml when the strength is measured after 7, 14, 28 days the calculated value is increased 41.37%, 35.93% and 31.42% respectively. But with 10^6 cells/ml when the strength is measured after 7, 14, 28 days the value is found to be increased 34.48%, 34.06% and 26.28% respectively.

Fig. 5 Analogy of flexural strength of control concrete and concrete mixed with *Bacillus cereus*
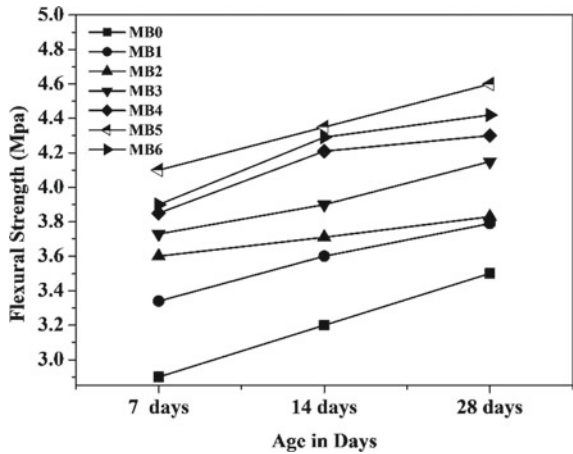
The strength gradually increases upto 10^5 cells/ml and then decreases. The decreased value of strength obtained at 10^6 is still higher than that obtained at 10^4 cells/ml. Overall concrete added with *Bacillus Cereus* provides more strength than control concrete.

4 Conclusions

Based on the above results following conclusions may be drawn.

- When a comparison is done between Split tensile strength, flexural strength and compressive strength of concrete containing bacterial specimen and control mix, better results are seen in case of concrete having *Bacillus cereus* bacterial species.
- Compressive, flexural strength along with split tensile strength of concrete show noticeable increment when cells concentrations of bacterial species are increased gradually increased from 10 cells/ml to 10^5 cell/ml, 10 times at a time. Increment in strength is shown up to 10^5 cells/ ml cell concentration and decrement at 10^6 cells/ml.
- Concrete shows increment in strength upto specific cell concentration of bacteria, and gradually decreases after that.
- Highest compressive strength, flexural and split tensile strength is obtained when cell concentration of bacteria is 10^5 cells/ml.
- *Bacillus cereus* bacterial species can form calcium carbonate precipitate that plugs the path of pores and small, big cracks, therefore when added in concrete give best result and show optimal increment in strength.

References

1. de Muynck WD, de Belie N, Verstraete W (2010) Microbial carbonate precipitation in construction materials: a review. EcolEng 36(2):118–136
2. Tiano P, Biagiotti L, Mastromei G (1999) Bacterial biomediated calcite precipitation for monumental stones conservation: methods of evaluation. J Microbiol Meth 36(1–2):139–145
3. Gollapudi UK, Knutson CL, Bang SS, Islam MR (1995) A new method for controlling leaching through permeable channels. Chemosphere 30(4):695–705
4. Finnerty WR, Singer ME (1983) Microbial enhancement of oil recovery. Nat Biotechnol 1:47–54
5. Castanier S, Le Metayer-Levrel G, Perthuisot JP (1999) Ca-carbonates precipitation and limestone genesis—the microbiogeologist point of view. Sediment Geol 126(1–4):9–23
6. De Muynck W, K Verbeken, De Belie N, Verstraete W (2010) Influence of urea and calcium dosage on the effectiveness of bacterially induced carbonate precipitation on limestone. Ecol Eng 36(2):99–111
7. Mitchell JK, Santamarina JC (2005) Biological considerations in geotechnical engineering. J Geotech Geoenviron Eng 131(10):1222–1233
8. MacLeod FA, Lappin-Scott HM, Costerton JW (1988) Plugging of a model rock system by using starved bacteria. Appl Environ Microbiol 54(6):1365–2137

9. Rodriguez-Navarro C, Rodriguez-Gallego M, Chekroun KB, Gonzalez-Muñoz MT (2003) Conservation of ornamental stone by myxococcus xanthus-induced carbonate biomineralization. Appl Environ Microbiol 69(4):2182–2193

10. Hammes F, Verstraete W (2002) Key roles of pH and calcium metabolism in microbial carbonate precipitation. Rev Environ Sci Biotech 1(1):3–7

11. Bachmeier KL, Williams AE, Warmington JR, Bang SS (2002) Urease activity in microbiologically-induced calcite precipitation. J Biotechnol 93(2):171–181

12. Achal V, Mukherjee A (2015) A review of microbial precipitation for sustainable construction. Constr Build Mater 93:1224–1235

13. Siddique R, Chahal NK (2011) Effect of ureolytic bacteria on concrete properties. Constr Build Mater 25(10):3791–3801

14. Wang JY, Ersan YC, Boon N, Belie ND (2016) Application of microorganisms in concrete: a promising sustainable strategy to improve concrete durability. Appl Microbiol Biot 100(7):2993–3007

15. Bang SS, Lippert JJ, Yerra U, Mulukutla S, Ramakrishnan V (2010) Microbial calcite, a bio-based smart nanomaterial in concrete remediation. Int J Smart Nano Mater 1(1):28–39

16. Snehal K, Das BB (2019) Mechanical and permeability properties of hybrid fibre reinforced porous concrete. Indian Concrete J 93(1):54–59

17. Snehal K, Das BB, Kumar S (2020) Influence of integration of phase change materials on hydration and microstructure properties of nano silica admixed cementitious mortar. J Mater Civil Eng ASCE 32(6)

18. Snehal K, Das BB (2020) Effect of phase-change materials on the hydration and mineralogy of cement mortar. In: Proceedings of the institution of civil engineers-construction materials, pp 1–11

19. Das BB, Kondraivendhan B (2012) Implication of pore size distribution parameters on compressive strength, permeability and hydraulic diffusivity of concrete. Construct Build Mater 28(1):382–386

20. Godbole KM, Sawant PH, Das BB, Dhanuskar JR (2015) Prediction of service life of concrete structure from half-cell potentiometer data—validation based on case study. Int J Appl Eng Res 10(14):34420–34427

21. Sumukh EP, Goudar SK, Das BB (2021) Predicting the service-life of reinforced concrete by incorporating the experimentally determined properties of steel-concrete interface and corrosion. Recent trends in civil engineering. Springer Publications, pp 399–417

22. Snehal K, Das BB, Archana Dinesh T (2018) Experimental investigation on the influence of phase change material (pcm) on the properties of cement mortar. In: 4th UKIERI concrete congress-concrete: the global builder

23. Snehal K, Das BB (2021) Application of Andreassen and modified andreassen model on cementitious mixture design: a review. Recent developments in sustainable infrastructure. Springer, pp 729–750

24. Sumukh EP, Goudar SK, Das BB (2020) A review on the properties of steel-concrete interface and characterization methods. In: Select proceedings of SMTS 2019. Springer Publications Pte. Ltd., pp 167–202

25. Farsana C, Das BB, Snehal K (2020) Influence of fineness of mineral admixtures on the degree of atmospheric mineral carbonation. Smart technologies for sustainable development. Springer Publications, pp 118–136

26. Goudar SK, Das BB, Arya SB (2019) Combined effect of marine environment and pH on the impedance of reinforced concrete studied by electrochemical impedance spectroscopy. Sustain Construct Build Mater 635–649

27. Snehal K, Das BB, Akanksha M (2020) Early age, hydration, mechanical and microstructure properties of nano-silica blended cementitious composites. Construct Build Mater 233

28. Wu M, Johannesson B, Geiker M (2012) A review: self-healing in cementitious materials and engineered cementitious composite as a self-healing material. Constr Build Mater 28(1):571–583

29. Huang HL, Ye G, Qian CX, Schlangen E (2016) Self-healing in cementitious materials: materials, methods and service conditions. Mater Des 92:499–511
30. Wang J, Dewanckele J, Cnudde V, van Vlierberghe S, W Verstraete, De Belie N (2014) X-ray computed tomography proof of bacterial-based self-healing in concrete. Cem Concr Compos 53(7):289–304
31. Bang SS, Galinat JK, Ramakrishnan V (2001) Calcite precipitation induced by polyurethane-immobilized *Bacillus pasteurii*. Enzyme Microb Technol 28(4–5):404–409
32. Ramachandran SK, Ramakrishnan V, Bang SS (2001) Remediation of concrete using micro-organisms. ACI Mater J 98(1):3–9
33. Jonkers HM (2007) Self-healing concrete: a biological approach. In: Van der Zwaag S (ed) Self-healing materials: an alternative approach to 20 centuries of material science. Springer Inc., The Netherlands, pp 195–204
34. Jonkers HM, Thijssen A, Muyzer G, Copuroglu O, Schlangen E (2010) Application of bacteria as self-healing agent for the development of sustainable concrete. Ecol Eng 36(2):230–235
35. Luo M, Qian CX, Li RY (2015) Factors affecting crack repairing capacity of bacteria-based self-healing concrete. Constr Build Mater 87:1–7
36. Luo M, Qian CX (2016) Influences of bacteria-based self-healing agents on cementitious materials hydration kinetics and compressive strength. Constr Build Mater 121:659–663
37. Ersan YC, Verbruggen H, De Graeve I, Verstraete W, De Belie N, Boon N (2016) Nitrate reducing CaCO3 precipitating bacteria survive in mortar and inhibit steel corrosion. Cem Concr Res 83:19–30
38. Ramakrishnan V, Ramesh KP, Bang SS (2001) Bacterial concrete. In: Smart materials and MEMS. International Society for Optics and Photonics, pp 168–176
39. Achal V, Mukherjee A, Reddy MS (2011) Microbial concrete: way to enhance the durability of building structures. J Mater Civ Eng 23:730–734
40. Ghosh P, Mandal S, Chattopadhyay B, Pal S (2005) Use of microorganism to improve the strength of cement mortar. Cement Concrete Res 35:1980–1983
41. Jena S, Basa B, Panda KC (2020) Effect of *Bacillus cohnii* bacteria on the properties of concrete. In: Recent developments in sustainable infrastructure: select proceedings of ICRDSI 2019. Springer, pp 597–606
42. Jena S, Basa B, Panda KC (2020) Bacterial concrete for the development of sustainable construction—a review. In: Recent trends in civil engineering: select proceedings of ICRTICE 2019. Springer, pp 587–600
43. Achal V, Pan X, Özyurt N (2011) Improved strength and durability of fly ash-amended concrete by microbial calcite precipitation. Ecol Eng 37:554–559
44. Erşan YÇ, Da Silva FB, Boon N, Verstraete W, De Belie N (2015) Screening of bacteria and concrete compatible protection materials. Construct Build Mater 88:196–203
45. Chahal N, Siddique R, Rajor (2012) Influence of bacteria on the compressive strength, water absorption and rapid chloride permeability of fly ash concrete. Construct Build Mater 28:351–356
46. Gavimath C, Mali B, Hooli V, Mallpur J, Patil A, Gaddi D, Ternikar C, Ravishankera B (2012) Potential application of bacteria to improve the strength of cement concrete. Int J Adv Biotechnol Res 3:541–544
47. Maheswaran S, Dasuru S, Murthy ARC, Bhuvaneshwari B, Kumar VR, Palani G, Iyer NR, Krishnamoorthy S, Sandhya S (2014) Strength improvement studies using new type wild strain *Bacillus cereus* on cement mortar. Curr Sci 50–57
48. Jena S, Basa B, Panda KC, Sahoo NK (2020) Impact of Bacillus subtilis bacterium on the properties of concrete. Mater Today Proc
49. Khaliq W, Ehsan MB (2016) Crack healing in concrete using various bio influenced self-healing techniques. Construct Build Mater 102:349–357
50. IS: 8112 (1989) Indian standard, 43 grade ordinary portland cement specification, (First Revision). Bureau of Indian Standards, Manak Bavan, 9 Bahadur Shah Zafar Marg, New Delhi, India

51. IS: 383 (1970) Indian standard specification for coarse and fine aggregates from natural sources for concrete, (Second Revision). Bureau of Indian Standards, New Delhi
52. IS: 10262 (1982) Recommended guidelines for concrete mix design. Bureau of Indian Standards, New Delhi, India

Effect of Mechanical and Chemical Activation of Fly Ash on the Properties of Fly Ash Bricks

Zulker Nain, Bibhu Prasad Nayak, and Sudeep Kumar Patel

1 Introduction

Fly ash is a byproduct that results from the burning of pulverized coal in electric power generating plants. Production of coal waste (slag and FA) from industrial processes is increasing rapidly, and every year more than 365 million tons of FA is produced worldwide. According to the report of [1], about 196.44 million tons of FA generated in the year 2017–18 from 167 thermal power stations on which 131.87 million tons (67% of total generation) of FA could be used for various purposes. About 9.01% of total utilization was used for manufacturing of brick.

Fly ash utilization in the field of civil engineering can cause several environmental benefits includes; (i) reduction in amount of green house and other adverse gases emission by simply replace or displace the use of cement [4, 16] (ii) conservation of other natural resources and materials (iii) reduction in amount of disposed coal products [2] (iv) improving concrete durability and life span of the structures [10, 11].

Recently many works upon the use of FA in the field of civil engineering has been reported. Efficient, affordable and eco-friendly products are the main priority of these researches. Application of FA products like geopolymers, lightweight concrete, mineral filler for asphalt roads, Soil stabilization, waste stabilization/treatment etc. are being the major step towards the ultimate success in this field. Among all geopolymers production using FA was a great achievement as it helps to minimize the environmental threats and shows cementitious behavior simultaneously. It is an inorganic polymeric material formed under ambient curing temperature followed by chemical reaction between alumino-silicate oxides and alkali metal silicate solutions under highly alkaline conditions. The most proposed mechanism for formation of geopolymer contains four steps moving in a parallel direction (i) dissipation of Si and Al from the aluminosilicate sources in presence of highly alkaline aqueous solution,

Z. Nain (✉) · B. P. Nayak · S. K. Patel
Silicon Institute of Technology, Sambalpur, Odisha, India

(ii) formation of oligomers species (geopolymers precursors) consisting of polymeric bonds of Si–O–Si and/or Si–O–Al type, (iii) formation of three-dimensional polymeric framework during polycondensation of oligomers, (iv) constitution of bond of undissolved solid particles within the geopolymeric network and hardening of the whole network into solid polymeric structure.

Geopolymerization process depends on many parameters including chemical and mineralogical composition of source material, curing procedure, dosage of alkali activator, concentration of alkaline solution etc. There are several references that define the importance of the parameters while going through geopolymerization process. Many researchers [3, 5, 12, 13, 15] conducted the study upon the change in mechanical activation of FA keeping respectable alteration in other variables during geopolymerization and found that increasing the fineness of FA is unquestionably an easiest way to heighten and control reactivity [12–14].

Chemical activation is also considered as a significant method in order to change the reactivity of FA. It can be done by several method such as alkali activation, sulphate activation, composite activation and activation by high molecular materials. Among all of them alkali activation is most compatible and easier to perform by the helps of reagent like NaOH, KOH etc. Extensive research in this field has been carried out by several authors [6–8] throughout the world and found that the increase in concentration of NaOH increases the compressive strength of the product while maintaining the solid to liquid and NaOH to Na_2SiO_3 ratio taking other value as constant. The addition of Sodium Silicate to Sodium Hydroxide helps to enhance the reaction between the source material (FA) and the solution and hence used for geopolymerization process.

Lime utilization while producing FA brick is a traditional process. It helps to the bind the particles of bricks and hence suggested by IS 12894: 2002. Musmade et al. [9] have broached the compressive and tensile behavior of lime added geopolymer concrete by casting $150 \times 150 \times 150$ mm FA cubes with 3 categories of lime (quick lime, slaked lime and hydrated lime) at different percentages such as 5%, 10%, 15%, 20% and 25%. Chemical activation is done for the geopolymerization process. Among all of them the mix containing 10% slaked lime shows maximum compressive strength with respect to the load.

Hence, this experiment targets towards the analysis on the properties of FA brick produced by geopolymerization introducing several variables like percentage of lime activation, percentage of mechanical activation and percentage of chemical activation etc.

2 Materials

The materials used in this investigation include FA, sand, lime, Sodium Silicate and sodium hydroxide. All the materials were procured from the local areas nearer to Sambalpur.

FA used in this study was low calcium class-F unprocessed type obtained from Hindalco power and steel, Sambalpur. It has density of 1300 kg/m^3 and Specific gravity of 2.42. This FA was mechanically activated by grinding with a ball mill to three different fineness values such that 32%, 18% and 6% of total FA mass retains on 40-micron sieves. The chemical composition of FA used is listed in Table 1. Similarly, the sand and slaked lime was also procured from the local market. The sand used here was fine graded river bed sand having fineness modulus of 2.18, Specific gravity of 2.64 and water absorption of 0.22%. Further, the sodium silicate solution was prepared by mixing distilled water maintaining a ratio of SiO_2 to Na_2O as 2.10 and sodium hydroxide solution was prepared by dissolving the commercial grade sodium hydroxide pellets with 98% purity in distilled water. The concentration of the NaOH solution was taken 8 M, 11 M and 14 M for this experiment. This alkaline solution was prepared one day prior to the manufacturing of the brick.

3 Experimental Procedure

This investigation is divided into two stages. In the first stage all the three mechanically activated FA samples were activated with 5%, 10% and 15% of lime. Hence, totally nine numbers of mixes were prepared to check the optimum proportion. Further, the optimum level of lime was kept constant at 10% and the FA samples with three different mechanical activations were activated with alkali solution of three different NaOH molarities i.e. 8 M, 11 M and 14 M. The ratio of NaOH solution and Na_2SiO_3 solution was maintained at 0.4. Hence another nine numbers of mixes were prepared to achieve the optimum mix having superior properties. For, all the 18 mixes the proportion of sand to FA was maintained at 3.0 by weight. The detailed mix proportion is presented in Table 2. The data presented in Table 2 represent the quantity of raw materials required for the preparation of 10 numbers of 0.23 m × 0.11 m × 0.07 m size bricks in each batch.

The naming of the samples is done in such a way that it can be easily identified. In the naming the letter "L" represents the levels of lime activation. It has three levels i.e. 5%, 10% and 15% represented by the digit 1, 2, and 3 in Table 2. Similarly, "M" represents the levels of mechanical activation. It has three levels i.e. with fineness of 32%, 18% and 6%. These are represented with digits 1, 2, and 3 in Table 2. Again, "N" represents the levels of chemical activation. It has four levels i.e. no chemical activation, activation with 8 M alkaline solution, activation with 11 M alkaline solution and activation with 14 M alkaline solution. These are represented by the digits 0, 1, 2 and 3 in Table 2. For example, LMN120 indicates the lime

Table 1 Composition of fly ash

Composition	SiO$_3$	Al$_2$O$_3$	Fe$_2$O$_3$	CaO	Na$_2$O	K$_2$O	TiO$_2$	MgO	P$_2$O$_5$	SO$_3$	LOI
Percentage	53.36	26.49	10.86	1.34	0.37	0.80	1.47	0.77	1.43	1.70	1.39

Table 2 Mix design

Samples	Fly ash (kg)	Sand (kg)	Lime (kg)	Water content	Wt. of NaOH and water for solution		Wt. of Na_2SiO_3 and water for solution	
					Water (Lt)	NaOH (kg)	Water (Lt)	Na_2SiO_3 (kg)
LMN110	11.178	33.533	0.559	4.024				
LMN120	11.178	33.533	0.559	4.024				
LMN130	11.178	33.533	0.559	4.024				
LMN210	11.178	33.533	1.118	4.024				
LMN220	11.178	33.533	1.118	4.024				
LMN230	11.178	33.533	1.118	4.024				
LMN310	11.178	33.533	1.677	4.024				
LMN320	11.178	33.533	1.677	4.024				
LMN330	11.178	33.533	1.677	4.024				
LMN211	11.178	33.533	1.118		0.871	0.279	1.437	1.437
LMN212	11.178	33.533	1.118		0.798	0.351	1.437	1.437
LMN213	11.178	33.533	1.118		0.737	0.413	1.437	1.437
LMN221	11.178	33.533	1.118		0.871	0.279	1.437	1.437
LMN222	11.178	33.533	1.118		0.798	0.351	1.437	1.437
LMN223	11.178	33.533	1.118		0.737	0.413	1.437	1.437
LMN231	11.178	33.533	1.118		0.871	0.279	1.437	1.437
LMN232	11.178	33.533	1.118		0.798	0.351	1.437	1.437
LMN233	11.178	33.533	1.118		0.737	0.413	1.437	1.437

percentage of category 1, mechanical activation of category 2 and chemical activation of category 0 that means no chemical activation.

Further, the bricks prepared by using the raw materials as per the Table 2. were cured under sprinkler curing for 14 days and tested for compressive strength and water absorption to draw the conclusion.

4   Results and Discussion

4.1   Compressive Strength of Brick

In mixes LMN110, LMN21 and LMN310, the mechanical activation of FA is constant (32%), no chemical activation is present and lime content are 5%, 10% and 15% respectively. Hence, it can be observed from Fig. 1 that the increase in lime percentage leads to increase the compressive strength by 12% for 10% lime and decrease the
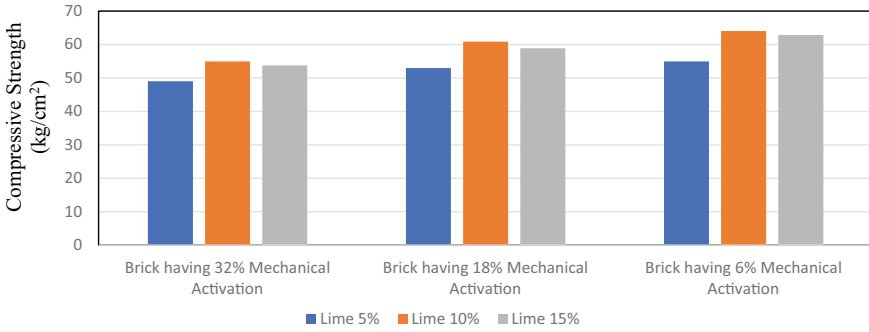
Fig. 1 Compressive strength of brick due to variation in lime content at different level of mechanical activation

result by 9.6% for 15% lime as compared to 5% lime i.e. used in LMN110. Further, the results follow the same patter for the mixes prepared with 18% and 6% mechanical activation. The sample prepared with 10% lime obtains peak value of strength due to the chemical reaction between FA, lime and water which generates sufficient amount of heat for curing itself in normal day temperature. But in case of 15% lime surplus amount heat delays the formation of bond with in the particles.

Similarly, by considering LMN110, LMN120 and LMN130, where the lime is fixed at 5% of total mass of FA and no chemical activation is present. It can be seen in Fig. 2 that the increase in fineness of FA increases the values of strength by 12% for LMN120 and 8.05% for LMN130 with respect to LMN110. The results follow the same pattern for the mixes containing similar changes like LMN210, LMN220, LMN230 and LMN310, LMN320, LMN330. This indicates that the increase in fineness of FA increases the compressive strength of brick due to increase in the reactivity of the FA and enhanced geopolymerisation reactions. Mechanical activation tends to decrease the dimension and increase the specific surface area of FA which can cause lesser void ration and higher compaction value within the bricks.
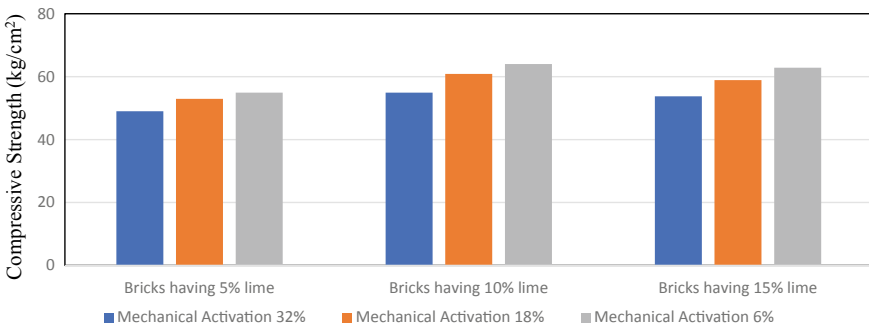
Fig. 2 Compressive strength of brick due to variation in level of mechanical activation at different lime content
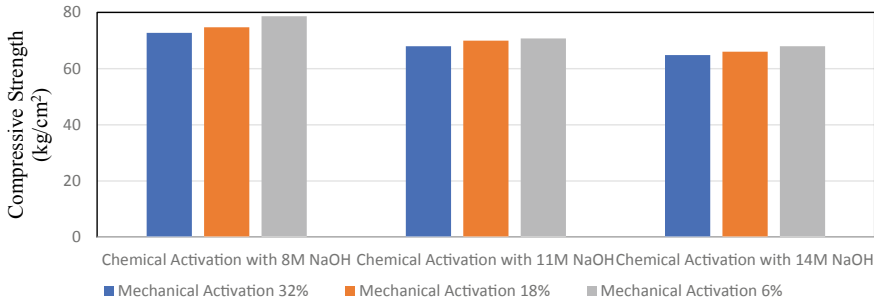
Fig. 3 Compressive strength of brick having 10% lime due to different level of mechanical activation

Considering the mixes LMN211, LMN221, LMN231 where the chemical activation of FA is fixed i.e. 8 M NaOH and lime content is 10% of total mass of FA the only change in the fineness of the particle tends to change the result and increases the strength of brick by 2% for LMN221 and 8.1% for LMN231 w.r.t LMN211 (Fig. 3). The results follow the similar pattern for the batch of mixes with 11 M NaOH (LMN212, LMN222, LMN232) and 14 M NaOH (LMN213, LMN223, LMN233). This tends to indicate that the fineness of FA has a greater impact on the activation process and can cause higher strength of brick.

By Considering the mix LMN211, LMN212, LMN213 and LMN210 when the mechanical activation of FA is fixed at 32% and lime content at 10%, the only change in the molarity of NaOH tends to change the result and increases the strength of brick by 32.3% for LMN211, 23.7% for LMN212 and 17.9% for LMN213 w.r.t LMN 210 (Fig. 4). Similar trend is also observed for mixes with 18% and 6% mechanical activation. This indicates that the sample having lower concentration of NaOH solution possess higher compressive strength with respect to the sample having high concentration of NaOH or having no chemical present. This is because high amount of OH concentration accelerate the dissolution of FA and polycondensation was hampered.
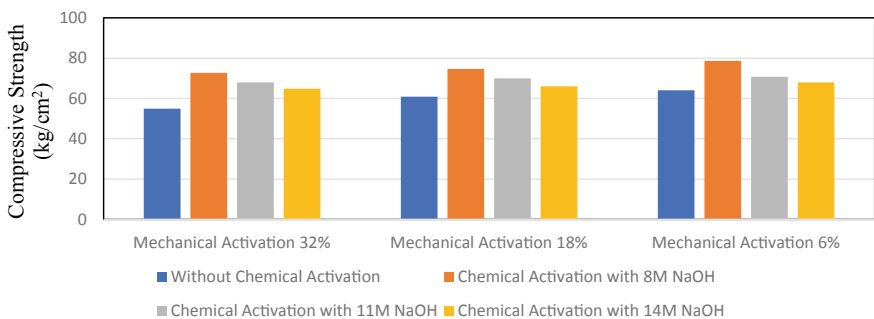
Fig. 4 Compressive strength of brick having 10% lime due to different level of chemical activation
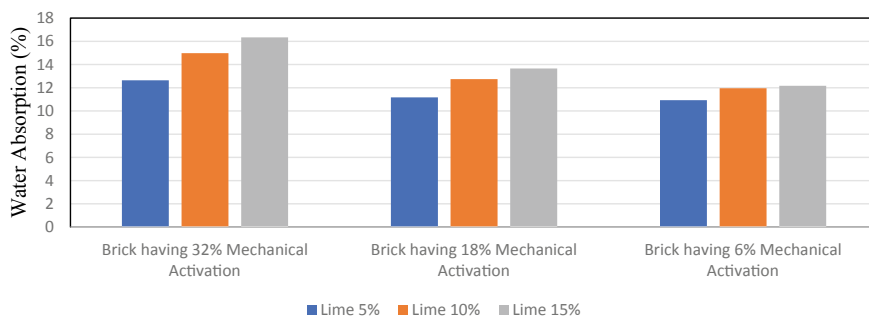
Fig. 5 Water absorption of brick due to variation in lime content at different level of mechanical activation

Rise in alkali concentration tends to increase the strength of geopolymer, but in presence of excess hydroxide ion concentration the alumina silicate gel precipitates at the very early stage, leading lower strength of geopolymer.

Among all the brick samples LMN231 i.e. with 10% lime of total mass of FA and 6% of the FA retained on the 40μ sieve and chemical activation with NaOH concentration of 8 M achieved the highest strength which is 60.4% higher than LMN 110.

4.2 Water Absorption of Brick

In mixes LMN110, LMN210, and LMN310 the mechanical activation of FA is fixed at 32% and no chemical activation is present. It can be seen from Fig. 5 that, the increase in lime percentage leads to increase the water absorption by 18.51% for 10% lime and 29.22% for 15% lime as compared to 5% lime i.e. used in LMN110. This indicates that the increase in lime percentage increases the water absorption of the FA brick due to formation of calcium silicate hydrate. Calcium silicate hydrate is a compound formed from the reaction between lime and FA which has a high physical water absorption capacity.

Similarly, by considering LMN110, LMN120 and LMN130 where the lime is fixed at 5% of total mass of FA and no chemical activation is present, the increase in fineness of FA decrease the values of water absorption by 11.65% for LMN120 and 13.52% for LMN130 with respect to LMN110 (Fig. 6). The results follow the same pattern for the mixes containing similar changes like LMN210, LMN220, LMN230 and LMN310, LMN320, LMN330. This indicates that the increase in fineness of FA decreases the water absorption of brick due to increase in the reactivity of the FA and enhanced geopolymerisation reactions. Mechanical activation tends to decrease the size of pore and increase the specific surface area of FA which can cause lesser void ratio and compacted hardly.
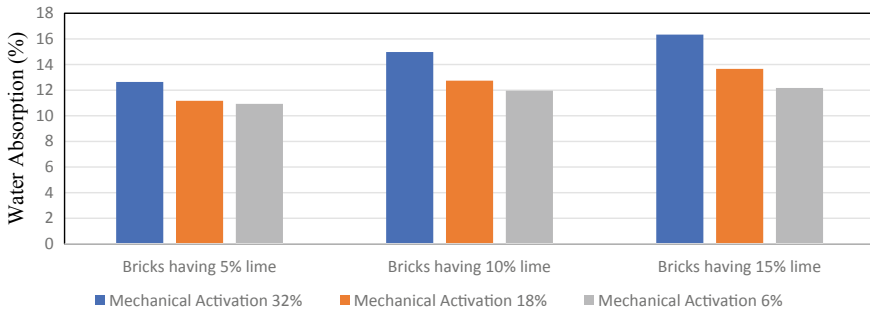
Fig. 6 Water absorption of brick due to variation in level of mechanical activation at different lime content
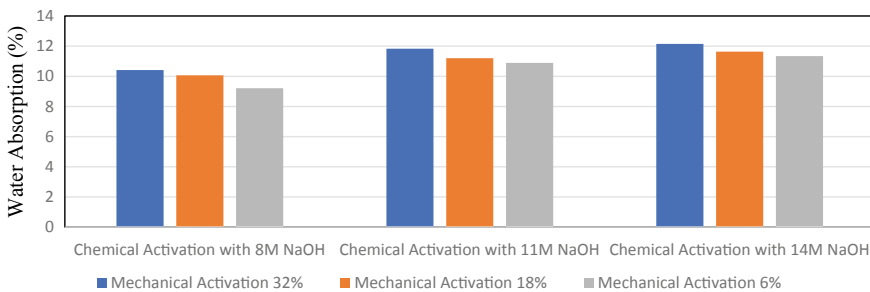
Fig. 7 Water absorption of brick having 10% lime due to different level of mechanical activation

Considering batch LMN211, LMN221, LMN231 where the chemical activation of FA is fixed i.e. 8 M NaOH and lime content is 10% of total mass of FA, the only change in the fineness of the particle tends to change the result and decreases the water absorption of brick by 3.35% for LMN221 and 11.6% for LMN231 with respect to LMN211 (Fig. 7). The results follow the similar pattern for the batch of mixes LMN212, LMN222, LMN232 and LMN213, LMN223, LMN233. This tends to indicate that the increase in fineness of FA decreases the specific surface area and void ratio respectively hence the water absorption decreases.

By Considering the mix LMN211, LMN212, LMN213 and LMN210 when the mechanical activation of FA is fixed at 32% and lime content is 10% of total mass of FA the only change in the molarity of NaOH tends to change the result and decreases the water absorption of brick by 30.44% for LMN211, 21.05% for LMN212 and 18.93% for LMN 213 with respect to LMN 210 (Fig. 8). For batch of mixes LMN221, LMN222, LMN223 w.r.t LMN220 and mixes LMN231, LMN232, LMN 233 w.r.t LMN230, the result follows the same pattern as previous. This indicates that the sample having lower concentration of NaOH solution possess lower water absorption with respect to the sample having high concentration of NaOH or having no chemical
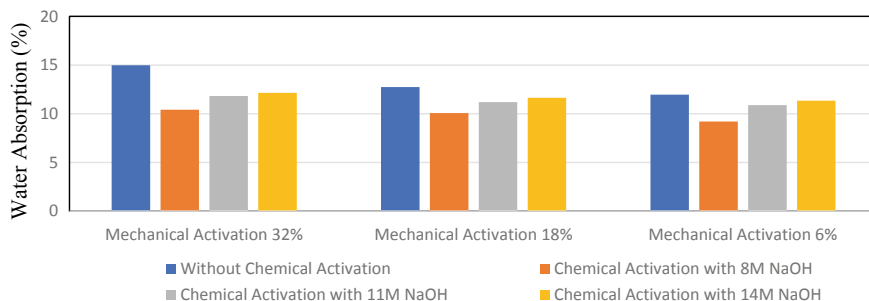
Fig. 8 Water absorption of brick having 10% lime due to different level of chemical activation

present. This is because of geopolymerization which binds the FA particles very closely reducing the voids present in the sample resulting a smooth uniform surface.

5 Conclusion

The conclusions that can be drawn out of the above discussions are.

- In absence of chemical activation, use of 10% lime may be considered as the optimum dosage for the development of highest strength of brick.
- The strength of brick increases and water absorption decreases as the fineness of FA increases.
- The brick with finer FA particles with less amount of NaOH concentration shows better result i.e. both compressive strength and water absorption as compared to other.
- Out of all the samples prepared in this experiment the bricks under the mix LMN231 possess higher strength of 78.66 kg/cm^2 and satisfies the requirement of 2nd class brick. It

References

1. Central electricity authority (2019) Report on Fly ash generation at Coal\Lignite based thermal power stations and its utilization for 1st half of the year 2018–19. Central electricity authority, New Delhi
2. Das BB, Pandey SP (2011) Studies on influence of fineness of fly ash on the carbonation and electrical conductivity of concrete. J Mater Civ Eng ASCE 23(9):1365–1368
3. Somna K et al. (2011) NaOH-activated ground FA geopolymer cured at ambient temperature. Fuel 90.6:2118–2124
4. Farsana C, Das BB, Snehal K (2021) Influence of fineness of mineral admixtures on the degree of atmospheric mineral carbonation. Smart Technol Sustain Develop 117–136

5. Fernández-Jiménez A et al. (2019) Mechanical-chemical activation of coal FAes: an effective way for recycling and make cementitious materials. Front Mater 6:51
6. Hardjito D, Vijaya Rangan B (2005) Development and properties of low-calcium FA-based geopolymer concrete
7. Panias D, Giannopoulou IP, Perraki T (2007) Effect of synthesis parameters on the mechanical properties of FA-based geopolymers. Colloids Surf A Physicochem Eng Aspects 301(1–3):246–254
8. Phoo-Ngernkham T et al. (2018) A mix design procedure for alkali-activated high-calcium FA concrete cured at ambient temperature. Adv Mater Sci Eng
9. Musmade RD, Hake SL (2019) Compressive and tensile behavior of lime added geopolymer concrete. J Struct Eng Manage 6.3:1–11
10. Sahoo S, Das BB, Mustakim S (2017) Acid, alkali and chloride resistance of concrete composed of low carbonated fly ash. J Mater Civil Eng ASCE 29(3)
11. Sahoo S, Das BB, Rath AK, Kar BB (2015) Acid, alkali and chloride resistance of high volume fly ash concrete. Indian J Sci Technol 8(19):72266
12. Shivaprasad KN, Das BB, Renjith R (2018) Influence of fineness of fly ash on compressive strength and microstructure of bottom ash admixed geopolymer mortar. Indian Concrete J 92(3)
13. Shivaprasad KN, Das BB (2018) Determination of optimized geopolymerisation factors on the properties of pelletized fly ash aggregates. Construct Build Mater 163
14. Shivaprasad KN, Das BB (2018) Effect of duration of heat curing on the artificially produced fly ash aggregates. In: IOP conference series: materials science and engineering, vol 431, no 9. IOP Publishing, p 092010(1–8)
15. Sharath BP, Shivaprasad KN, Athikkal MM, Das BB (2018) Some studies on sustainable utilization of iron ore tailing (IOT) as fine aggregates in fly ash based geopolymer mortar. In: IOP conference series: materials science and engineering, vol 431, no 9. IOP Publishing, p 092013(1–8)
16. Snehal K, Das BB, Akanksha M (2020) Early age, hydration, mechanical and microstructure properties of nano-silica blended cementitious composites. Construct Build Mater 233

Utilization of Air-Cooled Ferrochrome Slag in Lime Additive Blended Cement-Based Concrete

Prasanna Kumar Acharya and Sanjaya Kumar Patro

1 Introduction

Lime as a binding material has been using since time immemorial. Monuments built thousands of years ago using lime mortar are still standing without any major structural defect. Lime is found abundant as a natural resource. Huge limestone dust is generated worldwide due to major quarry operations. Use of limestone dust in a small dosage as explored in this study for partial replacement of cement would not only reduce the environmental burden but also reduce carbon-di-oxide (CO_2) emission and energy consumption due to less production of cement. It is also expected that there may be a possibility of development in strength properties due to long-term pozzolanic reaction on the availability of calcium hydroxide from lime and silicon oxide from PPC and PSC. ACFS slag is a non-ferrous crystalline slag obtained as a waste material at the rate of 1–1.2 tonnes from the smelting process during the production of each tonne of ferrochrome products. ACFS bears desired mechanical and engineering properties of coarse aggregate, for which its potential use in the preparation of green concrete is investigated in the study. The utilization of ACFS in concrete will help in the conservation of non-renewable natural sources.

2 Literature Study

Limestone powder is a product of carbonate rocks due to crushing. The use of limestone dust in cement and concrete has hugely increased in the last few years [1]. The

P. K. Acharya (✉)
School of Civil Engineering, KIIT DU, Bhubaneswar, Odisha, India

S. K. Patro
Department of Civil Engineering, VSS University of Technology, Burla, Odisha, India

use of limestone powder as filler in concrete preparation is observed as a general practice in many European countries. Technical, economic and ecological benefits are achieved due to the addition of limestone powder in cement. Limestone powder helps in developing the rate of hydration rate, controls the bleeding and increases the early days' strength of concrete. Limestone powder possesses good packing ability in the granular skeleton of cement and large dispersions in grains of cement [2]. The limestone powder does not have a pozzolanic character. On the other hand, it has the property of filling which makes the matrix denser. It also strengthens the interfacial transition area between paste and aggregate [3]. The setting times and porosity reduce on blending of limestone powder in pozzolanic cement. The free lime content and combined water content increase with limestone powder content. The carboalumi-nate formed due to limestone powder occupies the pores between particles of cement and accelerates the setting time. The blending of limestone powder reduces the diffu-sion coefficient of chloride ions, improves the compressive strength and increases the heat of hydration [4]. At 15% lime content minor differences in performance were observed in comparison to normal concrete at the same water-cement ratio. The decrease in strength properties observed with an increase in limestone powder content. Modulus of elasticity and flexural strength increased with lime content. Up to 25%, lime content permeation and durability properties increased [5].

The setting time of cement containing limestone powder 0–30% is reported to be less than that of the normal concrete. The compressive strength such as concrete that contained 0–30% limestone power decreased with increasing the dosage of limestone powder. The rate of diffusion increased with age. The diffusion coefficient decreased with a dosage of limestone powder 10–20% [6]. The slump decreased with the lime dust content 0–30%. The compressive strength and flexural strength got increased with a dosage of lime dust up to 10% and thereafter got decreased. After 15% of limestone powder, the absorption was reported to increase. Drying shrinkage got increased up to 10% limestone powder and content and decreased with a further increase in dosage [7]. The workability, compressive strength, sorptivity and chloride permeability of limestone powder concrete were reported similar to that of normal concrete. The dosage of limestone powder of 20% was considered as optimum as far as the matter of protection against corrosion is concerned. When the freezing–thawing behavior of concrete with limestone powder concrete was found inferior to normal concrete, the carbonation depth and total porosity characteristics were found superior [8]. The strength, acid resistance and sulphate resistance increased in concrete made of blended cement that contained natural coarse aggregates and lime up to 7% on replacement of cement [9].

Ferrochrome slag has angular particles, high specific gravity, good impact value and satisfactory crushing strength required for use as coarse aggregate of concrete. The slag is found alkaline but satisfies the durability criteria with sodium sulphate. The target compressive strength was achieved on the replacement of natural coarse aggregate by ferrochrome slag [10]. The physicochemical properties of air-cooled ferrochrome slag coarse aggregate are better than virgin aggregates. It is reported to be used as in granular layers of highway pavements [11]. The leaching of elements from the ferrochrome slag to the groundwater reported low except for potassium

[12]. The structure of the ferrochrome slag is glassy and crystalline partly. Major phases of ferrochrome slag are amorphous glass, Mg–Al-silicate, forsterite, Fe–Mg–Cr–Al-spinels, and metal alloy. The products of ferrochrome slag are reported to be chemically stable [13]. The left out chromium in the ferrochrome slag remained immobilized as trivalent chromium in stable phases such as chromite or magnesiochromite/magnesium aluminum chromite and inhibited chromium leaching from slag under ambient condition [14]. The ferrochrome slag as an alternative coarse aggregate in the concrete making is found suitable with mechanical strength equal to or even more than normal [15]. The use of ferrochrome slag as alternate coarse aggregate and ferrochrome ash with lime as supplementary cementitious material enhances the properties of concrete [16].

2.1 Significance of the Study

The blended types of cement (PPC and PSC) that are produced using fly ash and ground granulated blast furnace slag are rich in silicon oxide (SiO_2) and aluminum oxide (AL_2O_3). These two elements in combination with calcium hydroxide ($CaOH_2$) play a vital role in producing calcium-silicate-hydrate (C–S–H) gel through a pozzolanic reaction. It is anticipated that this pozzolanic reaction can be made continued for a longer period on additional supply calcium hydroxide ($CaOH_2$) due to the supplementation of lime. Considering the mechanical advantages of ACFS over natural aggregates and obtaining long term pozzolanic reaction due to the use of lime, it is expected to achieve a sustainable green concrete. The present knowledge on the combined effect of lime as supplementary cementitious material and ACFS as alternate coarse aggregate is not visible. The preparation of green concrete with a waste stream material like ACFS as alternate coarse aggregate may be another step towards a sustainable path. The result of the study may be a step ahead in bridging the knowledge gap.

3 Experimental Program

3.1 Materials

PSC and PPC conforming to Indian standard specifications IS: 455-1989 [17] and IS: 1489-1991 (Part-1) [18] are used in this work. The various properties of cement are presented in Tables 1 and 2. Hydraulic lime was collected from the local market and used on partial replacement of cement. Natural river bed sand and natural granite stone conforming to the requirements of IS: 383-1970 [19] used as fine and coarse aggregates. AFCS as presented in Fig. 1, was collected from an operating ferrochrome plant of Odisha and used as an alternate coarse aggregate on total replacement of

Table 1 Physical properties of PSC and PPC

Property	Results				Requirements	
	PSC	PPC	PSC + Lime	PPC + Lime	PSC	PPC
Standard consistency (%)	34	35	37	38	–	–
Setting time—initial (min)	94	60	84	54	≥ 30	≥ 30
Setting time—final (min)	219	178	196	134	≤ 600	≤ 600
Soundness (mm)	0.5	1	1	1	≤ 10	≤ 10

Table 2 Chemical properties of PSC and PPC

Properties	Results		Requirements	
	PSC	PPC	PSC	PPC
Sulphide sulphur (%)	0.17		≤ 1.5	
Chloride content (%)	0.01	0.016	≥ 0.1	≤ 0.1
Insoluble residue (%)	2.33	26.1	≤ 4	FA % +4(100−FA %)/100
Magnesium oxide (%)	4.48	2.4	≤ 10	≤ 6
Sulphur trioxide (%)	2.58	2.2	≤ 3	≤ 3
Loss in ignition (%)	1.43	2.3	≤ 5	≤ 5

Fig. 1 ACFS coarse aggregate

Table 3 Properties of aggregates

Aggregates	Specific gravity	Water absorption (%)	Flakiness index (%)	Elongation index (%)	Impact value (%)	Crushing value (%)	Abrasion resistance
NCA	2.83	0.2	18.5	13.5	15.3	20.1	18.6
ACFS	2.84	0.63	9.83	10.5	11	17.89	18.19
FA	2.7	0.73	–	–	–	–	–

NCA = Natural coarse aggregate, ACFS = Air-cooled ferrochrome slag coarse aggregate and FA = Fine aggregate
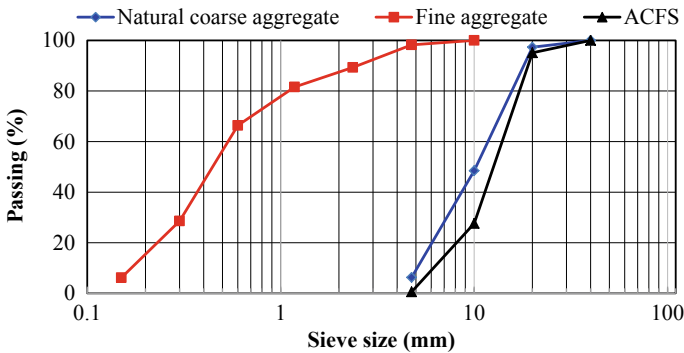
Fig. 2 Particle size distribution of aggregates

virgin coarse aggregate. The properties and particle size distribution of fine coarse aggregates are presented in Table 3 and Fig. 2.

3.2 Items of Investigation

The effect of lime on blended cement (PSC and PPC) mortars were examined on properties like consistency, setting time and soundness. The effect of on workability of blended cement-based concrete using ACFS as an alternate to coarse aggregate was studied using the slump test. The effect of lime and ACFS on mechanical properties was studied by conducting compressive, flexural and splitting tensile strength tests at the end of 4, 13 and 26 weeks (28, 91 and 182 days). Sorptivity test as a measure of the durability of such concrete was conducted at the same age.

Table 4 Concrete mix ingredients

Mix designation	Unit	PSN	PSF	PPN	PPF
Cement	kg/m^3	330	307	330	307
Lime	kg/m^3	0	23	0	23
Fine aggregate	kg/m^3	660	660	660	660
Natural coarse aggregate	kg/m^3	1320	0	1320	0
ACFS coarse aggregate	kg/m^3	0	1320	0	1320
W/C ratio		0.45	0.45	0.45	0.45
Super plasticizer	kg/m^3	1.65	1.65	1.65	1.65
Lime	%	0	7	0	7
ACFS coarse aggregate	%	0	100	0	100
Slump	mm	90	45	68	25

3.3 Mix Proportion

A total of 4 concrete mixtures were prepared, named as PSN, PSF, PPN and PPF. The first two (PSN and PSF) belonged to the Portland slag cement (PSC) group while the last two (PPN and PPF) belonged to the portland pozzolana cement (PPC) group. The concrete sample PSN contained PSC, lime and natural coarse aggregates while PSF contained PSC, lime and ACFS coarse aggregates. Similarly, PPN contained PPC, lime and natural coarse aggregates while PPF contained PPC, lime and ACFS coarse aggregates. The details of the mixture ingredients are presented in Table 4. A water-cement ratio of 0.45 was adopted. The dosage of superplasticizer was 0.5% by weight of cement.

3.4 Mixing, Test Specimen and Curing

As per the mix proportion mentioned in Table 4, the various components were weighed. The binding materials, cement and hydraulic lime were blended properly till a uniform colour was obtained. Then the required quantity of superplasticizer was mixed with water. The binding materials and the aggregates were dry mixed in a pan type mixture machine. Then half of the superplasticizer mixed water was mixed with the dry mix to have a semi-solid mix. Then the rest of the water mixed with superplasticizer was mixed to the semi-solid mix to have a homogenous mix. Cubes of 15 cm size for compressive strength test; prisms of $100 \times 100 \times 500$ mm size for flexural strength and cylinders of 150 mm dia $\times$ 300 mm long for split tensile strength tests were cast. For the test of sorptivity samples of 100 mm dia and 50 mm thick were required. These samples were prepared by cutting from the cylindrical samples of 100 mm dia and 200 mm long. The test samples were cast in three successive layers and compacted using a vibrating table for two minutes. The samples were

covered with wet hessian cloth and kept for 24 h at ambient temperature. Thereafter the samples were released from moulds and allowed to remain to cure in water.

3.5 Test Procedure

Properties of cement were determined as per the procedure of IS 455:1989 [17] and IS 1489:1991 (Part-I) [18]. Properties of coarse and fine and coarse aggregates were ascertained using IS: 383:1970 [19] and IS: 2386(Part 1)-1963 [20]. Setting time was obtained using the guidelines of IS: 5513–1996 [21] and IS: 8142-1976 [22]. The workability was studied through the slump test using the procedure of IS: 7320-1974 [23] and IS: 1199-1959 [24]. Consistency test was done as per IS: 5513-1996 [21]. The soundness test was performed as per the provisions of IS: 5514:1996 [25] and IS: 4031(Part-3)-1988 [26]. The compressive strength and flexural strength were conducted as per the guidelines of IS: 516-1959 [27]. The split tensile strength test and sorptivity test were conducted as per IS: 5816-1999 [28] and ASTM C-642-06 [29]. The computation of results was done considering the average result of three samples.

The term sorptivity of concrete is the ingress of water inside the pores of concrete caused due to capillary action in a saturated condition. From this sorptivity data, the pore system of concrete is studied. The sorptivity of concrete is determined by the increase in weight due to the ingress of water within a particular period. For the test of sorptivity, the concrete samples were dried in an oven at 105 °C. Then the side surface of the specimen was coated with wax to avoid the sorption through side faces. The weight of the specimen was taken at ambient temperature before sorption. Then the specimens were kept in a tray of water over tiny supports in such a way that only 5 mm of the specimen from the bottom was immersed in water. The test setup procedure was followed as reported by the authors in the past [30]. The specimens were weighed after 9, 49, 100, 169, 256 and 361 min of sorption. For easy understanding and plotting of results, the interval of study time was selected as if the square root of time ($\sqrt{t}$) to be a whole number. The absorbed water is calculated by finding the difference between the weight of the specimen after sorption and initial weight in a particular time interval (t). Then sorptivity (S) is derived using the equation $S = {}^i\!/\!{\sqrt{t}}$.

Where, S = sorptivity, i = absorbed water (g/mm^2), t = time of sorption (min). S is determined through a linear regression analysis of i versus $\sqrt{t}$.

4 Results and Discussion

4.1 Consistency, Setting Times and Soundness

Due to the blending of lime (7%) on replacement of cement, the consistency of blended mixes of PSC and PPC increased. The increase in water demand is due to the occurrence of the early hydration process because of lime. The setting times got reduced in presence of lime in both the blended mixes containing PSC and PPC. The soundness remained almost consistent. The results are presented in Table 1.

4.2 Workability

The workability ascertained in terms of slump values. Due to the blending of lime and incorporation of ACFS in concrete mixes PSF and PPF, the slump values reduced, for which the addition of 0.5% superplasticizer was considered to maintain workability. The negative impact on workability is due to a quick chemical reaction because of lime and higher water absorption capacity of ACFS in comparison to natural coarse aggregates. The slump values are presented in Table 4.

4.3 Compressive Strength

The compressive strength of concrete mixes PSN, containing natural coarse aggregate was found 33.55, 39.70 and 41.42 MPa at 28, 91 and 182 days. The same for PSF was found 36.72, 42.96 and 44.46 MPa. There is appreciable strength development in both mixes with age. The strength development in PSN is found 23.5% between 28 and 182 days. The same in PSF is calculated 21% during the same period. The late age strength development in both the mixes is found more than 20% and this is for continued pozzolanic reaction due to the presence of lime and more utilization $Ca(OH)_2$. The compressive strength development of PSF over PSN is 9.45, 8.20 and 7.3% at 28, 91 and 182 days respectively. The result shows the almost uniform rate of strength development which establishes uniform and positive impact of ACFS. ACFS has some mechanical advantages in comparison to natural coarse aggregate for which it improved the mechanical strength. Moreover, physically ACFS has a rough surface which helped in improving bond at the interfacial transition zone of aggregate and in turn enhancement of strength.

The compressive strength of concrete mixes PPN with PPC, containing natural coarse aggregate was found 33.11, 37.76 and 39.62 MPa at 28, 91 and 182 days. The same for PPF was found 33.99, 40.60 and 43.50 MPa. The strength enhancement in PPN is found 19.6% between 28 and 182 days. The same for PPF is reported as 27.98%. Results indicated development in the strength of mixes with age, which may
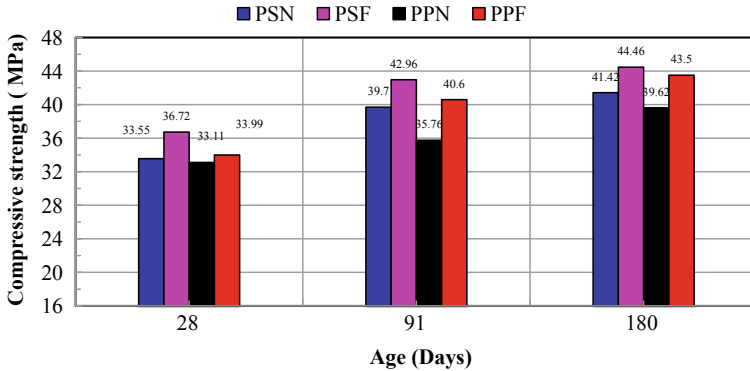
Fig. 3 Compressive strength

be considered as an effect of lime on continued pozzolanic reaction. The compressive strength improved due to the inclusion of ACFS. Due to the inclusion of ACFS, the compressive strength development in PPF in comparison to PPN is calculated 2.65, 13.50 and 9.80% at 7, 28, 91 and 182 days. The result shows strength development in all curing periods which establishes utilization of lime and surplus $Ca(OH)_2$ in the creation of C–S–H gel.

When comparing the results of mixes with PSC with those of PPC, it is observed that mixes with PSC offered more strength. Thus it can be concluded the influence of lime and ACFS is more positive in PSC in comparison to PPC. The results are presented in Fig. 3.

4.4 Flexural Strength

The flexural strength of PSN that contained 7% lime, PSC and natural coarse aggregates was recorded 6.4–9.8 MPa during 28–182 days. The flexural strength enhanced with age and the enhancement recorded at 182 days is more than 50% in comparison to the strength of 28 days. This encouraging development is due to lime as a filler material and its involvement in continued pozzolanic reaction utilizing surplus $Ca(OH)_2$. On the use of ACFS in the mix PSF, the flexural strength increased in comparison to PSN and found 9–10.8 MPa during 28–182 days. The increase in PSF over PSN caused due to ACFS is calculated as more than 40% at 28 days and 10% at 182 days. The strength of PSF also improved with age and the improvement is estimated at up to 20% between 28 and 182 days.

Concrete mix made with PPC using natural coarse aggregate (PPN) exhibited flexural strength 5.2–8.8 MPa in between 28 and 182 days. Due to the positive impact of lime in pozzolanic activity and the creation of further C–S–H gel, this mix gained appreciable strength with age and up to 182 days the strength gain is 69% over 28 days strength. Concrete mix made with PPC and ACFS (PPF) offered
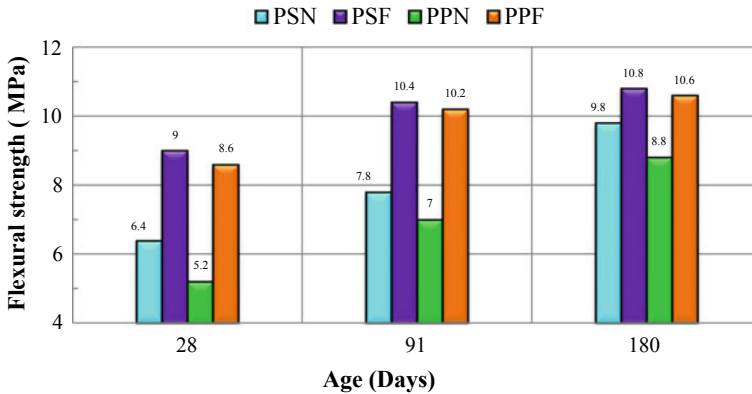
Fig. 4 Flexural strength

flexural strength 8.6–10.6 MPa. The increase in PPF over PPN caused due to ACFS is calculated as more than 65% at 28 days and 20% at 182 days. The positive impact of lime in enhancing the flexural strength with age is visible from the result. The flexural strength got improved up to 23% at 182 days over the strength of 28 days. Comparing the results of concrete mixes made of PSC (PSN and PSF) and PPC (PPN and PPF), it is observed that the results of PPC lag behind those of PSC. Thus it can be concluded that the combined effect of lime and ACFS is more positive on PSC based concrete. The results are presented in Fig. 4.

4.5 Split Tensile Strength

The split tensile strength of PSN varied 3.68–4.81 MPa in between 28 and 182 days. The same of PSF varied 4.53–5.30 MPa. The results are presented in Fig. 5. The results showed continuous strength development in both the mixes in all curing periods, which may be attributed to the influence of lime as narrated in previous sections. The strength of PSF is found 23 and 10% more than PSN at 28 and 190 days respectively. This may be attributed to the positive impact of ACFS. The physical characteristics of ACFS such as rougher surface and angular shape helped in developing bonds between paste and aggregate and enhanced the tensile strength.

The split tensile strength of PPC based mix PPN was recorded between 3.25 and 4.38 MPa in 28–182 days. The increase in strength during these days is calculated around 35%. This heavy increase is not only due to the filling effect of lime but also its effective role in the pozzolanic reaction. The PPC based mix PPF, containing ACFS as coarse aggregate exhibited split tensile strength 3.95–5.23 MPa during 28–182 days. The strength development during these days is 32%. The rate and reason for such development are similar to PPN. Due to the replacement of virgin aggregate
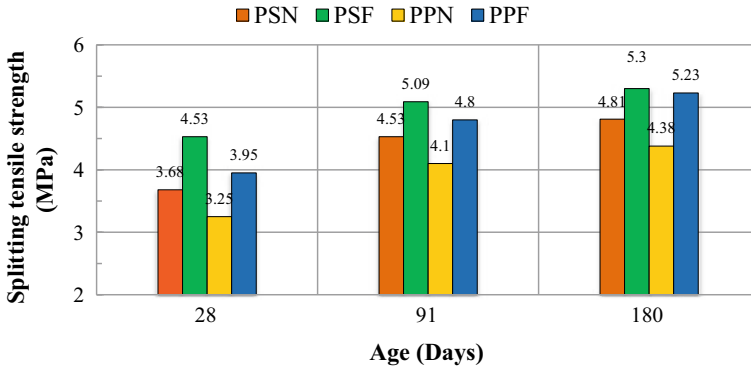
Fig. 5 Split tensile strength

by ACFS, the strength enhanced 21and 19% in 28 and 182 days. The reason for enhancement is similar to PSF as explained earlier.

Like other properties, the combined effect of lime and ACFS is more on more on PSC based concrete mixes than PPC based.

4.6 Sorptivity

The ingress of water due to capillary suction was studied after the completion of 28, 91 and 182 days for all concrete mixes. After 28 days, for mix PSN, the sorption of water after 9, 49, 100, 169, 256 and 361 min was recorded 0.545, 0.672, 0.866, 1.054, 1.100 and 1.250 mm. It was 0.396, 0.464, 0.692, 0.781, 0.890 and 0.988 mm for concrete mix PSF. The ingress of water for PPN during the above period was noted 0.591, 0.705, 0.972, 1.102, 1.222 and 1.750 mm. The same for mix PPF was reported 0.436, 0.564, 0.902, 1.098, 1.178 and 1.366 mm. The sorptivity for PSN, PSF, PPN and PPF is calculated as 0.045, 0.039, 0.067 and 0.060 as per the procedure explained in test procedure section. The results are reported in Fig. 6.

After 91 days of the curing period, in mix PSN, the sorption of water after elapse of 9, 49, 100, 169, 256 and 361 min was recorded 0.500, 0.625, 0.820, 1.010, 1.060 and 1.210 mm. It was 0.355, 0.425, 0.650, 0.730, 0.850 and 0.950 mm for concrete mix PSF. The ingress of water for the mix PPN during the above period was noted 0.560, 0.670, 0.935, 1.060, 1.160 and 1.700 mm. The same for mix PPF was reported 0.400, 0.530, 0.870, 1.050, 1.120 and 1.320 mm. The sorptivity for PSN, PSF, PPN and PPF is estimated as 0.045, 0.039, 0.065 and 0.048. The results are reported in Fig. 7.

After 182 days, for mix PSN, the sorption of water after immersion of 9, 49, 100, 169, 256 and 361 min was recorded 0.450, 0.600, 0.780, 0.980, 1.000 and 1.182 mm. It was 0.325, 0.400, 0.620, 0.705, 0.800 and 0.910 mm for concrete mix PSF. The ingress of water for PPN during above period was observed 0.540, 0.630,
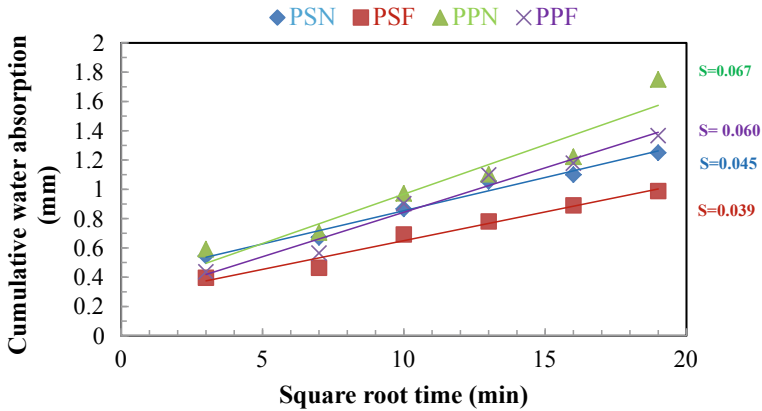
Fig. 6 Sorptivity at 28 days
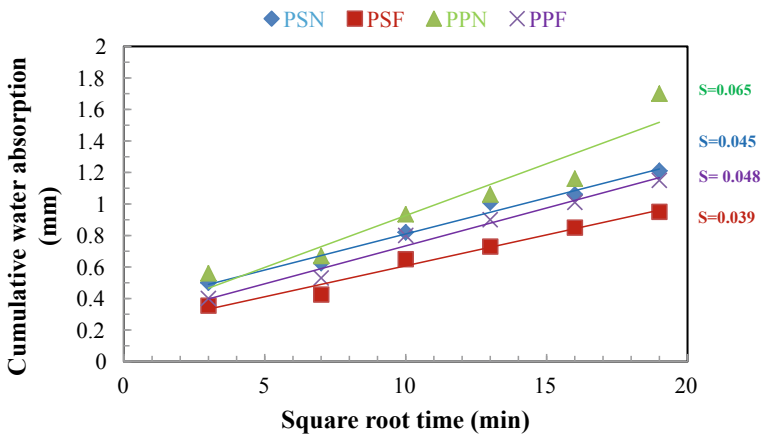
Fig. 7 Sorptivity at 91 days

0.900, 1.020, 1.110 and 1.660 mm. The same for mix PPF was reported 0.360, 0.500, 0.755, 0.840, 0.970 and 1.100 mm. The sorptivity for PSN, PSF, PPN and PPF is calculated as 0.044, 0.038, 0.064 and 0.047. Results are reported in Fig. 8.

The sorptivity of all mixes reduced with age which may be due to the formation of more gel and therefore the improvement in the transition zone and dense structure. The sorptivity also reduced when natural coarse aggregate is replaced with ACFS due to better bonding between constituent materials of concrete. The sorptivity of PSC based concrete is found less than that of PPC based concrete. Thus the influence of lime and ACFS is found positive on both the types of cement but more positive on PSC.

◆ PSN   ■ PSF   ▲ PPN   ✕ PPF
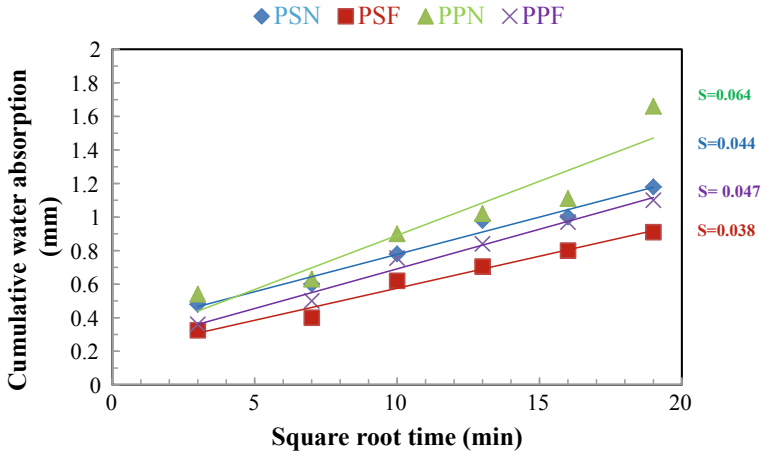
Fig. 8 Sorptivity at 182 days

5   Conclusions

Based on the results, the following conclusions are derived from the present study:

- On inclusion of 7% lime to PSC and PPC, the consistency of blended mixes increases, the setting time decrease and the soundness remain the same.
- On blending of 7% lime in PSC and PPC as partial replacement of cement and ACFS as an alternate coarse aggregate to virgin coarse aggregate, the workability of produced concrete decreases.
- The influence of lime and ACFS on blended cement-based concrete is found positive on mechanical properties like compressive, flexural and split tensile strengths.
- The sorptivity is reduced on the use of lime as partial replacement of cement and ACFS as a total replacement of natural coarse aggregates.
- The effect of lime and ACFS is more positive on PSC based concrete in comparison to PPC based.

References

1. Vuk T, Gabrovs R, Kauc V (2002) Cem Concr Res 32:943–948
2. Bonavetti V, Donza H, Menendez G, Cabrera O, Irassar EF (2003) Cem Concr Res 33:865–871
3. Liu S, Yan P (2010) J Wuhan Univ Technol 25:328–331
4. Heikal M, El-Didamony H, Morsy MS (2000) Cem Concr Res 30(11):1827–1834
5. Dhir RK, Limbachiya MC, McCarthy MJ, Chaipanich A (2007) Mater Struct 40(5):459–473
6. Moon HY, Jung HS, Kim JP (2004) J Korea Concr Inst 16(6):859–865
7. Tahir C, Khaled M (1996) Cem Concr Res 26(7):1121–1130

8. Tsivilisa S, Batis G, Chaniotakis E, Grigoriadis G, Theodossis D (2000). Cem Concr Res 30(10):1679–1683
9. Acharya PK, Patro SK (2016). J Inst Eng (India) Ser A 97(2):71–79
10. Das BB, Das SK, Parhi PK (2014). Paper presented at all India seminar on advances in construction technology, Bhubaneswar, Odisha, India
11. Alten Y, Mustafa K (2010) Mater Struct 43:309–317
12. Lind BB, Fallman AM, Larsson LB (2001) Waste Manage 21:255–264
13. Kauppi M, Niemela P (2007). Paper presented at Info XI, Outokumpu, Tornio Works, Tornio, Finland
14. Panda CR, Mishra KK, Panda KC, Nayak BD, Nayak BB (2013) Construct Build Mater 49:262–271
15. Patro SK, Mohanty T, Mohanty MK (2013). Int J 3R's 4(4):637–641
16. Acharya PK, Patro SK (2016). Waste Manage Res. https://doi.org/10.1177/0734242X16654751
17. IS: 455-1989. Portland slags cement specification. Bureau of Indian Standards, New Delhi, India
18. IS: 1489-1991 (Part-1). Specification for Portland pozzolana cement-specification. Bureau of Indian Standards, New Delhi, India
19. IS: 383-1970. Specifications for coarse and fine aggregates from natural sources for concrete. Bureau of Indian Standards, New Delhi, India
20. IS: 2386(Part-1)-1963 (Reaffirmed 1997). Methods of test for aggregates for concrete, Part-1 Particle size and shape. Bureau of Indian Standards. New Delhi, India
21. IS: 5513-1996. Vicat apparatus—specification. Bureau of Indian Standards, New Delhi, India
22. IS: 8142-1976. Methods of test for determining setting time of concrete by penetration resistance. Bureau of Indian Standards, New Delhi, India
23. IS: 7320-1974. Specifications for concrete slump test apparatus. Bureau of Indian Standards, New Delhi, India
24. IS: 1199-1959. Methods of sampling and analysis of concrete. Bureau of Indian Standards, New Delhi, India
25. IS: 5514-1996. Apparatus used in Le-Chatelier test-specification. Bureau of Indian Standards, New Delhi, India
26. IS: 4031-1988. Methods of physical tests for hydraulic cement. Bureau of Indian Standards, New Delhi, India
27. IS: 516-1959. Indian standard code of practice-methods of test for strength of concrete. Bureau of Indian Standards, New Delhi, India
28. IS: 5816-1939. Splitting tensile strength of concrete-Test method. Bureau of Indian Standards. New Delhi, India
29. ASTM C 642-06. Standard test method for density, absorption and void in hardened concrete. American Society for Testing of Materials
30. Acharya PK, Patro SK (2016) Constr Build Mater 120:241–250

Evaluation of Pre-cast Prestressed Concrete System: For the Housing Projects

Nathnael Azmeraw Workeluel and Tribikram Mohanty

1 Introduction

Housing in the twenty-first century, from urban expansion to overcrowding, became a worldwide epidemic. Whilst housing is one of the three primary necessities of existence, there is still chaos in underdeveloped economies which have large populations of both quantity as well as quality (Shaw and Hagemans 8) to satisfy the mentioned housing demand and a more efficient, quick, and sustainable construction approach is considered necessary to meet the above-mentioned demand (Ding et al. 2015).

While the complexity of structural, serviceability and highly common quality issues is a precise appropriate preventive construction, it is exciting to take the enormous opportunity that such a fresh start would offer. Where there is an area for machinery and processing, structural concrete components can be cast and cured at the bottom in a regulated manner. This could be seen as a function of the precast prestressed construction process except in some of the world's impoverished communities, precast pre-stress building has been extensively used. Studies of buildings (Rogan et al. 2000) show that the advantages of the premises are enhanced by efficiency, construction time is increased by 50%, waste reduction by 70%, project costs savings of up to 10%, and the benefit of a just delivery to the site.

Designing and handed over residential condos with near serviceability, protection, time, and high-quality standards are sneeded to fulfill the constantly growing housing demand. As rapid economic development demands population growth, construction without any kind of loss of quality and no project delay, project cost outfit in labor shortages, or similarly associated building instability, construction firms have the first step towards this difficulty.

N. A. Workeluel · T. Mohanty (✉)
Structural Engineering, SCE, KIIT DU, Bhubaneswar, India
e-mail: tmohantyfce@kiit.ac.in

163

The integrated approach of pre-stressed units for the housing project would allow the designer to adjust the structural arrangements in an excellent aesthetic and structural versatility in such a manner to prevent the members' span serve as a constraint. Those projects will therefore be rapidly completed and start to generate revenue faster by making pre-pressurization applications feasible. Therefore, implementing the pre-pressed concept in the housing project will further promote the construction rate.

The successful implementation of the precast concrete system for housing projects in the construction industry system would provide the solution for project delay, boost the conventional construction followed by the advanced technical system, demonstrate the structural benefit, resistance, and availability of the precast concrete system to create an environmentally sustainable system. It facilitates the growing building industry through the provision of alternative and cost-effective design, timely implementation, and the use of high-tech buildings.

The scope of this paper focuses on the contrast of the construction of the beam and the ribbed architectural modification slab with the precast and typical concrete systems on the design of frames on the base reaction and the output columns of two systems of quality, quantity, and time.

2   Methodology

Prestressed concrete: Components of precast concrete are reinforced with either conventional reinforcement bars, high-lasting chains, or a combination of both. Inside the shape, the strands are pre-tensioned until the concrete is poured. The strands are cut (detention) until the concrete has healed to a particular intensity. As the strands intend to recover their original untensioned length, having bonded to the concrete, they bind to the concrete and apply a compressive force. This "precompression" increases the load-carrying ability of the components and helps regulate cracking to particular limits allowed by building codes (precast concrete components are reinforced with either traditional reinforcement bars, high-lasting strands, or a combination of both. Before the concrete is poured, the strands are pre-tensioned in the form. As they bind to the concrete, they plan to recover the untensioned original length, bind to the concrete, and add a compressive force. This "precompression" increases the capacity of the components to bear loads and helps control cracking to some limits authorized by building codes.

Concrete casting process: Pre-stressed members may be classified as cast in-situ, pre-cast, and composite structural members, depending on the concrete casting mechanisms. These studies follow the composite protocol procedure. The pre-cast elements in a composite construction structure can be joined together more easily than those in a pre-cast structure. Through composite construction, much of the shape and false-work needed for complete cast-in-place construction can be saved. The suitability of each form, however, must be studied concerning the specific condition of the structure given.

Fig. 1 Parabola- rectangular stress distribution under compression
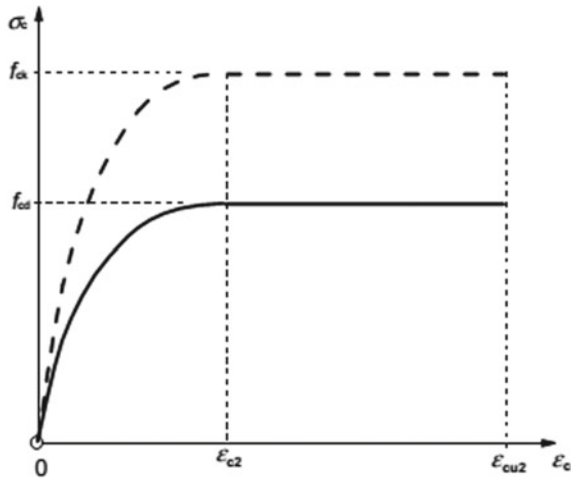
Materials for Prestressed Concrete

- **Concrete** Prestressed concrete requires concrete that, at a relatively early age, has high compressive strength with a comparatively higher tensile strength than ordinary concrete. Minimum 28-cube day cube strength recommended for pre-tensioned members in euro code manual C40/50(Euro code 2 section 1-1 1992).

Initially, concrete's stress–strain activity under uniaxial compression is linear and elastic. The action becomes nonlinear and inelastic with the formation of micro-cracks. The resistant pressure decreases with an increase in strain after the specimen exceeds the pick tension. Parabola- It is possible to display a rectangular diagram using the above interaction and it is shown in the Fig. 1.

- **Prestressing Steel**: The pre-stressing steel used meets the actions of high strength, sufficient ductility, high bond with low loss relaxation, and minimal corrosion.

Analysis and Design of the Housing Projects using Conventional Reinforced Concrete

A Representative of the G + 12 condominium housing project with a certain architectural modification contrasted the conventional and pre-stressed prefabricated concrete framework and the study and design of the structure used with Excel 2010 using SAP2000.

According to the Euro code, the material characteristics and load combination are defined by accounting for self-weight, imposed dead load, live load, and earth rapid load with a combination of load case, seismic data, and combinations. aspects of modeling and design are:

- As per EBCS-1.1995 table 1.3, the load combination factor was added.
- Stiffness modification factor as per EBCS-1.1995 table 3.4

- Inter story drifts is checked according to conditions fulfilled in Euro code 8 EN 1998–1 sections 4.4.3.2 and EBCS 8 1995 section 2.4.3.2.
- Second-order effects (P-Δ effects) are verified in compliance with the requirements met by the Euro code 8 EN 1998–1 section 4.4.2.2 and EBCS 8 1995 section 2.4.2.2.
- Live load reduction is considered as per EBCS-1 for every story of the building with Stiffness modification factors that were adjusted in accordance.

Analysis and Design of the Housing Projects using Precast Prestressed Concrete Units

The major difference between conventional reinforced and pre-stressed precast concrete is that by merely bringing them together and making them function together as they might prefer, reinforced concrete incorporates concrete and steel bars but Prestressed concrete, on the other hand, "actively" incorporates high-strength steel. By tensioning the steel and holding it against the concrete, this is done, thereby bringing the concrete into compression. A much stronger behavior of the two materials results in this active combination. Steel is ductile and is now pre-stressed for high tension action.

The major difference between conventional reinforced and pre-stressed precast concrete is that by merely bringing them together and making them function together as they might prefer, reinforced concrete incorporates concrete and steel bars but Prestressed concrete, on the other hand, "actively" incorporates high-strength steel. By tensioning the steel and holding it against the concrete, this is done, thereby bringing the concrete into compression. A much stronger behavior of the two materials results in this active combination. Steel is ductile and is now pre-stressed for high tension action. With its tensile capacity now strengthened by being compressed, Concrete is a brittle product, although its compressive capacity is not harmed. Prestressed concrete is therefore an optimal mix of modern materials of high strength. Dill of Nebraska tried high-strength steel bars coated in the production of pre-stressed concrete in 1925 to avoid bonding with concrete. The steel rods were tensioned and anchored to the concrete using nuts after the concrete had hardened. But these approaches have not been applied solely for economic reasons. While Freyssient also attempted the pre-tensioning scheme where the steel was bonded to the concrete without end anchorage, Hoyer of Germany first made practical application of this process. The Hoyer device consists of extending wires several hundred feet apart between two buttresses, putting shutters between the units, inserting the concrete, and cutting the wires after hardening the concrete. Freyssient invented conical wedges for end anchorages in 1939 and created double-acting jacks that tensioned the wires and then moved the male cones to anchor them onto the female cones. In 1940, Belgium's Professor Magel created a magnet device in which two wires were extended at a time and anchored at each end with a simple metal wedge. Prestressed concrete started to gain significance about that time, but it did not come to the fore until around 1945.

Analysis and Design for the Slab Panels: Ribbed slab, T-section, according to the Euro code manual, the minimum dimension with material properties is carried out per the structural design. The compressive strength of concrete for C50 is used

for the construction of the ribbed slab concrete transfer for 7 days. The detailed parameters of the design are described below.

- Model parameters for the slab panel of prestressed concrete
- Elastic sectional modularization
- Adjusted construction loads for the beams of pre-stressed concrete
- Determination of eccentricity and prestressing forces
- Calculation of short and longer losses
- Resistance Bending Moment and estimation of minimum reinforcement
- Tendon spacing and design of Shear
- Adjusted construction loads for the beams of pre-stressed concrete.

Girder Beam Analysis and Design: The ribbed slab is supported by an arrangement in the girder beam and then linked to the column to give an overall frame. The shape of the girder beam should be such that the support of the rib slabs (T sections) is convenient and a smooth, serviceable floor surface is created (Fig. 2).

The initial data for the width and depth of the inverted flange is taken from the PCI design manual (8), the frame is analyzed using SAP 2000 software for the precast prestressed concrete unit, and the analyzed result is used to design the girder beams. The design for the beams should be done in such a way when using precast units, with similar floor system, the analysis result is taken for the design of girder beam, but in the case where the analysis differs in an enormous amount, for a particular member with engineering judgments, special design is done. At each level of the floor, the following model considerations were in use;

- A pin is a link between the wall and the framed structure.
- Rigid floor diaphragms
- The live load reduction factor is done as per code
- Stiffness modification factors were adjusted.
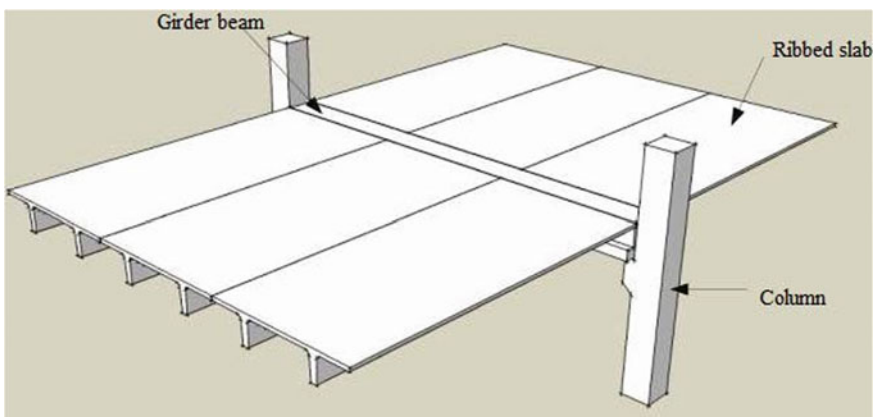
Fig. 2 The demonstration of the ribbed slab to girder beam and girder beam to column connection

The specification for girder beams is performed using the same design process, and the measurement is presented in the same way as the ribbed slab was performed.

Connections and Detailings: and while this study is followed based on the previous study for connections and dealings, French et al. (1981) created connectors to connect the beams to columns using post-tensioned bars. The post-tensioned bars were designed to shift the interface away from the yield. In the 1980s, Rockwin Company created a "drop-in" beam system using a monolithic concrete technology by constructing precast concrete frames with member splices away from predicted regions of inelastic action.

Economic Analysis: The industrialization of the construction industry has offered an important solution to the problems of modern and land infrastructure projects. The use of prefabricated units may be one of the possible solutions. If a comprehensive analysis of the cost of the installation of such an industry is performed in-depth, pre-cast prestressed concrete has the potential to change the industry. A contrast of reinforced concrete with the economic aspect of this method is discussed in the evaluation of the existing use of pre-stressed concrete in terms of efficiency, time, and expense.

Time: Building projects are distinctive in many distinctive efforts, one of which is a time delay, which raises the overall cost and contributes to unforeseen expenses. These delays can arise for reasons relating to financial suppliers, suppliers of materials, and conditions of the site and controls at hand. Compared to conventional reinforced concrete, these explanations for eradication are that their construction is speedy using pre-cast units. This is mostly because there is no loss of time when curing floors and time is eliminated concerning the installation of formwork.

Quality: The key factor in the performance of building projects is quality. Performance of projects specifically related to the life cycle of the project and the project management framework. The condo housing projects are primarily intended to tackle the low-cost project with vaguely optimum quality assurance. Compared to using premanufactured units, handling the continuous intended concrete mixes and concrete grade at the site is not a simple job. When using pre-cast units, concrete mixes are managed and engineered to meet the necessary grade and achieve the required quality in an ascetically pleasing atmosphere.

Cost: For assessment.

- For both conventional reinforced and Pre-cast prestressed concrete systems, the proposed condo house design was analyzed using SAP 2000.
- The quantity is estimated for the ribbed slab, girder beam, and column, and both conventional and precast units have been compared.
- Finally, the discrepancy was made by removing the maintenance costs in Ethiopian currency for both.

3   Discussion

The girder beam and column 10% for transport are added from the overall cost of pre-cast pre-stressed in the discussion of the paper for a fair-and-square comparison between the pre-cast prestressed concrete and reinforced concrete total cost of the slab.

- For slabs: pre-cast prefabricated prestressed concrete has a lower cost with a good method, efficiency, and quality for the condo housing projects. It noted that the application of ribbed pre-cast pre-cast concrete slab had a major impact on condo house projects in time, quality, and quantity of projects.
- For the girder beams: even if it is more difficult to conclude because of connections, but for longer beams, pre-cast pre-stressed concrete, they are advantages in giving freedom for architectural design and quality control to offer longer span.
- For columns: It seems to be consistent with no substantial cost difference for columns, but it offers space for designers and architects to provide their design with the required space without restriction and interruption (Fig. 3).

Housing Projects Comparison using Typical Reinforced Concrete and Precast Prestressed Concrete

Conventional Reinforced concrete: use of normal strength materials with lower section modifiers and complete section capability is not used, homogeneous joints are easily accomplished, cracks may not be controllable, the dimensions of the components are higher than the pre-stressed unit, structural layouts are restricted mostly on the maximum permissible column dimensions and depth of the beam, the resemblance of the construction members, the lower form of equipment compared to the
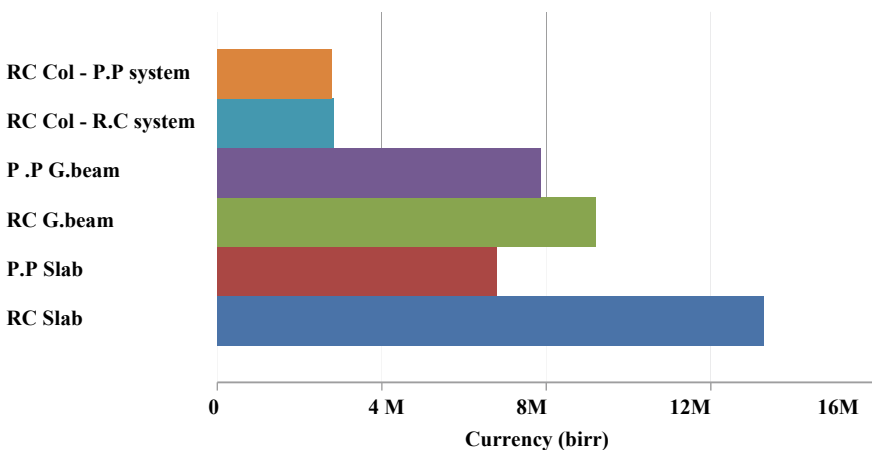
Fig. 3 The demonstrated figure on price comparison between pre-cast prestressed concrete and normal reinforced concrete

precast prestressed units, the lower demand for qualified labor than the reinforced concrete unit, the higher cost of formwork with maintenance than precast systems.

Pre-cast prestressed concrete: uses high strength materials with a higher value of section modifiers and full capacity of the section is utilized, construction of joints might not be easy, the occurrence of Cracks is controllable, Member dimensions are reduced in a significant quantity with Layout flexibility, the similarity of structural members to be suitable for the pre-cast industry is necessary, cranes and other machines are mandatory, skilled laborers' are needed as compared to the reinforced concrete system, the form-work cost is reduced and molds are used, expensive detailing of joints and manufacturing site with mixing silos are required, quality control and high fire resistance property are easily achieved.

4   Conclusion

It can be inferred as follows from the outcomes and discussion:

- In housing projects, the use of precast prestressed concrete slabs will save 54% of the reinforced concrete ribbed slab cost.
- Using pre-cast pre-cast concrete girder beam in housing projects can save 21% of the cost of reinforced concrete beams without taking into account the cost of connexion costs and actual transport, although a compressive study on the use of pre-tensioned cast-in-situ concrete to minimize the use of costly connexion information is required.
- The cost of columns is consistent with the conventional reinforced concrete structural arrangement with the precast prestressed structural arrangement.
- Application of pre-cast pre-stressed ribbed slabs for improved project management on condo housing projects should be considered.
- It is advisable to go hand in hand with the architectural design with the structural engineer for pre-cast structures to prevent uneconomical layouts and to ease the construction process.
- In contrast to the conventional one, which is the important thing in the design of residential apartment buildings, it offers design versatility in column spacing.
- As it provides minimum timing for projects, by speeding up construction in correspondence with the contribution to the cost of precast implementation of the housing project, it will minimize the total project time, allowing the construction industry to expand at an enormous rate.

References

1. Standard AA (2011) Building code requirements for structural concrete (ACI 318-11). In: American Concrete Institute
2. Rahman AB, Leong DC, Saim AA, Osman MH (2006) Hybrid beam-to-column connections for precast concrete frames. In: Proceedings of the 6th Asia-Pacific structural engineering and construction conference, Kuala Lumpur, Malaysia, pp 5–6
3. Bond AJ, Brooker O, Harris AJ, Harrison T, Moss RM, Narayanan RS, Webster R (2006) How to design concrete structures using Eurocode 2. Concrete Centre
4. Moss RM, Brooker O (2006) How to design concrete structures using Eurocode 2:3. Slabs. Concrete Centre
5. Sengupta AK Department of Civil Engineering. Indian Institute of Technology Madras Module. Prestressed Concrete Structures
6. Rochefort A (2008) Analysis and design of prestress concrete members to Eurocodes (EC2) considering the temperature. Dissertation submitted in total fulfillment of the requirements of the degree of M.Sc structural engineering, School of engineering and the building environment Napier university
7. Walraven JC, Stoelhorst D (eds) (2008) Tailor made concrete structures: new solutions for our society (Abstracts Book 314 pages + CD-ROM full papers 1196 pages). CRC Press
8. Shaw KS, Hagemans IW (2015) 'Gentrification without displacement' and the consequent loss of place: The effects of class transition on low-income residents of secure housing in gentrifying areas. Int J Urban Reg Res 39(2):323–341
9. Mittal A (2010) Prestressed concrete wire and stands specification manual
10. Adamu A. Prestressed concrete structures, lecture note, Department of civil and environmental engineering. Addis Ababa institute of technology, Addis Ababa, Ethiopia
11. Beeby AW, Narayanan RS (2009) Designers' guide to Eurocode 2: design of concrete structures. London
12. CSI educational services (1995) From start to finish: model, design and optimize a multi-story concrete structures using ETABS. University Avenue Berkeley, California, United states of America
13. Mehetre AJ, BR N (2013) Analysis of pre-stressed floor grid system. Int J Eng Res Appl (IJERA) 3(4)
14. Ritz P, Matt P, Tellenbach C, Schlub P, Aeberhard HU (1985) Post-tensioned Slabs, 4.2 report series. VSL International LTD, Berne, Switzerland
15. Braconi A, Bursi OS, Fabbrocino G, Salvatore WA, Tremblay R (2008) Seismic performance of a 3D full-scale high-ductility steel–concrete composite moment-resisting structure—Part I: design and testing procedure. Earthquake Eng Struct Dyn 37(14):1609–1634
16. European standard (2001) Eurocode 1: actions on structures-part 1-1: General ations densities, self-weight, imposed loads for buildings, pr EN 1991-1-1
17. British Standards Institution (2004) Eurocode 2: design of concrete structures: Part 1-1: general rules and rules for buildings. British Standards Institution
18. De Normalisation CE (2004) Eurocode 2: design of concrete structures—Part 1–1: general rules and rules for buildings. Belgium, Brussels
19. Bentz E, Collins MP (2001) Response-2000, user manual. University of Toronto, Toronto, Ontario, Canada
20. Bentz E (1999) Response 2000, Shell 2000, Triax 2000 and Membrane 2000. User Manual. Version. 2001; 1. Published by Center for advanced engineering, New Zealand
21. Group of the New Zealand concrete society and the New Zealand society for Earthquake Engineering, Guidelines for the use of structural precast concrete in buildings, 2nd edn
22. Parastesh H, Hajirasouliha I, Ramezani R (2014) A new ductile moment-resisting connection for precast concrete frames in seismic regions: an experimental investigation. Eng Struct 1(70):144–157
23. Bachmann H, Steinle A (2011) Precast concrete structures. Ernst & Sohn, Berlin

24. Irish precast concrete association IPCA, Precast concrete frames guide, Newlands Business park, Clondalkin, Dublin 22
25. Maya LF, Albajar L (2012) Beam-column connections for precast concrete frames using high performance fiber reinforced cement composites. In: High performance fiber reinforced cement composites 6. Springer, Dordrecht, pp 347–354
26. ACI Committee, International Organization for Standardization. Building code requirements for structural concrete (ACI 318–08) and commentary. American Concrete Institute
27. Englekirk RE (2002) Design-construction of the Paramount-A 39-story precast prestressed concrete apartment building. PCI J 47(4):56–71. ACI Committee. Building code requirements for structural concrete (ACI 318–05) and commentary (ACI 318R-05). American Concrete Institute
28. Englekirk RE (2002) Design-construction of the Paramount-A 39-story precast prestressed concrete apartment building. PCI J 47(4):56–71
29. Ding KW, Zhang X (2012) Literature review of precast concrete frame structures in civil engineering. In: Advanced materials research 2012, vol 568. Trans Tech Publications Ltd, pp 3–6
30. Song LL, Guo T, Gu Y, Cao ZL (2015) Experimental study of a self-centering prestressed concrete frame subassembly. Eng Struct 1(88):176–188
31. Ermed MW. Addis ababa integrated housing development program: a strategy for urban poverty reduction and sustainable socio-economic transformation, presentation. Addis Ababa, Ethiopia
32. Proestos GT (2018) Modelling reinforced and prestressed concrete structures subjected to shear and torsion. Doctoral dissertation, University of Toronto, Canada
33. Collins MP, Mitchell D (1997) Prestressed concrete structures. Response Publications
34. Krishhna Raju N (2007) Prestressed concrete, 4th edn. The Mc-Graw-Hill Publishing Company Limited, New Delhi
35. PCI Design Handbook: Precast and Prestressed Concrete (5th Edition) by PCI Concrete Handbook Committee (1999–04–03) [PCI Concrete Handbook Committee]
36. Platform European concrete (2008) Eurocode 2 worked examples. Published by the European concrete platform ASBL
37. Harry H. Design-construction of the paramount–a 39-story precast prestressed concrete apartment building
38. Council FF (1974) National research council. Expansion joints in buildings: technical report no. 65. National Academies Press
39. Nakaki SD, Englekirk RE, Plaehn JL (1994) Ductile connectors for a precast concrete frame. PCI J 39(5):46–59
40. Lin TY, Burns NH. Design of prestressed concrete structures

A Life Cycle Analysis Based Framework to Promote Circular Economy in the Building Sector

J. S. Smitha and Albert Thomas

1 Introduction

The need and awareness for sustainable development have been growing high in the last few decades, and therefore, methods for lowering the environmental impacts are an important consideration in almost every industry in these days. The construction industry also strives to achieve sustainable growth as it has been identified as a leading sector in the consumption of energy and other natural resources [19]. During construction, a large amount of raw materials, water, fossil fuels and energy is utilized and correspondingly huge quantities of waste are generated [9, 14, 28, 29]. Manufacturing process of these construction materials involves lot of energy needs and disposal of harmful by-products [34, 1]. Similarly, construction phase also requires deployment of machineries and equipment, transportation needs and other site activities [6]. Likewise, operational phase of built environment is associated with energy consumption for lighting, heating, cooling and ventilation, and for signaling and control systems in infrastructure [32]. In addition, maintenance, repairs and refurbishment also have environmental impacts due to the use of more materials, and the disposal of harmful waste. Similarly, at the end of life, demolition and disposal of waste causes additional impacts. Hence any form of construction has substantial environmental impacts due to its resource and energy intensive nature, and efforts are to be made in building design and techniques for reducing these impacts.

Discussions on sustainability in buildings is mainly focused on analysis of energy consumption and alternate building materials having lower energy demand

J. S. Smitha · A. Thomas (✉)
Department of Civil Engineering, IIT Bombay, Mumbai, India
e-mail: albert@iitb.ac.in

J. S. Smitha
e-mail: 194048003@iitb.ac.in

[30]. Towards this, both operational energy (OE) and embodied energy (EE) of buildings had been studied and methods to reduce them have been proposed. Analysis of EE and OE on different building façade systems of tall buildings points out the necessity of considering EE along with OE in assessing the environmental effects [10]. Similarly, evaluation of greenhouse gas emissions associated with energy consumption of building materials is also analyzed [25]. Likewise, Mathiyazhagan et al. [22] framed a model for selection of sustainable material considering the environmental, economic and social aspects. In addition to these efforts, the demolition phase and reduction of impacts in disposal of construction waste and recycling potential of materials are also gaining interest. [3]. Overall, there has been a concentrated effort in understanding the energy impacts of construction materials.

The construction sector is heavily material intensive and consumes maximum natural resources, and about 40% of natural stone quarried is used for construction works [20]. As a result, the construction industry produces a large amount of waste every year and nearly 80% comes from the cities, accounting for 3000 million tons worldwide [12, 13]. Construction and Demolition Waste (CDW) contributes to 30–35% of the global waste and its main constituent is concrete, which is the second most-consumed material worldwide [27]. In India the amount of CDW generated in a year is estimated as 300 million tons on an average and it is only on a rising trend [12]. Therefore, disposal of waste after demolition of buildings at their end of life is another major problem faced by the society today. Recycling construction waste helps to cut down the consumption of natural resources and energy, as it reduces solid waste generation, pollution of air and water, and eventually decreases greenhouse gas emission [27, 33]. This could be a solution to two problems at the same time, as it would decrease the amount of waste disposal and reduce the natural resources consumed. The awareness of environmental effects of dumping this waste at the landfill sites and scarcity of dumping areas to accommodate large volume of such waste necessitated the search for alternatives. Research for proving the benefits and feasibility of utilizing waste materials in construction is active and studies now investigate the recycled content and end of life recycling scenarios of building materials [8, 36].

When a building is demolished at its end of life, most of the components could be recycled or reused through a marketing system. Many components of building are reusable which could be considered as down cycling and demolition waste could be recycled by converting it to new construction materials. Metals such as reinforcement steel and aluminum can be recycled completely as they are collected as scrap, melted and used for manufacturing new metal parts, the recycling percentage depending on the collection rate. Doors, windows and other carpentry are removed carefully so that they can be reused in some other buildings. Masonry and flooring are demolished carefully to separate the bricks, blocks and tiles to be used again for construction. In general, the component which does not have any scope of circularity is painting, polishing and similar finishing works. But the structural concrete, mortar remains and concrete floor are dumped in landfills which also involve long distance transportation. Therefore, the major volume in the building, after its useful life, is discarded as waste which pollutes the environment and this can be avoided by recycling this inert waste.

It has been suggested through several studies that recycled aggregates obtained from demolition of old buildings and rework at construction site is a good alternative for natural aggregates [8, 18, 35]. This process of recycling waste will reduce both landfilling quantity and at the same time exploitation of new resources from nature. This becomes more significant in the context that aggregates are in short supply in countries such as India where the demand is increasing [12]. The aggregate obtained from CDW is termed as recycled aggregate (RA) and the concrete prepared from such aggregates is recycled aggregate concrete (RAC). The procedure of converting demolition waste to aggregates to be used again for construction and thereby avoiding landfill, is in line with the newly evolving principle of 'circular economy'(CE).

The concept of circular economy promotes the corporate social responsibility and is becoming popular in many sectors such as automobile industry [31, 37], textile industry [24], electronics and plastics [23] and water sector [16]. In this concept, organisations are encouraged to not only consider their economic growth, but also fulfil their responsibilities to the society. Organizations should not only thrive for their own betterment, but should consider the goodwill of the community and different industries in a region should work together. For instance, the waste from one industry can be used for manufacturing new products in the same sector or a different sector. This is the idea of circular economy by which waste disposal can be reduced and utilisation of maximum materials is possible. In the building sector, the demolition waste can be recycled and used for production of new building materials, in line with circular economy concept. This led to the development of a new concept of considering existing buildings as material bank and not as waste materials to be dumped to landfill sites, at the end of life [14, 15, 21]. Circular Economy is the new drift for sustainable development where construction industry has immense scope. The CE model can potentially convert the end of life phase to a system of regenerating resources and reusing those in construction activities thereby reducing demand for virgin materials [2].

2 Motivation

Various approaches were attempted through the years to render the built environment more sustainable or green. Still the building sector remains a pioneer in the consumption of natural resources and production of inert waste [12, 14]. The extraction and processing of construction materials consumes a lot of energy, are highly polluting and cause natural resource depletion. Concrete is the major contributor to the adverse environmental impacts from the construction sector [27] and more than 75% of it consists of aggregates, extracted from the nature. Natural aggregates, both coarse and fine are becoming scarce and in urban regions the distance of transportation is increasing as nearby sources are waning [13].

While the construction industry is facing the problem of resource depletion on one side, there are issues regarding handling of demolition waste on the other side, aggravated by legal measures that ban dumping of construction waste in metropolitan

areas. Conversion of CDW to RA for preparation of fresh concrete in new construction works provides a good solution and introduces circular economy to construction sector. Shifting from linear economy to circular economy shall transform the construction sector to a more resilient system, which is less dependent on virgin raw materials [11]. In linear economy, raw materials extracted from nature are used for construction and at the end of life, the demolished waste ends up in dumping yards. But in circular economy, the buildings are considered as 'material bank' and at end of life, demolition waste is processed to produce construction materials that are used in new buildings. Closing the loop to create a circular economy, alone does not establish the environmental efficiency of a system and to confirm that, it has to be tested for the net impacts [9]. Efficiency of circularity will depend on the system and process of recycling and the impact due to the recycling process should not be more than the avoided impacts. There should be a systematic study to analyse the environmental impacts to confirm the feasibility of a new circular system and the whole exercise of recycling can be considered to have environmental benefits only if the credits of using recycled material is more than the burden caused by recycling process [38]. To ensure sustainability in construction field, the impacts caused to the environment have to be measured and compared [7].

Life cycle assessment is an effective tool for analysing sustainability and environmental performance of built environment [26]. LCA methodology enables to decide the feasibility of replacing natural virgin materials with recycled materials [2]. Environmental design is possible by performing environmental assessment which gives information, verifies claims and facilitates improvement by quantifying the changes caused by a process in the environment [5]. There were several studies that used LCA methods to understand the recyclability aspects. Pradhan et al. [27] used LCA to compare the impacts while using different mix design methods for concrete made of recycled aggregate (RA) and natural aggregate (NA). Jain et al. [13] studied the environmental benefits of recycling CDW by avoiding landfilling. Even though few studies focus on the mix design and strength analysis of RAC [8, 35], there are not many studies that use LCA methods to evaluate impacts in the field of circular economy and recycling of CDW in buildings, specifically in an Indian context.

Overall, this study compares the environmental impacts of a case study building using Natural Aggregate Concrete (NAC) and Recycled Aggregate Concrete (RAC). In building construction supporting circular economy, concrete shall be prepared using RA in place of NA. The percentage of replacement varies and can be determined as per the strength requirements and site conditions. According to many studies, 100% replacement is not recommended for structural members but is suitable for PCC, flooring and pavement blocks. 30% replacement by RA is recommended in high strength concrete for structural components as it does not affect the strength characteristics [18, 35]. The concrete components in the building shall be identified and suitable replacement strategy shall be considered.

The CDW is transported to the plant, segregated, crushed and sieved using dry or wet processes to convert it to aggregates for required size. Concrete is prepared with suitable replacement ratios and the impacts of NAC and RAC with various replacement ratios can be evaluated. RAC is used for different components of the

building with different proportions of RA and NA and hence the net effect can be assessed using LCA tool.

Therefore, the main objective of this study is to utilise the systematic methods of life cycle assessment for analysing the environmental impacts due to introduction of circular economy in the building construction industry. The major part of demolition waste that goes into landfill consist of concrete and masonry and hence recycling of these materials are considered. Demolition waste can be converted to recycled aggregates and the different scenarios of using in new construction work are analysed and their impacts are assessed using an LCA approach.

3 Methodology

Overall, the methodology for this study mainly involves performing a life cycle analysis for a case study building with varied scenarios. In the sections below, the assumptions for LCA as well as the details of the case study building and the scenarios performed are explained in detail.

3.1 Life Cycle Assessment

Life cycle assessment (LCA) is a systematic tool for analysing the impacts of any product or system, based on ISO 14040 and ISO 14044 guidelines [27, 38]. Open LCA is an open source software tool that makes LCA calculation easy and fast for sustainability assessment. There are various databases such as eco-invent that have documented life cycle inventory data sets for many industries, including construction materials. Open LCA Version 1.6.3 is used in this study, along with the eco-invent 3.6 database.

ISO 14040 provides a methodological framework for life cycle studies and it divides LCA into four steps: (i) Goal and scope—including defining the system boundary and functional unit (ii) Inventory analysis (iii) Impact assessment (iv) Interpretation of results. The main steps related to the current study are discussed below:

Goal and scope definition: The first step in any LCA is to identify the goal and scope of study. The purpose of current study is to compare the environmental impacts of using natural aggregates and recycled aggregates for concrete in a building.

System Boundary and functional unit: The activities from extraction of natural materials to preparation of concrete for NA and transportation and recycling activities to preparation of concrete for RA are considered for comparison. After preparation of concrete, the activities such as mixing and placing of concrete in building will remain the same for both the cases and hence not considered in this study for comparison. Concrete used in one building is the functional unit and a case study building is considered.

Inventory Analysis: The input and output flows for recycled aggregate was obtained from literature review. This data of energy and material was used for defining the process of recycled aggregates in Open LCA. Inventory for natural aggregates was taken from the existing eco-invent database.

Impact Assessment: The LCIA method used in the study is eco-indicator 99 which considers the impact factors such as ecosystem quality, human health and resources. These are macro categories and allow comparison of environmental effects of RA and NA [33], and eco-indicator 99 is the comprehensive weighing method [3] used in this study. A report generated in Open LCA also provides a comparison chart for the selected options.

3.2 Analysis

For evaluating the environmental impacts for preparation of NAC, the processes to be considered are extraction from nature, transportation, crushing of natural aggregates and mixing of concrete. In the case of using recycled aggregates in concrete, processes such as transporting CDW to the recycling plant, crushing and sieving activities at the recycling plant have to be considered. The data set of natural aggregates is available in eco-invent database, but for recycled coarse and fine aggregates, processes are created in Open LCA. The data of energy and material consumption for recycling of CDW to RA are given in Table 1 [13]. As shown in the table, in Jain et al. [12], the environmental assessment for CDW going to landfill and recycled into aggregates is carried out and the study gives a summary of recycling data pertaining to the two major CDW recycling plants in India.

In Open LCA, flows and processes are defined for NAC and RAC and a project is created for their comparison. A building in line with circular economy shall use recycled aggregate concrete, considering a suitable replacement ratio depending on

Table 1 Recycling data

Parameter	Unit	Recycling plant values
Total capacity of 2 plants	Tons per day	2500
Share of aggregate and sand recovered	%	50% coarse aggregate, 25% fine aggregate, 25% soil
Average collection distance	km	7.5
Truck capacity	t	9–15
Plant diesel consumption	kg/t	0.4–1
Electricity consumption	kWh/t	6–10
Water requirement for wet process	L/t	20
Life time	yrs	20

Adapted and modified from [11]

the type of concrete and structure. As mentioned earlier, up-to 30% replacement shall be assumed for structural members and 100% replacement for PCC. Environmental impacts caused due to construction of the building for the total concrete quantity are compared for the two cases of using NAC and RAC.

A case study building is considered for examining the concrete use and evaluating the impacts of using RAC for a building. The case study building is an academic building, having framed structure of ground plus three floors and external aluminum façade, consisting of class rooms, laboratories and administration office space. From the bill of quantities, the type and quantity of concrete components in the building is obtained. M40 reinforced cement concrete is used in the structural members of super structure and sub structure; M15 plain cement concrete is assumed for below footing and in floors. A summary of concrete quantities used in the building is given in Table 2.

For PCC, 100% replacement of NA by RA is assumed and material requirement for 1 cum concrete is obtained as per IS 109. Impact of M15 concrete using NA and using RA are compared in Open LCA and eco-indicator 99 as given in 'Fig. 1'.

Table 2 Summary of concrete quantity

Sr. no	Quantity	Description	Unit	Replacement ratio
1	420	PCC M15 below footing, foundation and floor	Cum	100% RA
2	1300	RCC M40 in substructure	Cum	30% RA 70% NA
3	1200	RCC M40 in substructure	Cum	30% RA 70% NA
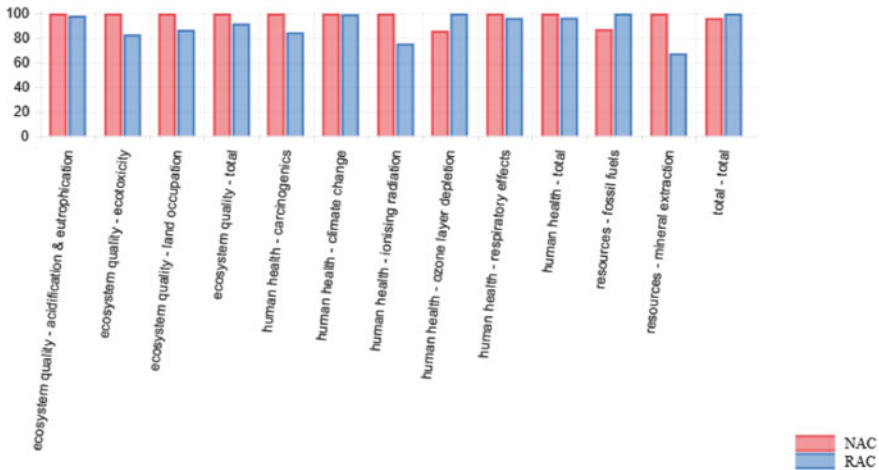
Fig. 1 Relative indicator result for PCC with 100% replacement by RA
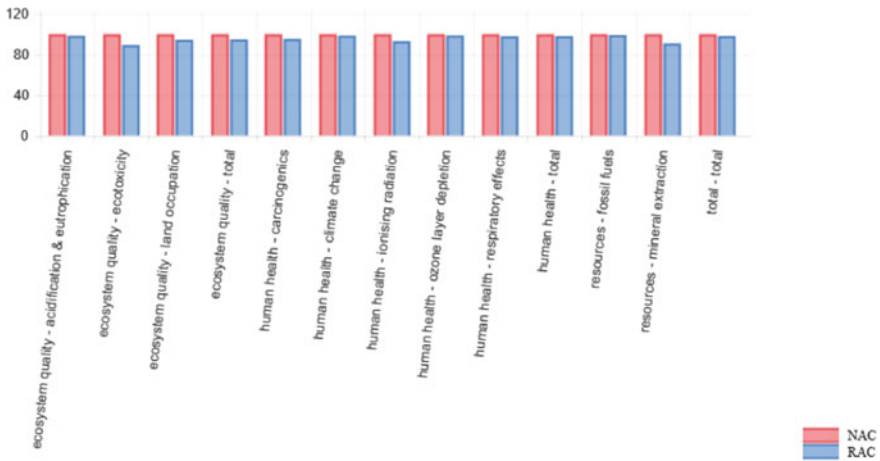
Fig. 2 Relative indicator result for RCC with 30% replacement by RA

The results in Open LCA with eco-indicator 99 LCIA, shows points in y-axis obtained by setting 100% for maximum value and calculating the relative results for other values.

In case of RCC in M40 for superstructure and substructure, 30% replacement with RA is assumed to be completely replacing NA. The material quantities are obtained as per IS 10262 [17] considering 30% RA and 70% NA. The comparison is obtained as in 'Fig. 2'.

The case study building has a total of 420 cum PCC in M15 and 2500 cum RCC M40. Considering the total volume of concrete in one building, the environmental impacts of using RA instead of NA shall be compared as shown in 'Fig. 3'.

4 Discussion

From the analysis carried out in a small building of G + 3, it can be seen that there is a substantial reduction in environmental impacts when RAC is used. Eco-indicator 99 considers the impact factors related to ecosystem quality, human health and resources and it proves to be environmentally beneficial. In this study only 30% replacement ratio is considered for structural members. This proportion shall be increased with better mix design using fly ash or other admixtures. Use of fly ash in concrete also supports the theory of circular economy. As there is growing scarcity of natural aggregates, use of RA shall be promoted. Even after considering the processing required to convert CDW to RA, it proves to be environmentally friendly. Active discussions are happening recently regarding the promotion of circular economy in the construction industry with the main aim of reducing the dependence on natural resources. But recycling process itself may have negative environmental impacts.
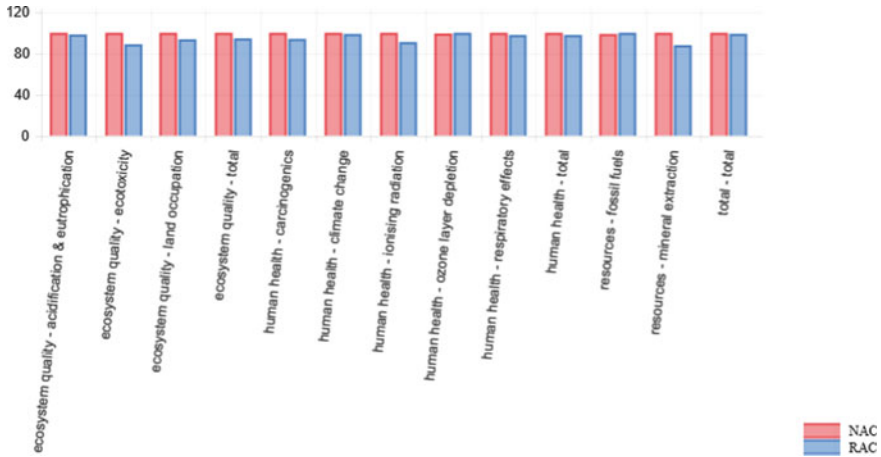
Fig. 3 Relative indicator result as per eco-indicator 99 for case study building with RAC

Therefore, a thorough life cycle study has to be carried out before we could affirm the benefits of circularity. LCA can be effectively used for deciding the feasibility of the recycling process. Open LCA is an open source software and can be effectively used for the assessment of environmental impacts in the construction field.

5 Conclusion

The concept of circular economy is gaining popularity in the construction industry as in many other sectors. Recycling of a material often involves processing before it can be utilised in the next stage. These processes and transportation prove to be energy consuming and can sometimes nullify the advantage of recycling. Therefore, a thorough life cycle analysis shall be carried out for examining the environmental performance of circular loops. In the construction field, use of RA in concrete provides a solution to two problems of shortage in natural resources and pollution due to landfilling. In this study, the life cycle impacts of using NAC and RAC in a building are compared and it is found that there is an overall gain in environmental performance when RAC is used. The research is to be taken forward with different construction materials for analysing their recycling potential in the building.

References

1. Aneesh NR, Shivaprasad KN, Das BB (2018) Life cycle energy analysis of a metro station building envelope through computer-based simulation. Sustain Cities Soc 39:135–143

2. Bauwens T, Hekkert M, Kirchherr J (2020) Circular futures: what will they look like? Ecol Econ 175:106703
3. Blengini GA (2009) Life cycle of buildings, demolition and recycling potential: a case study in Turin, Italy. Build Environ 44(2):319–330
4. Carlisle S, Friedlander E (2016) The influence of durability and recycling on life cycle impacts of window frame assemblies. Int J Life Cycle Assess, 21(11):1645–1657
5. Crawford R (2011) Life cycle assessment in the built environment. Taylor & Francis
6. Devi P, Palaniappan S (2014) A case study on life cycle energy use of residential building in Southern India. Energy Build 80:247–259
7. Ding GKC (2008) Sustainable construction—the role of environmental assessment tools. J Environ Manage 86(3):451–464
8. Duan ZH, Poon CS (2014) Properties of recycled aggregate concrete made with recycled aggregates with different amounts of old adhered mortars. Mater Design 58:19–29
9. Eberhardt L, Birgisdottir H, Birkved M (2019) Comparing life cycle assessment modelling of linear vs. circular building components. In: IOP conference series: earth and environmental science, vol 225, no. 1. IOP Publishing
10. Giordano R et al. (2017) Embodied energy and operational energy evaluation in tall buildings according to different typologies of façade. Energy Procedia 134:224–233
11. Giorgi S, Lavagna M, Campioli A (2019) LCA and LCC as decision-making tools for a sustainable circular building process. In: IOP conference series: earth and environmental science, vol 296, no. 1. IOP Publishing
12. Jain S, Singhal S, Jain NK (2018) Construction and demolition waste (C&DW) in India: generation rate and implications of C&DW recycling. Int J Construct Manage 1–10
13. Jain S, Singhal S, Pandey S (2020) Environmental life cycle assessment of construction and demolition waste recycling: a case of urban India. Resour Conserv Recycl 155:104642
14. Jayasinghe LB, Waldmann D (2020) Development of a BIM-based web tool as a material and component bank for a sustainable construction industry. Sustainability 12.5:1766
15. Kakkos E et al. (2019) Environmental assessment of the Urban Mining and Recycling (UMAR) unit by applying the LCA framework. In: SBE19 Brussels-BAMB-CIRCPATH 'Buildings As Material Banks-A Pathway for A Circular Future', 1, 012049. Paper Presented at SBE19 Brussels-BAMB-CIRCPATH 'Buildings as Material Banks-A Pathway for A Circular Future', 5–7 Feb 2019, Brussels, Belgium
16. Kakwani NS, Kalbar PP (2020) Review of circular economy in urban water sector: challenges and opportunities in India. J Environ Manage 271:111010
17. Kanth GSK, Ashok Kumar S (2017) Durability studies on recycled coarse aggregate concrete of grade M40
18. Karakaš N et al. (2018) Potential use of recycled aggregate in structural concrete elements. In: 9th international congress of Croatian society of mechanics
19. Kirankumar G, Saboor S, Vali SS, Mahapatra D, Setty ABTP, Kim KH (2020) Thermal and cost analysis of various air filled double glazed reflective windows for energy efficient buildings. J Build Eng 28:101055
20. Kirankumar G, Saboor S, Vali SS, Mahapatra D, Setty ABTP, Kim KH (2020) Thermal and cost analysis of various air filled double glazed reflective windows for energy efficient buildings. J Build Eng 28:101055
21. Leising E, Quist J, Bocken N (2018) Circular economy in the building sector: three cases and a collaboration tool. J Cleaner Prod 176:976–989
22. Mathiyazhagan K, Gnanavelbabu A, Lokesh Prabhuraj B (2019) A sustainable assessment model for material selection in construction industries perspective using hybrid MCDM approaches. J Adv Manage Res
23. Metzger BL (2003) Design for recycling: influencing product design using the Recyclability Index. Diss. Massachusetts Institute of Technology
24. Muthu SS et al. (2012) Recyclability potential index (RPI): the concept and quantification of RPI for textile fibres. Ecol Indicators 18:58–62

25. Nautiyal H, et al. (2018) Life cycle assessment of an academic building: a case study. Environmental carbon footprints. Butterworth-Heinemann, pp 295–315
26. Pomponi F, Moncaster A (2017) Circular economy for the built environment: a research framework. J Clean Prod 143:710–718
27. Pradhan S, et al. (2019) Comparative LCA of recycled and natural aggregate concrete using particle packing method and conventional method of design mix. J Clean Prod 228:679–691
28. Praseeda KI, Venkatarama Reddy BV, Mani M (2015) Embodied energy assessment of building materials in India using process and input–output analysis. Energy Build 86:677–686
29. Rames T, Prakash R, Shukla KK (2010) Life cycle energy analysis of buildings: an overview. Energy Build 42(10):1592–1600
30. Reddy BV, Jagadish KS (2003) Embodied energy of common and alternative building materials and technologies. Energy Build 35(2):129–137
31. Sakai S et al. (2014) An international comparative study of end-of-life vehicle (ELV) recycling systems. J Mater Cycles Waste Manage 16.1:1–20
32. Shifad S, Pati P, Das BB (2021) A multi-dimensional study on impact of energy efficiency on life cycle cost of a single-family residential building. In: Das BB, Nanukuttan SV, Patnaik AK, Panandikar NS (eds) Recent trends in civil engineering. Lecture notes in civil engineering, vol 105. Springer, Singapore
33. Simion IM et al. (2013) Comparing environmental impacts of natural inert and recycled construction and demolition waste processing using LCA. J Environ Eng Landscape Manage 21(4):273–287
34. Surekha B, Hegde MN, Jagadish KS (2016) Energy and building materials. Int J Civil Eng 5:13–24
35. Thomas J, Thaickavil NN, Wilson PM (2018) Strength and durability of concrete containing recycled concrete aggregates. J Build Eng 19:349–365
36. Tošić N, Jelena D, Vedran C (2016) Use of recycled and waste materials in concrete—A Serbian perspective. Researchgate.net
37. Tsuji A et al. (2006) Recyclability index for automobiles. In: Proceedings of the 99th annual meeting and exhibition of the air and waste management association, New Orleans, LA
38. van der Harst E, Potting J, Kroeze C (2016) Comparison of different methods to include recycling in LCAs of aluminum cans and disposable polystyrene cups. Waste Manage 48:565–583

Effective Criterion for Equipment Management in Construction Industry

Dolasankar Sahu and Mohibullah

1 Introduction

Since past couple of decades it's been clear that reliance upon equipment and machineries had increased tremendously not only because of rise of labour cost or their short supply but for profitability by increasing productivity [1]. Every construction projects requires different kinds of equipment and machineries designed for executing their respective construction tasks. For instance the shorter equipment usage for residential projects and usage of equipment and machineries are goes to moderate level for commercial projects and intense and high utilization for heavy and industrial projects [2]. Achieving efficiency and productivity from those equipment and machineries is vital for gaining profit in construction. Equipment management is very crucial in making profit out of construction projects as it varies from 5 to 30% of total cost of the construction project [3]. In context of construction, perceptible benefits of raised mechanization are self-evident that their application emboldens to perform towards higher productivity, reducing the cost and enhanced competitiveness between contractors [4]. Significant sum of capital are invested by the firms on numerous construction equipment to raise the magnitude of annual construction. Investments involves acquisition cost, operations, maintenance and replacement over lifespan of the equipment or machineries. Receiving such huge capital, construction equipment management must make sure the mentioned liabilities are undertaken efficiently and avert delays, inferior quality of work and cost overruns respectively [5]. On that account two key critical factors for managing equipment and machineries i.e. criteria for selection, maintenance must be considered strategically to improve productivity in construction. Proper equipment selection process is crucial which makes sure the effectiveness of proper equipment also cost effective and less time consuming during construction [6]. During equipment's downtime, due to cost of

D. Sahu (✉) · Mohibullah
Faculty of School of Civil Engineering, KIIT Deemed To Be University, Bhubaneswar, India

repair and other consequential cost firms suffers huge loss of capital for that suitable equipment maintenance management is essential to keep all the equipment and machineries fit and workable at all-time [7]. Therefore, equipment management having effectual selection and maintenance criteria is essential for generating maximum savings in construction industry.

In construction equipment management, there are many studies have done by several researchers where some developed some techniques, tools or models. According to the report by Day (1991) equipment selection is controlled by several constraints imposed by work and contractual obligations [8].

Samee and Pongpeng (2012) recommended a method for selecting appropriate type of equipment for contractors by first analyzing need for the type of equipment, capacity and appropriate quantity as for project. Then for each type of equipment cost-benefit analysis performed for buying, leasing and renting. Then selection factors for each equipment type and for every mode of procurement are formed out of which all required equipment are acquired [5].

Harris (1988) suggested crucial criteria for selection for earth moving equipment; machine capacity, function to be performed, operation method, method limitation, cost of the method, with other method cost comparison and possible alteration to project design under consideration [9].

Alkass et al. (2003) using queuing theory proposed a computer model for selecting earth moving equipment, then model examined on following criteria: equipment availability; equipment capacity; productivity, safety and cost of the equipment; and dimensions of equipment [10].

Shapira and Goldenberg (2007) taken into account the following factors for construction cranes selection; company policy regarding owning and renting, project forecast of the company, ground condition of the site, method for procurement and subcontracting, commercial considerations,, project specialization of the company, day rentals administration, dependence on outsourcing, responsibility shifting to external party, timetable and plan of progress, night shifts, interactions with other equipment, past experience, tradition, equipment pieces to manage, staging areas coverage by cranes, labour availability, site obstacles, site congestion, site accessibility, noise levels, owner and client satisfaction, heavy traffic, poor visibility due to weather conditions, reliability and equipment age, obstruction of crane operator view [11].

A computer model developed by Alkass et al. (1993) for selecting concrete transportation and placement equipment. Factors considered for evaluation are: vehicle capacity, site characteristics, output of the vehicle, weather conditions, rental cost, efficiency of operator and temporary haul on roads. Also suggested for accounting operation continuity, time restrictions, temporary works, effect of permanent work and concrete specifications [12].

A system developed by Chan et al. (2001) by four important factors for selection of material handling equipment (conveyors, industrial trucks, overhead conveyor cranes, automated guided vehicles, storage/retrieval systems): performance measures, economic aspects, technical aspects, strategic aspects [13].

A model suggested by Burt et al. (2005) for selecting mining equipment (trucks), the incorporated factors in the model includes characteristics of the mine material, requirement of haul route, loading equipment, maneuvering space, capacity, dumping conditions, power and altitude limitations of engine, mechanical drives gear ratios to final drive, size of the tire, three-axle or two-axle configuration choice, electrical or mechanical drive system choice, tread and ply rating [14].

Significant effort have made by earlier researchers to minimize downtime of equipment and machineries by providing models and theoretical frameworks. A health-monitoring framework developed by Said et al. (2014) for telematics-based equipment to gather performance parameters of important equipment to detect possible failure signs by assessing the condition of equipment regularly [15].

Prasertrungruang and Hadikusumo (2009) suggested a model which means to facilitate the relationship between operational practice, acquisition condition, quality of maintenance, disposal practice and consequences for downtime of heavy equipment [16].

For earth-moving wheel trucks Marinelli et al. (2012) examined several parameters (age, capacity, kilometers, maintenance) effect on deterioration process using discriminant analysis methodology. Also an Artificial Neural Network based model presented by Marinelli et al. (2014) for predicting condition level of earth-moving wheel trucks using mentioned parameters [17, 18].

A model introduced by Mohideen et al. (2011) which handles unpredictable breakdown issues in plants to reduce downtime and enable faster recovery, predicated from breakdown parameters obtained from earlier history of work records [19].

A comparative study presented by Yip et al. (2014) on General Regression Neural Network (GRNN) model and Box-Jenkins time series models to forecast construction equipment maintenance cost [20].

A methodology proposed by Curcuru et al. (2010) which reduces maintenance cost by figuring out the on which time decision must be taken and maintenance procedure starting date [21].

Sahexnayder and Hancher (2009) discovered that appropriate attention has not been given to maintenance of equipment as it should and as it contributes around 40% cost overrun of the total construction project [22].

In this paper, a vivid discussion has been done about two key critical factors for managing equipment and machineries i.e. criteria for selection, maintenance to improve productivity in construction.

2 Equipment Selection

Prime agenda to select any equipment is to achieve maximum productivity, flexibility in operation with consideration to viable economy. Based on the earlier studies it cannot be opposable that selecting an appropriate equipment is more of a strategic decision for any construction phase. Several factors proposed by Blundon (1980) which affect construction equipment selection [23]. These factors included

equipment maintainability; equipment costs; availability of market-work analysis; availability of equipment and parts for replacement; needs-specific requirements of contractor for current or future projects; assembly, dismantling time, transportability and logistics; versatility, mobility and adaptability; fuel, energy consumption policy; existing fleet compatibility to balance interdependent equipment; site conditions, influence of climatic conditions and time scheduled for the project; equipment reliability and durability; expected economic life and obsolescence; operator skills and training required; company bidding strategy–equipment costs; service and reputation of backup dealer; equipment capacity and power; brand name loyalty of equipment; trained service personnel availability; availability of proper support equipment and tools; available equipment options; operator convenience; salvage value of new equipment and safety and environmental protection standards.

2.1 Sustainable Criteria for Equipment Selection

Growing need for mechanization purpose to increase efficiency, quality and productivity, most of the time while selecting equipment and machineries environmental and social aspects are ignored. Concept of sustainability of construction has emphasized energy conservation, green environment, efficiency, economy and human well beings. Sustainability should be comprehensive and it must include the basic categories i.e. environmental, social, economic and technical aspects of sustainable construction [24, 25]. Based on research holistic guidelines proposed for sustainable criteria development which should be applicable for broad options with openness and practicability [26] (Fig. 1).

Environmental, social, economic and technical measures were emphasized by previous researchers for sustainable performance and their performance measures are direction to develop a broad and effective criterion includes fundamental aspects for sustainable equipment selection (Table 1).

2.2 Analytical Hierarchy Process (AHP)-Based Equipment Selection

AHP developed to help in making decisions where various interrelated characters involved with contending aspects or factors. Primary feature of this process is it deals systematically with larger tangible and objective factors as well as intangible and no quantifiable elements. Hierarchy construction is decomposing the complexity by identifying small factors which are organized in hierarchy like structure those creates big problem and planning their mutual relationship and then 'synthesizing the relations' by analyzing the relative weights of the factors and clustering their cumulative effect compared with a particular decision criteria. In this case, primary
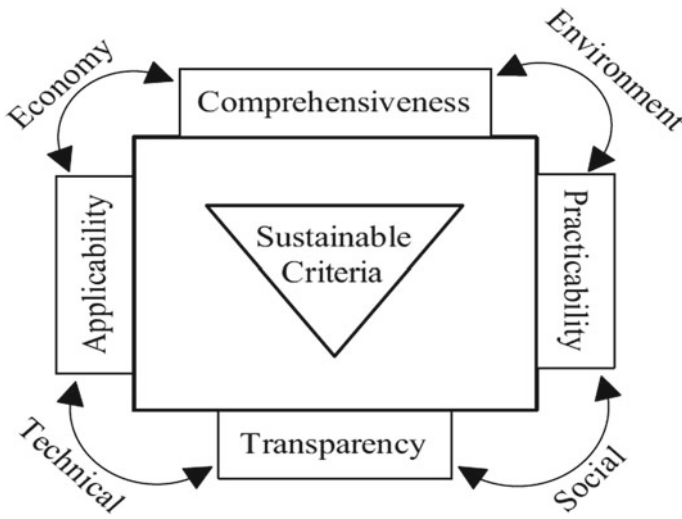
Fig. 1 Flow sheet for development of sustainable criteria

problem is comprises in several levels followed by set of attributes in each level. Like selection of equipment with respect to economy, efficiency, schedule and safety which are attributes of first level and so on. Five basic AHP elements such as hierarchy construction, pairwise comparison, Relative-Weight calculation, Aggregation of relative weight and Consistency ratio are required to be determined. The mentioned model 3 primary modules are comprised; cost evaluation of alternatives, benefit evaluation of alternatives and total evaluation of alternatives [12].

Process of selection starts with priliminary phase that is gathering information and feasible alternative generation and so on for each level since thegoal is to obtain the best possible production system (Figs. 2, 3).

2.3 Soft Factors for Equipment Selection

Selection criteria classified in two factors; tangible and intangible. Technical specifications, cost consideration and site conditions are grouped as tangible (hard) factors and intangible (soft) factor are changes with situation, environment, company, authorities, regulations etc. Soft factors considered for selecting equipment for major construction projects plays a crucial role in wise decision making especially for project planning team and project manager. Soft factors for equipment selection are;

Table 1 Sustainable criteria list for selection of construction equipment [2]

Engineering criteria	Socio-economic criteria	Environmental criteria
Equipment age	Ownership cost	Greenhouse gas emissions
Equipment capacity	Operational cost	Fossil fuel consumption
Equipment reliability	Local skilled operator availability	Energy saving
Equipment efficiency	Operator health	Noise control
Equipment operating life	Operator view and comfort	Vibration control
Equipment productivity	Safety features	Quantity of particulate matter
Fuel efficiency	Operator proficiency	Oil/lube leakage control
Implement system	Training needs for operator	Use of sustainable fuels
Traction system	Relationship with dealer/supplier	Use of biodegradable Lubricants and hydraulic oil
Structure and suspension system		Environmental statutory compliance
Power train system		
Control and information system		
Compliance with site operating conditions		
Meet job/operational requirements		
Meet haul road condition		
Versatility of equipment		
Easy repair and maintenance		
Machine/equipment standardization		
Spare parts availability		

1. Policy of company regarding owning and renting	2. Ground condition at site	3. Project forecast of the company
4. Commercial consideration	5. Sub-contracting and procurement procedure	6. Project specialization of company
7. Day rental administration	8. Outsourcing dependence	9. Responsibility shifting to external party
10. Night shift work	11. Timetable and progress plan	12. Interaction between other equipment
13. Past experience, tradition	14. Equipment pieces to manage	15. Staging area coverage by crane
16. Congestion at site	17. Obstacles on site	18. Availability of labor

(continued)

(continued)

1. Policy of company regarding owning and renting	2. Ground condition at site	3. Project forecast of the company
19. Noise level	20. Site accessibility	21. Heavy traffic
22. Owner/client satisfaction	23. Poor visibility due to weather condition	24. Reliability and equipment age
25. Strong wind	26. Overlapping of crane work envelope	27. Obstruction of crane operator view

The mentioned state-of-the-art equipment selection model could be beneficial for selecting building construction equipment [27] (Fig. 4).

3 Downtime of Equipment

Downtime is defined as machine unable to perform for any cause i.e. maintenance or breakdown. Maintenance leads to direct cost for equipment downtime and indirect cost from construction delay, client goodwill loss and reduction in profit margin [28, 29].

3.1 Downtime Factors

Site factors—Unprecedented site condition due to lack of data or improper site investigation, environmental condition may differ during operation [28, 30]. Site location may restrict the size and type of equipment to transport to site [8]. However equipment's repair time may affect due to improper communication or promptness in procuring the parts because of remoteness of work site.

Equipment factors—Equipment breakdown risk connected to sophistication and complexity of mechanical and hydraulic system of equipment [30, 31]. In terms of site management it is crucial to have accurate knowledge of capacity, technical suitability and complexity of equipment under different conditions.

Crew-level factor—Human aspects of crews plays important role in operation, maintenance and process of production. Skill of the operator is crucial factor which affects performance of operator and through efficiency of work direct cost of downtime also [30–32]. Equipment misuse caused by operator negligence and improper training may lead to increased frequency and downtime cost [33]. When management at site tries to increase rate of work by extensive overtime and putting pressure on crews to avoid downtime impact, morale and motivation of the crews may have negative impact and as consequence can have negative effect on productivity [34, 35].
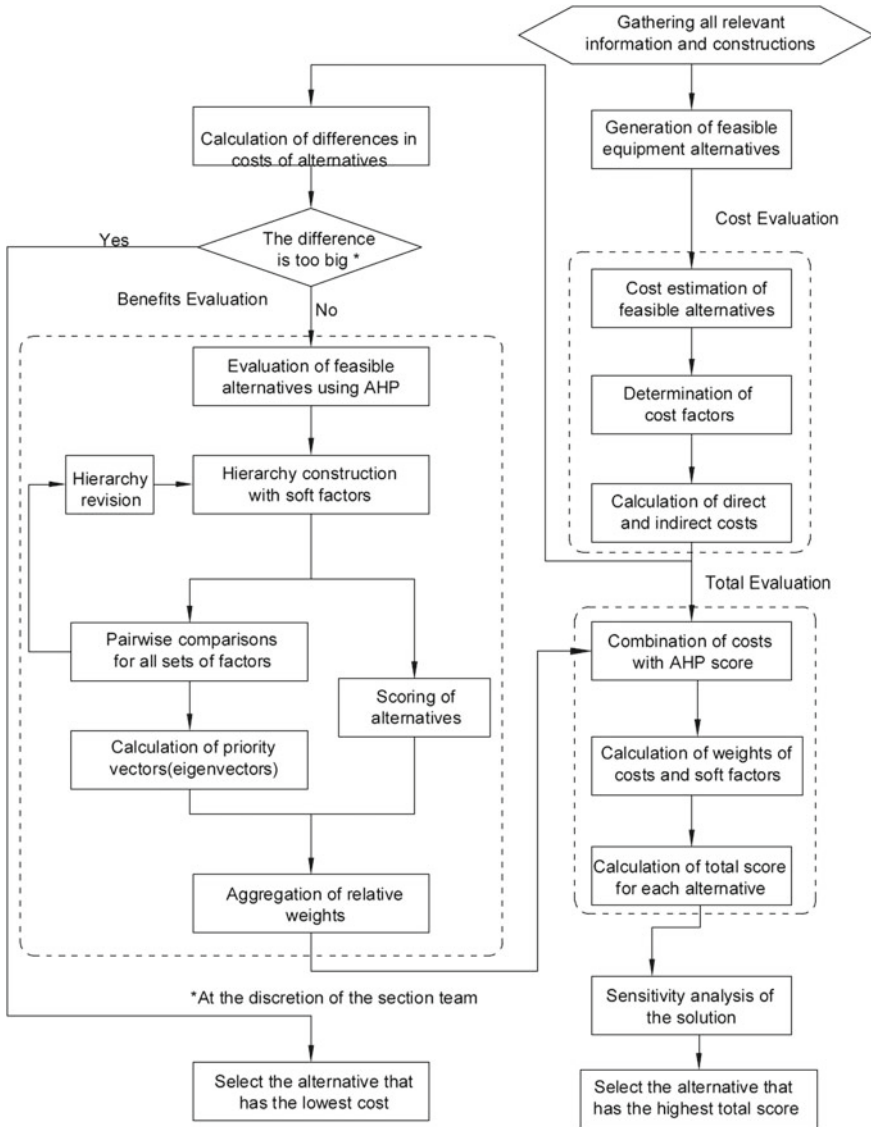
Fig. 2 Equipment selection process

Force majeure—This category related to natural events and calamities which are unprecedented participants on the project and which may result in equipment maintenance delay and affect performance of project as well. Seasonal events should be anticipated by contractors and adapt required precautions to reduce likely impact on downtime [33].
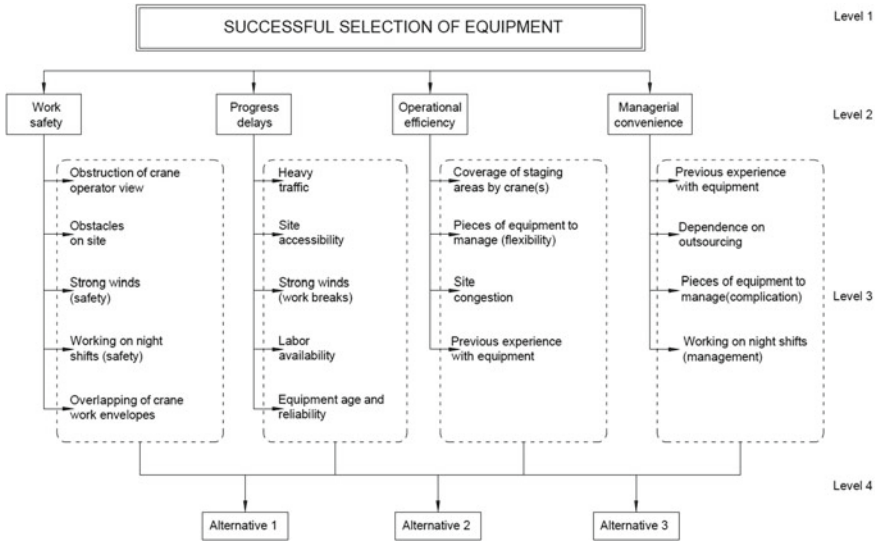
Fig. 3 Equipment selection hierarchy
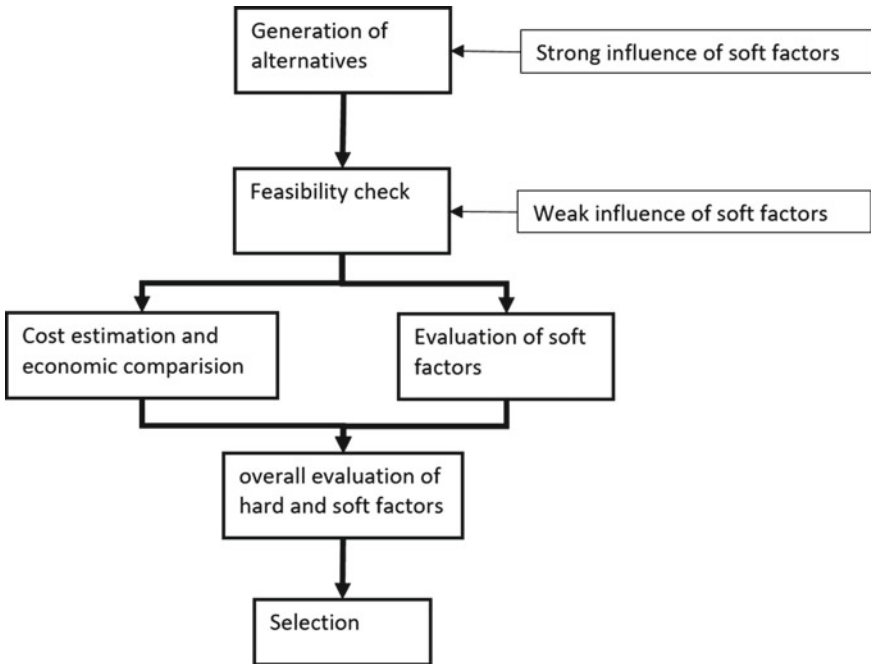
Fig. 4 Equipment selection process

Procedures and policies of company—Construction firms' equipment policies mirror the priorities set by management and strategic planning and resource allocation as well [36]. Mostly it is strategic importance for a company to keep a proper equipment fleet, contract award also based on condition to equipment availability.

Factors at project-level—spare parts availability, rental facilities, resources, workshop sophistication and its location, on hand substitute equipment and other specific requirement are significant to downtime. Delay in skilled mechanics to arrive on site may stop the work.

Actions of site management—Downtime may influenced by management at site in many ways such as wait for fractured equipment to be repaired, replace the equipment that broken, changing or adding resources, quicken the activities, crew transfer to other site or operations, changing work sequence. Executing mentioned actions properly may reduce downtime impact and improper application may aggravate the situation. As a result project suffers loss of productivity.

Downtime and consequences—Equipment and crews' idleness, disruption of work, delays of activity and productivity loss are some downtime consequences. These consequences may act according to actions of site management, procedures and policies of company, crew level factor and factors at project level. Thus management at site should understand the event of downtime and its likely impact on project and its performance in proper way (Fig. 5).
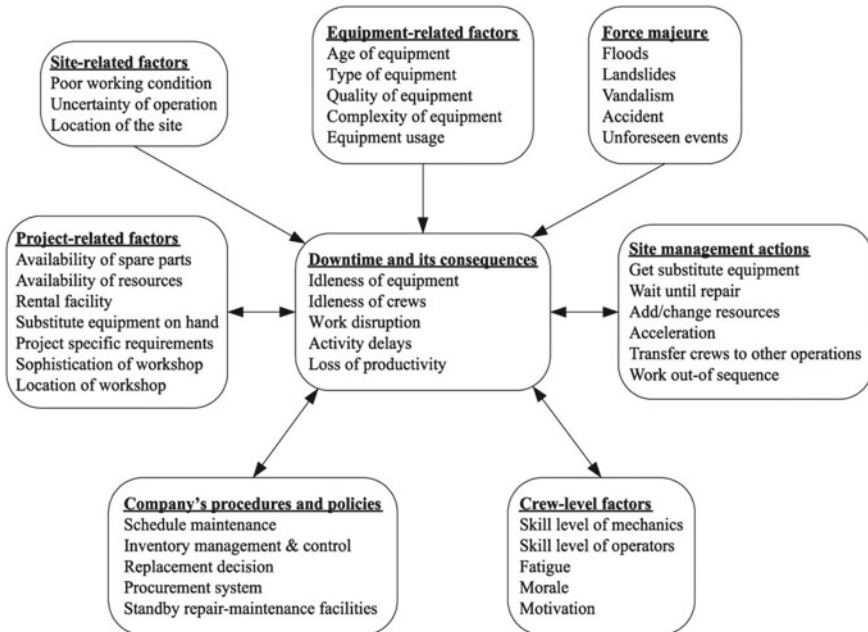
Fig. 5 Analysis of downtime factor

4 Downtime Impact Computation

Definition of downtime can be expressed as unavailability of equipment for the period it assigned to work due to breakdown. Downtime percentage is calculated as for planned work hours;

Downtime percentage = (Total down time hours/Total planned workhours) ∗ 100

Downtime costs can be grouped in two groups: Tangible cost and Intangible cost [37]. Labor cost, resources for equipment repairing, wages of operator, production loss by equipment are under tangible cost. Increased cost resulting from production loss of different resources starved of production, labor productivity loss, stretched overhead cost, in some situations late-completion charges and liquidated damages [33, 38]. Sum of all categories cost are downtime cost of equipment.

Repair cost: consist of three items cost such as Labor (helpers/mechanic), materials and spare parts for repair.

Idle cost for supervisors, operators and laborers: Cost occurs for human resource idle time.

Wages of workers will continue to be paid who are idle when equipment fails.

Equipment Idle cost: This cost incorporates idle cost of broken equipment and any dependent stays idle result of it. Equipment should be use productively and earn revenues adequately to retrieve its investment cost which is the prime focus in equipment financing.

Equipment substitution cost: This cost added when management decides for substitution of fractured equipment either from their own fleet (contractor would have employed the equipment in other project or lend it on rent) or form agency outside.

Labor productivity loss: Work disruption, crowding of workers, accelerated work, extended overtime, learning curve effects and so on are seeded by downtime [39–43].

Project associated cost: Liquidated damages, late completion penalties and additional claims are under this category.

Other costs: Overtime costs, encouragement paid to workers, accelerations cost and miscellaneous expenses are indirect costs related to downtime event.

Based on aforementioned categories

Percentage of downtime cost for any project
= (Total downtime cost/Budgeted Project Cost) ∗ 100
Downtime impact cost = Total downtime cost/Total downtime hours

5 Equipment Maintenance

Cost of maintenance should not be considered as burden but an investment towards future revenue increment of the company (Robert et al. 2006). The invested amount while purchasing the equipment should recover within their useful period only if it is kept under smooth working condition through effective maintenance strategy.

5.1 Preventive Maintenance

It can be expressed as equipment maintenance before defect occurs. Maintenance prime goal is to avoid the equipment failure consequences. Prevent failure before defect actually occurs to preserve reliability of equipment is by replacing worn-out part/components before complete failure. Along with lubrication to equipment should take place routinely. Due to routine preventive maintenance equipment downtime minimizes, likely liability reduces, equipment life increases.

5.2 Personnel Training

Operators of different equipment and machineries should know about maintenance and is beneficial so that whenever equipment shows sign of fault they can be self-help or assist to maintenance personnel for repairs. Maintenance knowledge and skill development training in the company is a great way to ensure that operators gather sufficient skills, proficiency and remain motivated.

5.3 Administration for Equipment Parts

Adequate spare parts administration is important for getting suitable parts at the time when equipment fails and need to be replaced.

6 Discussion

Principal functions of plant managers or construction managers are to plan, procure, organize and control. Objective of operation manager to make right decisions to obtain the appropriate plant and machineries for accomplishment of proposed work. Mechanization in construction industry has been driven by two aspects which are output maximization and operating cost minimization with respect to each input.

At the time of selecting constructional equipment requirement for a most sensible criteria, it is essential having a favorable impact on productivity, operational efficiency, cost minimization, and human and environmental wellbeing.

AHP model includes context and particular conditions of project and it allows user experience and subjective perception manifestation while getting structured process framework and satisfying consistency in solution.

Several factors and processes interrelate one-another results downtime and lessen or worsen its effect on project performance. Construction firms required to manage equipment and maintenance strategy proactively to minimize the effect of downtime. Several factors mentioned may cause downtime and consequences so to counteract these, special efforts are required to reduce the impact like caused factor of downtime should identify, importance to crew-level factors, downtime consequence can take place by producing feedback structure by actions and decisions at management level, contractor's part in controlling the downtime, detecting the cause of downtime and its effect on performance of the project.

For Safety, higher output, better productivity and more effectiveness, equipment and machineries must be maintained properly.

7 Conclusion

Construction firms requires to embrace management of equipment and machineries proactively to avoid nontrivial influence because of equipment issues in construction performance.

Mentioned sustainable criteria are forecasted to contractors in selection and deployment of equipment and machineries that fulfil the TBL framework of sustainability i.e. profit, people, Planet. AHP-based model proven to be convenient and user-friendly tool, particularly given the relatively complex process it is applied to here, its built-in facility to force the user into orderly, methodical thinking, and its inherent capacity to unveil the tacit knowledge of the competent, experienced user.

Right equipment selection is pivotal for project success. Therefore it is of significant importance to have extreme understanding and realization of issue of soft consideration and the criticality of their structured integration in the process of selecting the equipment. State of the art equipment selection process is mentioned includes verity of soft factors for current construction environment which could be beneficial to selection of equipment.

Enough stock of fast breaking and wearing parts to be kept in inventory. Also definite or fixed percentage of expenditure or funds be made for spare parts while new equipment being purchased. When shift ends or at the weekend when machine not performing work, prior to failure replacing worn parts can improve the availability time of equipment.

For supervisors and operators training is necessary to possess the knowledge thoroughly of equipment like functionality and capacity. Extremely skilled mechanics are required at workplace to guarantee of quality maintenance.

References

1. And HFC, Mccaffer R (1991) Management of construction equipment. Macmillan, London
2. Waris M, Liew MS, Khamidi MF, Idrus A (2014) Criteria for the selection of sustainable onsite construction equipment. Int J Sustain Built Environ 3:96–110
3. Prasannasangeetha A, Alan S (2015) Equipment management in construction sector. Int J Sci Eng Res 3(6)
4. Lynn M (1996) Buildings decline and fall. Management Today 28–32
5. Samee K, Pongpeng J (2015) Structural equation model for construction equipment management affecting project and corporate performance. KSCE J Civil Eng 1–15
6. Phogat VS, Singh AP (2013) Selection of equipment for construction of a hilly road using multi criteria approach. Soc Behav Sci 104:282–291
7. Manikandan M, Adhiyaman M, Pazhani KC (2018) A study and analysis of construction equipment management used in construction projects for improving productivity. Int Res J Eng Technol 5(3):1297–1303
8. Day DA, Benjamin NBH (1991) Construction equipment guide. John Willey & Son Inc., New York
9. Alkass S, Harris F (1988) Expert system for earthmoving equipment selection in road construction. J Construct Eng Manage ASCE. 114:426–440
10. Alkass S, El-Moslmani K, Alhussein M (2003) A computer model for selecting equipment for earthmoving operations using queuing theory. In: Annual conference of the international council for research and innovation in building and construction (Cib), Auckland, New Zealand, W78
11. Shapira A, Goldenberg M (2005) AHP-based equipment selection model for construction projects. J Constr Eng Manage 131(12):1263–1273
12. Alkass S, Aronian A, Moselhi O (1993) Computer-aided equipment selection for transportation and placing concrete. J Constr Eng Manage 119(3):445–465
13. Chan FTS, Ip RWL, Lau H (2001) Integration of expert system with analytic hierarchy process for the design of material handling equipment selection system. J Mater Process Technol 116(2–3):137–145
14. Burt C, Caccetta L, Hill S, Welgama P (2005) Models for mining equipment selection. In: Proceedings of the Modsim 2005 international congress on modelling and simulation, pp 1730–1736
15. Said H, Nicoletti T, Perez-Hernandez P (2014) Utilizing telematics data to support effective equipment fleet-management decisions: utilization rate and hazard functions. J Comput Civil Eng 04014122:1–11
16. Prasertrungruang T, Hadikusumo BHW (2009) Modeling the dynamics of heavy equipment management practices and downtime in large highway contractors. J Constr Eng Manage 135(10):939–947
17. Marinelli M, Lambropoulos S, Petroutsatou K (2014) Earthmoving trucks condition level prediction using neural networks. J Qual Maintenance Eng 20(2):182–192
18. Marinelli M, Lambropoulos S, Pantouvakis JP (2012) Investigation of earthmoving trucks deterioration using discriminant analysis. Int J Project Organization Manage 4(4):397–413
19. Mohideen A, Ramachandran M, Narasimmalu RR (2011) Construction plant breakdown criticality analysis—part 1: UAE perspective. Benchmarking: Int J 18(4):472–489
20. Yip H, Fan H, Chiang Y (2014) Predicting the maintenance cost of construction equipment: comparison between general regression neural network and box-Jenkins time series models. Autom Constr 38:30–38
21. Curcurù G, Galante G, Lombardo A (2010) A predictive maintenance policy with imperfect monitoring. Reliab Eng Syst Saf 95(9):989–997
22. Schexnayder PE, Hancher F (2009) The true cost of equipment failure, 3rd edn. Netta Hook, Germany
23. Blundo GH (1980) Comparison of methods for evaluating construction equipment acquisition. Master Thesis, Concordia University, Quebec, Canada

24. Chen EA, Okudan GE, Riley DR (2010) Sustainable performance criteria for construction method selection in concrete building. Autom Constr 19(2):235–244
25. Singh RK, Murty HR, Gupta SK, Dikshit AK (2007) Development of composite sustainability performance index for steel industry. Ecol Ind 7(3):565–588
26. Akadiri OP, Olomolaiye OP (2012) Development of sustainable assessment criteria for building materials selection. J Eng Constr Archit Manage 19(6):666–687
27. Shapira A, Goldenberg M (2007) Soft considerations in equipment selection for building construction projects. J Constr Eng Manage 133:749–760
28. Edwards DJ, Holt GD, Harris FC (1998) Maintenance management of heavy duty construction plant and equipment. Chandos Publishing, Current and future construction plant research, pp 121–124
29. Edwards DJ, Holt GD, Harris FC (1998) Predictive maintenance techniques and their relevance to construction plant. J Qual Maintenance Eng 4(1):25–37
30. Arditi D, Kale S, Tangkar M (1997) Innovation in construction equipment and its flow into the construction industry. J Constr Eng Manage 123(4):317–380
31. Elazouni AM, Basha IM (1996) Evaluating the performance of construction equipment operations in Egypt. J Constr Eng Manage 122(2):109–114
32. Edwards DJ, Holt GD, Harris FC (2000) A model for predicting plant maintenance costs. Constr Manage Econ 18:68–75
33. Pathmanathan V (1980) Construction equipment downtime costs. J Constr Div 106(4):604–607
34. Cooper KG (1994) The $2,000 hour: how managers influence project performance through the rework cycle. IEEE Eng Manage Rev 22(4):12–23
35. Roberts EB, Alfred P (1974) A simple model of R & D project dynamics. R & D Manage 5(1):1–15
36. Sözen Z, Giritli H (1987) Equipment policy as one of the factors affecting construction productivity: a comparative study. In: Lansley PR, Harlow PA (eds) Managing construction worldwide: productivity and human factors in construction, 5th international symposium. CIOB, CIB, London, pp 691–696
37. Vorster MC, De La Garza JM (1990) Consequential equipment costs associated with lack of availability and Dt. J Constr Eng Manage 116(4):656–669
38. Tsimberdonis AI, Murphee EL Jr (1994) Equipment management through operational failure costs. J Constr Eng Manage 120(4):522–535
39. Construction Industry Institute (CII) (1995) Quantitative effects of project change. Project Management Research Team, Publication, Austin, TX, pp 43–52
40. Eden C, Williams T, Howick S (2000) The role of feedback dynamics in disruption and delay on the nature of disruption and delay in major projects. J Oper Res Soc 51:291–300
41. Halligan DW, Demsetz LA, Brown JD, Pace CB (1994) Action-response model and loss of productivity in construction. J Constr Eng Manage 120(1):47–64
42. Horner RMW, Talhouni BT (1995) Effects of accelerated working, delays and disruption on labour productivity. The Chartered Institute of Building, Ascot
43. Schwartzkopf W (1995) Calculating lost labour productivity in construction claims. Wiley Law Publications, Wiley, New York, NY

Development in Sustainable Infrastructure—Correlation of Concrete Core Data

Shrushti Faldessai and K. G. Guptha

1 Introduction

The in-place compressive concrete strength is primarily assessed utilizing different non-destructive test methods on existing concrete structures. There are different available test methods to evaluate the quality of the existing concrete structures [1, 2]. These tests vary from completely non-destructive to partially destructive tests. The most widely used test method for the assessment of the strength of concrete is by core drilling and testing [3, 4]. Though the coring process is time-consuming and very costly, it gives accurate results of the actual condition of the structures [5]. Whereas rebound hammer and UPV tests give approximate results [6]. Non-destructive methods such as rebound hammer test and ultrasonic pulse velocity test show indirect measurements of concrete strength as compared to the semi destructive test of core testing which provides a direct assessment of concrete quality [7–9]. The concrete quality is mainly controlled by core diameter, L/D ratio and its shape.

2 Materials and Methodology

2.1 Materials

Ordinary Portland cement (OPC) of grade 53 (Dalmia cement) having specific gravity of 3.15 was used in this research analysis. It was also confirmed that the water content used was satisfying the stipulations provided in IS 10262(2009). Manufactured sand (M sand) passing through 4.75 mm sieve was used in this research study. The standard sand used was following the requirements as per IS 650:1991. The specific gravity

S. Faldessai (✉) · K. G. Guptha
Goa Engineering College, Farmagudi 403401, India

Fig. 1 Rebound hammer

of the sample was 2.76 and was under the zone II category. Coarse aggregates having different sizes (6 mm, 10 mm, and 20 mm) were used in this experiment.

2.2 Methodology

2.2.1 Schmidt's Hammer Test

Rebound Hammer test is an independent field test that measures the exterior surface stiffness and quality of the concrete. Rebound Hammer consists of a plunger that was pushed against the concrete perpendicular to the exposed surface. The main principle of this test is that the impact spring-mass bounces back when the plunger of the device is pressed against the hard surface with a fixed amount of energy. When the hammer rebounds, it shows the rebound index which is recorded on a graduated scale. This rebound number indicates the surface hardness of the concrete. If the rebound number is less than 20, it indicates that the quality of the concrete is very bad and if more than 40, the quality of the concrete is very good (Figs. 1, 2).

2.2.2 Ultrasonic Pulse Velocity Test

This testing device consists of transducers that are in contact with two opposite faces of the specimen being tested that transmits and receives the ultrasonic waves generated from one end to another. The time taken for the ultrasonic waves to travel between the two probes was noted in microseconds. Distance between the transducers was also recorded. Once the distance and time were known, pulse velocity was calculated by the following formula: **Velocity = distance/Time in km/s**.

Higher the pulse velocity, better is the quality of the concrete and it should be more than 4 km/s. If less than 3.0 km/s it indicates, poor quality of the concrete (Fig. 3).

Fig. 2 UPV instrument

Fig. 3 Core cutting machine
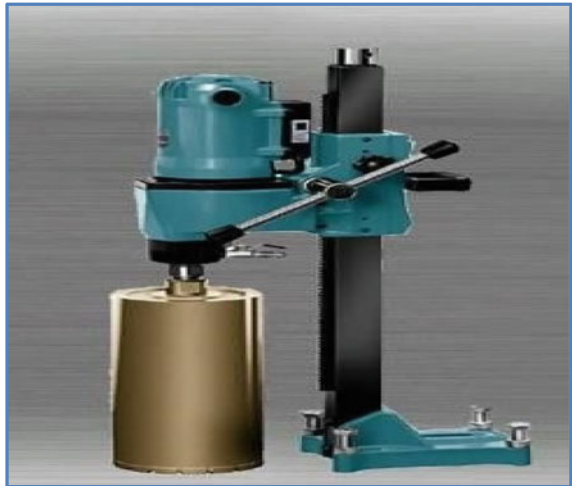
2.2.3 Core Compression Test

Cores are either extracted from the existing concrete structures or removed from the concrete blocks. These cores were taken out by core cutting machines having diamond bits and testing was done as per ASTMC 42–77. All the samples were then cured for 28 days. During the coring process, the machine gets heated up, to prevent this water was added for the smooth operation of the process. When the cores were taken out, their ends were not even and before testing it.

Should be properly capped with a suitable material like molten sulfur. Capping of cores was required so that the loads were uniformly applied at the ends.

3 Experimental Work

All the experimental work was conducted at Dilip Buildcon Ltd (DBL) at Cortalim-Goa. The moulds were prepared from the waste plywood on the site having different dimensions that are given in the Table 1. The various diameters used were of sizes 69 mm, 100 mm and 150 mm with H/D ratio of 1.5. Keeping the H/D ratio fixed height was calculated for various diameters used (Fig. 4).

A total of 3 trials were carried out by varying core diameter and aggregate sizes. The slenderness ratio (H/D) of the core was kept constant throughout the work. For each mix design trial, 6 cores were removed out of which 3 were tested for compression testing and the remaining 3 for water absorption of cores. From the 4 cubes cast 3 were tested for compression testing and remaining 1 for water permeability test on cubes. Different physical tests such as specific gravity tests on cement, fine and coarse aggregates, water absorption test on fine aggregates and coarse aggregates and particle size distribution test on fine sand was carried out (Tables 2, 3 and Figs. 5, 6).

Table 1 Material properties

Grade of concrete	M25
Slump	100 mm
Water cement ratio	0.45
Gradation of F.A	Zone II
Specific gravity of cement	3.15
Specific gravity of F.A	2.76
Specific gravity of C.A	2.83
M.S.A	20 mm
Water absorption of M sand	1.93%
Water absorption of C.A	0.80%

Fig. 4 Moulds of different sizes

Table 2 Core diameters and mould dimensions

Description	Core diameter (mm)	Mould dimensions L × B × H (mm)
1	150	500 × 340 × 225
2	100	340 × 230 × 150
3	69	250 × 170 × 103.5

Table 3 Final mix proportions

Material	Kg/cum
Cement	350
Water	183
F.A	731
C.A	1291

Fig. 5 Front view of cores with varying diameters and heights

Fig. 6 Top view of cores with varying diameters and heights

4 Results and Discussions

4.1 Water Absorption and NDT Test on Cores

The water absorption value increases from 2.26% to 3.72% as aggregate size decreases from 20 to 6 mm. When the maximum size of aggregates increases, the surface area to be wetted by water per unit volume reduces, which can be seen from the table that the smaller size aggregates absorbs more water compared to bigger size aggregates. **The permissible limits of water absorption are 1.5 to 3% for natural river sand, whereas it is 2% to 4% for manufactured sand**. The water absorption value for 20 mm, 10 mm and 6 mm size aggregates are within the acceptable limits. The difference in the percentage from 20 to 10 mm size aggregates was 0.7% and 0.76% for aggregate size of 10–6 mm (Fig. 7).

Referring to Fig. 8, it is observed that, the ultrasonic pulse velocity values increases as aggregate size increases from 6 to 20 mm. The concrete quality for all the three sizes of aggregates (6, 10 and 20 mm) was found out to be very good to excellent. There was not much difference observed for UPV values when tested on 3rd and 28th days. The variation in the UPV values from 6 to 10 mm size aggregates was observed to be 34.4% and from 10 to 20 mm it was 47.9%. The above figure shows a linear increase in the UPV readings obtained for different sizes of coarse aggregates. The deviation in the UPV values for 20 mm size aggregates was seen to be 2.98% between 3rd and 28th days of concrete and it was 3% to 4% for natural sand.

Referring to Fig. 9, it can be seen that, as the size of aggregates increase, rebound number also increases. The concrete quality for 20 mm size aggregates was very good and the variation in the rebound number on 3rd and 28th days was very less. The increase in the percentage was estimated to be 28.9% for aggregate size varying from 6 to 10 mm and 11.2% for 10 mm to 20 mm. The fluctuations in the rebound number for 20 mm size aggregates was measured to be 3.89% between 3rd and 28th days of concrete, whereas it was 7–10% for river sand.
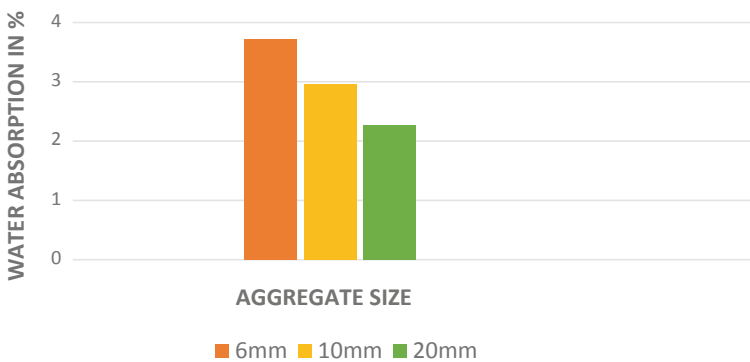
Fig. 7 Water absorption for 6 mm, 10 mm and 20 mm aggregate sizes
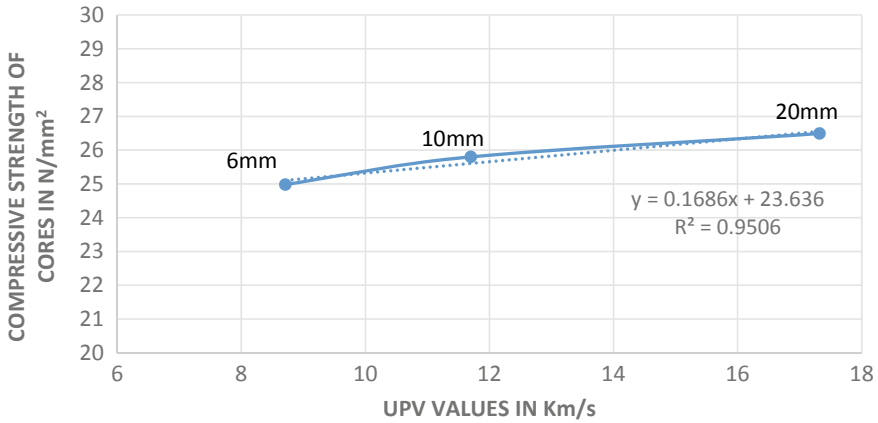
Fig. 8 UPV values for varying aggregate sizes
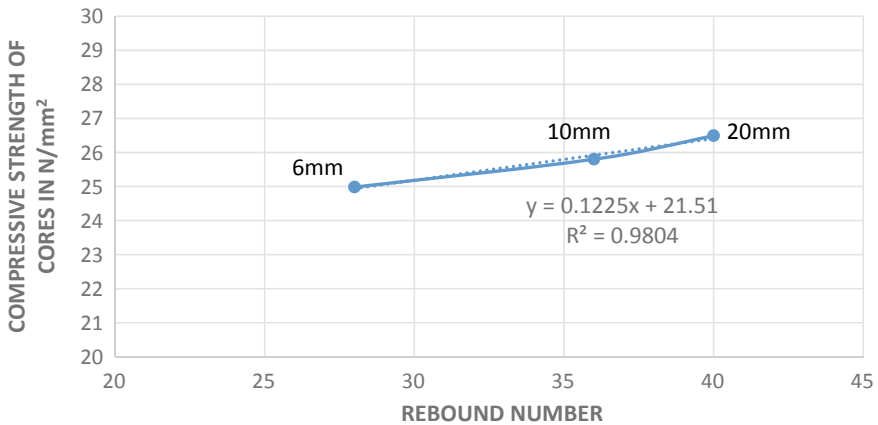
Fig. 9 Rebound number for varying aggregate sizes

4.2 Compressive Strength of Cubes, Cores and Water Penetration

The results presented below in Fig. 10, shows that, as the maximum size of aggregate increases, its compressive strength of cubes also increases. The highest compressive strength was observed for 20 mm size aggregate. The variation in the compressive strength for 6 mm to 10 mm and for 10 mm to 20 mm size aggregates was increased by 9.46% and 7.68% respectively after 3 days of curing. The increase in the percentage of strength was 3.11% and 3.74% for aggregate size 6 mm to 10 mm and 10 mm to 20 mm respectively after 7 days. Similarly the increase was 1.96 and 2.44% for aggregate size 6–10 mm and 10–20 mm after 28 days. Whereas in case of natural
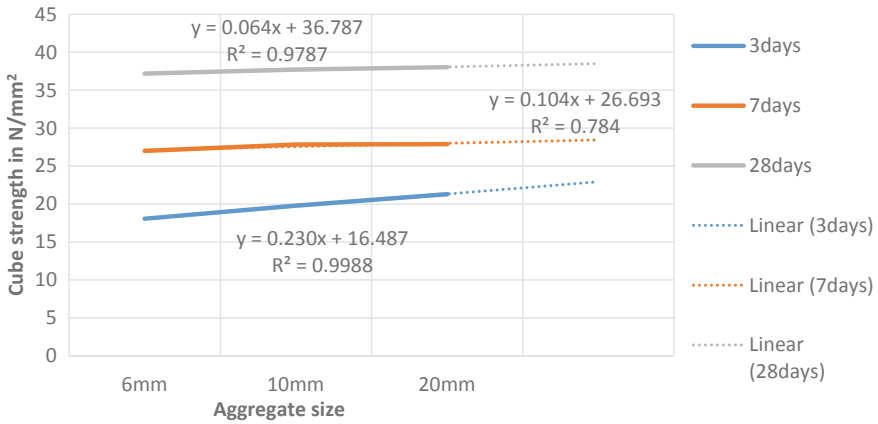
Fig. 10 Compressive strength of cubes at 3, 7 and 28 days

river sand, the increase in the percentage was estimated to be 15.71% for 10–20 mm size aggregates.

Referring to Fig. 11, it can be concluded that there is a linear relationship between corrected compressive strength of cores and core diameter. The compressive strength of the core increased, as the core diameter increased from 69 to 150 mm. The highest compressive strength was achieved for core diameter of 150 mm. The difference in the compressive strength was noticed to be 6.04% and 13.81% when core diameter increased from 69 to 150 mm after 28 days and 3 days respectively. For concrete with 20 mm size aggregate and having natural river sand, 69 mm diameter core has been tested to give 6% to 7% lower values than with 100 mm diameter cores. Whereas, the decrease in the strength is 3.28% for 100 to 69 mm diameter core when used with manufactured sand.
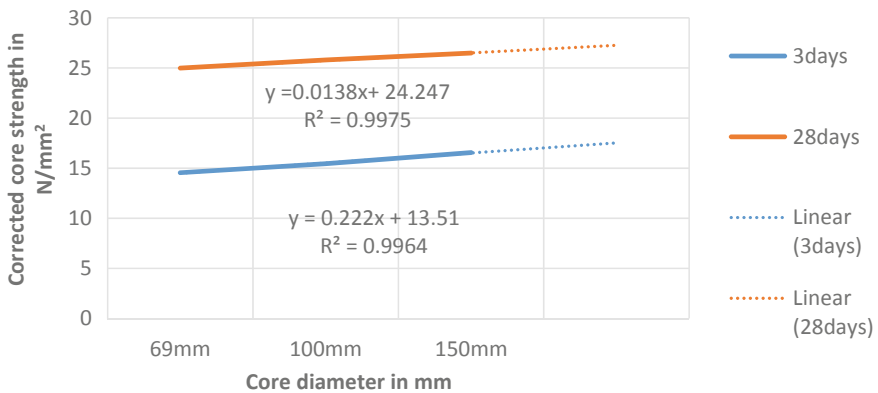
Fig. 11 Compressive strength of cores v/s core diameter

The above Fig. 12, shows cube strength and corrected strength of cores after 28 days of concrete. The difference in the strength variation between cubes and cores after 3 days of testing was found out to be 24.2%, 27.9% and 28.2% for core diameter of 69 mm, 100 mm and 150 mm respectively. After 28 days, the strength variation was 48.83%, 46.20% and 43.60% for core diameters of 69 mm, 100 mm and 150 mm respectively. For river sand the strength variation between core strength and cube strength is estimated to be 25%.

Referring to Fig. 13, it is observed that the depth of penetration decreases as aggregates size increases from 6 to 20 mm. The rise in the percentage was found to be 21.42% for aggregate size varying from 20 to 10 mm and 23.52% for 10–6 mm. The depth of penetration achieved for manufactured sand was marginally higher compared to river sand. Water penetration results for various sizes of aggregates
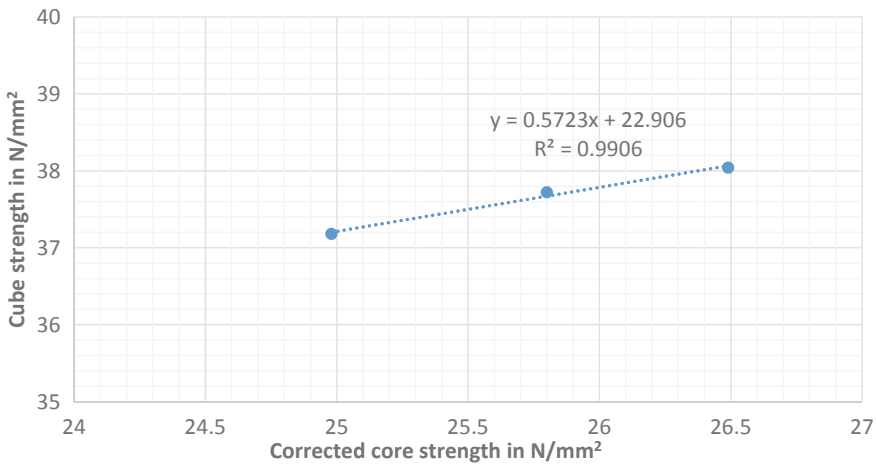
Fig. 12 Corrected cores strength v/s cube strength at 28 days
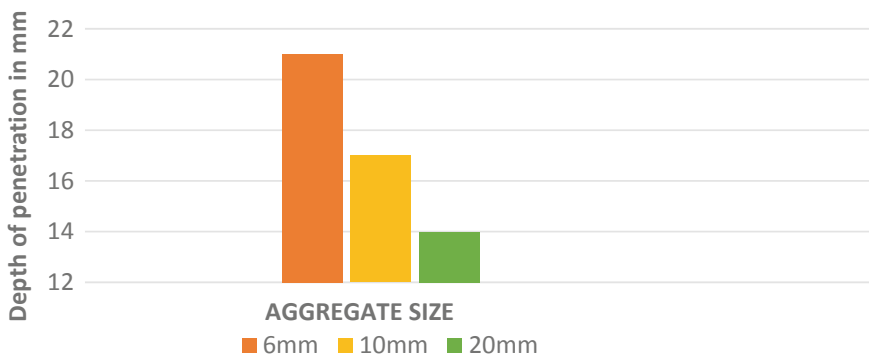
Fig. 13 Water penetration test on cubes

Table 4 Comparison of natural sand and m sand

Parameter	Natural sand	M sand	Increase or decrease w.r.t. Natural sand	Remarks
Water absorption	1.5%–3%	2%–4%	0.5%–1%(↑)	Greater W.A for M sand
Cube strength	28.85 N/mm^3	38.04 N/mm^3	31.85%(↑)	High strength obtained with M sand
Core strength	23.08 N/mm^3	25.80 N/mm^3	11.78%(↑)	Comparatively higher strength with M sand
Density	1.44 kg/m^3	1.75 kg/m^3	21.52%(↑)	Density achieved is more for M sand
Rebound values	36	40	11.11%(↑)	Better quality control with M sand
UPV values	10.5	17.3	64.76%(↑)	Excellent quality achieved with M sand
Specific gravity	2.3–2.7	2.5–2.9	2.93%(↑)	S.G obtained for M sand is more
Permeability	12 mm	14 mm	16.7%(↓)	Marginally higher for M sand

was within the permissible limits, which is 25 mm. There are several factors like water-cement ratio, compaction of concrete, curing of concrete and other factors that influence permeability of concrete to a great extent (Table 4).

5 Conclusions

The water absorption value increases from 2.26% to 3.72% as aggregate size decreases from 20 to 6 mm. The difference in the percentage from 20 to 10 mm size aggregates was 0.7% and 0.76% for aggregate size varying from 10 to 6 mm. The UPV values increases as aggregate size increases from 6 to 20 mm.The variation in the UPV values from 6 to 10 mm size aggregates was observed to be 34.4% and from 10 to 20 mm it was 47.9%. As the size of aggregates increase, rebound number also increases. The increase in the percentage was estimated to be 28.9% for aggregate size varying from 6 to 10 mm and 11.2% for 10 mm to 20mmAs the maximum size of aggregate increases, its compressive strength of cubes also increases. The variation in the compressive strength for 6 mm to 10 mm and for 10 mm to 20 mm size aggregates was increased by 1.46% and 1.0% respectively after 28 days of curing.

It was also observed that there is a linear relationship between corrected compressive strength of cores and core diameter. The difference in the compressive strength was noticed to be 13.81% and 6.04% when core diameter increased from 69 to 100 mm and from 100 to 150 mm after 3 and 28 days respectively. The difference in the strength variation between cubes and cores after 28 days of testing was found to

be 48.83%, 46.20% and 43.60% for core diameter of 69 mm, 100 mm and 150 mm respectively.

It can be concluded that concrete produced by using M sand has (15–20%) higher compressive strength compared to natural sand for the same grade of concrete. The concrete quality achieved with M sand is comparatively better than natural sand. It was seen that rebound and UPV values increases by 11.11% and 64.76% respectively compared to natural sand. The physical properties of concrete such as Specific gravity, Density, water absorption and permeability are more or less similar to natural sand. The specific gravity, density, water absorption and permeability values increases by 2.93%, 21.52%, 0.5% to 1% and 16.7% respectively compared to river sand.

References

1. Souidania A (2018) Aggregate size and lateral dimension effects on core compressive strength of concrete. Lisbon/Portugal
2. Kumavat HR, Patel VJ, Tapkire GV, Patil RD (2017) Utilization of combined NDT in the concrete strength evaluation of core specimen from existing building. Int J Innov Res Sci Eng Technol 6(1)
3. Patil SG, Shivkumar (2017) Correlation between actual compressive strength of concrete and strength estimated from core. 14(2)
4. Hanim M, Alaraji WA, Aziz Saim A, Nor Atimi W, Majid WA (2014) In-situ strength of concrete using the correlation of different NDT test methods. Int J Appl Eng Res 9
5. Bhosale N, Salunkhe PA (2016) To establish a relation between destructive and non- destructive tests on concrete. Int J Eng Res Gen Sci
6. Agarwal PK, Sharma S, Naval S, Sharma S (2013) Experimental study of core diameter varying H/D ratio on concrete core strength. Int J Eng Res Technol
7. Guptha S (2018) Comparison of non-destructive and destructive testing on concrete: a review. Trends Civil Eng Arch
8. Khoury S, Aliabdo AAH, Ghazy A (2014) Reliability of core test-critical assessement and proposed new approach. Alexandria Eng J 53:169–184
9. Suzuki S, Kage T, Seko S (2011) Influence that ratio of length to diameter of high strength concrete core to the compressive strength of concrete. Int Conf Durability Build Mater

Moving Load Identification on the Bridge by Accelerometer Transducer

Aman Prakash and Ganesh Hegde

1 Introduction

Bridges play a vital role in the transport system which support financial and social growth, are therefore regarded as one of the most significant and indispensable infrastructures. The data of the load exerted on the bridge is essential for sustaining good serviceability of the bridge. The load which changes its magnitude and positions concerning time is termed as dynamic moving load. The heavy vehicle loads creating vibration which may significantly change the local and global dynamic behaviour of the bridge and affect the fatigue life of the bridge. The reaction generated by the structure (like strain, acceleration, bending moment etc.) can be extracted by using "transducer" which is placed under the span of the bridge to identify the load approaching on the bridge. The accelerometers typically give us the data of force and acceleration which are exerted upon the sensor due to movement and force detection. The accelerometer transducer shown in Fig. 1 has the crystal placed between a solid base and force sensing arm. When pressure is increased on the top surface of the crystal a potential difference is developed across its opposite ends which are connected to the output terminals.

The vehicle load identification principle is shown in Fig. 2. As the vehicle moves over the deck of the bridge, the axle of the vehicle moves over the transducer and it senses the load and further, the load is converted into the current signals as shown in the Fig. 2 the tri-axial accelerometer transducer measured the vibration in all three axes. The capacitance and acceleration records are transferred to the A/D converter which is used as data acquisition. Then microcontroller which is used for data processing controls the linear and non-linear signals from the transducer. The load is displayed and transmitted to the output device which is monitored by the computer. And another hand there is the handset device is also there which used

A. Prakash (✉) · G. Hegde
Department of Civil Engineering, Goa College of Engineering, Farmagudi, Goa, India
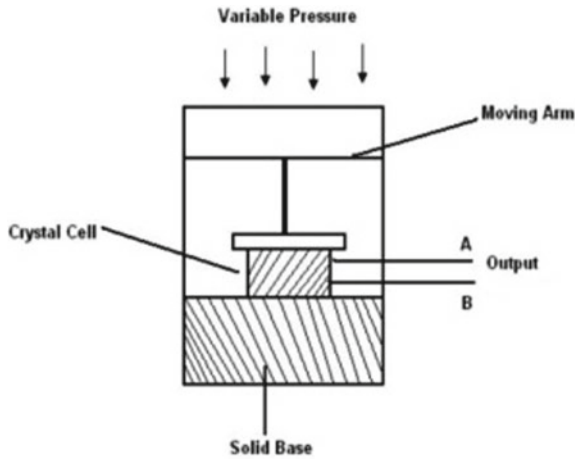
Fig. 1 Accelerometer transducer working
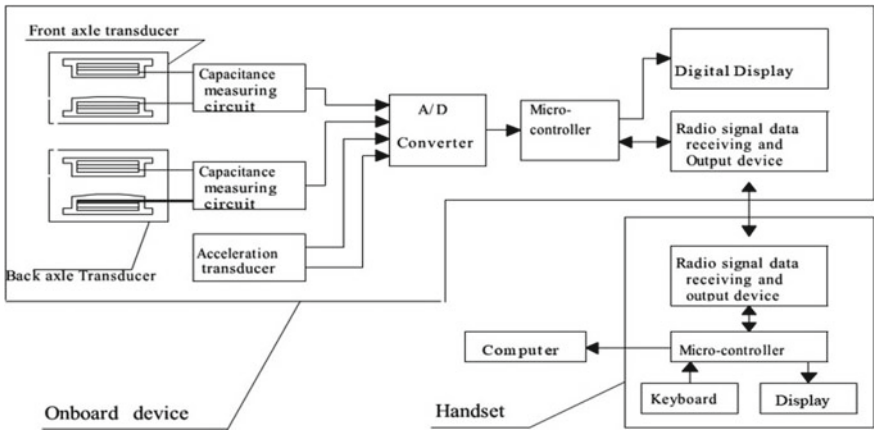
Fig. 2 Operational system

to display the data on the bridge inspector and the data is transmitted by the radio frequency.

2 Literature Review

Krylov [1] and Timoshenko [2] has found the theoretical formulation to identify the moving load. They took an example of simply supported beams on which they applied

a moving load with the velocity with different parameters. They governed Bernoulli–Euler's differential equation, for a beam with a constant mass and cross-section per unit length,

$$EJ\frac{\partial v^4(x,t)}{\partial x^4} + \mu\frac{\partial v^2(x,t)}{\partial t^2} + 2\mu\omega_b\frac{\partial v(x,t)}{\partial t} = \delta(x-ct)F(t) \qquad (2.1)$$

where F(t) is the applied load, E is Young's modulus, J is the constant moment of inertia of the beam cross-section, x is the length coordinate from the left-hand end of the beam, t is the time coordinate with t = 0, the instant of the force arriving upon the beam. In Eq. (2.1), $v(x, t)$ is the beam deflection at the point x and time t, μ is the constant mass per unit length, is the circular frequency of the beam, l is the span length, c is the constant speed of load motion, and δ(x) is the Dirac delta function.

O'Connor and Chan [3] developed the Interpretive Method I, which utilizes the response from inertial and damping forces to compute the dynamic vehicle-bridge Interaction forces. The bridge deck is modeled as an assembly of lumped masses interconnected by massless elastic beam elements. Chan et al. [4] later developed Interpretive Method II which is similar to Interpretive Method I, but utilized Euler's equation of beams to model the bridge deck. The interpretive method I is independent of vibration modes but Interpretive method II needs at least the first three modes to accurately identify more than one moving load. Both Interpretive methods I and II are less accurate in identifying moving loads than time domain and frequency-time domain methods. All the above-discussed methods can be ill-conditioned due to insufficient structural response measurements and regularization techniques are generally utilized to overcome this difficulty.

Yu and Chan [5] has described as per their study that the time domain method (TDM) and the frequency-time domain method (FTDM) gave precise value than the interpretive method I (IMI) and the interpretive method II (IMII) by law, chan. Later and Zhu and Law found that the TDM was widely accepted because it gives high precise value and accurate theory, which can be used to identify the load history of vehicle moving on bridge deck without hampering the traffic flow. A double integration method of measured acceleration value is used to identify the displacement and the applied load magnitudes in time-domain method.

3 Methodology

3.1 Influence Line Calibration

Influence lines are frequently used to analyse the vehicle load and that they are an important method for analysis. Results of influence line gives the accurate load identification and behaviour of the bridge. So for this strain data are used for the calibration which is extracted from the field test.
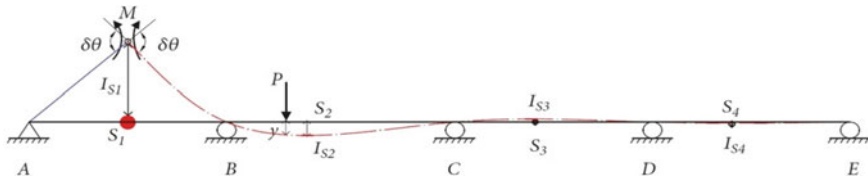
Fig. 3 Representation of the cross-section area

Method 1

Influence values are extracted from the analysed girder of the bridge. S_1 is the cross-section area used for identification of the load where the transducers are placed,

According to the Euler's—Bernoulli Theorem, $\varepsilon = \frac{MY}{EI}$ "ε" is the normal strain at the chosen cross-section S_1, M is the bending moment about the section, Y is the distance between the point and the neutral axis, I is the moment of inertia of the section and E is the young modulus. To explain this method a pictorial representation is given above in Fig. 3 which indicates that the bridge model consists of 4 spans whose length are 32 m, naming as S_1, S_2, S_3, S_4 and the A, B, C, D, E are the restraint. As 'A' is the hinge support and 'B', 'C', 'D', 'E' are the rotational support which allows to rotation of the beam in two portion. A load 'P' is applied on the bridge deck and the moment 'M' is generated. A displacement is induced by the moving load, which divide the section into two parts which are having the linear and cubic curve of the displacement.

According to the virtual work, the moment 'M' and the virtual load 'P' are equated to zero.

Equation is, $M \cdot \delta\theta - P \cdot Y = 0$, where, $M = P \cdot \frac{Y}{\delta\theta}$

$\delta\theta$ is the rotational displacement, Y is the vertical displacement from where load P is applied. Equation $\frac{Y}{\delta\theta}$ denotes the influence line diagram for the bending moment at the cross-section where the transducers are placed and displacements are represented in influence line.

Method 2

The measured value I represent displacement influence line diagram which is shown in the Fig. 3 and it is obtain from the field test at the different location like S_1, S_2, S_3, S_4. These results are calibrated with the known weighted vehicle which is tested many times on the bridge at different locations and the results are being calibrated.

A mechanism of virtual work is applied here in this method in which 'P' is the vehicle load and is being written as $P = W*g$ where 'W' is the weight of vehicle and g is the acceleration of gravity. The flow chart representing the calibration is given in Fig. 4.

A time history data is being recorded by the fixed transducer when vehicle is moving on the bridge deck. The deflection I_1, I_2, I_3, I_4 occurred by the calibrate load vehicle at the different positions S_1, S_2, S_3, S_4 are measured and it is easy to fit

Fig. 4 Flow diagram of the calibrated weight

Strain data recorded from the calibrated vehicle

Strain data recorded from known vehicle

Stress Distribution factor calculation

ILD calculation

Speed calculation

Axle Weight calculation

S_1 S_2 S_3 S_4
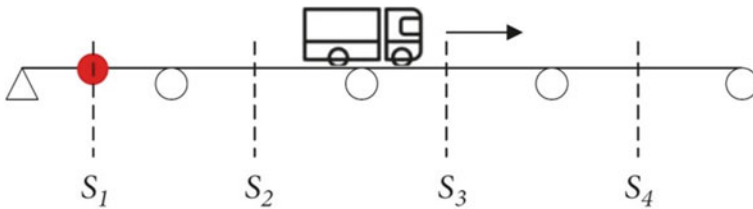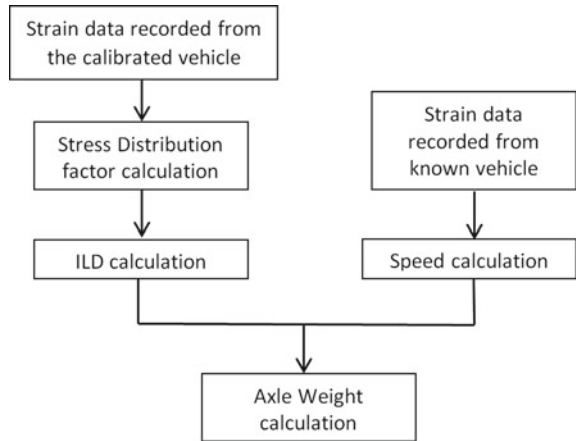
Fig. 5 Vehicle moving with known weight

the influence curve on the different position as shown in Fig. 3. The strain data of the influence line is computed to get the relationship between the vehicle weight in motion and the bridge weight. The equation is $V_W = \frac{I_S}{W}$

Where V_W are the strain developed by the weight of the vehicle and the where influence line is created (Fig. 5).

This calibrated method has advantages like calculations which are done in MS Excel and its data shown in Fig. 6 and 7, operations are easily handled and also there is no requirement of the traffic flow on the bridge. The representation of the displacement influence line diagram of the bridge is the simplest way of representing the real bridge condition under the moving vehicle load.

3.2   Calibration Method and Special Adjustments

Calibration is an important for each deployment at every site. Results from deployment one proved that calibration factors at permanent sites should not be employed at portable sites, as inaccurate WIM measurements result. New calibration factors must be discovered using test-trucks. The portable WIM controller was successfully
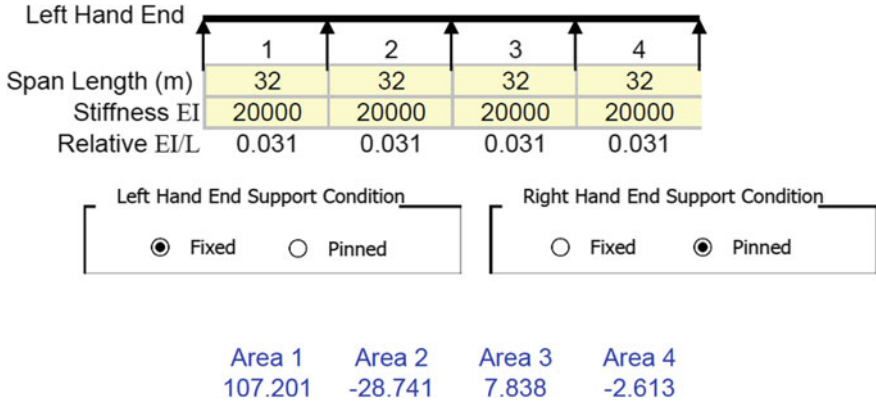
Fig. 6 Excel data sheet
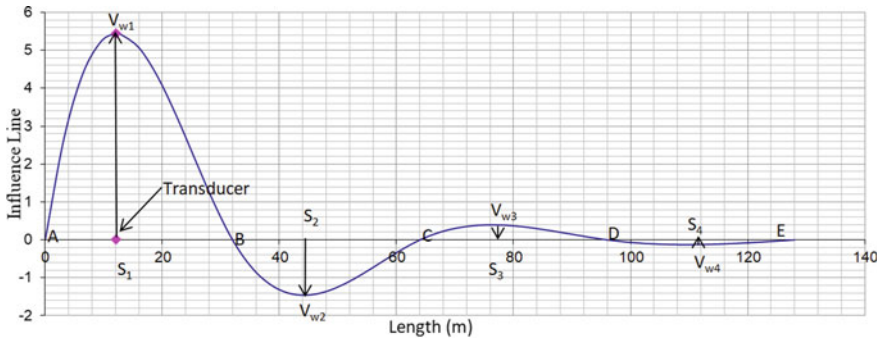
Fig. 7 Influence line diagram

calibrated immediately after highway bridge deployment. Results were consistent and repeatable. More details are provided in the following sections.

A truck loaded with sand and known weight and length was used for testing. The test-truck velocity at the time of transducer overpass is an important factor for calculating the truck weight. Hence, the WIM controller must accurately measure truck weight prior to the start of the calibration process. WIM's velocity should match driver-reported test-truck velocity. This method considers the human factor error. Majorly, radar technology was used when available as an alternative method for obtaining more accurate vehicle velocity measurements.

Front axle weight (FXW) and gross vehicle weight (GVW) were calibrated by driving the test-truck multiple times over the transducers and then inputting average WIM readings into the following calibration factor equation:

$$\mathrm{NewCF} = \frac{\mathrm{ActualGVM}}{\mathrm{AverageWIMGVM}} * \mathrm{CurrentCF}$$

During weight calibration, both FXW and GVW parameters can be adjusted. A trade-off between these two exists, as FXW may adversely impact overall GVW, and GVW may adversely influence FXW. Accordingly, a balance between these two parameters was achieved by adaptively adjusting parameters during calibration. Calibration factors were identified for different speed to obtain improved WIM measurements. Although the same factors could be used for all speed, it is important to know that WIM measurements will deviate from their true actual values.

The equation used to calibrate GVW can also be used to calibrate FXW. This procedure is required to obtain accurate overall weight measurements.

3.3 Bridge Vehicle Interaction

For the modeling and analysis of the bridge structures considered, it is desirable to have a finite element method. Finite element bridge models having the dimensions and properties were constructed using CSI Bridge. The models are used to analysis in various moving loading conditions, dynamic loads and vehicular loads moving across the span at a different speed.

The main aim is to identify the moving load on FEM model of a pre-stressed bridge. A FEM model bridge deck is created in the software and vehicle is made to move with different velocities. The acceleration and displacement time history signature of the bridge deck are obtained at pre-determined locations. Transducers are also placed in the longitudinal direction to identify the velocity of the vehicle. The length of the deck is 67.05 m which consist of one pier and 2 abutment walls and also it consists of 2 lanes total widths of 10.97 m. Concrete Grade M 20 material is used in this simulation (Fig. 8).

The time history of displacement and acceleration is extracted at centre of each span when vehicle is moving with different velocity of 40 km/hr. From the analysis it is observed that acceleration largely increased by the increasing in the speed of vehicle. Time history (displacement and acceleration) is extracted at predetermined joints of the bridge.
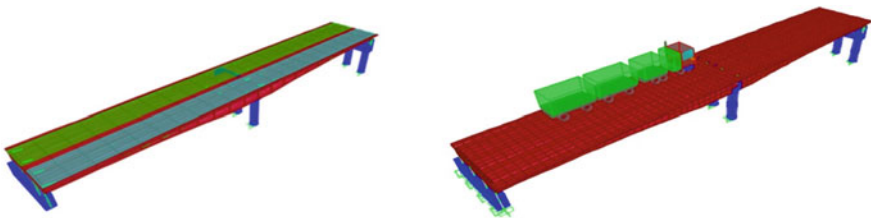
Fig. 8 Finite element model of the pre-stress bridge

3.3.1 Considering the Vehicle (iRC–A) is Moving on the Deck from One Direction

Displacements and acceleration are recorded at the different joint of the lane when vehicle (IRC-A) is moving on the bridge with different velocities. Displacement and acceleration response are analyzed for velocities of 40 km/hr. Vertical displacement and acceleration are measured at joint 165 & 524 as these joint are the centre joint of the both span of lane 1 (Fig. 9).

The data are recorded in tabular form as shown in Tables 1 and 2 Displacement.
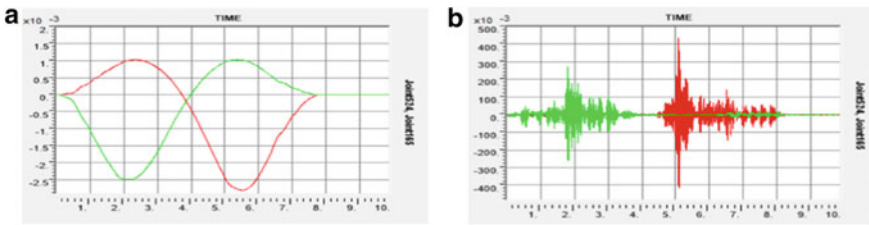
Fig. 9 **a** Displacement-speed 40 km/hr. **b** Acceleration-speed 40 km/hr

Table 1 Accelerations

Speed	Joint no	Accelerations			
		Max		Minimum	
		Value (mm)	Time (s)	Value (mm)	Time (s)
40 km/hr	165	0.2709	1.80	−0.2581	1.81
	524	0.4350	5.090	−0.4149	5.100
72 km /hr	165	0.6476	1.740	−0.6498	1.730
	524	0.6070	3.310	−0.5890	3.320

Joint 165—Centre of first span, Joint 524—Centre of second span

Table 2 Displacements

Speed	Joint mo	Displacements			
		Max		Minimum	
		Value (mm)	Time (s)	Value (mm)	Time (s)
40 km/hr	165	0.1031	5.370	−0.2500	2.190
	524	0.1033	2.340	−0.2814	5.540
72 km/hr	165	0.1039	3.000	−0.2520	1.210
	524	0.1049	1.260	−0.2829	3.090

Joint 165- Centre of first span, Joint 524- Centre of second span
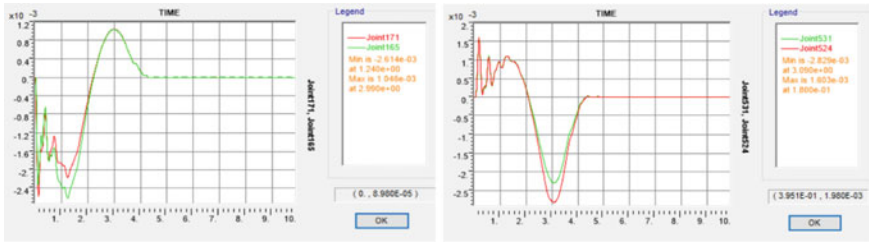
Fig. 10 Displacement graph for joint 165,171, 531 and 524 at velocity of 40 km/hr
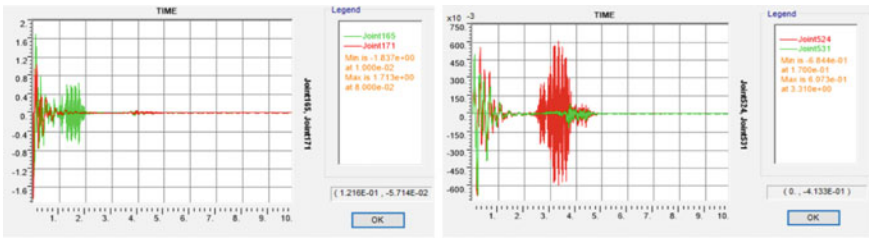
Fig. 11 Acceleration graph for joint 165,171, 531 and 524 at velocity of 40 km/hr

3.3.2 Considering Two Vehicles (IRC-A) Moving from Both Directions.

Again simulation result of IRC A vehicles, when they are moving on the bridge deck from both direction with the velocity of 40 km/hr. Displacement and acceleration graph are recorded at the mid of the both span for both lane (Figs. 10, 11).

Acceleration and Displacement are increasing with increasing the velocity from 40 to 180 km/hr. These acceleration and displacement records along with influence line diagram are being used to develop the novel method for identifying moving loads on the bridge deck. The method will be used to identify the moving load using measured acceleration records.

4 Conclusion

Calibration factors and configuration will be conducted to acquire accurate WIM measurements. WIM accuracy analyses conducted under a controlled environment in which a truck (hereafter known as test-truck) with known axle weight and dimension will be used to evaluate system performance. Test-truck axle weight, spacing, velocity and classification performance parameters are reported. Many factors influence the accuracy of the WIM measurements. If transducer are not installed properly then error, noise are identified when vehicular movement took place. In turn, the WIM controller detects and registers a large number of ticks due to one axle impact.

This results in either over counting or misdetection, depending on the WIM configuration—in particular, the tick filtering threshold. A method to apply the transducer on the bridge deck is developed and proved successful. These techniques provided extended periods of deployments with acceptable portable WIM measurement and data quality. Default calibration factors used for transducer embedded on the bridge deck are not suitable for on-ground. Doing so causes significant weight error and inaccurate vehicle classification. Hence, portable WIM systems should be calibrated at deployment site. A new calibration is required each time the portable WIM site is changed. It is advised to use calibration factors per velocity, acceleration and displacement to increase weight accuracy.

References

1. Krylov AN (1905) Mathematical collection of papers of academy of sciences. Math Ann 61:211
2. Timoshenko SP (1922) On the forced vibrations of bridges. Philosoph Magazine 6(43):1018
3. O'Connor C, Chan THT (1988) Dynamic loads from bridge strains. J Sound Vib 114:1703–1723
4. Law SS, Chan THT, Zeng QH (1999) Moving force identification a frequency and time domains analysis. J Dyn Syst Measur Control 121:394–401
5. Yu L, Chan THT (2003) Moving force identification based on the frequency-time domain method. J Sound Vib 261(2):329–349
6. Law SS, Chan THT, Zeng QH (1997) Moving force identification: a time domain method. J Sound Vib 201(1):1–22
7. Law SS, Bu JQ, Zhu XQ, Chan SL (2004) Vehicle axle loads identification using finite element method. Eng Struct 26(8):1143–1153
8. Law SS, Chan THT, Zhu QX, Zeng QH (2001) Regularization in moving force identification. J Eng Mech 127:136–148
9. Zhu XQ, Law SS (2002) Practical aspects in moving load identification. J Sound Vib 258(1):123–146
10. Moses F (1979) Weight-in-motion using instrumented bridges. J Transport Eng 105(3):233–249

Time—History Analysis of Bridge's Deck Subjected to Vehicular Load Considering Road Roughness

Uddhav U. Naik and Ganesh Hegde

1 Introduction

The transportation systems are considered as the foundation for the growth of country's economy. There are many new highway networks are being constructed across the country and bridges are part of these highway network. Highway bridges are subjected to continuous traffic loads due to increased need of transportations of goods, movement of people across country. Deck is a basic requirement of all type of Bridges. The deck is integral part of bridge which transfers the vehicle load to piers. There are many new and recently constructed bridges in Goa. There are speed and load restrictions enforced on some of the bridges in Goa due to weakening performance of bridges decks. The bridge deck experiences load which include the weight of the vehicles and the dynamic loads that are introduced from movement of the vehicles. The dynamic forces might occur from "Bouncing" or from striking a joint or potholes on bridge deck. Because of this every day dynamic loads the deck may develop some cracking because of excessive stress accumulation. As road surface on the bridge degrades over a time, the lane surface irregularity profile also varies accordingly. The conflicting surface irregularity will give rise to increased dynamic loads on the bridge deck through dynamic interaction between surface irregularity and vehicles. The situation may further worsen when overweight trucks are running on the rough bridge surface. The increase in dynamic force leads to increased stress on bridge deck. It is also noticed that on many of the bridges in Goa there are speed restriction imposed without considering the bridge deck dynamics which get modified according to road roughness condition.

The road roughness is another factor which affects the dynamic actions of the girder. So in order to predict the bridge deck performance (i.e. displacement and stress) to modified dynamic loads due to roughness, detailed dynamic analysis has

U. U. Naik (✉) · G. Hegde
Department Of Civil Engineering, Goa College of Engineering Farmagudi, Ponda, Goa, India

to be carried out considering road roughness. The results help in making decision on speed limits on bridges in Goa and health monitoring of the bridges and road surfaces.

2 Simulation of Road Surface Unevenness

Road roughness plays an important role within the investigation of motor-vehicle-bridge interaction, which has been a standard concern of the researchers. According to Ding et al. [1] conclusions, the roadway unevenness only leads to a jump in suspensions of motor-vehicles, and its impact can be omitted in bridge-vehicle interaction analysis. Deng and Cai [2] suggested that, because of the highway surface deterioration of present bridges, the impact factors measurements might be greater than the values laid out in design codes that mainly goal new bridge design. So it's far necessary to consider pavement roughness in analysis. The detailed studies conducted are discussed in the subsequent section.

3 Methods of Roughness Measurement

The Roughness is recorded by using two methods (1) Field Assessment and (2) Simulating Numerically [3].

3.1 Field Assessment

The field assessment is done by taking a support of Profilometer. The instrument consists of profiling sensor (Laser) device which is designed for Quality Control and inspection of surface of the road, which help in measuring different road profiles. The sensors used in the instrument are Optocator 2207 and LMI/Selcom [4]. Laser used may be having frequency of 62.5 kHz. An encoder was assembled with a magnet on the left rear wheel of a car, giving precision on the distance measured. In this way different profiles of road irregularities can be measured on the field with various levels of roughness.

3.2 Numerical Simulation

Here the PSD function formula is used to described road roughness. The road roughness is modeled by a Zero-Mean Stationary Gaussian Random Process. The road surface roughness (r_x) is given by [5–12].

$$r_x = \sum_{i=1}^{n} \sqrt{2s(\bar{Q}k)\Delta\bar{Q}} \cos(2\pi\bar{Q}k \; xp + \theta_k) \tag{1}$$

where,

n   No. of Points in the Inverse Fourier Transform.

xp   Location on the road surface.

θ_k Random Phase Angle with a uniform distribution between 0 and 2π.

$\bar{Q}$ Power Spectral density function suggested by Liu Xian-Dong et al., which is given by,

$$\bar{Q}(n) = \bar{Q}(n_o) \; (n/n_o)^{-w} \tag{2}$$

where,

n   spatial frequency {cycle/meter}.

n_o Reference spatial frequency.

$\bar{Q}(n_o)$ Road Roughness Coefficient {cubic meter/cycle}.

w   Dimensionless Frequency Index.

Using the International Roughness Index (IRI), the road roughness coefficient is predicted,

$$\bar{Q}(n_o) = 6.1972 \times 10^{-9 \times} \; e^{\;(IRI/0.42808)} + 2 \times 10^{-6} \tag{3}$$

The IRI is calculated at time 't' using equation given below,

$$IRI = 1.04e^{gt} \; IRI_0 + 263 \; (1+SNC)^{-5}(CESAL)_t \tag{4}$$

where,

IRI_0 Initial roughness value.

t   time in year.

η environmental coefficient.

SNC   Structural number.

$\{CESAL\}_t$ Traffic estimator at time 't' in millions.

4   Methodology

4.1   Bridge Information

The three continuous spans highway bridge is model using CSI bridge software having span length of 22.1 m, 29.5 m and 22.1 m respectively. The bridge has total
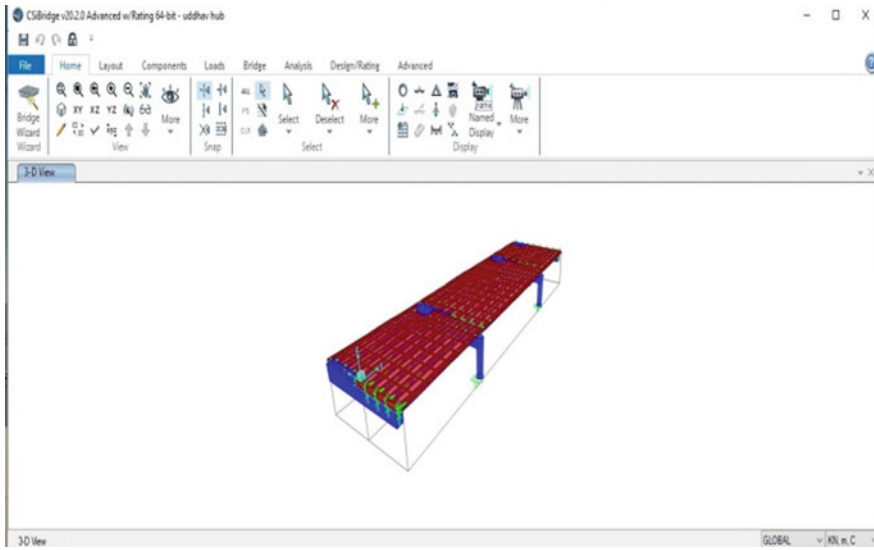
Fig. 1 Development of bridge finite element model

length of 73.66 m and total width 18.76 m respectively. The deck has total thickness of 0.20 m and is supported by eight parallel pre-stressed concrete I—girders with a 1.5, 0.20 m in depth. The girders are spaced equally at the distance of 2.419 m. The girders are reinforced longitudinally at the tops of the cross sections and are braced with stirrups. The junctions between adjacent girders, supported by the pier cap, are embedded in a concrete diaphragm creating an integral and fixed connection. Each column contains standard longitudinal reinforcement, and transverse confinement. The integral abutment is adopted for this bridge.

4.2 Development of Bridge Finite Element Model

The typical Finite Element bridge model in CSI bridge is shown in the Figure (Fig. 1). The bridge deck is divided into small plate elements having a rectangular shape. The Bridge deck is connected to bridge girders through rigid link elements.

4.3 Traffic Flow Simulation

Hsn-44 truck is allowed to move on the bridge at the speed of 30, 80 and 150 km/hr in order to take into account the dynamic effects of the moving vehicles when they
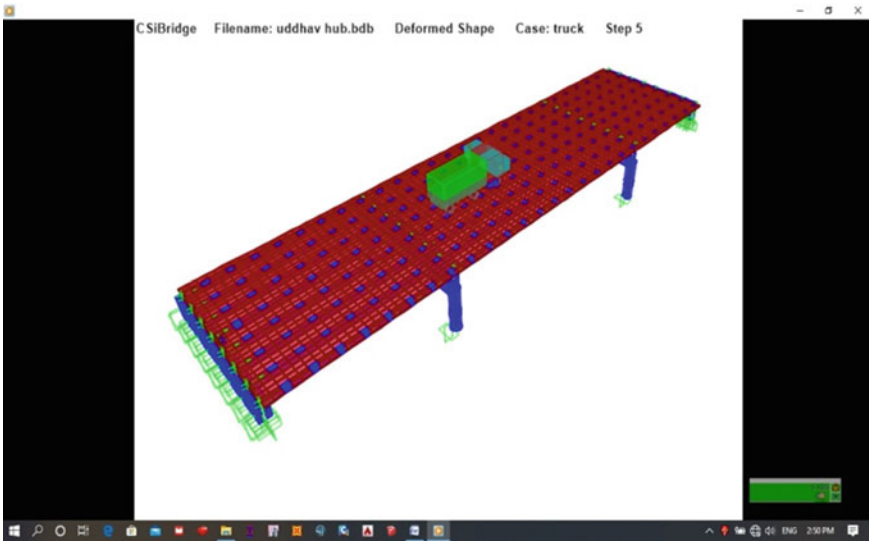
Fig. 2 Traffic flow simulation

enter the bridge and fully running on the bridge. The simulated running vehicle on the bridge is shown in the (Fig. 2).

4.4 Simulation of Road Surface Roughness

In this study two typical Road Surfaces is taken, i.e. one with the good surface having $\phi(w_o) = 1 \text{cm}^3$ and second is with very poor surface having $\phi(w_o) = 256 \text{cm}^3$. Through the spectral representation approach, road surface roughness is simulated as a single-variate stationary random process. The simulation result is given below (Figs. 3 and 4).
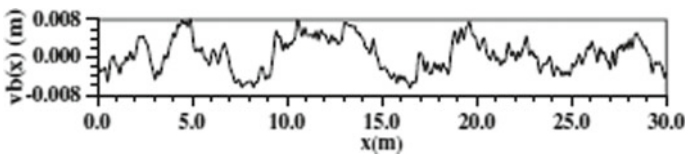
Fig. 3 Simulation results of good surface road (GSR), $\phi(w_o) = 1 \text{ cm}^3$
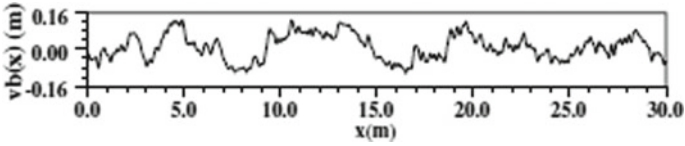
Fig. 4 Simulation results of very poor surface road (VPSR), $\phi (w_o) = 256$ cm^3

5 Results and Discussion

In order to study the deck response, three representative deck joints are selected with joint No. 142, 399 and 655 at the centre of first span, centre of second span and centre of third span respectively. The time-history responses at joints are illustrated below.

5.1 The Time-History of Displacement with Roughness and Without Roughness

5.1.1 Comparative Displacement Time History at the Speed of 30 km/hr

See Figs. 5 and 6.
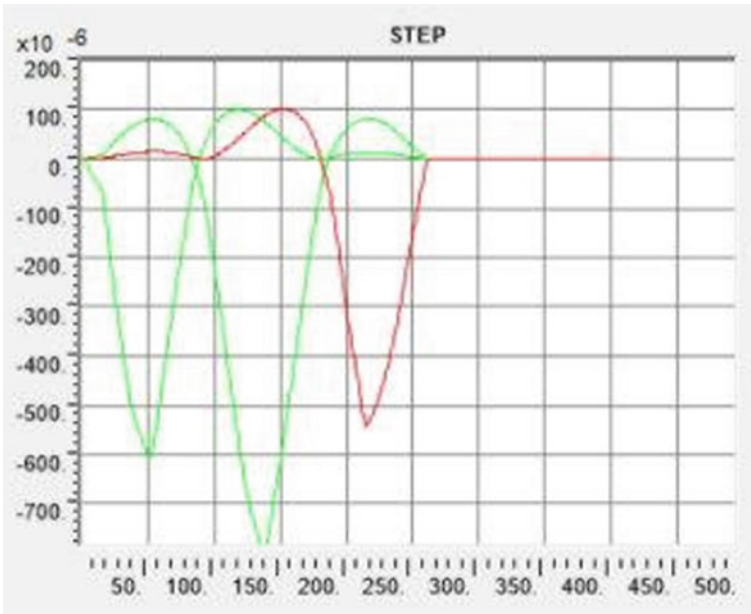
Fig. 5 Displacement time history plot for road without roughness at the speed of 30 km/hr
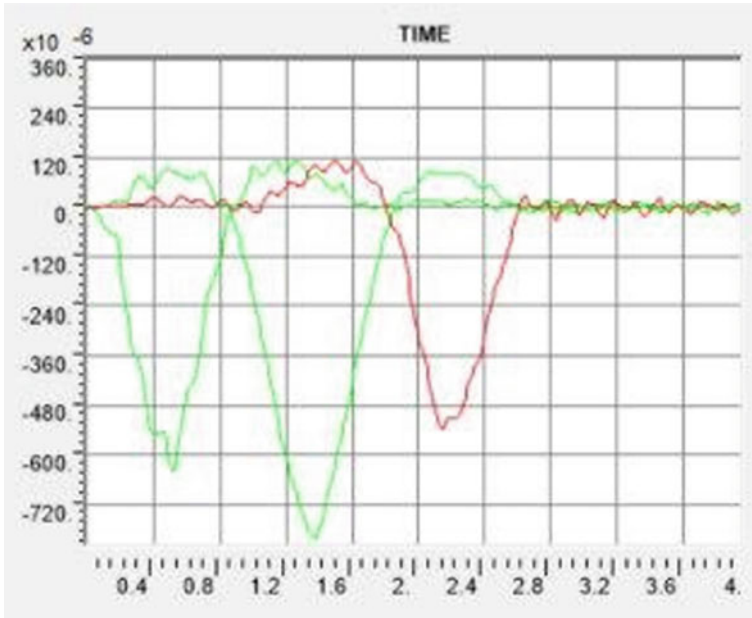
Fig. 6 Displacement time history plot for road with roughness at the speed of 30 km/hr

5.1.2 Comparative Displacement Time History at the Speed of 80 km/hr

See Figs. 7, 8.

5.1.3 Comparative Displacement Time History at the Speed of 150 km/hr

See Figs. 9 and 10.

5.2 The Time-History of Acceleration with Roughness and Without Roughness

5.2.1 Comparative Acceleration Time History at the Speed of 30 km/hr

See Figs. 11, 12 and Tables 3 and 4.
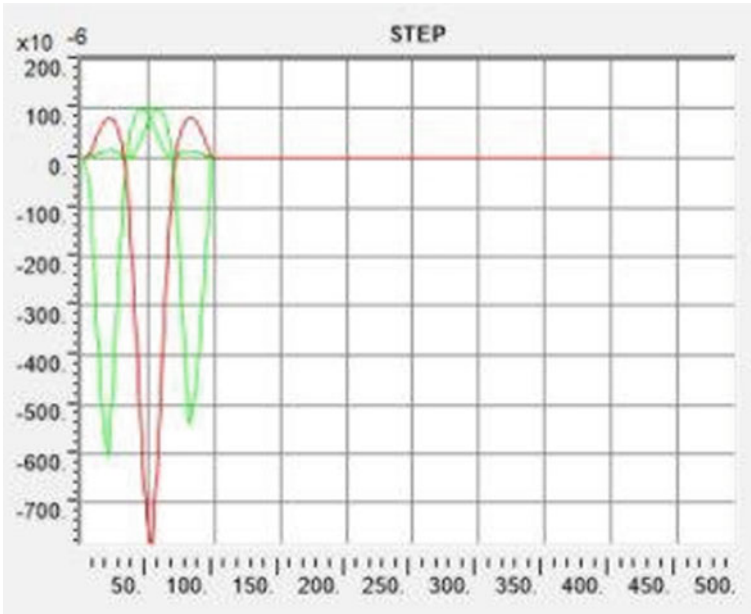
Fig. 7 Displacement time history plot for road without roughness at the speed of 80 km/hr
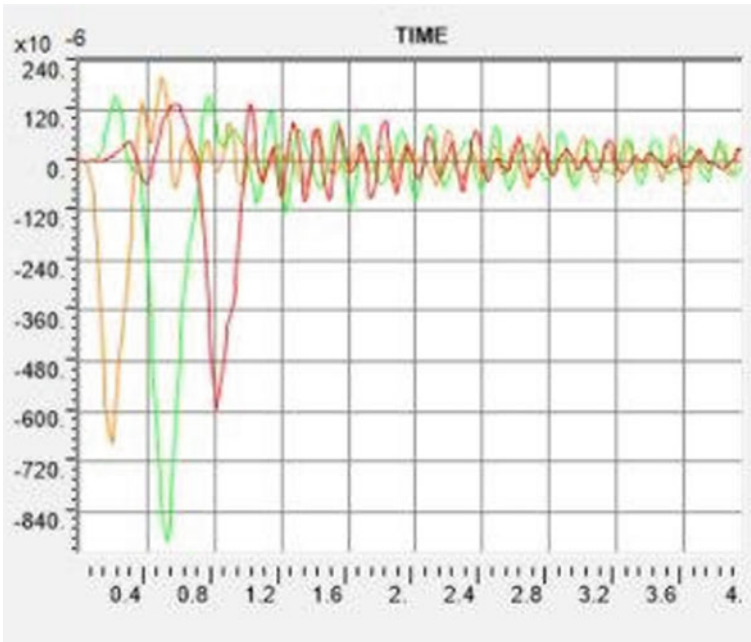
Fig. 8 Displacement time history plot for road with roughness at the speed of 80 km/hr
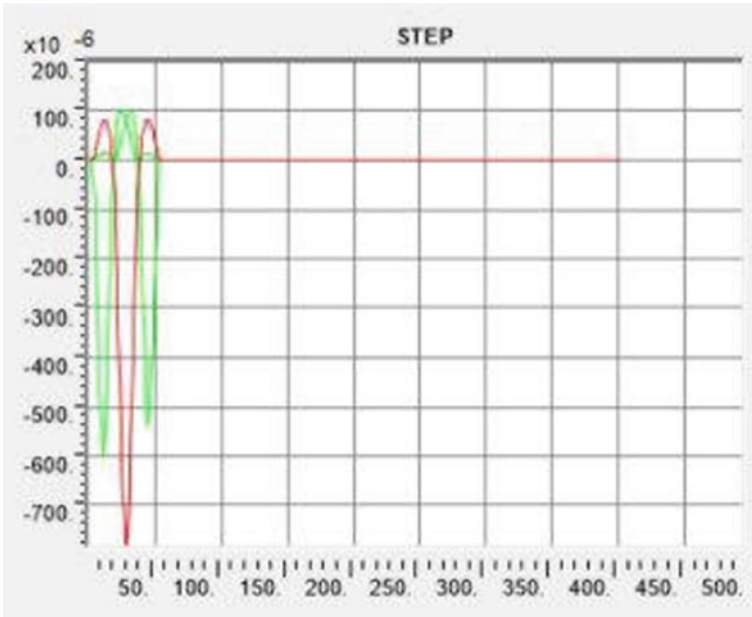
Fig. 9 Displacement time history plot for road without roughness at the speed of 150 km/hr
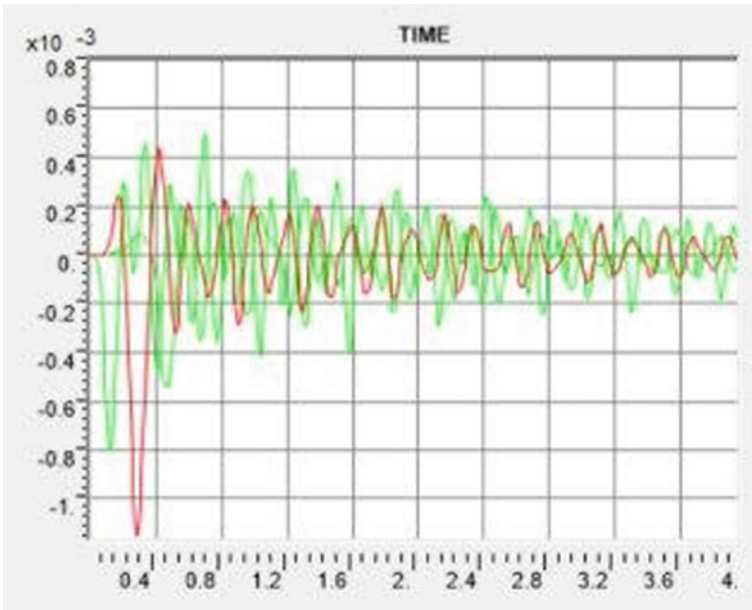
Fig. 10 Displacement time history plot for road with roughness at the speed of 150 km/hr
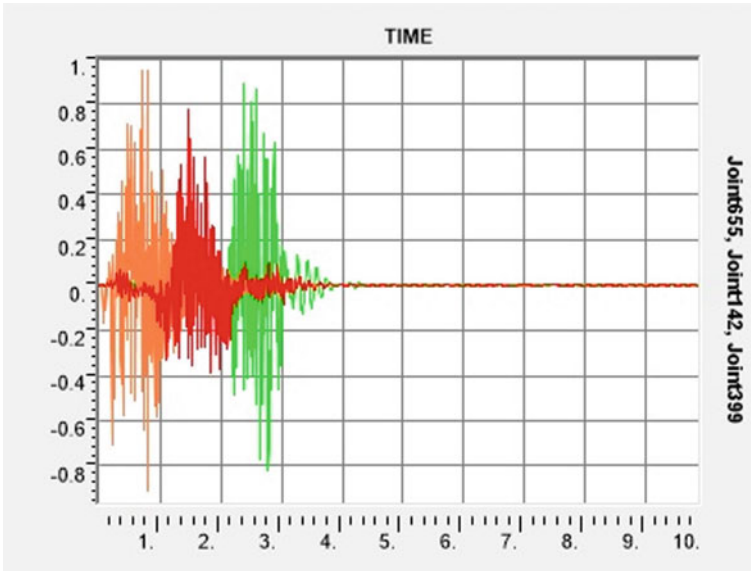
Fig. 11 Acceleration time history plot for road without roughness at the speed of 30 km/hr
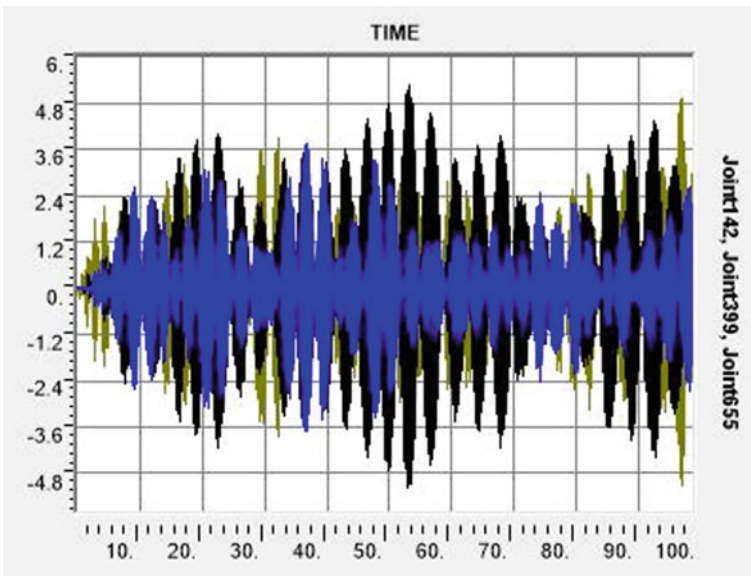
Fig. 12 Acceleration time history plot for road with roughness at the speed of 30 km/hr
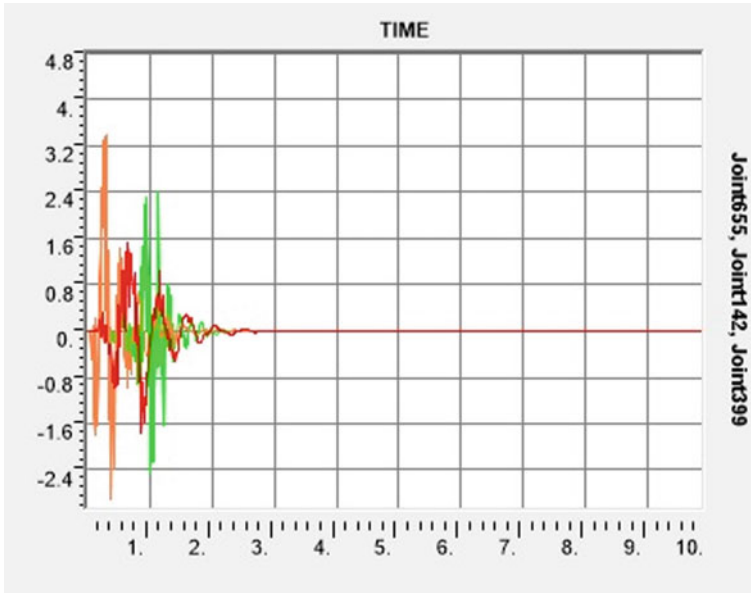
Fig. 13 Acceleration time history plot for road without roughness at the speed of 80 km/hr

5.2.2 Comparative Acceleration Time History at the Speed of 80 km/hr

See Figs. 13 and 14.

5.2.3 Comparative Acceleration Time History at the Time Speed of 150 km/hr

See Figs. 15 and 16.

Acceleration and Displacement are increasing with increasing the speed from 30 to 150 km/hr. Also it is seen that this acceleration and displacement results which is tabulated in Tables 1, 2, 3 and 4 respectively, is varies from the good surface roughness to very poor surface roughness. These acceleration and displacement records along with influence line diagram are being used to develop the novel method for determining dynamic response of the bridge deck. The measured acceleration records are used to get the displacement by direct integration. The displacement obtained at different joints are used to prepare influence diagram. Thus help in determining the dynamic performance of the bridge deck. This study of determining bridge deck performance is developed considering the road roughness.
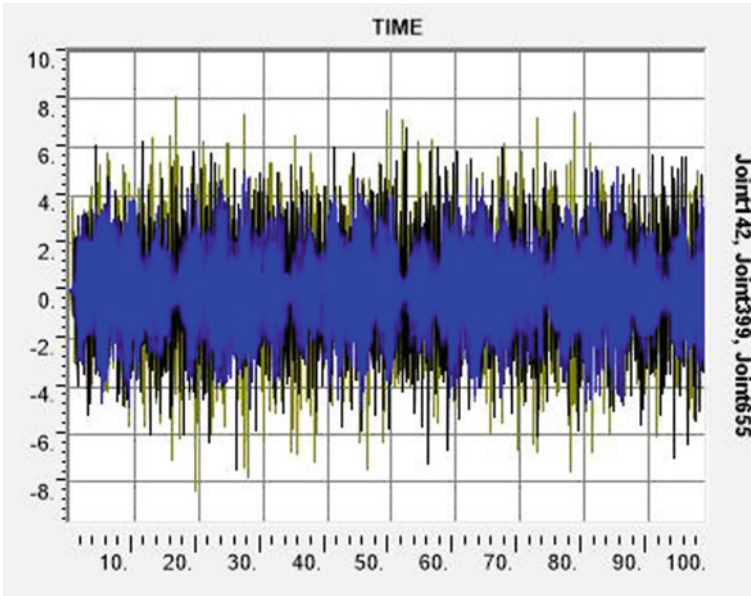
Fig. 14 Acceleration time history plot for road with roughness at the speed of 80 km/hr
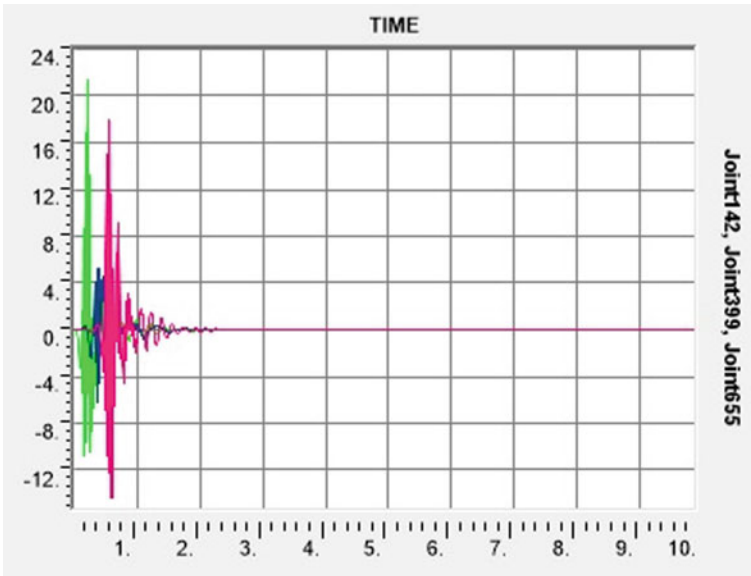
Fig. 15 Acceleration time history plot for road without roughness at the speed of 150 km/hr
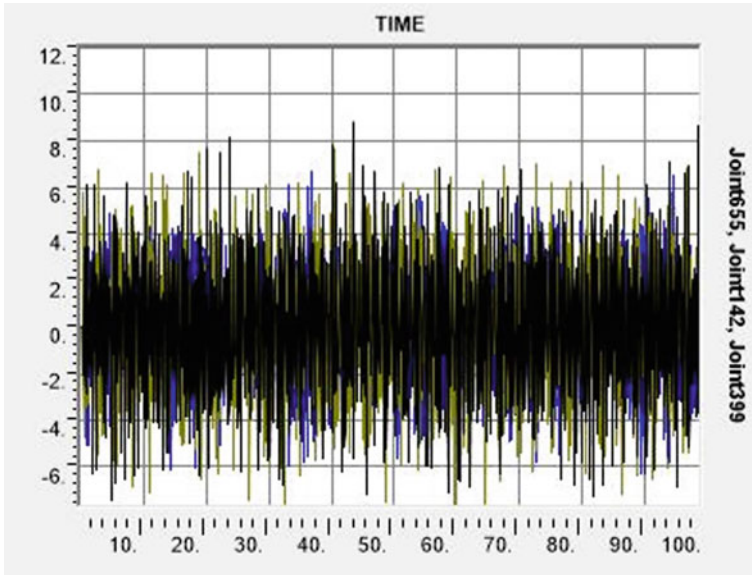
Fig. 16 Acceleration time history plot for road with roughness at the speed of 150 km/hr

Table 1 Displacements without roughness

Speed (km/hr)	Joint No	Displacements without roughness			
		Maximum		Minimum	
		Value (mm)	Time (s)	Value (mm)	Time (s)
30	142	1.005e–04	1.180e+02	−6.041e–04	5.200e+01
	399	8.211e–05	2.160e+02	−7.992e–04	1.380e+02
	655	1.016e–04	1.538e+02	−5.442e–04	2.150e+02
80	142	1.003e–04	4.500e+01	−6.033e–04	2.800e+01
	399	8.210e–05	8.200e+01	−7.945e–04	5.200e+01
	655	1.013e–04	5.800e+01	−5.400e–04	8.100e+01
150	142	1.001e–04	2.400e+01	−6.018e–04	1.100e+01
	399	8.200e–05	4.400e+01	−7.895e–04	2.800e+01
	655	1.011e–04	3.100e+01	−5.400e–04	4.400e+01

Joint 142-Centre of First Span, Joint 399—Centre of second span, Joint 655—Centre of Third span

Table 2 Displacements with roughness

Speed (km/hr)	Joint No	Displacements with Roughness			
		Maximum		Minimum	
		Value (mm)	Time (s)	Value (mm)	Time (s)
30	142	1.116e–04	1.145e+00	−6.406e–04	5.200e–01
	399	9.597e–05	4.800e–01	−8.038e–04	1.380e+00
	655	1.134e–04	1.490e+00	−5.359e–04	2.150e+00
80	142	1.984e–04	4.900e–01	−6.755e–04	1.900e–01
	399	1.567e–04	7.600e–01	−9.110e–04	5.200e–01
	655	1.384e–04	1.010e+00	−5.948e–04	8.100e–01
150	142	4.607e–04	3.300e–01	−7.973e–04	1.200e–01
	399	4.397e–04	4.100e–01	−1.155e–03	2.800e–01
	655	5.002e–04	6.900e–01	−5.394e–04	4.800e–01

Joint 142—Centre of First Span, Joint 399—Centre of second span, Joint 655—Centre of Third span

Table 3 Accelerations without roughness

Speed	Joint No	Accelerations without roughness			
		Maximum		Minimum	
		Value (mm)	Time (s)	Value (mm)	Time (s)
30 km/hr	142	9.548e–01	7.100e–01	−9.116e–01	7.900e–01
	399	7.808e–01	1.450e+00	−3.894e–01	1.830e+00
	655	8.926e–01	2.370e+00	−8.220e–01	2.780e+00
80 km/hr	142	3.387e+00	2.900e–01	−2.894e+00	3.700e–01
	399	1.519e+00	6.300e–01	−1.750e+00	8.600e–01
	655	2.417e+00	1.130e+00	−2.462e+00	1.010e+00
150 km/hr	142	2.137e+01	2.000e–01	−1.074e+01	1.600e–01
	399	5.268e+00	4.000e–01	−6.234e+00	3.600e–01
	655	1.794e+01	5.600e–01	−1.432e+01	5.800e–01

Joint 142—Centre of First Span, Joint 399—Centre of second span, Joint 655—Centre of Third span

5.3 Stress Response on the Bridge Deck

The following stress responses are obtained on the bridge deck when the vehicle is allowed to run on the bridge with two different speeds i.e. 30 and 80 km/hr with roughness and without roughness.

Table 4 Accelerations with roughness

Speed (km/hr)	Joint No	Accelerations with Roughness			
		Maximum		Minimum	
		Value (mm)	Time (s)	Value (mm)	Time (s)
30	142	4.928e+00	9.710e+01	−5.108e+00	9.700e+01
	399	5.258e+00	5.310e+01	−5.186e+00	5.280e+01
	655	3.758e+00	3.680e+01	−3.721e+00	3.670e+01
80	142	7.707e+00	4.050+01	−7.619e+00	5.950e+01
	399	6.801e+00	5.230e+01	−7.470e+00	2.580e+01
	655	5.166e+00	8.520e+01	−4.933e+00	2.790e+01
150	142	8.125e+00	1.640e+01	−8.382e+00	1.940e+01
	399	8.809e+00	4.340e+01	−7.396e+00	5.000e+00
	655	6.732e+00	3.690e+01	−6.272e+00	8.950e+01

Joint 142—Centre of First Span, Joint 399—Centre of second span, Joint 655—Centre of Third Span

5.3.1 Stress Response on the Bridge Deck at the Speed of 30 km/hr

See Figs. 17, 18 and Table 5.
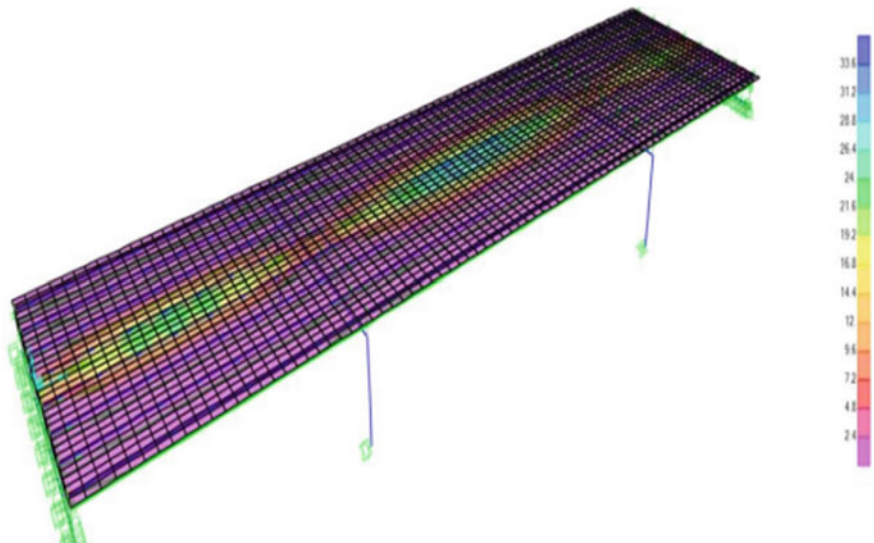
Fig. 17 Stress response on the bridge deck for road without roughness at the speed of 30 km/hr
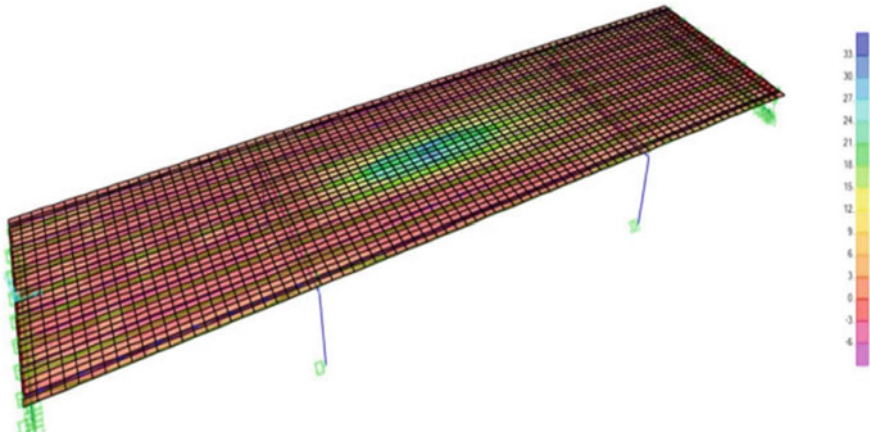
Fig. 18 Stress response on the bridge deck for road with roughness at the speed of 30 km/hr

Table 5 Transverse stresses on bridge deck for roads with and without roughness

Speed (Km/hr)	Transverse stresses on bridge deck			
	Without roughness		With roughness	
	Maximum (N/m^2)	Minimum (N/m^2)	Maximum (N/m^2)	Minimum (N/m^2)
30	33.6	−2.4	35.646	−6.804
80	32.713	−9.238	48	−5.6

5.3.2 Stress Response on the Bridge Deck at the Speed of 80 km/hr

See Figs. 19 and 20.

From the table it is seen that transverse stresses are increasing as there is increased in speed i.e. from 30 to 80 km/hr. Also it is seen that stress value is minimum on the smooth surface where as, as the surface is getting poorer this stress value is significantly increasing which may lead into surface cracking of the bridge. Thus affecting working life of the bridge.

6 Conclusion

This study investigates bridge deck dynamic responses such as displacement, stress under moving load considering road roughness. The analysis is carried out by starting with a detailed FEM modeling of the bridge including bridge deck. Two typical Road Surfaces is taken, i.e. one with the good surface having $\phi(w_o) = 1 \text{ cm}^3$ and second is with very poor surface having $\phi(w_o) = 256 \text{ cm}^3$. Through the spectral representation approach, road surface roughness is simulated as a single-variate stationary random
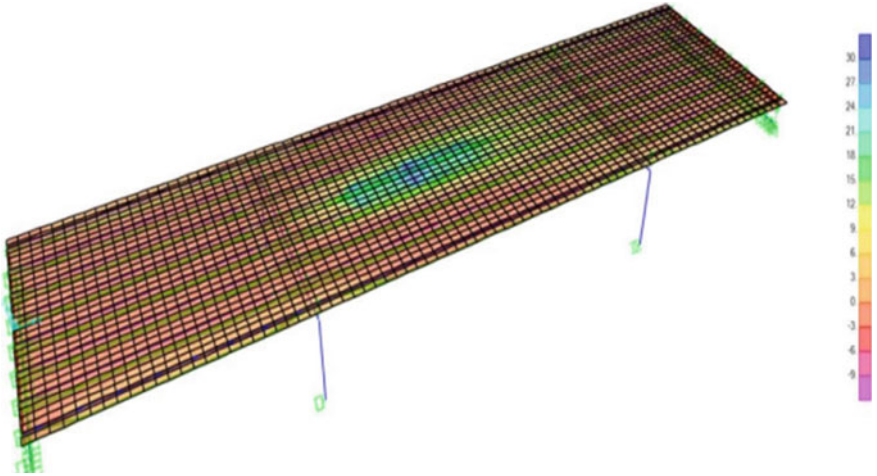
Fig. 19 Stress response on the bridge deck for road with roughness at the speed of 80 km/hr
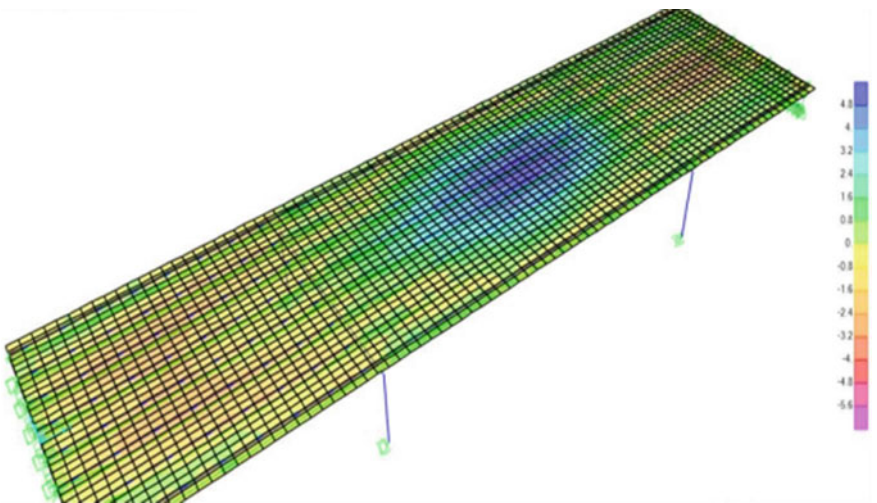
Fig. 20 Stress response on the bridge deck for road with roughness at the speed of 80 km/hr

process. Hs-n 44 truck is allowed to move on the bridge with three different speed i.e. 30 km/hr,80 km/hr and 150 km/hr respectively and dynamic analysis is carried out. The deck responses such as displacement, acceleration are thus obtained. So the conclusion can be made that as the speed of the vehicle increased the deflection of the deck is also increased and the deflection position also shifts. It is also concluded that when the surface is good there will be less displacement and as the surface is getting poorer the displacement will increased. The results of this which will turn

into reducing the working life of the Bridge. The method to study dynamic response of bridge deck is being developed considering road roughness.

References

1. Ding L, Hao H, Zhu X (2009) Evaluation of dynamic vehicleaxle loads on bridges with different surface conditions. J Sound Vib 323(3–5):826–848
2. Deng L, Cai CS (2010) Development of dynamic impact factor for performance evaluation of existing multi-girder concrete bridges. Eng Struct 32(1):21–31
3. Huang D (2012) Vehicle-induced vibration of steel deck arch bridges and analytical methodology. J Bridge Eng 17(2):241–248
4. Nassif HH, Liu M (2004) Analytical modeling of bridge-road-vehicle dynamic interaction system. J Vib Control 10(2):215–241
5. Dodds CJ (1972) BSI proposals for generalized terrain dynamic inputs to vehicles. Int for Stand ISO/TC/108/WG9, Document No 5
6. AASHTHO (1998) Load and resistance and factor design: bridge design specification, 2nd edition. American Association of state Highway and Transportation Officials
7. Chen SR, Wu J (2010) Dynamic performance simulation of long-span bridge under combined loads of stochastic traffic and wind. J Bridge Eng 15(3):219–230
8. Chen S, Wu J (2011) Modeling stochastic live load for long-span bridge based on microscopic traffic flow simulation. Comput Struct 89(9–10):813–824
9. Wang CH (2007) Study on the impact force acted on highwaybridges by moving vehicle loads. PhD thesis. Harbin Institute of Technology, Harbin, China
10. González A, O'Brien EJ, Cantero, et al (2010) Critical speed for the dynamics of truck events on bridges with a smooth surface. J Sound Vib 329(11):2127–2146
11. Lee HP (1996) Dynamic response of a beam with a moving mass. J Sound Vib 191(2):289–294
12. Liu Y, Qian Z-D (2008) Review of road roughness and vehicle vibration model

Interference Effects Between Twin Tall Buildings Under Wind Excitation

Suresh Kumar Nagar, Ritu Raj, and Nirendra Dev

1 Introduction

With the availability of high-strength materials and modern design and construction techniques, the number of tall and super tall buildings is increasing. However, with the use of lightweight materials and increased height, tall buildings are becoming more flexible and hence sensitive to wind effects. In modern cities, a large number of high-rise buildings are being constructed in groups with close proximity. Due to mutual interference, the buildings' flow pattern is different from those for isolated buildings, which may result in significant variation in wind loads on the building. Wind load on a building may increase up to 80% in the presence of an interfering building (Khanduri et al. 1998). An increase or decrease in wind load mainly depends on the interfering building's geometry and position, angle of wind incidence, and upstream terrain conditions. Hence it is difficult to provide a comprehensive and generalized set of guidelines for modifications in the wind effects due to interference effects. Therefore the interference effects due to the interfering buildings on wind loads should be appropriately assessed.

Many researchers have investigated the interference effects between two or more high-rise buildings [1–14]. Xie and Gu [4] proposed the simplified formulas for interference between three tall buildings based on the investigation done on the effects of the relative heights of the interfering buildings and the spacing between two and three buildings. Kim et al. [6] studied the interference effects on local peak pressure coefficients between two buildings with various configurations and different height ratios of an interfering building. Hui et al. [7–9, 12] investigated the interference effects between two high-rise buildings with square and rectangular shapes on the peak pressure coefficients. The results showed that interference effects much depend

S. K. Nagar (✉) · R. Raj · N. Dev
Delhi Technological University, Delhi, India
e-mail: snagar@rtu.ac.in

upon wind direction and building shapes and their relative positions. Kar and Dalui [15] studied the variation of pressure at the faces of an octagonal plan shaped tall building due to interference effects arises in the presence of two and three square tall buildings of the same height. Kim et al. [10] studied the interference effects between two buildings on overall wind loads and local wind loads through a series of wind tunnel tests for various height ratios and interfering building locations. Interference effects between twin-tall buildings with aerodynamics modification were investigated by Yan and Li [11] with both High-frequency force balance (HFFB) and synchronous multi-pressure sensing system (SMPSS) techniques. The results showed that the dynamic wind loads and responses are significantly increased for critical tandem and staggered arrangements of the twin-tall buildings. Hui et al. [12] studied the wind-induced torsional loads under interference effects on two adjacent high-rise buildings. It was observed that mean torsion under interference effects can be tripled for the isolated case, whereas extreme torsion was 1.8 times that for isolated building. Yu et al. [13] studied interference effects on wind-induced acceleration responses in along-wind and crosswind directions between two high-rise buildings for different breadth ratios of interference building.

2   Experimental Setup

Experiments were carried out in the boundary layer wind tunnel in the Department of Civil Engineering at the IIT Roorkee, Roorkee. Tests were carried out under a simulated wind flow of the terrain category II as per IS 875: part 3 at a geometric scale of 1:300, where the mean wind speed profile followed the power-law with a power exponent of 0.22. The mean wind velocity profile is shown in Fig. 1. The mean wind speed at the roof height of the building model was 9.87 m/s. Two building models of identical sizes and shapes were used in the experiments.

Measurements were made on a pressure model made of a transparent Perspex sheet, referred to as the principal building, while the other model was made of wooden, which was not installed with any instrument, referred to as the interfering building. Both building models had a square plan form of breadth B = 200 mm. The height-to-breadth ratio was H/D = 3. At the target geometric scale 1:300, the models represented full-scale buildings of height 180 m and width 60 m. A total of 140 pressure taps, 20 on each level (Fig. 2b), were installed on the walls of the principal building, which were located at seven different heights levels of 10, 60, 180, 300, 420, 540, and 590 mm from the bottom as shown in Fig. 2a to obtain a proper distribution of wind pressure on all the faces of models. The principal building was tested in isolated and with interfering building placed at various locations. Figure 3 shows the different configurations of the interfering building. Three interference conditions were created by placing interfering building at various positions. In the first arrangement, the interfering building was placed in line with the principal building with full blockage interference condition. Distance (x) between the principal building and the interfering building was kept equal to 60 mm (1/10th) of the height of the

Fig. 1 Mean velocity profile
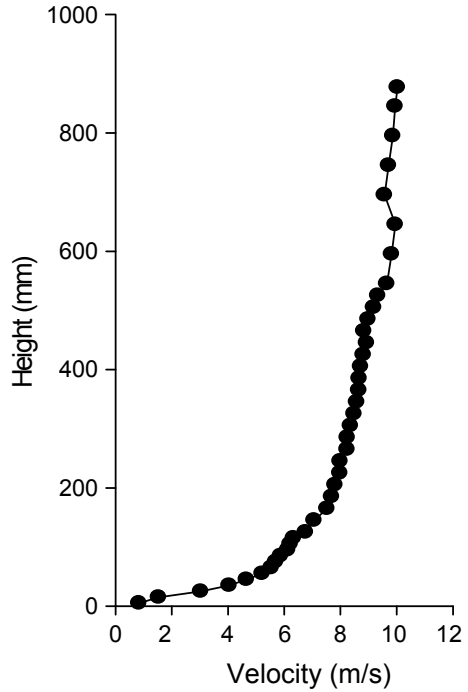
principal building model) for all cases. In the second and third arrangements, the interfering building was placed in oblique configuration, creating a half blockage and no blockage conditions for the principal building, respectively.

3 Results and Discussions

Mean pressure coefficients for square building in isolated and three interference conditions are evaluated and presented here. Mean pressure coefficients are presented at all the faces along with the height and along the building's perimeter at different levels and compared for isolated and three interference conditions. To quantify the effects of the presence of interfering building at three different locations, interference factors are calculated and compared at all four faces of principal building for three interference conditions.
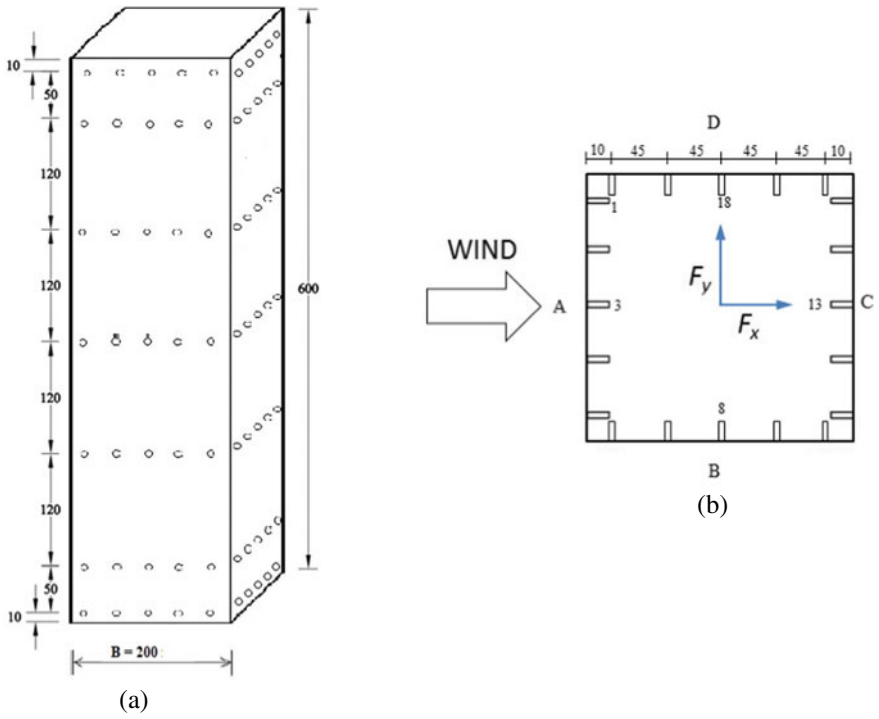
Fig. 2 **a** Measurement levels. **b** Pressure taps distributions at each level
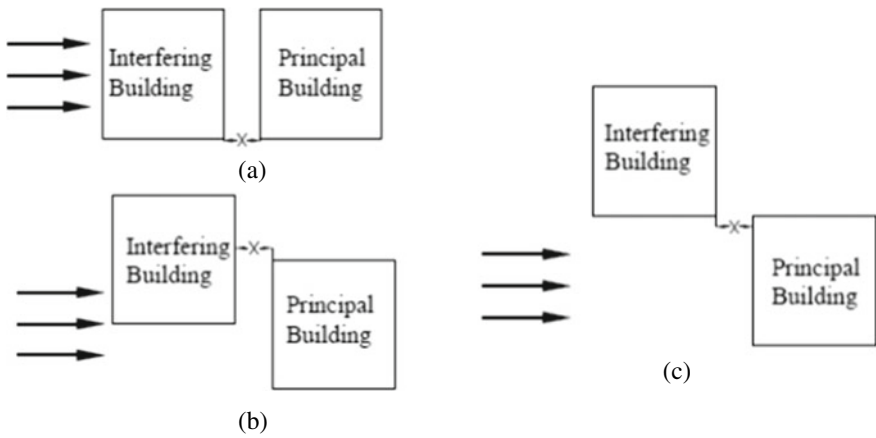
Fig. 3 Interference conditions **a** Full **b** Half **c** No blockage

3.1 Mean Pressure Coefficient

The value of mean pressure coefficient ($C_{p,mean}$) at any pressure measuring point is calculated by normalizing the measuring pressure at the corresponding measuring point based on the following equation:

$$\overline{c}_P = \frac{\overline{P} - P_{static}}{P_{dyn}} \tag{1}$$

where $\overline{P}$ is mean pressure; P_{static} is the static pressure at reference height; P_{dyn} is the dynamic pressure at reference height given by $\frac{1}{2}\rho_a U^2$, where U is the reference velocity, at reference height. Figure 4 show the variation of mean pressure coefficients ($C_{p,mean}$) at the centerline of all faces for isolated and three interference conditions. The windward face pressure is positive for isolated and no blockage interference conditions with similar distributions. Windward face experience suction in case of full blockage and half blockage interference conditions. Distribution along height is parabolic in isolated and interference conditions. Suction at the right side face is reduced significantly because full and half blockage conditions and the distribution along height are almost straight lines and merged. For no blockage interference condition, suction is almost similar to the isolated case. On the leeward face, suction is reduced in case of all three interference conditions. The distribution pattern in isolated and interference conditions is almost the same with the lowest suction in case of full and half blockage conditions. The changing location of the interfering building most influences the left side face. Suction is highest in isolated building case. Suction is reduced significantly as the blockage is increased from no blockage to full and lowest in full blockage.

Variation of $C_{p,mean}$ along the perimeter at different measuring levels is presented and compared in Fig. 5 for isolated and three intereference conditions. Positive
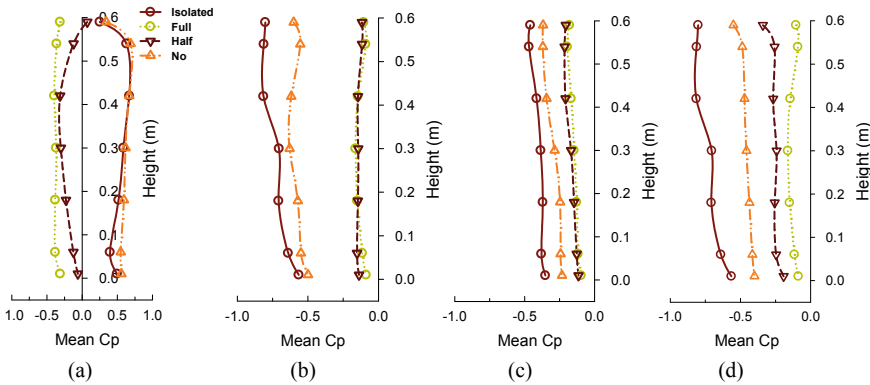
Fig. 4 Mean C_p along the centerline of the face **a** Face A **b** Face B **c** Face C **d** Face D

(a)   (b)

(c)
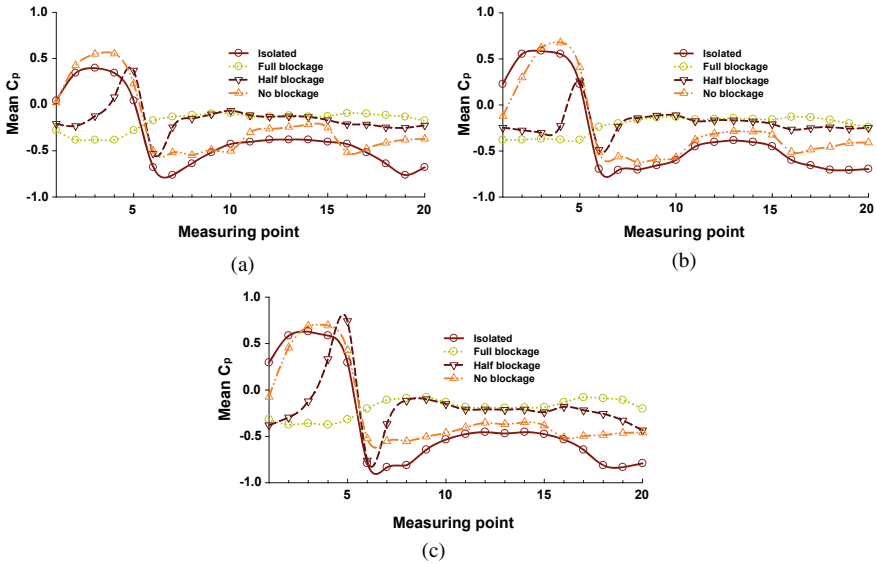
Fig. 5 Mean C_p along the measuring points at levels **a** 540 mm **b** 300 mm **c** 60 mm

pressure increases at the center of the windward face in case of isolated and no blockage interfering conditions and changes smoothly from negative to positive from the left edge to the right edge in half blockage. The whole windward side is under suction in case of a full blockage condition. Suction near windward edges of side faces is higher due to separation of flow at edges in all cases. Suction almost keeps constant throughout the perimeter till measuring point 20 in case after the center of the right face (measuring point 8) in case of full and half blockage interfering conditions.

3.2 Interference Factor

The interference factor (I.F) at four faces of the principal building model for various interference conditions is evaluated by using:

$$I.F = \frac{mean\ pressure\ at\ interference\ condition}{mean\ pressure\ at\ isolated\ condition} \tag{2}$$

The interference factor at a face is obtained by taking a weighted area average of all pressure taps at the face. The interference factors at all four faces for three different interference conditions are presented in Fig. 6. The value of I.F at face A is −0.88 in full blockage interference condition, which shows that the principal building's complete windward side emerges in the wake of the principal building.

Fig. 6 Interference factor of mean C_p at each face
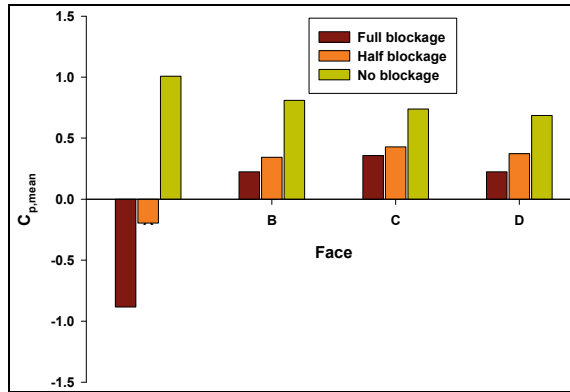
In no blockage condition, I.F almost equal to 1 indicates the negligible effect of the interfering building at the principal building's windward side. Interference factors at the side and leeward faces are less than unity, which shows the reduction in suction at these faces for all interference conditions. Reduction in suction is higher in the full blockage condition compare to the other two conditions.

4 Conclusions

Experiments were carried out to investigate the interference effects on mean wind pressures between square twin-tall buildings for various locations of the interfering building on the principal building's windward side. Mean pressure coefficients for different interference conditions were evaluated. Interference effects were presented in the form of interference factors at each face for three interference conditions. Mean pressure at the windward face is almost equal to the isolated case for no blockage conditions, while for the other two conditions, it is affected by the wake of the interfering building, but the absolute value is reduced. The maximum reduction is in half blockage condition. At the side and leeward faces, suction is reduced considerably for all three interference conditions. A maximum reduction is in the case of full blockage condition.

References

1. Bailey PA, Kwok KCS (1985) Interference excitation of twin tall buildings. J Wind Eng Ind Aerodyn 21(3):323–338
2. Khanduri AC, Stathopoulos T, Bedard C (2000) Generalization of wind-induced interference effects for two buildings. Wind Struct 3(4):255–266
3. Xie ZN, Ming Gu (2004) Mean interference effects among tall buildings. Eng Struct 26(9):1173–1183

4. Xie ZN, Ming Gu (2007) Simplified formulas for evaluation of wind-induced interference effects among three tall buildings. J Wind Eng Ind Aerodyn 95(1):31–52
5. Lam KM, Leung MYH, Zhao JG (2008) Interference effects on wind loading of a row of closely spaced tall buildings. J Wind Eng Ind Aerodyn 96(5):562–583
6. Kim W, Tamura Y, Yoshida A (2011) Interference effects on local peak pressures between two buildings. J Wind Eng Ind Aerodyn 99(5):584–600
7. Hui Y, Tamura Y, Yoshida A (2012) Mutual interference effects between two high-rise building models with different shapes on local peak pressure coefficients. J Wind Eng Ind Aerodyn 104:98–108
8. Hui Y, Yoshida A, Tamura Y (2013) Interference effects between two rectangular-section high-rise buildings on local peak pressure coefficients. J Fluids Struct 37:120–133
9. Hui Y et al (2013) Pressure and flow field investigation of interference effects on external pressures between high-rise buildings. J Wind Eng Ind Aerodyn 115:150–161
10. Kim W, Tamura Y, Yoshida A (2015) Interference effects on aerodynamic wind forces between two buildings. J Wind Eng Ind Aerodyn 147:186–201
11. Yan B, Li Q-S (2016) Wind tunnel study of interference effects between twin super-tall buildings with aerodynamic modifications. J Wind Eng Ind Aerodyn 156:129–145
12. Yi H, Tamura Y, Yang Q (2017) Analysis of interference effects on torsional moment between two high-rise buildings based on pressure and flow field measurement. J Wind Eng Ind Aerodyn 164:54–68
13. Yu X, Xie Z, Gu, Ming (2018) Interference effects between two tall buildings with different section sizes on wind-induced acceleration. J Wind Eng Ind Aerodyn 182:16–26
14. Sharma A, Mittal H, Gairola A (2019) Wind tunnel and delayed detached eddy simulation investigation of interference between two tall buildings. Adv Struct Eng 22(9):2163–2178
15. Kar R, Dalui SK (2016) Wind interference effect on an octagonal plan shaped tall building due to square plan shaped tall buildings. Int J Adv Struct Eng (IJASE) 8(1):73–86

Analytical Behaviour of Multi-storeyed Building with Tuned Mass Damper as Energy Dissipater

K. Soujanya, Chhabirani Tudu, and P. K. Parhi

1 Introduction

Tuned mass damper is the oldest passive energy dissipating device [1, 2]. There are different types of passive control devices like metallic yield dampers, friction dampers viscoelastic dampers, viscous fluid dampers, tuned liquid dampers and tuned mass dampers [2–4]. A Tuned mass damper as shown in Fig. 1 consists of a secondary mass with spring and a damping element to increases the damping in the primary structure. Its basic purpose is to reduce the response of main system by tuning an additional vibrating mass to a frequency close to the resonant frequency of the main system, there by dissipating the vibration energy of the structure through damping [5, 6]. The TMD is effective in reducing the vibrations induced due the dynamic loads like wind load and earthquake loads [3, 7–9].

1.1 Soft Storey

A soft/weak storey is defined as one in which the storey's lateral strength is less than 80% of that in the storey above/below as per IS 1893 part 1. The delicate story idea has specialized and useful preferences over the traditional development. First is the decrease in unearthly speeding up and base shear because of increment of common time of vibration of structure as in a base disconnected structure.

K. Soujanya · C. Tudu (✉) · P. K. Parhi
Department of Civil Engineering, College of Engineering and Technology, Bhubaneswar, Odisha, India
e-mail: chhabiranice@cet.edu.in

P. K. Parhi
e-mail: pkparhi@cet.edu.in

Fig. 1 Schematic diagram
of mass damper
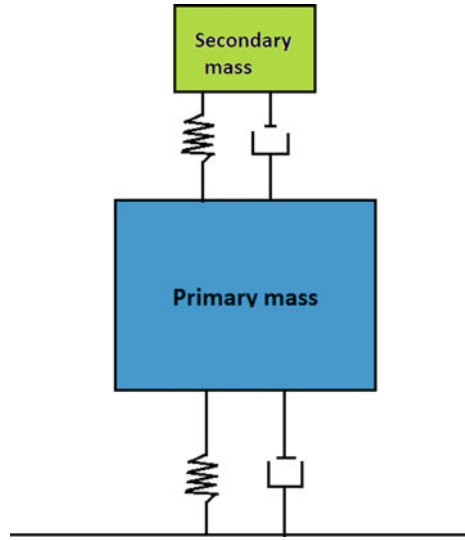
Fig. 2 Plan of the structure
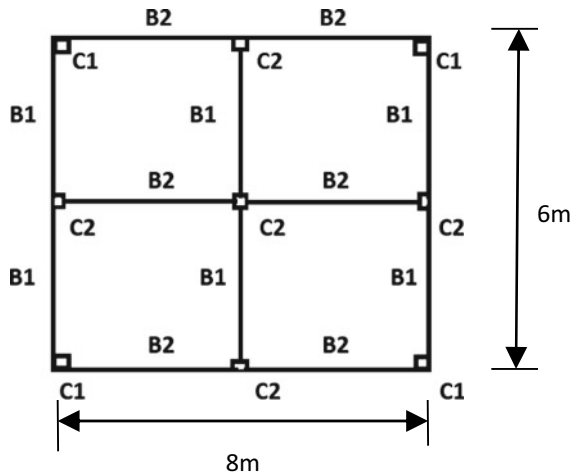
Table 1 Detailing of
structure

Column name	Column size in mm	Beam name	Beam size in mm
C1	230 × 230	B1	230 × 400
C2	230 × 400	B2	230 × 400

In this work the structure with and without TMD were modelled and compared
for different earthquake data. The plan and details of the structure to be considered

for analysis are shown in Fig. 2 and Table 1 respectively. The isometric view of the structure with and without TMD is shown in Figs. 3 and 4.

Fig. 3 Structure without TMD
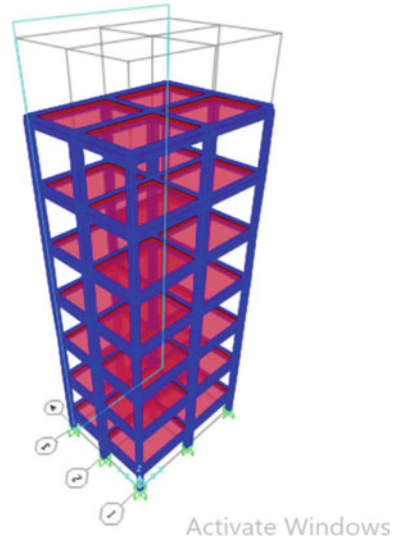
Fig. 4 Structure with TMD
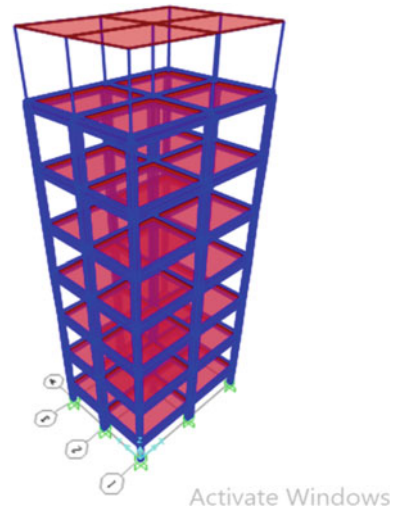
2   Optimum TMD Parameters

The optimum TMD parameters are obtained by using three different methods in terms of frequency ratio, damping ratio and stiffness of secondary structure. Among which the best method is adopted for the analysis. In Sadek's Method, he concluded that for a TMD to be effective, the damping ratios in the two complex modes of vibration, ξ1 and ξ3 should be approximately equal to the average damping ratios of the structure and the TMD as in Eq. (1) [5], i.e.

$$\xi 1 \cong \xi 3 \cong (\frac{\beta + \xi}{2}) \qquad (1)$$

Den Hartog also derived closed form expressions for optimum damper parameters. He assumed no damping to be present in the main mass to facilitate the derivations. Warburton tabulated numerically searched optimum values of absorber parameters for certain values of absorber to main mass ratio and main mass damping ratio. It is an extension of the Den Burtons method as in this method the formulations for designing the optimum values of the absorber parameters, by subjecting the harmonic loading to the undamped single degree of freedom system. This formulation is derived based on the white noise excitation for a single degree freedom system.

Figure 5a shows graph of variation of frequency ratio in different methods, wherein it's quite clear that the Den Hartog method frequency ratio is more pronounced with decrease in the mass ratio. It is quite evident as per Fig. 6 that in terms of damping ratio the results of Sadek's method are more pronounced. The conventional ideology is that the TMD is generally placed at the storey with maximum deflections, i.e. at the topmost floor as shown in Fig. 9. Thus the optimum parameters of TMD are obtained as directed in the Sadek's method are shown in the Table 2.

In order to tune the TMD to the structural frequency the optimum frequency ratio is used and the details of the soft storey obtained are shown in the Table 2.

Fig. 5   Variation of b among methods
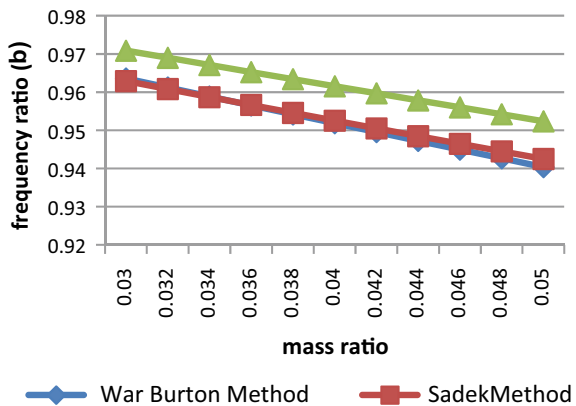
Fig. 6 Variation of ξ among methods
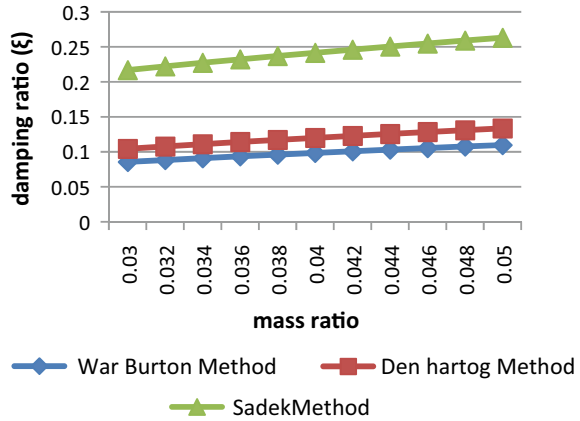
Table 2 Optimum frequency ratio and height

Mass ratio	Optimum frequency ratio	Height of the damper calculated (m)
0.03	0.96292	3.2
0.05	0.942503	3.7

3 Structural Response for Time History Values

Figure 7 shows the behaviour of the different storey of the building for various mass ratios. This particular graph is obtained by subjecting the models to Taft earthquake data and performing a time history analysis of the structural responses. It has been seen that the reduction of displacements due to 5% mass ratio ranges from 20 to 57%, where as the reduction of displacements due to the 3% mass ratio ranges from 4 to 35% approximately. In the graph shown in Fig. 8, the model with 5% mass ratio

Fig. 7 Displacements for different mass ratio subjected to Taft earthquake data
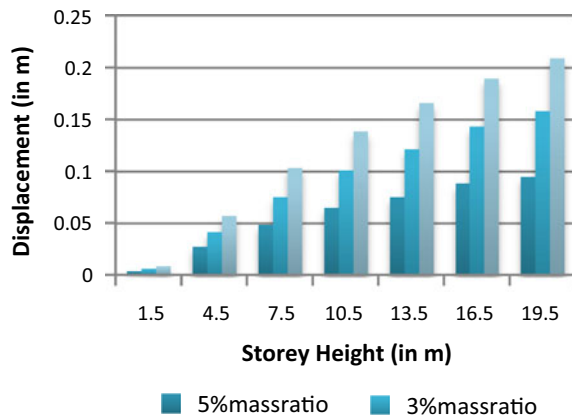
Fig. 8 Displacements for different mass ratio subjected to Bhuj earthquake data
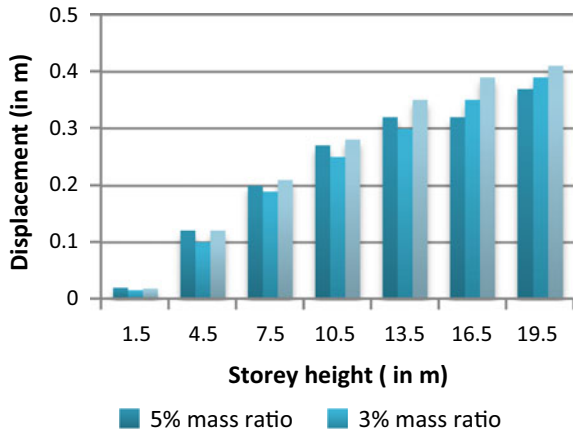
shows a non linear trend as compared to the other mass ratio. The percentage of reduction for 5% mass ratio ranges from 4 to 17% whereas for 3% mass ratio the reduction ranges from 4 to 16%.

   This particular graph shown in Fig. 9 is obtained by subjecting the models to Loma Preita earthquake data and performing a time history analysis of the structural responses. The reduction in the joint displacements of 5% mass ratio ranges from 13 to 32% where as the reduction for 3% mass ratio ranges from 3 to 9%. As the mass ratio increases the reduction in the displacement also increase, this is because as the mass ratio increases the TMD becomes more robust and effective. The model with a single TMD installed at the top storey with 3 and 5% mass ratio are subjected to Taft earthquake. These models are further subjected to two other earthquakes for the comparison of results. The displacement of the structure without the TMD and with TMD is shown in Fig. 10. The percentage of reduction in drift is calculated as follows:

Fig. 9 Displacements for different mass ratio subjected to Loma Preita earthquake data
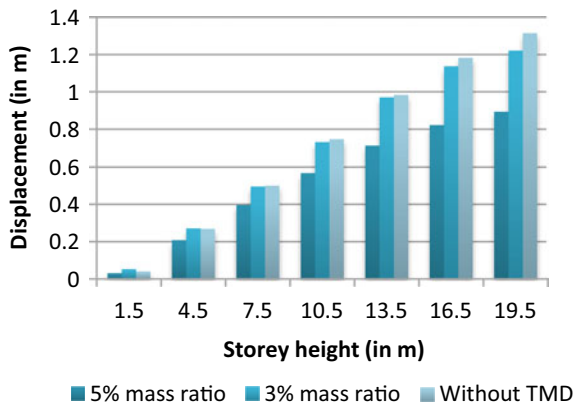
Fig. 10 Sway with and without damper

TMD at the top most floor having maximum deflection

Sway without TMD   **Sway with TMD**
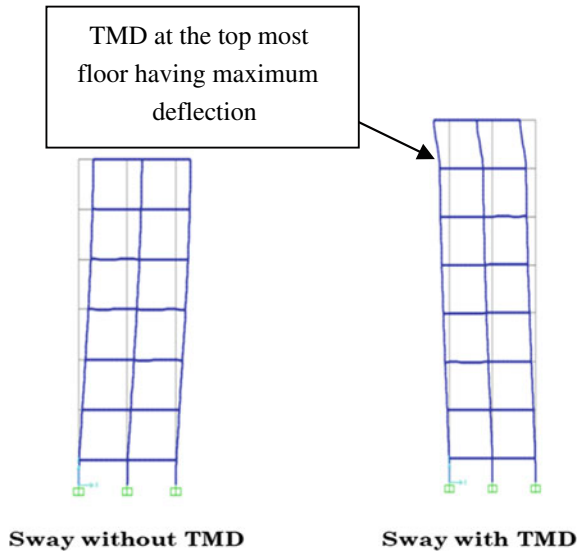
Percentage reduction in drift

$$= \frac{\text{Difference in the drift of model with and without TMD}}{\text{Drift in the model without TMD}} \qquad (2)$$

The percentage reduction is calculated for each storey level from Eq. (2) and represented in a graphical format in Fig. 11 for clear comparisons, and also to observe the clear trend seen in different model as compared.

The model with a single TMD installed at the top storey with 3 and 5% mass ratio are subjected to Taft earthquake. The model with 3% mass ratio reduces the drift by a maximum value of 44% approximately whereas the model with 5% mass ratio reduces the drift by a maximum value of 26%. Also the percentage reduction of drift also increases with the increase in the mass ratio of the structure or models considered. The variation of percentage reduction of drift by 3% and 5% TMD is shown in Fig. 12

Fig. 11 Damping per storey level for Taft
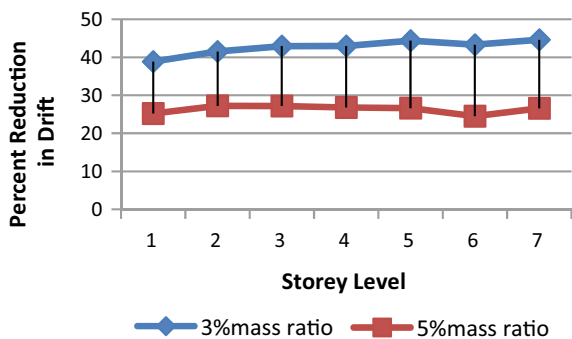
Fig. 12 Damping per storey
level for Bhuj
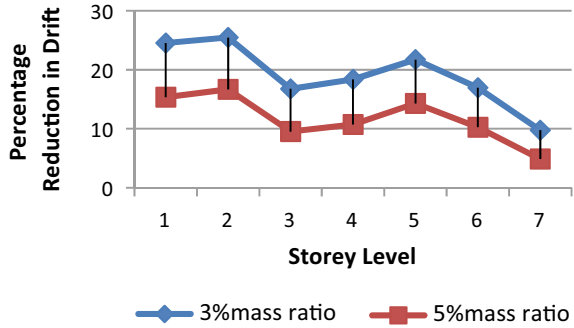
Fig. 13 Damping per storey
level for Loma
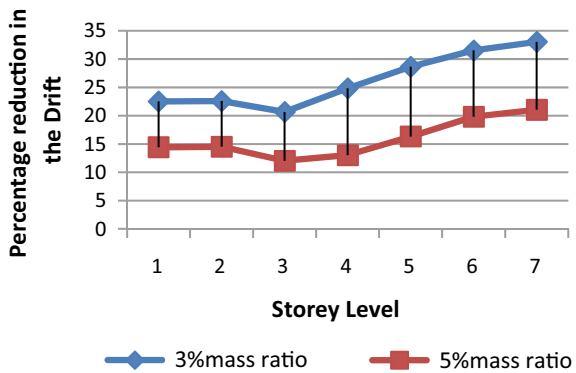
graph. In this case the models are subjected to Bhuj earthquake. The model with 3%
mass ratio reduces the drift by a maximum value of 25% approximately whereas the
model with 5% mass ratio reduces the drift by a maximum value of 17%. In this case
the difference in the percentage reduction of drift in the two models, decreases with
the increase in the storey level. Thus the device is similarly effective in reducing the
top floor displacements.

The percentage reduction in model with 3% mass ratio is higher as compared to
the percentage reduction in model with 5% mass ratio as seen in Fig. 13. The model
with 3% mass ratio reduces the drift by a maximum value of 33% approximately
whereas the model with 5% mass ratio reduces the drift by a maximum value of 21%.
In this case the models are subjected to Loma Preita earthquake.

4   Conclusions

The overall objective of this paper was to determine the optimum parameters of
tuned mass dampers that result in a considerable reduction in the displacement. This
investigation has led to the following conclusions:

- The behaviour of the structure is simulated by subjecting the model to an earthquake ground motion based on dynamic and mathematic model of the structure. It was found that the TMD was effective in reducing the structural induced vibrations.
- Among all the methods the Shadek method and the War Burtons methods show nearly similar results, but the Den Hartog method shown a slight variation. The damping ratio is more pronounced in case of the Shadek's approach.
- By comparing various analysis results it was found that the maximum reduction in the structural displacements from as less as 3–57%. Thus it was observed that TMD can be helpful in limiting the impact induced due to different time history data.
- As the mass ratio increases the TMD becomes more robust and effective.
- The reduction in the storey drift decreases with increase in the storey height. The maximum percentage reduction in the drift for all the three-time history values ranges from 17 to 44%.
- With the increase in mass ratio the percentage reduction in the displacement increases with increase in the mass ratio, thus the TMD with 5% mass ratio is more effective as compared to the TMD with 3% mass ratio.
- The frequency ratio obtained from all the methods decrease with increase in the mass ratio of the TMD of a structure.
- The maximum displacement is observed at the top most storey of the structure, thus is the effective position of placement of the TMD.

References

1. Bekdas G, Nigdeli SM (2018) Mass ratio factor on optimum TMD design in frequency domain. Int J Theor Appl Mech 3:68–73
2. Jabary RN, Madabhushi GSP (2017) Tuned mass damper positioning effects on the seismic response of a soil-MDOF-structure system. J Earthq Eng 22(2):281–302
3. Zhou Z, Najm H, Vasconez R (2016) Effectiveness of tuned mass dampers in mitigating earthquake ground motions in low and medium rise buildings. J Eng Archit 4. No 2:11–27
4. Carolina T, Oscar AL (2004) Effect of the position and number of dampers on the seismic response of frame structures. In: 13th world conference on earthquake engineering, paper no. 1044
5. Sadek F, Mohraz B, Taylor A, Chung R (1997) A method of estimating the parameters of tuned mass dampers. Earthq Eng Struct Dyn 26:617–635
6. Rana R, Soong TT (1998) Parametric study and simplified design of tuned mass dampers. Eng Struct 20(3):193–204
7. Warburton GB, Ayorinde EO (1980) Optimum absorber parameters for simple systems. J Int Assoc Earthq Eng 8(3):197–217
8. Rana R (1996) Response control of structures tuned mass damper and their generalisation. In: 11th world conference on earthquake engineering, paper no. 498
9. Hadi MNS, Arfiadi Y (1998) Optimum design of absorber for MDOF structures. J Struct Eng 12(11). ASCE

Evaluation of Ultimate Torque and Twist of Ferrocement Strengthened "U" Wrapped Beams: Different Approaches

Gopal Charan Behera

1 Introduction

Man made havocs and natural calamities facade problems for all categories of structures and creates a threat to human life. Havocs and natural calamities induce variable stresses which have necessitated constant attention, maintenance and upgradation of infrastructures. Strengthening of distressed structures is absolutely necessary when these structures are unable to resist the induced forces or incapable to meet the updated codal requirements. Concrete structures can be strengthened by retrofitting and "U" wrap is most suitable method of retrofitting for structures with extension of flanges. Retrofitting using fiber reinforced polymer (FRP) is costly and requires skilled workmanship for application. For developing countries ferrocement wrap is a better solution over FRP. Concrete structure strength can be enhanced by FRP wrapping [1, 2]. Different repair materials require different wrapping strategy. According to the wrapping material, wrapping method is to be finalized. Karayannis et al. [3] pointed out material, wrapping cost and availability of repair infrastructure and person decides wrapping strategy. Strength of weak members can be enhanced by FRP wrapping. There is substantial increase in strength when FRP wrapping is done and also change in mode of failure of sections is noticed [4]. If a section is fully wrapped, there is increase in strength. It is not always practicable to wrap a full section. In many cases it is found better to go for "U" wraps. Research papers on determination of torque and twist are found for FRP wraps on all four sides [5]. Chalioris [6] worked on increase in strength of "U" wraps. FRP wrapping requires high cost and skilled workers for which it more popular in high economic group of people or areas [7]. In the contrast, ferrocement wrapping has the capacity to increase the strength as reported from the works of [8]. Taking consideration of cost and strength, ferrocement can be utilized as a wrapping material in place of FRP. Ferrocement has the properties like water

G. C. Behera (✉)
Government College of Engineering, Kalahandi, Bhawanipatna, India

259

proofing and also strength in tension, compression and bending is more than concrete [9]. In many cases as wrap on all sides may not be feasible, in that case "U-wrap" is a better choice. The above literature proofs application of ferrocement as wrap in place of FRP.

Ferrocement is formed by taking smaller diameter wires in two perpendicular directions with this mortar matrix on both sides of mesh. This higher percentage of reinforcement evenly distributed over entire surface helps to enhance the strength. Ferrocement wrap is found to be water proof, have the ability to resist sulphate attack and corrosion. Ferrocement structure is able to arrest the cracks formed at the initial stage [10]. Chalioris et al. [11] proved stirrups of "U" shape has capacity to enhance strength and stiffness of beams. All these literature have enough evidence of enhancement of strength and stiffness of "U" wrap.

1.1 Significance of Present Study

Torsional load induces shear stress. Stirrups on all four sides can better resist the torsion. When reinforcement in all four sides cannot be provided, "U" type is a better choice [12]. Torsional strength of "U" wrapped beams is predicted by Deifalla et al. [13]. Chalioris [6] noticed the failure is due to bond failure at the interface of FRP and concrete. Strength of a "U" wrap cannot be same as that of a full wrap. Torque and twist at ultimate stage of ferrocement "U" wrap beam are reported experimentally and with support of analytical model by Behera et al. [14]. Determination of torque and twist at ultimate stage by experimental and analytical method has been reported in Behera [15]. From the various works mentioned above prove that ferrocement can be a wrapping material in place of FRP. No such single equation is derived from the experimental results to predict ultimate torque and twist at ultimate torque of RC beams of different sections or with different materials. Analytical method is tedious and time taking to predict the torsional strength. This challenge inspired to find a solution to predict cracking torque and twist with easy method. Here, with the help of soft computing, solution is found out. The output of the present study is to determine torsional parameter such as ultimate torque and twist at ultimate torque of RC beams with medium and higher grade concrete.

2 Methods to Predict Torque and Twist at Ultimate Stage

2.1 Experimental Program

Beams tested by this author during his doctoral program are taken into consideration. Cross sections of all beams are of 125 mm wide and 250 mm depth. Lengths of the beams are 2 mt. Material and material properties for the casting of beams are

presented in Table 1. Figure 1 presents the cross section and torsion test rig. All the beams were of dimension 125 mm × 250 mm. Width was taken 125 mm to accommodate 25 mm ferrocement wrap on three sides, longitudinal bars and stirrups as shown in Fig. 1. Taking aspect ratio 2, depth was fixed to 250 mm. Ten beams were cast. The beams were designated with alphabets only. First alphabet represents grade of concrete (M for medium M35 grade and H for high strength M60). Second alphabet represents state of torsion (P-plain beam, no reinforcement in core; control specimen for medium strength Beams, U-under reinforced, L-longitudinal over reinforced, T-torsionally over reinforced, C-completely over reinforced). Outer ferrocement wrap was cast initially and allowed to set. After setting of ferrocement wrap, concrete was filled in core portion (75 mm × 225 mm) then the core concrete was cast with core reinforcement. Torsional test is done by torsion test rig. This is reported in Fig. 1.

Table 1 Beam designation and material properties

S.N	Designation	Compressive strength ferrocement matrix	Compressive strength concrete (MPa)	Longitudinal steel		Transverse rein	
				ϕ (dia in mm), nos.	Yield strength (MPa)	ϕ (dia in mm), spacing mm	Yield strength (MPa)
1	MP	40	35	"_"	"_"	"_"	"_"
2	MU	40	35	6, 4	350	6, 100	350
3	ML	40	35	12, 4	440	6, 100	350
4	MT	40	35	6,4	350	8, 100	465
5	MC	40	35	12, 4	440	8, 100	465
6	HP	55	60	"_"	"_"		"_"
7	HU	55	60	6, 6	350	6, 70	350
8	HL	55	60	12, 6	440	6, 70	350
9	HT	55	60	6, 6	350	10, 70	445
10	HC	55	60	12, 6	440	10, 70	445
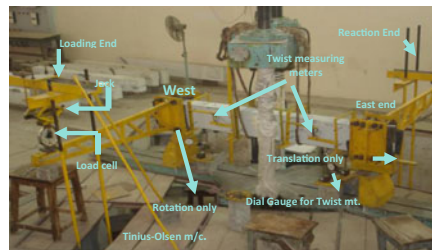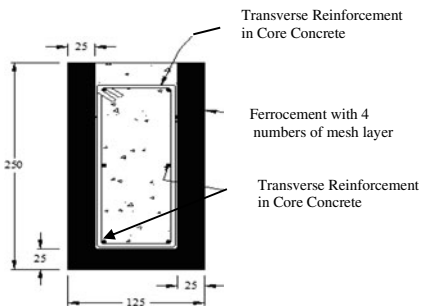
Fig. 1 Beam cross section and torsion testing

2.2 Analytical Model

Experimental program was time consuming and the process involves destruction of proto type specimen. To avoid prediction of torque and twist by experimental method, analytical model using softened truss theory and applying modifications in material properties was developed by author which was fully covered Behera et al. [14, 15].

2.3 Soft Computing Method

Experimental method employed to evaluate torque and twist at ultimate stage is a time consuming process as demolition of specimen is involved. For analytical procedure, programming is required and also a time taken procedure. For computation of torque and twist at ultimate stage of different beams with different material and properties, there is necessity some other method which will be easier and quick one. To overcome these problems soft computing method is employed which provides some equations for the prediction of parameters.

2.3.1 Multivariate Adaptive Regression Spline (MARS)

This multivariate adaptive regression spline (MARS) provides simple equations to predict the desired parameters. This method was developed by Friedman [16]. Some researchers name it as black box while others call it white box. In this method, the output is obtained in the form of an equation. This does not provide any basic thing how the final equation is derived. Approximately 70% of experimental results are taken as fitting and others are used for testing. No such basic assumptions are required for this method. The performer is unable to find the relation between various parameters.

$$
\begin{aligned}
T ultimate = {}& 6.75 - maximum[0,\ 0.32265\text{-}spacing\ of\ longitudinal\ reinforcement] \\
& * 2.7323\text{-}maximum[0,\ 350\text{-}Fty] * 0.002276 \\
& + maximum[0,\ Mortar\ strength\text{-}40] * 0.07677
\end{aligned}
$$

θ_{ultimate}(rad/m) = 0.03558-maximum of [0, Fly-350] * 0.0003376-maximum [0, 350-Fly] * 0.00008786 + maximum [0, spacing of stirrup] * 0.00102665.

2.3.2 WASPAS Method

Weighted aggregated sum product assessment (WASPAS) method was developed by Zavadskas et al. [17]. This method is used for solving multi-criteria decision-making problems (MCDM). The method is the grouping of weighted sum method (WSM)

Table 2 Ultimate torque and twist values

Ultimate torque (kNm)				Twist at ultimate torque (rad/m)			
Beams	Expt	Analytical	MARS	WASPAS	Expt	Analytical	MARS
MP	5.546	5.54	5.074	4.791	0.00530	0.00530	0.00480
MU	6.01	5.8902	6.458	5.644	0.14000	0.13000	0.13820
ML	6.939	6.92	6.752	7.321	0.11220	0.10973	0.10786
MT	7.38	7.427	6.463	7.453	0.13480	0.13483	0.13825
MC	9.426	9.3728	9.426	9.129	0.11000	0.10299	0.10780
HP	6.52	6.52	6.226	6.341	0.00546	0.00560	0.00483
HU	7.68	7.729	7.904	7.472	0.13050	0.13736	0.10745
HL	7.87	7.828	7.904	9.165	0.05600	0.05500	0.07706
HT	8.86	8.58	7.904	9.553	0.09210	0.09158	0.10745
HC	12.91	12.98	12.91	11.246	0.07540	0.07361	0.07706

and weighted product method (WPM). The various steps of WASPAS procedure are taken Alireza and Javad [18] and Madic et al. [19, 20]. Initialization of matrix is first step of this method, after which matrix is normalized. The next step is calculation of relative importance. The 4th step is the application of WPM and final step is to optimize the value. Table 2 shows the torque and twist at ultimate stage, found experimentally and predicted by MARS and WASPAS.

3 Interpretation of Test Results

Ultimate torque and twist found from various methods were discussed in this section.

3.1 Behaviour of "U" Wrap Beams

Ten beams were cast and tested. Two beams MP and HP are as control specimens for medium and high strength RC beams having no reinforcement in core. Four beams covering four states of torsion were cast with M35 and M60 grade concrete. All the cracks were found having an inclination of 45° to the longitudinal steel. This may be due to induced shear from torsional loading.

3.2   Ultimate Torque of Medium and High Strength Beams

The beams MP and HP failed after initiation of micro crack on longer face and formation of macro crack. After cracking, these beams sustain further some load up to ultimate failure. For other type of beams, after initiation of crack, beams are able to resist further more load due to participation of reinforcement in the core. So, ultimate torque depends on amount of reinforcement in both direction and also on ferrocement wrap. The ultimate torques of beams MP, MU, ML, MT, MC, HP, HU, HL, HT and HC were found be experimentally 5.546 kNm, 6.01 kNm, 6.939 kNm, 7.38 kNm, 9.426 kNm, 6.52 kNm, 7.68 kNm, 7.87 kNm, 8.86 kNm and 12.91 kNm respectively. The predicted values by soft computing method and by analytical methods were reported in Table 2 and also in Fig. 2. For medium concrete beams ultimate torque carrying capacity increases 69.96% with respect to its control specimen while the same for high strength beam it was found to be increasing 98.01%. Maximum increase in strength was reported in HC (high strength over reinforced beams). Over reinforced beams have more amount of reinforcement, so also resist more torque. Transversely over reinforced beams resist more torque than longitudinally over reinforced beams for both medium and high strength beams. This may be due to participation of transverse reinforcement to resist torque. The same has been presented in Fig. 2. The percentage increase of torque in longitudinally over reinforced beam for ML and HL are found to be 25.12% and 20.71% over their control specimen MP and HP respectively. The same for transversely over reinforced beam MT and HT are found to be 33.07% and 35.89% over their control specimen MP and HP respectively. Increase in ultimate torque for under reinforced beams were limited to 8.37% and 17.79% over their control specimen for medium and high strength ferrocement "U"
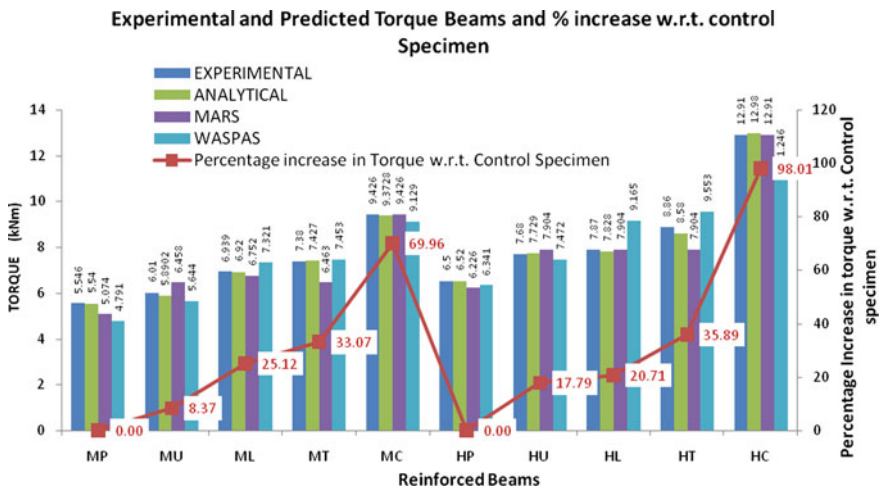
Fig. 2 Experimental and predicted torque for various beams with % increase in torque w.r.t. control specimen
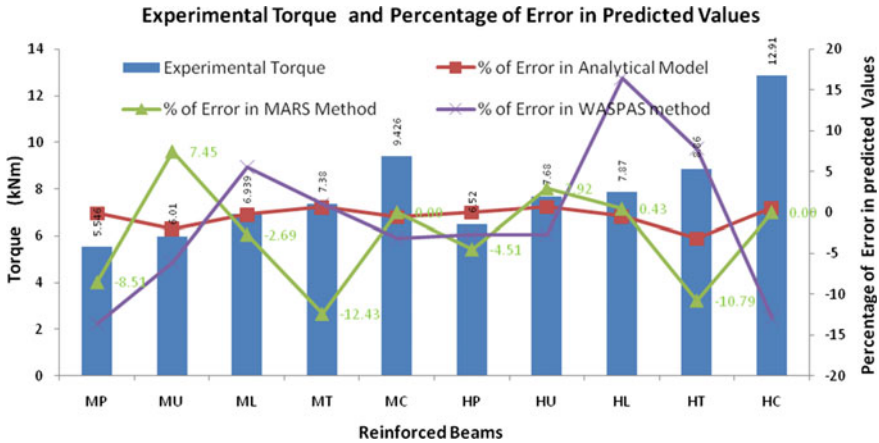
Fig. 3 Experimental ultimate torque with percentage of errors in predicted values

wrap beams. Figure 3 represents the errors found in predicted values. Maximum error was reported in beam HT by analytical model which was only −3.16%. Percentage of error in MARS method was found to be less than 10 except for beams MT and HT. The prediction of ultimate torque by WASPAS varies within 10% of experimental values expect for beams MP, HL and HC. The maximum error was found in WASPAS method for beam HL i.e. 16.45%.

3.3 Ultimate Twist of Medium and High Strength Beams

Torque and twist are the main parameters to be considered when a section is loaded under torsion. The previous section deals with torque. Percentage of error in some beams as found more in WASPAS method, this method is not included for prediction of twist. Twist at ultimate torque of beams MP, MU, ML, MT, MC, HP, HU, HL, HT and HC was found experimentally 0.0053 rad/m, 0.14 rad/m, 0.1122 rad/m, 0.1348 rad/m, 0.11 rad/m, 0.00546 rad/m, 0.0921 rad/m, 0.056 rad/m, 0.0921 rad/m, 0.0754 rad/m respectively. Under reinforced beams MU and HU exhibited maximum twist at ultimate torque. As the stiffness of under reinforced beams are less, they exhibit more rotation. As the rotation capacity is more, the toughness which is the area under torque twist diagram will be more. Under reinforced beams in both medium and high strength concrete category were found to have 2541.51% and 2290.11% increase in twist over their control specimens respectively. This proves twist at ultimate torque is influenced more in states of torsion. Next to under reinforced beams, transversely over reinforced beams twist more than other categories in both medium and high strength concrete ferrocement "U" wrapped beams. MT and HT exhibit 25.43 and 16.87 times more twist with respect to their control specimens. Figure 4 shows the
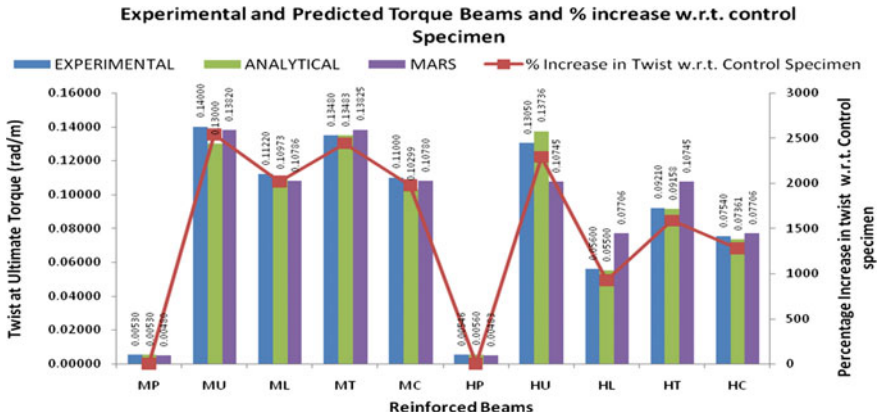
Fig. 4 Experimental and predicted twist at ultimate torque for various beams with percentage of increase in twist w.r.t. control specimen

variation of twist at ultimate torque of different beams and percentage of increase in twist with respect to control specimen.

Prediction of twist is more accurate in analytical model. Maximum error was noticed as -7.14% for MU. Errors are within 5% of the experimental values. The experimental and errors in predicted values are reported in Fig. 5. Torque and twist values more accurately predicted by softened truss model.
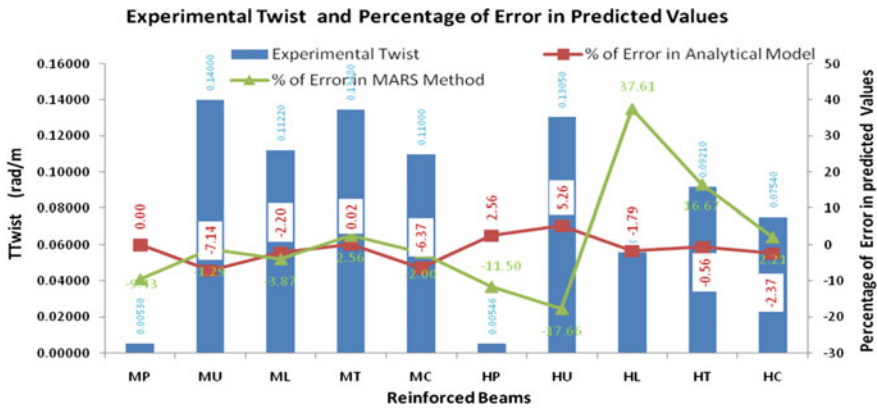
Fig. 5 Experimental twist at ultimate torque with percentage of errors in predicted values

4 Conclusions

In this research activity, medium and high strength RC beams are constructed with "U" wrap of ferrocement. Torque and twist capacity at ultimate stage were found after the testing of beams. Analytical and soft computing methods were employed to predict the same. The following conclusions were drawn from this research work.

A. For prediction of both torque and twist at ultimate stage, analytical model is more suitable when experimental results are not available. Predicted values for ultimate torque by the methods of soft computing such as MARS and WASPAS are very close to test values. However, WASPAS method is not suitable for prediction of twist at ultimate stage.

B. Both torque and twist at ultimate stage are more influenced by the amount of steel provided in core concrete.

C. Maximum torque carrying capacity is observed in beams having more reinforcement both longitudinal and transverse direction than balance section. High strength beams are able to sustain more torque than medium strength ferrocement wrapped beams. Completely over reinforced medium and high strength beams are able sustain 69.96 and 98.01% more torque than to their control specimen.

D. Maximum twist capacity is observed in under reinforced beams. High strength beams are found with less twist with respect to their medium strength ferrocement wrapped beams. MU has the maximum rotation capacity which is 26.42 times more than its control specimen. Next to under reinforced category beams, transversely torsionally over reinforced beams have better rotation capacity than other categories of beams.

References

1. Dong H-L, Wang DY, Wang ZY, Sun YL (2018) Axial compressive behavior of square concrete columns reinforced with innovative closed-type winding GFRP stirrups. Compos Strcut 192(15):115–125
2. Muhammad T, Wang ZY, Wang DY (2018) Axial compressive behaviour of square concrete columns reinforced with CFRP sheet strip stirrups. Submitted to: Constr Build Mater
3. Karayannis CG, Chalioris CE, Sirkelis GM (2008) Local retrofit of exterior RC beam-column joints using thin RC jackets—an experimental study. Earthq Eng Struct Dyn 37(5):727–746
4. Isleem HF, Wang DY, Wang ZY (2018) Axial stress-strain model for square concrete columns internally confined with GFRP hoops. Mag Concr Res 70(20):1064–1079
5. Yasmeen TO, Ahmed MA, Ashteyat (2020) Performance of RC beam strengthened with NSM-CFRP strip under pure torsion: experimental and numerical study. Int J Civ Eng 18:585–593
6. Chalioris CE (2008) Torsional strengthening of rectangular and flanged beams using carbon fibre-reinforced-polymers—experimental study. Constr Build Mater 22(1):21–29
7. Deifalla A (2015) Torsional behavior of rectangular and flanged concrete beams with FRP reinforcements. Journal of Structural Engineering 141(12):50–68
8. Li B, Lam ESS, Wu B, Wang YY (2000) Experimental investigation on reinforced concrete interior beam-column joints rehabilitated by ferrocement jackets. Eng Struct 56:897–909

9. ACI Committee 549 (1979) Ferrocement-materials and applications. In: ACI symposium proceedings SP-61. Farmington Hills, Michigan
10. Shannag MJ, Mourad SM (2012) Flowable high strength cementitious matrices for ferrocement applications. Constr Build Mater 36:933–939
11. Chalioris CE, Thermou GE, Pantazopoulou SJ (2014) Behaviour of rehabilitated RC beams with self compacting concrete jacketing—analytical model and test results. Constr Build Mater 55:257–273
12. Behera GC, Rao TDG, Rao CBK (2008) Torsional capacity of high strength concrete beams jacketed with ferrocement U wraps. Asian J Civ Eng 9(4):411–422
13. Deifalla A, Ghobarah A (2010) Full torsional behavior of RC beams wrapped with FRP: analytical model. J Compos Constr 14(3):289–300
14. Behera GC, Rao TDG, Rao CBK (2014) Analytical model for torsional response of RC beams strengthened with ferrocement U-Wraps. SEI, IABSE Struct Eng Int 24(4):509–520
15. Behera GC, Rao TDG, Rao CBK (2014) A study on post cracking torsional behaviour of high strength reinforced concrete beams with ferrocement "U" wraps. Slovak J Civ Eng 22(3):1–12. https://doi.org/10.2478/sjce-0012
16. Friedman J (1991) Multivariate adaptive regression splines. Annals Stat 19:1–141
17. Zavadskas EK, Turskis Z, Antucheviciene J, Zakarevicius A (2012) Optimization of weighted aggregated sum product assessment. Elektron. Elektrotech 122:3–6
18. Alireza A, Javad K (2019) New methods and applications in multiple attribute decision making (MADM) 1–233
19. Madic M, Gecevska V, Radovanovic M, Petkovic D (2014) Multicriteria economic analysis of machining processes using the WASPAS method. J Prod Eng 17:1–6
20. Madic M, Antucheviciene J, Radovanovic M, Petkovic D (2016) Determination of manufacturing process conditions by using MCDM methods: application in laser cutting. Eng Econ 27:144–150

Performance of Optimal Sensor Placement Strategies for Damage Detection in Civil Engineering

Swagato Das and Purnachandra Saha

1 Introduction

Structural Health Monitoring in civil engineering structures is achieved with the use of sensors and different damage detection methods which can indicate structural damage [1]. Sensors are the electronic devices which are installed on the structures to obtain detailed information on strain, stress, acceleration, deformation, etc. The data obtained are utilized by system identification methods to identify the structural parameters, such as natural frequencies and mode shapes [2]. These identified parameters can be utilized for SHM using different methods such as change in mode shape, frequency response method, optimization methods, etc. [1, 3]. The main factors for data acquisition using sensors are number of sensors to be placed to the available sensor network and the source of power for the sensors to work [4]. However, the issue of sensor placement draws attention of different researchers. The sensors installed in the structures are permanent. Due to the design of complex structures, the number of sensors to be placed is more. Therefore, more the number of sensors placed on a structure, more detailed information is obtained which improves the SHM process [5, 6]. Hence cost of data acquisition is higher [7]. In order to reduce the cost, the number of sensors to be installed needs to be reduced. The sensors must be placed such that all the structural parameters are sensed without missing any important data. Therefore, the placement of sensor is difficult. The sensor locations were usually determined from the past experience and knowledge of the vibration occurrence. In many health monitoring situations, there was a need for analysis of the measured data to obtain result of unmeasured parts [8]. There are two types of error: false positives, which

S. Das (✉)
Civil Engineering Department, C.V. Raman Global University, Bhubaneswar, Odisha, India

P. Saha
School of Civil Engineering, KIIT, Deemed to be University, Bhubaneswar, Odisha, India

denotes false damage to the structure, and false negatives, in which the damage is missed [9]. Therefore, optimal placement of sensor is necessary for higher accuracy.

In this scenario, different techniques have been developed for optimal sensor placement (OSP). These techniques mainly include the System—Realization method and Optimization Method. The System—Realization method uses and compares the identified structural parameters between the reduced sensor data and real parameters to determine the optimal number of sensors required for SHM and their appropriate placement in the structure [8]. The Effective Independence (EFI) Method, which is popular among researchers for OSP, uses the truncated mode shapes to determine the placement of sensors [7]. These methods are based mainly on the iterative calculations. Also, the sensor noises have not been considered [10]. Optimization Algorithms have been introduced in civil engineering for the purpose of optimal structural design and health monitoring [2, 11, 12]. The optimization techniques have been introduced for OSP in order to determine the sensor placement in complex structures using objective functions based on structural parameters such as natural frequencies and mode shapes [13]. This technique has been introduced as in case of complex structures; the iterative calculations required for placing the sensors increases.

This paper deals with the development of different OSP techniques used for civil SHM. The study mainly focusses on the different OSP techniques used till date and a detailed comparison among these techniques based on the advantages and disadvantages.

2 Different Methods of OSP Used for Civil SHM

Optimal sensor placement has been the key strategy of the civil engineers to monitor the health of complex structures, such as high-rise buildings, bridges, off-shore structures, etc. This technique helps to place the sensors, such as strain sensor, accelerometers, etc., on the structure such that the structural parameters, natural frequency and mode shape, of the civil engineering structure may be identified using minimum number of sensors. This in-turn reduces the cost of SHM and improves the efficiency of monitoring. The OSP techniques are mainly divided into two groups: System Realization Method and Optimization Method.

2.1 System Realization Method

The system realization method mainly uses the mode shapes obtained from the sensed sensor data and compares it with the real mode shapes to identify the probable sensor locations. Some of the common System Realization Methods are Effective Independence (EFI) Method, Kinetic Energy Method, Eigenvalue Vector Product and Variance Method.

2.1.1 D-Optimal Criteria

An OSP algorithm using D-optimality criteria has been used which uses the maximum determinant of Fisher Information matrix to verify the optimal sensor placement [14]. The D-optimal algorithm has a decoupling effect in which the optimal sensor placement problem and modal identification problem can be solved in an independent manner (Eq. 1) [15].

$$\beta* = \text{Arg}, \max_{\beta} \left(\prod_{i=1}^{N} \left(\prod_{k=1}^{M} \beta_k \frac{\left(r_k^T \Phi_i\right)^2}{\psi_k^2} \right) \right)$$ (1)

where N is the number of structural mode shapes, M is the points that describers a particular mode shape, r_k is the vector associated with the location of kth sensor, Φ is the mode shape vectors for N flexible body, ψ_k is the noise spectrum associated with kth sensor and β is composed of 0s, when the particular point in the mode shape is not included in the output, and 1s, if otherwise. Hence the input required for determination of OSP is the natural mode shapes, which can be obtained using finite element modelling. The algorithm has been tested on truss bridge using two sensors. The algorithm was able to rank the optimal location of sensors and also provide an alternate location. This feature is handy in the case where the first sensor fails and the second sensor acts as a back up detecting damage in structure. The algorithm however requires a long computational time owing to the number of possible combinations.

2.1.2 Effective Independence Method

The Effective Independence Method (EFI) is one of the popular methods used by researchers for formulating sensor placement strategies [10]. The sensor placement for large space structural system using finite element model (FEM) based effective independence (EFI) method was carried out [10]. The locations have been ranked according to their contribution and the sensor candidate set was revised using iterative method according to this contribution. The EFI method has found its use in many aspects of OSP as it works on the principle of linear independency of identified modes by reducing the covariance matrix between estimated modal displacement and modal coordinate. This method maximizes the Fisher Information Matrix to quantify the independence between the two or more reduced mode shapes to determine the suitable sensor locations [7]. The measured structural response vectors are used to estimate the error in results and is represented as:

$$J = E[(q - \hat{q})(q - \hat{q})^T)] = \left[\frac{1}{\sigma^2} \varphi^T \varphi \right]^{-1} = Q^{-1}$$ (2)

where q is the coefficient of response vector, φ is the FEM target mode shapes matrix, σ^2 is the noise variance in each sensor, E is the Young's Modulus and Q is the Fisher Information Matrix [16]. Fisher Information matrix obtained from the measure mode shapes, has been considered for linear estimate. Therefore, the best estimation of q is obtained when Q is maximized. The maximization process is done by deleting the candidate sensor positions such that the FIM determinant is maximum. The deletion of sensor location is carried out depending upon the value of EFI value, 0 indicating no contribution of sensor to the measurement system. An iterative process is performed employing the Effective Independent Distribution to evaluate the sensor location configuration is developed [10].

The EFI method was applied for ranking sensor locations in a space station considering truss model [10]. The selection of sensor candidate was based on the modal kinetic energy and the process was carried out using FORTRAN program. Out of the 200° of freedom (DOFs) targeted on the structure, 70 DOFs were calculated by the EFI technique, after 7 iterations, to be critical for sensor location, shown in Fig. 1. The algorithm has been tested successfully for structural truss. This EFI method gives good estimates of target modes by maximizing the retained independence information and minimizing the estimate errors.

An error analysis for sensor placement has been deviced using EFI method [18]. The error occurring may be due to the model error which comprises incorrect modelling techniques, incorrect input parameters, small linearities or unmodelled dynamics. The error analysis assumes that the target mode shape contains both real mode shapes and corresponding errors. The positive definite net information matrix of sensor configuration indicates the ability of the sensor to independently identify the real target modes. The algorithm was used on space station truss, as used by Kammer [10], to make intelligent decisions on sensor placement for identification of real modes using the net information matrix. Also, the bounds of suitable size for
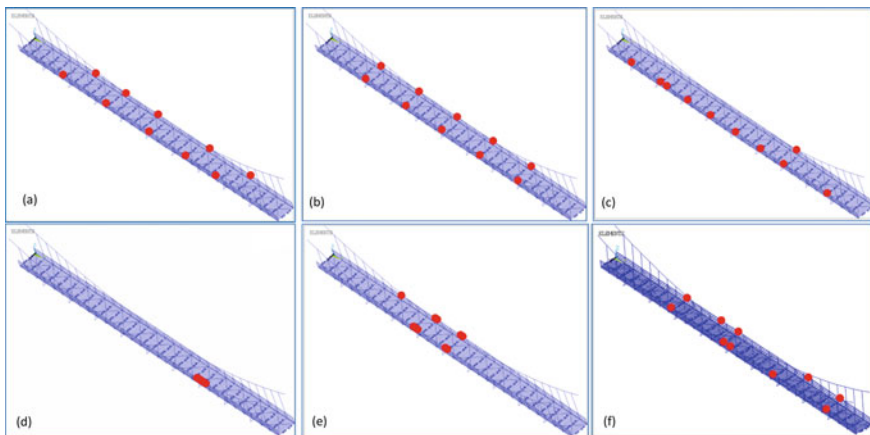
Fig. 1 OSP using: **a** EFI method, **b** EFI-EFI—Driving Point Residue method, **c** KEM method, **d** EVP method, **e** NODP method and **f** VR method (Red dots indicate the sensor locations) [17]

the errors to occur have been defined using bound theory so that the net information matrix is positive. The method showed an error of 15% as the algorithm may be conservative in defining the derived positive definiteness condition. Even so, the method can be used to get a rough estimate of the sensor location.

Research has been carried out to develop a formal relationship between system-realization algorithm and EFI sensor placement technique in order to develop a technique which can detect damage as well as locate sensors [19]. The system realization algorithm depends on observability matrix which indicates the number of target modes, or sensors placed, in the system. With use of EFI, the optimum sensor configuration will be achieved thus reducing the size of observability matrix and size of Hankel data matrix required for modal identification. The technique has been successfully implemented for sensor location in large dynamic civil structures [20].

The EFI method faces a problem with the sensor locations with low energy content as there is loss of information. In order to overcome this limitation, The EFI method has been combined with the Driving Point Residue (DPR) method [21]. However, the algorithm does not consider the sensor noise. Also, the final set of sensor location is suboptimal as the algorithm is iterative in nature. The actual field results may be different from the FEM results for large structures where modal density is high [7].

2.1.3 Energy Based Method

The Kinetic Energy Method (KEM) maximizes the measure of kinetic energy in the structure to find the reduced sensor placement configuration [17]. For the need to identify mode shapes using higher signal to noise ratio, a new area was researched by maximizing the kinetic energy of structural system. The difference between the EFI and KEM is that the former maximizes the FIM, whereas the KEM maximizes the kinetic energy of the structure. The kinetic energy is directly related to the mode shapes as is given as:

$$KE = \varphi^T M \varphi \tag{3}$$

where M is the mass matrix of the structure. Guyan reduction is used to obtain the reduced mass and stiffness matrices [22]. These reduced mass and stiffness matrices can be used to estimate the reduced mode shapes, thus computing the sensor locations.

Eigenvalue Vector Product (EVP) is another energy based technique which considers the evaluation of EVP vector to select suitable sensor locations and is expressed as [23]:

$$EVP_i = \prod_{j=1}^{N} |\varphi_{ij}| \tag{4}$$

where N is the total number of modes. In this technique, the sensor with largest EVP values is selected to maximize the vibration energy and prevent the selection of sensors on nodal lines of vibration node.

Another energy based method used for OSP is the non-optimal drive point (NODP) method which is used to find the optimal excitation point. The vibration measured by sensor is considered as the function of the relative sensor positions and the mode shape nodal lines. This iterative algorithm unselects the candidate sensor position having the smallest displacement and is represented as [24]:

$$NODP_i = \min_j \left| \varphi_{ij} \right| \tag{5}$$

2.1.4 Variance Method

The Variance Method (VM) is an improvement of most informative subset (MIS) technique which considers the coefficients of the covariance matrix [25]. The covariance relation is given as:

$$V_r = \sum_{i=1}^{M} \frac{c_{ij}}{Dep_i} \tag{6}$$

where M is the number of sensor locations, c_{ij} is the covariance coefficient, Dep_i is the sum of the off-diagonal terms in c_{ij} matrix. Maximization of V_r gives the probable distribution of sensors.

2.1.5 Time Domain Parameter Estimation

A backward elimination scheme was developed using Time Domain parameter estimation method which can determine the appropriate placement of sensors [26]. The algorithm uses the Time Domain method which is effective for complex structures having large number of modes and for modes which are closely spaced.

The algorithm has been tested with eight bay truss from NASA Langley Research Center [27] for both experimental and simulated cases which shows less error in estimates.

The System-Realization methods have been compared for sensor placement in a FEM modelled Nottingham suspension bridge using GPS sensors [28]. EFI method, EFI—Driving Point Residue (DPR) method, KEM method, EVP method, NODP method and VR method has been compared to compute the location of sensors in a FEM modelled bridge [17, 29]. The sensor location results have been shown in Fig. 1 and shown as red dots. It can be concluded from the results that the EFI—Driving Point Residue method shows good location results. The EFI method shows

a fairly uniform location along the bridge as seen from Fig. 1a. The EFI—FPR method, as shown in Fig. 1b, gives a quasi-uniformly spaced and symmetrical sensor placement, which gives full set of modal data. The KEM results, shown in Fig. 1c, gives sensor locations only on one side of bridge handrails. Hence, the results need to be extensively verified with real life structure. The EVP method gives the sensor locations concentrated in a small area of the bridge, as shown in Fig. 1d, which causes a serious doubt on the accuracy of mode shape determination. The NODP method places the sensors mainly in the bridge mid span, as in Fig. 1e. The VR method shows sensors placed randomly along both sides of the bridge, as in Fig. 1f. This method does not consider the symmetry of the bridge. Hence the EFI-DPR method shows better OSP results than the rest of the methods, as was observed from the mean square error between the mode shape obtained and the FE model mode shape.

Similar comparative study was conducted by Liu et al. [30] in which the EFI, EFI-DPR and KEM have been considered for sensor placement. The results obtained showed that the EFI-DPR showed accurate sensor placement than KEM.

3 Optimization Method

Optimization algorithms have been introduced for OSP due to the ease by which the iterative mathematical calculations can be solved and the maximum possible information about the structural system can be obtained. The different objective functions used for OSP depend mainly on the mode shapes of the structure. The different optimization techniques implemented for OSP have been shown in Table 1.

4 Discussion

The optimal sensor placement techniques have been divided into System—Realization technique and optimization technique.

The system realization technique uses mainly the identified mode shapes of the structure to device the OSP strategies. D-optimality criteria uses the maximum determinant of Fisher Information matrix to verify the optimal sensor placement. This method ranks the optimal location of sensors and provide an alternate location. The algorithm however requires a long computational time owing to the number of possible combinations. In order to deal with the computational time, Effective Independence Method was introduced. This method uses the maximization of Fisher Information Matrix to quantify the independence between the two or more reduced mode shapes to determine the suitable sensor locations. The method gives good estimation of target modes by maximizing the retained independence information and minimizing the estimate errors. The EFI method has been combined with the Driving Point Residue (DPR) method to overcome the problem of the sensor locations with low energy content as there is loss of information. This EFI-DRP method

Table 1 Optimization methods used for OSP

Optimization method	Objective function	Application	Remark
Modified Monkey Algorithm [31]	MAC based—maximization of MAC off-diagonal values and average value of off-diagonal elements	Dalian world trade building	In order to reduce the random nature of the MA, modification has been made by introducing Euclidean distance operator and the OSP results show good sensor placement
Niching Monkey Algorithm (NMA) [32]	Maximization of MAC off-diagonal values	Dalian World trade building	The sensor placement of Monkey Algorithm (MA) and NMA is compared and it was observed that the NMA proved to be superior
Genetic Algorithm [33]	Modal fitness function—modal fitness, deformation energy, curvature mode	Tai Zhou Bridge [34]	Fitness functions considering the Deformation Energy shows good sensor placement as it shows symmetric distribution
Discrete Artificial Bee Colony (ABC) algorithm [5, 6]	Modal Assurance Criteria (MAC) based-Least square summation and maximization of MAC off-diagonal values	27 bar truss bridge [5, 6], 21 storey building [35], Canton tower [36]	MAC based objective function which considers summation of least squares showed good sensor placement locations
Improved ABC Algorithm [37]	Maximization of MAC	Ha-Qi long span railway bridge	The improved ABC showed better speed as compared to the basic ABC in accurately determining the sensor locations

showed good sensor placement results than other sensor placement techniques. The EFI algorithm do not consider the sensor noise and the final set of sensor location is suboptimal as the algorithm is iterative in nature. Therefore, where modal density is high, actual field results may be different from the FEM results for large structures. In order identify mode shapes using higher signal to noise ratio, maximizing the kinetic energy of structural system was introduced. Time Domain Parameter Estimation algorithm has been used for effective sensor placement in complex structures having large number of modes and for modes which are closely spaced.

In order to overcome the problem of iterative calculations, optimization techniques have been employed for the purpose of OSP. Monkey Algorithm has been modified and applied for OSP in Dalian World trade building using objective functions based on MAC. This method gave good estimation results. Genetic Algorithm, when applied on Tai Zhou Bridge using fitness based objective function, showed symmetric and well defined sensor placement. Artificial Bee Colony algorithm has also been modified and applied for sensor placement in buildings, like Canto tower, and bridges, like Ha-Qi long span railway bridge. The method also showed symmetric reduced sensor placement without compromising the information obtained from the structures.

5 Conclusion

Out of the different optimal sensor placement strategies, System-Realization based and optimization-based techniques have been discussed in the manuscript.

(1) Out of the different System—Realization techniques, Effective Independence Method—Driving Point Residue have been widely used by the researchers for OSP. This method shows reliable and symmetric sensor placement such that the structural parameters can be identified.

(2) The optimization technique has also been applied for OSP. These techniques have been applied for solving OSP using different objective functions based on mode shapes in complex structures, such as Canton tower, Tai Zhou Bridge, Dalian World trade building, etc.

References

1. Das S, Saha P (2016) Damage identification in a multi-storeyed building using modal based health monitoring techniques. Struct Eng Convention (SEC-2016) CSIR-SERC, Dec 2016
2. Das S, Saha P (2020) Performance of hybrid decomposition algorithm under heavy noise condition for health monitoring of structure. J Civ Struct Health Monitor. https://doi.org/10.1007/s13349-020-00412-5
3. Das S, Saha P (2018) A review of some advanced sensors used for health diagnosis of civil engineering structures. Measurement 129:68–90
4. Das S, Saha P (2018) Structural health monitoring techniques implemented on IASC–ASCE benchmark problem: a review. J Civ Struct Health Monitor 8(4):689–718
5. Sun H, Büyüköztürk O (2015) Identification of trafficinduced excitations of truss bridges through heterogeneous data fusion. Smart Mater Struct 24(075032)
6. Sun H, Büyüköztürk O (2015) Optimal sensor placement in structural health monitoring using discrete optimization. Smart Mater Struct 24(125034):16
7. Rao ARM, Lakshmi K, Krishnakumar S (2014) A generalized optimal sensor placement technique for structural health monitoring and system identification. Procedia Eng 86:529–538
8. Li ZN, Tang J, Li QS (2004) Optimal sensor locations for structural vibration measurements. Appl Acoust 65:807–818

9. Flynn EB, Todd MD (2010) A Bayesian approach to optimal sensor placement for structural health monitoring with application to active sensing. Mech Syst Signal Process 24:891–903

10. Kammer DC (1991) Sensor placement for on-orbit modal identification and correlation of large space structures. J Guidance 14(2):251–259

11. Das S, Saha P (2021) Performance of swarm intelligence based chaotic meta-heuristic algorithms in civil structural health monitoring. Measurement 169(108533)

12. Roy S, Kundu CK (2020) State-of-the-art review on the use of optimization algorithms in steel truss. Int J Sci Technol Res 9(3):160–165

13. Yi TH, Li HN (2012) Methodology developments in sensor placement for health monitoring of civil infrastructures. Int J Distrib Sens Netw 2012(612726):11

14. Tongco EC, Meldrum DR (1994) Optimal sensor placement for identification of large flexible space structures automatic control in aerospace, Palo Alto, California, USA

15. Bayard BS, Hadaegh FY, Meldrum DR (1988) Optimal experiment design for identification of large space structures. Automatica 24(3)

16. Dowski E (2002) Fisher information and Cramer-Rao bound. Colorado University

17. Heo G, Wang ML, Satpathi D (1997) Optimal transducer placement for health monitoring of long span bridge. Soil Dyn Earthq Eng 16:495–502

18. Kammer DC (1992) Effect of model error on sensor placement for on-orbit modal identification of large space structures. J Guidance, Control, Dyn 15(2):334–341

19. Kammer DC (1996) Optimal sensor placement for modal identification using system-realization methods. J Guidance, Control, Dyn 19(3):729–731

20. Rao ARM, Anandakumar G (2008) Optimal sensor placement techniques for system identification and health monitoring of civil structures. Smart Struct Syst 4(4):465–492

21. Meo M, Zumpano G (2005) On the optimal sensor placement techniques for a bridge structure. Eng Struct 27:1488–1497

22. Guyan RJ (1965) Reduction of stiffness and mass matrices. Am Inst Aeron Astronaut J 3(2):380

23. Larson CB, Zimmerman DC, Marek EI (1994) A comparison of modal test planning techniques: excitation and sensor placement using the NASA 8-bay truss. In: 12th international modal analysis conference

24. Imamovic N (1998) Model validation of large finite element model using test data. PhD, Imperial College London

25. Fedorov V, Hackl P (1994) Optimal experimental design: spatial sampling. Calcutta Stat Assoc Bull **44**(March–June):173–174

26. Liu C, Tasker FA (1995) Sensor placement for multi-input multi-output a dynamic identification. In: 36th structures, structural dynamics and materials conference, AIAA, Washington, DC

27. Kashangaki TAL (1992) Ground vibration tests of a high fidelity truss for verification of on orbit damage location techniques NASA technical memorandum 107626

28. Roberts GW, Cosser E, Meng X, Dodson AH, Morris A, Meo M (2003) A remote bridge health monitoring system using computational simulation and single frequency GPS data. In: Proceedings of the 16th international technical meeting of the satellite division of the institute of navigation

29. Worden K, Burrows AP (2001) Optimal sensor placement for fault detection. Eng Struct 23:885–901

30. Liu KL, Yan RJY, Soares G (2018) Optimal sensor placement and assessment for modal identification. Ocean Eng 165:209–220

31. Yi TH, Li HN, Zhang XD (2012) A modified monkey algorithm for optimal sensor placement in structural health monitoring. Smart Mater Struct 105033:9

32. Yi TH, Li HN, Gu M, Zhang XD (2014) Sensor placement optimization in structural health monitoring using Niching Monkey algorithm. Int J Struct Stab Dyn 14(5):1440012 (1440018pp)

33. Han LZ, Zhang JQ, Yang Y (2014) Optimal placement of sensors for monitoring systems on suspension bridges using genetic algorithms. Appl Mech Mater 530–531:320–331

34. (1997) Highways department of Hong Kong, Lantau fixed crossing and ting Kau bridge wind and structural health monitoring. Master Plan. Flint and Neill Partnership

35. Celebi M, Toksöz N, Büyüköztürk O (2014) Rocking behavior of an instrumented unique building on the mit campus identified from ambient shaking data. Earthq Spectra 30:705–720
36. Yi TH, Li HN, Gu M (2011) Optimal sensor placement for structural health monitoring based on multiple optimization strategies. Struct Des Tall Spec Build 20:881–900
37. Yang J, Peng Z (2018) Improved ABC algorithm optimizing the bridge sensor placement. Sensors 18(2240):18
38. Das S, Saha P, Patro SK (2016) Vibration based damage detction techniques used for health monitoring of structrues: a review. J Civ Struct Health Monit 6(3):477–507
39. Das S, Saha P, Satapathy SC, Jena JJ (2020) Social group optimization algorithm for civil engineering structural health monitoring. Eng Optim. https://doi.org/10.1080/0305215X.2020.1808974

The Influence of Red Mud on the Performance Characteristics of High Strength Self Compacting Concrete

B. Ritish Reddy, Md. Zakir Hussain, S. Keerthi, and B. Narendra Kumar

1 Introduction

The rapid growth in construction industry brought a lot of new materials to experiment and replace, as to reduce the environmental impact of the materials. Among them Red Mud (RM) is the material that we are replacing which is derived from Alumina. As the rate of production of alumina is being increased at 1% per annum since last decade the production of RM is also increasing. RM is fine powdered mud which adversely affects the air, land, and water. So with this reference it is needed to use this RM in some way, so to compensate this production of RM some amount of it used in place of admixture to prepare concrete. The current research study is focused on effect of RM on the properties of High Strength Self Compacting Concrete (HSSCC).

RM has high pH between 10–14 which retains passive environment near reinforcement and prevents corrosion as well as it reduces the heat of hydration since some amount of cement is replaced by RM. It also consumes calcium hydroxide which is byproduct of hydration which remains as waste, so this RM reacts with calcium hydroxide to form C–S–H gel. These can be seen as some of the advantages of RM but simultaneously there are some disadvantages also which should be studied to make the utilization of RM profitable. Among them one of the drawbacks is setting time using RM is more than that of ordinary cement.

B. Ritish Reddy (✉) · Md. Zakir Hussain · S. Keerthi · B. Narendra Kumar
Department of Civil Engineering, VNR VJIET, Hyderabad, India

2   Materials Used

Concrete cube specimens of size 150 mm × 150 mm × 150 mm were prepared. Here quartz sand is used as fine aggregate. In the concrete mix super plasticizer and viscosity modifying agents are also added.

2.1   Red Mud

Red Mud (RM) is a reddish-brown sludge byproduct produced through the Bayer process in the aluminum industry. When 1 ton of alumina is produced, 1–1.5 tons of RM is generated as a byproduct. RM can be repurposed as a cement admixture material in concrete, ready-mixed concrete, cement and ceramic products. Neutralized RM is prepared by adding sulfuric acid to liquefied RM.

2.2   Quartz Powder

Quartz powder is a chemical compound consisting of 1 part silicon and 2 parts oxygen. Quartz powder is obtained from Quartz which is the most abundant mineral found on the Earth's surface. Its major constituent is silicon dioxide. Specific gravity of it lies between 2.6–2.7. Its specific area depends upon its particle size which may be 1100, 2300, 3500 cm^2/gm.

3   Experimental Investigation on SSC

3.1   Mix Proportions

The mix proportions of the normal SSC and HFHSSCC made replacing cement with red-mud areshown below in Table 1. Here 2.5, 5, 7.5 and so on is the percentage of RM replaced with cement.

3.2   Fresh Properties

Tests are conducted to determine the fresh properties of the mixes and the results are tabulated as shown in Table 2 and graphs are plotted as shown in Figs. 1, 2 and 3.

Table 1 Mix proportions of the current work in kg per cubic meter

Mix designation	Cement (kg/m^3)	Red mud	Quartz powder (kg/m^3)	Quartz sand (kg/m^3)	Coarse aggregate (kg/m^3)	SP (% of P.C)	VMA (% of P.C)	W/P ratio
SCC	450	–	–	810	776	1.3	0.5	0.28
HFHSSCC-2.5	351	9	90	810	776	1.3	0.5	0.28
HFHSSCC-5	342	18	90	810	776	1.3	0.5	0.28
HFHSSCC-7.5	333	27	90	810	776	1.3	0.5	0.28
HFHSSCC-10	324	36	90	810	776	1.3	0.5	0.28
HFHSSCC-12.5	315	45	90	810	776	1.3	0.5	0.28
HFHSSCC-15	306	54	90	810	776	1.3	0.5	0.28
HFHSSCC-17.5	297	63	90	810	776	1.3	0.5	0.28
HFHSSCC-20	288	72	90	810	776	1.3	0.5	0.28
HFHSSCC-22.5	279	81	90	810	776	1.3	0.5	0.28

Table 2 Fresh properties for the mixes

Mix designation	Flow table		V-funnel		L-box
	Diameter (mm)	T50 (seconds)	Tf (seconds)	T5 min (seconds)	
SCC	660	2.4	10	12	0.96
HFHSSCC-2.5	650	3.1	11	13	0.91
HFHSSCC-5	640	3.9	12	14	0.89
HFHSSCC-7.5	630	4.9	13	15	0.87
HFHSSCC-10	620	5.2	13	16	0.85
HFHSSCC-12.5	600	5.8	14	18	0.84
HFHSSCC-15	590	6.2	14	20	0.82
HFHSSCC-17.5	580	7.1	16	22	0.79
HFHSSCC-20	570	8.2	17	23	0.77
HFHSSCC-22.5	550	9.4	18	25	0.73

3.2.1 Slump Cone Test

The results of slump cone test are represented as follows in Fig. 1.

3.2.2 V-Funnel Test

The results of V-Funnel test are represented as follows in Fig. 2.
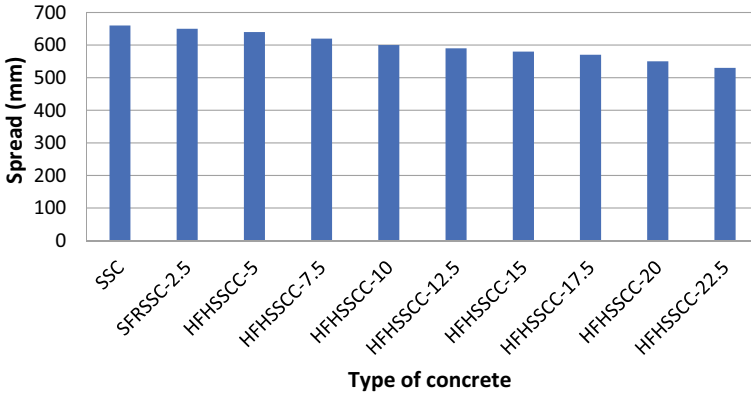
Fig. 1 Graphical representation of slump flow
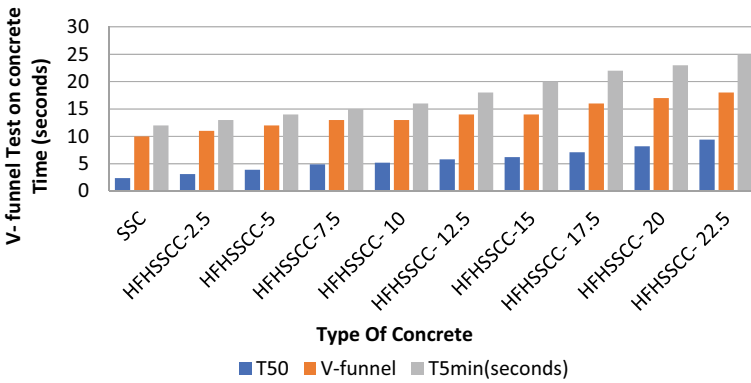
Fig. 2 Graphical representation of V-funnel test

3.2.3 L-Box Test

The results of L-Box test are represented as follows in Fig. 3.

3.3 Hardened Properties

The tests such as compressive strength, split tensile strength, flexural tensile strength of concrete are conducted on all the mixes, the results are tabulated as shown in Table 3.
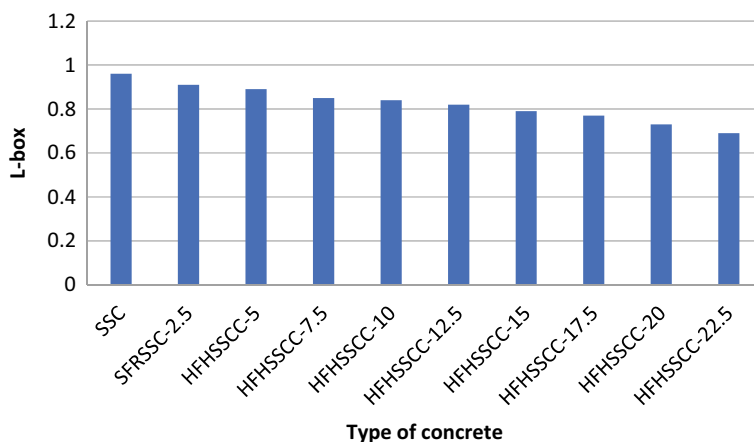
Fig. 3 Graphical representation L-box test

Table 3 Hardened properties for the mixes

Mix designation	Compression strength values (N/mm^2)		Split tensile strength values (N/mm^2)		Flexural strength values (N/mm^2)	
	7 days	28 days	7 days	28 days	7 days	28 days
SCC	48	54	5.28	6.21	6.72	7.99
HFHSSCC-2.5	54.25	59.62	6.13	7.03	8.08	9.36
HFHSSCC-5	58.82	63.79	6.82	7.78	9.11	10.33
HFHSSCC-7.5	61.34	66.93	7.36	8.36	9.81	11.11
HFHSSCC-10	64.12	69.40	7.88	8.88	10.57	11.93
HFHSSCC-12.5	68.13	71.46	8.58	9.43	11.65	12.86
HFHSSCC-15	69.24	73.54	9	10.07	12.39	13.75
HFHSSCC-17.5	71.82	74.65	9.69	10.67	13.35	14.48
HFHSSCC-20	73.56	76.82	10.29	11.52	14.12	15.36
HFHSSCC-22.5	72.12	73.86	9.95	10.34	13.7	14.1

3.3.1 Compressive Strength

The results of compressive strengths of concrete are represented as follows in Figs. 4 and 5.

3.3.2 Split Tensile Strength

The results of split tensile strengths of concrete are represented as follows in Figs. 6 and 7.
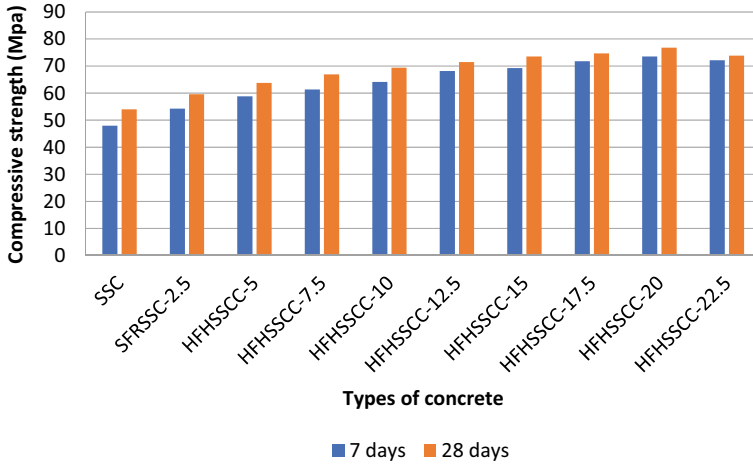
Fig. 4 Graphical representation of compressive strength
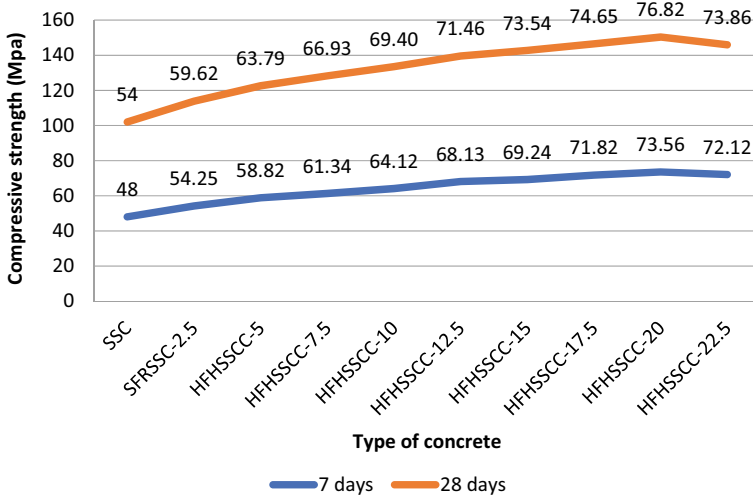
Fig. 5 Plot of compressive strength

3.3.3 Flexural Strength

The results of flexural tensile strengths of concrete are represented as follows in Figs. 8 and 9.
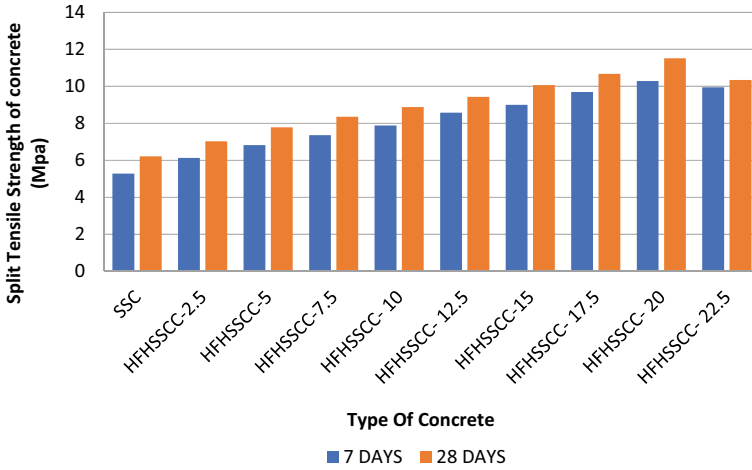
Fig. 6 Graphical representation of split tensile strength
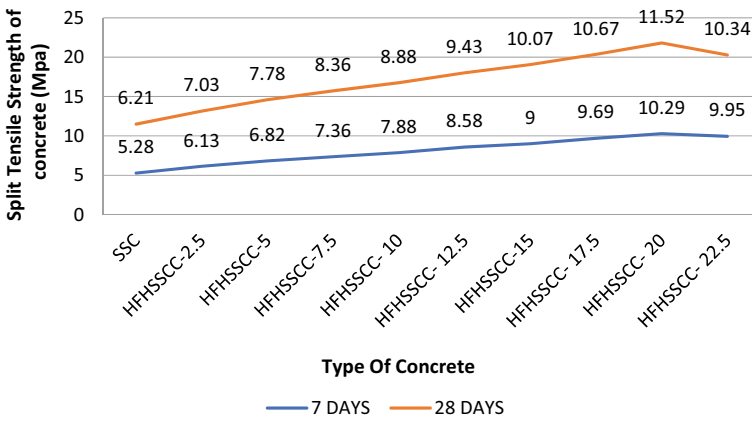
Fig. 7 Plot of split tensile strength

4 Results and Discussions

4.1 Slump Cone Test

As per IS10262-2019, to know the workability of RM concrete slump cone test was performed. The workability decreases with increase in RM replacement and this is indicated in Fig. 1. The reason behind the decrease in workability was because of the water been absorbed by the RM particles.
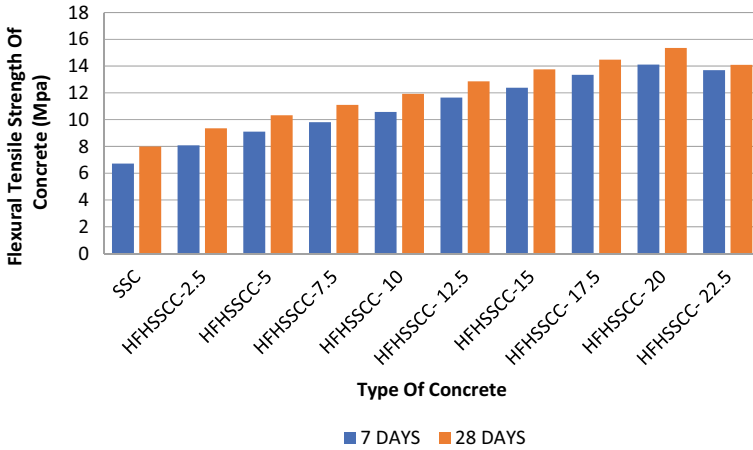
Fig. 8 Graphical representation of flexural strength
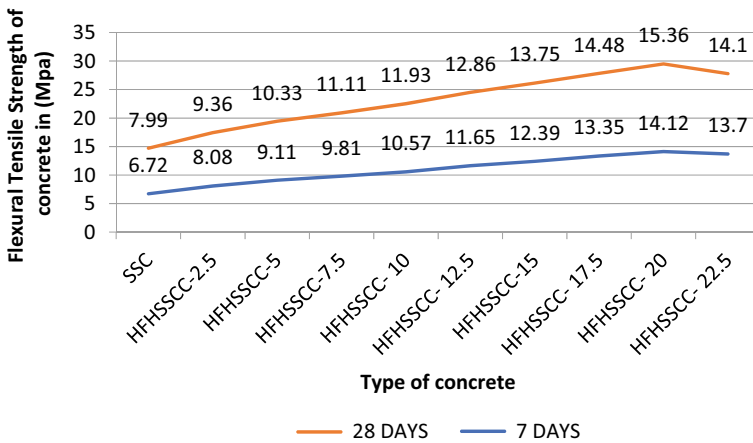
Fig. 9 Plot of flexural strength

4.2 V-Funnel Test

As per IS10262-2019, to know the ease in concrete flow of RM concrete V-Funnel test was performed. The ease of concrete flow decreases with increase in RM replacement and this is indicated in Fig. 2. The reason behind the decrease of ease in concrete flow was because the same reason as mentioned for slump cone test.

4.3   L-Box Test

As per IS10262-2019, to know the blocking ratio of RM concrete L-Box test was performed. The blocking ratio decreases with increase in RM replacement and this is indicated in Fig. 3. The reason behind the decrease in blocking ratio was because the finer RM particles filled the pores inside.

4.4   Compressive Strength

Compressive testing machine was used to test all the concrete samples to find the compressive strength and this is indicated in Figs. 4 and 5. The replacement of cement with RM in concrete is from 0 to 22.5% with an increment of 2.5% per sample, and these concrete samples are tested after 7 days and 28 days. The maximum compressive strength value is observed at 20% and after that compressive strength value got decreased but not less than the normal SCC value.

4.5   Split Tensile Strength

Split tensile test was performed on all the concrete samples to find their tensile strength and this is indicated in Figs. 6 and 7. The replacement of cement with RM in concrete is from 0 to 22.5% with an increment of 2.5% per sample, and these concrete samples are tested after 7 days and 28 days. The maximum tensile strength value is at 20% and after that tensile strength value gets decreased but not less than the normal SCC value. The increment in the tensile strength is due to the finer particle size of RM and Quartz powder which reduces the minor cracks and increases the tensile strength.

4.6   Flexural Strength

Flexural strength test was performed on all the red-mud concrete samples to find their flexural strength and this is indicated in Figs. 8 and 9. The replacement of cement with RM in concrete is from 0 to 22.5% with an increment of 2.5% per sample, and these concrete samples are tested after 7 days and 28 days. The maximum flexural strength value is at 20% and after that flexural strength value gets decreased but not less than the normal SCC value.

5 Conclusions

On the current study on RM the following results were observed:

- The results of fresh properties were less than the normal SCC which refers that use of RM reduces the workability of the concrete.
- There was a gradual increase in the hardened properties till 20% addition of RM; from there it was a decrease in the values.
- Split tensile strength values at the age of 7 days and 28 days were varying from 11–15% for the respective compressive strength values.
- Flexural strength values at the age of 7 days and 28 days were varying from 14–20% for the respective compressive strength values.

References

1. Persson B (2001) A comparison between mechanical properties of Self-compacting concrete and the corresponding properties of normal concrete. Cem Concr Res 31:193–198
2. Su N, Hsu K-C, Chai H-W (2001) A simple mix design method for self-compacting concrete. Cem Concr Res 31:1799–1807
3. Bouzoubaa N, Lachemi M (2001) Self-compacting concrete incorporating high volumes of class F fly ash preliminary results. Cem Concr Res 31:413–420
4. Sri Ravindrarajah R, Siladyi D, Adamopoulos B Development of high-strength self compacting concrete with reduced segregation potential, vol 1, 1048 pp. ISBN 2-912143-42-X, soft covers
5. Okamura H, Ouchi M (2003) Self-compacting concrete. J Adv Concr Technol 1:5–15
6. Aggarwal P, Aggarwal, Gupta SM (2008) Self-compacting concrete—procedure for mix design. Leonardo Electron J Pract Technol 12:15–24
7. Girish S, Ranganath RV, Vengala J (2010) Influence of powder and paste on flow properties of SCC Constr Build Mater 24:2481–2488
8. Todorova E, Chernev G, Chernev G (2013) Influence of metakaolinite and stone flour on the properties of self-compacting concrete. J Chem Technol Metall 48(2):196–201
9. Druta C (2003) Tensile strength and bonding characteristics of self-compacting concrete. B.S. (Mechanical Eng.), Polytechnic University of Bucharest, 1995 August 2003

Development in Sustainable Infrastructure—Influence of Sustainable Development Goals on the Redevelopment Planning for Industrial Townships in India

Abantika Sengupta and Parthiba Chakraborty

1 Introduction

Since their launch in 2015, UN Sustainable Development Goals (Agenda 2030) have been integral to any industry, innovation, and infrastructure to achieve a better and more sustainable future for all [19]. The key targets for 2030 include about reduction in greenhouse gas emissions, awareness about renewable energy, and improvement in energy efficiency [14]. By the Intergovernmental Panel on Climate Change (IPCC) Special Report of 2019, global warming is likely to reach 1.5 °C between 2030 and 2050 at the current rate of raise, which may lead to a very high risk of severe, widespread and irreversible impacts globally [9]. Human activities are most likely to be blamed for this change in the ecosystem. In order to mitigate the climate-related risks for natural and human environments it is essential to put a check on the misuse of the earth's resources right away and follow the path of SDGs to reach a world with lower carbon footprint. A study on the implementation of the SDG in Indian context shows its highest focus on Industry innovation and infrastructure [8]. The 2030 goals set by UN can broadly be divided into five categories viz., environmental, economic, human rights, education, and health [7]. In this paper we have focused on parameters such as indoor air quality, temperature, humidity, ventilation, lighting, acoustics, ergonomic design, and safety to achieve SDGs 3, 7, 9, 11, 13 and 17. SDG 3 refers to good health and well-being for all at all ages, hence protecting the environment and improving life expectancy. SDG 7 refers to affordable

A. Sengupta
Faculty of Engineering Technology, Department of Civil Engineering, KU Leuven, Technology Campus, Ghent, Belgium
e-mail: abantika.sengupta@kuleuven.be

P. Chakraborty (✉)
Department of Architecture, KIIT School of Architecture and Planning, Bhubaneshwar, Odisha 751024, India
e-mail: parthiba.chakraborty@kiit.ac.in

and clean energy. Energy forms the core of every earth aspect which inherently affects climate change, jobs, increasing incomes or food production. SDG 9 refers to industry, innovation and infrastructure, the development of which is utterly crucial for empowering communities across the world. SDG 11 refers to sustainable cities and communities. Cities of every nation form the groundwork for social, cultural and economic advancement. SDG 13 refers to climate action which is an imminent subject in every country these days. Climate change occurs globally and has a heavy impact on people, communities and national economies. SDG 17 refers to partnerships to achieve the goal. A study maps the interactions between the goals [1, 10].

Studies on the inclusion of the SDG into the planning of township shows the importance of data driven re-development planning [12]. In India, the deterioration of environmental and water quality can be mitigated by implementing the SDGs [16]. The industrial townships holds great potential in implementing the SDGs [2, 13, 20]. Indian planning and energy policies are being revamped to mitigate climate change and achieve, energy reduction goals and SDGs. Indian Green Building Council (IGBC) has set up rating systems for the development of green townships [6]. Building energies and envelopes are being re-aligned according to the Energy Conservation Building Code (ECBC) [5]. Understanding the linkages between multiple targets of redevelopment planning of Industrial townships and the SDGs may help to integrate and develop coherent cross-sectoral policy to explore synergies [3, 8, 11, 17].

2   Materials and Methods

Agenda 2030, the Sustainable Development Goals sets a plethora of agendas which on being implemented envisions for a healthier, sustainable and more inclusive space for all. The redevelopment of the township was planned with the Sustainable Development Goals in mind. With advent of time, the industrial townships need for an expansion in terms of area as well as workforce. Assessment of the existing conditions of the built environment, air quality, infrastructure, transport, water, sanitation and safety of the township is the key parameter for setting the re-development goals.

Even though the industrial townships are self-contained with sufficient infrastructure, i.e. residential, non-residential and institutional buildings, arterial and internal roads for efficient transport, water and sewerage treatment plants, underground drainage systems utilising the natural contours for rainwater dispersion, but the growth of these township in an unplanned manner with unplanned settlements in any available land ignoring the planning principles as well as the safe distance of the township from the steel plant to maintain the resident ambient air quality as well as the existing layout of the sewerage, led to jeopardizing the planned nature of the township. Due to this, these industrial townships faces acute issues of substandard residential units for employees, electrical break downs, transport issues, water logging and sewerage disposal issues. The re-development of the township

aims to revive the planning principles and upgrade it keeping the existing infrastructure and adding on to it. Health, well-being, infrastructure, access to clean energy and transport and safety of the residents along with providing them with state-of-the-art facilities are the primary goals.

Sustainable Development Goal 3—Good Health and Well-being was the key objective while drafting the re-development plan of the township. User-perception survey on the existing attributes of the township plays a vital role in determining the requirements of the future vision of the township. The township needs an upgradation to equip itself in terms of physical and social infrastructure and housing to accommodate the expansion. Rehabilitation of existing residents would be one of the first tasks of the re-development planning. For an efficient planning, thus data collection of the existing conditions is the key step. The entire case study can be compartmentalized into 2 stages:

1. Data Collection
2. Data Analysis
3. Proposal.

2.1 Data Collection

Achieving well-being and good health for the residents of the re-developed township is one of the main objectives of the study. Sustainable Development Goal 3 is closely related to the mental and physical well-being of the people, this includes, air quality, visual and thermal comfort, efficient transport system, clean water supply, safety, cleanliness and maintenance.

To assess the existing condition of the township and identify the intervention areas and levels, the first step is to collect the data of the existing condition of the township. This is in the form of the total station survey, user-perception survey and the socio-economic survey of the existing conditions of these townships.

Total station survey of entire existing township area with all details including built form, movement corridors, vegetation, Air Pollution level and air-borne particles, levels and contours, drainage system, existing infrastructure including electricity lines, lighting, sewerage, telephone etc. **User Perception Survey** as an Assessment study of existing conditions of prevailing township zone of all pockets. Assessing the physical infrastructure is not enough to comprehend the existing issues. A user-perception survey on the attributes such as—housing, travel mode, amenities and facilities, education, medical infrastructure, safe places, preferred location and mode of recreation. A thorough analysis on these attributes identifies the areas of intervention. **Socio – economic survey** of the Township. Demographic and socio-economic survey is done to identify the existing number of working employees and the future projections to design the housing and the township to be able to accommodate the future expansion. The employees were surveyed on basis of rank and age to comprehend the number of housing typology required.

2.2 Data Analysis

The data collected by the total station survey, user perception survey and the socio-economic survey has been analyzed under the following attributes:

1. *Existing Land use characteristics*: The acquisition of the existing land use data is one of the first tasks for re-development planning (Figs. 1 and 2).
2. *Urban Design Scenario*: The urban design of the redevelopment planning needs to based on the imageability of the existing township which includes its landmarks, pathways and nodes and also identifying the blighted areas of the township [4]. Areas have to be identified for total change, partial remodelling and minimal change according to the degree of Blight conditions, they have reached. Besides, the general topography, form, shape, size, pattern, density of structures,

Fig. 1 Land use of existing Burnpur industrial township. *Source* Redevelopment of ISP Burnpur Industrial Township, IIT Kharagpur
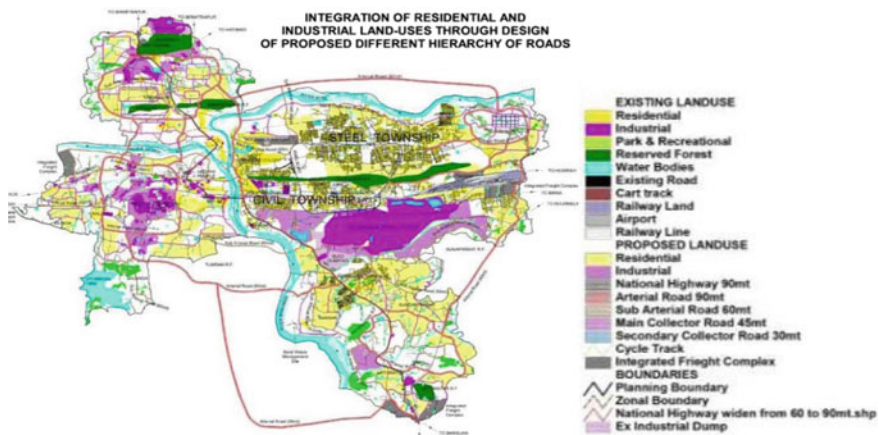
Fig. 2 Proposed land use of Rourkela industrial township. *Source* Rourkela Master Plan 2031 Draft Report, Rourkela Master Plan 2031 Maps [15]

Fig. 3 Identified imageability and blighted areas of the exiting township

texture and grain of built environment, landscape or vegetative characteristics also contribute to construct the overall public imageability of a township (Fig. 3).

3. *Housing*: The present gross residential density is expected to increase due to expansion of industrial activities and new employees for industrial townships. The number of present employee who are allotted the residential units within the industrial township needs to be evaluated. The number of obsoleter residential units needs to be assessed. This gap between the expected housing and the actual housing scenario is mainly due to the dilapidated condition of a major portion of housing stock. The walking distance to basic amenities is often high (Fig. 4).

4. *Transportation*: The number of entry points to the residential area of the existing township needs to evaluated. If found insufficient-there are two possibilities to explore in future—one, augmenting the connectivity and another to the propose Ring Road proposed in the land use development pattern planning.

A study on the existing traffic flow assessement of Burnpur Township indicates peaking behaviour, particularly during morning 8–9 a.m., and afternoon
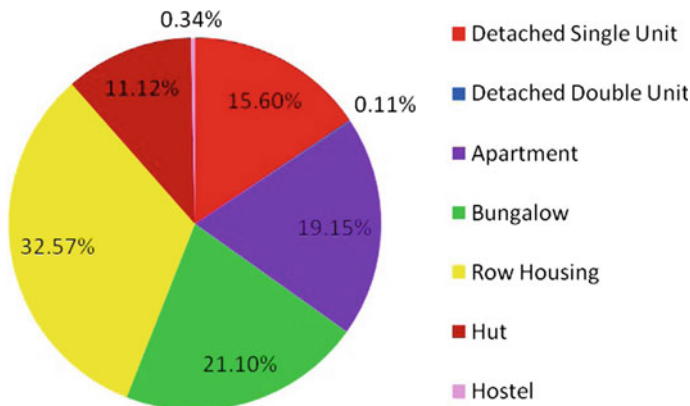
Fig. 4 Existing housing scenario of Burnpur industrial township. Township, IIT Kharagpur *Source* Redevelopment of ISP Burnpur Industrial
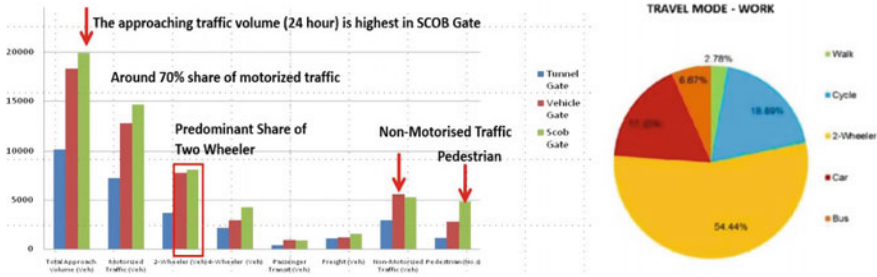
Fig. 5 Existing transport scenario of Burnpur industrial township. Township, IIT Kharagpur. *Source* Redevelopment of ISP Burnpur Industrial

2–3 p.m. The share of motorized traffic is predominantly 2-wheeler based. The share of non-motorised traffic, mostly cycle, is significant. With rising income and changing mode preference a shift can be expected to even larger share of 2-wheeler traffic. There are many pockets of non-residential functions which attract lot of outside traffic within the residential township, generating lot of thorough traffic through internal roads. There is a lack of parking facilities in many locations, especially commercial zones, educational facilities zones etc. On-street parking often creates impedance to the traffic flow during certain hours-leading to loss of mobility (Fig. 5).

5. *Physical Infrastructure*: Assessment on the data collected for existing (a) water supply (b) drainage network (c) sanitation system (d) solid waste management (e) power supply and other infrastructure like telephone, gas, fibreoptics for internet etc. gives a scenario of the existing issues and the infrastructure conditions. Assessment can be made to retain the existing infrastructure and upgradations needed for the future planning.

6. *Social Infrastructure*: Social infrastructures like education, health, socio-cultural, recreational and commercial needs to be evaluated. The number of each kind, population it is catering to and the distance of these facilities from residential and industrial zone needs to be assessed.

7. *Environment*: The existing environmental conditions needs to be assessed on the basis of the—(a) Ambient Air Quality (b) Surface and ground water quality (c) Noise level (d) Soil characteristics and (e) Flora and fauna. Suspended Particulate Matter(SPM), Respirable Particulate Matter (RPM), Sulphur dioxide (SO_2), Nitrogen oxides (NOx) and Carbon monoxide (CO) needs to be evaluated for summer, winter and post monsoon seasons. The noise levels at the residential, healthcare and educational institutions during day time and night time must be in limits of industrial area, prescribed by the Schedule III, Rule 3 of Environmental Protection Rule [18]. Water has to be treated with conventional treatment prior to supply to meet the drinking water quality standard.

2.3   Proposal

To achieve the SDG 3 (good health and wellbeing), 7 (affordable and clean energy), 9 (industry, innovation and infrastructure), 11 (sustainable cities and communities), 13 (climate action) and 17 (partnerships to achieve the goal), redevelopment planning caters to high impact. In industrial townships in India, since the population and the people it is catering to are already in an estimated amount, the proposals can be formulated to achieve the SDGs. These industrial townships can cater to smart planning and can also impact the energy and carbon footprint reduction goals. The focus of re-development planning to cater to the SDGs can be formulated in the following initial ideas, based on the assessment and evaluation done via data collection and analysis of the existing conditions:

- Smart, compact, self-contained walkable sectors with mixed land use
- Natural and technology driven check on surveillance
- High rise structures with low ground coverage
- Green and energy efficient buildings
- Sufficient recreational facilities and open spaces
- A zero—waste status
- Rain Water Harvesting
- Grid Connected Roof Top Solar Power Generation
- Efficient Sanitary Systems
- Smart Metering for electricity and water supply
- Energy, water and waste management
- e-governance
- Smart health care and communications
- Smart transportation (Fig. 6).

Proposal for Master plan, Circulation Plan and Conceptual service plan is based on the well- being and the good health of the residents of the township

- An Integrated Urban Design Structure Plan (IUDSP) for the proposed industrial townships with corresponding strategies for urban renewal and new development parcels. Formulate urban design guidelines (a set of restrictive and prescriptive guidelines on built form and its safe distance from steel plant in terms of air pollution level, streetscape and street furniture and hardware, signage, color palette. and building regulations) for development parcels, open space system and streets. This would also include relevant architectural control guidelines if required for certain area to preserve the quality or characteristics of the same. To offer a futuristic urban setting befitting modern industrial township.
- In the proposed township design special planning strategies will be taken to revitalize the blighted areas with appropriate development inputs including augmentation of existing facilities and infrastructure in most sustainable manner. Functional inputs along with the aesthetic considerations in all the physical design elements will be the major initiative towards the future proposal of the new township. To provide state-of-art facilities and amenities for ensuring world class quality of
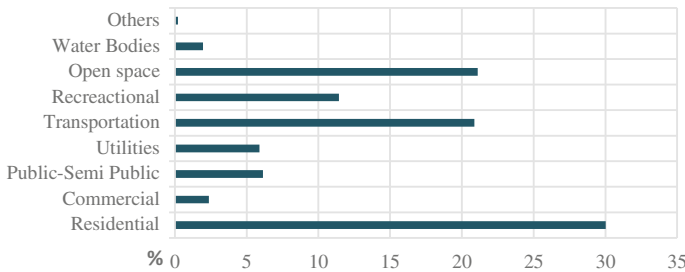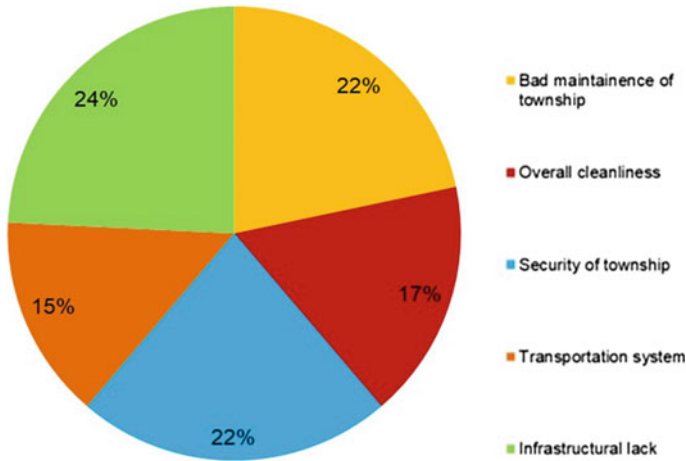
Fig. 6 Identified issues ofthe existing Burnpur Industrial Township. *Source* Redevelopment of ISP Burnpur Industrial Township, IIT Kharagpur

life to the residents. To optimize land utilization by planning future residential zones through compact high rise structures. To plan an effective and efficient circulation network, promoting vehicular routes, walkable streets, bicycle lanes and encourage more use of non-polluting public modes of transport.

- To reduce carbon footprint of township through 3R (Reduce, Re-use and Recycle) and thus promoting Zero Discharge Township.
- Architectural by-laws—a set of development control guidelines and a plan showing the proposed footprints of important structure.
- Landscape plan: Overall landscape master plan, indicating type of plantation, suggestive civil structure, land cover, decorative elements. To maximize green space and reduce ground coverage. To maintain the environmental quality and ecological balance by restoring and preserving the natural environment, topography and natural resources like river, water bodies, natural drainage channels, tree cover. To create open spaces and green buffers as Lung Spaces for the urban habitat.
- Total Integrated service layout showing water supply line, sewerage, telegraph and IT with phasing out of existing services. Water supply, sanitation system, storm water drainage, electrical and tele-communication, integrated solid waste management, housing strategies achieving energy certifications (GRIHA Level 3).
- To encourage social bonding and inculcate a feeling of community and a sense of belongingness towards the township amongst the residents by creating more and more public spaces and buildings of different scale facilitating more interaction.
- To create a centralized database of utilities and services, for IT-linked management of infrastructure and services.

3   Conclusions

The main Challenge during the design a township that is commensurate with state of the art plant and yet retain essence and imageable existing components. The main ordeal during a re-development planning is to assess the existing condition in terms of assets, living conditions and environment compliance and plan to retain the usable infrastructure and align the planning principles with existing energy reduction goals and SDGs for the welfare of all. The industrial townships in India, which are in need for re-development planning holds great potential in implementing the Sustainable development Goals and contribute towards energy and carbon footprint goals. Green township developments are beneficial to the individual and community. Mixed land use and compact planning are the characteristic of a green development, which reduces dependency on automobiles and associated greenhouse emissions. The outdoor air quality is enhanced by providing landscaped areas, encouraging the use of clean fuels for vehicles. Noise levels are reduced by provision of vegetative buffer. Green buildings and energy efficient infrastructure further aid in reducing the greenhouse gas emissions. Public landscaped areas, walkable streets, bicycling lanes, community gardens and public spaces encourage physical activity and help in improving public health.

References

1. Allison EH, William WL, Dey MM, Halpern S, Mccauley DJ, Smith M, Vaitla B, Myers SS (n.d.) Map the interactions between sustainable development goals
2. Betti G, Consolandi C, Eccles RG (2018) The relationship between investor materiality and the sustainable development goals: a methodological framework. https://doi.org/10.3390/su1 0072248
3. Burford G, Hoover E, Velasco I, Janoušková S, Jimenez A, Piggot G, Podger D, Harder MK (2013) Bringing the 'missing pillar' into sustainable development goals: towards intersubjective values-based indicators 3035–3059. https://doi.org/10.3390/su5073035
4. Chapman EH, Lynch K (1962) The image of the city. J Aesthetics Art Criticism 21(1):91. https://doi.org/10.2307/427643
5. ECBC Standard 2017 (2017) Government of India
6. Green Townships—IGBC green townships in India|IGBC (n.d.). Accessed 20 September 2020. https://igbc.in/igbc/redirectHtml.htm?redVal=showGreenTownshipssigninscope-content
7. Griggs D (2015) Sustainable development goals for people and planet 5–7
8. Id SA, Hussain T, Li B (2018) The implementation of sustainable development goals in 'BRICS' countries. https://doi.org/10.3390/su10072513
9. IPCC 2019 (n.d.) IPCC, Special 1.5 Global Warming Report 2019. https://report.ipcc.ch/sr15/pdf/sr15_spm_final.pdf
10. Leal W, Luiz O, Quelhas G, Luiz D, Nascimento DM, Avila LV (2018) A literature-based review on potentials and constraints in the implementation of the sustainable development goals Rodrigo Goyannes Gusm A 198:1276–1288. https://doi.org/10.1016/j.jclepro.2018.07.102

11. Mainali B (n.d.) Evaluating synergies and trade-offs among sustainable development goals (SDGs): explorative analyses of development paths in South Asia and Sub-Saharan Africa. https://doi.org/10.3390/su10030815

12. Marcovecchio I, Thinyane M, Estevez E, Fillottrani P (2015) Capability maturity models towards improved quality of the sustainable development goals indicators data

13. Moldavska A, Welo T (2019) A holistic approach to corporate sustainability assessment: incorporating sustainable development goals into sustainable manufacturing performance evaluation. J Manuf Syst 50(December 2018):53–68. https://doi.org/10.1016/j.jmsy.2018.11.004

14. Priorities, Five (2015) Five priorities for the UN sustainable development goals 7–8

15. Rourkela Master Plan 2031 Draft Report, Rourkela Master Plan 2031 Maps (n.d.). Accessed 30 October 2020. https://affordablehousing.live/rourkela-master-plan-2031-draft.html

16. Roy A, Pramanick K (2019) Analysing progress of sustainable development goal 6 in India: past, present, and future. J Environ Manage 232(November 2018):1049–1065. https://doi.org/10.1016/j.jenvman.2018.11.060

17. Science, Environmental (2018) Integrating disaster risk reduction with sustainable development goals: mechanism analysis and readiness of stakeholders integrating disaster risk reduction with sustainable development goals: mechanism analysis and readiness of stakeholders

18. The Environment Protection Schedule III. (n.d.) Accessed 27 October 2020. http://www.lawsindia.com/IndustrialLaw/k57.htm#sSCHEDULE_III

19. United Nations Sustainable Development—17 Goals to Transform Our World. (n.d.). Accessed 20 September 2020. https://www.un.org/sustainabledevelopment/

20. Yakovleva N, Kotilainen J, Toivakka M (2017) The extractive industries and society Re Fl Ections on the opportunities for mining companies to contribute to the united nations sustainable development goals in Sub-Saharan Africa. Extr Ind Soc 4(3):426–433. https://doi.org/10.1016/j.exis.2017.06.010

Adaptive Reuse, Reduce and Monitoring Systems in Structural Engineering

K. Suresh Babu, B. N. Rao, and Srinivas Reddy

1 Introduction

We are all aware of the fact that in a building, safety comes first and then comes comfort. It is apparent to explain to reassure that a building's prima facia purpose is to house its inhabitants in a safe and secure way from the calamities that exists outside the realm of the building. Current scenario of sustainability and having a green outlook on everything we do, we are in a time–space continuum where we look at things from a sustainability perspective. The reason for this sustainability perspective is multi-fold, interdisciplinary, and existential for everyone on this planet. We see environmental preservation, conservation, and restoration as the various facets of bringing sustainable living in every walks of our lives. How do we see this in a perspective from a structural engineering point of view is the deliberation in this article. How do we see sustainability for the current situation?

Sustainability is explained as—for the living, the progression of life should yield an optimized effort in bringing a situation that the current generation's living needs will not deplete the resources for future generations and sustain the resources on this planet earth—as a phenomenon in every generation. Sustainable concepts include various methods, like Adaptive Reuse, Reduce, which are examined from the existing practices and reviews. With the monitoring systems that are already making a significant contribution in automobile and aerospace also has a significant role in the civil engineering field which has not impacted as much as it should have been, are also studied and a correlation of the three aspects of the study is attempted in this paper.

K. Suresh Babu · B. N. Rao (✉)
Department of Civil Engineering, Indian Institute of Technology Madras, Chennai, India
e-mail: ce17d301@smail.iitm.ac.in

S. Reddy
Department of Mechanical Engineering, Indian Institute of Technology Madras, Chennai, India

2   Adaptive Reuse

Every work or deliberation of humankind uses the energy of some sort of earth resources. This usage of resources is paramount and critical if the attempt to make or build is non-existent previously and which will improvise as a pioneering attempt for the future. It becomes an act of depleting the resources if we tend to use the resources of mother earth and repeat the act of building or making something to make our sustenance of living in this planet earth. How do we stop the attempt to deplete the resource is the question here. Adaptive Reuse- may be the solution for the said concern of depleting the natural resource (Fig. 1).

Any building structural safety is the first criteria to assess the suitability of the building for any use implied on it. Though there are further aspects to assess the suitability of the building for the re-assignable uses, the prima-facia aspect to check for the various suitability of uses, is the structural engineering aspect—that is the stability of the structure in the discussion. One of the examples reviewed is the research paper, Adaptive Reuse-A Case of Lal Baradari, Lucknow, by Pradeep Singh[1], Architect, Urban Node, Lucknow and Mohammad Laraib Ahmad[2], Architect, Studio for Planning Architecture and Design, Lucknow[2], The paper deals with the explanation of the adaptive reuse done strategically at Lal Baradari building in Lucknow and the various methods used to facilitate the reuse of the building.

2.1   Adaptive Reuse—A Case of Lal Baradari, Lucknow [3]

The objective of the paper is to find a reuse strategy of Lal Baradari Building in Lucknow, which is under the control of the State Lalit kala Academy which is part of the state government of Uttar Pradesh in India. This building is known as a summer house building of 12 doors and in the time tested condition, finding adaptive reuse

Fig. 1 Lal Baradari **a** [1], **b** [2]

that also brings the sense of place of the building with its architectural edifice in a strategic way with the help of the case studies was the aim of the paper.

The framework used in the study is to identify the purpose of Adaptive Reuse as a practice in current times. Adaptive Reuse brings the sustainable principle to the limelight for the simple fact that such adaptive reuse, uses the building which has the embodied energy, which is not to be demolished. The life of the building is extended and further utilized. Further, with the resource preserving idea, such re-use is also helping the economy and also the heritage of the place by preserving its past history associated with the building. The research paper is trying to answer the reason for the adaptive reuse and it explains predominantly with the cultural aspect and heritage aspect and to bring the past to present connectivity through experimentation and ideas transgression with respect to the scientific, philosophical, and architectural aspects.

2.1.1 The Principles of Adaptive Reuse

1. Redesign building should perform well as per the functional requirement.
2. Should adapt changes and alterations done and should create a connection to the new users.
3. Respond well to the existing surroundings and enhance its context.
4. Should create a visual statement by providing visual coherence and please users and passers-by Sustainable, least-polluting, energy-efficient, easily accessible, and have a minimum environmental impact.

The above principles of adaptive reuse as mentioned in the paper, do not mention the aspect of structural safety in detail which is the paramount criteria and beyond which if once the structural stability is established, further the other aspects of comfort and functional aspects can come into purview. The advantages as explained in the paper also do not bring this aspect of structural stability. There is this need to reaffirm the structural stability aspect in order to carry forward with the reusability, with the need for the functional aspect present in the context now. However, the paper discusses the deliberations of the quality materials used in the olden days, the comfort that is achieved because of the thickness of the shell of the building from the surrounding harsh climatic condition, and the reinforcing of the sense of place that the building brings with its heritage and its past values. The impact of the adaptive reuse with the surrounding—which is called brown fields—is also expressed in the paper, as lesser chemical and physical contamination to the environment by not demolishing and rebuilding. This is an appreciable attempt to reinstate the adaptive reuse ideas.

2.1.2 Case Studies for Reference

The Re-Use strategy adapted is done technically, strategically, and typologically. To arrive at technical know-how or a intelligent approach or even understanding the

typological aspect of the building references are drawn from case studies done on similar grounds. These case study references are the following buildings—Adaptive reuse and restoration of a Chettinadu mansion, Pudukottai, Tamil Nadu, India, Kasturbhai Lalbhai Museum, Ahmadabad (Rahul Mehrotra Architects) and Church into a Book Store—Location: Maastricht, Netherlands, Europe Architect (book installation): Merkx + Girod. In all these case studies, only in the adaptive reuse of the church into a bookstore, the factor of the structural system is considered an important aspect and deliberated. In the other two Indian buildings, the structural systems are assumed to be stable and with no further analysis, the adaptive reuse is considered with respect to the heritage and cultural values and the need of the present time which are all again a time-bound approach rather than a systematic approach to establish the reuse of a building.

2.1.3   Historical Background

Lal Baradari—The history behind the building was explained further and how it narrowly escaped the canons of the British to house the throne of the ruler in the yesteryears. The location and the plan of the building are further explained in the article. And in the existing usage of the building, the article clearly explains the current situation of usage where the insensitive approach to the structural aspect of the building explained, raises further concerns about its future. The building is a load-bearing structure constructed with Lakhauri bricks and lime mortar. The arches are spanning larger spaces with double storied height, which were all mutilated by improper application of concrete slabs, iron girders to support the superstructure. The usage of modular bricks with cement mortar and creating of false ceiling and partitions that hamper the light passage from an upper glass floor slab—all explains the precarious approach primarily to the structural integrity of the building. The following paragraph explains the application of structural engineering aspects into the building for its current usage clearly.

2.1.4   Structural Aspects

"Structure of the building is load-bearing with arches carving out the opening to various places and helping in reducing the load as well as in the equal transfer of load. The vaulted slab system with iron girders has been used in the ceiling to divide a large span into smaller parts and helps in distributing the load. Due to heavy load added to the structure by laying of concrete on the roof, there might be some structural issues that arise in the future."—[3] The current condition of the walls, Finishes and Plaster, Roofs, Slabs, Flooring, Openings, and Structural Systems are explained in detail. It is an outcome of what existed in the past and what level of intervention happened by the authorities who had tried to input a usage into the building with their alternations and modifications to the fabric of the building by using modern materials that had suffocated the existing old materials from breathing that leads to

dampness and overloading due to self-weight etc., which are all dangerous symptoms to hold the same building as and is for the future.

The structural engineering aspect of the building is explained as follows. An I-Section has been used which runs through each end of the vault acting as a tension member and a load of the vaulted slab is then transferred to the columns which is a compression member. New columns with I-section girders have been added to provide extra support to the structure in the basement. As the structure dates back to 1870 materials such as Lakhauri bricks and lime mortar has been used which is important with respect to this region and establishes the construction techniques at that time in this region." [3]. The reuse approach to the building is explained in three major categories or strategies as part of the guidelines for Lal Baradari. They are, "Typological: Before the reuse of the building, a Literature study is a must about the original and new uses to be incorporated.

Technical: Structural study and analysis with dimensions should be known and noted in the building.

Strategy: The building along with its surroundings should be taken into context thus reusing the building while keeping in mind the 'character, sense, and spirit' of the place."—[3]. The other aspects of guidelines include use and function; Quality of Design; Materials and Technology; Flexibility and reversibility are all discussed. In this, The material and Technology aspect mentioned is an in-between approach between the old and the new existing Technology.

3 Reduce—A Sustainable Strategy

Taking a cue from the previous paper study of Adaptive reuse, it is a natural inquisitiveness to seek methods that are already in use and that may still help and establish the factor of sustainability in every step of its approach. A notion of "reduce" is seen further beyond the adaptive reuse to cross-verify its pattern of approach within the realm of structural engineering is the next step. For this, the following papers are studied and understood as follows. Having tried adaptive reuse, the concept of "reduce" plays an important role in the area of structural design from the perspective of sustainability. However, more focus is given to the material property than the reduction of the material itself in most of the journal papers. No quantification is given to the aspect of how much reduction in the material is achieved by the 'reduce' measures and also achieving the desired effect (Figs. 2, 3 and 4).

3.1 Hollow Core Slabs

A comprehensive study of the various methods to achieve thermal comfort using hollow-core slabs and achieving fewer energy resources for the operational aspect
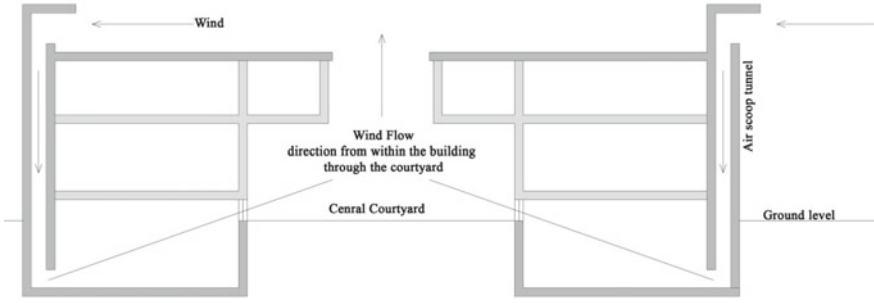
Fig. 2 Natural ventilation flow in buildings—a section of the dwelling with scoop and integral ventilation pathway
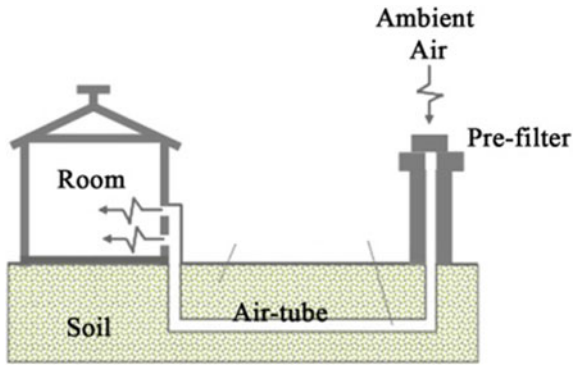
Fig. 3 Schematic diagram of earth cooling/heating system
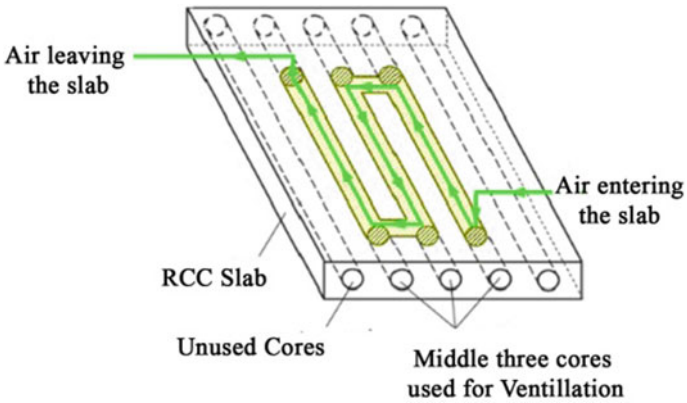
Fig. 4 Hollow core slab illustrated to show the air entering the hollow cores and leaving the hollor cores facilitating heat gain or lose from the slab

of the building and its simulation are explained in this paper—Research and application of active hollow core slabs in building systems for utilizing low energy sources written by Xinhua Xua, Jinghua Yua, Shengwei Wangb, Jinbo Wang, published in the year 2014 [4]. This paper explains the review of the technologies used in Europe to achieve the thermal balance in the building through ways to use the difference in the diurnal temperature difference in the atmosphere and as well as the ground thermal source. These technologies usages are more contextual and climatic conditions within the context play a major role in establishing the relevance of the adopted technological ways and means to achieve efficiency through the methods adopted. There is an experimental study conducted and explained to ascertain the comfort conditions achieved using these hollow-core slabs. Again the common thread being, the structural stability is assumed to be worked out and the next immediate preposition being the comfort conditions for which the testing and simulations are conducted. let us see in detail the methods adopted by the paper to ascertain certain aspects of these hollow-core slabs.

3.1.1 Thermal Comfort

There is a substantial heat transfer between the concrete slab and the air cavity inside the slab under both heat gain or loss conditions, along with other methods used like ground thermal mass transfer through air pipes or recovery process heat. The main focus of the paper is to illustrate the utilization of hollow core slab that would yield a lesser energy utilization and eventually various experiments are conducted to ascertain the lesser carbon footprint and overall cost reduction due to the use of hollow-core slabs, is very well established in this paper. A comparison that explains the various experiments conducted from 1970 till 2013 by various authors and in all these experiments, the heat transfer is discussed that leads to the consumption of lesser energy in the building. However, the hollow core slab consuming lesser material, whose embodied energy usage reduction is not quantified nor the reduction in the carbon footprint because of the use of the hollow core slab is not discussed. This quantification will encourage future usage of hollow-core slabs as a common practice in slab design and construction. The one dimension, two dimensions, three-dimension of finite element modelling, and the steady-state and dynamic state of heat flow are measured and evaluated. However, the embodied energy of the material and the reduced usage of material due to the hollow void volume are not elaborated.

3.2 Adaptive Re-use in Urban Scenario

Another paper reviewed is Encapsulating sustainability principles for the structural design of buildings published in the year 2008, by Timothy J McCarthy, Neaz Sheikh, Anne Gardner [5]. This paper draws the advantage of the adaptive re-use principle in developing a sustainable urban environment. Here the methods in which the buildings

have to be designed structurally so that any adaptive reuse strategy in the future will be carried out in ease without disturbing the core characteristics of the building. There are articles that would explain how hollow-core slabs will be appropriate in bringing out the thermal comfort in a building. However, this article explains how the hollow core slabs can be pertinent in bringing out the 'adaptive reuse' to the buildings by taking measures that will be useful for the future generation's requirement and usage. These precast hollow core slabs use the pre-tensioned or post-tensioned rods to establish the long spans with space, which can be adaptively reused for various functions in the future.

Further, this article talks about the economic benefits and social benefits that arise because of the usage of hollow-core slabs. The 'reduce' in the usage of a material is apparent, however, the advantage of reduction that which is not used is not quantified. The usage of hollow-core slabs focuses on adaptive reuse and the outcome of adaptive reuse is quantified through the effectiveness of features like its layout and optimization factors are given and structural elements used, etc. In this adaptive reuse, if there is any change in core and establishing core-cuts in future need of a staircase implementation, then it becomes difficult in such slabs. This is considered as the disadvantage of precast hollow-core slabs with pretension or post-tension rods and such adaptive reuse may not be a correct approach.

3.3   Net-Zero Energy Buildings

A research paper—Sustainable Design of a Nearly Zero Energy Building Facilitated by a Smart Micro grid, is reviewed to relate to the earlier reviews of a sustainable building approach. The nearly zero-energy buildings are the new age phenomenon for creating a sustainable environment. In these lines, how would be the approach of sustainable structural engineering will play a role is analysed. This paper explains the various aspects of the net-zero building. The importance of the architecture design and the envelope design and the aspects of the passive designs are discussed. In these aspects of envelope design, considering the adaptive reuse and the reduced phenomenon, using the hollow core slabs, one tends to achieve a reduction in the consumption of energy and in the usage of reduced energy demand will be a successful strategy towards sustainability. Though the paper focuses on achieving nearly zero energy consumption building through alternative energy sources, it cannot be undermined or neglected, in the approach to use sustainable practices even in the structural design aspects. More often, this has been an overlooked area that may need further attention, research, and formalization.

4 Structural Health Monitoring (SHM) System

The structural health monitoring system helps in identifying the structural failure in advance and thereby eradication of the adversity is made possible. Here SHM complements the sustainable principles in a way that, when the structures are designed for stability and safety, SHM makes itself a supporting partner that will prove its stability or raise an alarm to showcase the adversity. In either case, we are trying to safeguard the environment or human loss which is irreversible. Further, the life of the building that is either put to adaptive reuse or being designed with the 'reduce' concept will be depending on SHM in the future to alert in case of any unexpected natural calamities that may occur [6]. In this paper, the importance of the SHM as a new normal aspect of structural engineering practice has been established. Further, the rationale of various practices of SHM and the need for establishing standards for future practices of structural design, management, and maintenance are explained.

SHM formalizes the understanding and evaluation of a structure from the point of view of traditional experimental or theoretical structural mechanics, combined with material sciences and electronics and information and communication technologies of the present day. When sustainability is the new norm everywhere, how this SHM plays a role in re-establishing the sustainable principles are also to be considered, and to be dealt with in the emerging times. Further to monitoring the structure 24×7, a newly emerging field of formalization of the adaptive smart structural systems is in the offering. The adaptive smart structural system is the intervention that is to be applied to the structures which are already built and instead of demolishing them and going for newer construction, these buildings can be put to reuse using structural retrofit solutions and SHM plays an important role in this new structural intervention to further monitor the system and raise an alarm if so required. In this way, the building is put to maximum use of its lifetime or even made to have an extended lifetime through proper maintenance done through monitoring.

In developing countries, most of the structures are built post 2nd world war. The progression of society is determined by infrastructural development. Any deterioration due to various climatic factors is going to be a major setback for the human resource and for further revamping the infrastructural facilities. For all these reasons, SHM can be a solution where, the problem to the structure is first identified and the concern raised will give data about the solution addressing system and also the various facts about the material, environment and the design implementation and so forth, are all feed as the data. Most of the structures post-world war II are all steel, reinforced, composite or pre-stressed concrete structural systems. The steel in the RCC is prone to corrosion of reinforcing steel induced by chloride ion ingress into concrete. Other less common causes of deterioration in concrete are carbonation induced corrosion, freeze–thaw attack, alkali-silica reaction, and external and internal chemical attack. Besides corrosion, fatigue is also one of the causes for the degradation of the structure due to constant vibration caused by the moving loads in the components of the infrastructure [6].

4.1 Types of SHM

Figure 5 explains clearly the various parts of SHM. The extended lifetime due to the proper maintenance or avoiding the degradation due to periodically monitored maintenance will result in an extended lifetime of the structure. There are two types of SHM in practice. One is Permanent Monitoring and the second is Periodic Monitoring.

Permanent Monitoring establishes from the initial construction stage and periodical monitoring is done from time to time for a shorter span of time. The positives and negatives of both permanent and periodical monitoring are as explained below. Both the systems capture data about the material degradation, environmental factors, structure response to the static and dynamic loads, the data captured from the initial construction stage needs a separate data accumulation system architecture that involves data transmission, management, and permanent storage. However, with the periodical monitoring, the quantum of data analyses is not as high. Hence the cost involved in establishing a permanent monitoring system is high compared to a periodical monitoring system and evaluation into the system. However, the periodical monitoring system may not capture the incidents that may lead to the effect which is monitored at a given time and assumptions will have to be made of any random incidents prior to monitoring which is a deviation from the ideal condition.

There is definitely an advantage in the permanent monitoring system as it can facilitate online and multistage processing of data and any unexpected structural behaviour can be identified. Such online processing of data can also rise warnings and alarms to avert any calamities in real-time. Table 1 explains the difference between the two as follows. The type of algorithms used in the SHM is Diagnostic and Prognostic methods. The diagnostic method uses the responses from the structural system based on its behaviour to the sensors and how it responds to the signals and so forth. Prognostic methods estimate the further life period left in the structure and use two types of finding them out. They are the finite element method and the heuristic method. The finite Element Modelling method uses the material degradation models where the static and dynamic parameters are optimized in order to reflect the
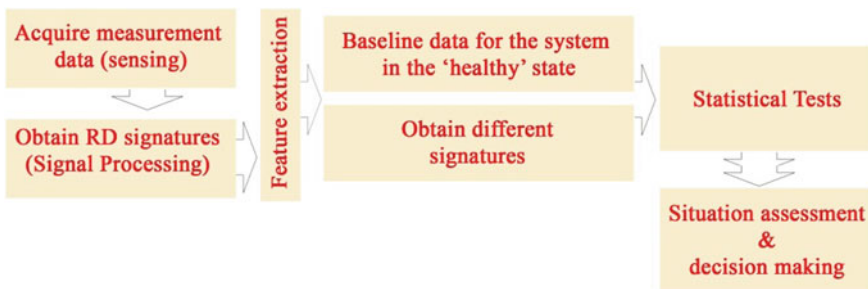
Fig. 5 A typical structural health monitoring system

Table 1 Characteristics of permanent monitoring and periodic monitoring

Evaluation characteristics	Permanent monitoring	Periodic monitoring
Sensor types	>>Extended	>>Restricted
Data management	>>Complex	>>Simple
Accidental events	>>Recorded	>>Not recorded
Damage identification	>>Online	>>Offline
Warning of alarms	>>Real-time	>>Deffered
Fatigue life evaluation	>>Direct	>>Indirect
Installation costs	>>High	>>Low
Operational costs	>>High	>>Low

structural response and the evolution of structural conditions. The Heuristic model uses the updated lifetime functions to predict the lifespan left out in the structure.

"The effectiveness of a diagnostic algorithm can be measured in terms of (a) length of the reference period, (b) minimum detectable damage for a given signal to noise ratios, (c) time of observation after damage needed for detection, (d) capability of locating damage, (e) capability of determining the intensity of damage, (f) capability of identifying multiple damages occurring at different locations, and (g) reliability."—[6] With respect to the guidelines and standards for SHM—though there are few guidelines and standards formalized like recently in Russia in Russia (GOST P 53,778 2010 Building and Structures—Technical inspections and monitoring regulations), the other guidelines are the official international standards are the ISO 14963:2003—Mechanical Vibration and shock—Guidelines for dynamic test and investigations on bridges and viaducts and the ISO 18649:2004—Mechanical vibrations—Evaluation of measurement results from dynamic tests and investigations on bridges. Further practical applications of SHM is not as pronounced as it could have been only because of the lack of standards and guidelines as of now. However, the factor of safety that is calculated for the structural systems can come down predominantly if SHM can be implemented and there is definitely scope in formalizing SHM to a greater extent.

The reason for less use of SHM in the civil engineering field is as follows, as mentioned by Andrea E. DEL GROSSO Professor of Engineering University of Genoa Genoa, Italy. "Extreme diversity of the players involved in the civil engineering sector, including facility owners, designers, and contractors, in terms of economic interests, size, and technical skills. Extreme diversity of the structural typologies and situations involved in the construction industry, Lack of understanding of the potential benefits induced by the use of SHM techniques, Extreme diversity of the players in the SHM market." [6] SHM may open out questions of all the theoretical and environmental assumptions made on the material and structure and also on the durability, maintenance, and life cycle costs involved with the structure. In this, the interesting point which is in line with our discussion is the life cycle costs which

Fig. 6 Optimum design solution based on life-cycle cost minimization with and without monitoring
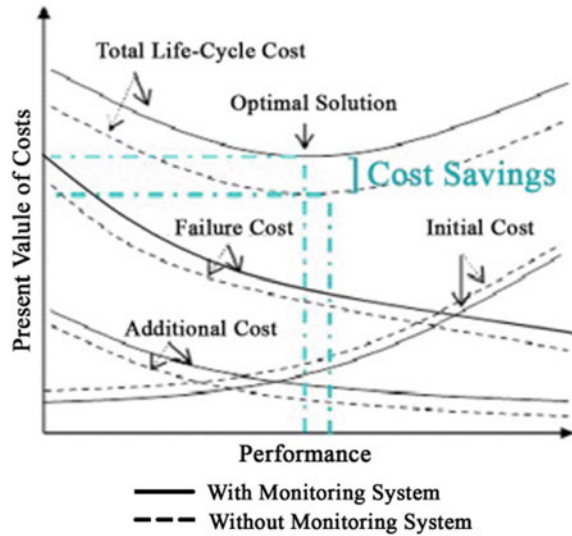
play an important role in reducing the carbon footprint of the building. For this very reason, the reduced concept can also go hand in hand with the SHM in order to bring out a best practice in the area of structural engineering in the future. Figure 6 [6] explains clearly the importance of informed procedures with the help of SHM.

5 Conclusion

It can be understood that the technological aspect used in the refurbishing of Lal Baradari is still not the latest one but a kind of prevalent technology which is already getting obsolete. The emerging technological advancement is not assumed to play an integral part of the reuse of Lal Baradari. However an attempt is taken to establish the need for adaptive reuse of the existing old buildings, understanding its various characteristics and appreciating the structural and material integrity for further use, infused into the building without damaging the architectural characteristics, is a welcome sign for a future formalization and establishment of a clear structural—methodological approach that is very essential for any historical or old building that is in the realm of adaptive reuse for the present and future times. In such a scenario, there is plenty of scope for establishing the monitoring system in the building and that has not been utilized to the maximum so far due to various reasons. In fact the adaptive reuse and reduce—the phenomenon of sustainability will need SHM to reinstate the sustainability conditions. There is another scope of SHM, is that in order to optimize the usage of materials the safety factors applied earlier in the structural designs can be reduced intelligently and can be monitored periodically, for the sustenance of the building. SHM also monitors the environmental changes

which will complement the structural intervention to make informed decisions with respect to building stability and safety.

References

1. http://navrangindia.blogspot.com/2019/01/historic-lal-baradart-once-sanctified.html
2. http://wwwgeorgeherbertsheperdlko.blogspot.com/2015/10/lal-baradari-bhawan-under-repair. html
3. Singh P, Ahmad ML (2019) Adaptive reuse—a case of Lal Baradari, Lucknow. Int Res J Eng Technol (IRJET) 06(03):2395–0056
4. Xua X, Yua J, Wangb S, Wanga J (2014) Research and application of active hollow core slabs in building systems for utilizing low energy sources. Appl Energy 116:424–435
5. McCarthy TJ, Neaz Sheikh M, Gardner A (2008) Paper No: 383 Encapsulating sustainability principles for the structural design of buildings. In: Conference on passive and low energy architecture, Dublin
6. Shiryayev O (2008) Improved structural health monitoring using random decrement signatures. Thesis for: PhD in engineering, University of Alaska

Case Study of Successful Repairs of Retaining Wall at Curtorim Goa Using Sustainable TGSB Technology

Leonardo Souza and Purnanand P. Savoikar

1 Introduction

Goa gets the heaviest average yearly rainfall in India. By August to September the ground is so soaked that the soil is almost at a state of collapse equilibrium. This is the most crucial and critical period in the year for soil stability. Most landslides and retaining wall collapses occur during this period. Many different option are available for soil stabilization and retention but when a collapse occurs in this highly critical state the emergency measures must be both effective and lasting.

TGSBs (Traditional Goan Saraswat Bunds) uses ancient technology that has survived dynamic and static loading and the worst of rainfall, and flooding till today. This multi-use technology was used for land reclamation and hill-stabilization. It is slowly losing the ground to more expensive but more appealing modern techniques which unfortunately are not sustainable and fail easily.

1.1 Methods of Slope Stabilization

A number of methods can been used to stabilize slopes. Each of them is found to be appropriate for a particular set of geological and climatic conditions. They are broadly classified as: soil stabilization, soil retention, excavation and slope modification, drainage and water control, vegetation, etc (Table 1).

L. Souza · P. P. Savoikar (✉)

Department of Civil Engineering, Goa Engineering College, Farmagudi 403 401 Goa,, India

Table 1 Slope stabilization methods

Methods	Types	
Soil stabilization	Chemical	Lime, cement, bitumen, ash, proprietary chemicals, nano-fines or blends
	Mechanical	Rollers, rammers, vibration, blasting
Soil retention	Reinforcement Natural or geo-synthetic	Soil netting, skeleton sheeting, inexpensive soil bracing system, facing walls, retaining walls, secant pile walls, sheet pile walls, tiebacks, soil nailing, ground anchors, reticulated piling, jet grouting and prefabricated geo-elements
Excavation and/or slope modification	Additive	Toe bund, rock toe
	Subtractive	Slope angle, berms, loose soil removal
Drainage and/or water control	Water diversion	Contour drainage, slope drainage
	Water removal	Dewatering, pumping, sumps
Vegetation	Slope top	Coconut trees, Vetiver grass
	Slope surface	Grasses, herbs
	Slope bottom	Tall tap root trees

1.2 Measures of Soil Stabilization

There are many ways to stabilize the soil. They may be divided into chemical, mechanical and reinforcement methods. These may be used individually or in combination with each other. Chemical methods are lime, cement, bitumen, ash, proprietary chemicals, nano-fines or blends of these. Chemical processes can be used to alter soil properties such as strength, compressibility, hydraulic conductivity, swelling potential and volume change properties. The additives are combined with the help of machines or hand mixed.

Mechanical methods are compaction or vibration. Mechanical Stabilization uses the mechanism of improving the properties of the soil by changing its gradation. This process includes soil compaction and densification by application of mechanical energy using various sorts of rollers, rammers, vibration techniques and sometime blasting. Reinforcement methods are either natural or synthetic. Soil reinforcement is performed by placing tensile elements in the soil to enhance its natural stability and strength. TGSBs uses a combination of lime-coconut leaf ash combined with light tamping and natural soil reinforcement to stabilize soils.

1.3   Measures of Soil Retention

There are many methodologies used to retain the soil. Earth retention techniques include: skeleton sheeting, inexpensive soil bracing system, soil netting, facing walls, retaining walls, secant pile walls, sheet pile walls, tiebacks, soil nailing, ground anchors, reticulated piling, jet grouting, and prefabricated geo-elements. They may be used singly or in combination with each other. TGSB uses a facing of coursed rubble facing wall to retain soils.

1.4   Measures of Soil Vegetation

There are many methodologies used to strengthen the soil by vegetation. Earth retention Techniques include: slope top vegetation, slope surface vegetation, slope bottom vegetation. The type of vegetation used is subject to much debate but certain types are suited for certain functions depending on root morphology, height, leaf mass and branching patterns. TGSB uses coconut trees on the top of the slope to stabilize the slope.

2   Location and Case History

For purpose of actual verification of the earth modification and strengthening techniques used by ancients Saraswats in TGSB, a damaged retaining wall for a two storey house of Dr. Vijay Borges which lies on a steep hilly area at Curtorim in Salcette taluka of South Goa was chosen. The downhill side had a steep vertical cut 3 to 4 m in height 2 m away from the house. The soak pit of the septic tank was located in this area. The hill-cut which faced the neighbour was supported by a single-layer 25 cm thick Lateritic masonry wall joined by cement mortar with a few weep-holes. Figure 1 shows the Google map location of the site and the collapsed retaining wall.

3   Site Investigation

In order to ascertain the proper course of action to be taken a site inspection was undertaken. Photographs of the collapsed wall and soil samples were taken. A rough sketch (Fig. 2) was drawn for further reference. Whatever measurements that could be taken were taken. The double storey house was found to be 1.5 m away from the boundary. There was a gutter/drain on the side of the house for surface water. The neighbour's house was 2.5 m away on the lower side. The wall had collapsed on the neighbour's soak pit. The soil was wet and tension cracks were developing owing to

Fig. 1 **a** Google satellite image showing the location of the house of Dr. Vijay Borges uphill of the Curtorim Church Cemetery **b** collapsed masonry portion **c** proximity of completed wall to the Borges house and neighbours house
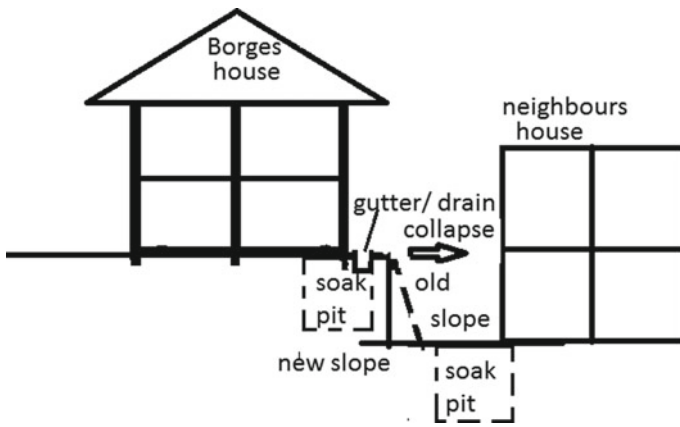
Fig. 2 Rough sketch the proximity of the houses and the problem of the soak pits

surcharge pressure from the foundation of the house on the top. The side-wall had fully collapsed damaging completely the temporary wood store of the neighbour.

4 Problem

The original hill side consisted of many terraced berms. When the neighbour purchased the adjoining property he cut off the berm to make place for his house construction. The new facing wall was constructed of lateritic coursed masonry 30 cm thick with a 50 cm deep foundation (Fig. 3). The total height of the slope was changed from 1.5 to 3 m. and the wall which was originally made from sloping random rubble masonry was now changed to smooth vertical coursed dressed masonry without proper drainage arrangement for the backfill of the wall. The dry masonry that allowed for easy drainage was now replaced by cement mortar filled joints that
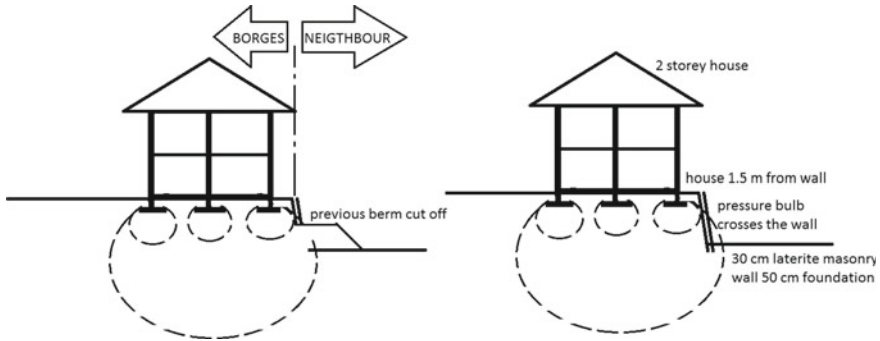
Fig. 3 The pressure bulb of the structure on the retaining wall

blocked drainage. There were soak pits both sides of the wall. The pressure bulb which was once within the soil now was outside the soil. This combined with the slope modification and excessive presence of putrescible organic matter led to a very dangerous geotechnical situation. The smooth laterite masonry wall used to repeatedly collapse in the past, in parts, and was subsequently repaired in parts and patches.

This time the wall of the boundary adjacent to the house fully collapsed during the rainy season damaging the back garden and wood storage hut of the neighbour and not missing but luckily not damaging the neighbour's house. The temporary structure had absorbed the shock of the collapse sparing the main structure behind. As there was incessant rains the mud was getting washed off and the foundations of the Borges house were getting exposed. Plastic sheets were placed to avoid soil loss but there was urgent need to repair the wall to avoid damage even collapse of the Borges house and consequent damage to the neighbour's house.

5 Previous Repairs

The collapsed wall was constructed of single layer coursed lateritic masonry in cement mortar. This was damaged every rain and annually it was repaired by temporary patchwork of masonry or mortar. This hotchpotch repairs had led to the ultimate collapse of the entire wall within five years of its construction. Rebuilding a laterite masonry wall was the first option explored by the house owner. But this was just a fascia and did not play any part in containing the soil. The apprehension expressed by the owner and several other engineers he consulted led to rejection of the idea.

Fig. 4 Different options explored by the owner

6 Different Options Explored by the House Owner

The next option was a standard plum-concrete gravity retaining wall. The exorbitant cost combined with the fact that it was neither feasible nor advisable to build such a wall at the height of the monsoon season led to the scuttling of that idea too. The next option was a standard plumb-concrete gravity retaining wall. The contractor was in favour of this as it involved a hefty commission not to mention convenience of construction. The exorbitant cost combined with the fact that it was neither feasible nor advisable to build such a wall at the height of the monsoon season led to the scuttling of that idea too. Figure 4 shows the different options explored by the owner for repairs of the retaining wall.

The idea of soil nailing was explored but access to the site was difficult. The most common concept put forward by his ex-colleagues and Geotechnical experts of Goa Engineering College was a Gabion Retaining wall. The space constraints caused by the width of a Gabion, and the close proximity of the house to the boundary meant that the house was in danger of damage due to loss of support to the foundation if further excavation was carried out to accommodate the Gabion. This led to the elimination of this idea too.

The option of a thinner cantilever retaining wall was similarly abandoned due to practical on-site difficulties and the temporal expediency of the matter. Finally, after much convincing (despite the reluctance of the contractor) and mainly due to the economics (time, materials, money and labour) involved the owner decided to adopt the TGSB approach.

7 Geotechnical Investigations and Evaluations

Soil samples were taken and tested in the laboratory to find out the density and shear values needed for analysis [SP36-1, SP36-2]. The soil was silty sand with fine to coarse ratio of 35:65. The bulk density was 18.5 kN/m^3 and the saturated density was 21 kN/m^3. The geotechnical properties of soil are presented in Table 2.

Table 2 Geotechnical properties of soil at Borges house in Curtorim

Soil properties	γ kN/m^3	γ_{sat} kN/m^3	c kN/m^2	$\phi(°)$	Fines (%)	Coarse (%)
Bottom soil	18.5	21	12	32	35	65

From the earth pressure bulb we can see that there is a surcharge pressure of P at the top of the soil and an additional horizontal pressure of 0.1P at the bottom of the wall and 0.05P at the centre of the wall (Fig. 4).

Lateral earth pressure can be found by adding components for horizontal pressure, pressure bulb and surcharge (Eqs. 1 and 2).

$$P = \frac{1}{2}K_o\gamma H^2 + \frac{1}{2}(0.1)pH + pH \tag{1}$$

$$K_o = 1 - \sin\phi \tag{2}$$

As the wall is too thin (30 cms) to resist by gravity the resistive action is the shear strength of the wall (Eq. 3). Shear area of the wall is (0.3H).

$$\tau = c_{wall} + \sigma \cdot \tan\phi_{wall} \tag{3}$$

$$P_{wall} = 0.3H\tau \tag{4}$$

As obviously seen from above, the factor of safety dramatically decreases due to the presence of the house on the top. Table 3 shows the quantities required for estimation of factor of safety. Soil pressure from the house is assumed at 55 kN/m^2. The factor of safety is given by Eq. 5:

$$FoS = \frac{P_{wall}}{P} \tag{5}$$

Table 3 Earth pressure parameters required for factor of safety

Symbol	Unit	Condition	
		Dry	Wet
$K_o = 1 - \sin\phi$		0.470	0.470
H	m	3.000	3.000
γ	kN/m^3	18.500	21.000
$\sigma = \gamma_{wall}. H/2$	kN/m^2	36.000	36.000
τ	kN/m^2	130.207	130.207
p	kN/m^2	55.500	63.000
P_{wall}	kN	117.0	117.0
P	kN	213.953	242.865

The factor of safety obtained for the lateritic wall is 0.546 in dry conditions and 0.482 in wet conditions. Hence, it is observed that the conventional solution used was a recipe for failure. Thus, the wall failed every monsoon.

By using a TGSB approach, the soil action was changed from the retaining failure to slope failure.

By Culmann's method (Fig. 5) of wedge [], the parameters needed for calculation of factor of safety are given by Eqs. 6–10. Table 4 shows the parameters needed for calculation of factor of safety:

$$\theta_{crit} = \frac{1}{2}(90 + \phi) \tag{6}$$

$$FoS = \frac{C + N\tan\phi}{T} \tag{7}$$

$$W_{house} = 6p \tag{8}$$
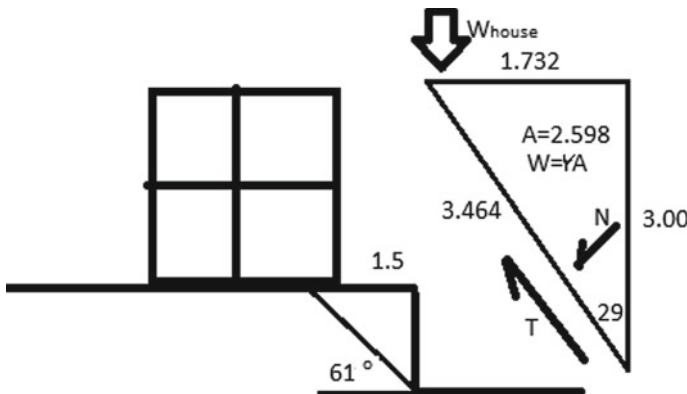
Fig. 5 Wedge for Culmann's method

Parameter	Unit	Condition	
		Dry	Wet
θ_{crit}	°	61.000	61.000
W_{house}	kN	330.000	330.000
W	kN	48.063	54.558
N	kN	320.547	326.105
T	kN	200.335	203.777
c + N. tanϕ	kN	212.277	203.750

Table 4 Wedge parameters required for factor of safety

$$N = (W + W_{house}) \cdot \cos \phi \qquad (9)$$

$$T = (W + W_{house}) \cdot \sin \phi \qquad (10)$$

The factor of safety obtained from the parameters given in Table 4 for the lateritic wall is 1.059 in dry conditions and 0.999 in wet conditions which is almost 1 therefore on threshold of critical. The factor of safety increases when the coconut tree roots are considered due to their additional cohesive component to soil, thus, demonstrating the utility of TGSB. We see from above calculations that the factor of safety has almost doubled.

8 Final Solution and Strategy Adopted

Based on the above calculations the final solution from economy and safety was the TGSB technology. The wall had to be built at the same time as the debris was cleared. There was not much space available to neither shift demolished materials nor store new materials. The foundation of the house was being stressed due to exposure so the full wall could not be cleared in one stage. First the foundation needed to be dug 50 cm below Ground level while clearing the old wall and its foundation. It was decided to excavate the full foundation of the wall in phases (1.5 m stretch at a time).

A trench of width 50 cm and depth 50 cm was dug. A 20 cm bed of Plain Cement Concrete was laid. A coursed dry lateritic rubble masonry 50 cm wide (double stone) was used for first 1 m, and then 30 cm wide masonry (single stone) was used for the remaining height as shown in Fig. 6a, b. Some of the previous stones with mortar removed were also used in between (mainly at the back) to reduce cost and environmental impact.

As each course was laid, the mud was back filled. A layer of about 10% coconut leaf ash and 4% lime was raked in. It was not possible to mix as ideally needed since the mud was wet in the rains and difficult to handle. Then a layer of rice paddy straw
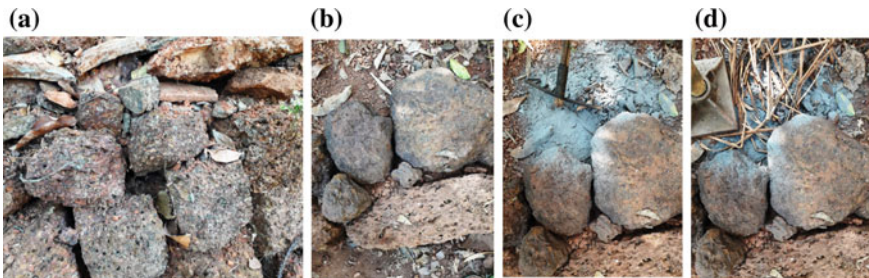
Fig. 6 **a** Coursed dry lateritic rubble masonry **b** two layer of rubble per course **c** stabilized backfill **d** reinforce and compact with rammer

was placed and the soil was rammed by 25 blows of 10 kg hand held rammer as shown in Fig. 6c, d.

As this was being done the adjacent 1.5 m strip was excavated and the process repeated (Table 5). Meanwhile the second course or rubble was laid on the first strip and the steps were repeated. In this manner the wall was raised and compacted in stages. A backward slope of 50 cm in 3 m height was maintained in the wall (Fig. 7).

Though the looks of the wall are not exceptionally aesthetical it is fully functional. Additionally there are some coconut trees along the wall whose roots will grow into the repaired area and anchor to the facing stones will further enhance the strength of the wall. Even though the monsoon season of 2019 was exceptionally long and delayed with heavy rains falling up to November, the wall showed little damage when inspected. This year too, the monsoon has exceeded the rains of last year. The wall is still performing its geotechnical-functions. This is a testimony to the sustainability and utility of TGSB technology.

Table 5 Steps in laying TGSB

Steps	Process
1	Lay two layer of rubble and fill gap with smaller stones to pack them
2	Back fill with lateritic soil
3	Add approximately 10% ash and 4% lime by volume
4	Use the hand rake and mix the stabilizers in the mud
5	Lay a thin layer of rice straw
6	Ram uniformly with 25 blows of 10 kg hand-rammer

Fig. 7 Two views of the completed wall built using TGSB technology

9   Conclusions

People are reluctant to use traditional methods and prefer to use modern methods for geotechnical purposes. The ancient methods are economic, have a smaller carbon footprint and are sustainable. The current case study has shown that TGSB technology can be successfully used to repair a damaged retaining wall and stabilize the slope. When we change from a thin facia wall of lateritic masonry to TGSB technology the mechanism of failure changes from retaining failure to slope failure and the factor of safety dramatically increases from 0.546 to 1.059 in dry conditions and from 0.482 to 1 in wet conditions.

References

1. SP:36-1 (1987) Compendium of Indian standards on soil engineering Part-1 laboratory testing of soils for civil engineering purposes. Bureau of Indian Standards New Delhi
2. SP:36-2 (1988) Compendium of Indian standards on soil engineering: Part-2 field testing of soils for civil engineering purposes. Bureau of Indian Standards New Delhi

Evaluation of the Effectiveness of Euler's Buckling Load for the Analysis of Concrete Filled Steel Tube Slender Columns

K. S. Dhananjaya, Chetan S. Kumar, and Nandeesh M. Sreenivasappa

1 Introduction

Columns are the most important part of any structure like buildings, bridge decks, flyovers etc., which transfer the loads to foundations and further transmitted to subsoil. Conventionally the loads or forces in a column transferred axially so that Columns undergo compressive stress, but in most of the cases Columns are subjected to eccentric loading transverse forces and bending moment depending upon its supporting conditions or constraints at the ends of it.

Loads on columns will usually act at the ends of the member, producing axial compressive stresses within the column which is resisted by the confinement effect produced by longitudinal and transverse reinforcement. But these confinements are just for interior concrete not for the outside cover concrete, hence when load is applied, cracks will appear in outer concrete which can propagate to interior concrete and leads to failure of column. To over-come this drawback, confinement of concrete was introduced. Providing confinement enhances the support for the whole concrete core material thereby utilising the complete strength of concrete under axial compression, since the entire concrete is encased the situation of concrete cracking does not arise and hence material does not fail easily. Therefore, to provide complete confinement to concrete, we can use mild steel tubes with concrete. These composite materials are called as concrete filled Steel tubes which will have more advantages over RCC columns. Due to the presence of Steel Tube the confinement pressure exerted on the smaller section of concrete, will enhance the load carrying capacity and also reduce creep and shrinkage compared to RCC columns.

By providing the Steel tubes around concrete the stiffness of a column is increased compared to the RCC column. Due to the enhanced load carrying capacity as a result of confining effect, the cross-sectional area of a CFST column is smaller

K. S. Dhananjaya · C. S. Kumar · N. M. Sreenivasappa (✉)
M S Ramaiah Institute of Technology, Bengaluru, India
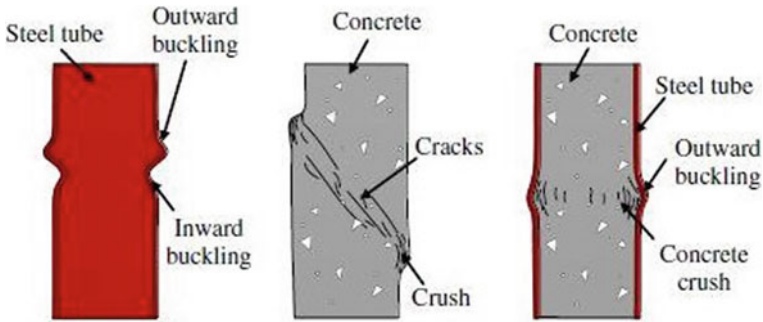
Fig. 1 [1] Schematic failure modes of hollow steel tube, concrete and CFST stub columns

than conventional RCC columns for the same load carrying capacity. Due to which reduction in area the columns might become slender.

Due to the enhanced behaviour of CFST columns compared to the RCC column, it is used in earthquake zones, where structures are subjected to heavy cyclical loading, load from traffic, load due to storage tank, decks of multi storey building.

These CFST structures are more popular in seismic prone countries like Japan, China, Nepal etc. because of its enhanced load carrying capacity, seismic processing properties, ductility and energy dissipation. CFST are mostly utilised in tall buildings, viaduct and in bridges like Brazil Japan and also in other countries.

The failure modes of CFST column is generally ductile in nature due to encasing steel possessing higher strength and ductility properties when compared to traditional RCC columns. The failure modes observed in CFST columns are as shown below (Fig. 1).

Acknowledging the advantages of CFST, We have conducted analytical study on long columns under axial compression using ANSYS with varying L/d, D/T ratios and different grades of concrete.

2   Finite Element Method

Finite Element Analysis is a method to simulate loading conditions on a design and determine the design's response to those conditions. The design is modelled using discrete building blocks called elements. Each element will have exact equations, which will describe how it responds to a certain load. The "sum" of the response of all elements in the model gives the total response of the design. The elements have a finite number of unknowns; hence it is called finite elements.

2.1 Advantages of Using Finite Element Method

- FEA are used to reduce the amount of prototype testing—computer simulation allows multiple "what-if" scenarios to be tested quickly and effectively.
- To simulate designs which cannot be sui.
- for prototype testing.
- It helps in reduced testing and redesign costs thereby shortening of product development cycle.
- To Identify issues in designs before product is produced.
- Optimize performance before prototyping.

2.2 ANSYS

In this paper we have made use of Finite Element Software ANSYS 2019 R3 to perform the analytical investigation

ANSYS is a commercial FEM package having the capabilities ranging from a simple, linear, static analysis to a complex, nonlinear, transient dynamic analysis. It is available in modules. Each module is applicable to specific problem.

3 Specimen Modelling

A total of 98 specimens were modelled and analysed using the ANSYS software. The locally available diameters of specimens (8 different diameters were chosen from 101.6 to 193.7 mm) for 4 different specimen lengths (2500, 3000, 3500, 4000 mm) and for 3 different Grades of concrete (M30. M40, M50) were modelled. All these specimens were modelled, analysed to find out the Buckling load values. The Euler buckling load were obtained using the formula [1] The ANSYS buckling load values were compared to that of Euler buckling load and checked its suitability and the trends were observed.

3.1 Assumptions Made

Following are the material specifications which were assumed to model all the 98 specimens (Table 1).

Table 1 Material
specifications for modelling
ANSYS specimens

Grade of structural steel	250 MPa
Young's modulus of steel	200 GPa
Poisons ratio of steel	0.3
Density of steel	7800 kg/m^3
Grade of concrete	M30, M40, M50
Young's modulus of concrete	25,000 MPa
Poisons ratio of concrete	0.16
Density of concrete	2400 kg/m^3
Boundary conditions	@ bottom end fixed @top end hinged support (Leff = 0.7 L)

4 Euler Buckling Load

The Euler Buckling load was calculated by using the following Formula 1

Formula 1 : **Euler Buckling Load formula**

$$P_{cr} = \frac{\pi^2 E I_{eff}}{L_{eff}^2}$$

$$EI_{eff} = E_s I_s + C_1 E_c I_c$$

$$C_1 = 0.6 + 2\frac{A_s}{A_s + A_c} < 0.9$$

P$_{cr}$ Euler Critical Buckling load
 E   Modulus of Elasticity
I   Moment of Inertia
L   Effective Length of the specimen
Es   Modulus of Elasticity of Steel
Ec   Modulus of Elasticity of Concrete
Is   Moment of inertia of Steel section
Ic   Moment of inertia of Concrete section
As   Area of cross-section of Steel
Ac   Area of cross-section of Concrete

5 Results

Table 2 shows the dimensions and notations meanings. Table 3 shows the Euler Buckling load and ANSYS results obtained from modelling 98 specimens.

Table 2 Specimen dimensions notations meanings

Notation	Meaning	Dimensions mm
L1	Length 1	2500
L2	Length 2	3000
L3	Length 3	3500
L4	Length 4	4000
D1	Diameter 1	101.6
D2	Diameter 2	114.3
D3	Diameter 3	127
D4	Diameter 4	139.7
D5	Diameter 5	152.4
D6	Diameter 6	165.1
D7	Diameter 7	168.3
D8	Diameter 8	193.7

6 Discussions

The Graphs 2, 3, 4 shown in Figs. 2, 3 and 4 respectively shows the variation in the load carrying capacities of specimens of different slenderness ratio for grades M30, M40 and M50 concrete respectively. It is also observed that the Euler's buckling load results are very comparable to that of ANSYS loads. This trend is observed for all slenderness ratios.

The Graph 5 in Figure 5 shows the variation of the load carrying capacities of specimens as found from modelling using ANSYS software of different slenderness ratio for grades M30, M40 and M50 concrete respectively. Following are the results observed.

- The load carrying capacity of CFST column decreases with increase in slenderness ratio for all grades of concrete which are considered.
- The load carrying capacity of CFST column increases with increase in grade of concrete. However, the percentage increase is higher for lower grade of concrete and lower for higher grade of concrete.

7 Conclusion

- For a given confinement ratio, the load carrying capacity of CFST column decreases with increase in slenderness ratio for all grades of concrete which are considered.
- For a given slenderness ratio, the load carrying capacity of CFST column increases with increase in confinement ratio for all grades of concrete which are considered.

Table 3 Analytical Specimen Euler Buckling Load and ANSYS results

Specimen Name	Slenderness Ratio $\lambda=L/d$	Euler's Buckling Load	Ansys Buckling Load
M30/L1/D1	24.61	1341.95	1424.1
M30/L1/D2	21.88	1988.01	2317.7
M30/L1/D3	19.69	2825.95	3330.5
M30/L1/D4	17.9	3885.89	4505.9
M30/L1/D5	16.41	5931.35	6303.84
M30/L1/D6	15.15	8654.11	9627.7
M30/L1/D7	14.86	10145.2	11070.4
M30/L1/D8	12.91	17620.1	21152.9
M30/L2/D1	29.53	931.911	989.34
M30/L2/D2	26.25	1380.56	1609.3
M30/L2/D3	23.63	1962.46	2308.8
M30/L2/D4	21.48	2698.53	3226.5
M30/L2/D5	19.69	3610.83	3839.6
M30/L2/D6	18.18	4722.54	5275.4
M30/L2/D7	17.83	5036.96	5521.2
M30/L2/D8	15.49	8084.18	9856.6
M30/L3/D1	34.45	684.669	727.55
M30/L3/D2	30.63	1014.29	1175.2
M30/L3/D3	27.56	1441.81	1704.3
M30/L3/D4	25.06	1982.6	2389.7
M30/L3/D5	22.97	2652.86	2826.8
M30/L3/D6	21.2	3469.62	3825.2
M30/L3/D7	20.8	3700.62	4033.2
M30/L3/D8	18.07	5939.4	7257.4
M30/L4/D1	39.38	841.009	892.647
M30/L4/D2	35	1333.44	1523.45
M30/L4/D3	31.5	2015.45	2362.31
M30/L4/D4	28.64	2930.34	3494.43
M30/L4/D5	26.25	2031.09	2167
M30/L4/D6	24.23	2656.43	2947
M30/L4/D7	23.77	2833.29	3120.2
M30/L4/D8	20.66	4547.35	5737.6

Specimen Name	Slenderness Ratio $\lambda=L/d$	Euler's Buckling Load	Ansys Buckling Load
M40/L1/D1	24.61	1388.14	1477
M40/L1/D2	21.88	2062.27	2419.7
M40/L1/D3	19.69	2939.27	3485.2
M40/L1/D4	17.9	4051.76	4720.8
M40/L1/D5	16.41	6166.31	6560.95
M40/L1/D6	15.15	8977.37	10067.2
M40/L1/D7	14.86	10492.8	11598.8
M40/L1/D8	12.91	18230.5	22292.3
M40/L2/D1	29.53	963.983	1026.1
M40/L2/D2	26.25	1432.13	1679.6
M40/L2/D3	23.63	2041.16	2415.2
M40/L2/D4	21.48	2813.72	3385
M40/L2/D5	19.69	3610.83	3839.6
M40/L2/D6	18.18	4722.54	5275.4
M40/L2/D7	17.83	5036.96	5521.2
M40/L2/D8	15.49	8084.18	9856.6
M40/L3/D1	34.45	708.233	754.66
M40/L3/D2	30.63	1052.18	1226
M40/L3/D3	27.56	1499.63	1783.7
M40/L3/D4	25.06	2067.22	2508.6
M40/L3/D5	22.97	2652.86	2826.8
M40/L3/D6	21.2	3469.62	3825.2
M40/L3/D7	20.8	3700.62	4033.2
M40/L3/D8	18.07	5939.4	7257.4
M40/L4/D1	39.38	856.562	917.035
M40/L4/D2	35	1358.54	1560.15
M40/L4/D3	31.5	2053.95	2411.95
M40/L4/D4	28.64	2986.97	3585.27
M40/L4/D5	26.25	2031.09	2167
M40/L4/D6	24.23	2656.43	2947
M40/L4/D7	23.77	2833.29	3120.2
M40/L4/D8	20.66	4547.35	5737.6

Specimen Name	Slenderness Ratio $\lambda=L/d$	Euler's Buckling Load	Ansys Buckling Load
M50/L1/D1	24.61	1428.83	1523.3
M50/L1/D2	21.88	2127.69	2508.5
M50/L1/D3	19.69	3039.1	3620
M50/L1/D4	17.9	4197.89	4908.6
M50/L1/D5	16.41	6373.31	6829
M50/L1/D6	15.15	9262.17	10390.3
M50/L1/D7	14.86	10799.1	11833.7
M50/L1/D8	12.91	18768.3	22559.5
M50/L2/D1	29.53	992.24	1058.6
M50/L2/D2	26.25	1477.57	1740.8
M50/L2/D3	23.63	2110.49	2508
M50/L2/D4	21.48	2915.2	3523.1
M50/L2/D5	19.69	3917.36	4213.2
M50/L2/D6	18.18	5144.05	5787.5
M50/L2/D7	17.83	5491.9	5986.2
M50/L2/D8	15.49	8879.25	10930
M50/L3/D1	34.45	728.993	778.62
M50/L3/D2	30.63	1085.56	1270.2
M50/L3/D3	27.56	1550.56	1852.9
M50/L3/D4	25.06	2141.78	2612.1
M50/L3/D5	22.97	2878.06	3101.4
M50/L3/D6	21.2	3779.3	4198.6
M50/L3/D7	20.8	4034.87	4408.5
M50/L3/D8	18.07	6523.53	8044.8
M50/L4/D1	39.38	870.264	929.528
M50/L4/D2	35	1380.66	1584.31
M50/L4/D3	31.5	2087.86	2448.85
M50/L4/D4	28.64	3036.87	3624.2
M50/L4/D5	26.25	2203.51	2377.4
M50/L4/D6	24.23	2893.53	3224.6
M50/L4/D7	23.77	3089.19	3380.3
M50/L4/D8	20.66	4994.58	6370.6
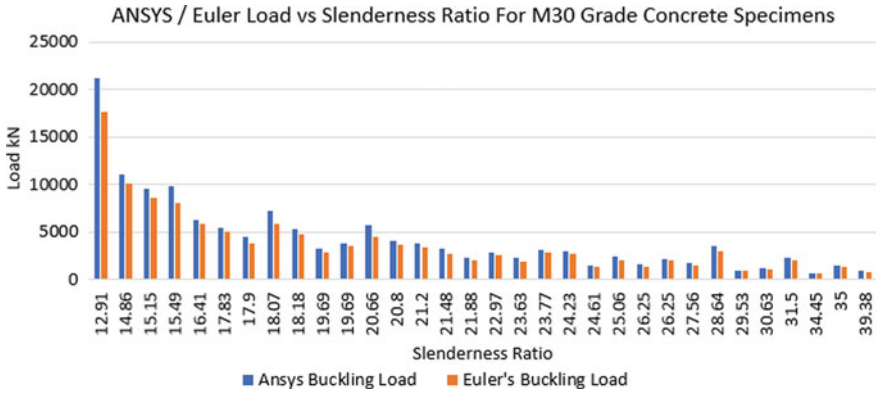
Fig. 2 Graph of ANSYS & Euler Load vs Slenderness ratio for M30 Grade of concrete
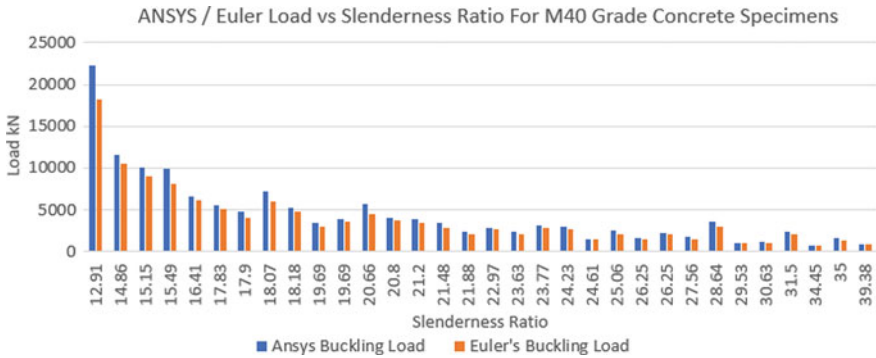
Fig. 3 Graph of ANSYS & Euler Load vs Slenderness ratio for M40 Grade of concrete
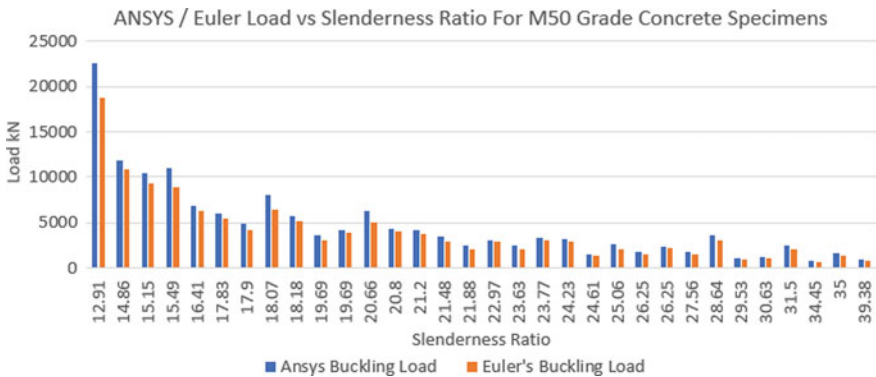
Fig. 4 Graph of ANSYS & Euler Load vs Slenderness ratio for M50 Grade of concrete
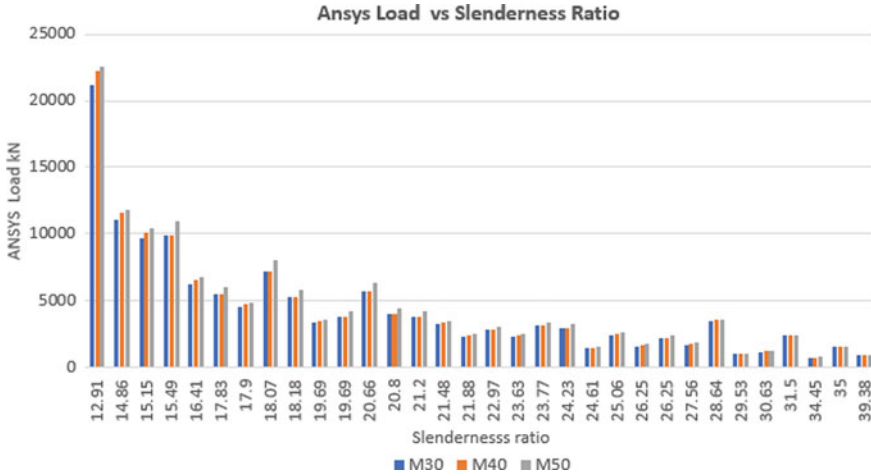
Fig. 5 Graph of ANSYS Slenderness ratio for M30, M40 & M50 Grades of concrete

- The load carrying capacity of CFST column increases with increase in grade of concrete. However, the percentage increase is higher for lower grade of concrete and lower for higher grade of concrete.
- As confinement ratio increases, there is an increase in deviation of buckling value obtained from ANSYS package when compared with Euler's formula.
- As slenderness ratio increases, there is a decrease in deviation of buckling value obtained from ANSYS package when compared with Euler's formula.
- Overall Euler's formula is found to underestimate the buckling load by about 5% for samples with lower confinement ratios and this deviation increases for specimen with confinement ratio value and above.

8 Scope for Further Studies

- In the present study we observe that with increase in slenderness ratio there is sudden increase and decrease in the Buckling load values both from ANSYS and Euler's Buckling load. It does not follow a general decreasing pattern. The reason for which is to be studied.
- In this analytical study, varying confinement ratio (d/t) with even thickness is considered. For further investigation this thickness can be varied to find out the effect of thickness on confinement for even diameter CFST columns.
- In this analytical study, M30, M40 and M50 are the grades of concrete used. Further investigation can be done for higher grades of concrete.
- In this analytical study, the grade of steel considered is E350. Further investigation can be done for higher grades of steel and different types of steel.

- The planned experimental work could not be completed. So, for further investigation, the results from this analytical work can be verified by conducting experimental investigation.

References

1. Han LH, Weili L, Bjorhovde R (2014) Developments and advanced applications of concrete filled steel tubular structural members. J Constr Steel Res. https://doi.org/10.1016/j.jcsr.2014.04.016
2. Giakoumelis G, Lam D (2014) Axial capacity of circular concretefilled tube columns. J Constr Steel Res. https://doi.org/10.1016/j.jcsr.2013.10.001
3. Karasin A, Günaslan SE, Öncü ME (2014) Models for confined columns with fiber composites. Int J Advanc Res Eng Technol
4. Patil BH, Mohite PM (2014) Parametric study of square concrete filled steel tube columns subjected to concentric loading. Int J Eng Res Applications 4(8):109–112
5. Geetha H, Swedha T (2015) An Experimental study on Concrete Filled Tubular Columns Using Varying Steel Materials. Int J Innovative Sci
6. Bedage SD, Shinde DN (2015) Concrete filled steel tube subjected to axial compression of long Column. Int J Res Eng Technol
7. Raghu KS, Ramesh Babu E, Dr Manju Prasad M, Dr Kumar NS (2013) Buckling behavior of concrete filled steel tube under finite element method. Int J Emerg Trends Eng Dev
8. Ajel HA, Abbas AM (2015) Experimental and analytical investigations of composite stub columns. Int J Innovative Res Sci
9. Sreenivasappa NM, Reddy ARP, Jagannatha Reddy HN, Prabhakara R (2021) Dynamic Response of RC Slab Under Drop Test Retrofitted with CFRP Strips Using NSM Technique. In: Recent Trends in Civil Engineering. Lecture Notes in Civil Engineering, vol 77. Springer, Singapore. https://doi.org/10.1007/978-981-15-5195-6_5
10. Duarte APC, Silva BA, Silvestre N, De Brito J, Júlio E, Castro JM (2015) Experimental study on short rubberized concrete-filled steel tubes under cyclic loading Composite Structures. Frontiers of civil and structural engineering

Influence of Various Factor Associate with Claims on Construction Industry

Bittu Ghosh, Mohibullah, and D. K. Bera

1 Introduction

Construction of any nation plays a predominant job in upgrading financial growth and improvement of the nation. The construction business has contributed an expected US$3000 billion to the national GDP (PPP) in 2011–12 (a portion of around 19%).

Today, with globalization and urbanization, construction sectors development tasks are done all over world. Construction practice started from an ancient period. Construction sector is a vast field. Construction does not only involves building a structure but also involves alter, repairs, demolish of structure as well as it focus on pre-construction and post construction phase. The construction venture includes numerous members with alternate points of view and necessities [1].

Construction is an un-persistent field. Construction sector faces the worst recession and performance with many failing of project. A construction sector faces various challenging jobs in its pathway [2–8]. In construction sectors there is no exact solution for one problem as well as problem also differ by companies, location, work environment, department by department, person to person, countries and state.

Claim acts a crucial role in task cost and time overwhelms, regularly changing correspondence among partners and structure conduct; this underscores the significance of claim management. A right technique for compelling claim management is that the utilization of better-known cases with the assistance of past mastery. All in all, a claim in construction comes and may occur as an aftereffect of numerous reasons which will add to deferring a task and additionally expanding its costs. Claims involve

B. Ghosh (✉) · Mohibullah · D. K. Bera
School of Civil Engineering, KIIT Deemed To Be University, Bhubaneswar, India
e-mail: 1854004@kiit.ac.in; mohibullah.fce@kiit.ac.in

D. K. Bera
e-mail: dberafce@kiit.ac.in

worry for all contracting parties engaged with a construction venture. In the accomplishment of a task, participation between invested individuals is required over the span of the undertaking; these gatherings are the proprietor, consultant, and contractual worker, even the provider. In any case, these gatherings have various interests and objectives with the goal that contentions/debates frequently happen due to variations throughout task planning and execution. The logical inconsistencies that happen can possibly incite claims. The amount of claims and claims is extending and could be a burden inside the construction venture. Indian construction venture crisis are driven by disrupted claims, for example, 85% of cases raised are as yet pending and average settlement time is about 6–6.5 years [9]. A claim is a debatable argument for coverage or compensation to the claimant for the activities which was deviated from the agreement and has incurred for the time and/or cost. Conflict is a contradiction between the different necessities and dispute happens when the parties differ about the effects of a conflict [10]. A dispute is common and not always well managed [11]. Disputes are additionally come about because of the indistinguishable resolutions of claims, which are attributes as consequences of poor administration of disputes. In the event that disputes are not settled expeditiously, they will in general become prolonged and escalated, making an increasingly convoluted and less manageable situation [12]. As detailed by the Business Standard on April 26, 2012, the National Highways Authority of India (NHAI) is thinking about claims arriving at INR 1,108 million in disputes and arbitration. Out of the all outdisputess, 1,099 disputes adding up to INR 1,021.9 million are in councils and 536 disputess adding up to INR 86.54 million are in different courts. Most of these disputes are in the (EPC) ventures. As of late, out of 1,263 highway ventures, 297 and 350 detailed a period or cost invades, separately, and 103 tasks confronted both time and cost overwhelms [13]. It has been observed that the actual cost increases by 2.42–13.42% due to claims [13]. Claim can happen both from clients or contractual worker because of discernment contrasts from the underlying understanding that has been expressed in a construction agreement. A claim could also be drawn as a management equipment to deal with failure that happens within the construction procedure.

Construction claims are considered by many task members to be one of the most problematic and upsetting occasions of a project [14]. Ventures in the construction business have been faced with an extraordinary volume of claims, which contrarily sway the construction business condition [15]. A Construction Claims: part of hypotheses and zone of concerns spotted claims union strategies and systems to look for Construction Contracts, best practices to take care of such issues between all construction venture partners [16]. Claims are unpredictable, so identifying the most common claims from past experiences and their root-causes could be a sound policy for the proper claim management process [17]. The uses of good claim management will most likely keep away from disputes that will affect cost overwhelm and time invade [18]. The dispute instances of the construction business have represented 10% and, particularly, the quantity of dispute claims identifying with the foreign sector has likewise expanded in extent (for example from 46.2% in 2012 to 48.5% in 2013). The quantity of dispute cases identifying with the construction area has been essentially expanding as of present years (VIAC1 2014, VIAC2 2014, VIAC3

2014) [19]. "In 2016, the average value of construction disputes stood at 42.8 million U.S. dollars [20]. A claim is a solicitation for time and additionally financial pay for damages caused by any party to the agreement [21]. Claim and dispute occasions in Indian roadway construction undertakings have turned into an intermittent marvel causing time and cost invades for most of construction projects under execution [13]. In this multidisciplinary condition, claims seem to obstruct the consummation of construction and cause delays in conveying ventures [22]. At the point when there are delays, contractual workers will in general submit delay claim looking for time and cost acclimation to their agreements [23]. Construction contract conditions assume a vital role in the organization and goals of claims and disputes [24].

Claims are regular, inescapable, and for sure an imperative piece of present day contract framework. The study contributes to various claim occurrences in the construction sector and the intensity by measuring there means score from various reputed paper. This will help project participants to have a proper claim management approach and concerning criteria in the project cycle. The crucial phase in construction for proper strategic governance can be taken up for the project. The paper have categorized the claim in various components such as changes, delay, technical issues, and contractual relationship, financial with the obtained of the reputed paper for the various countries and tried to conclude the most critical factors have to be concern for claim in the construction venture.

2   Research Approach

The first stage in this investigation was to perceive the claims in construction sector through literature study. Construction agreement claims are tedious, cost including and in all likelihood prompting unacceptable outcomes [25]. Initially comprehensive literature survey was studied to outline Claims in construction, based on stated sub-components reasons were further categorized in wide components. In view of the review factors of claims in the construction sector, it was sorted in five wide groups. These are introduced in Table 1.

Executing a task is typically connected with cooperation of various players who have had different objective and interests bringing about debates and differences. Claims normally relate to project risk. In construction activities, claims are being emerged to remunerate damages brought about by claimant organization, in expansion to a look at it's profitably. Along these lines, each factor making damage contractual worker's or proprietor's association and keeping them from arriving at their objectives associated with venture, can convince them to claim [25].

The classification was done basically from the various reasons of claims that take place in constructions sector. The factors which arises claims in construction venture were initially studied by the comprehensive literature study then it have been categorized as the terms of the factors that basically denotes the actual cause of the components. Each case has distinctive main cause. In light of the survey of related

Table 1 Construction claim broad components

Construction claim components	
Changes	Due to owner/client
	Due to law
	Due to site condition
	Due to economy and market
	Due to material
	Due to quantity variation
Delay	Due to contractor
	Due to client/owner
	Due to finanace
	Due to suspension/termination of work
	Due to late approval/instruction/site possession
	Due to damage of property
Technical issues	Contract/specification
	Design and dwg
	Pre-investigation
	Eot claim
	Safety
	Execution
	Planning
	Quality
Contractual relationship	Government/politics
	Natural hazards
	Public/local
	Conflict
	Staff incompetent
	Communication
Financial	Escalation
	Crises
	Bid amount

literature in the construction venture, of claims were recognized and arranged. These are presented in Table 2 nearby the composition sources.

These categorized is done on practical construction terms which is generally used in the sector to denote the various problems. Here in this study data collection have been done with respect to various countries to know the occurrences of various claims in the construction sector and its impact have given by the questionnaire survey of their respective countries. This paper has taken the impact parameters of reputed

Table 2 Claim components with sources

Broad components		Sub-components	Sources
Changes	Due to owner/client	Changes in owner's requirements	Kemala Hayati et al. [18], Majid Parchami Jalal et al. [17], Long Le-Hoai et al. [19], Essam K. Zaneldin et al. [22], Nor Azmi Bakharya et al. [26], Mohammed Taha Al-Qershi et al. [9]
		Changes of design from owner during the post-tender award stage	
		Changes in employer's/user's requirements arising during the post-tender award stage	
		Change or variation orders	
		Oral change orders by owner	
		Change of project scope by owner	
		Change or variation orders due to new requirements from client	Sadi Assaf et al. [15], Wenxin SHEN et al. [27], Malek Mishmish et al. [21], Mohammed Taha Al-Qershi et al. [9]
		Last minute changes initiated by the client	
		Change orders	
		Oral change orders by client	
	Due to law	Change in government regulations	Long Le-Hoai et al. [19], Malek Mishmish et al. [21], Mohammed Taha Al-Qershi et al. [9]
		Change in code (such as governmental laws, national standard)	
	Due to site condition	Change of site condition	Long Le-Hoai et al. [19], Mohammed Taha Al-Qershi et al. [9]
	Due to economy and market	Changes in material and labor costs	Essam K. Zaneldin et al. [22], Sadi Assaf et al. [15], Kemala Hayati et al. [18], Nor Azmi Bakharya et al. [26], Mohammed Taha Al-Qershi et al. [9]
		Influence of market price fluctuations on subcontractors and suppliers	
		Change in material/labor costs	
	Due to material	Materials out of specification	Sadi Assaf et al. [15], Long Le-Hoai et al. [19]
		Change in material due to unavailability	
	Due to quantity variation	Variations in quantities due to new requirements from client	Essam K. Zaneldin et al. [22], Sadi Assaf et al. [15], Malek Mishmish et al. [21], Mohammed Taha Al-Qershi et al. [9]
		Variations in quantities	

(continued)

Table 2 (continued)

Broad components		Sub-components	Sources
Delay	Due to contractor	Delay caused by contractor	Long Le-Hoai et al. [19], Essam K. Zaneldin et al. [22], Malek Mishmish et al. [21], Sadi Assaf et al. [15], Mohammed Taha Al-Qershi et al. [9]
		Delay of subcontractors	
		Due to lack of contractor's resources	
		Delay in mobilization time by the contractor	
		Delay of subcontractors	
	Due to client/owner	Delays caused by client	Long Le-Hoai et al. [19], Essam K. Zaneldin et al. [22], Parchami Jalal et al. [15], Sadi Assaf et al. [15], Malek Mishmish et al. [21], Mohammed Taha Al-Qershi et al. [9]
		Owner's need of much time for decision making	
		Non-availability of land on time due to client's occupation	
		Delays due to The employer or employer's agents' negligence to fulfill their liabilities to the contractor	
		Delay caused by owner	
	Due to finanace	Delay in payments by owner	Sadi Assaf et al. [15], Long Le-Hoai et al. [19], Essam K. Zaneldin et al. [22], S. H. Hasheminasab et al. [25], Sadi Assaf et al. [15], Malek Mishmish et al. [21], Kemala Hayati et al. [18], Mohammed Taha Al-Qershi et al. [9]
		Delay in payment of contractor for subcontractors or suppliers	
		Disagreements arising during negotiations	
		Client delayed payment	
		Delay of certified payment by the client	
		Disagreement on the mode of payment under preliminaries/general items	
		Delays in sub-contractor's payment	
		Untimely payment	
	Due to suspension/termination of work	Termination of work	Long Le-Hoai et al. [19],Sadi Assaf et al. [15], Essam K. Zaneldin et al. [22], Malek Mishmish et al. [21], Mohammed Taha Al-Qershi et al. [9]
		Suspension of work	
		Contractor's stop of on-site works	

Table 2 (continued)

Broad components	Sub-components		Sources
	Due to late approval/ instruction/site possession	Contractor's late completion of progress milestones	Long Le-Hoai et al. [19], Malek Mishmish et al. [21], Sadi Assaf et al. [15], Mohammed Taha Al-Qershi et al. [9]
		Delay in issuing detail work plans and schedules	
		Late handover of construction site for other construction organizations	
		Delay in granting possession of site	
		Late issue of instruction/clarification	
		Delay in mobilization time by the contractor	
	Due to damage of property	Damage to neighbouring installations when performing work	Long Le-Hoai et al. [19]
		Damage to owner's installations during performing contract	
Technical issues	Contract/ specification	Inadequate definition and/or specification of the precise scope of contract	Long Le-Hoai et al. [19], Wenxin SHEN et al. [27], Sadi Assaf et al. [15], Nor Azmi Bakharya et al. [26], S. H. Hasheminasab et al. [25], Essam K. Zaneldin et al. [22], Malek Mishmish et al. [21], Kemala Hayati et al. (2019), Mohammed Taha Al-Qershi et al. [9]
		Poorly written contracts	
		Double meaning in specification	
		Client incorporates changes in scope during construction	
		Acceptance of unclear/imprecise tender offers without proper clarifications, negotiations, recording of changes	
		Dispute regarding Contract Interpretation	
		Error/defect/contradiction in designs/specifications/contract	
		Misinterpretation of the contract by the contractor	
		Unclear scope of works	
		Undefined/vague scope of work	
		Unclear technical specification	

Table 2 (continued)

Broad components	Sub-components	Sources
	Design and dwg	Incomplete and/or uncoordinated design	Kemala Hayati et al. [18], Nor Azmi Bakharya et al. [26], Sadi Assaf et al. [15], S. H. Hasheminasab et al. [25], MajidParchami Jalal et al. [17], Long Le-Hoai et al. [19], Essam K. Zaneldin et al. [22], Malek Mishmish et al. [21], Mohammed Taha Al-Qershi et al. [9]
		Error/defect/contradiction in designs/specifications/contract	
		Inconsistencies in the drawings and specifications	
		Design changes being introduced at the post-tender award stage	
		Specifications and drawings inconsistencies	
		Change of design during construction to suit site conditions	
		Omissions in the design documents, requiring changes in the shop-drawing	
		Double meaning in specification/design	
		Design-related issues (such as design change)	
		Design errors or omissions	
		Lack of clarity in the owner's requirements and/or inadequacy of the design brief	
		Non-compliance of as-built work with design	
	Pre-investigation	Inadequate investigation before bidding	Long Le-Hoai et al. [19], Malek Mishmish et al. [21], Nor Azmi Bakharya et al. [26], Kemala Hayati et al. [18]
		Time in the contract is too short	
		Lack of available information from site investigation	
		Project being implemented in short time period with inadequate site investigation, design works, tender and contract documents	
	Eot claim	Failure by the contractor to comply with the contractual requirement for EOT application	Malek Mishmish et al. [21], Norazian Mohamad Yusuwana et al. 2013, Mohammed Taha Al-Qershi et al. [9]
		Different perceptions in methods for assessing the extension of time	
		Permissible period of time extension	

Table 2 (continued)

Broad components		Sub-components	Sources
	Safety	Accidents	Long Le-Hoai et al. (2018 [19], Essam K. Zaneldin et al. [22], Sadi Assaf et al. [15], Malek Mishmish et al. [21], Mohammed Taha Al-Qershi et al. [9]
		Accidents on site	
		Accidents as a consequence of negligence	
		Problems in safety management	
	Execution	Incorrect application of technology	Long Le-Hoai et al. [19], S. H. Hasheminasab et al. [25], Malek Mishmish et al. [21], Kemala Hayati et al. [18], Mohammed Taha Al-Qershi et al. [9]
		Lack of accuracy in request for subcontracted work and quantity	
		Differing site conditions	
		Reworks	
		Construction defects	
		Defective work by contractor	
		Defects in works	
		Excessive extra work	
		Difficulties in detecting any problems during the work due to high workload	
		Execution errors	
		Influence of site congestion on subcontractors' works	
		Poor site lay-out coordination or organizing	
		Shortcuts in construction procedure	
	Planning	Planning errors by contractors because of uncertainties	Sadi Assaf et al. [15], Long Le-Hoai et al. [19], Essam K. Zaneldin et al. [22], Malek Mishmish et al. [21], Mohammed Taha Al-Qershi et al. [9]
		Inadequate documentation	
		Estimating errors	
		Due to planning and scheduling errors	
		Scheduling errors	
		Underestimation of project duration by contractor	
		Lacking or poor planning and scheduling	
		Too optimistic in planning and scheduling	

Table 2 (continued)

Broad components	Sub-components		Sources
	Quality	Bad quality of contractor's work	Sadi Assaf et al. [15], Long Le-Hoai et al. [19], Essam K. Zaneldin et al. [22], Mohammed Taha Al-Qershi et al. [9]
		Defects during the construction stage that become apparent during liability period	
		Contractor rendering poor quality work	
		Failure to meet quality requirements	
Contractual relationship	Government/ politics	Negative effects of political factors	Kemala Hayati et al. [18], Long Le-Hoai et al. [19], Essam K. Zaneldin et al. [22], S. H. Hasheminasab et al. [25], Malek Mishmish et al. [21], Mohammed Taha Al-Qershi et al. [9]
		Political factors	
		Government regulations	
		External Risks (Political, Social and cultural, Economical) Occurrence during construction contract	
		Violation of government area regulations	
		Public disorder	
	Natural hazards	Acts of God (such as hurricane, storm)	Long Le-Hoai et al. [19], Wenxin SHEN et al. [27], Malek Mishmish et al. [21], Mohammed Taha Al-Qershi et al. [9]
		Incidental events during construction stage (such as land slide, destruction of property adjacent to project)	
		Act of God	
		Natural hazards	
	Public/local	Disruption due to third-party access to contractor's works	Malek Mishmish et al. [21], Long Le-Hoai et al. [19], Mohammed Taha Al-Qershi et al. [9]
		Protest of local people during project implementation process	
		Lack of knowledge about legal local systems	
		Third-party interference	
	Conflict	Lack of coordination between Participants due to Discord within project participants	Sadi Assaf et al. [15], MajidParchami Jalal et al. [17], Long Le-Hoai et al. [19], Malek Mishmish et al. [21], Mohammed Taha Al-Qershi et al. [9]
		Subcontractor problems due to mismanagement by main contract	
		Lack of co-ordination between different teams	
		Discord within the project participants	

Table 2 (continued)

Broad components		Sub-components	Sources
		Unsuitable behaviour of contractor's employees to other stakeholders	
	Staff incompetent	Frequent absence of key personnel of contractor from site or meeting	Long Le-Hoai et al. [19], Malek Mishmish et al. [21], Kemala Hayati et al. [18], Mohammed Taha Al-Qershi et al. [9]
		Insufficient contract knowledge by site staff	
		Due to lack of qualified personnel/inadequate supervision on site	
		Inadequacy of workers as committed in contract agreement	
		Inadequacy of personnel (such as engineers, managers) as committed in contract agreement	
		Incompetent contractor staff	
	Communication	Bad communication between parties	Essam K. Zaneldin et al. [22], Kemala Hayati et al. [18], Long Le-Hoai et al. [19], Mohammed Taha Al-Qershi et al. [9]
		Poor communication between site and head office	
		Poor communication	
Financial	Escalation	Sudden swings in economic and market conditions	Long Le-Hoai et al. [19], Kemala Hayati et al. [18], Essam K. Zaneldin et al. [22], Nor Azmi Bakharya et al. [26], Mohammed Taha Al-Qershi et al. [9]
		Influence of market price fluctuations on subcontractors and suppliers	
		Inflation	
	Crises	Financial problem of owner organization	Long Le-Hoai et al. [19], Essam K. Zaneldin et al. [22], Sadi Assaf et al. [15], S. H. Hasheminasab et al. [25], Kemala Hayati et al. [18], Mohammed Taha Al-Qershi et al. [9]
		Contractor financial challenges	
		Inadequate financial strength on part of a contractor and failure in obligations	
		Financial problem of contractor organization	
	Bid amount	Low price contract due to fierce competition among contractors	Sadi Assaf et al. [15], Long Le-Hoai et al. [19], Malek Mishmish et al. [21], Mohammed Taha Al-Qershi et al. [9]
		Low profitability from project	
		Low price due to high competition resulting in financial problems	
		Underestimation of project cost by contractor	

papers and has done a mean score as standard parameter for analyzing impact of the respective claims.

2.1 Changes

When the client issues oral/written instruction/order that are at variance with the stipulated contained specification agreement of the project. This order may either be communicated at site or through meeting or via mail without preparing any supportive documents. The scarcity of material in market as specified in the contract can be a major source of claim. When contractor bid for the project, they quote the tender based on the material available in the market, at the time of bidding. In this course if some of the material is unavailable, the contractor is faced to seek alternative to the material presently available in the market. Even an increase in the cost of material as per specified in the agreement due to production or non-production-related issues such as a nation-wide increase in cost (e.g. taxes, custom clearance, cost of diesel, petrol, power or water). Change in the quantities is varied as per the volume of work which can vary the cost of the project. In that situations claims can be developed. More specially if the quantity of the material is imported or material with long lead time will undoubtedly leads a cause for the contractor to raise a claim. Claim arises when the condition of the site changes then the data provided in the agreement which leads to a major claim factor for the project. The change of law by the government is a crucial cause for the claim to arise as certain rules may hike the project cost or certain technology can be ban which leads to a major cause of claim.

2.2 Delay

At the point when the contractual worker disregards or late in activating the task, the client may think about it as a pointer of the temporary worker's reluctance or inability to lead the assignment. Delay can likewise emerge when the customer neglects to issue the running bill installment on the due date, bringing about the undertaking errand can be led. Deferred running bill installment can be because of budgetary crises of the client that makes the client the contrast in installment. On the off chance that any harm to the private property caused because of proprietor/contractual worker can held the venture length which may prompts debate among the gatherings for the remuneration of the harm. At the point when the customer issues oral/composed/email guidance that are variances with the agreement. Late in issuing endorsement from the client point of view can hold up the venture action that can cost the temporary worker for retention the undertaking. Based on working connection between two gatherings this could may stand a potential wellspring of question. Thusly, the customer can find a way to evade future issues by retention the propelled installment or through ending the agreement. The end or suspension of assignment provoked by different

reasons, including non accessibility of land, apparatuses, mishap, sub-temporary workers prompts cessation of work [28–30].

2.3 Technical Issues

At the point when the extent of the undertaking is misty or unknown appropriately it has been seen that the claim occurrence in most event. Notwithstanding when the Errors in plans or particular can be a factor for emerging of claims. On the opposite side, exclusions are factors that are not demonstrated. It is more often than not to encounter the blunders or exclusions in enormous ventures. Some of the time the different frameworks don't fit consistently as a result of lacking consideration being coordinated to the coordination procedure by the team leader, who is frequently the engineer. This absence of coordination could likewise come from increasing speed forced by the clients allowing for the review procedure. Pre-examination of the tasks now and again is vary from the real condition while executing the action this prompts a noteworthy change in the technique or even in the supplies and materials. Now and again venture have been started in brief span without site examination or sought after that might be prompts misty proviso in understanding between gatherings which prompts augmentation of time claim. In site mishaps may happens as a results of clients or temporary workers carelessness of well-being related issues, power majeure, hazardous structure or ill-advised access before handover. Executing the movement with inappropriate procedure or imperfections in construction has the significant commitment to the claim. The easy route taken while construction may now and again be unseemly might be a reason for revamps or the site contrast from the understanding perspective an elements for claim. The vulnerabilities encompassing construction activities make legitimate arranging a troublesome objective to accomplish, especially without data. This reason emerges when the action executed by the temporary worker not satisfy the guidelines as explained in the agreement [30, 31].

2.4 Contractual Relationship

Activities need to pursue the administration rules and guidelines, in such intrigue political impedance happens in the task which may drives different changes that may not be indicated according to the agreement that has the potential for claims. Neighborhood Bodies have different impedance in the undertaking that temporary worker or even the client get rule and need to satisfy their interest if there should arise an occurrence of specific structures or regions because of their convention or need to mightily give certain pay off to execute the task. The staff of the contractual worker might be uncouth to execute the movement or the poor correspondence among temporary workers and subcontractors or among clients and temporary workers prompts claim [32].

2.5 Financial

At the point when the agreement have been taken the agreement depends on the present market an incentive with certain thought however in the event that there is a sure real expansion that have been happened while executing the task that assume an essential job in financial part of the project. The variety if goes past the presumption prompts claim as the agreement clause. The bid worth is now and again taken by the contractual worker in under-cost to improve their opportunity of winning the bid. They adopt this practice since they foresee the age of benefit through the issuance of claims during the construction stage. In the event that the client expels the claims as baseless, the contractual worker may wind up in troublesome conditions. The client or the temporary worker might confront money related crises inside which influences the undertaking as the postpone installment impacts the task execution in both the forthright factors.

Each claim has different root causes. Based on the review of related literature in the construction industry, of claims were identified and categorized. These are presented in Table 2 along with the literature sources (Table 3).

3 Summary and Discussion

This paper centers chiefly on distinguishing and surveying the most incessant purposes behind claims, and their basic main causes, for construction projects in the different nations. This paper gives a significant commitment to specialists and professionals as it distinguishes the reasons for cases in construction projects and structures a valuable reason for further improvement for maintaining a strategic distance from or limiting construction claims in that nations. Information with respect to the claim is normally kept secret by contractual workers, specialists and customers, and it is generally hard to accumulate solid information because of its private nature. In light of the consequences of this examination, it is prescribed that alleviation techniques be created to maintain a strategic distance from or limit guarantees in development extends in the different nations.

A Change is the most regular reason for cases in the construction ventures. It has been seen that the Indonesia is mostly affected by this followed by Saudi Arabia, UAE, India, Vietnam. During the construction stage, clients demand a varieties to the settled upon venture scope. Contractual workers think about that they are entitled for repayment for the extra work, while clients think about that the work is incorporated into the agreement's extension and is hence part of the offered cost. This predictable with different examinations that demonstrated change request claims as the most successive. Figure 1 demonstrates the effect of change claim in construction part of different nations.

Contractor worker's deferral is the second most incessant reason for cases in the construction ventures. It has been seen that Indonesia has its most effect followed by Saudi Arabia, UAE and India as similar state then Vietnam among different

Table 3 Score of claim components

Broad components		UAE	Indonesia	Vietnamese	Saudi Arabia	India
Changes	Due to owner/client	3.18	4.67	2.31	3.9	3.56
	Due to law	2.53		2.24		2.98
	Due to site condition			2.73		2.78
	Due to economy and market			2.88	3.05	3.19
	Due to material			3.23	3.2	
	Due to quantity variation	3.65			3.7	3.69
Delay	Due to contractor	3.37		2.38	3.7	3.38
	Due to client/owner	2.65		2.3	3.5	3.15
	Due to finance	2.8	4.33	3.06	3.3	3.38
	Due to suspension/ termination of work	2.78		2.58	3.05	2.84
	Due to late approval/ instruction/site possession	3.08		3.15		3.75
	Due to damage of property			2.96		
Technical issues	Contract/specification	3	4.29	2.81	3.3	3.30
	Design and dwg	3.08	4.05	2.86	3.6	3.35
	Pre-investigation	3.31	4.29	3.04		3.25
	EoT claim	3.31				
	Safety	2.49		3.42		
	Execution	2.78	3.76	3.17		2.76
	Planning	2.92		2.98	3.05	3.30
	Quality	3.1		2.75	3.25	2.80
Contractual relationship	Government/ politics	2.1	2.95	2.495		
	Natural hazards/extreme climate	2.55		2.61		2.95
	Public/local	3		2.181		3.08
	Conflict	3.33		3.21	3.4	
	Staff incompetent	2.78	4.38	2.99		3.03
	Communication		3.86	3.13	3.15	3.10
Financial	Escalation		3.24	2.21		2.95
	Crises		2.9	2.17	3.3	3.12
	Bid amount	3.08		2.14	3.5	3.32
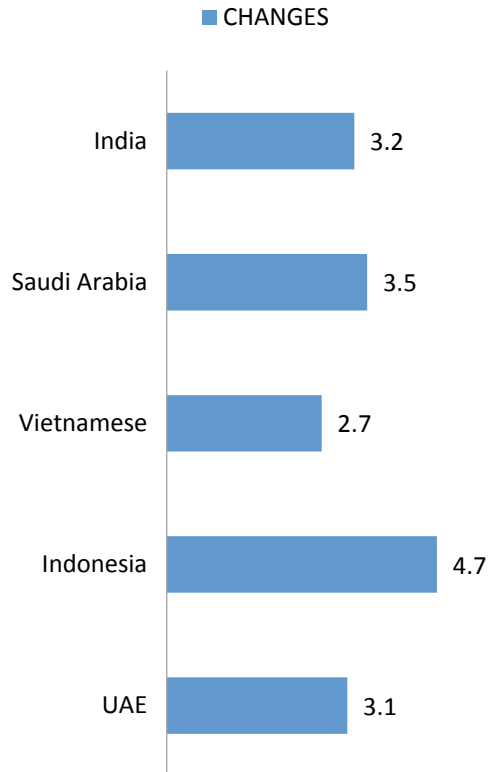
nations after its effect on changes as top-most. Late issuance of guidelines as well as explanations by the specialist during construction the reason for claims. Figure 2 demonstrates the effect of delay claim in construction division of different nations.

A Technical issue is the third most regular reason for cases in the construction ventures. It has been seen that Indonesia is generally affected pursued by Saudi Arabia, India then the Vietnam and UAE remain at comparable position. Insufficient documentation, deficient time considered contract plan, An ineffectively composed contract, When the agreement reports are so ineffectively drafted that they don't depict the commitments/privileges of each gathering fittingly, Inadequate site examination before offering, Some of the key contract arrangements might miss, irregularities in detail and drawings, The principle purposes behind this claim are the utilization of agreement particulars/drawings arranged for a past contract that are not explicit to the present contract pursued by ambiguities, During construction, different utilities are experienced which are not appeared on the agreement drawings, coming about in either occupying the utilities or moving the proposed works, Time impediments during configuration bring about fragmented structures requiring late changes in the construction archives which lead to disparities in documentation reason for claim in the construction. Figure 3 demonstrates the effect of Technical issues claim in construction division of different nations.

Fig. 2 Impact of delay in construction of countries

DELAY

Country	Value
India	3.1
Saudi Arabia	3.4
Vietnamese	2.7
Indonesia	4.3
UAE	3.1
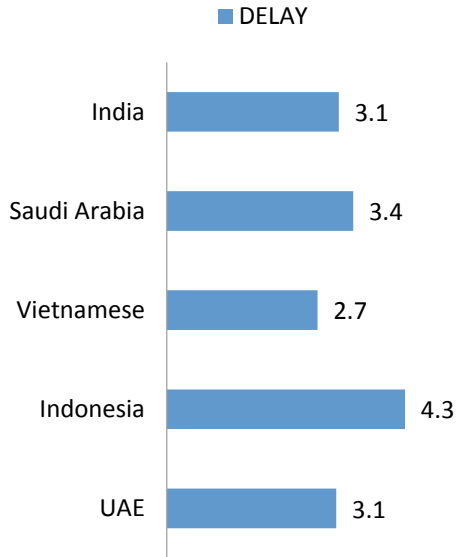
Fig. 3 Impact of technical issues in construction of countries

TECHNICAL ISSUES

Country	Value
India	3.1
Saudi Arabia	3.3
Vietnamese	3.0
Indonesia	4.1
UAE	3.0
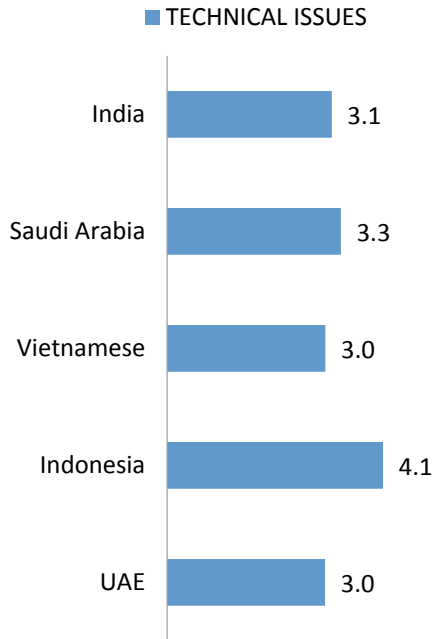
Fig. 4 Impact of contractual relationship in construction of countries

■ CONTRACTUAL RELATIONSHIP

India — 3

Saudi Arabia — 3.3

Vietnamese — 2.8

Indonesia — 3.7

UAE — 2.8
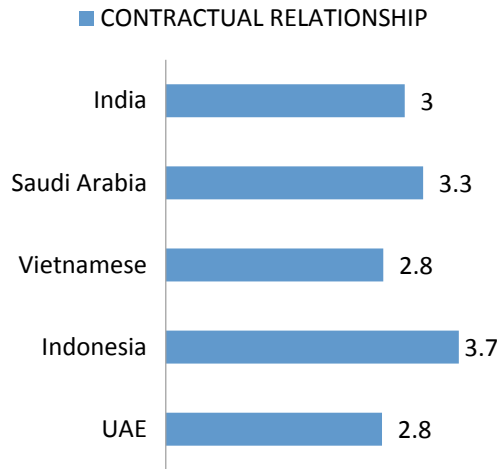
Contractual Relationship is the fourth reason for claim in the Construction Projects among the other criteria as discussed. This claim has most impact in Indonesia followed by Saudi Arabia, India and then the Vietnam and UAE stands at similar state. The fundamental explanation behind this claim is the absence of staff pursued by various observations between the specialist and the contractual worker of unexpected conditions, Third gathering impedance, interruption to the temporary worker because of outsider (experts/different contractual workers/customers' representatives), delay in acquiring the No Objection Certificate (NOC) to complete the works. Figure 4 demonstrates the effect of Contractual relationship claim in development area of different nations.

Finance is the fifth reason for claims in the Construction Projects. Because of high challenge, contractual workers will in general submit preposterously low costs. The money related crises of client/contractor may be a factor and the acceleration in rates are the claim cause. This prompts budgetary issues during venture execution which thus prompts claims. This crises is mostly affected in Saudi Arabia followed by India, UAE and Indonesia at similar situation then Vietnamese. Figure 5 demonstrates the effect of finance claim in construction division of different nations.

The results were also analyzed based on the factors impact of various countries. Figure 6 presents the overall ranking of the causes of claims of various countries.
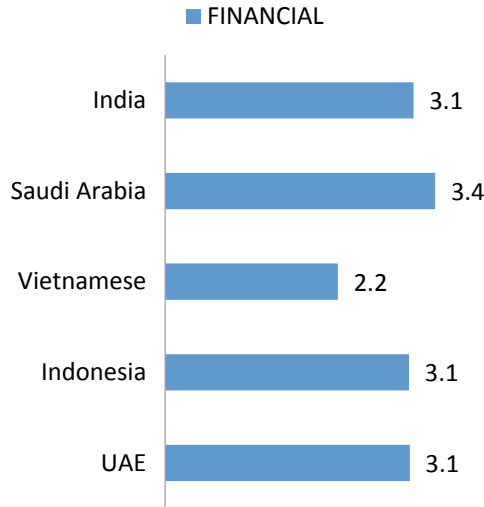
Fig. 5 Impact of finance in construction of countries
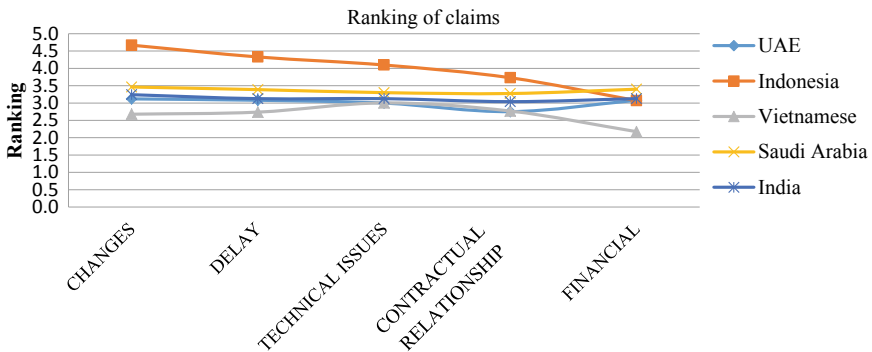
Fig. 6 The overall impact of the causes of claims of various countries

4 Conclusion

This investigation of each wide parts with various country demonstrated that the most successive claims emerges in changes sought after by delay, technical issues, contractual relationship factor then the finance. The most affected nation according to study expresses that Indonesia pursued by Saudi Arabia, India, UAE and Vietnam. With this investigation we presume that claim impact-fully affects construction tasks to which a suitable claim management framework must be actualized to beat number of claims. This study shows the area where in claim is more prominent which has to be managed with effective claim management system to avoid any conflict in the construction projects.

References

1. Wang C, Yap JBH, Wood LC, Abdul-Rahman H (2019) Knowledge modelling for contract disputes and change control. Prod Plan Control 30(8):650–664
2. Pandey A, Chaudhary PK, Das BB (2021) Productivity analysis of shuttering works for sewage treatment plant. In: Select proceedings of TMSF 2019. Springer Publications Pte. Ltd. A Book Chapter
3. Akhil RP, Das BB (2019) Cost reduction techniques on MEP projects. In: Select proceedings of ICSCBM 2018. Springer Nature Singapore Pte Ltd., pp 495–517. A Book Chapter
4. Hegde AL, Jain A, Das BB (2021) Resource buffers in construction projects. In: Select proceedings of TMSF 2019. Springer Publications Pte. Ltd. A Book Chapter
5. Paul B, Tondihal S, Das BB (2021) Safety stock in inventory management and wastage analysis at construction sites. In: Select proceedings of TMSF 2019. Springer Publications Pte. Ltd. A Book Chapter
6. Upadhya PR, Das MS, Das BB (2021) Multi criteria decision making approach for selecting a bridge superstructure construction method. In: Select proceedings of TMSF 2019. Springer Publications Pte. Ltd. A Book Chapter
7. Pradeep RC, Das BB (2019) Methods to monitor resources and logistic planning at project sites. In: Select proceedings of ICSCBM 2018. Springer Singapore Pte Ltd., pp 793–802 A Book Chapter
8. Shekhar S, Shukla P, Das BB (2021) Developing a standard template for activity linkage and resource estimation of MEP works. In: Select proceedings of TMSF 2019. Springer Publications Pte. Ltd. A Book Chapter
9. Al-Qershi MT, Kishore R (2017) Claim causes and types in Indian construction industry—contractor's perspective. Am J Civ Eng Arch 5(5):196–203. https://doi.org/10.12691/ajcea-5-5-3
10. Phillips-Alonge OK (2018) The influence of partnering on the occurrence of construction requirement conflicts and disputes. Int J Constr Manag. https://doi.org/10.1080/15623599.2018.1435236
11. Duchaussoy Q (2019) Disputes in construction contracts: commonly experienced but not fully understood? PM World J VIII(II) (February)
12. Saeb A, Danuri MSBM, Zakaria NB, Mohamed OB (2019) A case study of dispute resolution methods pertaining to the construction standard form in Iran. Int J Constr Educ Res. https://doi.org/10.1080/15578771.2019.1575937
13. Parikh D, Joshi GJ, Patel DA (2019) Development of prediction models for claim cause analyses in highway projects. J Leg Aff Disput Resolut Eng Constr © ASCE. ISSN 1943-4162
14. Nasirzadeh F, Carmichael DG, Jarban MJ, Rostamnezhad M (2018) Hybrid fuzzy-system dynamics approach for quantification of the impacts of construction claims. Eng Constr Arch Manag © Emerald Publishing Limited 0969-9988. https://doi.org/10.1108/ECAM-08-2017-0150
15. Assaf S, Hassanain MA, Abdallah A, Sayed AMZ, Alshahrani A (2019) Significant causes of claims and disputes in construction projects in Saudi Arabia. Built Environ Proj Asset Manag. https://doi.org/10.1108/.BEPAM-09-2018-0113
16. Abdel-Khalek HA, Aziz RF, Abdellatif IA (2019) Prepare and analysis for claims in construction projects using Primavera Contract Management (PCM). Alex Eng J
17. Parchami Jalal M, Noorzai E, Roushan TY (2019) Root cause analysis of the most frequent claims in the building industry through the SCoP3E Ishikawa diagram. J Leg Aff Disput Resolut Eng Constr. © ASCE. ISSN 1943-4162
18. Hayati K, Latief Y, Rarasati AD (2019) Causes and problem identification in construction claim management. IOP Conf Series Mater Sci Eng 469:012082
19. Le-Hoai L, Dang CN, Lee SB, Lee YD (2018) Benchmarking claim causes against contractors in emerging markets: empirical case study. Int J Constr Manag. https://doi.org/10.1080/15623599.2018.1435156

20. Zhao W (2019) The root cause of claims and disputes in construction industry and solution analysis. PM World J VIII(V)
21. Mishmish M, El-Sayegh SM (2016) Causes of claims in road construction projects in the UAE. Int J Constr Manag 18(1):26–33. https://doi.org/10.1080/15623599.2016.1230959
22. Zaneldin EK (2006) Construction claims in United Arab Emirates: types, causes, and frequency. Int J Project Manage 24(2006):453–459
23. Perera BAKS, Wijewickrama MKCS, Goonawardana PJA, Jayalath C (2021) Improving the efficacy of delay notification process of construction projects in Sri Lanka. Int J Constr Manag 21(7):755–768. https://doi.org/10.1080/15623599.2019.1581593
24. Barakat M, Abdul-Malak M-A, Khoury H (2019) Sequencing and operational variations of standard claim and dispute resolution mechanisms. J Leg Aff Disput Resolut Eng Constr. © ASCE. ISSN 1943-4162
25. Hasheminasab SH, Mortaheb MM, Ahmadian A (2014) Causes of common and frequent claims in oil, gas and petrochemical projects of Iran. KSCE J Civ Eng 18(5):1270–1278. https://doi.org/10.1007/s12205-014-0422-5
26. Bakhary NA, Adnan H, Ibrahim A (2015) A Study of Construction Claim Management Problems in Malaysia. Procedia Econ Financ 23(October 2014):63–70. https://doi.org/10.1016/S2212-5671(15)00327-5
27. Shen W, Tang W, Yu W, et al. (2017) Causes of contractors claims in international engineering-procurementconstruction projects. J Civ Eng Manag 23(6):727–739. https://doi.org/10.3846/13923730.2017.1281839
28. Bisoka AN, Giraud C, Ansoms A (2019) Competing claims over access to land in Rwanda: legal pluralism, power and subjectivities. Geoforum, pp 1–10
29. Lee GY, Shi P (2019) A dependent frequency-severity approach to modeling longitudinal insurance claims. Insur Math Econ. https://doi.org/10.1016/j.insmatheco.2019.04.004
30. Maiyo JK, Evers SJTM (2019) Claim-making in transnational land deals: discourses of legitimation and stakeholder relations in central Uganda. Geoforum. https://doi.org/10.1016/j.geoforum.2019.04.014
31. Ram Mohan MP, Kini ER (2019) Right of recourse claims based on latent defects in the nuclear energy sector in India: brace yourself for fact-intensive disputes. Indian Institute of Management W. P. No. 2019-05-01
32. Van Over beek F (2018) Claim-making through subjectivation: a governmentality analysis of associational performance to claim land in the hybridity of peri-urban Bukavu. Geoforum. https://doi.org/10.1016/j.geoforum.2018.04.007

Analysis of Risk Assessment and Management of Wastewater Treatment Plants

Zoalfikar Ismaiel and Akshaya Kumar Verma

1 Introduction

Defining the risk management process is complex due to the multiplicity and inter-dependence of the different scientific and economic fields in which it is applied comprehensively. It can be defined in a simplified form as an integrated process to determine the best way to diagnose and monitor potential risk control. Risk management and assessment should result in the risk being reached at an acceptable level that is not harmful [5]. The risk assessment should lead to a specific situation in which the management of the treatment plants is aware of the presence of hazards identified in (ERA) during the operation of the plant takes into account its size, level such that it does not exceed the acceptable risk limit. In WWTPs, risk management can be described as the prevention of negative damage during operation and maintenance and the emphasis on reducing the size of the damage caused after the occurrence of such events. Risk management is divided into two basic stages: risk assessment and risk monitoring (Table 1). The components of assessment are identifying and assessing risks and determining the level of acceptance or not. Risk monitoring includes monitoring wastewater treatment processes, plant maintenance status and monitoring general changes [8].

Z. Ismaiel · A. K. Verma (✉)
Department of Civil Engineering, Institute of Technical Education & Research, Siksha O Anusandhan (Deemed To Be University), Bhubaneswar 751030, India
e-mail: akshayakumarverma@soa.ac.in

Table 1 Stages of risk management and assessment

Stages	Actions taken and results
Risk identification	– Introducing all types of risks – Explain the cause of the danger – Identify the threatened components at risks – Identify failure causes
Risk analysis	– Determine the severity of the risk—the impacts resulting from the risk – Provide risk analysis and modeling methods – Description of risk management tools
Risk assessment	– Accurate measurements of actual risk level – Scaling framework – Evaluate the ability of treatment plant officials to implement an integrated risk management policy – Suggest possible variables to enable proper management – Analysis of costs and expenses
Risk management	– Determine the tools to limit and mitigate the effects – Give priority to one tool as well as the other – Comparison of management variables and the use of alternative tools
Control and monitoring	– Exposing the impacts of the risk assessment process – Increase the effectiveness of solutions by reviewing the environmental risk assessment report – Continuous field measurements – Suggest alternatives to increase efficiency

1.1   Identification

The reference method for describing risks for municipal wastewater treatment plants is the analysis of historical data, during which one must focus on all events causing damage at all potential levels. There is a wide variety of threats that may adversely affect wastewater treatment plants and the environment. These threats can be divided into three categories: (1) malicious threats, those caused by human activities that aim to harm the assets, (2) natural threats caused by natural phenomena such as severe weather and (3) threats unintended, caused by human activities, and their consequences are accidental or unintended [1]. The main objective of identifying risks is to distinguish precisely the mechanism of operation of each facility, to enable the inventory of risk factors and the types and levels of risks that cause them. Risks can be identified for the following stages:

- Determine the characteristics of the facility for which the risk assessment is to be conducted.
- Specialist conversations with the facility manager and employees who are in direct contact with operations.
- Analyze data associated with on-site damaging events.
- Verify the results obtained in several ways (practically, guesses, and with experience).

Table 2 Sample scheme of a risk map

Frequency of appearance	Rare	Risk rarely occurring and causing high losses	Risk rarely occurring and causing low losses
	Often	Risk often occurring and causing low losses	Risk often occurring and causing high losses
		Amount of losses	

1.2 Risk Estimation

Risk estimation consists of determining its amount, which depends on the definition of risk, data availability, validity, and expected results. Several theories of estimation can be distinguished:

- Quantitative numbers—determine the exact numerical value of the risk, such as probability, frequency of occurrence and value of losses, which is to be comparable and standardized.
- Qualitative variables—the risk value is determined based on experience as a relative amount on agreed criteria, the results are presented in a descriptive form.
- Single numbers—focus on just one parameter such as water quality parameters.
- Mixed methods are the most effective strategies, and involve the simultaneous use of quantitative, qualitative, and numerical methods.

An example of a risk identification matrix for the so-called risk assessment map (Table 2):

1.3 Risk Admissibility

In the case of WWTPs, the admissibility of risks is based on the approved legal controls and standards. These are the restriction criteria [6, 7] whose investigation confirms that all events resulting from wastewater treatment will not cause pollution or serious harming as shown in Fig. 1.

- Acceptable risk (low level)—an event unrelated to the overall performance of the facility as being a "daily hazard"; It does not require extreme precautions
- Tolerable risk (medium level)—conditional acceptable risk, when risk mitigation costs are significant or its cost exceeds the cost of losses resulting from the risk.
- Unacceptable risk (high level)—directly related to the critical threats to the environment, health and human life, requiring immediate intervention without regard for costs.

Frequency of appearance	Rare	Risk rarely occurring and causing high losses	Risk rarely occurring and causing low losses
	Often	Risk often occurring and causing high losses	Risk often occurring and causing low losses

Color scale	
Acceptable risk (low level)	
Tolerable risk (medium level)	Amount of losses
Unacceptable risk (high level)	

Fig. 1 Risk hierarchy for the risk map

1.4 Risk Assessment

Determining environmental hazards is a precautionary process to avoid the occurrence of harm or reduce the impact/minimizing injury risk/workers catching disease and causing harm to facilities, equipment and the environmental incubator [5]. These measures enable the achievement of commitment and complete protection in a healthy and safe workplace in all environmental aspects. It is necessary to define the nature of potential risks within the framework of the ability to take solutions to eliminate or mitigate them and control them within the desired levels (Fig. 2).

This is a process that takes place in succession according to arranged stages to clarify the facts to decision-makers and guide them to an effective integrated system for identifying, evaluating and controlling risks. The stages can be mentioned as follows:

- Risk assessment: actual and potential risks, classifying the risks associated with the event according to: probability of occurrence and severity (magnitude).
- Risk Control—includes undermining the risk associated with the event.
- Providing comprehensive information with education and training of employees directly facing risks and supervising and controlling risks.
- Review risk assessment and monitoring of elimination and mitigation processes.

After the evaluation and discussion processes, officials and employees are provided with lists and tables that focus on accurately describing the risks in which the category and the measure of probability and severity are specified, through which the employee is able to objectively distinguish the event and the resulting risk and determine the level of probability and severity on their own. The probability range is 1–5, ranging from an unlikely to a near-certain (predominant) level. While the value scale of severity is 1–5 it ranges from neglected severity to marginal (critical) intensity after assessing the risk value it is matched with the risk assessment matrix.

Level	Likelihood	Actual or expected occurrence frequency
1	Rare	Minor events, exceptional events, no previous cases to be mentioned, errors of non-compliance.
2	Unlikely	Occur occasionally, less than 25% chance of occurrence, uncomplicated process, imbalance checks and balances.
3	Possible	Unknown time of occurrence; chance of occurrence: 25-50%; Previous surveys indicate non-compliance; Interconnected processes with diverse checks and balances; the reasons are outside the control of the station.
4	Likely	Susceptibility to occur at any time; chance of occurrence: 50-75%; Interconnected processes with diverse checks and balances; the reasons are outside the control of the station.
5	Certainly	It happens within expectations, most circumstances happen; chance of occurrence: more than 75%, Interconnected processes with diverse checks and balances; the reasons are outside the control of the station

Fig. 2 Description of likelihood level

The risk assessment measurement is based on the risk value. The description of the severity, timing and persistence of the risk is made through these measurements. Specifically, risk measures are a final summary to identify practical confrontations and harmful actions within the framework.

1.5 Rating the Risk

Risk categorization is a way to get the stage of auditing the size of the risk and indicating the most harmful events, which gives a clear view of the ranking of risk levels. The priority for dealing with the greatest risk is by paying attention to indicators of severity and likelihood. Rating can be easily dealt with by creating a list arranged according to the most severe threat to the least.

Two basic factors can be distinguished in the classification:

- Severity of exposure - the extent of the effects resulting from the risk.
- Probability The possibility of the event occurring due to exposure to risk.

Fig. 3 Simple risk assessment matrix

1.6 Risk Calculations

There are different types of risks to the facilities in the plant. The main focus here is the "health risks" due to mechanical failure of the facility, specifically operational failure and large fluctuations in water quality after treatment during the exposure period [5]. The results of the risk assessment highlighted in the risk matrix are essential for making a sound decision in order to keep the risk under control (Fig. 3). Quantitative risk assessment can be done using the following formula and can be represented by Table 3.

Risk (R) = Likelihood (L) × Severity (L).

L: probability that an adverse event will occur.

S: consequences of the adverse event.

1.7 Risk Communication and Risk Perception

Reporting risks and notifying the authorities is an important part of the risk management and analysis process, with the participation of: management evaluators, employees and the public (Fig. 4).

1.8 Types of Risk in a Municipal Sewage Treatment Plants

Environmental hazards must be considered broadly in all respects, as in addition to the risks related to the operation of the plant and the technological work system,

Table 3 Description of severity level

Level	Characterization of exposure severity
1	• Harmless regular injuries (not causing disability) are recorded and reported to the authority • inor damage to facilities • Natural environmental impact (there is no possibility to address it) • Plant productivity (outflow, water quality) decreased slightly • No risks outside the framework • No public or media concern
2	• Serious injuries at the site causing brief disability (physical, pathological) • Mechanical damage from 1 to 20 times the normal level • Controlled environmental impact (no lasting impact on the food chain, no concern for wildlife or aquatic life) • Curable environmental impacts • Decrease in production from 1 to 20 times the required level • Light level effect outside the station (noise, smoke, odor, obstruction to traffic) • Negative opinions consensus about the public inconvenience • Media reference to environmental impacts
3	• Potential fatal accidents • An operational failure leads to permanent failure • Utilities damage from 20 to 50 times the normal level • Unacceptable environmental impact (it takes one month at most to reduce it) • Little impact on the food chain, concern for wild or aquatic life • Production losses from 20 to 50 times the required level • Controllable impact off-site (special facilities: slight harm, population: curable health impact) • Negative public reaction and media concern
4	• Death at work • Permanent injuries health disability • Facility damage from 50 to 200 times the normal level • High severity environmental risk (6 months maximum to treat and eliminate) • Harmful impact on the food chain, wildlife and aquatic life • Production losses from 50 to 200 times the required level • Significant off-site damage (private facilities: material or operational losses, population: short-term health damage or temporary disability injuries) • Media concern at the country level
5	• Frequent deaths at the site • Permanent injuries (four or more) at the site resulting in permanent disability • Utility damage is more than 200 times the normal level • Wide environmental impact (more than 6 months to reduce or eliminate, up to years) • Production loss is more than 200 times the required level • Severe off-site damage (property, off-site deaths, long-term health impact (epidemic) • Strict public reaction, demands to shut down the operation of the station and the concern of the international community

Fig. 4 Risk analysis model

the wastewater treatment plant is defined by the authorities as a company or service facility and is treated with the same controls and restrictions. The task of assessing environmental risks, in addition to determining the types and characteristics of hazards, also deals with side effects in the event that events are linked in a series that lead to the occurrence of the risk, so the types of risks must be dealt with in a coherent manner (risk entanglement). In practical terms, it is possible for two or more events to occur that have neglected the risk (no effect) and in connection with them create the potential for an actual risk that threatens the environmental components [8].

During hazard characterization the following hazards must be mentioned:

- Financing risks.
- Legal risks.
- Regulatory risks.
- International political risks.
- Technological risks.

2   Methodologies

The type and essence of the research varies over scattered periods of time because the process of collecting historical data and following up the variables takes place simultaneously (a certain period) [5]. The General methodology for managing risks for environmental health is represented by Fig. 5.

The primary objective of conducting a risk assessment is to make decisions about the needs and nature of risk management. Their decision makers are empowered to set priorities and conserve resources in a systematic and comprehensive manner [2]. Observations and interviews are used in obtaining data; this is done with the help of the authorities, employees and the population surrounding the framework (direct confronters). Depending on the type of station and the operations and activities in which it takes place [8], the element to be examined must be determined and the
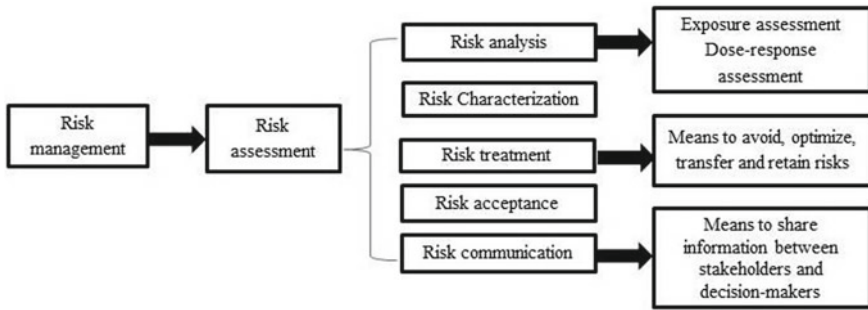
Fig. 5 General methodology for managing risks for environmental health

possible threats and future risks identified. An appropriate identification method for each type must be adopted and linked at the end. This study is based on experiences, observations and investigations. In addition, the focus of the study is descriptive research and an integrated formulation of environmental risk assessment. The research does not make comparisons between station types or links between operations. This study objectively describes the events that threaten the environment. This paper focuses on the reasons that should be studied to identify the threats, classify the level of resulting risks and evaluate the risks in the water treatment process. Two types of data can be distinguished:

Primary data: obtained through studying the current reality (observation and detection) and interviewing workers.

Secondary data: general description of the treatment plant, operation protocols, operational bases, number of workers, tools used and how to store them, and hazardous materials if any.

These data are useful for finding ways to eliminate hazards and reduce occupational risks within the plant environment.

– Based on the information after observation and interviews, the risk is described, its likelihood, level, and consequences.
– The effectiveness of assessing potential hazards in a water treatment plant is by identifying hazards according to the current situation and treatment operations being carried out during the study period (Table 4).

3 Results and Discussions

An integrated operational risk assessment framework is necessary for mechanical and biological processes in the treatment plant. The method of measuring, forecasting and describing the potential risks in more detail that occurs during operations independently and interrelated simultaneously is described to obtain the final product and meet the needs without causing a catastrophic risk to all environmental factors,

Table 4 Steps of risk assessment

Step		Justifications
1	Carry out a risk assessment	The risk assessment decision can be made because:
		• Adding new equipment or materials to existing ones or modifying operating methods
		• A change in the work plan or tasks required at the station
		• Increase the level of the surveillance and public safety program
		• Indicates hazards
		• Detection of a specific event that causes any risk
2	Create a risk assessment team	• A team of experienced and trained professionals is familiar with all aspects of environmental risk assessment
		• The team consists of 6 people at most
		• Developing a plan as an integrated risk assessment team with the participation of representatives who are in direct contact with the plant's operating system
3	Characterization of risks	• Asking questions that can predict common risks
		• Questioning the existence of a risk or problem (energy supply, technical equipment, mechanical operations, human errors, external factors, etc.)
4	Review the risk assessment progress for previous steps (verification)	Working group meeting and discussing the following:
		• The potential severity of the risk (determine the consequences)
		• The potential for risk causing loss (loss of production, environmental components, human factor …)
5	Risks in order of priority	• The severity and probability are presented in the risk matrix to rank the risks in order of priority as follows:
		• E: Catastrophic risks; Immediate intervention is required
		• H: High risk; Urgent administrative action
		• M: Medium risk; Administrative procedure as quickly as possible
		• L: Low risk; Long term procedure
6	Improving action plans	Priority is given to the risks identified for taking control actions and measures. A hierarchy is created to mitigate risks.to a minimum:
		• Elimination
		• Substitution
		• Engineering restrictions
		• Warning signs/explanatory signs and/or administrative controls
		• Personal protective equipment

(continued)

Table 4 (continued)

Step		Justifications
7	Results	Notify the results of the risk assessment to all concerned persons. Existing and new employees working in the workplace assessed should be sensitized to risks and trained in mitigation and prevention measures

as mentioned previously [3]. Risk assessment, analysis and management will effectively define standards and procedures that must be applied within the framework to ensure safe and healthy working conditions. Therefore, it will be the responsibility of all employees and supervisors to be familiar with the standards and procedures followed in any incident within the wastewater treatment plant and how to deal with them in the methods specified in the environmental risk assessment report [4]. The identification of risks resulting from the approved environmental activities must be based on all environmental components (water, soil, air, plant and animal life and human health). Speaking of the authorities' norms of water quality, they should not exceed the critical values (threshold values) for all parameters. Environmental hazards leading to nitrogen and phosphorous pollution of ground and surface water resources should be prohibited. Environmental protection operations are carried out by controlling all polluted sites (periodic samples, continuous monitoring, and scheduled maintenance) to provide a safe working environment inside and outside the site. Risk levels are improved with appropriate treatment over time, so it is important as a result of following the assessment and mitigation stages to reach the desired results [3]. It should be noted that in any element that will be examined and placed under the status of environmental risk assessment, in the selected period of time that will be analyzed, the element is placed under supervision in case it exceeds the quality indicators set by the authorities (correct design, construction, operation and maintenance [8]). This will result in lists in which notes are recorded and the method of treatment for all hazards. This will facilitate the officials to deal with the risks that threaten the components of the treatment plant at any time [5]. For site and design risks to soil, a cumulative risk assessment should be developed after the plant is put into operation based on several major risks related to the site and soil characteristics including soil suitability, seepage volume, and the specific distances between different soil types around the site. Each type of soil individually, and determining the slope that helps determine the direction of the path of pollutants, containing areas exposed to floods [3]. Risks associated with the wastewater treatment plants have been summarized in Table 5.

4 Conclusion

Hazard identification is the essential and essential stage of the risk assessment process in every infrastructure. One must be familiar with the characteristics of the part to be assessed for errors, and knowledge of the detailed operational processes. By analyzing the risk map results, it is possible to observe the events representing the highest likelihood (intensity) of occurrence in the treatment plant and distinguish its location whether it is in the zone of acceptable/undesirable/hazardous risks. The proposed risk assessment method is effective only for wastewater treatment plants that have a structured archive containing high-resolution historical data (detailed, continuously modified, regularly collected, and coherent), as it is the basis for the

Table 5 Events that lead to risks associated with wastewater treatment plants

Element/Action	Event	Factor	Type of risk	Effect (Potential Risk)	Required/suggested actions
Control room	Electrical Hazard	Internal	Qualitative, operational	Fatality, disaster	Permanent maintenance, backup generators
Bar screen	Partial or complete blockage of the barriers	Outside	Qualitative	Changes in inflow, loss of productivity	Regular cleaning of retained materials
Grit chamber	A rise in the sediment layer	External	Qualitative	clogging of grease chamber outflow	Unclogging the outflow
Coagulation	Contact with chemicals, Work at a height off the ground	Internal	Qualitative, operational	Falling from a height (bruises, fractures), Permanent injury up to fatality	Provide workers with safety equipment
Filtration	Working at height around sand filter	Internal	Qualitative, operational	Drowning, Falling, Permanent injury up to fatality	Instruct and warn workers, Provide workers with safety equipment
Backwash pump room	Noise, fracture of the spindle	Internal	Qualitative, operational	Amputations, fractures, hearing disturbance	Ongoing maintenance, checking constantly that pumps are ready
Chlorination	Crash inside the site, leakage of chlorine from the tank	Internal	Qualitative, operational, financial	Staff contact with chlorine, out of service station, Fatality accident	Carefully handle chlorine, protective equipment, regular maintenance
Acid materials	Strong acid vapor	Internal	Qualitative, operational, financial	Inhalation, skin contact might lead to respiratory disorders, Skin sores	Carefully handle, protective equipment
Reservoir	Confined space hazard	Internal	Qualitative, operational	Absence of O_2, hazardous toxic gases	Ongoing maintenance, checking constantly

risk assessment process. Incorporating risk assessment techniques lead to a more standardized approach to assessing and managing systems on site.

References

1. Bavani EB, Tabesh M (2012) Risk assessment and management of wastewater treatment plants (WTPs) using a fuzzy multi-attribute decision-making (FMADM) approach. In: 10th international conference on hydroinformatics HIC, Hamburg, Germany
2. Berglund K, Claesson H (2010) A risk assessment of reusing wastewater on agricultural soils-a case study on heavy metal contamination of peach trees in Ouardanine, Tunisia, Lund University
3. Carroll SP, Goonetilleke A et al (2006) Integrated risk framework for onsite wastewater treatment systems. Environ Manage 38(2):286–303
4. El-Quliti SA, Basarwan R et al (2016) Procedure for hazard Identification and Risk Assessment in Waste-water Treatment Planting Saudi Arabia. Int J Sci Tech Res Eng 1(2):1–10
5. Falakh F, Setiani O (2018) Hazard identification and risk assessment in water treatment plant considering environmental health and safety practice, 06011. In: E3S web of conferences 31, 2018
6. Łój-Pilch M, Zakrzewska A et al (2019) Risk assessment analysis in a municipal wastewater treatment plant. In: Proceedings of the ISMO 2019-innovations-sustanaibility-modernity-openness conference (ISMO' 19), Bialystok, Poland, 22–23 May 2019
7. Łój-Pilch M, Zakrzewska A et al (2019) Risk assessment in municipal wastewater treatment plant. In: E3S web of conferences 100, park 00050
8. Łój-Pilch M Zakrzewska A et al (2018) Risk identification on the example of municipal sewage treatment plant. In: E3S web of conferences 44

Supervisory Leadership in Construction—Critical Review

Pramod Kumar Misra and Jitendra Mohanty

1 Introduction

In assessing an organization's accomplishment or loss, successful leadership plays a significant part. Whenever people operate in communities, leadership's position is illustrated. This is the mechanism by which a community or entity forms and determines its priorities and culture. Leadership is essentially a mechanism of control including leaders' several important functions like empowering, guiding, organizing, and encouraging employees. The emergence of an organizational hierarchy seems to suggest that leadership is not necessarily part of the structure flow. Later Belbin proposed that regardless of structure, unique value of leadership can be developed [1]. In the last decades, project-driven paradigm along with innovative expertise (technical) seems to appear as the major traits of effective construction supervisory leadership (ECSL) in the significant building sector [2]. Conversely, ECSL is responsible for a broad variety of engineering procedures and administrative activities for each construction project (CP). Apart from this, the timely successful accomplishment of the whole project along with its required resource's allocation dependence on ECSL render them as CP's primary decision-maker [3–9]. The plethora of ECSL roles including subordinate's/subcontractor's empowerment, engagement, direction, structured training, constructive criticism, teaching out-of-box thinking, encouragement and so on enhanced with effective discharge of the CP manager's responsibility. The impetus of prevailing milieu, trait and expertise, and their circumstance's characteristics determines the degree of ECSL in CP manager [10, 11]. The present research aims to summarise the leadership literature available in the context of construction

P. K. Misra (✉)
Talent Management, G R Infraprojects Ltd., Gurgaon, India

P. K. Misra · J. Mohanty
School of Management, KIIT (Deemed To Be University), Bhubaneswar, India

industry, explore ECSL style practiced in CP as well as, the best ECSL and style in different construction sector was identified.

2 Literature Review of Leadership Style in the Context of Construction Industry

The industries' crucial aspect, ECSL style (leader's characteristic with relatively enduring trait bundle) helps employees to stay focused and more dedicated to CP [12]. Timely accomplishment of CP is a combined effect of its leadership abilities including emotional intelligence, communication, reward recognition, supportiveness, beliefs [13]. Rowlinson et al. explored CP managers' leadership trait and reported migration of supportive style to directive style along with the migration of stages from the initial to the main stages of CP [14]. Post thorough assessment of connection between leadership, organizational team work and success of project, Odusami et al. reported leadership as a key to projects' successful accomplishment [15].

Using principal component analysis and varimax orthogonal rotation statistical technique Ademola et al. explored the dependence of Nigerian workers' morale on leadership styles (LS) and reported democratic as most practiced LS whereas laissez-faire style least practiced. workers' morale experienced positive effect of democratic LS and indicated an increment in the productivity and satisfaction of workers. Furthermore, communication loss among managers and workers may happen in Autocratic LS, even though it can yield fast results. laissez-faire LS found responsible for development of belongingness and team spirit among workers. Also, they reported articulate, Self-confident, self-assurance, determination, persistence and dependability as top five traits of leader through Relative Importance Index statistical analysis [16].

At various construction jobsite, site supervisors team including foremen, frontline leaders, contractors and worker execute the CP work. With the progresses of CP, complexities arise due to the frequent change of the combination of CP team and that pose challenge during the inception of safety standard including maintaining the safety culture and its promotion awareness [17].

Schwatka et al. imparted 2.5 h customized training based on safety leadership to enhance occupational safety of CP supervisors' including foremen and other frontline leaders' ECSL skill. They analysed the pre and post training feedback from the participants through quasi-experimental prospective switching replications and linear mixed modelling statistical technique and evidenced enhanced ECSL skill after 4-weeks of participation in short-term training [18].

Heavy-duty equipment maintenance workers' and supervisors' communication LS based on occupational safety improved through imparting the Zohar developed coaching-module based on constructive-criticism from different stake holders and
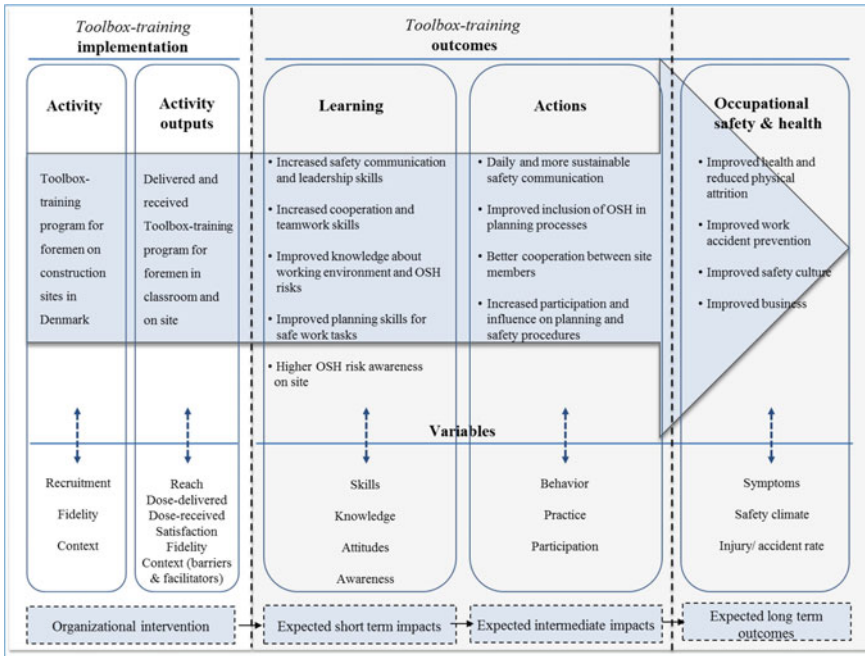
Fig. 1 Organisation of "Toolbox-training program". Courtesy [20]

participants. Also, author reported the rates of accident dropped significantly, awareness improved on use of ear plug along with an enhanced perceptions safety climate for worker [19].

Excluding accumulation of outcome data, in Denmark Jeschke et al. has identified an effective execution of a 22.5-h construction supervisor (CS) training programme "Toolbox-training program" (Refer Fig. 1), which covered subjects such as conflict resolution, communication and occupational safety, in a recently published assessment of the process [20].

During the safety walk-arounds (Participants—supervisors from five healthcare companies, multi-faceted intervention, duration—six-months) assessment, Bronkhorst et al. analyzed the online feedback accumulated. The authors evidenced a remarkable safety participation and safety climate awareness among the participating CS [21].

"Improving Supervisory Leadership" was described as a primary predictor of a good workplace safety environment by CP industry participants of "Safety climate/culture workshop – 2013". Apart from this, in order to enhance the industrial safety standard, they also recommended to designate site-supervisors (with transformational LS in context of safety) as active safety practitioner [22].

From the descriptive analysis, Kreiner et al. reported that the leadership traits plays key role in the selection of leader in Serbian textile industry. Furthermore, importance to specific managerial roles along with influential leadership trait, enhance effective

organizational outcome. Also, from the survey, age of leader was reported as 46 years (most recurrent) and 46.3 years (average). Apart from this, from the factor analysis, author also ranked the different factors as per the following: [23].

1. University degree
2. Organizer, Lawyer, Engineer, and Economist
3. Leadership structure according to social origin
4. The leaders' activities (strategic, operational, internal and external), and their social status
5. Significance of the managers' remarkable performance measures
6. Leaders' attitudes on the role of such managerial positions
7. Thorough assessment of importance of individual ranks
8. Certain stakeholders' interest to be met based on assessment in point 7.

Randeree et al. examined employees' 'commitment to the organization' and 'job satisfaction' of construction sector in the United Arab Emirates (UAE) with response to various LS through case study and reported 'consensus' and 'consultative' as the prevalent LS. Furthermore, in order to improve the employees' retention, authors recommended "fixed-term renewal contracts and structured pay scales" (Beneficiary: junior staff Asian people men, and youngsters; Key issue: security and salary), as well as, "autonomy, flexible working practices and flatter organizational structures" (Beneficiary: citizens of Emirate and Europe, senior staff and women; Key issue: nature of work). Also, they reported impact and efficacy of LS on employee's job satisfaction (strong correlation) and commitment to organization (moderate to strong correlation) significantly dependent on industry type (public or private) and size of organization. Apart from this, for LS assessment and leaders' selection, authors recommended to keep managerial selection mechanism robust with suitable recruitment policies including interview and implementation of psychometric tests or similar. Table 1 represent the top—3 LS chosen by UAE based CP workers whereas the Fig. 2 illustrates presence of LS in UAE based CP industry [24].

Opoku et al. identified sustainability endorsing primary leadership roles in construction industry (Refer Fig. 3), as well as, reported the devising (policies), enactment (procedures) and dissemination (best practices) as three major traits of sustainable CP leadership in UK (Refer Fig. 4). Also, authors recommended such supervisors actions should not be limited the employer only, but also, they need to act as consultant for other industry to promote delivery of sustainable CP. For sustainable

Table 1 Top three LS preferred by employees. Courtesy [24]

Overall	Organization type		
	Consultant	Contractor	Client
D	CT	D	TM
CS	CS	TF	D
TM	TM	CS	CT

Legend: Democratic—D; Team management: TM; Transformational: TF; Consensus—CS; Consultative—CT
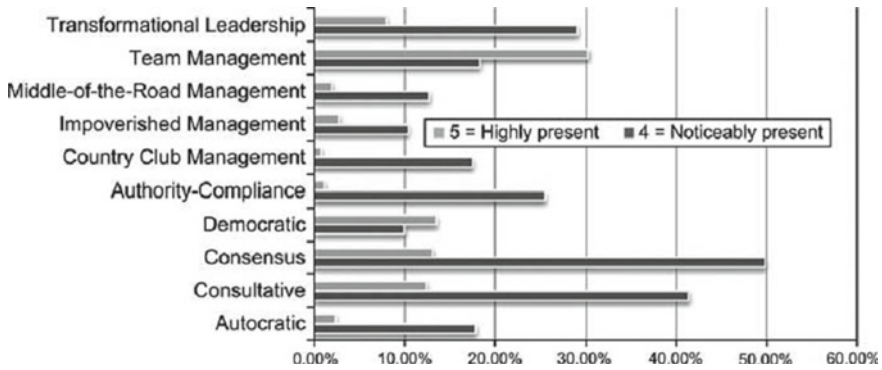
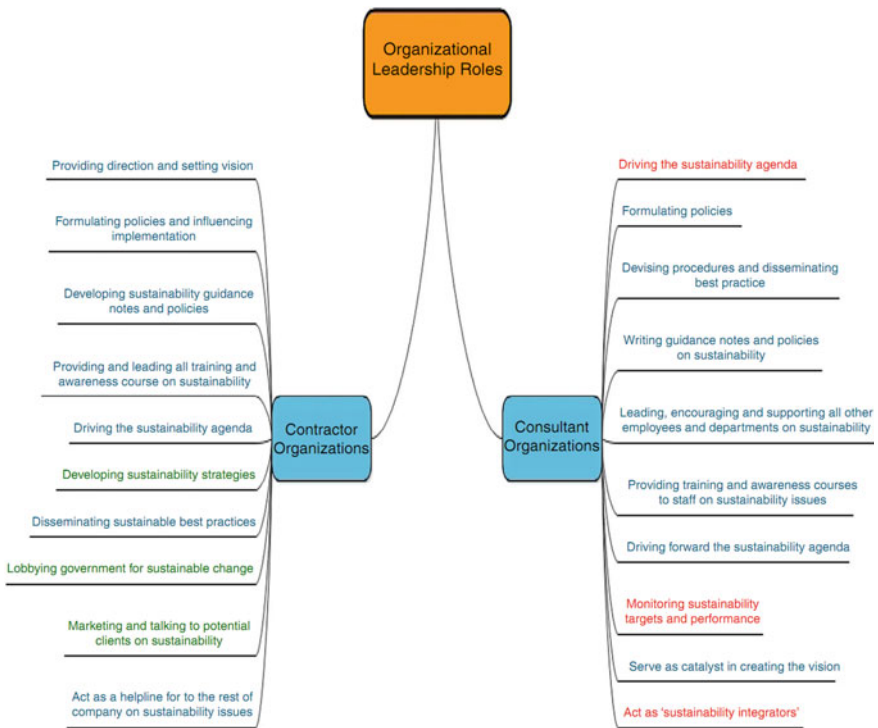**Fig. 2** Illustration of presence of LS in UAE based CP industry. Courtesy [24]

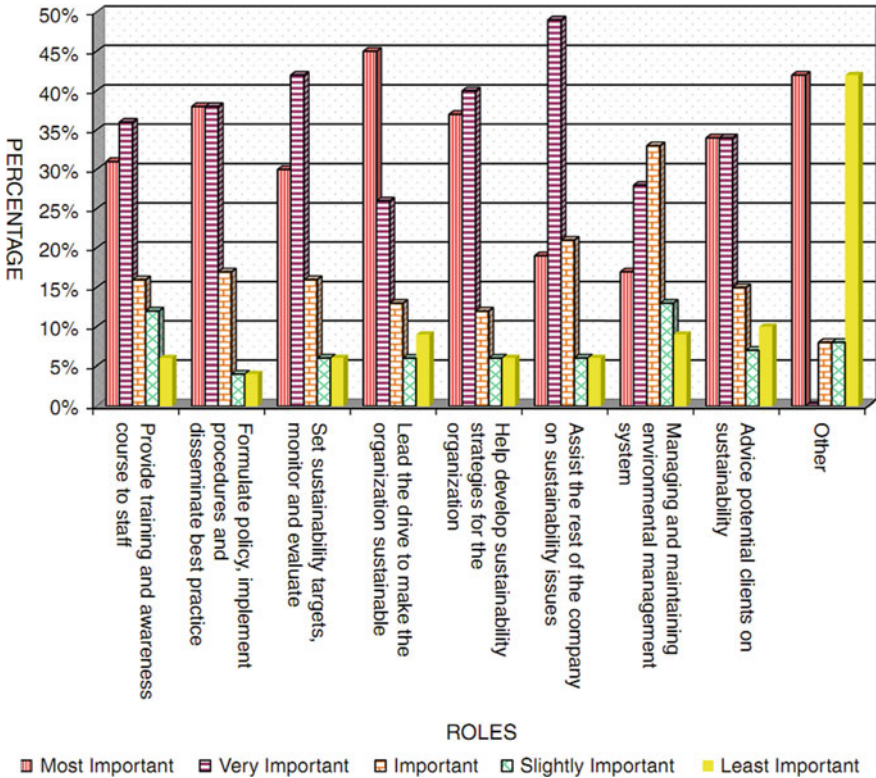**Fig. 3** Roles in construction leaderships endorsing sustainability [25]

Fig. 4 Importance of roles in sustainability of construction leaderships [25]

construction, these leaders required to be visionary, impetus and influential; develop awareness through coaching (policies and guidance notes materials); spearheading in policy making; disseminate best practice by devising appropriate mechanism [25].

Guterresaa et al. developed an empirical relationship model between input variable (education-training and leadership style) output variable (employee performance) mediating variable (work motivation). They applied the Structural Equation Modelling with the Partial Least Square to obtained data (participants: 86) through survey questionnaires from Civil Servants employees (population size: 436) in Ministry of Education, Ti-mor-Leste to analyse the developed model, as well as, used no probability sampling with Purposive-judgment sampling technique. The report shows Education-training programs in the organization helped employees to develop superior leadership style (problem solving and highly skilled) exhibiting enhanced employee performance through work motivation [26].

Daniel et al. identified issue of 57% non-value adding activities (NVA) due to traditional approach to CP faced by construction site at Gibraltar and its contributing factors. Using a combination of quantitative and qualitative research approach, authors modelled Last Planner System (LPS) to minimize NVA based on data

collected through 7 semi-structured interviews and a survey of 31 questionnaires. They highlighted schedules (unrealistic in nature), training (poor core-competency), authorization procedure (remains overdue) and work interruption (community cause) as contributing factors to NVA. They found, for NVA minimization, some LPS principles including pre-planning, regular review and meeting with enhanced communication with all the stakeholders align with the recommendations offered by construction professional. Furthermore, the authors advised to explore possibility to include sub-contractors in the decision-making process in the current practices [27].

Nidadhavolu examined the leadership styles used by the higher-management levels (senior managers, construction engineers, worker supervisors) of three construction companies in India (company A, B and C), and reported the effect of leadership styles through descriptive statistics (60 participants, 25 questions) of on both job satisfaction, as well as, organizational commitment. The results show that the higher-management of company A uses transformational leadership style and the employees are satisfied with the job and committed to the organization. However, employees of company B (laissez-faire leadership style and low supportive—low directive style) and C (laissez-faire leadership style and middle-of-the-road management) were dissatisfied with the organizational leadership trait that leaded to both poor job satisfaction and poor organizational commitment [28].

Opoku et al. surveyed the UK based Construction industries to and reported presence of intra-organisational LS including transactional, transformational, laissez-faire, charismatic, strategic and democratic (Refer Fig. 5). However, strategic LS was found mainly responsible for encouraging sustainability construction practices in the UK based industry. Authors also reported the various behavioural effects appear as the result of diverse LS and for all the circumstances, single LS would not be effective. Hence, the LS needs to be flexible and situational to match all requirement [29].

Liphadzi et al. examined correlation, impact and efficacy between South African CP LS and their project success. They evidenced a strong correlation between LS including transformational, transactional and success of the CP. Also, they found delivery of project is strongly corelated with transformational LS whereas least corelated to democratic LS. However, no correlation was evidenced for South African CP success with autocratic and laissez fair LS. Authors reported the LS is responsible for successful CP accomplishment [30].

Zheng et al. reported high degree of transactional or transformational LS congruence with culture of organization responsible for innovative trait in Chinese construction industry. Further, in contrast with the CP crew with lower innovative trait and stronger organizational culture at higher levels LS, results incongruity of asymmetric type. Under organization culture's innovation scale, the said state can be seen directly. Conversely, if the harmony culture is less than two LS is responsible for higher innovative trait value [31].
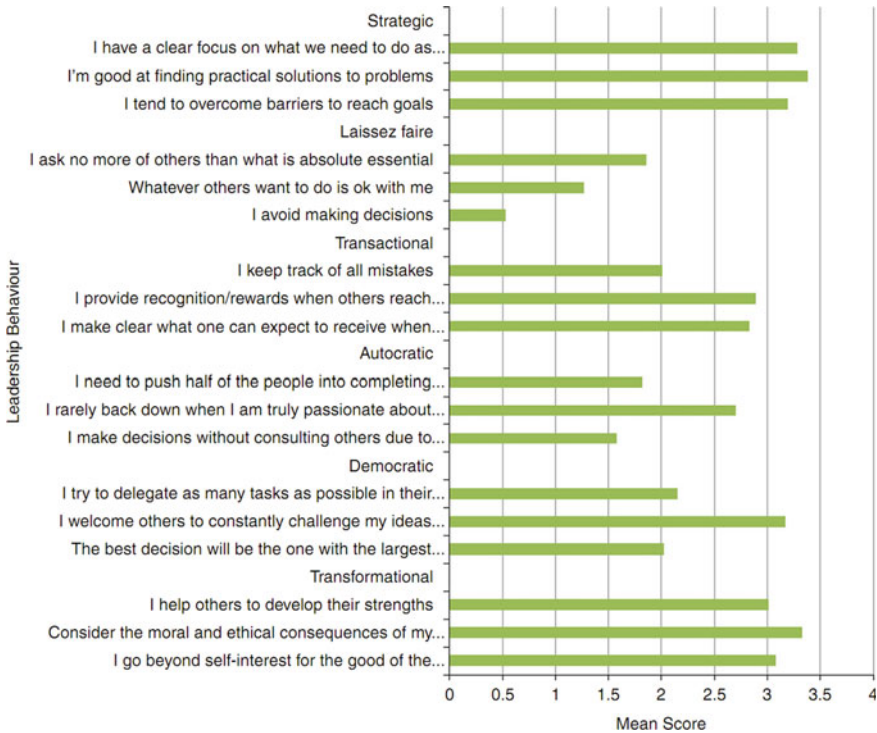
Fig. 5 LS impacting sustainability of construction leaderships [29]

3 Conclusions

The present research summarised the leadership literature available in the context of construction industry, explored ECSL style practiced in CP as well as, the best ECSL and style in different construction sector was identified. It was found that ECSL ensures achievement of organizational goals along with professional achievement and promotion of individual employee in construction industry leading to the productive participation of employees. In construction, different ECSL leadership styles are needed in different situations. Full Range Leadership, Contextual Leadership, Transformational Leadership, Transformational Leadership in context of Occupational Safety, Transactional Leadership, Servant Leadership, and Charismatic Leadership are the various leadership practices were found to be implemented significantly in construction projects. After all, industrial echelons must be able to recognise and apply the requisite leadership styles for firms, circumstances, groups and individuals to be successful among other construction industries and project managers. In addition to that, they need mobility and flexibility, they need to respond to change and at times conflicting circumstances. Thus, ECSL impact everyone from the executive to the newest intern. Diverse styles of ECSL practiced by the leaders

may affect the effectiveness or success of organisations. This comprehensive study provides the ECSL of CP leaders.

References

1. Belbin RM (1997) Team roles at work. Butterworth-Heinemann, Oxford, Boston
2. Pries F, Doree A et al (2004) The role of leaders' paradigm in construction industry change. Constr Manag Econ 22(1):7–10
3. Pandey A, Chaudhary PK, Das BB (2019) Productivity analysis of shuttering works for sewage treatment plant. In: Select proceedings of TMSF 2019. Springer Publications Pte. Ltd. A Book Chapter
4. Akhil RP, Das BB (2019) Cost reduction techniques on MEP projects. In: Select proceedings of ICSCBM 2018. Springer Nature Singapore Pte Ltd. A Book Chapter, pp 495–517
5. Hegde AL, Jain A, Das BB (2021) Resource buffers in construction projects. In: Select proceedings of TMSF 2019. Springer Publications Pte. Ltd. A Book Chapter
6. Paul B, Tondihal S, Das BB (2021) Safety stock in inventory management and wastage analysis at construction sites. In: Select proceedings of TMSF 2019. Springer Publications Pte. Ltd. 2021. A Book Chapter
7. Upadhya PR, Das MS, Das BB (2019) Multi criteria decision making approach for selecting a bridge superstructure construction method. In: Select proceedings of TMSF 2019. Springer Publications Pte. Ltd. A Book Chapter
8. Pradeep RC, Das BB (2019) Methods to monitor resources and logistic planning at project sites. In: Select proceedings of ICSCBM 2018. Springer Nature Singapore Pte Ltd. 2019, pp 793–802. A Book Chapter
9. Shekhar S, Shukla P, Das BB (2021) Developing a standard template for activity linkage and resource estimation of MEP works. In: Select proceedings of TMSF 2019. Springer Publications Pte. Ltd. 2021. A Book Chapter
10. Ismail M, Fathi MS (2018) Leadership in construction: leadership styles practiced in construction project—a review. J Adv Res Bus Manag Stud 13(1):24–30
11. Messick DM, Kramer RM (2004) The psychology of leadership: new perspective and research. Lawrence Eribaum Associates, Publishers. New Jersey
12. Odusami KT, Iyagba RRO et al (2003) The relationship between project leadership, team cooperation and construction project. Int J Project Manage 21:519–527
13. Muller R, Turner RJ (2007) Matching the project managers' leadership style to project type. Int J Proj Manag 25(1):21–32
14. Rowlinson S, Ho T, Yun PK (1993) Leadership styles of construction managers in Hong Kong. Constr Manag Econ 11:455–565
15. Odusami KT, Iyagba RRO et al (2003) The relationship between project leadership, team composition and construction project performance in Nigeria. Int J Project Manage 21(7):519–527
16. Ademola AJ, Olugbenga AO et al (2017) Leadership styles of selected construction managers in Nigeria. Br J Environ Sci 5(4):1–10
17. Lehtola MM, van der Molen HF et al (2008) The effectiveness of interventions for preventing injuries in the construction industry. Am J Prev Med 35:77–85
18. Schwatka NV et al (2019) A training intervention to improve frontline construction leaders' safety leadership practices and overall jobsite safety climate. J Saf Res 70:253–262. https://doi.org/10.1016/j.jsr.2019.04.010
19. Zohar D (2002) Modifying supervisory practices to improve submit safety: a leadership-based intervention model. J Appl Psychol 87(1):156–163
20. Jeschke KC, Kines P et al (2017) Process evaluation of a toolbox-training program for construction foremen in Denmark. Saf Sci 94:152–160. https://doi.org/10.1016/j.ssci.2017.01.010

21. Bronkhorst B, Tummers L et al (2018) Improving safety climate and behavior through a multi-faceted intervention: Results from a field experiment. Saf Sci 103:293–304. https://doi.org/10.1016/j.ssci.2017.12.009
22. CPWR: The Center for Construction Research and Training (2013) Workshop: safety culture and climate in construction: bridging the gap between research and practice. https://www.cpwr.com/safety-culture/workshop-safety-culture-and-climate-construction.
23. Kreiner J, Sajfert D, Terek E, Petrovic N (2018) Determination of personality traits and character of leaders, their selection and efficiency in the textile industry. J Eng Manag Compet (JEMC) 8(2):121–128
24. Randeree K, Chaudhry AG (2012) Leadership—style, satisfaction and commitment an exploration in the United Arab Emirates' construction sector. Eng Constr Archit Manag 19(1):61–85
25. Opoku A, Cruickshank H et al (2015) Organizational leadership role in the delivery of sustainable construction projects in UK. Built Environ Proj Asset Manag 5(2):154–169
26. Guterresa FDC, Armanu L et al (2020) The role of work motivation as a mediator on the influence of education-training and leadership style on employee performance. Manag Sci Lett 10(7):1497–1504
27. Daniel EI, Garcia D et al (2020) Improving construction management practice in the Gibraltar construction industry. In: Pasquire C, Hamzeh FR (eds) 27th annual conference of the international group for lean construction (IGLC), Ireland, pp 539–550
28. Nidadhavolu A (2018) Impact of leadership styles on employee job satisfaction and organizational commitment—a study in the construction sector in India. Masters Theses & Specialist Projects, School of Engineering and Applied Sciences, Western Kentucky University, Bowling Green, Kentucky. https://digitalcommons.wku.edu/theses/2090
29. Opoku A, Ahmed V et al (2015) Leadership style of sustainability professionals in the UK construction industry. Built Environ Proj Asset Manag 5(2):184–201
30. Liphadzi M, Aigbavboa C et al (2015) Relationship between leadership styles and project success in the South Africa construction industry. Procedia Eng 123:284–290
31. Zheng J, Wu G et al (2019) Leadership, organizational culture, and innovative behavior in construction projects: the perspective of behavior-value congruence. Int J Manag Proj Bus 12(4):888–918

Integration Enabled by Virtual Real (VR) Time Simulations of Construction Projects as Lean Application

Jyoti Trivedi, Parth Parihar, and N. Sunil

1 Introduction

Project was defined as: an attempt in which 5Ms i.e. Men, material, money, machinery and methods are organized in a innovative way, to undertake a distinctive scope of work, of given specification, within constraints of cost and time, to achieve constructive change defined by quantitative and qualitative objectives.

Mixed Reality viz; Augmented Reality (AR) and Virtual Reality (VR) are technologies of paramount importance for the Architecture, Engineering and Construction (AEC) sectors as the built environment is inherently associated to three-dimensional (3D) space and AEC professionals depend heavily on visualisation for communication. VR and AR—to a lesser degree—have been used by built environment professionals to support the visualisation of design, construction and city operations since around 1990s [1].

AR and VR are dignified to evolve towards many industries. Important research efforts are made in other fields ranging a wide spectrum from aerospace and advanced manufacturing to medical, psychology etc. These efforts should be processes and taken into consideration to upgrade future AR and VR research efforts. Research gap that identifies the requirements and work needed to make AR and VR more accessible to the AEC sectors [1].

Dunston et al. [2] investigated a VR system for design review information process of hospital patient rooms. The authors indicated that VR-enabled design reviews

J. Trivedi (✉) · P. Parihar
Faculty of Technology, CEPT University, Ahmedabad, Gujarat, India
e-mail: jyoti@cept.ac.in

N. Sunil
Department of Civil Engineering, GITAM Deemed To Be University, Visakhapatnam, Andhra Pradesh, India
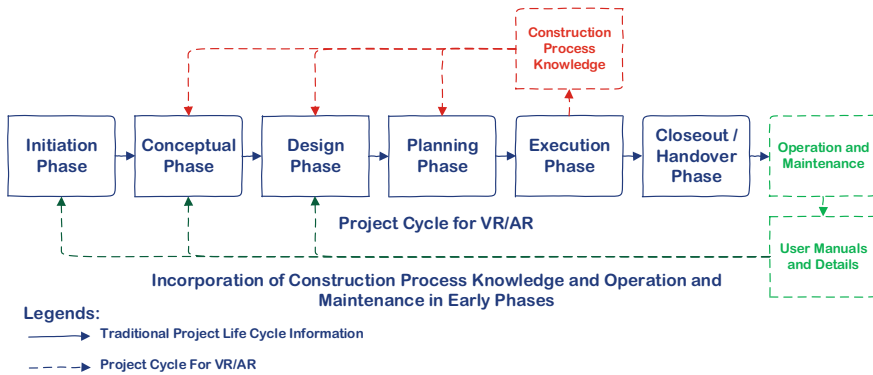e-mail: snandipa@gitam.edu

Fig. 1 Project cycle (PC) for VR/AR

improve interaction and have a higher effect on design decision-making. Boton [3], re-produced a method to support constructability analysis meetings using VR environments. The method upgrades BIM-based construction simulations to be converted into a VR application for visualisations. Authors faced constraints to design support, the main constraint of using AR and VR for design review include the challenge to convert design changes to BIM models and to document the experiences and discussions that the users had within the AR and VR background. A two-way streamline and automatic communication between BIM models used for construction and AR and VR models is required. These constraints have been partially addressed by the work of [4] which proposed a set of theory and categories that enables a bi-directional connection between BIM model and VR application. Thus, this study aims to develop a modest lean based integrated framework of simulation models. The project cycle (PC) of VR/AR itself is an in-build lean construction process knowledge incorporated in early phases of operation and maintenance as given in Fig. 1.

Development of construction project venture control might be viewed as a standout amongst the most complex effort in industry. A task, particularly for a project, has three fundamental concepts. Initially, it is unique: no task previously or after will be the same. Besides, it is attempted utilizing novel procedures: no task previously or after will utilize a similar approach. At last, it is transient: it has a start and an end. Development ventures are normally performed in a changing situation by a wide range of kinds of works [5].

Controlling the development of construction project venture has a lot of vulnerability and is liable to the impact of critical occasions. In this manner, accomplishing successful control for the construction project is exceptionally troublesome.

Specialists engaged with overseeing development manage the creation parts of understanding an office e.g., development of a petrochemical plant, a mine, or an interstate expressway. In this setting, engineers are engaged with creating and effectively planning gainful techniques and procedures for unearthing's and banks, arrive recovery, pipe establishment, passages, streets, and other common works. At the point when ventures turn out to be substantial or complex, they turn out to be harder

to oversee utilizing existing strategies. PC re-enactment procedures are exceptionally compelling in this space at giving the instruments required to outline and examine development forms paying little mind to many-sided quality or size. Utilizing PC recreation instruments, models can be manufactured that speak to the general rationale of different exercises required to develop an office, the assets engaged with doing the work groups, gear, administration, and so on., and nature under which the undertaking is being assembled e.g., climate, ground conditions, work pools, advertise circumstance, and so forth.

The models speak to the way toward building an office and also its condition, and in that capacity can be utilized to grow better undertaking designs, to upgrade asset use, to limit expenses or venture term, and to enhance general development venture administration.

Construction industry is one of the most challenging sectors and involves considerable amount of risks with respect to time, money, health and environment [6–12]. Construction projects are very complex in nature as it involves huge investment, large workforce, and resources and affects stakeholders which are susceptible to failures with respect to quality, budget and schedule. The challenge is to deliver the project of desired quality on time and within the estimated cost.

Controlling the development of construction project venture has a lot of vulnerability and is liable to the impact of critical occasions. In this manner, accomplishing successful control for the construction project is exceptionally troublesome.

Virtual Reality or Real Time Simulations are used majorly in research and study purpose but are not implemented in the construction industry as in manufacturing industry. Animations can only follow Critical Path Method (CPM) as it will follow the same activity flow once created and for any uncertainty it should be added as an activity. The use of CPM is far behind now to move forward is to work on simulations. The Randomness of a simulation by which we can get a new and different result every time and by some sample collection we move towards a result.

The problems solved by Simulation Games can be used to overcome the problems faced by us in our simulations and managing systems for construction industry by generating interactive construction simulation. Thus the study framework is created to develop VDC of site and formulate use of Virtual Reality to create simulations.

The research study of VDC construction operational project cycle (PC) for VR/AR is divided in distinct stages highlighting Sect. 1 as use of discrete event simulation and explaining simulation phases of the modules Figs. 1 and 2, Sect. 2 about Lean production and its approach for construction operation, Sect. 3 Lean Integration application Figs. 4 and 5, Sect. 4 about VR application, Sect. 5 Formulation of simple framework for VR integration and altered with adding the input and output requirements of VR/AR integration in Lean Construction Simulation environment as given in Figs. 6, 7, 8, 9, 10 and 11 as the final result output.
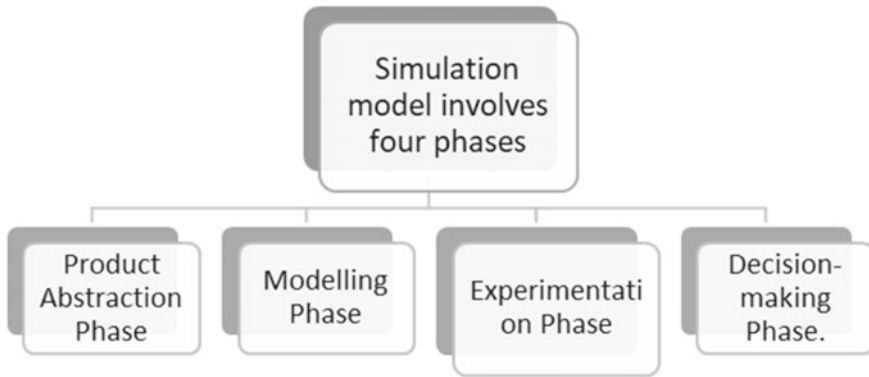
Fig. 2 Phases/stages of simulation model

2 Discrete Event Simulation

Discrete-event simulation can be utilized to demonstrate and break down complex development tasks. This innovation has been accessible since the 1960s and has constantly developed in capacities and programming support. The index of academic distributions identified with DES in development is significant, and numerous analysts know about the innovation. Nonetheless, critical parts of DES right up 'till the present time are broadly misconstrued as for the idea of the tasks that can be examined. In particular, DES is proficient, and especially suited, for tasks that are perplexing. Complex activities, thusly, are hard to approve and subsequently experience issues picking up validity among specialists and chiefs.

The innovation coming about because of as of late finished up look into named DES-based virtual reality (or DES based VR). This is finished with the assistance of circumstances that is sufficiently little to be displayed in adequate detail, yet shows complexities reasonable for DES demonstrating, to represent how the innovation can essentially enhance the approval of complex models (Source: "Discrete-Event Simulation-Based Virtual Reality Environments for Construction Operations: [13]).

The developing of a simulation model framework involves four stages/phases:

- The product brief stage specifying the product to be develops;
- The process brief and modelling stage in which processes, resources, environment, etc., are developed to the product brief and reduced to models;
- The experimentation stage in which the simulation is carried out and the models are experimented; and the decision-making stage as given in Fig. 3.

Despite the fact that the arranging and control methods utilized as a part of arranging development at the task and activity levels are extraordinary, both can profit generously from dynamic three-dimensional (3D) representation. Distinctive individuals in development in this manner comprehend diverse things by the expression "perception". Therefore, the term has been utilized as a part of the writing to allude

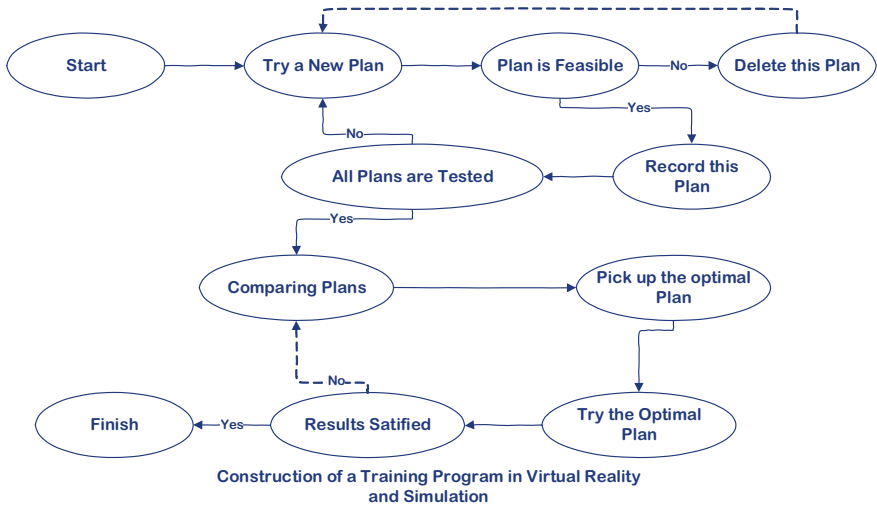Construction of a Training Program in Virtual Reality and Simulation

**Fig. 3** Experimentation stage to decision stage process

to any sort of arrangement of successive PC outlines without thinking about their root or substance. As a result, various PC based visual exercises that can be specifically or by implication utilized for development arranging might be suitably named representation. These are not restricted to the liveliness of development plans [i.e., four-dimensional project cycle (PC) supported outline (4D CAD)], outline examination of development gear in physical re-enactment conditions (e.g., Working Model), perception of get together arrangements and continuous virtual intelligent demonstrating of development hardware (e.g., IV++), situation creation and movement for obstruction investigation (e.g., Bentley Dynamic Artist), development website show based data access over the web utilizing VRML, and dynamic 3D representation of discrete-occasion activities reproductions [14].

3 Lean Production and Integration

Activity Level versus Operations Level Construction Visualization

Representation examine endeavours at the undertaking or action level are roused by the deficiencies of conventional booking and control systems, for example, bar graphs and basic way strategy (CPM) in having the capacity to speak to all parts of development essential for venture level arranging. Perception is accomplished by connecting a 3D computer aided design display speaking to the plan of the office and a development plan. This type of perception has famously turned out to be known as 4D computer aided design. 4D computer aided design centres around the representation of the development item finished the time of its development.
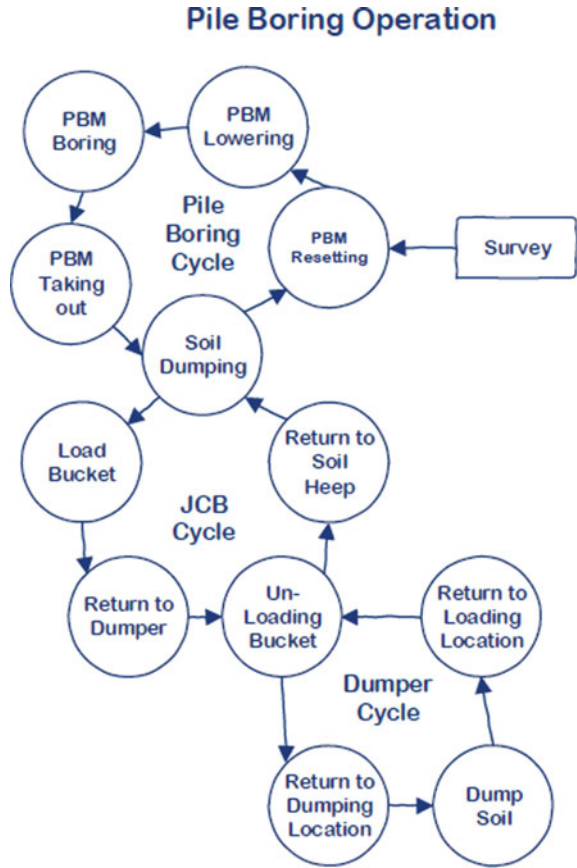
As time progresses, singular parts (computer aided design components) of the office are added to the visual model in their last position and frame as directed by the timetable. 4D computer aided design models consequently pass on what physical segments are manufactured where and in which time allotment. Various research contemplates have investigated and abused such powerful undertaking level 3D perception and recorded its favourable circumstances and advantages.

Conversely, picturing development at the activities level, notwithstanding envisioning the advancing item, includes having the capacity to see the cooperation of the different assets as they assemble the item or play out a help benefit. These assets incorporate, yet are not constrained to, transitory structures, materials, gear, and work as they make the item. At this level of detail, perception of the advancing development item can be accomplished as a side-effect if the activity envisioned is of long length.

To envision an activity, it is important to see, notwithstanding the physical segments of the office, the gear, work force, materials and brief structures required to assemble it. In addition, it is important to delineate the developments, changes,
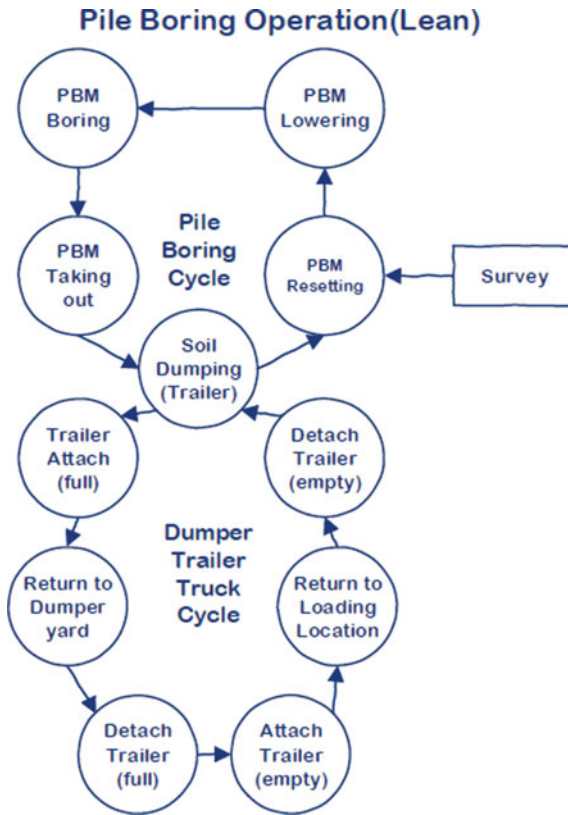
Pile Boring Operation(Lean)

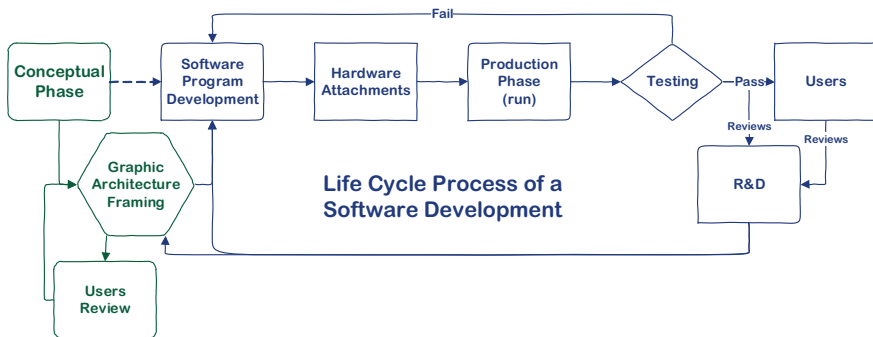**Fig. 5** Cyclone system after application of lean

Fig. 6 Life cycle process of a software development
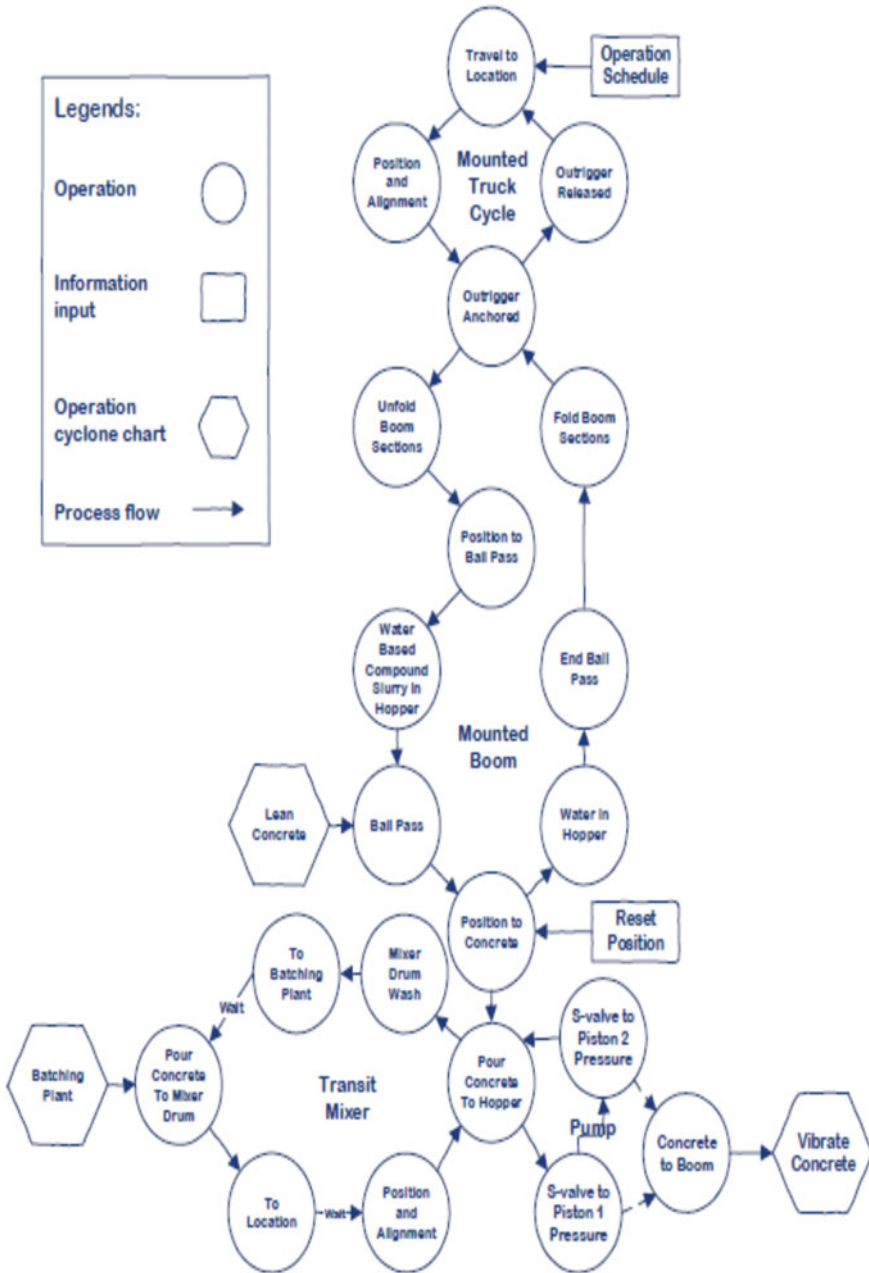
Fig. 7 Existing process

Fig. 8 Alternate process 1
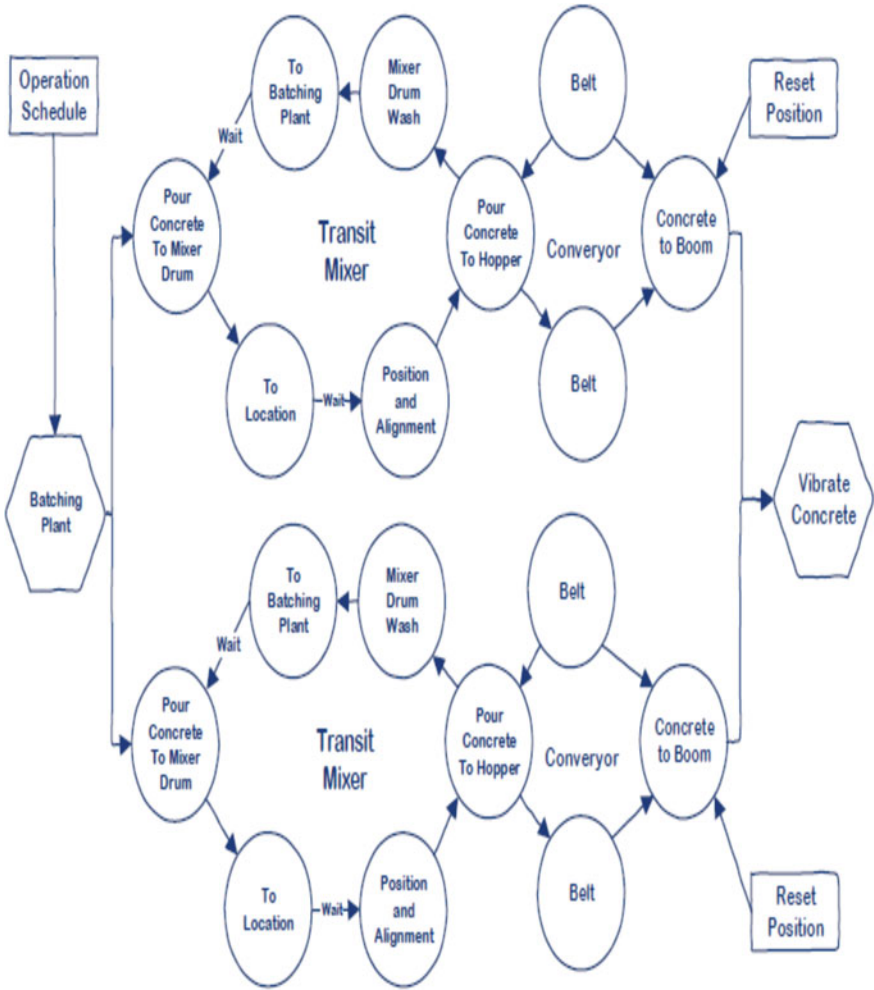
and collaborations between these perception components. The developments and changes must be spatially and transiently precise. To portray smooth movement, visual components must be appeared at the correct position and introduction a few times each second. Issues, for example, directions in 3D space, speed, and increasing speed should be considered [14].
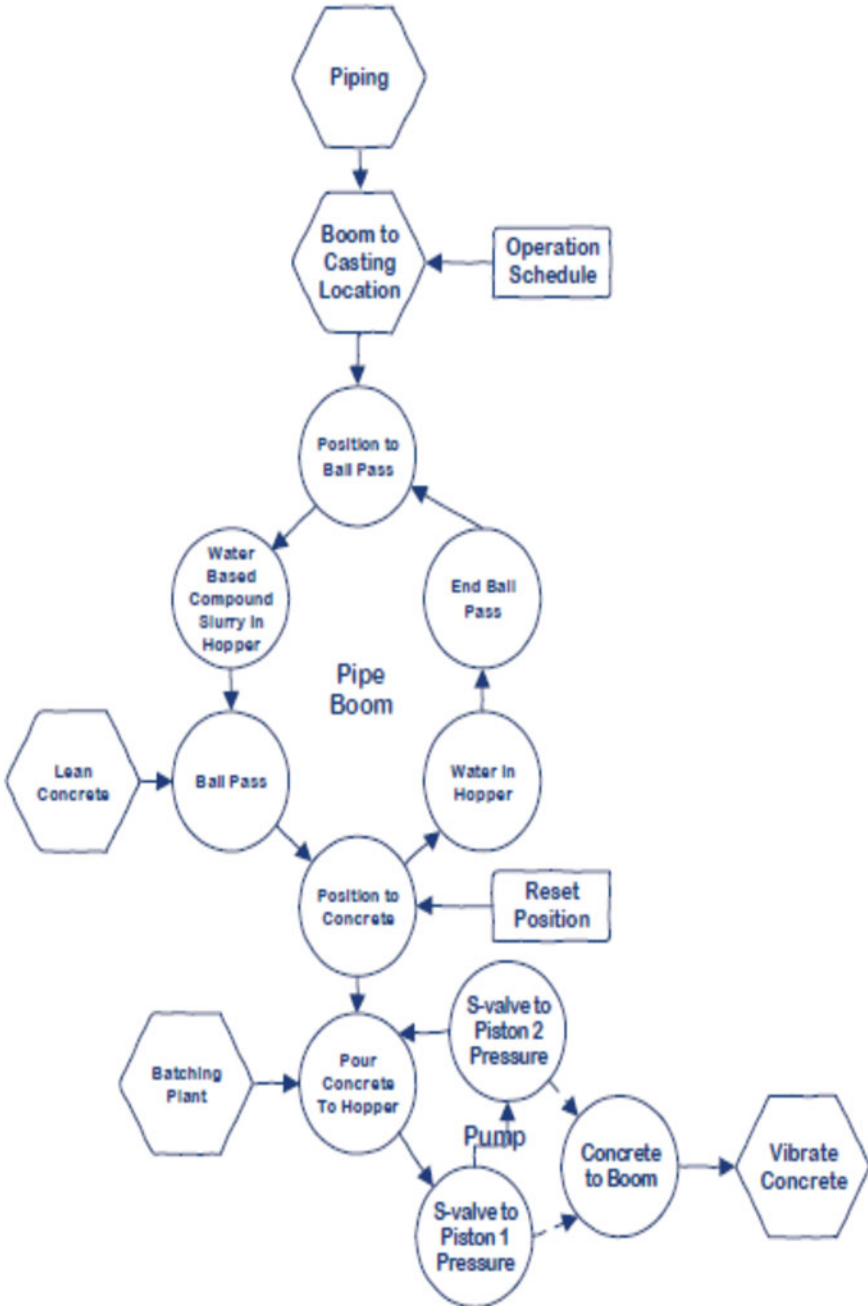
Fig. 9 Alternate process 2

4 Integration as Lean Application

The Cyclone Systems is a way to deal with demonstrating, investigating, and controlling or enhancing development activities depends on a basic stream charting technique that encourages displaying of redundant procedures (e.g., burrowing, black-top clearing, street building, and segmental extension development). Two-dimensional (2D) graphical models are utilized to reproduce gainful yield and to recognize potential lop-sidedness in the utilization of key assets in any given creation process [15].

Recreation activities prompt the upcoming age of PC displaying frameworks for development, where re-enactment assumes a basic part in a cutting-edge vision of mechanization. An example is shown in Figs. 4 and 5.

The above cyclone system shows the existing operation cycle of equipment's for pile boring activity. PBM—Pile Boring Machine.

The above cyclone system shows how the existing operation cycle of equipment is for pile boring activity could be reduced to less equipment's for the same activity, which reduces wastage in equipment, manpower and time as well as takes less amount of space on site by using Lean approach in construction operations. PBM—Pile Boring Machine later to develop the VR integrated lean approach is explained in case studies for metro project Figs. 4 and 5.

5 Virtual Realty Applications

Virtual Reality (VR) is entirely another innovation. It is all the more precisely an arrangement of more established innovations combined. These innovations are basically PC designs/shows, human PC interfaces and reproduction. Virtual the truth is additionally alluded to as Virtual Conditions.

There are various definitions for virtual reality, some of them are expressed underneath:

- A PC was created for reproduction of this present reality.
- The fantasy of support in an engineered domain as opposed to outside perception of such a situation.
- A PC produced reproduction of three-dimensional condition, in which the client can both view and control the substance of that condition.

Virtual reality can likewise be portrayed as the exploration of coordinating man/people with process and data. It comprises of three-dimensional, intuitive, project cycle (PC) produced condition. These situations can be models of genuine or conjured up universe.

5.1 Virtual Reality Systems Can Be Divided into Two Main Categories

5.1.1 Desktop Virtual Reality

PC based virtual reality frameworks are normally classed as Work area frameworks. Work area virtual reality has risen up out of verified PC supported plan. With these frameworks the client sees and associates with the PC spindle to picture on a customary PC realistic screen.

5.1.2 Immersive Virtual Reality

The primary contrast between immersive virtual reality frameworks and work area frameworks is that in immersive virtual reality the PC screen is superseded with a head mounted show unit. Immersive virtual conditions can be depicted as a framework which "drenches" or encompasses the member in a domain. With this framework the client (watcher) feels as in a common habitat. Equipment and programming for this framework are more costly and more modern than immersive virtual reality. This framework requires equipment, for example, super PCs, High determination Silicon Illustrations screens, position GPS beacons, control gloves and head- mounted presentations. Programming can be reason made. For example, a pilot training program which is arranged in a room encompassed by wide edge projection screens.

5.1.3 Virtual Reality Applications

The VR will empower the task group to embrace economical practices of significant development procedures and test different execution techniques in a close reality sense, preceding the genuine beginning of development. It is critical to help the professionals to discover circumstances modelling the development procedure and to create strategies for illuminating them. VR gives a perfect domain to do those works and prepare professionals for the development business. Saying VR perfect simply has the accompanying reasons:

- Virtual the truth is completely intuitive, where the administrators choose what will be done straightaway and how. VR requires the administrators to act and respond and all articles in VR could be effortlessly comprehended.
- Virtual the truth is novel in its accentuation on the experience of the human member. VR centres the administrators' consideration around the experience while suspending mistrust about the strategy for making it.
- Operators associate with virtual reality in the way they would with this present reality. Unique aptitudes don't need to be educated for working the PC.
- Virtual reality gives an energizing and animating instrument for preparing.

VR can be performed over and again. Along these lines, the blunder or crashes can be effectively rectified till an ideal plan is figured it out.

In the development business, late endeavours to utilize Virtual Reality focused on the procedure of outline and development. The principal utilization of VR in the development part was the advancement of walkthrough frameworks. Other conceivable applications have been distinguished in spite of the fact that at various phases of trials and advancements.

In design; Preliminary and detailed design, Space modelling, Interior design, Lighting design, Heating Ventilation and Air Conditioning design, Ergonomics and functional requirements, Space selling, Fire/Safety/Access assessments, landscaping

In construction; Site layout and planning, Planning and monitoring of construction processes, Evaluation of construction scenarios, Rehearsing Erection sequence, Planning Lifting operations, Progress and monitoring, Inspections and Maintenance, Safety Training and skills.

6 Simple Framework for Integration

PC based virtual reality frameworks are normally classed as Work area frameworks. Work area virtual reality has risen up out of verified PC supported plan. With these frameworks the client sees and associates with the PC spindle to picture on a customary PC realistic screen. Thus on the live case study of metro project simple framework for integration were developed as follows:

i.   Identifying various Level of schedule for construction process.
ii. 4D Parametric simulation with respect to time.
iii. Generating Virtual Reality and Augmented Reality scenario for the project life cycle.
iv. Conceptualize the architecture of the software which could be used in a project.

Cases are taken from real scenarios of life cycle process of software development is shown how the issues could be solved using VR/AR in Fig. 6.

6.1 Software Modules

The whole software was divided into 4 Modules Fig. 10.

1. Engine
2. Model
3. Schedule/Planning and Simulation
4. Real Time Simulation.

6.2 VR Simulation Construction Application on Metro Project

This can be used in all phases of construction Conceptualisation, Designing, Planning, Execution, Management, Handover/Close-out and Operations and Maintenance Stage. Which current digitization and automation can't do.

6.2.1 Integrated Concurrent Engineering

All the models of Architecture, structure MEPs, permanent machines and equipment's are modelled on the same platform by which the whole building component's gets integrated.

6.2.2 Client Goals and Project Objective (Case Description-Metro Project)

An observation done at Metro-Link Express for Gandhinagar and Ahmedabad (MEGA), East-West Corridor (Thaltej Gram to Commerce Six road), Pier Casting at Gurukul Junction. Data Collection in consultation with project manager.

According to the existing process and creating alternate simulation process 1 and 2 by Cyclone System chart is prepared in Figs. 7, 8 and 9 which also shows alternate process 1 and 2 for the same activity by changing the operations by Lean approach as explained in Table 1.

Alternate Process 1 the results as by using conveyor plugin transit mixer with 7 cum drum capacity will take 25 min to take position, align, empty concrete and move out of position and more than 1 transit mixer can pour concrete to it, let us suppose 2 transit mixers will pour concrete at same time by standing on either sides of the casting location. So 14 cum concrete will be poured in 25 minutes. For 1 pier concrete round taken will be = 81.68/14 = 5.84 nos. Alternate Process 2, gives us results as by using piping system directly by batching plant in nearby location of approx. 30 cum per hr with a discharge pump of 100 cum per hr. Time taken to cast the pier = 81.68/30 = 2.72 h. Solution depicts less no of resources (equipment) are required for concrete casting. So the final output of pier casting existing process time taken of 10 hours the alternate process 1 and 2 reduction time taken is 2.43 h and 2.72 hours respectively.

6.3 VR Simulation Integrated Software Modules

See Figs. 10 and 11.

Table 1 Case assessment: pier casting process

| Case assessment	Project details-planning assumptions	Output	Issues behind the actual time-solution by Lean Simulation
Pier casting activity = existing process	• Pier cross-section = circular • Diameter of pier = 2 m • Height of casting = 7 m (from top of pile cap) starter height = 0.5 m • Total volume of concreting to be done in pier = 3.14 * 2 * 2 * (7 − 0.5) = 81.68 cum • Boom placer: putzmeister boom placer m36-4 • Pumping capacity = 100 cum per hr • Vol. capacity of a truck = 7 cum number of trucks required to cast the pier = 81.68/7 = 11.66 or 12 number of trucks • Cycle time of 1 truck = 20 min • Cycle time of 12 trucks = 20 * 12 = 240 min = 4 h	• Time taken by boom placer to cast the pier = 81.68/100 = 0.8168 h = 49 min • Time taken by transit mixers to cast the pier = 4 h • Actual time taken to cast the pier = **10 h** (morning 0500 h to afternoon 1500 h)	The reasons behind this actual time: i.i. Traffic management on the junction ii. Traffic barricading of the junction iii. Equipment management like location and position for casting the pier iv. Safety measures taken care-off due to live traffic movement v. Operational planning not done in planning phase which took Site engineers more time vi. Truck movement was difficult at that location
Alternate-process-1 **Module 1**: engine by planning equipment location and routing prior by cyclone chart formulation-lean operation adoption	In this option it gives us the results as by using conveyor plugin transit mixer with 7 cum drum capacity will take 25 min to take position, align, empty concrete and move out of position and more than 1 transit mixer can pour concrete to it, let us suppose 2 transit mixers will pour concrete at same time by standing on either sides of the casting location. So 14 cum concrete will be poured in 25 min. (https://www.youtube.com/watch?v=GRojfcaqna4) For 1 pier concrete round taken will be = 81.68/14 = 5.84 nos	• Time taken for 5.84 rounds of double transit mixers will be = 5.84 * 25 = 146 min. or **2.43 h**	Solution; less number of resources (equipment) are required for concrete casting

(continued)

7 Conclusions

This study shows that VDC construction operational project cycle (PC) for VR/AR can be used in various ways throughout the entire project life cycle of a built asset; which have been formulated in a 5 stage simple framework with use case of metro

Table 1 (continued)

| Case assessment	Project details-planning assumptions	Output	Issues behind the actual time-solution by Lean Simulation
Alternate process 2	Results as by using piping system directly by batching plant in nearby location of approx. 30 cum per hr with a discharge pump of 100 cum per hr	• Time taken to cast the pier = 81.68/30 = **2.72 h**	Solution; less number of resources (equipment) are required for concrete casting

Fig. 10 Software modules
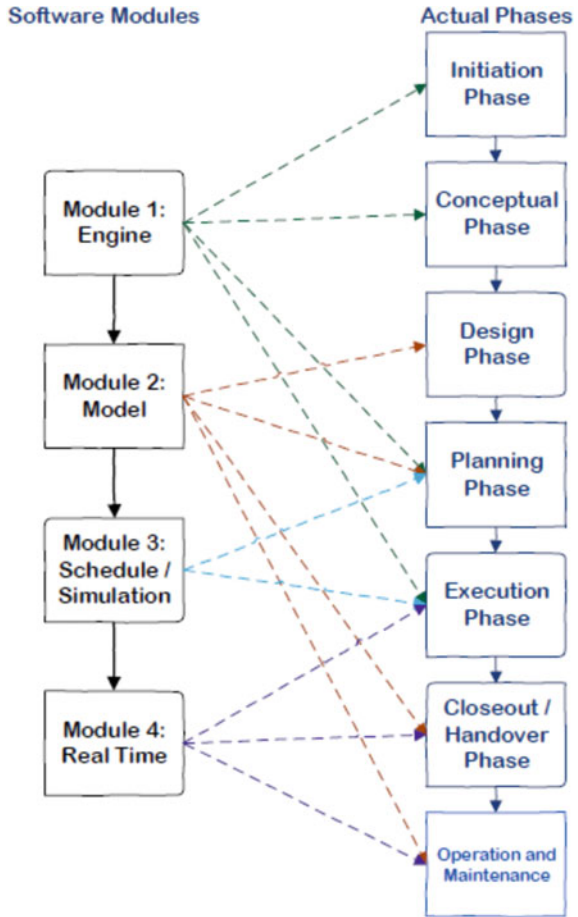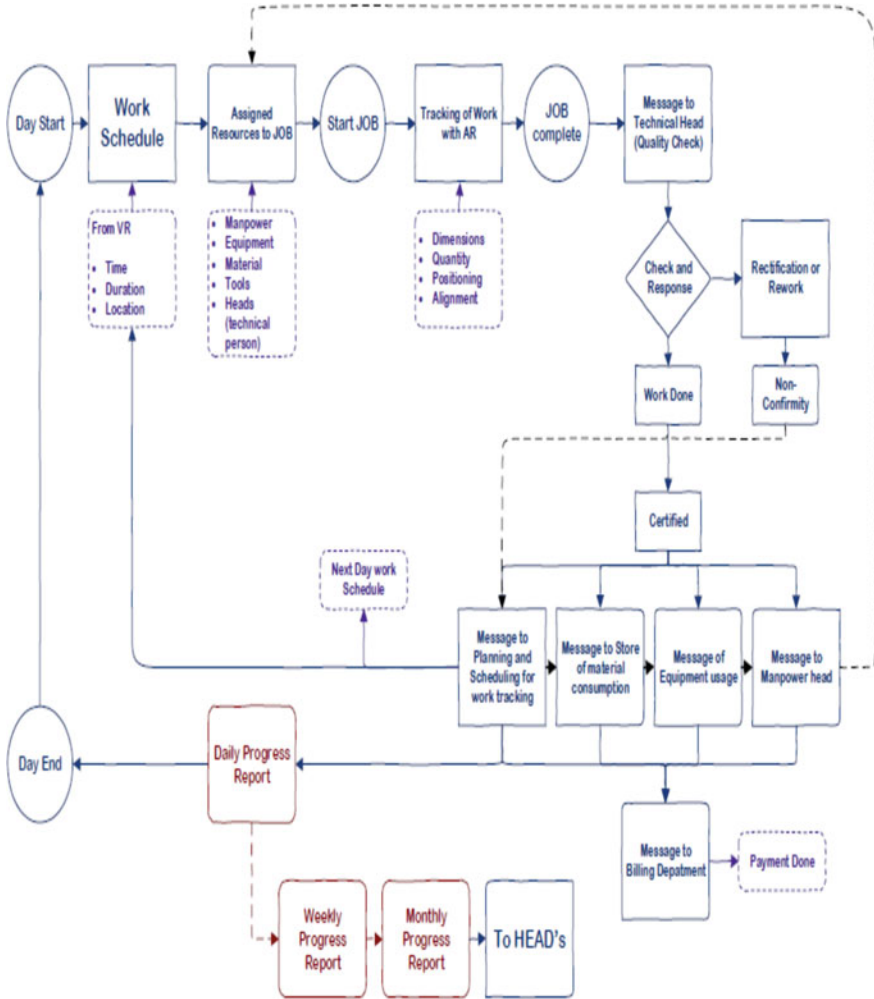
Fig. 11 MIS Flow sample module-4

project: highlighting stage-1 as use of discrete event simulation and explaining simulation phases of the modules Figs. 1 and 2, stage 2 about Lean production and its approach for construction operation, stage 3 Lean Integration application Figs. 4 and 5, Sect. 4 about VR application, stage-5 Formulation of simple framework for VR integration and altered with adding the input and output requirements of VR/AR integration in Lean Construction Simulation environment as given in Figs. 6, 7, 8, 9 and 10 as the final result output. Despite the low levels of adoption, there is an indication that construction companies have a high interest in investing in AR and VR technologies.

The true meaning of simulation for construction projects is to reach the maximum level of schedule with respect to the level of development of model from conceptual phase to the closeout phase and even in operational and maintenance period of the project (Fig. 10).

The 4D parametric simulation has many variables like in real world like uncertainties which gives the idea of actual execution work which is to be done on site in its prior phases so that the constructability of model can be attain and the planning and scheduling can be done accordingly, and every single component gets its values which is going to be the part of project (Figs. 3 and 4, Table 1 case assessment). The results According to the existing process and creating alternate simulation process 1 and 2 by Cyclone System chart is prepared in Figs. 7, 8 and 9 which also shows alternate process 1 and 2 for the same activity by changing the operations by Lean approach as explained in Table 1. Solution depicts less no of resources (equipment) are required for concrete pier casting. So the final output of pier casting existing process time taken of 10 h the alternate process 1 and 2 reduction time taken is 2.43 h and 2.72 h respectively. So similar simulations can be done for Issues of safety, site layout, material and equipment management and management information system etc.; can also be easily solved as they are also the part of model, they also have their planning, and schedule a sample of MIS flow of module-4 is shown in Fig. 11.

Lean can be easily applied on operations of an activity and can be benefited to contractors with the help of cyclone charts as discussed in table-1 and also in Figs. 4 and 5, which gives a reduction in wastes like time, equipment, manpower, space etc.

This study also establishes that AR and VR are not explored in the construction industry and requires research and development. This study presents an predominant research agenda that can be helpful to practitioners on the best way to prepare exploring their control and monitoring efforts to simulation game development. Also, it presents a fundamental lean construction operation simulation concept that sets the direction for exploring necessary research to enable the successful adoption of AR and VR in the construction industry.

References

1. Delgadoa JMD, Oyedelea L, Demianc P, Beachb T (2020) A research agenda for augmented and virtual reality in architecture, engineering and construction. J Adv Eng Inform 45(2020)
2. Dunston PS, Arns LL, Mcglothlin JD, Lasker GC, Kushner AG (2011) An immersive virtual reality mock-up for design review of hospital patient rooms. Collaborative design in virtual environments. Springer, Netherlands, Dordrecht, pp 167–176. https://doi.org/10.1007/978-94-007-0605-7_15
3. Boton C (2018) Supporting constructability analysis meetings with immersive virtual reality-based collaborative BIM 4D simulation. Autom Constr 96:1–15. https://doi.org/10.1016/J.AUTCON.2018.08.020
4. Dris AS, Lehericey F, Gouranton, Arnaldi B (2019) Open BIM based IVE ontology: an ontological approach to improve interoperability for virtual reality applications. Advances in informatics and computing in civil and construction engineering. Springer International Publishing,

Cham, pp 129–136. https://doi.org/10.1007/978-3-030-00220-6_16

5. Li G-C, Ding L-Y, Wang J-T (2013) Construction project control in virtual reality: a case study. J Appl Sci 6(13)
6. Pandey A, Chaudhary PK, Das BB (2021) Productivity analysis of shuttering works for sewage treatment plant. In: Select proceedings of TMSF 2019. Springer Publications Pte. Ltd. A Book Chapter
7. Akhil RP, Bhusan DB (2019) Cost reduction techniques on MEP projects. In: Select proceedings of ICSCBM 2018. Springer Nature Singapore Pte Ltd., pp 495–517. A Book Chapter
8. Hegde AL, Jain A, Das BB (2021) Resource buffers in construction projects. In: Select proceedings of TMSF 2019. Springer Publications Pte. Ltd. A Book Chapter
9. Paul B, Tondihal S, Das BB (2021) Safety stock in inventory management and wastage analysis at construction sites. In: Select proceedings of TMSF 2019. Springer Publications Pte. Ltd. A Book Chapter
10. Upadhya PR, Das MS, Das BB (2021) Multi criteria decision making approach for selecting a bridge superstructure construction method. In: Select proceedings of TMSF 2019. Springer Publications Pte. Ltd. A Book Chapter
11. Pradeep RC, Bhusan DB (2019) Methods to monitor resources and logistic planning at project sites. In: Select proceedings of ICSCBM 2018. Springer Nature Singapore Pte Ltd., pp 793–802. A Book Chapter
12. Shekhar S, Shukla P, Das BB (2021) Developing a standard template for activity linkage and resource estimation of MEP works. In: Select proceedings of TMSF 2019. Springer Publications Pte. Ltd. A Book Chapter
13. Rekapalli PV, Martinez JC (2011) Discrete-event simulation-based virtual reality environments for construction operations: technology introduction. J Constr Eng Manag 137(3)
14. Kamat VR, Martinez JC, Fischer M, Golparvar-Fard M, Peña-Mora F, Savarese S (2011) Research in visualization techniques for field construction. J Constr Eng Manage 137(10)
15. AbouRizk S, Halpin D, Mohamed Y, Hermann U (2011) Research in modeling and simulation for improving construction engineering operations. J Constr Eng Manag 137(10)

Experimental Investigation of Artificial Fiber Reinforced Concrete

Biswabhusan Parida, Ch. Sirajudheen, and Pravat Kumar Parhi

List of Abbreviations

GF   Glass Fiber
GFRC   Glass Fiber Reinforced Concrete
FRC   Fiber Reinforced Concrete
SF   Steel Fiber
SFRC   Steel Fiber Reinforced Concrete

1   Introduction

Concrete is the commonly accepted versatile construction material. It is used extensively in all structural application. It develops strength with age. At the same time, it loses its strength in the form of durability. Concrete was considered to be a durable material. But in recent years, the durability of concrete is being threatened by constant changing environmental conditions. The durability of concrete is major concern [1]. There are various limitations of concrete are low tensile strength, flexural strength, reduced resistance to opening of crack and its propagation. As it's a known fact that because of the brittleness of concrete, the cracks find a way for propagation within it. Hence for overcoming such a situation, the research fraternity has come up with the idea of addition of short, multidirectional and close spaced fibers with the concrete system. Fibers are reinforcing material which possesses various properties. The distribution of discrete fibers plays an important role in the development

B. Parida (✉) · Ch. Sirajudheen · P. K. Parhi
CET, Bhubaneswar, India

P. K. Parhi
e-mail: pkparhi@cet.edu.in

of concrete. They are enhancing the properties of weak, brittle building material [2]. The enhancement of these properties includes ductility, flexural strength, tensile strength, corrosion resistance, lightweight, toughness, damage tolerance, resistance to impact and cracking, durability, permeability and fatigue resistance. It eliminates cracking due to plastic shrinkage and drying shrinkage. In this experimental investigation, the properties of FRC which comprises of artificial fibers like glass fibers and steel fibers were used. The aims and objective of this experimental study is to describe the present state of knowledge and technology of fiber reinforced concrete. In the current study convectional concrete and fiber reinforced concrete are prepared, and the response of the concrete structure to fibers are studied in terms of fresh and mechanical properties.

1.1 Fiber Reinforced Concrete (FRC)

The FRC consists of two phases, i.e. fiber phase and matrix phase. Fiber phase provides strength, in matrix phase fibers are embedded. The matrix phase holds the fiber in the purposive position by giving the FRC its structural integrity. The performance of the FRC determined by the concrete and fiber. The properties of fiber depend on type, geometry, orientation, surface, distribution and concentration of fiber. The fibers in normal concrete have little or no effect on its pre cracking behavior but enhance after post cracking [3]. Fiber is little active during the initiation of a crack but it is very active after the crack by bridging across the crack. It can transfer the force in between both faces of a crack, thus providing strength after the crack. The fibers can hold the concrete together even after considerable cracking. The fibers help concrete to become ductile after the post-cracking. This transformation of concrete from brittle material to ductile material develops other characteristics like energy absorption characteristics.

1.1.1 Glass Fiber

Glass fiber reinforced plastic composites are made of resins, reinforcements, fillers and additives. It exhibits hardness, corrosion resistance, low maintenance requirement, low coefficients of thermal expansion, high fire resistance, lightweight and alkali resistant. It is highly resistant to chemicals. The properties are the same across and along the fiber. As these are resistant to alkali, they exhibit as a kind of reinforcing material but won't corrode like steel fibers. These fibers gets dispersed easily and uniformly within the concrete system and influences a slight improvement towards its compressive strength whereas its more on toughness and impact resistance [4].

1.1.2   Steel Fiber

Steel fibers are fiber reinforcing material, which in combination with concrete provides particular advantages in comparison with traditional steel rebar reinforcement. Steel fiber is cheaper and more comfortable to use than conventional steel rebar. It is short, a discrete length of steel wire having an aspect ratio from about 20–100. The stiffness and tensile strength of concrete increases. The fibers obstruct the propagation of crack by holding both faces of the crack, so deflection becomes minimum in structure. In some cases, steel fiber can completely replace the steel reinforcement in concrete. The usage of steel fiber in high volume should be avoided. It includes the problem of electrical conductivity, corrosion, and high magnetic field.

1.2   Literature Review

Mahmoud Mazen Hilles and Mohammed M. Ziara [5] in their paper entitled "Mechanical behavior of high strength concrete reinforced with glass fiber" have studied the effects of alkali-resistant glass fiber with different contents of 0.3, 0.6, 0.9 and 1.2% by weight of cement. They tested for compressive, splitting tensile and flexural strengths of high strength concrete. The maximum compressive strength was achieved at 1.2% of fiber i.e. 13.14% increase over the control mix. The splitting tensile strength has achieved at 1.2% fiber i.e. 63.22% increase. The flexural strength was achieved at 1.2% fiber i.e. 52.36% increase.

J. D. Chaitanya Kumar et al. [6] in their paper entitled "Experimental Studies on Glass Fiber Concrete" have studied fiber of 0.5, 1, 2 and 3% of cement by adding as an admixture. The addition of 1% glass fiber shows increase in workability. The compressive strength, flexural strength, split tensile strength increases for M-20 concrete at 7 and 28 days.

Syed Mazharul Islam et al. [7] in their paper entitled "Fiber Reinforced Concrete Incorporating Locally Available Natural Fibers in Normal and High Strength Concrete and a Performance Analysis with Steel Fiber-Reinforced Composite Concrete" have studied the properties of FRC consisting of steel and coconut fibers for both normal strength concrete (NSC) and high strength concrete (HSC) of 0, 0.5 and 1.0% fiber volume. The compressive strengths at 28 days were taken as 28 MPa for normal strength concrete and 48 MPa for high strength concrete. The workability of fresh concrete reduces due to addition of fibers. In the case of CFRC, the workability reduces excessively depending on the absorption, surface area, shape and size of the fiber. The flexural strength of NSC was increased by 0.5 and 1.0% coir fibers. The flexural and tensile strengths of HSC was increased by 0.5% coir fibers.

Job Thomas and Ananth Ramaswamy [8] in their paper entitled "Mechanical Properties of Steel Fiber-Reinforced Concrete" have studied the influence of steel fibers on mechanical properties of concrete. They have considered three grades of concrete, namely, normal strength (35 MPa), moderately high strength (65 MPa), and high-strength concrete (85 MPa) with various fiber dosages 0, 0.5, 1.0, and 1.5%.

The 10% steel fiber increases the overall properties of concrete. There was a 40% increase of tensile strength and 30% increase of strain corresponding to the peak compressive strength.

2 Experimental Programme

2.1 Materials Used

Cement: 53 Grade ordinary Portland cement (Mahasakti Cement) is used. It is conforming to IS 4031 and IS 12269–2013.

Water: It is the essential ingredient of the concrete. It is free from impurities like oil, alkalinities, acids.

Coarse Aggregate (CA): the locally available machine crushed aggregate of 20 mm down and 10 mm down are used. The coarse aggregate is tested for various properties. It is confirming to IS 383-2016.

Fine Aggregate (FA): The locally available fine aggregate isused. It is tested for different properties as per IS 383-2016 (Tables 1 and 2).

Table 1 Physical properties of cement

Name of test		Result
Fineness (m^2/kg)	Specific surface	295
Specific gravity		3.17
Setting time (minutes)	Initial setting time	165
	Final setting time	240
Soundness test	Le Chatelier method (mm)	1.0
	Auto clave (%)	0.074
Compressive strength (MPa)	3 days	38
	7 days	48
	28 days	60

Table 2 Physical properties of aggregate

Particulars	Fine aggregate	Coarse aggregate
Sieve analysis	Zone III	Table-7 of IS 383:2016
Fineness modulus	3.348	7.468
Specific gravity	2.62	2.82
Water absorption (%)	0.9	0.2
Free (surface) moisture (%)	1.2	5

Table 3 Physical properties of fibers

Characteristics	Description of fiber	
	Glass fiber	Steel fiber
Type	AR glass fiber	Crimped micro SF
Tensile strength	7200 MPa	1100 MPa
Length	12 mm	25 mm
Diameter	0.5 mm	0.50 mm
Aspect ratio	24	50

Super Plasticizer (SP): Sikaplast 4231 NS was used as an admixture.

Glass Fiber: Monika International, Jaipur, Rajasthan manufacture the Alkali Resistant MONEX glass fibers. Cem-FIL was used in the experimental investigations and was purchased from Monika International. This fiber was included at four different percentage i.e. 0, 0.5, 0.7 and 0.9%.

Steel Fiber: The crimped micro steel fiber was purchased from Sudheswar Enterprises, Rajgangpur, Odisha (India). This fiber was included at four different percentage i.e. 0, 0.5, 1 and 1.5% (Table 3, Figs. 1 and 2).

Fig. 1 Glass fiber

Fig. 2 Steel fiber

Table 4 Quantity of material per cubic meter of concrete

Cement	413 kg/m^3
Water	165 L/m^3
FA	625 kg/m^3
CA	1320 kg/m^3
SP	2.1 L/m^3
W/C	0.40

Table 5 Mix designation

Fiber	Control mix	Glass			Steel		
Fiber content (%)	0	0.5	0.7	0.9	0.5	1	1.5
Mix Designation	CC	GF 0.5	GF 0.7	GF 0.9	SF 0.5	SF 1	SF 1.5

2.2 Mix Proportion

Mix design of M-30 concrete is based on IS 10262-2009. In FRC, the percentage of fibers by mass of cement was added to the mix and the same amount of coarse aggregate was deducted from the total (Tables 4 and 5).

2.3 Tests on Concrete

The tests on concrete are corresponding to IS: 516-1959.

Workability: Slump cone method is used to measure workability. The test procedures are in accordance with IS 1199-1959.

Compressive strength: 150 mm × 150 mm × 150 mm cube size was selected for this test. This test was conducted on the digital compression testing machine of 3000 KN capacity (Fig. 3).

Compressive stress (MPa) = load at failure (N)/surface area of the cube (mm^2).

Flexural Strength: 500 mm × 100 mm × 100 mm beam size was selected. Two-point loading was applied at the middle third of the span. The following formula was used to calculate the flexural strength (Fig. 4).

f = PL/bd^2.

Where; P = ultimate load applied (N),

L = the effective length of the specimen i.e. 400 mm,

b = breadth of the specimen i.e.100 mm,

d = depth of the specimen i.e. 100 mm.

Split Tensile Strength: A cylinder of 150 mm diameter and 300 mm height was selected. The following formula was used to calculate the split tensile strength (Fig. 5).

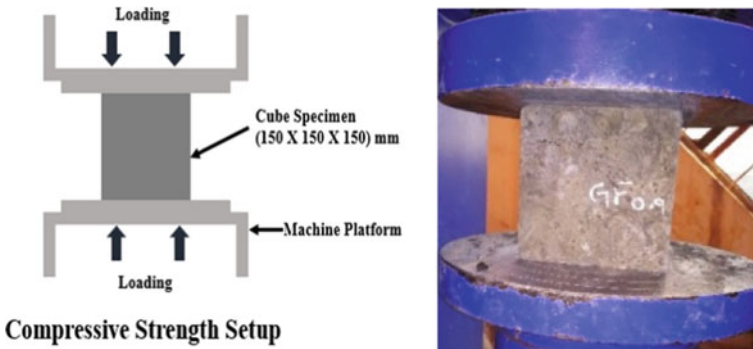Split tensile strength = 2P/πdL.
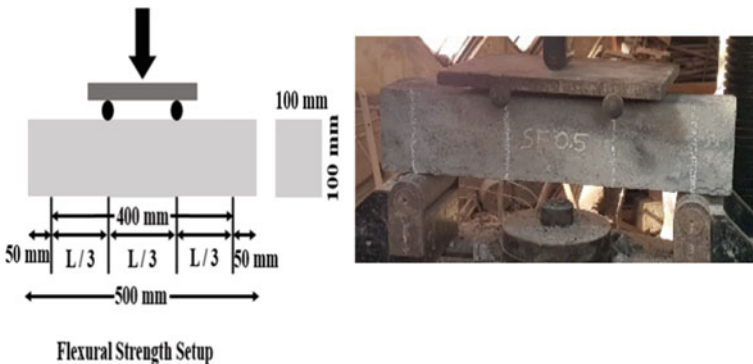

Fig. 3 Compressive strength of cube

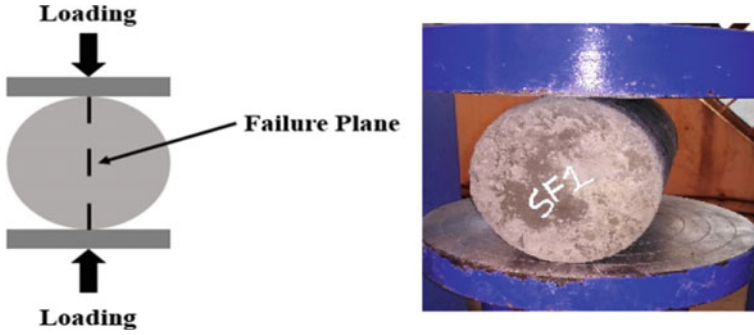
Fig. 4 Flexural strength of beam

Fig. 5 Split tensile strength of cylinder

Where; P = ultimate load (N),
D = Diameter of the cylinder i.e. 150 mm,
L = Length (or) height of the cylinder i.e. 300 mm.

3 Results and Discussions

3.1 Workability

The increase of fiber content decreases the workability of concrete. The workability was maintained at medium level. The average decrease of workability in comparison with the control mix was about 17.05% for GFRC and 20.16% for SFRC. The workability reduces due to the higher surface area of glass and steel fiber (Fig. 6, Table 6).
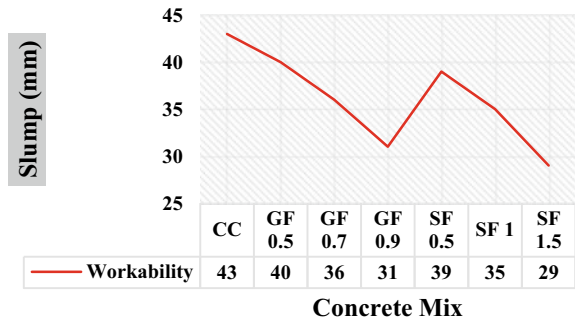

Fig. 6 Variation of workability

	CC	GF 0.5	GF 0.7	GF 0.9	SF 0.5	SF 1	SF 1.5
Workability	43	40	36	31	39	35	29

Concrete Mix

Table 6 Slump value

Mix	Slump (mm)	Drop
CC	43	–
GF 0.5	40	7%
GF 0.7	36	16%
GF 0.9	31	28%
SF 0.5	39	9%
SF 1	35	19%
SF 1.5	29	33%

3.2 Compressive Strength

From the Table 7, the 7 and 14 days strength of GFRC and SFRC are more than normal concrete except 0.5 and 0.7% glass fiber and 1.5% steel fiber. When steel fiber content increases beyond 1%, the strength decreases. In case of glass fiber, at 0.5 and 0.7% fiber content the strength decreases.

The increase of fiber content increases the compressive strength of GFRC. The crack arresting ability of glass fiber increases the compressive strength. The uniform distribution of glass fibers reduces crack. The glass fibers are not effective in concrete matrix at 0.5 and 0.7%.

The increase of fiber content decreases the compressive strength of SFRC. When steel fiber content increases beyond 1%, the strength decreases. The compressive strength decreases due to the pull out of fibers and more fibers than optimum fibers create extra voids in concrete (Fig. 7, Table 7).

Table 7 Compressive strength

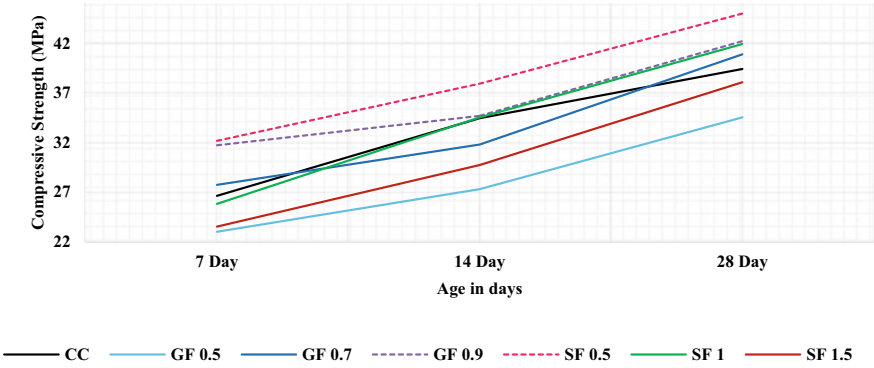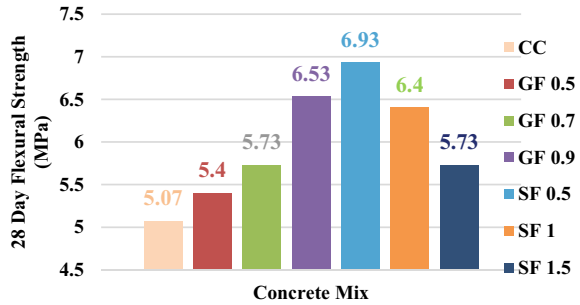| Mix	Compressive strength (MPa)			
	7 days	14 days	28 days	% Change of 28 days strength
CC	26.59	34.44	39.41	–
GF 0.5	22.96	27.26	34.52	−12.41
GF 0.7	27.7	31.78	40.89	3.76
GF 0.9	**31.7**	**34.67**	**42.22**	**7.13**
SF 0.5	**32.15**	**37.93**	**45.01**	**14.21**
SF 1	25.78	34.52	41.93	6.39
SF 1.5	23.48	29.7	38.07	−3.40

Fig. 7 Variation of compressive strength

Fig. 8 Variation of flexural strength

3.3 Flexural Strength

The flexural strength is governed by the loading rate, length of fiber, shape, size and length of the span, bond stress between the matrix. The strength is maximum at 0.9% glass fiber content and 0.5% steel fiber content. The fibers were fully utilized in the post-cracking stage, then it increases the ductility and toughness of all kinds of FRC. The concrete took full advantage of fibers in flexure. So, in every fiber content, the flexural strength increases over the flexural strength of normal concrete (Fig. 8, Table 8).

3.4 Split Tensile Strength

The shorter fiber with optimum fiber content achieves proper distribution in the matrix. It resists cracking due to tensile load in the cylinder. The strength is maximum at 0.9% glass fiber content and 0.5% steel fiber content. The more abundant fiber with more fiber content gives void in the concrete. As a result, multiple cracking

Table 8 Flexural strength

Mix	Flexural strength (MPa)		Difference of 28-day strength
	7 day	28 day	
CC	3.87	5.07	–
GF 0.5	4	5.4	6.51%
GF 0.7	4.6	5.73	13.02%
GF 0.9	**5.2**	**6.53**	**28.80%**
SF 0.5	**5.6**	**6.93**	**36.69%**
SF 1	4.93	6.4	26.23%
SF 1.5	4.27	5.73	13.02%

is present in the cylinder. Similarly, a shorter length of fiber with less fiber content provides less bond strength, which may pull out from the fractured portion of the cylinder. The increase of fiber content increases the split tensile strength of GFRC. The increase of fiber content decreases the split tensile strength of SFRC (Fig. 9, Table 9).
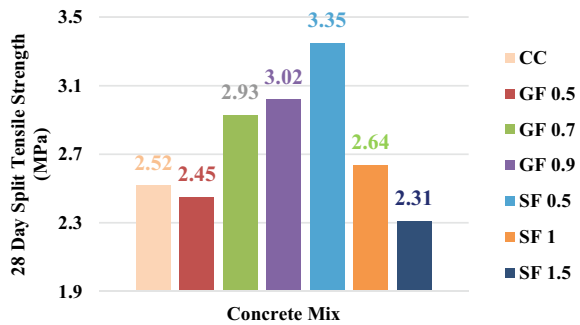
Fig. 9 Variation of split tensile strength

Table 9 Split tensile strength

Mix	Split tensile strength (MPa)		Difference of 28-day strength
	7 day	28 day	
CC	1.82	2.52	–
GF 0.5	1.89	2.45	−2.78%
GF 0.7	2.1	2.93	16.27%
GF 0.9	**2.29**	**3.02**	**19.84%**
SF 0.5	**2.31**	**3.35**	**32.94%**
SF 1	1.89	2.64	4.76%
SF 1.5	1.67	2.31	−8.33%

4   Conclusion

In this research, different fiber such as glass and steel is investigated. The fibers are added with the percentage by cement mass. The experiments have been performed to investigate the various fresh and mechanical properties of fiber reinforced concrete. The fresh properties are workability in terms of slump cone test. The mechanical properties are compressive strength, flexural strength, and split tensile strength. These properties are also compared with those of ordinary concrete.

The fresh properties reveal:

In GFRC and SFRC, the workability remains at medium level. The workability was maintained throughout the experiment using admixtures. It reduces bleeding of water and segregation of coarse aggregate by giving a homogenous mixture.

The mechanical property shows that:

The compressive, flexural and tensile strength of FRC can be increased by 0.9% glass and 0.5% steel fibers.

The compressive strength, flexural strength and split tensile strength of 0.9% GFRC improved by 7.13%, 28.80%, and 19.84% respectively than that of normal concrete. The glass fiber improves crack arresting ability of concrete.

The compressive strength, flexural strength and split tensile strength of 0.5% SFRC improved by 14.21%, 36.69%, and 32.94% respectively than that of normal concrete. The steel fiber improves the cracking due to a tensile load of the cylinder.

These fibers increase the overall performance of concrete without any design changes. These fibers fill up the extra voids in concrete. It increases the durability of concrete by preventing the entry of chemical and other substances. It restricts the growth of crack under load.

References

1. Sumukh EP, Goudar SK, Das BB (2021) Predicting the service-life of reinforced concrete by incorporating the experimentally determined properties of steel-concrete interface and corrosion. In: Select proceedings of TMSF 2019. Springer Publications Pte. Ltd., pp 399–417. A Book Chapter
2. Yadav S, Das BB, Goudar SK (2019) Durability studies of steel fibre reinforced concrete. In: Select proceedings of ICSCBM 2018. Springer Nature Singapore Pte Ltd., pp 737–745. A Book Chapter
3. Goudar SK, Shivaprasad KN, Das BB (2019) Mechanical properties of fiber reinforced concrete using coal-bottom ash as replacement of fine aggregate. In: Select proceedings of ICSCBM 2018. Springer Nature Singapore Pte Ltd., pp 863–872. A Book Chapter
4. George RM, Das BB, Goudar SK (2019) Durability studies on glass fiber reinforced concrete. In: Select proceedings of ICSCBM 2018. Springer Nature Singapore Pte Ltd., pp 747–756 A Book Chapter
5. Hilles MM, Ziara MM (2019) Mechanical behavior of high strength concrete reinforced with glass fiber. Eng Sci Technol Int J

6. Chaitanya Kumar JD, Abhilash GVS, Khasim Khan P, Manikanta Sai G, Taraka Ram V (2016) Experimental studies on glass fiber concrete. Am J Eng Res (AJER) 5(5):100–104
7. Islam SM, Hussain RR, Abu Zakir Morshed Md (2011) Fiber-reinforced concrete incorporating locally available natural fibers in normal- and high-strength concrete and a performance analysis with steel fiber-reinforced composite concrete. J Compos Mater 1–12
8. Thomas J, Ramaswamy A (2007) Mechanical properties of steel fiber-reinforced concrete. J Mater Civ Eng ASCE
9. Rai A, Joshi YP (2014) Applications and properties of fibre reinforced concrete. J Eng Res Appl 4(5): 123–131. ISSN 2248-9622 (Version 1)
10. Dawood ET, Hamad AJ (2013) High performance lightweight concrete reinforced with glass fibers. In: 12th scientific conference 4–5 May 2013, AL-Mansour Journal/No.20/Special Issue
11. Dawood ET, Ramli M (2018) Production of durable high strength flowable mortar reinforced with hybrid fibers. Chall J Concr Res Lett 9(1):10–20
12. Dsouza N, Patil NN, Rajashekhar Swamy HM (2018) Strength and durability aspects of steel fibre reinforced concrete. Int J Civ Eng Technol 9(7):948–957
13. Report on fiber reinforced concrete reported by ACI Committee 544

Wet Press Technique for Precast Concrete Products

Uddesh U. Gaude and K. G. Guptha

1 Introduction

Conventional method of production of precast concrete products such as pavers, kerb stone, drainage cover, etc. is slow and labour intensive leading to substantial overheads. Wet press is the process used for producing precast concrete unit with better strength and durability has become popular in overcoming foresaid deficiencies. Careful aggregates selection is of vital importance for achieving better quality products [1, 2]. The dust or 'fines' are used for achieving close-texture and smooth surface on the finished product [3–5]. Unlike conventional concrete mixing process water-cement ratio is not critical in these types because extra water is drained off during pressing. While a required quantity of water for cement hydration and to ensure mix flows into the moulds easily without vibrations is added. Immediately after pressing the product achieves sufficient strength to be able to handle and stack. This property of removing from mould immediately after pressing makes the mould available for next unit, which increases the production rate. The pressing time generally ranges from 10 to 30 s. This means that moulds can be reused within 50 s; where as in conventional type it requires time to harden and de-moulded only next day of casting. To achieve highest productivity within confined manufacturing space, wet press manufacturers can employ turntable style station machines (carousel) for accomplishing the mould-filling, pressing/drainage, and de-moulding phases. Lifted products can be stacked on edge close to each other (not touching). Property of stacking on the vertical edge also makes it possible to cure in minimum space. These concrete units are stacked in dry area for overnight curing and then transferred to stacking area for normal completion of curing [6].

U. U. Gaude (✉) · K. G. Guptha
Department of Civil Engineering, Goa College of Engineering, Farmagudi, Goa, India
e-mail: kgg@gec.ac.in

Although these units proves to be better in many ways over the conventional methods do require some improvements or certain properties to enhance certain presentable qualities of the product. Normal problems observed in this technique are listed as follows:

1. Difficulty in pressing RCC drain slab
2. Avoid escape of cement and fine particles while pressing.
3. Bonding and finishing
4. Improve green strength of concrete
5. Strength improvement, etc.

Current study was to analyse the above problems and improve quality of the products. Better bonding and green strength of concrete were improved by use of chemicals and revision of RCC design and use of macro synthetic fibre tuff helped in improving overall strength. In absence of the literature availability the authors have to depend only on the limited information available as listed in the references.

2 Materials

Typical material matrix used in the production of precast wet pressed concrete products per batch is presented in Table 1.

2.1 *Chemical Admixtures*

The chemical admixtures used for improving bonding and workability include the following.

2.1.1 Nano Chemicals

Chemicals such as Terrasil and Zycobond were added to improve the quality of the products. These are based on Nano-technology. Terrasil was used to improve cohesiveness and Zycobond is used for bonding. Addition of these chemicals improved strength, workability and density of concrete.

Table 1 Mix proportion currently in use

Cement kg	20 mm kg	10 mm kg	6 mm kg	Fines kg	Water lts
90	100	130	100	300	50–53

Table 2 Reinforcement details

Sr. No	Position	Main	Distribution
1	Bottom	Tor 12@90mmc/c	Tor 10@170mmc/c
2	top	Tor 10@170mmc/c	Tor 10@250mmc/c

2.1.2 Dynamon

This is an accelerator cum super plasticizer used to reduce the initial setting time to avoid cracks during stacking.

2.2 Steel Reinforcement

Steel reinforcement of Fe500 grade is used as tension reinforcement. Two meshes one each at bottom and top for 150 mm thick drain slab was used and top steel was provided simply to assist lifting mechanisms. Bottom steel is only responsible for resisting tensile strength. No shear reinforcement was seen. Reinforcement details are as shown in Table 2.

2.3 Bajaj Macro Synthetic Fibre Tuff

Synthetic macro Fibre Tuff 36 mm long was used to enhance shear strength of concrete and also to reduce shrinkage and temperature cracks. These are also believed to improve permeability, explosive spalling and plastic settlement.

3 Machinery

Basic machinery involved in the wet press concrete production includes:

(a) Batching system for weighing the materials
(b) Conveyer Belt and Trolley arrangement for transferring weighed material into the mixer mechanically
(c) Cement and water dispensers for adding cement and water respectively
(d) Electrically operated concrete mixer for mixing, fitted with discharge nozzle for mould filling
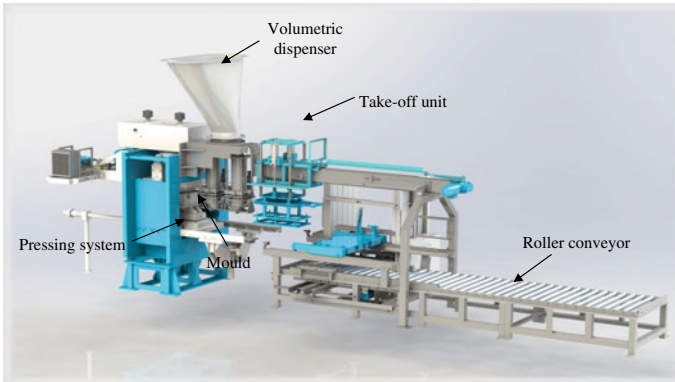(e) Pressing unit.

Fig. 1 Single mould wet press machine

3.1 Hydraulic Press Machinery

Hydraulic wet press machinery comes with a complete assembly of volumetric material dispenser, single stage or three stage mould, pressing system, Ejector station and handling system as shown in Fig. 1 [6].

3.2 Volumetric Measuring Dispenser

These dispensers are attached to the bottom of the mixer for mould filling directly from the mixer. Volume to be dispensed into the mould is pre fixed based on kind and size of the product to be pressed [6].

3.3 Moulds

These machines are available in two varieties viz., one with a single mould system and the other with three moulds system. The single mould press gives more cost effective tooling or set up option to that of triple mould system. It is still a 400 Ton power machine and is capable of producing any product that the triple mould one can output. Single moulds are used for low quantity special products. Triple mould pressing process has the rotary table system for filling and pressing operations. These are used for higher production requirements [6]

3.4 Pressing System

Filled moulds are pressed with hydraulic pressure of 400 Ton to expel out the excess water used for mixing concrete and to achieving desire workability. Pressing ram automatically starts pressing the wet concrete filled in the mould. Pressing time varies based on size and kind of the product and generally ranges from 10 to 30 s. Quick drainage of excess water while pressing operation is achieved with the help of vacuum [6].

3.5 Ejector Arm

Ejector arm automatically releases and extends the pressed product out of the mould. From where it is lifted by applying suction pressure on the top surface and moved to waiting pallet for stacking [6].

3.6 Handling System

This system consists a take-off unit which may be manually operated, semi-automatic or fully automatic. When the ejector arm presses the product out of the mould; take-off-unit takes over and lifts the product by applying suction pressure on to the top surface of the product. Pressed unit is then carried on to a stacking product and stacked along with previously casted products which is then shifted for curing.

4 Methodology

Manufacturing process of wet pressed concrete products involves following operations. Figure 2 shows the flow chart of the manufacturing process.

4.1 Process

Irrespective of the single stage or three stage press machine, the process is basically the same for both i.e. filling moulds with wet concrete into the mould, pressing the concrete to squeeze out the extra water, ejecting, stacking and curing the finished product are major steps.

A most economical concrete mix design for the production is achieved by using locally available material as far as possible. These materials are weighed precisely
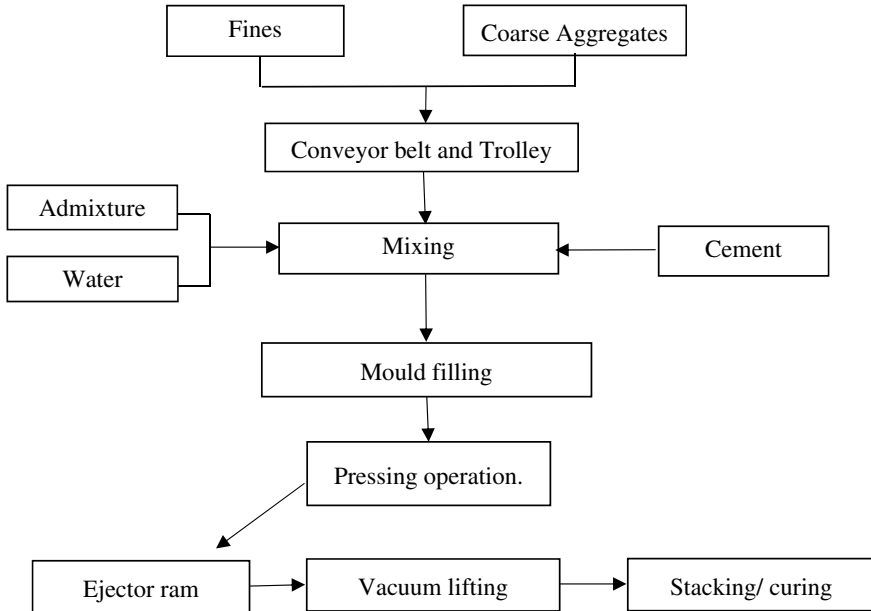
Fig. 2 Manufacturing process flow diagram

and batched according to mix design requirement and then transferred it to a mixer using electrically operated trolley. Cement, chemical admixture if any and water required for cement hydration and to form slurry that flows into the mould without any vibration is directly added into the mixer. Mixer is run till a good slurry is formed which is inspected with inspection window provided on the mixer. Fines are used to obtain close texture and better finish on the surface of the product. To prevent the escape of fine particles along with water as the pressure is applied to expel the excess water, a sheet of porous paper is placed at the bottom of the mould.

A measured amount of wet mix is then dispensed through hopper into the mould. The mix easily runs and fills the mould without vibration, and another filter paper is placed on the top. The press is then actuated and the hydraulic ram presses down into the mould squeezing out the excess water immediately after pressing. The product is strong enough to be handled at the end of this stage. The ejector ram automatically extends the pressed product out of the mould immediately after pressing. Pressed product is then lifted by applying a vacuum pressure on to the surface of the product. Carrier then transfers it to a stacking pallet along with previously casted products. This is continued till the pallet gets filled. Once the pallet is filled it is lifted by using a fork lift truck and stacked within the building for overnight curing. The products are then stacked outside into the stacking area for normal completion of curing [5]. The flow diagram is shown in Fig. 2 [5, 6].

4.2 Visual Observations

Based on visual observations following data was recorded for ongoing production.

1. Cement to total solid ratio was observed to be 1/8 which
2. 33.3% of fines (powder) used to obtain good texture and smooth surface on the finished product.
3. Aggregate quality, grading, packing and quantity of water affect the pressing time.
4. Pressure applied is for 15–22 s.
5. During pressing, water carries very marginal quantum of fine dust and cement particles along with it leaving pores on the slab edges.
6. Main issue was with RCC unit due to steel which is believed to undergo some bending under hydraulic pressure.
7. No shear reinforcement was provided.

4.3 Other Tests Carried Out

Following physical tests were performed on the concrete specimen.

4.3.1 Compressive Strength

Core samples of 100 mm diameter and 150 mm length were extracted to find compressive strength of concrete [7]. Test data is tabulated as in Table 3. Average compressive strength observed as 28.16 N/mm^2. This confirms the strength achieved is in tune with mix design carried out.

Table 3 Compressive strength of concrete

Sample	L/D	C/S area (mm^2)	Load (N)	Correction factor	Corrected compressive strength (N/mm^2)	Equivalent cube strength (N/mm^2)
1	1.5	7854	190,000	0.943	22.81	28.52
2	1.5	7854	185,000	0.943	22.22	27.76
3	1.5	7854	188,000	0.943	22.57	28.21

4.3.2   Transverse Strength Test

(a)   Using chemical admixtures

Loading arrangement for the test is shown in Fig. 3. Test photograph is shown in Fig. 4.

Drain cover slabs were tested using universal testing machine for finding bending and shear strength of specimen under the point load at centre. In this test the slab was placed as simply supported with sufficient bearing. Centre of span was marked and load was applied at the centre. Load was increased gradually till specimen fails. Load at which specimen failed was recorded. Precast unit tested with and without chemical admixture are tabulated in Table 4.
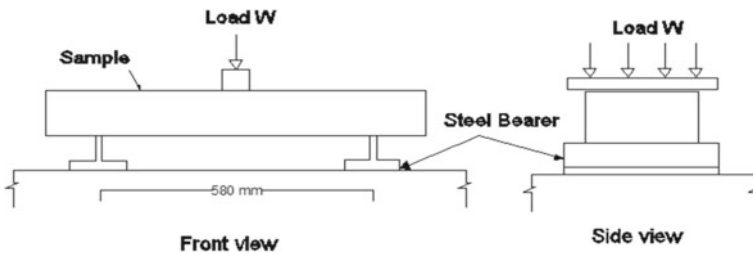

Fig. 3   Transverse strength test experimental setup

Fig. 4   Transverse strength testing

Table 4   Transverse strength test

Specimen (0.75 × 0.4 × 0.15) m		Span (m)	Load (Kn)	Avg (Kn)	Moment (Kn m)	SF (Kn)	Avg (Kn)	% improvement
Without chemicals	1	0.58	155	149	22.42	77.5	75	–
	2	0.58	143		20.73	71.5		
With chemicals	1	0.58	175	165	25.38	87.5	86	14.66
	2	0.58	169		24.5	84.5		

Table 5 Transverse strength

Specimen (0.75 × 0.4 × 0.15) m		Span (m)	Load (Kn)	Avg (Kn)	Moment (Kn m)	SF (Kn)	Avg (Kn)	% improvement
Without chemicals	1	0.58	185	181.5	26.825	92.5	90.75	–
	2	0.58	178		25.81	89		
With chemicals	1	0.58	205	210.5	29.725	102.5	105.25	15.97
	2	0.58	216		31.32	108		

(b) **Use of macro synthetic Fibre Tuff**

Improvement in shear strength and reduction in shrinkage and temperature cracks in concrete was achieved by adding Bajaj Macro Synthetic Fibre Tuff. As cited in literature, fibre introduction is believed to reduce permeability, explosive spalling and plastic settlement too. These were used along with steel reinforcement. Transverse strength results are tabulated in Table 5.

5 Discussions

In the light of the experiments conducted and the results obtained, the sole factor considered was to not to increase the overall cost. To achieve this, presence of fibres was taken and their quantity was optimized in tune with bonding and accelerators chemicals used. Incorporation of fibres prompted the reduction of steel reinforcement to an extent of 20%. This phenomenal change prompted use of chemical admixtures without further surging in costs.

It was observed that fine particles of cement and certain fines in fine aggregates were marginally escaping during the process of hydraulic pressing making the product to lose its aesthetics. Use of nano-chemicals viz., terrasil and zycobond in addition to dynamon SP508 have improved bonding such that increase in the size of particles made it difficult by the process of agglomeration prevented escape of fine particles through the filter paper made the product aesthetically pleasing. The very nature of admixtures assisted the product in its green state to improve the desired strength.

Use of fibres has improved compressive strength and tensile strength acting as reinforcement in the concrete matrix. These fibres indirectly act as obstruction during the pressing operations thereby improving in preventing finer particles. It was also observed that the deposition of fines on to the fibres due to the presence of bonding agents reduced pressing time from 21 to 17 s (23% reduction in pressing time.) by saving energy charges.

It was also observed and confirmed improvement in transverse strength to the tune of 15% with use of chemical admixtures alone and overall 40% increase is possible by addition of chemical admixtures and fibres.

6 Conclusion

Following conclusions were drawn.

1. Wet press technique is a good option for improving quality and productivity of precast concrete units.
2. Addition of chemical admixture and fibres improves transverse strength by about 40%.
3. Aesthetics of the finished products when compared with and without chemicals showed a phenomenal improvement with the chemicals.
4. There was no additional cost involved in improving the product aesthetic and quality.
5. A phenomenal reduction in the pressing time by about 25% is attributed to the use of chemicals and fibres.

References

1. Shivaprasad KN, Das BB (2018) Determination of optimized geopolymerisation factors on the properties of pelletized fly ash aggregates. Constr Build Mater 163. Elsevier
2. Goudar SK, Das BB (2021) Influence of particle size of bottom ash on mechanical properties of M30 grade concrete. In: Select proceedings of TMSF 2019. Springer Publications Pte. Ltd. A Book Chapter
3. Snehal K, Das BB, Akanksha M (2020) Early age, hydration, mechanical and microstructure properties of nano-silica blended cementitious composites. Constr Build Mater 233. Elsevier
4. Snehal K, Das BB (2020) Application of Andreassen and modified Andreassen model on cementitious mixture design: a review. In: Select proceedings of ICRDSI 2019. Springer Publications Pte. Ltd., pp 729–750 A Book Chapter
5. Rieder KA et al (2015) Wet press concrete slab manufacturing, 26 May 2015
6. Forest press hydraulics FPH. Single Mould Press. http://www.forestpresshyd.com/FPH_HOMEPAGE.html
7. IS 516:1959—method of tests for strength of concrete

Structural Performance and Characteristics of Concrete with Crushed Glass as Partial Replacement of Sand

Binaya Patnaik, Thomas Bezabih, and Mehretu Gabrie

1 Introduction

Concrete is the leading construction material in the world. It is vigorously consumed in the construction of simple to complex civil engineering structures. Concrete is a quasi-brittle composite material obtained from carefully proportioned mixture of cement, fine aggregates, coarse aggregates and water. The chemical reaction between cement and water binds the aggregate particles to form a solid mass. Admixtures, where necessary, may be added to modify certain properties in the fresh or hardened states of concrete. It is an established fact that the compressive strength of concrete is influenced by, among other things, the quality and proportion of fine and coarse aggregate, the cement paste and the paste-aggregate bond characteristics. The compressive strength of concrete, like that of natural stone, is high which makes it suitable for members primarily subjected to compression [1]. The facility with which, while plastic, it can be made to fill forms or molds of almost any practical shape and its high fire and weather resistance is another evident advantage of concrete material. The compressive strength of concrete as per EBCS-EN-1992-1-1:2013 [2] is related to the characteristics cylinder strength fck or cube strength fck, cube, determined at 28 days. Aggregates (fine and coarse) occupy roughly three-fourths of the volume of concrete. Therefore, the properties of aggregates have considerable importance to the quality, strength and durability, of concrete. The sources of aggregates, fine and coarse, are either naturally occurring or crushed stone. The parent materials of aggregates are derived mainly from volcanic activity. The dominant rock for coarse aggregate production in Ethiopia is generally basalt while ignimbrite is most commonly used for masonry stone. On the other hand the majority of sand is collected

B. Patnaik (✉)
Department of Civil Engineering, Gambella University, Gambella, Ethiopia

T. Bezabih · M. Gabrie
Department of Civil Engineering, Hawassa University Institute of Technology, Hawassa, Ethiopia

from riverbeds. It is an obvious fact that it takes millions of years for the formation of these naturally occurring constituents of concrete. Ethiopia is a country blessed with enormous natural resources. Due to this, wasteful utilization of resources is observed from past to present. Recycling and the reuse of natural materials have been traditionally of low priority and often nonexistent in the country. However, this should no longer be true where consumption of resources is mounting which in turn aggravates depletion of natural resources. In developing countries like most of African countries, the demand for civil engineering works is inexhaustible. Hence, concrete is in high need which results continuous demand of concrete constituent materials. Naturally occurring materials like sand, obtained from river beds, are depleting eventually, whereas production of cement is capital intensive in addition to not being environmental friendly due to high emission of CO_2. One of the substitute material that comes to mind as a solution to this concerning problem is the use of recycled concrete. The other and yet very effective and most conclusive solutions to overcome this problem is practice of concrete usage made from recycled materials. In recent times, replacement of recycled materials (from disposal sites or industry wastes) and agricultural wastes as partial and/or full replacement of concrete constituents is being studied worldwide. Replacements of waste powder granite, waste marble powder, fly ash (Rashik Mustafa et al. 2018) bottom ash [3], and residual wastes of agricultural products like Rice husk ash, Rise straw ash are some of the proved significant replacements of sand and cement in concrete. Crushed glass is being studied for use in concrete for partial replacement of cement, sand and aggregates. It is used in crushed form as fine or coarse aggregates and in powdered form as cement. In addition to all these, some more industrial rejections like aluminium refinery residue, termed as Red Mud [4] which was stabilized using another industrial material commonly known as ground granulated blast furnace slag for the purpose of road construction. Bottom ash, which is also a common waste generated from thermal industries, which needs a proper disposal otherwise it leads to leaching of heavy metals to the groundwater table. Various studies are available in developing a concrete by using it as partial replacement to river sand. Also a concrete of grade M-30 can be achieved and a substantial improvement can be observed in it characteristic properties [5, 6]. Therefore, it can be observed that there are various industrial wastes are available for developing a recycled concrete and a lot of useful inferences can be drawn from past experimental studies. This research aims at investigating the optimum percent replacement (0–100%) of crushed glass in concrete as partial replacement of sand and the performance of concrete with different levels of sand replacement.

2 Materials

In this experimental study, the high strength concrete C50 (HSC) was used. The concrete test specimens were casted by replacing sand with crushed glass at 0, 20, 40, 60, 80 and 100% in volume and cured for strength and durability property investigations. The cement used was Dangote Ordinary Portland Cement (OPC) with

Table 1 Physical properties of fine aggregates, coarse aggregate and crushed glass

Physical properties	Sand	Crushed glass	Coarse aggregate
Specific gravity	2.64	2.7	2.68
Absorption (%)	1.3	0	1.2
Moisture content (%)	2.62	2.3	2.46
Unit weight (kg/m^3)	1300	1515.9	1636.3

42.5R grade. The fine and coarse aggregates used were locally available materials which were collected from Dimtu and Monopole around Hawassa city respectively. Crushed glass was collected from Addis Ababa glass and Bottles share company. Since it was aimed to study the effect of glass when used in concrete, an appreciably homogeneous raw material is needed. Hence, only one color of glass was used in this study so as to identify the properties of the glass. Light green color crushed glass was used. The crushed glass which was coarser than the expected grading limit was re-crushed using hammer and a simple technique adopted from Thurston County solid waste, 2011. Several physical tests were conducted to identify the properties of the fine aggregate, coarse aggregate and crushed glass have been presented in Table 1.

The fineness modulus of the crushed glass was found to be 2.7 and its chemical properties, which was tested in Geological Survey of Ethiopia laboratory, is shown in Table 2.

The mix proportions for the high strength concrete which were designed as per (ACI 211.1–81, 1985) and (ACI 211.4R-93, 1998) respectively are summarized in Table 3.

Table 2 Chemical composition of light green glass

Description	Composition (% by mass)
Silica, SiO_2	71.51
Alumina, Al_2O_3	1.35
Iron Oxide, Fe_2O_3	0.25
Calcium Oxide, CaO	10.57
Magnesium Oxide, MgO	0.51
Sodium Oxide, Na_2O	13.94
Potassium Oxide, K_2O	0.87
F	0.51
SO_3	0.51
Total	100.00

Table 3 Mix proportions used for high strength concrete

Grade	Cement (kg/m^3)	Fine aggregate (kg/m^3)	Coarse aggregate (kg/m^3)	W/C ratio	Water (kg/m^3)
C-50	519.05	408.55	1162	0.42	218

Compressive strength testing	Flexural strength testing	Concrete at high temperature
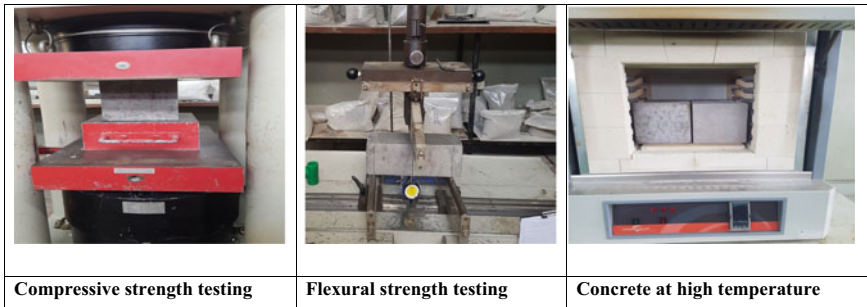
Fig. 1 Test setup of the concrete specimens

3 Experimental Methods

Slump test for workability was carried out as per (ASTM C 143/C 143M-00, 2000) for the high strength concrete C50. The compressive strength of cube 15 cm size concrete specimens were tested as per (ASTM C 39/C 39M-01, 2001) for each crushed glass replacement case. Three test specimens were tested for each selected curing ages, 7th and 28th day, of concrete and averaged out for considering the final value. The flexural strength of 10×10 cm cross sectional size with 30 cm clear span length plain concrete specimens were tested as per (ASTM C 293-02, 2002) for each crushed glass replacement case of the high strength concrete C50. For thermal analysis cube 15 cm size concrete specimens were exposed to elevated temperatures such as 200 and 600 °C for 4 h in a muffle furnace and tested for loss of weight and strength compared to the initial weight and strength at ambient temperature. Various test setup have been presented in the Fig. 1.

4 Results and Discussions

Effect of crushed glass on the workability of concrete

Slump cone test was conducted to examine the workability of concrete and has been presented in the Table 4. The experimental results shows that as the level of glass replacement increases, the slump increases significantly. The consistency of the mix was improving as more percentage of sand by weight was being replaced by crushed glass. This is mainly because of the low water absorption property of crushed glass.

Table 4 Slump test result

Mix	Glass replacement (%)	w/c ratio	Slump (mm)
Treatment-1	0	0.42	22
Treatment-2	20	0.42	28
Treatment-3	40	0.42	51
Treatment-4	60	0.42	86
Treatment-5	80	0.42	88
Treatment-6	100	0.42	116

Table 5 Compressive strength test result

Treatment	Glass replacement (%)	Compressive strength (MPa) at 7th day	Compressive strength (MPa) at 28th day
Treatment-1	0	39.65	54.29
Treatment-2	20	39.74	55.27
Treatment-3	40	40.40	55.28
Treatment-4	60	40.06	55.32
Treatment-5	80	42.16	58.70
Treatment-6	100	34.88	52.01

Effect of crushed glass on the compressive strength of concrete

The experimental results of the compressive strength test at 7th and 28th day of each treatment are shown in Table 5. The results demonstrates that the maximum compressive strength for both at 7th and 28th day was attained at 80% inclusion of crushed glass in concrete.

Compressive strength of all the specimens increased with time and exceeded the intended compressive strength value at 28th days of casting age. As a result, it is fair to say that inclusion of crushed glass in concrete up to 80% has a significant importance for the improvement in compressive strength of concrete. This, in some way, is different than the optimum compressive strength which was reported by previous studies [7, 8]. However, at 100% replacement of crushed glass by weight of sand in concrete, the compressive strength test result both at 7th and 28th days showed a decrement. It is conjectured that at a point, after it attained its optimum compressive strength value (80% crushed glass replacement), the strength has began to fall down. This could be resulted from the missing of sand as constituent in concrete since there is no sand used in the concrete mix (Treatment-6). Hence, full replacement of sand could cause the concrete to lose the binding effect it gets from sand. This statement can be incorporated with the very high slump of concrete attained at 100% replacement of sand by crushed glass (Table 4). However, in the long term, the pozzolanic reaction between glass particles and cement could modify and enhance the leading to an obvious increase in compressive strength. Figure 2 shows the comparison between
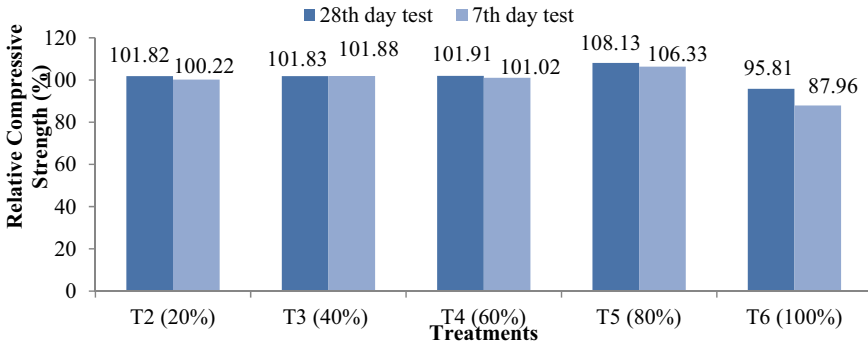
Fig. 2 Relative compressive strength percentage results at 7th and 28th day test

treatments was made in percentage increment of compressive strength results of treatments with controlled specimen.

Effect of crushed glass on the flexural strength of concrete

The flexural strength test result at 7th and 28th day of each treatment is shown in Table 6. It can be observed that the flexural strength of concrete specimens improved as inclusion of crushed glass in concrete got higher until it reached 80%. At 100% replacement of crushed glass by weight of sand (Treatment-6), the flexural strength at 7th day showed a small decrement compared to the controlled specimen. However, at 28th day test, although it showed decrement than the strength at 80% replacement, it was somehow higher than the controlled specimen. Therefore, it can be said that, at 28th day of casting age, when crushed glass fully replaced sand (100%) in concrete, flexural strength of concrete improved.

Figure 3 shows the comparison between treatments was made in percentage increment of flexural strength results of treatments with controlled specimen.

Thermal Analysis

When the test samples were subjected elevated temperature, significant change in colour was observed in all concrete specimens at 600 °C temperature exposure. Some

Table 6 Flexural strength test result

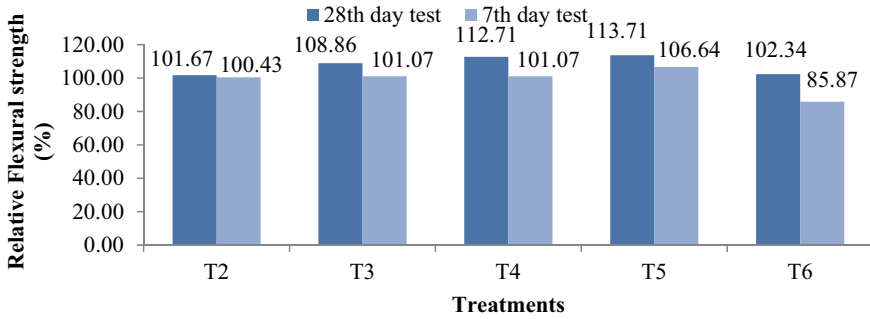| Treatment	Glass replacement (%)	Modulus of rupture (MPa) at 7th day	Modulus of rupture (MPa) at 28th day
Treatment-1	0	4.67	5.98
Treatment-2	20	4.69	6.08
Treatment-3	40	4.72	6.51
Treatment-4	60	4.72	6.74
Treatment-5	80	4.98	6.80
Treatment-6	100	4.01	6.12

Fig. 3 Relative flexural strength percentage results at 7th and 28th day test

concrete specimens exposed to 600 °C exhibited spalling or breaking up of pieces. This effect was attributed with the study by Olofinnade et al. [9], who reported that, spalling of the concrete with glass powder at elevated temperature, could be caused by the dehydration of the C–S–H gel and expansion of the concrete due to the heating. Severity of the spalling and even cracks depends on the level of temperature in which the samples were exposed to heating, hence no specimen, at 200 °C, showed spalling or breaking up of pieces from the concrete. Results of mass loss and residual compressive strength are described below. Temperature exposures of 200 and 600 °C are referred as T-200 and T-600 throughout the discussion.

Mass Loss

The result of mass loss computed in percentage is illustrated in Fig. 4 (Mass before heating/ Mass after heating). Generally, the test result shows that mass loss of all concrete specimens has increased as the temperature in which the samples were exposed to is increased. Mass loss of concrete when exposed to elevated temperature could be because of the evaporation of materials like water from the concrete when high amount of heat is exerted. Mass loss for all sample specimens is significantly higher at 600 °C than at 200 °C. This result can be incorporated with the report by Mousa [10], who indicated that weight loss of silica-fume and recycled rubber-filled high strength concrete increased with increasing temperature.

Fig. 4 Effect of crushed glass on mass loss of concrete with increasing temperature
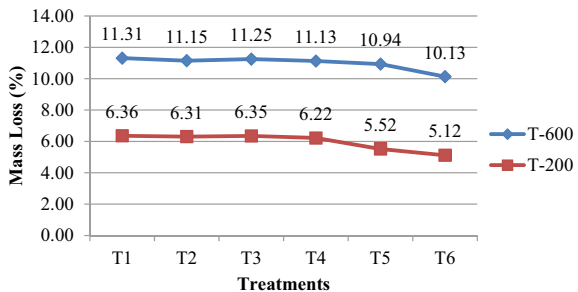
It can be seen from the above Fig. 4 that mass loss was decreasing as crushed glass replacement in concrete was increasing both at 200 and 600 °C. Moreover, specimens exposed to 600 °C temperature showed higher percentage mass loss. For instance, the control specimen exhibited 6.36% mass loss after heating at 200 °C while 11.31% mass loss was observed when 600 °C heating temperature was exerted.

Residual compressive strength

The effect of the heating temperature on the strength of concrete cubes produced without inclusion of crushed glass, as control specimen, and concrete cubes containing crushed glass content as sand replacement in percentage levels of 0–100% are shown in Fig. 5. The results show that there is clearly decrement in the compressive strength of concrete as the temperature increases. This can be incorporated with the results reported by previous studies on the performance of concrete containing glass subjected to elevated temperatures ([9, 10], Ali 2016). It is shown in Fig. 5 that Treatment-2 exhibited the maximum compressive strength when exposed up to 200 °C temperature. Although at higher temperature, all concrete specimen shows decrement in compressive strength as compared to control. However, it is reported in this study that, at room temperature, the control concrete specimen possessed a lower compressive strength than all the other concrete samples containing crushed glass up to 80% percentage replacements by weight of sand (Table 5).

Furthermore, relative comparison of the residual strength of concrete, in terms of mechanical strength ratio, which is computed from the residual compressive strength of concrete specimens at elevated temperature to the strength of control specimen after heating, is illustrated in Figs. 6 and 7. The diagrams presented, for the sake of relative comparison, shows that control specimen and treatment-2 (20% glass inclusion) possesses nearly the same, although the strength obtained was greater than control, residual compressive strength at 200 °C. All other treatments show small decrement in their compressive strength property both at 200 and 600 °C.
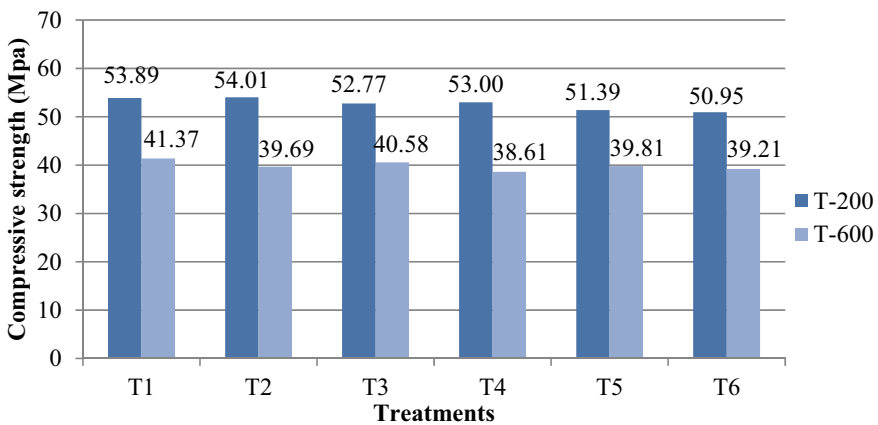

Fig. 5 Residual compressive strength of concrete after heating

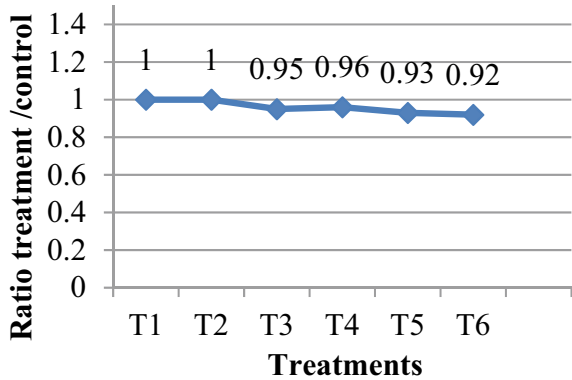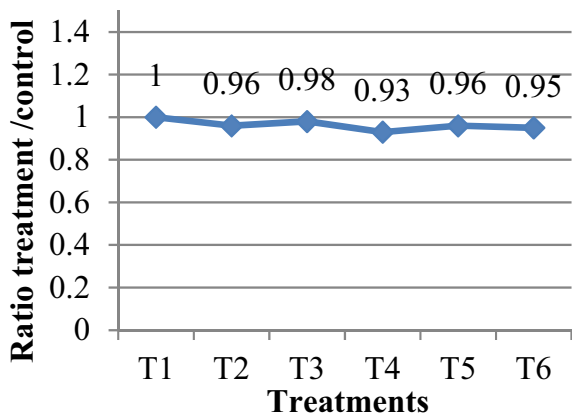**Fig. 6** Relative comparison of residual compressive strength at 200 °C in ratio

Fig. 7 Relative comparison of residual compressive strength at 600 °C in ratio

5 Conclusions

In this study, recycled crushed glass was used to replace natural sand as fine aggregates in concrete of compressive strength of 50 MPa. The following conclusions can be drawn from the experimental results that have been carried out in this study.

- Glass inclusion in concrete had a significant effect on fresh property (workability) of concrete. Slump of fresh concrete was increasing drastically as crushed glass inclusion in concrete was increasing. Therefore, workability enhancer chemical admixtures are not needed in a concrete mix of grade C50 when crushed glass is included.
- Up to 80% glass replacement ration in concrete, compressive strength of concrete has increased at early stage as well as 28th day of casting age. After that, the compressive strength has decreased. Thus, optimum compressive strength was attained at 80% replacement of glass by weight of sand.

- Flexural strength of concrete was improved up to 100% replacement of sand by crushed glass. Although the maximum flexural strength was attained at 80% ratio.
- Performance of concrete under elevated temperature was nearly similar for the tested specimens. Mass loss was decreasing as glass inclusions increased although mass loss was getting higher as temperature to which the specimens were exposed to have increased. Residual compressive strength showed decrement at elevated temperature. Glass inclusion has led to decrement in residual compressive strength. However, no significant negative influence of glass inclusion in concrete at elevated temperature was observed.

In summary, recycled crushed glass can be incorporated into concrete as fine aggregates up to 80% replacement ratio without deleterious effect on concrete properties that has been studied.

References

1. Nilson AH, Darwin D, Dolan CW (2010) Design of concrete structures, 4th edn. The McGraw-Hill Companies, New York, USA
2. EBCS EN 1992-1-1:2013. Ethiopian Building Code Standard
3. Renjith R, Shivaprasad KN, Das BB (2018) Properties of heat cured bottom ash based geopolymer mortar admixed with fly ash of different fineness. Advances in concrete, structural and geotechnical engineering. Bloomsbury Publishing Plc., pp 603–607. A Book Chapter
4. Kudachimath N, Raviraj HM, Das BB (2021) Effect of GGBS on strength of aluminium refinery residue stabilized by alkali solution. In: Select proceedings of TMSF 2019. Springer Publications Pte. Ltd., pp 331–339. A Book Chapter
5. Goudar SK, Shivaprasad KN, Das BB (2019) Mechanical properties of fiber reinforced concrete using coal-bottom ash as replacement of fine aggregate. In: Select proceedings of ICSCBM 2018. Springer Nature Singapore Pte Ltd., pp 863–872. A Book Chapter
6. Goudar SK, Gedela SK, Das BB (2021) A review on mechanical and microstructure properties of reinforced concrete exposed to high temperatures. In: Select proceedings of ICRDSI 2020. Springer Publications Pte. Ltd., pp 719–728. A Book Chapter
7. Iqbal Malik M, Bashir M, Ahmad S, Tariq T, Chowdhary U (2013) Study of concrete involving use of waste glass as partial replacement of fine aggregates. IOSR J Eng 3(7)
8. Rubini K, Joy LS, Sanjana (2016) An experimental study on crushed glass material for the partial replacement of natural sand in concrete. Int J Eng Tech Res (IJETR) 4(3)
9. Olofinnade OM, Ede AN, Ndambuki JM (2017) Experimental investigation on the effect of elevated temperature on compressive strength of concrete containing waste glass powder. Int J Eng Technol Innov 7(4):280–291
10. Mousa MI (2017) Effect of elevated temperature on the properties of silica fume and recycled rubber-filled high strength concretes (RHSC). HBRC J

The Effect of Elitism in Solving Resource Leveling Problem in Construction Projects

Gopinath Selvam and T. Ch. Madhavi

1 Introduction

Resource management is essential for the successful completion of construction projects. Resource management results in effective usage of resources. Resource management involves the process of estimating and procuring the materials, manpower and machineries and controlling the operations till closure of the project. Challenges in the resource management are categorized with duration and resource constraints [1–7]. Resource management problem with time constraint is resource constrained project scheduling problem and the later is termed as resource leveling problem (RLP) [8].

Resource leveling problem (RLP) assures uniform utilization of resources in the project. Resource leveling involves shifting of non critical activities with its available float days to reduce resource variation between consecutive days. There by, the duration of the project is not increased. RLP belongs to combinatorial problem; the number possible solution increases in exponential form with increase in non-critical activities [9]. RLP is still complex and challenging problem—several researchers proposes different problem solving approaches to solve RLP.

Mathematical, heuristic, meta heuristic, hybrid, and hyper heuristic approaches were used by the researchers to solve RLP. Among these approaches genetic algorithm optimisation approach is used in notable instances by the researchers to solve RLP. Genetic algorithm is a stochastic optimisation approach [10]. Genetic algorithm

G. Selvam (✉)
College of Engineering and Technology, Department of Civil Engineering, SRM Institute of Science and Technology, SRM Nagar, Kattankulathur, Chengalpattu District, TN 603203, India
e-mail: gopinats@srmist.edu.in

T. Ch. Madhavi
Faculty of Engineering and Technology, Department of Civil Engineering, SRM Institute of Science and Technology, Bharathi Salai, Ramapuram, Chennai, TN, India

optimism approach works on the operators of selection, recombination, mutation, and elitism [11].

Selection operator selects set of parents randomly from the population; recombination operator cross over the genes of the selected parents to generate a new population; mutation operator mutates a particular or set of genes in the next generation and produce distinct feature over the parents; elitism operator retains the elite chromosome (parent/children) in the population. Among these operators, elitism is a special operator. Elitism leads to determine the optimal solution in lesser number of generation. This study aims at analysing the influence of elitism operator in genetic algorithm optimisation approach to solve resource leveling problem.

2 Methodology

In addition to other operators a fitness function is included in genetic algorithm optimisation approach. The objective of fitness functional is to drive the problem search space towards optimal solution. Different type of fitness functions were mentioned in the literature [12]. Some of the mostly adopted fitness functions are Minimization of the sum of the absolute deviations in daily resource usage and minimization of the sum of the square of daily resource usage.

Set of activities from a residential building project was considered to evaluate the proposed study (Tables 1 and 2). Resource leveling problem was attempted to solve as minimization problem. Value of elitism operator were considered from 0.1 with an incremental value of 0.1 upto the maximum value of 1.0. The values of other operators were adopted from the literature [13]. With each value of elitism operator, the fitness value was calculated. Resource levelling metrices [14] such as fitness value, resource moments, resource levelling index, minimum and maximum resource requirement, standard deviation, and squared deviation were calculated to ascertain the optimal solution. Genetic algorithm optimisation approach is coded in MATLAB R2016a.

Table 1 Activity details

S. No	Task name	Duration	Predecessors	T.F	F.F	Int.F	Ind.F
1	Marking for column	4 days		–	–	–	–
2	Lift wall reinforcement	5 days	1SS + 1 day	–	–	–	–
3	Column starter	3 days	1,2SS + 1 day	2	2	–	–
4	Column shuttering and concreting	8 days	3SS + 2 day,2	2	–	–	–
5	Shuttering for roof slab	11 days	4SS + 4 days,3	1	–	–	–
6	Reinforcement	8 days	5SS + 4 days,4	1	–	–	–
7	Others	2 days	6SS + 6 days,5	–	–	–	–
8	Concreting	2 days	6,7FS + 1 day	–	–	–	–

Table 2 Resource requirement

I.D	Task name	Duration	Mason	Helper	Carpenter	Fitter	Bhisti
1	Marking for column	4 days	3	12	–	–	–
2	Lift wall reinforcement	5 days		15		15	–
3	Column starter	3 days	1	4	2	–	1
4	Column shuttering and concreting	8 days	2	24	5	–	7
5	Shuttering for roof slab	11 days	–	14	5	–	–
6	Reinforcement	8 days	–	12	–	20	–
7	Others	2 days	–		–	–	–
8	Concreting	2 days	11	92	–	–	45

Day wise resource requirement is obtained after allocating the resources to the activities. Total resource requirement was considered to in resource levelling. Based on the nature and values of float days, chromosomes were developed. Chromosome represents the genes, in this study, flexibility of free float days was considered as genes. Decoding mechanisms were developed as a separate function to convert the optimal chromosome representation into logical solutions.

2.1 Fitness Function

The fitness function drives the optimisation approach towards reaching the optimal solution. Minimization of the sum of the square of daily resource usage proposed by Hiyassat [15] was considered in this study. On every generation, the fitness value is calculated with incremental value of elitism operator. The optimal fitness value in each trial is recorded.

$$Z = \min \sum_{i=1}^{T} (R_i)^2$$

R_i Deviation in resource requirement on ith day.
T Overall project duration.

.

3 Results and Discussion

Resource requirement profile before levelling indicates in multiple instances, the minimum resource requirement is zero (Fig. 1). The minimum resource requirement is reduced to a single instance after performing resource levelling (Fig. 2). In addition,
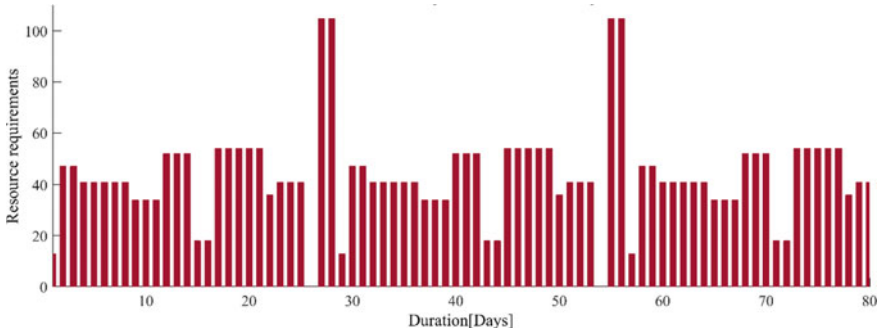
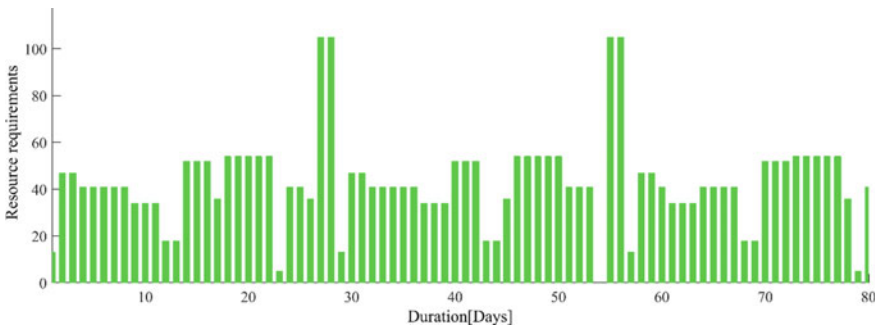**Fig. 1** Resource requirement—before leveling

Fig. 2 Resource requirement—after levelling

certain deviations in the resource requirement is reduced after levelling the resources. Different fitness values were obtained with incremental values of elitism (Table 3). With an incremental value of elitism in every trial, the best chromosome is considered

Table 3 Ellitism rates and fitness values

Trial No	Er	Fitness value
1	0.10	181,950
2	0.20	183,024
3	0.30	184,140
4	0.40	183,882
5	0.50	183,688
6	0.60	187,800
7	0.70	186,324
8	0.80	188,836
9	0.90	193,266
10	1.00	210,506
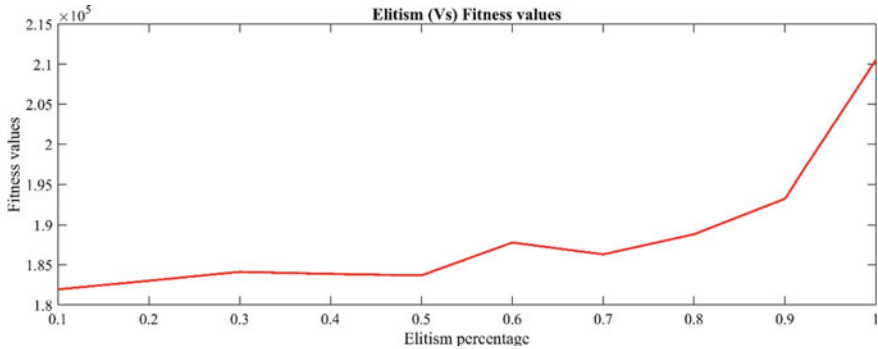
Fig. 3 Fitness value with different elitism rate

Table 4 Resource levelling metrices

S. No	Metrices	Before leveling	After leveling
1	Fitness value	220,843	210,506
2	Moment of histogram	334,776	333,498
3	Minimum resource demand	0	0
4	Maximum resource demand	105	105
5	Resource leveling index: per period resource difference between actual and the average resource usage	3839	3630
6	Standard deviation	21	22
7	Squared deviation	455	465

as elite and it is stored in the search space. More the value of elitism rate, more elites are stored. Since most of the chromosomes were considered as elites in the trial with probability of elitism was considered as 1, the optimal solution is obtained with the same trial (Fig. 3). Five percent reduction in the fitness value and resource levelling index were observed after levelling the resources. The moment value of before and after levelling were not significantly different. Minimum and maximum resource remained with identical values; since, the available precedence relationships does not produce more flexibility in the schedule (Table 4).

4 Conclusion

Elitism operator in genetic algorithm optimisation approach is studied with incremental values to solve resource leveling problem. The proposed idea is evaluated with set of activities from a residential building project. For a minimisation problem, the maximum value of elitism operator produced optimal solution. Compared to mutation operator, consideration of maximum value of elitism will provide optimal

solution. Even though higher probability of elitism provided optimal solution in this study, it is advisable to study the different probability of elitism in every project, before fixing its value.

References

1. Pandey A, Chaudhary PK, Das BB (2021) Productivity analysis of shuttering works for sewage treatment plant. In: Select proceedings of TMSF 2019. Springer Publications Pte. Ltd. A Book Chapter
2. Akhil RP, Das BB (2019) Cost reduction techniques on MEP projects. In: Select proceedings of ICSCBM 2018. Springer Nature Singapore Pte Ltd., pp 495–517 A Book Chapter
3. Hegde AL, Jain A, Das BB (2021) Resource buffers in construction projects. In: Select proceedings of TMSF 2019. Springer Publications Pte. Ltd. A Book Chapter
4. Paul B, Tondihal S, Das B (2021) Safety stock in inventory management and wastage analysis at construction sites. In: Select proceedings of TMSF 2019. Springer Publications Pte. Ltd. A Book Chapter
5. Upadhya PR, Das MS, Das BB (2021) Multi criteria decision making approach for selecting a bridge superstructure construction method. In: Select proceedings of TMSF 2019. Springer Publications Pte. Ltd. A Book Chapter
6. Pradeep RC, Das BB (2018) Methods to monitor resources and logistic planning at project sites. In: Select proceedings of ICSCBM 2018. Springer Nature Singapore Pte Ltd., pp 793–802. A Book Chapter
7. Shekhar S, Shukla P, Das BB (2021) Developing a standard template for activity linkage and resource estimation of MEP works. In: Select proceedings of TMSF 2019. Springer Publications Pte. Ltd. A Book Chapter
8. Selvam G, Madhavi Tadepalli TCh (2019) Genetic algorithm based optimization for resource leveling problem with precedence constrained scheduling. Int J Constr Manag 1–10. Taylor & Francis. https://doi.org/10.1080/15623599.2019.1641891
9. He L, Zhang L (2013) Dynamic priority rule-based forward-backward heuristic algorithm for resource levelling problem in construction project. J Oper Res Soc 64(8):1106–1117. Nature Publishing Group. https://doi.org/10.1057/jors.2013.33
10. Leu S et al (1999) A fuzzy optimal model for construction resource leveling scheduling. Can J Civ Eng
11. Tran H-H, Hoang N-D (2014) A novel resource-leveling approach for construction project based on differential evolution. J Constr Eng 2014:1–7. https://doi.org/10.1155/2014/648938
12. Damci A, Polat G (2014) Impacts of different objective functions on resource leveling in construction projects: a case study. J Civ Eng Manag 20(4):537–547. https://doi.org/10.3846/13923730.2013.801909
13. Ponz-Tienda JL et al (2013) The resource leveling problem with multiple resources using an adaptive genetic algorithm. Autom Constr 29(January):161–72. Elsevier B.V. https://doi.org/10.1016/j.autcon.2012.10.003
14. Kyriklidis C et al (2014) Hybrid nature-inspired intelligence for the resource leveling problem. Oper Res Int J 14(3):387–407. https://doi.org/10.1007/s12351-014-0145-x
15. Hiyassat MAS (2001) Applying modified minimum moment method to multiple resource levelling. J Constr Eng Manag 127(June):192–198

Free Vibration Analysis of Natural Fiber Laminated Composite Beam

Jaylalita Mohanta and Madhusmita Biswal

1 Introduction

The fibers collected from various animals and plants are known as natural fiber. The common plant-based natural fibers are sisal fiber, jute fiber, bamboo fiber, hemp fiber and flax fiber. The natural fibers are light weight, easily available, low cost, biodegradable, high specificity and nonabrasive processing characteristics, sound-absorbing, and low in density. So the natural fiber has used in the replacement of synthetic fiber like carbon fiber and glass fiber. Now a day's composite is widely used for its good strength, efficiency, and durability. The natural fiber composite (NFC) is the composite, in which fibers are green, biodegradable, and recyclable. The NFC beam is mainly used in aerospace, harbours, duck, infrastructure, the roof of the load-bearing structure for its lightweight properties. The manufacturing process of composite beam is easy, less time consumption, easy to handle, transfer, and repair. So now a day the demand of a composite beam is very high.

The previous study on the properties of natural fiber was reviewed by Ku et al. [5]. The studies based on the improvement, application and problem faced on the use of natural fiber composite were reviewed by Ticoalu et al. [11], Dittenber and Ganga Rao [2] and Faruk et al. [3]. The investigation on impact, tensile and dynamic property of coconut sheath/sisal hybrid composite was done experimentally by Kumar et al. [6]. The study on free vibration characteristic of composite beam made up of banana and sisal fiber reinforced hybrid polymer was done by Rajesh and Pitchaimani [10]. The Buckling and free vibration analysis of bidirectional natural fiber composite and axial compression was investigated by Rajesh and Pitchaimani [9]. Free vibration analysis of composite beam made up of short bamboo fiber based polymer was

J. Mohanta (✉) · M. Biswal
Department of Civil Engineering, CAPGS, BPUT Rourkela, Rourkela, India

M. Biswal
e-mail: capgs.madhusmita@bput.ac.in

observed by Jena [4]. Buckling and dynamic analysis of natural fiber sandwich beam with synthetic foam core under axial compression was observed by Wadder et al. [13]. The study had develop based on a procedure used to determine the dynamic damp behaviour of glass fiber reinforce composite beam by Tita [12] and Matsunaga [7]. The study developed on sandwich composite plate with a circular cut-out to observe the dynamic behaviour by Mondal et al. [8]. Free vibration behaviour of flat and curved sandwich beam with face and core deboned was studied by Baba and Thoppul [1].

As per the current environment condition and the growing pollution rate the main focus in biodegradable material as well as the eco-friendly structure. So the natural fiber composite beam is perfect formation as per our current requirement. But the beams are subjected to various dynamic loading during its life time; hence it is necessary to know the frequency rate before designing the structure. So the free vibration analysis of natural fiber laminated composite beams is necessary.

2   Finite Element Modeling of the Composite Sandwich Plate

Finite element method (FEM) based model has developed and analyzed using ANSYS software with the different natural fiber property in natural fiber laminated composite beam. The material properties of the natural fiber laminated composites are chosen from previous study and model has been developed.

2.1   Dynamic Responses of Laminated Composite Beam

The equation of equilibrium of the laminated composite beam structure under deformation can be written as

$$[M]\{\ddot{x}\} + [C]\{\dot{x}\} + [K]\{x\} = \{P(t)\} \qquad (1)$$

where, [M], [C], [K] are the mass matrix, damping, and stiffness matrix respectively. The $\{\ddot{x}\}$, $\{\dot{x}\}$, $\{x\}$ are relative accelerations, velocities and displacement respectively.
{P (t)} is the equation of motion.
For free undamped vibration, the equation reduce to

$$[M]\{\ddot{x}\} + [K]\{x\} = \{P(t)\} \qquad (2)$$

The actual value of natural frequency and the corresponding mode shape are deriving from the normalizing undamped equation of motion in finite element model-based software ANSYS Workbench 16.0. The required equation is

$$\{[K] - \omega^2[M]\}\{\varphi_i\} = \{0\} \tag{3}$$

where φ_i = corresponding mode shape,

ω_i = angular natural frequency in radian/sec = $\sqrt{\frac{K}{M}}$.

2.2 Numerical Simulation

In the current research, the jute and sisal fiber laminated composite beam of length 250 mm has been analysed with different layer thicknesses such as four layers, eight layers, twelve layers, and sixteen layers. The different aspect ratios such as 2.5, 5, 10, 15, and 20 have also taken for the free vibration study under different boundary conditions. The material properties of jute, sisal and glass fiber has been found from the previous study and described in Table 1.

The properties of glass fiber and polyurethane has considered from Baba and Thoppul [1]. The properties of polyvinyl foam is taken from Mondal et al. [7]. The properties of foam materials are represent in Table 2 and the density of all composite fibers with their corresponding thickness of one layer is represent in Table 3 respectively.

The mode shapes of the S/J/S laminated composite cantilever beam and curve sisal laminated composite fixed beam has shown in Fig. 1 and Fig. 2 respectively.

Table 1 Physical properties of jute, sisal and glass fiber

Natural fiber	E1 Gpa	E2 Gpa	E3 Gpa	Nu12	Nu13	Nu23	G12 Gpa	G13 Gpa	G23 Gpa
Sisal	1.16	1.16	1.16	0.34	0.34	0.34	0.79	0.79	0.79
Jute	0.70	0.70	0.70	0.32	0.32	0.32	0.53	0.53	0.53
Glass	10.16	10.16	10.16	0.3	0.3	0.3	3.00	3.00	3.00

Table 2 Physical properties of polyvinyl and polyurethane

Materials	E1 Gpa	Nu12
Polyvinyl foam	0.119	0.3
Polyurethane foam	0.115	0.3

Table 3 Thickness and density of composite materials

Materials	Thickness of one layer (mm)	Density (kg/m^3)
Sisal	0.875	1170.40
Jute	0.625	1300
Glass	0.762	1869
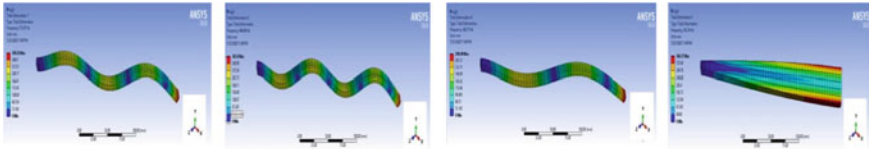
Fig. 1 Mode shapes of S/J/S cantilever beam
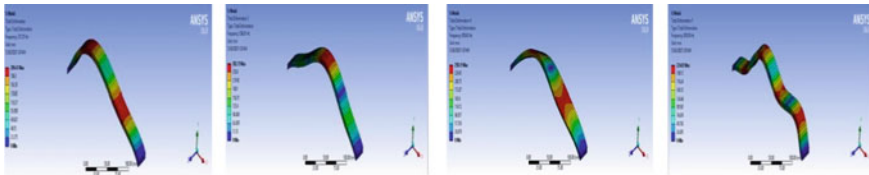

Fig. 2 Mode shapes of curved fixed beam

3 Results and Discussion

3.1 Comparison with Previous Studies

The accuracy of analysis with the software is necessary to validate for the study. The analysis has been carried out with the property of existing literature and compared to create a good argument. The finite element based software ANSYS 16.0 is validated by comparing with previous literature property and result. In the present investigation, the vibration analysis has done with the tensile properties of a previous study by Tita [11] as given in Table 4 and the density of the fiber is 1976 kg/m^3. The beam has made up of 0/90° layer orientation of E-glass cloth with ten layers sequences. The comparison between previous analysis and present analysis has shown in Table 5.

Table 4 Properties of glass/epoxy composite cantilever beam mentioned in previous study [11]

Dimension of the sample (mm)	E1 GPa	E2 GPa	E3 GPa	Nu12	Nu13	Nu23	G12 GPa	G13 GPa	G23 GPa
25 * 2 * 400	24.40	24.40	10.66	0.28	0.20	0.20	4.94	4.47	4.47

Table 5 Comparison of natural frequencies of ten layers glass fiber laminated cantilever beam with previous study [11]

Modes	Natural frequencies by (Tita, 2001) (Hz)	Natural frequencies by present method (Hz)
1	5.11	5.16
2	31.96	32.34

3.2 Layer Effects on Fundamental Natural Frequency of Natural Fiber Laminated Composite Beams

In this part of study, the jute (J) and sisal (S) fiber laminated composite beam had been analyzed with different number of layers such as four layers, eight layer, twelve layer, and sixteen layers in cantilever, simply supported and fixed beam. The result of first natural frequency with numbers of the layers is shown in the Fig. 3.

Figure 3 shows that the fundamental natural frequency is higher in sixteen layers sisal fiber laminated composite fixed beam as compared to the other beams. As per the analysis, the sixteen layers sisal fiber laminated composite fixed beam has 25.241 times and 9.088 times, 12.650 times and 4.555 times, 8.444 times and 3.049 times, 6.340 times and 2.301 times more first natural frequency than the cantilever and simply supported sisal fiber laminated composite beam in four layers, eight layers, twelve layers, and sixteen layers respectively, whereas for fixed beam has 3.931 times, 1.977 times, 1.325 times more fundamental natural frequency than the four layers, eight layers and twelve layers respectively. Similarly, the same beam has 47.990 times, 17.255 times and 7.481 times, 24.032 times, 8.639 times, and 3.735 times, 16.038 times, 5.771 times and 2.509 times, 12.038 times, 4.341 times and 1.888 times more first natural frequency than the cantilever, simply supported and fixed jute fiber laminated composite beam (JFLCB) in four layers, eight layers, twelve layers, and sixteen layers respectively. The sisal fiber laminated composite
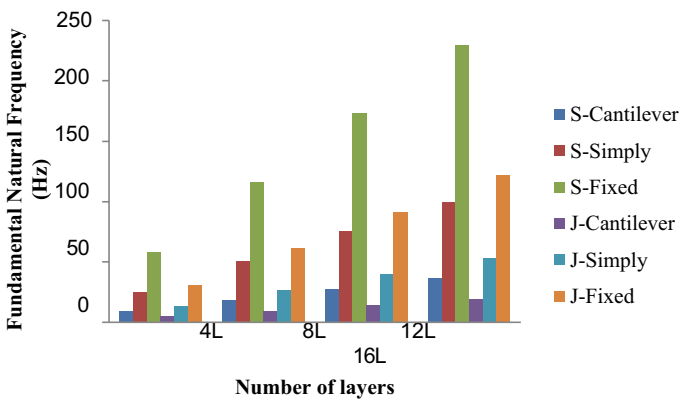
Fig. 3 Layer effect on fundamental natural frequency of different type of beams

Fig. 4 Effect on first natural
frequency with the aspect
ratios
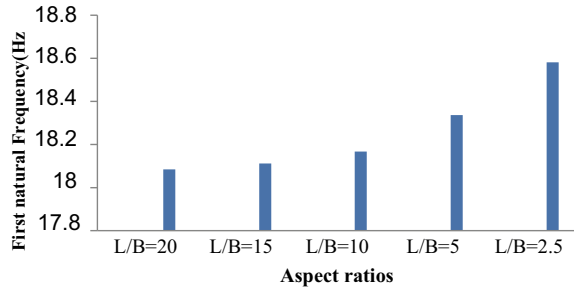
beam (SFLCB) has more fundamental natural frequency than the JFLCB for its
greater tensile properties. Due to the increase of numbers of layer, the fundamental
natural frequency has increased. The fundamental natural frequency of four layers
SFLCB has increased by 49.87, 66.65, and 74.87% in eight, twelve, and sixteen
layers cantilever beam.

3.3 Effects of Aspects Ratio on Fundamental Natural Frequency of Sisal Fiber Laminated Composite Beam (SFLCB)

The effects of different values of aspect ratios (l/b ratio) such as 2.5, 5, 10, 15, and
20 on fundamental natural frequency of sisal fiber laminated composite SFLCB is
presented in Fig. 4.

Figure 4, concludes that the first natural frequency of the sisal fiber laminated
composite cantilever beam has increased with the decreased aspect ratio. As per the
analysis, the fundamental natural frequency at the aspect ratio of 2.5 has 1.34, 2.27,
2.59, and 2.74% more than the aspect ratio of 5, 10, 15 and 20.

3.4 Effects on Natural Frequencies of Natural Fiber (NF) and Synthetic Fiber (SF) Laminated Hybrid Composite Beam

The three layers laminated cantilever composite beam has hybridized with the natural
fiber and glass fiber. The result of the hybridization with jute and sisal fiber laminated
composite cantilever beam and the hybridization of jute fiber with glass fiber and
sisal fiber with glass fiber laminated composite beams are shown in Fig. 5.

Figure 5 shows that, the only sisal fiber laminated composite cantilever beam has
more frequencies and only jute fiber laminated composite cantilever beam has the
less. The hybridization of jute fiber and sisal fiber, increases the first natural frequency
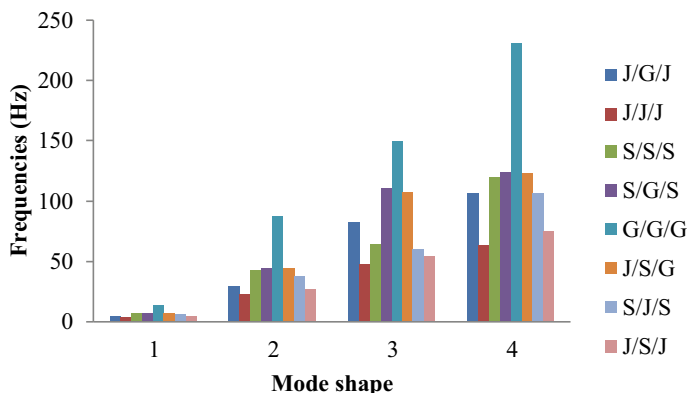
Fig. 5 Effects on frequencies in natural and synthetic fiber laminated composite cantilever beam

of jute fiber laminated composite cantilever beam by 57%, but a 17% decreases the fundamental natural frequency of sisal fiber laminated composite cantilever beam. Only glass fiber laminated composite cantilever beam has observed the maximum natural frequencies and the only jute fiber laminated composite beam has observed the minimum natural frequencies. The fundamental natural frequency of jute fiber and sisal fiber laminated beam has increased by 30.689 and 3.580% by the hybridization with glass fiber in the laminated composite beam. The combination of layers in jute fiber with the glass fiber laminated composite beam gives the good outcome as compare to the layer sequences of sisal and glass fiber.

3.5 Effects on Natural Frequencies in the Sandwich Composite Cantilever Beam

Formation of a sandwich beam with 30 mm thick PV foam and polyurethane as core material, four layer jute, sisal and glass fiber is used as face material of the sandwich composite laminated cantilever beam. The result of the analysis with the sandwich beam is represented in Fig. 6.

From Fig. 6, the sandwich analysis with PV foam and polyurethane as a core material, it has been found that the sandwich cantilever beam made up of PV foam and the sisal fiber has more natural frequency as compared to the jute and polyurethane. The highest natural frequencies have observed in G/PV/G laminated beam and lowest in J/U/J fiber laminated composite cantilever beam. The formation of sandwich has increased the natural frequencies of sisal and jute fiber laminated composite beam. The comparison study has developed in the basis of natural frequencies in between the glass fiber laminated sandwich beam and the natural fiber laminated sandwich composite beam. The PV is taken as core and the jute and sisal laminated composite sandwich beam has 59.215% and 51.686% less fundamental natural frequencies
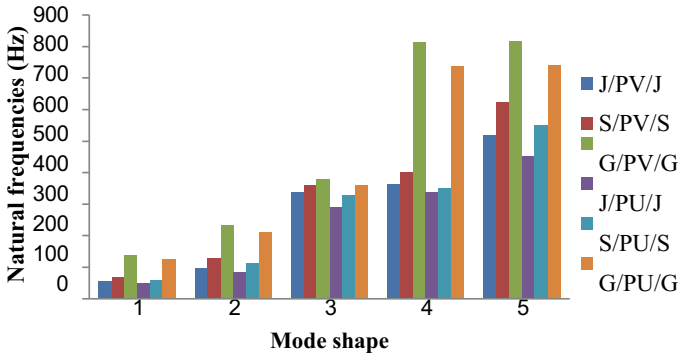
Fig. 6 Effect on natural frequencies in natural fiber and synthetic fiber laminated sandwich Cantilever beam

than the glass fiber laminated composite sandwich beam respectively. Similarly the polyurethane as core layer and jute and sisal fiber as face layer in sandwich composite beam has 61.426% and 53.707% less fundamental natural frequency than the glass fiber laminated composite sandwich beam respectively.

3.6   Effect on Natural Frequencies in the Curved Fixed Beams

In this part of the analysis, eight layers of sisal fiber laminated composite fixed beam with various angles at the support have taken. Figure 7 shows the natural frequencies of first five mode in 0°, 30°, 45°, and 60° curved fixed beams.

From Fig. 7, it is found that the fundamental natural frequency is more in 30° curved fixed beams. The fundamental natural frequency of 30° curved fixed beams has 10.83%, and 35.80% more than the 45°, and 60° curved fixed beams respectively. The 30^0 curve gives 2.597 times more fundamental natural frequency than the flat beam. Curved in the beam has increased the stiffness of the beam, but after certain

Fig. 7 Natural frequencies in curve fixed beams
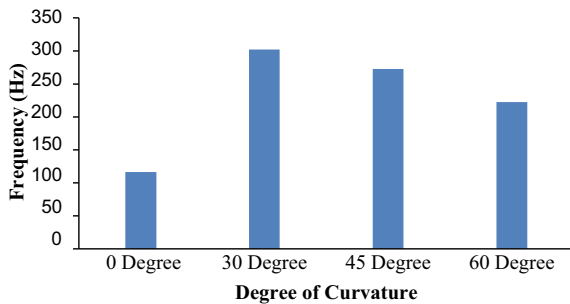
curves it tends to break. Mainly the 30° curve beam gave the best result as compare to the other angle of the curved beam.

4 Conclusions

- The first natural frequency of natural fiber laminated composite beam increases with increasing of layer due to increasing the stiffness.
- Sisal fiber laminated composite beam has more fundamental natural frequency as compared to the jute fiber laminated composite beam.
- The natural fiber laminated fixed beam has observed the maximum fundamental frequency than the cantilever and simple supported beam.
- The first natural frequency of natural fiber is inversely proportional to the aspect ratio.
- In case of natural fiber laminated hybrid composite beam, the fundamental natural frequency of jute fiber laminated composite beam has increased but sisal fiber laminated composite beam has decreased due to hybridization.
- The fundamental natural frequency of natural fiber laminated composite beam has improved by hybridization with synthetic fiber.
- The combination of sisal fiber and polyvinyl foam in a sandwich composite beam has performed a good result.
- The 30° curve fixed beam has more fundamental natural frequency than the flat fixed beam.

References

1. Baba BO, Thoppul S (2009) Experimental evaluation of the vibration behavior of flat and curved sandwich composite beams with face/core debond. Compos Struct 91(1):110–119
2. Dittenber DB, Ganga Rao HVS (2012) Critical review of recent publications on use of natural composites in infrastructure. Compos Part A Appl Sci Manuf 43(8):1419–1429
3. Faruk O et al (2012) Biocomposites reinforced with natural fibers: 2000–2010. Progress Polym Sci 37(11):1552–1596
4. Jena PC (2018) Free vibration analysis of short bamboo fiber based polymer composite beam structure. Mater Today Proc 5(2):5870–5875
5. Ku H et al (2011) A review on the tensile properties of natural fiber reinforced polymer composites. Compos Part B Eng 42(4):856–873
6. Kumar KS et al (2014) Tensile, impact, and vibration properties of coconut sheath/sisal hybrid composites: effect of stacking sequence. J Reinforced Plast Compos 33(19):1802–1812
7. Matsunaga H (2001) Vibration and buckling of multilayered composite beams according to higher order deformation theories. Journal of Sound and Vibration, 246(1):47–62
8. Mondal S et al (2015) Dynamic performance of sandwich composite plates with circular hole/cut-out: a mixed experimental–numerical study. Compos Struct 131:479–489
9. Rajesh M, Pitchaimani J (2017) Experimental investigation on buckling and free vibration behavior of woven natural fiber fabric composite under axial compression. Compos Struct 163:302–311

10. Rajesh M, Pitchaimani J, Rajini N (2016) Free vibration characteristics of banana/sisal natural fibers reinforced hybrid polymer composite beam. Procedia Eng 144:1055–1059
11. Ticoalu A, Aravinthan T, Cardona F (2010) A review of current development in natural fiber composites for structural and infrastructure applications. In: Proceedings of the southern region engineering conference (SREC 2010). Engineers Australia
12. Tita V, de Carvalho J, Lirani J (2001) A procedure to estimate the dynamic damped behavior of fiber reinforced composite beams submitted to flexural vibrations. Mater Res 4(4):315–321
13. Waddar S et al (2019) Buckling and vibration behaviour of syntactic foam core sandwich beam with natural fiber composite facings under axial compressive loads. Compos Part B Eng 175:107133

Experimental and Numerical Studies on Free Vibration of Natural Fiber Laminated Composite Plates

Tanushree Dalai and Madhusmita Biswal

1 Introduction

Now a days the research emphasis on composite with green technology to avoid the use of artificial fiber in composite. Natural fibers are achievable substitution for conventional fibers in most of engineering applications such as structural, aerospace, automobile, mechanical due to their excellent unique properties. Composite material provides chance towards the engineer as well as designer to enhance efficiency of material, superior use of resources and ensuing in cost diminution.

The main objective of this paper is to improvement, analysing and characterization of woven fabric natural composite laminated plates to know their suitability and adaptability for various structural applications and determine the natural frequency of vibration by vibration analysis so as to prevent damages in structure due to the phenomenon of resonance. Vibration analysis can be used to locate, identify and roughly enumerate defect in natural fiber composite. Natural frequencies caused by vibration are a sign to identify an unseen deficiency that produce in the plate specimen. Mainly these inspections were concentrated on experimental as well as analytical testing of composite laminated plate structure.

Many researchers have investigated vibration characteristics such as, Gowda and Naidu [1] studied dynamic characteristics of jute and sisal laminated composite plate. It is concluded that the damping factor of sisal laminated plate was 1.52 times greater than jute. Sai et al. [2] investigated dynamic study on hybrid sisal/bagasse/epoxy composite plates experimentally. They found out that the fundamental frequency of hybrid plate is 1.15 time higher than that of sisal plate. Kadbhane and Kharate

T. Dalai
Nilachal Polytechnic, Bhubaneswar, Odisha, India

M. Biswal (✉)
Centre for Advanced Post Graduate Studies, BPUT, Rourkela, Odisha, India
e-mail: capgs.madhusmita@bput.ac.in

453

[3] preformed damping behavior of conventional and composite laminated sandwich plates. It was observed that natural frequency of plate increase by increase in number of modes and the simply supported condition preferred more natural frequency than cantilever condition. Ali [4] investigated vibration characteristics and mechanical properties of sisal natural fiber reinforced composite laminated plate. It is observed that the composite having high volume fraction of fiber and less volume fraction of matrix provide greater young' modulus with high strength value. Shah et al. [5] presented vibration study on unidirectional natural fiber composite for determine natural frequency with various boundary condition. They concluded Hemp/sisal fiber reinforced polymer composite hold maximum natural frequency as well as greater mechanical strength followed by Sisal FRPC and Hemp FRPC. Deli [6] presented experimental and numerical investigation on vibration of date palm composite plate. Sawant and Mache [7] presented experimental and numerical investigation on damping properties of natural fiber reinforced composites. From the existing literature it was noticed that only limited works were reported on free vibration characteristics of natural fiber laminated composite plates. The main objective of this paper is to establish an investigation over free vibration of laminated composite plates with pure natural fiber and its hybrid separately. In this experiment it will consider various parameters of natural fiber composite plates as per the research demand.

2 Materials and Methods

In this work the woven fabric type natural fiber are used. There are three types of natural fiber are used as jute (bidirectional in nature), sisal fiber (bidirectional in nature) and banana fiber (unidirectional in nature) as shown in Fig. 1. These fibers are purchased from Go green Products, Chennai, Tamil Nadu, India. Resin and hardener are used as catalyst of Araldite brand from Kolkata, West Bengal, India.

Fig. 1 Woven fabric natural fiber

Fig. 2 Preparation of plate specimen

2.1 Fabrication of Natural Composite Plates by Hand Lay-Up

Composite laminates were prepared by hand lay-up technique supported with two sets of ply. In between the two ply the composite plates are placed with proper fabrication then by application of load it was rest for two to three days. The each laminate of size 250 mm lengths and 250 mm breadth was made as shown in Fig. 2. First up all fiber and matrix was measured in the ratio 50:50 by weight.

2.2 Determination of Material Constants

In this present study tensile test is determined to found out the Young's modulus of elasticity. The tensile test specimen is prepared according to the ASTM D3039 standard and tensile testing carried out using INSTON 8862 as shown in Fig. 3. The cross head velocity or rate of loading of this machine is 1 mm/min. The strips cut down from the casted plate for this testing were of the dimension 250 mm length and 2.5 mm breadth.
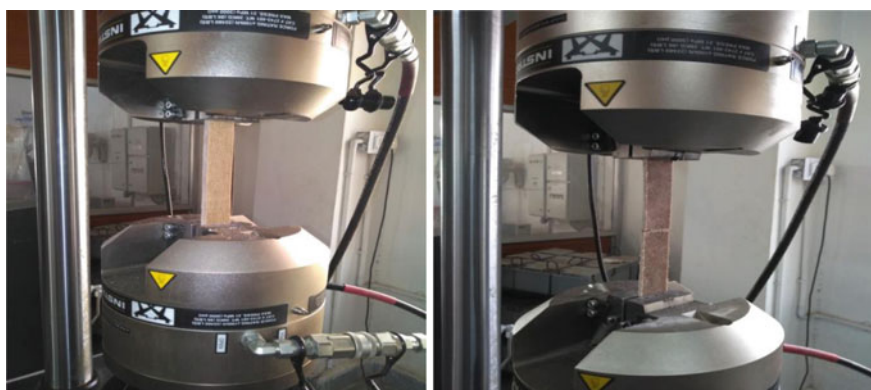
Fig. 3 Tensile test set up before and after failure of strip sample

Fig. 4 Various boundary condition of plate for vibration test by FFT

2.3 Determination of Natural Frequency by FFT Analyzer

The experiments of natural composite plates are to be done by FFT analyzer. The vibration analyzer will receive the signs from the impact hammer and accelerometer sensed resulting vibration systematically. Both the input and output indications was investigated by spectrum analyzer. Hence a curve will be generated as graphical shape known as Frequency Response Function (FRF).

The plates were adjusted according to the preferred boundary condition. The output result was displayed on computer screen through pulse lab shop software. As per various numbers of modes of excitation given to the plate various FRF are measured. The various boundary conditions are CFFF, SSSS, CFCF and CCCC as shown in Fig. 4.

2.4 Determination of Physical Properties of Plate Specimen

The physical properties of fabricated composite plates are measured perfectly. The thickness of the laminated composite plate sample was measured by vernier callipers having a least count of 0.1 mm. The weighing machine is used to measure the weight of the casted plate which is required to calculate the density of the plate as shown in Table 1.

2.5 ANSYS Modelling of Plate Specimen

In this part numerical analysis of different natural composite plate are evaluated by using the finite element software ANSYS 17.2 model. All laminated plates are modelled in ANSYS with various boundary conditions then analysis done to find out natural frequencies of different composite laminated plate. The ANSYS modelling solved by (SHELL 8 node 281) with various load application as per different boundary condition as shown in Fig. 5.

Table 1 Physical properties of fabricated composite plate specimen

Material type	No. of layers	Length (m)	Width (m)	Thickness (m)	Mass (kg)	Density (kg/m^3)
Jute/Epoxy [0°/90°]2S	4	0.235	0.235	0.0025	0.182	1318.50
Jute/Epoxy [0°/90°]3S	6	0.235	0.235	0.0033	0.237	1300.50
Jute/Epoxy [0°/90°]4S	8	0.235	0.235	0.0043	0.303	1284.40
Jute/Epoxy [45°/45°]4S	8	0.235	0.235	0.0041	0.305	1174.45
Sisal/Epoxy [0°/90°]2S	4	0.235	0.235	0.0035	0.227	1174.50
Sisal/Epoxy [0°/90°]3S	6	0.235	0.235	0.0052	0.336	1170.40
Sisal/Epoxy [0°/90°]4S	8	0.235	0.235	0.0075	0.469	1132.35
Sisal/Epoxy [45°/−45°]4S	8	0.235	0.235	0.0070	0.466	1205.45
Jute/Banana/Sisal/Epoxy Hybrid	8	0.235	0.235	0.0061	0.317	941.00
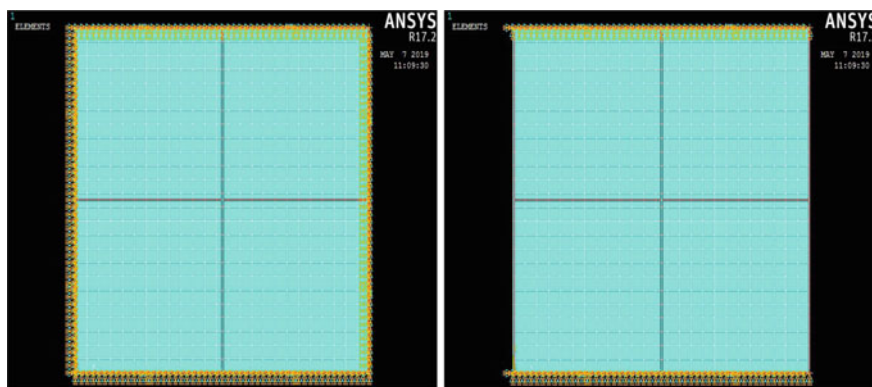
Fig. 5 ANSYS modelling of plates with various boundary conditions

3 Results and Discussions

In this part all the experimental results through FFT analyzer and numerical values through ANSYS software to determine natural frequencies of woven fiber natural laminated composite plates. It also defined the brief comparison in between experimental and numerical values.

Table 2 Material properties by tensile test

Materials types	No. of layer	E1 (GPa)	E2 (GPa)	G12 (GPa)	μ12
Jute	8	0.70	0.70	0.53	0.32
Sisal	8	1.16	1.16	0.79	0.34
Hybrid	8	3.20	3.20	1.63	0.30

3.1 Elastic Constants Obtained from Tensile Test

All the parameters are observed by eight Layer woven fiber natural laminated composite plates. From the tensile test results i.e.; tabulated in Table 2. It is observed that the average value of young's modulus of hybrid specimen was greater while compared to plain jute and sisal.

3.2 Layer Effect on Fundamental Frequency of Natural Fiber Laminated Plates

In this part the variation of natural fundamental frequency with variation in number of laminates was studied for 4 layer, 6 layer and 8 layer with variable thickness of jute and sisal square plate as shown in Figs. 6 and 7.

It is observed that the natural fundamental frequency of jute laminated plate for 4 layers and 6 layers is decreased by 43.94 and 25.21% with respect to 8 layers whereas in case of sisal plate the natural fundamental frequency is decreased by 44.86 and 22.08% overall. As a whole it is identified that the more in thickness of the plate structure have extensive optimistic effect on natural frequency in different end configuration.
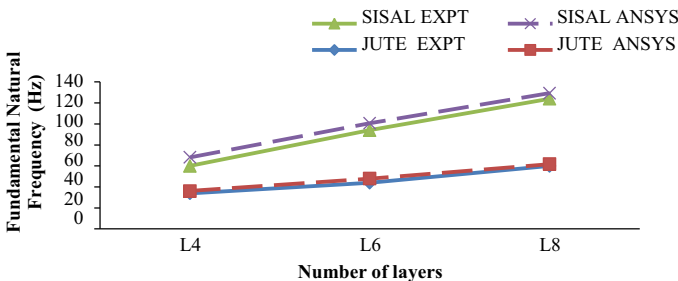
Fig. 6 Layer effect on FNF of Jute and Sisal plate with CFCF BC
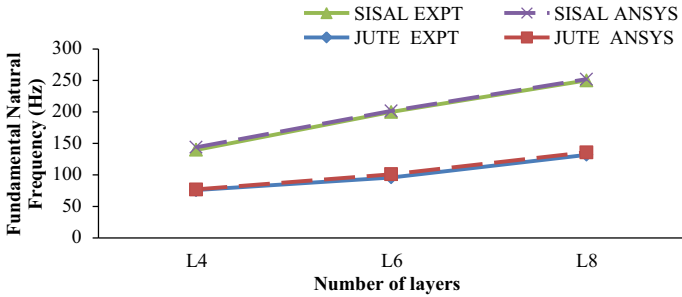
Fig. 7 Layer effect on FNF of Jute and Sisal plate with CCCC BC

3.3 Orientation Effect on Fundamental Frequency of Natural Fiber Laminated

The influence of orientations on vibration characteristic of cross ply composite having fiber orientation [0°/90°]4S and [45°/−45°]4S of eight plies are taken into consideration. Both the experimental and numerical fundamental frequency of laminated composite plate under various boundary conditions is shown in Fig. 8.

It is found out that fundamental natural frequency of angle ply is decreased by 9.66% and 5.96% with respect to cross ply of jute and sisal plate respectively in both experimental as well as analytical method. Hence it is observed that the free vibration natural frequency of woven fabric laminated natural composite plates are increasing by changing the lamination stacking sequence from symmetric angle ply to symmetric cross ply.
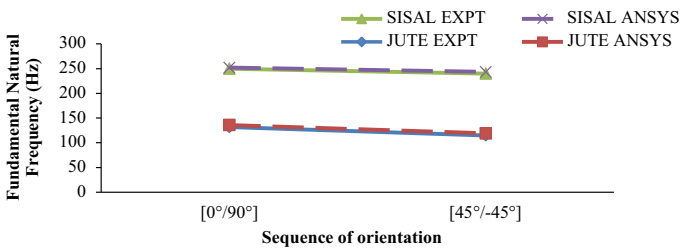
Fig. 8 Orientation effect on FNF of jute and sisal plate with CCCC BC
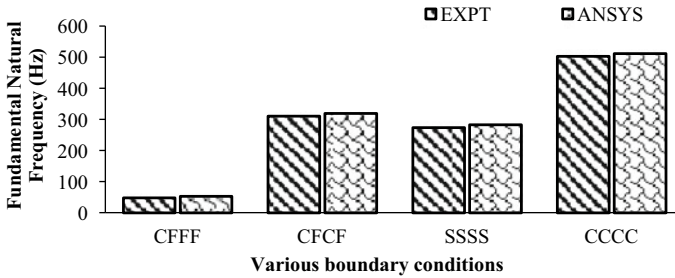
Fig. 9 Effect of boundary condition on FNF of hybrid plate

3.4 Effect of Boundary Condition on Fundamental Frequency of Hybrid Plate

The influence of boundary conditions on fundamental frequencies of laminated composite plates four types of boundary conditions are considered in this investigation such as CFFF, CFCF, SSSS, CCCC as shown in Fig. 9.

The natural fundamental frequency of hybrid laminated plate under CFFF, CFCF and SSSS boundary conditions are decreased by 84.84, 56.81 and 60.7% with respect to four side clamped boundary condition in both experimental as well as numerical study. So that it is observed that the fundamental frequency of laminated plate structure is significantly depend on stiffness of any end configurations.

3.5 Effect of Fiber Verity on Fundamental Frequency of Laminated Composite Plate

There are three different laminated plates such as plain jute, plain sisal and hybrid are taken in this present work to examine the influence of fiber type as shown in Fig. 10.

It is found out that the fundamental frequency of jute and sisal laminates are found to decrease by 73.69 and 47.07% than hybrid plate but in comparison between jute and sisal shows that the fundamental frequencies of sisal laminate increases by 50.06% than jute laminated plate. It is clear that hybridized composite material possess more strength as compare to monolithic materials due to the high young's moduli.
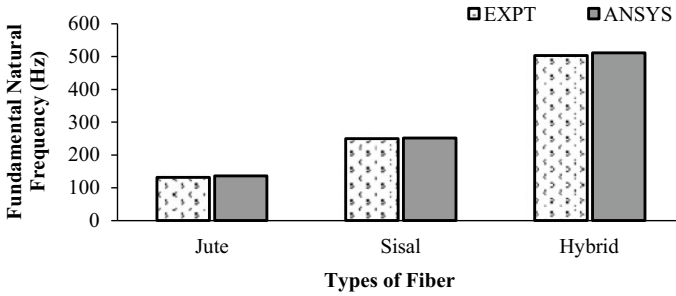
Fig. 10 Effect of fiber type on FNF with CCCC BC

4 Conclusions

The comparisons performed between experimental studies and numerical predictions have good correlation with each other. The fundamental natural frequency of woven fabric natural fiber laminated composite plate increases with the increasing in number of layer under all boundary conditions. The fundamental frequency is decreased in symmetric angle ply as compare to symmetric cross ply. The plate with four side clamped boundary condition gives highest fundamental frequency as compared to other boundary conditions. The hybrid laminated plates possess highest fundamental frequency than single sisal and jute laminated plate with respect to four different boundary condition.

References

1. Gowda TM, Naidu ACB (1999) Experimental study of dynamic characteristics of natural fiber reinforced polymer composite materials. In: Proceedings of NACWET-99, S. J. C. Institute of Technology, pp 277–284
2. Sai NV, Kishore PN, Kumar CP (2014) Investigation on dynamic behavior of hybrid sisal/bagasse fiber reinforced epoxy composites. IJIRAE 357–360
3. Sayali CK, Kharate NK (2016) Damping evaluation of conventional and composite plates using different structures. IJREST 21–32
4. Ali ZAA (2016) Sisal natural fiber reinforcement influenced with experimental and numerical investigation onto vibration and mechanical properties of composite plate. IJEE, pp 497–508
5. Shah M, Khatri J, Patolia H (2018) Vibration analysis of natural fiber composite beam under various end condition. IJERT 7:6–12
6. Deli AA (2016) Experimental and numerical investigation of date palm fiber effect on natural frequency of composite plate with different boundary conditions. IJISET 5:1163–1174
7. Sawant S, Mache A (2018) Experimental and numerical investigation of damping properties of natural fiber reinforced composites. IJMTE 8:611–622

Characteristics of Sugarcane Bagasse Ash as a Pozzolanic Material—A Report on Present Knowledge

Amaresh Tripathy and Prasanna Kumar Acharya

1 Introduction

Ordinary Portland Cement (OPC) is the one of the most widely used construction materials. Along with advantages there is a big drawback in its usage as it contributes in global CO_2 emissions, which approximately is about 4–8% [30]. With the expected consumption of cement projected to rise in future years, which indicates that the associated CO_2 emission will also go up [10, 28]. Hence it is very essential to find methods to utilize substitute Supplementary Cementitious Materials (SCM) that cam impart sustainability in concrete construction [12, 25, 27, 29]. Large amount of agro industrial wastes are being generated in India on daily basis [4, 20]. The major industrial waste locally available are rice husk ash, sugarcane bagasse ash etc. These agro-industrial wastes are the cause of disposal problems and associated environmental degradability issues [5].

Sugarcane production has increased over the years and India produced 376.9 million ton of sugarcane in 2019. Considering the mammoth magnitude in which sugarcane is produced in India it will be a humongous task to dispose such exponential quantities of bagasse ash.

Bagasse ash comprises of highly reactive silica and hence can be utilized as pozzolanic material. Studies suggest that there is a silica content in range of (55–80%) in addition to various other chemical oxides, some of which are summarized in Table 1, hence can be used as a SCM. Objective of this paper is to enlist and virtually compare the effects of the various treatment procedures adopted on bagasse ash before being utilized as a SCM. A gist of the various recent studies like X-ray fluorescent (XRF), X-ray powder diffraction (XRD), Scanning electron microscopy (SEM), Thermogravimetric analysis (TGA) etc. on the bagasse ash is presented for

A. Tripathy · P. K. Acharya (✉)
School of Civil Engineering, KIIT DU, Bhubaneswar, Odisha, India

Table 1 Oxide composition of sugarcane bagasse ash

Author(s)	SiO$_2$	Al$_2$O$_3$	Fe$_2$O$_3$	CaO	MgO	K$_2$O	Na$_2$O	TiO$_2$	MnO	P$_2$O$_5$	SO$_3$	LOI
Arif et al. [1]	78.50	7.27	3.85	1.28	1.28	1.41	0.70				1.55	NR
Bahurudeen and Santhanam [2]	72.95	1.68	1.89	7.77	1.98	9.28					4.45	21.00
Bahurudeen et al. [3]	75.67	1.52	2.29	6.62	1.87	9.59	0.12					3.00
Chusilp et al. [5]	54.45	6.06	3.23	15.41	1.37						0.04	19.39
Cordeiro et al. [8]	80.80	5.10	1.60	3.10	0.00	6.30		0.30	0.10	0.80	1.50	0.40
Deepika et al. [11]	75.67	1.52	2.29	6.62	1.87	9.59	0.12					0.06
Frías et al. [13]	55.97	12.44	6.50	0.84	0.48	0.90		2.67		0.98	1.00	17.98
Ganesan et al. [14]	64.15	9.05	5.52	8.14	2.85	1.35	0.92					4.90
Joshaghani and Moeini [17]	55.70	2.86	3.51	15.34	4.08	6.10	0.37					8.92
Kazmi et al. [17]	85.17	1.69	2.73	2.59	0.69	0.36	0.29				0.17	3.55
Pereira et al. [22]	78.59	4.47	4.88	1.34	1.03	2.37	0.22	1.16			0.66	4.40
Rajasekar et al. [23]	86.79	2.45	1.75	3.42	1.46	3.83					0.30	0.70
Ríos-Parada et al. [24]	66.12	15.00	7.16	2.57	1.19	3.52	0.54	1.13	0.22	1.14	0.26	9.00
Singh et al. [26]	63.16	9.70	5.40	8.40	2.90						2.87	6.90
Yadav et al. [31]	69.7	9.23	4.67	3.85	0.07	3.71	0.88	0.57		2	1.67	16.7

ready reference covering the various physical, chemical properties as well as micro analytical studies.

2 Properties of Sugarcane Bagasse Ash

2.1 Chemical Properties

Generally, the chemical composition is ascertained buy using XRF test on bagasse ash sample. Silica (SiO_2), alumina (Al_2O_3) and iron oxide (Fe_2O_3) are the main constituents in a material which determine and contribute towards its reactivity. Table 1 provides the data from some of the literatures studied along with the loss of ignition (LOI).

The chemical composition of bagasse ash reveals that it comprises of about 50–80% of silicon dioxide (SiO_2), 1–10% of iron oxide (Fe_2O_3) as well as 1–15% of aluminium oxide (Al_2O_3). Alongwith these major constituents there are several other minor oxide components are also available which are present in very negligible quantities. Some of the such chemical oxides are calcium oxide (CaO), potassium oxide (K_2O), sodium oxide (Na_2O), Sulphur trioxide (SO_3), magnesium oxide (MgO) etc. A trend of high LOI is observed which may be attributed to the inefficiency of boilers in the thermal power plants of the sugar mills where the calcination process progresses unevenly resulting in bagasseash with partially burnt as well as unburnt fractions [26]. Chusilp et al. [5] cited that a high LOI for any sugarcane bagasse ash will result in a mortar with decreased strength parameters tested at early ages. Montakarntiwong et al. [18] observed the super plasticizer requirement to increase when they replaced OPC with bagasse ash with a relatively high LOI of 20%. The reported chemical compositions of bagasse ash were found to varying from country to country e.g. Brazil [13] to India [2, 31] to Australia [1] etc. as well as on the calcination temperature and combustion period of bagasse ash as reported by Cordeiro et al. [6, 7], Joshaghani and Moeini [16]. The various properties are also believed to be varying depending on various other factors such as crop species, agricultural and harvesting conditions and quality control.

2.2 Physical Properties

Bagasse ash generally has a specific gravity (SG) which between 1.25 and 2.6. Specific gravity values as reported are marginally higher than ordinary Portland cement. The SG plays an important part in determining the amount water required for standard consistency.

The specific surface area (SSA) of any pozzolanic material serves as a determinant of its reactivity. The raw sugarcane bagasse ash has been studied to have a higher

SSA [31] but at the same time with the structure of the particles being not regular as well as hollow it has been observed to increase the water demand. Ganesan et al. [14] observed the SSA of their collected raw bagasse ash sample was approximately about 3 times higher than OPC.

Generally, the samples studied by researchers have coarse fractions. Coarser materials are lesser reactive. For a great supplementary cementitious material, it should match the fineness characteristics of OPC.

3 Processing Methodologies and Their Effects

Bagasse ash tend to have a varied particle size distribution and are generally available in the coarser fraction. Hence to increase the pozzolanic properties researchers have tried to grind the material to increase its fineness and suggested the process being effective long back [5, 14]. The raw bagasse ash has been studied to contain number of impurities like volatile substances, carbon etc. which are leftovers from incomplete combustion in the power plants. Researchers [19, 21] studied the effects of incineration of the raw bagasse ash to reduce these impurities. Reduction of the various impurities by means of the incineration process resulted in the increase in reactivity of the pozzolanic materials.

3.1 Effect on Physical Properties of Sugarcane Bagasse Ash

Grinding is observed to increase the SG of bagasse ash. Bahurudeen et al. [3] observed in their experiments that the processed bagasse ash prepared by them had a lower SG which led to increase in powder volume and subsequent increase in water requirement for maintaining same workability. Chusilp et al. [5] found the SG to increase from 2.08 to 2.29 when used a ball mill machine for grinding with the objective of particle retained on a 45 µm sieve was less than 5% depicted by Fig. 1a, b. Cordeiro et al. [6, 7] observed that grinding of bagasse ash resulted in changing of tubular shaped porous particles into denser particles depicted by Fig. 2a, b. Cordeiro et al. [9] during their experimentation work grounded the as-received bagasse ash using mechanism of ball mill and for total duration of 4 h which resulted in reduction of mean particle size from 300 µm to 4.7 µm.

Researchers [11] upon their physical ball mill grinding process found that SG increases from 1.91 to 2.12, whereas SSA increased from 145 to their target of 300 matching the fineness of OPC. Montakarntiwong et al. [18] when tested the SG of two variety of bagasse ash prior and after the grinding process, which targeted a less than 5% retention on 45 µm sieve, observed that the SG of the material with low LOI increased from 2.22 to 2.47 whereas that with high LOI increased from 2.09 to 2.16.
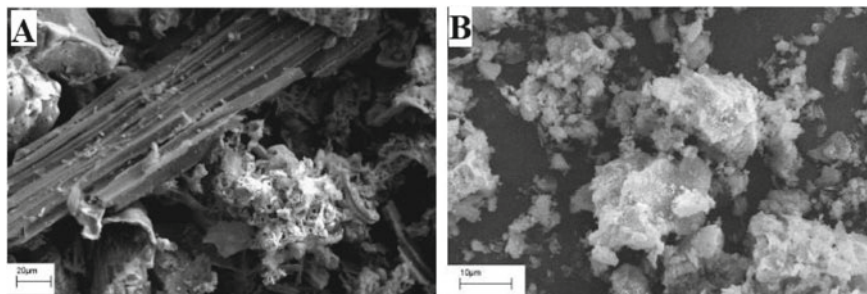
Fig. 1 Images obtained from scanning electron microscope for **a** raw sugarcane bagasse ash **b** grounded sugarcane bagasse ash [5]
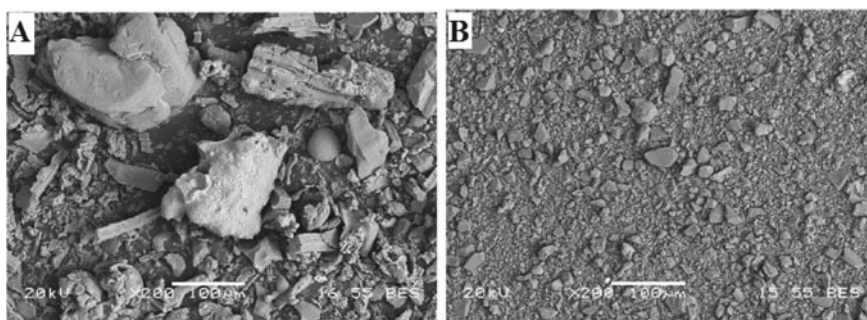

Fig. 2 Images obtained from scanning electron microscope for sugarcane bagasse ash after **a** grinding time of 8 min **b** grinding time of 240 min [6, 7]

Cordeiro et al. [6, 7] upon incinerating the raw bagasse ash at different temperatures of 400, 500, 600, 700 and 800 °C for 3 h periods concluded of not finding any major difference in terms of particle size and had similar physical packing. Bahurudeen and Santhanam [2] observed the peak of SG and SSA at 600 °C and on further increase in temperature both of the values decreased. However, all calcined specimen possessed a higher SG and a lower SSA as compared to raw bagasse ash (Table 2).

3.2 Effect on Chemical Properties of Sugarcane Bagasse Ash

Calcination temperature as well as duration has a direct effect on the various chemical properties of the bagasse ash material. The changes in the oxide contents of different chemicals driven by changes in LOI are evident and has been reported by various researchers, few of which have been summarized in Table 3. It has been concluded by Cordeiro et al. [6, 7] that a temperature of above 600 °C is enough to expel the carbon

Table 2 Effect of processing methodologies on various physical properties

Author(s)	Description/Calcination temperature	50% passing (d$_{50}$)	Specific gravity	Specific surface area (m^2/g)	Consistency (%)	IST (min)	FST (min)	PAI (%)
Yadav et al. [31]	As received raw BA		1.94	24.83	50	170	350	57.04
	BA calcined		2.14	14.47	45	125	300	69.27
	BA calcined + grounded		2.26	21.85	37	90	275	94.74
Bahurudeen and Santhanam [2]	Raw BA		1.91	145				73
	600		2.07	136				74
	700		2.05	131				86
	800		2.03	118				77
	900		1.93	110				67

Table 3 Effect of processing methodologies on oxide composition and LOI

Author(s)	Temp (°C)	Period (min.)	SiO$_2$	Al$_2$O$_3$	Fe$_2$O$_3$	CaO	Na$_2$O	K$_2$O	SO$_3$	MnO	MgO	TiO$_2$	P$_2$O$_5$	LOI
Cordeiro et al. [9]			53.20	13.90	4.40	2.40		1.60	1.50	0.10		0.80	1.30	20.90
	600	180	69.60	15.70	5.70	1.30		2.20	1.50	0.10		0.90	0.90	2.10
Rajasekar et al. [24]	550	60	86.79	2.45	1.75	3.42		3.83	0.30		1.46			7.00
Deepika et al. [11]			72.95	1.68	1.89	7.77	0.02	9.28			1.98			21.00
	700	90	75.67	1.52	2.29	6.62	0.12	9.59			1.87			3.00
Joshaghani and Moeini [16]	500	30	54.10	2.86	3.32	14.10	0.29	5.70			3.86			11.46
	600	30	54.80	3.12	3.75	13.80	0.29	5.60			3.98			10.34
	700	30	54.00	2.80	3.42	14.40	0.32	6.00			4.03			10.58
	800	30	55.70	2.86	3.51	15.34	0.37	6.10			4.08			8.92
	1000	30	53.40	2.91	3.46	14.50	0.37	6.00			4.05			12.10
Frías et al. [13]	300		55.97	12.44	6.50	0.84	0.00	0.90	1.00		0.48	2.67	0.98	17.98
	800		66.61	9.46	10.08	1.43	0.22	3.19	0.10		0.92	2.44	1.04	4.27
	800	60	69.40	11.26	5.41	2.51	0.09	3.45	1.83		1.28	1.38	1.61	1.56
Chusilp et al. [5]			54.10	5.69	3.54	15.37			0.03		1.41			19.36
	550	45	77.37	3.59	4.66	7.81			0.15		1.32			5.08
Cordeiro et al. [6, 7]	600	180	60.96	0.09	0.09	5.97	0.70	9.02		0.48	8.65		8.34	5.70
Morales et al. [20]	800	20	58.61	7.32	9.45	12.56	0.92	3.22	0.53		2.04	0.34	2.09	2.73
	1000	20	59.35	7.55	9.83	12.89	0.96	3.41	0.72		2.10	0.37	2.15	0.81
Ganesan et al. [14]	650	60	64.15	9.05	5.52	8.14	0.92	1.35			2.85			4.90

content as well as the volatile compounds from bagasse ash and by the process have increased the pozzolanic performance of the materials.

The optimum range of temperature for proper calcination varies between 600 and 800 °C depending on the characteristics of the material for reducing the LOI, which also depends upon the calcination duration as with increase in the calcination temperature, duration of calcination has to be less and vice versa. As per Bahurudeen and Santhanam [2] It is preferable not to increase the temperature for calcination exceeding beyond 800 °C, otherwise there is a possibility of amorphous silica getting transformed into crystalline cristobalite, which in hindsight retards the pozzolanic reactivity. Cordeiro et al. [9] established that as the silica content increases with reduction in LOI, there will be an increase in pozzolanic reactivity.

3.3   Effect on Microstructural Properties

3.3.1   Thermogravimetric Analysis (TGA) Study and Differential Thermal Analysis (DTA) Study of Sugarcane Bagasse Ash

TGA is carried out by measuring the mass of a substance under a controlled temperature within a controlled environment as a function of temperature/ time. It is a measure of the loss in form of decomposition, solvent mass loss, oxidation, mass loss in form of water etc. Researchers have carried out the studies and endothermic reactions have been observed in the TGA curves [17, 22, 31]. Figure 3 represents some of the curves as reported by various researchers.

The very first endothermic curve occurring till 300 °C has been reported to be associated to the hygroscopic nature of bagasse ash particles [31]. Between 300 and 550 °C second endothermic reaction is found to take place which is reported to be due to the combustion of organic matter [31]. Endothermic reaction, the third one, occurring between 550 and 850 °C has been attributed to reorganizing of arrangement at structural levels starting with burning of quartz minerals [31]. The last and fourth endothermic reaction occurs till 1200 °C, which is a sharp one, is predicted to be caused by intense change in the arrangement of Si–O–Si bonding [31]. Frías et al. [13] observed weight loss of 1.69% for bagasse ash prepared in laboratory, 1.98% and 9.085 for bottom bagasse ash and filter bagasse ash respectively as obtained from sugar industry. They observed in their analysis, an endothermic peak at 572 °C, which they predicted to be due to carbonate decomposition. Another peak reported by Frías et al. [13] was due to adsorbed water loss. Jagadesh et al. [15] concluded presence of sufficient reactive minerals, formed above calcination temperature as they also marked endothermic reactions in their research work.

From their TGA curves, Kazmi et al. [17] observed that till 700 °C there is a mass loss of about 6%; whereas the mass loss of 22% between 700 and 1000 °C was quite sudden. The DTA curves obtained by Kazmi et al. [17] as per Fig. 3c showed that there is an endothermic peak at 81 °C which was predicted is due to removal of absorbed water along with the exothermic peak which was observed between 400
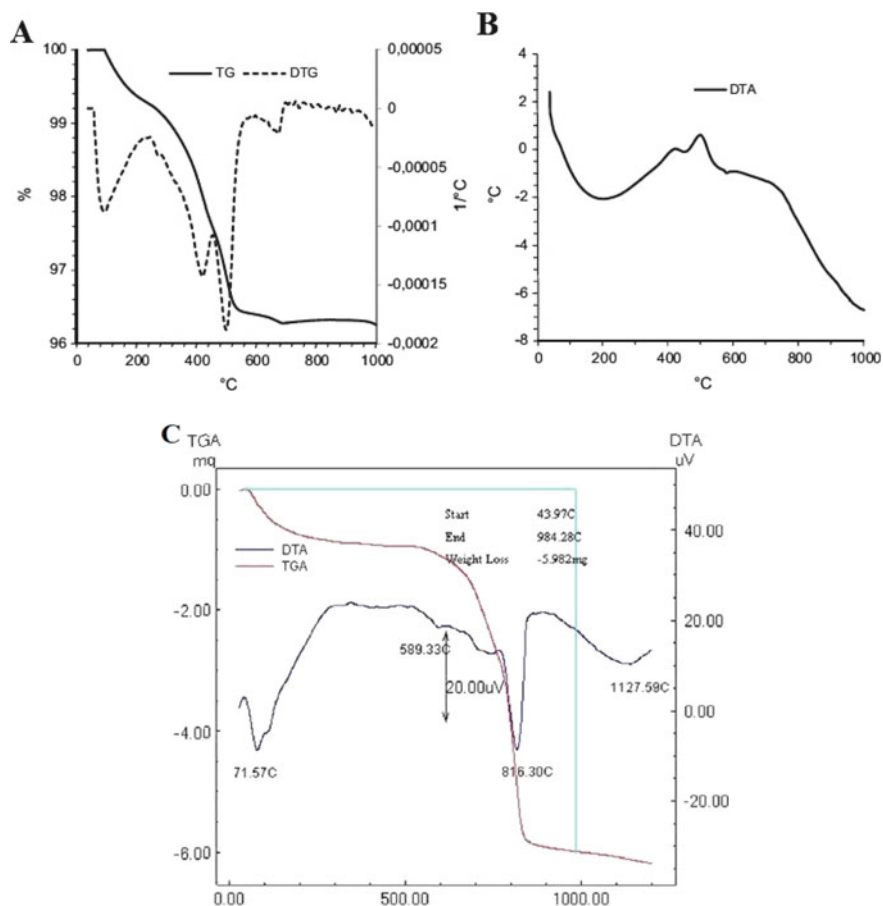
Fig. 3 a TG and DTG curves for sugarcane bagasse ash [22], **b** DTA curve for sugarcane bagasse ash [22], **c** TGA and DTA curve of 20% bagasse ash incorporation [17]

and 500 °C was predicted due to CSH as well as the last endothermic peak was observed at 815 °C and concluded that it might be due to $CaCO_3$ combustion [17].

Pereira et al. [22] observed their major mass loss was in the range of 350–550 °C with prediction that it was due to organic matter depicted via Fig. 3a, b. The DTG curves had first peak at 417 °C followed by another peak at 497 °C predicting the occurrence due to a different oxidation/volatilization processes. A relatively small peak was also observed at 671 °C by Pereira et al. [22] due to carbonate decomposition.

3.3.2 Scanning Electron Microscope (SEM) Study and Energy Dispersive X-ray Analysis (EDAX) Study of Sugarcane Bagasse Ash

Researchers have conducted morphological analysis of bagasse ash with the use of a scanning electron microscope (SEM) device. Surface of bagasse ash has been observed to contain oval shaped elongated particles which contains large number of pores as depicted in Fig. 4e. This results in more water absorption and subsequent increase in more water demand. It has been observed from the reported data that on an average the addition of sugarcane bagasse ash results in about 20% increase in water demand when compared to that of OPC.

Yadav et al. [31] studied the morphology of various bagasse ash samples. As per Fig. 4d, they found that it mainly consists of unburnt, elongated and oval shaped particles with numerous pores and concluded that the bagasse ash has sponge characteristic and are good water absorbent. This signifies that the temperature in boilers is lesser than required hence the particles have not been able to convert into non-porous type. They visualized bulk amount of amorphous particles as depicted in Fig. 4c. Irregular shaped particles with smooth surface were also observed as per Fig. 4b, which are more of prismatic tetrahedral in shape. In addition to the above various spherical as well as irregular and fibrous particles were also observed as per Fig. 4a.

The findings of the EDAX analysis carried out by Yadav et al. [31] are tabulated as per Table 4. For the fibrous particle the EDAX analysis results showed that the bagasse ash material contained major elements of 40.86% of Carbon (C), 37.27% of Oxygen (O), 13.36% of Silicon (Si), 2.54% of Aluminium (Al), 1.92% of Potassium (K). Other elements like Calcium (Ca) was 0.53%, Magnesium (Mg) was 0.52% and Iron (Fe) 0.02%.

Morphological study of the structure of bagasse ash in as received as well as calcined form had also been carried out by Bahurudeen and Santhanam [2]. By studying the SEM images they found that a variety of shapes e.g. fibrous, spherical, prismatic as well as irregular. Fibrous and irregular shaped particles are of more common occurrence in bagasse ash but with due calcination they transform into prismatic and spherical particles. Spherical shape particles are also amorphous in nature and are formed by the high temperature melting of organic matter. Due to their presence in coarser size, the fine fibrous particles, having a cell structure with intercellular network were also being able to be detected. These particles had a huge quantity of carbon which exceeded 80% as per the EDAX analysis. Some of the coarser unburnt fibrous particles had a carbon portion which was incombustible covered by a rich silica layer. These particles also had a huge quantity of carbon which was about 78.29%. The authors concluded that the calcination process is quite essential for diminishing the carbon content.
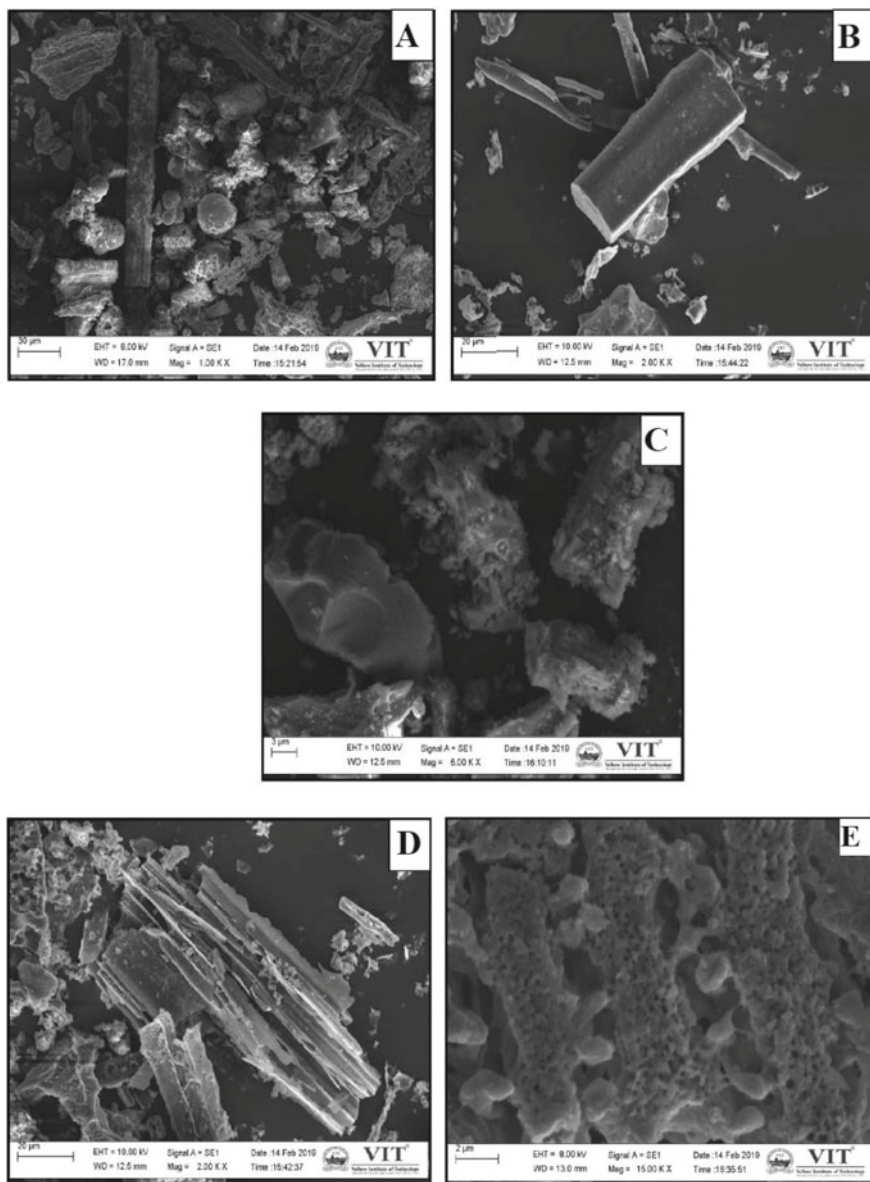
Fig. 4 Sugarcane bagasse ash SEM images for **a** particles of different shapes, **b** prismatic particle, **c** amorphous particle, **d** unburnt bagassse fiber particle, **e** unburnt highly porous particle [31]

Table 4 EDAX data [31]

Shape of particle	Source	Major element(s)	Minor element(s)	Figure
Fibrous coarser particles	Improper burning	Si and C	Al, Fe and Ca	Figure 5e
Prismatic	Moderate burning	Si	Al and K	Figure 5b
Irregular	Moderate burning	Si	Mg, Fe, Al and K	Figure 5c
Spherical	Melting at high temperature	Si	Mg, Fe, Ca, Na and K	Figure 5d
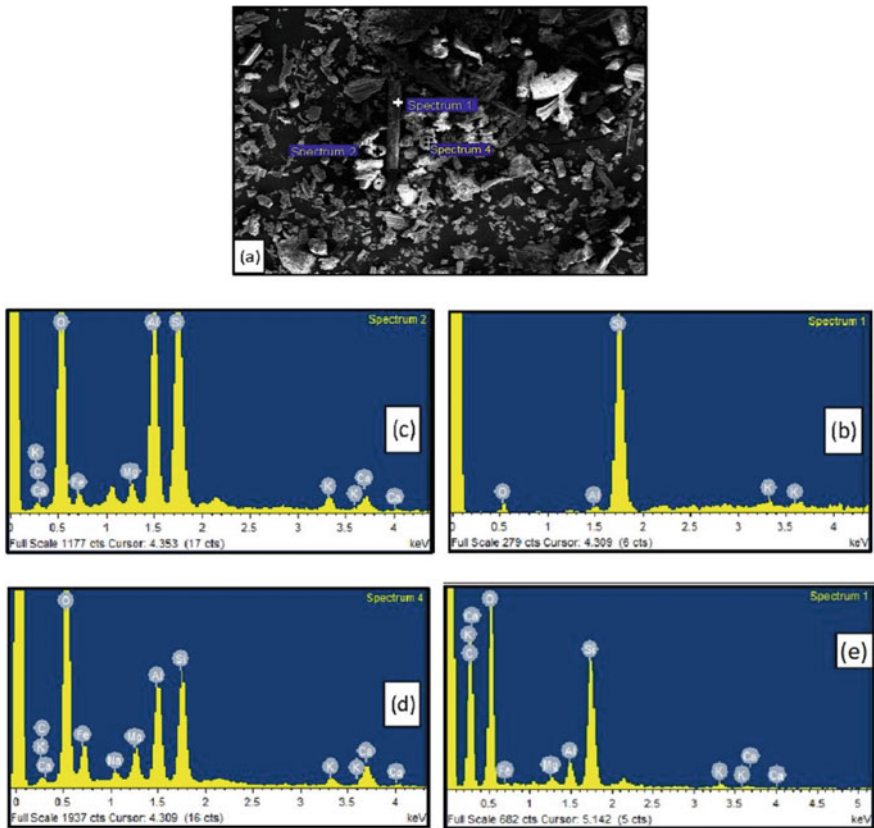
Fig. 5 **a** SEM image for EDAX analysis, **b** spectrum 1—particle with prismatic shape, **c** spectrum 2—particle with irregular shape, **d** spectrum 4—particle with spherical shape, **e** fibrous particle [31]

3.3.3 X-ray Diffraction (XRD) Study of Sugarcane Bagasse Ash

The XRD technique is a method that analyses and determines the structure of crystalline materials and the crystalline phases are identified which reveal crucial chemical information. From various studies [8, 9, 14, 31] it was established that most of the diffraction angle (2θ) for the raw sugarcane bagasse ash falls in the range of $15°$ to $35°$. The most commonly occurring mineral found in bagasse ash is quartz. In addition to quartz, crystobalite phase of silica is also found majorly, which occur in form of elongated spheres.

Yadav et al. [31] observed that quartz was the most abundantly available mineral which signified that silica present is the as received bagasse ash was quartz which is due to presence of sand. They also observed an increase in the amorphous content with calcination as per Fig. 6d, which confirmed by means of increase in non-diffracting component. The combined process of grinding and calcination resulted in tracing of kyanite, silicon oxide, boehmite as well as corundrum in very lesser magnitudes. They concluded that 700 °C was the optimum temperature to derive a requisite amount of amorphous silica without the crystalline state getting converted into crystobalite.

Cordeiro et al. [9] observed the presence of quartz and microcline (potassium rich alkali feldspar) as crystalline phases in both as received as well as calcined bagasse
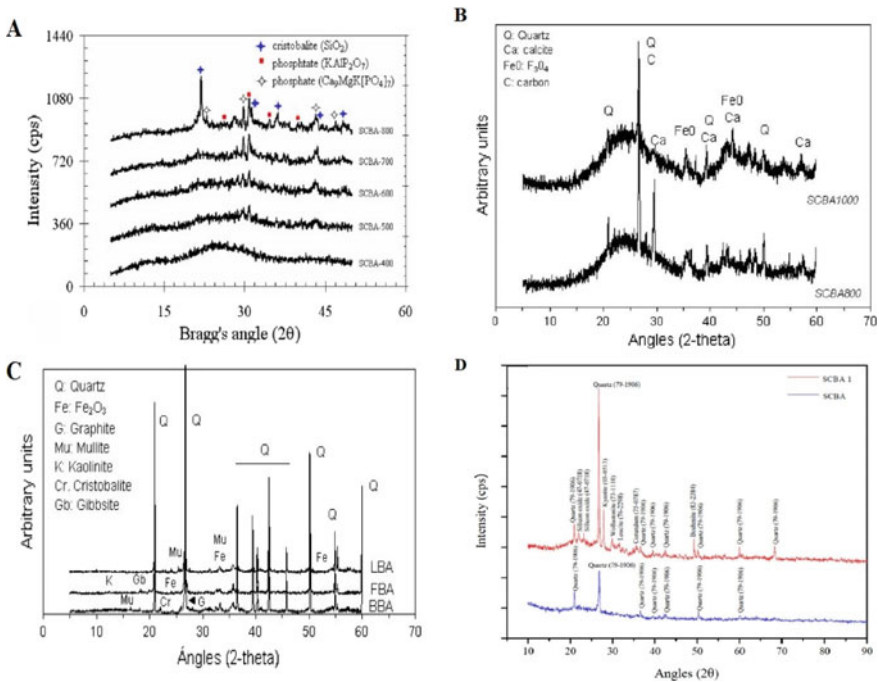
Fig. 6 3 X-ray diffraction patterns for sugarcane bagasse ash **a** Cordeiro et al. [6], **b** Morales et al. [19], **c** Frías et al. [13], **d** Yadav et al. [31]

ash, which they attributed to soil contamination of the sugarcane. Cordeiro et al. [8] observed the additional presence of crystobalite, which they predicted was due to lengthy time frame of calcination at high temperature which facilitated crystallization of the original amorphous silica. Cordeiro et al. [6] observed in a study which focused on controlled burning of sugar cane bagasse that at temperature of about 800 °C that crystobalite formation gets initiated and prior to this temperature the silica stays in amorphous state mostly as depicted in Fig. 6a. The amorphous state silica works as the determinant of pozzolanic reactivity and with the increase in temperature beyond the threshold of 700–800 °C the amorphous content changes into its crystalline variant of silica majorly occurring in form of crystobalite. The same theory and results were also established by Morales et al. [19] depicted as Fig. 6b, where they found quartz as main component but did not observe any major differences in the crystalline and vitreous phase fractions for calcining temperatures of both 800 °C as well as 1000 °C. Frías et al. [13] from their research on fly bagasse ash (FBA), bottom bagasse ash (BBA) and laboratory bagasse ash (LBA) work found that all of the types of ashes had predominantly quartz along with some amounts of iron oxide and mulite but in addition to that FBA had kaolinite and gibbsite whereas BBA had crystobalite represented as Fig. 6c.

Arif et al. [1] observed that at temperature about 573 °C the quartz is having a change in form from a low temperature system to a high temperature system. On further increase in temperature, at 870 °C it is getting converted into tridymite, if there is availability of any impurity. At temperature of about 1470 °C it gets converted into cristobalite, which finally melts at temperature of 1705 °C. They also observed the process being reversible in case of the temperature rise is imparted slowly to the material.

3.3.4 Transmission Electron Microscope (TEM) Study of Sugarcane Bagasse Ash

TEM is a procedure where a beam of electrons is propagated through a material sample to form an image which provides its morphologic and crystallographic information. Morales et al. [19] carried out studies on the characteristics by TEM analysis of calcined sugarcane bagasse ash and also compared the same with Energy-dispersive X-ray spectroscopy (EDAX) which were represented as shown in Fig. 7a–d.

Morales et al. [19] by their studies discovered that there exists a difference in morphology between different grain types of bagasse ash. Particles with non-porous as well as irregular structures are observed in Fig. 7a. They were observed to be rich in calcium which was validated by the EDAX test results spectrum as per Fig. 7b. As shown in Fig. 7c particles which are uncalcined bear a spongy texture, which has an abundance of presence of silicon which was validated by the EDAX test results spectrum as per Fig. 7d.
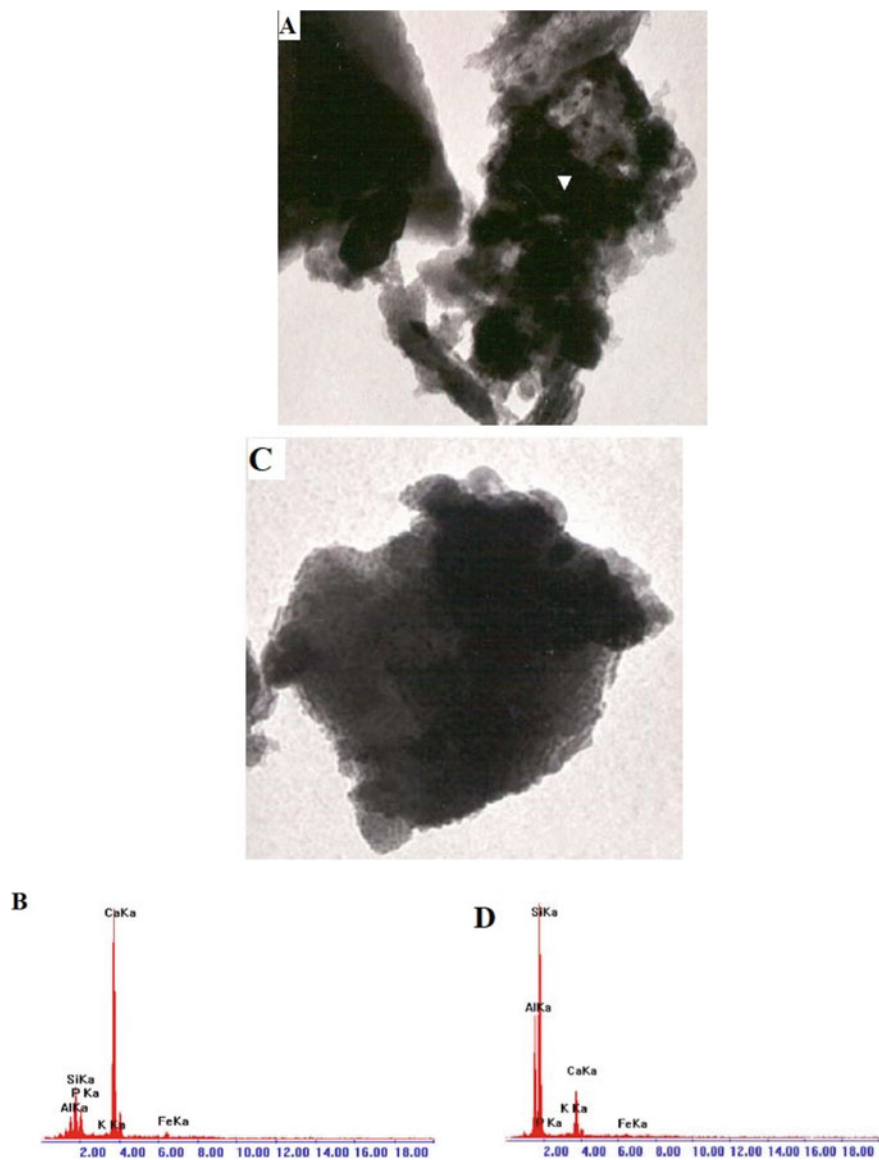
Fig. 7 TEM results from bright field images of bagasse ash enriched in **a** calcium oxides, **c** silicon oxide, **b** XEDS spectrum of **a**, **d** XEDS spectrum of **c** [19]

4   Conclusion

From the reviewed literatures, it may be concluded that there exist sufficient studies which establishes the positive effects of calcination, grinding and their combined effects on the characteristics of bagasse ash. These beneficial effects are the determinant of bagasse ash being undertaken as a SCM with sufficiently good pozzolanic properties. The grinding process has established to be reducing the SSA and thereby increasing the reacting capability by making the particles finer. The calcination process has been observed to remove the variety of discussed impurities, reduce the LOI and increase the amount of reactive amorphous materials. Hence these processes together contribute to the increase in pozzolanic reactivity of the sugarcane bagasse ash. Pozzolanic reactivity of any material is directly linked to the performance enhancement of any mortar or concrete incorporating the SCM up to a certain replacement level. The usage of sugarcane bagasse ash as a SCM has provided an alternative solution and remedy to the waste management issue and environmental hazards created by disposal of the materials.

References

1. Arif E, Clark MW, Lake N (2016) Sugar cane bagasse ash from a high efficiency co-generation boiler: applications in cement and mortar production. Constr Build Mater 128:287–297
2. Bahurudeen A, Santhanam M (2015) Influence of different processing methods on the pozzolanic performance of sugarcane bagasse ash. Cement Concr Compos 56:32–45
3. Bahurudeen A, Kanraj D, Dev VG, Santhanam M (2015) Performance evaluation of sugarcane bagasse ash blended cement in concrete. Cement Concr Compos 59:77–88
4. Chethan Kumar B, Yaragal S, Das BB (2020) Ferrochrome ash—its usage potential in alkali activated slag mortars. J Clean Prod 257
5. Chusilp N, Jaturapitakkul C, Kiattikomol K (2009) Effects of LOI of ground bagasse ash on the compressive strength and sulfate resistance of mortars. Constr Build Mater 23(12):3523–3531
6. Cordeiro GC, Toledo Filho RD, Fairbairn EMR (2009) Effect of calcination temperature on the pozzolanic activity of sugar cane bagasse ash. Constr Build Mater 23(10):3301–3303
7. Cordeiro GC, Toledo Filho RD, Tavares LM, Fairbairn EDMR (2009) Ultrafine grinding of sugar cane bagasse ash for application as pozzolanic admixture in concrete. Cem Concr Res 39(2):110–115
8. Cordeiro GC, Tavares LM, Toledo Filho RD (2016) Improved pozzolanic activity of sugar cane bagasse ash by selective grinding and classification. Cem Concr Res 89:269–275
9. Cordeiro GC, Barroso TR, Toledo Filho RD (2018) Enhancement the properties of sugar cane bagasse ash with high carbon content by a controlled re-calcination process. KSCE J Civ Eng 22(4):1250–1257
10. Dalinaidu A, Das BB, Singh DN (2007) Methodology for rapid determination of pozzolanic activity of materials. J ASTM Int (JAI) 4(6)
11. Deepika S, Anand G, Bahurudeen A, Santhanam M (2017) Construction products with sugarcane bagasse ash binder. J Mater Civ Eng 29(10):04017189
12. Farsana C, Das BB, Snehal K (2020) Influence of fineness of mineral admixtures on the degree of atmospheric mineral carbonation. In: Smart technologies for sustainable development, Springer Publications, pp 117–136
13. Frías M, Villar E, Savastano H (2011) Brazilian sugar cane bagasse ashes from the cogeneration industry as active pozzolans for cement manufacture. Cement Concr Compos 33(4):490–496

14. Ganesan K, Rajagopal K, Thangavel K (2007) Evaluation of bagasse ash as supplementary cementitious material. Cement Concr Compos 29(6):515–524
15. Jagadesh P, Ramachandramurthy A, Murugesan R, Sarayu K (2015) Micro-analytical studies on sugar cane bagasse ash. Sadhana 40(5):1629–1638
16. Joshaghani A, Moeini MA (2017) Evaluating the effects of sugar cane bagasse ash (SCBA) and nanosilica on the mechanical and durability properties of mortar. Constr Build Mater 152:818–831
17. Kazmi SMS, Munir MJ, Patnaikuni I, Wu YF (2017) Pozzolanic reaction of sugarcane bagasse ash and its role in controlling alkali silica reaction. Constr Build Mater 148:231–240
18. Montakarntiwong K, Chusilp N, Tangchirapat W, Jaturapitakkul C (2013) Strength and heat evolution of concretes containing bagasse ash from thermal power plants in sugar industry. Mater Des 49:414–420
19. Morales EV, Villar-Cociña E, Frías M, Santos SF, Savastano H Jr (2009) Effects of calcining conditions on the microstructure of sugar cane waste ashes (SCWA): influence in the pozzolanic activation. Cement Concr Compos 31(1):22–28
20. Mustafa R, Shivaprasad KN, Das BB (2019) Effect of various additives on the properties of fly ash based geopolymer mortar. In: Sustainable construction and building materials, Springer Nature Singapore, pp 707–715
21. Payá J, Monzó J, Borrachero MV, Díaz-Pinzón L, Ordonez LM (2002) Sugar-cane bagasse ash (SCBA): studies on its properties for reusing in concrete production. J Chem Technol Biotechnol Int Res Process Environ Clean Technol 77(3):321–325
22. Pereira A, Akasaki JL, Melges JL, Tashima MM, Soriano L, Borrachero MV, ... Payá J (2015) Mechanical and durability properties of alkali-activated mortar based on sugarcane bagasse ash and blast furnace slag. Ceram Int 41(10):13012–13024
23. Rajasekar A, Arunachalam K, Kottaisamy M, Saraswathy V (2018) Durability characteristics of ultra high strength concrete with treated sugarcane bagasse ash. Constr Build Mater 171:350–356
24. Ríos-Parada V, Jiménez-Quero VG, Valdez-Tamez PL, Montes-García P (2017) Characterization and use of an untreated Mexican sugarcane bagasse ash as supplementary material for the preparation of ternary concretes. Constr Build Mater 157:83–95
25. Sahoo S, Das BB, Mustakim S (2017) Acid, alkali and chloride resistance of concrete composed of low carbonated fly ash. J Mater Civil Eng, ASCE 29(3)
26. Singh NB, Singh VD, Rai S (2000) Hydration of bagasse ash-blended portland cement. Cem Concr Res 30(9):1485–1488
27. Snehal K, Das BB (2019) Techniques for preparation and dispersion of nano-SiO$_2$ in cementitious system—a review. In: Sustainable construction and building materials, Springer Nature Singapore, pp 397–407
28. Snehal K, Das BB, Akanksha M (2020) Early age, hydration, mechanical and microstructure properties of nano-silica blended cementitious composites. Construct Build Mater, Elsevier 233
29. Snehal K, Das BB, Kumar S (2020) Influence of integration of phase change materials on hydration and microstructure properties of nano silica admixed cementitious mortar. J Mater Civil Eng ASCE 32(6)
30. Yadav AL, Sairam V, Muruganandam L, Srinivasan K (2020) An overview of the influences of mechanical and chemical processing on sugarcane bagasse ash characterisation as a supplementary cementitious material. J Clean Prod 245:118854
31. Yadav AL, Sairam V, Srinivasan K, Muruganandam L (2020) Synthesis and characterization of geopolymer from metakaolin and sugarcane bagasse ash. Construct Build Mater 258:119231

Analysing Construction and Demolition Waste Practices: An Indian Case Study

J. S. Sudarsan, A. A. Abhyankar, Aayushi Parashar, and Sistla Vinay Krishna

1 Introduction

Constant urbanization, developing infrastructure and the growing population in India, the Construction sector is at its peak in the country. The effect of around 52.6% declining in the GDP of the last quarter i.e., from March–June of the total 23.9% decrease ranking it third in the economic growth contributor category. Construction Sector in India plays a huge role in the nation's Gross Domestic Product (GDP). As India is a developing nation, the development of the nation is proportional to the infrastructure of the country, where most of it is in the construction phase. On account of these construction activities, repair, remodelling and demolition of the old buildings and structures were recognised in many cities [1–7]. Thus, these activities lead to the generation of Construction and Demolition Waste (CDW) in significant amounts which have a greater potential to be recycled and reused. Construction and Demolition Waste (CDW) can be classified into fragmented Building material, Architecture Sediment and Unrecoverable Construction waste. And then can be further dropped down into recyclable, mixed backfill and landfill [8, 9]. Concrete, Bricks and Mortar has accounted for around 90% of the total waste generated. Also, C&D waste is capable to uphold the economy by reducing the use of virgin resources [10]. The Construction and Demolition Waste (CDW) management has been poor in India despite its greater reuse value and positive effects on the environment leading to a sustainable construction by implementation of lean practices. Technology such as Building Information Modelling (BIM), Geographic Information System (GIS), BIG DATA and prefab construction and implementation of human related factor such as

J. S. Sudarsan (✉) · A. A. Abhyankar · A. Parashar · S. V. Krishna
National Institute of Construction Management and Research (NICMAR) Pune, Pune 411045, Maharashtra, India
e-mail: ssudarsan@nicmar.ac.in

diversion climate and culture can be fruitful development in case of C&D waste management [11].

Waste management improvement is crucial for the construction sector. Generation of Construction waste can be classified into two categories namely natural causes and man-made activities. Manmade destruction in order to have new building construction work, public infrastructure, and renovation, other is natural source due to earthquake, floods and other natural disaster [12]. Nearly 15–20% of the materials ordered go down as waste thus impacting the profitability and project cost with reference to some estimates. The C&D waste is not defined properly and as the building is made by different materials and for different usages and when demolished the material is not used wisely i.e. there is lack of detail and accurate waste management philosophies [13]. The Government has also started tightening the threads in-order to keep a check on the landfill dumping by inclusion of stringent local regulatory measures and took measures to make sure that including a waste management plan to be a part of the project planning. There are technology and methodology that can be used with regard to construction waste but those aren't implemented by construction stakeholders. A need of effective govt policies is there to manage such waste. Otherwise, this wide problem for achieving a sustainable environment will never be achieved [14]. Construction waste generated during operational and design stages sum up to be around 20–30% of the purchased material. It was found that 1 out of 10 units of material purchased goes into landfill as waste [9].

Lean construction can be a solution to the above-mentioned problems of handling the construction and demolition wastes. It is not only cost effective but also a very efficient technique for the successful waste management and develop a sustainable environment. Lean practices should be implemented in the feasibility study stage and the planning stage, such that an effective impact can be observed on the project throughout its life time. There is high need for development of practices for decision making process for CW generation through the life cycle of project with LCA approach for a sustainable project [15]. Since the efficiency and skillset of the working staff plays a role on the quantity of waste being generated, construction firms shifted their focus on to lean construction practices that reduce waste in the first place rather than to worry about handling when generated. The promotion of C&D activities should be there not only in the case of green building projects but as a genuine case of sustainable development and the Illegal ways of dumping should be stopped across country [16].

Lean practices not only target the waste minimization but also used to cut down those resources allotted to non-value adding activities. To maximise the value and minimize the waste are the two important focuses of the Lean technology. For an efficient Construction and Demolition Waste (CDW) management by Lean, involvement and participation of all the stakeholders is extremely important. Almost all the Stakeholders are said to be equally important contributor for C&D waste be it contractor, Designer, Supplier, Owner, Site Manager, Manufacturer [17]. This gives a clear idea about which process and who are adding value to the project, thus helping them in identifying the non-value adding services, in other words waste, can be controlled. The 5S's that define Lean are Sort, set in order, Shine, Standardize and Sustain. Thus,

Lean Construction practices not only reduce the wastes but also play a crucial role in making the process productive.

2 Methodology

The methodology followed for this research contains. Data Collection through multiple sources broadly classified as Primary and Secondary data. For Secondary Data collection, the Journals, Research papers, and the latest trends in the industry were considered and the practices that are followed worldwide for construction waste management were looked upon and the differences with the practices followed in India were mapped. Primary Data Set comprises the data collected through surveys and construction practitioner's interviews regarding the waste disposal methodologies adopted in the industry. A detailed questionnaire designed, which was intended to extract information and support activities associated with construction waste management was floated and the responses recorded Fig. 1. Demographic information and individual knowledge related to waste management was enclosed from this survey and efforts to grouping waste vessels through variable interrogation was made in-order to find the chastisement that engenders the foremost waste on construction sites, and therefore it's benefit to using second-hand material on construction sites. Finally, the data collected was analysed to identify the problem, thus giving us the
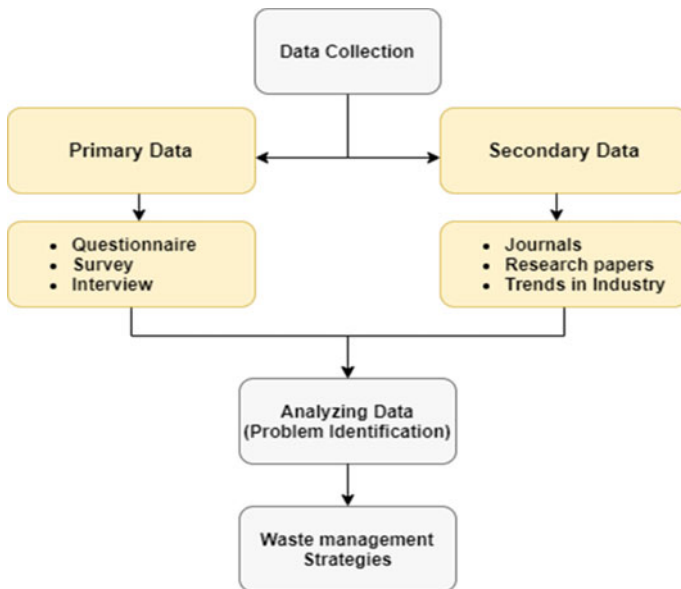
Fig. 1 Methodology

most suitable strategy and plan for Construction Waste Management at the sites may be adopted for an economical and sustainable environment.

3 Results and Discussions

As a part of this is research work for the collection of data, a questionnaire was floated among professionals and practitioners to understand the awareness and practices followed in industry for Construction and Demolition waste management and adoption of Lean practices. The questionnaire was shared among major cities of Maharashtra like Nasik, Pune and Mumbai. The population was noted 115 that was all the consulting and contracting firm registered constituted to the sample frame of study. However, the sample size determined by Leslie Fisher's Formulae came out to be 48 firms. A total of 150 copies of questionnaire was shared and 92 questionnaires were correctly filled and analysed for further study.

The questionnaire contained several questions relating to background and waste handling processes followed in respondent's organization. A descriptive statistic was conducted by using Statistical Package for the Social Science (SPSS) software package because of the nature of research question. The data was presented with the help of Charts for which the Importance Index was calculated for each aspect with the help of degree of importance and ultimately giving overall ranks to all the options on the basis of Importance Index Table 1 [18].

The majority responders (47%) had more than 10 years of experience, increasing the reliability of the analysis. Most of the respondents were associated to construction of High-rise building (67%) and Housing estate. It was found that the construction waste generated per day for a project was 1–5 tonnes. Out of that, Wood/Timber

Table 1 Important waste materials generated on site (generation on importance index)

Construction waste materials	Degree of importance					Importance index	Overall rank
	5	4	3	2	1		
Asphalt	2	2	3	9	14	0.3933	9
Brick/Block	10	10	7	0	3	0.7600	2
Cardboard	1	2	6	10	11	0.4133	8
Concrete	10	7	5	1	7	0.6800	4
Drywall/Wallboard	0	6	8	11	5	0.5000	6
Glass	3	5	4	8	10	0.4867	7
Masonary/Mortar	12	5	7	5	1	0.7467	3
Metals	5	10	6	4	5	0.6400	5
Wood/Timber	11	10	6	3	0	0.7933	1

Importance Index of the Waste Materials Generated on Site
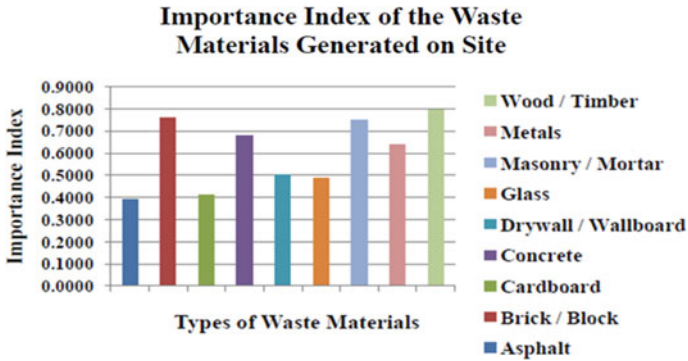
Fig. 2 Importance index of waste materials generated on site

covered was ranked first followed by Bricks and Masonry/mortar Fig. 2. Also, Demolition was the main cause for the production of construction waste. Most of the participants believed that out of all the waste generated only 10–25% will be recycled in further stage.

The ranking of waste material which are frequently recycled are given in the figure below. It was found that metals such as steel and aluminium have the highest recycling rates among the materials recovered from the construction and demolition sites. While on the other hand, concrete is seldom to be recycled Fig. 3.

It is observed that metals that possesses the highest importance while cardboard has the lowest recycling cost Fig. 4. Although metals are expensive to recycle, there are many advantages of metals recycling. By recycling metal such as aluminium and steel, it helps to reduce greenhouse gas emission and also decrease environment damage that caused by mining.

As per the respondents, the method of waste minimization adopted by their organization to minimise the wastes were careful evaluation of materials to cut down the

Importance Index of Frequently Recycled Waste Materials

Fig. 3 Importance index of frequently recycled waste materials
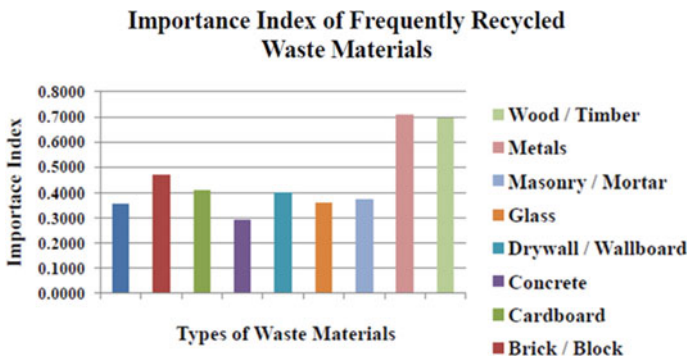
Importance Index of Waste Materials Based on Their Recycling Cost
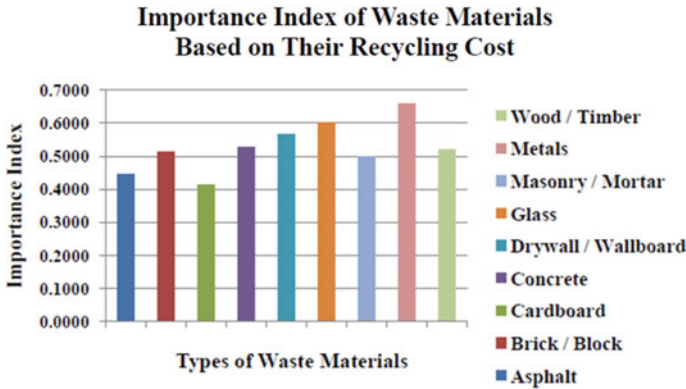
Fig. 4 Importance index of waste materials based on their recycling cost

over-ordering which impacts the wastage and the practice of just-in-time delivery to avoid damages during the storage period which also impacts the waste Fig. 5.

Also, practitioner's preferred dumping of the waste material followed by landfill activity of the material. While quite few choose to burn material into open air Fig. 6. Burning in open air is an illegal practice.

It was agreed by the respondents that main advantage of recycling is help to reduce environmental impacts. Conversely, the respondents were in the opinion that minimizing the waste by recycling did not contribute much on the increase landfill life Fig. 7.

While only 10–25% of the generated is believed to be reused for waste management, the main problem faced by the industry was difficulty in storing, transporting and disposal of the material associated by difficulty in collection and transportation Fig. 8.
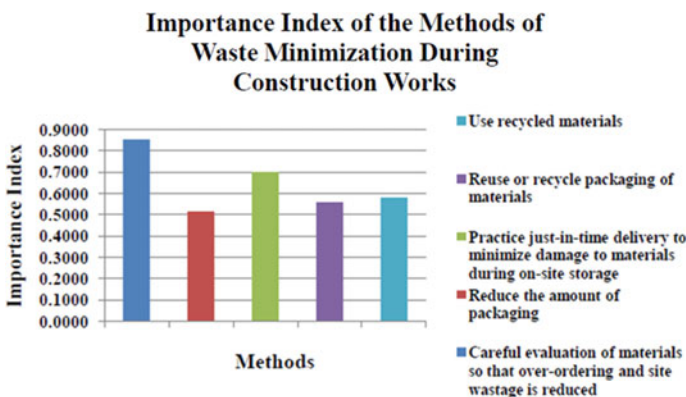
Importance Index of the Methods of Waste Minimization During Construction Works

Fig. 5 Importance index of the methods of waste minimization during construction works

Importance Index of the Methods Used to Dispose of the Waste Materials
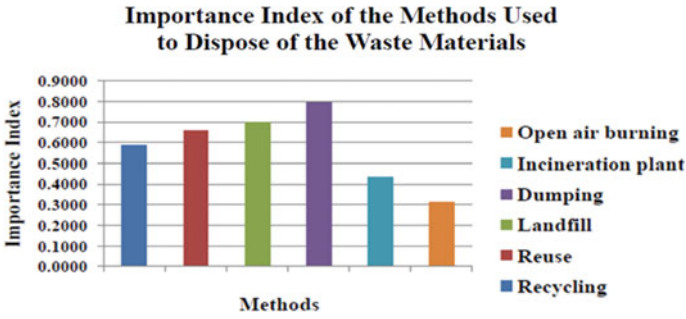
Fig. 6   Importance index of the methods used to disposal of the waste materials

Importance Index of the Effects of Waste Minimization by Recycling
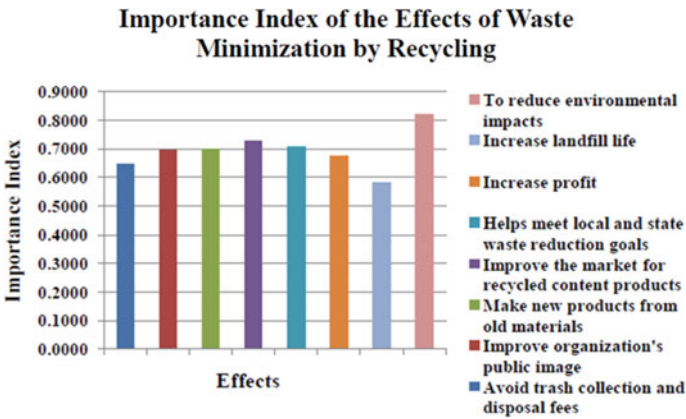
Fig. 7   Importance index of the effects of waste minimization by recycling

Importance Index of the Main Problems in Recycling of Construction Wastes

Fig. 8   Importance index of the main problems in recycling of construction wastes
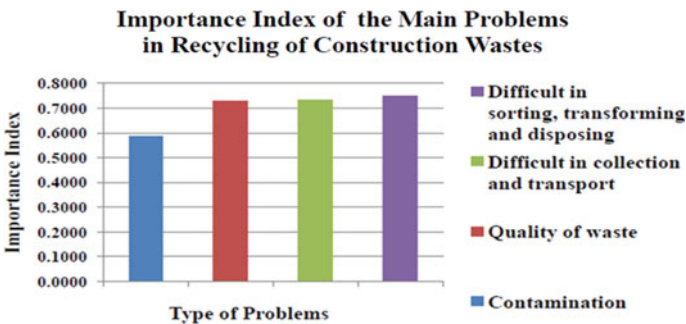
Importance Index of the Factors to
Encourage Construction Waste
Recycling
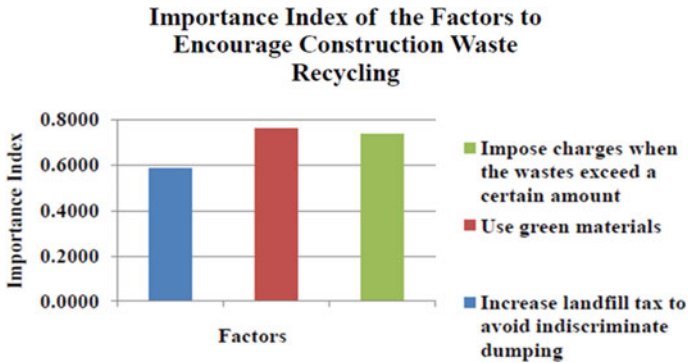
Fig. 9 Importance index of the factors to encourage construction waste recycling

The use of green material was the main factor ranked by respondents which encouraged recycling of construction waste on the other hand the many believed that increment in landfill tax to avoid Indiscriminate dumping was not a very encouraging factor to motivate practitioners to adopt recycling practices for generated construction waste Fig. 9.

4 Conclusion

The outcome from this investigation has settled that selection of Sustainable and Lean Construction (SLC) practices in the Indian development industry and it also proves the need supporting the fact that major problem in India is the unregulated usage of non-renewable resources. The awareness of construction stakeholders and the process of construction and demolition (C&D) is surprisingly high but the implementation is the trouble part.

Applying sustainability in the processes and in organization provides quality of life for all stakeholders and contributes towards the betterment of society and economy, in addition to environment conservation. Lean's goal is to reduce waste and add value to the Stakeholder's goal. Lean practices like Target Value Design, practices design delivery to deliver customer values and develops design with project constraints. Traditionally, Value engineering is used only when it is necessary to cut down the project cost.

The Lean Project Delivery (LPD) system is eminent in industry for its collaborative project organization, relational contract and lean operational system to align and integrate key participants and encourage a collaborative environment while promoting Concurrent Engineering. Concurrent engineering is well described as execution of various task by the collaborative approach of multidisciplinary teams with a common goal to obtain product with desired quality and functionality.

The paper discusses the implications of the different perspectives and argues that they lead to different improvement approaches each reflecting different paradigms for the nature of the change. This also propose that result-focused improvement programs along with lack of support from the public sector, mainly regarding the inspection of destination of C&D waste disposal, incentives regarding ethical waste disposal practices from the government may be a barrier to the adoption of Lean Construction. AEC professionals and their organizations should set their own clear goal in regard to sustainability and take initiatives which goes beyond just environment Sustainability towards the social and economic sustainability.

For future research it can be looked into what drives a stakeholder to establish a result or process focused program. It appears that specialty contractors are more familiar with the process-perspective because of their familiarity with productivity improvement studies.

Future research also needs to

(1) Develop and validate a suitable framework for the optimal usage of the Construction wastes
(2) Further examine the behaviour of improvement process over time.

References

1. Hegde AL, Jain A, Das BB (2019) Resource buffers in construction projects. In: Select proceedings of TMSF 2019, Springer Publications Pte. Ltd. 2021
2. Pandey A, Chaudhary PK, Das BB (2019) Productivity analysis of shuttering works for sewage treatment plant. In: Select proceedings of TMSF 2019, Springer Publications Pte. Ltd. 2021
3. Shekhar S, Shukla P, Das BB (2019) Developing a standard template for activity linkage and resource estimation of MEP works. In: Select proceedings of TMSF 2019, Springer Publications Pte. Ltd. 2021
4. Upadhya PR, Das MS, Das BB (2019) Multi criteria decision making approach for selecting a bridge superstructure construction method. In: Select proceedings of TMSF 2019, Springer Publications Pte. Ltd. 2021
5. Paul B, Tondihal S, Das BB (2019) Safety stock in inventory management and wastage analysis at construction sites. In: Select proceedings of TMSF 2019, Springer Publications Pte. Ltd. 2021
6. Reddy CP, Das BB (2018) Methods to monitor resources and logistic planning at project sites. In: Select proceedings of ICSCBM 2018, Springer Nature Singapore Pte Ltd. 2019, pp 793–802
7. Akhil RP, Das BB (2018) Cost reduction techniques on MEP projects. In: Select proceedings of ICSCBM 2018, Springer Nature Singapore Pte Ltd. 2019, pp 495–517
8. Ginga OJ (2020) Materials circular economy on construction and demolition waste: a literature review on material recovery and production. Materials 13:10–18 (2020)
9. Islam R, Tasnai N, Yuniarto A, Uddin ASM (2019) An empirical study of construction and demolition waste generation and implication of recycling. Waste Manage 95:10–21
10. Jin YR, Chen Q (2018) Science mapping approach to assisting the review of construction and demolition waste management research published between 2009 and 2018. Resour Conserv Recycl 140:175–188
11. Menegaki M, Damigos D (2018) A review on current situation and challenges of construction and demolition waste management. Curr Opin Green Sustain Chem 13:8–15
12. Chen X, Lu W (2016) Identifying factors influencing demolition waste generation in Hong Kong. J Clean Prod 141:799–811

13. Saadi N, Ismail Z, Alias Z (2016) A review of construction waste management and initiatives in malaysia. J Sustain Sci Manage 11:101–114
14. Magalhaes R, Danilevicz A, Saurin T (2017) Reducing construction waste: a study of urban infrastructure projects. Waste Manage 67:265–277
15. Bansal, Bishoni S (2016) Recycling and reuse of construction and demolition waste sustainable approach. In: The 7th international conference on sustainable built environment
16. Bossink, Brouwers H (1996) Construction waste: quantification and source evaluation. J Construct Eng Manage 112:55–60
17. Rafidah R, Abd MZ, Rina S, Adilah NA (2018) Relative importance index of sustainability design and construction activities criteria for green highway. Chem Eng Trans 63:151–156
18. Job T, Wilson JPM (2013) Construction waste management in India. Am J Eng Res (AJER) 2:6–9

Effect of Edge Configuration on Rectangular and Plus Plan Shape Buildings Having Same Plan Area (300 m^2) and Height (50 m)

Arun Kumar and Ritu Raj

1 Introduction

Wind flow is a complex phenomenon and it has a typical behavior to exert differential velocity and pressure, due to its gusting nature, around any bluff body coming in its way of flow direction. In high rise buildings above the height of 60 m (approx.) the height factor is so pronounced that the effect of wind becomes more prominent than the seismic effect while considering the horizontal load. The generalized estimation of magnitude of wind is carried out by defining pressure coefficient (C_{Pe}). C_{Pe} is influenced by various factors like, shape and geometry, incident wind profile, angle of attack, terrain roughness, turbulence in the wind etc. Baines [1] firstly depicted the effect of velocity distribution due to wind and its flow pattern on tall buildings. The contour of the mean wind pressure was intuitively demonstrated as positive pressure on windward side and negative pressures on sides, top and back surfaces of a square shaped building. Various research papers in the field of wind engineering on different shape of high-rise buildings have been published by researchers. Gomes et al. [2] investigated wind pressure distribution on the faces of 'L' and 'U' plan shape tall buildings by using Wind Tunnel Test as well as Computational Fluid Dynamics (CFD) models. Mendis et al. [3] studied the interreference effect as well as along wind and across wind effects for tall buildings using wind tunnel tests and CFD. Amin and Ahuja [4] studied wind induced pressure on buildings of various geometries. Tanaka et al. [5] presented aerodynamic characteristics of different irregular plan shaped tall buildings by wind tunnel tests. Amin and Ahuja [6] investigated the effect of different side ratios on a rectangular building model of same area and height. Chakraborty and Dalui [7] presented a paper on a numerical study of pressure distribution on

A. Kumar (✉) · R. Raj
Department of Civil Engineering, DTU, New Delhi, India

R. Raj
e-mail: rituraj@dtu.ac.in

491

different faces of square plan shaped tall buildings under 0°, 30° and 45° wind angles using Ansys (Fluent). Bhattacharyya et al. [8] studied pressure distribution of various faces of 'E' plan shaped tall building through physical and analytical wind tunnel for various wind angles. Kheyari and Dalui [9] have studied the wind load on a tall building under interference effects through CFD. Roy and Bairagi [10] studied wind pressure and velocity pattern around stepped tall building comprising of rectangular, square and triangular shape placed one above each other. Study of wind pressure and velocity pattern around 'N' plan shaped tall building was conducted by Mukherjee and Bairagi [11]. Bairagi and Dalui [12] studied the pressure distribution of square tall building with 20% setback at h/2 and 10% setback each at h/3 and 2 h/3.

In this paper a brief description is being presented to evaluate C_{Pe} through ANSYS (CFX) and assess the effect of edge configuration around buildings of equal plan area and height. The pressure coefficients with the two models of same height (500 mm) and plan area (30,000 mm^2) but with different edge configuration viz rectangular and plus plan shapes under identical ABL (Atmospheric Boundary Layer) wind conditions is evaluated as depicted in Figs. 1 and 2.

Fig. 1 Rectangular model
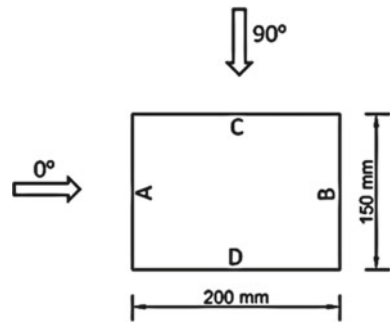
Fig. 2 Plus shape model
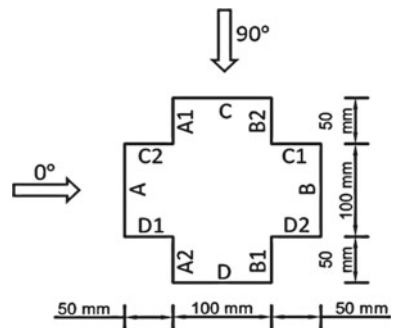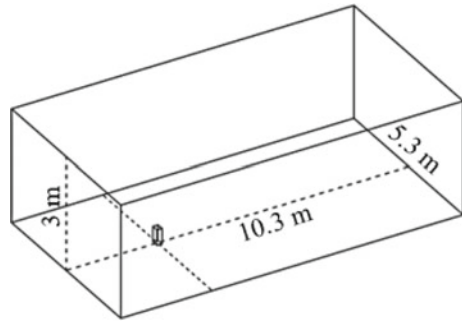
2 Model and Computational Domain

The size of the computational domain in all the three directions, model within the domain and the appropriate boundary condition to cut off the model from the surroundings is created to achieve good similarity with that of the real situation flow condition. Domain size is kept as suggested by Revuz et al. [13] so that velocity fluctuations, uplift force and backwash, vortex generation in the wake region etc. are effectively created in the simulation. The rectangular and plus shape models of height 500 mm and plan 30,000 mm^2 each (1:100 scale) are placed inside the domain of size L = 10.3 m, B = 5.3 m and H = 3.0 m as shown in the Fig. 3.

3 Computational Grid

The result of the simulation depends significantly on the discretized grid of the computational domain and the model. The resolution of the grid is specified to capture important physical parameters such as pressure on the model surface, vortices created, separation and reattachment of the flow etc. to a precise extent. The discretization of geometry of the model is finer than that of the computational grid. Greater the number of cells, better the CFD results. But, increase in number of cells increases the calculation time and also enhanced computing resource is required [14]. In the present study meshing with automatic method and face sizing are adopted with element size 90 mm for the domain volume, 40 mm for the ground and 20 mm for the model walls and roof. Smooth inflation for the model is given so that the grid from the domain touches the walls orthogonally for better simulation results. The total no of nodes created are in the order of 460,000 and the total number of elements are in the order of 2,500,000.

Table 1 Flow parameter

Description	Parameter
Solver	CFX
Flow analysis type	Steady state flow
Flow regime	Subsonic air at 25 °C with reference pressure of 1 (atm)
Turbulence model	k-ε model
Inlet condition	Velocity of flow = normal speed by Power Law with 5% turbulence intensity
Power law	$U = U_{Ref} \times (Z/Z_{Ref})^{\alpha}$ where U is the horizontal wind speed at an elevation Z $U_{Ref} = 0.5$ m/s, $Z_{Ref} = 0.1$ m and $\alpha = 0.143$ for terrain category II (As per IS 875 (Part 3): 2015) [15]
Outlet condition	Average static pressure with relative pressure = 0 (Pa)
Domain side walls, top wall and model roof top	Free slip walls i.e. $U_{wall} = 0$, $\tau_w = 0$ Where U_{wall} is velocity normal to the wall and τ_w is the wall shear stress
Ground and model walls	No slip wall i.e. $U_{wall} = 0$
Model wall roughness	Smooth wall

4 Boundary Condition and the Flow Parameter

The boundary condition for the computational domain and the model and the flow parameter are taken as shown in the Table 1.

5 Result and Discussion

The face averaged value of surface pressure coefficients (C_{Pe}) for different faces of the rectangular model and plus shape model at 0° and 90° angles are presented in Table 2 and 3 respectively. Positive pressure coefficients occur at the wind ward faces due to wind energy dissipation and drag force, whereas suction occurs at the leeward faces due to vortex generation and backwash. The side faces are subjected to negative pressure due to flow separation and sidewash. However, in the plus shape

Table 2 C_{Pe} on faces of rectangular model

Wind angle	C_{Pe} face A	C_{Pe} face B	C_{Pe} face C	C_{Pe} face D
0°	0.78	−0.28	−0.58	−0.59
90°	−0.58	−0.56	0.66	−0.31

Table 3 C_{Pe} on faces of plus shape model

Wind angle	Face Av. C_{Pe}			Face Av. C_{Pe}			Face Av. C_{Pe}			Face Av. C_{Pe}		
	A1	A	A2	B1	B	B2	C1	C	C2	D1	D	D2
0°	0.29	0.81	0.30	−0.37	−0.33	−0.37	−0.41	−0.57	0.21	0.15	−0.57	−0.40
90°	0.14	−0.6	−0.39	−0.39	−0.55	0.10	0.29	0.81	0.30	−0.37	−0.30	−0.36

model the windward side faces are subjected to positive pressure due to interference effect from the adjoining windward faces.

5.1 Rectangular Model

The pressure contour on faces for 0° wind angle in rectangular model are shown in Fig. 4a–d. That for 90° wind angle are shown in Fig. 5a–d. Wake generation, vortex generation and wind patterns are shown in Fig. 6a–b for 0° wind angle and for 90° wind angle the same are shown in Fig. 7a–b. C_{Pe} central vertical faces and that along

(a) Face A   (b) Face B   (c) Face C   (d) Face D
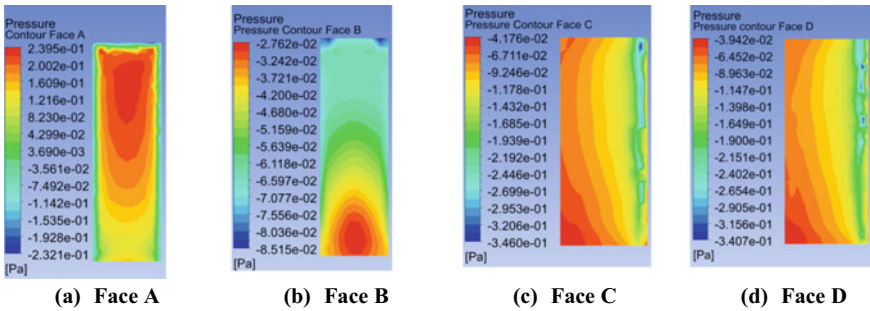
Fig. 4 Pressure contour 0° wind angle rectangular model

(a) Face A   (b) Face B   (c) Face C   (d) Face D
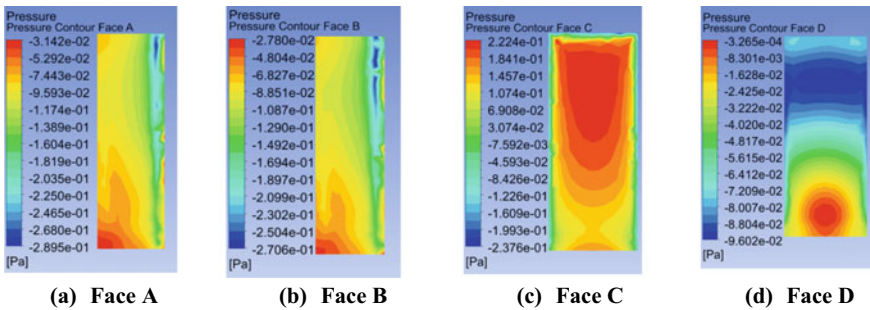
Fig. 5 Pressure contour 90° wind angle rectangular model
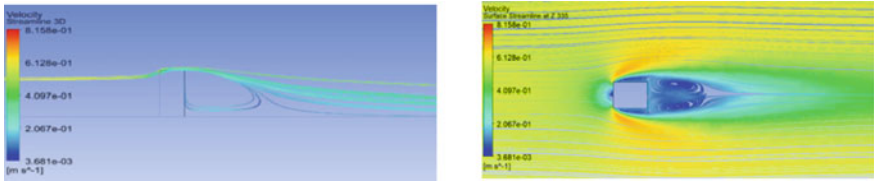
Fig. 6 a Wake generation in rectangular model at 0° wind angle. **b** Wind pattern at 2/3rd height of model in rectangular model at 0° wind angle
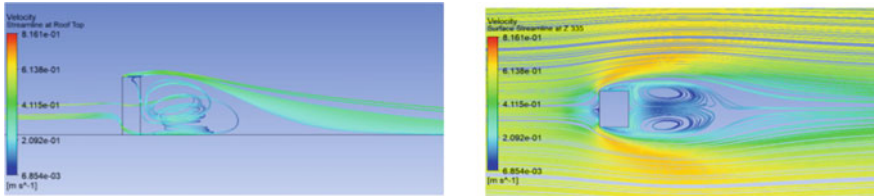
Fig. 7 a Wake generation in rectangular model at 90° wind angle. **b** Wind pattern at 2/3rd height of model in rectangular model at 90° wind angle
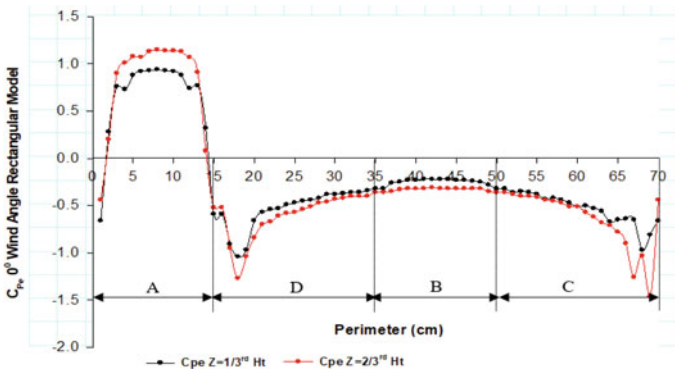
Fig. 8 C_{Pe} along perimeter for 0° wind angle rectangular model

the perimeter at 1/3rd and 2/3rd height of the models are shown in Figs. 8, 9, 10 and 11. On the basis of the above, characteristics of wind pressure are summarized as follows.

5.1.1 0° Wind Angle

Referring to Figs. 4 and 8 it is seen that face A, being the windward, is subjected to maximum positive pressure. The pressure is more pronounced in the upper middle level of the face and centered from the edges. The pressure at the edges are negative
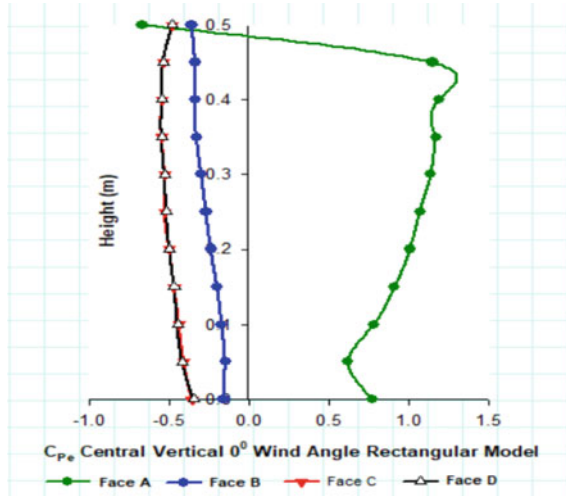
Fig. 9 C_{Pe} central vertical 0° wind angle rectangular model
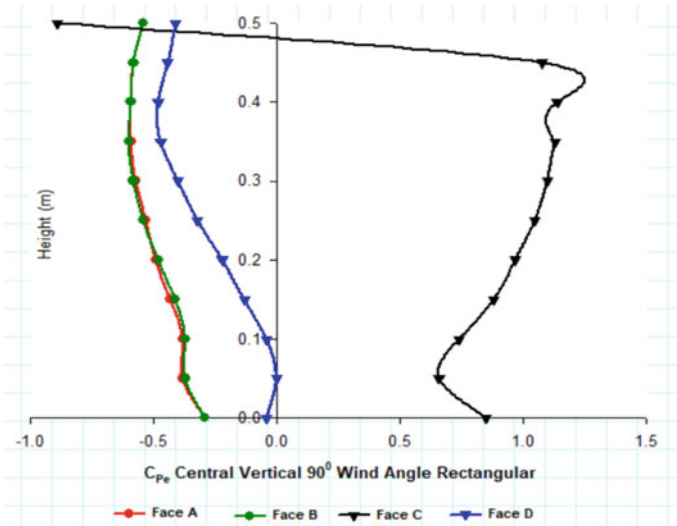
Fig. 10 C_{Pe} central vertical 90° wind angle rectangular model

due to flow separation occurring at the edges. It is also be seen in Fig. 9 that the C_{Pe} is increasing after a certain height due to increase in energy dissipation. At the roof level it becomes negative due to uplift force. The maximum C_{Pe} on face A is 1.23 and the minimum is −1.19. Face B being the leeward face is subjected to negative pressure due to creation of vortex in the wake region. The suction pressure is increasing along the height of face B due to generation of greater uplift force from
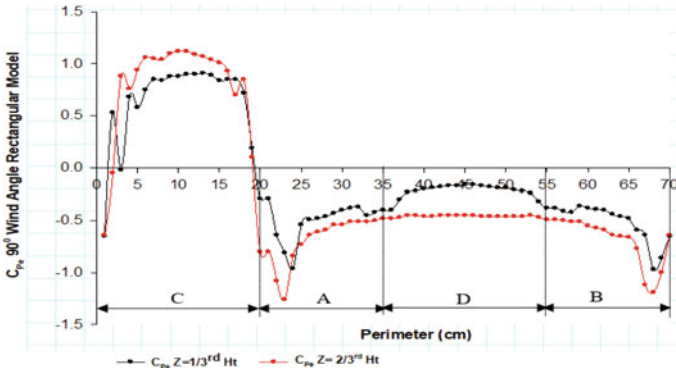
Fig. 11 C_{Pe} along perimeter for 90° wind angle rectangular model

the backwash created by the vortex (Fig. 6a). The maximum value of C_{Pe} on face B is −0.14 and the minimum is −0.43. Face C and D being the side faces are subjected to negative pressure due to flow separation from the edges of face A. The intensity of negative pressure is more near the edges of face A and reduces towards the edges of leeward face B. The variation in the C_{Pe} along the central vertical lines on face C and D are almost constant (Fig. 9). The maximum and minimum C_{Pe} on these faces are −0.21/−0.20 and −1.77/1.74 respectively.

5.1.2   90° Wind Angle

For 90° wind angle similar situation is created for the windward face C, leeward face D and the side faces A and B. Face C, being the windward side, is being subjected to maximum positive pressure (Fig. 11). The pressure is more pronounced in the upper middle level of the face and centered from the edges. The maximum C_{Pe} on face C is 1.14 and the minimum is −1.22. The variation compared to 0° wind angle is attributed to the change in side ratio. On the leeward face D, it is 0.00 and −0.49 respectively. An important observation is that the pressure at the lower height of the leeward face D is almost nil (Fig. 10) as compared to the 0° wind angle situation on the leeward face B. Suction pressure is increasing as the height increases and become almost constant above 2/3rd height. This is due to creation of backwash of more intensity and uplift pressure due to vortex generation in the leeward side (Fig. 7a). The variation of C_{Pe} along the vertical central lines on side faces A and B are more than that on the side faces C and D of 0° wind angle. The maximum and minimum value of C_{Pe} on these faces are −0.16/−0.14 and −1.48/−1.39 respectively.

5.2 Plus Shape Model

5.2.1 0° Wind Angle

The pressure contours (Figs. 12 and 13a–l) on the symmetrical faces are identical and hence only faces A, D1, A2, D, B1, D2 and B are discussed for 0° angle of attack. Being the windward side, face A, and A2 are experiencing positive pressure due to energy dissipation and drag force. C_{Pe} on face A and A2 is increasing after a certain height due to increase in energy dissipation. At the roof level it becomes negative due to uplift force (Fig. 14). Face D, D2, B1 and B2 are all experiencing negative pressure throughout the height. Face A is having a symmetrical positive pressure distribution along the vertical center line and across its width with maximum pressure around the middle (Fig. 12). The pressure is positive throughout the height and width of the model except near the roof top where it is negative due to uplift force. Unlike in the rectangular model, the pressure at the edges are also positive and not negative. The maximum positive value of C_{Pe} is 1.23 and the negative value is −0.65. Due to interference effect of face A2, face D1 is subjected to positive pressure up to a certain height and then it suffers suction immediately before the roof top due to uplift force (Fig. 14). It is relevant to mention that the side faces in rectangular model are subjected to negative pressure. The value of pressure coefficient for face D1 at 1/3rd height of the model is between 0.13 and 0.24 and at 2/3rd height of model is between 0.18 and 0.31. Max pressure is concentrated towards the corner of face D1 and A2 at both the heights. Face A2 is predominately subjected to positive pressure. At 1/3rd height of the model it is between 0.24 and 0 and at 2/3rd height it is between 0.31 and 0.11 showing that the pressure is reducing towards the edge of face A2 and D. Face D is subjected to negative pressure with maximum suction concentrated towards the edge of face A2 and D and gradually reducing towards edge of face D and B1. The pressure on face B1 is completely negative and almost constant. The C_{Pe} is in the range of −0.36 to −0.4. The pressure on face D2 is also negative in nature
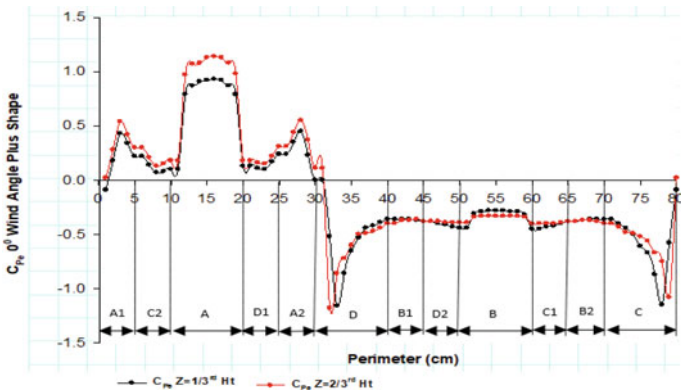
Fig. 12 C_{Pe} along perimeter for 0° wind angle plus shape model
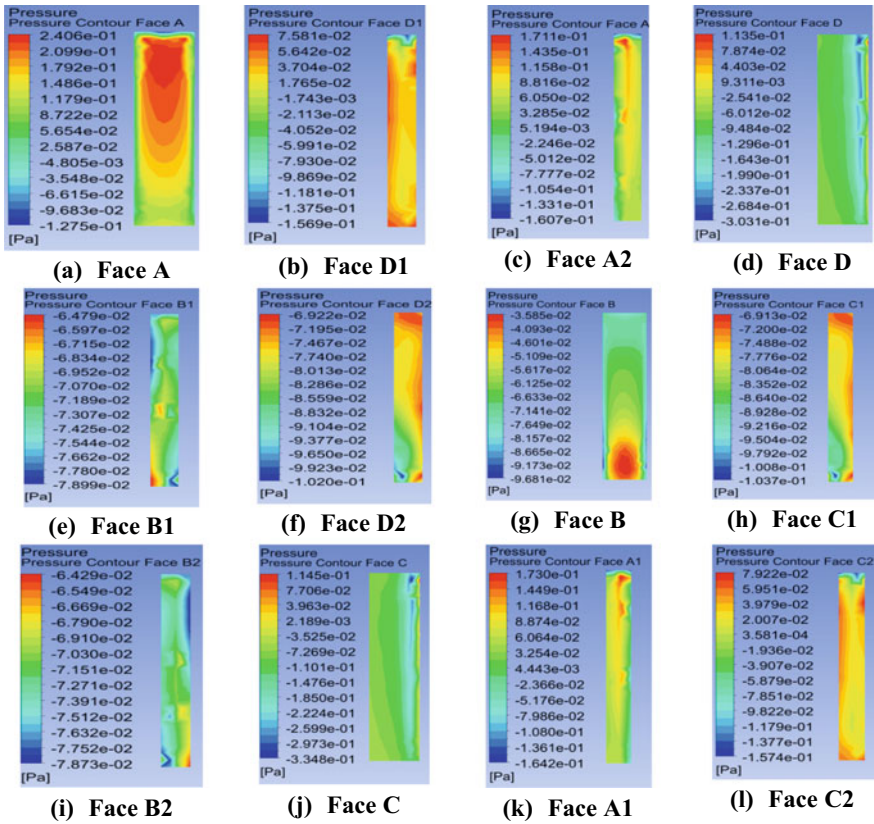
Fig. 13 Pressure contour 0° wind angle plus shape model

throughout. The C_{Pe} is in the range of -0.36 to -0.44. The pressure on face B is also negative. The suction is more towards the edges and also at roof top due to creation of vortex and backwash. The value of C_{Pe} is between -0.2 and -0.4 (Fig. 15).

5.2.2 90° Wind Angle

The scenario in this case is identical to that of plus shape model 0° wind angle discussed above. The only changes are that the faces in the 0° wind angle case may be read as face C, A1, C2, A, D1, A2 and D in place of A, D1, A2, D, B1, D2 and B respectively. The wake generation and wind pattern have been shown in Fig. 16a and b respectively.
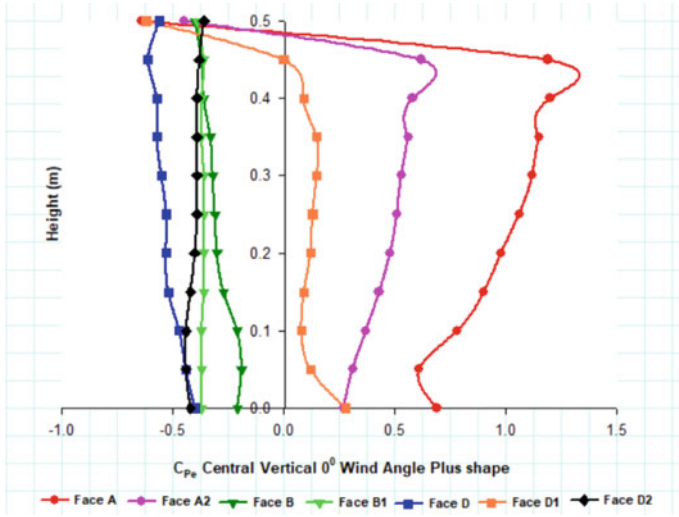
Fig. 14 C_{Pe} central vertical 0° wind angle plus shape model
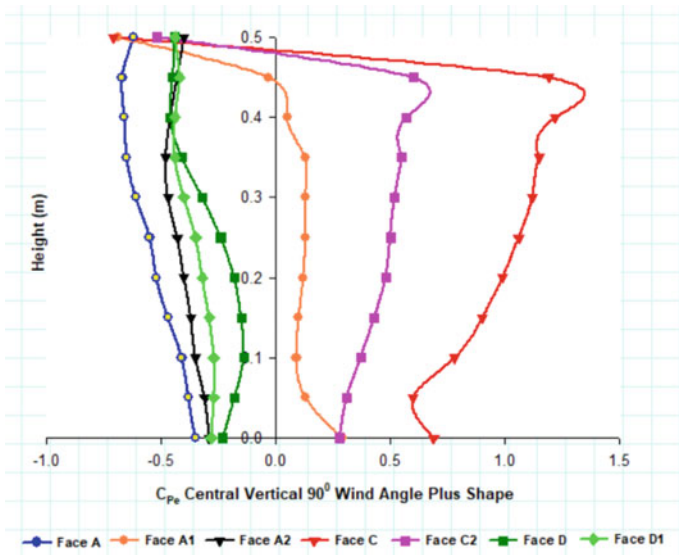
Fig. 15 C_{Pe} central vertical 90° wind angle plus shape
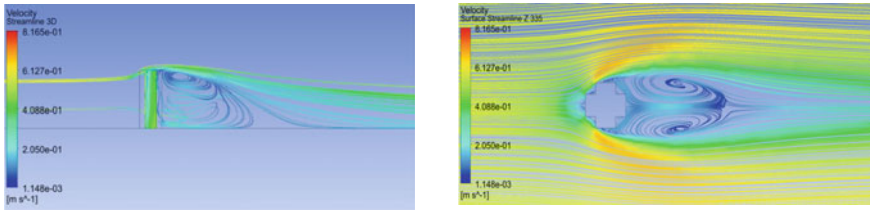
Fig. 16 a Wake generation in plus shape model at 0° wind angle. **b** Wind pattern in plus shape model at 0° wind angle

6   Conclusion

The wind pressure measurements represented herein lead to identification of influence of edge configuration on wind pressure distribution of a rectangular and plus shape building and is summarized below.

- While the average pressure distribution on all the leading faces (windward, leeward and side faces) are almost identical in both the cases, pressure at the edges and corners in the plus shape model makes difference in better ventilation planning and structural design in the prototype building.
- On the windward face A in plus shape model, the pressure is positive throughout the width as against that in the rectangular model in which case suction occurs due to flow separation at the edges.
- Also, on the corner cut faces (plus shape), the pressure at the corners are relatively more in magnitude than that at the free edges.
- The side faces adjacent to the windward face in plus shape are experiencing positive pressure due to interference effect from the corner cut windward faces. The flow reverses after hitting the corner cut windward faces and results in generation of positive pressure on the corner cut side faces.
- The data taken from the simulation may be of great importance for the architects and structural designers.

References

1. Baines WD (1952) Effect of velocity distribution on wind loads on a tall building. Technical paper, University of Toronto, 6203
2. Gomes A, Rodrigues AM, Mendes P (2005) Experimental and numerical study of wind pressure on irregular-plan shapes. J Wind Eng Ind Aerodyn 93:741–756
3. Mendis P, Ngo T. Haritos N, Hira A, Samali B, Cheung J (2007) Wind loading on tall buildings. EJSE: Load Struct 7:51–54
4. Amin JA, Ahuja AK (2011) Experimental study of wind-induced pressure on buildings of various geometries. Int J Eng Sci Technol 3(5):1–19

5. Tanaka H, Tamura Y, Ohtake K, Nakai M, Kim YC, Bandi EK (2013) Experimental investigation of aerodynamic forces and wind pressure acting on tall buildings with various unconventional configuration. J Wind Eng Ind Aerodyn 107–108:179–191
6. Amin JA, Ahuja AK (2013) Effects of side ratio on wind induced pressure distribution on rectangular buildings. J Struct Hindawi 12. Publishing Corporation. Article ID 176739
7. Chakraborty S, Dalui SK (2013) Numerical study of surface pressure on square plan shape tall building. In: Symposium on sustainable infrastructure development (SID), Feb 8th to 9th, (2013), pp 252–258
8. Bhattacharyya B, Dalui SK, Ahuja AK (2014) Wind induced pressure on 'E' plan shaped tall buildings. Jordon J Civil Eng 8(2):120–134
9. Kheyari P, Dalui SK (2015) Estimation of wind load on a tall building under interference effect: a case study. Jordon J Civil Eng 9(1):84–101
10. Roy K, Bairagi AK (2016) Wind pressure and velocity around stepped unsymmetrical plan shape tall building using CFD simulation—a case study. Asian J Civil Eng (BHRC) 17:1055–1075
11. Mukherjee A, Bairagi AK (2017) Wind pressure and velocity pattern around 'N' plan shape tall building—a case study. Asian J Civil Eng (BHRC) 18(8):1241–1258
12. Bairagi AK, Dalui SK (2020) Distribution of wind pressure around different shape tall building. Adv Struct Syst Mater 31–38
13. Revuz J, Hargeaves DM, Owen JS (2012) On the domain size for the steady state CFD modeling of a tall building. Wind Struct 15(4):313–329
14. Franke J, Hirsch C, Jensen A, Krus H, Schatzmann M, Westbury P, Miles S, Wisse J, Wright NG (2004) Recommendation on the use of CFD in Wind Engineering. In: COST action C14: impact of wind and storm on city life and built environment. Von Karman Institute for Fluid Dynamics
15. IS 875 (Part 3)-2015 Design loads (other than earthquake) for building and structures—Code of Practice Part 3 Wind Loads (Third Revision)

Rice Husk Ash as a Sustainable Cementing Material for Concrete in Ethiopia

Binaya Patnaik, Gatbel Buony, and Zelalem Mekuria

1 Introduction

Rice is one of the major crops grown in various countries across globe. The rice production trends in Ethiopia indicates high increasing rate especially since 2006. The rice producing farmer increase from 32 thousand in 2006 to 119 thousand in 2013, the area allocated increase from 6 thousand hectares in 2006 to 58 thousand hectares in 2013 and the production of rice increased from 11 thousand tons in 2006 to 184 thousand tons in 2013. Rice Husk is one of the waste material produced from the crop after the rice is taken out. The husk is used as a fuel by factories and locals and at times dumped unused. The ash being a pozzolanic material possesses the property of cementing material which can help purposeful utilization of agricultural waste and also reduce the consumption of energy used in the production of cement [1–5]. Therefore rice husk is an agro based product which can be used as a substitute of cement without sacrificing the strength and durability of concrete. Since rice husk has negligible protein content, it is not useful for animal feeding. Rice husk ash is obtained from controlled burning of rice husk at about 650 °C. In this research, an extensive study conducted on the fresh, strength and durability properties of concrete by partially replacing cement with rice husk ash by means of carrying out various experiments. Test were conducted both at fresh and hardened state. The tests conducted at fresh state were workability (slump) test and density test. At hardened state the compressive strength and tensile strength were measured and from durability perspective the water absorption and chloride permeability of RHA based concrete were studied.

B. Patnaik (✉) · G. Buony
Department of Civil Engineering, Gambella University, Gambella, Ethiopia

Z. Mekuria
Department of Civil Engineering, Hawassa University Institute of Technology, Hawassa, Ethiopia

2 Materials

Ordinary portland cement (OPC) of 42.5 grade and RHA from local factories in Hawassa, Ethiopia, were used for this study. The rice husk obtained from the factory was further burnt at 650 °C for an hour to bring down the carbon content and further ground to pass through 90 μm sieve. A sample of rice husk, the burning process and a sample of rice husk ash is shown in Fig. 1. The chemical properties of RHA was tested in Geological Survey of Ethiopia laboratory. The physical and chemical properties of cement and RHA are presented in Tables 1 and 2.

Locally available angular crushed granite metal having a maximum size of 20 mm was used as coarse aggregate having fineness modulus of 7.63 and sp. gr of 2.65, bulk density of 1468 kg/m³ at compacted state and the water absorption of 1.2% respectively. River sand with specific gravity 2.5, fineness modulus 2.8, bulk density of 1700 kg/m³ at compacted state and the water absorption of 2.04% respectively was used as fine aggregate. Clean, impurities free (acids, alkalis and oils etc.); generally speaking, potable water used for mixing concrete and curing.

As per the code book ACI 211, the mix design was carried out and the quantity of materials were designed. To find the optimum percentage of RHA in concrete as a partial replacement of cement, five type of mixes (RH0, RH10, RH20, RH30 and RH40) were arranged by partially replacing cement with RHA from 0 to 40%. Concrete test specimens such as cubes, cylinders and discs of above mentioned mixes were casted and tested for their compressive, tensile strength and rebound hammer at

Fig. 1 RHA from Hawassa local factory

Table 1 Physical properties of cement and RHA

Material	Specific gravity	Fineness (μm)	Specific surface (m²/kg)	Mean grain size
OPC	3.15	82	300	21
RHA	1.71	90	890	5.2

Table 2 Chemical properties of cement and RHA

Material	SiO_2	Al_2O_3	Fe_2O_3	CaO	MgO	Na_2O	K_2O	SO_3	LOI
OPC	21.55	5.69	3.39	64.25	0.85	0.33	0.59	2.47	1.80
SCBA	86.73	0.04	0.61	0.39	0.08	1.32	9.76	–	0.54

Table 3 Mix design and proportion of C30 grade concrete

Grade	Cement (Kg/m^3)	Fine aggregate (kg/m^3)	Coarse aggregate (kg/m^3)	W/C ratio	Water (kg/m^3)	Mix proportion
C-30	350	680	1040	0.54	170	1:1.94:2.97

7, and 28 days and RCPT along with water absorption at 28 days. The mix proportions have been presented in Table 3.

3 Experimental Procedure

For preparation of good concrete, the vital factors are appropriate mixing, compaction and sufficient curing which were adopted during the test sample preparation process. Pan mixture was used for mixing process and the time for mixing was kept for 3–4 min. To examine the workability properties of fresh concrete, slump test was performed. 24 h after casting the test samples were demoulded and adequately cured using potable water. Sample of fresh concrete and test sample casting have been shown in Figs. 2 and 3 respectively.

The test specimens were tested for their compressive strength and tensile strength at three different age i.e. 7 days, 14 days and 28 days by using cube samples (150 mm × 150 mm × 150 mm) and cylinder samples (150 mm dia × 300 mm ht) respectively. The test setup for compressive strength and tensile strength have been shown in Figs. 4 and 5 respectively. Each test result were averaged out from three test specimen test results.

Fig. 2 Fresh concrete

Fig. 3 Workability of
concrete testing

Fig. 4 Compressive strength
test setup

As part of non-destructive testing, the rebound hammer test was conducted using concrete cubes (150 mm × 150 mm × 150 mm) at 28 days of curing period. The rebound hammer test setup has been shown in Fig. 6. Each test result were averaged out from three test specimen test results.

The rapid chloride permeability test (RCPT) was conducted using concrete discs (100 mm dia × 50 mm ht) at 28 days of curing period. The rapid chloride permeability test setup has been shown in Figs. 7 and 8. Each test result were averaged out from three test specimen test results.

The water absorption test was performed by using concrete cube samples of size 150 mm × 150 mm × 150 mm at 28 days curing period. The water absorption test setup has been shown in Figs. 9 and 10. Each test result were averaged out from three test specimen test results.

Fig. 5 Tensile strength test setup

Fig. 6 Rebound hammer testing on concrete

Fig. 7 Concrete discs curing for RCPT

Fig. 8 RCPT test setup

Fig. 9 Concrete cubes for water absorption

Fig. 10 Concrete cubes in oven for drying

Table 4 Slump values of different concrete mixes

Sr. No	Proportions of RHA (%)	Concrete slump (mm)
1	0	32
2	10	25
3	20	12
4	30	0
5	40	0

4 Results and Discussions

The test results of concrete fresh properties, strength properties and durability properties have been presented below and discussed.

4.1 Effects of RHA on Fresh Properties of Concrete

The effect of replacement of cement by RHA partially from 0 to 40% on workability of concrete is shown in Table 4.

It can be observed from Table 4 that the workability of RHA concrete is reduced with increased replacement of cement with RHA. In this study replacement of RHA above 20% were not possible due to high water demand. Since these tests were conducted based on the RHA-W method, it increased the volume of concrete which results from its low density of RHA this leads to increasing the water demand. But the tests were not conducted for that zero slump, there were additional water to get the workable concrete.

4.2 Effects of RHA on Compressive Strength of Concrete

The effect of replacement of cement by RHA partially from 0 to 40% on compressive strength of concrete at different ages is shown in Table 5.

It can be clearly seen from Table 5 that the compressive strength of concrete is rising from normal concrete (0% replacement) to the concrete with 10% of RHA as partial replacement of cement. By further rising the RHA content as replacement of cement the compressive strength is reducing. Similar tendency of strength difference can be observed at different age of testing i.e. 7 days, 14 days and 28 days. It can also be seen that, with increase in the age from 7 days to 14 and 28 days, the compressive strength increases for all type of mixes which is especially due to the delayed pozzolanic effect of RHA in concrete. The causes for compressive strength development in RHA blended concretes and the rise in compressive strength up to 10% cement replacement of RHA may be to the high silica content, amorphous phase,

Table 5 Effect of RHA on compressive strength of concrete

Mix	% RHA replacement	Density (kg/m³)	Compressive strength at different age		
			7 days	28 days	90 days
C30	0	2120	28.03	29.52	31.32
	10	2009	26.04	30.04	34.02
	20	1868	26.10	28.20	30.29
	30	1823	15.18	18.31	21.43
	40	1738	8.84	10.86	12.87

fineness, degree of reactivity of RHA, specific surface area and pozzolanic reaction between reactive silica in RHA and calcium hydroxide in an alkaline environment. Based on the above test results, it has been established that 10% of RHA is the optimum to be used as a partial replacement of cement in manufacturing of concrete from compressive strength perspective.

4.3 Effects of RHA on Tensile Strength of Concrete

The effect of replacement of cement by RHA partially from 0 to 40% on tensile strength of concrete at different ages is shown in Table 6.

It can be clearly seen from Table 6 that the tensile strength of concrete is rising from normal concrete (0% replacement) to the concrete with 10% of RHA as partial replacement of cement. By further rising the RHA content as replacement of cement the tensile strength is reducing. Similar tendency of strength difference can be observed at different age of testing i.e. 7 days, 14 days and 28 days. It can also be seen that, with increase in the age from 7 days to 14 and 28 days, the tensile strength increases for all type of mixes which is especially due to the delayed pozzolanic effect of RHA in concrete. Based on the above test results, it has been established that 10% of RHA is the optimum to be used as a partial replacement of cement in manufacturing of concrete from tensile strength perspective.

Table 6 Effect of RHA on tensile strength of concrete

Mix	% RHA replacement	Density (kg/m³)	Tensile strength at different age		
			7 days	28 days	90 days
C30	0	2120	1.5	2.92	3.30
	10	2009	1.6	3.72	4.17
	20	1868	1.31	2.29	2.95
	30	1823	1.22	2.01	2.66
	40	1738	1.19	1.88	2.10

Table 7 Effect of RHA on rebound number

Mix	% RHA replacement	Density (kg/m^3)	Rebound number
C30	0	2120	35.2
	10	2009	39.22
	20	1868	34.044
	30	1823	24.085
	40	1738	17.751

4.4 Effect of RHA on Rebound Number

The effect of replacement of cement by RHA partially from 0 to 40% on rebound number of concrete at different ages is shown in Table 7.

It can be clearly seen from Table 7 that the rebound number of concrete is rising from normal concrete (0% replacement) to the concrete with 10% of RHA as partial replacement of cement. By further rising the RHA content as replacement of cement the rebound number is reducing. The rebound number is analogues to compressive strength of concrete and the trend for rebound number shows similar as that of compressive strength. This indicates non-destructive testing approach is viable for measuring the compressive strength of RGA based concrete rather than adopting destructive testing.

4.5 Relation Between Compressive Strength and Rebound Number

Mathematical equations have been derived to express rebound number strength and compressive strength of concrete with different percentage of RHA. Figure 11 shows the relationship between rebound number and compressive strength at 28 days. The equation obtained as below:

For 0 up-to 40% replacement of RHA,

$$RN = 0.5906 * CS + 3.1253 \text{ and } 'R^2' = 0.9424$$

where RN = Rebound Number, CS = Compressive Strength, R^2 = Correlation Coefficient.

Relationship between Compressive Strength and Rebound Number

$y = 0.5906x + 3.1253$
$R^2 = 0.9424$
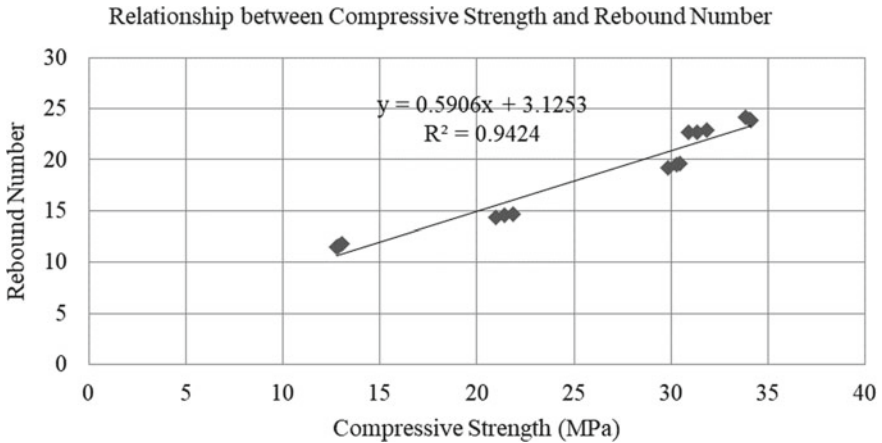
Fig. 11 Relationship between compressive strength and rebound number

4.6 Effect of RHA on Water Absorption of Concrete

The water absorption of controlled concrete and RHA concrete measured over a period of three days. The saturated water absorption in percentages for controlled concrete and RHA concrete is presented in Table 8.

It can be observed from Table 8 that the saturated water absorption of concrete is decreasing with the increase of rice husk ash replacement by cement up to 20%, indicating a decrease in permeable pores in the concrete. The water absorption of 30 and 40% rice husk ash concrete is higher when compared to their respective normal concrete and other replacement of rice husk ass concrete. The minimum water absorption is also found in case of 20% RHA mix and the value at 28 days is found to be 1.32%, while the maximum water absorption is found in case of 40% RHA concrete mix and the value at 28 days is found to be 3.12%. This shows that rice husk ash concrete can be considered to be good from the durability perspective with respect to water absorption up to 20% RHA replacement by cement because porosity of concrete reduced at higher RHA concrete.

Table 8 Saturated water absorption of controlled and RHA concrete

Grade	% RHA	Weight of oven-dried sample (kg)	Weight of saturated sample (kg)	Saturated water absorption at 28 days (%)
C-30	0	8.370	8.525	1.85
	10	7.955	8.087	1.66
	20	7.890	7.994	1.32
	30	7.775	7.941	2.14
	40	7.390	7.621	3.12

Table 9 Chloride penetration in concrete mixes

Type of mix	Charge passed in coulombs	Chloride ion penetrability as per ASTM C1202
RCPT-0	2240	Moderate
RCPT-10	1860	Low
RCPT-20	1465	Low
RCPT-30	1545	Low
RCPT-40	2370	Moderate

4.7 Effect of RHA on Chloride Penetrability of Concrete

The effect of replacement of cement by RHA partially from 0 to 40% on charge passed by Columbus and chloride permeability of concrete at 28 days curing period is shown in Table 9.

From Table 9, it can be observed that, with partial replacement of cement with RHA up to 30%, the permeability of concrete is decreasing compared to the controlled concrete. However, beyond 30% of cement replacement with RHA, the permeability of concrete is increasing as compared to the controlled concrete. The decrease in the charge passed with the increase in RHA is mainly because of the pozzolanic effect of RHA which makes the concrete impervious by consuming the calcium hydroxide produced from hydration of cement and a main cause of making concrete pervious. The level of chloride ion penetration for concrete with RHA of 10–30% as partial replacement of cement remains in the "Low" range as per ASTM C1202 and thus demonstrating that these has a good ability to resist chloride ion penetration. It is also expected that with increase of age when most of the hydration of concrete with RHA completes, the chloride permeability of concrete to be decreased drastically.

5 Conclusions and Recommendations

On the basis of the present experimental investigation carried out, following conclusions have been made.

- Use of RHA as a partial replacement of cement in concrete helps in addressing the waste management issues of rice husk ash and reduces environmental impacts.
- The optimum percentage of RHA in concrete as partial replacement of cement in concrete from strength perspective is found to be 10%.
- Non-destructive testing can be an ideal way of measuring the compressive strength of rice husk based concrete. A good correlation can be seen between compressive strength and rebound number of RHA based concrete.
- Water demand of RHA blended concrete increases with an increase in the RHA content.

- The density of concrete decreases with inclusion of RHA in concrete and make the concrete light weight.
- The water absorption capacity of the concrete decreases by inclusion of RHA up to 20% as a partial replacement of cement.
- With inclusion of RHA as a cementing material in concrete up to 30% as partial replacement of cement, the chloride permeability of concrete decreases as compared to the controlled concrete.

References

1. Farsana C, Das BB, Snehal K (2020) Influence of fineness of mineral admixtures on the degree of atmospheric mineral carbonation. In: Smart technologies for sustainable development, Springer Publications, pp 117–136
2. Mustafa R, Shivaprasad KN, Das BB (2019) Effect of various additives on the properties of fly ash based geopolymer mortar. Sustain Constr Build Mater, Springer Nature Singapore, 707–715
3. Snehal K, Das BB (2019) Techniques for preparation and dispersion of nano-SiO_2 in cementitious system—a review. Sustain Constr Build Mater, Springer Nature Singapore, 397–407
4. Snehal K, Das BB, Akanksha M (2020) Early age, hydration, mechanical and microstructure properties of nano-silica blended cementitious composites. Constr Build Mater Elsevier 233
5. Snehal K, Das BB, Kumar S (2020) Influence of integration of phase change materials on hydration and microstructure properties of nano silica admixed cementitious mortar. J Mater Civil Eng ASCE 32(6)

Risk Assessment in Construction Industry Using a Fuzzy Logic

Purnajit Bhowmik, Gaurav Udgata, and Shivanshi Trivedi

1 Introduction

In this fast-developing world, construction is becoming more and more complex day by day [1–7]. With the increase in construction complexity, Risk management creates a need for an alternative solution to be addressed instead of using the traditional risk management method. To address such problems researches are coming up with new innovative techniques to mitigate the void that has been created and successfully address the problem. In this aeon of progressive development, it is extremely difficult to avoid risks in our day to day life. Risk management is a dynamic topic and hence needs to address a wide range of problems and achieve a tangible benefit.

Many researchers have successfully implemented FIS (Fuzzy Inference System) into risk management within different industries. Our work whirls around the use of FIS to identify different risks which categorize them from very low, low, medium, medium–high to high and obtain a crisp value which helps in better understanding of the risk.

P. Bhowmik (✉) · G. Udgata · S. Trivedi
School of Civil Engineering, KIIT Deemed to be University, Bhubaneswar, India

G. Udgata
e-mail: gaurav.udgatafce@kiit.ac.in

1.1 Fuzzy Inference System

Fuzzy Inference System is a methodology used for implementing fuzzy logic. The Mamdani fuzzy inference system uses fuzzy set theory to map input (fuzzy classification features) to output (fuzzy classification classes). The fuzzy rule is a collection of linguistic values which show how the FIS would be making decisions based on the classification of input or controlling an output. Here is a sample which helps represent the system Figs. 1 and 2 ("Fuzzy Sets and Pattern Recognition," 2020).
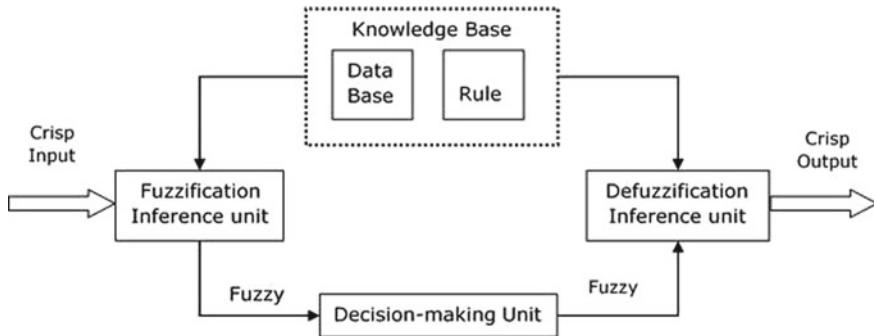
Fig. 1 Representation of the fuzzy inference system
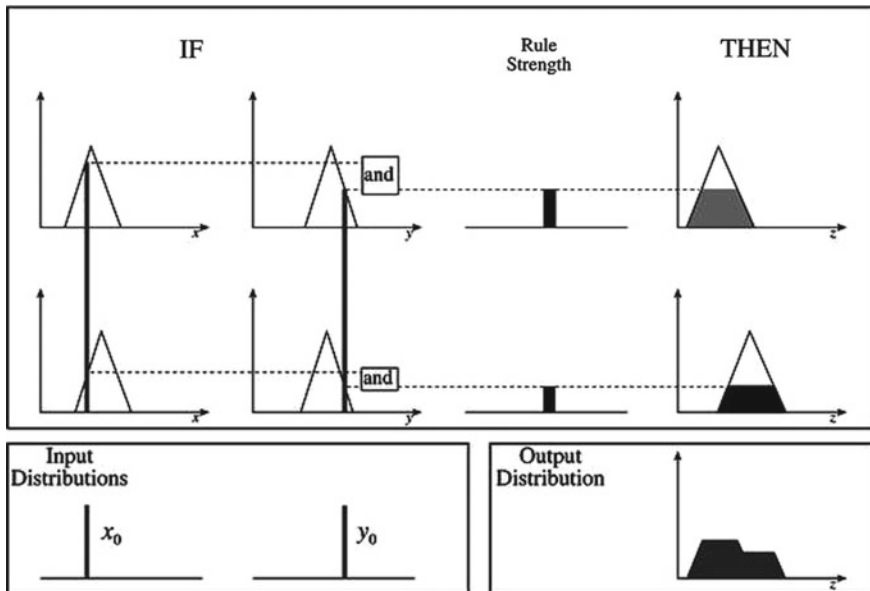
Fig. 2 A two input, two rule Mamdani FIS with a fuzzy input

2 Literature Review

Risk management is a crucial and analytical task as it is analogous to the cost of the project, time of completion, and quality of construction and to evade the risks or reduce the severity proper management should be enforced. From past experience, it is evident that the construction industry has a distinct and broad range of risks that has to handled properly otherwise the project failure is inevitable.

Keshk et al. [8] a study on construction project risks suggested that there should not be only one strategy to dodge all the risks in a project as the strategy depends upon the magnitude and the type of risk. Keshk et al. [8] added that the best way to avoid risks should come with conscious project planning. Nieto-Morote and Ruz-Vila [9] stated that the initial step should be to identify the type of risk and then analyzing it. The identification could be done on the ground of the likelihood of the risk and the ranking of the risk should be considered very important. Shojaei et al. [10] proposed that every construction project is unique and would have different challenges and the major task is to fill the void between the literature and practicality of implementation of effective risk management which could be done by applying analytical tools in decision making.

Construction projects need proper implementation of planning which aims that the project does not deviate from its objective. Various methods and techniques have been used in the past to come up with the most efficient risk estimation methods. Nabawy et al. [11] recommended that for the construction of megaprojects, the best technique to adopt is the Monte Carlo analysis. Monte Carlo analysis has been extensively used for the risk evaluation in scheduling and budgeting. Nabawy et al. [11] also proposed another quantitative technique namely, Sensitive analysis, can be implemented when the main focus is to locate the critical risk that would lead to direct failure of the project.

The construction projects can be complex, where the risk is uncountable, the information is inadequate or not precise. Hence, there is a need to adopt a new methodology to estimate the risks with satisfactory results. Nieto-Morote and Ruz-Vila [9] used a fuzzy risk assessment technique in which the risk is categorized on the ground of its likelihood and severity. His approach allowed to assess the risk in linguistic variables rather than real numbers. Samantra et al. [12] quantified risk using fuzzy set theory. The linguistic terms were expressed by different fuzzy numbers in different fuzzy functions including triangular and trapezoidal. The approach helped to generalize the risk at different levels and the results showed that it is more realistic and reliable when compared to conventional statistical methods. Dikmen et al. [13] applied influence diagrams with fuzzy sets for the real case study on international construction projects in Turkey. The study proposed that if the methodology is used then the risk level at the start of the project and the actual cost value can be determined. The approach was efficient and user friendly, can be used by less experienced staff for calculating the risk in international projects.

Fuzzy Inference System (FIS) is used to calculate the risk through the concept of fuzzy set theory. FIS is an efficient technique to achieve precise outputs. FIS is

Fig. 3 Research stage

utilized to classify and organize risk according to its sensitivity. Raeihagh et al. [14] applied FIS on a case study of inter-phase pipelines of the South Pars gas field and the results showed that the system can predict the upcoming faults and failure in the project. Fuzzy Inference systems depict the practical and more flexible results compared to conventional risk assessment methods. Michael et al. [15] combined FIS with the first optimization stage to redesign the recycling supply chain in Cuba. Incorporating two processes, 225 redesign solutions were obtained and the designers got a variety of options to adopt a solution.

3 Research Methodology

3.1 General

The motive of the work is to study different types of Construction risks and incorporate it with FIS instead of using tradition risk analysis. Here an effort has been made to categorize risks into 4 parts (low, medium, medium–high, high) and to get a crisp value for each type of risk for better understanding and evaluation.

3.2 Research Stage

The method selected for conducting risk management is distributing a questionary survey to various personals from the Construction industry. A risk analysis is assessed using Fuzzy Inference System (Fig. 3).

3.2.1 Objective and Scope of the Project

The study is carried out with the following objective:

- Implementation of Mamdani fuzzy inference system using Matlab for risk assessment.
- Classify Risk into different categories and to obtain a crisp value using Fuzzy InferenceSystem.

3.2.2 Designing of the Questionnaire

The information Collection process was achieved by two essential strategies first being Distribution of Questionnaire and second through individual discussion with the help of video Conference. As a result, the types of risks that influence a Construction project was found which is listed below

- Technical Risks
- Financial Risks
- Management Risks
- Political Risks
- Environmental Risks.

3.2.3 Data collection

To successfully achieve the objective of our study it was important to collect the right information. Data collection was a crucial part which was successfully achieved by sending questionnaires to Construction Industry Personals through e-mail. As mentioned, the collection of data was achieved through a questionnaire which had the option of likelihood and severity in a form of 5 choices (very low, low, moderate, high, very high) and (Negligible, Low, moderate, high, catastrophic) respectively.

3.2.4 Risk Assessment—Fuzzy Inference system

Fuzzy Inference System involves the assessment of the linguistic value of likelihood and severity of various risks and identifying the type of risk with a crisp value for better understanding and improving the performance of the project. We use the form of the risk matrix which shows the likelihood and severity mapped onto a risk-based grid. A total of 25 rules have been identified and used for performing the risk assessment (Fig. 4).

Severity	5	MH	MH	MH	H	H
	4	M	M	MH	MH	H
	3	M	M	M	MH	MH
	2	L	L	L	M	MH
	1	L	L	L	M	MH
		1	2	3	4	5
				Likelihood		

Fig. 4 Risk matrix proposed by Wu et al. [16]

Linguistic Value		Graphical Representation (MF)
Risk Categories		
1.Low(L)	0,1,2	
2.Medium(M)	1,2,3	
3.Medium High(MH)	2,3,4	
4.High(H	3,4,5	
Severiety Categories:		
1.Negligible(N)	0,0.5,1.5	
2.low(L)	0.5,1.5,2.5	
3.Moderate(M)	1.5,2.5,3.5	
4.High(H)	2.5,3.5,4.5	
5.Catastrophic (c)	3.5,4.5,5	
Likelihood Categories		
1.Very Low (LV)	0,0.5,1.5	
2.low (L)	0.5,1.5,2.5	
3.Moderate(M)	1.5,2.5,3.5	
4.High (H)	2.5,3.5,4.5	
5.Very High (VH)	3.5,4.5,5	
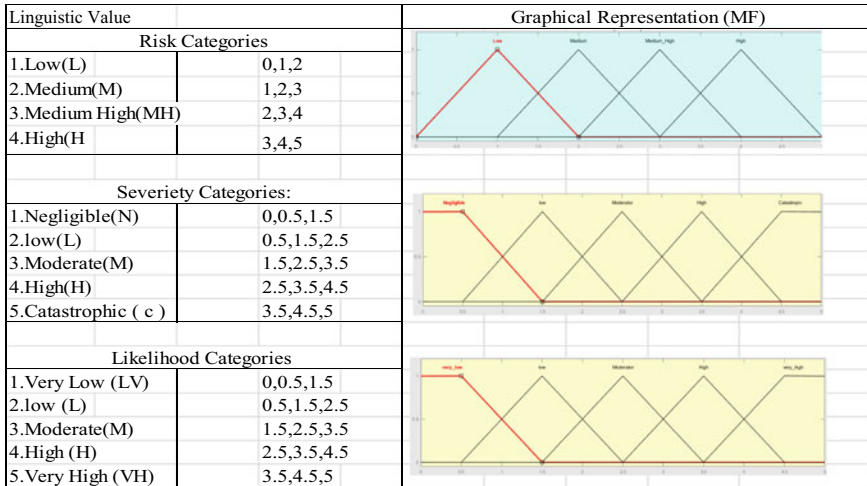
Fig. 5 Conversion of linguistic data to fuzzy data using triangular MF

4 Results and Analysis

The risk matrix uses a dual input and a single output for calculating the risk index. By using this technique, data of the probability of likelihood and severity of risk for each factor is collected in form of linguistics value. The next step is to convert linguistic value to the coded linguistic variable. Now the linguistic variable is converted to fuzzy data. This process is done by using a triangular MF as shown in Fig. 5. After the conversion, a crisp value (numerical value) for the type of risk is found using Matlab by performing Mamdani's FIS as shown in Table 1 (Figs. 6 and 7).

5 Conclusion

The main purpose of the study was to implement FIS into risk assessment for better identification of risk. The survey results on the types of Construction risk showed that:

- The Fuzzy Inference System can help address the shortcomings of the traditional risk assessment method.
- The correlation between input and output data in the proposed fuzzy system was described as a linguistic variable. This is more realistic in depicting actual condition in comparison to the classical model.
- Based on the results, it can be said that scope, inadequate site investigation, relation with stakeholder, clashes within the employee and resource allocation should be given topmost priority.

Table 1 Type of risks

Sl no		Coded linguistic variable		Code	Numerical value		
		Likelihood	Severity		Likelihood	Severity	Risk
1	Type of contract	3	3	**Likelihood**	2.5	2.5	2
2	Delay in design phase	2	3	1. Very Low 2. Low	1.5	2.5	2
3	Inadequate site investigation	5	4	3. Moderate 4. High	4.5	3.5	4
4	Change in project scope	4	5	5. Very High **Severity** 1. Negligible	3.5	4.5	4
5	Design errors and faults	4	4	2. Low 3. Moderate	3.5	3.5	3
6	Improper scheduling	4	3	4. High 5.	3.5	2.5	3
7	Delay in release of funds	3	3	Catastrophic	2.5	2.5	2
8	Delay in worker wage	2	5		1.5	4.5	3
9	Currency exchange rate	2	2		1.5	1.5	1
10	Relation with stakeholder	5	5		4.5	4.5	4
11	Unsatisfactory skilled staff	3	4		2.5	3.5	3
12	Clash within the employee	4	4		3.5	3.5	4
13	Delay in resource allocation	5	4		4.5	3.5	4
14	Communication problem	4	2		3.5	1.5	2
15	Change of interest within ruling party	2	3		1.5	2.5	2
16	Acquiring permission/approval	4	2		3.5	1.5	2
17	Natural disaster	2	5		1.5	4.5	3
18	Weather and seasonal variation	1	4		0.5	3.5	2

- It can also be noted that risk doesn't follow a trend and is unique for each project with the change in geographical conditions
- Historical documents should be maintained by the individual contractors and construction companies, as it helps for predicting risks and reducing the chances of high-level risks.
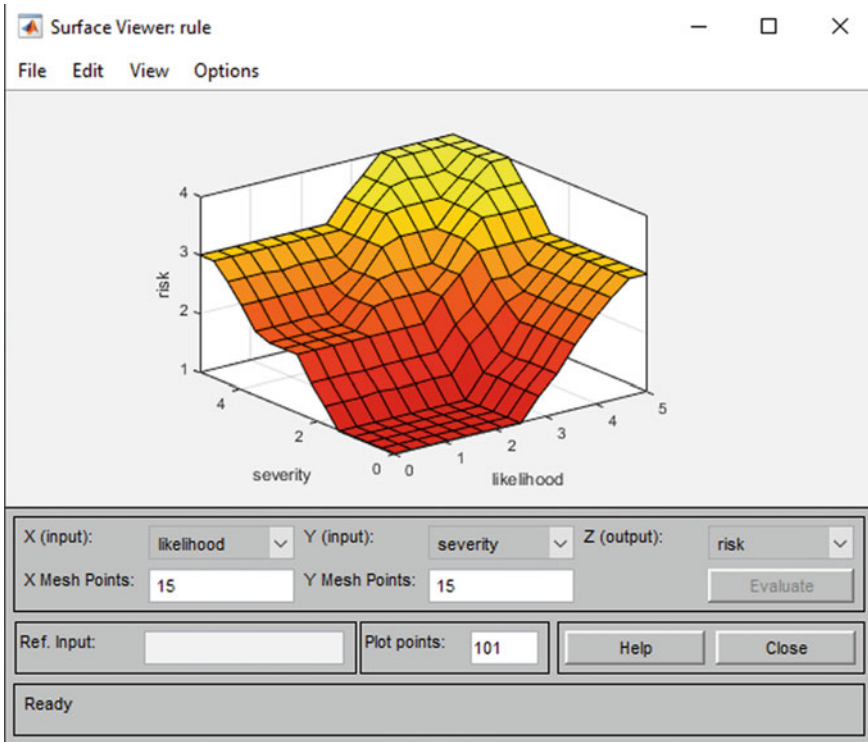
Fig. 6 Surface viewer: rule using MATLAB

Finally, it can be concluded that the implementation of Fuzzy Inference System in Construction does add value to Risk management in comparison to the Classical model in terms of classifying, understanding and visualising risk.
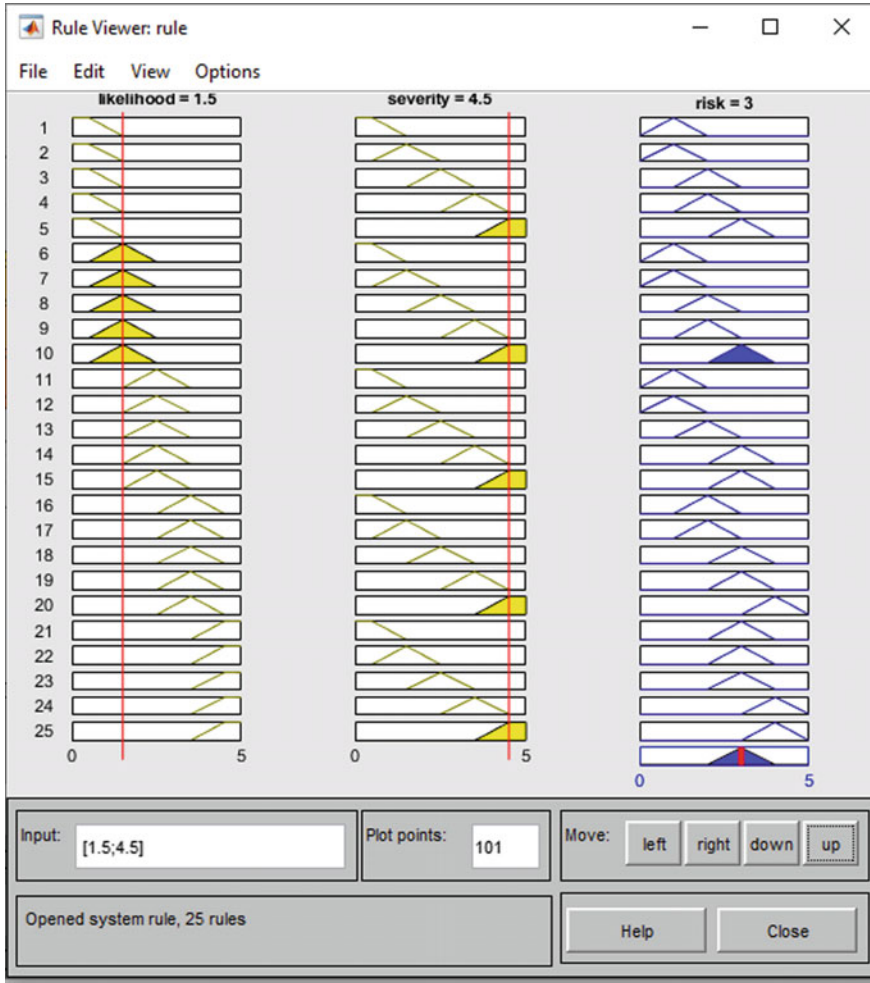
Fig. 7 Analysis of the type of risk using rule viewer in MATLAB

References

1. Akhil RP, Das BB (2018) Cost reduction techniques on MEP projects. In: Select proceedings of ICSCBM 2018, Springer Nature Singapore Pte Ltd. 2019, pp 495–517
2. Reddy CP, Das BB (2018) Methods to monitor resources and logistic planning at project sites. In: Select proceedings of ICSCBM 2018, Springer Nature Singapore Pte Ltd. 2019, pp 793–802
3. Pandey A, Chaudhary PK, Das BB (2019) Productivity analysis of shuttering works for sewage treatment plant. In: Select proceedings of TMSF 2019, Springer Publications Pte. Ltd. 2021
4. Hegde AL, Jain A, Das BB (2019) Resource buffers in construction projects. In: Select proceedings of TMSF 2019, Springer Publications Pte. Ltd. 2021
5. Paul B, Tondihal S, Das BB (2019) Safety stock in inventory management and wastage analysis at construction sites. In: Select proceedings of TMSF 2019, Springer Publications Pte. Ltd. 2021

6. Upadhya PR, Das MS, Das BB (2019) Multi criteria decision making approach for selecting a bridge superstructure construction method. In: Select proceedings of TMSF 2019, Springer Publications Pte. Ltd. 2021
7. Shekhar S, Shukla P, Das BB (2019) Developing a standard template for activity linkage and resource estimation of MEP works. In: Select proceedings of TMSF 2019, Springer Publications Pte. Ltd. 2021
8. Keshk AM, Ibrahim M, Annany Y (2018) Special studies in management of construction project risks, risk concept, plan building, risk quantitative and qualitative analysis, risk response strategies. Alexandria Eng J 57(4):3179–3187
9. Nieto-Morote A, Ruz-Vila F (2011) A fuzzy approach to construction project risk assessment. Int J Project Manage 29(2):220–231
10. Shojaei P, Amin S, Haeri S (2019) Development of supply chain risk management approaches for construction projects: a grounded theory approach. Comput Indus Eng 128:837–850
11. Nabawy M, Khodeir LM (2020) A systematic review of quantitative risk analysis in construction of mega projects. Ain Shams Eng J, In press
12. Samantra C, Datta S, Mahapatra SS (2017) Fuzzy based risk assessment module for metropolitan construction project: an empirical study. Eng Appl Artifi Intell 65:449–464
13. Dikmen I, Birgonul MT, Han S (2007) Using fuzzy risk assessment to rate cost overrun risk in international construction projects. Int J Project Manage 25(5):494–505
14. Raeihagh H, Behbahaninia A, Aleagha MM (2020) Risk assessment of sour gas inter-phase onshore pipeline using ANN and fuzzy inference system-case study: the south pars gas field. J Loss Prevent Process Indus 68:104238
15. Michael C, Costa Y, Pishvaee MS, Castro RC (2021) A fuzzy inference based scenario building in two-stage optimization framework for sustainable recycling supply chain redesign. Expert Syst Appl 165:113906
16. Wu W, Cheng G, Hu H, Zhou Q (2013) Risk analysis of corrosion failures of equipment in refining and petrochemical plants based on fuzzy set theory. Eng Failure Anal 32:23–24

Application of CFRP in Concrete Culvert Bridges

Jitendra Pratap Singh, Amit Kumar, and Ajay Kumar

1 Introduction

Every nation is aspiring for the Economic development which requires development of the infrastructure and transportation. Industrial development lays down the foundation for setting up the industries, commercial hubs and educational institutions. These focal points of the economic activities are connected by the means of transportation and communication. Road and railways mode of transportation incorporates a major chunk of the distribution of goods and services which in turn vitalises the economic activities. Rivers, lakes and canals causes obstruction and discontinuity in the path of the road or railway. Culverts are used for continuity of road over small obstruction like canal.

Whenever there is an obstruction like canal or lake, the culvert is made to connect the two shores of the canal or the lake. Smallest distance between two parallel shores of the canal is the perpendicular line which makes restricts the geometry of the slab to be a rectangle. However, the road may have an inclination with respect to the canal flow. The rectangle shape of the culvert will force the road to have a curve so that it can deviate from its original trajectory to align itself with the rectangular culvert. Skew culverts provide the solution to that problem. With skew culverts, the road can maintain the inclination with canal direction without introducing the additional curves.

Historically, the bridges made of wood and ropes were used as culvert. Such bridges were very unstable and fragile. they undergo a lot of vibration for the loads like moving traffic load and wind loads, which caused uneasiness. With the development

J. P. Singh (✉)
Kamla Nehru Institute of Technology, Sultanpur, India
e-mail: jitendra.singh@knit.ac.in

A. Kumar · A. Kumar
National Institute of Technology Patna, Patna, India

of the concrete, wood has been replaced by the concrete as the construction material. Concrete culverts provide a rigid deck which does not vibrates under the action of moving traffic load and wind load. However, the problem with the concrete is that the concrete is weak in tension and undergoes a brittle failure which is sudden in nature. The problem can be solved to some extent by the use of reinforced concrete. Reinforced concrete has got Steel reinforcement which can take the tensile stress developed in the slab. Steel is very strong in tension and the failure of steel is gradual and ductile. Hence the reinforced concrete culverts are advantageous over the plain concrete culverts. Prestressed concrete culverts have started gaining the popularity as well. In the prestress concrete culverts, the steel is pretensioned to a specific amount of stress so that is can counterbalance the bending stresses developed due to loading. Performance of the prestressed concrete culvert bridges in vibration and deflection is superior to reinforced concrete bridges.

Reinforced concrete culvert faces the challenge of corrosion because they are under the contact of water directly or indirectly by the seepage. When the water comes in the contact of steel reinforcement, corrosion of the reinforcement takes place. The product of corrosion are the oxides of the iron which don't have the tensile strength. They are brittle and acquire more volume. The extra volume of the reinforcement causes the bursting of the concrete. Hence due to steel corrosion reinforced concrete or prestressed concrete structural member may degrade, breaks structural integrity or cause catastrophic failure.

Many researches have been done and the use of Carbon Fibre Reinforced Polymer (CFRP) as a substitute of instead of steel for reinforcement or prestressing tendons is studied. CFRP has very high strength and rigidity. It is noncorrosive in nature. CFRP contains the carbon fibre embedded in the matrix of polymer. The orientation of the carbon fibre will change the properties of CFRP. Hence CFRP is anisotropic in nature. By suitable changing the angle of inclination, we can change the properties of the CFRP composite structure. Hence it is used in reinforced and prestressed concrete structures as it gives reliable structure efficiently.

2 Literature Review

Sharma et al. gave the prediction of ultimate flexural capacity of laterally loaded reinforced concrete skew slab and concludes that actual crack pattern and ultimate flexural capacity of slab specimens tested in the laboratory are found in a good agreement with the theoretical predictions and simulated results for all slabs having aspect ratio greater than or equal to unity and the hypothetical collapse mechanism for skew slabs was found to be in a good agreement [1].

Naresh and Muthu carried analysis of a simply supported reinforced concrete skew slab by using finite element software ANSYS and calculated load deflection behaviour under the action of uniform distributed load and compare the results with the experimental results and it has been found that theoretical results closely concur with experimental results [2].

Raj and Phani studied the design and study on the behaviour of skew slab bridges with various skew angles using STAD PRO and analysis is as per Indian codes IRC 6:2014 and concluded that load-carrying capacity increases with the increase in tilting angle, maximum deviation of inclined skew slabs decreases with the increase in the inclination angle, up to 15° inclined angle skew slabs behave like normal slabs and also by comparing results with the experimental results it shows load deflection same [3].

Lal and Vedpal carried out the analysis of reinforced concrete girder bridges with different skew angles and find the effect of skewness on design parameters i.e. B.M, shear force and Maximum Reaction and concluded that the increase in BM up to 40-degree skew angle is less. At a higher skew angle, a sharp increase is observed. Torsion, with an increase of skew angle, increases appreciably in all directions [4].

Anusreebai and Krishnachandran studied FEM analysis using ANSYS software on skew slabs by taking different reinforcement pattern and compared the results with the experimental results and concluded that the slab with main reinforcement parallel to the free edge and distribution reinforcement perpendicular to the free edge has more cracking load and ultimate load-carrying capacity [5].

Vaibhav and Pranesh carried out the seismic analysis of skew bridges using the finite element method (SAP2000) taking different skew angles and concluded that skewness affects the seismic response of the bridge. i.e. large skewness increases deck acceleration and bearing reaction of the bridge. Axial forces in the exterior girders increase more than that of interior girders [6].

Deepak and Sabeena carried out research on finite element analysis of skew slabs by using skew angles from 0° to 30° and find the effect of skew angles on the uplift of acute corners and concluded that with the increase of skew angles uplift of acute corners increases but load carrying capacity also increases [7].

Gholamreza and Zahed carried out three-dimensional finite –element analysis on continuous composite skew slab girder bridges with different skew angles and compared with the non-skew bridges as well as with to AASHTO standard specifications and AASTHO LRFD specifications and concluded that as the skew angle increases, the support moment in interior and exterior girders rapidly decreases [8].

Menessa et al. compared the effect of skew angles with reference to straight bridge and reported that the bridges with the skew angles less than 20° can be designed as non-skew as moments are almost same for both [9].

Bhatt carried out the theoretical analysis and compared with the experimental results on the behaviour of reinforced concrete skew slabs designed by the Direct Design Method and concluded that the method can be used for the practice [10].

3 Methodology

The main objective of the research paper is as follow

1. To study the behaviour of the CFRP in the Skew Slab

2. To study the effect of the skewness of the slab
3. To understand the effect of CFRP in controlling the maximum stress in the slab
4. To understand the effect of the CFRP in controlling the maximum deflection of the slab.

For the analysis of the Skew Slab, the material properties of the slab elements are as follows:

Concrete

Density   2500 kg/m^3
Grade of Concrete   M25
Modulus of Elasticity   25000 MPa

Steel Reinforcement

Density   7850 kg/m^3
Grade of Concrete   Fe415
Modulus of Elasticity   200000 MPa

CFRP Polymer Composite

E11   170000 MPa
E22   9000 MPa
Poisson Ratio (μ12)   0.34
G12   4800 MPa
G13   4800 MPa
G23   4500 MPa

The geometric Properties of the Slab, reinforcement and CFRP are as follows:

1. SLAB: 1000 × 1000 × 120 mm
2. CFRP: 950 × 50 mm
3. Reinforcement: 950 mm.

For the analysis the Slab is modelled as the 3-D Solid Element with size 1000 × 1000 mm along with the required inclination. The Slab is modelled as the 3-D Deformable Solid element with the required angle of skewness. The CFRP composite is modelled as the shell element with the required angle of skewness. The length of the CFRP is adjusted so that it can give a clear cover of 25 mm from all the sides as shown in Fig. 1.

The Slab and CFRP and Steel Reinforcement are assembled in such a way that the CFRP and the steel reinforcement would carry the tensile stresses while the concrete will carry the compressive stress. The centre to centre spacing of the reinforcement is 100 mm as per IS 456 2000 [11]. Similarly, for the CFRP the centre to centre spacing is 100 mm (Fig. 2).

The loading of the Slab is in accordance to IRC 36-2002. The Standard Class AA loading which is 70 tonnes is applied on the road on an area of 3600 × 800 mm. The pressure developed per wheel is 0.122 MPa. This pressure is applied uniformly on the slab to analyse its effect on the slab for flexure stress and deflection. The ends
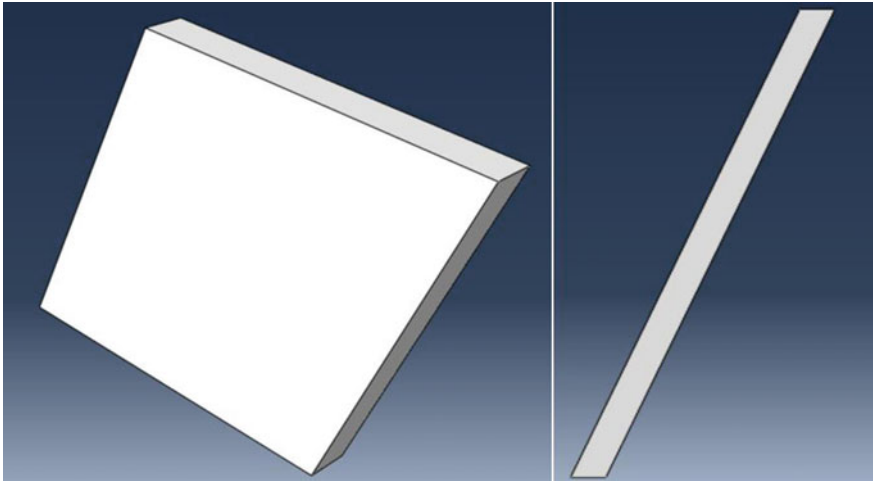
Fig. 1 CAE model of slab and CFRP composite
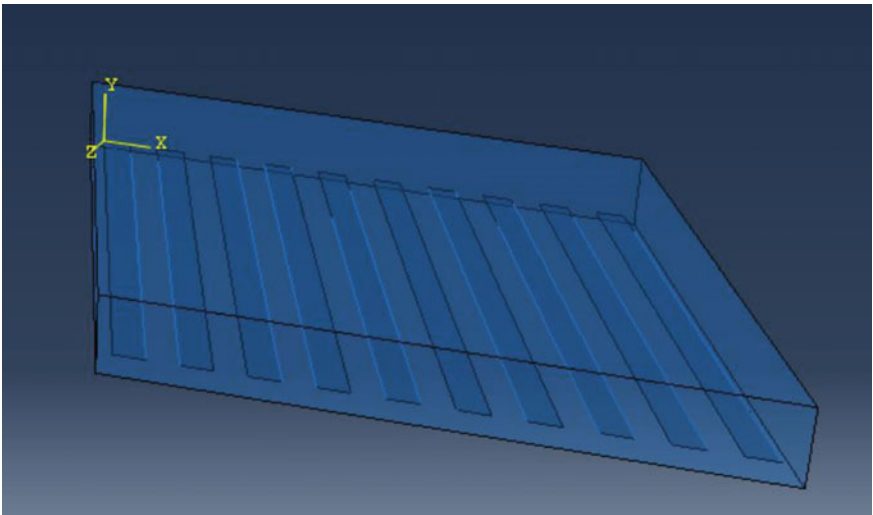
Fig. 2 CFRP and steel reinforcement assembly

are modelled as the hinged supports. The loading is applied on the top surface of the slab as follows (Fig. 3).

The interaction between the CFRP and the Steel Reinforcement is modelled as the embedded region. It is because both steel and the CFRP composites are embedded in the Slab. The loading is applied on the slab and the slab transfer the stresses to the CFRP and Steel reinforcement by the action of cohesive surface bonding. The Steel
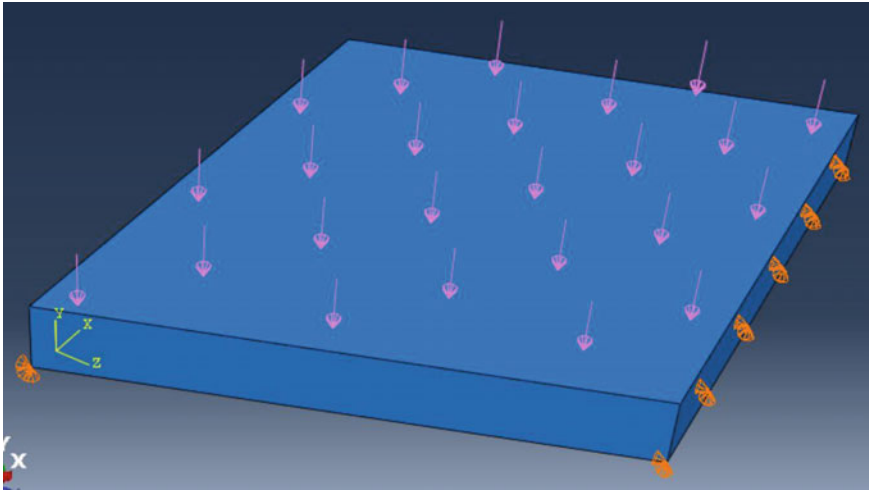
Fig. 3 Loading on the slab

and CFRP will take the tensile stresses till they fail. The also add up to the stiffness of the slab. The embedded interaction of the slab and the CFRP and Steel

Reinforcement is as shown in Fig. 4.

The meshing is done on the slab so that the region which require more detailed meshing are partitioned in such a way that the smaller regions are addressed effectively. The thickness of the slab is such a region which require more detailed meshing
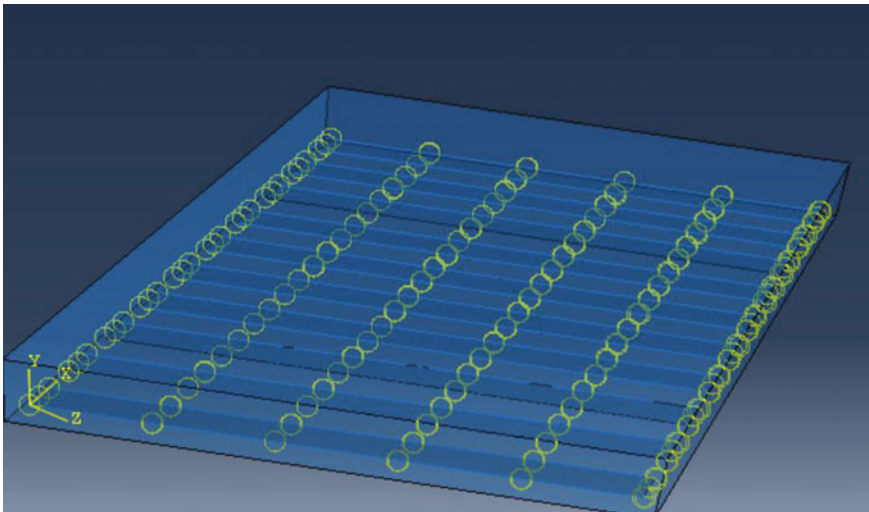
Fig. 4 Embedded interaction of CFRP, reinforcement and slab

than the overall region of the slab. The meshing is chosen for FRP in such a way that the total integral points in the calculation of the material properties of the CFRP composite Shell will be three. The messing of the slab is shown in Fig. 5.

The analysis is done and Static General Step is created for the analysis. The results are produced in the forms of stresses and the deflection. The maximum deflection and the maximum Stresses are calculated and noted for each of the CFRP composite profile arrangement. The stresses and the deflection are shown in Figs. 6 and 7. The stresses in the slab can be seen to form the Arch structure.
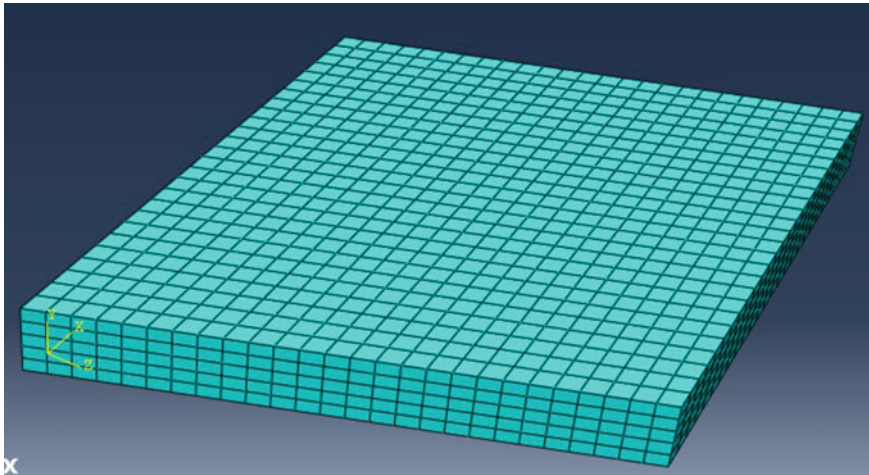
Fig. 5 Meshing of the slab
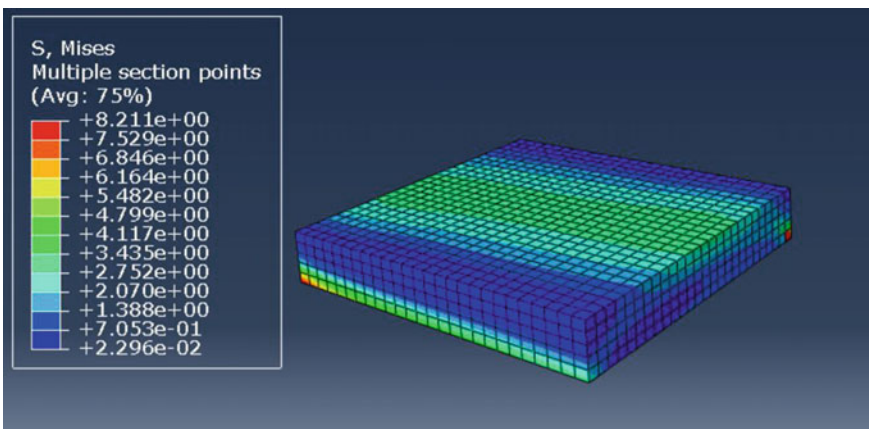
Fig. 6 Stresses in the slab
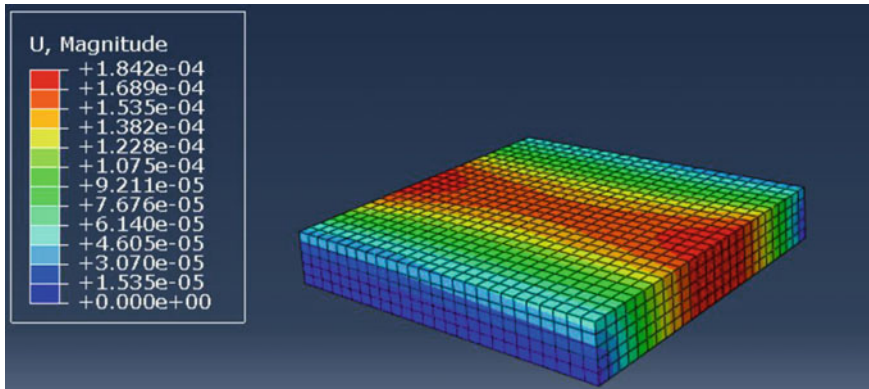
Fig. 7 Deflection of the slab

4 Results

The Slab is analysed for the following six different types of arrangement of the CFRP composite. Each arrangement has different inclination of the fibre, different thickness and different structure so a to give us an idea about the variation of the strength and serviceability of the slab with respect to these profiles (Fig. 8).

ABAQUS analysis is done for the given sets of Carbon Fiber Reinforced Polymer composites and the maximum stress and maximum displacement is plotted with respect to the Skew angle of the plate (Figs. 9, 10, 11, 12, 13 and 14).

5 Conclusion

ABAQUS analysis has been performed for the given culvert slab reinforced with CFRP composite. When the angle of Skewness of the slab is changed, the perpendicular length of the slab becomes shorter which decreases the deflection of the slab, which can be seen in the results. The increase in the stress is accounted for additional transverse stresses due to skewness of the slab.

Increasing the thickness of the CFRP Composites will decrease both the Stress and the deflection because of the additional increase in the rigidity of the structure. Amongst the various arrangements, the Forty-five-degree angle of inclination of fibres of the CFRP composite has performed the best. It is followed by the conventional (0/90)n fibre arrangement. Hence, the use of CFRP as a substitute of the steel reinforcement can be recommended. Total replacement of the steel reinforcement is discouraged because the CFRP doesn't have ductility as better as steel reinforcement.
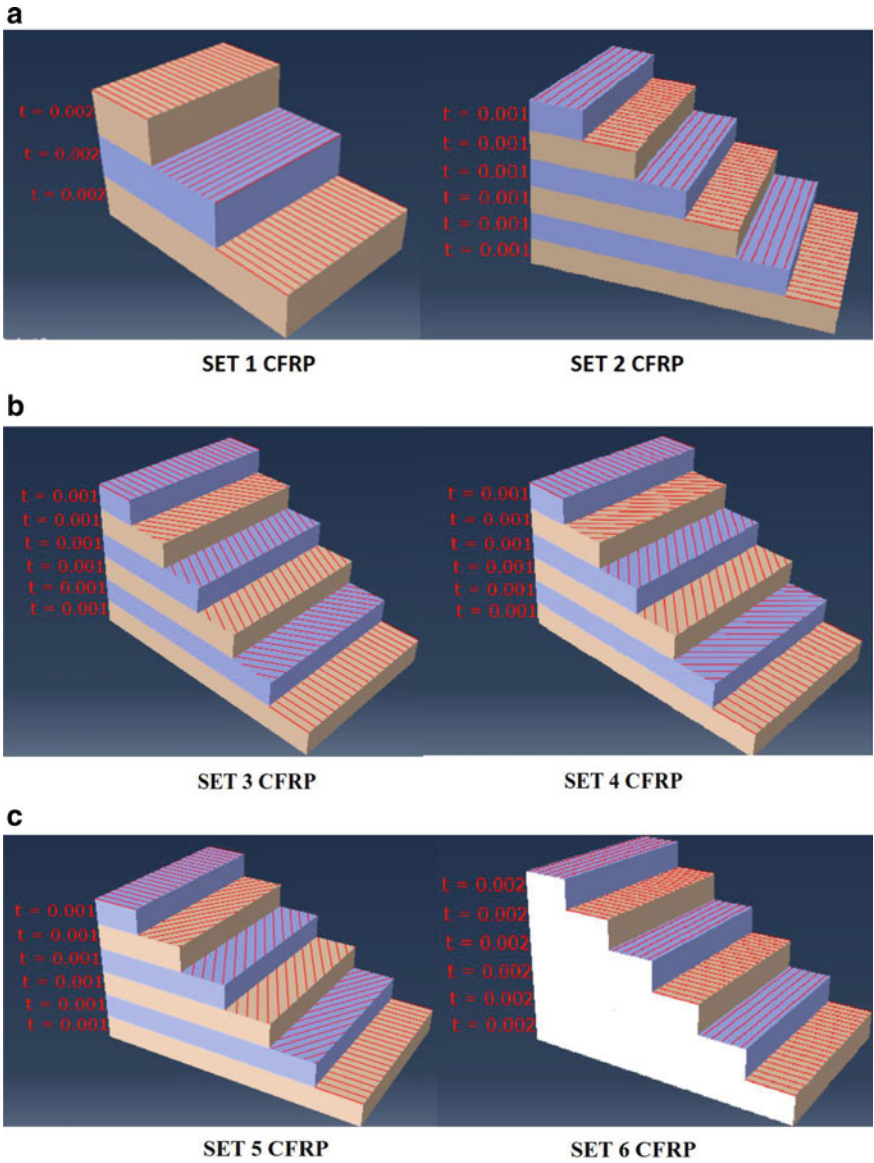
Fig. 8 **a** Set 1 and set 2 CFRP arrangement. **b** Set 3 and set 4 CFRP arrangement. **c** Set 5 and set 6 CFRP arrangement
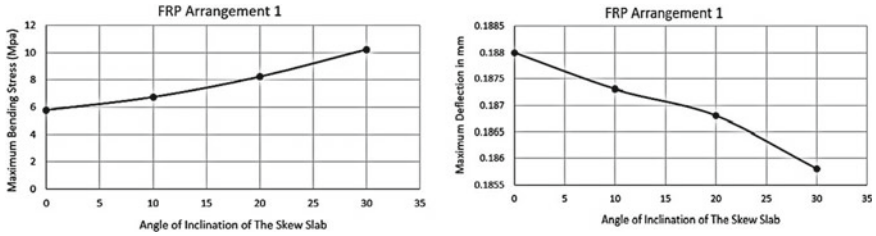
Fig. 9 Maximum stress and deflection for set 1 CFRP arrangement
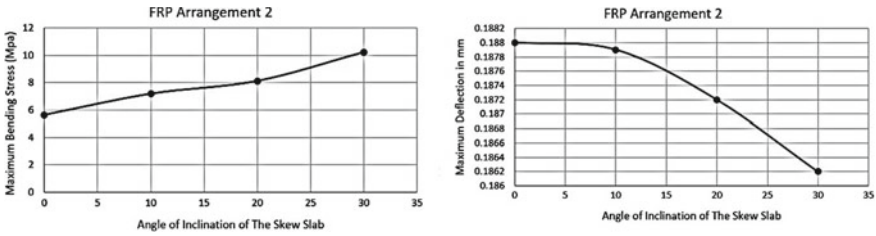
Fig. 10 Maximum stress and deflection for set 2 CFRP arrangement
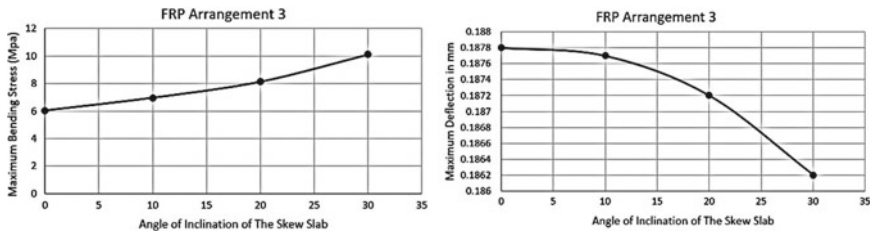
Fig. 11 Maximum stress and deflection for set 3 CFRP arrangement
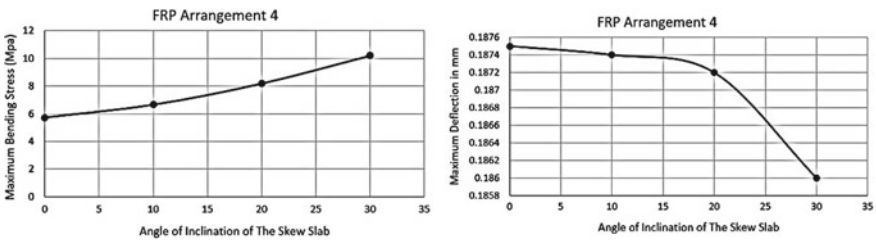
Fig. 12 Maximum stress and deflection for set 4 CFRP arrangement
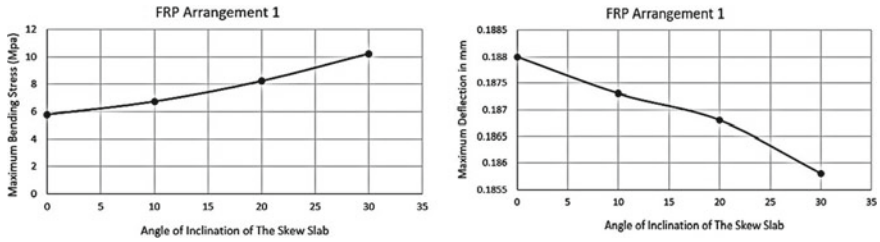
Fig. 13 Maximum stress and deflection for set 5 CFRP arrangement
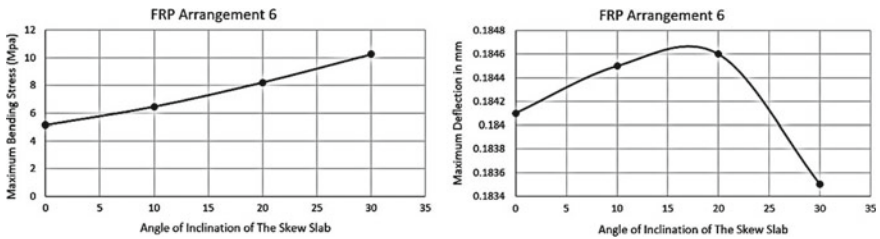
Fig. 14 Maximum stress and deflection for set 6 CFRP arrangement

References

1. Sharma M, Kwatra N, Singh H (2019) Predictive modelling of RC skew slabs: collapse load. Struct Eng Int 443–452
2. Naresh GN, Muthu KN (2017) Analysis of simply supported reinforced concrete skew slabs. Int J Civil Eng Technol 8:121–128
3. Raj KK, Phani RG (2017) Design and study on behavior of skew slab bridges with various skew angles. J Appl Sci Innov
4. Lal M, Vedpal RK (2016) Study of skewness angles in reinforced concrete girder bridges. Int J New Technol Res 2:06–10
5. Anusreebai SK, Krishnachandra VN (2016) Effect of reinforcement pattern on the behaviour of skew slab. Int Res J Eng Technol 3
6. Vaibhav K, Pranesh M (2015) Seismic analysis of skew bridges. J Civil Eng Environ Technol 2:71–76
7. Deepak C, Sabeena MV (2015) Effect of skew angle on uplift and deflection of RCC skew slab. Int J Res Eng Technol 4
8. Gholamreza N, Zahed A (2012) Influence of skew angles on continuous composite girder bridge
9. Menessa C, Mabsout M, Tarhini K, Frederick G (2007) Influence of skew angles on reinforced concrete slab bridges. J Bridge Eng 205–214
10. Bhatt P (1988) Direct design of reinforced concrete skew slabs. Comput Struct 30:477–484
11. Sinha BN, Sharma RP (2009) RCC box culvert methodology and designs including computer method. J Indian Roads Congress. academia.edu

Risk Assessment and Management in Construction Industry

Lisyna Priyadarshini and Prasanta Roy

1 Introduction

At present, the construction industry is quite possibly the most unique, risky and very demanding or challenging business. Due to it's complexity and uniqueness of such construction projects, the risks prevail in the system. For every construction project risk management has become a significant part of the project. In every industries the risk management practice shows that the risk management has the obvious function for increasing the efficiency of the project implementation, saving the expense and further developing the project benefit [1]. It is a organized process of identifying, assessing, analyzing, responding the project risk and setting preference for risk mitigation [2]. Basically, risk is a choice in an environment instead of a destiny. Project risk can be explain as an uncertain event that prompts neglecting to achieve something like one task objective and control the probability and impact of unfortunate events or to boost the acknowledgment of chances. Risk management's goal is to ensure that uncertainty doesn't redirect the undertaking from the business objectives [3–5]. The process of risk management can further develop the project execution by controlling the results of risky events on project objectives [6]. It is perceived that it is possible to manage risks but not eradicate them [7]. Organized and dynamic risk management practices are required to handle and manage risks so that the success of projects can be established [8].

L. Priyadarshini (✉)
School of Civil Engineering, KIIT Deemed to be University, Bhubaneswar, India

P. Roy
Civil Engineering Department, Amity University, Kolkata, India
e-mail: proy2@kol.amity.edu

2   Concept of Risk and Risk Management

Risk management has become an undeniably challenging activity [9]. It has become an necessary demand for the construction projects. Risk management process contains Risk identification, Risk assessment and Risk control. Risk is assessed by Qualitative Methods and Quantitative Methods. Risk management is the organized process of identifying, analyzing, and responding to project uncertainties or risk, and it incorporates to expanding the probability and consequences of positive attributes and limiting the probability and consequences of properties unfavourable to project objectives [10, 11]. In current construction management literature, various risk identification and assessment or evaluation procedure have been offered within which the normal recognized techniques is identifying risks that may arise during the projects execution, assigning ratings to identified risk factors thinking about their probability of occurrence and effect, and finally calculating the general risk rating to assess the general effect of risk factors on the project for the good outcomes [8]. For a long time, risk management in construction projects has been moved toward utilizing a reductionist methodology that produces helpless outcomes and limits the nature of project management. For example, a number of the times risk is managed through the use of contingencies (money) or floats (time) that are not resolved dependent on a comprehensive examine of the risks that can influence a specific project, and that in many cases are clearly inadequate to cover the consequences of risks that do occur during the project realization. Then, in most of the cases projects end with costs invade and late [12–19].

The following flow chart is showing how the Risk, Conflict, Additional Claim, Dispute and Project Completion are interlinked and corelated (Fig. 1).
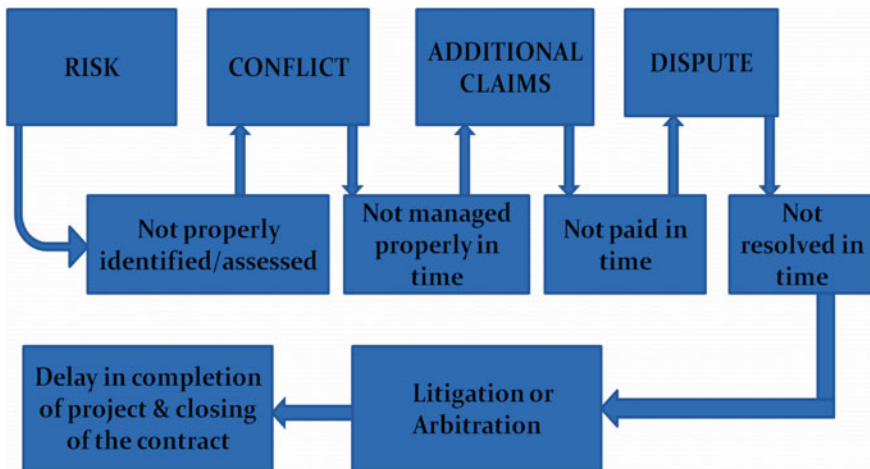
Fig. 1 Flow chart of risk, conflict, claim and dispute relationship

2.1 Sources of Risk in Construction Projects

There are numerous uncertainties present in the construction projects, which include the performance of the contractor(s), consultant(s), owner(s), availability of resources, conditions of the environment, other parties involvement (sub contractors, suppliers and vendors), contractual relations, change in Designs and drawings and, Inadequately co-ordinated work, imperfect estimates, Roles and responsibilities are not define properly, Natural hazards, Untalented staff, Legal and political problems [11].

2.2 Risk Management Process

Manager can plan their strategy based on four step of risk management process.

1. Risk identification
2. Risk assessment
3. Risk response
4. Risk monitoring and control (Fig. 2).

3 Methodology

The present studied was aimed to identify, assess and mitigate the significant risks involved in the project. The research methodology is based on collection of data, analysis and validation of the data and report on findings and results. This comprised of comprehensive literature review, followed by open interviews in person and over phone and distributing questionnaire surveys to the experienced personnel in the industry and various agencies e.g. contractors, consultants and owners of the projects. Figure 3 shows the research methodology flow chart which has been used for this study.

4 Method of Surveying

To examine and check the sensitivity of owners, consultant, and contractors, to the root causes and resolutions of risk in construction industries a questionnaire was prepared. Factor making risk in construction industries were first identified and analyzed through questionnaire. To identify the causes and mitigation in construction industries, a good number of literature review and case studies were carried out and a questionnaire was prepared and distributed to major construction companies (Consultant, Owner and Contractor) in different countries. For each of the risk
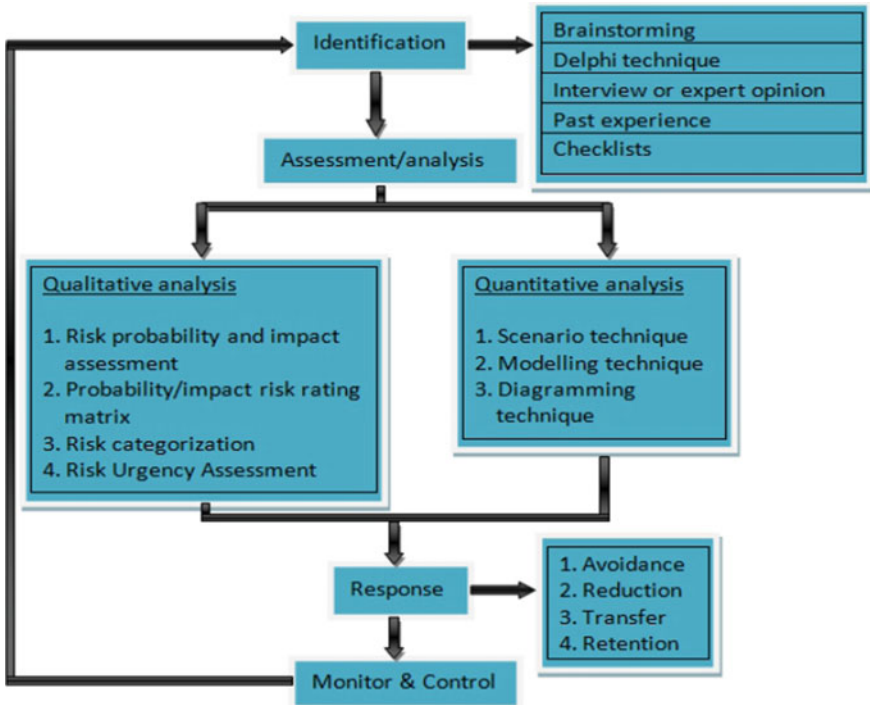
**Fig. 2** Flow chart of risk management process
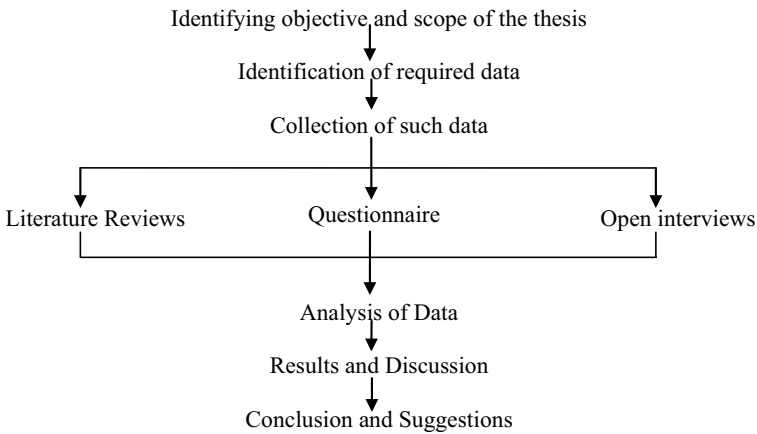
Fig. 3 Research methodology flow chart

and resolutions, the respondent was requested to judge the several factors of it in construction industries. Using the sampling technique, the questionnaire survey was distributed among the participants. The response rate of survey was 36%.
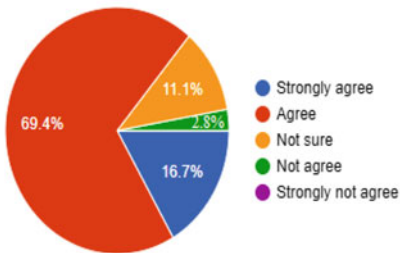
4.1 Bar Chart

The observations are displayed below in the form of bar chart for each question separately taking the value from frequency table and representing them in terms of percentage.

Knowledge of risk management is essential for execution of Projects?

Did you participate in risk assessment exercise?
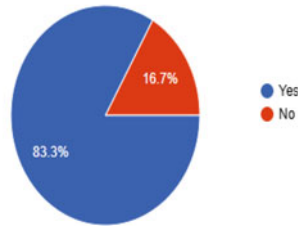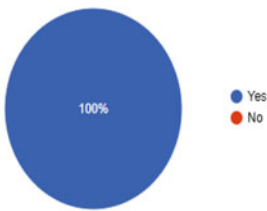
Any risk identified?

Has the risks been assessed?
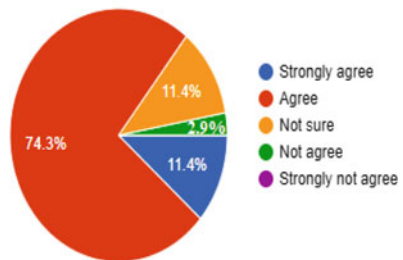
Any plan to mitigate the risks?

- Strongly agree
- Agree
- Not sure
- Not agree
- Strongly not agree
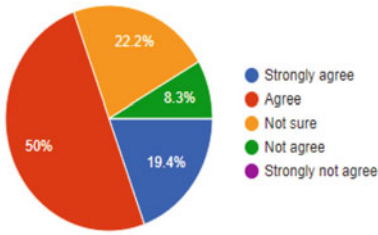
Risk management process in construction industry
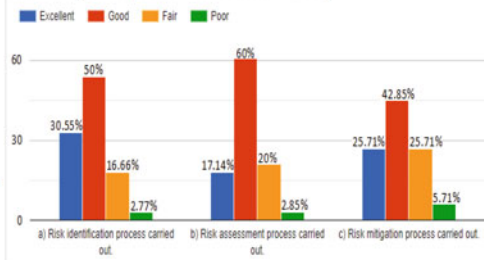
Who are involved in risk management process?
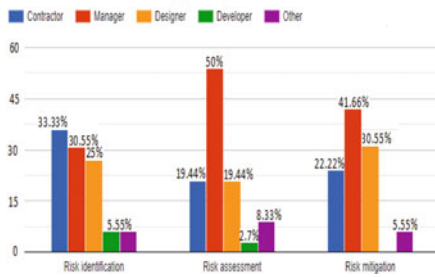
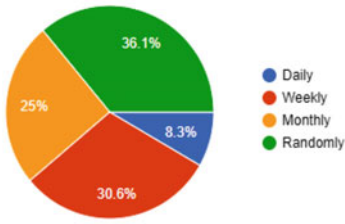## The following risk identification techniques has been used?

- Brainstorming
- Checklist
- Past experience
- Interviews
- All the above
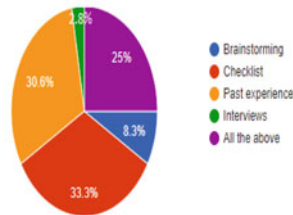
Which techniques has been used for risk assessment?

- Top ten risks tracking
- Expert judgment
- Decision tree analysis
- Sensitivity analysis
- All the above
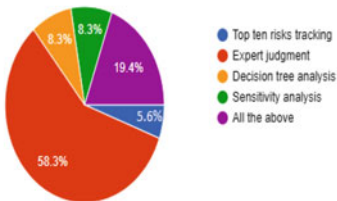
Which technique has been used for risk monitoring?

- Traffic lights monitoring method
- Graphic monitoring
- Monitoring schedule by timely
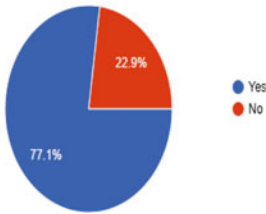- Risk assessment checkpoints
- All the above
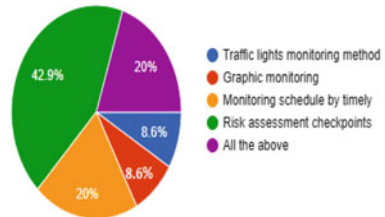
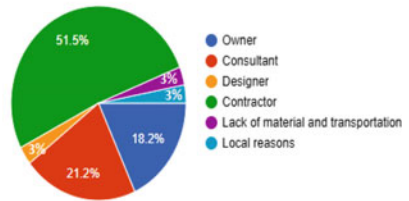How frequently the risk management team members meet to monitoring the risks?

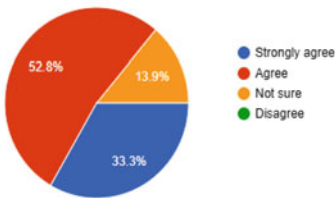Percentage progress of risks resolution in the current project.
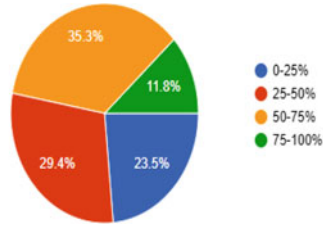
Has there been any gap between the planed progress and actual progress at the site?
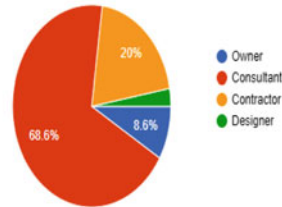
Who is responsible for the delay in the progress for the current projects?

Application of proper software is beneficial for risk management process?
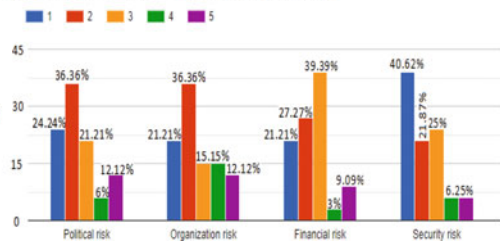
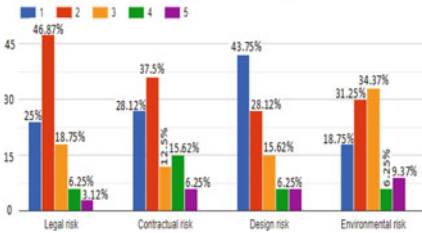The statistical reports of risk management is prepare by
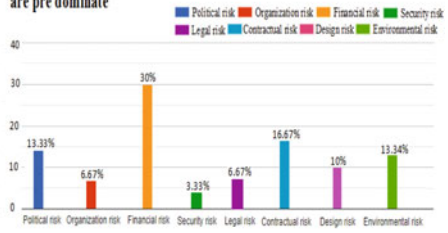
What does the statical reports contains?

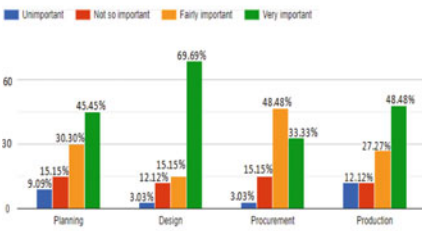Frequency of occurrence of risk (5 times or more).

Frequency of occurrence of risk (5 times or more).

In your project which of the risk(s) are pre dominate

Assess the importance of risk management in the different phase of the project.

Who carried out the following risk management process in different phases of project? A) Planning
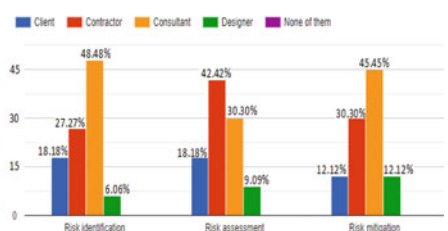
Design & Engineering
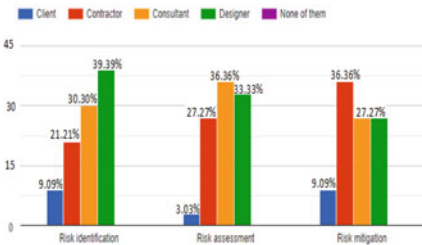
Procurement
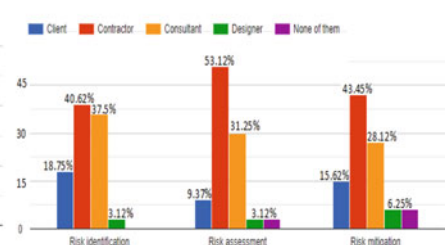
Execution
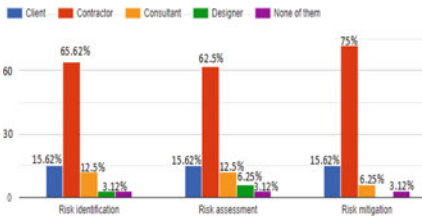
Pre-commission
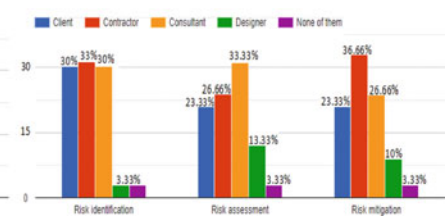
commission
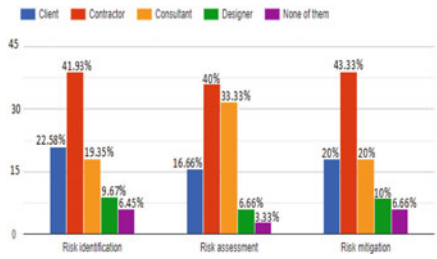
Production
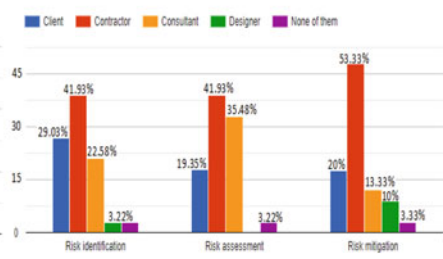
Who has managed the following risk in the project you have executed? A) Financial risks

Design & Engineering risk

Organizational/contractual risk

Execution Risks

Production risks

This research explored a better understanding of risk management through the set of questionnaire survey of 36 different construction projects.

1. The risk management process consists of risk identification, risk assessment, risk monitoring and risk mitigation. The first step in the process of risk management is risk identification. This identification process consists of various techniques like brain storming,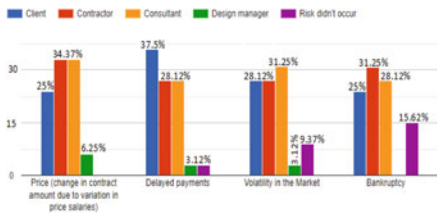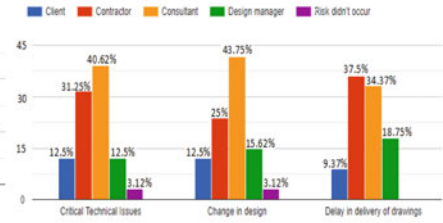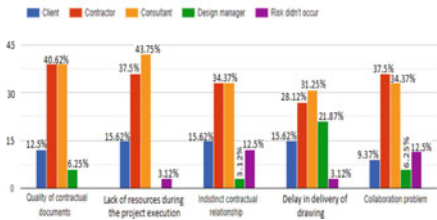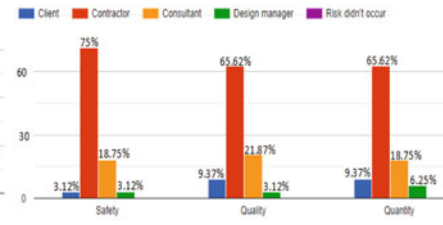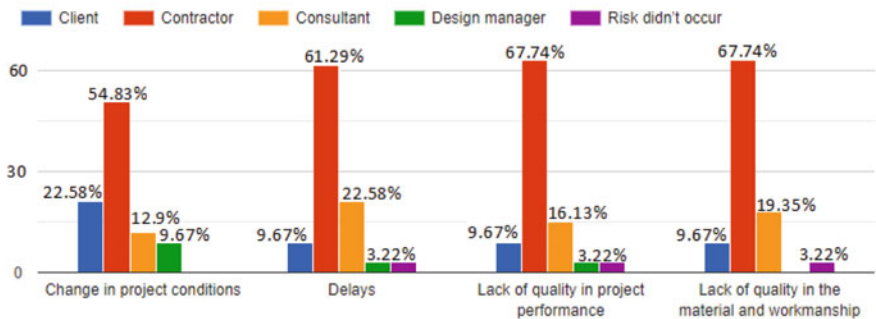 Delphic technique, Checklist, Interview, Past experience etc. According to the survey conducted for the present thesis, the maximum respondents (33%) agreed that they have used "Checklist" and very few respondents (2.8%) agreed that they identified the risk through interview or expert opinion.

2. According to the risk management technique, the next process involved is the assessment of risk. This process can also be termed as quantification or analysis stage This analysis is done generally through top ten risk tracking, probability and impact assessment, scenario technique—Monte Carlo simulation, decision tree analysis, sensitivity analysis and expert judgment methods. Among all these methods, majority (58%) as per our survey report have accepted that they use in general the Probability and Impact matrix Assessment method which is a qualitative method of analysis. Only 8.3% respondents have expressed that they use quantitative method of decision tree analysis for risk assessment process.

3. Risk monitoring is the last stage and integral part of risk management process. It is the important step of risk management process where all possible and potential risks are frequently monitored to identify any change in status or in case they turn into an issue. This method consists of various techniques e.g. traffic light monitoring method, graphic monitoring, monitoring schedule by timely and risk assessment check point etc. Maximum respondents (43%) agreed that they use risk assessment check point method and minimum respondents (8.3%) agreed that they use traffic light monitoring and graphic monitoring method.

   The monitoring process carried out "randomly" by risk management team members have been accepted by maximum respondents (36%), whereas, less number (8.3%) says that they carried out their meeting on "daily basis".

4. From the survey conducted for this thesis, it was observed that in maximum projects, the security risk was substantially low (03%), whereas, the financial risk is quite high (30%).

5 Validation Through Questionnaire Survey

A questionnaire is prepared to validate the root causes and remedies of Risk and disputes in construction industries. The questionnaires follow a five point Likert scale response mechanism. Likert scale is a psychometric response scale basically used in questionnaires to derive respondent's inclinations or level of concurrence with a statement or set of explanation. Respondents are asked to indicate their level of agreement with a given explanation by way of an ordinal scale.

The format of the scale utilized here for each question is as per the following:

i.   Strongly disagree (1)
ii.   Disagree (2)
iii. Neutral (3)
iv.   Agree (4)
v.   Strongly agree (5).

The numbers in the brackets indicate the rank of the correctness from lower to higher order each having same interval between them. It means that the greater the rank is the respondents have more consent on the mentioned policy. This ranking will also be useful later for calculation and analysis, which will be done on SPSS software. The questionnaire consists of 24 questions. Now, these responses are analyzed using the software SPSS. SPSS stands for Statistical Packages for Social Science. It is the most widely used software for research in management and social science around the globe. There are two types of data sheet we need to fill up in IBM SPSS. One is data view and the other one is variable view. In data view, we have to record the responses from the respondents. But, for that we have to fill up the variable view sheet first which defines the properties of each variables i.e. questions. In the field of variable name, we just put the question numbers instead of full questions as we cannot use space or any special character there. The variable names are written as Q1, Q2, Q3 … Q22 and Q24. Now, moving to the next column in the variable view tab i.e. type of variable. As we are using numbers to represent the responses we simply select numeric. As there is no need for decimals, we select '2' for all the questions. Then, in the label option we write down the full questions. Putting the values is very important here because our analysis depends upon the values we put in the column. We put previously decided Likert scale values here. If any respondent does not answer or forget to answer a question then, it can be said that the value is missing. For these missing cases, SPSS has solution. We can assign a value that we are not going to use in the data view sheet. Here, we assigned the value '0'. Whenever there is a missing response we put the value 0 against that certain variable. Finally, in the measure column we select the ordinal scale as individual responses are generally treated as ordinal data The Variable view window of SPSS software is shown in the above figure (Figs. 4 and 5).

To validate the root causes and remedies of Risk and disputes in construction industries through questionnaire of survey, the following two methods were used:

1.   Reliability analysis
2.   Test of hypothesis using student t-test approach.

5.1   Reliability Analysis

Cronbach's Alpha is the most common method to check internal consistency or reliability for reliability analysis. It is also used to measure scale reliability. Cronbach's alpha is one way of measuring the strength of that consistency.
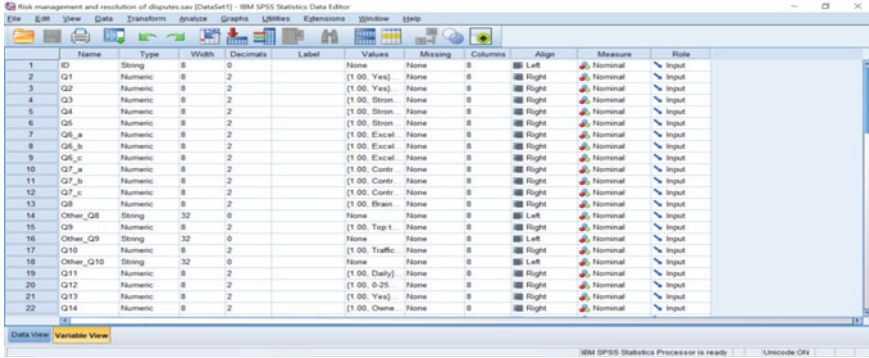
Fig. 4 Variable view window of SPSS software after input
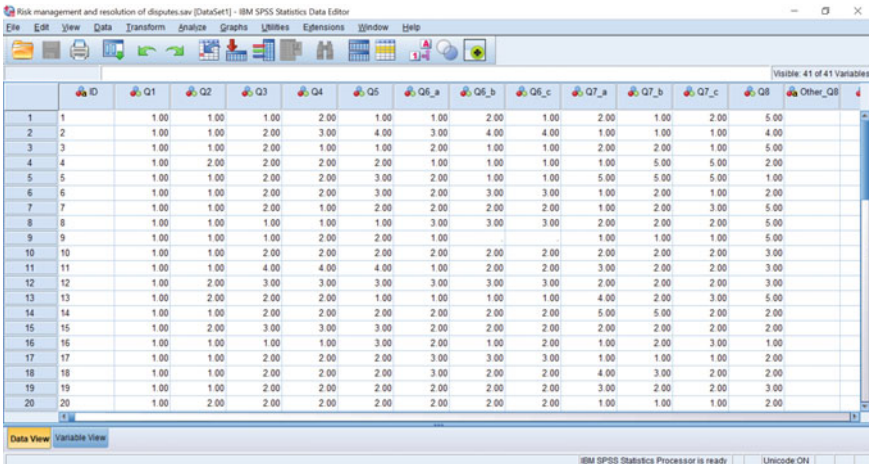
Fig. 5 Data view window of SPSS software after response are recorded

Cronbach's alpha can be expressed as a function of the number of test items and the average inter-correlation among the items. It is given by the formula:

$$\alpha = \frac{K}{K-1}\left(\frac{1 - \sum_{i=1}^{K}\sigma_{Yi}^2}{\sigma_X^2}\right)$$

where k mention to number of scale items.

σ_{Yi}^2 is the variance with item i.

σ_X^2 is the variance connected with observed total score.

Alternatively, Cronbach's Alpha can be expressed as the

Table 1 Cronbach's alpha values and their reliability

Cronbach's alpha	Reliability/Internal consistency
$\alpha \geq 0.9$	Excellent
$0.9 > \alpha \geq 0.8$	Good
$0.8 > \alpha \geq 0.7$	Acceptable
$0.7 > \alpha \geq 0.6$	Questionable
$0.6 > \alpha \geq 0.5$	Poor
$0.5 > \alpha$	Unacceptable

$$\alpha = \frac{K \times \overline{C}}{\overline{V} + (K - 1)\overline{C}}$$

where K is a number of scale item.

$\overline{C}$ is the average to all co-variances between items.

$\overline{V}$ is the average variance of each item.

The resulting α component of reliability ranges from 0 to 1 in providing this overall assessment of a measure's reliability. If all of the scale items are entirely independent from one another (i.e., are not correlated) then $\alpha = 0$ and if all the items have high co-variances, then α will approach 1 as the number of items in the scale approaches infinity. In other words, higher the α coefficient the more the items have shared co-variance and probably measures the same underlying concept.

Although the standards for what makes 'good' α coefficient are entirely arbitrary and depend on theoretical knowledge of the scale in question, a commonly accepted rule for interpreting Cronbach's Alpha given below (Table 1).

The following steps are followed in SPSS to the reliability test:

$$\text{Analyze} \rightarrow \text{Scale} \rightarrow \text{Reliability Analysis}$$

The initial reliability analysis is shown in Table 2. So the questions have acceptable consistency. This means questions have more shared co-variances and measures the same underlying concept. So the questionnaire is feasible.

Table 2 Reliability statistics from SPSS software for management of risk and resolution of disputes

Cronbach's alpha	No. of items
0.784	33

5.2 Test of Hypothesis Using Student t-test Approach

Analysis using t-test method is the most common measure of survey to determine whether it is statistically significant or not. The t-test compares the values of two averages (means) of samples, and shows whether they are different from each other or not. The t-test also shows how significant the differences are.

Scores are provided for each reply of a commuter on the basis of a hierarchy including strongly agree, agree, not sure, disagree and strongly disagree that are mentioned as 0.9, 0.7, 0.5, 0.3 and 0.1, respectively.

The responses are analyzed using the software Excel Sheet. In the present thesis, the responses have been recorded in two sheets. In one of the sheets the responses from India (B) and in another sheet the responses from outside India (C) (Nepal, Bhutan) are recorded. The mean (average) for the data of India and outside India for each question is calculated.

Then the following steps have been carried out for t-test.

1. Calculate the deference $(E = B - C)$ between the two observations on each pair, making sure you distinguish between positive and negative deference's.
2. Calculate the sum ΣE
3. Calculate the square of each difference E^2
4. Calculate the sum of square difference ΣE^2
5. Calculate the square of sum of difference $(\Sigma E)^2$
6. Use the following formula to calculate T value

$$T = \frac{\left(\frac{\Sigma D}{N}\right)}{\sqrt{\frac{\Sigma D^{2-\left(\frac{(\Sigma D)^2}{N}\right)}}{(N-1)N}}}$$

7. Use tables of the t-distribution to compare your value for T to the $tn - 1$ distribution. This will give the $t_{theoretical}$ value for the t-test (Table 3).

From the above analysis, it is evident that the $t_{calculated}$ value is smaller than the $t_{theoritical\ value}$. This indicates that there is significant difference in opinion of professionals engaged in the construction sectors between India and outside India. The observations are displayed below in the form of bar chart for each question separately taking the value from frequency table and representing them in terms of percentage.

Table 3 Significance statistics from SPSS software for Management of risk and resolution of disputes	$t_{calculated}$ value	$t_{theoretical}$ value
	0.895	2.037

6 Conclusion

This paper mainly aimed towards the exploring of the causes that lead to the risk in major construction projects, assessing it's magnitude and recommendations on how it can be mitigated in the most efficient manner.

For this purpose, previous work on similar research topics, journals, conference papers and also different case studies have been reviewed carefully. From research work it has also been seen that risk is a reality in almost every construction project and inevitable in construction industry. If the projects are not properly managed then it can takes place at any point of time during the project progression. Apart from the theoretical analysis, a detail survey work has been conducted with 33 questions in two parts which were sent to various industry professionals in India and abroad. The survey reports were analyzed and found to be feasible through reliability tests. Through T-test analysis, it was evident that there are significant differences in opinion of professionals engaged in the construction sectors in regard to the process of risk management.

7 Future Work

In future, this research work can be further advanced by collecting and analyzing the various statistical data from various projects which have been completed. We would also like to recommend further study on particular live projects and their risk management processes including the procedures the company follows for mitigating their risks throughout the project life span and thereby collecting all the data and analyzing them.

8 Recommendations

Based on the survey report, analysis and studies, the following items are recommended to minimize the potential Risks in a project.

1. For successful execution of major projects, implement an effective risk management process or system and ensure that the team handling the risk management process should have sufficient knowledge and experience about this process.
2. The risk management processes i.e. risk identification, risk assessment, risk response and risk monitoring should be continuously assessed, followed up on regular basis and timely actions are taken in time throughout the entire span of the project in order to keep track and minimize all the potential risks.

3. During the planning stage itself, a full fledged risk assessment about the project should be made as an effective measure to avoid risks during the execution stage.

4. Everybody who is in the planning process relating to the project should mandatorily identify and understand the risks.

5. The risks and contractual disputes are evident in the construction industries. However, such risks could be minimized by following proper mitigation processes and resolved in time.

6. The risk management team should be open minded, proactive with huge industry experience along with the sound knowledge on projects risks and contract.

7. The client, consultant, designer, and the contractor must work together hand in hand in a major project starting from its feasibility phase through the construction and commissioning phases until the successful completion and handover of the project to address the potential risks in time along with the recommendation of their mitigating actions.

8. Financial risk for major projects is a global phenomena and this risk should be handled carefully by engaging the competent and reputed financial consultants since this cannot be handled by engineers alone.

9. Another important aspect in risk identification is that the organizations involved in the contract should adopt a continuous learning approach. Past projects and past events are real-life scenarios from which to gain experience that might stand the parties in good stead in the future so that probable risks that might be encountered in a new project can be identified beforehand and necessary measures could be taken in order to avoid triggering those risks.

10. Safety (HSE) and occupational health are considered to be one of the most potential sources of major risks in major construction projects. Therefore all necessary action to be taken and proper procedures as per international codes and practices are to be strictly adhered in order to ensure the zero LTI (loss time injure)

11. Risk Register should be used in each project to identify, assess and mitigate the risks.

12. The Contractors should be aware of RMP (risk management process) otherwise the organization (owner/client) should train them to get them the knowledge of RM.

13. In assessing the time limit for the completion of any construction project, pragmatic procedure or solution should be adopted. The situation of Force majeure should be taken into consideration. Country's political situation also contributes a lot towards the managing of the project; therefore, it should also be taken into consideration. The bar chart and CPM should also be taken into consideration.

14. Detail geotechnical exploration including soil testing and geological information must be carried out at site prior to the design and engineering. The design

and engineering of complicated and major projects should be carried out by experienced and competent consultant. The owner as well as the contractor must study the drawing carefully issued by the consultant to ensure a flawless project.

References

1. Zhou LF, Yuan GH (2011) The risk assessment model of BT construction engineering project financing. In: 2011 international conference on risk and project management, pp 169–173
2. Jayasudha K, Vidivelli B, Surjith ERG (2014) Risk assessment and management in construction projects. Int J Scient Eng Res 387–396
3. Mark W, Cohen PE, Glen RP (2004) Project risk identification and management. AACE Int Trans INT.01 1–5
4. Morote AN, Vila FR (2011) A fuzzy approach to construction project risk assessment. Int J Project Manage 220–231
5. Islam MS, Nepal MP, Skitmore M, Attarzadeh M (2017) Current research trends and application areas of fuzzy and hybrid methods to the risk assessment of construction projects. Adv Eng Inf 112–131
6. El-Karim MSA, Nawawy OAM El, Alim AMA (2017) Identification and assessment of risk factors affecting construction projects. Housing and Building National Research Center, pp 202–216
7. Farooq MU, Thaheem MJ, Arshad H (2018) Improving the risk quantification under behavioural tendencies: a tale of construction projects. Int J Project Manage 414–428
8. Yildiz AE, Dikmen I, Birgonul MT (2014) Using expert opinion for risk assessment: a case study of a construction project utilizing a risk mapping tool. Procedia—Social Behav Sci 519–528
9. Hsueh SL (2007) On-line multi-criterion risk assessment model for construction joint ventures in China. Automat Constr 607–619
10. Azevedo RC, Ensslin L, Jungles AE (2014) A review of risk management in construction: opportunities for improvement. Mod Econ 367–383
11. Taroun A (2014) Towards a better modelling and assessment of construction risk: insights from a literature review. Int J Project Manage 101–115
12. Salawua RA, Abdullahb F (2015) Assessing risk management maturity of construction organisations on infrastructural project delivery in Nigeria. Procedia—Social Behav Sci 643–650
13. Hegde AL, Jain A, Das BB (2019) Resource buffers in construction projects. In: Select proceedings of TMSF 2019, Springer Publications Pte. Ltd., 2021
14. Pandey A, Chaudhary PK, Das BB (2019) Productivity analysis of shuttering works for sewage treatment plant. In: Select proceedings of TMSF 2019, Springer Publications Pte. Ltd., 2021
15. Shekhar S, Shukla P, Das BB (2019) Developing a standard template for activity linkage and resource estimation of MEP works. In: Select proceedings of TMSF 2019, Springer Publications Pte. Ltd., 2021
16. Upadhya PR, Das MS, Das BB (2019) Multi criteria decision making approach for selecting a bridge superstructure construction method. In: Select proceedings of TMSF 2019, Springer Publications Pte. Ltd., 2021
17. Paul B, Tondihal S, Das BB (2019) Safety stock in inventory management and wastage analysis at construction sites. In: Select proceedings of TMSF 2019, Springer Publications Pte. Ltd., 2021

18. Pradeep RC, Das BB (2019) Methods to monitor resources and logistic planning at project sites. In: Select proceedings of ICSCBM 2018, Springer Nature Singapore Pte Ltd., 2019, pp 793–802
19. Akhil RP, Das BB (2019) Cost reduction techniques on MEP projects. In: Select proceedings of ICSCBM 2018, Springer Nature Singapore Pte Ltd., 2019, pp 495–517

Chemical Attacks on Lightweight Concrete Made with Industrial Waste

Durga Chaitanya Kumar Jagarapu and Arunakanthi Eluru

1 Introduction

POS is a sort of thick waste created all through the extraction of palm oil. Normally, this left-over material is developed stocks and abandoned in the territory of the palm oil mills [1]. Palm oil natural products are red to brown when appropriate and it is practically round, ellipsoid fit. Each natural product comprises of a hard seed inside it. The seeds can be formed, ready, dried, and utilized as coarse aggregate [2]. It has been making that POS strong waste can be given off a role as coarse total for the creation of primary lightweight concrete [3]. POS is a cultivating strong waste making from the palm oil industry. It has been shown that high strength lightweight total cement has a compressive strength of normally somewhere in the range of 34 and 69 MPa through the blend of numerous pozzolans and water reductants [4–7]. The natural effect of oil palm cultivating is an amazingly provocative subject. POS are horticultural strong end harvests of oil palm producing courses [8]. Primary lightweight cement has been utilized for various years; one might say that SLWC is like ordinary lightweight cement with the exception of their thickness is lower [9]. POS is lighter than the customary coarse total. Likewise, the resulting substantial will be lightweight. Lightweight substantial utilizing POS as coarse total can collect cements with compressive qualities of more than 25 Mpa [10].

D. C. K. Jagarapu (✉) · A. Eluru
Department of Civil Engineering, JNTU Anantapur, Ananthapuramu 515002, Andhra Pradesh, India

557

Table 1 Physical properties of cement, GGBS, and POFA

S. No	Description	OPC	GGBS	POFA
1	Fineness (m^2/kg)	340	416	980
2	Normal consistency (%)	31	–	–
3	Setting time (minutes)			
	1. Initial	40 min	55 in	–
	2. Final	6 h	9 h	–
4	Specific gravity	3.15	2.98	2.2

Table 2 Chemical analysis of GGBS and POFA

Binder	Cao	Sio_2	Al_2o_3	Mgo	Mno	Tio_2	K_2o	N_2o	So_3	P_2o_5	Fe_2o_3	CI	LoI
GGBS	33.77	33.77	13.24	8.46	0.05	0.58	0.37	0.27	<0.1	<0.1	0.65	<0.1	<0.1
POFA	4.35	63.4	5.51	3.78	0.16	0.34	6.35	0.15	0.93	3.75	4.2	0.46	6.19

Table 3 Properties of aggregates

Fine aggregates	POS	Coarse aggregates
Silt content—0.25% Fineness modulus = 2.2 Bulking of sand –23% Bulk density—1625 kg/m^3 Specific gravity—2.66	Specific gravity—2.2 Bulk density—966 kg/m^3 Surface area—980 m^2/kg	Specific gravity −2.63 Bulk density—1.54 gm/cc Water absorption—0.53%

2 Materials and Material Properties

The POS Concrete was obtained by mixing different combinations of cement, GGBS, POFA, Fine aggregates, Coarse aggregates, and POS. The properties of the materials are shown in Tables 1, 2 and 3. The formation of POS and POFA are Explained in Fig. 1. The binding materials a aggregates are shown in Figs. 2 and 3.

3 Mix Proportions

As per IS: 10262-2009 and IS: 456-2000 codes and using all the above material properties M30 grade lightweight fiber reinforced concrete mix is advanced for different replacements. In this total 12—different mixes are designed with up to 50% replacement of Binding materials and coarse aggregates. All 12-mixes with different percentage replacements are shown in Table 4. All these 12 mixes are designed as per Indian standards and presented in Table 4.
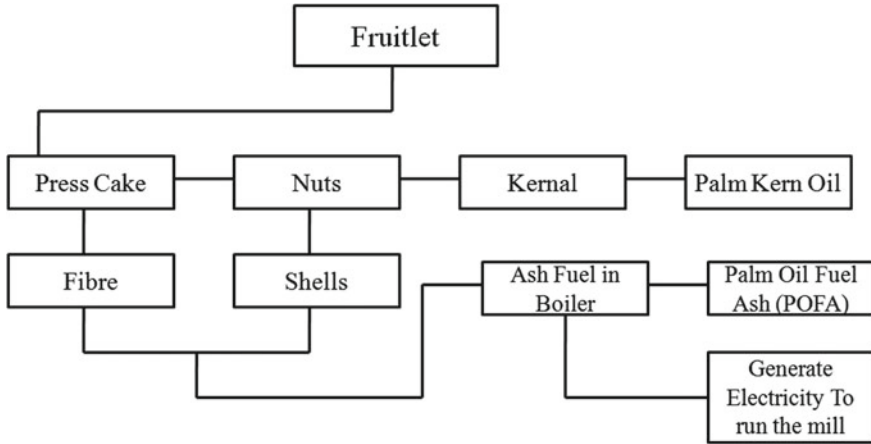
Fig. 1 Formation of POS and POFA

Cement   *GGBS*   *POFA*

Fig. 2 Binding materials

Fine aggregates   Coarse Aggregates   Palm oil Shells

Fig. 3 Aggregates

4 Experimental Investigation

The strength studies like compressive, split tensile, bending strengths, and Youngs modulus of the all 12-mixes are considered as per the Indian standards and those are existing in Table 5.

Table 4 Percentages of material replacements

MIX	Percentage	Proportions (C: GGBS/POFA: F.A: C. A: POS)
N1	Conventional Mix	1:0: 2.03:3.52:0
N2	Conventional + G F	1:0: 2.03:3.52:0
G1	10%—GGBS and 10%—POS	1:0.11: 1.82: 2.84:0.14
G2	20%—GGBS and 20%—POS	1:0.25: 2.04: 2.83:0.31
G3	30%—GGBS and 30%—POS	1:0.43: 2.33: 2.83:0.53
G4	40%—GGBS and 40%—POS	1:0.67: 2.71: 2.82:0.83
G5	50%—GGBS and 50%—POS	1:1: 3.25: 2.82:1.24
P1	10%—POFA and 10%—POS	1:0.11: 1.81: 2.82:0.14
P2	20%—POFA and 20%—POS	1:0.25: 2.01: 2.8:0.31
P3	30%—POFA and 30%—POS	1:0.43: 2.28: 2.77:0.52
P4	40%—POFA and 40%—POS	1:0.67: 2.64: 2.75:0.81
P5	50%—POFA and 50%—POS	1:1: 3.1: 2.72:1.20

Table 5 Strength characteristics of the mixes

MIX ID	Compressive strength (MPa)	Split tensile strength (MPa)	Bending strength (MPa)	Modulus of elasticity (Gpa)
N1	42.24	3.8205	2.7607	32.49615
N2	43.56	3.962	3.0513	33.00
G1	31.24	3.113	2.4701	27.94638
G2	35.2	2.264	2.3248	29.66479
G3	30.36	2.547	2.1795	27.54995
G4	24.64	1.981	1.3077	24.81935
G5	18.04	1.415	1.453	21.23676
P1	30.36	2.83	1.8889	27.54995
P2	31.24	2.264	0.7265	27.94638
P3	23.32	1.8395	0.4359	24.14539
P4	17.16	1.132	0.2906	20.71232
P5	14.08	0.9905	0.26154	18.76166

For durability studies standard sizes of cubes, 150 mm × 150 mm × 150 mm is equipped. The specimens are cast as per the standard procedure and leave hardening. After 24-h the specimen is Demould and reserved for normal water curing. After 28 days of water curing, the specimens are taken out furthermore cleaned with running water, and kept for 2-h air drying. Before placing specimens for solutions curing the specimen's weights is taken. After that, the specimens are placed in Magnesium sulfate, Sodium chloride, and Sulphuric acid solutions shown in Fig. 4. After 28, 56, and 90 days of curing period in all 3—chemical solutions, and the specimens are
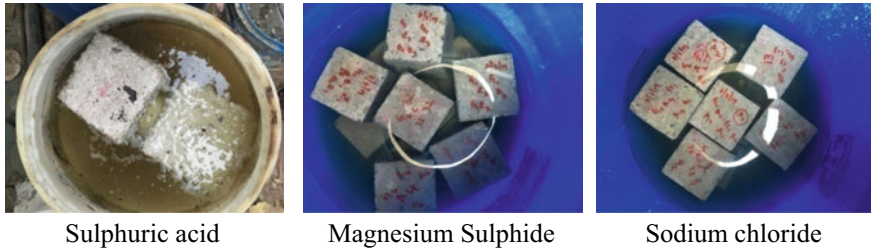
Sulphuric acid   Magnesium Sulphide   Sodium chloride

Fig. 4 All 3—chemical curing's

Table 6 Details of chemical attacks

S. No	Acid attack	Sulfide attack	Chloride attack
Chemical	Sulphuric acid (H_2So_4)	Magnesium sulfate ($MgSo_4$)	Sodium chloride (NaCl)
Percentage	3	5	3.5
pH Value	8	2	7

taken out and cleaned with running water, after that kept for air drying. After air-drying, the weight of the specimens is recorded and tested for compressive strength [11, 12]. For each curing period on a standard of 3-cubes are experienced. Details of all attacks are presented in Table 6.

After all the experiments the results are initiated. From the above chemical attacks, the compressive strength of the specimens for individual attacks is calculated.

4.1 Weight Variance

All specimens (N1 to P5) cured in H_2So_4, $MgSo_4$ and NaCl are weighed before curing and also weighed before testing for 28, 56, and 90 Days. Both the weights are compared for weight variance in all curing ages. The clear statistics represented as follows. The Acid curing is shown clearly in Fig. 5. Renaming 2—attacks, there is no physical change in the specimens.

- Specimens which are cured in H_2So_4, they are losing their weight in all the 12-mixes.
- It is observed in all the acid curing ages, specimens that are taken out, the coarse aggregates, and POS are exposing to the environment.
- Binding material is replaced with POFA showing less weight loss compared to the GGBS replacement in all the curing ages.

| During Curing | After curing | After washing |

Fig. 5 Process of acid curing

- The weight loss is a minimum of 4.39% and a maximum of 20.28% in GGBS replacement. Whereas POFA replacement weight loss is a minimum of 0.1% and a maximum of 7.91%.
- It is observed that specimens that are cured in the MgSo4 and NaCl solution are gaining their weight after curing.
- A maximum of 5.2% weight is gained in GGBS replacement and a maximum of 5.99% weight is gained in POFA replacement.
- In GGBS specimens the weight variance is a maximum of 6.197% and POFA specimens 5.96%.
- All the 3- attacks weight variances are shown in Figs. 6, 7, and 8.
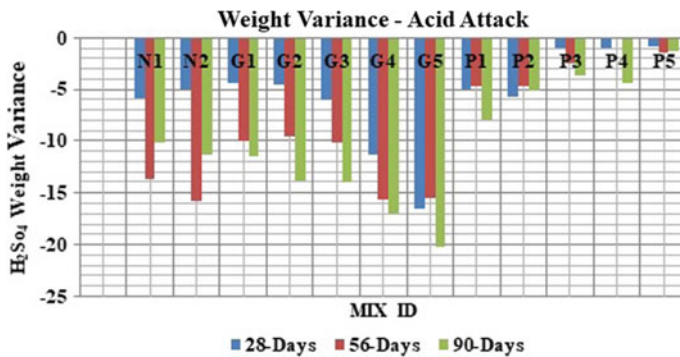
Fig. 6 Acid attack weight variance
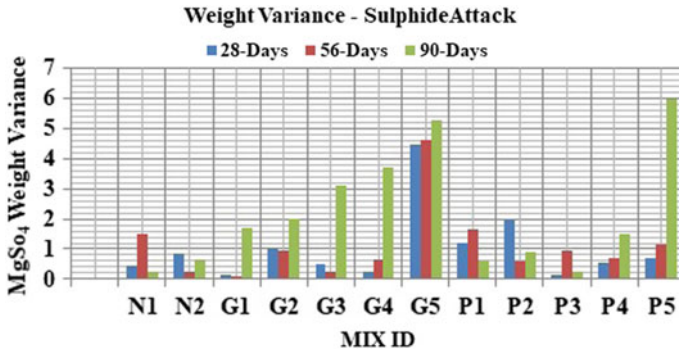
Fig. 7 Sulphide attack weight variance
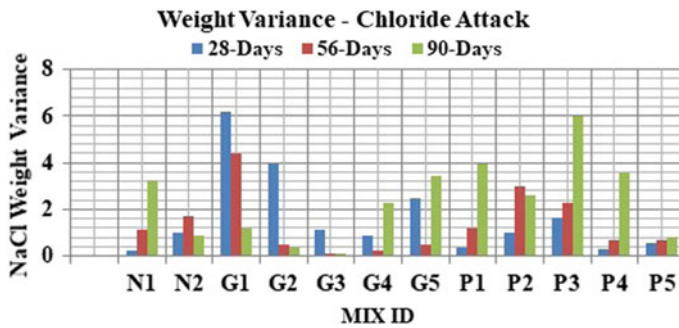
Fig. 8 Chloride attack weight variance

4.2 *Effect of Compressive Strength*

The compressive strengths are calculated for different chemical attacks (H_2So_4, $MgSo_4$, and NaCl) for different curing periods under the Compressive Testing Machine (CTM). The effect of all chemical attacks is explained in Figs. 9, 10, and 11, the X-Axis is representing the Mix Id and the Y-axis is Represented the Compressive strength of all 12-Mixes.

5 Conclusion

From above all durability studies for 12—concrete mixes the following conclusions are drawn:

- It is strongly recommended that POS and POFA can be used as a construction building material to produce the light weight concrete.
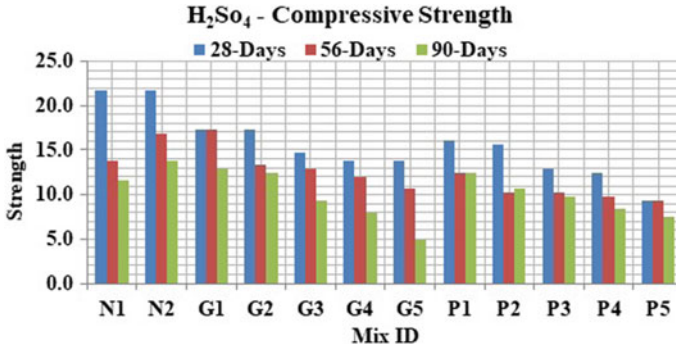
Fig. 9 Acid attack compressive strength

Fig. 10 Sulphide attack compressive strength

Fig. 11 Chloride attack compressive strength

- To achieve the LWFRC up to 30% of POS replacement in coarse aggregates is suggested.
- Surge the percentage of replacement materials (POS, GGBS, and POFA) the density and strength are decreases.
- In Acid Attack the density is declining and for Sulphide and magnesium attacks swelling the density with curing age and proportion of POS.
- Nearly in all the chemical attacks the compressive strength of concrete is fewer with likening to the normal water curing.
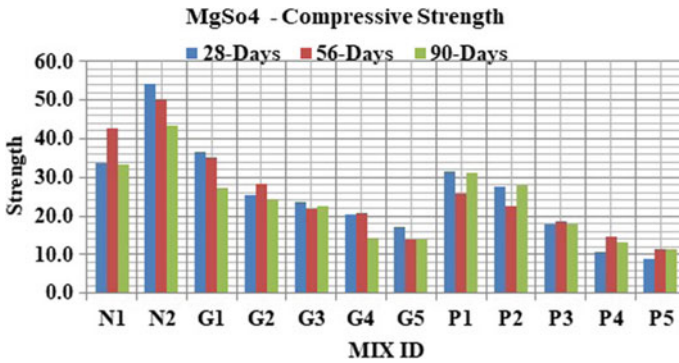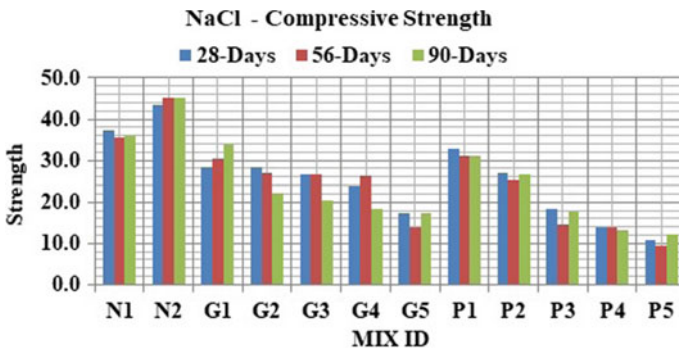- The LWFRC is suggested for structural elements construction but up to 30% of POS replacement is permitted.

References

1. Chia et al (2017) Durability characteristics of polyvinyl alcohol–treated oil palm shell concrete. J Mater Civ Eng 29(10):1–9
2. Almograbi (2010) Durability study of lightweight concrete material made from date palm seeds (DPS). High-Perform Struct Mater 112:69–75
3. Teo et al (2010) Durability of lightweight OPS concrete under different curing conditions. Mater Struct 43:1–13
4. Ming et al (2014) Effects of heat treatment on oil palm shell coarse aggregates for high strength lightweight concrete. Mater Des 54:702–707
5. Snehal K, Das BB, Kumar S (2020) Influence of integration of phase change materials on hydration and microstructure properties of nano silica admixed cementitious mortar. J Mater Civil Eng ASCE 32(6)
6. Snehal K, Das BB, Akanksha M (2020) Early age, hydration, mechanical and microstructure properties of nano-silica blended cementitious composites. Constr Build Mater, Elsevier 233
7. Das BB, Pandey SP (2011) Studies on influence of fineness of fly ash on the carbonation and electrical conductivity of concrete. J Mater Civ Eng ASCE 23(9):1365–1368
8. Ming et al (2014) Effects of oil palm shell coarse aggregate species on high strength lightweight concrete. Scient World J 1–22
9. Ming et al (2018) Enhancement of durability properties and drying shrinkage of heat-treated oil palm shell species high-strength lightweight concrete. Nanosci Nanotechnol 2(1):1–11
10. Khairunisa et al (2015) Acid resistance of oil palm shell lightweight aggregate concrete containing palm oil fuel ash. Appl Mech Mater 754–755:326–330
11. Sahoo S, Das BB, Mustakim S (2017) Acid, alkali and chloride resistance of concrete composed of low carbonated fly ash. J Mater Civil Eng ASCE 29(3)
12. Sahoo S, Das BB, Rath AK, Kar BB (2015) Acid, alkali and chloride resistance of high volume fly ash concrete. Ind J Sci Technol 8(19):72266

The Effects of Ground Granulated Blast-Furnace Slag Blending with Fly Ash Based Self Compacting Geo-polymer Concrete on the Workability and Strength Properties at Ambient Curing

Subodha Kumar Rautaray, Dillip Kumar Bera, and A. K. Rath

1 Introduction

Next to automobile, the second largest CO_2 is generated due to production of Portland cement which causes environmental pollutions to the maximum extent. The cement industries are mostly responsible for about 6% of total CO_2 emissions to the atmosphere and so to say as the major promoter of global warming. Besides, a large quantity of energy is consumed for its production next to steel and aluminum industry. Approximately 1.89 billion tons of cement is being produced worldwide annually against the requirement of about 2.60 billion ton per year. Also the lime stone which is the main source of its production, may come to an end after 25–30 years. Fly ash (FA), a waste product from Thermal Industries is simply dumped on the earth which occupies large valuable space and also causes air pollution. An alternative binder like "Geopolymer", a new group of materials using fly ash was developed by Joseph Davidovits in St. Quentin, France, in the 1970s. Fly ash based geo-polymers are part in the Geo-polymer family and playing major role since the 1990s. Fly ash based geo-polymer is one of the best promising alternative to challenge the Portland cement concretes [1–3]. Furthermore, the fly ash based geopolymer mortar needs heat curing for the achievement of its desired properties by limiting its practical application upto ambient curing conditions. Past experimental studies have inferred that for the accomplishment of application of these fly ash based geopolymers, without any heat curing, requires the inclusion of ground granulated blast furnace slag as

S. K. Rautaray · D. K. Bera (✉) · A. K. Rath
School of Civil Engineering, KIIT Deemed To Be University, Campus-3, Bhubaneswar 751024, India
e-mail: dberafce@kiit.ac.in

A. K. Rath
e-mail: akrathfce@kiit.ac.in

a partial substitute to fly ash in geopolymer mortars, cured in ambient conditions [4–7], wherein finally it was concluded that it is very much possible for achieving the required characteristic properties and also it is analogous to ordinary portland cement.

Self compacting concrete is the modern day's requirement for quick operation resulting in saving time and avoiding vibration for its compaction. Self-compacting geopolymer concrete (SCGC) is again a challenging concept in concrete technology that not only allows concrete to be placed in complex structural formwork, but also uses industrial waste to produce high-value concrete, completely eliminating the use of conventional Portland cement (OPC) [8]. Increasing the molarity of NaOH increases the compressive strength of SCGC to 12 M. Beyond 12 M the strength decreases. But fresh properties are inversely proportional to the increase in molarity [9]. The liquid part of the concrete i.e. the alkaline solution, super plasticizer and extra water should be mixed properly before being added to the dry mix for getting better workability of SCGC.

2 Experimental Details

2.1 Materials Used

Fly ash: Fine spherical dry fly ash particles were collected at NTPC, Kaniha, Odisha, India. Details of physical and chemical properties are shown in Table 1.

The class F type fly ash is used in this research work in accordance to the requirement of ASTM C618-08. The average size of fly-ash was 86.82% passing 45μ sieve. A low loss on ignition (LOI) value represents a high value of pozzolanic behavior and a lower water requirement.

GGBFS: Slag is a bi-product of iron and steel making industry. It is a non metallic material that mainly contains silicate, calcium, aluminate and various bases. It is obtained in the form of flakes which is ground to get a fine powder of having a fineness of 400–450 m^2/kg and is called as GGBFS (Ground Granulated Blast Furnace Slag). In our present experiment, the slag was obtained from JSPL, Kalinga nagar in the Jajpur region of Odisha and ground it in the laboratory of the KIIT Civil Engineering to get GGBFS.

Super plasticizers: Master Glenium Sky 8233 of BASF brand super plasticizer has been used to enhance the workability of self compacting geo-polymer concrete.

Aggregates: Coarse aggregate: Hard granitecrushed stone with fraction of 20–10 mm 50% and 10–4.75 mm 50% was taken. Fine aggregate: It was in confirming to Zone-III grading with respect to IS: 383-1970. The physical properties of aggregates are shown in Table 2.

Alkali activator solutions: An alkali-activated liquid is formed by mixing sodium hydroxide (NaOH) of various molarities with a sodium silicate solution (Na_2SiO_3).

Table 1 Chemical and physical properties of fly ash and GGBFS

| Materials | Chemical composition (%) | | | | | | | | | | Physical properties | |
Oxides	CaO	SiO₂	Al₂O₃	Fe₂O₃	SO₃	Na₂O	K₂O	MgO	P₂O₃	LOI (85 °C)	Specific gravity	Blain area (m²/kg)
Cement (PPC)	43.5	31.3	7.2	2.8	2.5	0.45	0.35	1.35	–	1.5	3.15	325
Fly ash	1.91	57.06	26.94	5.66	0.04	0.06	1.09	0.72	0.87	2.89	2.24	350
GGBFS	35.40	31.90	19.32	0.36	0.23	0.80	0.35	8.41	–	–	2.90	400

Table 2 Physical properties of aggregates

Property	Specific gravity	Fineness modulus	Water absorption (%)	Unit weight (kg/m^3)
Fine aggregates	2.55	2.23	0.6	1676
Coarse aggregates	2.63	6.58	0.8	1622

Ratio of NaOH to Na$_2$SiO$_3$ (NH/NS) solution is taken in this paper as 1:2.5 and the concentration of NaOH is varied in the range of 8 M (molarity), 10 M, 12 M and 14 M.

Sodium hydroxide (NaOH) solution: Flakes of sodium hydroxide (NaOH) of 97%-98% purity was purchased in bulk quantity in bags of 50 kg each from local supplier of M/S Grasim Industries Ltd. The NaOH solution was made by dissolving flakes of NaOH in water 24 h prior to the casting of theself compacting Geo-polymer concrete. The solid mass of NaOH depends on the concentration of the solution.

Sodium silicate (Na$_2$SiO$_3$) solution: Sodium silicate liquid was purchased from same local supplier of M/S Grasim Industries Ltd. (Na$_2$O = 13.7%, SiO$_2$ = 29.4%, and water = 55.9% by mass) and whose bulk density was 1.5 kg/l.

Cement: In this study, Portland pozzolana cement (PPC)-43 grade with Blaine specific surface 325 m^2/kg complying with (IS 1489-1991) Part-I (fly ash based) was used. The chemical and physical compositions of cement are mentioned in Table 1.

2.2 Methodology

2.2.1 Mix Design

For M-30 grade SCC, various trial mixes have been studied for both flowablility and mechanical properties by adding SP varying from 0.5 to 2% as shown in Table 3 and it was found that the mix proportion of 1:1.78:2.36 shows good results. Hence, the same ratio has been chosen for the present experiment for SCGC. Basing on this proportion fly ash has been taken as 420 kg/m^3. Some of the authors have taken alkali solution by fly ash ratio as 0.5 [9–14] and others have taken this ratio as 0.45 [8, 15–22]. For economic point of view, we have chosenalkaline solution by fly ash

Table 3 SCC mix proportion

SCC mix proportion (Kg/m^3) of normal casting				
Sample	Cement	Fine aggregate	Coarse aggregate	SP
PC0.5	420	747.6	991.2	2.1
PC1	420	747.6	991.2	4.2
PC1.5	420	747.6	991.2	6.3
PC2	420	747.6	991.2	8.4

Table 4 SCGC mix proportions

SCGC mix proportion in kg/m^3

Sample	Fly ash	GGBFS	NaOH	Na$_2$SiO$_3$	FA	CA	SP
M 2	420	–	54 (12 M)	135	747.6	991.2	8.4
M 4	420	–	54 (12 M)	135	747.6	991.2	16.8
M 6	420	–	54 (12 M)	135	747.6	991.2	25.2
M 7	420	–	54 (12 M)	135	747.6	991.2	29.4
M 8	420	–	54 (12 M)	135	747.6	991.2	33.6
SCGC 8M	420	–	54 (8 M)	135	747.6	991.2	25.2
SCGC 10M	420	–	54 (10 M)	135	747.6	991.2	25.2
SCGC 12M	420	–	54 (12 M)	135	747.6	991.2	25.2
SCGC 14M	420	–	54 (14 M)	135	747.6	991.2	25.2
SCGC 12M-10%	378	42	54 (12 M)	135	747.6	991.2	25.2
SCGC 12M-20%	336	84	54 (12 M)	135	747.6	991.2	25.2
SCGC 12M-30%	294	126	54 (12 M)	135	747.6	991.2	25.2
SCGC 12M-40%	252	168	54 (12 M)	135	747.6	991.2	25.2
SCGC 12M-50%	210	210	54 (12 M)	135	747.6	991.2	25.2

ratio as 0.45. Similarly, most of the authors have taken sodium silicate by sodium hydroxide ratio as 2.5 [8–15, 17–22]. Here the same ratio of 2.5 has been taken.

In this work superplasticizer (SP) has been used and varied from 2 to 8% by weight of FA for making self compacting concrete [27, 29] as mentioned in Table 3. It is seen that at 6% of SP the flowability is satisfactory in accordance with EFNARC values and taken the same percentage for further studies. Similarly effect of variation of molarity of NaOH has been studied from 8 to 14 M. It has been seen that optimum strength is achieved at 12 M and taken the same molarity for further studies with variation 10–50% of GGBFS [20, 22, 24–26], details has shown in Table 4. Almost all authors have taken extra water percentage as 12 for flowability. The same 12% have been taken for better flowability [20, 27–26].

2.2.2   Mix Procedure

For self compacting concrete mix design, the coarse aggregate selected was of two types 50% of 10–20 mm and 50 % of less than 10 mm. In the mixer the coarse aggregates were spread well of desired quantity. Then fine aggregates followed by pozzolonaic materials (fly ash and GGBFS) were mixed. These materials were mixed in a dry state. Required quantity of geo-polymeric solution (Sodium hydroxide and Sodium silicate solution) was weighed and the required percentage of the Super plasticizers and extra water was added to it and stirred well. One day before the casting the sodium hydroxide solution was prepared at lab. After getting a proper dry mix of the constituent materials of the concrete which can be confirmed by seeing a

uniform colour of the mixture, solution of water and super plasticizer prepared was added. Then the mixture machine was rotated for about 3 min to get a homogeneous mix.

Self compacting properties have been studied at lab for workability properties with the help of slump flow, L-box and V-funnel tests methodologies to satisfy the filling, passing and segregation resistance properties of fresh state concrete. These tests have been carried out at fresh state within a period of 30 min after mixing. The mix was then properly mixed after the fresh test process was over. The uniform mix was then placed into the moulds and was left for 36 hours for the final setting time. After that these were de-moulded and left for 7, 28 and 56 days respectively in ambient curing.

2.2.3 Casting of Specimen

Required amount of prepared NaOH and Na_2SiO_3 solutions are mixed prior to the casting.The cube moulds were well coated with lubricants on their inner surface. The required amount of pozzolonaic material (Fly ash and GGBFS), fine and coarse aggregates are then taken with proper weight with the help of weighing machine. The materials were first mixed thoroughly in dry condition. Alkali solutions of different molarities i.e. 8 M, 10 M, 12 M and 14 M and 6% super plasticizer and 12% extra water were mixed thoroughly at a container to obtain a good consistent solution. Then the solution was added to the dry mix and mixed in a mixer for about three minutes until a homogeneous concrete was obtained. The fresh state of this homogeneous mix was then taken for slump flow, L-box and V-funnel tests and measurement had been taken to study the degree of workability of mix as per the EFNARC specification and guidelines [29]. Concrete was then poured into the $150 \times 150 \times 150$ mm cube, 100 mm diameter and 300 mm height cylinder and $100 \times 100 \times 500$ mm prism moulds for studying compressive, split tensile and flexural strengths respectively. The moulds were safely demoulded after 36 hours and were kept in a dry place for ambient curing [31].

2.2.4 Curing

Curing was carried out at room temperature, that is, at $25 \pm 20°$ C and 50% relative humidity. After 36 h, the samples were taken out of the moulds and kept at this ambient conditions for the desired days i.e. 7 days, 28 days and 56 days of strength tests for different mixes in accordance with the IS: 456-2009.

2.2.5　Compressive Strength of Geo-polymer Concrete

The average compressive, flexural and split tensile strength tests were calculated out of three samples of a mix at 7, 28 and 56 days in ambient curing. These results of SCC and SCGC for various Molarities are shown in Figs. 4, 5 and 6.

3　Results and Discussion

3.1　Fresh Properties: Workability

The fresh state of mixes as mentioned in Tables 3 and 4 were undergone for slump flow, L-box and V-funnel tests as per the EFNARC specification and guidelines. The results of slump flow, L-box and V-funnel tests of the cement concrete and geo-polymer concrete mixes have been shown in the Figs. 1, 2 and 3 including EFNARC limits [29] respectively. The results are under EFNARC limits are nominated as self compacting concrete. Therefore M6, M7 and M8 are to be considered as SCC and M6-10 s, M6-20S and M6-30S are also be considered as self compacting geo-polymer concrete as all the three test values are within the EFNARC limits. The next phase of test is to make the optimum mix which should have maximum strength values.

Out of four mixes PC-0.5 i.e. 0.5% addition of SP mix is not coming in the range of EFNARC limits as shown in Figs. 1, 2 and 3 M6-10S, so except PC-0.5 mix others are PC-1.0, PC-1.5 and PC-2.0 is coming under self compacting concrete as per EFNARC guidelines. Similarly for geo-polymer concrete M2 (2% addition of SP) and M4 (4% addition of SP) are not coming under the limits of EFNARC but at 6%, 7% and 8% addition of SP samples are in the limits of EFNARC. Therefore 6% addition of SP is taken as the optimum dosage of SP in geo-polymer concrete in the same way at 1% addition of SP (PC-1.0) in cement concrete samples taken as

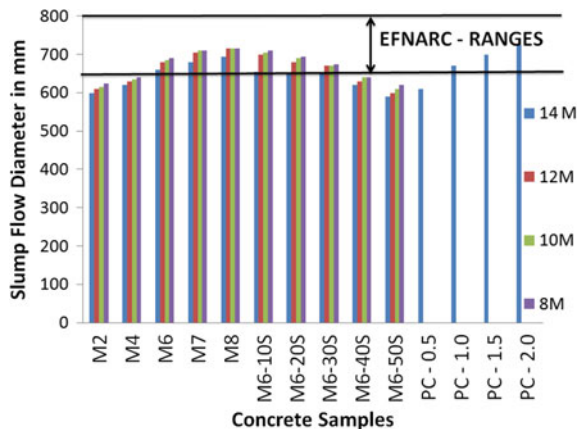Fig. 1 Slump flow test values of SCC and SCGC

Fig. 2 L-box test values of
SCC and SCGC
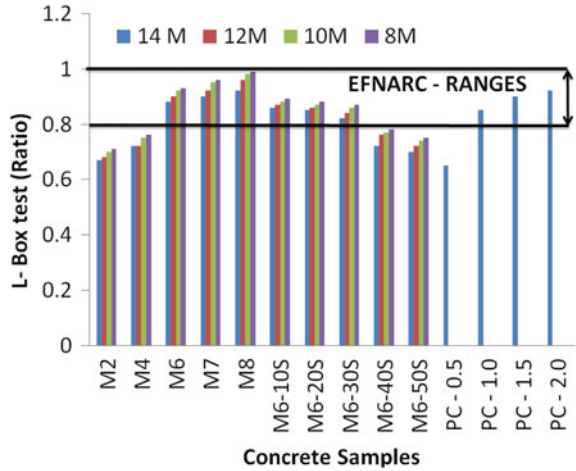
Fig. 3 V-funnel test values
of SCC and SCGC
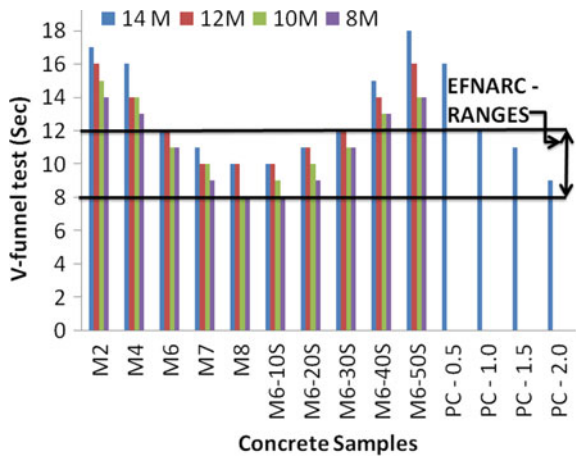
optimum dosage of SP for further studies. Later part, the geo-polymer concrete with
6% SP (M6) with partial addition of GGBFS as 10, 20, 30, 40 and 50% by replacing
FA have been studied for fresh and strength properties. The fresh properties of the
same samples like: M6-10S, M6-20S, M6-30S, M6-40S and M6-50S results are also
shown in Figs. 1, 2 and 3. It is seen that M6-10S, M6-20S and M6-30S mixes are
coming under the EFNARC limits so these mixes are called as self compacting geo-
polymer concrete. Therefore M6-40S and M6-50S specimens are not studying for
strength properties.

3.2 Compressive Strength Test

The specimens such as PC-0.5, M2, M4, M6-40S and M6-50S do not show the properties of self compacting in fresh state. Therefore the mechanical properties of those specimens have not been studied here. It is found out that, though the fresh properties of PC-2.0 are comparatively better than the specimen PC-1.0. Therefore, 1% of SP has been designed for SCC. Similarly, though the fresh properties of M7 and M8 are better than M6, therefore M6 has been taken for future studies with partial replacement of GGBFS. 6% of SP has been optimised both from the strength and economic point of view. The SCGC with replacement of FA with GGBFS has been designed with 6% SP for testing of mechanical properties. Likewise, it is also seen that the compressive strength is increased with the increase of GGBFS percentages. The best result for SCGC is achieved at M6-30S at 12 M in 7, 28 and 56 days with 6% SP.

3.3 Flexural and Split Tensile Strength

From the Figs. 4, 5 and 6 it can be seen that the maximum strength is achieved on 12 molar samples. Therefore, 12 M concentration of NaOH solution have been taken for further tests of flexural and split tensile strength. The results of flexural and split tensile strength are shown in Figs. 7 and 8 respectively. As seen from the results it is seen that, the development flexural and split tensile strength is identical to that of compressive strength. The increase in percentage of GGBFS increases both the flexural and split tensile strength. The maximum strength is occurred at 30% replacement of GGBFS (M6-30S) with respect to PC-1.0 (SCC at 1% SP) and other replacement of GGBFS and plain M6 values.
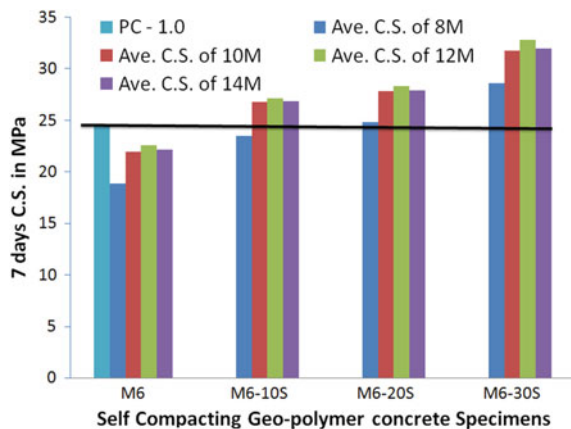

Fig. 4 Compressive strength of SCGC at 7d

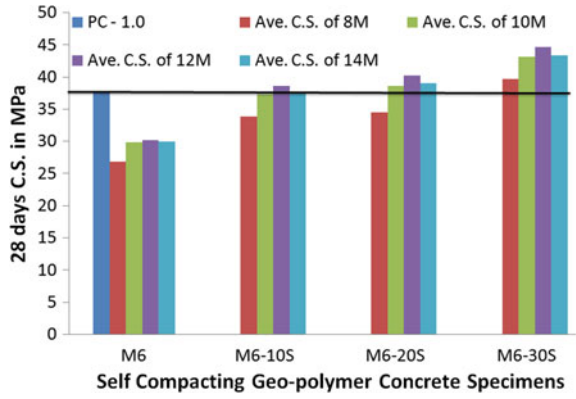**Fig. 5** Compressive strength of SCGC at 28d

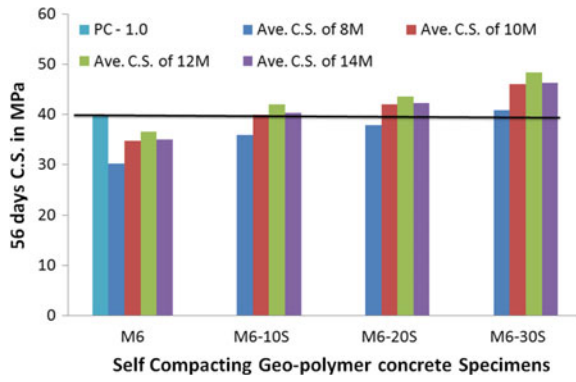**Fig. 6** Compressive strength of SCGC at 56d
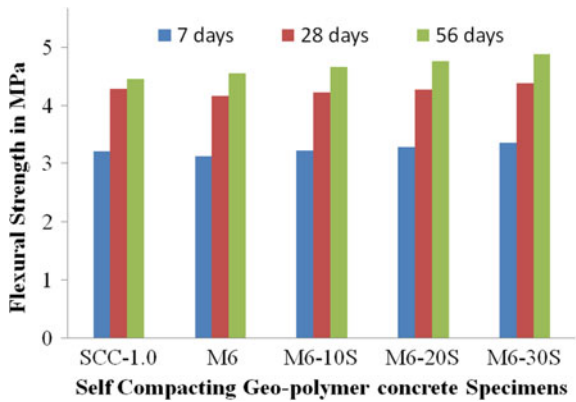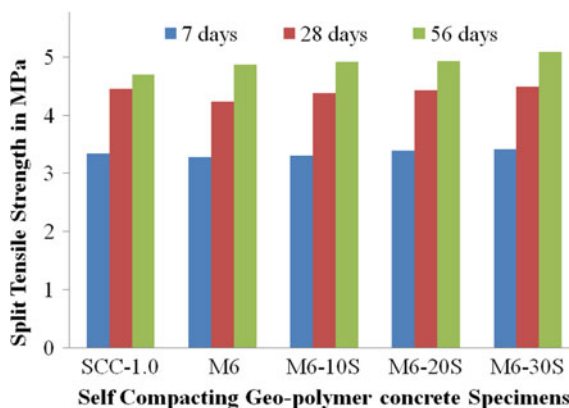

Fig. 7 Flexural strength of SCGC

Fig. 8 Split tensile strength of SCGC

4 Conclusions

This paper has tried to design a mix proportion by varying the concentration of NaOH (molarity from 8 to 14 M), dosage of SP percentages (0–8%) and GGBFS partial replacement percentages (10–50%) of self compacting geo-polymer concrete with respect to fresh and hardened properties of SCC. The following points are to be incurred from the studies; as molarity increases the compressive strength of SCGC is also increased but decreased the flowability of fresh SCGC. The increase in the percentage of SP helps to increase the flowability of SCGC. Increase in percentage of GGBFS decreases the flowability of the SCGC. Beyond 30% of GGBFS the specimen stops to show the character of self compacting. The increase in the percentage of GGBFS increases the compressive strength of SCGC. 12 M is the optimum concentration for getting better strength of SCGC. Beyond 12 M it tends to lose the charter of self compacting. Percentage increase of compressive strength of 12M—M6-30S specimen values is 18–21% increased with respect to SCC-1.0 (PC-1.0) at 28 and 56 days of maturation respectively.

References

1. Hardjito D, Wallah SE, Sumajouw DMJ, Rangan BV (2004) On the development of fly ash-based geo-polymer concrete. ACI Mater 467–472
2. Hardjito D, Wallah SE, Sumajouw DMJ, Rangan BV (2004) Factors influencing the compressive strength of fly ash-based geo-polymer slag geo-polymer concrete. Civil Eng Dimens 6(2):88–93
3. Al Bakria AMM, Kamarudin H, Hussain MB, Nizar IK, Zarina Y, Rafiza AR (2011) The effect of curing temperature on physical and chemical properties of geo-polymers. Phys Procedia 22:286–291
4. Prasanna KM, Tamboli S, Das BB (2019) Characterization of mechanical and microstructural properties of FA and GGBS-based geopolymer mortar cured in ambient condition. In: Select proceedings of ICRDSI 2019, Springer Publications Pte. Ltd., 2020, pp 751–768

5. Renjith R, Shivaprasad KN, Das BB (2018) Properties of heat cured bottom ash based geopolymer mortar admixed with fly ash of different fineness. In: Advances in concrete, structural and geotechnical engineering. Bloomsbury Publishing Plc, pp 603–607

6. Mustafa R, Shivaprasad KN, Das BB (2018) Effect of various additives on the properties of fly ash based geopolymer mortar. In: Select proceedings of ICSCBM 2018, Springer Nature Singapore Pte Ltd. 2019, pp 707–715

7. Prasanna KM, Theodose I, Shivaprasad KN, Das BB (2019) Fast setting steel fibre geopolymer mortar cured under ambient temperature. In: Select proceedings of ICRDSI 2019, Springer Publications Pte. Ltd., 2020, pp 769–787

8. Anuradha R, Thirumal RB, John PN (2014) Optimization of molarity on workable self-compacting geo-polymer concrete and strength study on SCGC by replacing fly ash with silica fume and GGBFS. Adv Stru Geot Eng 03(01):11–18

9. Memon FA, Nuruddin MdF, Demi S, Shafiq N (2011) Effect of curing conditionson strength of fly ash based self-compacting geo-polymer concrete. IJCESCAE 5(8):342–345

10. Nuruddin MF, Demi S, Ahmed MF, Shafiq N (2011) Effect of superplasticizer and NaOH molarity on workability, compressive strength and moisture properties and microstructure properties of self-compacting geo-polymer concrete. IJECEGGE 5(3):187–194

11. Memon FA, Nuruddin MdF, Demi S, Shafiq N (2012) Effect of super-plasticizer and extrawater on workability and compressive strength of self-compacting geo-polymer concrete. Res J Appl Sci Eng Technol 4(5):407–414

12. Demi S, Nuruddin MF, Shafiq N (2013) Effects of microstructure characteristics of interfacial-transition zone on the compressive strength of self-compacting geo-polymer concrete. Const Build Mater 41:91–98

13. Henigal AM, Sherif MA, Hassan HH (2017) Study on properties of self-compacting geo-polymer concrete. IOSR-JMCE 14(2):52–66

14. Jeyaseela J, Vishnuram BG (2015) Study on workability and durability characteristics of self-compacting geopolymer concrete composites. Int J Adv Tech Eng Sci 3(1):1246–1256

15. Memon FA, Shafiq N (2013) Effect of silica fume on the fresh and hardened properties of fly ash based self-compacting geo-polymer concrete. Int J Mine Metall Mat 20(2):1–9

16. Sashidhar C, Jawahar JG, Neelima C, Kumar DP (2016) Preliminary studies on self-compacting geo-polymer concrete using manufactured sand. Asian J Civil Eng (BHRC) 17(3):277–288

17. Ahmed MF, Nuruddin MF, Shafiq N (2011) Compressive strength and workability characteristics of low-calcium fly ash based self-compacting geo-polymer concrete. Int J Civil Env Eng 3(2):72–78

18. Ushaa TG, Anuradha R, Venkatasubramani GS (2015) Flexural behaviour of self-compacting geo-polymer concrete using GGBFS with various replacements of R-sand and M-sand. ARPN J Eng Apld Sci 10(14):6157–6166

19. Ushaa TG, Anuradha R, Subramani GSV (2015) Performance of Self- Compacting Geo-polymerconcrete containing different mineral admixtures. Ind J Eng Mat Sci 22:473–481

20. Memon FA, Nuruddin MF, Khan S, Shafiq N, Ayub T (2013) Effect of sodium hydroxide concentration on fresh properties and compressive strength of self-compacting geo-polymer concrete. J Eng Sci Technol 8(1):44–56

21. Shivaranjan NS, Kumar KSS, Babu DLV, Nagaraj VK (2016) A study on self-compacting geo-polymerconcrete with various water to geo-polymer solids ratios. IRJET 3(7):2064–2069

22. Demie S, Nuruddin MF, Ahmed MF, Safiq N (2011) Effects of curing temperature and super-plasticizer on workability and compressive strength of self-compacting geo-polymer concrete. IEEE 1884–1887

23. Abdollahnejad Z, Mastali M, Mastali M, Dalvand A (2017) Comparative study on of the effects of recycled glassfiber on drying shrinkage rate and mechanical properties of the self-compacting mortar and fly ash slag geo-polymer mortar. J Mat Civil Eng 29(8):04017076:1–11

24. Saifuddin KP, Purohit BM, Jamnu MA (2014) Effects of super plasticizer on self-compacting geo-polymer concrete using fly ash and ground granulated blast furnace slag. J Int Acad Res Formultidisciplinary 2(3):290–294

25. Manjunath R, Narasimhan MC (2018) An experimental investigation on self-compacting alkali activated slag concrete mixes. J Build Eng 17:1–12
26. Dhavamani A, Sundararajan R (2018) Effects of fly ash and blast furnace slag on the performance of self compacting geo-polymer concrete. IJCIET 9(1):953–964
27. Kamseu E, Ponzoni C, Tippayasam C, Taurino R, Chaysuwan D, Sglavo VM, Thavorniti P, Leonelli C (2016) Self-compacting geo-polymer concretes: effects of addition of aluminosilicate-rich fines. J Build Eng 5:211–221
28. Nuruddin MF, Demie S, Shafiq N (2011) Effect of mix composition on workability and compressive strength of self-compacting geo-polymer concrete. Canad J Civil Eng 38:1–8
29. EFNARC, Specification and guidelines for self-compacting concrete, February 2002
30. Reddy KM, Kumar GN (2017) Experimental study on self compacting geo-polymer concrete. IRJET 4(1):953–957
31. Nagaraj VK, Babu DLV (2018) Assessing the performance of molarity and alkaline activator ratio on engineering properties of self-compacting alkaline activated concrete at ambient temperature. J Build Eng 20:137–155

Analytical and Numerical Study of Fractured Isotropic and Composite Plates Under Mode-I Crack Extension

Danish Fayaz, S. N. Patel, and Rajesh Kumar

1 Introduction

Plates are widely used as a principal structural component in aerospace, mechanical, civil engineering, and marine applications and industrial design such as ships, aircraft, plants, bridges, machines, etc. [5]. The use of isotropic plates and orthotropic composite laminates play a significant role in the structures mentioned above based upon their application and usage as a structural component. A component in a structure may be prone to one, two, or more kinds of failure. Some of the common causes of failure are gross plastic deformation (yielding), deflection beyond a particular stage, elastic instability (buckling), large elastic deformation (jamming), tensile instability (necking), fatigue, fracture, creep, environmental degradation, impact, wear, etc. The fracture is often overlooked as a potential mode of failure at the expense of an overemphasis on strength. Hence, the knowledge of these kinds of failures is necessary to avoid a structural component's catastrophic failure. Engineered structures are exposed to a series of events involving loading, environment, and damage threats.

Fracture in a material is defined by the presence of a crack in it. Fracture mechanics is based on the assumption that there exists a crack in a component. In composite laminates, the fracture mainly depends upon lamination order and ply-orientation. A composite can fail due to fiber-breakage, debonding, delamination, formation of matrix microcracks. These defects may result from residual stresses due to the curing process, external impact damage, and environmental degradation or may develop in fabrication or service, causing structural degradation at stresses well below the strength levels expected for defect-free material. The composite materials exhibit superior properties; hence a crack in a composite structure may significantly lose strength and stiffness. As a result of this mechanism, the fracture characterization of composites structures acquires remarkable relevancy. A dangerous crack may be

D. Fayaz (✉) · S. N. Patel · R. Kumar
Department of Civil Engineering, Birla Institute of Technology and Science, Pilani, Pilani, India

nucleated and grown during the component′s service, causing catastrophic failure of the entire structure. Hence the study of flaws or cracks in a structural element is necessary to avoid sudden failure, causing loss of life and property.

Different researchers have dealt with the different theoretical approaches for the calculation of various parameters in cracked plates. A direct relation has been put forward between the Westergaard stress function for crack problems and a newly-introduced stress function for a line crack problem by Brussat and Westmann [3]. Buckling loads were estimated for an isotropic plate with different cracks (edge and central cracks) under uniaxial compressive load, biaxial load, and in-plane shear load Kumar and Paik [9]. Buckling analysis of different cracked plates under tension and compression using the Finite Element Method was studied by Brighenti [2]. A comparative study has been done by Hüsnü Dirikolu and Aktaş[7] to determine the SIF for carbon-epoxy composite plates with different inbuilt holes of different diameters. Experimental data, analytical approaches and FE fracture analysis tool (FRANC2DL) have been used to compare the SIF values. Another FE based software ANSYS has been used by Jabur [8] to calculate SIF for mode-I and mode-II central crack for a plate subjected to uniform tensile load with different crack lengths and orientations. Numerical analysis was compared with the theoretical results, which revealed a good agreement in-between. A general mixed boundary element approach based on displacement and traction integral equations for anisotropic media is presented and SIF were computed for crack opening displacement (COD) [6]. The effects of biaxial loading on the central cracked plate established by Meek and Ainsworth [11, 12] in the form of J-integral values have been computed. A boundary collocation method was presented for SIF computations for an internal crack in a finite anisotropic plate [15]. Analytical stress analyses are presented for orthotropic composite materials containing a through crack under uniaxial normal loads (mode I) [10]. 2D crack problems for homogenous, anisotropic, linearly elastic materials are solved by Azhdari et al. [1] using Riemann-Hilbert method. Anisotropic materials subjected to in-plane and anti-plane loadings were considered and the problem was formulated based on Lekhnitskii's complex variable approach [4]. Solutions for half-plane problems and elliptical crack cavity problems were also derived.

A systematic study has been conducted on an isotropic plate and a composite plate with a central crack subjected to uniform tension. Efforts have been made in three aspects: theoretical model development, computer simulation using finite element based software (ABAQUS/Standard), and analytical evaluation using Westergaard's approach [using Cauchy-Riemann conditions in the form of $Z(z) = \text{Re}(z) + i\,\text{Im}(z)$] and Irwin's approach. The finite element method is extensively used in the stress analysis of the isotropic steel plate and unidirectional laminates in this study using ABAQUS/Standard. The plate responses with a central crack under the effect tensile load is performed using ABAQUS/Standard and analytically. Near field crack-tip stresses are mainly taken into consideration. Different types of damages in the matrix, as well as in fibers, are also studied.

2 Theory

In this section, the analytical solution for the case of plane stress problem for cracked isotropic as well as the orthotropic/anisotropic plate has been presented. The case of uniform tensile pressure has also been taken into account in this section.

2.1 Isotropic Plate

For plane problems, the equilibrium equation can be written as [3]

$$\frac{\partial^4 \phi}{\partial x^4} + \frac{2\partial^4 \phi}{\partial x^2 \partial y^2} + \frac{\partial^4 \phi}{\partial y^4} \tag{1}$$

For Mode I problems, one way to solve the biharmonic equation is to express ϕ in terms of the complex function $Z_z(z)$ and can be expressed as

$$\phi = \mathrm{Re}\left(\overline{\overline{Z}}\right) + i\mathrm{Im}(\overline{Z}) \tag{2}$$

where $Z_z(z)$ is a complex-valued function of the complex variable $z = x + iy$, which satisfies Cauchy-Riemann conditions (Fig. 1).

The boundary conditions for a cracked body can be written as

For $-a < x < a$ and $y = 0$; $\sigma_{yy} = 0$ and $\tau_{xy} = 0$

For $z \to \infty$; $\sigma_{xx} = \sigma_{yy} = \sigma$

The stress function should satisfy the above boundary conditions and by putting $Z = \frac{\sigma z}{\sqrt{z^2 - a^2}}$ in Eq. (2), we get
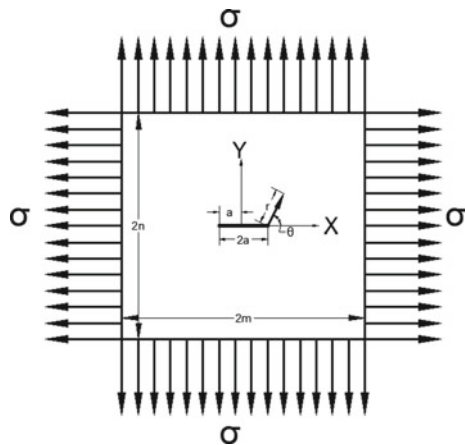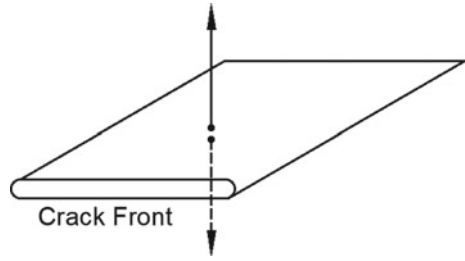
Fig. 1 Central crack in a plate

Fig. 2 Crack front (mode I)

Crack Front

$$\sigma_{xx} = \frac{K}{\sqrt{2\pi r}}\left[\cos\frac{\theta}{2}\left(1 - \sin\frac{\theta}{2}\sin\frac{3\theta}{2}\right)\right] \qquad (3)$$

$$\sigma_{yy} = \frac{K}{\sqrt{2\pi r}}\left[\cos\frac{\theta}{2}\left(1 + \sin\frac{\theta}{2}\sin\frac{3\theta}{2}\right)\right] \qquad (4)$$

In the above equations when $r \rightarrow 0$, the stress field has a singularity of $\sqrt{r}$ at the crack tip and $K = \sqrt{\sigma a}$ is the stress intensity factor (SIF).

3 Results and Discussion

This section starts with the problem description in which finite analytical model of the problem has been presented, followed by the convergence and validation study and the discussion on the results.

3.1 Problem Description

Two central cracked (isotropic and composite laminated) square plate $(2m \times 2n)$ with crack length $(2a)$ is considered for the analysis in the present investigation, as shown in Fig. 1. The crack is aligned along the principal X-axis as shown in Fig. 1 and the mode I crack front is shown in Fig. 2. The crack length is kept constant $(2a = 20\,\text{mm})$. The dimensions of the plate are taken as 200 mm × 200 mm and 400 mm × 400 mm. Isotropic plate used is made of steel of overall thickness 1 mm with the mechanical properties tabulated in Table 1. The composite plate consists of 3 layers of plies with the 0-degree orientation of fibers, and the thickness of each

Table 1 Mechanical properties of isotropic plate

Property	Magnitude
Longitudinal modulus (E_1)	200,000 MPa
In-plane Poisson ratio (μ_{12})	0.3

Table 2 Mechanical properties

Property	Orthotropic composite plate
Longitudinal modulus (E_1)	142,000 MPa
Longitudinal modulus (E_2)	7800 MPa
In-plane shear modulus ($G_{12} = G_{13}$)	4000 MPa
Out-of-plane shear modulus (G_{23})	2800 MPa
In-plane Poisson ratio (μ_{12})	0.34

Table 3 Hashin damage parameters

Property	Magnitude (MPa)
Longitudinal tensile strength	2606
Longitudinal compressive strength	1682
Transverse tensile strength	72.4
Transverse compressive strength	299
Longitudinal shear strength	116
Transverse shear strength	112

Table 4 Damage evolution parameters

Property	Magnitude (N/mm)
Longitudinal tensile fracture energy	146.7
Longitudinal compressive fracture energy	106.3
Transverse tensile fracture energy	2.33
Transverse compressive fracture energy	2.33

ply is 1 mm. The mechanical properties of isotropic and composite laminated plates are tabulated in Tables 1 and 2, respectively.

The damage parameters required for damage evolution law and damage stabilization during simulation for composite plate are tabulated in Tables 3, 4 and 5.

Table 5 Damage stablization parameters

Property	Magnitude
Viscosity coefficient in longitudinal tensile direction	1.4
Viscosity coefficient in longitudinal compressive direction	1.4
Viscosity coefficient in transverse tensile direction	1.4
Viscosity coefficient in transverse compressive direction	1.4
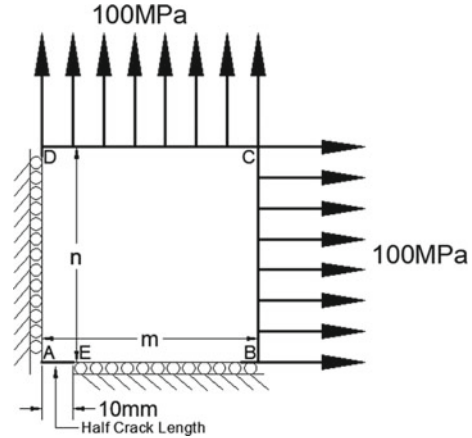
The finite element software ABAQUS/Standard is used to carry out the numerical simulation for determining the different parameters such as stress intensity factors and damage scale factors. Owing to the symmetry, the only one-quarter plate is modeled as shown in Fig. 3. S4R type mesh elements are used in ABAQUS/Standard to carry out the analysis. A uniform in-plane biaxial tensile pressure of $\sigma = 100$ MPa is applied on the plate as shown in Fig. 3. The boundary conditions of the quarter model are imposed by constraining the edge AD in the x-direction ($u = 0$) and edge EB in the y-direction ($v = 0$) to account for the planes of symmetry of the full model. Numerical results are presented for square plates of 200 × 200 mm and 400 × 400 mm (length × width).

3.2 Convergence and Validation Study

For the convergence and validation study, an isotropic steel plate is taken into consideration. The plate dimensions are taken as 200 mm × 200 mm along the length and width and the thickness is kept 1 mm. A crack of length 2a (20 mm), as shown in Fig. 3, is made at the center with negligible thickness. For the present case, a uniform in-plane tensile pressure of $\sigma = 100$ MPa is applied to sides BC and DC in x and y directions, respectively. Although the analytical solution can be implemented for an infinite plate configuration subjected to uniform in-plane tensile loading, the dimensions of the plate considered for analysis are restricted to 200 mm × 200 mm. The problem is solved using FEM software ABAQUS/Standard and the results are compared with the available results. The dimensional normalized stresses $\left(\sigma_{yy}/\sigma_{applied}\right)$ for the different mesh sizes are calculated, and the values are plotted with respect to distance from the crack tip along the crack axis as shown in Fig. 4. It is observed in Fig. 4 that almost all the mesh sizes are converged. The results from the present FEM analysis are also compared with the available results of Tada et al.
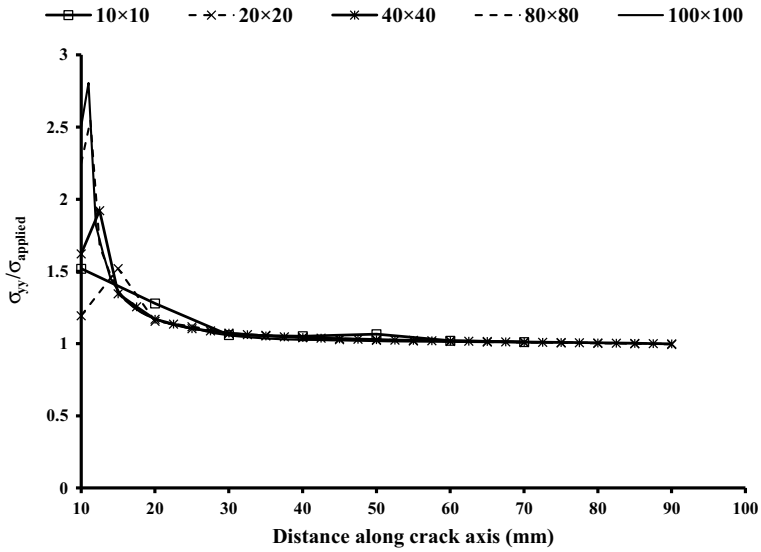
Fig. 4 Dimensionless normal stress by FEM

[13] and Westergaard [14]. It is found that the FEM results are matching well with the available results (Fig. 5).

After the convergence and validation study, the stress intensity factor for both the plates is studied using ABAQUS/standard. The mesh size for the present problem is
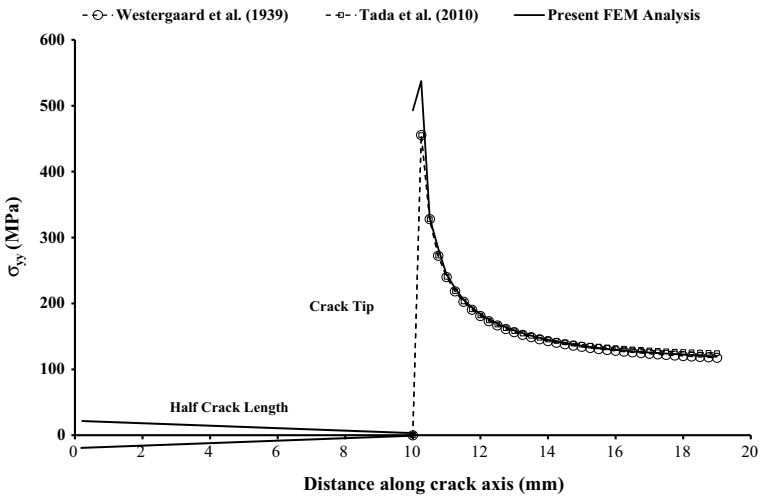

Fig. 5 Normal stress along the crack axis

taken as 100×100. The stress intensity factors and the damage factors are studied and discussed in the following sections.

3.3 Stress Intensity Factors

The stress intensity factor (K_I) at different locations along the crack axis is studied for the isotropic and composite plate for two different aspect ratios. It is found that the stress intensity is decreased while moving away from the crack tip along the crack axis. It is also found that the stresses while calculating analytically at the crack tip approaches to infinity because the stress field has a singularity of $\sqrt{r}$. The crack tip stress shows finite values (higher values of stresses) in finite element software. Figures 6, 7, 8 and 9 shows the stress intensity factors for both plates for different aspect ratios computed from the finite element software. The stress intensity factors are calculating at each node along the crack axis from stresses S_{11} and S_{22}. Figures 10 and 11 shows the normalized stress intensity factors $\left(K/K_I\right)$ for isotropic and composite plates with different aspect ratios. The values of K and K_I in all the figures are defined by $K = \sigma\sqrt{\pi a}$, where σ is the applied load and $K_I = \sigma_{xx}\sqrt{\pi a}$ or $K_I = \sigma_{yy}\sqrt{\pi a}$, where σ_{xx} and σ_{yy} are the stresses obtained in x and y directions respectively.
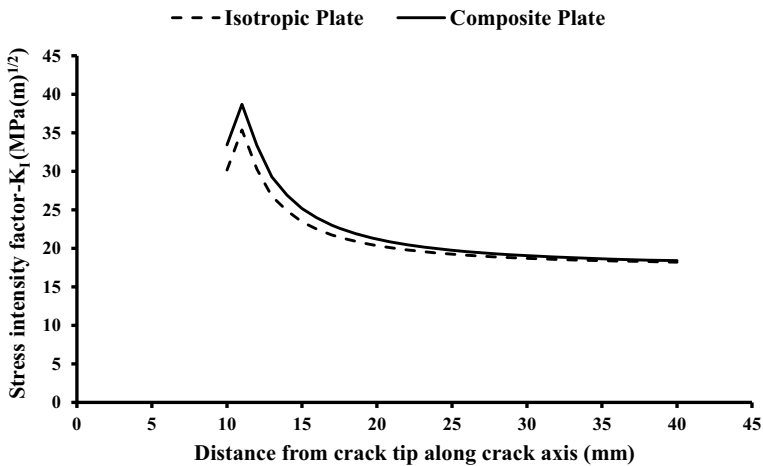
Fig. 6 SIF considering S_{11} stresses (200×200 mm)
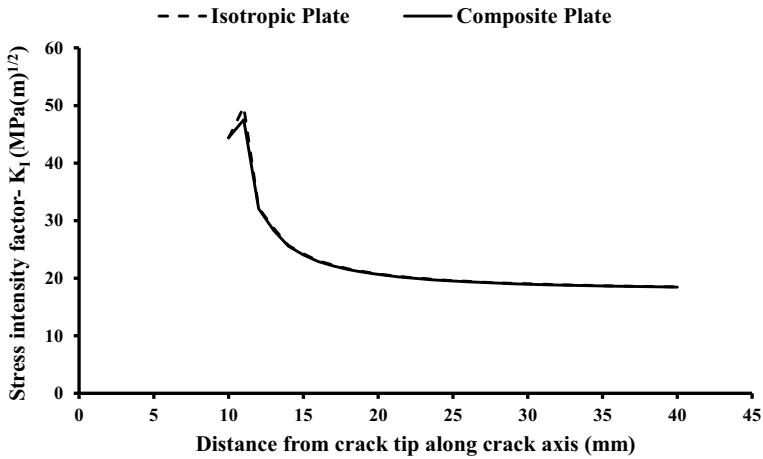
Fig. 7 SIF considering S_{22} stresses (200×200 mm)
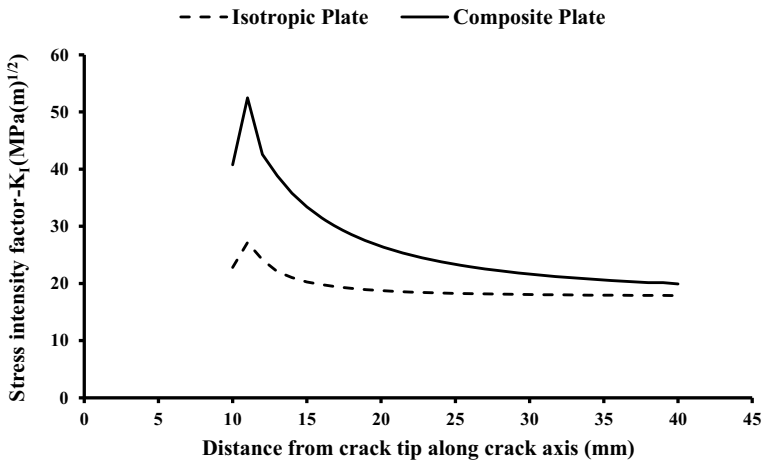
Fig. 8 SIF considering S_{11} stresses (400×400 mm)

3.4 Damaged Material Response

Different modes of damage like damage mode in fiber tension, in fiber compression, in matrix tension, and matrix compression for the composite plate are studied. Out of all the modes, it is found that the plate fails in matrix tension near the crack tip as shown in Fig. 12. The damage scale can vary from 0 (no damage) to 1 (complete damage). In other words, fracture will occur when damage scale factor equals to 1. A simple progressive damage model is applied to retrieve the degradation factors and to calculate the nominal stresses. Hashin damage failure initiation criteria is
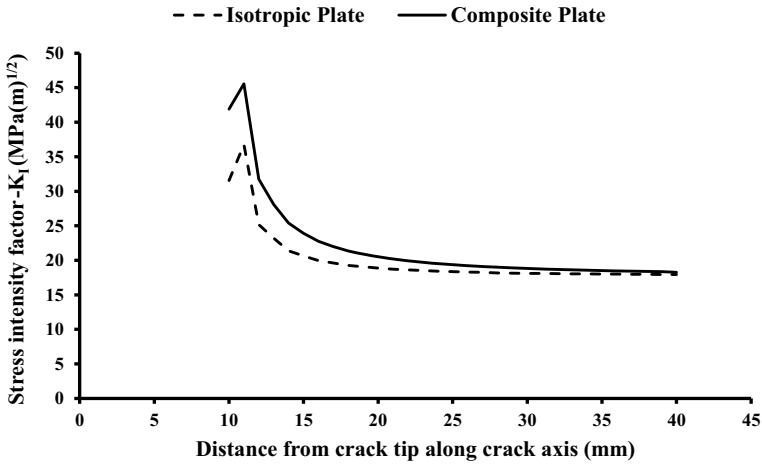
Fig. 9 SIF considering S_{22} stresses (400×400 mm)
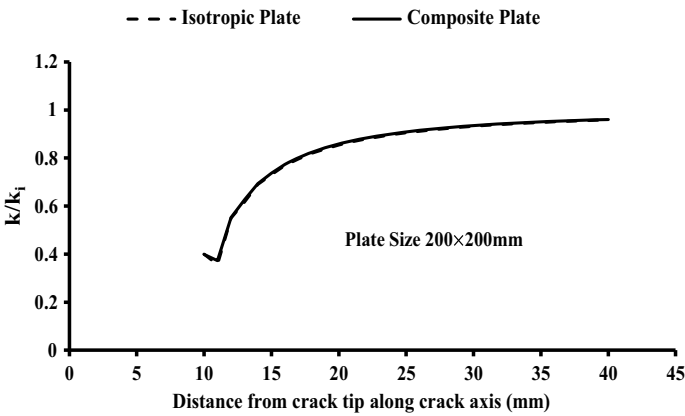
Fig. 10 K/K_I considering S_{22} stresses for K_I (200×200 mm)

used to calculate the damage scale of the composite plate. Damage initiation criteria tells about which of the available failure criteria is used to determine whether an element is failed or not. The different parameters for damage evolution and damage stabilization are defined in Tables 3, 4 and 5. The damage evolution is specified either in terms of fracture energy. Damage evolution law tells what happens to the element after failure. Figure 13 shows the full modeled plate with crack and damage scale.
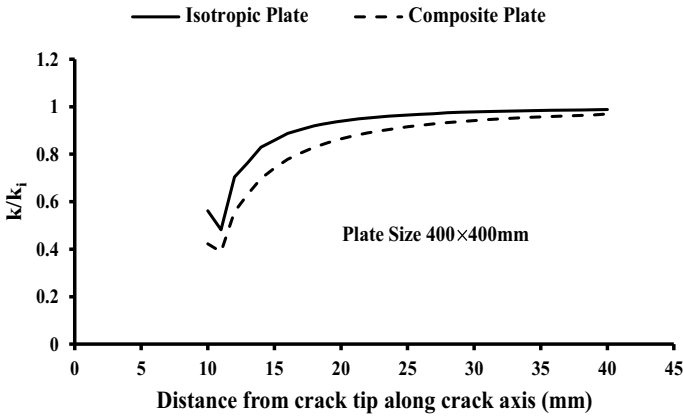
Fig. 11 K/KI considering S_{22} stresses for KI (400 × 400 mm)
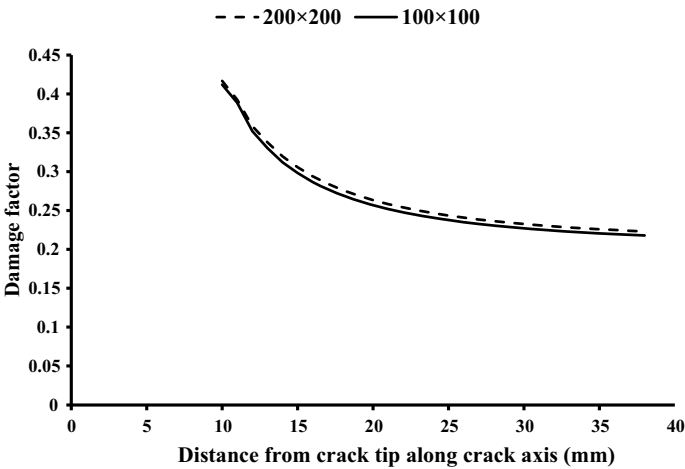
Fig. 12 Damage scale for composite plate

4 Conclusions

Based on the results obtained from analytical and numerical (FEA) efforts, the following conclusions have been reached:

1. The proposed analytical models can be used to provide predictions for anisotropic composite plates and an isotropic plate subjected to tensile load with a centre crack. These predictions include the normal stress and shear stress calculations at the different sections of the plate.

2. The crack tip stresses tends to become higher and the far field stresses are converging equivalent to the applied load.
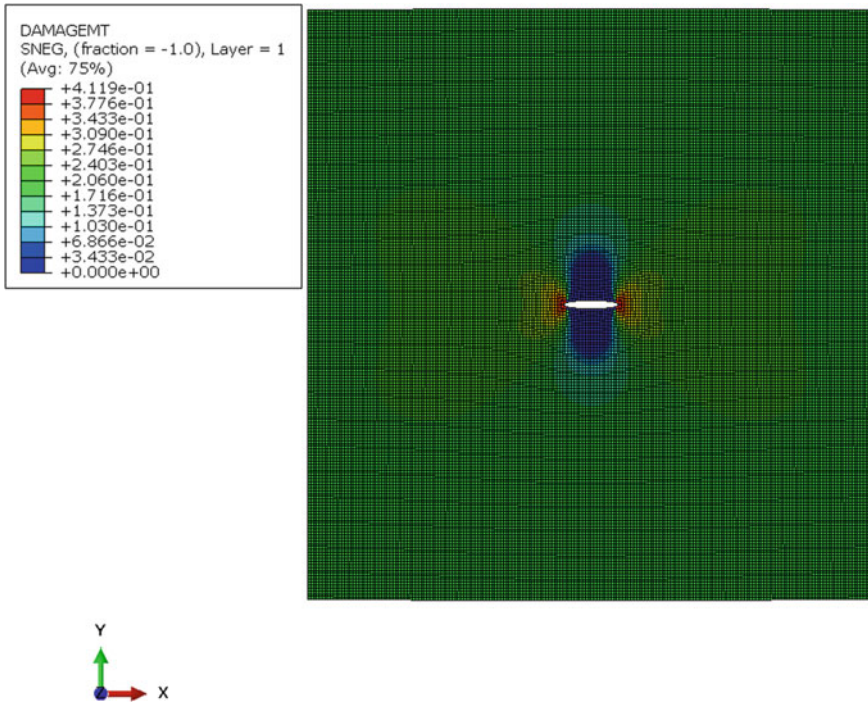
Fig. 13 Cracked plate model presenting damage scale

3. The matrix fails in tension with a higher value of damage scale as 0.4119 for 100 × 100 mm composite plate and 0.4166 for 400 × 400 mm composite plate.

References

1. Azhdari A, Obata M, Nemat-Nasser S (2000) Alternative solution methods for crack problems in plane anisotropic elasticity, with examples. Int J Solids Struct 37(44):6433–6478. https://doi.org/10.1016/S0020-7683(99)00137-7
2. Brighenti R (2005) Numerical buckling analysis of compressed or tensioned cracked thin plates. Eng Struct 27(2):265–276. https://doi.org/10.1016/j.engstruct.2004.10.006
3. Brussat TR, Westmann RA (1975) A Westergaard-type stress function for line inclusion problems. Int J Solids Struct 11(6):665–677. https://doi.org/10.1016/0020-7683(75)90019-0
4. Chiang CR (2009) Some elasticity problems of a general anisotropic solid subjected to anti-plane loadings. Acta Mech 203(1–2):49–61. https://doi.org/10.1007/s00707-008-0030-x
5. Deb Nath SK (2013) Effects of fiber orientation and material isotropy on the analytical elastic solution of a stiffened orthotropic panel subjected to a combined loading. Adv Mater Sci Eng. https://doi.org/10.1155/2013/710143
6. García F, Sáez A, Domínguez J (2004) Traction boundary elements for cracks in anisotropic solids. Eng Anal Boundary Elem 28(6):667–676. https://doi.org/10.1016/j.enganabound.2003.08.005

7. Hüsnü Dirikolu M, Aktaş A (2000) Analytical and finite element comparisons of stress intensity factors of composite materials. Compos Struct 50(1):99–102. https://doi.org/10.1016/S0263-8223(00)00083-0

8. Jabur LS (2015) Theoritical and numerical analysis of central crack plate with different orientation under tensile load. Int J Ind Eng Technol 5(4):7–18

9. Kumar YVS, Paik JK (2004) Buckling analysis of cracked plates using hierarchical trigonometric functions. Thin-Walled Struct 42(5):687–700. https://doi.org/10.1016/j.tws.2003.12.012

10. Liu CD (1986) Analytical solution for orthotropic composite plate containing a mode I crack along principle axis. Int J Fract 76(1):21–38. https://doi.org/10.1007/BF00034028

11. Meek C, Ainsworth RA (2014) Fracture assessment of centre-cracked plates under biaxial loading. Procedia Mater Sci. Elsevier B.V. 3:1612–1617. https://doi.org/10.1016/j.mspro.2014.06.260

12. Sih GC, Chen EP (1981) Mechanics of fracture, cracks in composite materials. Martinus Nijhoff Publishers

13. Tada H, Paris PC, Irwin GR (2010) Stress analysis results for common test specimen configurations. In: The stress analysis of cracks handbook, 3rd edn, pp 39–80. https://doi.org/10.1115/1.801535.ch2

14. Westergaard MH (1939) Bearing pressures and cracks. Trans AIME J Appl Mech 6:49–53

15. Woo CW, Wang YH (1993) Analysis of an internal crack in a finite anisotropic plate. Int J Fract 62(3):203–218. https://doi.org/10.1007/BF00012539

Extralab: A New Way of Management Remote Laboratory in Real Time and in Network: Strengthens, Weakness and Next Challenges

Paul Floury and Jean-Louis Roubaty

1 Introduction: Extralab Story Telling

The water quality monitoring world market is anticipated to be worth around \$4.7B by 2025, increasing at a compound annual growth rate of around 4.5% between 2020 and 2025. The increase of this market is influenced by stringent government policies, initiatives toward lowering the water pollution level, and increasing industrial applications pushing the sector for improved water testing and analysis products (marketsandmarkets.com).

Online measurement has been developing for many years in the fields of industry and the environment. It benefits from the standardization of processes and a maturation of analytical instruments. In situ and continuous analysis meet many industrial needs in terms of process control to optimize consumption of reagents and raw materials and to maintain the quality of finished products are justified in an economic and regulatory context more and more demanding.

In 2012 a French Research CNRS scientific program launched a prototype called Remote Lab and RiverLab. They are new instruments solutions to deploy a full laboratory for the water quality monitoring online automatically and continuously. This is a concept of "Lab in the Field" aiming to transfer laboratory instruments in a solution directly to the field.

After 5 years of research, the analytical performances of the Remote Laboratory (RL) are usually better than in the laboratory under standard analysis conditions, showing the benefit of transporting the laboratory devices to the field. Moreover RL

P. Floury (✉) · J.-L. Roubaty
Extralab Society, Paris, France
e-mail: floury@extralab-system.com
URL: https://www.extralab-system.com

P. Floury
IPGP, Université Paris Diderot, Paris, France

prototype is a connected laboratory and allows an access on real time to all water quality parameters measured and to performed number of remote interventions and expertise.

This represents an innovation in the water quality monitoring and opens a great potential of application to the research infrastructures and industrial applications. The success of RiverLab prototype is thanks to a close partnership between research institutes (CNRS, IPGP and INRAE) and companies as provider an assembly of the prototype.

ExtraLab is a start up benefiting of the legacy of the successful partnerships between research institutes and companies partners and extend the concept to a larger business. ExtraLab opens new opportunities in the field of water quality monitoring. ExtraLab is the start-up project based on a scientific project, part of a research program started in 2012 called Critex, a scientific program from public research grants via AllEnvi, CNRS. The project is based on a collaboration of 5 Research Institutes and Universities in France. This program has also received funding and human support from each of the 5 Research Institutes involved. Critex is a scientific program launched in 2012. Critex is an Excellency equipment project funded by ANR within the framework of "Investment for Future" French government program. Critex is funded by ANR via AllEnvi (7M€) in 2012.

Extralab offers a new concept of full remote decentralized laboratory solution. This solution allows deploying a full laboratory directly on the field to measure natural water quality in real time. Today, Extralab is collaborating with research institutes all around the Word (Europe, China, USA). Here, we present a proof-of-concept study of a "lab in the field" called the "Remote Lab" (RL), based on the idea of permanently installing a suite of laboratory instruments in the field.

2 Hardware Solution: Remote Laboratory (Riverlab, Compact Lab and Lab Mobil)

Extralab makes water quality monitoring accessible everywhere in real time. Extralab aims to develop Hardware solutions: full online remote laboratory directly deployed on the field.

2.1 Hardware Solution

The concept of the Remote Laboratory (RL) is to deploy a full laboratory solution directly on the field: River, industries, building, underground water… This gives a complete analysis of dissolved species continuously at high frequency (20 minutes is needed for a complete analysis). All the instruments of the RL are isolated at 24 °C $\pm$ 2 °C. The RL has been designed around a primary circuit, which pumps the

unfiltered water analyzed. A process automatically managed provides filtered water to instruments. Solutions deployed by Extralab are under patents. Here is some examples of instruments deployed in the remote laboratory:

- ICP-MS: able to analyzed all metals and trace elements dissolved in water
- Ionic Chromatography for all major dissolved species and some trace elements measurable
- Dissolved Gas in water
- VOC gazes measurable using mass spectrometer
- Online ATP analyzer: Biological activity
- ^{13}C, ^{18}O, D/H Isotopes
- SiO_2 analyzer
- COD analyzer
- Alkalinity (Fig. 1).

The analytical performances achieved in RL are the same find in a conventional laboratory. Moreover, instruments are working under constant measurements and the same matrix. This allows achieving a better analytical performance [1].

A multivalve installed upstream of the interments allows us to check the drift of the instruments and the background signal by regular introduction of calibration solutions and pure distilled water. Pure distilled water automatically generated is
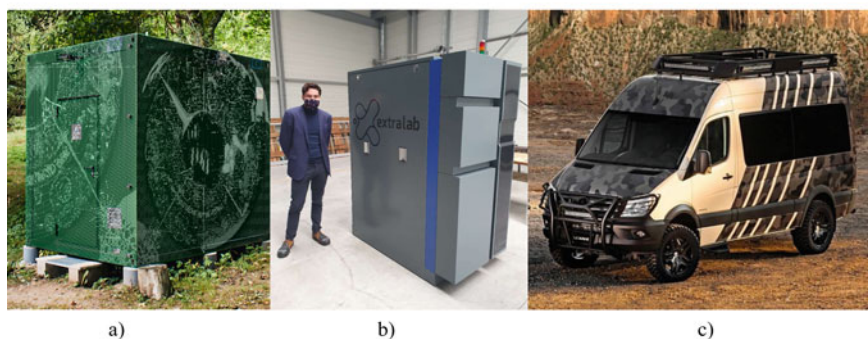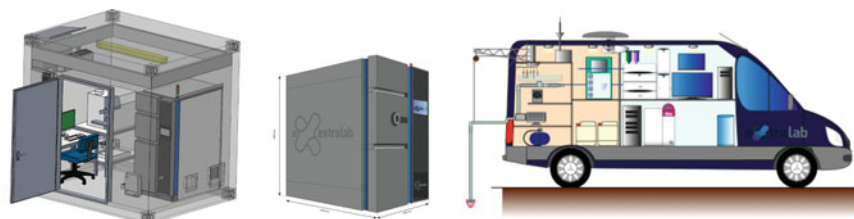

Fig. 1 Remote Laboratory solutions developed by Extralab. **a** Riverlab: a full remote laboratory deployed on the field. **b** Compact Laboratory: process and instruments are compacted side. The system is less than 500 kg. **c** LabMobil: the aim of LabMobil is to be deployed quickly for environment emergency

regularly introduced to check the residual noise. Generally two sets of calibration solutions are prepared to cover the entire range of chemical variation.

Several parameters of the RL can be remotely monitored such as pump activity, pressure, flow and temperature in the primary circuit; activation of the tangential filtration cleaning system, instrument connection, and temperature in the bungalow. A set of alarms and sensors controls each key point of the system. An email is automatically sent in case of dysfunction. Under normal operating conditions, the RL needs human intervention only once per week.

2.2 *Analytical Performances of the RL*

The reliability of the system was assessed through 5 different tests (accuracy, drift, precision of the whole system, cross-contamination and reproducibility). The cross contamination has been tested through several tests. Results are presented in a devoted paper: [1]. The aim of the RL solutions is to achieve very high-frequency measurements of river chemistry over long periods of time (from few days to many years). To compensate for any long-term drift, the instruments are calibrated with a new set of solutions regularly. However, calibration drift can occur over timescales shorter than two months, resulting in systematic and/or random errors in concentration measurements. Results from tests show that the RL is able to capture long-term fine chemical variations with no drift and a precision significantly better than conventionally achieved in the laboratory (up to ± 0.5 % for all major species for over a day and up to 1.7 % over two months). The first results from the RL reveal a significant improvement in reproducibility compared to conventional sampling and analysis techniques.

3   Software: Extralab Platform

3.1 *Platform Presentation*

Extralab has developed full software online to perform the full laboratory works continuously and in real time. The Extralab platform allows users to have access at any time to the data recorded and make exploration directly on the data recorded. The software comprises 5 blocks:

- Datathèque. A database where all data are presented and can be viewed and selected for scientific exploration.
- Dashboard: A private board only accessible to people allowed to work on the remote laboratory.

- Protocol, Method. This section is developed to apply a control and a method to validate the data recorded. A space where user can write rules of selection and filtration on raw data.
- ExtraPlot: A free plot library where users can create their own reporting.
- ExtraCode: An IDE to directly code on data in real time. The language can be chosen between Python or R and soon other languages depend on the request of the users (Matlab…). Scientific models can be calculated in real time and helps for decision making.

All personal comments, data, plots, reporting and model through the platform are loaded in a dedicated space. The space represents a personal, unbreakable and secure space where the user can performed its entire works. Using the 5 blocks of the platform, the whole work of the data from measurements to scientific expertise can be done continuously and directly on the remote laboratory (Fig. 2).

The dashboard is specific for each remote laboratory and exclusively devoted to the teams working on the remote laboratory. The team can decide to give a public access on lecture. The decision is made by the headmaster the campaign of the remote laboratory. The dashboard allows a perennial access to all events, remarks and interventions made on the laboratory. Tis will also helps the users for the data validation and qualification.
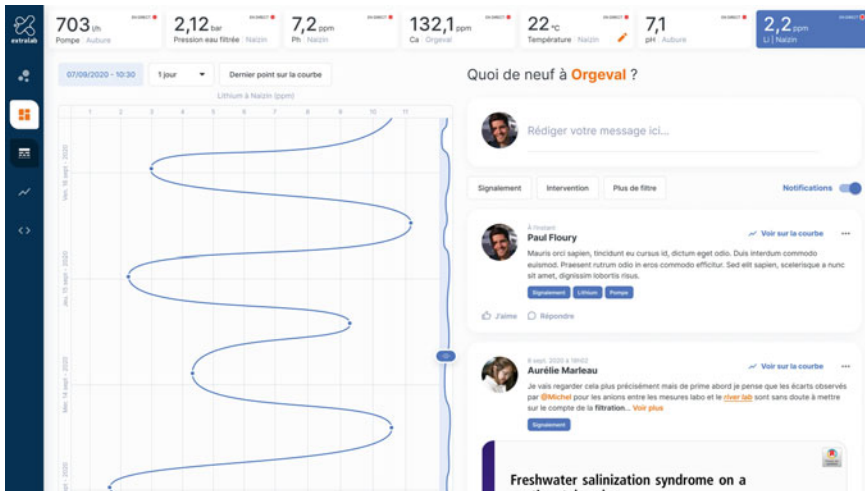
Fig. 2 Screen shot of the Extralab dashboard. The dashboard is a journal connected to the remote laboratory. The user chooses a parameter and can see on the right panel all remarks, photos, files, interventions on the feeds
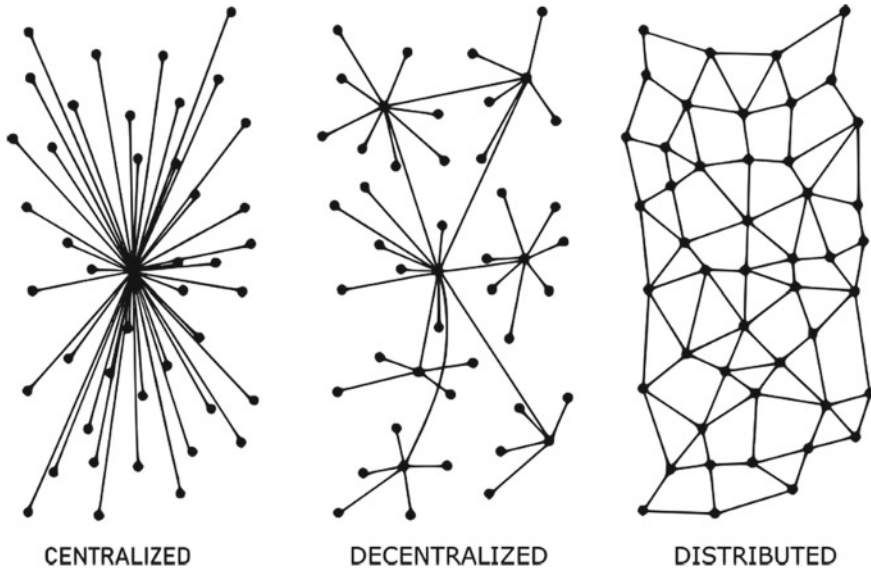
Fig. 3 Example of network architecture. Each node represents a Riverlab or a compacted laboratory or a Lab Mobil. The architecture of Extralab database is decentralized

3.2 Architecture of the Network

The database collected in the distributed network is connected to the IDE where scientist can directly performed scientific model. Moreover this allows the deployment of machine learning solution. The machine learning can be performed using a neuronal network directly append on the platform.

Each Remote Laboratory represents a node in the network. The network constituted is not fully distributed. It is partially distributed: decentralized. The architecture of the network is dependents on the user and the environmental question. The decision to be connected with the rest of the network is depending on each customers and the type of data collected (Fig. 3).

3.3 Scientific Expertise in Real Time

The last point is the environmental expertise and scientific exploration helped by machine learning. All this expertise is directly performed continuously and in real time through the platform. This allows strong reactivity for decision maker and save precious time: No delay between the sampling and the expertise results.

The machine learning can be trained on a database already collected on other spot of measurements. Hence results coming from the machine learning can be compared and apply in a new spot of measurements. This makes a powerful tool to
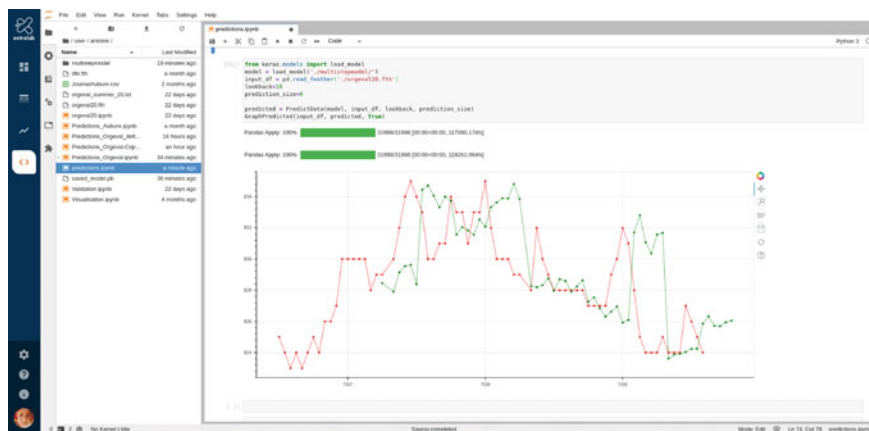
Fig. 4 Example of Machine Learning model performed in real time on a dataset. Here the example of a model performed on a French river on the conductivity data recorded by the Riverlab. The red data are the data collected by the Riverlab. The green data are the data predicted by the machine learning system. The ML model predicts step by of 6 h in futur regarding the last 12 h in the past

already perfumed prediction in a new environment close to the system. For example in environmental emergency, this can provide a first prediction (Fig. 4).

4 Conclusion

Extralab presents a new way of managing a full laboratory entirely remotely. The solutions proposed by the Extralab Company are able to provide a scientific expertise on water quality in real time. The solutions is in two parts: (1) hardware solutions with solutions like the Riverlab, the Compact Lab or the Lab Mobil and (2) a Software online Extralab platform. Remote Laboratory are able to deployed a full solution with numbers of instruments connected online by a process. Secondly the online software has been developed comprising 5 parts. Each part reports the whole work that we can find in a conventional laboratory for water analyses but in real time. Combination of Hardware solution with the software gives the possibility of deployed the system in several cases and many industries: where water quality is a challenge. Moreover the Lab Mobil Solution is devoted to the environmental emergencies. Finally, thanks to a huge amount of data collected and available, the software of Extralab allows to remotely calculated models for expertise. This is gives access to a scientific expertise directly on the platform and on the data collected in real time. This represents a power tools for decisions makers and water emergencies. This offers a strong solution dress to situation where the water quality is an emergency and where the time delay is precious and decisions can't be waited.

Reference

1. Floury P, Gaillardet J, Gayer E, Bouchez J, Tallec G, Ansart P, Koch F, Gorge C, Blanchouin A, Roubaty J-L (2017) The potamochemical symphony: new progresses in the high frequency acquisition of stream chemical data. Hydrol Earth Syst Sci Discuss 1–41. https://doi.org/10.5194/hess-2017-12

Effect of Various Waste Materials on Hydration Process Binding Materials

Aakash Kumar Gupta and Prasanna Kumar Acharya

1 Introduction

Hydration is a process of cement hardening in presence of water which explains the development of the microstructure of the cementitious material. During the process of hydration, the fluid suspension is transformed into a rigid solid form. Cement hydration is a continuous chemical reaction phase in which the main cement compounds form chemical bonds with water molecules that favors the growth of crystalline and semi-crystalline hydration products known as hydrates. It is very important to estimate cement hydration, as there is a good relationship of hydration with porosity, hydration heat, production of strength, chemical shrinkage that can later cause a severe crack [1–4]. Various activities are being undertaken to minimize carbon dioxide emissions as well as energy and raw material consumption by cement industry to reduce the environmental impact [5]. In addition, it is commonly agreed to use cements in which portion of the clinker has been substituted by other materials that are chemically active in the hydrating cement system [6, 7] . In the cement industry, supplementary cement materials (SCMs) typically include industrial waste products, pozzolans and active minerals with either hydraulic or pozzolanic characteristics [8–11].

This paper investigated various authors past papers which uses different types of supplementary cementitious materials (SCMs) such as ground granulated blast furnace slag (GGBS), fly ash (FA), red mud (RM), limestone powder, palm oil fuel ash (POFA), rice husk ash (RHA), those have been used as replacement of cement in concrete production, their physical properties and compositions of chemicals of cements and cementitious materials are critically reviewed and compared in this report.

A. K. Gupta · P. K. Acharya (✉)
School of Civil Engineering, KIIT DU, Bhubaneswar, Odisha, India

In power plants, fly ash is produced by coal combustion as by products and fly ash characteristics are specifically affected by the form of coal used and the conditions of combustion [12]. Authors [6] reported that the introduction of fly ash as SCMs affects the kinetics of cement hydration and also Fly ash spherical grains serve as agents to enhance the rheological properties of the mixtures of fresh concrete [4]. Fly ash responds to $Ca(OH)_2$ and the products of this reaction helps in void filling, functioning as micro-fillers, leading to the formation of a more compact structure and obtaining greater composite cement ash strength [13, 14]. Sun et al. [12] have prepared high volume fly ash (HVFA) concrete by replacing FA with ratios 40, 55 and 70% by mass and reported that 40% FA replacement in HVFA concrete displays a comparable compressive strength of 180 days to the control concrete.

Ground granulated blast furnace slag (GGBS) occurs when coke reduces iron ore at about 1350–1550 °C in a blast furnace . As a cement substitute material, GGBS is being used widely, reducing carbon emissions of cement while potentially enhancing technological efficiency. However, requirements only consider slag composite cement hydration at 20 °C, that may not be suitable for use in warm regions [15]. The mechanical properties of cement are reduced significantly if GGBS replacement is greater than 50%, particularly at an early age [16]. Authors [17] have investigated that Partial replacement of Portland cement with slag is usually appropriate for structures subjected to sea-water because slag significantly increases concrete's resistance to the entry of chloride delaying the time until the embedded reinforcement starts to corrode. Angulo-Ramírez et al. [16] have evaluated the effect of the alkaline activator (NaOH, Na_2SiO_3) and its concentration in hybrid cements relying on granulated blast furnace slag (80%) on mechanical properties and reaction products at different ages. Ogirigbo and Black [15] reported the temperature will have a much stronger impact on the slag's reactions than the chemical composition difference.

Limestone powder is produced from limestone quarry as a by-product and the characteristics of cement can influence materials through filling, nucleation, dilution and chemical effects. Adu-Amankwah et al. [18] investigated on Sulfate interactions within composite cements of ternary slag-limestone and the effects of sulfate dose on hydration kinetics, hydrated phase assemblies and micro-structural have been reported. Mehdipour et al. [19] have done Investigation of the synergistic effects between PLC and SCM in terms of enhancing strength in PLC systems stated that SCMs are more efficient compared to OPC systems. Authors [20] studied the Impact of powdered minerals on normal strength concrete hydration process and products for hydration and confirmed that the origin of heat seems to have been impacted by the use of powdered minerals.

Rice husk produced from agricultural products as a by-product, which has disposal challenges, consisting of high silica content, and worldwide, over 150 million tons are produced every year [1, 2, 5, 7, 10, 11, 21]. The rice husk is a silica-rich fibrous substance and certain organic compounds, such as lignin and cellulose. Rice husk has been used for cogenerating electricity due to its high melting point and poor protein content t [16, 18, 22]. The presence of RHA as SCMs in concrete materials enhances the characteristics, including enhanced flexural and compressive strengths, decreased permeability, improved concrete workability, and also makes commercial use of the

commodity and thus creates cheaper materials for low-cost building materials. Vieira et al. [23] have evaluated Evolution of Concrete of high-strength compressive strength with rice husk ash (RHA) and hydration effect of RHA measured with isothermal calorimetry and thermogravimetry. They reported that compressive strength was affected by RHA particle size until 28 days, while replacement material became the important factor at 91 days. Authors Liu et al. [21] reported that to improve the equal use of raw materials and boost MPC characteristics, rice husk ash (RHA) can be applied to magnesium phosphate cement (MPC).

Red mud is a highly alkaline waste that is a reddish-brown sludge because during through the Bayer process in the aluminum industry of large quantities of ferric oxide by-products produced. The processing of 1.0 tons of alumina produces 1.0–1.5 tons of red mud as a by-product [24]. Many scholars have performed comprehensive research on the use of red mud in recent decades. Authors Kang et al. [24] by applying liquefied red mud to sulfuric acid (LRM, pH 10–12), prepared neutralization of red mud (LRM + S; pH 6–8), which could facilitate its use as a construction material, stated that the maximum hydration peak heat had a low calorific value and was delayed for the cement paste with LRM compared to Plain. Authors Chen et al. [25] investigated Gangue-cemented paste backfill (GCPB) macroscopic strength and micro-structural evolution through uniaxial compression studies, XRD, SEM, and FTIR tests and concluded that RM has a major impact on GCPB strength and hydration products. Authors Li et al. [26] have used Red mud (RM), fly ash (FA) and desulphurised gypsum (DG) to prepare non-burnt bricks based on red mud (RMNB) and based on investigation they concluded that the formation of Ettringite (Aft) can be encouraged by adding desulphurised gypsum to non-brunt brick. Optimum Aft formed sulphate The pore size is refined and the strength is increased, while excessive sulphate produced by Aft damages the internal structure and decreases the strength.

2 Materials Reviewed

This paper studied the past authors works on hydration characteristics of various cementitious materials. Authors like Ogirigbo and Black [15], Angulo-Ramírez et al. [16], Yio et al. [17], Skibsted and Snellings [11] have reported on ground granulated blast-furnace slag (GGBS), characteristics of Fly ash is studied by Pacewska and Wilinska [6], Sun et al. [12]. The study on Rice husk ash is reported by Liu et al. [21], Vieira et al. [23]. Characteristics on Red mud is published by Kang et al. [24], Chen et al. [25], Li et al. [26]. Similarly, works on Limestone powder are reported by Adu-Amankwah et al. [18], Mehdipour et al. [19], Tikkanen et al. [20]. Most of the authors have used fly ash as supplementary cementitious materials blended with cement. The oxide composition of chemical of these raw materials are determined by X-ray fluorescence (XRF) test is listed in Table 1.

Table 1 Oxide composition of OPC and SCMs composition

References	Materials	Oxide compositions (wt%)											
		SiO$_2$	Al$_2$O$_3$	Fe$_2$O$_3$	CaO	MgO	SO$_3$	TiO$_2$	Na$_2$O	K$_2$O	MnO	P$_2$O$_5$	LOI
Sun et al. [12]	Fly ash (FA)	59.1	21.63	3.85	5.93	2.26	0.84	0.91	2.5	1.18	–	0.78	0.85
	OPC	20.7	4.87	3.37	61.26	1.54	3.5	0.24	0.4	0.66	–	–	3.15
Ogirigbo and Black [15]	GGBS	36.58	12.23	0.48	38.24	8.55	1	0.83	0.27	0.65	0.64	0.06	(+1/06)a
	OPC	19.1	5.35	2.95	62.38	2.37	3.34	0.25	0.05	1.05	0.03	0.1	2.54
Angulo-Ramírez et al. [16]	GGBS	31.99	14.54	1.12	46.86	1.05	0.82	–	–	–	–	–	1.82
	OPC	19.13	4.42	4.32	57.7	1.6	2.32	–	–	–	–	–	9.78
Adu-Amankwah et al. [18]	Slag	34.9	11.6	0.5	41.8	5.8	3.1	1.1	0	0.5	0.3	0	(+1.45)
	Limestone	2	0.8	0.3	53.1	0.6	0	0	0	0.1	0	0	42.3
	OPC	20.4	5.6	2.5	62.1	1.7	3.5	0.3	0	0.7	0	0.1	2
Mehdipour et al. [19]	Limestone	16.31	3.62	2.81	58.24	0.91	3.16	–	–	–	–	–	4.45
	Class C FA	35.64	23.76	4.95	27.72	4.95	2.47	–	–	–	–	–	0.51
	OPC	19.32	16.31	3.15	62.53	2.63	3.31	–	–	–	–	–	1.46
Tikkanen et al. [20]	Limestone	9.2	1.9	0.87	40	9.1	–	0.06	0.18	0.43	0.03	0.02	–
	OPC	20.9	5.2	3.4	65.1	2.8	0.7	–	0.8	0.9	–	–	–
Vieira et al. [23]	RHA	89.85	4.79	0.86	0.79	–	1.34	–	–	1.38	0.24	0.22	0.53
	OPC	15.25	4.64	3.39	67.25	–	4	–	–	0.98	0.13	–	4.35

(continued)

Table 1 (continued)

References	Materials	Oxide compositions (wt%)											
		SiO_2	Al_2O_3	Fe_2O_3	CaO	MgO	SO_3	TiO_2	Na_2O	K_2O	MnO	P_2O_5	LOI
Li et al. [26]	Red mud	29.18	30.01	8.71	15.96	0.893	2.73	2.7	8.22	0.795	–	–	–
	Fly ash (FA)	34.6	25	8.67	17.2	0.684	10	1.39	0.309	1.2587	–	–	–
	OPC	24.6	10.6	1.25	53.6	3.33	1.8	0.599	0.385	0.976	–	–	–
Kang et al. [24]	LRM	17.6	25.6	30.4	1.83	0.21	0.29	6.27	13.2	–	–	–	–
	LRM + S	17	25.4	29.2	1.84	0.21	4.48	5.99	10.7	–	–	–	–
	OPC	21.7	5.7	3.2	63.1	2.8	2.2	–	–	–	–	–	2.44

3   Analysis of Properties

3.1   *Heat of Hydration*

3.1.1   Fly Ash

Pacewska and Wilinska [6] have carried out Isothermal calorimetry tests to measure earlier cement hydration heat with 80% fly ash and CEM I 42.5R and stated that the initiation time was significantly shorter, the impact of hydrate precipitation was more extreme and the heat energy released was also higher compared to the findings for the same sample with CEM I 32.5. Author [12] have reported that High-volume fly ash (HVFA) cement blends observed overall far less heat released Other than the reference sample, particularly for the first 24 h, suggesting fewer hydrates developed in HVFA cement pastes due to too little cement material, which results in the production of High-volume fly ash (HVFA) concrete at 3 days of minimal compressive strength.

3.1.2   Ground Granulated Blast Furnace Slag

Ogirigbo and Black [15] measured the heat flow produced throughout cement paste hydration using a TAM Air calorimeter on cement paste of 9 g for a duration of 28 days at 20 and 38 °C, which was done to determine the filler effect by swapping the slag portion mixes of equal fineness as the slags of quartz in the slag. They recorded that a slight movement of the Alite (C_3S) hydration resulted from the addition of either quartz or slag to the CEM I. Angulo-Ramírez et al. [16] have performed hydration heat tests in blends using the isothermal calorimetry method on a Cal Metrix I-8000 calorimeter at a temperature of 25 °C for 48 h and recorded that 80% of alkali activated OPC/GBFS cements have less cumulative heat at 48 h than 100% OPC, so low hydration heat can be considered.

3.1.3   Limestone Powder

Tikkanen et al. [20] have performed Semi-adiabatic studies of calorimetry on blends of concrete casted into the cylinder-shaped insulated containers made from expanded polystyrene stated that the degree of hydration of concrete containing minerals additives at the same age was Higher than the regular concrete that contains just cement from Portland Concrete. Adu-Amankwah et al. [18] prepared 9 g of paste containing a 0.5 w/b ratio and conducted isothermal calorimetry test which was consistently tested at 20 °C for 28 days using TAM Air calorimeter, the impact of sulphate concentration in Portland ternary composite clinker-slag-limestone cements and reported that the content of sulphate affected the Clinker, slag, and calcareous hydration material properties, though C_3S was not significantly impacted.

3.1.4 Rice Husk Ash

The hydration heat release process is analysed by the TAM-air hydration calorimeter and the sludge hydration heat blended with 7% RHA is stated to be less than that of pure magnesium phosphate cement (MPC) prior to 1 h. The total hydration volume is reduced and the hydration heat is decreased, but the total quantity of hydration products increases steadily with the continuous hydration reaction [21].

3.1.5 Red Mud

Kang et al. [24] used multi-channel microcalorimeter for hydration heat flow analysis for liquefied red mud (LRM and LRM + Sulfuric acid (S)), which is introduced to water and then combined with cement. They stated that when LRM is neutralized with sulfuric acid and applied to cement paste, irrespective of the added number, an initially strength greater than that of LRM can be achieved.

3.2 Chemical Shrinkage

3.2.1 Limestone Powder

To assess chemical shrinkage with dilatometry, 15 gm of paste prepared with a 0.5 w/b ratio and before being poured into a plastic beaker, the paste was mixed by hand for 2 min, 34 mm in dia. and 68 mm in height, and parallel measurements were made on samples where quartz of similar fineness was replaced with slag to distinguish the filler effect from the supplementary cementitious materials reaction [18].

3.3 Thermo-gravimetric Analysis

3.3.1 Fly Ash

Through the application of the Thermo analyser SDT 2960, TG and DTG curves, 100 heating threshold C / min, sample mass: 9–13 mg, atmospheric nitrogen. Pacewska and Wilinska [6] reported that in the context of CEM I 42.5 R and cement mixtures, the consistency of the cement paste comprising fly ash can initially be greater than that of the cement paste containing fly ash cement CEM I 32.5 R, while these variations would diminish at a later date. Sun et al. [12] performed the analysis of thermo-gravimetric (TG) using a thermal gravimetric analyzer with a constant heating rate of 10 °C/min under nitrogen flow from 40 to 1000 °C, it was reported that the pozzolanic

FA reaction progresses substantially at the later healing time and consumes significant quantities of nitrogen flow and CH with supplementary C–S–H secondary gels, resulting in more dense and morphological healing.

3.3.2 Ground Granulated Blast Furnace Slag

Angulo-Ramírez et al. [16] conducted using the TA Instruments SDTQ600 around 1100 °C, the TG test with a 10° C/min rate, nitrogen as liberate gas and alumina crucibles confirmed that the use of activator like NaOH in the hybrid system gives a quicker early reaction than the reference system. and the SS + NaOH hybrid system. However, compared with the loss of weight in the other systems after 28 days of healing, in the NaOH system, the rise in weight loss is minor. Ogirigbo and Black [15] performed a simultaneous thermal analysis (STA) with the aid of the Stanton Red croft 780 sequence and the findings demonstrated the temperature of the reactivity of slags had a much greater effect than the disparity in chemical composition.

3.3.3 Limestone Powder

Adu-Amankwah et al. [18] performed TGA test on a Stanton Red croft 780 sequence evacuated at 58 ml/min under a nitrogen gas environment, with approx. at a rate of 20 °C/min, 6–18 mg of extra grounded powdered sample was heated to 1000 °C in a platinum crucible and stated that for the first 90 days, Calcite reactions were limited to approx. 3 gm per 100 gm of binder. Calcite's early reaction was delayed at elevated sulfate levels, yet deviations were typically smaller than the error of measurement. Mehdipour et al. [19] used a thermal analyzer Netzsch STA 409 PC to classify and measure the number of phases that are found in mortars and Reduction of mass (TG) and differential loss of mass (DTG) residues for 7 days were used for the calculation of the remaining CH content present in the unit. Furthermore, the non-evaporative amount of water obtained to predict the level of cement hydration, TGA/DTG was used for the single OPC and PLC systems. According to TG results of Tikkanen et al. [20] the amount of $Ca(OH)_2$ that's been generated was not significantly affected by 10–20% cement containing mineral powder. This may be due to a faster rate of cement hydration and also to the variations in w/c which can be related to the available room for the expansion of hydration products, which improves when w/c is increased by substituting MP for cement.

3.4 X-ray Fluorescence

3.4.1 Ground Granulated Blast Furnace Slag

Yio et al. [17] determined the compositions of oxide of unspecified slag, cement, and aggregates by X-ray fluorescence (XRF) and the combination of the composition of the concrete was further characterized by considering the balance of mass and providing solutions to series of linear equation.

3.4.2 Red Mud

Li et al. [26] have checked the oxide content of the oxides by using X-ray fluorescence (XRF) and the mechanical output was tested by the automatic pressure machine and the loading rate was 6 kN/s.

3.5 Compressive Strength

3.5.1 Fly Ash

Sun et al. [12] demonstrates The increase in compressive strength of the two mixtures, calculated at 3, 7, 28, 56, 90 and 180 days, and the results showed that high volume fly ash (HVFA) concrete exhibits much lower compressive strength than control concrete at 3 and 7 days Owing to the dilution effect of Fly ash, the proportion of cement decreases and the hydration of HVFA cement mixtures slows down.

3.5.2 Ground Granulated Blast Furnace Slag

Ogirigbo and Black [15] used a Toni pact 3000 concrete cube crusher. The development of Unconfined Compressive Strength (UCS) at 20 and 38 °C was shown to measure compressive strength at 1, 7, 28, 90 and 180 days and the results indicated that curing at high temperature resulted in higher strength up to 7 days, however, with marginal gain from strength beyond 28 days, the power of the samples cured at 20 °C was ultimately higher than that of the 38 °C samples cured.

3.5.3 Limestone Powder

Mehdipour et al. [19] investigated the compressive strengths of mortars at 1, 3, 7, 28, 56, and 91 days using 50 mm cubes. All mortar samples were preserved in lime saturated solution at $21 \pm 2°$ C after demolding at 24 h, before testing and the

results reflect the average of three samples repeated. The coefficient of variation in the compressive strength for the investigated mixtures was found to be less than 6% among triplicate specimens. Adu-Amankwah et al. [18] studied compressive strength development as a consequence of the sulphate component in the cement that has two opposing effects i.e. raised ettringite volume improves the strength of compression and decreases CSH phase density that reduces the strength. Tikkanen et al. [20] reported on average, the compressive strength of concrete powdered minerals were 4.1 N/mm^2 higher than normal concrete, measured at 28 days, which is also consistent with the higher degree of hydration of these mixtures.

3.5.4   Rice Husk Ash

Vieira et al. [23] assessed the compressive strength development of high strength concrete containing rice husk ash as a consequence of RHA particle size, porosity and Substitute material. Results suggested that compressive strength was affected by RHA particle size until 28 days, while replacement material became the important factor at 91 days. Liu et al. [21] results have shown that when the RHA content is 5 percent, the compressive strength hits the peak value and then decreases with the rise in RHA content. The compressive intensity increased by 39.2% at 3 h, 39.7% at 1 d and 25.7% at 7 d, comparison to the control group.

3.5.5   Red Mud

Chen et al. [25] reported the uni-axial compressive strength values of gangue-cemented paste backfill (GCPB) samples were 0.23 and 0.95 MPa after 7 days and 28 days of curing, which were 7% and 13% higher than those of control samples, and indeed the compressive strength of GCPB samples first enhanced and then reduced with an increase in the proportion. Kang et al. [24] concluded for the cement paste with LRM, the compressive strength at the age of 28 d was found to be as poor as 55% of Plain's compressive strength, whereas the cement paste with LRM + S displayed a strength ratio of up to 99%.

4   Micro-structural Analysis

4.1   X-ray Diffraction

4.1.1   Fly Ash

For better comparison, the X-ray diffraction patterns of each sample were evaluated for 1, 3, 7, 28, 56, 90, 180 days and the peaks were selected in the 5–40 range. After

180 days of hydration, anhydrous phases, including alite, belite and ferrite, were still detectable in all samples. The details of the X-ray diffraction analysis also showed that the major crystalline hydrate phases were CH and Aft [12].

4.1.2 Ground Granulated Blast Furnace Slag

Ogirigbo and Black [15] performed XRD analysis after hydration at 20 and 38 °C for 1, 7 and 28 days, to analyze the effect of temperature on hydration and phase assemblage produced from both slag blends. Angulo-Ramírez et al. [16] obtained X-ray diffraction patterns for Hybrid cements activated by GBFS/OPC 80/20 with SS + NaOH and NaOH at 1- and 28-day curing ages, as well as the reference content diffractogram (OPC/GBFS) are shown. Quartz, calcite, aragonite, and hydrated gehlenite are available, among many other hydrates that vary depending on the type of activator used. To devitrify the unreacted slag, the sample is activated at 950–1050 °C, it was then combined with 10% CaF_2 and analyzed by XRD. The maximum intensity ratio of melilite/CaF_2 is calculated to predict slag content and compared with those of activated slag mixtures from the same source as the calibration [17].

4.1.3 Limestone Powder

Adu-Amankwah et al. [18] performed XRD scans by collecting information from a PAN alytical MPD Pro, a Cu Ka anode fitted with 40 kV and 40 mA is used on fresh ground specimens without hydration cessation, using a step over a range of 5–80 °2 with an X'Celerator tracker. The XRD results suggest that the calcite response, particularly at the early stages, was moderately affected by the early sulphate material, as was evident by hemicarboaluminate precipitation once sulphate was no longer present. Mehdipour et al. [19] performed analysis of X-ray diffraction (XRD) on powdered cementitious mixtures using a Philips X'pert after 7 days of hydration diffractometer with Cu Ka (k = 1.54 Å) radiation in a $\theta - \theta$ configuration. Samples were scanned in continuous mode between 5° and 90° (2θ) with an integrated phase scan of 0.025° (2θ) using a Pixel detector with a time of 150 s per move. According to XRD results of Tikkanen et al. [20] the amount of $Ca(OH)_2$ that's been generated was not significantly affected by 10–20% cement containing mineral powder. This may be due to a higher cement hydration rate and also to the differences in w/c that can be attributed to the available space for hydration products to expand, which increases when w/c is increased by replacing cement with MP.

4.1.4 Red Mud

Kang et al. [24] concluded that unlike the case of the LRM study, the cement paste with 20% LRM + S displayed a $Ca(OH)_2$ peak after only 1 h in the XRD analysis, close to the case of Plain. Moreover, no new items were found due to the addition

of red mud. Li et al. [26] noted that AFt and a small number of sodium aluminum silicate hydrate (N–A–S–H), which are known to have outstanding potential for Na+ and heavy metals solidification,are the hydration products with the improve quality. Chen et al. [25] clearly noticed from the XRD patterns that the amount of hydration products were higher than those of other classes from the GCPB samples when the percentage of RM was less than 1/3.

4.2 Scanning Electron Microscopy

4.2.1 Ground Granulated Blast Furnace Slag

Angulo-Ramírez et al. [16] electron microscopy scanning suggested that due to the presence of hydrate C–S–H and gehlenite, which are characteristic of this material type and due to the quick hydration that occurs in these alkali-activated cements, small cracks develop, the hybrid cements (cement-slag 20/80) had a relatively compact structure; this phenomena must be controlled. Yio et al. [17] used the SEM technique was operated in high vacuum, at an acceleration voltage of 10 kV 193 and a working distance of 10–15 mm, using a Camscan Apollo 300 field-emission SEM for imaging. Samples were viewed at 500 magnification, which provides a field of view of 240 × 192 μm per frame for 194. Ogirigbo and Black [15] concluded that at 7 days, the degree of hydration of slag 1 and slag 2 at 38 °C was greater than that of 20 °C by around 14 and 11%, respectively, and according to BSE-SEM image examination. By 28 days, for slag 1 and slag 2, this gap had dropped to around 8 and 5% respectively.

4.2.2 Limestone Powder

Adu-Amankwah et al. [18] performed SEM analysis in backscattered electron mode, using a Zeiss EVO MA15 SEM fitted with an detection system 80 mm^2 and the apparatus was run at 15 keV. Analysis of SEM points was conducted for the 90-day composition, on C–S–H and hydrated slag rims.

4.2.3 Rice Husk Ash

Vieira et al. [23] evaluated the composition of RHA samples using a Hitachi—TM 3000 micro-scope by scanning electron microscopy. The specimens were splashed and coated with gold in a sample holder.

4.2.4 Red Mud

Chen et al. [25] used the gangue-cemented backfill paste samples that were analyzed using SEM with zero and optimal red mud material i.e. APREO electron microscope for high and low vacuum scanning provided by the American FEI company, in order to observe the internal microstructure more conceptually. Li et al. [26] studied an EDS scan for the assessment of the constituent elements of the components of hydration which means that these zones comprised predominantly elementary Ca, Si, Al, S and O. It is concluded that the micrograph of the specimens consisting of elongated rod shaped AFt and cluster CSH gel, integrating the key elements of EDS and other study findings.

4.3 Fourier Transform Infrared Spectroscopy (FTIR)

4.3.1 Ground Granulated Blast Furnace Slag

Angulo-Ramírez et al. [16] conducted Fourier Transform Infrared spectroscopy using the IR-100 Perkin Elmer device in frequency transmittance mode from 4000 to 400 cm^{-1} and concluded that the wide bands in the spectrum of reference cements as well as hybrid cements between 3450 and 3300 cm^{-1} and 1640 and 1650 cm^{-1} related to the tension and bending motions of the fundamental O–H bond in the water.

4.3.2 Rice Husk Ash

Liu et al. [21] used the Infrared Spectrum (FTIR, Nicolet iS50 Thermo Scientific, USA) to describe the RHA was added. The precise surface area, distribution of size and accumulation of RHA have been obtained using the Laser Particle Size Analyzer BT-9300S.

4.3.3 Red Mud

Chen et al. [25] used FTIR spectroscopy to explored the impact of red mud on GCPB and in particular, to investigate and identify the suitable quantity of red mud, the chemical compositions of the samples that were processed. Li et al. [26] conducted FTIR analysis to investigate the bond activity, present in samples and molecular group bands. The findings suggest that the quantity of Aft rises with the rise in DG ($CaSO_4$ $0.2H_2O$) dose and the disparity in strength can be assumed to be primarily correlated with the shape of Aft.

5 Conclusion

In this review, hydration characteristics blended types of cement produced due to the blending of various supplementary cementitious materials (SCMs) like fly ash, ground granulated blast furnace slag, limestone powder, rice husk ash, red mud etc. are reviewed. It is observed that different techniques such as isothermal calorimetry, X-ray diffraction (XRD) and thermogravimetric (TG), scanning electron microscopy (SEM), Fourier Transform Infrared spectroscopy (FTIR) were mainly used to study the hydration characteristics of cement paste. Based on review, following a few conclusions have been drawn:

1. This review indicate that the alkaline activation (sodium silicate + NaoH) is extremely useful for blended Portland cements as it increases the material's power and leads to the production of a denser microstructure, properties with higher longevity.
2. The inclusion of fly ash as SCMs, especially in its initial stages, results in hydration retardation. When high volumes of fly ash are used, it is extremely noticeable and is beneficial to establish high volume fly ash binder activation methods, effectively enhancing setting, hardening and mechanical strength in the initial stages.
3. Review revealed that the limestone powders in concrete as well as cement paste impact the evolution of heat. At an age equivalent to that measured by semi-adiabatic calorimetry, the degree of hydration of concrete containing mineral additions was above the level of standard concrete containing only Portland Composite cement.
4. The introduction of blast furnace slag into concrete at various substitution rates increases the rate of chemical shrinkage and hydration from the very first hour, which gives additional strength and denser microstructure when activated with alkaline, resulting in better durability characteristics.
5. Addition of the rice husk ash material mainly mesoporous, where micro and macropores are also present influences the main features of RHA samples, including pozzolanic behaviour, distinctive surface area and soluble fraction, by the volume of pores on these three bands.
6. Addition of red mud used partially instead of Portland cement (PC) for gangue-cemented backfill paste (GCPB) in coal mining, which not only helps to reduce the filling expense of the mines, as the filling materials prepared have strong mechanical characteristics, which contribute to enhancing the protection of the working face of the filling.
7. The SEM, XRD and FTIR microstructure studies observed that different SCMs such as GGBS, fly ash, RHA, RM, limestone and the pore structure of the cement paste has been optimized, resulting in a denser microstructure due to the development of a more polymerized C–S–H gel, ideal for toughness and high strength.

Finally, this overall review reached the conclusion that the use of various additional cement materials in concrete manufacturing can affect concrete characteristics, such as hydration rate, strength, durability, workability, etc.

Correspondingly, by eliminating waste materials, these SCMs will protect natural resources and this eco sustainable concrete offers good scope for the future.

References

1. Snehal K, Das BB, Kumar S (2020) Influence of integration of phase change materials on hydration and microstructure properties of nano silica admixed cementitious mortar. J Mater Civ Eng ASCE 32(6)
2. Snehal K, Das BB (2020) Effect of phase-change materials on the hydration and mineralogy of cement mortar. In: Proceedings of the institution of civil engineers-construction materials, pp 1–11
3. Snehal K, Das BB. Influence of incorporating phase change materials on cementitious system—a review. In: Recent trends in civil engineering. Springer, pp 33–63
4. Snehal K, Das BB, Akanksha M (2020) Early age, hydration, mechanical and microstructure properties of nano-silica blended cementitious composites. Constr Build Mater (Elsevier) 233
5. Shivaprasad KN, Das BB (2018) Determination of optimized geopolymerisation factors on the properties of pelletized fly ash aggregates. Constr Build Mater (Elsevier) 163
6. Pacewska B, Wilińska I (2013) Hydration of cement composites containing large amount of waste materials. Procedia Eng 57:53–62
7. Sahoo S, Das BB (2019) Mineralogical study of concretes prepared using carbonated fly ash as part replacement of cement. In: Sustainable construction and building materials. Springer Nature Singapore, pp 519–529
8. Dalinaidu A, Das BB, Singh DN (2007) Methodology for rapid determination of pozzolanic activity of materials. J ASTM Int (JAI) 4(6)
9. Das BB, Singh DN, Pandey SP (2012) Rapid chloride ion permeability of OPC and PPC based carbonated concretes. J Mater Civ Eng ASCE 24(5):1–5
10. Goudar SK, Das BB, Arya SB (2019) Microstructural study of steel-concrete interface and its influence on bond strength of reinforced concrete. In: Advances in civil engineering materials, vol 8(1). ASTM International, pp 171–189
11. Skibsted J, Snellings R (2019) Reactivity of supplementary cementitious materials (SCMs) in cement blends. Cement Concr Res 124:105799
12. Sun J, Shen X, Tan G, Tanner JE (2019) Compressive strength and hydration characteristics of high-volume fly ash concrete prepared from fly ash. J Therm Anal Calorim 136(2):565–580
13. Das BB, Kondraivendhan B (2012) Implication of pore size distribution parameters on compressive strength, permeability and hydraulic diffusivity of concrete. Constr Build Mater (Elsevier) 28(1):382–386
14. Das BB, Singh DN, Pandey SP (2010) A comparative study for determining pore volume of concrete. Indian Concr J 84(12):7–12
15. Ogirigbo OR, Black L (2016) Influence of slag composition and temperature on the hydration and microstructure of slag blended cements. Constr Build Mater 126:496–507
16. Angulo-Ramírez DE, de Gutiérrez RM, Puertas F (2017) Alkali-activated Portland blast-furnace slag cement: mechanical properties and hydration. Constr Build Mater 140:119–128
17. Yio MHN, Phelan JC, Wong HS, Buenfeld NR (2014) Determining the slag fraction, water/binder ratio and degree of hydration in hardened cement pastes. Cem Concr Res 56:171–181
18. Adu-Amankwah S, Black L, Skocek J, Haha MB, Zajac M (2018) Effect of sulfate additions on hydration and performance of ternary slag-limestone composite cements. Constr Build Mater 164:451–462

19. Mehdipour I, Kumar A, Khayat KH (2017) Rheology, hydration, and strength evolution of interground limestone cement containing PCE dispersant and high volume supplementary cementitious materials. Mater Des 127:54–66
20. Tikkanen J, Cwirzen A, Penttala V (2014) Effects of mineral powders on hydration process and hydration products in normal strength concrete. Constr Build Mater 72:7–14
21. Liu R, Pang B, Zhao X, Yang Y (2020) Effect of rice husk ash on early hydration behavior of magnesium phosphate cement. Constr Build Mater 263:120180
22. Kolani B, Buffo-Lacarrière L, Sellier A, Escadeillas G, Boutillon L, Linger L (2012) Hydration of slag-blended cements. Cement Concr Compos 34(9):1009–1018
23. Vieira AP, Filho RDT, Tavares LM, Cordeiro GC (2020) Effect of particle size, porous structure and content of rice husk ash on the hydration process and compressive strength evolution of concrete. Constr Build Mater 236:117553
24. Kang S, Kang H, Lee B (2020) Effects of adding neutralized red mud on the hydration properties of cement paste. Materials 13(18):4107
25. Chen S, Du Z, Zhang Z, Yin D, Feng F, Ma J (2020) Effects of red mud additions on gangue-cemented paste backfill properties. Powder Technol
26. Li Z, Liu X, Li Y, Ren Y, Wang Y, Zhang W (2020) Effects of sulfate on the mechanical performances and hydration characteristics of red mud based non-burnt brick. Constr Build Mater 262:120722

Performance of Functionally Graded Concrete Made of Layered Technique—A Review

Sangram K. Sahoo, Benu G. Mohapatra, Sanjaya K. Patro, and Prasanna K. Acharya

1 Introduction

The concrete consists of cement as its main constituent and the same is source of 5% of CO_2 emission globally. It is the useful material next to water declared by U.S. Geological Survey [1]. Scientists and engineers are continuously investigating for improvement in concrete properties and less CO_2 emission [2–5]. Typically, concrete in structural elements is cast using a homogeneous mixture [6, 7]. A specified set of materials are mixed in a suitable ratio for a non-homogeneous concrete mix to meet the basic requirements. Functional grading non-homogeneous concrete mix can be achieved in two ways, the first one by continuous grading and the second one by stepwise layering Stepwise layered concrete is easy to cast and cost economy. The present paper focuses on present knowledge of functionally graded concrete (FGC) with layers, its properties and behavior.

Nazari and Sanjayan [8] experimented with the functionally graded structures fabricated with extrusion of layers in the cementitious materials including the formation of functionally graded interfaces. It is beneficial in stress reduction due to changes of properties gradually in concentrated form at the place of interfaces with more laminated properties. The strength of functionally graded region in geopolymeric specimens depends upon the fracture strength of constituent layers which is related to the surface energy and elastic modulus of that graded region as presented in Fig. 1. Nazari and Sanjayan [9, 10] reported that the mechanical property and durability got enhanced in geopolymer FGC structures with fewer greenhouse gases emission and lower embodied energy.

S. K. Sahoo · B. G. Mohapatra · P. K. Acharya
School of Civil Engineering, KIIT Deemed to be University, Bhubaneswar, Odisha, India
e-mail: bmohapatrafce@kiit.ac.in

S. K. Patro (✉)
Department of Civil Engineering, VSS University of Technology, Burla, Odisha, India
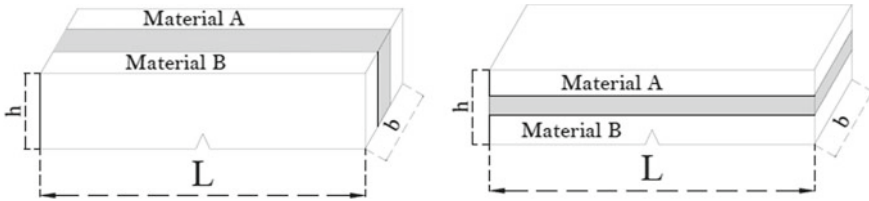
Fig. 1 Diagrammatic presentation of crack configuration in FGC structure (Nazari et al. 2014)

Ning et al. [11] reported that the elastic load-bearing capacity of the ideal functionally graded lining and two-layered functionally graded linings are higher than the conventional single-layered lining detected by the elasto-plastic analysis which they presented through Fig. 2. Nazari and Sanjayan [9, 10] reported that the compressive strength of the FGC specimen is higher than that anticipated from the rule of the mixture when the applied load is parallel to functionally graded layer. The position of the functionally graded layer is the governing factor of strength in FGC specimens. Kurugol et al. [12] reported that the coarse aggregate fraction with lightweight aggregate and its increment decreases Young's modulus of elasticity (MoE) of concrete. The composite of lightweight concrete with steel fiber reinforced lightweight concrete in a two-phase concrete material predicted best in the Hashin-Hansen model when compared with the experimental results. Composite structure studied by Hussein et al. [13] as presented through Fig. 3 using normal or high strength concrete and ultra-high performance fiber reinforced concrete in layer reported that the shear and flexural capacity is successfully enhanced. It is 1.6–2.0 times higher than normal/high strength concrete structures and delivering the addition of shear connectors is unnecessary.

Nogata et al. [14] and Amada et al. [15] studied that natural systems like bones in animals and stems in plant through the structural grading, serve as a role model for engineered functionally graded materials as presented in Fig. 4. Heinz et al.
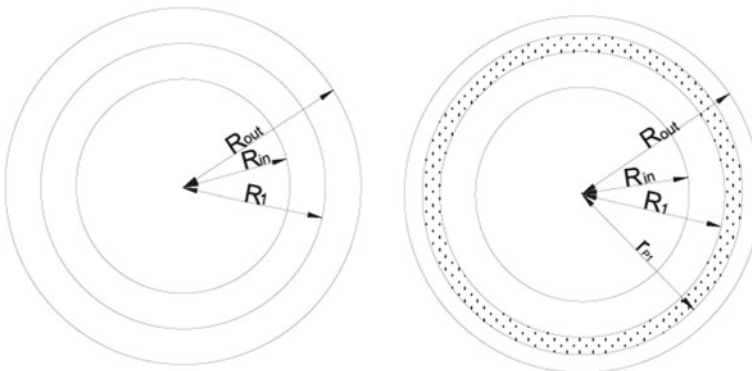

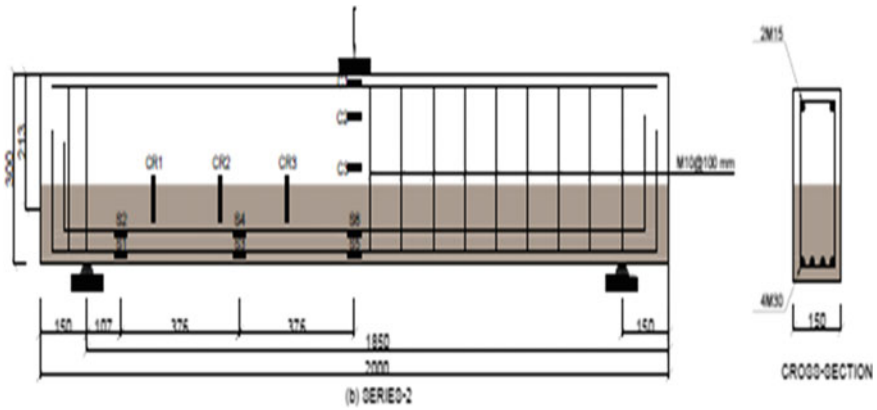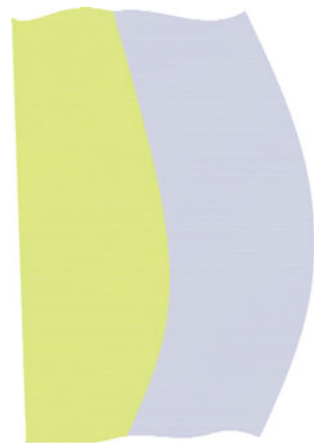**Fig. 2** Two layered lining concrete in situ stress [11]

Fig. 3 Testing procedures and reinforcement details of beam specimen [13]

Fig. 4 Non-uniform distribution of fibers in a cross-section of a bamboo culm (Amada et al. 2001)

[16] experimented with thin slabs in two different concrete mixes of same densities (Fig. 5) and found the instability due to fresh stage because of weight difference was minimized. Kieback et al. [17] and Maalej et al. [18] experimented with the notions of functionally grading and found its wide use in the area of energy aerospace and Bio-engineering. Mahamood et al. [19], Jha et al. [20] and Markworth et al. [21] analyzed functionally graded materials and reported that it can be used in a pressure vessel and space applications. Koijumi [22] and Kawasaki et al. [23] have reported extensive use of functionally graded concrete as a thermal barrier and thermal gradients respectively. Nature is reported to be the mother of concept functionally graded materials. However, functionally graded concrete finds very little attention in the field of concrete construction. The main reason behind this is the relatively more cost of concrete and the lack of efficient methods to detect functionally graded concrete

(FGC) elements. Presently, technological advancements have contributed more to optimize the use of the FGC element.

2 Principles and Methodology

This paper deals with the categorization of non-homogeneous concrete based on the topology of layered concrete shown in Fig. 5.

Layered concrete

Layered non-homogenous concrete with a layered structural differentiation in the configuration is presented in Fig. 6. Many experiments have been conducted on the functional benefits of layered concrete on double-layered horizontally cast elements of the prism form.

   The functional advantages have been studied by various researchers in two-layered prismatic specimens cast horizontally with or without longitudinal reinforcements. Details of specimens, objectives and casting methodology are presented in Table 1.
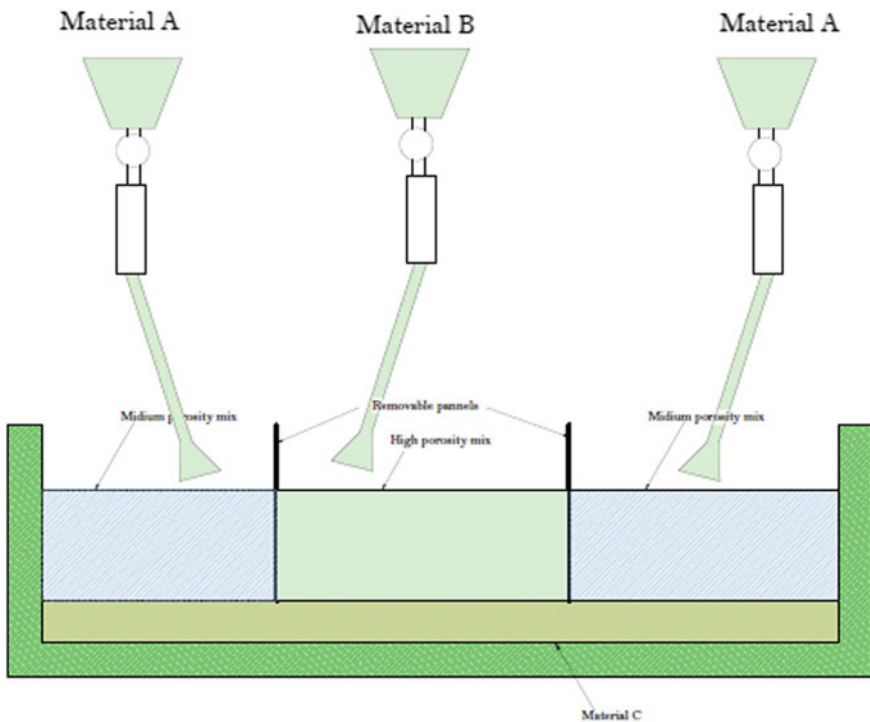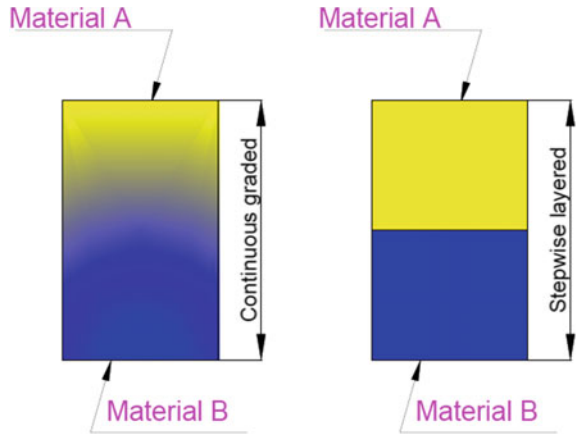

Fig. 5 Linear concrete gradation methods adopted by Heinz et al. [16]

Fig. 6 Diagrammatic presentation of continuous graded and layered concrete

Through detailed research in the field of layered concrete beams, it has been found out that careful computation of mixture ratio can improve the performance of concrete. A double-layered unreinforced concrete beam having regular concrete in the top and high volume fly-ash concrete (HVFC) in the bottom layer was prepared and studied by Bajaj et al. [31] as presented in Fig. 7. He concluded that tensile stresses near the area having fly-ash of 35% in HVFC permits the less requirement of cement. Nes and Qverli [24] brought up a dual-layered reinforced structure having normal density concrete at top and low-density fiber-reinforced at the bottom layer. It was concluded that in contrast to a homogeneous sample of regular concrete this sample had a weight 42% lessened by itself. Functionally grading can be used to improve the breaking property of unreinforced concrete. Roesler et al. [32] analyzed the breaking of fiber based reinforced concrete and regular concrete. He cut a notch of thickness having 1/3rd of the sample into the bottom surface to carry out the crack mouth opening displacement (CMOD) test. Functionally graded concrete also enhances the longevity of reinforced concrete structures, whose most common problem is the corrosion in steel reinforcement as reported by Ahmad [33] and Papadakis [34]. The authors studied that the major causes of corrosion are concrete carbonation and absorption of hostile substances like chlorides and acid gasses. Ahmad [33] and Lepech [35] experimented that the absorption of hostile matters can be detained by reducing the permeability in concrete, range of crack and its width. The following longevity properties are basically required in the bordering areas of the spatial element as these regions are more exposed to the hostile substances.

The concrete of Low permeability at its outer layer was scrutinized by Dias et al. [36] to shield steel reinforcement. Particularly, they explored the correlation among the width of shielding layer and the co-sequencing to protect the corrosion. Wen et al. [37] experimented with chloride absorption test and tests on corrosion of steel bar conducted on reinforced concrete samples having shield covers of different widths as presented through Fig. 8. Li and Xu [25] analyzed the flexural characteristics of double-layered RC beams with a base layer of ultra-high toughness cementitious

Table 1 Research data of the past researchers

References	Specimen type	Specimen size in mm	Top/parallel layer material	Bottom/parallel layer material	Objective	Improvement in target	Casting mould and equipment	Methodology adopted
Nazari et al. [9]	Prisms	100 × 100 × 650 (b × h × l)	G2	G1	Stress intensity factor and fracture toughness	Experimental stress intensity is more than analytical in FGG structures	Prism moulds and table vibrator for 15 Hz	Horizontally step wise layered one after another. EDS analysis for finding of graded layer
Nazari et al. [8]	-do-	-do-	-do-	-do-	Fracture strength. Modulus of elasticity and surface energy of FGG structure	Improvement in crack configurations is + 3.23%, in flexure + 1.72% and in surface energy + 1.45%	-do-	Testing with two configurations, and EDS analysis. CP1 exhibit more results than CP2
Ning et al. [11]	400 and 300 mm dia concrete hollow cylinder	Inner layer dia-300 Outer layer dia-500	Mixture of $E_1, \mu 1, \sigma_{c1}$ (normal concretse)	Mixture of E_2, μ_2, σ_{c2} (fiber reinforced concrete)	Stress distribution improvement in composite concrete lining by changing the mechanical properties	Improvement in elastic limit as well as poisson's ratio. 25% more in pressure bearing data	Cylindrical mould of 300 mm and 400 mm dia and 2300 mm long	Inverse analysis for stress distribution under hydrostatic load of 30 MPa and axial load by six 300-ton jacks

(continued)

Table 1 (continued)

References	Specimen type	Specimen size in mm	Top/parallel layer material	Bottom/parallel layer material	Objective	Improvement in target	Casting mould and equipment	Methodology adopted
Nazari et al. [10]	Cubes	50 × 50 × 50 mm	G2	G1	Compressive strength and role of graded layer	Compressive strength of graded specimens more than analytical. It is just 12.5 and 33% more than G1	Cube moulds and table vibrator for 15 Hz	Measurement of compressive strength and comparison it with result of rule of mixtures
Kurugol et al. [12]	Prism	100 × 100 × 400 mm (b × h × l)	FL/PLF	NL/PL	Modulus of elasticity and its relation with coarse aggregate and fiber reinforcement	MoE of 35.6, 36.8% obtained more in FRNC and FRLC respectively	Prism moulds of 100 × 100 × 400 mm	Parallel phase model game more results in MoE
Hussein et al. [13]	Prism with reinforcement	1284 × 150× 300 mm	NSC/HSC	UHPFRC	Increment of shear strength and flexure strength	Composite structure strength posses 1.7–2.0 times more strength than single layered of NSC/HSC	Beam mould of 1284 × 150 × 300 mm and needle vibrator	Composite beams of UHPFRC-NSC/HSC gave more results

(continued)

Table 1 (continued)

References	Specimen type	Specimen size in mm	Top/parallel layer material	Bottom/parallel layer material	Objective	Improvement in target	Casting mould and equipment	Methodology adopted
Kieback et al. [17]	Cube	$150 \times 150 \times 150$ mm	M_{20}/M_{30} in parallel	Fly-Ash blendedconcrete of M_{20}/M_{30} in parallel	Increment of compressive strength and bond strength	Compressive strength obtained 18% more and bond strength is more in comparison with normal concrete	Cube mould of $150 \times 150 \times 150$ mm and table vibrator of 15 Hz	Cube of 75 mm $M_{20}/M_{30} + 75$ mm FA blended concrete gave ultimate strength
Maalej et al. [18]	Prism with reinforcement	$102 \times 152 \times 914$ mm (b × h × l)	Normal concrete	Engineered cementitious concrete (51 mm thick)	Improvement in durability	Crack width reduction obtained 80%	Prism mould of $914 \times 152 \times 102$ mm and needle vibrator	Smaller crack width due to layered concrete
Nes et al. [24]	Beam with reinforcement	$3000 \times 150 \times 250$ mm (l × b × h)	Normal concrete	Fiber-reinforced light weight concrete (FRLWC) (200 mm thick) (200 mm thick)	Reduction in weight	Achievement of weight reduction about 42%	Beam mould of $3000 \times 150 \times 250$ mm and needle vibrator	Measurement of weight reduced due to use of light weight fiber

Table 1 (continued)

References	Specimen type	Specimen size in mm	Top/parallel layer material	Bottom/parallel layer material	Objective	Improvement in target	Casting mould and equipment	Methodology adopted
Li et al. [25]	Beam with reinforcement	2000 × 120 × 120 mm (l × b × h)	Normal concrete	Ultra-High-Toughness cementitious concrete (15/20/25/35/50 mm thick)	Improvement in flexure, ductility and durability with cost minimization	Improvement of strength about 30% with 80% less crack width with 70% increase in deflection	Beam mould of 2000 × 80 × 120 mm and needle vibrator	Measurement of flexure and crack width with related to deflection in layered concrete using UHTCC
Chan et al. [26, 27]	Prism	500 × 150 × 150 mm (l × b × h)	Recycle aggregate concrete (RAC)/FRC	Normal concrete/FRC	Energy content and cost minimization	Achievement in carbon content reduction about 48%, cost reduction about 43% with 21% strength reduction	Prism mould of 500 × 150 × 150 mm and table vibrator of 15 Hz	Measurement in carbon reduction and cost minimization
Liu et al. [28]	Prism	700 × 80 × 150 mm (l × b × h)	Fiber reinforced concret/Normal concrete	Fiber reinforced concret/Normal concrete (100 mm thick)	Improvement in fracture	Relative fracture energy improved up to 108% with 2 mm displacement	Prism mould of 700 × 80 × 150 mm and table vibrator of 15 Hz	Measurement of fracture stiffness

(continued)

Table 1 (continued)

| References	Specimen type	Specimen size in mm	Top/parallel layer material	Bottom/parallel layer material	Objective	Improvement in target	Casting mould and equipment	Methodology adopted
Maalej et al. [29]	Beam with reinforcement	2500 × 210× 240 mm (l × b × h)	Normal concrete	Ductile fiber reinforced concrete (DFRCC) (45 mm thick and more)	Improvement in durability	Steel loss in more time about 70% for achievement to a recommended level	Beam mould of 2500 × 210 × 240 mm and needle vibrator	Measurement of time required for steel loss
Naghibdehi et al. [30]	Beam	1350 × 300 × 100 mm (l × b × h)	Steel FRC/polypropylene fiber RC	Steel FRC/polypropylene fiber reinforced concrete(50 mm thick)	Strength improvement with less cost	Fracture toughness increases up to 480%	Beam mould of 1350 × 300 × 100 mm and vibrator	Measurement of fracture toughness
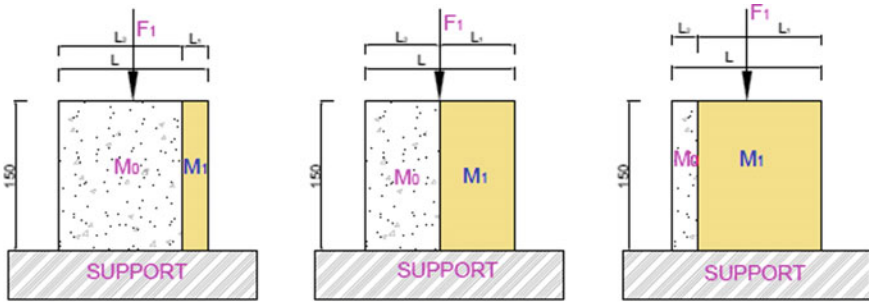
Fig. 7 Double layered concrete specimens with normal concrete and HVFAC [31]
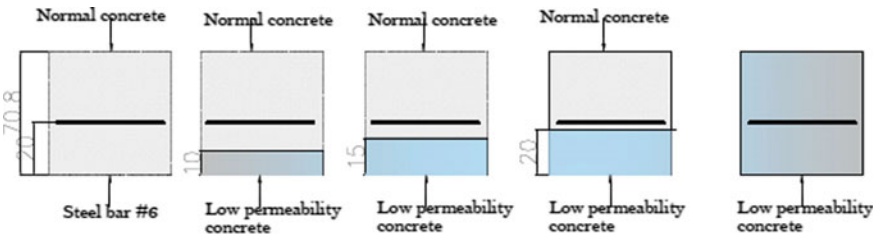

Fig. 8 Homogeneous normal-concrete, 10 mm/15 mm/20 mm thick protective layer and homogeneous low permeability concrete layers in reinforced concrete specimens [37]

composite (UHTCC) and the upper layer of regular concrete. Testing was done on beams of the various base widths. Such beams showed enhanced ductility and load-resisting capacity and compared to regular concrete. Samples having a base layer of thickness 35 mm showed crack depth below 0.5 mm, 30% more load-bearing ability and 70% more deformation capacity. There were no notable benefits in ductility and crack on RC beams having the wider UHTCC layer. Therefore, it was concluded the maximum thickness of UHTCC cover to be above the reinforcement. These showed that the application of mixtures having low in permeability and various cracking functions contributes to the longevity of the spatial elements by detaining the entrance of hostile matters.

An investigation on the behavior of double-layer unreinforced concrete using various materials was done by Han et al. [38] which is presented in Fig. 9. He found that if two mixtures of different stiffness and compressive strength are utilized together then the strength of the resulting specimen is similar to the strength of the weakest material whereas its stiffness is in between the stiffness of both mixtures. Heinz et al. [16] tried to understand the effect of reinforced concrete substances made up of layers along longitudinal and cross-sectional direction of various mixtures to reduce the cement content as well as the net weight of concrete beams. The density was modified and the cement amount was further reduced by using cement mixtures of different porosities, the inclusion of foam and by using low mass mixtures. The

Fig. 9 Lateral and cross-sectional view of unreinforced concrete cylinder [38]
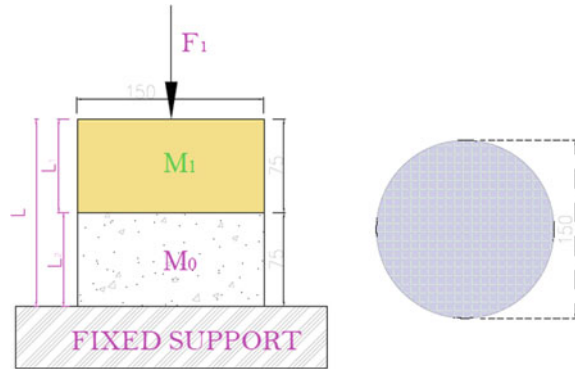
concluded results exhibited that the computed flexural and shear resistance values were fulfilled by the layered beam with a 34% reduced weight.

3 Casting Technology

Layered concrete substances are categorized into two main classes based on casting methods such as the Fresh-on-hardening method and the Fresh-on fresh method.

(a)   Fresh-on-hardening method:

In fresh-on-hardening methods as the name suggests there is an addition of a new layer of concrete only when the previous layer has hardened. It is generally found in the precast concrete plants where the unmoved concrete layer is added on the precast part to get complex structural members. It is used to enhance the properties of spatial elements in areas exposed to mechanical stresses. Utilization in ultra-high performance fiber reinforced concrete (UHPFRC) which increases the strength and longevity of bridge decks was studied and reported by Silfwerbrand [39] and Denarie et al. [40]. Graybeal [41] reported that this method is also used to get functionally gradation of the interface between two hardened elements. To connect the precast elements, concrete mixtures having high performance properties are mainly used in-situ to qualify the basic requirements. Fresh-on-hardened techniques on concrete helps in the exact monitoring of each interface while preparation. Neville [42] studied that it makes simpler by the utilization of a single concrete mixture to produce layered components. Despite these it has a limitation of greater tome consumption as a new layer is cast only after the previous layer has hardened. It also possesses a disadvantage in terms of drying shrinkage which can achieve a value up to 4×10^{-3}, with the development of the volume within the first few months of drying. There is also a risk of a poor bond between the layers.

(b)   Fresh-on fresh method:

In the fresh-on-fresh casting method, there is a simultaneous casting method and hardening of several concrete mixtures. Many researchers today are now being held on the fresh-on-fresh casting techniques. It is further categorized into two classes: (i) Horizontal layers, (ii) Vertical layers.

(i)   Horizontal layers:

Coussot [43], Tattersall [44] and Banfill [45] experimented that while fresh concrete acts like a yield stress fluid in which the threshold shear stress is very weak and hence doesn't allow the materials to move, rather fill the mould. This has helped in preparation of non-homogenous concrete elements by pouring layer wise horizontally. The factors such as mix compatibility, deposition method, rheology, vibration process, casting sequence and time between castings of each layer affect the stability of the component in both wet and hardened state.

(ii)   Vertical layers:

There is very little discussion using fresh-on-fresh methods for casting vertical layers. These depend on provisional panels between two vertical layers. The factors such as height, mixture density and rheology affect the stability of the vertical layer mixture elements. Fresh-on-fresh pouring methods have benefit of very little time consumption. There also exists a good bond among the layers, though, a challenge faced in the utilization of fresh-on-fresh concrete is the how to check on the flow of local concrete at interface among the components at the fresh condition of concrete. Many analysts Chan et al. [26, 27], Maalej et al. [18] have found a resolution to this problem by having a time gap of 20 to 60 min in between mixing and developing two layers. Maimouni et al. [46] and Torelli et al. [47] studied that there is a chance of local concrete flow when the stiffness of the mixtures are quite weak to resist the shear stresses. A vertical drawback for the use of the fresh-on-fresh pouring method is the absence of well-known calculative and analytical techniques. Moreover, in vertical layers, there is a vital problem in casting layers as their interfaces crosses the reinforcing bars. The utilization of provisional plates causes horizontal arrangements which may lead to an interface after panel removal. Therefore further experiments and analysis in these fields are required to sort out the drawbacks.

4   Design and Analysis at Fresh and Hardened State

The intrinsic physiographical complication of Functional Graded Concrete elements is having the analytical challenges and influences on specific design on both fresh and hardened stage of concrete.

Fresh state behaviour:

The growth of shear stresses in regions where structural differences in the material composition are related to material density there is a flow of heavier materials under lighter materials which is called as global instability in the fresh state as shown in Fig. 10. Roussel [48] dealt with exact knowledge of the association of the density of materials, rheological properties, global instability and geometry is important to check the fresh stage behavior of FGC and related manufacturing methods. In the production of homogeneous concrete elements, the fresh stage properties of the mixture are modified to the desired pouring technique. Torelli et al. [47] experimented that mixtures for 3D printing are fluent enough to be pumped and expelled out of the nozzle but stiff enough to bear their own weight. Torelli and Lees [49] studied the universal unreliability process in layered of FGC. Tattersall et al. [50, 44] studied that in regular concrete casting, the material flows to fill a mould which is gained by applying vibration in stiff concretes. Vibration provisionally reduces the yield stress of fresh concrete. Buswell [51] experimented that excess vibration can lead to local instabilities like segregation. But if the material is sufficiently smooth to move under its own weight then vibration is not required. These substances are known as self-compacting concrete (SCC). In the matter of concrete spraying, the mixture chosen need to be sufficiently smooth to be pumped and sprayed but sufficient stiff to keep away from local uncertainty occurrences. In the case of 3D printing, the fresh state material properties are cautiously modified. The scientists explored the basic problem of stability of concrete prism in fresh state made up of two vertical layers as shown in Fig. 11. It was found that there is an enhancement of stability in fresh
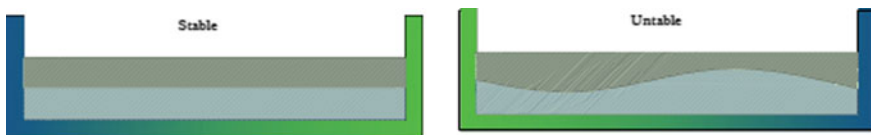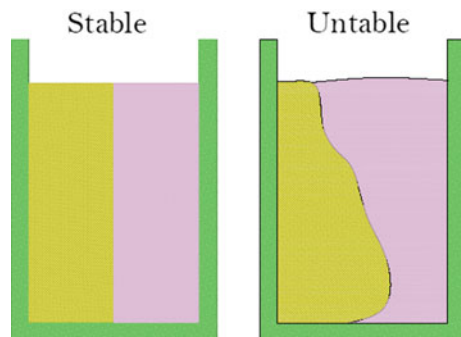

Fig. 10 Diagrammatical illustration of stable and unstable horizontal layered concrete by Roussel [48]

Fig. 11 Diagrammatical illustration of stable and unstable vertical layered concrete by Roussel [48]

state of two concrete columns with the growing amount of stresses in yielding of two materials and reducing the variability of density. It also showed that the plastic approach can be applied to numerous physiographic.

Harden state behaviour:

CEB-FIP model code for concrete structures [52] and Fib model code [53, 54] decided that layered concrete elements are studied utilizing a stepwise variation in substance configuration which helps in the easier analysis of material properties. Moreover, the popular utilization of layered techniques in concrete precast element construction resulted in the growth of the quality of structural design of layered components. Evangelista et al. [55] and Park et al. [56] studied the material configuration by classifying different homogeneous properties to separate class of finite elements that shows a separate layer.

5 Experimental Results

The details of material used in the various specimen are presented in Table 2 and different mixes used by the previous authors are presented in Table 3. The experimental and theoretical compressive strength of specimens as reported by the authors Nazari and Sanjayan [9, 8, 10] are presented in Fig. 12, the compressive strength of specimens used by Ning et al. [11] and Bajaj et al. [31] in Fig. 13 and Hussein et al. [13] and Chan et al. [26, 27] Fig. 14. The modulus of elasticity (MOE) has been presented in Fig. 15 and 16.

6 Conclusion

The main objectives of FGC are to improve the structural behavior, design strength, controlling the fractural behavior and failure of the structure. FGC structure is associated with the reduction of energy consumption, reduction in carbon emissions and improved thermal performance as an insulating concrete. Steel corrosion is delayed in FGC due to low permeability in peripheral regions. Crack is minimized due to less hydration of heat in mass structures. There is the possibility of savings up to 40% of materials cost through FGC. That strength of FGC is affected by the position of the graded layer and the thickness of constituent layers. On account of their popular use, fresh-on-harden pouring techniques are advanced while fresh-on-fresh pouring techniques are slowly finding their wide use in the field of civil engineering. The fresh-on-fresh concrete has the merit of having a strong bond among the layers and lessening the production time. But they do have a disadvantage of checking their deformations in the fresh state. More analysis is required in the field of fresh-on-fresh concrete to assure an increase in manufacturing. There is also a need of increased exploration in the area of vertically layered, horizontally layered and continuously

Table 2 Details of materials used in specimens

Ref. No	Mix specimen type	Cement in kg	Sand	Polymer in kg	Aggregate in kg	L.W. aggregate in kg	Fly ash type I in kg	Fly ash type II in kg
Nazari et al. [8,9]	G1						1286	
-do-	G2							1315
-do-	FGG1						257	1052
-do-	FGG2						514	789
-do-	FGG3						772	526
-do-	FGG4						1029	263
Ning et al. [11]	M1	390	585		1325			
-do-	M2	467	702		1040			
-do-	M3	546	819		795			
-do-	M4	686	1029					
-do-	M5	686	1029					
-do-	M6	686	1029					
Kurugol et al. [12]	N	350	795		971			
-do-	L	350	795		971/701.2/431.6/161.8/0	0.0/70.9/141.8/212.7/255.2		
-do-	P	350	795	0.0/20.21/40.42/60.63/80.85	971	255.2		

(continued)

Table 2 (continued)

Ref. No	Mix specimen type	Cement in kg	Sand	Polymer in kg	Aggregate in kg	L.W. aggregate in kg	Fly ash type I in kg	Fly ash type II in kg
-do-	F	350	795		971			
-do-	PL	350	795	0.0/20.21/40.42/60.63/80.85		255.2		
-do-	LF	350	795		950/686.6/422.6/0.0	0.0/69.4/138.8/249.9		
-do-	FL	350	795			255.2/253.4/251.7/249.9/248.1		
-do-	PLF	350	795	0.0/20.21/40.42/60.63		249.9		
Hussein et al. [13]	D	712	1020		211	231 (silica fume)		

Ref. No	Alkali activator in kg	Sodium silicate in kg	NaOH solution in kg	NaOH flakes in kg	Water reducer in kg	Fiber in kg	Water in kg
Nazari et al. [8,9]	643	459	184	103			81
-do-	658	470	188	105			83
-do-	655	468	187	105			82
-do-	652	466	186	104			82
-do-	649	464	185	104			81
-do-	646	461	185	104			81
Ning et al. [11]					8.775	8 (polypropylene)	156
-do-					10.508	–	187

(continued)

Table 2 (continued)

Ref. No	Alkali activator in kg	Sodium silicate in kg	NaOH solution in kg	NaOH flakes in kg	Water reducer in kg	Fiber in kg	Water in kg
-do-					12.285	4	218
-do-					17.493	4	255
-do-					17.493	8	255
-do-					17.493	12	255
Kurugol et al. [12]							192.5
-do-							192.5
-do-							192.5/173.25/154/13.75/115.5?
-do-						(steel) 0/19.6/39.25/58.9/78.5	192.5
-do-						–	192.5/173.25/154/134.75/115.5
-do-						58.9	192.5
-do-						0.0/19.6/39.25/58.9/78.5	192.5
-do-						58.9	192.5/173.25/154/134.75
Hussein et al. [13]					30.7 (superplasticizer)		109

Table 3 Specimen details

Specimen	Authours and year			
	Nazari et al. [8–10]	Ning et al. [11]	Hussein et al. [13]	Bajaj et al. [31]
G1	G1 (100)%			
G2	G2 (100)%			
FGG1	G1 (80)% + G2 (20)%			
FGG2	G1 (60)% + G2 (40)%			
FGG3	G1 (40%) + G2 (60)%			
FGG4	G1 (20)% + G2 (80)%			
M1		M1 (100)%		M1 (100)%
M2		M2 (100)%		M2 (100)%
M3		M3 (100)%		M3 (100)%
M4		M4 (100)%		M4 (100)%
M5		M5 (100)%		M5 (100)%
M6		M6 (100)%		M6 (100)%
NS			Normal strength concrete (100%)	
HS			High strength concrete (100%)	
UN1			UHPFRC with 1% fiber + Normal strength concrete (N + U)	
UN1.5			UHPFRC with 1.5% fiber + Normal strength concrete (N + U)	
UN2			UHPFRC with 2% fiber + Normal strength concrete (N + U)	
UH1			UHPFRC with 1% fiber + High strength concrete (H + U)	
UH1.5			UHPFRC with 1.5% fiber + High strength concrete (H + U)	

Table 3 (continued)

Specimen	Authours and year			
	Nazari et al. [8–10]	Ning et al. [11]	Hussein et al. [13]	Bajaj et al. [31]
UH2			UHPFRC with 2% fiber + High strength concrete (H + U)	
M7				M7 (100)%
M8				M8 (100)%
S1				M1 (83.33)% + M2 (16.67)%
S2				M1 (50)% + M2 (50)%
S3				M1 (16.67)% + M2 (83.33)%
S4				M1 (83.33)% + M3 (16.67)%
S5				M1 (50)% + M3 (50)%
S6				M1 (16.67)% + M3 (83.33)%
S7				M1 (83.33)% + M4 (16.67)%
S8				M1 (50)% + M4 (50)%
S9				M1 (16.67)% + M4 (83.33)%
S10				M5 (83.33)% + M6 (16.67)%
S11				M5 (50)% + M6 (50)%
S12				M5 (16.67)% + M6 (83.33)%
S13				M5 (83.33)% + M7 (16.67)%
S14				M5 (50)% + M7 (50)%
S15				M5 (16.67)% + M7 (83.33)%
S16				M5 (83.33)% + M8 (16.67)%
S17				M5 (50)% + M8 (50)%

(continued)

Table 3 (continued)

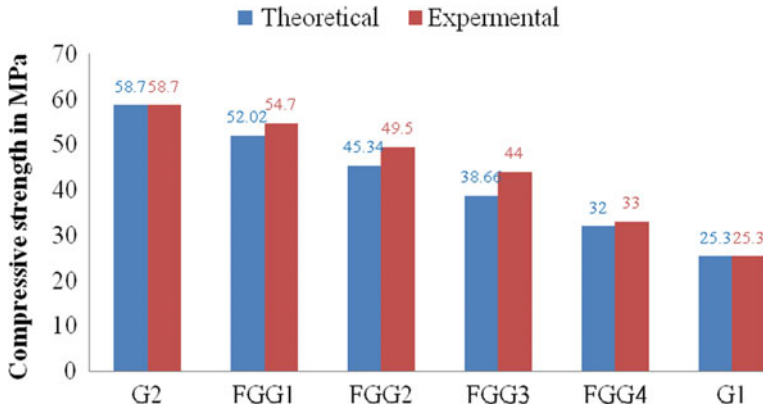| Specimen	Authours and year			
	Nazari et al. [8–10]	Ning et al. [11]	Hussein et al. [13]	Bajaj et al. [31]
S18				M5 (16.67)% + M8 (83.33)%

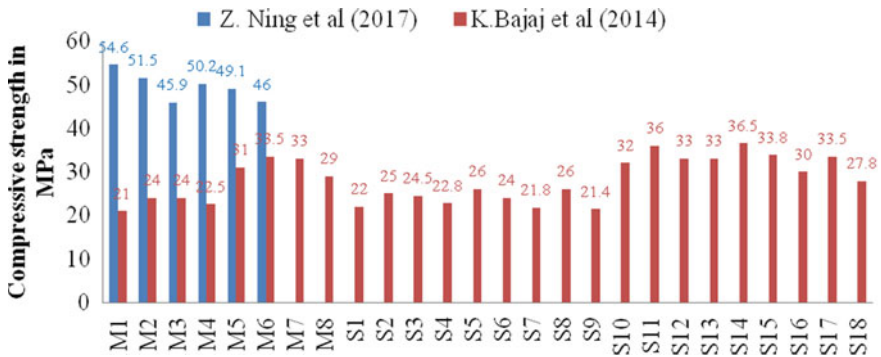**Fig. 12** Compressive strength [8–10]

Fig. 13 Compressive strength [11, 31]

grade concrete. The expansion of elementary logical methods to model FGC would unfasten the hurdle for execution in the construction industry and bring an alteration in essence towards cement reduction.
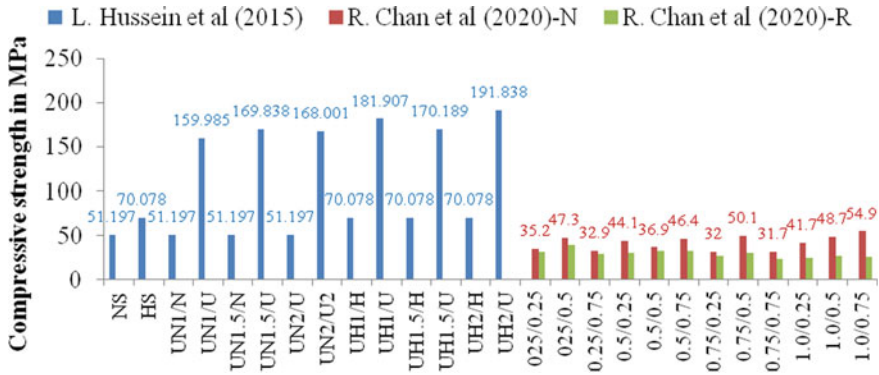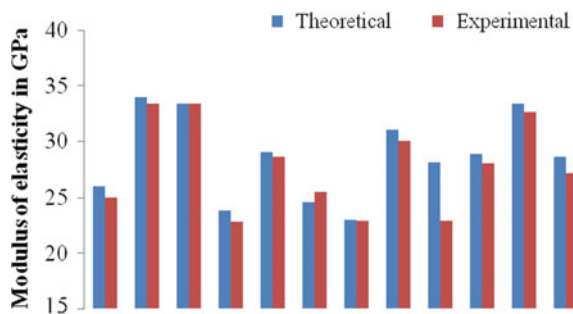
Fig. 14 Compressive strength [13, 26, 27]
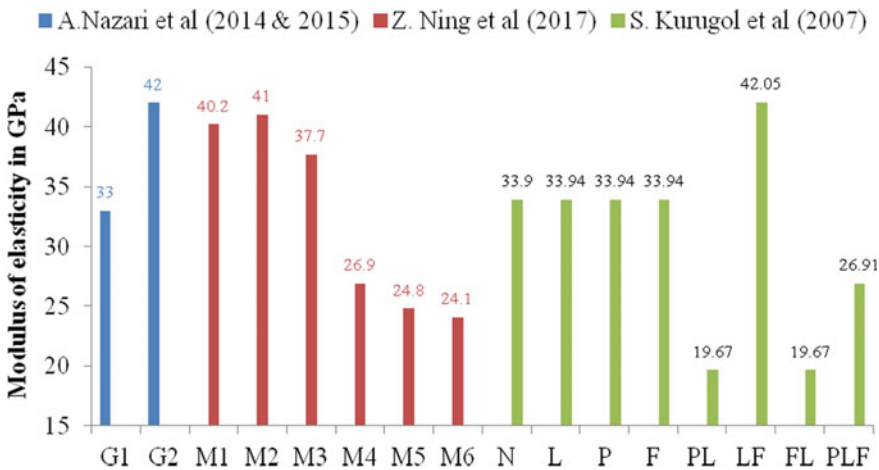
Fig. 15 Modulus of elasticity (Nazari et al. 2014, 2015) [11, 12]

Fig. 16 Modulus of elasticity [31]

References

1. U.S. Geological Survey (2015) Mineral commodity summaries; Cement. http://mineral.s.usgs.gov/mineral.s/pubs/comodity/cement/. U.S. Geological Survey
2. Farsana C, Das BB, Snehal K (2020) Influence of fineness of mineral admixtures on the degree of atmospheric mineral carbonation. In: Smart technologies for sustainable development. Springer Publications, pp 117–136
3. Sahoo S, Das BB, Mustakim S (2017) Acid, alkali and chloride resistance of concrete composed of low carbonated fly ash. J Mater Civ Eng ASCE 29(3)
4. Snehal K, Das BB, Akanksha M (2020) Early age, hydration, mechanical and microstructure properties of nano-silica blended cementitious composites. Constr Build Mater (Elsevier) 233
5. Das BB, Pandey SP (2011) Studies on influence of fineness of fly ash on the carbonation and electrical conductivity of concrete. J Mater CivEng ASCE 23(9):1365–1368
6. Snehal K, Das BB (2021) Application of Andreassen and modified Andreassen model on cementitious mixture design: a review. In: Recent developments in sustainable infrastructure. Springer, pp 729–750
7. Snehal K, Das BB (2019) Mechanical and permeability properties of hybrid fibre reinforced porous concrete. Indian Concr J 93(1):54–59
8. Nazari A, Sanjayan JG (2014) Modelling of fracture strength of functionally graded geopolymer. Constr Build Mater 58:38–45
9. Nazari A, Sanjayan JG (2015) Stress intensity factor against fracture toughness in functionally graded geopolymer. Arch Civ Mech Eng 15:1007–1016
10. Nazari A, Sanjayan JG (2015) Compressive strength of functionally graded geopolymers: role of position of layers. Constr Build Mater 75:31–34
11. Ning Z, Aizhong L, Charlie C, Li, Zhou J, Zhang X, Wang S, Chen X (2017) Support performance of functionally graded concrete lining. Constr Build Mater 147:35–47
12. Kurugol S, Tanacan L, Ersoy HY (2007) Young's modulus of fiber-reinforced and polymer-modified lightweight concrete composites. Constr Build Mater
13. Hussein L, Amleh L (2015) Structural behaviour of ultra-high performance fiber reinforced concrete-normal strength or high strength concrete composite members. Constr Build Mater 93:1100–1116
14. Nogata F, Takahashi H (1995) Intelligent functionally graded material: bamboo. Comps Eng 5:743–751
15. Amada S, Unda OS (2001) Fracture properties of bamboo, J Compos Part B Engg 32:451–459
16. Heinz P, Herrmann M, Sobek W (2012) Production method and application of functionally graded components in construction (Herstellungsverfahren und Anwendungsbereiche fur functional gradierte Bauteile im Bauwesen). Fraunhofer IRB Verlag, Stuttgart
17. Kieback B, Neubrand A, Riedel H (2003) Processing techniques for functionally graded materials. Mater Sci Eng A 362:81–106
18. Maalej M, Li VC (1995) Introduction of strain-hardening engineered cementitious composite in design of reinforced concrete flexural members for improved durability. ACI Struct J 92:167–176
19. Mahamood RM, Akinlabi ET (2017) Functionally graded materials. Springer. https://doi.org/10.1007/978-3-319-53756-6
20. Jha DK, Kant T, Singh RK (2013) A critical review of recent research on functionally graded plates. Compos Struct 96:833–849. https://doi.org/10.1016/J.COMPSTRUCT.2012.09.001
21. Markworth AJ, Ramesh KS, Parks WP (1995) Modelling studies applied to functionally graded materials. J Mater Sci 30:2183–2193. https://doi.org/10.1007/BF01184560
22. Koijumi M (1997) FGM activities in Japan. Compos Part B Eng 28:1–4. https://doi.org/10.1016/S1359-8368(96)00016-9
23. Kawasaki A, Watanabe R (1997) Concept and P/M fabrication of functionally gradient materials. Ceram Int 23:73–83. https://doi.org/10.1016/0272-8842(95)00143-3
24. Nes LG, Qverli JA (2016) Structural behaviour of layered beams with fiber-reinforced LWAC and normal density concrete. Mater Struct 49:689–703

25. Li Q, Xu S (2009) Experimental investigation and analysis on flexural performance of functionally graded composite beam crack-controlled by ultra-high toughness cementitious composite. Sci China Ser E: Technol Sci 52:1648–1664
26. Chan R, Liu X, Galobardes I (2020) Parametric study of functionally graded concrete incorporating steel fibers and recycled aggregates. Constr Build Mater 242:118180
27. Chan R, Liu X, Galobardes I (2020) Parametric study of functional.ly graded concrete incorporating steel fibers and recycled aggregates. Constr Build Mater 242:118186
28. Liu X, Yan M, Galobardes I, Sikora K (2018) Assessing the potential of functionally graded concrete using fibre reinforced and recycled aggregate concrete. Constr Build Mater 171:793–801
29. Maalej M, Ahmed SFU, Paramsivam P (2003) Corrosion durability and structural response of functionally-graded concrete beams. J Adv Concr Technol 1:307–316
30. Naghibdehi MG, Mastali M, Sharbatdar MK, Naghibdehi MG (2014) Flexural performance of functionally graded RC cross-section with steel and PP fibers. Mag Concr Res 66:219–233
31. Bajaj K, Shrivastava Y, Dhoke P (2014) Experimental study of functionally graded beam with fly ash. Inst Eng India Ser A 94(4):219–227
32. Roesler J, Paulino G, Gaedicke C, Bordelon A, Park K (2007) Fracture behavior of functionally graded concrete materials for rigid pavements. J Transp Res Board 40–49. Transportation Research Board of the National. Academies, Washington, D.C. https://doi.org/10.3141/2037-04
33. Ahmad S (2003) Reinforcement corrosion in concrete structures, its monitoring and service life prediction—a review. Cem Concr Compos 25:459–471. https://doi.org/10.1016/S0958-9465(02)00086-0
34. Papadakis VG (2000) Effect of supplementary cementing materials on concrete resistance against carbonation and chloride ingress. Cem Concr Res 30:291–299. https://doi.org/10.1016/S0008-8846(99)00249-5
35. Lepech M, Li VC (2005) Water permeability of cracked cementitious composites. Adv Civ Eng Mater Res Lab Univ Michigan
36. Dias CMR, Savastano Jr H, John VM (2010) Exploring the potential of functionally graded materials concept for the development of fiber cement. Constr Build Mater 24:140–146
37. Wen X, Tu J, Gan W (2013) Durability protection of the functionally graded structure concrete in the splash zone. Constr Build Mater 41:246–251
38. Han A, Gan BS, Pratama MMA (2016) Effects of graded concrete on compressive strengths. Int J Technol 7:732–740
39. Silfwerbrand J (1990) Concrete bond in repaired bridge decks. Concr Int 12:61–66
40. Denarie E, Bruhwiler E (2006) Tailored composite UHPFRC-concrete structures. In: Measuring, monitoring and modeling concrete properties: an international symposium dedicated to Professor Surendra P. Shah, Northwestern University, U.S.A. Springer, Dordrecht, pp 69–75. https://doi.org/10.1007/978-1-5104-3_8
41. Graybeal B (2014) Design and construction of field-cast UHPC connections. The United States Federal Highway Administration
42. Neville AM (1995) Properties of concrete, 4th and final edn
43. Coussot P (2014) Yield stress fluid flows: a review of experimental data. J Nonnewton Fluid Mech 211:31–49. https://doi.org/10.1016/j.jnnfm.2014.05.006
44. Tattersall GH, Baker PH (1988) The effect of vibration on the rheological properties of fresh concrete. Mag Concr Res 40:79–89. https://doi.org/10.1680/macr.1988.40.143.79
45. Banfill PFG (2006) Rheology of fresh cement and concrete. Rheol Rev 61–130. The British Society of Rheology
46. Maimouni JG, Lac E, Pringuey T, Boujlel J, Chateau X (2016) Rayleigh-Taylor instability in elastoplastic solids: a local catastrophic process. Phys Rev Lett 116. https://doi.org/10.1103/PhysRevLett.116.154502154502
47. Torelli G, Fernandez MG, Lees JM (2020) Functionally graded concrete: design objectives, production techniques and analysis methods for layered and continuously graded elements. Constr Build Mater 242:118040

48. Roussel N (2012) Understanding the rheology of concrete. Woodhead Publishing
49. Torelli G, Less JM (2019) Fresh state stability of vertical layers of concrete. Cem Concr Res 120:227–243. https://doi.org/10.1016/J.CEMCONRES.2019.03.006
50. Tattersall GH, Baker PH (1989) An investigation on the effect of vibration on the workability of fresh concrete using a vertical pipe apparatus. Mag Concr Res 41:3–9. https://doi.org/10.1680/macr.1989.41.146.3
51. Buswell RA, Leal de, Silva WR, Jones SJ, Dirren BJ (2018) 3D printing using concrete extrusion, a road map for research, J Cem Concr Res 112:37–49.
52. CEB-FIP (1990) Model code for concrete structures. Comite Euro-International. du Beton, Secretariate Permanent, Case Postale 88, CH-1015 Lausanne, Switzerland
53. fib. Model Code 2010—Final draft, vol 1. Fib Bull 2012;1
54. fib. Model Code 2010—Final draft, vol 2. Fib Bull 2012;2
55. Evangelista F, Roesler J, Paulino G (2009) Numerical stimulations of fracture resistance of functionally graded concrete materials. J Transp Res Board 122–131
56. Park K, Paulino GH, Roesler J (2010) Cohesive fracture model for functionally graded fiber reinforced concrete. Cement Concr Res 40:956–965

Approaches to Slope Stability Analysis Considering the Effects of Dilatancy and Strength Non-linearity: A Review

J. Nihar Ranjan, Benu G. Mohapatra, and Manal Alali

1 Introduction

Slope stability analysis is an important problem in geotechnical engineering. The widely used Limit Equilibrium Method (LEM) does not require the dilatancy angle [1] and is usually based on a linear Mohr–Coulomb failure criterion. However, studies by authors have pointed out the limitations of the LEM. These limitations include the possible kinematic inadmissibility of the solutions and an inaccurate Factor of Safety (FoS) [1–4]. In comparison, the Limit Analysis Method (LAM) based on Upper Bound (UB) and Lower Bound (LB) solutions can bracket the true FoS [2, 3, 5]. LAM can be used only if the flow rule is associated ($\psi = \phi$), while practically, soils do not always follow the associated flow rule assumption [2, 5–9]. Strength reduction finite element analyses are increasingly being used in slope stability problems [2]. For these analyses, an associated flow rule overpredicts the factor of safety [1, 10] while a nonassociated flow rule may result in numerical problems if the friction angle is large and the dilatancy angle is very small [2, 11]. In such cases the FoS fluctuates making it difficult to determine a unique value.

The strength envelope nonlinearity of soils in σ-τ stress space is well known [12–18]. Using the linear Mohr–Coulomb strength assumption may result in unsafe assessment of slope stability [12–14, 17, 18]. The present paper reviews the works of previous authors on the effects of dilatancy and nonlinearity and approaches to incorporate these in slope stability analysis.

J. Nihar Ranjan · B. G. Mohapatra (✉) · M. Alali
School of Civil Engineering, KIIT Deemed to be University, Bhubaneswar, Odisha, India
e-mail: bmohapatrafce@kiit.ac.in

J. Nihar Ranjan
e-mail: 1943005@kiit.ac.in

2 Dilatancy and Slope Stability Analysis

2.1 Dilatancy

Dilatancy is the behaviour observed in soils whereby volumetric expansion occurs during shearing. It is usually measured in terms of the dilatancy angle ψ. Dilatancy angle ψ is given as the ratio of increase in volumetric strain to increase in major principal strain [18]

$$\tan \psi = \left(\frac{d\varepsilon_v}{d\varepsilon_1} \right) \tag{1}$$

where ε_v= volumetric strain, ε_1= major principal strain.

The dilatancy angle in the triaxial test is measured as [20]

$$\sin \psi = \frac{-d\varepsilon_v}{2d\varepsilon_a - d\varepsilon_v} \tag{2}$$

where $d\varepsilon_v$ = volumetric strain increment, $d\varepsilon_a$ = axial strain increment.

Dilatancy varies with relative density of the soil and becomes more significant for dense sands and overconsolidated clays. Bolton [21] gave an expression for maximum dilatancy angle

$$\psi_{max} = 0.3I_R [21] \tag{3}$$

where

$$I_R = I_D(10 - \ln p') - 1 \tag{4}$$

I_D is the relative density.

Andersen and Schjetne [20] determined the values of ψ_{max} based on Eq. 3 and compared it with empirically determined values for $p' = 150$ and 600 kPa as shown in Fig. 1.

Dilatancy affects the shear strength of soils thus playing an important role in the understanding and prediction of soil behaviour [10, 18].

2.2 Effects of Dilatancy

The dilatancy angle is not used in the traditional limit equilibrium method (LEM) based on Mohr–Coulomb strength criterion [1]. However, on account of several limitations in the LEM [1–4,21], the finite element strength reduction method and limit analysis method are being increasingly used for slope stability problems.
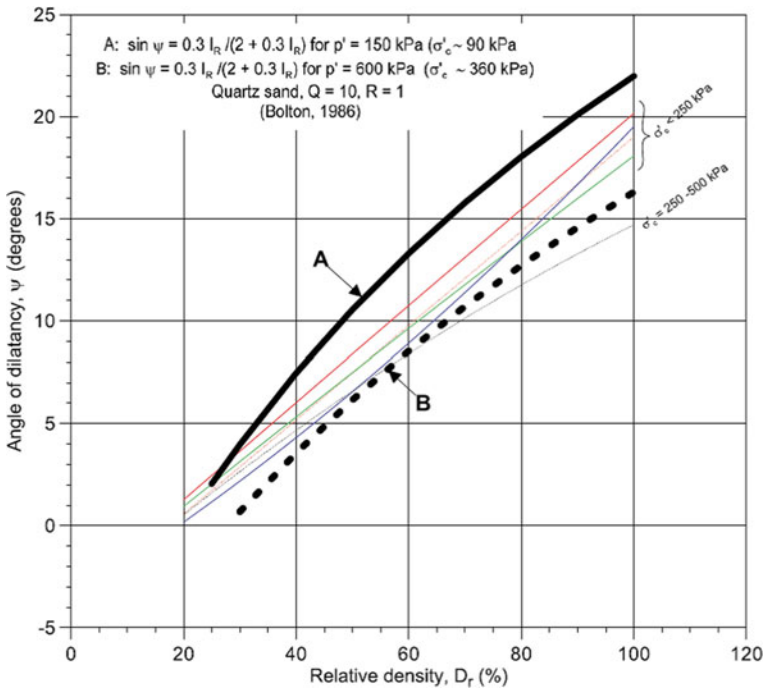
Fig. 1 Tangent dilatancy angle at peak shear stress compared with [21] by Andersen and Schjetne [20]

The limit analysis method is based on the normality condition or the associated flow rule [2, 5–9, 21]. For Mohr–Coulomb failure criterion, in case of an associated flow rule the velocity vector makes an angle of ϕ with the velocity discontinuity line or the rupture surface, where ϕ is the angle of friction for the soil. For the flow rule to be nonassociated the above angle becomes equal to ψ, where ψ varies between 0 and ϕ [3, 9, 24]. A nonassociated flow rule cannot be used in the traditional limit analysis. However, the associated flow rule assumption is not realistic and overpredicts the dilation of soil and safety condition of the slope [2, 5–10].

In a strength reduction finite element analysis based on Mohr–Coulomb yield criterion, the dilatancy angle does not significantly affect the solutions obtained because of the unconfined nature of the slope stability problems [24, 26]. But studies by authors showed that the effect of dilatancy angle becomes significant with high values of ϕ [11, 28]. As per Tschuchnigg et al. [11], the flow rule becomes significant at friction angles larger than 35°, while Tschuchnigg et al. [28] reported a range of 40°–45°. Using the associated flow rule ($\phi = \psi$) leads to overestimations, while setting $\psi = 0°$ gives conservative estimates [1, 10]. Using nonassociated flow rules in a 2D finite element analysis, as the degree of nonassociativity (ϕ-ψ) increased, Tschuchnigg et al. [11] reported numerical difficulties and fluctuating values of FoS as shown in Fig. 2.

Fig. 2 Predicted factor of safety [11]
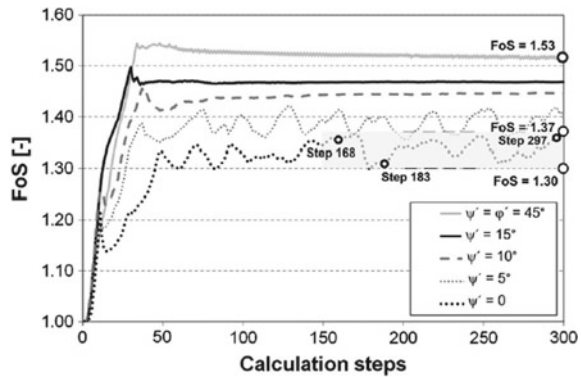
Lin et al. [1] investigated the effect of dilatancy angle on FoS using a 3D finite element model and compared the results with Tschuchnigg et al. [11]. As shown in Fig. 3, using the associated flow rule they observed fluctuations in FoS. They concluded that associated flow rule was not suitable for 3D finite element analysis.

Kumar [9] studied the effect of dilatancy on stability factor in the presence of pore-water. Based on data from Kumar [9], Fig. 4 shows the percentage reduction in stability factor when the flow rule is changed from associated to nonassociated ($\psi = 0°$), for slope of angle of 55°, at three different pore-water pressure ratios.

Ganjian et al. [30] investigated the effect of dilatancy angle on 3D safety factors for slopes under static and seismic conditions. Based on their work, Figs. 5 and 6 show the percentage reduction in FoS when the flow rule is changed from associated
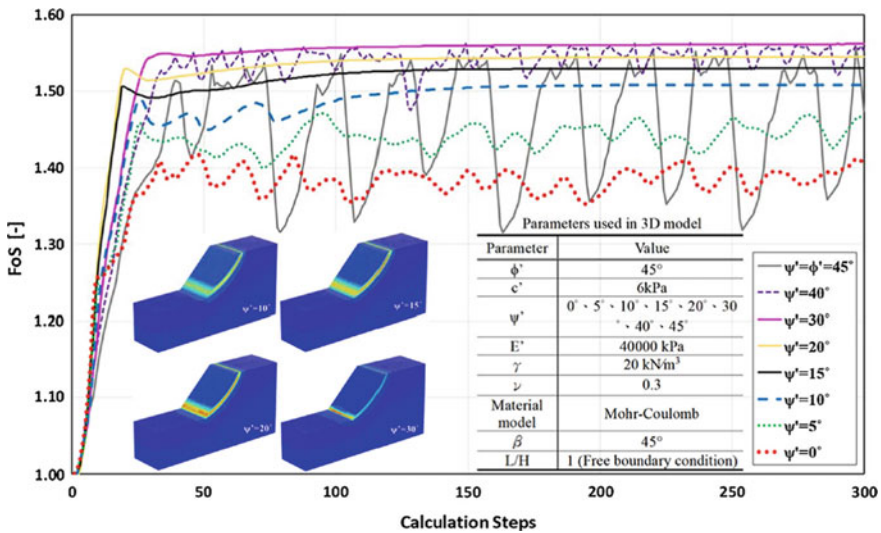

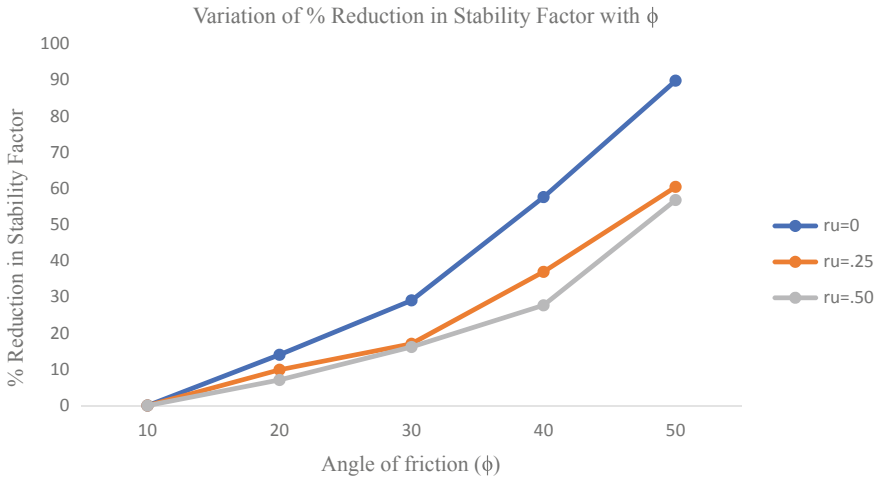**Fig. 3** Comparisons of 3D slope model FoS for different dilatancy angles [1]

Fig. 4 Effect of dilatancy on stability factor

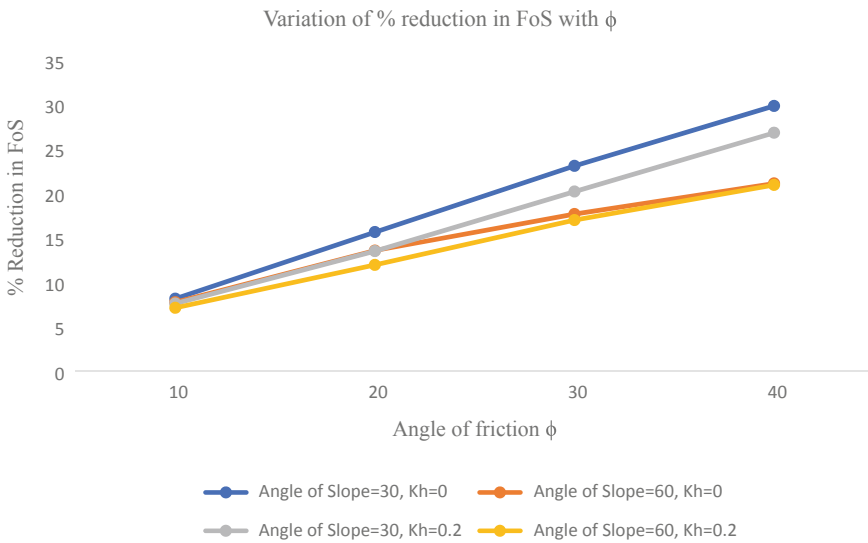**Fig. 5** Effect of dilatancy on 3D factors of safety, without local surcharge load on slope

to nonassociated ($\psi = 0°$). In Fig. 5 no local surcharge load on slope was considered, while Fig. 6 considers local surcharge load on slope. In Figs. 5 and 6, two slope angles 30° and 60° were considered under both static($k_h = 0$) and seismic($k_h = 0.2$) conditions.

Eskandarinejad and Shafiee [7] investigated the seismic stability of reinforced slopes considering nonassociated flow rule. Based on their work, Fig. 7 shows the
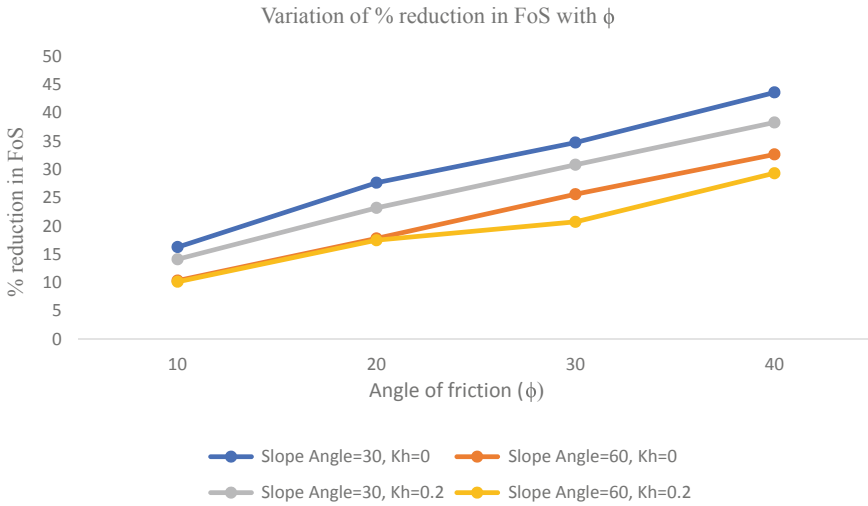
Variation of % reduction in FoS with ϕ

Fig. 6 Effect of dilatancy on 3D factors of safety, with local surcharge load on slope

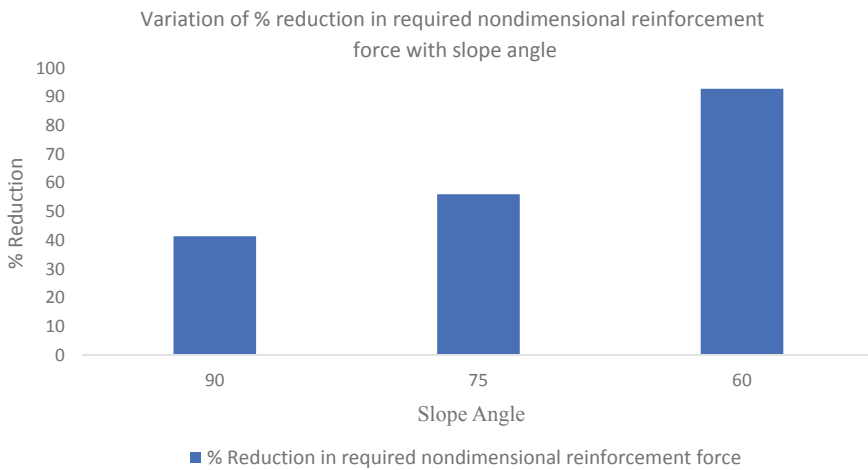Variation of % reduction in required nondimensional reinforcement force with slope angle

Fig. 7 Effect of dilatancy on required reinforcement force under seismic condition

percentage reduction in the required nondimensional reinforcement force when the flow rule is changed from nonassociated($\psi = 0°$) to associated, at friction angle of 45°. Three slope angles of 90°, 75° and 60° were considered in Fig. 7.

2.3 Incorporating a Nonassociated Flow Rule in Stability Analysis

Several researchers have worked in the area of incorporating nonassociated flow rule in limit analysis. In this regard, reduced effective strength parameters (c^*, ϕ^*) have been suggested to be used along with the associated flow rule to conduct limit analysis of slope stability problems [7, 8]. This method has been referred to as the Davis Approach in the literature [1, 2, 5, 11]. According to the Davis approach [11]

$$c^* = \beta c'$$
(5)

$$\tan \phi^* = \beta \tan \phi'$$
(6)

$$\beta = \frac{\cos \psi' \cos \phi'}{1 - \sin \psi' \sin \phi'}$$
(7)

where ϕ', c', ψ' are given parameters.

c^*, ϕ^* are reduced parameters.

β is the reduction factor.

The original Davis approach is applicable where the FoS is obtained in terms of the maximum load that can be applied for a given soil strength. For strength reduction approach to FoS modified Davis approaches have been recommended to be used [11]. The modified approaches named as Davis B and Davis C depend on iterative procedures to arrive at the relevant reduced strength parameters. The reduction factors in these methods as given in Oberhollenzer et al. [2] are as follows:

Davis B

$$\beta_{failure} = \frac{\cos\left[arctan\left(\frac{\tan \psi'}{FoS}\right)\right] \cos\left[arctan\left(\frac{\tan \phi'}{FoS}\right)\right]}{1 - \sin\left[arctan\left(\frac{\tan \psi'}{Fos}\right)\right] \sin\left[arctan\left(\frac{\tan \phi'}{Fos}\right)\right]}$$
(8)

Davis C

$$\beta_{failure} = \frac{\cos\left[arctan\left(\frac{\tan \phi'}{FoS}\right)\right] \cos \psi'}{1 - \sin\left[arctan\left(\frac{\tan \phi'}{FoS}\right)\right] \sin \psi'}$$
(9)

Important differences between Davis A, B and C are given in Table 1.

Oberhollenzer et al. [2] have observed that even though the modified approaches are still conservative when compared with the results obtained from strength reduction finite element analysis, they are in better agreement with strength reduction analysis as compared to the original Davis approach. Davis B approach has been

Table 1 Tschuchnigg et al. [11]

	Davis A	Davis B	Davis C
Comparison of different procedures			
β	Constant $\beta_{\text{failure}} = f(\varphi', \psi')$	Varies $\beta_{\text{failure}} = f(\varphi'_{\text{failure}}, \psi'_{\text{failure}})$	Varies $\beta_{\text{failure}} = f(\varphi'_{\text{failure}}, \psi')$
ψ'	Constant	Varies	Constant
Note:	φ^* could theoretically smaller than ψ'	φ^* cannot smaller than ψ'	φ^* could theoretically smaller than ψ', but β increase with decreasing φ'. Limit: $\beta \leq 1.0$

recommended to be used with finite element limit analysis. This approach can also resolve the observed numerical instabilities while using a nonassociated flow rule [2].

3 Nonlinearity and Slope Stability Analysis

3.1 Nonlinearity and Its Effects on Slope Stability

Linear Mohr–Coulomb (MC) failure envelopes, which use a linear approximation to fit the experimental data, are widely used in slope stability analysis. However, it has been observed that strength envelopes of soils have nonlinear forms, especially at low normal stress ranges [12–18]. As Jiang et al. [14] have pointed out, usual experimental investigations for field applications do not cover very low effective normal stresses and extrapolation is done to obtain data not covered in experimental assessment. This may lead to overestimation of soil shear strength at low normal stress ranges. Nonlinearity is important in slope stability calculations since for many practical problems critical slip surfaces are shallow and normal stress acting on such surfaces is small [14, 16–18]. Studies have found that nonlinear parameters have significant impact on problems of slope stability and the predicted slip surface and use of linear Mohr–Coulomb (MC) may yield unsafe solutions [12–14, 17, 18]. Baker [18] observed that the nonlinear (NL) strength envelope gives better description of experimental findings as compared to the linear MC envelope, even for sands and normally consolidated clays which are usually taken to be linear frictional materials. The basic objective of NL strength criterion is not to have a better curve fitting of experimental information, but rather to arrive at a more conservative estimate of strength as compared to the linear MC criterion at normal stresses that are not covered in the experimental normal stress range [18]. An additional advantage of nonlinear strength envelopes in slope stability analysis has been pointed out by Gregory and Bumpas [26]. They observed that with the nonlinear strength envelope explicit consideration of the fully softened zone may not be necessary since the maximum depth of the critical slip surface will be automatically restricted to depths typically observed for shallow slides in highly plastic clays.

Various nonlinear envelopes have been suggested by authors to better fit the experimental data and represent the curved failure envelopes of soils. They include bilinear functions, trilinear functions and various power law relations [14]. Among these the power law failure envelopes have been widely applied to slope stability analysis [12, 16, 17, 28, 30]. One type of power law failure criterion is the simple power law failure criterion, where the failure envelope passes through the origin. Another type is the general power law failure criterion which possesses an initial cohesion at zero normal stress and is more appropriate for cohesive soils [17]. The following form of general power law failure enveloped has been widely used by authors [12]:

$$\tau = c_0 \left(1 + \frac{\sigma_n}{\sigma_t} \right)^{1/m} \tag{10}$$

where c_0 = cohesion at zero normal stress.

σ_n = normal stress.

σ_t = tensile stress at zero shear stress.

m = nonlinearity coefficient.

The value of m depends on the geotechnical material involved [30]. Zhao et al. [30] have discussed the range of m suggested by various authors and the widest range is given to be from 1 to 2.

3.2 Incorporating Nonlinearity in Slope Stability Analysis

As has been observed by [14, 16, 32–37], the nonlinear strength criterion cannot be directly used in stability analysis since the shear strength of soils is a nonlinear function of stress. With the power law failure criterion broadly two approaches are used in stability analysis. In one approach the applicable equilibrium and energy dissipation equations are written in terms of the nonlinear power law failure criterion. Then mathematical tools like variational calculus, numerical approaches, iterative procedures, dynamic programming, Taylor series expansion etc. are used to solve the governing nonlinear equations. But these procedures are mathematically relatively more complicated. In the second approach instantaneous Mohr–Coulomb parameters are determined from the nonlinear failure criterion by the tangential technique. These parameters are used in the analysis and then optimization is done to arrive at the required solutions.

4   Conclusion

Study of literature has revealed that dilatancy and soil strength nonlinearity have significant effect on problems of slope stability. Approaches have been developed by authors to use a nonassociated flow rule in limit analysis. In strength reduction method even though for small friction angles the dilatancy angle setting does not have much effect on the solution, as the friction angle increases and assumes high values the significance of flow rule increases and cannot be neglected in the analysis. Nonlinearity of strength envelope has significant effect on the solutions obtained from stability analysis and the corresponding failure mechanisms. This is especially relevant since in many slope problems the normal stresses on the failure surface fall in low ranges. Hence dilatancy and nonlinearity effects should be incorporated into analyses for obtaining better solutions to slope stability problems.

References

1. Lin H-D, Wang W-C, Li A-J (2020) Investigation of dilatancy angle effects on slope stability using the 3D finite element method strength reduction technique. Comput Geotech 118:103295
2. Oberhollenzer S, Tschuchnigg F, Schweiger HF (2018) Finite element analyses of slope stability problems using non-associated plasticity. J Rock Mech Geotech Eng 10:(1091–1101)
3. Wang Y-J, Yin J-H, Lee CF (2001) The influence of a non-associated flow rule on the calculation of the factor of safety of soil slopes. Int J Numer Anal Meth Geomech 25:1351–1359
4. Qian ZG, Li AJ, Merifield RS, Lyamin AV (2015) Slope stability charts for two-layered purely cohesive soils based on finite-element limit analysis methods. Int J Geomech 15(3):06014022:1–14
5. Li C, Jiang P, Zhou A (2020) Non-associated plasticity analysis of slope stability under steady unsaturated flow conditions. Comput Geotech 128:103786
6. Mizuno E, Chen WF (1983) Plasticity analysis of slope with different flow rules. Comput Struct 17(3):375–388
7. Eskandarinejad A, Shafiee AH (2011) Pseudo-dynamic analysis of seismic stability of reinforced slopes considering non-associated flow rule. J Cent South Univ Technol 18:2091–2099
8. Drescher A, Detournay E (1993) Limit load in translational failure mechanisms for associative and non-associative materials. Geotechnique 43(3):443–456
9. Kumar J (2004) Stability factors for slopes with nonassociated flow rule using energy consideration. Int J Geomech 4:264–272
10. Manzari MT, Nour MA (2000) Significance of soil dilatancy in slope stability analysis. J Geotech Geoenviron Eng 126:75–80
11. Tschuchnigg F, Schweiger HF, Sloan SW (2015) Slope stability analysis by means of finite element limit analysis and finite element strength reduction techniques. Part I: Numerical studies considering non-associated plasticity. Comput Geotech 70:169–177
12. Wu D, Gao Y, Chen X, Wang Y (2021) Effects of soil strength nonlinearity on slip surfaces of homogeneous slopes. Int J Geomech 21(1):06020035:1–11
13. Eid HT (2010) Two and three-dimensional analyses of translational slides in soils with nonlinear failure envelopes. Can Geotech J 47:388–399
14. Jiang J-C, Baker R, Yamagami T (2003) The effect of strength envelope nonlinearity on slope stability computations. Can Geotech J 40:308–325
15. VandenBerg DR, Castellanos BA, McGuire MP (2019) Comparison and use of failure envelope forms for slope stability analysis. Geotech Geol Eng 37:2029–2046

16. Li YX, Yang XL (2019) Soil-slope stability considering effect of soil-strength nonlinearity. Int J Geomech 19(3):04018201:1–10
17. Gao Y-F, Wu D, Zhang F, Qin H, Zhu D (2016) Effects of nonlinear strength parameters on stability of 3D soil slopes. J Cent South Univ 23:2354–2363
18. Baker R (2004) Nonlinear Mohr envelopes based on triaxial data. J Geotech Geoenviron Eng 130:498–506
19. Banerjee A, Puppala AJ, Kumar P, Hoyos LR (2020) Stress-dilatancy of unsaturated soil. Geo-Congress 2020 GSP 319:420–429
20. Andersen KH, Schjetne K (2013) Database of friction angles of sand and consolidation characteristics of sand, silt and clay. J Geotech Geoenviron Eng 139:1140–1155
21. Bolton MD (1986) The strength and dilatancy of sands. Geotechnique 36(1):65–78
22. Liu X, Cheng XH, Scarpas A, Blaauwendraad J (2005) Numerical modelling of nonlinear response of soil. Part 1: Constitutive model. Int J Solids Struct 42:1849–1881
23. Tschuchnigg F, Schweiger HF, Sloan SW (2015) Slope stability analysis by means of finite element limit analysis and finite element strength reduction techniques. Part II: Back analyses of a case history. Comput Geotech 70:178–189
24. Krabbenhoft K, Karim MR, Lyamin AV, Sloan SW (2012) Associated computational plasticity schemes for nonassociated frictional materials. Int J Numer Methods Eng 90:1089–1117
25. Chang Y-L, Huang T-K (2005) Slope stability analysis using strength reduction technique. J Chin Inst Eng 28(2):231–240
26. Griffiths DV, Lane PA (1999) Slope stability analysis by finite elements. Geotechnique 49(3):387–403
26. Gregory GH, Bumpas KK (2013) Post-peak fully-softened strength and curved strength envelope in shallow slope failure analysis. Geo-Congress 2013:255–268
28. Tschuchnigg F, Schweiger HF, Sloan SW, Lyamin AV, Raissakis I (2015) Comparison of finite-element limit analysis and strength reduction techniques. Geotechnique 65(4):249–257
29. Deng D, Li L (2019) Coupling nonlinear strength criterion and double-strength reduction technique. Int J Geomech 19(6):04019052:1–13
30. Ganjian N, Askari F, Farzaneh O (2010) Influence of nonassociated flow rules on three-dimensional seismic stability of loaded slopes. J Cent South Univ Technol 17:603–611
31. Zhao L, Cheng X, Dan H, Tang Z, Zhang Y (2017) Effect of the vertical earthquake component on permanent seismic displacement of soil slopes based on the nonlinear Mohr-Coulomb failure criterion. Soils Found 57:237–251
32. Li D, Cheng Y (2012) Lower bound limit analysis using nonlinear failure criterion. Procedia Earth Planet Sci 5:170–174
33. Li X (2007) Finite element analysis of slope stability using a nonlinear failure criterion. Comput Geotech 34:127–136
34. Yang X, Chi S (2013) Upper bound finite element analysis of slope stability using a nonlinear failure criterion. Comput Geotech 54:185–191
35. Drescher A, Christopoulos C (1988) Limit analysis slope stability with nonlinear yield condition. Int J Numer Anal Methods Geomech 12:341–345
36. Deng D, Zhao L, Li L (2015) Limit equilibrium slope stability analysis using the nonlinear strength failure criterion. Can Geotech J 52:1–14
37. Yang X-L, Yin J-H (2004) Slope stability analysis with nonlinear failure criterion. J Eng Mech 130(3):267–273

Effective Utilization of Eragrostis Teff Straw in Adobe Units for Sustainable Construction in Ethiopia

Binaya Patnaik, Benu G. Mohapatra, Getnet Kassahun, and Temesgen Gebreyesus

1 Introduction

Ethiopia is one of the developing countries in the world and currently facing many challenges in the form of faster population growth, deforestation and uncontrolled urbanization. The burn beating of the land to gain larger areas of cultivation and grazing for the livestock, the demand of firewood and the high timber content in traditional house building techniques in combination with high population causes deforestation, which in the long run leads to extremely high pressure on the lands of surrounding towns and cities. In these situations, it is highly imperative to adopt a low-cost and sustainable housing construction technique. Soil with wood (Chika Bet) is widely used in many rural areas of Ethiopia as a traditional house building technique. However, these house construction technique consumes a lot of wood and also have serious durability issues along with termite attack is a biggest concern. Even though natural fibres are being used by the local community to enhance the strength and durability of the Chika-Bet houses, but the improper addition of fibres and water to the soil leads to more damage to these houses. There are several low cost housing techniques have been tried across world out of which adobe construction technique is very well suited to application in developing countries for its less cost, simple method of construction and use of locally available materials. Adobe house construction technique uses mixing of soil, fibre and minimum amount of binders which are generally available locally and also very much affordable to people. This construction technique generally solves economic, social and environmental related problems in

B. Patnaik (✉)
Department of Civil Engineering, Gambella University, Gambella, Ethiopia

B. G. Mohapatra
School of Civil Engineering, KIIT, Bhubaneswar, India

G. Kassahun · T. Gebreyesus
Department of Civil Engineering, Wolaita Sodo University, Sodo, Ethiopia

Fig. 1 Woods used from forest for rural house construction in Ethiopia

developing countries. In past few researchers have tried preparing adobe units using various locally available materials such as banana fibres, sugarcane bagasse, coir etc. as reinforcing agents and the results have been promising in terms of enhancing the strength and durability of adobe units. In this current research an attempt has been made to utilize teff straw which is one of the major agro waste produced in Ethiopia as a reinforcing material along with a suitable binder based on the soil characteristics in preparing adobe units and investigating their mechanical and various durability properties (Fig. 1).

2   Materials and Methodology

The materials used for this study were locally available soil, teff straw fibre, cement and water.

2.1   *Laboratory Tests on Soil and Eragrostis Teff Straw Fibre*

The soil samples used to prepare adobe units were taken from Wolaita Sodo area, around Wolaita Sodo University, Ethiopia. The soil was taken from 1 m depth below the natural ground level by removing the soil rich in artificial organic matter. Soil tests were carried out by using ASTM standard procedures and soil classifications are identified according to the unified soil classification system (USCS). Several experimental investigations were also carried out to determine the physical properties of the soil. The experimental test carried out were water content, specific gravity, grain size analysis, plastic, and liquid limit, maximum dry density and optimum water content. The results of these tests are shown that the soil is CL as per the

Table 1 Soil properties

Natural moisture content (%)	19.18
Air-dry moisture content (%)	15.28
Specific gravity	2.63
Liquid limit (%)	49.1
Plastic limit (%)	26.77
Plastic index	22.33
Maximum dry density (kN/m^3)	13.17
Optimum moisture content (%)	32.39
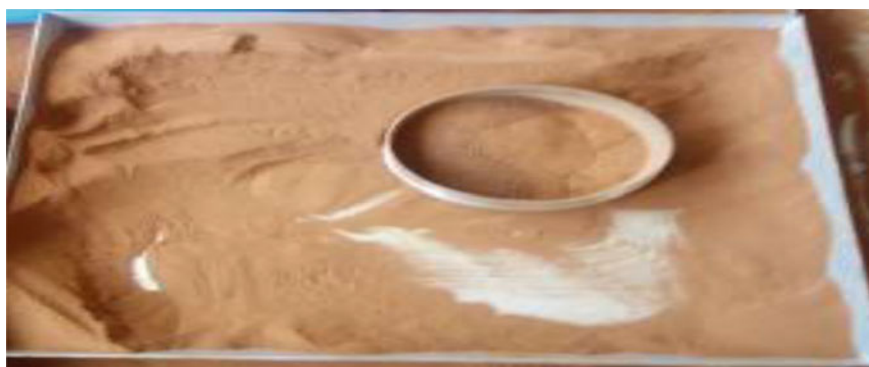
Fig. 2 Screened clay soil for preparing adobe specimen

USCS standard. Based on the test results on the soil, cement was chosen as the stabilizing material because of the limits of plasticity index from 7 to 29% and the liquid limit ranges from 25 to 50%. Based on physical properties of the soil and reviewed previous studies, this soil was found to be appropriate for adobe earth house construction. The soil properties have been presented in Table 1 (Figs. 2 and 3).

The eragrostis teff straw fibre is an agriculture waste plentily available in Ethiopia. Eragrostis teff straw is a durable, easily applicable, accessible, cheap and not chemically hazardous material. The average length of the eragrostis teff straw fibre used in this research is 30 mm. The experimental investigations carried out for eragrostis teff straw fibre are water content analysis, specific weight analysis, and water absorption rate analysis. The experimental test results are tabulated in Table 2.

The cement used for this research was PPC Dangote cement having a compressive strength of 32.5 MPa. PPC cement is highly durable, less cost, and emits less carbon dioxide than OPC cement. Water is one of the major materials in the production of adobe units. Water used in this study was free from all forms of contaminants, taste and odour less i.e. in general potable water.

Fig. 3 Laboratory tests for soil properties

Table 2 Eragrostis teff straw fibre properties	Cross-section	Circular
	Length (mm)	30
	Range of diameter (mm)	0.1–1
	Specific weight (g/cm^3)	0.18
	Natural moisture content (%)	13.84
	Water absorption in 5 min (g/min)	0.73
	Water absorption in 10 min (g/min)	0.375
	Water absorption in 1 h (g/min)	0.063

2.2 Preparation of Adobe Unites and Mix Proportions

All adobe units prepared for this research have prisms shape. One hundred forty-four (144) adobe units were prepared and cured by air-drying. Adobe unit samples were prepared with the dimension of 190 mm × 90 mm × 90 mm as per Indian Standards (IS: 4332-1, 1967). All prepared adobe units were from soil, soil plus 3.5% cement, soil plus 3.5% cement plus 0.5, 1, 1.5, 2% straw fibre by weight of soil. Adobe units mixed were arranged according to maximum dry density (MDD) and optimum moisture content (OMC) from standard proctor test. The soil was sieved and screened

by 1.18 mm sieve before ready to mix. Then the soil and cement mixed in the dry state, the straw fibre is added and mixed properly until it becomes uniformly arranged. Mixing of materials were done with hands properly with the addition of water till to optimum moisture content. The soil, soil–cement, and soil–cement-straw fibre mix mechanically compact with 30 blows in equal three layers in the timber molds. The sample specimens were taken out from the timber moulds after 7 days, cured and air-dried at normal temperature for different periods of time. The unstabilized and unreinforced, stabilized and unreinforced, and stabilized and reinforced sample specimens were subjected to different laboratory tests. For each type of adobe units, four-sample tests were taken for all strength and durability tests. The test results were the average of four test results. The variation of more than 5% was not considered in the calculation of the test results. This research study incorporated production and testing of unstabilized unreinforced sample specimens (0% cement plus 0% straw fibres), stabilized unreinforced samples (3.5% cement plus 0% straw fibres) and stabilized reinforced sample specimens (3.5% cement plus 0.5, 1, 1.5, 2% straw fibre by weight of soil). The mixture proportions are listed in Table 3 (Fig. 4).

Table 3 Mix proportions of different adobe mixes

Sr. No.	Denotation	Soil (%)	Cement (%)	Teff straw (%)	OMC (%)
1	A	100	Nil	Nil	32.39
2	B	96.5	3.5	Nil	28.81
3	C	96	3.5	0.5	
4	D	95.5	3.5	1	
5	E	95	3.5	1.5	
6	F	94.5	3.5	2	

Fig. 4 Preparation of adobe units

Fig. 5 Compressive strength test

2.3 Strength Tests

2.3.1 Compressive Strength Tests

The compressive Strength test was carried out to determine the amount of compressive load the adobe units can bear without before fracturing, as well as describe stress carrying capacity of adobe units. The equipment used was a compressive testing machine of maximum load carrying capacity of 2000 KN. Compressive strength test was carried out for all treated and untreated adobe units. Compressive strength sample specimens were prism with the dimensions of 190 mm * 90 mm * 90 mm as per Indian standards (IS: 4332-1, 1967) [23]. The compressive load was applied at the rate of 0.04 N/mm^2/s until adobe units fractured. The compressive strength test and stress carrying capacity tests of adobe unit specimens were conducted after 14, 28, and 56 days of air curing and drying (Fig. 5).

2.3.2 Water Strength Tests

The water strength test is the determination of the water strength coefficient for wet and dry compressive strength of adobe unit sample specimens. The water strength coefficient is the ratio of wet compressive strength to dry compressive strength after immersion in clean water. This test was conducted for all adobe units sample specimens after 28 days of curing and air drying. The equipment used for this test was compressive testing machine, metallic plates, and flat-bottomed bucket.

3 Results and Discussions

3.1 Soil Test Results

Table 4 shows that, the test results of the standard proctor test of soil–cement mix with varying with cement amount of 3, 3.5, and 4%. It shows that, the maximum dry

Table 4 Standard proctor tests to find optimum amount of cement

Mixes	Maximum dry density (kN/m^3)	Optimum moisture content (%)
Soil	13.17	32.39
Soil + 3% cement	12.73	27.63
Soil + 3.5% cement	13.53	28.81
Soil + 4% cement	13.45	32.96

Fig. 6 Standard proctor compaction test for soil–cement mix

density increasing with an increase in cement amount up to 3.5% and maximum dry density decrease in further addition of 4% cement. Therefore, the addition of 3.5% cement is an optimum value that will be used in adobe mixes, because it has given maximum dry density. These tests were used 3.5% cement as a stabilizer for soil (Fig. 6).

3.2 Compressive Strength Test Results

From the analysis of test results of the compressive strength presented in Fig. 7, it can be seen that, for 14 days curing period, the maximum early gain in strength is shown by mix A (Soil + 0% Cement + 0% Teff straw fibre) and followed by mixture E, D, C, F, B. The compressive strength of mix B (Soil + 3.5% Cement + 0% Teff straw fibre) is less than the other mixes because of the curing period was not enough to increase the compressive strength. For 28 and 56 days of curing period, the maximum gain in strength are shown by mix E (Soil + 3.5% Cement
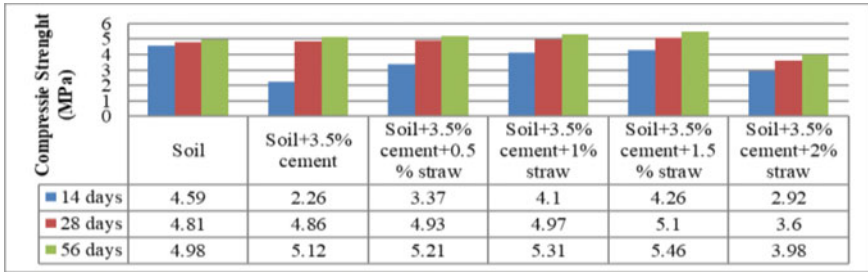
	Soil	Soil+3.5% cement	Soil+3.5% cement+0.5 % straw	Soil+3.5% cement+1% straw	Soil+3.5% cement+1.5 % straw	Soil+3.5% cement+2% straw
■ 14 days	4.59	2.26	3.37	4.1	4.26	2.92
■ 28 days	4.81	4.86	4.93	4.97	5.1	3.6
■ 56 days	4.98	5.12	5.21	5.31	5.46	3.98

Fig. 7 Compressive strength of adobe unit specimens at 14, 28 and 56 days of curing

+ 1.5% Teff straw fibre) and followed by mixture D, C, B, A, F. So it can be concluded that, the addition of 3.5% cement and inclusion of teff straw fibre (0–2%) in the soil mix increases the compressive strength after 28 and 56 days of curing and drying period. The compressive strength of 28 and 56 days of mixture E (Soil + 3.5% Cement + 1.5% Teff straw fibre) is 5.1 and 5.46 MPa. The increment in compressive strength for 28 and 56 days of curing period of mix E is 5% and 9.64% respectively. According to Spence and Cook (1983) the average earth brick strength, range from 3 to 3.5 MPa for load-bearing requirements of normal two-story buildings. The study results confirmed that adobe unit specimens stabilized with cement and reinforced with teff straw fibre enhance the compressive strength and can be adopted for important construction works, especially mixes of soil and 3.5% cement stabilizer with 1.5% teff straw reinforcement. The compressive strength value required by Indian standards for traditional Mud brick is 1 MPa. However, the maximum value of 28 days compressive strength from this research was found to be 5.1 MPa. This implies that the local soil and teff straw can be used for preparing Adobe units for house construction.

3.3 Water Strength Test Results

Water strength is the ratio of wet compressive strength to dry compressive strength for adobe unit specimens. The minimum permissible value of this coefficient has been taken as 0.5. From water strength tests, mix E (Soil + 3.5% Cement + 1.5% Teff straw fibre) has the highest water strength value of 0.56. Adobe unit specimens of mixes D and C have a considerable value of 0.52 and 0.5 respectively. These values are fitted with permissible limit 0.5. Unreinforced adobe unit samples do not have water strength because the samples are immediately deteriorated and break when immersed in water. These test shows that, adobe unit specimens stabilized with cement and reinforced with teff straw fibre enhance the durability compared with unreinforced adobe unit specimens (Fig. 8).

These tests were the ratio of wet compressive strength to dry compressive strength for all adobe unit specimens after 14 days of immersion in water. The mix E (Soil +
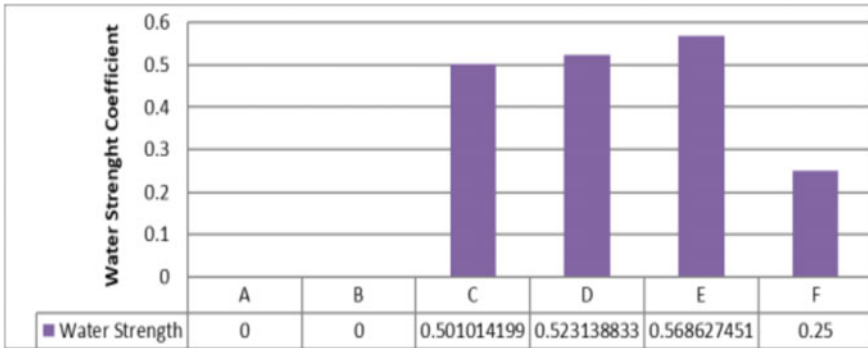
Fig. 8 Water strength test result

3.5% Cement + 1.5% Teff straw fibre) shows that, the highest water strength value of 0.169 in 1 day of air drying followed by mix F, D, and C with the values of 0.144, 0.135, and 0.124 respectively. The results obtained from laboratory tests, for mix E (Soil + 3.5% Cement + 1.5% Teff straw fibre) has the highest water strength value of 0.943 in 7 days of air drying followed by mixes D, C, and F with the values of 0.926, 0.915, and 0.694 respectively. This test shows that stabilized and reinforced adobe unit specimens get 94.3% of the compressive strength after 14 days of immersion within 7 days of drying, especially mix E (Soil + 3.5% Cement + 1.5% Teff straw fibre) (Fig. 9).
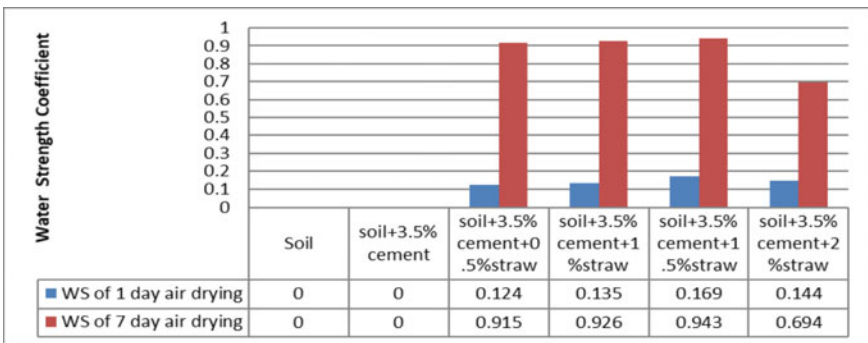
Fig. 9 Compressive strength at 14 days of immersion in water

4 Conclusions

This research provides a new and simple construction technique called adode technique for rural housing construction in Ethiopia by enhancing the strength and durability properties of earthen units. This research also provides the optimum quantities of constituent materials of adobe units. The experimental results shows that, the stabilized and reinforced soil samples helps in improving the strength and durability of earthen houses compared with unstabilized and unreinforced soil houses.

- The 28 and 56 days of curing strength of mix E (Soil + 3.5% Cement + 1.5% Teff straw fibre) was recorded the highest value with about 5% and 9.64% respectively compare with mix A (Soil + 0% Cement + 0% Teff straw fibre).
- After 24 h of immersion in water for water strength test indicated that, mix E (Soil + 3.5% Cement + 1.5% Teff straw fibre) has a higher water strength value of 0.56. So that, mix E (Soil + 3.5% Cement + 1.5% Teff straw fibre) has maximum improvement in strength as compared with other mixes.
- After 14 days of immersion in water, the test result shows after 1 and 7 days of drying, mix E (Soil + 3.5% Cement + 1.5% Teff straw fibre) has the higher water strength coefficient of 0.17 and 0.943 respectively. This shows Mix E (Soil + 3.5% Cement + 1.5% Teff straw fibre) has a maximum water strength and gets back around 94.3% of the compressive strength after 7 days of drying.

The appropriate mix of adobe units is suggested to be containing soil (95%), cement (3.5%), and teff straw fibre (1.5%) with a water content of 28.81%. Therefore, mix E (Soil + 3.5% Cement + 1.5% teff straw fibre) can be considered to be the efficient mix for preparing strong and sustainable adobe units for rural house construction in Ethiopia.

References

1. Standard test method for specific gravity of solid soils by water pycnometer, ASTM D 854-00
2. Standard test method for laboratory compaction, ASTM D 698
3. Varum H, Costa A, Fonseca J, Furtado A (2015) Behavior characterizaton and rehabilitation of adobe construction. Procedia Eng 714–721
4. Manette N, Oyawa W, Nyomboi T. Effects of hand compaction on compressive strength and water absorption of compressed stabilized earth blocks, vol 3. JKUAT, Kenya
5. Darshan P, Vivek P, Viresh R, Hardik S, Dipesh V (2014) Comparison of brick made from black cotton soil with various admixture to the normal bricks. IJIRST 1(7)
6. Habib A, Begum R, Abdus Salam Md (2015) Effect of stone dust on the mechanical properties of adobe bricks. IJISET 2(9)
7. Egenti C, Khatib JM, Negim E (2015) Performance of compressed earth brick in comparison with the prevailing sand-cement wall construction in Nigeria. IJERR 3(4):37–41
8. Danso H, Brett Martinson D, Ali M, Williams JB (2015) Effect of sugarcane baggase fiber on the strength properties of soil bricks. In: First international conference on bio-based building materials, Portsmouth, United Kingdom
9. Sharma V, Vinayak HK, Marwaha BM (2015) Enhancing sustainability of rural adobe houses of hills by addition of vernacular fiber reinforcement. Int J Sustain Built Environ 4:348–358

10. Sharma V, Marwaha BM, Vinayak HK (2016) Enhancing durability of adobe by natural reinforcement for propagating sustainable mud housing. Int J Sustain Built Environ 5:141–155
11. Patnaik B, Gebreyesus T, Kassahun G (2019) Sustainability of adobe structures. JETIR 6(6)

Analytical Investigation on Retrofitted Masonry Wall

A. Meenachi, R. Malathy, and R. Syed Rishvana

1 Introduction

Masonry is a composite building element built by grouping the bricks or stones embedded by means of mortar. There are two types of masonry, reinforced masonry and unreinforced masonry. Reinforced masonry (RM) is defined as masonry wall reinforced with rebar, steel sections, mesh etc. Un reinforced masonry (URM) is masonry wall that is built without any reinforcement as mentioned above and it is the most conventional type in practice. Most of the buildings are unreinforced masonry buildings and it is the most traditional and oldest method of construction as it is evolved in its natural way of construction. Collective advantages of URM buildings are heat, aesthetics and sound insulation, fire resistance, economic considerations and its mechanical properties, contribute to its appearance and also the most opted option for construction of houses. These walls during their service life will have extensive damage due to lateral loads [1]. Since it is brittle in nature it doesn't give any warning before failure. The aim of our project is to propose analytical model with the experimental data with retrofitting methods for URM walls and study its behavior analytically static load.

Generally failures of URM walls occurred due to continuous vertical joint, longer corner stones, improper verticality, etc. These failure occurs in the masonry structures due to In plane bending and Out of plane bending. It is type of bending means the wall bends in its own plane (i.e.) along its length of wall. The resistance for this bending should be developed along the length of the wall. It is the type of bending caused by out of plane forces i.e. acting along the width of the masonry wall. Since

A. Meenachi (✉) · R. Malathy
Department of Civil Engineering, Sona College of Technology, Salem, Tamilnadu, India
e-mail: meenachia@sonatech.ac.in

R. Syed Rishvana
Rebar Design and Detailing, Chennai, India

width is smaller than length the resistance developed is minimum [2]. The In-plane failure is categorized by a diagonal tensile crack pattern, and out-of-plane failure, where cracks are primarily along the mortar bed joints. In plane bending doesn't cause sudden failure but out plane bending do and it is critical too [3].

Retrofitting is defined as modifying or strengthening the existing building with new components. Retrofit may include the process of repair or rehabilitation or strengthening the structure along with structural system. Retrofitting can be done for both failure structure and the structure about to fail. Retrofitting is aimed to increase the maximum capacity of the buildings. The aim of retrofitting is to enhance the ultimate strength of the building by improving the structures ability to absorb inelastic deformation. This can be achieved by changing the structural system such that the energy is transferred along alternative load paths, or alternatively, increasing the ductility As discussed earlier, masonry structure have suffered extensive damage due to both In plane bending and out of plane bending. To minimize the damage to some extent retrofitting is provided to withstand such bending. An analytical model has been developed for the unreinforced masonry wall based on the experimental work. The failure load at which the walls failed had been loaded with the analytical model for its validation.

2 Experimental Program

2.1 Compressive Strength of Brick

Size of the brick is measured and placed in compression testing machine as shown in Fig. 1. Compression load is gradually applied on brick and the load at failure is measured. Compressive strength of the brick is calculated and tabulated in Table 1.
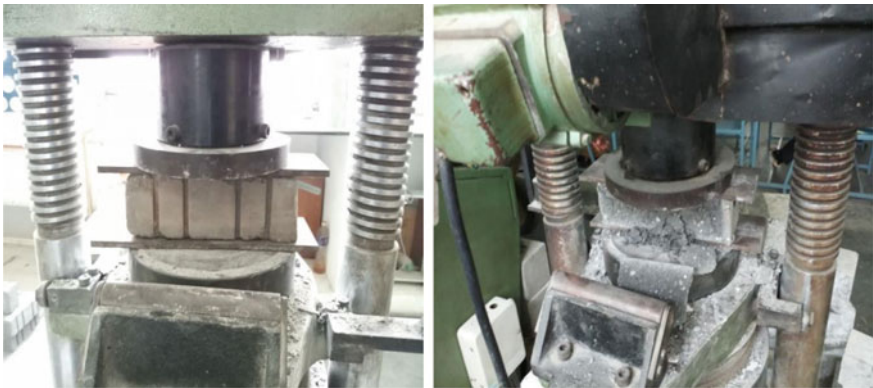

Fig. 1 Compression test on bricks

Table 1 Compression test on brick

S. No.	Size of brick (mm × mm × mm)	Area of loading face (mm × mm)	Ultimate load (kgf)	Compressive strength (N/mm^2)
1	230 × 110 × 75	230 × 110	17,500	6.78
2	230 × 110 × 75	230 × 110	16,950	6.57
3	230 × 110 × 75	230 × 110	17,650	6.84

The value of compressive strength is 6.73 N/mm^2. As per IS 3495 (Part II)—1992 the standard value of compressive strength of first class brick is 10 N/mm^2 and second class brick is around 7 N/mm^2. So our brick is second class brick.

2.2 Testing of Masonry Wall

Experimental investigation on masonry [4, 5] walls was tested under static loading condition. Five number of masonry wall were constructed and retrofitted in rectangular and diagonal pattern with gabion and crimped wire mesh as shown in Fig. 2. Out of five, one wall is plain masonry without any retrofitting to have a comparison on standard behaviour. Masonry wall was constructed in a size of 1.16 m × 1 m of thickness 230 mm, by using brick of size 230 mm × 110 mm × 75 mm. The walls were loaded with static load and loaded up to failure. The failure loads for the five masonry walls are tabulated in Table 2. The pattern and material for retrofitting were chosen based on literatures.

Diagonal Retrofitting   Rectangular retrofitting

Fig. 2 Retrofitted masonry walls

Table 2 Experimental failure loads of masonry walls

Type of masonry	Ultimate load (kN)
Plain masonry	160
Gabion retrofitted masonry in rectangular pattern	260
Gabion retrofitted masonry in diagonal pattern	250
Crimped wire retrofitted masonry in Rectangular pattern	300
Crimped wire retrofitted masonry in diagonal pattern	280

3 Analytical Program

3.1 Modelling and Material Properties

Finite element modelling [6, 7] is analysing the structural component by dividing into number of small elements. ABAQUS is used for the formulation of the analytical model. Initially in creating parts of elements, creation of elements such as brick (Header and stretcher) of size 230 mm × 110 mm × 75 mm, queen closer of size 230 mm × 55 mm × 75 mm, Mortar, gabion mesh and crimped wire mesh of diameter of 2 mm. Assigning material properties such as young's modulus, density, Poisson's ratio [4] for all elements is tabulated in Table 3. Then sections such as brick, mortar and mesh should be created and assigned to its properties.

Assembly of the wall is done by merging all elements and made into wall of size 1.16 m × 1 m × 0.23 m. as per the experiments conducted. Boundary condition is assigned to wall as fixed at base depict the rigidly in experimental work. Meshing should be done for the wall for the analysis work. Meshing should be done by creating seed instance. For the analysis purpose meshing is done by creating 50 mm seeds. In the output file the variation of behavior of the wall will be shown in each seed. Depending upon the properties of meshing material, the behavior will change under loading. Also depending upon the pattern of retrofitting such as rectangular as well as diagonal the behavior will vary as shown in Fig. 3.

Table 3 Properties of material

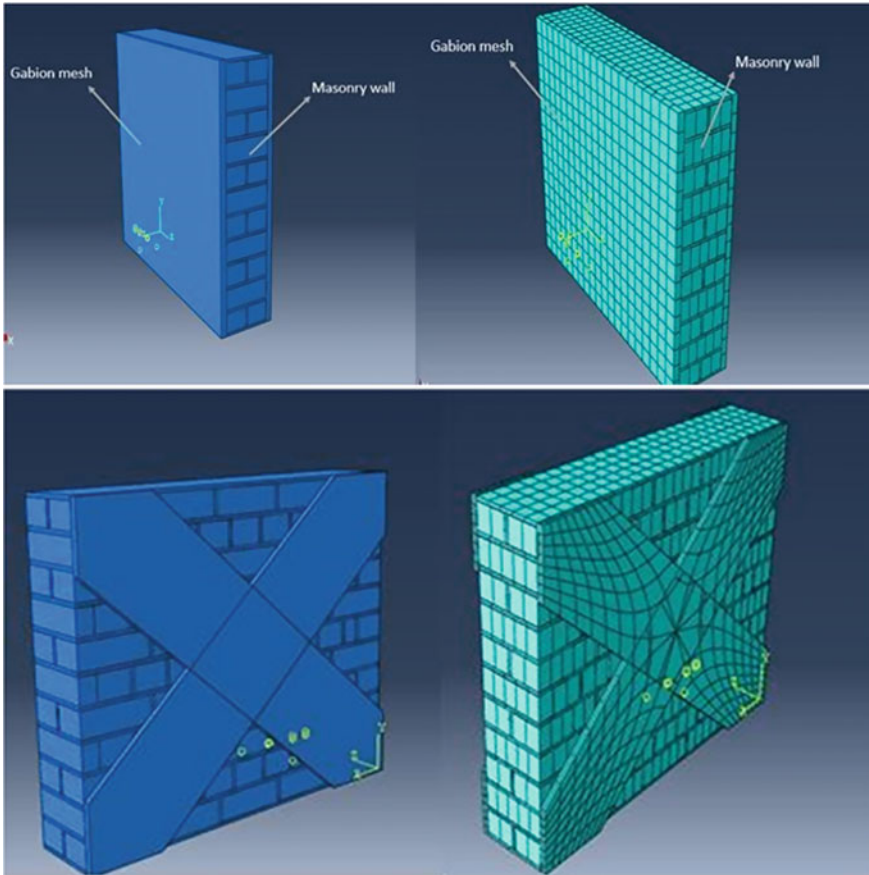| Properties	Brick	Cement mortar	Gabion mesh	Crimped wire mesh
Young's modulus (N/mm^2)	1.18×10^5	0.35×10^5	1.89×10^5	1.89×10^5
Density (kg/m^3)	2000	2080	7750	8000
Poisson's ratio	0.15	0.2	0.305	0.265

Fig. 3 Modeling of the masonry wall with rectangular and diagonal retrofitting

4 Results and Discussion

By applying the experimental load of 160 kN on the plain masonry wall, shows that the complete masonry is subjected to maximum stress and top portion subjected to ultimate stress. The colour difference in the top layer shows the variation of stress from maximum to minimum.

Similarly for gabion mesh retrofitted (rectangular pattern) masonry the ultimate load which is obtained from experimental work is 260 kN. The analytical result indicates maximum stress only occurred at mesh part compared to masonry part. Hence, it is much viable than plain masonry. But when the same wall retrofitted in diagonal pattern, the stress was distributed uniformly throughout the top layer and mesh provided at diagonal pattern the behavior doesn't that much effective as rectangular retrofitted masonry. So, the masonry also subjected to maximum stress [8].
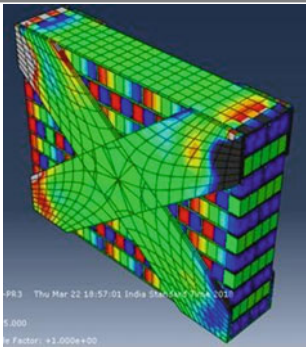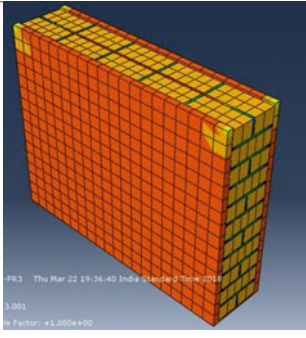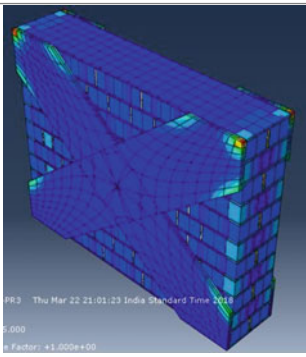
Crimped wire retrofitted masonry in rectangular pattern under an ultimate load of 300 kN was applied in the model. The aperture distance of crimped wire mesh is less than the gabion mesh, which results in good bearing capacity. Here maximum stress at mesh part only, masonry doesn't undergo that much stress because retrofitting was provided at full face of wall, so load was evenly distributed. The same in diagonal pattern under an ultimate load of 280 kN shows maximum stress acting at both mesh part and top portion of masonry. Because retrofitting provided only at diagonal face of masonry which is not that much effective to withstand the axial loading. The stress of all five masonry walls is tabulated in Table 4.

Table 4 Benaviour of all masonry wall

Type of masonry	Ultimate Load (kN)	Behavior of masonry	Analytical result
Plain masonry	160	Complete masonry subjected to maximum stress and top portion subjected to ultimate stress	
Gabion retrofitted masonry in rectangular pattern	260	Maximum stress only at mesh part. Masonry doesn't undergo that much stress	

(continued)

Table 4 (continued)

Type of masonry	Ultimate Load (kN)	Behavior of masonry	Analytical result
Gabion retrofitted masonry in diagonal pattern	250	Maximum stress acting at major portion of masonry wall as well as on mesh	
Crimped wire retrofitted masonry in Rectangular pattern	300	Maximum stress acting at mesh part and mortar joints. Masonry doesn't undergo that much stress	
Crimped wire retrofitted masonry in diagonal pattern	280	Maximum stress acting at major portion of masonry wall as well as on mesh and moderate stress at edges of the wall	

5 Conclusions and Future Suggestions

By analysing above results, crimped wire retrofitted masonry in rectangular pattern achieved good behaviour under an ultimate load of 300 kN. Because, for static loading the resistance should be created on the full face rather than in diagonal face of masonry wall. At the same time aperture distance between crimped wire mesh is smaller than the gabion mesh. So crimped wire retrofitted masonry in rectangular pattern

have shown best results in both experimental and analytical investigation. Thus the developed model can be further analysed for seismic and other vulnerabilities.

References

1. Shrestha H, Pradhan S, Guragain R (2012) Experiences on retrofitting of low strength masonry buildings by different retrofitting techniques in Nepal. In: 15th world conference on earthquake engineering, Lisbon, Portugal
2. Santa Maria H, Alcaino P, Luders C (2006) Experimental response of masonry walls externally reinforced with carbon fiber fabrics. In: Proceedings of the 8th US national conference on earthquake engineering
3. Chuang S-W, Zhuge Y, McBean PC (2004) Seismic retrofitting of unreinforced masonry walls by cable system, pp 1–6
4. ElGawady MA, Lestuzzi P, Badoux M (2005) In-plane seismic response of URM walls upgraded with FRP. J Compos Constr 9(6):524–535
5. ElGawady MA, Lestuzzi P, Badoux M (2005) Aseismic retrofitting of unreinforced masonry walls using FRP. Compos B Eng 37(2–3):148–162
6. ElGawady MA, Lestuzzi P, Badoux M (2006) Analytical model for the in-plane shear behavior of URM walls retrofitted with FRP. Compos Sci Technol 66(3–4):459–474
7. ElGawady MA, Lestuzzi P, Badoux M (2006) Shear strength of URM walls upgraded with FRP. Eng Struct 28(12):1658–1670
8. Alcaino P, Santa-Maria H (2008) Experimental response of externally retrofitted masonry walls subjected to shear loading. J Compos Constr 12(5):489–498
9. ElGawady MA, Lestuzzi P, Badoux M (2007) Static cyclic response of masonry walls retrofitted with fiber-reinforced polymers. J Compos Constr 11(1):50–61

Design of Energy Efficient Educational Institutional Building

Kavyaa Senthilkumar and Gulshan Taj

1 Introduction

Structures are the significant marker of social advancement of the province. Each human wants to claim agreeable structure. It is estimated that one person spends his two-third of his lifetimes in the structures. Institutional structures are the storage facility of information advancement. They are a major wellspring of creating information. Furthermore, Sustainability has gotten progressively significant in the structure business lately. The structure is generously answerable for 33% of energy utilization. The point of the undertaking is to investigate and plan of an Institutional structure which meets the energy productivity. The arranging is done according to Indian standard code arrangements. Energy efficiency is likewise a significant rule that needs unique consideration while planning the structures [1–3]. Examination says that 55 million understudies go through their days in organizations. A new and quickly developing pattern is planning those foundations with the particular purpose of giving sound, agreeable, and beneficial learning conditions. By developing a supportable Institutional structure number of understudies get will prepared for filing their fantasy life through examinations. Furthermore, it's gives a stage to develop their transporter in an ecological well-disposed manner. Hence, while considering the load opposing and dependability measures in a structure it is additionally imperative to actualize energy efficient methodology too [4]. Here, A plan of R.C working of G+2 (Civil Block) story outline work is taken up. The dimension of the structure is (168 ft * 204 ft) comprises of segments fabricated solidly framing an organization. The size of building is 40 m × 28 m. It is energy productive instructive structure. The plan is made utilizing programming on primary investigation plan (E-Tabs). The structure exposed to both the vertical loads just as flat loads. The vertical loads comprise of

K. Senthilkumar (✉) · G. Taj
Department of Civil Engineering, Sona College of Technology, Salem, India
e-mail: kavyaa.17civil@sonatech.ac.in

dead load of primary parts, for example, beams, columns, slabs and so on and live loads. In this way, building is intended for dead loads, live loads and wind loads and earthquake load according to IS 875 and IS 1893. The structure is planned as two-dimensional vertical frame and maximum and minimum bending moments and shear forces by experimentation techniques according to IS456-2000 [5–8]. The assistance is taken by programming accessible in foundation and the calculations of loads, moments and shear forces and acquired from this product. At that point building will be planned according to green building concepts by integrating day light which will be analysed using Ecotect-2011 software.

2 Need of the Project

- The advantages of bringing daylight into a space can be invalidated by ill-advised treatment of the sunlight being presented.
- Make uniform conveyance of daylight to diminish awkward high splendour proportions of light.
- Take into consideration client change and abrogate.
- Guarantee satisfactory light to all occupants of the daylight space.
- Give view and association with the outside.
- Totally organize with the compositional enunciation of the structure in general. Totally fuse with other structure systems—HVAC, Electrical, Lighting, Structural, Interiors.
- Control direct daylight when necessary and utilize beneficial passive solar strategies when appropriate.
- Execute inside all around improvement monetary arrangement of the undertaking. Achieve huge energy saving by diminishing lighting energy costs and related cooling energy costs.

3 Scope of the Project

The main objective of this Project is to explore the sustainability analysis.

- The main objective of our project is to understand and implement the various design criteria like planning, analysis and design of institutional building of acres
- To implement green concept to make the building more energy efficient
- To plan in AutoCAD
- To Analyse and design in Etabs
- To analyse energy efficiency in Ecotec software.

4 Data Availability Statement for Structure

4.1 Statement of Project

1. Length of (g+2) building—206 ft
2. Width of (g+2) building—168 ft
3. Height of (g+2) building—52 ft
4. Typical storey height—4.2 m
5. Bottom story height—4.2 m
6. Density of concrete—25 KN/m^2
7. Grade of concrete—M30 KN/m^3 and
8. Grade of steel—HYSD415
9. Thickness of slab—0.35 (m)
10. Zone 3 (Z.F. = 0.16)
11. wind speed = 44 m/s.

4.2 Dimension of Structural Member of Building

1. Main beam—0.3 m × 0.45 m
2. Main Column—0.4 m × 0.4 m
3. Slab thickness—0.35 m.

5 Loading Pattern

Gravity loads act a comparable path as gravity

- **Dead load according to IS 875-Part-1**

The principle vertical loads that is considered is dead loads. Dead loads are constant loads which are moved to structure for the duration of the life expectancy of the structure. Dead loads is basically a direct result of self-weight p permanent partition walls, fixed permanent equipment and weight of different materials. It essentially includes the weight of roofs, beams, walls and beams.

- **Live load according to IS 875-Part 2**

Live loads are either moving loads with no acceleration. These loads are believed to be conveyed by the arranged use or inhabitancy of the structure including loads of portable segments or furniture and so on. The base assessments of live loads to be acknowledged that are given in IS 875.

- **Loading combination**

Fig. 1 and 1a Site Plan of building(G+2) in AutoCad and Floor plan of (G+2) building

SITE PLAN
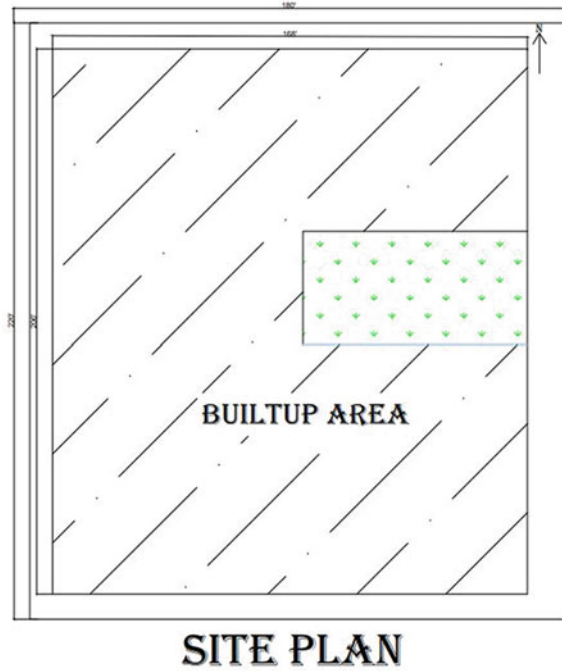
As per the limit state design of reinforced concrete structures the following load combination has been considered:

1(D.L of g+2 building + L.L of g+2 building)

1.5(D.L of g+2 building + L.L of g+2 building)

1.2(D.L of g+2 building + L.L of g+2 building + W.L of g+2 building)

1.2(D.L of g+2 building + L.L of g+2 building + E.L of g+2 building).

6 Layout of Structure

See Figs. 1, 1a, 2, 3, 3a, 4, 5, 6 and 7.

7 Results and Discussions

See Figs. 8, 9 and 10.

The structure is plan subject to the E-Tabs, and the theory of limit state method which invigorate satisfactory strength, serviceability, and durability besides the economy. The displacement, shear force, bending moment variation are designed and
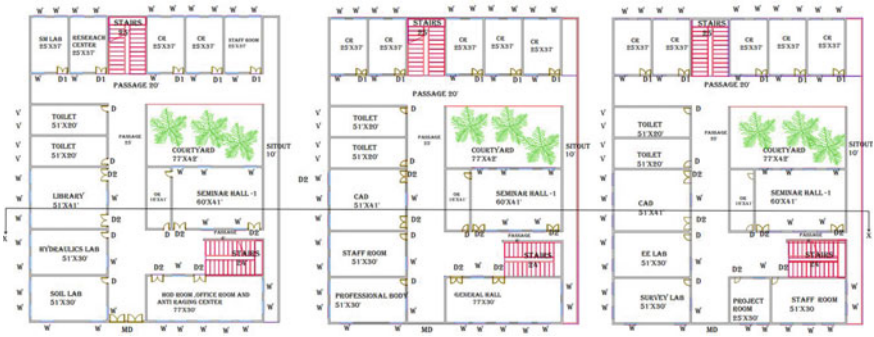
Fig. 1 and 1a   (continued)
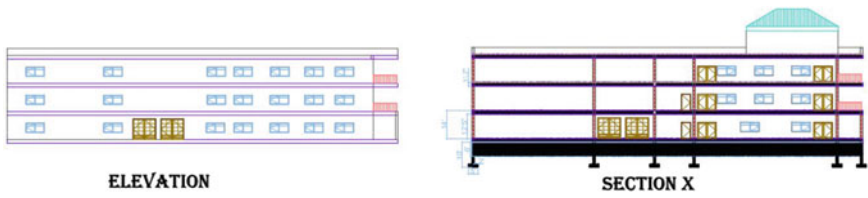
Fig. 2   Elevation and sectional details of building

Fig. 3 and 3a   Beam column layout and column centerline marking
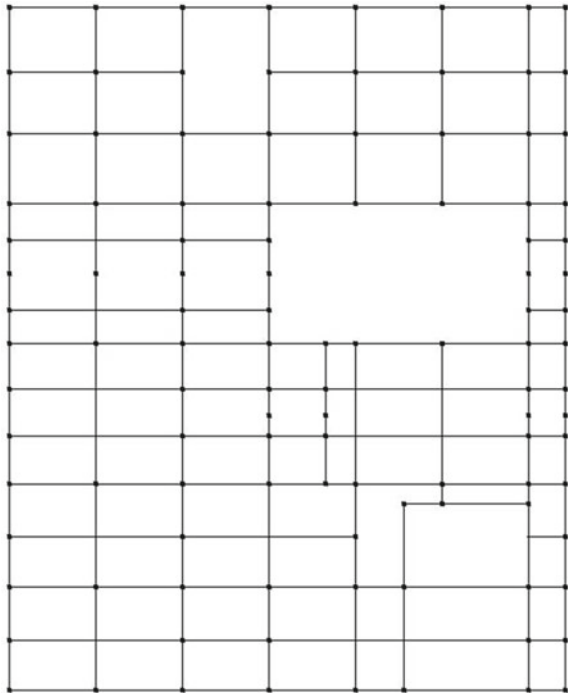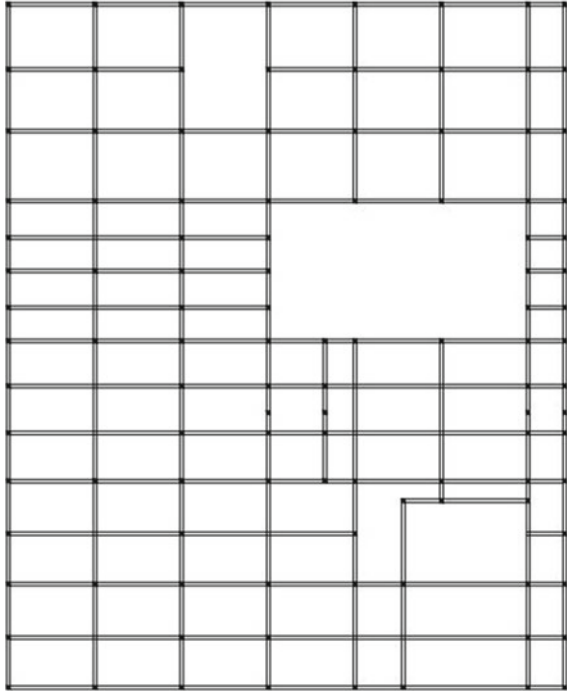
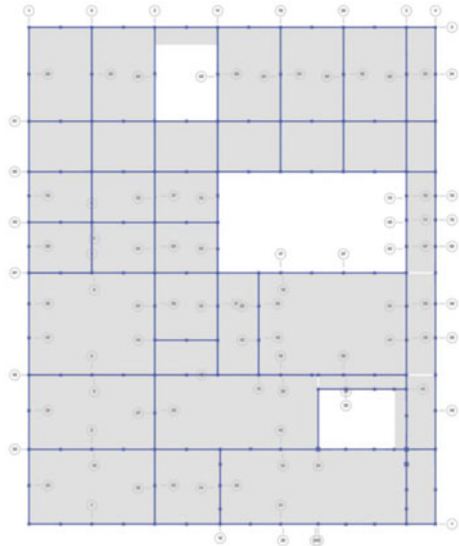**Fig. 3 and 3a** (continued)

Fig. 4 Modelling in Etabs

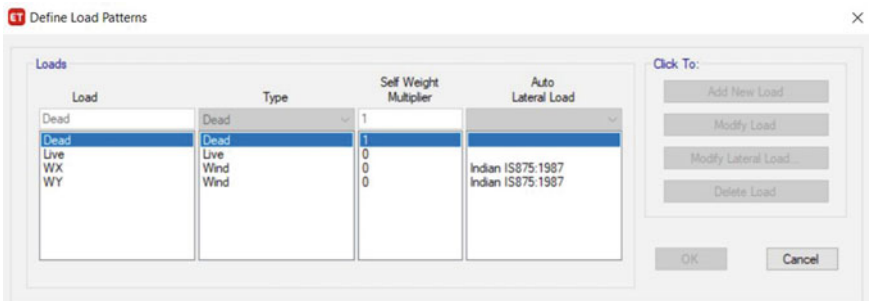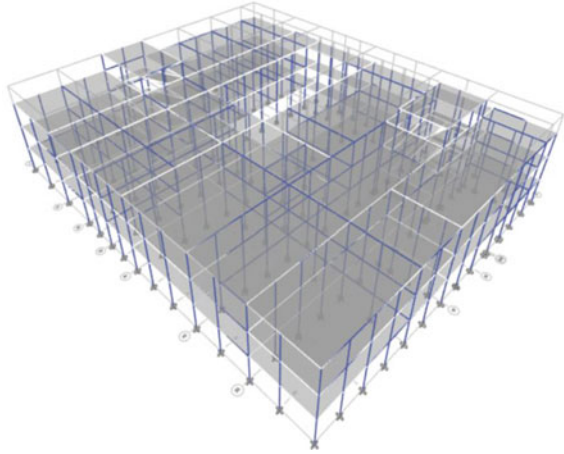**Fig. 5** 3d-Modelling of structure in Etabs

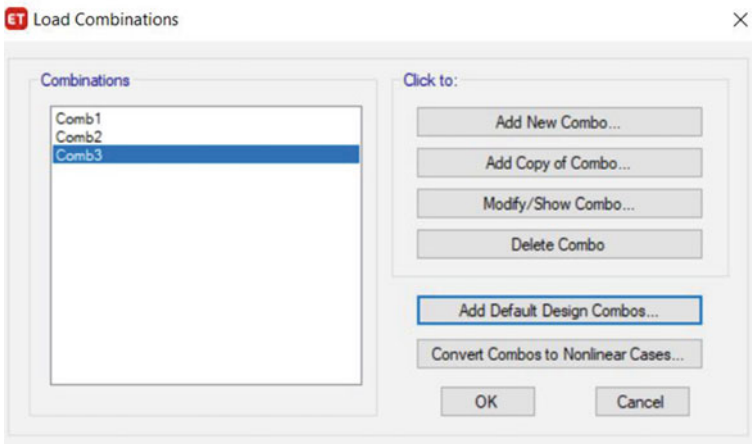**Fig. 6** Assigning loads

Fig. 7 Assigning load combinations
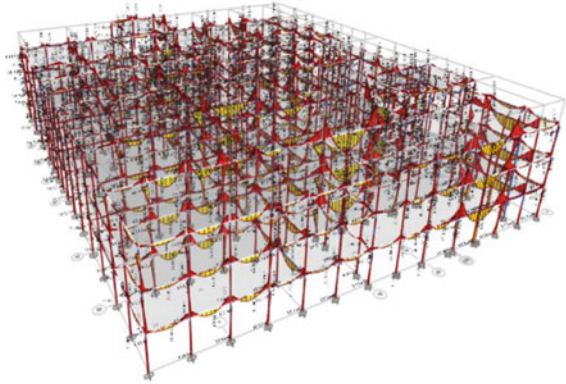
Fig. 8 Member force for
frames of (g+2) building

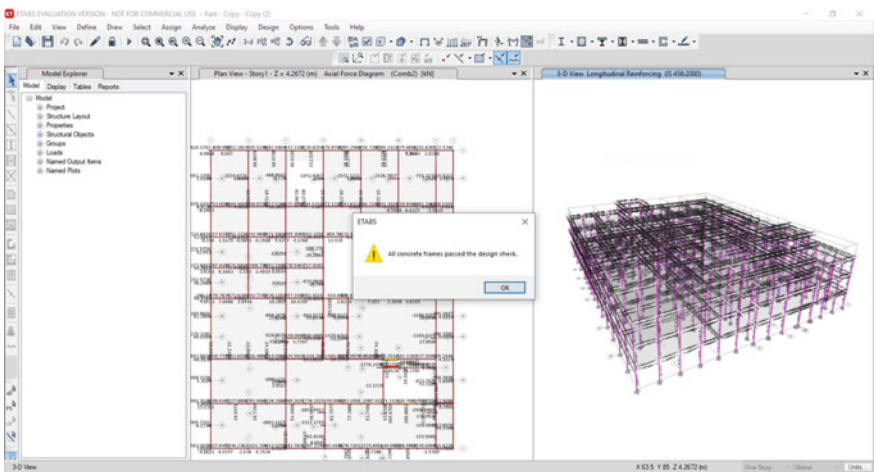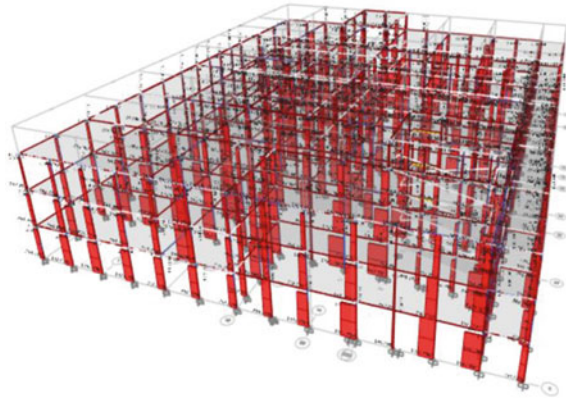**Fig. 9** Axial force of (G+2)

**Fig. 10** Design check verification

analysed utilizing E-tabs. It has been showed up in figure that that all concrete frames are passed under given material property and loading conditions. Different significant outcomes like bending moments, shear force and deflection, displacements, are analysed and shown all are safe under given loading conditions.

8 Purpose of Ecotect-2011 Software

Ecotect-2011 is an achievable and maintainable plan examination programming which is an exhaustive plan to detail commonsense structure setup gadget. The Ecotect-2011 was generally used during determined stage and structure headway time of the endeavor. It offers building energy assessment supportiveness that can improve efficiency of both existing structures and new structure plans. If any alternations need to be carryout, it awards architects to go for alternative plan. This gives appropriate information about various assessments, for instance, light examination, shadow assessment, thermal properties s, concealing gadgets, and solar radiation, shadows and reflections so on.

9 Methodology of Day Light Analysis

The main purpose of this analysis is to know how Ecotect-2011 Daylight simulation provides energy efficient and performance to the (g+2) building contingent depends on materials, direction etc.
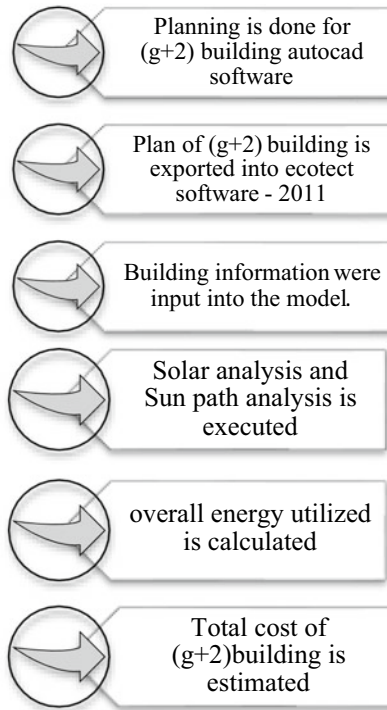
Methodology chart 1: Light analysis procedure

Planning and expelled in AutoCAD software and a short time later exported into Ecotect-2011. Building information for instance, site region, direction, elevation, wind investigation and landscape were imported to the model. Sunlight based assessment and path of Sun is examined will give us a further analysis which is totally planned in Ecotect-2011. This software is totally organized with Ecotect-2011 and can be used to make daylight-based.

10 Proposed Solution

Utilizing Ecotect-2011 software modeling of (g+2) educational institutional building, is done. Dimensions of the building (G+2) are taken and the orientation of building is noted and then modeled in Ecotect-2011 software. 'Fluoro lamp strip' units of 40w are installed, in which case the illumination level is to be 250 lux (Fig. 11).
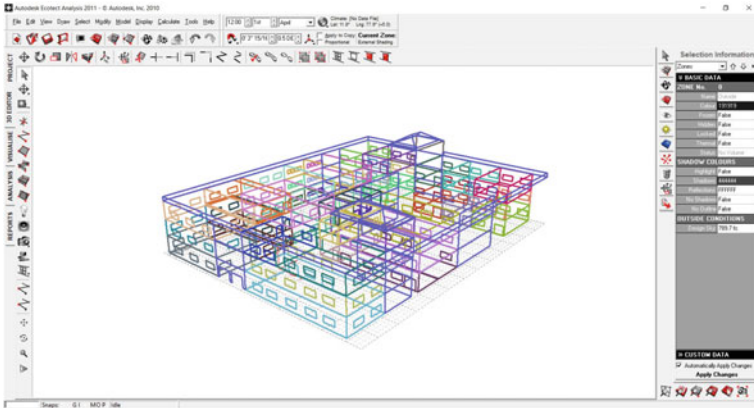
Fig. 11 Modelling in Ecotect-2011

11 Software Execution

The Lighting analysis of (g+2) building is estimated. Daylight factor of (g+2) building, electric lights of (g+2) building and daylight levels of g+2 building are calculated using Ecotect-2011 software. This analysis is calculated without using blinds for the windows of (g+2) building (Figs. 12, 13, 14, 15 and 16).

The results shows the daylight light analysis in the building is done for various conditions. The band color shows that daylight factor in the (g+2) building which is in the range of 2.86–54.82% and the higher value lies near the windows and courtyards.
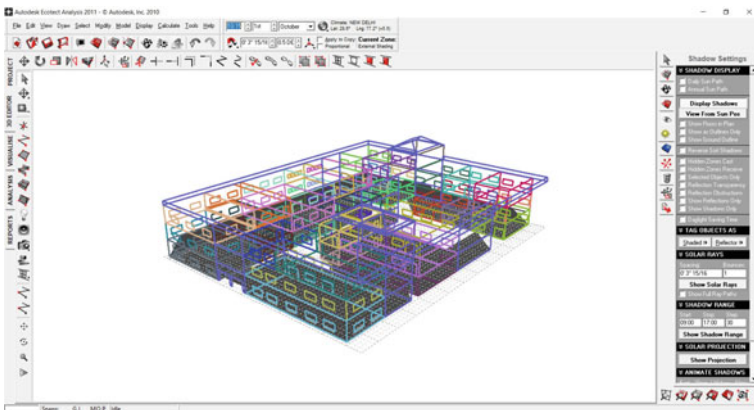
Fig. 12 Shadow investigation

Fig. 13 Grid analysis
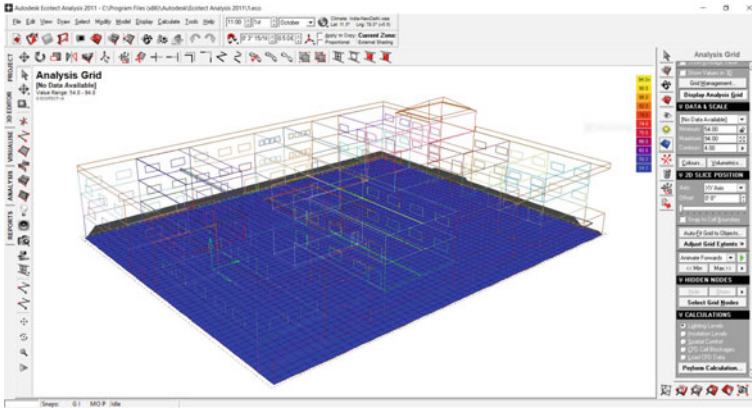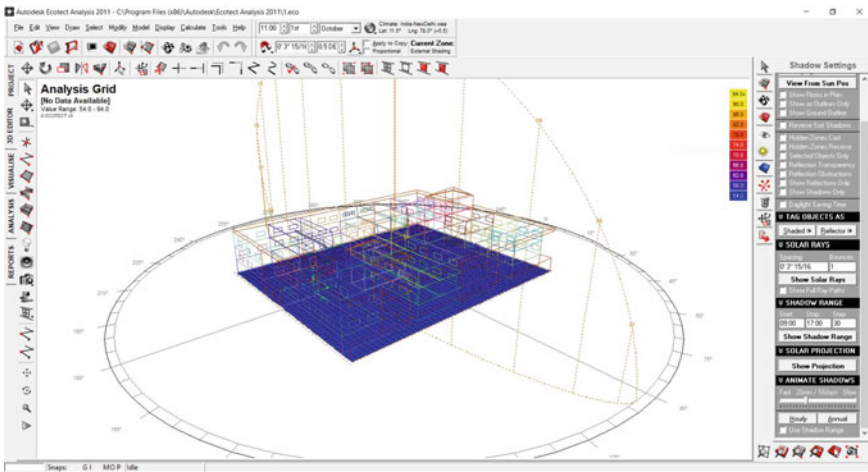

Fig. 14 Daily Sun-path

12 Results and Discussion

Modeling of the building of G+2 is done in Ecotect-2011 software

- **Shadow analysis for the (g+2) building**

Shadow analysis show the point by point day lighting assessment and execution of the structure hourly where maximum daylight will be fallen can be achieved accurately.

- **Light Analysis for the (g+2) building**
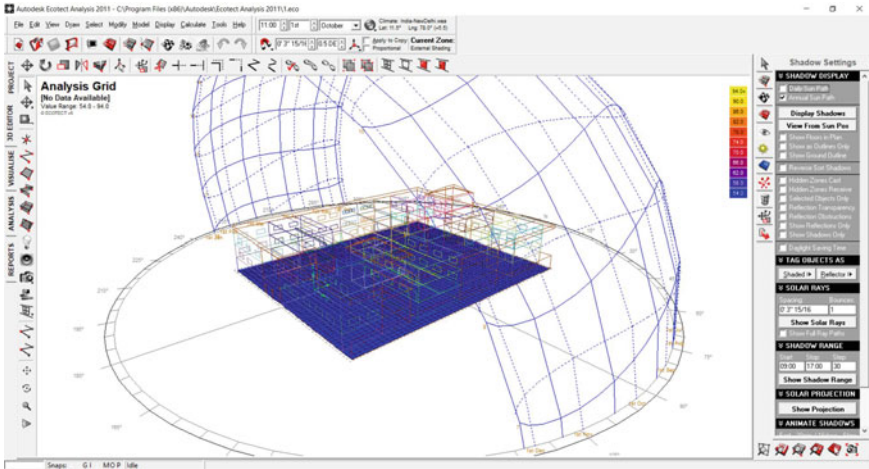
Fig. 15 Yearly Sun path
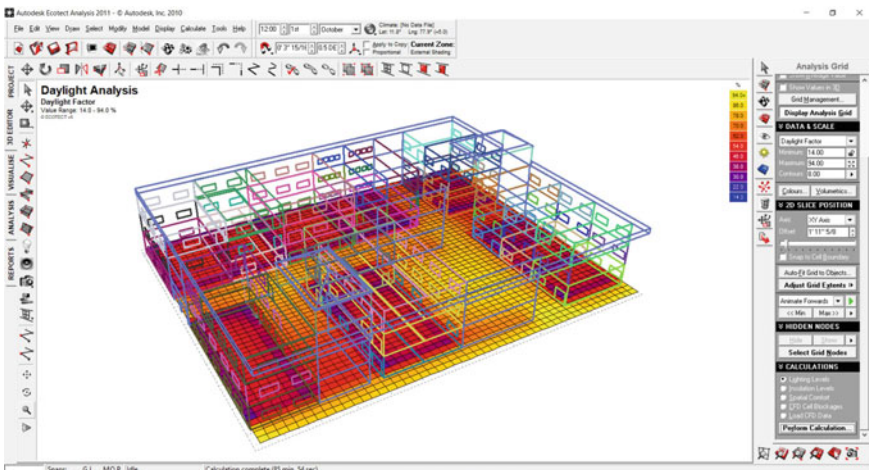
Fig. 16 Day light analysis

Without utilizing the blinds light level fluctuates between 2.86 and 54.82% relying upon the distance from the window since daylight arrives at various segments of the room. Sunlight level of g+2 building range is seen to be in 480–5380 lux. The Artificial Electric lighting of g+2 building level in building is ranging between 12 and 556. The overall lighting of g+2 building ranging fluctuated from 420 to 6420 lux.

13 Occupants Portal

An application will be created and, in that occupants, can have login and they can screen the energy use from the information gathered from Ecotect-2011 programming. And furthermore, sensors will be actualized in the structure and temperature, water level in tank, energy usage, each one of those stuffs can be hindered and transferred those subtleties in application. With the goal that occupants can use it in effective way.

14 Conclusion

Planning by utilizing Software's takes after E-tabs decreases package of time in arrangement work. Subtleties of every single underlying part can be gotten utilizing E-tabs. All the List of failed beams can be obtained and furthermore Better Section can be changed by utilizing E-tabs. Exactness is Improved by using programming the status of the endeavor has given an extraordinary opportunity to rise we in arranging and planning of multi-storeyed (G+2) Building. Configuration was done by using ETABS programming and successfully checked by IS 456-2000. The examiner and configuration results got from programming are secured and all concrete frames are passed. Configuration was finished by utilizing ETABS programming and effectively confirmed according to IS 456-2000. The examination and configuration results got from programming are protected and all concrete frames are passed. Ecotect-2011 is novel according to various assessment contraptions, that it centres around the promptest periods of (g+2) building, when direct decisions may influence the convincing result of an endeavour. Later on, it is essential to ensure that the g+2 building orchestrating to be intelligent and more pleasing, eco-accommodating as well as energy saving working condition. This is needed to create understanding and portray the neighbourhood ecological data for extra investigation.

References

1. Aneesh NR, Shivaprasad KN, Das BB (2018) Life cycle energy analysis of a metro station building envelope through computer-based simulation. Sustain Cities Soc 39:135–143
2. Mahapatra D, Ashok Babu TP (2020) Variation of time lag, decrement factor and inside surface temperature with solar optical properties of building envelope in different climatic zones of India. In: Reddy A, Marla D, Simic M, Favorskaya M, Satapathy S (eds) Intelligent manufacturing and energy sustainability. smart innovation, systems and technologies, vol 169. Springer, Singapore
3. Shifad S, Pati P, Das BB (2021) A multi-dimensional study on impact of energy efficiency on life cycle cost of a single-family residential building. In: Das BB, Nanukuttan SV, Patnaik AK, Panandikar NS (eds) Recent trends in civil engineering. lecture notes in civil engineering, vol 105. Springer, Singapore
4. Trisnawan D. Ecotect design simulation on existing building to enhance its energy efficiency

5. Sallal AK. Design and analysis ten storied building using ETABS software-2016
6. Guleria A. Structural analysis of a multi-storeyed building using ETABS for different plan configurations
7. Panchal, Marathe PM. Comparative method of study for RCC, in a G+30 story commercial building
8. Naga Sai Gopa KS, Lingeshwaran N. Analysis and design of (g+5) residential building by using Etabs

Influence of Contact Time to Magnetic Field of Mixing Water on Fresh and Hardened Properties of Concrete

Ramalingam Malathy, Narayanan Karuppasamy, and U. Vinitha

1   Introduction

Water plays a traditional role in concrete, with significant influences on its engineering properties. The magnetic water treatment received some attention from the scientist community [1]. Researchers from industrialized countries have showed that increase fresh and hardened properties of concrete and Freeze–thaw resistance was due to magnetic treated water in concrete [2, 3]. Due to applying a strong magnetic field, water will behave as Diamagnetism, as a result, water molecules are oriented in certain direction [4]. Magnetization improves negative ionic hydration, thus intensifying the damaging effect on the water crystal structure [5]. While mixing process, hydration process will takes place on the surface of the cement particles and hydrated product is formed. Further hydration hinders the development of mechanical strength of concrete. In case of magnetic water, water molecules gets soften easily penetrate into cement particles and allowing complete hydration process occurs and enhances the strength parameters [6]. The amount of improvement to the concrete strength is 10%, savage of cement by 5% [7]. The hardness of water caused by calcium and magnesium initially gets decreased after the magnetic treatment of the water [8]. On the other side, Concrete becomes denser and develops resistance for drying shrinkage by replacing cement by GBFS for improving the structure of concrete [2, 3, 9]. Reduction of surface tension will make molecules more dynamic and fluid, which in turn gives better bonding of materials added to water [1]. Magnetized water overcomes environmental pollution without the usage of chemical admixtures. Magnetized water has been used in several application including health, environmental, agriculture, construction industry. Initially, the water gets magnetized after applying magnetic field in the mixing process followed by mixing of fine and coarse aggregate,

R. Malathy (✉) · N. Karuppasamy · U. Vinitha
Department of Civil Engineering, Sona College of Technology, Salem, TN, India
e-mail: malathycivil@sonatech.ac.in

cement. Magnetized water found its application in concrete, ready mix plants and construction sites and the operation is simpler to execute [10, 11]. The paper deals with the fresh and hardened concrete properties of concrete prepared with magnetic water with different contact time varying in magnetic field varying from 0 to 60 min respectively.

2 Experimental Details

2.1 Materials

Ordinary Portland cement Type I produced by ultra tech cement company was used. Crushed coarse aggregate with nominal size of 12 and 20 mm maximum size obtained locally. Fine aggregate (sand) was also sourced from a local supplier. Their physical properties are shown in Tables 1, 2 and 3 as per IS: 2386–1963 [12].

Table 1 Properties of cement

S. No.	Properties	Results
1	Normal consistency	36%
2	Initial setting time	32 min
3	Final setting time	5 h 37 min
4	Fineness (by sieve analysis)	4.5%
5	Specific gravity	3.15

Table 2 Properties of fine aggregate

S. No.	Properties	Result
1	Type	Uncrushed
2	Specific gravity	2.71
3	Fineness modulous	2.85
4	Grading	Zone-II

Table 3 Properties of coarse aggregate

S. No.	Properties	Result
1	Type	Crushed
2	Size	20 mm
3	Specific gravity	2.85
4	Water absorption	2.19%
5	Crushing value	25%
6	Impact value	18.85%

Fig. 1 Magnetic water set-up

Table 4 Properties of water

S. No.	Properties	Result		
		Before magnetization	After magnetization	Permissible limit
1	pH	7.6	8.1	6.5–8.5
2	Hardness	253 mg/l	75.33 mg/l	<600 mg/l
3	Cl	98.47 mg/l	67.47 mg/l	<500 mg/l
4	Iron	0.1 mg/l	0.1 mg/l	<1 mg/l

2.2 Magnetic Water

Preparation of magnetic water involves passing water through a PERMAG (N406) with 0.9 T of intensity as shown in Fig. 1. The water used for mixing and with quality shown in the Table 4 is produced by potable tap water in Salem district as per IS 3025–1987 [13].

2.3 Mix Composition

In the present research study, M25 grade trials were done on produced materials. To arrive the mix proportions, the Indian Standard mix design procedure was adopted (i.e., IS: 10262–2009) for M25 grade concrete [14]. The mix proportion is tabulated as shown in the Table 5.

Table 5 Mix proportion

	Cement	Fine aggregate	Coarse aggregate	W/C
Ratio	1	2.48	3.31	0.47

2.4 Experimental Variables

Tap water is exposed to magnetic field of 0.9 T for 60, 45, 30, 15 and 0 min denotes instant pumping through magnetic field. Both magnetic and normal water concrete specimens were cured in the temperature of 23 ± 1 °C for 7 and 28 days before the entire tests were performed.

2.5 Experimental Procedures

The slump measures the water cement ratio required to maintain the required consistency and to achieve the good workability with less water content. The slump test was conducted on fresh concrete as per IS 1199–1959 [15]. The Compressive test machine UTM-200 T was used for testing concrete samples as per IS 516–1959 [16].

3 Results and Discussion

3.1 Effect of Slump on Time of Contact to Magnetic Field

Figure 2 presents the various contact time of water circulated through a magnetic field. The increase in contact time of water to magnetic field increases the workability of the slump with increase in time duration upto one hour, but instant pumping itself provides water parameters ranges not beyond the normal water limits. The greatest increase in percentage of 61% arrived for contact time of 60 min duration. The increase in slump is due to following theory. Water is at Nano state, which exists in clusters, this clusters size depends upon the equivalent force in the water molecules.

Fig. 2 Slump versus time of contact to magnetic field (MF)
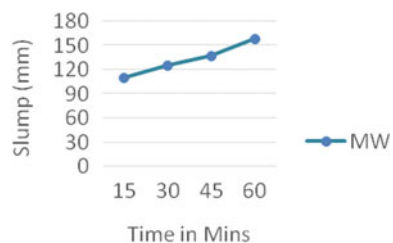
When water contact time to a magnetic field, cluster of molecules breaks down, decreases the bond angle between hydrogen atoms from 105° to 103° which arrived through macroscopic properties [17]. Water exposed to magnetic field will provide better dispersion and increase surface area of water for hydration with cement passed in concrete.

3.2 Effect on Compressive Strength

Figures 3 and 4 shows the values of the compressive strength of 7 and 28 days for different contact times. In the 7th and 28th day sample, we observed an amplification in compressive strength with magnetic water is 15.5 and 15.1% with increase in contact duration. The theme behind magnetic field treated water; chemical composition of scaling is reduced and produces more quantity of smaller water cluster. The range at which this strength is increasing due to contact duration of water on magnetic field is caused memory possessed by water. Disturbance in water occurred due to exposed of water to magnetic field after some time water starts orientation to this new form of magnetic water and there after mechanism will takes place [10, 11].

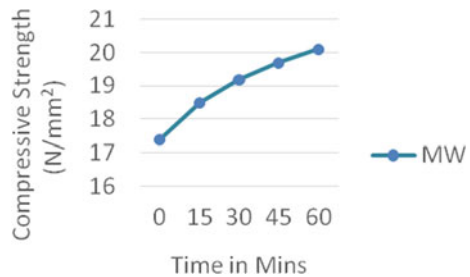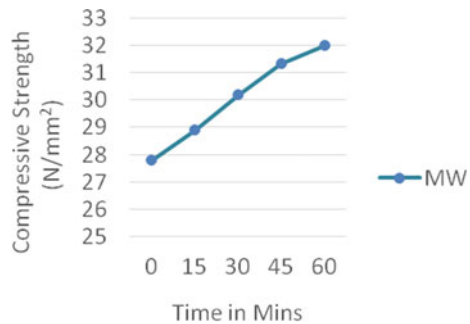**Fig. 3** 7 days compressive strength of magnetic water concrete in N/mm^2

Fig. 4 28 days compressive strength of magnetic water concrete in N/mm^2

4   Conclusions

From the experimental results, the following conclusions are arrived:

1. The chemicals parameters of water are enhanced through magnetic field treatment method.
2. The performance of slump value and compressive strength of magnetic water concrete increased with increase in contact time.
3. The workability of concrete is increased up-to 61%, for 60 min contact time of magnetic field.
4. The early age's strength increment attains through magnetic water.
5. The compressive strength of magnetic water concrete with maximum contact time increased by 15.5%.

References

1. Ahmed SM (2008) Effect of magnetic water on engineering properties of concrete. Al-Rafidain Eng 17:71–82
2. Su N, Wu C-F (2003) Effect of magnetic field treated water on mortar and concrete containing fly ash. Cement Concr Compos 25:681–688
3. Su N, Wu Y-H, Mar C-Y (2003) Effect of magnetic water on the engineering properties of concrete granulated blast-furnace slag. Cem Concr Res 30:599–605
4. Faris AS, Al-Mahaidi R, Jadooe A (2014) Implementation of magnetized water to improve the properties of concrete. Int J Civ Eng Technol (IJCIET) 5:43–57
5. Ali shynier, Mezher abed, Zaineb fouad (2014) Improving some of mechanical properties of concrete by magnetic water technology. Ministry of Science and Technology
6. Afshin H, Gholizadeh M, Khorshidi N (2010) Improving mechanical properties of high strength concrete by magnetic water technology. Arch Scientia Iranica 17:74–79
7. Hassan AF (2008) Effect of magnetized water on the properties of cement mortars at the earlier ages. Al-Qadisiya J Eng Sci 1:95–108
8. Banejad H, Abdosalehi E (2009) The effect of magnetic field on water hardness reducing. In: International water technology conference (IWTC), vol 13, pp 117–128
9. Goudar SK, Das BB, Arya SB (2019) Microstructural study of steel-concrete interface and its influence on bond strength of reinforced concrete. Adv Civ Eng Mater ASTM Int 8(1):171–189
10. Siva Konda Reddy B, Ghorpade VG, Sudarsana Rao H (2014) Influence of magnetic water on strength properties of concrete. Indian J Sci Technol 7:14–18
11. Siva Konda Reddy B, Ghorpade VG, Sudarsana Rao H (2014) Use of magnetic water for mixing and curing of concrete. Int J Adv Eng Res Stud 4:31–43
12. IS: 2386 (Part III)—1963: Methods of test for aggregate in concrete—specific gravity, density, voids, absorption and bulking
13. IS 3025 (Part 11) (1983, Reaffirmed 2002): Method of sampling and test (physical and chemical) for water and wastewater, Part 11: pH Value (First Revision). ICS 13.060.50
14. IS 10262–2009 (2009) Recommended guidelines for concrete mix, Bureau of Indian Standards New Delhi 1–14
15. IS 1199–1959 (2004) Methods of Sampling and Analysis of Concrete—Guidelines, Bureau of Indian Standards, New Delhi 1–44
16. IS 516–1959 (2004) Methods of tests for strength of concrete, Bureau of Indian Standards, New Delhi 1–24

17. Reddy BSK, Ghorpade VG, Rao HS (2013) Effect of magnetic field exposure time on workability and compressive strength of magnetic water concrete. Int J Adv Eng Technol 4:120–122

Experimental Study on the Mechanical and Durability Performance of Geopolymer Concrete Using GGBS and Metakaolin

A. Divya and S. Saranya

1 Introduction

The geopolymer technology is proposed by Davidovits which provides significant application in the concrete industry as an alternative material to the Portland cement [1]. In order to reduce the CO_2 emission from the cement manufacturing industry, geopolymer concrete is one of the best options to reduce environmental pollution [2–4]. It also helps in utilizing a huge amount of industrial waste effectively, to avoid disposal problems. The supplementary cementious material used in geopolymer concrete is rich in silicon and Aluminium [5–9]. These compounds react with the highly alkaline solution by geopolymerisation to produce the binding material [10–12]. The process comprises of chemical reaction in high alkaline conditions on Si–Al minerals to forms a three-dimensional polymeric chain and ring structure involving the Si–O–Al–O bonds [12–18]. Geopolymer concrete is the latest environment friendly construction material for sustainable development in construction industry. This attempt results in reducing CO_2 emission from the manufacturing industry and effective utilization of industrial waste by utilizing them as concrete material [1, 5, 6, 19–21].

A. Divya (✉) · S. Saranya
Department of Civil Engineering, Sona College of Technology, Salem, India
e-mail: divya.a@sonatech.ac.in

S. Saranya
e-mail: saranya@sonatech.ac.in

2   Geopolymer Concrete Materials

GGBS used in this experimental work was obtained from Local industry. Metakaolin with specific gravity 2.50 was utilized. Sodium silicate and sodium hydroxides were used as activators to react with the aluminium and the silica in GGBS and metakaolin. Sodium hydroxide solution of 12 M concentration was prepared by dissolving hydroxide flakes with 97% purity in the water. The river sand having the fineness modulus 2.76, specific gravity 2.54 and conforming to grading zone-II as per IS: 383-1970 was used. The coarse aggregate used in this research work was 20 mm of maximum size with fineness modulus and specific gravity are 6.45 and 2.60 respectively.

2.1   Construction of Geopolymer Concrete

For the design of geopolymer concrete, from the entire mass of concrete 75% of the concrete mass is considered by total aggregates (fine and coarse). Conventional concrete is casted in the similar way with aggregate range of 75–80% by the mass of concrete in which fine aggregate occupies 30% of the total aggregates. It is observed from the literature, the average density of geopolymer concrete is 2400 kg/m^3 similar to OPC concrete. With the density of concrete, the combined mass of alkaline liquid and cementious material is derived. The mass of alkaline liquid and GGBS was determined by assuming the ratios of alkaline liquid to GGBS as 0.35. The ratio of sodium silicate to sodium hydroxide solution was fixed as 2.50 approximately. In this present work, the concentration of NaOH solution is considered as 12 M. The mix ratio of corresponding proportion is given in the Table 1.

Table 1 Mix proportioning of geopolymer concrete

Mix ID	GGBS (kg/m^3)	Metakaolin (kg/m^3)	Fine aggregate (kg/m^3)	Coarse aggregate (kg/m^3)	NaOH solution (kg/m^3)	Na$_2$SiO$_3$ solution (kg/m^3)	Water (kg/m^3)	Super plasticizer (kg/m^3)
Mix 1	442.44	–	540	1260	45.1	112.6	39.43	11.83
Mix 2	398.2	44.24	540	1260	45.1	112.6	39.43	11.83
Mix 3	353.96	88.48	540	1260	45.1	112.6	39.43	11.83
Mix 4	309.71	132.73	540	1260	45.1	112.6	39.43	11.83
Mix 5	265.47	176.97	540	1260	45.1	112.6	39.43	11.83

2.2　Development of Geopolymer Concrete

Sodium hydroxide flakes of 480 g are liquefied in one litre of water to prepare sodium hydroxide solution of 12 Molarity. The mass of NaOH solids in a solution will be influenced by the concentration of the solution expressed in terms of molar. The mass of NaOH solids was measured as 361 g per kg of NaOH solution of M concentration. The alkaline solutions are mixed together one day prior to the casting of geopolymer concrete. The solid constituent aggregates, GGBS and Metakaolin were dry mixed manually for about 3 min. After one day the alkaline solution is mixed with other concrete materials in a controlled environment and transferred into the moulds as early as possible as the setting times are very less. It is observed that the concrete were very hard to handle.

2.3　Casting and Curing

The fresh concrete is immediately transferred into the mould after mixing. Cube specimen of size of $150 \times 150 \times 150$ mm, cylinders with diameter 150 mm and height 300 mm, and beams of 500 mm $\times$ 100 mm $\times$ 100 mm were made ready to study the compressive, tensile, flexural and durability study of geopolymer concrete. After casting, all the specimens were kept at room temperature to induce the geopolymerisation process till the date of testing. Figure 1 shows the Geopolymer cube specimen at 28 days.
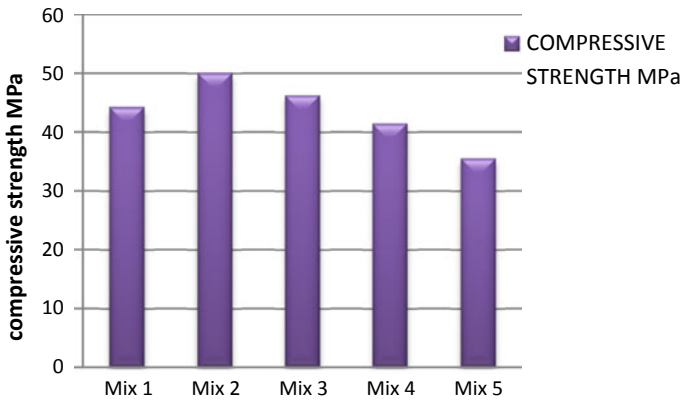
Fig. 1 Geopolymer cube specimen

Fig. 2 Compressive strength of geopolymer concrete

3 Experimental Investigation

3.1 Compressive Strength Test

The compressive strength of geopolymer concrete is determined by cube specimen. It is observed that the geopolymer concrete can withstand high load carrying capacity. From the graph it is observed that the concrete with GGBS and Metakaolin are acting as good binding materials. The compositions Mix 2 possess a higher compressive strength than the other combination. Figure 2 shows the comparison of the compressive strength of geopolymer concrete.

3.2 Tensile Strength Test

From the observation, it is noted that the tensile strength of geopolymer concrete increases with increase in percentage of GGBS at later days. It was found that split tensile strength shows improved strength of MPa for 10% replacement of metakaolin than the other mix. The tensile strength shows that the cementitious replacement gives equivalent strength as that of conventional concrete. Figure 3 shows the tensile strength of geopolymer concrete at 28 days.

3.3 Load Versus Deflection Behaviour of GPC Beams

The Geopolymer beams of size $1000 \times 100 \times 150$ mm with reinforced with two lower bars allowing for an effective depth of 130 mm with cover of 20 mm. The
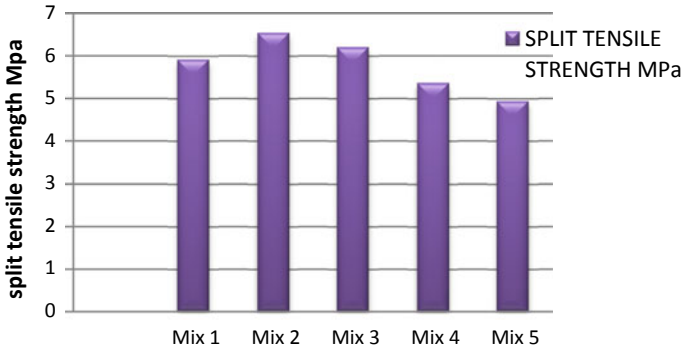
Fig. 3 Tensile strength of geopolymer concrete

beams were tested under ultimate load in two-point bending over a span of 900 mm and a shear span of 300 mm providing a shear span-to-depth ratio of 2. The load was applied in increments of 2 kN until the tensile reinforcement yielded. Deflection was observed for every corresponding load. The mid span deflection was recorded at each load step using a dial gauge which had a least count of 0.01.

When the maximum load was obtained, the concrete cover started to fall for the beams of Geopolymer and Conventional concrete in the compression zone. Figure 4 shows the failure pattern of the Geopolymer beam. It was observed that the first crack appeared close to the mid span of the beam.

Figure 5 shows the comparison of the load carrying capacity of geopolymer and conventional reinforced beam. The ultimate load of conventional and geopolymer beams are 72 kN and 91 kN respectively at the age of 28 days. It is observed that the initial and final crack capacity of Geopolymer concrete is higher than the conventional concrete.

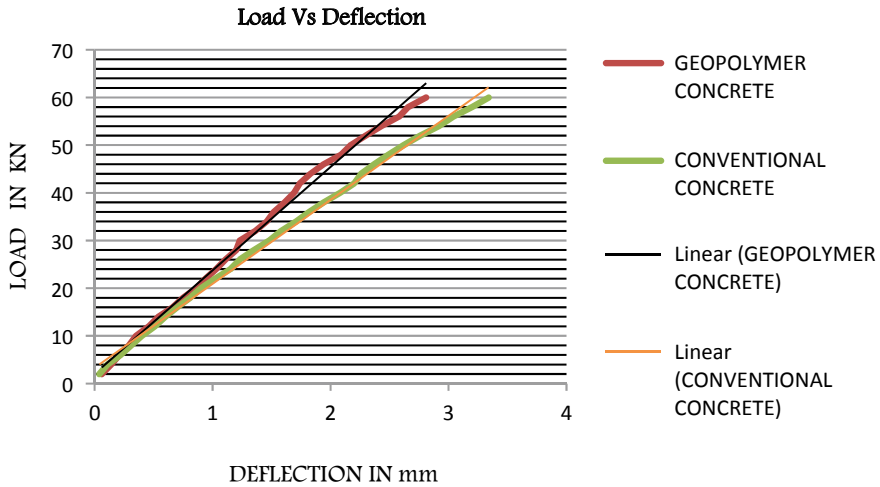**Fig. 4** Failure pattern of geopolymer concrete

Load Vs Deflection

GEOPOLYMER CONCRETE

CONVENTIONAL CONCRETE

Linear (GEOPOLYMER CONCRETE)

Linear (CONVENTIONAL CONCRETE)

Fig. 5 Load versus deflection behaviour of concrete

3.4 Half-Cell Potential Measurement

The half-cell potential measurement is an electrochemical technique used to determine the severity of corrosion in the reinforced concrete structures. After the initial curing of 28 days, the cylinder was again subjected to curing by salt water solution in the ratio 100:3.8 upto 2/3rd height of the cylinder. After 4 days, the water was removed and half-cell potential readings were taken. After the readings were taken the specimen were again subjected to salt water curing. By this way half-cell potential readings were taken every 4 days until it reached 90% probability of corrosion.

The corrosion behaviour of geopolymer and conventional concrete is shown in Fig. 6. In comparison to the values of ASTN C876, the experimental values obtained
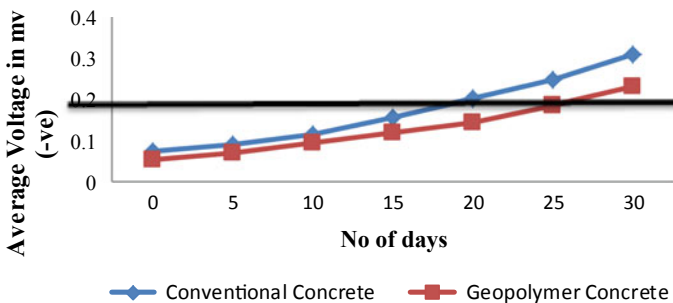

Fig. 6 Corrosion measurement by half-cell potential

from the cylinders shows that conventional concrete cylinder is subjected to corrosion earlier than Geopolymer concrete.

3.5 Accelerated Corrosion Test

An accelerated corrosion test is to determine the corrosion resistance of concrete. The salt water produces a corrosive attack to the concrete and corrosion is induced in a shorter time period by using digital multi meter.

The connection is made that the positive by is connected to the steel plate and the negative is connected to the steel reinforcement of the cylindrical specimen, which acts as electrode. Figure 7 shows the setup of accelerated corrosion test.

Figure 8 explains that the rate of corrosion of Geopolymer concrete is slower when compared to the conventional concrete.

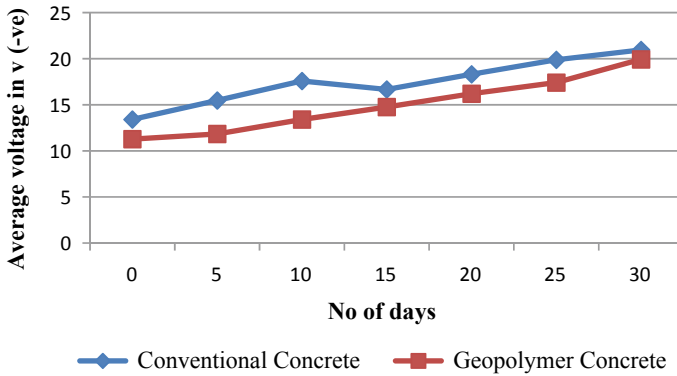**Fig. 7** Acceleration corrosion test

Fig. 8 Acceleration corrosion teat results

4 Conclusion

An attempt has been made to test the various properties of geopolymer concrete. Based on the experimental work, the following conclusions are made:

- The Compressive strength of the geopolymer concrete escalated with the increase in GGBS content in the concrete.
- The compressive strength of geopolymer concrete increases with an increase of age of concrete.
- The Ultimate load of the reinforced concrete beam for conventional concrete is 72 kN and Geopolymer concrete is 91 kN. The load carrying capacity of Geopolymer concrete RC beam is 23% higher than the conventional RCC beam.
- In half cell potential measurement, no corrosion occurs for Geopolymer concrete at 30 days as per ASTM C876 specifications.
- The Accelerated Corrosion test results shows that the current passing through the Geopolymer concrete is lower, when compared to the conventional mix.
- By proper proportioning of GGBS and Metakaolin and by selecting appropriate parameters, desirable strength of geopolymer concrete can be achieved.
- Since Geopolymer concrete exhibits good durability characteristics, it can be used as an alternate material to ordinary concrete.
- Geopolymer concrete is Eco-Friendly since complete replacement of cement is made.

References

1. Shivaprasad KN, Das BB, Renjith R (2018) Influence of fineness of fly ash on compressive strength and microstructure of bottom ash admixed geopolymer mortar. Indian Concr J 92(3)
2. Shivaprasad KN, Das BB (2018) Determination of optimized geopolymerisation factors on the properties of pelletized fly ash aggregates. Constr Build Mater (Elsevier) 163
3. Shivaprasad KN, Das BB (2018) Effect of duration of heat curing on the artificially produced fly ash aggregates. IOP Conf Ser: Mater Sci Eng 431(9):092010(1–8)
4. Sharath BP, Shivaprasad KN, Athikkal MM Das BB (2018) Some studies on sustainable utilization of iron ore tailing (IOT) as fine aggregates in fly ash based geopolymer mortar. IOP Conf Ser: Mater Sci Eng 431(9):092013(1–8)
5. Sharath BP, Das BB (2021) Production of artificial aggregates using industrial by-products admixed with mine tailings—a sustainable solution. In: Recent trends in civil engineering. Springer Publications, pp 383–397
6. Prasanna KM, Theodose I, Shivaprasad KN, Das BB (2021) Fast setting steel fibre geopolymer mortar cured under ambient temperature. In: Recent developments in sustainable infrastructure. Springer Publications, pp 769–787
7. Prasanna KM, Tamboli S, Das BB (2021) Characterization of mechanical and microstructural properties of FA and GGBS-based geopolymer mortar cured in ambient condition. In: Recent developments in sustainable infrastructure. Springer Publications, pp 751–768
8. Ganapati Naidu P, Prasad ASSN, Satayanarayana PVV (2012) A study on strength properties of geopolymer concrete with addition of GGBS. Int J Eng Res Dev 2(4)
9. Sundar Kumar S, Vasugi J, Ambily PS, Bharatkumar BH (2013) Development and determination of mechanical properties of fly ash and slag blended geo polymer concrete. Int J Sci Eng Res 4(8)
10. Krishnarao P (2013) Design of geopolymer concrete. Int J Innov Res Sci Eng Technol 2(5)
11. Parthiban K, Saravanarajamohan K, Shobana S, Ancha Bhaskar A (2013) Effect of replacement of slag on the mechanical properties of fly ash based geopolymer concrete. Int J Eng Technol 5
12. Palaniappan A, Vasantha S, Siva Prakasan S, Prabhu S (2013) GGBS as alternative to OPC in concrete as an environment pollution reduction approach. Int J Eng Res Technol 2(6)
13. Rajiwala DB, Patil HS (2011) Geopolymer concrete: a concrete of next decade. J Eng Stud Res 2(1)
14. Anuradha R, Sreevidya V, Venkatasubramani R, Rangan BV (2012) Modified guidelines for geopolymer concrete mix design using Indian Standard. Asian J Civ Eng 13
15. Sanni SH, Khadiranaikar (2012) Performance of geopolymer concrete under severe environmental conditions. Int J Civ Struct Eng 3
16. Bhattiwala QJ, Dabahekar K (2016) Effect of cementitious waste materials (GGBS) on concrete as a replacement in cement. Int J Sci Technol Eng 2(11)
17. Sutar M, Rameshwari, Tarannum, Shuruti (2015) Experimental studies on pozzolanic action of GGBS and strength properties of GGBS concrete. Int J Innov Res Sci Technol 1(12)
18. Prathap Kumar M, Srinivas V, Zoheb Nawaz M (2017) Experimental investigation on high strength concrete using GGBS, fly ash & sp-430 super plasticizer. Int Civ Eng Technol 8(9)
19. Tamilarasan VS, Perumal P, Mahaswari J (2012) Workability studies on concrete with GGBS as a replacement for cement with and without superplasticiser. Int J Adv Res Eng Technol 3(2)
20. Pithadiya PS, Nakum AV. Experimental study on geopolymer concrete by using GGBS. Int J Res Eng Technol
21. Vipul Naidu P, Pandey PK (2014) Replacement of cement in concrete. Int J Environ Res Dev 4

Feasibility Study on Metakaolin Boiler Ash Blended with M-Sand in Geo-polymer Concrete for Production of Building Blocks

D. Jegatheeswaran and S. Savitha Sree

1 Introduction

Pollution caused by emission of CO_2 into the atmosphere is increasing day by day. The depletion of fossils like coal, fuel and oil causes by various reasons. This is the main reason for the global warming causes the severe damage by weakens the heat trapping blanket that surrounding the earth. So there is need for the alternatives. The increase in the thermal power plants capacity the production of fly ash more. From which only 38% is productivity utilized in the construction industry and others are getting dumped the rivers and lake causing the contamination of water bodies. The emission of CO_2 from the concrete is directly proportional to the amount of cement in it; 900 Kgs of CO_2 is liberated into the atmosphere for the production of 1 tonnes of concrete [1]. So it's obvious that the usage of cement must be reduced, that it can be replaced with the other material having the same strength and durability. There is a shortfall of many building material, among which the brick production is major. According to the study in (TIFAC 2000), the production of brick is reduced by 25% per year in India [2].

In Asian countries especially in India the basic material for the construction is burnt clay brick. The major problem involved in the production of the clay brick is they required continuous removal of top. Soil which leads to the severe environmental problem. There is a need for the rate of using cost effective sustainable technologies using local material. For the manufacturing of 180 Billion tons burnt clay bricks it's require more than 340 Billion tonner of clay that is top soil is dug out from 5000 acre of land which causes the soil erosion. For overcoming this problem the usage of geopolymer concrete GPC blocks helps to some extreme the usage of GPC block in India increasing rapidly the demand for dwelling unit will be increases above 90 million in the future decades [3]. From various researches it is shown that the

D. Jegatheeswaran (✉) · S. Savitha Sree
Depatrment of Civil Engineering, Sona College of Technology, Salem, Tamil Nadu, India

geopolymer material shows better result than the Portland cement [4–6]. By various researches it is concluded the various property of geopolymer like no mechanism to form gypsum or ettringite from the main product of polymerization [7], good resistance to sulphate and acid solution [8, 9], thermal cures geopolymer bricks offer good benefits over the Portland cement [10]. This geopolymer technology reduced about 80% in the emission of CO_2 into the atmosphere [11]. The geo synthetic reaction of an alumina silicate type material with an alkaline solution at low temperature for a diverse group of ceramic material known as geopolymer. Geopolymer requires less energy for the synthesis process but acquires greater strength at required temperature in earlier time and also they are have more resistance to fine and chemical attack and also at the high temperature geopolymer undergoes a process similar to the sintering of ceramic material were the pores size reduced and helps in elevating the compressive strength [12–16].

The parameter like size and arrangement of the forerunner particles power the viscidity of the fresh state mixture which mainly affect the synthesis of geopolymer [17]. Thus geopolymer based on matakolin (MK) require larger amount of mixing due to the laminar arrangement and the maximum surface area of MK particles [18]. The water is required in minimum quantity for the spherical shape morphology of the fine aggregate [19, 20]. It is observed that when the MK is replaced by 20 and 30% of BS in the geopolymer with increment in the percentage there is increase in the strength and also it is observed that the long curing cause the decrease in the strength, also when during thermal curing temperature above 60 °C, the polymerization degree increase which contribute to the increase in the strength.

Lloyd and Rangan [5] conducted a study on geopolymer concrete with fly ash. For their study, they used low calcium (ASTM Class F) fly ash as their base material. The observations are made with the effect of water—geopolymer solids. They concluded that geopolymer is well adapted to manufacture precast concrete products that are essential in rehabilitation and retrofitting of structures after catastrophe as it possess magnificent properties Hardjito and Rangan [21] studied fly ash based Geopolymer Concrete. The material used was low calcium ASTM class F dry fly ash obtained from power station. The calcium content of the fly ash was about 2% in pile. They comment that statistics of compressive strength shows that the fly ash dependent geopolymer concrete has notable compressive strength and is suitable for structural implementation. The fly ash based geopolymer concrete also showed excellent resistance to sulphate attack and the elastic behaviour of hardened concrete and the strength of reinforced structural members are comparable to the Portland cement concrete [22]. The fresh geopolymer concrete was easily handled up to 120 min without any sign of setting. The addition of high range water reducing admixture improved the workability of concrete [23]. They concluded that higher concentration of sodium hydroxide solution and curing temperature in the range of 30–90 °C results in a higher compressive strength of geopolymer concrete. The higher compressive strength of geopolymer concrete depends on the larger concentration of sodium hydroxide. The rest period between casting of specimens and the commencement of curing up to 60 min has no effect on the compressive strength of geopolymer concrete. Rangan et al. [24] carried out experiments on Reinforced low—calcium fly ash based

Geopolymer concrete beams and columns. The excellent structural properties, less creep, minimum drying shrinkage, and higher resistance to sulphate attack, and acid resistant is obtained by Heat-cured low-calcium fly ash-based geopolymer concrete. And also they have very good compressive strength which is preferred for structural activities [25]. Kunal Kupwade-Patil and Erez Allouche [26] conducted test on the effect of alkali silica reaction in geopolymer concrete. In their study they observed that chemical reactions between hydroxyl ions in the pore water within the concrete matrix and certain forms of silica in alkali silica. This reaction could causes loss in strength, cracking, volume expansion and maximize the failure of the structure [21]. The results suggest that the extent of alkali silica reactions owing to the presence of reactive aggregates in fly ash based geopolymer concrete is substantially lower than OPC based concrete, and well below the ASTM specified threshold [27].

2   Objectives

The aims of the project are:

(i)   to develop structural grade Geopolymer concrete using indigenous source materials and alkaline liquids cured under heated regimes,

(ii)   to determine the short term mechanical properties viz. strength characteristics and elastic modulus,

(iii)   to establish the durability characteristics for different exposure conditions and assessment of geopolymer concrete against current durability performance criteria, and to develop and evaluate the geopolymer concrete products suitable for precast manufacture viz. products such as beams, sleepers and bricks.

3   Methodology

The work elements for the project are listed as below:

(i)   Source material, alkaline solutions, and other ingredients is recognised. The source material is bottom ash and the suitability of bottom ash from nearer power stations has been studied.

(ii)   The parameter such as particle size, LoI, and chemical composition. Material characterization of ingredients, is investigated.

(iii)   Strength tests such as cube compression test, cylinder compression test and split tension test at various time Studied as short-term and long-term mechanical properties

Studies on durability characteristics. In addition to the routine water absorption test and acid resistance tests, the following tests using corrosion analyser have been conducted:

i.   Open circuit potential test.
ii. Impedance test.
iii. LPR sweep test.
iv. Custom sweep test.
v.   Development of geopolymer precast products blocks. The development of high strength geopolymer concrete leads to the enlargement of scope incorporating the precast products like geopolymer building blocks. Further, millions of units of bricks are required for the building industry, and hence geopolymer bricks have been developed.
vi. Strength and behaviour tests on precast products.

4   Geopolymer Concrete

4.1   Preparation of Geopolymer Concrete

Low-calcium (ASTM Class F) fly ash obtained from coal-burning power stations can be suggested for the production of geopolymer concrete as they are produced as the by-product of burning anthracite or bituminous coal [28]. Low-calcium fly ash has silicon and aluminium oxides about 80% by mass, Si-to-Al ratio of about 2, iron oxide varies from 10 to 20% by mass and the calcium oxide constituted was less than 5% by mass [29], the carbon content of the fly ash, indicated by the loss on ignition by mass, was as low as less than 2% along with Coarse and fine aggregates used by the concrete industry are suitable to manufacture geopolymer concrete [27]. The alkaline liquid is prepared by the mixture of sodium silicate solution and sodium hydroxide (NaOH) solution and they should by mixed 24 h before to use.

4.2   Curing of Geopolymer Concrete

The ordinary cement concrete hardens due to hydration process in presence of water. The Geopolymer concrete revealed that cannot attain any strength by water curing since it hardens due to polymerization process in presence of heat. By mean of steam curing or hot air curing and the minimum curing period for 24 h the geopolymer concrete will harden. After casting the specimens, they are kept in rest period in room temperature for 2 days. The geopolymer concrete specimens are demoulded and then placed in steam curing chamber for 24 h at a temperature of 60 °C. The geopolymer concrete specimens are then allowed to cool in room temperature for 24 h [30].

If the geopolymer concrete is allowed to cure in ambient conditions, the strength development up to the full capacity will not take place [24]. To improve the strength development under ambient conditions, materials like silica fume and slag should be

added up to 30–40%. In that case, the geopolymer concrete is not fully based on fly ash and the cost will be more than that of concrete with ordinary Portland cement [31].

The class F fly ash collected from Mettur Thermal Power Station has been used for the development of geopolymer concrete. The fly ash and its constituents is shown in Fig. 1. XRF (mass percentage) is used to find the chemical composition of fly ash presented in Table 1.

M-sand with fineness modulus of 2.72 and specific gravity of 2.64 can be preferred. Coarse aggregates of size varies from 7 to 20 mm have been used. The different grades sodium silicate solution is available. A53 grade of sodium silicate with SiO_2-to-Na_2O ratio by mass 2, i.e., $SiO_2 = 29.4\%$, $Na_2O = 14.7\%$, and water $= 55.9\%$ by mass, is commonly used.

Fig. 1 The chemical composition of fly ash as determined by XRF

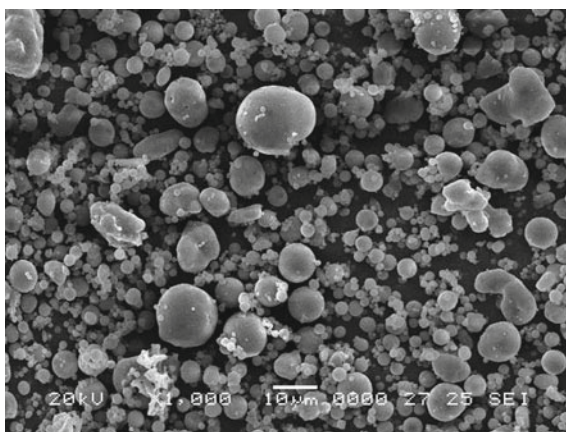**Table 1** Chemical composition of fly ash

Compound	Percentage (mass)
SiO_2	52.54
Al_2O_3	26.74
Fe_2O_3	11.12
CaO	1.28
Na_2O	0.47
K_2O	0.82
TiO_2	1.57
MgO	0.87
P_2O_5	1.53
SO_3	1.70
*LoI	1.36

* LoI—Loss on Ignition

The sodium hydroxide with 97–98% purity, in flake or pellet form, is commercially available. The solids must be dissolved in water to make a solution with the required concentration range between 8 and 16 Molar [32]. The Silicate and Aluminium compounds in the fly ash is desiccated by Sodium Hydroxide (NaOH) and Sodium Silicate (Na_2SiO_3) solutions.

5 Observation

5.1 Discussion on Strength of Geopolymer Concrete

Geopolymer concrete is a cement less concrete where the cement is replaced by fly ash and water is replaced by a combination of alkali activator solution. The alkali activator solutions are Sodium Hydroxide (NaOH) and Sodium Silicate (Na_2SiO_3). Different molarities of Sodium Hydroxide solution have been tried in this study [33].

It is found that the average compressive strength of Geopolymer concrete with 12 mol concentration of Sodium Hydroxide is 24.83 N/mm^2 which is very much suitable for minimum strength of concrete for Civil Construction suggested by IS: 456-2000. The average compressive strength of Geopolymer concrete of 8 mol Sodium Hydroxide is 20.92 N/mm^2. The reduction in concentration of Sodium Hydroxide reduces the strength of concrete. This strength is very well suited for M20 grade concrete [34]. The compressive strength of 8 M and 12 M concentration of NaOH Geopolymer concrete at later ages are showing 49% and 62% respectively increase at 9 months age in room temperature. From the case study 2, it is found that the average compressive strength of Geopolymer concrete of M 40 grade with 8 mol Sodium Hydroxide is 42.35 N/mm^2. This concrete is very much suitable for applications with high strength concrete.

A mix ratio of M 20 grade concrete obtained using IS: 10262-2009 was used (1:1.7:3.1) with a partial modification of replacement of cement and water by fly ash and different concentration of NaOH. The compressive strength of Geopolymer with 8, 10, 12 and 14 mol concentration of NaOH shows 30.75, 32.50, 37.50 and 20.50 N/mm^2. It is found that Geopolymer concrete with 12 M concentration of NaOH gives maximum compressive strength. A concrete mix with different concentrations of NaOH such as 8, 10 and 12 were tried with different ratio of AAS (sodium silicate plus sodium hydroxide) per fly ash as 0.40, 0.45, 0.50 and 0.55. Geopolymer Concrete with 8 M NaOH solution with AAS/fly ash ratio of 0.50 gives higher strength of 52.08 N/mm^2. Concrete of this strength is very much suitable for pre-stressing operations.

In this study, same mix ratio has been investigated for Geopolymer concrete with different ratios of alkaline solutions which is one of the main ingredients. The ratio of Sodium Silicate and Sodium hydroxide is kept as 2.5. The ratio of Alkali Activator solution (Na_2SiO_3 + NaOH) and fly ash is kept as 0.45. The strength properties of geopolymer concrete at different ages.

5.2 Acid Resistance Test on Geopolymer Concrete

Immersion technique was adopted to perform the acid attack studies. Cylinder specimens (100×200 mm) immersed in H_2SO_4 solution to perform the acid attack studies for 60 days. To maintain uniformity the solution is stirred at least for 2 days and also change with new solution in regular break to maintain the concentration in the medium [33, 35]. The surfaces were cleaned after removing the specimens from the medium to remove weak and loose material from the surface [36]. The percentage of mass increase when compared with initial mass for all geopolymer concrete. Hence, geopolymer concrete showed an excellent resistance to acid attack [37].

The compressive strength of GPC specimens immersed in H_2SO_4 about 60 days got reduced while increasing the concentration of acid. The 8 M NaOH specimen shows reduction in strength of 9.3, 18.1 and 31.8% in 0.5, 1, and 2% H_2SO_4 concentration respectively with respect to control specimen. The 10 M NaOH specimen shows reduction in strength of 13.7, 24.1 and 41.5% in 0.5, 1, and 2% H_2SO_4 concentration with respect to control specimen. The 12 M NaOH specimen shows reduction in strength of 18.41, 27.5 and 33.4% in 0.5, 1, and 2% H_2SO_4 concentration respectively with respect to control specimen. The 14 M NaOH specimen shows reduction in strength of 15.7, 21.0 and 26.4% in 0.5, 1, and 2% H_2SO_4 concentration respectively with respect to control specimen [38].

5.3 Sulphate Resistance Test on Geopolymer Concrete

The compressive strength of Geopolymer Concrete (GPC) specimens immersed in Na_2SO_4 about 60 days are reduced while increasing the concentration of acid. The strength of GPC specimen kept in Na_2SO_4 solution for 60 days shows reduction in strength in all the NaOH concentrated GPC specimens [39]. The compressive strength of 8 M, 10 M, 12 M and 14 M of NaOH, GPC specimens show 22.2, 12.5, 24.5 and 19.2% reduction in strength when it is immersed in Na_2SO_4 for 60 days [40].

5.4 Strength Tests

To test the geopolymer brick the strength test like compressive strength, flexural strength and tensile strength were. Country bricks and fly ash bricks of same size were also tested for comparison purpose. A comparison of strength of various bricks are presented in Figs. 2 and 3.
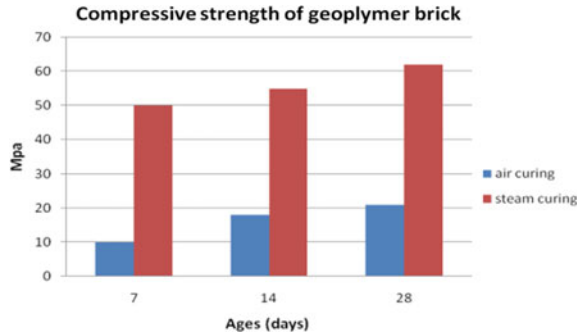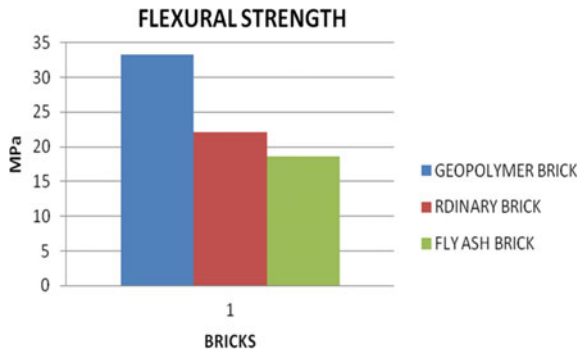
Fig. 2 Compressive strength
of geopolymer bricks

Fig. 3 Flexural strength of
bricks

5.5 Durability Tests

Acid resistance tests [41] were conducted on the three types of bricks namely
geopolymer bricks (with 10 M NaOH solution) country bricks and fly ash bricks by
immersing in different concentrations of sulphuric acid (H_2SO_4) and hydrochloric
acid (HCl). A comparison of weight loss is presented in Figs. 4 and 5.

Water absorption test were also conducted on the three types of bricks and the
test results are presented in and Fig. 6.
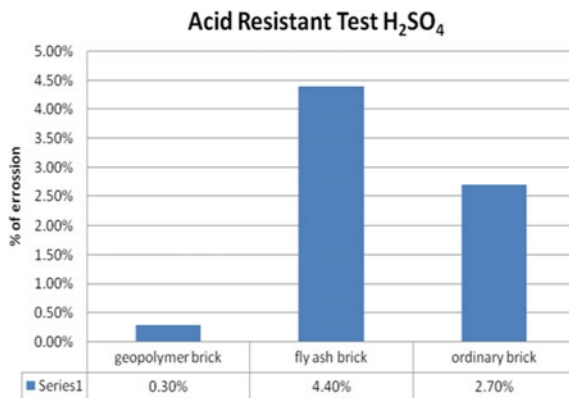
Fig. 4 Acid resistance test (H_2SO_4)
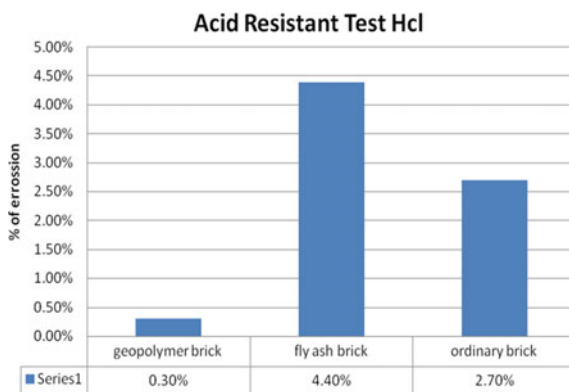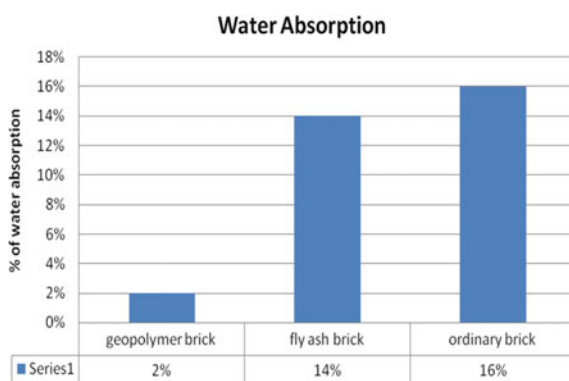

Fig. 5 Acid resistance test (HCl)

Fig. 6 Water absorption test

6 Conclusion

6.1 Environmental Benefits of the Technology

The use of fly ash as a source material has environmental advantages in addition to those presented by the replacement of Portland cement. The use of the industrial by-products such as fly ash in a high value product like concrete imparts better value-addition to these materials rather than low end usage as landfills and pavement sub-bases. It significantly decreases the use of natural resources and energy. The cement industry is the main culprit for the atmospheric pollution and mainly responsible for the emission of Green House Gases like CO_2. Production of one ton of cement approximately releases one ton of CO_2 into the atmosphere. Hence every million ton of fly ash used for geopolymer concrete helps the abatement of 1.0 million tons of CO_2 to atmosphere. It also obviates the problem of their safe storage and/or disposal. Presently, most fly ash is being handled in wet form and disposed off in ash ponds which are harmful for the environment and occupy a vast area. The World Bank has cautioned India that by 2015, disposal of coal ash would require 1000 km^2 or 1 m^2 of land per person [42]. Hence, use of geopolymer concrete helps us to increase the land available for agricultural and other purposes. Further, non toxic chemicals are used for the production of geopolymer concrete. These chemicals can be handled by land without any additional protection. Hence, geopolymer concrete developed using fly ash is an environment friendly green material.

6.2 Economic Benefits of the Technology

100% replacement of OPC by fly ash and hence geopolymer concrete is termed as cement less concrete [43] and also they are 10–30% cost esurient than the normal OPC. The heat-cured low-calcium fly ash based geopolymer concrete may yield additional economic benefits when it is utilized in infrastructure usage [44].

In the case of infrastructure applications, space available for keeping precast elements is very much restricted. Precast elements made out of normal concrete require 28 days for gaining full strength [45]. But at the same time, heat cured geopolymer concrete attains full strength in one day [25]. This results in savings in cost of expensive moulds and at the same time less space is required to keep the geopolymer concrete precast elements as they can be moved out of casting yard quickly [46]. Further, expensive steam curing chamber is not required at site. Cost effective steam curing arrangement made out of tarpaulins would be sufficient at site.

6.3 From the Experimental Investigation the Following Conclusion Are Made

Geopolymer concrete can be manufactured with low calcium fly ash with different molarities of NaOH. The steam cured geopolymer concrete beams with 8 Molarity NaOH solutions attain higher strength. Adequate curing temperature (60–75 °C) and adequate curing time (minimum 24 h) can give better results. The geopolymer concrete with steam curing at 75 °C increases the strength by 35–50% when compared to geopolymer concrete without steam curing.

Workability which influences the properties of the fresh concrete and cube compressive strength, flexural strength which influences the properties of the hardened concrete have been identified. Compressive strength of the Low-calcium fly ash-based geopolymer concrete has an excellent and is suitable for structural need due to the speedy polymerization process and aging of the alkaline liquid.

8 Molarity NaOH solution casted geopolymer specimen showed higher strength compared with other molarity specimens because when H_2O to $–Na_2O$ molar ratio increases which causes the decrease in the strength of geopolymer concrete.

Geopolymer binders have emerged as one of the possible alternative to OPC binders due to their reported high early strength and resistance against acid and sulphate attack apart from its environmental friendliness.

As geopolymer has better corrosion resistance, evidenced from corrosion tests, it can be used for making precast products like underground pipes, box culverts etc.

Since it is possible to produce geopolymer concrete of strength higher than 50 MPa it could be used for prestressed Concrete works.

Geopolymer bricks show very high compressive strength when compared to ordinary bricks. The strength of geopolymer bricks can be brought to the level of ordinary bricks by using lower molar solutions of NaOH.

References

1. Duxson P, Lukey GC, van Deventer JSJ (2007) Physical evolution of Na-geopolymer derived from metakaolin up to 1000 C. J Mater Sci 42(9):3044–3054. https://doi.org/10.1007/s10853-006-0535-4
2. Al-Bakri MM, Mohammed H, Kamarudin H, Niza IK, Zarina Y (2011) Review on fly ash-based geopolymer concrete without Portland Cement. J Eng Technol Res 3(1):1–4
3. Zhang Z, Yao X, Zhu H (2010) Potential application of geopolymers as protection coatings for marine concrete I. Basic properties. Appl Clay Sci 49(1–2):1–6. https://doi.org/10.1016/j.clay.2010.01.014
4. Nicholson C, Fletcher R, Miller N, Stirling C, Morris J, Hodges S, Mackenzie K, Schmucker M (2005) Building innovation through geopolymer technology. Chem New Zel 69(3):10–13
5. Lloyd RR, Provis JL, van Deventer JSJ (2011) Acid resistance of inorganic polymer binders. I. Corrosion rate. Mater Struct 45(1–2):1–14. https://doi.org/10.1617/s11527-011-9744-7
6. Duxson P, Fernández-Jiménez A, Provis JL, Lukey GC, Palomo A, van Deventer JSJ (2006) Geopolymer technology: the current state of the art. J Mater Sci 42(9):2917–2933. https://doi.org/10.1007/s10853-006-0637-z

7. Komnitsas K, Zaharaki D (2007) Geopolymerisation: a review and prospects for the minerals industry. Miner Eng 20(14):1261–1277. https://doi.org/10.1016/j.mineng.2007.07.011

8. Martínez-López C, Mejía-Arcila JM, Torres-Agredo J, Mejíade Gutiérrez R (2015) Evaluación de las características de toxicidad de dos residuos industriales valorizados mediante procesos de geopolimerización. DYNA 82(190):74–81. https://doi.org/10.15446/dyna.v82n189.43136

9. Buchwald A, Weli M, Dombrowski K (2005) Evaluation of primary and secondary materials under technical, ecological and economic aspects for the use as raw materials in geopolymeric binders. In: Proceedings of the 2nd international symposium of non-traditional cement and concrete, pp 32–40. ISBN: 80-214-2853-8

10. Duxson P, Provis JL (2008) Designing precursors for geopolymer cements. J Am Ceram Soc 91(12):3864–3869. https://doi.org/10.1111/j.1551-2916.2008.02787.x

11. Kovalchuk G, Fernández-Jiménez A, Palomo A (2008) Alkali activated fly ash. Relationship between mechanical strength gains and initial ash chemistry. Mater Constr 58(291):35–52. eISSN: 1988-3226

12. Renjith R, Shivaprasad KN, Das BB (2018) Properties of heat cured bottom ash based geopolymer mortar admixed with fly ash of different fineness. In: Advances in concrete, structural and geotechnical engineering. Bloomsbury Publishing Plc, pp 603–607

13. Prasanna KM, Tamboli S, Das BB (2020) Characterization of mechanical and microstructural properties of FA and GGBS-based geopolymer mortar cured in ambient condition. In: Select proceedings of ICRDSI 2019. Springer Publications Pte. Ltd., pp 751–768

14. Prasanna KM, Theodose I, Shivaprasad KN, Das BB (2020) Fast setting steel fibre geopolymer mortar cured under ambient temperature. In: Select proceedings of ICRDSI 2019. Springer Publications Pte. Ltd., pp 769–787

15. Kudachimath N, Raviraj HM, Das BB (2021) Effect of GGBS on strength of aluminium refinery residue stabilized by alkali solution. In: Select proceedings of TMSF 2019. Springer Publications Pte. Ltd., pp 331–339

16. Shivaprasad KN, Das BB, Renjith R (2018) Influence of fineness of fly ash on compressive strength and microstructure of bottom ash admixed geopolymer mortar. Indian Concr J 92(3)

17. Steveson M, Sagoe-Crentsil K (2005) Relationships between composition, structure and strength of inorganic polymers. J Mater Sci 40(16):4247–4259

18. Mehta PK (2002) Greening of the concrete industry for sustainable development. ACI Concr Int 24(7):23–28

19. Cembureau (2007) Cement in Cembureau countries statistics 2005–2007. http://www.cembureau.be/Documents/KeyFacts/STATISTICS/Cementpercent20inpercent20CEMBpercent20countries.pdf

20. Portland Cement Association (2006) World cement consumption growth expected to continue. In: Portland Cement Association executive report. http://www.cement.org/exec/1023-06.html

21. Hardjito D, Rangan BV (2005) Development and properties of Low calcium fly ash-based geopolymer concrete research report GCI. Faculty of Engineering Curtin University of Technology, Perth

22. Lieblang P (2009) Green Europe: emission trading on a largescale and individual green concrete housing on a small-scale. In: Katutz H (ed) Proceedings of international concrete conference and exhibition ICCX oceania "Concrete Solutions for Oceania", Sydney, Australia, pp 26–26

23. Mehta PK (2001) Reducing the environmental impact of concrete. ACI Concr Int 23(10):61–66

24. Rangan BV, Wallah SE (2006) Low-calcium fly ash based geopolymer concrete: long-term properties. Research report GC2. Faculty of Engineering Curtin University of Technology, Perth

25. Lloyd N, Rangan BV (2009) Geopolymer concrete—sustainable cementless concrete. In: Proceedings of tenth ACI international conference on recent advances in concrete technology and sustainability issues, Seville, pp 33–53

26. Karstensen KH (2006) Cement production in vertical shaft Kilns in China—status and opportunities for investment. UNIDO Contract RB-308-D40-8213110-2005

27. IPCC (2007) Climate change 2007: working group III: mitigation of climate change, emission trends (global and regional). http://www.ipcc.ch/publications_and_data/ar4/wg3/en/tssts-ts-7-2emissiontrends.html

28. Boden TA, Marland G, Andres RJ (2010) Global, regional, and national fossil-fuel CO_2 emissions. Carbon Dioxide Information Analysis Center, Oak Ridge National Laboratory, U.S. Department of Energy, Oak Ridge, Tenn., U.S.A. https://doi.org/10.3334/CDIAC/00001_V2010

29. Hardjito D, Wallah SE, Sumajow DMJ, Vijaya Rangan B (2009) On the development of fly ash based geopolymer concrete. ACI Mater J 101:52

30. Kupwade-Patil K, Allouche E (2011) Effect of alkali silica reaction in Geopolymer concrete. In: World of coal ash conference, May, 9-12-2011, Denver, CO, USA

31. Davidovits J (1994) High-alkali cements for 21st century concretes in concrete technology, past, present and future. In: Kumar Metha P (ed) Proceedings of V. Mohan Malhotra symposium. ACI SP-144, pp 383–397

32. Department of Environment and Water (2007) Industrial process sector greenhouse gas emissions projections 2007. http://www.climatechange.gov.au/projections/pubs/industrial2007.pdf

33. Stevenson M, Panian L (2009) Sustainability through strength. Concr Int 31(3):34:39

34. Poon CS, Lam L, Wong YL (2000) A study on high strength concrete prepared with large volumes of low-calcium fly ash. Cem Concr Res 30(3):447–455

35. ASTM Committee on Standards B611-2005 (Revised), Standard test method for abrasive wear resistance of cemented carbides

36. Mehta PK (2004) High performance, high volume fly ash concrete for sustainable development. In: Proceedings of international workshop on sustainable development and concrete technology, Beijing, China, pp 3–14

37. Davidovits J, Davidovits R, Davidovits M (2008) Geopolymer cement based on fly ash and harmless to use. PCT Publication WO 2008/01238, Indian Patent Application 1861 MUMNP/2009-05-15

38. ASTM Committee on Standards CSA/S413-1994

39. Malhotra VM (2002) High-performance high-volume fly concrete. Concr Int 24(7):30–34

40. Stern M, Geary AL (1957) J Electrochem Soc 104:56

41. ASTM Committee on Standards D2776, & G59, Volume 3.02. Metal Corrosion ASTM 2010 (Revised), test method corrosivity of water in the absence of heat electrical method

42. ASTM Committee on Standards C1543-10a, Standard test method for determining the penetration of chloride ion in to concrete by ponding

43. Sofi M, van Deventer JSJ, Mendis PA, Lukey GC (2007) Bond performance of reinforcing bars in inorganic polymer concrete (IPC). J Mater Sci 42(9):3107–3116

44. Sofi M, van Deventer J, Mendis PA, Lukey GC (2007) Engineering properties of inorganic polymer concretes (IPCs). Cem Concr Res 37(2):251–257

45. Australian Coal Association (2010) Coal and its uses-electricity generation. www.australian.com.au

46. Provis JL, Muntingh Y, Lloyd RR, Xu H, Keyte LM, Krivenko PV, van Deventer JSJ (2007) Will geopolymers stand the test of time? Ceram Eng Sci Proc 28(9):235–248

Finite Element Modelling of Reinforced Concrete Element Under Corrosion Effects

C. Rajendra Prasath, D. Vivek, and K. S. Elango

1 Introduction

Corrosion is a natural process that transforms a refined metal, including its oxide, hydroxide and sulphide, to a more chemically stable form It is the gradual deterioration of materials by their environment by chemical and/or electro chemical interactions [1]. The Finite Element Method (FEM) is a powerful technique designed specifically for solving complex problem of structural mechanics in statistics and econometrics, and it remains the method of choice for complex structures. In the FEM, a sequence of compatible finite elements interconnected at discrete points called nodes represents the structural system.

ABAQUS FEA is a finite element analysis and computer aided engineering software suite. ABAQUS/Standard, a finite element analyzer for special applications that employs an implicit platform of integration. ABAQUS/Explicit is a special purpose finite element analyser that has to use an explicit integration system to solve highly nonlinear systems under transient loads with many complex contacts. The uncorroded and corroded beams are modelled by using ABAQUS. In this modelling the stress strain behaviour and quality of beam will be obtained. The analysis consists of several steps: (a) Risk estimation (b) Computational load determination (c) Structural behaviour analysis (d) Structural system selection and (e) Structural behaviour evaluation.

C. R. Prasath (✉)
Department of Civil Engineering, PSNA College of Engineering and Technology, Dindigul, India

D. Vivek · K. S. Elango
Department of Civil Engineering, KPR Institute of Engineering and Technology, Coimbatore, India

1.1   Modelling Sequences in ABAQUS

There are three separate phases in every complete finite-element analysis:

Pre-processing or modelling: This stage includes the development of an input file containing the finite-element analyzer design of an engineer (also called a solver).

Processing or finite element analysis: This stage generates a visual file for performance.

Pre-processing: Postprocessor contains sophisticated routines used for shorting, printing and plotting selected results from a finite element solution. It is used to display the solutions in coloured contours, which assist the users to get a better understanding of the results.

Module

Part—Create individual parts by sketching their geometry or importing them.
   Property—Establish meanings of sections and materials and allocate them to component regions.
   Assembly—Build and assemble instances of the component.
   Step—Develop and describe the steps of analysis and associated requests for output.
   Interaction—Define the interaction between regions of a model, such as touch.
   Load—Assign loads, boundary conditions and fields.
   Mesh—Developing a mesh with a finite element.
   Optimization—Create an optimization task and configure it.
   Work—Apply a job and observe its progress for assessment.
   Visualization—View the outcome of the research and the model data extracted.

1.2   Objectives of This Study

The main objectives of the present study are the following:

- To compare the structural behaviour of uncorroded and corroded concrete beams with different corrosion rate using ABAQUS.
- To obtain the loss of steel area, different crack patterns and degradation strength in each corrosive model.

2   Review of Literature

Abdelatif et al. [2] have studied lap splice joints in concrete, the chloride stimulated corrosion technique. Calculate damage in concrete under different corrosion levels, corrosion current density, rust growth, expansion of corrosion products and stresses

were considered. Compared to numerical simulations, an experimental observation of corrosion-induced concrete cover cracking shows good correlation with their observations. Peng [3] have presented the effect of various stirrup arrangements on the accelerated corrosion of the rust properties of concrete members. Based on the research findings, the stirrup mode indicates that it has a major effect on the distribution of corrosion fractures, concrete cover damage and rebar corrosion features. Mechanical properties of corroded beam were prejudiced by stirrup arrangements and displays great resistance performance.

Juhui [4] have investigated chloride contaminated RC structures with non-uniform corrosion of reinforcement. RC structures definitely improve cracks in the chloride environment by the ingress of violent agents through chloride. The numerical finding implies investigating the mechanical impact of non corrosion product build-up around the bar in RC structures subjected to steel corrosion. Chen et al. [5] have inspected and develop a finite element model for corrosion to study crack propagation in concrete. Non uniform corrosion distribution around the steel cross section in reinforced concrete elements was influenced by chloride penetration from the member surface. Test results shows different crack pattern in reinforced concrete members were swayed by cover thickness on the crack widening.

Kallias and Imran Rafiq [6] have premeditated numerically 2D non-linear FE analysis to assess the structural performance of a series of RC beams—damaged by corrosion at different locations. FE models for the corrosion damaged RC members were developed and validated using experimental data. They reported that concrete compressive strength, bond deterioration and corrosion damage in the compressive region of the beams were similar to predicted response. Berra et al. [7] have investigated axisymmetric finite element analysis, modelling different levels of containment given by the transverse steel reinforcement, the bond strength of ribbed bars corrosion in reinforced concrete. Concrete cover cracking were caused by the corrosion product expansion to model. Such findings lead to a discussion of the various results of several experimental results. They concluded that the bond strength corroded bars is the main parameters in modelling to predict the properties of reinforcement.

Du et al. [8] have demonstrated in holes cast in concrete, simulated corrosion experiments with internal pressure were applied experimentally and the finite element model of the corroding reinforcement effects was considered. Test results on the surrounding concrete from reinforced concrete accelerated corrosion studies were confirmed against the predicted outcomes. Based on the above literatures tested more number of beams with different size of rebars for finding the beam is in safe in deflection and extracted the core theme of the study.

3   Methodology of the Study

3.1   Selection of RC Element

The beam of size 1500 × 150 × 200 mm was drawn with different reinforcement area of decreasing in reinforcement. The deflection is analysed using ABAQUS and compared with conventional specimen. The reinforcement detailing of beam is shown in Fig. 1.

3.2   Material Properties

3.2.1   Concrete Properties

As the hardened compressive strength and durability of concrete are controlled by these properties, the properties of workability, temperature density and age are considered to ensure the manufacture and placement of 'quality' concrete. The concrete mix was designed using maximum size of coarse aggregate as 10 mm, to achieve characteristics compressive strength 40 N/mm^2 at 28 days. The compressive strength of concrete was determined by simultaneous casting and testing cubes of size 150 mm × 150 mm × 150 mm, repair from the same concrete batch used for preparation of beam. The Poisson's ratio of concrete may vary from 0.1 to 0.3, in this study approximately 0.15 were selected. Density of concrete is taken as 25 kN/m^3 and Young's modulus is calculated from $5500\sqrt{fck}$. The value obtained 27,500 N/mm^2.

3.2.2   Steel Properties

Great formability and durability, good tensile yield strength and good thermal conductivity are the most significant properties of steel. The most distinctive feature of the stainless steel property is corrosion resistance, as well as these significant properties. The Poisson's ratio of steel is 0.3. The density and young's modulus of steel is 7850 kg/m^3 and 2.1 × 10^5 N/mm^2 respectively.
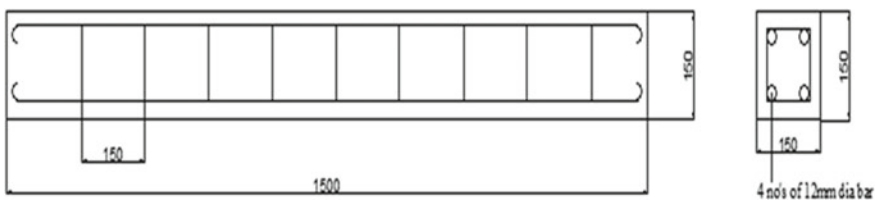

Fig. 1 Reinforcement detailing of beam

3.3   Finite Element Modelling of Beam

3.3.1   Static Analysis

Static analysis of the beams were executed under concentrated load and surface load applied in the vertical direction. Modelling procedure was shown in Figs. 2 and 3.

Deformation value of surface load and concentrated load were Compared and tabulated as shown in the Table 1.

Concentrated Load

Deformation of reinforced concrete beam with various diametres of rebar under concentrated load is shown in the Fig. 4.
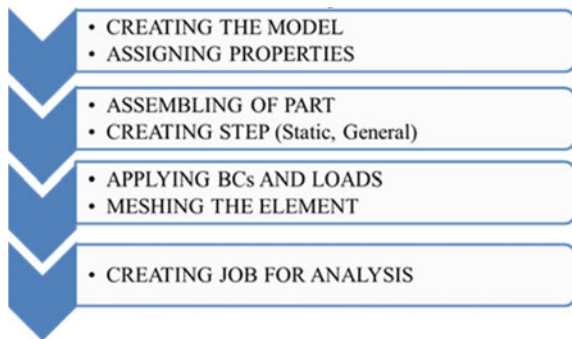
Surface Load

Deformation of reinforced beam with various diametres of rebar under surface load is shown in the Fig. 5.

3.3.2   Dynamic Analysis

A dynamic analysis often leads to the inertia forces that a structure develops when it is excited by abruptly applied dynamic loads. Modelling procedure was shown in Fig. 6. And also mode shape and frequency values of different diameter rebars was dispalced in Fig. 7.

After the dynamic analysis results shows Deformation of rebars having diametres of 12 and 10 mm in Figs. 8 and 9.

Fig. 2 Modelling procedure for static analysis

- CREATING THE MODEL
- ASSIGNING PROPERTIES

- ASSEMBLING OF PART
- CREATING STEP (Static, General)

- APPLYING BCs AND LOADS
- MESHING THE ELEMENT
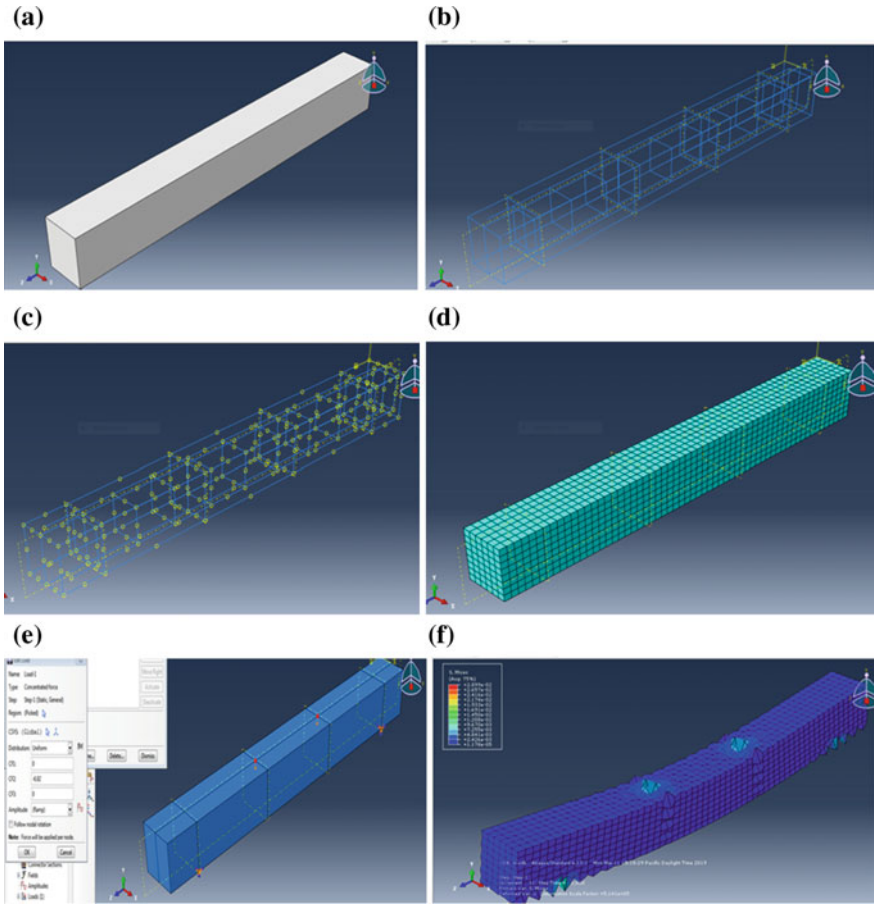
- CREATING JOB FOR ANALYSIS

Fig. 3 Modelling procedure **a** Solid model of beam, **b** Assembly of beam, main rod and stirrups, **c** Interaction of beam, main rod and stirrups, **d** Meshing, **e** Application of concentrated load, **f** Stress contour

Table 1 Deformation values under concentrated and surface load

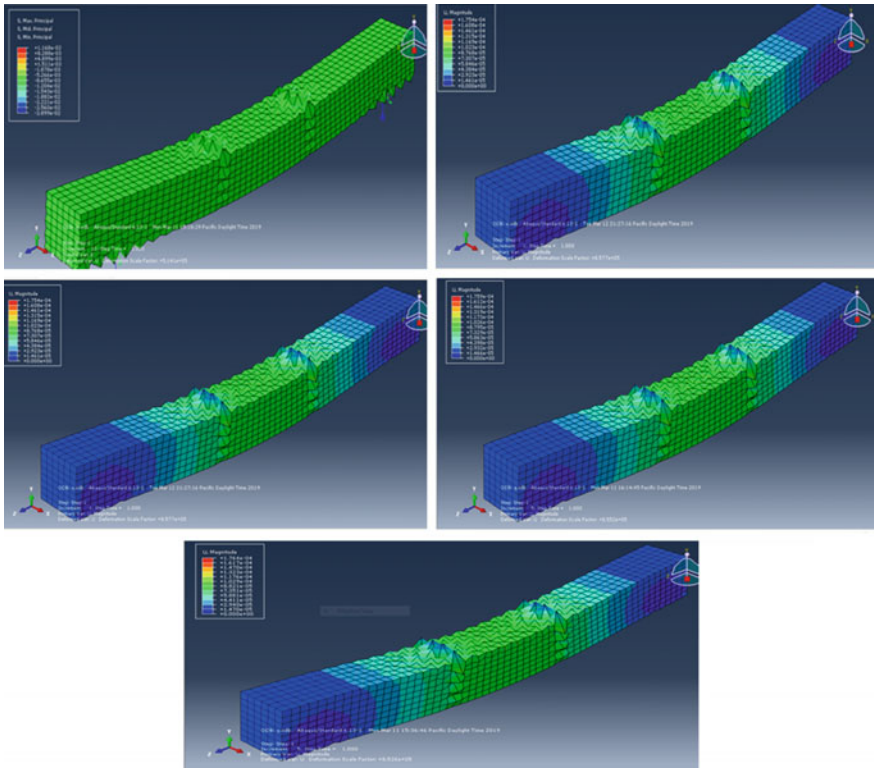| Size of the rebar diametres (mm)	Deformation (mm)	
	Surface load	Concentrated load
12	1.997	5.141
11.5	1.982	6.42
11	1.967	8.57
10.5	1.953	8.552
10	1.94	8.53

Fig. 4 Deformation of rebars having different diametres 12, 11.5, 11, 10.5 and 10 mm under concentrated load

Figures 7 and 8 represents the frequency value of each mode shape of 12 and 10 mm diameter rebars after the deformed shapes and mode shape for different rebar diameters were obtained from ABAQUS (in cycle/time).

4   Conclusion

In this investigation to observe the behaviour of RC beam under corrosion is very difficult and tedious so that ABAQUS was used to investigate the static and dynamic behaviour of RC element analytically. The following conclusions have been drawn from the analytical results:

- The beam with different bar sizes of 12, 11.5, 11, 10.5 and 10 mm was examined when comparing the finite element analysis (both static and dynamic) of all five models.
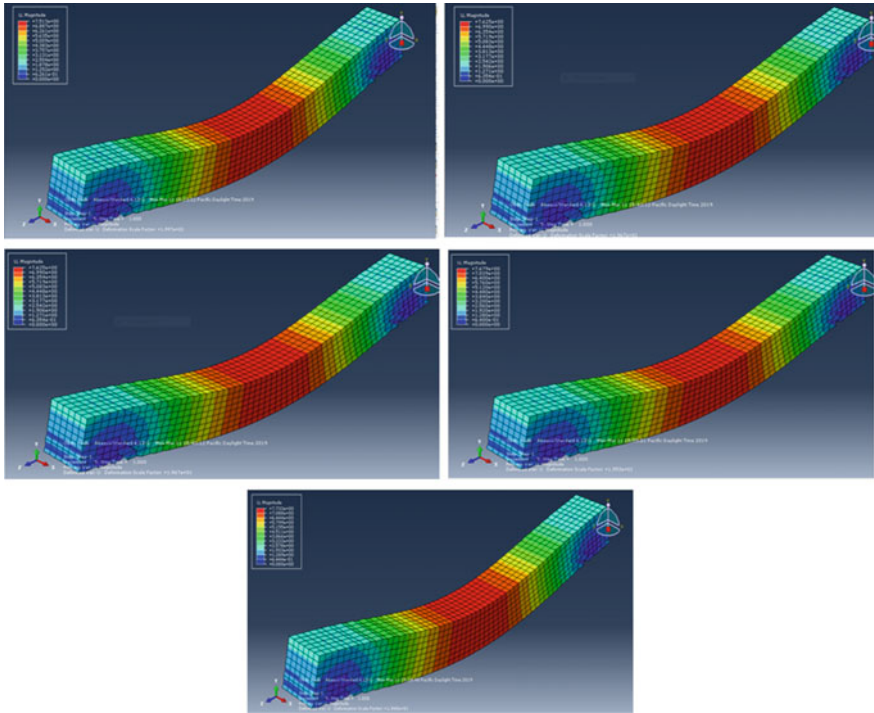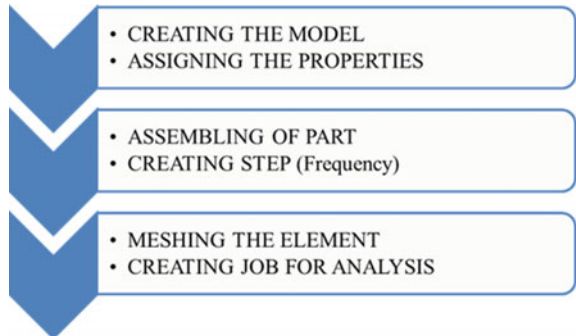
Fig. 5 Deformation of rebars having different diametres 12, 11.5, 11, 10.5 and 10 mm under surface load

Fig. 6 Modelling procedure for dynamic analysis

- CREATING THE MODEL
- ASSIGNING THE PROPERTIES

- ASSEMBLING OF PART
- CREATING STEP (Frequency)

- MESHING THE ELEMENT
- CREATING JOB FOR ANALYSIS

- From the analytical investigation shows that the decrease in the cross sectional area of reinforcement would the decrease the load carrying capacity and the deflection values were increased.
- From the dynamic analysis results, it can be observed that with the decrease in cross sectional area, the mode shape values increased.

1	Mode	1: Value = 121.43 Freq = 1.7538 (cycles/time)
2	Mode	2: Value = 295.33 Freq = 2.7351 (cycles/time)
3	Mode	3: Value = 491.36 Freq = 3.5279 (cycles/time)
4	Mode	4: Value = 793.93 Freq = 4.4845 (cycles/time)
5	Mode	5: Value = 951.73 Freq = 4.9099 (cycles/time)

1	Mode	1: Value = 121.44 Freq = 1.7539 (cycles/time)
2	Mode	2: Value = 294.47 Freq = 2.7311 (cycles/time)
3	Mode	3: Value = 492.93 Freq = 3.5336 (cycles/time)
4	Mode	4: Value = 796.24 Freq = 4.4910 (cycles/time)
5	Mode	5: Value = 948.69 Freq = 4.9021 (cycles/time)

1	Mode	1: Value = 3.04664E-10 Freq = 2.77799E-06 (cycles/time)
2	Mode	2: Value = 3.18755E-10 Freq = 2.84151E-06 (cycles/time)
3	Mode	3: Value = 3.22261E-10 Freq = 2.85709E-06 (cycles/time)
4	Mode	4: Value = 3.28872E-10 Freq = 2.88625E-06 (cycles/time)
5	Mode	5: Value = 3.48212E-10 Freq = 2.96990E-06 (cycles/time)

1	Mode	1: Value = 121.43 Freq = 1.7538 (cycles/tim
2	Mode	2: Value = 291.95 Freq = 2.7194 (cycles/tim
3	Mode	3: Value = 497.26 Freq = 3.5490 (cycles/tim
4	Mode	4: Value = 802.50 Freq = 4.5086 (cycles/tim
5	Mode	5: Value = 939.57 Freq = 4.8785 (cycles/tim

1	Mode	1: Value = 121.44 Freq = 1.7539 (cycles/time)
2	Mode	2: Value = 292.77 Freq = 2.7232 (cycles/time)
3	Mode	3: Value = 495.88 Freq = 3.5441 (cycles/time)
4	Mode	4: Value = 800.53 Freq = 4.5031 (cycles/time)
5	Mode	5: Value = 942.60 Freq = 4.8863 (cycles/time)

Fig. 7 Mode shape values of rebars having different diametres 12, 11.5, 11, 10.5 and 10 mm
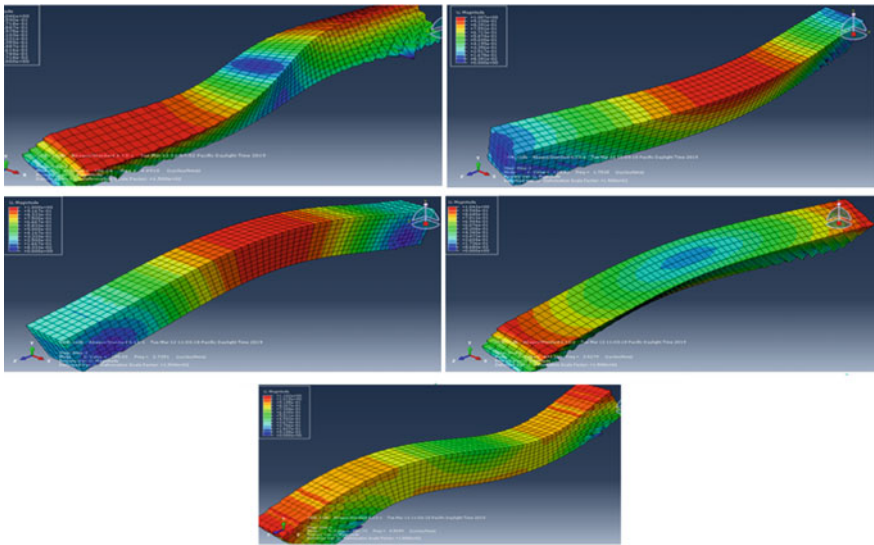

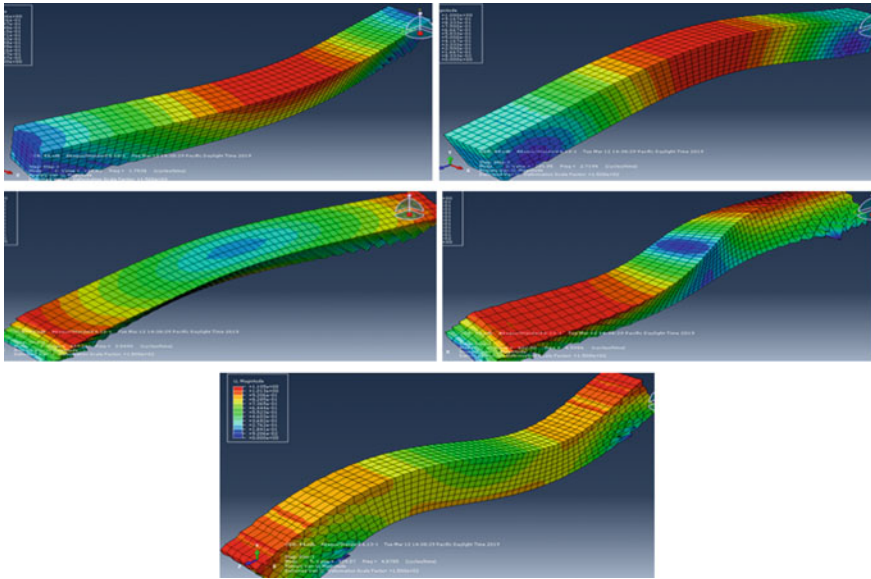**Fig. 8** Mode shapes of 12 mm diametre rebar

Fig. 9 Mode shapes for 10 mm diametre rebar

References

1. Sumukh EP, Goudar SK, Das BB (2021) Predicting the service-life of reinforced concrete by incorporating the experimentally determined properties of steel-concrete interface and corrosion. In: Select proceedings of TMSF 2019. Springer, pp 399–417
2. Abdelatif AO, Ozbolt J, Gambarelli S (2018) 3D finite element modelling of corrosion of lap splice joints in concrete. J Constr Build Mater 169:124–131
3. Zhao P, Xu G, Wang Q, Zhao J, Liu X (2018) Influence of stirrup arrangements on the corrosion characteristics of reinforced concrete members. J Constr Build Mater 192:683–695
4. Zhang J, Ling X, Guan Z (2017) Finite element modelling of concrete cover crack propagation due to non-uniform corrosion of reinforcement. J Const Build Mater 132:487–499
5. Chen E, Leung CKY (2015) Finite element modelling of concrete cover cracking due to non-uniform steel corrosion. J Eng Fract Mech 134:61–78
6. Kallias AN, Rafiq MI (2010) Finite element investigation of the structural response of corroded RC beams. J Eng Struct 32(9):2984–2994
7. Berra M, Castellani A, Coronelli D, Zanni S, Zhang G (2003) Steel-concrete bond deterioration due to corrosion: finite-element analysis for different confinement levels. J Mag Concr Res 55(3):237–247
8. Du YG, Chan AHC, Clark LA (2006) Finite element analysis of the effects of radial expansion of corroded reinforcement. J Comput Struct 84(13–14):917–929

Performance of Recycled Plastic Waste and Used Foundry Sand as a Replacement of Fine Aggregate in Concrete

Kanta Naga Rajesh and Ponnada Markandeya Raju

1 Introduction

In the construction sector concrete is a universally used material. In addition to cement, the production of concrete includes both sand and aggregate. The quarrying operations needed for sand and aggregate production are an energy-intensive process that results in a considerable amount of waste. In addition, the shortfall of sand (fine aggregate) and coarse aggregate has led to long-distance transportation and high costs in many countries like India, United States, etc. [1]. In recent years due to the global warming issues, environmental protection policies have led the construction sector to look for various alternatives for cement such as ground granulated blast furnace slag, fly ash, bottom ash, ferrochrome ash, etc. [2–9]. and sand such as used foundry sand (UFS), ferronickel slag aggregate crusher dust (CD), recycled plastic waste (RPA), etc., [10–12] and coarse aggregates such as construction demolition waste, industrial slag aggregates and tailings, etc. [13–15]. Today, there is a need and requirement to do research in the utilization of recycled HDPE (High Density Polyethylene) plastic waste (RPA) and used foundry sand (UFS) in various fields such as the construction sector, recycled plastic manufacturing units, etc. In addition to having useful and realistic application of plastics, contributes to improvement of energy efficiency of buildings, the cost of realization, enhancing the quality of life and conserve the environment. However, this method is not a leading method for disposing of the wastes. The present work is aimed to study the mechanical properties of concrete modified by RPA and UFS as FA replacements ranging from 5 to 30% by volume, to produce sustainable concrete [16].

K. N. Rajesh (✉)
GMR Institute of Technology, Rajam, Srikakulam, India
e-mail: nagarajesh.k@gmrit.edu.in

P. M. Raju
MVGR College of Engineering (A), Vizianagaram, India

2 Materials

In the present study, the materials used are cement, sand, coarse aggregate, water, used foundry sand and recycled HDPE plastic waste aggregate.

2.1 Cement

43 grade Ordinary Portland Cement (OPC) is used with fineness of 225 m^2/kg. The composition of chemical and mineralogical classification shown in Tables 1 and 2 are determined using X-ray Fluorescence (XRF) and EDX respectively. The mechanical properties of the cement are done confirming to IS 455:1989 [17] and the results are given in Table 3.

2.2 Recycled Plastic Waste Aggregates (RPA)/HDPE

RPA from waste/refused pipes as shown in Fig. 1 is brought from the Murthy industries in Visakhapatnam (India) are ground in a knife mill to produce aggregates smaller than 4.36 mm in size, RPA/HDPE properties is shown in Tables 4 and 5. RPA is used as a partial substitution of fine aggregate and is tested according to IS 2720 (Part 3), IS 2386 (Part 1 and 3) [18–20].

Table 1 Chemical composition of (OPC) cement

Component (%)	SiO$_2$	Al$_2$O$_3$	Fe$_2$O$_3$	CaO	K$_2$O	Na$_2$O	PAF	MgO	SO$_3$	Cl$^-$	H$_2$O
Cement	17.05	4.15	2.6	61.44	0.55	0.45	9.9	1.45	2.34	0.016	0.41

Table 2 Mineralogical composition of clinker (%)

Minerals	C$_3$S	C$_2$S	C$_3$A	C$_4$AF
Cement	62	16	7	13

Table 3 Mechanical properties of cement

Fineness (%)	Normal consistency (%)	Setting time (min)	Soundness (mm)	Specific gravity	Compressive strength (N/mm^2)
2	32	Initial = 48; Final = 252	2	2.93	44.6
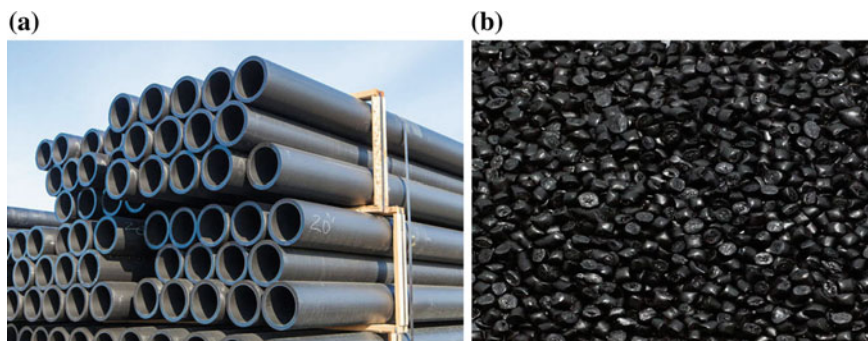
Fig. 1 **a** Corrugated tubes-HDPE, **b** HDPE waste

Table 4 Physical properties of fine aggregates

Sand (FA)	Natural	HDPE/RPA
Shape	Angular	–
Apparent volumetric mass (g/cm^3)	1.53	0.363
Actual density (g/cm^3)	2.64	0.923

Table 5 Mechanical properties of FA

FA	Fineness modulus	Specific gravity	Bulking (%)
Natural sand	2.27	2.54	6
UFS	2.45	2.7	8
HDPE/RPA	3.11	–	–

2.3 Used Foundry Sand (UFS)

UFS used in this study is obtained locally from ferrous foundry located in the Visakhapatnam, India, which produces metal/alloy components for the automotive industry. UFS is used as a partial replacement of fine aggregate and mechanical properties of same are given in Table 5 and is tested according to IS 2720 (Part 3), IS 2386 (Part 1 and 3) [18–20].

2.4 Natural Sand

Sand used in this study is obtained locally in Rajam, India. Sand size is less than 4.36 mm and the main properties of same are given in Tables 4 and 5 and is tested according to IS 2720 (Part 3), IS 2386 (Part 1 and 3) [18–20].

Table 6 Mechanical properties of CA

Fineness modulus	Specific gravity	Water absorption	Flakiness	Elongation
7.81	2.66	0.3%	4.81%	24.87%

2.5 Coarse Aggregate

CA used in this study is obtained locally in Rajam, India. The CA size is 20 mm down and the mechanical properties of the same are given in Table 6. The individual aggregates were blended to get the desired combined grading is tested according to IS 2720 (Part 3), IS 2386 (Part 1 and 3) [18–20].

3 Methodology

3.1 Mix Design

M20 grade concrete mix proportion of 1:1.63:3.19 design is done confirming to IS 10262:2009 [21]. A constant water to cement ratio (W/C) of 0.5 is used for all types of mixes, out of seven mixes, six mixes which are referred as non-conventional mix (NCM) are prepared by substituting natural sand with 5, 10, 15, 20, 25 and 30% of UFS and RPA and the rest of the mix is control mix (CM) without UFS and RPA. To simplify, all the seven mixes are labelled as CM, NCM5, NCM10, NCM15, NCM20, NCM25 and NCM30 and the detailed mix proportions are given in Table 7. For example, NCM5 indicates that the concrete mix containing cement, 95% natural sand, 5% of UFS and RPA a replacement of natural sand, coarse aggregate and water whereas CM indicates a mix with cement (OPC), natural/river sand, coarse aggregate and water.

Table 7 Concrete mix proportions

Ingredients	CM	NCM5	NCM10	NCM15	NCM20	NCM25	NCM30
Water (Kg/m^3)	186	186	186	186	186	186	186
Cement (Kg/m^3)	372	372	372	372	372	372	372
Fine aggregate (Kg/m^3)	609	609	609	609	609	609	609
Coarse aggregate (Kg/m^3)	1189	1189	1189	1189	1189	1189	1189
Used foundry sand (Kg/m^3)	–	30.45	60.9	91.35	121.8	152.25	182.7
Recycled plastic aggregate (Kg/m^3)	–	30.45	60.9	91.35	121.8	152.25	182.7

3.2 Preparation of Specimen

The concrete mixes are filled in cube moulds of size 150 mm × 150 mm × 150 mm in three layers and subsequently compacted in a table vibrator. Total of 21 specimens is prepared subjected to 3 for each type of mix. Later all specimens are covered with polythene sheets to avoid moisture loss and kept in room temperature for 24 h and thereafter demoulded, kept in curing tanks filled with water until the day of the test. The cube specimens of all types mixes are tested for compression capacity in compression testing machine (CTM—2000 kN capacity) according to IS 516:1959, IS 456:2000 [22, 23].

4 Result and Discussion

4.1 Workability

Slump cone test was used to determine the degree of workability of control and the non-conventional concrete mixes. The influence of UFS and RPA on the slump of mixes were shown in Fig. 2. From the figure, it was evident that workability reduced up to NCM30. The substitution effect of UFS and RPA in NCM5 and NCM10 on workability were insignificant and were comparatively equal to the CM, but there
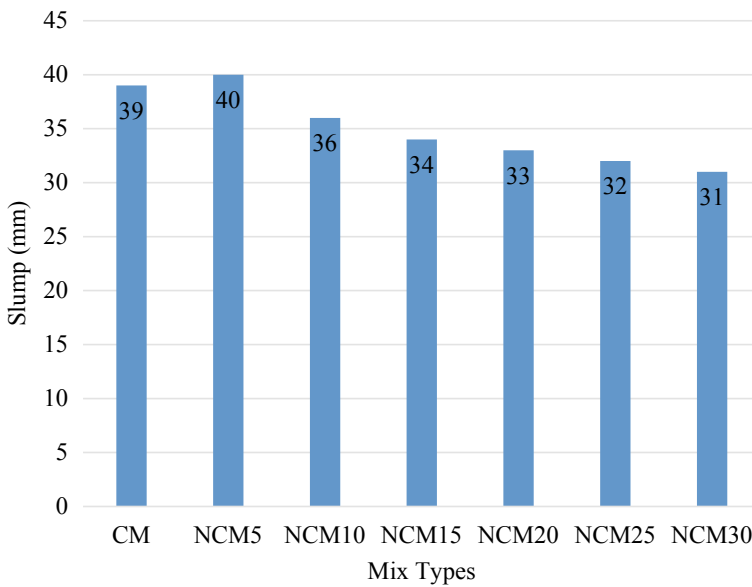

Fig. 2 Workability of all mixes—Comparison

was a higher loss in the workability for substitution rates of 15, 20, 25 and 30% was observed. The workability and fineness of the material were directly related, 8% of particles of UFS has a lesser size than 75 μm compared to natural sand and also UFS consists of particles of clay and ash, due to which water absorption of UFS was high and resulted in low slump values. Slump loss usually happens due to the hydration of water from the concrete. Based on the fineness of the substitution, the decision was made to adjust the water content to the mixes. However, the addition of RPA along with UFS does not lead to major water loss.

4.2 Compressive Strength

The compression capacity of all types of mixes for various curing days such as 7, 14, 28, 56 and 90 days was measured. The results were shown in Table 8 and the same were represented graphically in Fig. 3. It is evident from the results that 28 days compressive strength of the mix NCM5 (i.e., natural sand replaced by UFS and RPA at 5%) was 2.61% higher than CM. However, the 28 days compressive strength of all other mixes NCM10, NCM15, NCM20, NCM25 and NCM30 were 10.16, 38.87, 40.67, 43.17 and 45.26% respectively lower than CM. A decrease in concrete strength was observed in all the curing periods with the increment in the replacement rates of UFS and RPA. Presence of high silica in the UFS would help to enhance the process of hydration and increase the C3S formation considerably. However, the UFS fineness, decreases the concrete workability and the compressive strength and also simultaneous replacement of natural sand with RPA in concrete does not involve in the hydration process, after drying, the free water makes small channels, it results in tiny pores in the concrete [24] and thereby reduced the strength with increment in its substitution rate as shown in Fig. 4. (ASTM Type 1) ACI 209

Table 8 Compressive strength of all mixtures

| Mixture Id	Percentage replacement (%)	Experimental compressive strength (N/mm^2)					Calculated compressive strength (N/mm^2) as per ACI 209 (Type 1)	
		7 days	14 days	28 days	56 days	90 days	56 days	90 days
CM	0	17.18	22.46	28.35	30.54	31.05	30.77	31.70
NCM5	5	17.53	23.53	29.09	31.62	32.12	31.57	32.52
NCM10	10	16.7	18.48	25.47	26.97	27.62	27.64	28.48
NCM15	15	15.2	17.24	17.33	18.24	19.21	18.81	19.38
NCM20	20	13.4	16.73	16.82	18.05	18.52	18.25	18.80
NCM25	25	12.35	16.27	16.11	17.01	17.95	17.48	18.01
NCM30	30	12.12	14.32	15.52	15.74	17.12	16.84	17.35
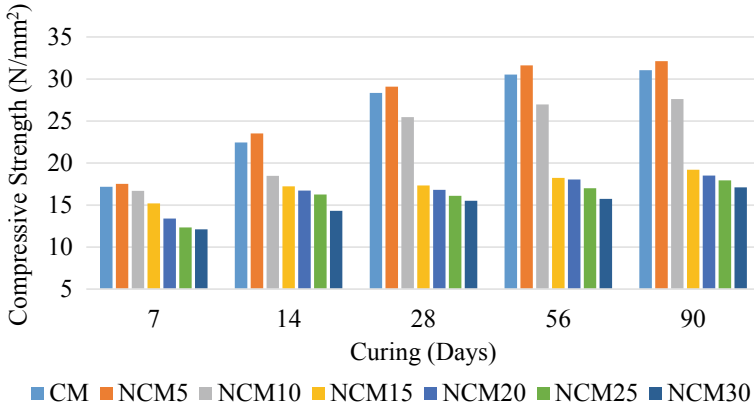
Fig. 3 Compressive strength of all mixes at various curing days—comparison
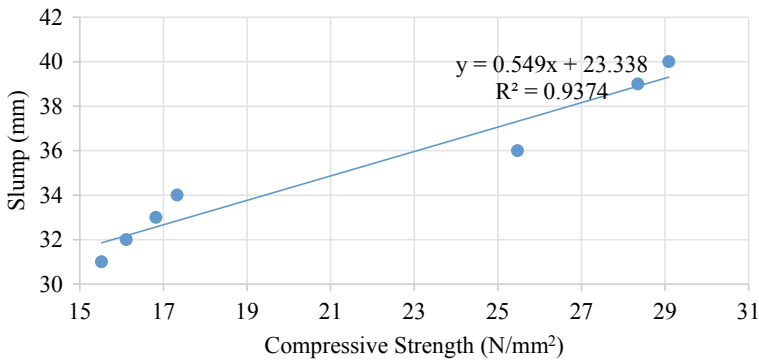

Fig. 4 Compressive strength (28 days) and slump

recommended the Eq. (1) to determine the strength of concrete in compression with time [25].

$$f_{cm}(t) = f_{c28}\left(\frac{t}{4 + 0.85t}\right) \tag{1}$$

where $f_{cm}(t)$ indicates average compressive at t days, f_{c28} indicates 28 days average compressive strength and t indicates age of concrete in days. The calculated compressive capacity of concrete for 56 and 90 days is computed using Eq. (1) and the values are presented in Table 8. The relation between experimental and calculated compressive strength of concrete for 56 and 90 days are shown in Fig. 5, it showed that the experimental and calculated values are in well agreement with $R^2 = 0.999$.
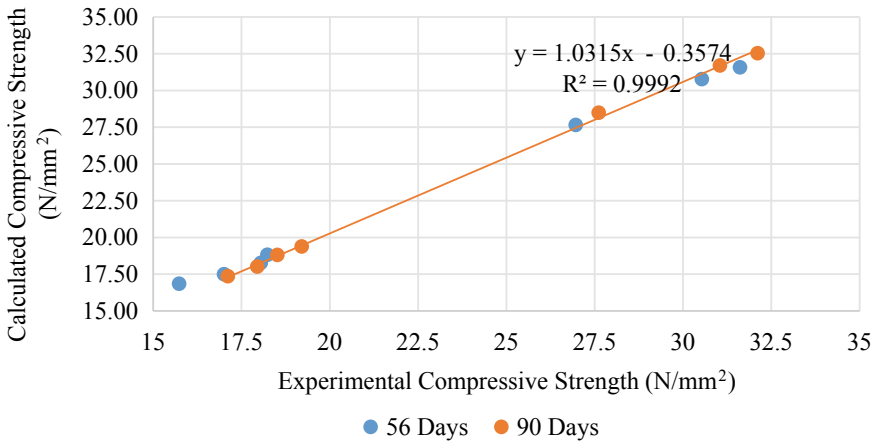
$$y = 1.0315x - 0.3574$$
$$R^2 = 0.9992$$

Fig. 5 Experimental and calculated compressive strength

According to IS 13311(Part 1):1992 [26], the durability property of all types concrete mixes at 28, 56 and 90 days were determined with Ultra Sonic Pulse Velocity (UPV). From the results, it was concluded that the measured NCM5 UPV values were slightly greater than CM UPV values, the values measured for mixes (NCM5 and NCM10) were higher than 3500 m/s, that was categorized as good, whereas for other mixes (NCM15, NCM20, NCM25 and NCM30) the measured UPV values were in between 3300 and 3500 m/s as RPA is not involved in a chemical reaction with cement resulted in voids and due that UPV values, these mixes were categorized as medium. Figure 6 demonstrates the relationship between the UPV and concrete compressive strength, wherein results were good agreement with $R^2 = 0.9189$. From the experimental results, it was evident that for producing good concrete, UFS and
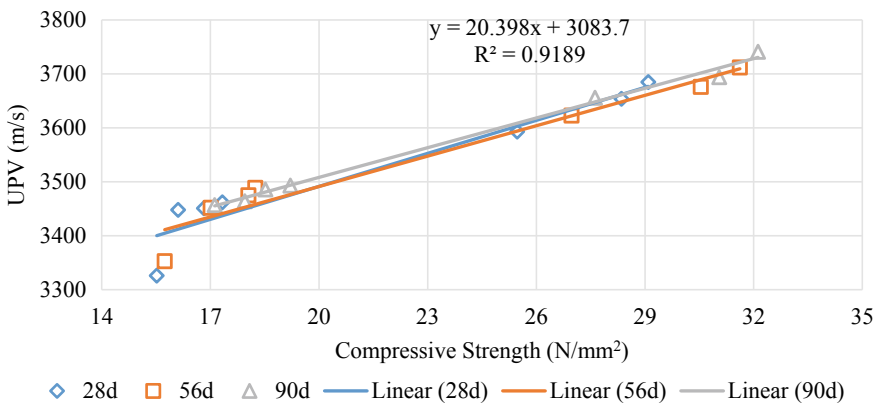

$$y = 20.398x + 3083.7$$
$$R^2 = 0.9189$$

Fig. 6 Compressive strength and UPV values of concrete at all ages

RPA up to 5% can be used as a fine aggregate without compromising the strength parameter.

4.3 Density of Concrete

The 28 days density of all mixes against the slump indicated that due to the increase in the porosity resulted in the poor workability of the mix and thereby causes a reduction in the compaction of the mix. From Fig. 7, it was evident that with an increase in porosity, concrete density reduced. It was also understood that due to the addition of RPA and UFS in concrete, which are lightweight compared with natural sand resulted in less dry density with the decrease in the slump value. In general, the concrete density was influenced by the material physical properties. Still in India, clay, sawdust and ash were used as binding agent in the foundry industries. The specific density of the material was reduced due to the presence of those particles. Due to the presence of RPA and it's less bonding in the concrete, its density decreased. The variation of dry density with compressive strength of concrete of all mixes at 28 days indicated with the increase in substitution rates of UFS and RPA reduced the compressive strength, which is directly related to the dry density as shown in Fig. 8 [27].

4.4 Elastic Modulus

The elastic modulus was predominantly effected by the elastic properties of aggregate and to a lesser extent on the age of concrete, type of curing, mix proportions and cement type. The modulus of elasticity was calculated from the compressive strength
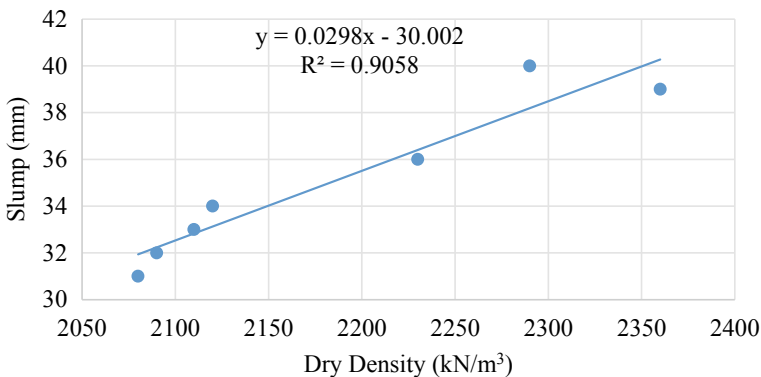

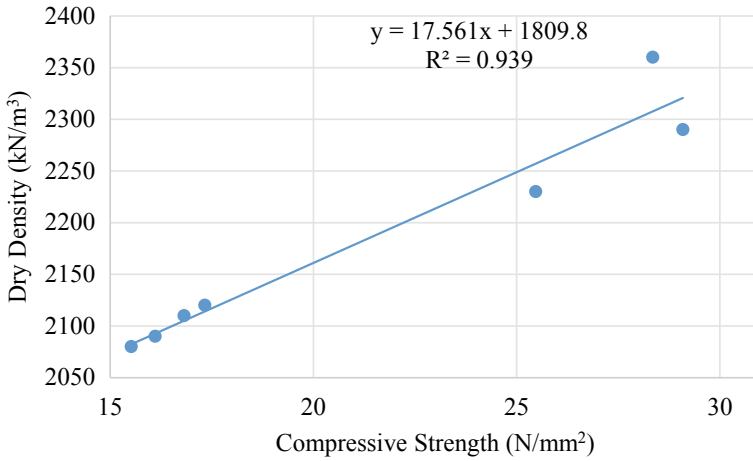**Fig. 7** Slump and dry density of concrete at 28 days

Fig. 8 Dry density and compressive strength of concrete at 28 days

obtained and UPV values using the Eqs. (2) and (3) recommended by IS 456:2000 and IS 13311(1):1992, respectively and is shown in Fig. 9.

$$E_c = 5000\sqrt{f_{ck}} \tag{2}$$

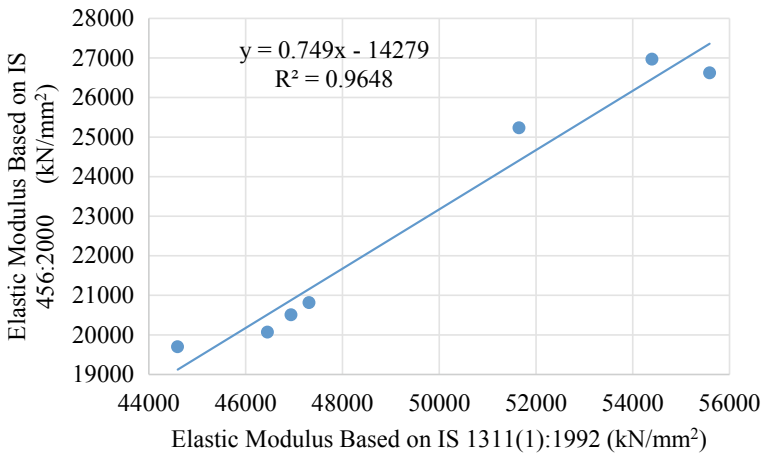$$E = \rho V^2 \frac{(1 + \mu)(1 - 2\mu)}{(1 - \mu)} \tag{3}$$

Fig. 9 Elastic modulus based on IS 1311(1):1992 and IS 456:2000 at 28 days

where E indicates dynamic elastic modulus (MPa), fck indicates compressive strength of concrete, ρ indicates density of concrete in kg/m^3, V indicates pulse velocity in m/s and μ indicates dynamic Poisson's ratio of the concrete. There was no substantial difference between the modulus of elasticity calculated using IS 456:2000 and IS 13311(1):1992, and the values were relatively similar ($R^2 = 0.9648$) [28, 29].

5 Conclusion

Based on the test results of the present work on the combined influence of UFS and RPA as a partial replacement of fine aggregate in the production of concrete, the following conclusions were drawn.

1. Compressive strength, slump and modulus of elasticity for 5% replacement of natural sand with combined UFS and RPA (i.e., NCM5) shown slightly higher values (i.e., 2.61, 2.56 and 1.29% respectively) when compared with control mix.
2. Dry density for 5% replacement of natural sand with combined UFS and RPA (i.e., NCM5) shown slightly lesser value (i.e., 2.97%) when compared with control mix.
3. Concrete mix (NCM5) of all ages (i.e., 28, 56 and 90 days) showed slightly higher values in durability like ultrasonic pulse velocity when compared with the control mix.
4. When compared to the CM, all the NCM mixes showed inferior values except NCM5, because of presence of fineness, clay, sawdust and ash in UFS and no reaction of RPA with cement matrix.
5. The mechanical and durability properties of NCM5 concrete mix showed slightly higher values compared with the control mix.
6. The experimental results showed that UFS and RPA can be effectively utilized up to 5% replacing natural sand in the concrete mix without affecting the concrete properties.

References

1. Langer WH (2011) Aggregate resource availability in the conterminous United States, including suggestions for addressing shortages, quality, and environmental concerns, Open-File Rep. 2011-1119. US Dept. of the Interior and USGS, Reston, VA

2. Saha AK, Khan MNN, Sarker PK (2018) Value added utilization of by-product electric furnace ferronickel slag as construction materials: a review. Resour Conserv Recycl 134:10–24. https://doi.org/10.1016/j.resconrec.2018.02.034

3. Saha AK, Sarker PK (2017) Sustainable use of ferronickel slag fine aggregate and fly ash in structural concrete: mechanical properties and leaching study. J Cleaner Prod 162:438–448. https://doi.org/10.1016/j.jclepro.2017.06.035

4. Sharan Kumar G, Shivaprasad KN, Das BB (2019) Mechanical properties of fiber reinforced concrete using coal-bottom ash as replacement of fine aggregate. In: Select proceedings of ICSCBM 2018. Springer, pp 863–872

5. Shivaprasad K N, B. B. Das and Renjith R, "Influence of Fineness of Fly Ash on Compressive Strength and Microstructure of Bottom Ash Admixed Geopolymer Mortar", Indian Concrete Journal, Vol. 92 (3), March 2018.

6. Prasanna KM, Tamboli S, Das BB (2020) Characterization of mechanical and microstructural properties of FA and GGBS-based geopolymer mortar cured in ambient condition. In: Select proceedings of ICRDSI 2019. Springer, pp 751–768

7. Sharan Kumar G, Das BB (2021) Influence of particle size of bottom ash on mechanical properties of M30 grade concrete. In: Select proceedings of TMSF 2019. Springer, pp 533–543

8. Chethan Kumar B, Yaragal S, Das BB (2020) Ferrochrome ash—its usage potential in alkali activated slag mortars. J Clean Prod 257

9. Chethan Kumar B, Yaragal S, Das BB Effect of elevated temperatures on ferrochrome ash based mortars. Indian Concrete J 93(10):14–20

10. De Barros Martins MA, Mambeli Barros R, Silva G, Silva Santos IF (2018) Study on waste foundry exhaust sand, WFES, as a partial substitute of fine aggregates in conventional concrete. Sustain Cities Soc. https://doi.org/10.1016/j.scs.2018.11.017

11. Badache A, Benosman AS, Senhadji Y, Mouli M (2018) Thermo-physical and mechanical characteristics of sand-based lightweight composite mortars with recycled high-density polyethylene (HDPE). Constr Build Mater 163:40–52. https://doi.org/10.1016/j.conbuildmat.2017.12.069

12. Hilal NN, Sahab MF, Mohammed Ali TK (2020) Fresh and hardened properties of lightweight self-compacting concrete containing walnut shells as coarse aggregate. J King Saud Univ Eng Sci. https://doi.org/10.1016/j.jksues.2020.01.002

13. Sáez del Bosque IF, Van den Heede P, De Belie N, Sánchez de Rojas MI, Medina C (2020) Carbonation of concrete with construction and demolition waste based recycled aggregates and cement with recycled content. Constr Build Mater 234:117336. https://doi.org/10.1016/j.conbuildmat.2019.117336

14. Yaragal SC, Chethan Kumar B, Jitin C (2019) Durability studies on ferrochrome slag as coarse aggregate in sustainable alkali activated slag/fly ash based concretes. Sustain Mater Technol e00137. https://doi.org/10.1016/j.susmat.2019.e00137

15. Sharath BP, Shivaprasad KN, Athikkal MM, Das BB (2018) Some studies on sustainable utilization of iron ore tailing (IOT) as fine aggregates in fly ash based geopolymer mortar. In: IOP conference series: materials science and engineering, vol 431, no 9. IOP Publishing, p 092013(1–8)

16. Rajesh KN, Raju PM, Mishra K, Madisetti PK A review on sustainable concrete mix proportions. In: IOP conference series: materials science and engineering, vol 1025. https://doi.org/10.1088/1757-899X/1025/1/012019

17. IS 455 (1989) (Reaffirmed 1995) Portland slag cement—specification. Bureau of Indian Standards, New Delhi

18. IS 2720 (Part 3) Methods of test for aggregates for—specification. Bureau of Indian Standards, New Delhi

19. IS 2386(Part 1) (1963) Methods of test for aggregates for concrete: Part 1 particle size and shape. Bureau of Indian Standards, New Delhi

20. IS 2386(Part 3) (1963) Methods of test for aggregates for concrete: Part 3 specific gravity, density, voids, absorption and bulking. Bureau of Indian Standards, New Delhi

21. IS 10262 (2009) Guidelines for concrete mix proportioning. Bureau of Indian Standards, New Delhi
22. IS 516 (1959) (Reaffirmed 2004) Method of tests for strength of concrete. Bureau of Indian Standards, New Delhi
23. IS 456 (2000) Plain and reinforced concrete code of practice. Bureau of Indian Standards, New Delhi
24. Sharma R, Bansal PP (2016) Use of different forms of waste plastic in concrete—a review. J Clean Prod 112:473–482. https://doi.org/10.1016/j.jclepro.2015.08.042
25. ACI 209.2R-08 Guide for modeling and calculating shrinkage and creep in hardened concrete
26. IS 13311(Part 1) (1992) Methods of non-destructive testing of concrete, Part 1: ultrasonic pulse velocity. Bureau of Indian Standards, New Delhi
27. Rai B, Rushad ST, Bhavesh KR. Duggal SK (2012) Study of waste plastic mix concrete with plasticizer. International scholarly research network, pp 1–5
28. Ganesh Prabhu G, Hyun JH, Kim YY (2014) Effects of foundry sand as a fine aggregate in concrete production. Constr Build Mater 70:514–521. https://doi.org/10.1016/j.conbuildmat.2014.07.070
29. Senhadji Y, Escadeillas G, Benosman AS, Mouli M, Khelafi H, Ould Kaci S (2015) Effect of incorporating PVC waste as aggregate on the physical, mechanical, and chloride ion penetration behavior of concrete. J Adhes Sci Technol 29(issue 7):625–640. https://doi.org/10.1080/01694243.2014.1000773

Study on the Mechanical Behaviour of Composite Beam with Headed and Channel Shear Connector

A. Divya and S. Hashni

1 Introduction

Steel concrete composite developments are popular among advanced countries. Nowadays it's gaining popularity in India also. Steel concrete composite construction is faster, conservative and eco-friendly. They have been widely utilized in development of high rise buildings as well as medium range bridge decks. By using steel concrete composite construction effective utilization of concrete and steel is achieved. In composite section composite action can be achieved by decreasing or preventing the corresponding displacement of steel and concrete at the interface [1]. To achieve the composite behavior mechanical connectors can be used for shear transfer. These connectors enable the two materials to behave as a single unit. Mechanical connectors are utilized to carry earthquake force between concrete and steel that are a part of lateral resisting system [2]. During the axial loads, mechanical connectors counterattack upward forces and the separation of steel and concrete element in vertical way. In composite structures force transfer depends on strength and stiffness of various component as well as shear connectors.

2 Shear Connectors

Shear connectors are categorized into rigid and flexible based on distribution of shear force, strength and deformation. Rigid shear connectors resist shear force by shearing in the front side and in the surrounding area of ultimate strength its deformation is insignificant. In the event of rigid connectors, stronger concentrated stress is produced which ends in the failure of concrete or weld [3]. At the connection point of steel

A. Divya (✉) · S. Hashni
Department of Civil Engineering, Sona College of Technology, Salem 636005, India

beam, the shear forces are resisted by tension, bending and shearing in flexible shear connectors. After reaching ultimate strength values, the connectors are subjected to plastic deformation. Compared to rigid connectors the flexible connectors are highly ductile. There are different types of shear connectors like headed stud, perfobond rib, Channel, T-rib connector, oscillating perfobond strip, waveform strip, T-connector, Pyramidal shear connector etc. [4]. Experimental test have been conducted to know the behavior of different types of shear connectors. In this paper an attempt has been made to compare the behavior of flexible type of shear connector experimentally.

2.1 *Headed Stud*

Headed studs are the most common and popular type of Shear connectors in composite construction. Headed studs subjected to axial and flexural forces resist interface forces by means of dowel action. They resist both longitudinal shear and vertical uplift. Headed studs are convenient for construction and have non-directional shear behaviour [1]. Due to high degree of automation in workshop and site they are commonly used worldwide.

2.2 *Channel Connector*

Channel connectors are based on highly reliable convention welding they do not require any bending test like headed stud. Channel connectors are welded on steel beam which helps the designer giving freedom for sizing to design for required force capacity with minimum number of connector compared to headed stud [5]. Channel connectors are easily available and cost of the connector is also much cheaper than other connectors.

3 Previous Research

3.1 *Channel Connector*

The experimental study on the performance of European style channel connector with different heights and lengths. A new equation has been developed to calculate the ultimate resistance of channel connector with reasonable accuracy. This work recommended that two channel connector results in higher load capacity for same channel length [6]. The exploratory investigation of channel shear connectors installed in solid concrete material slab under low cycle fatigue and monotonic loading Specimens made of plain concrete, reinforced concrete, fibre reinforced concrete and

engineered cementitious concrete were studied [7]. By using polypropylene fibre there is minor effect on shear strength capacity and load displacement performance. During reversed cyclic loading maximum specimens revealed 10–23% degradation in strength for the corresponding monotonic loading with same failure mode. It also concluded that by adding reinforcement bars in plain or fibre concrete strength can be increased substantially [8].

Related the study on the shear resistance of channel connector in light weight, plain and reinforced concrete were determined. The test result concluded that increase in length of connector can increase ductility and in general channel connector showed ductile behavior. By using reinforcement in concrete slabs ductility and shear capacity can be increased whereas in unconfined concrete composite system had brittle performance [9]. The proposed analytical research on the behaviour of channel shears connector using Finite element model. Parametric research using non-linear model are performed to examine the variation in strength of concrete, dimension of channel and channel orientation. It is observed that the ultimate strength of channel connector is directly proportional to square root of concrete compressive strength as Canadian code practices [10].

3.2   Headed Stud

The effective numerical model was proposed using FEM to simulate the push off test. The experimental test observed three modes of failure namely concrete cone failure, stud connector failure and joint stud and concrete failure. The push off test was carried to estimate the load-slip performance of headed stud in RC slab. The research presented that formulas in Euro code 4 had good correlation with finite element and experimental solution [11]. The behavior of shear connectors in solid and profiled steel sheeting slabs was observed to be modified by introducing the steel fibre to increase the strength and ductility of shear connection area in the slab. Solid slab had shear connection failure however profiled slab had concrete failure. The inclusion of steel fibre exhibited improvement in cracking load [12].

The paper determined the shear strength and stiffness of high strength steel stud connector by modified push-out test. It concluded that confinement of concrete with HSS stud predominantly improved the compressive and split resistance of concrete. The first failure mode was found in concrete followed by fracture of HSS stud connector. The shear strength of stud connectors was comparable with Euro code 4 values [13]. The Impact behaviour of stud shear connector in composite system was conducted through the static tests. The slip resistance of stud connector fulfilled the Euro code 4 and the design capacity provided conservative for welded stud

connector. The dynamic shear capacity of connectors found to be advanced by 33–63% compared with static response. It is summarized that more energy dissipated through specimens under impact load [2].

4 Preliminary Tests

4.1 Initial Test on Concrete

The compressive strength of concrete were firmed by testing the cube samples. The cubes were casted simultaneously while casting the specimen. The standard cubes of 150 × 150 × 150 mm were used. M-sand was preferred as fine aggregate in mix proportion with the fineness modulus and specific gravity of 3.7 and 2.7% respectively. Coarse aggregate of maximum nominal size 20 mm and specific gravity 2.8 was used. The cement utilized for all mixes was Ordinary Portland cement which corresponds to OPC 53 Grade. The test specimens were kept for curing under room temperature. After 28 days, the concrete cubes were tested in compression testing machine with a loading rate of 5 kN/s. The average compressive strength of concrete obtained was 26 N/mm^2 at 28 days.

4.2 Initial Test on Steel

Headed studs of diameter 20 mm and channel of ISMC 100 × 50 mm are used in this study. The stud and channel connector was made of Mild steel Fe250. Tensile test for both headed and channel connectors were conducted. A coupon sample of 6 mm thickness was made to determine the properties of connector material (Fig. 1). The dimension for coupon sample was adopted based on ASTM E8-04[12]. The samples were tested on Universal Testing Machine. From the tensile test of mild steel elastic modulus, yield stress, tensile strength and elongation for connector material was obtained (Fig. 2).

Fig. 1 Coupon specimens used in this study

Fig. 2 Stress–strain curve
for mild steel
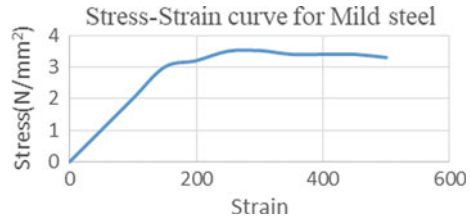
5 Description of Specimen

In this study four specimen with reinforcement was casted with headed and channel connectors. Totally four specimens with reinforced concrete was considered for testing in this study. Two specimens with headed connector and two specimens with channel connector were casted. M20 mix proportion of concrete was adopted. The specimens were casted with medium steel ISMB200 profile. The channel connector corresponds to ISMC 100 × 50 mm with flange and web thickness of 7.5 and 4.7 mm respectively. Headed stud connector of 20 mm diameter and 100 mm length was used as per codal provision. All the specimens have the same concrete block dimensions of 400 × 250 × 200 mm. Each beam flange was attached with channel and headed connectors. The specimens were reinforced with closed rectangular steel stirrup of 8 mm diameter and 10 mm diameter longitudinal bars at two sides of concrete block. Concrete cover of 25 mm was maintained in all the specimens.

When combined, the required concrete slab needed to be cast horizontally to replicate the real construction practice, this alignment creates problem during specimen assembly. Hence to overcome this difficulty the Specimens were cast transversely [10]. Even though this casting orientation is different from field condition it was believed to provide consisted quality of slab for both sides of the specimen without potentially obtaining denser concrete in push verses pull direction.

When different concrete slabs specimen were casted at different times, the concrete compressive strength of the slabs could differ during the push out test which will complicate the experimentally obtained behavior [14]. Hence all the concrete slabs were casted at the same time. Two concrete slabs of dimension 400 × 250 × 200 mm were connected by welding shear connectors to the flange of a steel ISMB200 beam. The same dimensions were adopted for both headed and channel connector. In case of headed connector welding was done on shaft and in channel connector welding was done on flange of the connector [15]. One channel was welded to each slab and two studs were welded on each slab with same slab dimensions. Beam, channel and headed sections used in this investigation were obtained from mild steel. The short length of channels used in the specimen was based on concrete slab size limitations. Figures 3 and 4 presents the side view of channel specimen and headed specimen, respectively. Picture of headed stud and channel connectors used in study are presented in Fig. 5.
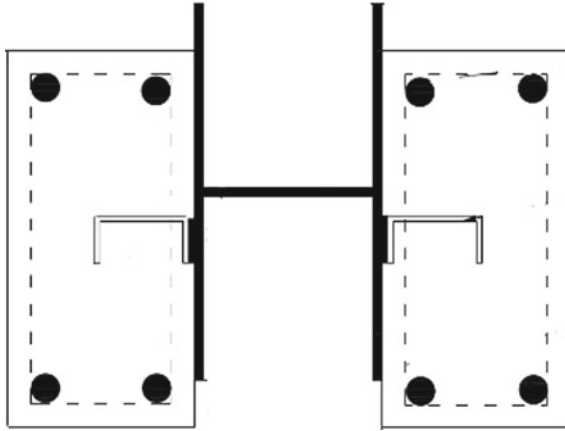
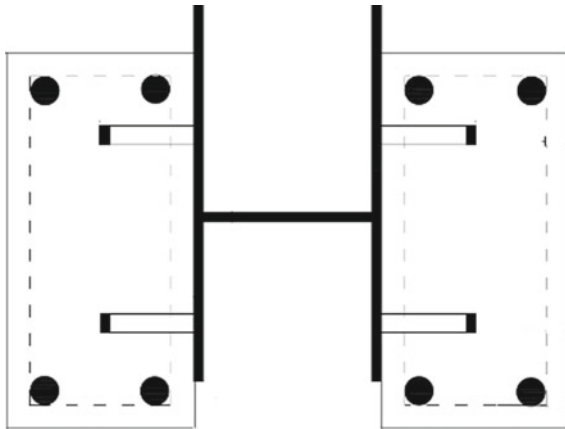**Fig. 3** Side view of channel specimen

Fig. 4 Side view of headed specimen

Fig. 5 Headed stud and channel connector

6 Loading and Test Procedure

In general the behaviour of shear connector can be obtained by conducting push-out tests. In specimen test setup concrete was attached to the two flanges of the steel I-beam The surface of concrete and steel beam were cleaned, smoothened and prepared at the points for dial gauge. The concrete surface was painted to know the first crack and steel beam was painted with red oxide to avoid corrosion. The specimens were tested under monotonic loading and load application was provided through a 100 T capacity Universal Testing Machine. The two concrete slabs of the specimen were kept on the fixed portion of the testing machine as shown in Fig. 6. Uniformly distributed load was applied on steel beams and concrete blocks were supported. The load was applied through base plate of 20 mm thickness which was kept at the top of steel beam. Monotonic loading was given by increasing the displacement until complete failure of specimen occurs. The test was continued till the ultimate load was reached without unloading.

Fig. 6 Experimental setup of the specimen

7 Experimental Behaviour of Tested Specimen

The outputs of monotonic push out trial of the entire specimen are depicted below. To explore the buckling behavior of channel and headed connector concrete block of the specimens were demolished. The failure mode witnessed in the push out specimens can be categorized into two types. The principal type is the connector fracture and alternative type is concrete cracking [3].

The cracks in concrete were observed from bottom to top. The concrete area surrounding the weld first crushed due to buckling of the connector. The typical characteristic observed in this failure mechanism was yielding and then rupture of connector near the bottom flange fillet. During testing the load was applied to steel beam section which uniformly distributes the load to the concrete. The concrete further transfers this load to the connector at the weld point [16]. Due to the load applied axially, the connector resists shear load primarily by buckling and transfers the load to concrete through bearing. This load distribution cause tensile crack in concrete by shearing, ripping and splitting, later displacement occurs at interface and the connector bends locally.

From experimental test the ultimate capacity of shear connector was determined from maximum load of push out test. It is observed that in two channel specimen and in one headed specimen concrete cracking has been the presiding failure mode. In one headed specimen stud fracture was the dominant failure. The peak load of channel connector was 630 kN and that of headed connector was 510 kN. Figures 7, 8 and 9 shows the image of crushing failure of concrete, load slip curves for headed connector and channel connector, respectively.

Fig. 7 Concrete crushing failure

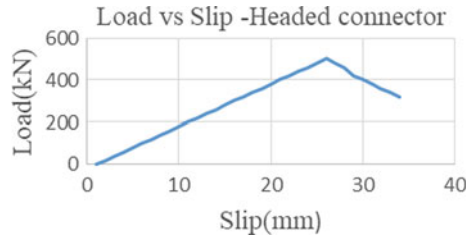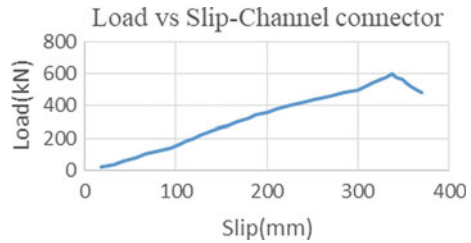**Fig. 8** Load slip curve for headed connector

Fig. 9 Load slip curve for channel connector

8 Results and Discussions

8.1 Failure Type for Connectors

From the study, Two different types of failure were observed in the tested specimen. The failure mode observed under monotonic loading for channel connectors was similar to headed connector with longitudinal crack along the slab. This crack opened further and developed along the slabs which results in the separation of steel beam and concrete slab when the load increased. It is to be noted that the channel connector specimens exhibited a different crack behaviour concentration near the connector along the concrete crushing at the front side of the connector.

Excepting one specimen in all the other specimens concrete fracture happened for both channel and headed connectors. The failure mode in most specimens were followed by forming a longitudinal crack along with the slab opening more and further proceeded with loading. On further loading the tests exhibited buckling of connector in most cases. The channel connectors were subjected to displacement at the lower part of web and the headed connectors are subjected to displacement at the shank. Table 1 presents the experimental results and buckling of connector is shown in Fig. 10.

Table 1 Experimental result of the specimens

Specimen	Concrete strength	Exp. result (kN)	Failure mode
1	24.5	520	Concrete
2	22	500	Stud
3	27	640	Concrete
4	25.7	600	Concrete

Fig. 10 Buckling of connector

8.2 Load Slip Curve

When monotonic load is applied to steel beam movement happens between concrete and steel. The behaviour of shear connectors in the composite beam can be described by load slip curve. By using the load-slip curve the maximum slip and shear load capacity for the specimens can be achieved. The load-slip curve for headed and channel connector is shown in Fig. 7. The response curve consist of three different stages such as elastic, plastic and descending stage. The elastic stage is linear in which slip increases as the load increases. When peak load was reached the connector yielded and moved into plastic stage. After peak load was reached large deformation occurred in concrete and connector in the descending stage. By comparing the load-slip curve for headed and channel connector it is observed that the channel connector had more stiffness than headed connector. The load carrying capacity of channel connector is also higher than headed connector. From this response it can be

Fig. 11 Comparison of load displacement behaviour for channel and headed connector
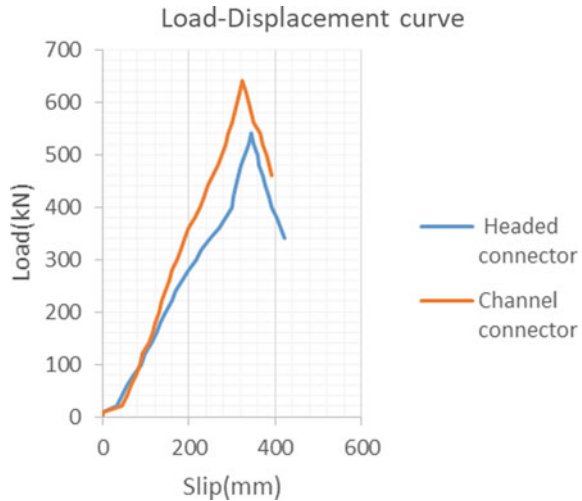
concluded that channel connectors are more ductile than headed connector. Comparison of load displacement behaviour for channel and headed connector is shown in Fig. 11.

9   Conclusion

A sequence of test were conducted on channel and headed connector. The specimens were casted without any admixtures and fibres which resembled the practical sections employed in bridges and high rise building.

- The failure modes observed in Headed and Channnel connector are: Connector fracture and concrete cracking.
- The tension capacity of reinforcing steel provides greater strength with higher loading capacity to the specimen with connector failure followed by concrete crushing.
- Load-slip curve plotted from the push out test show that specimen with channel connector had higher ultimate load compared to headed connector specimen.
- The shear capacity of two headed studs on each side of the beam was less compared to one channel connector on each side for all specimens having the same dimension.
- From load-slip curve it can be seen that the deflection of channel connector is high so the ductility of channel connector is high.
- As previous reserch works have suggested from this experimental analysis it can be concluded that composite section with channel connector have greater load carrying capacity and it can replace few number of headed studs.

References

1. Revathi S, Arul Mary S, Bangarumythili S (2016) An experimental investigation on performance of headed stud connectors in steel-concrete composite beams. Int J Eng Res Technol 4
2. Huo J, Wang H, Zhu Z, Liu Y, Zhong Q (2018) Experimental study on impact behaviour of stud shear connectors between concrete slab and steel beam. J Struct Eng 144(2):04017203
3. Ataei A, Zeynalian M, Yazdi Y (2019) Cyclic behaviour of bolted shear connectors in steel-concrete composite beams. Eng Struct 198
4. Shariati A, Ramlisulong NH, Suhatril M, Shariati M (2012) Various types of shear connectors in composite structures: a review. Int J Phys Sci 7(22):2876–2890
5. Qian Y, Jie J-P (2011) Experimental study on stud shear connectors with large diameter and high strength
6. Baran E, Topkaya C (2012) An experimental study on channel type shear connectors. J Constr Steel Res 74:108–117
7. Shariati M, Ramli Sulong NH, Suhatril M, Shariati A, Arabnejad Khanouki MM, Sinaei H (2013) Comparison of behaviour between channel and angle shear connectors under monotonic and fully reversed cyclic loading. Constr Build Mater 38:582–593
8. Maleki S, Bagheri S (2008) Behaviour of channel shear connectors Part-I: experimental study. J Constr Steel Res 64:1333–1340
9. Shariati M, Ramli Sulong NH, Arabnejad MMKH, Mahoutian M (2011) Shear resistance of channel shear connectors in plain, reinforced and lightweight concrete. Sci Res Essays 6(4):977–983
10. Maleki S, Bagheri S (2008) Behaviour of channel shear connectors Part-II analytical study. J Constr Steel Res 64:1341–1348
11. Lam D, El-Lobody E (2005) Behaviour of headed stud shear connectors in composite beam. J Struct Eng 131:96–107
12. Mirza O, Uy B (2009) Effects of steel fibre reinforcement on the behaviour of headed studs shear connectors for composite steel-concrete beams. Adv Steel Constr 5:72–95
13. Amar Prakash N, Anandavalli CKM, Lakshmanan N (2012) Modified push-out tests for determining shear strength and stiffness of HSS stud connector—experimental study. Int J Compos Mater 2(3):22–31
14. Maleki S, Mahoutian M (2009) Experimental and analytical study on channel shear connectors in fibre-reinforced concrete. J Constr Steel Res 65:1787–1793
15. Pavlovic M, Markovic Z, Veljkovic M, Budevac D (2013) Bolted shear connectors vs. headed studs behaviour in push-out tests. J Constr Steel Res 88:134–149
16. Sai Shraddha P, Sudha C, Lakshmipathy M (2017) Study on ductility behaviour of different types of shear connectors in composite structural elements. Int J Civil Eng Technol 8:339–353

Up-Gradation of Unreinforced Masonry Infill Square Reinforced Concrete Frame of Ferrocement Cover with External Prestressing to Cater Seismic Forces

M. Soundararajan, K. Prakash, and S. Thirumurugan

1 Introduction

Unreinforced masonry walls (URM) are one of the significant parts of the building. In this world mostly old historic and modern buildings are made up of URM walls. Some times URM buildings are not constructed as per the codal provisions, so that these buildings are generally not capable to withstand the seismic forces. Hence these seismic forces on URM buildings subjected to damage and it leads to loss of human beings and their properties [1]. URM walls are basically weak in in-plane action of wall. The vulnerability of this kind of URM buildings are to be improved by adopted with appropriate retrofitting methods [2]. There are several methods were adopted in the field to improve the performance of the building against the seismic forces such as surface treatment, grout injections on the infill along with external reinforcement, Glass Fibre Reinforced Polymer (GFRP Sheets), welded wire mesh, Carbon Fibre Reinforced Polymer (CFRP Sheets), tie rods, Engineering Cementitious Properties (ECC shotcrete), Poly propylene Band (PP band) [3, 4].

Different methods have been proposed in recent decades to improve the shear strength of masonry walls, such as grout injections, reinforced plasters, fiber-reinforced composite applications. The grout injection is a form of filling the masonry voids with cement mortar or grout. The reinforced plaster technique consists of applying a reinforced concrete coating on both wall faces and binding them together by steel bars that pass through the masonry. The reinforced plaster technique was also commonly used and showed good efficacy, but serious problems of corrosion of steel meshes were caused after 10–15 years after the application. Recently, methods have been proposed to add sheets or meshes of composite materials based primarily on carbon and glass fibers, but also on polypropylene to the wall faces. Via diagonal compression tests of six unreinforced and twelve reinforced walls, ferro-cement

M. Soundararajan (✉) · K. Prakash · S. Thirumurugan
Department of Civil Engineering, Sona College of Technology, Salem, India

welded wire mesh and micro-concrete coating were tested in order to research the effectiveness of this technique in improving the shear and ductility ability of masonry. Experiments were performed on a CFRP (Carbon Fibre Reinforced Polymers) reinforced wall that showed that the strength of retrofitted masonry panels could be increased by up to 70% and deformability by up to 10%. The capabilities of sprayed ECC shotcrete (Engineered Cementitious Composite) were analyzed to show that both the in-plane strength and ductility can be enhanced by ECC [5]. It was also illustrated that for one and two leaf walls, the efficacy of the externally bonded reinforcement is the same, but decreases rapidly for thicker walls. Walls with a GFRP-reinforced mortar coating (Glass Fibre Reinforced Polymer) were tested. These walls were made with various styles and thicknesses of masonry, and GFRP connectors connected the coatings together. Compared to the unreinforced ones, the tests showed major changes in the bending and shear strength of reinforced walls [6].

In this study, the behaviour of URM and RM-S walls are involved with additional provisions to with stand the static and dynamic forces caused by the earthquake. Hence in this research paper mainly focus on strengthening of URM walls by retrofitting method using steel fibres, ferrocement and steel rods of 16 mm dia rod. In this experiment the walls are subjected to compressive force on the square frame diagonal, before and after retrofitting the frame. The above study allows us to know the behavior and assessment of the safety of the masonry unit structure when it is subject to seismic forces.

2   Specimens Features

Two Unreinforced specimens were tested. In particularly one of that specimen were constructed as conventional structure such as Infill masonry wall i.e. Wall constructed within the RC square frame. Specimen consists of Brick wall of 1.2 m × 1.2 m which surrounded by Reinforced concrete frame of M20 grade. RC Frame size about 0.228 m × 0.152 m. The RC frame has reinforcement of 12 mm dia rod as Main reinforcement and 8 mm dia as stirrups as shown in Fig. 1. The Second specimen was constructed in same size but the reinforcement in the specimen was tied with chicken mesh for increasing the tensile strength of the wall (Fig. 2). In addition steel rods, fibres were added only at the corners of RCC square frame (Fig. 3). Brick work in the wall constructed using the C:M 1:5 and finally the plastering work were done with C:M 1:4 ratio at thickness of 30 mm. URM and RM-S are shown in Figs. 4, 5 and 6.

3   Testing of Specimen

Specimens were tested by 2000 kN Loading frame. The load applied to the specimen as a diagonal compression at the corners of test specimens as shown in Fig. 7. The
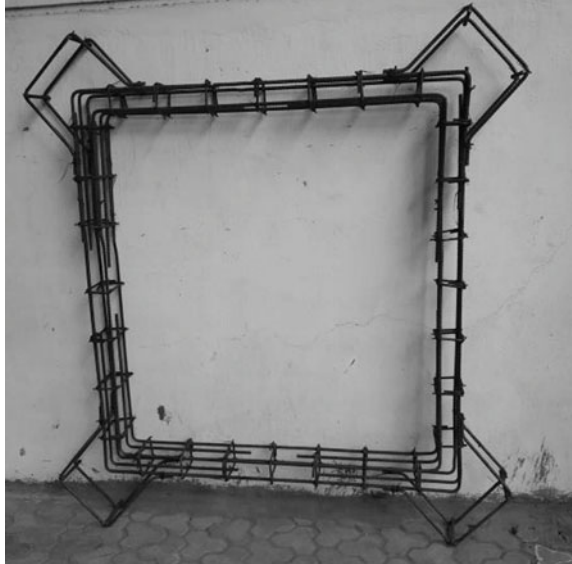
load setup is as shown in the Fig. 8. Dial gauges are fixed at the opposite direction of the loading corner faces to read the elongation on the specimen. The load applied to the specimen by using hydraulic jack which has the capacity of 2000 kN. Load is applied gradually on the specimen and the deflection induced on the dial gauges were noted at regular intervals of 30 kN loading [7]. Cracks at the walls were noted at regular intervals at different stages of loads on the specimen, first crack induced at 210 kN for URM and 270 kN for RM-S walls respectively.

Finally both the specimens were reached its ultimate load of 300 kN for URM and 360 kN for RM-S walls respectively. From this we can conclude that the pre-strengthened walls i.e. walls constructed by using the steel fibres in RC frame and chicken mesh tied with the reinforcement wrapped with walls took 60 kN more load than to that of the conventional wall.

Fig. 3 RC frame joint with steel fibre

Fig. 4 RC frame after plastering

4 Strengthening and Testing of Specimens

After the specimens were tested they need to be retrofitted by steel rods of 16 mm dia Steel rods were connected with channel section on both opposite faces by using bolt Connections as shown in Fig. 8. The bolt connections were designed as per load calculations [8, 9].

Fig. 5 RCC frame with masonry infill

Fig. 6 RCC frame infill after plastering

After the frames subjected to damage. Retrofitting techniques were applied to the RCC frame, then the frame again undergone through diagonal compression [10–13]. The load was applied to the frame with diagonal compression and the elongations were measured on the opposite diagonal of the specimens. The compressive load was applied at regular intervals of 30 kN loading. The ultimate load was noted for the retrofitting specimens, and it was 400 kN for URM and 480 kN for RM-S respectively. From these results we concluded that the frame after retrofitting with external prestressing along with ferrocement covering was carried higher load than to that of the URM walls [14].

Fig. 7 Load setup for the specimens

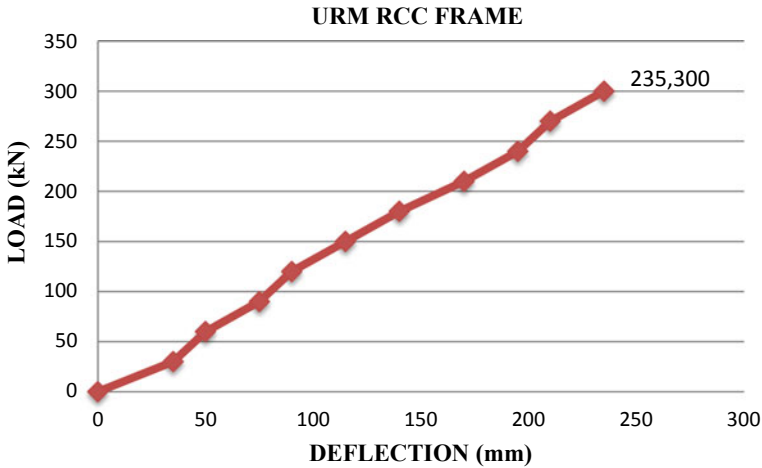**Fig. 8** Test set up for retrofitted specimen RM-S

Fig. 9 Load versus deflection for URM frame

5 Results and Discussion

The experiment was carried out on two types of masonry specimens (with and without external prestressing with 16 mm TOR steel rods). Diagonal compression tests were applied on frames and the deformation of the frame was measured on the opposite diagonal. During testing following results were observed.

The load versus deflections between the URM and RM-S showed that the differences in the strength of infill with and without ferrocement were plotted. Figures 9 and 10 showed the behaviour of the frames indicating the load versus deflection (diagonal elongation).

After the strengthening, the strength of the specimen was increased up to 33% for URM conventional structure and for the RM-S walls it increased up to 40%. Deflections for these specimens were noted and shown in the Figs. 11, 12 and 13.

6 Conclusion

The above tests on RC frame showed that the Frame with ferrocement cover along external prestressing steel rods showed better strength. After the strengthening, the strength of the specimens were increased up to 33% for URM conventional structure and for the RM-S walls it increased up to 40%. Deflections for these specimens were noted and shown in the Figs. 11 and 12.

Hence these test results indicate that the RC frames with infill along with ferrocement and additional external prestressing showed that the strength enhancement
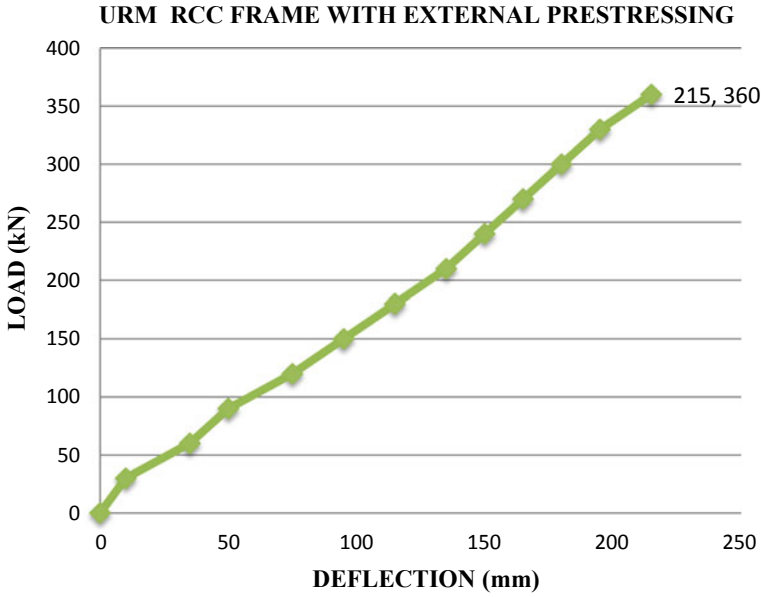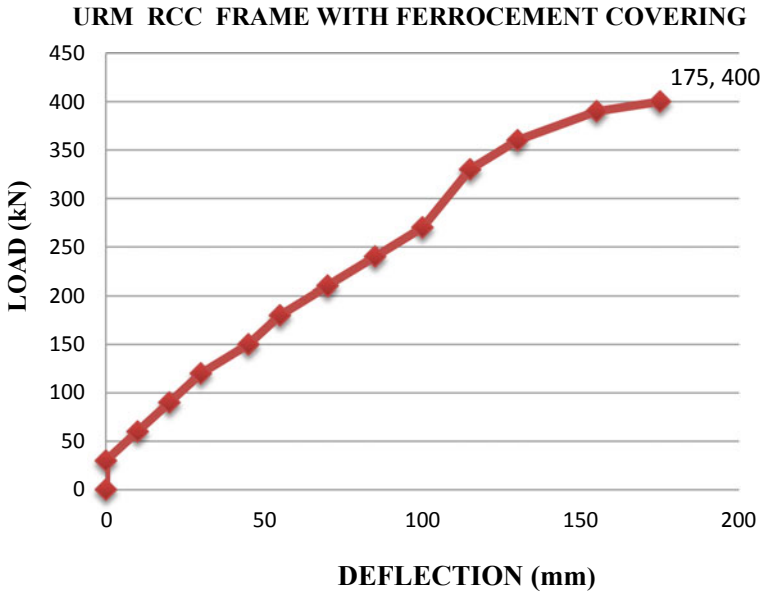
URM RCC FRAME WITH EXTERNAL PRESTRESSING

Fig. 10 Load versus deflection for URM frame with external prestressing

URM RCC FRAME WITH FERROCEMENT COVERING

Fig. 11 Load versus deflection for URM after retrofitting

SQUARE FRAME WITH RM-S
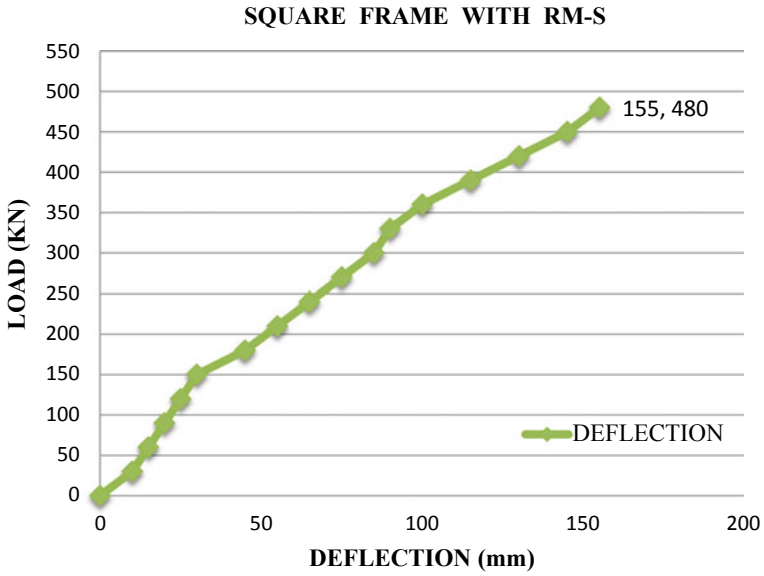
Fig. 12 Load versus deflection for RM-S frame with external prestressing
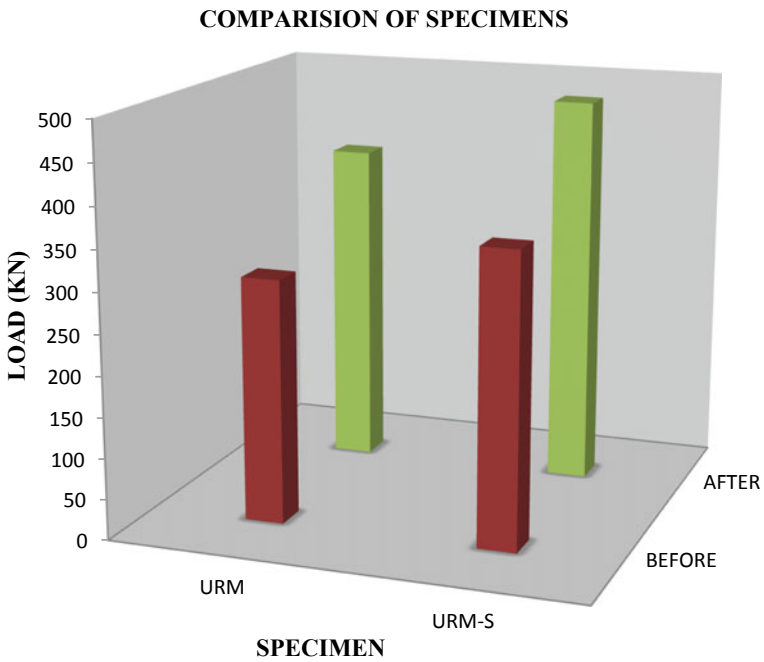
COMPARISION OF SPECIMENS

Fig. 13 Comparison of specimens before and after retrofitting

of RCC frame to cater seismic forces safely. This type arrangement of frames gives more safety to the human being as well as for infill RCC framed structures.

References

1. Kadam SB, Singh Y, Li B (2014) Strengthening of unreinforced masonry using welded wire mesh and micro-concrete–Behaviour under in-plane action. Constr Build Mater 54:247–257
2. Bhattacharya S, Nayak S, Dutta SC (2014) A critical review of retrofitting methods for unreinforced masonry structures. Int J Disaster Risk Reduct 7:51–67
3. Bischof P et al (2014) On the use of CFRP sheets for the seismic retrofitting of masonry walls and the influence of mechanical anchorage. Polymers 6.7:1972–1998
4. Lin Y-W et al (2014) In-plane strengthening of clay brick unreinforced masonry wallettes using ECC shotcrete. Eng Struct 66:57–65
5. Gattesco N, Boem I, Dudine A (2013) Behaviour of existing masonry strengthened with a GFRP reinforced mortar coating. In: Proceedings of the 14th CC2013 conference. Cagliari
6. Gattesco N, Boem I, Dudine A (2015) Diagonal compression tests on masonry walls strengthened with a GFRP mesh reinforced mortar coating. Bull Earthq Eng 13(6):1703–1726
7. ElGawady MA, Lestuzzi P, Badoux M (2005) Aseismic retrofitting of unreinforced masonry walls using FRP. Compos B Eng 37(2–3):148–162
8. Carozzi FG, Milani G, Poggi C (2014) Mechanical properties and numerical modeling of Fabric Reinforced Cementitious Matrix (FRCM) systems for strengthening of masonry structures. Compos Struct 107:711–725
9. Corradi M, Borri A, Vignoli A (2008) Experimental evaluation of in-plane shear behaviour of masonry walls retrofitted using conventional and innovative methods. Mason Int 21(1):29–42
10. D'Ambrisi A, Mezzi M, Caporale A (2013) Experimental investigation on polymeric net-RCM reinforced masonry panels. Compos Struct 105:207–215
11. D'Ambrisi A, Focacci F, Caporale A (2013) Strengthening of masonry–unreinforced concrete railway bridges with PBO-FRCM materials. Compos Struct 102:193–204
12. Borri A et al (2014) Masonry wall panels with GFRP and steel-cord strengthening subjected to cyclic shear: an experimental study. Constr Build Mater 56:63–73
13. Rinaldin G, Amadio C, Gattesco N (2017) Review of experimental cyclic tests on unreinforced and strengthened masonry spandrels and numerical modelling of their cyclic behaviour. Eng Struct 132:609–623
14. Nayak S, Dutta SC (2016) Failure of masonry structures in earthquake: a few simple cost effective techniques as possible solutions. Eng Struct 106:53–67

Performance of Recycled Coarse Aggregate Concretes with Basalt Fibers at Elevated Temperatures

Subhash C. Yaragal, Parameshwar N. Hiremath, M. Manoj Kalyan, Devesh Kumar, and P. P. Shiji

1 Introduction

The disposal problem of building demolition waste has become a serious issue both in the developing countries and developed countries. The consequence of rapid increase in infrastructure development is leading to a sharp decline in natural resources, shortage of land for waste disposal and increase in transportation costs that warrant urgent attention of researchers to provide remedial measures/solutions. The significant amount of construction and demolition waste going to dumping sites, in particular has drawn the attention of general public and environmentalists. There is a serious need to pave way towards waste free society. Therefore, the concept of recycling the waste material (waste minimization) and using it again in some form or the other has gathered momentum.

As regards to possible utilization of construction and demolition waste, this concrete debris should undergo crushing and screening processes in order to, obtain aggregate properties satisfying the limits of mixing gradation. As the construction waste is progressively increasing with the development of urban localities, study on the usage of discarded materials from demolished buildings is becoming very essential. Also, recycling of concrete not only addresses the issue of waste disposal, but it also reduces the cost and results in conservation of non-renewable natural sources [1, 2]. The environmental impact due to production of the raw ingredients of concrete (such as cement and coarse and fine aggregates) is considerable. Hence, maximizing the amount of recycled materials for use, in concrete is a very effective and promising approach towards sustainable construction.

Last decade has witnessed enormous increase in C&D waste [3, 4]. The use of Recycled Coarse Aggregate (RCA) in concrete is one of the ways of demolished waste utilization [5, 6].

S. C. Yaragal (✉) · P. N. Hiremath · M. M. Kalyan · D. Kumar · P. P. Shiji
Department of Civil Engineering, National Institute of Technology, Surathkal, Karnataka, India

The use of demolished waste was first carried out after Second World War in Germany [7]. However, the developed countries have started looking at waste as a resource, fulfilling part of their demand for raw materials [8]. While using recycled aggregates, care should be exercised to assess the quality of aggregates, as they have different sources, grades and ages [9].

Compressive strength of RCA based concrete is mainly dependent on, size of aggregate, strength of parent concrete, age of curing, severe inherent properties like adhered mortar, water absorption, replacement levels, and interfacial transition zone [10]. The most influencing factor that controls the strength of RCA based concrete is, increased water absorption of recycled coarse aggregate [11].

The option of C&D waste utilization is not fully in practice in developing countries, due to lack of sufficient knowledge and thorough regulatory guidelines, leading to waste being piled up causing disposal issues [12].

To improve the mechanical properties of recycled aggregate based concrete a different approach is required, that calls for further investigation in this field. Addition of fibers in concrete has major role in enhancement of structural properties of concrete [13–15]. Gokila et al. found the advantageous impact of basalt fiber in concrete with fiber dosages of 0.5 and 1%. Study indicates that 1% of basalt fiber has shown maximum increase in compressive strength at 28 days of curing. Nayan et al. [16] also observed increase in compressive strength of concrete with 2% basalt dosage.

Study carried out by Tumadhir [17] on mechanical properties of thermally treated basalt reinforced concrete indicates that, strength of concrete increase with increase in fiber content up to 0.3%. Later gradual reduction in strength was observed. Same observation was made by Elshafie [18].

Inclusion of basalt fiber in plain concrete has shown 14% increase in compressive strength. In case of RCA based concrete inclusion of basalt fiber has shown considerable increase in mechanical properties as suggested by Katkhuda [19]. The treated basalt fiber of 0.3% with HCL solution has shown increase in compressive strength, whereas untreated basalt fiber requires 0.5% fiber dosage to enhance the compressive strength of concrete. Jagadish et al. have studied the performance of basalt fiber in normal and high strength concrete with different proportion at elevated temperatures. Results indicate that, increase in compressive and split tensile strengths in high strength concrete is being more when compared to normal strength concrete. Yakhlat et al. have studied the mechanical properties of basalt fiber reinforced concrete. Results of the study noticed that there is about 6–18% increase in compressive strength with different proportion of basalt fiber. The maximum strength was observed for 0.3% basalt fiber.

Tabsheer Ahmed et al. studied the structural behavior of basalt fiber reinforced concrete. Outcome of the study implies that addition of 1% basalt fiber increases strength and inclusion of fibers does not affect the slump value significantly. Same observation was made by Gokila et al., among two basalt fiber dosage 0.5 and 1%, high compressive strength was obtained for 1% fiber dosage. With respect to above studies Rathod [16], presented compressive strength results of concrete with different proportions of basalt fibers. The maximum strength was observed for 2% fiber reinforced concrete. From the above research works it is clear that, the inclusion of

fibers aid in increase in strength of different types of concretes. Studies that address the elevated temperature exposure of RCA based concretes are scarce. Although, concrete is a bad thermal conductor, it exhibits virtuous thermal resistance. In the event of accidental fire exposure, several factors such as environmental and those associated with heating, significantly affect the residual concrete characteristics. The temperature of exposure, rate of heating and duration of exposure (soaking or retention period) are the major parameters controlling the performance of concretes at elevated temperatures. On other hand, parameters like dehydration of C–S–H gel, thermal incompatibility between the aggregate and the cement paste and the buildup of vapour pressure within concrete matrix are the main constituent's controlling factors.

There has been no significant research in the area of RCA based concrete's performance at elevated temperatures. Zega and Di Maio [2] have reported that the performance of RCA based concrete was better than conventional concrete with the utilization of lower w/c ratio. The co-efficient of thermal expansion of old and its affinity reduces the micro and macro cracking of the cement mortars. Researchers have studied the spalling behavior of RCA based concrete blocks, by varying the RCA replacement from 0 to 100% by volume. The concrete blocks were heated as per the Japanese Standard JIS A 1304 "Method of fire resistance test for structural parts of building". No spalling has been observed in both type of concretes such as RCA based concrete and conventional concrete. The results showed that the elevated temperature behavior of RCA based concrete was comparable with that of conventional concrete. Similar observations have been reported by Xiao and Zang. Viera et al., report no correlation between the residual mechanical properties of concrete with different percentage replacement of RCA in concrete. Further they have reported that RCA concretes exposed to 400, 600 and 800 °C, have shown similar trend of compressive strength reduction as those of conventional concretes at elevated temperatures. On other hand, study carried by Cree et al. [20] have reported that RCA based concretes perform better than conventional concretes at temperatures between 500 and 700 °C. From the above research works, there is need to take up detailed studies on the performance of RCA based concretes at elevated temperatures. This study reports the usage potential of basalt fiber in performance of RCA based concretes at elevated temperatures. Further the micro-structural investigation of RCA based concretes with basalt fibers at elevated temperatures is undertaken.

2 Materials

2.1 Materials

Ordinary Portland Cement of 53 grade was used in the present study. Naturally available river sand satisfying zone II gradation requirement as per IS 383-1970, with specific gravity of 2.6 was used as fine aggregate. Coarse aggregates of 20 mm down

Table 1 Properties of concrete ingredients

Sl. No.	Properties	Ingredients		
		Cement	Fine aggregate	Coarse aggregate
1	Specific gravity	3.15	2.6	2.7
2	Density (kg/m^3)	1440	1589	1684

Table 2 Properties of basalt fiber

Test parameter	Value
Diameter (μm)	5.8
Length (mm)	6.0
Density	2.75
Elongation at break	–
Melting point	1440 °C

and retained on 10 mm with specific gravity of 2.7, satisfying IS 383-1970 grading requirement was used. The specific gravity and density of cement, fine aggregate and coarse aggregates are tabulated in Table 1. The properties of basalt fibers used in this study are shown in Table 2.

2.2 Processing and Characterization of RCA

Processing or extracting RCA from demolished concrete involves, separating the adhered mortar to the extent possible and to bring the physical properties of RCA closer to or as similar to that of virgin/natural aggregates. The recycled coarse aggregates were obtained from the concrete cubes which were cast, cured for 28 days and then crushed to failure using a compression testing machine. RCA extracted from 28 days old concrete, was considered in the present study, as construction and demolished waste. By using hydraulic compression machine specimen were broken into small pieces of 20–40 mm. These pieces will have large content of mortar attached to them, which is not desirable so as to be used as coarse aggregates. Separation of this adhered mortar was the main challenge in obtaining RCA. Jaw crusher was used for processing RCA. The material discharged from the jaw crusher was sieved to size of 20 mm down and 10 mm holding, 10 mm passing and 4.75 mm holding as coarse aggregate. Later sieved material was washed manually with water, to remove the dust particles sticking to the surface of the aggregates. The washed material was then sun dried and stacked in the laboratory before use in the subsequent experiments as RCA. The properties of the RCA are as shown in Table 3.

Table 3 Properties of recycled coarse aggregates

SI. No.	Property	Results
1	Specific gravity	2.59
2	Water absorption	2.43%
3	Bulk density	
	I. Loose	1230 kg/m^3
	II. Compact	1490 kg/m^3

2.3 Mix Design

There are various methods of mix design available such as I.S. method, Road Note Method, British method etc. In this study AMBUJA METHOD for mix design was used, and UK method for calculation of fine and coarse aggregates in concrete. Water cement ratio of 0.45 was chosen. The obtained mix proportions are shown in Table 4.

2.3.1 Experimental Methodology

To generate construction and demolition waste, 60 numbers of 150 mm concrete cubes (1:1.8:2.7) were cast in the laboratory and crushed to failure, after 28 days of water curing. Later this crushed concrete C&D waste, is processed to obtain recycled coarse aggregates. Crushed concrete fragments were broken using a hammer to produce small pieces of size compatible for processing, using jaw crusher. Processing of recycled coarse aggregates is done using jaw crusher. The processed RCA is adopted in further experiments.

As the water absorption of the RCA being high, it is likely to absorb the water which is added for the concrete for cement hydration and workability. This will lead to less effective w/c ratio and less workability. Adding water to compensate for the absorption will also create problems as the effective w/c ratio will be very high and it will give high workability. Assessment of additional water to cater for RCA absorption is quite involved, complex and not that accurate. So, it was decided to soak RCA for 24 h before use, so that it does not absorb water during the process of mixing. This method of soaking was helpful to attain moderate workability of concrete without use of plasticizers. For performance studies of RCA, cubes were cast with different proportions of recycled coarse aggregate such as 0, 25, 50, 75 and 100%. For each mix three numbers of 100 mm concrete cubes were cast, cured for 28 days and then tested for their strengths using a compression testing machine.

Table 4 Mix proportion

Water (kg)	Cement (kg)	FA (kg)	CA (20 mm)
185.4	412	745	1118
0.45	1	1.8	2.71

Table 5 Mix proportion per cubic meter of RCA based concrete

Mix	RCA (%)	C (kg)	FA (kg)	CA (kg)	RCA (kg)	W (kg)
1	0	436	785	1182	0	211
2	25	436	785	882	300	209
3	50	436	785	591	591	207
4	75	436	785	300	882	206
5	100	436	785	0	1182	204

(C—cement, FA—fine aggregate, CA—coarse aggregate, W—water)

Table 6 Mix proportions per cubic meter of concrete (50% RCA) with basalt fiber

Dosage (%)	RCA (%)	Fibre (kg)	C (kg)	FA (kg)	CA (kg)	RCA (kg)	W (kg)
0	50	0	436	785	591	591	207
0.5	50	1.15	434.85	785	591	591	207
1.0	50	2.30	433.7	785	591	591	207
1.5	50	3.45	432.55	785	591	591	207
2.0	50	4.60	436	785	591	591	207

The dosage of chemical admixture (CONPLAST SP 430) has been suitably used to give slump in the range of 50–75 mm. The slump has been maintained constant for all proportions of RCA attempted. Table 5 presents the composition of various concrete mixes designed to achieve the objectives set forth.

For the performance enhancement studies of RCA based concretes, cubes were cast keeping the recycled aggregate as 50% replacement of natural/virgin aggregates and basalt fiber dosages (volume fraction) were varied from 0 to 2%. The aim was to find the optimum dosage of basalt fibers for strength enhancement. For each dosage three numbers of 100 mm concrete cubes were cast. The slump has been maintained constant for all fiber proportions. Table 6 presents the composition of various concrete mixes designed with 50% of RCA, for all fiber dosages. Similarly, performance enhancement of RAC with 100% of RCA by using basalt fiber is studied.

### 2.3.2 Test Facility for Elevated Temperature Exposure

Figure 1 shows a programmable electric furnace. Figure 2 shows time temperature build up curve.

The specimen were subjected to exposure tests for temperatures of (200, 400, 600 and 800 °C) with a retention period 30 min. After retention period, the specimen were furnace cooled. By furnace cooling, it is meant that, after completion of specified retention period at designated temperature, the furnace power supply is cut off and the door of the furnace shall not be opened till the specimen inside attain room

Fig. 1 Programmable electric furnace

Fig. 2 Time versus temperature build up curve for the furnace
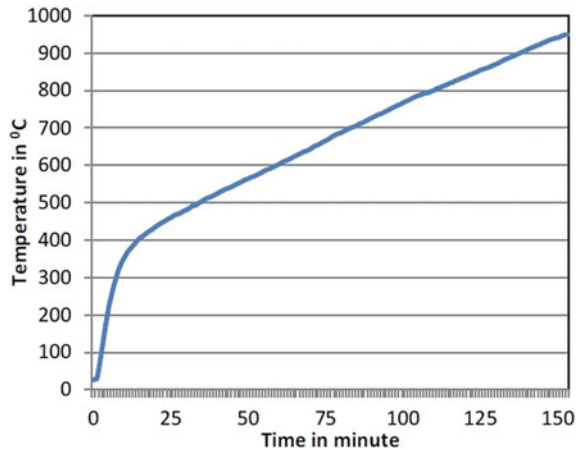
temperature. The interior of the furnace temperature can be monitored digitally from outside display panel.

2.3.3 Test on RCA Based Concretes

The properties of constituent materials such as the quality of aggregate, the quality of cement paste, and the bond between aggregate and cement paste, influence the strength of concrete. The concrete samples with RCA are tested at the age of 28 days. The testing of cubes was done in a 200 T compression testing machine. Microstructure analysis of RCA based concrete at different magnifications was carried out using

Scanning Electron Microscope (SEM). The study of the microstructure also includes the study of the morphology of a specimen of concrete to basis of RCA product with different proportions of the RCA with polypropylene and basalt fibers. The samples intended for the review by the SEM were collected from central part of the cube by using diamond saw cutter. The thickness of the sample for the observation through SEM was of approximately 5 mm and the spray of gold has been carried out on a dry surface of the sample of concrete. Then, the prepared samples were mounted on the heel of SEM using black carbon tape. The sample in a SEM has been bombarded by a beam of electrons at high speed with a voltage of acceleration of 10–20 kV headed directly on the sample. The SEM images have been taken at different locations on samples of concrete with different magnifications.

3 Result and Discussion

3.1 Fresh Properties of RCA Based Concretes

The standard slump cone test is used measure workability of concrete. With the increase in the percentage of the RCA in the concrete, the workability was observed to gradually reduce. The workability of the fresh concrete produced with 100% RCA had a value of slump close to zero mm. This is mainly due to the higher water absorption characteristics of RCA, the in comparison to the natural coarse aggregate.

The addition of water to compensate for this absorption was not a good option because the exact amount is difficult to be assessed. The other option of soaking RCA for 24 h before use, was adopted so that RCA does not absorb extra water during the process of mixing. The slump was maintained in the range of 50–75 mm, for all RCA mixes by using appropriate dosage of super plasticizer (CONPLAST SP 430). With increase in percentage of RCA in concrete, the super plasticizer dosage is also increased to maintain the slump in the range of 50–75 mm for all mixes. Table 7 shows the super plasticizer dosages of various mixes.

Table 7 Dosages (% by wt. of cement) of SP for different proportions

Basalt fiber (%)	SP dosage (RCA 50%)	SP dosage (RCA 100%)
0.5	0.24	0.40
1.0	0.34	0.64
1.5	0.46	0.82
2.0	0.54	0.96

3.2 Compressive Strength of RCA Based Concretes

The results of RCA based concretes with different levels of replacement are shown in Figs. 3 and 4. It can be observed that as the RCA level of replacement increases, the strengths are observed to gradually decrease. The reduction in strength for 25% of RCA replacement is 5% whereas for 50% of replacement, the loss of strength is around 12%.

The increase in percentage of RCA, increases porosity of ITZ between old and new matrix making it more weak, that causes reduction in concrete strength. At 75% RCA replacement, the decrease in strength is 19%, which is quite considerable.
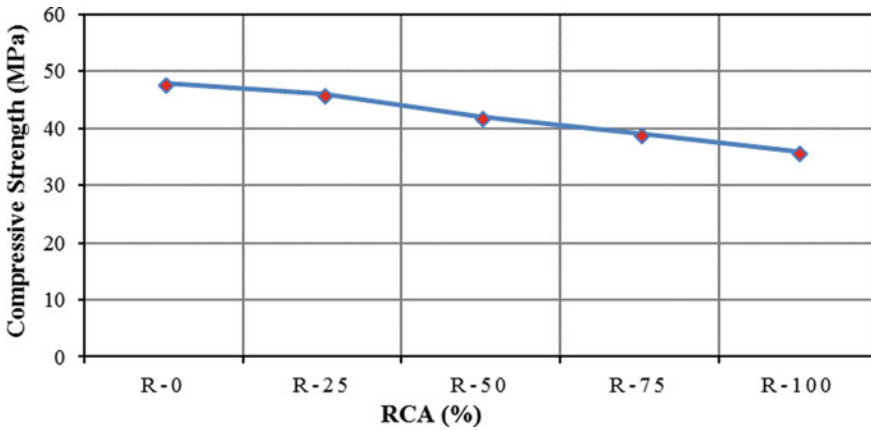
Fig. 3 Compressive strength variation with RCA (%)
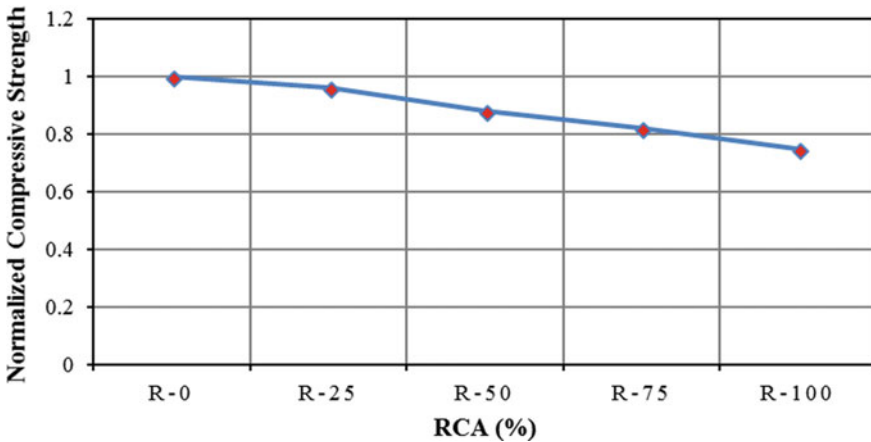
Fig. 4 Normalized compressive strength variation with RCA (%)

The drop in strength is mainly due to increased amount of adhered mortar quantity on RCA that decreases the bond between new and old matrix. RCA with 100% replacement has shown 25% reduction in compressive strength, nearly the same magnitude in strength reduction has been reported by Etxeberria et al. [21], Rahal [22] and Yand et al.

3.3   Microstructure of RCA Based Concretes

Microstructure of RCA based concrete is quite different and a little involved than conventional concrete especially in the Interfacial Transition Zone (ITZ). In case of normal concrete there is one ITZ that lies between coarse aggregate and cement mortar.

In RCA based concrete it has two ITZs, one is new ITZ that lies between recycled aggregate and new matrix and the other is old ITZ that lies between recycled aggregate and old adhered mortar. Hence, mechanical performance of RCA based concrete is a consequence of dual ITZs significantly influencing the strength.

From the experimental results, it can be observed that as RCA replacement increase from 0 to 100%, strength is observed to gradually decrease. This is mainly due to weak ITZ and presence of pores in adhered mortar on RCA. Figure 5a shows the ITZ of control concrete with dense microstructure. Figure 5b presents the microstructure of 50% RCA. It is observed that ITZ is comparatively porous than control concrete. This is the reason for reduced compressive strength of 50% RCA based concrete. As percentage of RCA increases, the amount of intrinsic pores, cracks and fissures are increasing to a considerable extent.

Poon et al. [23] investigated that as percentage of RCA increases, the quantity of loose and porous hydrates increase drastically leading to reduced strength of concrete. Figure 5c shows the weak ITZ of RCA based concrete with 75% replacement. Pores and cracks in ITZ are considerably more compared to control concrete. The porous nature of ITZ causes the reduction in elastic modulus and lowers the strength in that particular area. The SEM image of 100% RCA based concrete is shown in Fig. 5d. From SEM analysis, it is found that for 100% RCA very weak ITZ links are formed and these act as strength limiting phases. Further, thin wall between the matrix phase and coarse aggregate phase in concrete is observed. The number of new ITZ with old aggregate increase, with increase in percentage of RCA there by increasing the porosity of ITZ. Due to its poor micro structure, the stiffness of concrete gets reduced and that does not withstand the stress transfer across this. Therefore, 100% RCA based concrete has shown maximum reduced strength.
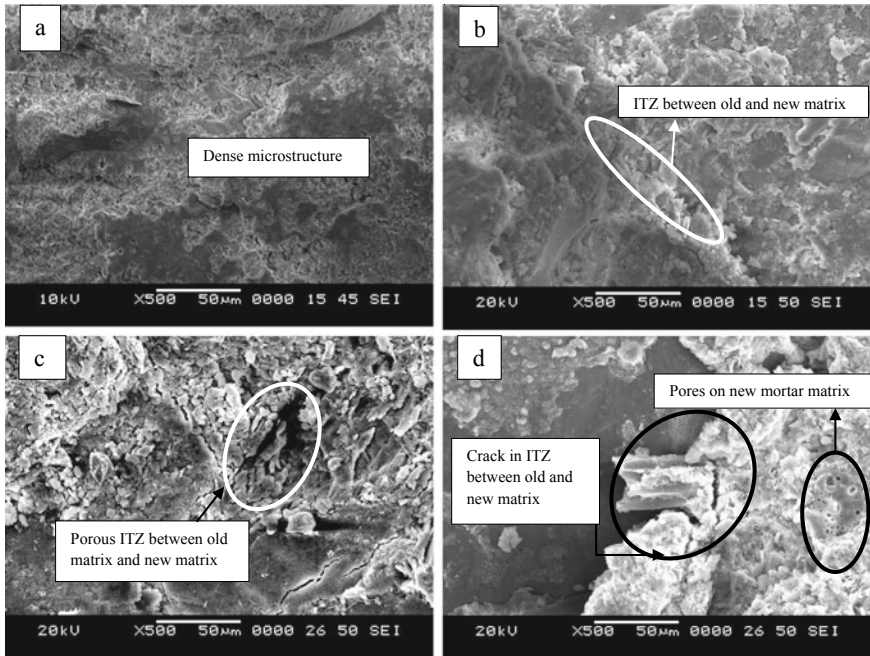
Fig. 5 RCA based concretes with replacement levels of **a** 0% **b** 50% **c** 75% and **d** 100%

3.4 Performance Enhancement of RCA Based Concretes Using Basalt Fibers

From the earlier section, it is observed that the strength of RCA based concretes decrease with increase in RCA content. The strength got decreased from 48 MPa (control mix) to 36 MPa for (100% RCA) based concrete. The strength reduction is 25% for 100% RCA based concrete. Therefore, attempts were made to obtain strength equal to or greater than, that of no RCA based concrete by incorporating basalt fibers. The results of performance enhancement of RCA based concrete by adopting basalt fibers is shown in Figs. 6 and 7.

It is observed that, with increase in fiber dosage, the compressive strength of 50% RCA based concretes increase at a steep rate. For 0.5% fiber dosage, the increase in compressive strength being 4% and for 1% dosage, the strength got increased by 8%. The increase in strength is attributed to high modulus of elasticity of basalt fibers. Basalt fibers, overcome/strengthen the weak ITZ portions by bridging the micro-pores. The maximum strength obtained for 1.5% fiber dosage was 13%. This is possibly due to, even distribution of fibers causing good bonding with concrete matrix leading to improvement in strength. However, for 2% of basalt fibers addition, the rate of strength gets considerably reduced, which renders more micro pores in the ITZ zone due to uneven orientation of high dosage of fibers. It is interesting to note
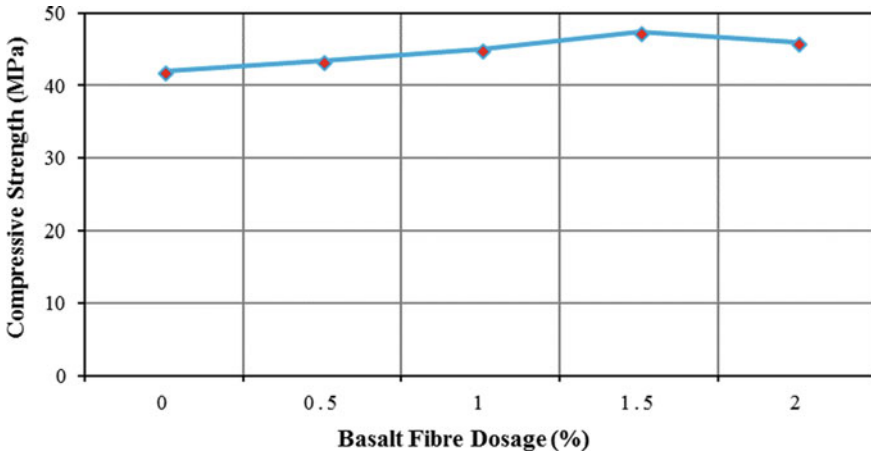
Fig. 6 Compressive strength variation of 50% RCA based concrete with basalt fiber
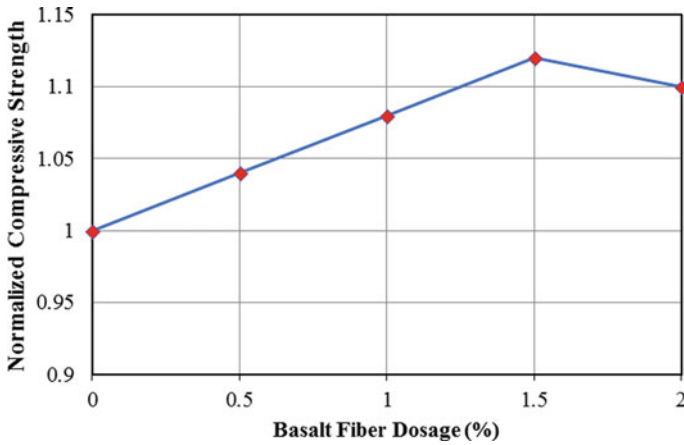

Fig. 7 Normalized compressive strength variation of 50% RCA based concrete with basalt fiber

that strength of 50% RCA based concrete can be best enhanced with 1.5% dosage of basalt fibers.

Similarly, experiments were conducted for performance enhancement of 100% RCA based concrete with basalt fibers. The results are presented in Figs. 8 and 9. Like the previous case, incorporation of fibers, has shown a steady increase in strength of concrete up to 1.5% fiber dosage. 0.5% fiber dosage has shown 6% increase in strength and 1% of fiber dosage has increased strength by 11%. Nearly 20% enhanced strength was obtained for 1.5% dosage of fibers. The increase in fiber dosage beyond 1.5% dosage has shown a decrease in strength like the previous case of 50% RCA
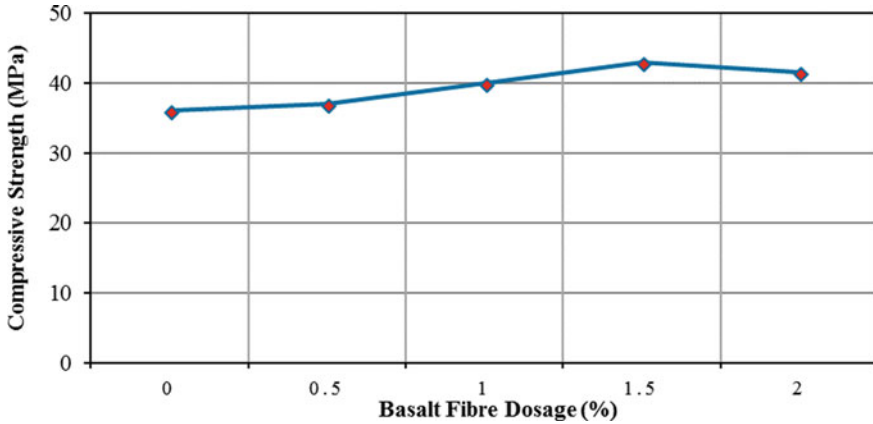
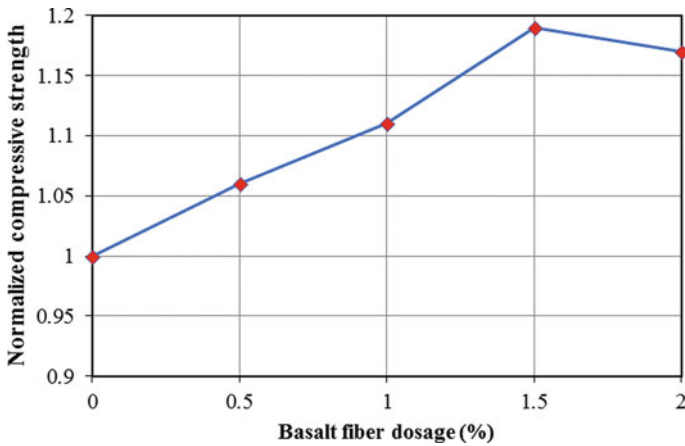**Fig. 8** Compressive strength variation of 100% RCA based concrete with basalt fiber

Fig. 9 Normalized compressive strength variation of 100% RCA based concretes with basalt fibers

based concrete. Figure 11 shows microstructure images of RCA based concrete with basalt fibers.

From Fig. 10a it can be observed that the fibers are laterally located making concrete matrix dense with improved bonding between new ITZ and old ITZ of aggregate and matrix phases. The enrichment of concrete matrix by basalt fibers can be observed in Fig. 10b, indicating strong bonding between basalt fiber and concrete matrix. This may be the reason for enhancement of RCA based concrete with basalt fibers. The increase in strength is also due to the high modulus of elasticity of basalt fibers that enrich the load carrying capacity of RCA based concrete.
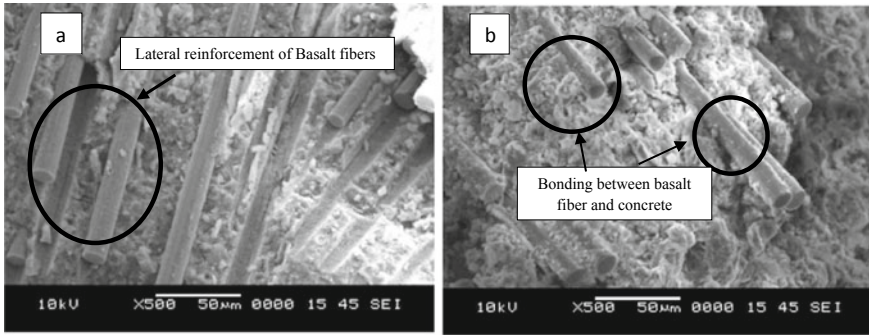
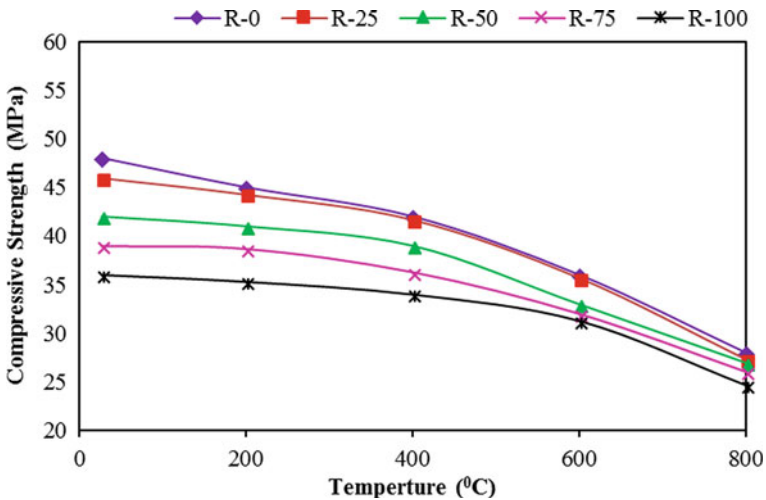**Fig. 10** Microstructure of RCA based concrete with basalt fibers

Fig. 11 Compressive strength variation with RCA at elevated temperatures

3.5 Performance of RCA Based Concretes at Elevated Temperatures

3.5.1 Compressive Strength

Compressive strengths of RCA based concretes, at different elevated temperatures are presented in Figs. 11 and 12. The residual strengths in the normalized form are also presented for ease of understanding and discussion. It can be observed that, with increase in temperature the strength gradually decreases for control concrete as well as, for other RCA based concrete mixes. Control concrete has shown 8, 12, 25 and 42%, reduction in compressive strength with increase in temperature. However, for
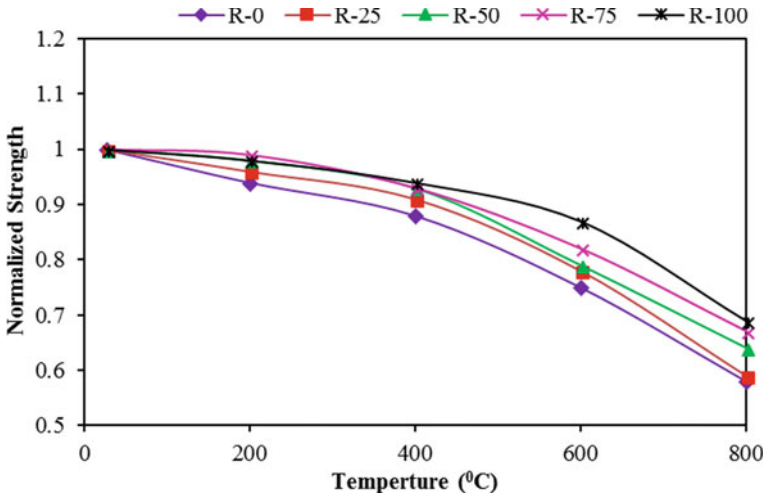
Fig. 12 Normalized compressive strength variation with RCA at elevated temperatures

the case of 100% RCA based concrete, the strengths are reduced by 2, 4, 13 and 21% for 200, 400, 600 and 800 °C respectively.

In other words, the higher values of residual strengths of 100% RCA based concrete is due to better thermal expansion properties between the aggregate and cement paste. Therefore, residual strengths, for recycled aggregate concretes were higher when compared to natural aggregate concretes at elevated temperatures.

RCA based concrete mixes have exhibited better elevated temperature endurance characteristics, as seen from their residual strengths after exposure. The better residual strength characteristics of RCA based concrete is due to the better thermal characteristics of RCA in the first place and also the increase in micro pores with increase in RCA, which assists in sustaining elevated temperatures when compared to no RCA based concrete.

Figure 13a, shows microstructure images of 50% RCA based concrete. It can be noticed that the presence of micropores on new matrix phases and gap between concrete phases, which allows steam pressure to be released, when RCA based concretes are exposed to elevated temperatures. The percentage of pores in matrix, increases with increase in percentage of RCA replacement. From Fig. 13b it can be observed that, the volume of pores increase in 100% RCA based concrete. Due to which, the chances of spalling of concrete at higher elevated temperatures will be reduced. That is RCA based concretes, exhibit better thermal characteristics. This may be the reason for improved residual compressive strengths of RCA based concretes at elevated temperatures.
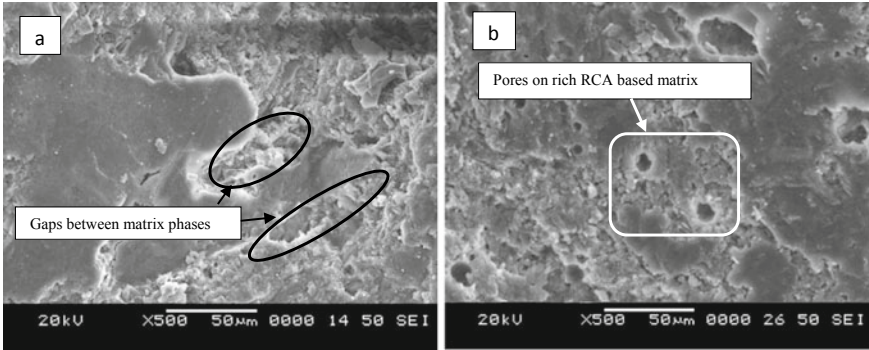
Fig. 13 Microstructure of RCA based concrete after exposure to elevated temperature

3.6 Performance of RCA Based Concretes with Basalt Fibers at Elevated Temperatures

The strength results of RCA based concretes, with basalt fibers at elevated temperatures are presented in Figs. 14 and 15. Basalt fibers in RCA based concretes, have shown considerable increase in strength when compared to RCA based concretes without fibers. The increase in compressive strength was observed for all RCA based concretes at 200 °C. The increment in strength was observed up to 400 °C, later there is gradual decrease in strength at higher elevated temperatures.
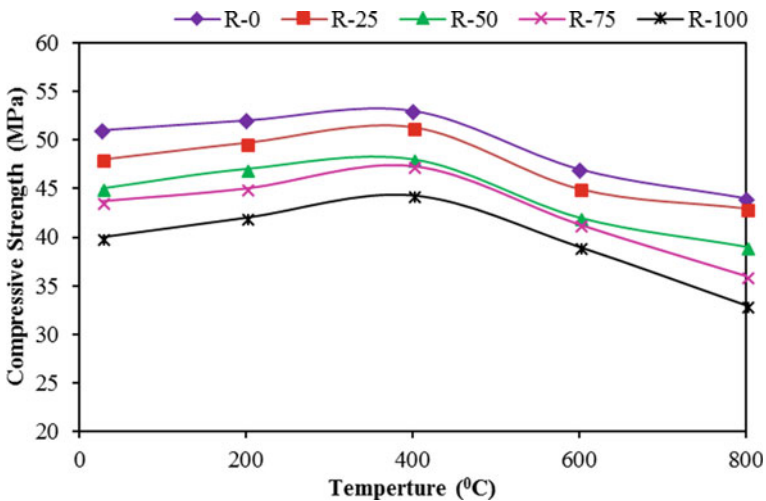

Fig.14 Compressive strength variation of RCA based concretes with basalt fiber versus elevated temperatures
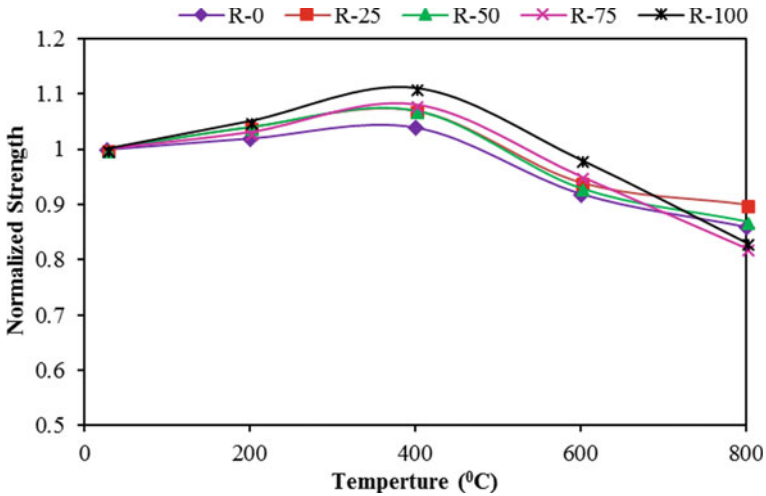
Fig.15 Normalized compressive strength variation of RCA based concretes with basalt fiber versus elevated temperatures

At microstructural level it is clearly observed (Fig. 16a, b) that, bonding between concrete and basalt fibers has a great influence on residual strength of RCA based concretes at elevated temperatures.

From Fig. 16a it can be observed that basalt fibers are cohesively bonded with RCA matrix. The fibers provide good bridging effect between the old and new matrix, even at elevated temperature of 400 °C. The basalt fibers are intact at 800 °C, even though the concrete exhibits disintegrated matrix as shown in Fig. 16b.
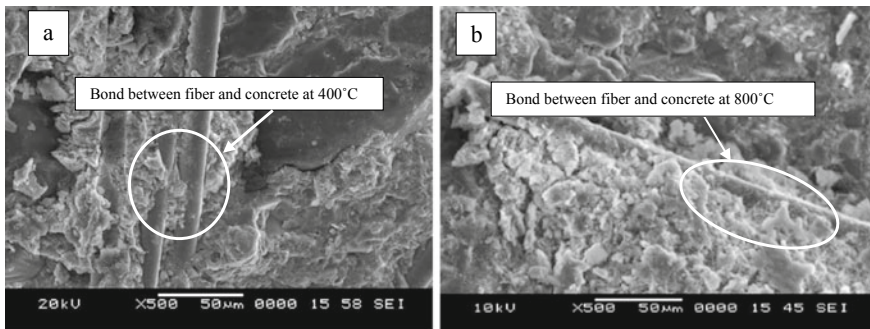

Fig. 16 Microstructure of RCA based concrete with basalt fibers after exposure to elevated temperature **a** 400 °C **b** 800 °C

4 Conclusions

Based on the detailed experimental investigation, the following are the important conclusions,

1. With increase in RCA, strength of concrete is observed to gradually decrease. For 100% RCA based concrete, 25% reduction in compressive strength is observed. Microstructure studies based on SEM images indicate that there is an increase in porosity of RCA based concrete due to increase in percentage of pores on adhered mortar.

2. Addition of basalt fibers, has a significant effect on strength enhancement of RCA based concretes. For both 50 and 100% RCA based concretes, 1.5% fiber dosage has resulted in higher enhanced compressive strengths, i.e., an increase in strength of 13 and 19%, for 50 and 100% RCA based concretes respectively.

3. Addition of basalt fiber is advantageous in strength retention of RCA based concretes at elevated temperatures.

4. For all replacement levels, the residual strengths of concrete with fibers are higher than the control concrete up to 400 °C. The loss in strengths is lower than 10 and 15% for exposure levels of 600 and 800 °C respectively.

References

1. Eguchi K, Teranishi K, Nakagome A, Kishimoto H, Shinozaki K, Narikawa M (2007) Application of recycled coarse aggregate by mixture to concrete construction. Constr Build Mater 21(7):1542–1551
2. Zega CJ, Di Maio ÁA (2011) Use of recycled fine aggregate in concretes with durable requirements. Waste Manag 31(11):2336–2340
3. Tabsh SW, Abdelfatah AS (2009) Influence of recycled concrete aggregates on strength properties of concrete. Constr Build Mater 23:1163–1167
4. Wagih AM, ElKarmoty HZ, Ebid M, Okba SH (2013) Recycled construction and demolition concrete waste as aggregate for structural concrete. HBRC J 9(3):193–200
5. Rao MC, Bhattacharyya SK, Barai SV (2011) Behavior of recycled aggregate concrete under drop weight impact load. Constr Build Mater 25:69–80
6. Rao MC, Bhattacharyya SK, Barai SV (2011) Influence of field recycled coarse aggregate on properties of concrete. Mater Struct 44(1):205–220
7. Khalaf FM, DeVenny AS (2004) Recycling of demolished masonry rubble as coarse aggregate in concrete. J Mater Civ Eng 16(4):331–340
8. Kou SC, Poon CS (2012) Enhancing the durability properties of concrete prepared with coarse recycled aggregate. Constr Build Mater 35:69–76
9. Padmini K, Ramamurthy K, Mathews MS (2009) Influence of parent concrete on the properties of recycled aggregate concrete. Constr Build Mater 23:829–836
10. Martínez-Lage I, Fernando M-A, Vázquez-Herrero C, Pérez-Ordóñez JL (2012) Properties of plain concrete made with mixed recycled coarse aggregate. Constr Build Mater 37:171–176
11. Panda KC, Bal PK (2013) Properties of self compacting concrete using recycled coarse aggregate. Proc Eng 51:159–164
12. Silva RV, de Brito J, Dhir RK (2014) Properties and composition of recycled aggregates from construction and demolition waste suitable for concrete production. Constr Build Mater 65:201–217

13. George RM, Das BB, Goudar SK (2019) Durability studies on glass fiber reinforced concrete. In: Sustainable construction and building materials. Springer, pp 747–756
14. Güneyisi E, Gesoğlu M, Akoi AOM, Mermerdaş K (2014) Combined effect of steel fiber and metakaolin incorporation on mechanical properties of concrete. Compos B Eng 56:83–91
15. Snehal K, Das BB (2019) Mechanical and permeability properties of hybrid fibre reinforced porous concrete. Indian Concr J 98(1):54–59
16. Rathod N, Gonbare M, Pujari M (2015) Basalt fibre reinforced concrete. Int J Sci Res 4(5):359–361
17. Tumadhir M (2013) Thermal and mechanical properties of basalt fibre reinforced concrete. World Acad Sci Eng Technol Int J Civil Environ Struct Constr Arch Eng 7(4):334–337
18. El-shafie S, Whittleston G (2015) A review of the effect of basalt fibre lengths and proportions on the mechanical properties of concrete. Int J Res Eng Technol 4(1):458–465
19. Katkhuda H, Shatarat N (2017) Improving the mechanical properties of recycled concrete aggregate using chopped basalt fibers and acid treatment. Constr Build Mater 140:328–335
20. Cree D, Green M, Noumowé A (2013) Residual strength of concrete containing recycled materials after exposure to fire: a review. Constr Build Mater 45:208–223
21. Etxeberria M, Vázquez E, Marí A, Barra M (2007) Influence of amount of recycled coarse aggregates and production process on properties of recycled aggregate concrete. Cem Concr Res 37:735–742
22. Rahal K (2007) Mechanical properties of concrete with recycled coarse aggregate. Build Environ 42(1):407–415
23. Poon CS, Shui ZH, Lam L (2004) Effect of microstructure of ITZ on compressive strength of concrete prepared with recycled aggregates. Constr Build Mater 18(6):461–468
24. Wagih AM, El-Karmoty HZ, Ebid M, Okba SH (2013) Recycled construction and demolition concrete waste as aggregate for structural concrete. HBRC J 9:193–200
25. Naidu AL, Jagadeesh V, Bahubalendruni MR (2017) A review on chemical and physical properties of natural fiber reinforced composites. Int J Adv Res Eng Technol (IJARET) 8(1):56–68

Wind-Induced Vibration Control on Transmission Tower

Swabarna Roy, Chinmay Kumar Kundu, and Bhagabata Jena

1   Introduction

Transmission towers are widely used for transmission of electric energy, which is essential in all the sectors. Tower structures are highly flexible structure having height much larger than its width. They are susceptible to strong wind excitations owing to their low damping [1, 2]. Wind turbulence cause a fluctuating load on the structure which then starts to vibrate. These dynamic vibration responses are of significant value and must be considered in the design stage. They are calculated either using codal design provisions or experimental procedure with the use of wind tunnel on an aeroelastic lattice tower model [3]. In order to determine the developed stresses in transmission tower members, wind load has been considered in the tower analysis [4, 5]. During strong wind loading, excessive vibration of transmission line tower system causes excessive acceleration and displacement along the hanging line which generates excessive tensile force on the cables, thus leading to structural failure [6]. So, in order to ensure stability and safety of structure, control of structural responses of the transmission towers under wind are required. The impact of element failure along with the failure modes should be realized. The uninterrupted operation and reliable transmission lines are a crucial need [7]. Failure of towers due to wind loads has been studies by many researchers [8–10]. The conclusion can be made from various literature studies that wind-induced vibrations are reason for several failures in transmission towers [11, 12]. In order to mitigate the dynamic response on transmission towers, different field measurement, experimental and theoretical

S. Roy (✉) · C. K. Kundu · B. Jena
School of Civil Engineering, KIIT University, Bhubaneswar, Odisha, India

C. K. Kundu
e-mail: chinmay.kundufce@kiit.ac.in

B. Jena
e-mail: bjenafce@kiit.ac.in

techniques have been introduced [13–15]. These techniques focus in enhancing the design parameters of the tower, such as ductility and stiffness, thus improving its dynamic performance. But the structure designed using the normal methods does not have the ability to resist strong wind excitations. Therefore, new techniques have been introduced over the traditional design methods which deals with the application of devices which can dissipate energy or absorb dynamic vibrations [16]. Control on the vibration can be achieved using devices like Viscoelastic damper (VE), Tuned Mass Damper (TMD), Magnetorheological (MR) Damper, Pounding Tuned Mass Damper (PTMD) and Friction Damper. These devices can be used to minimize the impact of external wind forces by controlling the vibration on towers. Viscoelastic damper has been used to reduce the acceleration of transmission tower top by a range more than 60% [17]. Viscous damper was utilized on a large-scale substation frame for controlling wind-induced effects [18]. Passive friction damper was used in an analytical control technique and was applied on transmission tower-line system and showed good control of excitations [19]. Finite Element (FE) models for transmission tower as well as tower-line system was analysed for vibration performance using Tuned mass dampers. The optimal damper parameters were determined which could effectively decrease the structural response under wind [20]. Semi-active devices like Magnetorheological damper can substantially supress the transmission tower dynamic response if the damper parameters are optimal determined [21].

This research article deals with the study of the application of various dampers for controlling wind-induced vibration in transmission towers. In order to ensure reliability and avoid failure of tower structure various control strategies has been adopted. This paper presents a zest of literature related to the damper behaviours in controlling the vibrational response. A good and accurate damper choice may lead to successful reduction in wind force vibrations. Hence, a comparative study has been performed based on the damping performance of these control devices.

2 Transmission Tower

The transmission tower structures essentially comprising of the supports, its foundations, ground-wires and the conductors placed at suitable height from ground with specified factor of safety to facilitate the flow of power energy from one place to another with safety and reliability. The height of the towers is determined based on various parameters such as minimum ground clearance, maximum sag, height of the ground-wire peak, vertical spacing between the cross arms, number of cross arms and other clearances. It is always advisable to keep the height minimum to the extent possible without sacrificing the safety and security of the tower.

2.1 Types of Tower

Generally, transmission towers are classified by voltage, number of circuits and type. The voltage classification of based on the voltage of line, a tower carries. In India the common voltage for transmission are 110, 220/230 and 440 kV. Based on the number of circuits, a transmission tower can be classified as single circuit, double or multi circuit. Tower configuration generally adopted in design are rectangular and square types. In case of broad-based towers, the square type is most commonly used. The right of way and the number of earth-wires also affect the configuration. Based on the type of the profile along the centre line of the transmission line route, towers are categorised as tangent tower, dead end tower and angle tower. Further based on the shapes, transmission towers are classified as corset tower, Barrel tower and Guyed towers.

2.2 Loads and Wind Induced Vibration on Tower

As specified in the design standard, the load conditions that are considered are dead load which consists of the weight of the structure and its attachments all considered as static load being applied on the structure [22]. Wind load is considered as a dynamic load acting on the structure. This wind load constitutes an important component of the total load on tower. At ground level, the wind intensity is less due to friction with the rough ground surface, the air flow is turbulent. But at higher altitude, the frictional influence becomes negligible and wind force increases with height. Then one of the important load is accidental load which involves unbalance load like broken wire condition. Other loads include weather load such as ice and earthquake loads, maintenance and construction load such as structure erection load, worker load.

2.3 Failure of Tower

The total collapse of transmission tower leads to many accidents, massive blackouts resulting in a great economic loss. Several failures have been reported due to wind load. Failure of the cross arms has been analysed using nonlinear Finite Element Analysis. It has been observed that the secondary bracing fails to restraint the main bottom cord member if the top tie member is not in tension [23]. Structural failure occurs when any one member starts to fail then redistribution of forces occurs amongst the remaining surviving member [24] (Fig. 1).
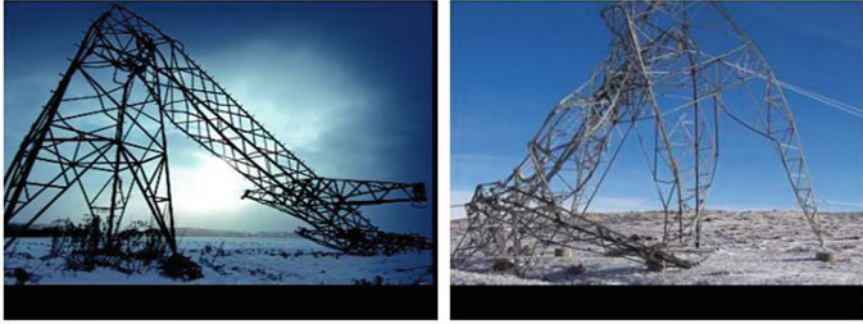
Fig. 1 Collapse of transmission tower during strong wind [25]

3 Vibration Control of Transmission Tower

Vibrational analysis on Finite element transmission tower model to determine the modal parameters, mode shapes, frequency, axial force, displacement. The Uncontrolled response and strain resultant of the tower due to wind load were obtained [26]. Modal analysis was done to determine the vibration characteristics of tower using computer software ANSYS [27]. Time history analysis is done to determine the vibrational response along with effect distributed on the conductor wires [28]. In order to control this vibrational response, various energy dissipating devices has been used. The equation of motion involving the damping force induced by the damping device is shown in Eq. 1.

$$[M_T]\{\ddot{x}(t)\} + [C_T]\{\dot{x}(t)\} + [K_T]\{x(t)\} = \{F_T(t)\} + V_B + F_{damp}(t) \qquad (1)$$

where $[K_T]$, $[C_T]$ and $[M_T]$ are the tower stiffness, damping and mass matrices respectively. The acceleration, velocity and displacement vectors are shown as, $\{\ddot{x}(t)\}$, $\{\dot{x}(t)\}$ and $\{x(t)\}$ respectively. $\{F_T(t)\}$, $F_{damp}(t)$ and V_B indicates the total wind load on the tower, the damping force induced by any device and base shear acting at the base of the tower. Different structural control devices have been developed for improving the wind resistance performance of the structure. Based on their energy dissipative nature, the control systems are categorised as Active, Semi-active, Passive and Hybrid system.

Passive control systems are widely used form of structural control. A number of researches have been carried out for wind-induced vibration control of transmission towers using this system. Passive control devices have shown excellent performance in controlling the vibration in structures [4, 5]. The advantage of passive devices is that they are energy efficient, requires no power source, and provides real time performance of structure. Passive energy dissipaters, such as Viscoelastic damper (VED) adds rigidity to the structure and changes its natural vibration characteristics. This energy dissipating device absorbs or divert part of the input energy, thus reducing

the energy dissipation demand of the main structure and minimizes the structural damage. It only provides additional damping to the structure without increasing the structural stiffness. Dissipation of input energy in the form of heat is the main significance of viscoelastic damper [29]. The Viscous damper which is based on damping energy principle was used vibration control [30]. The vibration acceleration of the tower with and without damper was obtained. The time domain and frequency domain characteristics value were obtained from the tower prototype to evaluate the control effect of the damper. The damping rate of crest value and the root mean square value was found to be 52–80% and 41–60% respectively. The optimized arrangement of the damper was analysed by numerical simulation on the transmission tower. This device is easy to age and increases the structural maintenance cost [31]. Mass dampers such as tuned mass dampers (TMD) comprises of an auxiliary mass elastically connected to the main structure. The relative motion between the damper and the structure partially cancels the external forces on the structure. Torsional response of a rectangular cross-sectional tower model with 10% geometrical eccentricity under wind load was controlled by Tuned Mass Damper (TMD) [32]. This damper owing to its passive nature can only encounter the tuned mode shape vibration and not the global dynamic responses. The conventionally used TMD, in combination with impact damper, makes use of tuned mass for absorption of vibrational energy and, in turn dissipation of these absorbed energy by the collision movement. This damper is known as PTMD, which is an improved form of TMD, and shows high resistance to wind [25]. Kaimal Spectrum was used for generation of wind field using the method of harmonic superposition. In order to examine the damper performance, the mean wind velocities of 20, 30 and 40 m/s were selected at a 10 m height (V_{10}). Table 1 shows the vibration reduction ratio for the three wind speeds as stated. Observations made were that the PTMD vibration reduction ratio maximizes with the increment in wind speed, therefore implying the effectivity of PTMD under strong wind force. Further, if the optimal parameter of PTMD is determined, the control performance can be improved. Figures 2 and 3 shows the displacement and acceleration responses for both uncontrolled and PTMD controlled vibrations, respectively at the tower top.

Friction dampers are structures similar to frictional rod which has resemblance to truss members, thus requiring no additional space for installation. Figure 4a shows the schematic diagram of Friction Damper installation in a model FE tower. Further, it can abate the dynamic response for both lower and higher vibrational modes. Friction damper has been installed on an analytical modelled transmission tower line system

Table 1 Wind speed variation along with maximum axial force [25]

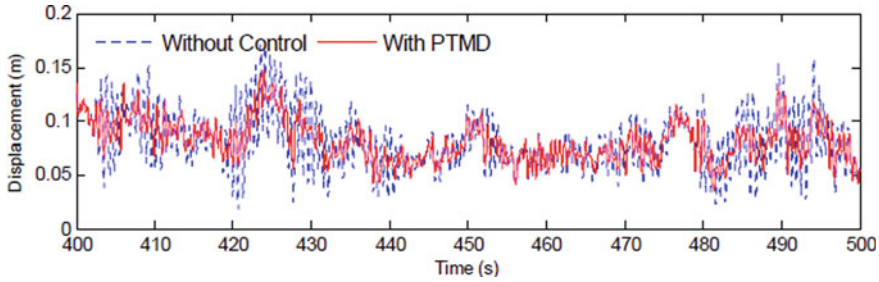| Wind speed (m/s)	RMS displacement (%)	RME acceleration (%)	Maximum displacement (%)	Maximum acceleration (%)	Max axial force (%)
20	31.0	22.8	12.5	9.9	12.4
30	36.2	30.1	14.3	16.4	16.9
40	39.8	35.3	17.9	24.6	21.1

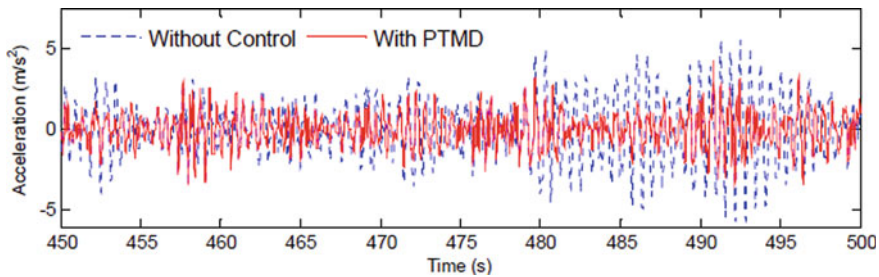**Fig. 2** Displacement response at the top of the tower at wind speed 40 m/s [25]

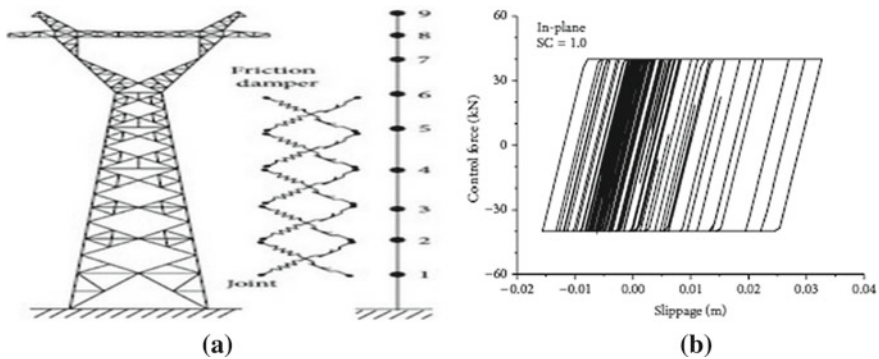**Fig. 3** Acceleration response at the top of the tower at wind speed 40 m/s [25]

Fig. 4 a Schematic diagram of friction damper installation in a FE tower model; **b** Hysteresis loop for in-plane vibration with stiffness coefficient (SC) 1 [33]

with lumped masses inter-connected with elastic elements [33]. Both the in-plane and out-plane vibrations are substantially dampened using this damper. A detailed parametric study shows 40 and 20 kN as the optimal value of control forces for out-plane and in-plane respectively, which shows best damper performance, irrespective of selected tower mass. The parametric investigation on damper stiffness clearly shows that with increment of the damper stiffness coefficient from 0 to 1, there is

reduction in dynamic response for vibration of in-plane as well as out-plane. The optimum stiffness coefficient found is 1. For a slipping force of 40 kN, the hysteresis loop of the friction damper for in-plane vibration with stiffness coefficient of 1 is shown in Fig. 4b.

An Active control system consist of sensors located on structure to measure excitation, processing unit and actuators to produce the required restoring force. They require considerable amount of external power to operate actuators that supply a control force to the structure. Active Mass Damper (AMD) is the most common used active control strategies. Traditional Tuned Mass Damper. by the addition of active control capacity, can act as an active control device which shows high efficiency and small damper's mass [34]. Such a system improves the efficiency of conventional TMD by increasing the operation frequency range and limiting the excessive mass movement. This active tuned mass damper (ATMD) can reduce about 50–60% wind induced vibrations by addition of 10% or more damping. To reduce this same level of vibration, a passive TMD would require two times the mass. However, increasing the friction coefficient deteriorates the ATMD performance, thus reducing the efficiency of the damper to mitigate vibration. The cost and maintenance of the active control devices are considerably higher than that of passive control devices.

In Semi-active control system, the semi active dampers combine both the passive and active dampers. This technique utilizes both passive and active control system to dissipate wind energy and control the structure. Electro Rheological (ER) damper, MR damper are few of the semi-active dampers. Fuzzy control approach which relies on clipped-optimal strategy was the control strategy used to examine the brace stiffness effect of MR damper, loading intensity of MR fluids and maximum yielding shear stress [21]. For improved control on wind induced vibrations, the optimal damper parameters were determined. MR dampers are semi-active smart damper that has been used to overcome the downfalls of dynamic absorbers. Similar to friction dampers, MR dampers are utilized as axial members that can be used instead of original steel truss members, therefore requiring no extra installation space. Thus, they can reduce the dynamic response of mode shapes without increasing the overall weight significantly. But the only difficulty in using this damper is the difficulty in fabrication of the practical design model due to its complicated configuration. Also, an additional supply of energy has to be supplied to the damper for control performance. This makes it difficult during tower operation hence, it is unsuitable.

4 Discussions

From the study it can be observed that transmission towers due to their height are susceptible to wind loads. They possess low structural damping and small stiffness. Due to strong wind, excessive vibration causes large defection of the structure leading to failure. Hence damping devices are used to abate the dynamic response. Various control analysis and design methodologies used in civil engineering structures have been determined using passive and active control systems. Passive devices have

been found to be suppressing wind-induced excitation but the parameters need to be defined correctly for increasing its effectiveness. Dynamic absorbers like Tuned mass dampers (TMD) reduce wind vibration efficiently but may require to be installed at one or more places for proper functioning. Experimental and analytical studies on TMD have shown that its effectiveness increases when the inherent structural damping was decreased in response to both cross-wind and along-wind directions. In case of transmission towers, finite element modelling is done and the lumped mass model is adopted where the control forces acts directly on one or two lumped masses of the tower. Active Mass Damper uses active control strategies along with TMD thus improving the efficiency of conventional TMD as its operation frequency range increases and the excessive mass movement is limited. Studies show that with increment in wind speed, the vibration reduction ratio of PTMD increases which implies that even under strong wind, efficiency of PTMD is not compromised. The Semi-active Magnetorheological damper has been installed in transmission tower line system because of its effective energy-dissipation capacity and easy configuration. But for its constant performance, an additional energy is needed to be supplied.

Friction damper is found to be advantageous as it can reduce the dynamic response for both high and low modes vibrations. Analytical method, using bi-mode method consisting of both the 2D lumped mass dynamic model and 3D finite element static model, has been used for determining the wind-induced response for a three-storey steel truss installed with friction damper. Further after obtaining satisfactory results, this bi-model method was carried out on a 339 m television tower. Variation of dynamic response along the height of the tower with and without the installed friction damper showing Peak displacement, Peak velocity, Peak acceleration is shown in Fig. 5. It can be observed that the displacement, velocity and acceleration of tower has been greatly controlled due to the installed friction damper. Control efficiency of the friction damper depends on the relative damper displacement and slip force. Also, the damper stiffness of the related elastic member plays a vital role in its energy dissipation ability. In order to achieve the maximum response reduction in structure, the damper parameters may be optimized using extensive parametric studies.

Hence control strategies using energy dissipating devices has been implemented. A comparative study has been done on basis of the damper performance for mitigating the wind-induced vibration. The performance comparison between the dampers is shown in Table 2. Substantial reduction in structural responses can be observed when using the VE dampers, even when exposed to heavy wind loads. PTMD damper is hybrid of VED and TMD and are large in size, thus reducing its mobility, thus making it difficult to install. An extra electrical energy is required to operate the semi-active MR damper. The active device AMD occupies a large space and requires a constant power supply for its functioning. Out of the all the control dampers, the friction damper is found to be most effective to control the wind-induced vibration in transmission towers. It uses hysteresis loop to dissipation energy capability and maintains a low level of residual displacement.

The location and parameters of the dampers can be designed optimally for fixed objective function using constrained conditions. Thus, higher level of performance can be achieved by parameter tuning of the dampers. Therefore, the passive dampers
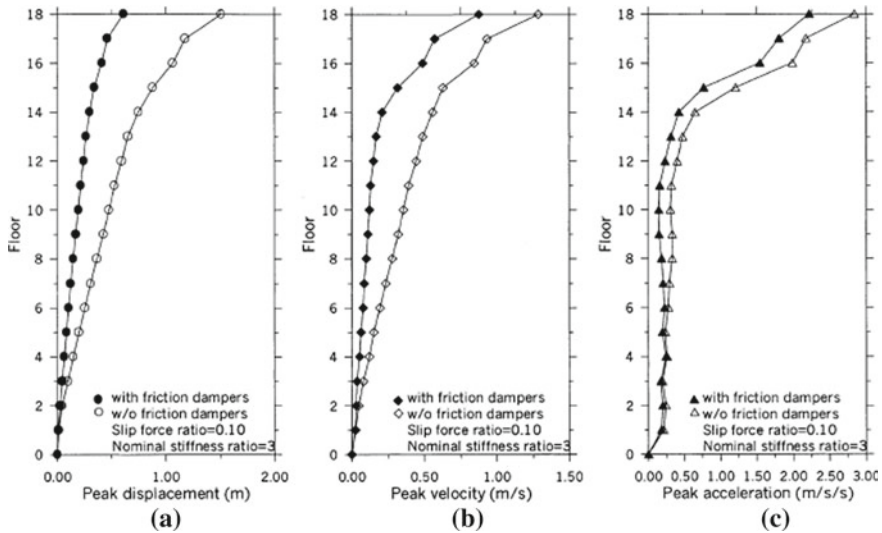
Fig. 5 Variation of dynamic response along the height of the tower; **a** Peak displacement, **b** Peak velocity, **c** Peak acceleration

Table 2 Comparison of control performance between dampers

Device name	Type	Disadvantages
Viscoelastic dampers [18]	Passive	It substantially weakens under harsh environment. Tower is placed in open air environment
Tuned mass damper [20]	Passive	Several additional masses which requires extra space occupancy
Pounding tuned mass damper [25]	Hybrid	Combination of TMD with VE damper, there is concern for fluid leakage and damping adjustment is difficult
Magnetorheological damper [21]	Semi-active	Configuration and fabrication are complicated and additional supply of energy is required for its control process
Friction damper [33]	Passive	Friction damper overcomes all other damper's disadvantages
Active tuned mass damper [34]	Active	It occupies a large space and requires constant power source. Hence cannot be implemented for all types of structures

have an edge over the other dampers in mitigating the structural responses in tower as they require no external power source. Moreover, the performance of these dampers can be improved by fine parameter tuning.

5   Conclusions

In this manuscript, observations made are that in transmission tower design, wind plays an important role as the towers are highly flexible having low damping. Different literatures show that control of tower owing to wind induced vibration is done with using dampers which are control devices. The following conclusions can be drawn from the above study,

(1)   A single tower failure may result in failure of the tower-line system as the tension forces developed by the inter-connected conductor wire may full down the adjacent towers.

(2)   In control study of transmission towers, a very few numbers of damping devices have been studied for reduction or control of structural responses.

(3)   The active damper, AMD, shows good control ability, but increases the weight of the structure installed as it is bulky in size and requires a constant power source for proper working. Hence it cannot be used in small structures or remote structures.

(4)   The semi-active damper, Magnetorheological Damper, requires complicated configuration and fabrication for proper installation and working. Also, the damper requires a constant power source effective working which limits the use of these dampers to remote locations.

(5)   Out of the all the control dampers, passive damper, the friction damper, is found to be most effective to control the wind-induced vibration in transmission towers as it works on the principle of relative damper displacement and slip force. Therefore, no external power source is required and the damper can be installed as a structural member in the towers.

As discussed in the above manuscript, friction dampers proved to be effective in case of control of transmission towers. Further, the parameters and location of this damper is to be optimally determined in order to achieve better control performance for the wind-induced vibration in case of transmission towers. Thus, practical study can be conducted in future to ensure accurate performance of dampers.

References

1. Bal HF, Yi TH, Li HN, Ren L (2012) Multisensors on-site monitoring and characteristic analysis of UHV transmission tower. Int J Distrib Sens Netw 2012:10p. Article ID 545148
2. Simiu E, Scanian R (1996) Wind effects on structures, 3rd edn. Wiley, New York, NY, USA
3. Belloli M, Rosa L, Zasso A (2014) Wind loads on a high slender tower: numerical and experimental comparison. Eng Struct 68:24–32
4. Roy S, Kundu CK (2021) Design and analysis of transmission tower under wind loading. In: Recent developments in sustainable infrastructure, Lecture notes in civil engineering, vol 75. Springer, Singapore, pp 231–241
5. Roy S, Das S, Saha P (2021) Seismic control and performance of passive hybrid damper under near-field earthquake. In: Advances in structural technologies, Lecture notes in civil engineering, vol 81. Springer, Singapore, pp 1–13

6. Balendra T, Wang CM, Cheong HF (1995) Effectiveness of tuned liquid column dampers for vibration control of towers. Eng Struct 17(9):668–675
7. Asgarian B, Eslamlou SD, Zaghi AE, Mehr M (2016) Progressive collapse analysis of power transmission towers. J Constr Steel Res 123:31–40
8. Battista RC, Rodrigues RS, Pfeil MS (2003) Dynamic behaviour and stability of transmission line towers under wind forces. J Wind Eng Ind Aerodyn 91:1051–1067
9. Savory E, Parke GAR, Zeinoddini M, Toy N, Disney P (2001) Modelling of tornado and microburst-induced wind loading and failure of a lattice transmission tower. Eng Struct 23(4):365–375
10. Xie Q, Sun L (2012) Failure mechanism and retrofitting strategy of transmission tower structures under ice load. J Constr Steel Res 74:26–36
11. Park J, Moon B, Min K, Lee S, Kim KC (2007) Cyclic loading test of friction-type reinforcing members upgrading wind-resistant performance of transmission towers. Eng Struct 29(2007):3185–3196
12. Xie Q, Zhang Y, Li J (2006) Investigation on tower collapses of 500kV renshang 5237 transmission line caused by downburst. Power Syst Technol 59–89
13. Lee PS, McClure G (2007) Elastoplastic large deformation analysis of a lattice steel tower structure and comparison with full-scale tests. J Constr Steel Res 63(5):709–717
14. Li HN, Tang SY, Yi TH (2013) Wind-rain-induces vibration test and analytical method of high-voltage transmission tower. Struct Eng Mech 48(4):435–453
15. Okamura T, Ohkuma T, Hongo E, Okada H (2003) Wind response analysis of a transmission tower in a mountainous area. J Wind Eng Ind Aerodyn 91(1–2):53–63
16. Housner GW, Bergman LA, Caughey TK, Chassiakos AG (1992) Structural control: past, present and future. J Eng Mech 123:210–216
17. Zhong WL, Wu LL, Wang W (2013) Wind-induced vibration suppression method for high-voltage transmission tower based on damping energy dissipation principle. J Central South Univ (Nat Sci) 44(1):397–402
18. Lan B, Yan K (2020) Wind-induced vibration control for substation frame on viscous damper. Comput Mater Contin 62(3):1303–1315
19. Zheng J, Chen B (2007) Wind-induced vibration control of transmission tower-line system by using passive devices. J Wuhan Univ Technol 29:80–92
20. Tian L, Wang Q, Yu Q, Xu N (2013) Wind-induced vibration optimal control for long span transmission tower-line system. Open Civil Eng J 7:159–163
21. Chen B, Zheng J, Qu W (2009) Control of wind induced response of transmission tower line system by using magnetorheological dampers. Int J Struct Stab Dyn 9(4):661–685
22. American Society of Civil Engineers (2010) ASCE Manual 74. Guidelines for electrical transmission line structural loading, 3rd edn. ASCE, New York
23. Rao NP, Mohan SJ, Lakshmanan N (2005) A study on failure of cross arms in transmission line towers during prototype testing. J Struct Stab Dyn 5(3):1337–1357
24. Natarajan K, Santhakumar AR (1995) Reliability-based optimization of transmission line towers. Comput Struct 55(3):387–403
25. Tian L, Gai X (2015) 1789 wind induced vibration control of power transmission tower using pounding tuned mass damper. J Vibro-Eng 17(7):3693–3701
26. Pasupuleti et al (2016) Dynamic analysis of electrical transmission tower using finite element technique. Int J Eng Res 4(5)
27. Jeng LJ, Jie SH (2014) Seismic response analysis of tower crane using SAP2000. Proc Eng 79:513–522
28. Li Q, Junjian Y, Wei L (2012) Random wind-induced response analysis of transmission tower-line system. Energy Proc 16(Part C):1813–1821
29. Samali B, Kwok KCS (1995) Use of viscoelastic dampers in reducing wind- and earthquake-induced motion of building structures. Eng Struct 17(9):639–654
30. Wang W, Zhao D, Zhong W, Xu J, Ling J, Xiao X (2013) Effect of wind-induced vibration's control for high-voltage transmission tower based on prototype measurement. J Central South Univ (Sci Technol) 44:3911–3917

31. Zhang CR, Zhang F (2015) Wind-induced vibration control of transmission tower based on SMA damper. Sci Technol Rev 33(7):74–78
32. Dutton R, Isyumov N (1990) Reduction of tall building motion by aerodynamic treatments. J Wind Eng Indus Aerodyn 36:739–747
33. Chen B, Xiao X, Li P, Zhong W (2015) Performance evaluation on transmission tower-line system with passive friction dampers subjected to wind excitations. Shock Vib 2015:13 p. Article ID 310458
34. Kwok KCS, Samali B (1995) Performance of tuned mass dampers under wind loads. Eng Struct 17(9):655–667

The Effect of Uniform and Non-uniform Torsion in Thin-Walled Structures

Lovely Sabat and Chinmay Kumar Kundu

1 Introduction

A thin-walled beam can be characterised as a flexible structure that has all three dimensions of different magnitude. The cross-sectional dimension (c) must be much smaller than the beam length (l) and the maximum thickness of the wall (h) must be much smaller than the cross-sectional dimension so that h/c ≪ 1 and the wavelength of the deformation along the beam, i.e. c/l ≪ 1 as can be seen in Fig. 1.

The cross-section of thin-walled beams can be of two types:

a. Open cross-section.
b. Closed cross-section.

The thin-walled beams can be analysed by using three dimensional theory but various thin-wall beam theories uses the h/c and c/l parameters to derive a one dimensional model which consists of one dimensional constitutive equations and is used in one dimensional equilibrium and kinematic equations and then used to analyse the original three dimensional structure and provides the approximate values of the three dimensional displacements, strains and stresses from one dimensional solution.

The Saint Venant theory is suitable for problems of pure torsion or uniform torsion only or for the members that do not warp under any loading and boundary conditions and it cannot be applied to all problems of torsion specifically for beams in which warping of the section occurs and the Saint Venant torsion is modified as uniform torsion and the mixed torsion originates only in members with section that can warp

L. Sabat (✉)
KIIT Deemed to be University, Bhubaneswar, India

C. K. Kundu
School of Civil Engineering, KIIT Deemed to be University, Bhubaneswar, India
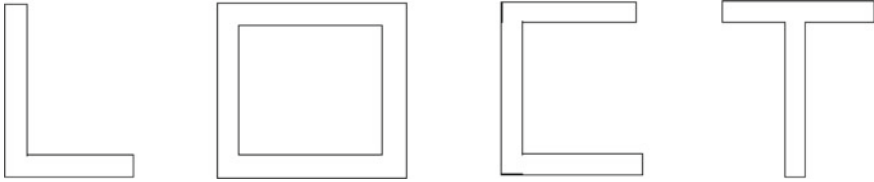e-mail: chinmay.kundufce@kiit.ac.in

Fig. 1 Thin-walled open and closed sections

under non-uniform torsion specifically for beams with one or more perfectly built in cross-section or other loading conditions [1]. The general theory of non-uniform torsion came when [2] considered the effect of restraining the warping of I beam at its end during lateral buckling [3]. The torsion analysis and the stress determination in steel members with thin-walled open cross-section can be done by 3 basic approaches:

1. Adopting the Vlasov theory of thin-walled elastic members.
2. Method based on modified bending and torsion analogy.
3. Simplified method supplying the torsion by the effect of couple of forces.

The torsional moment refers to the internal twisting moment about the longitudinal axis of the beam which is the summation of the Saint Venant torsional moment and the warping torsional moment whereas the warping moment refers to bending moment that occurs in the flanges due to the restraint of warping in the section. In open sections usually the arrangements are done so that the load would pass through the shear centre and there are no torsional effects but the torsional effects are seen due to eccentric loads and restraint conditions [4].

The non-uniform torsional behaviour of open thin-walled section is presented in various theories such those of Vlasov [5], Gjelsvik [3], and Prokic [6].

2   Literature Review

A theory for the analysis of elastic member with un-symmetric cross-section or single axis of symmetry was presented which includes both bending and torsion effects due to the applied varying torque by adopting the trigonometric series for solving the equations for stresses involving three different warping functions for the cross-section. The significance of the study of shear centre for such structures is studied as in general theory the resultant of the axial force stress acts at the centroid of the cross-section but the shear force resultants acts at the shear centre. As a result they concluded that the sense of shear centre does not exist formally and there is no single point in a general cross-section through which if lateral loads are applied anywhere along the beam will not result in twisting and the use of shear centre in the analysis of thin-walled cross-section gives an approximate results which may give more error when high strength materials are to be used [7]. The study of non-uniform torsion in a sandwich and a composite beam cross-section with

an analytical method based on the Reissner's variational principle for obtaining the optimum values of the adopted warping functions, torsional rotation and the measure of warping which are the unknowns was presented. Mathematical software, i.e. MATHACAD and HOMOGENE were adopted by the authors for solving the problems considered and the results obtained were that near the built in section for the contour or surface, the normal stresses are more important than the shearing stresses but at the core the normal warping stresses are not very important. Similarly a non-uniform warping beam theory including the effect of torsion and shear bending for a cantilever beam made of different cross-section using the displacement model and principle of virtual work by including the warping parameters associated to the warping functions corresponding to the torsion and shear force was developed. As a result, the three dimensional expression for normal and shear stresses are obtained and compared with the results of other classical theories and also presented the contribution of primary and secondary internal forces and the effect of the non-symmetrical of the cross-section on the structural behaviour [8]. The calculation of the warping constants for various thin-walled open sections is very tedious. The C_W values for some selective cold-formed steel sections are available in the AISI design manuals but the manual does not contains the values for all used sections so the authors Dung M. Lue and Jui-Ling Liu proposed a numerical method for calculating the warping constants by integration formulas for a general open thin-walled section through a computer program and showed some examples of channel sections and other open sections. As the result, it was seen that the proposed procedure is reliable and useful for calculation of warping constant as there was no difference between the calculated values and those listed in the AISI design manuals [9]. The work including the torsion analysis of steel members with thin-walled open cross-section was presented by taking an example of steel crane girder and derived the warping normal stress and shear stress and also the shear stress due to pure torsion by using three methods that are usually adopted to analyse such structures for torsion, i.e. the Vlasov's theory of thin walled elastic members secondly the modified bending and torsion analogy and finally used the simplest method of applying torsion by the effect of couple of forces. As a conclusion they found that the method of supplying torsion by the effect of couple of forces gives safe results at times and also stated that along with the load carrying capacity it is important to determine the deflections, strains and twist as such structures experiences large twist in plastic range and thus the plastic torsion theory should be avoided [10]. Similarly the warping analysis of concrete core walls as the already present methods for analysis were very complex to apply for practical applications. The author presented a simple method for calculating the longitudinal stresses on the core walls and header beams forces due to torsional loading by converting the header beam as a continuous beam element of equivalent thickness. The author also presented a case study of a tall concrete building and used the program WARPROP to obtain the section properties and stress calculations. From the results obtained it was observed that due to the torsional moment high longitudinal stresses are produced and the header beam forces are quite significant and cannot be neglected [11].

3   Uniform and Non-uniform Torsion

When a beam is subjected to equal and opposite torques at each end and the ends are free to warp out of their planes, then the ends of the beam will resist the torque at each cross-section by the shear stresses and the beam will twist about the longitudinal axis about the shear centre [12]. Such behaviour is called pure torsion or St. Venant torsion (Fig. 2).

Due to the uniform twisting, the circular cross-section bar of solid and hollow section will remain plane. But other type of sections will experience warping of the cross-section depending on the geometry of the cross-section i.e.

a.   In solid or hollow sections warping are very small and can be neglected.
b.   In double flange sections like I or channel sections, the warping effect is more significant.

Vlasov had developed the basic technical theory of thin-walled member with open cross-section by introducing the concept of sectorial coordinate and the term of mixed torsion in the analysis [13]. According to the Vlasov's theory, depending upon the type of cross section, the boundary conditions and type of loading two types of torsional behaviour may occur in thin-walled beam structures.

a.   Pure torsion or Saint Venant torsion which is characterised by pure torsion moment and results in pure torsion shear stresses, τ_t.
b.   Mixed Torsion which is the combination of pure torsion characterised by internal force (T_t) and resultant shear stress (τ_t) and warping torsion which is characterised by internal force (Bimoment = B) and warping torsion moment (T_ω) which results in warping normal stress (σ_ω) and warping torsion shear stress (τ_ω).

Saint Venant torsion can be used for members that do not warp under any loading and boundary conditions. If the section warps then the Saint Venant torsion is modified as uniform torsion, i.e., the circular sections warping do not occur [14]. Mixed torsion originates only in members with sections that can warp under non-section torsion, i.e., the thin-walled open cross-sections. Due the applied loading, the point load or uniformly distributed load, the external torque that will be applied on the section as
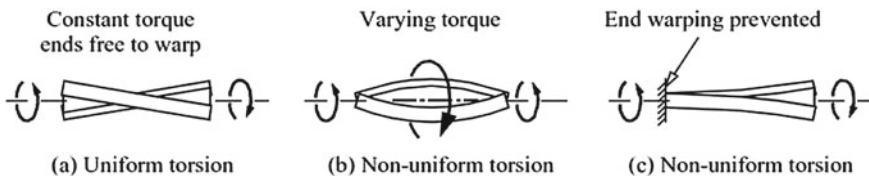
$$T_{ext} = P \cdot e \tag{1}$$

Constant torque ends free to warp   Varying torque   End warping prevented

(a) Uniform torsion   (b) Non-uniform torsion   (c) Non-uniform torsion

Fig. 2 Types of torsion

or

$$m_{ext} = p(x) \cdot e \tag{2}$$

The total internal torque T at any cross-section along the member will be
In case of pure torsion:

$$T = T_t$$

and in case of mixed torsion:

$$T = T_t + T_w \tag{3}$$

The differential equation for the mixed torsion for a prismatic member is

$$m_{ext.} = C_1 \frac{\partial^4 \phi}{\partial z^4} - C \frac{\partial^2 \phi}{\partial z^2} \tag{4}$$

where, $m_{ext.}$ = torque per unit length

$C_1 = EC_w$ = warping rigidity

$C = GJ$ = pure torsion rigidity

J = torsion constant

C_w = warping constant.

Considering the various boundary conditions, the angle of rotation $\phi(x)$ can be calculated easily and then after the internal forces can be calculated as.

The pure torsion

$$T_t = GJ \frac{\partial \phi}{\partial X} \tag{5}$$

The Bi-moment

$$B = -EC_w \frac{\partial^2 \phi}{\partial z^2} \tag{6}$$

The warping Torsion

$$T_w = -EC_w \frac{\partial^3 \phi}{\partial z^3} \tag{7}$$

4   Numerical Examples

To study the effect of uniform torsion and non-uniform torsion rectangular and channel sections are considered. The angle of twist per unit length are calculated by using approximate and experimental data for a shaft with a rectangular cross-section, with depth = 40 mm and thickness = 20 mm is subjected to a torque of 1 kN m and $G = 80$ GN/m^2 as shown in Fig. 3. The percentage of error is found to be 0.01%.

For approximate results
Using

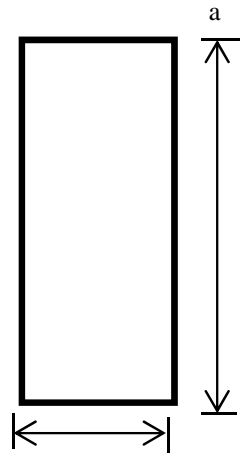$$k_1 = \frac{1}{3}\left(1 - 0.63\frac{b}{a}\right) \tag{8}$$

Maximum shear stress

$$\begin{aligned}
\tau_{max} &= \frac{T}{k_1 \times ab^2} = \frac{T}{ab^2} \times \left(3 + 1.8\frac{b}{a}\right)\\
&= \frac{1 \times 10^3}{0.040 \times (0.02)^2} \times \left(3 + 1.8 \times \frac{0.02}{0.04}\right)\\
&= 243.75 \text{ MN/m}^2
\end{aligned} \tag{9}$$

The angle of twist per unit length

$$\frac{\theta}{1} = \frac{42TJ}{GA^4} \tag{10}$$

Fig. 3 Rectangular section

where, $A^4 = (0.02 \times 0.04)^4 = 4.096 \times 10^{-13} \text{ m}^2$

$$J = I_{XX} + I_{YY} = \frac{ba}{12} \times (a^2 + b^2)$$
$$= \frac{0.02 \times 0.04}{12} \times (0.04^2 + 0.02^2)$$
$$= 1.33 \times 10^{-7} \text{ m}^4 \tag{11}$$

Now,

$$\frac{\theta}{l} = \frac{42 \times 1000 \times 1.33 \times 10^{-7}}{80 \times 10^9 \times 4.096 \times 10^{-13}}$$
$$= 0.1704 \text{ rad/m}$$
$$= 9.767 \text{ degree/m}$$

Using experimentally derived formulas:
Using the table data, Timoshenko [2], d/b = 40/20 = 2.

$$k_1 = 0.246$$

Maximum shear stress,

$$\tau_{max} = \frac{T}{k_1 \times ab^2}$$
$$= \frac{1 \times 10^3}{0.246 \times 0.04 \times 0.02^2}$$
$$= 254.06 \text{ MN/m}^2 \tag{12}$$

The angle of twist per unit length:

$$\frac{\theta}{l} = \frac{T}{k_2 \times db^3 G}$$
$$= \frac{1 \times 10^3}{0.229 \times (0.04) \times (0.02)^3 \times 80 \times 10^9}$$
$$= 0.1705 \text{ rad/m}$$
$$= 9.768 \text{ degree/m} \tag{13}$$

Therefore percentage error in shear stress calculation:

$$= \frac{254.06 - 243.75}{254.06} \times 100$$
$$= 4.05\%$$

Therefore percentage error in twist per unit length calculation:

$$= \frac{9.768 - 9.767}{9.768} \times 100$$
$$= 0.01\%$$

In the second example the angle of twist per unit length and the maximum shear stress for a extruded light alloy channel and I sections are considered. The dimensions of the channel section as shown in (Fig. 4) are 80 mm × 60 mm × 4 mm and the I section in (Fig. 5) is 100 mm depth and 100 mm width with thickness of web and flanges as 5 and 4.75 mm respectively is subjected to a torque of 20 Nm. $G = 30$ GN/m^2.

$$d_1 = 60 \text{ mm}$$
$$d_2 = 80 \text{ mm}$$
$$d_3 = 60 \text{ mm}$$
$$b_1 = b_2 = b_3 = 4 \text{ mm}$$

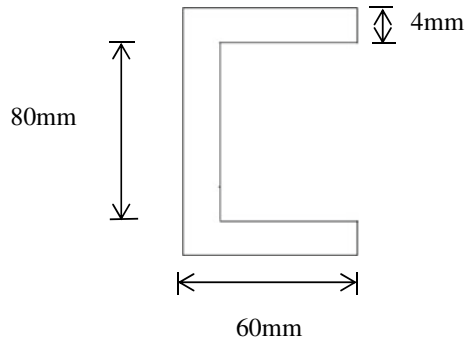**Fig. 4** Channel section

80mm

60mm

4mm

Fig. 5 I section

100mm

100 mm
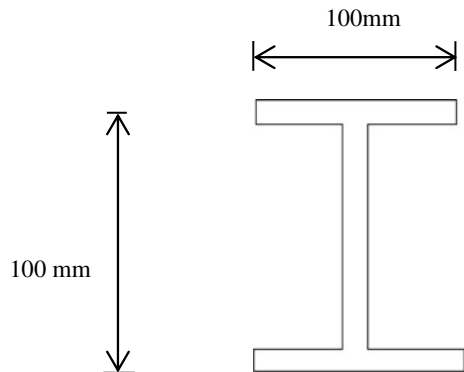
Total depth of the beam section d = 80 + 4 + 4 = 88 mm.

Ratio of d/b for the Timoshenko chart = 88/60 = 1.47.

From the table of d/b and k_1 and k_2 and by interpolating the values from the table, Timoshenko [2]

$$k_1 = 0.208 + \frac{0.231 - 0.208}{1.5 - 1.0} \times (1.47 - 1)$$

$$k_1 = 0.229$$

And similarly

$$k_2 = 0.141 + \frac{0.196 - 0.141}{1.5 - 1.0} \times (1.47 - 1)$$

$$k_2 = 0.192$$

Now,

Maximum shear stress,

$$\tau_{max} = \frac{T}{\Sigma k_1 \times db^2} = \frac{T}{Z'} \tag{14}$$

$$\begin{aligned} z' &= k_1 d_1 b_1^2 + k_1 d_2 b_2^2 + k_1 d_3 b_3^2 \\ &= 0.229 \times 60 \times 4^2 + 0.229 \times 80 \times 4^2 + 0.229 \times 60 \times 4^2 \\ &= 219.84 + 293.12 + 219.84 \\ &= 732.8 \text{ mm}^3 \end{aligned}$$

$$\tau_{max} = \frac{T}{Z'} = \frac{20}{732.8 \times 10^{-6}}$$

$$\tau_{max} = 27.292 \text{ MN/mm}^2$$

Angle of twist per unit length (θ/l):

$$\frac{\theta}{l} = \frac{T}{G \times (\Sigma k_2 \times db^3)} = \frac{T}{J_{eq} \times G} \tag{15}$$

$$\begin{aligned} J_{eq} &= k_2 d_1 b_1^3 + k_2 d_2 b_2^3 + k_2 d_3 b_3^3 \\ &= 0.192 \times 60 \times 4^3 + 0.192 \times 80 \times 4^3 + 0.192 \times 60 \times 4^3 \\ &= 2457.6 \text{ mm}^4 \end{aligned}$$

$$\frac{\theta}{l} = \frac{T}{J_{eq} \times G} = \frac{20}{2457.6 \times 10^{-12} \times 30 \times 10^9}$$

$$= 0.271 \text{ rad/m}$$
$$= 15.52 \text{ degree/m}$$

Ratio of d/b for the Timoshenko chart $= 100/100 = 1$

$$k_1 = 0.140$$
$$k_2 = 0.208$$

Maximum shear stress,

$$\tau_{\max} = \frac{T}{\Sigma k_1 \times db^2} = \frac{T}{Z'} \tag{16}$$

$$z' = k_1 d_1 b_1^2 + k_1 d_2 b_2^2 + k_1 d_3 b_3^2$$
$$= 0.140 \times 100 \times 4.75^2 + 0.140 \times 100 \times 5^2 + 0.140 \times 100 \times 4.75^2$$
$$= 981.75 \text{ mm}^3$$

$$\tau_{\max} = \frac{T}{Z'} = \frac{20}{981.75 \times 10^{-6}}$$

$$\tau_{\max} = 20.37 \text{ MN/mm}^2$$

Angle of twist per unit length (θ/l):

$$\frac{\theta}{1} = \frac{T}{G \times (\Sigma k_2 \times db^3)} = \frac{T}{J_{eq} \times G}$$

$$J_{eq} = k_2 d_1 b_1^3 + k_2 d_2 b_2^3 + k_2 d_3 b_3^3$$
$$= 0.208 \times 100 \times 4.75^3 + 0.208 \times 100 \times 5^3 + 0.208 \times 100 \times 4.75^3$$
$$= 4978.35 \text{ mm}^4$$

$$\frac{\theta}{1} = \frac{T}{J_{eq} \times G} = \frac{20}{4978.35 \times 10^{-12} \times 30 \times 10^9}$$
$$= 0.134 \text{ rad/m}$$
$$= 7.68 \text{ degree/m}$$

If we consider the same problem of a channel section but with one end fixed and then a torque M_t is applied at the other end which is free, it becomes the case of non-uniform torsion. The cross-sections are not free to warp. The angle of twist will not remain constant and in this case each cross-section will rotate with respect to the shear centre which is present on the horizontal axis of symmetry and there will
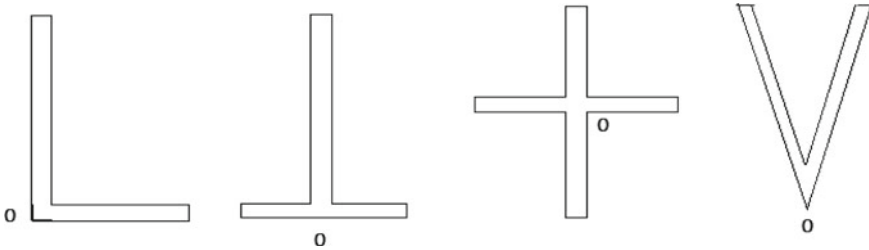
Fig. 6 Various thin-walled section with rectangle cross-sections

Table 1 Significance of St. Venant and warping torsion on various sections

Sl no.	Section type	St. Venant	Warping
1	Circular hollow sections	Significant	Does not present
2	Rectangular or elliptical hollow sections	Significant	Not significant
3	Angles, Tees and cruciform sections (+, L, T)	Significant	Not significant
4	Twin-flanged rolled and fabricated sections (I, [)	Significant	Significant
5	Thin cold-formed section (Z, Σ)	Not significant	Significant

be bending of flanges and also bending of web. So in such cases it is required to calculate the shear centre of the section first [15].

If the cross-section (Fig. 6) consists of thin rectangular elements that intersect at a common point and the axis of rotation is taken through the shear centre, then there will be no warping of the middle line due to torsion.

Different types of sections and the effects of Saint Venant torsion and warping torsion on these sections are presented in the Table 1.

The deflection in the flanges and web is required to be calculated from which the compressive force in the flanges due to the shear stress can be evaluated,

The compressive force in the flanges,

$$S = \frac{Eb^2h^4t_1}{48I_z} \times \frac{\partial^2 \phi}{\partial x^2} \qquad (17)$$

This force is further used for calculating the shear stresses in web and flanges and also M_t'' that balances these stresses. The shear force in the web reduces to zero and only the shear force in the flanges is considered.

The total shear force in the section will be;

$$V = \frac{b}{2}\frac{dS}{dx} + E \cdot \frac{h \cdot t \cdot b^3}{24} \times \frac{\partial^3 \phi}{\partial x^3} \qquad (18)$$

The torque that balances the shear force in flanges will be:

$$M_t'' = -\frac{Dh^2}{2} \times \left(1 + \frac{th^3}{4I_z}\right) \times \frac{\partial^3 \phi}{\partial x^3} \tag{19}$$

Therefore the total torque will be;

$$M_t = C \cdot \frac{\partial \phi}{\partial x} - \frac{Dh^2}{2} \times \left(1 + \frac{th^3}{4I_z}\right) \times \frac{\partial^3 \phi}{\partial x^3} \tag{20}$$

where,

$$C \cdot \frac{\partial \phi}{\partial x} = \text{St. Venant torsion}$$

$$\frac{Dh^2}{2} \times \left(1 + \frac{th^3}{4I_z}\right) \times \frac{\partial^3 \phi}{\partial x^3} = \text{Warping Torsion}$$

$$I_z = \frac{t_1 h^3}{12} + \frac{b + h^2}{2}$$

The values of ϕ', ϕ'', ϕ''' has to be solved for various loading and support conditions. It is a complex task to formulate the variation of angle of rotation (ϕ) for the general case for different end conditions where the total torque M_t varies along the beam.

So there are so many unknowns to be calculated for solving such problems like the value of e, C, D, I_z so it always better to solve such problems using computer programs or finite element analysis. Table 2 presented various constants for channel and I sections.

Table 2 Section properties of sections		Symmetric channel section	Double symmetric I section
	1. Torsion constant	$J = \frac{t^3}{3}(2b + h)$	$J = \frac{t^3}{3}(2b + h)$
	2. Shear centre	$e = \frac{b^2 h^2 t}{4I_z}$	Shear centre and the centroid coincides
	3. Warping constant	$C_w = \frac{tb^3 h^2}{12} \times \frac{3b+2h}{6b+h}$	$C_w = \frac{t_f h^2 b^3}{24}$
	4. Constant (a^2)	$a^2 = $ $\frac{Dh^2}{2C} \times \left(1 + \frac{th^3}{4I_z}\right)$	$a^2 = \frac{Dh^2}{2C}$

5   Conclusions

With many advantages of being light weight and economical structures and with superior designing, handling and installation systems, the application of thin-walled structures are increasing but the open sections like I, H or channel sections has less resistance against torsion from which torsional analysis of such section is important [16]. The open and closed thin-walled sections with non-zero warping rigidity will experience torsional warping and will include the variable rate of twist along the length of the beam. For such thin-walled open sections along with the load carrying capacity it is important to determine the buckling behaviour, deflections, strains and twist as such structures experiences large twist in plastic range using finite element method and other computer programs [17].

References

1. Freund J, Karakoc A (2016) Warping displacement of Timoshenko beam model. Int J Solids Struct 92:9–16
2. Timoshenko SP (1953) Strength of material. McGraw Hill
3. Gjelsvik A (1981) The theory of thin-walled bars. Wiley, New York
4. Sharman PW (1985) Analysis of structures with thin-walled open sections. Int J Mech Sci 27(10):665–677
5. Vlasov VZ (1961) Thin-walled elastic beams, 2nd edn. Israel Program for Scientific Translation, Jerusalem
6. Prokic A (1993) Thin-walled beams with open and closed cross-section. Comput Struct 47(6):1065–1070
7. Brown EH, Burgoyne CJ (1994) Non-uniform elastic torsion and flexure of members with asymmetric cross-section. Int J Mech Sci 36(1):39–48
8. El Fatmi R (2007) Non-uniform warping including the effects of torsion and shear forces. Part-I: a general beam theory. Int J Solids Struct 44:5912–5929
9. Lue DM, Liu JL, Lin CH (2007) Numerical evaluation on warping constants of general cold-formed steel open sections. Steel Struct 7:297–309
10. Melcher J, Karmazinova K (2012) On problems of torsion analysis of steel members with open cross section. Proc Eng 40:262–267
11. Mendis P (2001) Warping analysis of concrete cores. Struct Des Tall Build 10:43–52
12. Sapountzakis EJ, Mokos VG (2003) Warping shear stresses in non-uniform torsion by BEM. Comput Mech 30:131–142
13. AnikoPluzsik A, Kollar LP (2006) Torsion of closed section, orthotropic thin-walled beams. Int J Solids Struct 43:5307–5336
14. Justin M, Mehdi BA, Vladimir G, Vladimir K, Juraj P, Juraj H (2018) Effect of non-uniform torsion on elastostatics of a frame of hollow rectangular cross-section. J Mech Eng 68(2):35–52
15. Kumar SA, Reddy JK (2016) The influence of warping and Winkler-Pasternak soil on the torsional vibrations of thin-walled open section beams with guided-end conditions. Int J Res Eng Technol 4(Issue 1):15–28
16. Gotluru PW, Schafer BW, Pekoz T (2000) Torsion in thin-walled cold-formed steel beams. Thin-Walled Struct 127–145
17. Timoshenko SP, Goodier JN (1970) Theory of elasticity, 3rd edn. McGraw Hill

Study the Permeability Behaviour of Pervious Geo-polymer Concrete at Ambient Temperature

Jagannath Patel, Dillip Kumar Bera, and A. K. Rath

1 Introduction

Concrete is the single most commonly consumed building material across the globe for its wide applicability. Conventional cement is the principal constituent and binder for the modern concrete, which is not judged as an environmental hostile material as cement producing is energy consuming as well as liberating large quantity of CO_2 to the environment [1].

Due to the rapid growth of urbanization permeable grassland and forested areas are increasingly converted to large impervious surfaces like buildings and pavement. This pattern significantly reduces the infiltration which minimizes groundwater recharge and increases storm water runoff into surface, thus causing urban floods [2]. This trend has a significant impact on the quality and quantity of water and hydrological cycle of an area [3]. In addition, impervious layer makes it very trouble sum to interchange the soil moisture and heat wave with the atmosphere. The humidity and temperature of the landscape of the urban area cannot be managed and hence this causes the occurrence of heat island in urban areas [4].

On the other hand growing amount of industrial as well as agricultural waste and its safe disposal is a severe headache for most of the countries. Significant damage being caused to the Mother Nature due to accumulation of these waste materials since of most of these wastes possess complex composition and characteristics and hence their safe management and disposal is become necessary.

These situations have led to a demand for innovative solution which may have help to minimize the problems, and probably reverse the various damage that has

J. Patel (✉) · D. K. Bera · A. K. Rath
School of Civil Engineering, Campus-3, KIIT Deemed to be University, Bhubaneswar 751024, India

D. K. Bera
e-mail: dberafce@kiit.ac.in

already done. It can be easily identified that we need an unconventional binder which can replace the OPC and a way to which helps to reduce the waste. Further we have to find a method to reduce and control the storm water runoff. The storm water could be managed by the application of pervious concrete. On the other hand cement binder could be replaced by geo-polymer binder which is also a mean of waste utilization [5–10].

In recent days, geo-polymer concrete has evolved as one of the best feasible alternatives to conventional Portland cement concrete for the construction world.

French scientist Joseph Davidovits is the first person to developed and reported about the formation of geo-polymer material and which is formed by the reaction of silica and alumina-rich solids with a high alkaline solution [11, 12].

Alkaline liquids and Si–Al reach source materials are the two principal constituents of geo-polymer binder. Geo-polymer binder is an eco friendly binding material with respect to conventional cement binder due to less emission of green house gases and also utilize large amount of industrial waste materials during its production. In addition to eco friendly behaviour geo-polymer also shows several outstanding performances of mechanical and durability properties [13].

Pervious concrete is another form of concrete which used to control and manage the storm water and helps to recharge the ground water due to its high porosity. This is also coined as porous and no-fine concrete.

Typically, pervious concrete has significantly high permeability due to the interconnected pores, ranging from 2 to 8 mm. It has also a void content ranging from 15 to 35%, and compressive strengths ranging from 2.8 to 28.0 MPa [14].

Usually, pervious concrete contain cement, coarse aggregate, admixture and no or little fine aggregate. The use of no-fines concrete these days limited to as a pavement material due to its low mechanical strength. However, pervious concrete had been employed as structural application in European countries at the nineteenth century [15].

Pervious concrete applications helps water infiltration and produce almost zero runoff [2]. Vehicle noise can also be absorbed by pervious concrete pavement.

Furthermore, by accumulating heat, pervious concrete surfaces can modify the temperature and humidity of the earth's surface, resulting in a comfortable environment [4]. In addition, the use of pervious concrete reduces the requirement for detention and retention ponds, as well as sewage and other traditional storm water control technologies.

It's one of the EPA's (Environmental Protection Agency) recommended Best Management Practices (BMPs). The use of pervious concrete on the construction site can also help the building qualify for LEED certification (Leadership in Energy and Environmental Design) and Green Building Rating System credits [3].

Pervious Geo-polymer concrete (PGC) may be an innovative approach to deal with those various problems that has been already discussed. Basically PGC is pervious concrete with geo-polymer binder. It contains geo-polymer binder and coarse aggregate. This is relatively a new emerging concept to minimize the issues related with storm OPC production, storm water management and waste management. There are very few studies have done on Pervious geo-polymer concrete [16–18]. Till date very

few works has done on pervious geo-polymer concrete and that too using the elevated temperature curing. But in the in-situ or practical condition it is very difficult create that kind of environment i.e. curing at elevated temperature.

There have been few investigations on pervious geo-polymer concrete with low calcium fly ash. It is reported by Thoin et al. [19] that pervious concrete can be produce by using high-calcium fly ash geo-polymer binder. The properties are satisfactory and similar to the traditional pervious concrete [20]. Zaetang et al. [17] claimed that the compressive strength of PGC is between 5.7 and 8.6 MPa and the density between 1466 and 1502 kg/m^3. Sata et al. [16] used recycled aggregate to manufacture PGC and get acceptable properties.

In this paper work, low calcium fly ash was employed as a source material, and an alkaline liquid was made by mixing sodium hydroxide and sodium silicate solution to make a geo-polymer binder.

Various sizes of crush granite stones were used as coarse aggregate. The equipment and technology currently available to manufacture conventional pervious concrete were used to produce pervious geo-polymer concrete. Mostly the curing of PGC samples were done at ambient temperature instead of conventional elevated temperature curing. The properties included compressive strength, flexural strength, void content and permeability has been studied in this work. The effect of several factors on these properties was also studied. The methods and equipment currently available to measure the properties conventional pervious concrete were similarly used for pervious geo-polymer concrete.

2 Experimental Program

2.1 Materials Used

2.1.1 Cement

The cement used in the experiment was Ramco 43 grade Ordinary Portland Cement (IS: 8112-1989). Table 1, lists the chemical and physical properties of cement and fly ash.

Table 1 Cement and fly ash chemical and physical properties

Materials	Chemical oxides (%)								Physical properties		
	CaO	SiO$_2$	Al$_2$O$_3$	Fe$_2$O$_3$	SO$_3$	Na$_2$O	K$_2$O	MgO	LOI	Density	Plain area
									(%)	(g/cc)	m^2/kg
Cement	63.5	20.3	2.2	1.8	2.1	0.45	0.35	1.1	1	3.15	300
Fly ash	1.3	54.41	30.40	8.44	0.1	1.0	1.98	1.53	–	2.1	350

Fig. 1 Pictures of materials used

In Fig. 1 images of materials used are mentioned i.e. (a) Cement, (b) Fly ash (c) NaOH pallets, (d) Na_2SiO_3 Solution, (e) Coarse Aggregates and (f) NaOH Solution.

2.1.2 Fly Ash

Fly ash with low calcium content (class F) was used as a source material in this investigation. National Thermal Power Corporation, Talchar, Odisha, India provided fly ash for this work.

Table 1, shows the chemical oxides of the fly ash. According to IS: 3812 (Part I), this fly ash was low calcium (Class F) fly ash or Siliceous fly ash since the sum of the percentages by mass of oxides, Silicon dioxide (SiO_2), aluminium oxide (Al_2O_3), and iron oxide (Fe_2O_3) is substantially more than 70.

2.1.3 Alkaline Liquid

The alkaline solution was prepared by adding both sodium hydroxide and sodium silicate solutions with a definite proportion right before mixing. A local source provided the sodium silicate solution ($Na_2O = 13.7\%$, $SiO_2 = 29.4\%$, water $= 55.9\%$ by mass) and sodium hydroxide (NaOH) in pellet form with 98 percent purity. One day prior to casting, NaOH solution of required concentration (molarity) was prepared.

2.1.4 Aggregates

Coarse aggregates ranging in size from 4.75 to 20 mm were utilized in a saturated surface dried condition. These were granite aggregates that had been crushed at Tapang stone query in district of Khorda. The aggregates' sieve examination reveals that they meet the requirements of IS: 383-1970. Aggregate specific gravity and fineness modulus were 2.7 and 2.48, respectively.

Table 2 Mix proportion of pervious cement and geo-polymer concrete

Sample	FA (kg/m^3)	Cement (kg/m^3)	Aggregate (kg/m^3)	Sodium silicate solution (kg/m^3)	Sodium hydroxide solution (kg/m^3)
PCC	–	300	1500	–	–
PGC 10	300	–	1500	96.5	38.5
PGC 12	300	–	1500	96.5	38.5
PGC 14	300	–	1500	96.5	38.5

2.2 Mix Proportions

In this mix proportion, binder to aggregate ratio by mass was taken as 1:5, ratio of sodium silicate (SS) to sodium hydroxide (SH) by mass was 2.5, the concentration (molarity) of sodium hydroxide solutions were 10, 12 and 14 M and ratio of alkaline solution-to-fly ash, by mass, was taken as 0.45. The aggregate contains 60% retained samples between 4.75 and 10 mm and 40% retained samples between 10 and 20 mm. The details of mix proportions are mentioned in Table 2.

2.3 Mixing and Casting

A revolving pan mixture was utilised for mixing. The solid elements of PGC, namely coarse aggregates and fly ash, were dry mixed in the mixer for 2–3 min to prepare PGC. The alkaline liquid, which is a mixture of sodium silicate and sodium hydroxide solution, is then added to the dry material and mixed for another 3–4 min.

The fresh PGC mix has a gleaming aspect, a dark colour, and is cohesive. After mixing, the fresh concrete was immediately poured into the moulds. Before pouring the concrete into the moulds, the interior surfaces were sprayed with oil. The tamping rod was used for a small quantity of tamping. After 24 and 72 h, the standard pervious concrete and PGC were demolded, respectively.

2.4 Curing of the Specimens

For the conventional pervious cement concrete (PCC) normal water curing was done. In this work, two forms of curing were used for the PGC: one was heat curing and the other was ambient curing. For heat curing oven was used. Heat curing was done at 75 °C temperature for 48 h and then the specimens were left in ambient condition. The ambient curing was done in the sunlight.

3   Methodology

3.1   Compressive Strength

Compressive strength of the PGC was obtained by performing compressive strength test as per as stated in IS 519:1959. As per IS 456:2000, 150 mm cube specimens were used to conduct this test. Compressive strength test was executed at 7, 28, 56 and 90 days for all the mix proportions.

3.2   Flexural Strength

Flexural strength of the PGC was obtained by performing flexural strength test as per IS 519:1959. $100 \times 100 \times 500$ mm prism specimens were used to conduct this test as. This test was performed at 7 and 28 days for all the mixtures.

3.3   Void Content

The void content of PGC specimens is calculated according to the ASTM C1688. Three cube specimens for every different mix proportions were used and average value of these three specimens are taken to determine void content. The void content of pervious concrete is computed using following equation:

$$\text{Void content } (\%), \ V_T = \frac{(T - D)}{T} \times 100$$

Density (D) is the net mass of the concrete by the volume of the measures 'Vm', $D = \frac{Mc - Vm}{Vm}$ where, Mc—mass of the concrete plus mass of the mould, Mm—Mass of the mould (measures).

'T' is Theoretical density, $T = \frac{Ms}{Vs}$ 'Ms' is the total mass of materials batched, 'Vs' is total sum of absolute volume of materials.

3.4   Water Permeability

The water permeability of PGC specimens was tested as per literature published by Sata et al. (2015). Cylindrical specimen of 10 cm height and 15 cm diameter were casted for permeability test. The permeability test is conducted by permeameter. Permeameter is not readily available in market, so a similar type of permeameter was developed in laboratory. A schematic diagram of the permeameter shown in

Fig. 2, in the same way an in-house permeameter was developed for permeability test shown in Fig. 3. The coefficient of water permeability (k) is calculated by using Darcy's law:

$$\text{i.e., } k = \frac{QL}{HAt};$$

where, 'k' is the coefficient of water permeability in cm/s, 'Q' is the quantity of water collected in cm^3, 't' is water collection time in sec, 'L' is the length of specimen in cm, 'H' is the water head in cm, and 'A' is the cross sectional area of specimen in cm^2.

4 Result and Discussion

Each of result of the test represents the average of three test specimens. The behaviour of pervious geo-polymer concrete is analysed and discussed in comparison to conventional pervious concrete (PCC). PGC and conventional pervious concrete strength and water permeability are also calculated, compared, and discussed.

The density, void content, compressive strength, and permeability correlations between PGC and PCC were formulated and discussed.

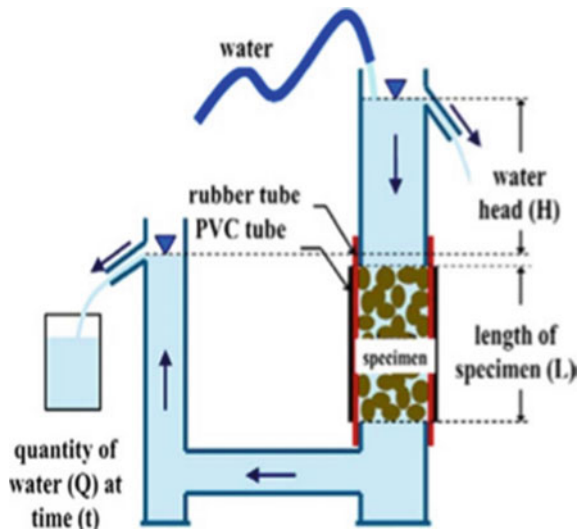**Fig. 2** Schematic diagram of permeameter
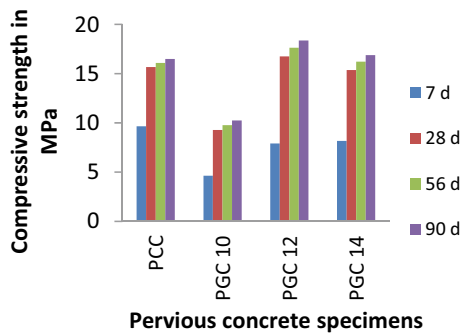
Fig. 3 In-house developed permeameter

Fig. 4 Compressive strength test results

4.1 Compressive Strength and Flexural Strength Tests

The figure clearly illustrates that at later days; most pervious geo-polymer specimens had higher compressive strength than Portland cement pervious concrete. The rate of gain of early strength of PGC was lower than the PCC but its rate of gain of later strength was more than the PCC i.e. 56 and 90 days as shown in Fig. 4. The specimen of 12 M concentration was found maximum strength after 28 days. PGC samples have a 7-day strength that was about 0.4 to 0.45 times that of 28-day samples but for PCC samples it was 0.6 to 0.65 times that of 28 days samples. From data mentioned in Table 3, it was concluded that the early rate of gain of strength is low in PGC specimens.

Table 3 Test results of compressive and flexural strengths, density, void content and permeability

Mix	Compressive strength (MPa)				Flexural strength (MPa)		Density (kg/m^3)	Void content (%)	Permeability (mm/s)
	7 d	28 d	56 d	90 d	7 d	28 d			
PCC	9.65	15.37	16.32	16.98	1.76	2.54	1902	27.85	12.65
PGC 10	4.64	9.28	9.87	10.34	0.84	1.89	1885	26.68	11.15
PGC 12	7.91	16.75	17.08	17.56	1.22	2.57	1905	24.35	9.53
PGC 14	8.17	15.36	15.89	16.61	1.24	2.34	1898	26.12	10.95
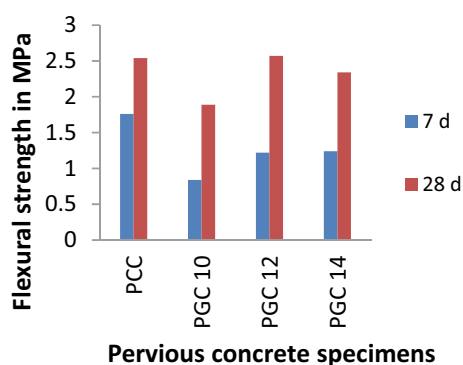
Fig. 5 Flexural strength test results

The percentage gain of strength in PGC after 28 days of ambient curing is more than PCC that is nearly 5 to 7%.

PGC samples have a 7-day flexural strength that was about 0.44 to 0.52 times that of 28-day samples but for PCC samples it was 0.65 to 0.69 times that of 28 days samples. From this data it was concluded that the early rate of gain of flexural strength is low in PGC but comparatively more than the compressive strength results. This may be happened due to exposure of more surface area of the prism than cube specimens to face the sunlight during ambient curing Fig. 5.

4.2 Void Ratio (%), Density and Permeability

The water permeability test results of the PCC and PGC are shown in Table 3. The water permeability of pervious cement concrete is higher than the PGC samples
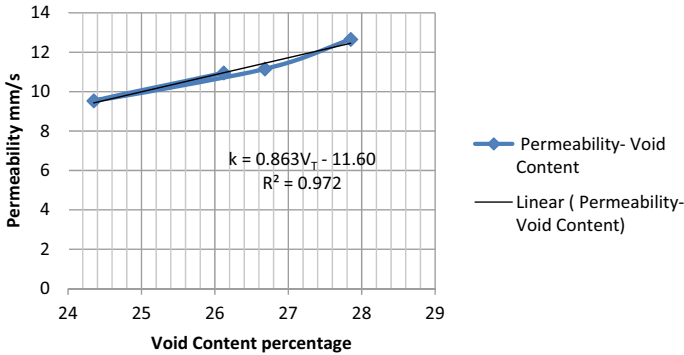
Fig. 6 Relation between permeability and void content

for same aggregate sizes and binder to aggregate ratio. However it can be observed PGC12 shows better water permeability than PCC [21].

Density of 12 M pervious geo-polymer concrete specimen (PGC12) is slightly higher than pervious cement concrete but the difference is not significant and also maximum among the PGC other specimens as shown in Table 3. On the other hand PCC have substantially higher amount of void content than PGC specimens. This may be the reason of higher permeability of PCC than PGC. We may also observed from Table 3, that higher the density of the specimens lesser the amount of void content. The co-relationship between coefficient of permeability and void ratio of all PGC specimens values are plotted as shown in Fig. 6. A simple linear curve was fitted nicely over the graph and the R^2 value was found out as 0.97, which indicates a strong relationship between coefficient of permeability (k) and total void ratio (V_T), i.e. $k = 0.863V_T - 11.60$. Similar nature of results is also reported by previous authors [16]. Thus it is clear that density and void content are related to each other and void content is inversely proportional with the density of pervious cement concrete as well as pervious geo-polymer concrete.

5 Conclusion

In order to investigate the effect of various parameters on strength and water permeability of PGC, 3 different type of pervious geo-polymer mixes were prepared, with respect to variable NaOH concentration (10, 12, 14 M).

On the basis of the experimental work and test results that are reported in this study, the following conclusions can be drawn.

Pervious concrete can be successfully manufactured by using geo-polymer binder in ambient curing temperature of compressive strength more than 15 MPa.

The porosity of the concrete, its age, and the binder material type all influence the compressive strength and water permeability of pervious geopolymer concrete. It has

been seen that ambient cured PGC shows very low strength gain at early age but it gains substantial strength after 7 days with age. The compressive strength increased with an increase in sodium hydroxide concentration up to a value of 12 M, and when NaOH is further increased, the compressive strength decreases. The optimum water permeability of PGC is obtained using the 12 M NaOH solution. The results of permeability and void ratio of PGC samples are strongly correlated each other. Further studies can be carried out to enhance the compressive strength by using other industrial waste as granulated blast furnace slag and micro silica etc.

References

1. Mehta PK (2002) Greening of the concrete industry for sustainable development. Concr Int 24(7):23–28
2. Freeborn JR, Sample DJ, Fox LJ (2012) Residential stormwater: methods for decreasing runoff and increasing stormwater infiltration. J Green Build 7(2):15–30
3. Sansalone J, Kuang X, Ranieri V (2008) Permeable pavement as a hydraulic and filtration interface for urban drainage. J Irrig Drain Eng 134(5):666–674
4. Yang J, Jiang G (2003) Experimental study on properties of pervious concrete pavement materials. Cem Concr Res 33:381–386
5. Mustafa R, Shivaprasad KN, Das BB (2019) Effect of various additives on the properties of fly ash based geopolymer mortar. In: Select proceedings of ICSCBM 2018. Springer, pp 707–715
6. Renjith R, Shivaprasad KN, Das BB (2018) Properties of heat cured bottom ash based geopolymer mortar admixed with fly ash of different fineness. In: Advances in concrete, structural and geotechnical engineering. Bloomsbury Publishing Plc, pp 603–607
7. Prasanna KM, Tamboli S, Das BB (2020) Characterization of mechanical and microstructural properties of FA and GGBS-based geopolymer mortar cured in ambient condition. In: Select proceedings of ICRDSI 2019. Springer, pp 751–768
8. Kudachimath N, Raviraj HM, Das BB (2021) Effect of GGBS on strength of aluminium refinery residue stabilized by alkali solution. In: Select proceedings of TMSF 2019. Springer, pp 331–339
9. Shivaprasad KN, Das BB, Renjith R (2018) Influence of fineness of fly ash on compressive strength and microstructure of bottom ash admixed geopolymer mortar. Indian Concr J 92(3)
10. Sharath BP, Shivaprasad KN, Athikkal MM, Das BB (2018) Some studies on sustainable utilization of iron ore tailing (IOT) as fine aggregates in fly ash based geopolymer mortar. In: IOP conference series: materials science and engineering, vol 431, no. 9. IOP Publishing, p 092013 (1–8)
11. Davidovits J (1988a) Soft mineralogy and geo-polymers. In: Proceedings of the geo-polymer, first European conference on soft mineralogy. The Geo-polymer Institute, Compiegne, France, pp 19–24
12. Davidovits J (1988b) Geo-polymer chemistry and properties. In: Proceedings of the geo-polymer, first European conference on soft mineralogy. Compiegne, France, pp 25–48
13. Hardjito D, Wallah SE, Sumajouw DM, Rangan BV (2004) On the development of fly ash-based geo-polymer concrete. ACI Mater J 101(6):467–472
14. American Concrete Institute (ACI) (2008) Report on pervious concrete. ACI-522-R-08
15. Snehal K, Das BB (2019) Mechanical and permeability properties of hybrid fibre reinforced porous concrete. Indian Concr J 93(1):54–59
16. Sata V, Chindaprasirt P, Wonga A (2013) Properties of pervious geo-polymer concrete using recycled aggregates. Constr Build Mater 42:33–39
17. Zaetang Y, Sata V, Chindaprasirt P, Wonga A (2015) Use of coal ash as geo-polymer binder and coarse aggregate and coarse aggregate in pervious concrete. Constr Build Mater 96:289–295

18. Omer A, Bzeni DKH, Zangy RRA, Arioz E (2020) Properties of slag-based geopolymer pervious concrete for ambient curing condition. Mater Sci Eng 737:1–9
19. Tho-in T, Sata V, Chindaprasirt P, Jaturapitakkul C (2012) Pervious high calcium fly ash geo-polymer concrete. Constr Build Mater 366–371
20. Shah DS, Pitroda J (2014) An experimental study on hardened properties of pervious concrete. J Int Acad Res Multidiscip 2(3):332–338
21. American Society for Testing and Materials (ASTM) (2008) Standard test method for density and void content of freashly mixed pervious concrete. ASTM C1688/C 1688 M-10 a. Annual book of ASTM standard (04.02). West Conshohcken

Ferrochrome Powder as a Partial Replacement of Cement

Asish Kumar Pani, Prasanna Kumar Acharya, and Jayaram Tripathy

1 Introduction

Cement concrete is considered as the second most consumed material next to the water. The demand for concrete and thereby the demand for cement is also increasing day by day. Cement production consumes huge natural resources and non-renewable energy, on the other hand, produces huge carbon dioxide. As such due to the production of cement not only the natural resources are depleted but also the environment is polluted. According to Sanjuan et al. [1] cement manufacturing accounts for 7.4% of world carbon dioxide emissions, or around 825–890 kg of CO_2 per tonne preparation of cement clinker. Various waste products are blended with cement as supplemental cementitious materials to reduce carbon dioxide emissions caused by cement manufacture [2–8]. Sanjuan et al. [1] have reported that manufacturing of blended cement using alternative materials to clinker and other methods like substitute raw materials, fuel alternatives etc., the carbon dioxide emission can be reduced to 630 kg per tonne of cement produced. An abnormally high requirement for concrete is the main cause of massive cement production, that results in significant loss of energy and emission of greenhouse gas. Scientists are striving around the world to identify alternative materials of cement with superior properties in order to rescue the earth from an ecological standpoint. Scientists are also working for developing substitute raw materials, reducing consumption fossil fuel, reducing consumption of energy, using substitute clinker and so on [9].

The reuse of waste stream materials is accepted as raw materials of concrete. Researchers around the globe are working hard continuously to reduce, reuse and sustainably recycle the waste materials to achieve a circular economy [10–12]. In recent past years, many industrial waste materials are reported to be used as substitute cementitious materials and aggregates of concrete. Ferrochrome powder (FP) is a

A. K. Pani · P. K. Acharya (✉) · J. Tripathy
School of Civil Engineering, KIIT DU, Bhubaneswar, Odisha, India

waste material obtained from the stainless steel producing industry. The production of ferrochrome requires mostly of 2.5 MT of chromite ore for producing 1 MT of ferrochrome, because of which, about 1–12 MT of waste gets generated Chethan et al. [13]. It has gained some engineering properties because of which it can be used as a supplementary cementitious material.

Mohanty et al. [14] has used a combination of FP and Fly ash (FA) for replacement of OPC and reported that the compressive strength is maximum with a dosage of 30% FA + 3% FP on replacement with cement. The compressive strength increased 39 and 49% in between 7–28 and 7–56 days respectively in optimum use of 30% FA + 3% FP. The flexural strength also increased proportionally with compressive strength. Dattani et al. [15] used FP and lime in self-compacting concrete and reported that maximum compressive strength is obtained with the use of 30% FP and 10% lime. They reported up to 50% use of FP with lime enhanced the compressive, flexural and tensile strength. The Workability and fresh density increased because of the inclusion of FP with lime. The sorptivity of self-compacting concrete (SCC) is also found less than the normal concrete. The authors have recommended the use of 50% FP with lime for self-compacting concrete. Mohanty et al. [16] investigated the structural performance of cement concrete beams containing varying contents of FP and FA as partial cement replacement. The authors replaced 10, 20, and 30% of the fly ash with 3% FP. According to the authors' findings, the concrete with 30% FA and 3% FP has the highest load-carrying ability of all the beam samples. Furthermore, the FA and FP beam samples are reported to have greater ductility than standard concrete. Due to the combined effect of 30% FP and 10% GP with OPC, Mohanty and Parhi [17] observed that the usage of FP and gypsum powder (GP) has favourable implications that are noticeable on early age strength and 28d strength. According to the authors, concrete containing ferrochrome ash FP and GP is environmentally benign, has a good fireproofing capability, and may be used for a variety of applications.

FP has been dubbed flue dust by Rao et al. [18], who claim that the dust obtained from the ferrochrome plant is one such waste material that contains chromite minerals. Flue dust from the ferrochrome production is harmful due to the poisonous nature of trivalent and hexavalent chromium. According to Acharya and Patro [19], when FP is used 40% and lime is used 7%, the water requirement increases, the flowability and setting times decreases, and the soundness remains constant. Compressive strength develops with age. At all ages, the replacement of 47% OPC with FA and lime achieves the strength of regular concrete. The addition of FP and lime boosts the ultrasonic pulse velocity and impermeability.

Because of the addition of FP and lime, the slump value decreased and density increased marginally, according to Acharya and Patro [20]. With the addition of FP and lime, strength qualities improved, and this trend remained with age. The addition of lime and FP lowered the sorptivity. The ability to withstand acid and sulphate attacks has improved. In compared to their counterparts without FP and lime, the degree of hydration measured at 28 days is higher in mixes with FP and lime. With the addition of FP and lime, the bond between aggregates and matrix strengthened, and the breadth of micro gaps shrank. The finest qualities are obtained by a concrete mix comprising 10% FA and 7% lime, according to the scientists. The

finest qualities are obtained by a concrete mix comprising 10% FA and 7% lime, according to the scientists. The combined effect of FCA and lime on compressive strength development is observed to be considerable at an early age, comparable at 28 days, and noteworthy at a late age, according to Acharya and Patro [20]. At all ages, the flexural strength and bond strength of concrete containing FCA and lime, which replaced OPC by up to 47%, improved dramatically. The use of FCA and lime improves the abrasion resistance. The addition of FCA and lime to concrete improves the abrasion resistance of the material. At all ages, the sorptivity of concrete mixes including FCA and lime was shown to be lower than the control mix [21]. Acharya and Patro According to the study, replacing up to 47% of OPC with ferrochrome ash (FCA) 40% and lime 7% has a comparable favourable impact on 28-day strength and a significant influence on long-term strength qualities. The use of 40% FCA and 7% lime in replacement of an equal amount of cement has a positive effect on the different mix proportions required for different types of concrete projects. Because to the beneficial effects of FCA and lime, the overall void content got reduced.

The study of the literature showed that not many works have been published on the use of FP in concrete. Authors of the past have used FP with lime, gypsum and fly ash. FP is also used in making geopolymer concrete. The use of FP alone as supplementary cementitious material is scary to see. The present work is intended to help fill this gap.

2 Materials and Methods

2.1 Cement

OPC-33 grade cement with various properties as shown in Table 1 was used in this study.

Table 1 Properties of OPC-33 grade

Physical properties	Test result obtained
Soundness (mm)	0.7
Initial setting time (Min)	150
Final setting time (Min)	250
3 days compressive strength (MPa)	17.5
7 days compressive strength (MPa)	24.6
28 days compressive strength (MPa)	38.5
Standard consistency (%)	28.1
Fineness (M^2/Kg)	317

Table 2 Chemical composition of FP

Name of the elements	%
Cr_2O_3	12.4
SiO_2	19.6
Al_2O_3	11.1
MgO	15.6
Fe_2O_3	6.06
CaO	4.22
CL	9.4
ZnO	2.59

2.2 Ferrochrome Powder

Ferrochrome powder was procured from Balasore Alloys Limited located in Balasore. The chemical composition of FP is presented in Table 2.

2.3 Aggregates

For the preparation of cement concrete sand was collected from nearby area river conforming to the standard—Zone-III as mentioned in IS: 383-1970 [22]. Black hard crusher broken coarse aggregate of 10–20 mm size confirming to the standards of IS: 383-1970 [22] was collected from nearby crushers.

2.4 Water

Clean portable water was used for mixing and curing purpose, properties of which are presented in Table 3.

Table 3 Properties of water

Parameters	Values
Sulphates (mg/l)	74
Suspended solids	0
MPN value/100 ml	0
pH value	7.1
Chlorides (mg/l)	20
Dissolved solids(mg/l)	290

2.5 Methods

2.5.1 Mix Proportion

A mix of M-30 grade concrete was prepared based on the guide lines of IS 10262:2009 [2]. For this purpose 410 kg of OPC 33 grade cement, 660 kg of fine aggregates, 1280 kg of coarse aggregates and 164 kg of water were used. The normal concrete using the above quantities of materials was named as R0. The concrete mixes prepared replacing 10, 20, 30 and 40% of OPC were named as R1, R2, R3 and R4 respectively.

2.5.2 Sample Preparation and Curing

Cubical samples of size 150 mm were prepared for compressive strength test, cylindrical samples of size 150 mm diameter and 300 mm height for split tensile test and prismoidal samples of 100 mm × 100 mm × 500 mm for flexural strength tests were prepared. After 24 h, the specimen was opened from the moulds immersed in water till their testing at the age of 7, 28 and 91 days.

2.5.3 Procedure

The compressive and flexural strength were tested as per IS: 516-1959 [3]. The test of split tensile strength was conducted as per IS: 5816-1999 [4]. The average result of the three samples was considered as the final result of the mix.

3 Results and Discussion

3.1 Compressive Strength

The compressive strengths of all mixes were as curtained at the age of 7, 28 and 91 days. The normal concrete (R0) showed a strength of 33.68, 38.49 and 42.76 MPa at 7, 28 and 91 days. The concrete mix R1 with 10% FP showed a decrease of strength 23, 13 and 22% at 7, 28 and 91 days respectively. The concrete mix R2 with 20% FP showed a decrease of strength 22, 19 and 28% at 7, 28 and 91 days respectively. At the same age of testing, the mix with 30% of FP (R3) suffered loss of strength 23, 18 and 19% respectively. Similarly, the mix with the highest 40% FP content (R4) obtained less strength 42, 25 and 20% at 7, 28 and 91 days respectively in comparison to normal concrete. The trend of results of R3 and R4 is found different from that of R1 and R2. The results indicated that with the increase in FP content and age the reduction % of strength got lowered. This may be due to the availability of pozzolanic materials and continued pozzolanic reaction up to late age. The results

Fig. 1 Compressive strength
of concrete mixes
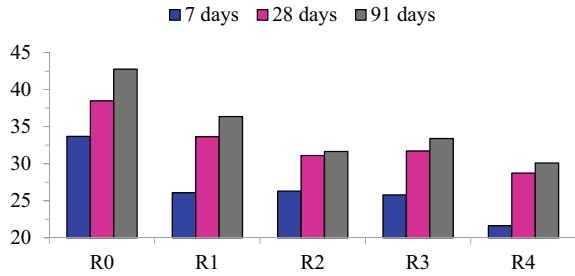
are presented in Fig. 1. The results indicated that due to supplementation of FP, there is no improvement in strength, rather there is the loss of strength. Perhaps from this point of view authors of the past have taken some other mineral mixtures with FP. The reason of declination of strength on replacement of cement by FP may be attributed to the deficiency of lime in the blended mix. The study of the result revealed another aspect that the mix with the lowest dosage of FP (10%) and the highest dosage of FP (40%) obtained strength around 39 and 29 MPa at 28 days. The normal concrete mix which was prepared for a characteristic strength of 30 MPa with a target strength of 43 MPa, showed the result of 39 and 29 MPa at 28 days on replacement of 10 and 40% OPC by FP. Using 40% FP, thereby saving 40% OPC and getting the strength of 29 MPa may also be considered important from a waste utilization point of view and circular economy. The concrete having the strength of 29 MPa can be used for many general and medium strength structural concrete.

3.2 Flexural Strength

The flexural strengths of all mixes were ascertained at the age of 7, 28 and 91 days. The normal concrete (R0) showed a strength of 7.00, 7.30 and 7.60 MPa at 7, 28 and 91 days. When 10% cement was replaced by FP in concrete mix R1 the flexural strength got decreased 21, 5 and 7% at 7, 28 and 91 days respectively. The concrete mix R2 with 20% FP showed a decrease of strength 31, 33 and 22% at 7, 28 and 91 days respectively. At the same age of testing, the mix with 30% of FP (R3) suffered the loss of strength up to 36%. The mix with the highest 40% FP content (R4) obtained less strength up to 40% in between 7 and 91 days in comparison to normal concrete. The results are shown in Fig. 2. The results showed that due to the inclusion of FP, as like compressive strength, the flexural strength got decreased. The reason may be attributed to the fact due to supplementation of FP, the blended mix suffered from calcium oxide deficiency. FP has less calcium oxide content than OPC.

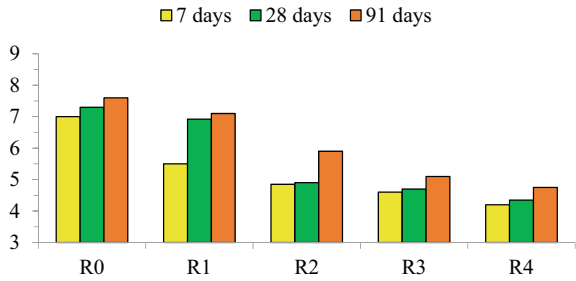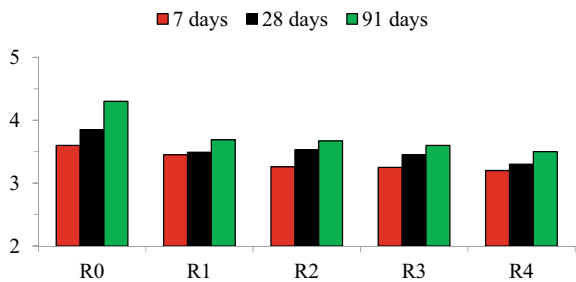Fig. 2 Flexural strength of concrete mixes

Fig. 3 Splitting tensile strength of concrete mixes

3.3 Split Tensile Strength

The split tensile strength of all mixes was ascertained at the age of 7, 28 and 91 days. The control concrete (R0) showed a strength of 3.60, 3.85 and 4.30 MPa at 7, 28 and 91 days respectively. The concrete mix R1 showed a strength of 3.45, 3.49 and 3.69 MPa at at the same age. The concrete mix R2 with 20% FP exhibited strength 3.26, 3.53 and 3.67 MPa at 7, 28 and 91 days respectively. At the same age of testing, the mix with 30% of FP (R3) showed a result of 3.25–3.60 MPa in between 7 and 28 days. The same for the mix R4 was measured 3.20–3.50 MPa in between 7 and 28 days. The results are presented in Fig. 3. Results showed that there is a declination of split tensile strength on the supplementation of FP. Due to the supplementation of FP, the proportioning of oxide contents got unbalanced and the lime saturation factor got reduced for which the strength properties got reduced.

4 Conclusion

Based on the materials used and parameters studied, the following a few conclusions are derived from the current study:

- Due to the inclusion of 40% FP, the compressive strength at 28 days got reduced by around 25% than conventional concrete.

- The mix containing 40% FP exhibited the compressive strength 29 MPa, which can be considered as a medium-strength concrete.
- Thus saving in 40% cement due to the utilization of a waste stream material like FP and obtaining a medium-strength concrete may be considered important as far as economy and ecology are cocerned.
- There is a reduction in tensile strength due to the supplementation of FP.

References

1. Sanjuan MA, Andrade C, Mora P, Zarogoza A (2020) Carbon dioxide uptake by cement based materials: a Spanish case study. Appl Sci 10:339. https://doi.org/10.3390/app10010339
2. Snehal K, Das BB, Kumar S (2020) Influence of integration of phase change materials on hydration and microstructure properties of nano silica admixed cementitious mortar. J Mater Civil Eng ASCE 32(6)
3. Snehal K, Das BB, Akanksha M (2020) Early age, hydration, mechanical and microstructure properties of nano-silica blended cementitious composites. Constr Build Mater Elsevier 233
4. Snehal K, Das BB (2019) Techniques for preparation and dispersion of nano-SiO$_2$ in cementitious system—a review. In: Select proceedings of ICSCBM 2018. Springer, pp 397–407
5. Snehal K, Das BB (2021) Experimental set-up for thermal performance study of phase change material admixed cement composites—a review. In: Select proceedings of SMTS 2019. Springer pp 137–149
6. Snehal K, Das BB (2020) Application of Andreassen and modified Andreassen model on cementitious mixture design: a review. In: Select proceedings of ICRDSI 2019. Springer, pp 729–750
7. Snehal K, Das BB (2021) Influence of incorporating phase change materials on cementitious system—a review. In: Select proceedings of TMSF 2019. Springer, pp 33–63
8. Das BB, Snehal K (2018) Engineering properties of nano-particles admixed concrete—a review. In: Advances in concrete, structural and geotechnical engineering. Bloomsbury Publishing Plc, pp 190–195
9. Sanjuan MA, Argiz C, Mora P, Zarogoza A (2020) Carbon dioxide uptake in road map 2050 of the Spanish cement industry. Energies 10:3452. https://doi.org/10.3390/en13133452
10. Renjith R, Shivaprasad KN, Das BB (2018) Properties of heat cured bottom ash based geopolymer mortar admixed with fly ash of different fineness. In: Advances in concrete, structural and geotechnical engineering. Bloomsbury Publishing Plc, pp 603–607
11. Goudar SK, Shivaprasad KN, Das BB (2019) Mechanical properties of fiber reinforced concrete using coal-bottom ash as replacement of fine aggregate. In: Select proceedings of ICSCBM 2018. Springer, pp 863–872
12. Goudar SK, Das BB (2021) Influence of particle size of bottom ash on mechanical properties of M30 grade concrete. In: Select proceedings of TMSF 2019. Springer, pp 533–543
13. Chethan Kumar B, Yaragal S, Das BB (2020) Ferrochrome ash—its usage potential in alkali activated slag mortars. J Clean Prod 257
14. Mohanty T, Majhi S, Saha P, Das B (2019) Combined effect of fly-ash and ferrochrome ash as partial replacement of cement on mechanical properties of concrete. In: E3S web of conferences, CGEEE 2018. https://doi.org/10.1051/e3sconf/20199302008
15. Dattani KR, Bhuva PK, Borad CV (2017) Performance of ferrochrome ash (FCA) with lime as partial replacement of cement in self compacted concrete. J Emerg Technol Innov Res 4(4):269–277
16. Mohanty T, Saha S, Saha P, Das B (2019) Structural behaviour of concrete with fly-ash and ferrochrome ash as partial replacement of cement. Int J Rec Technol Eng 8(4):11086–11091

17. Mohanty S, Parhi PK (2017) Impact of ferrochrome ash and gypsum powder on properties of concrete. Int J Eng Res Technol 6. https://doi.org/10.17577/IJERTV6IS070016
18. Rao DS, Angadi SI, Muduli SD, Nayak BD (2010) Valuable waste. Mineral processing, English Edition, vol 51, pp 2–6
19. Acharya PK, Patro SK (2015) Effect of lime and ferrochrome ash (FA) as partial replacement of cement on strength, ultrasonic pulse velocity and permeability of concrete. Constr Build Mater 94:448–457
20. Acharya PK, Patro SK (2016) 457Acid resistance, sulphate resistance and strength properties of concrete containing ferrochrome ash (FA) and lime. Constr Build Mater 120:241–250
21. Acharya PK, Patro SK (2016) Strength, sorption and abrasion characteristics of concrete using ferrochrome ash (FCA) and lime as partial replacement of cement. Cement Concr Compos 24:16–25
22. Acharya PK, Patro SK (2016) Use of ferrochrome ash (FCA) and lime dust in concrete preparation. J Clean Prod. https://doi.org/10.1016/j.jclepro.2016.05.042

Seismic Performance of Steel Frames with Shape Memory Alloy (SMA) Bracing System

Thaer Alkateeb and Asheena Sunny

1 Introduction

The ease of applicability and comparably less weight, steel frames are being widespread key element used in structural projects. Several models have used to uplift the performance of frames in terms of seismic resistance targeting increasing elasticity, dissipation energy and reducing drift storey and permanent deformation. Therefore, Shape memory alloys, or SMA in short, is a suitable material aiming to have well-performed braces. Uniquely special traits well-known as super elasticity or Pseudo elasticity (SE/PE), SMA has a potential ability restoring sizeable elasticity after removal of loads and with its hysterical loop behavior [1–6]. According to its structure, it primarily correspond to both the stress state and the temperature, which the letter pertain to the chemical composition and the heat treatment process. It can be observed 'Fig. 1' in turn of non-stressed SMA alloy the two fundamental transformation processes:

1—Martensite phase: This phase is ranging between two temperature values, Ms as initial point and Mf as lasting one. Amid this range, it is Stable at high pressure values and low temperatures.

2—Austenite phase: This phase is ranging between two temperature values, beginning at A_s and ending at temperature A_f, and it is stable at low pressure values and high temperature.

Looking at previous works [8], the principle was to analyze the performance of steel building in hilly areas where regarded to earthquake incidences faced by X-knee-braced tires with SMA built-in. As a result, it had shown reducing in storey drift but the storey displacement remains the same. With same methodology, Jalili et al. [9] had designed and tested the impact of seismic relating to SMA bars as

T. Alkateeb · A. Sunny (✉)
School of Civil Engineering, KIIT-DU, Bhubaneswar, India
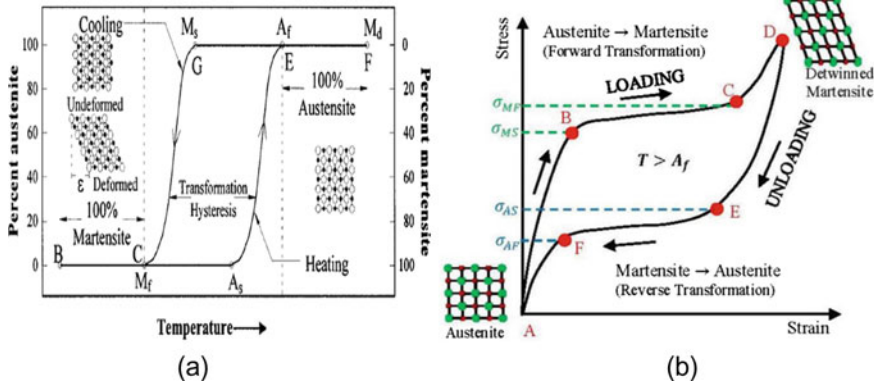e-mail: Asheena.sunnyfce@kiit.ac.in

Fig. 1 **a** Thermal transformation processes of SMA **b** Stress and strain curve [7]

shaped called X-Knee Braces Frames or (X-KBFs). This experiment placed super-elastic elements between the joints (beam column) and knee members for many storey buildings (3–5–7) and resulting to lessen the storey displacement as well as a significant increase in the re-centring capacity of the structure.

2 Objectives

The present study focus on the following objectives:

(1)   To compare the steel frames with and without SMA braces.
(2)   To analyze the performance of steel frames with 3 configuration of SMA braces using ABAQUS.

3 Finite Element Analysis

The present study was conducted using the software ABAQUS 2020. The suggested 2D steel frame of 3 storey is shown in 'Fig. 2'. The aim of this study is to improve the seismic performance of the steel frame by testing three models shown in 'Fig. 3'. The first model consisting of reinforcing the joints with rods made of SMA. At second model, X-brace SMA is used. Thirdly model configuration is v-brace mirrored SMA. The work mainly will be focused on:

- Behaviour the frame under cyclic loading
- Seismic behaviour comparison between three models

The frame contains three storey having a distance between the columns (3 m in length each) with same length for each storey. In Table 1, there are section properties
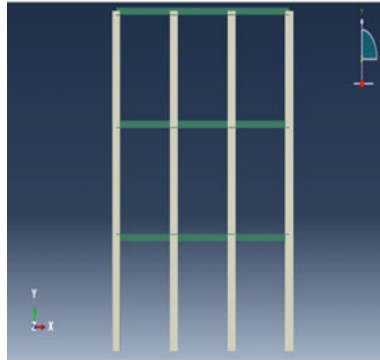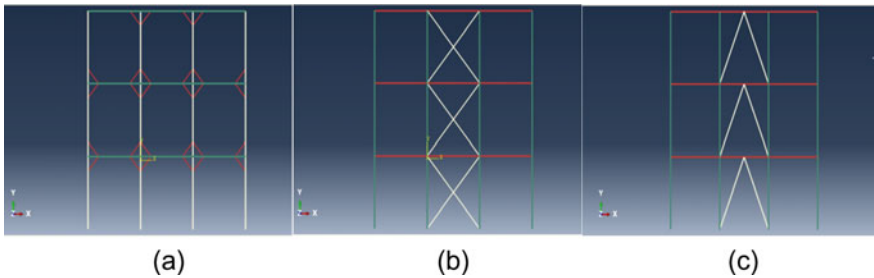
Fig. 2 Bare frame

Fig. 3 **a** First model **b** second model **c** third model

Table 1 Section properties

Element	Section	Depth of the section, d (mm)	Width of the flange, b_f (mm)	Thickness of flange, t_f (mm)	Thickness of web, t_w (mm)
Column	ISWB 400	400	200	13	8.6
Beam	ISLB 200	200	100	7.3	5.4

assigned to the frame. Moreover, both steel and SMA's mechanical properties are described in 'Tables 2 and 3' respectively.

In ABAQUS 2020, the element B21 is used for modelling column as well as beam. This element is a linear component consisting of two nodes in the same plane. Additionally, for SMA modelling, T2d2 element is used which is a truss composed

Table 2 Steel properties

Modules of elasticity	Poisson's ratio	Yield stress
210,000 MPa	0.3	250 MPa

Table 3 Mechanical properties of SMA [9]

Quantity	Symbol	Value
Austenite to martensite starting stress	$\sigma sA \rightarrow M$	414 MPa
Austenite to martensite finishing stress	$\sigma fA \rightarrow M$	550 MPa
Martensite to austenite starting stress	$\sigma SM \rightarrow A$	390 MPa
Martensite to austenite finishing stress	$\sigma fM \rightarrow A$	200 MPa
Modulus of elasticity for austenite	EA	27.6 GPa
Maximum residual strain	εL	3.5%

Fig. 4 Truss element T2D2 [10]
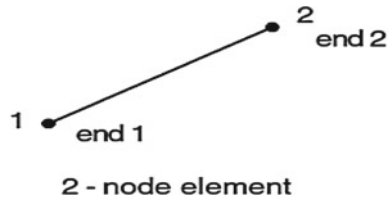
one element and two nodes with two degrees of freedom for each node, shown in 'Fig. 4'.

4   Non-liner Static Analysis

It is a model in which analysis is performed under permanent vertical loads and lateral loads are gradually increased to estimate the deformation and wear pattern of the structure. Recentering refers to the ability of a material to return to its original undeformed shape upon unloading. For this, a lateral load in the direction of slope (X-direction) is applied cyclic load on the right top-most portion of the test frame, is depicted in 'Fig. 5'.

Fig. 5 Diagram cyclic load
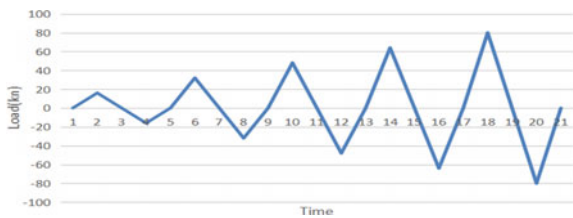
5   Results and Discussion

The stress results obtained from FEM analysis is used for the present study. For the bare frame, it can be seen that the overshooting the stress verge by about 20% of yield stress which is 250 MPa and recorded at 298 Mpa shown in Fig. 6. Therefore, it has reached a phase of plasticity. The second model configuration i.e., reinforcing the joints with rods made up of shape memory alloy (SMA) shown in Fig. 7 experiences the drop of stress value and reduced to 215.9 Mpa which means that the frame remains
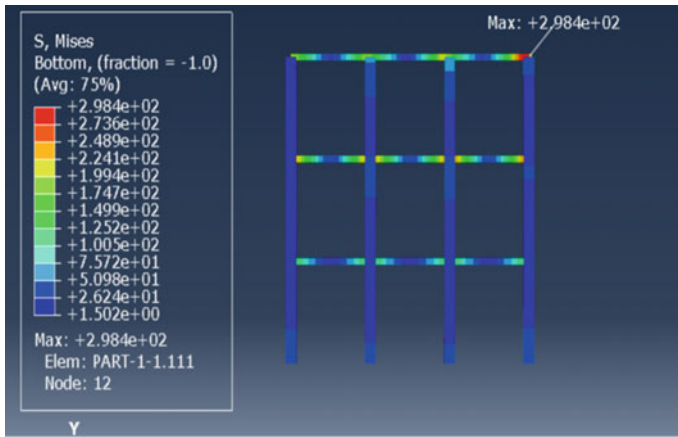
Fig. 6 Bare frame stress
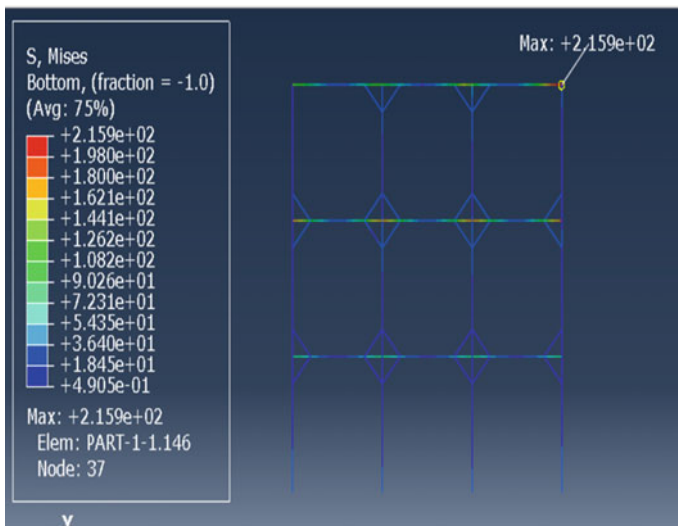
Fig. 7   Joints reinforcement (model 1) stress

within the permissible stress and elasticity phase. Tuning into the stress results of second model shown in Fig. 8, the usage of X-brace SMA frames are shown a little improvement about 5% from 250 to 238.9 Mpa. Lastly, the third model deploying v-brace mirrored SMA shown in Fig. 9, has a negative impact by increasing stress beyond yield stress, about 12%.

The comparison between bare frame and used models in terms of maximum stress is represented in Table 4.

In overall perspective, the bar chart compares the reduction in stress between SMA braced systems with bare frame and depicted in Fig. 10. It can be seen the superiority of first model with up to a one-quarter percentage of in total stress of
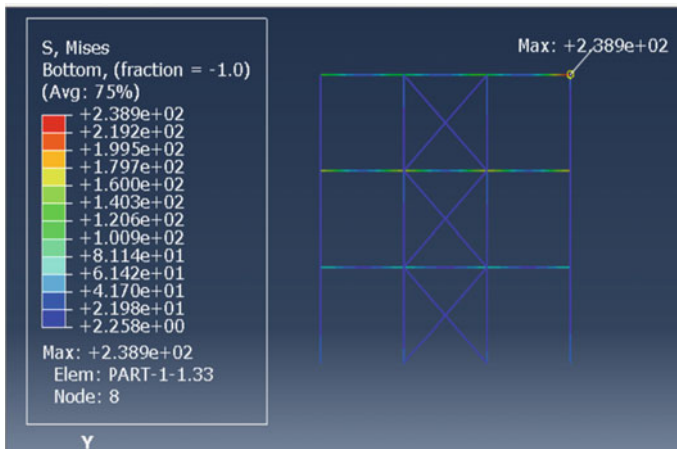

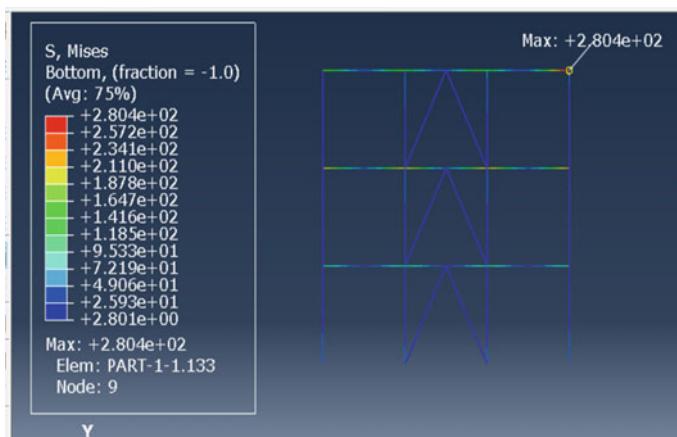Fig. 8 X-brace frame SMA (model 2) stress

Fig. 9 V-brace mirrored SMA (model 3) stress

Table 4 Comparison of stress

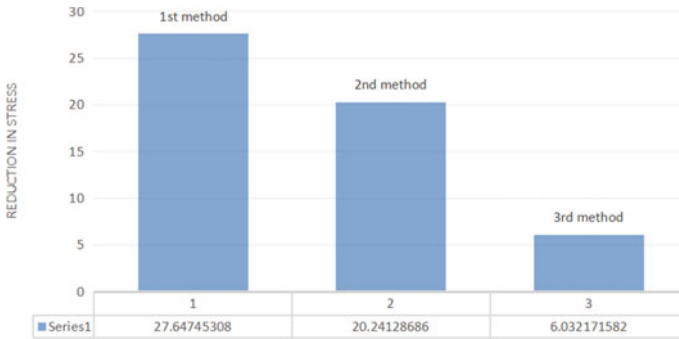|	Bare frame	First-model (SMA)	Second-model (SMA)	Third-model (SMA)
Stress (S) Mpa	298.4	**215.9**	238.9	280.4

Fig. 10 Graphical comparison of percentage reduction in stress

Bare frame. Followed by the second and then third model with reduction of 20 and 6% respectively

6 Conclusion

A finite element analysis with the use of ABAQUS was carried out in a 3 bay portal frame with and without braced systems by performing nonlinear static analysis. The study was conducted by considering different configurations of bracings with SMA and leads to the flowing conclusions:

- Using SMA can improve seismic performance in steel frames by energy dissipation and reducing stresses.
- In the first model consisting of SMA reinforcement at the joints provided the highest reduction in stress comparison with other models used hence it can be concluded that model 1 is more effective.

The present study was only focused on stress analysis in steel frames and further the study can be extended to storey drift analysis of braced SMA in 3D steel buildings. It is also required to conduct experimental study to validate the conceptualization.

References

1. Omidian P, Saffari H (2018) Comparative analysis of seismic behavior of RC buildings with shape memory alloy rebar in regular, torsional irregularity and extreme torsional irregularity cases. J Build Eng 20:723–735
2. Shaji G (2016) Seismic control of structures using shape memory alloys. IOSR J Mech Civil Eng (IOSR-JMCE) 54–58
3. Asgarian B, Moradi S (2011) Seismic response of steel braced frames with shape memory alloy braces. J Constr Steel Res 67(Issue 1):65–74
4. Qiu C-X, Zhu S (2017) Performance-based seismic design of self-centering steel frames with SMA-based braces. Eng Struct 130:67–82
5. Bartera F, Giacchetti R (2004) Steel dissipating braces for upgrading existing building frames. J Constr Steel Res 60(Issues 3–5):751–769
6. Ghowsi AF, Sahoo DR (2020) Seismic response of SMA-based self-centering buckling-restrained braced frames under near-fault ground motions. Soil Dyn Earthq Eng 139:106397. https://doi.org/10.1016/j.soildyn.2020.106397
7. Alam MS, Youssef MA, Nehdi M (2007) Utilizing shape memory alloys to enhance the performance and safety of civil infrastructure: a review. Can J Civ Eng 34(9):1075–1086
8. Sreenivas R (2020) Seismic performance of steel X-knee-braced frames equipped with shape memory alloy bars in step back buildings on hillside slope. 7(issue 7)
9. Jalili M, Mahmoudi M, Montazeri S (2018) Seismic performance of steel X-knee-braced frames equipped with shape memory alloy bars. J Constr Steel Res 147C:171–186. https://doi.org/10.1016/j.jcsr.2018.03.019
10. Hasan H, Almnini L, Hasan H, Al-Helwani A (2015) Seismic performance of steel frames equipped with buckling restrained brace. Int J Eng Res Sci Technol 4